Food Engineering Series

José Miguel Aguilera
Gustavo V. Barbosa-Cánovas
Ricardo Simpson · Jorge Welti-Chanes
Daniela Bermúdez-Aguirre *Editors*

Food Engineering Interfaces

Springer

Food Engineering Series

For other titles published in this series, go to
www.springer.com/series/5996

José Miguel Aguilera • Gustavo V. Barbosa-Cánovas • Ricardo Simpson • Jorge Welti-Chanes • Daniela Bermúdez-Aguirre
Editors

Food Engineering Interfaces

Springer

Editors
Prof. José Miguel Aguilera
Pontificia Universidad Católica de Chile
Dept. de Ingeniería Química y
Bioproceso
Vicuña Mackenna 4860
Santiago
Chile
jmaguile@ing.puc.cl

Dr. Ricardo Simpson
Universidad Técnica Federico
Santa María
Depto. Procesos Químicos,
Biotecnológicos y Ambientales
Av. España 1680
Valparaíso
Chile
ricardo.simpson@usm.cl

Dr. Daniela Bermúdez-Aguirre
Washington State University
Dept. Biological Systems Engineering
213 LJ Smith Hall
99164-6120 Pullman
Washington
USA
daniela@wsu.edu

Dr. Gustavo V. Barbosa-Cánovas
Washington State University
Dept. Biological Systems
Engineering L.J. Smith Hall 220
Pullman, WA 99164-6120
USA
barbosa@wsu.edu

Dr. Jorge Welti-Chanes
Director de Post y Pregrado
División de Biotecnología y Alimentos
Instituto Tecnológico y de Estudios
Superiores de Monterrey
Av. Eugenio Garza Sada 2501 Sur
Col. Tecnológico
64849 Monterrey
N.L. México
jwelti@itesm.mx

ISSN 1571-0297
ISBN 978-1-4419-7474-7 e-ISBN 978-1-4419-7475-4
DOI 10.1007/978-1-4419-7475-4
Springer New York Heidelberg Dordrecht London

Preface

The articles included in *Food Engineering Interfaces* are based on the presentations made by invited speakers of the 10th International Congress on Engineering and Food (ICEF 10) held in Viña del Mar, Chile, in April 2008. All the chapters were significantly upgraded from the original presentations and were later peer-reviewed and copyedited. This book was conceived well ahead of the event in order to make sure that readers would have the opportunity to get a taste of the challenges that lie ahead. At the same time, efforts were made to cover, with a high degree of detail, specific topics that are very relevant at the present time. As a result, this book is an excellent addition to the literature as the topics are well blended and clearly expand old food engineering boundaries.

The book is divided into five parts: selected topics in food engineering, advances in food process engineering, water management in food, food microstructure, and food packaging. All the 28 chapters have been written by renowned professionals working in food engineering and related disciplines. The first chapter of the book deals with the history and future of food engineering, and the remaining chapters in Part I deal with topics such as microbial risk assessment using new engineering tools, the development of eco-indicators to monitor the environmental impact on selected food industries, the mathematical simulation of gastric digestion, the engineering challenges posed by incorporating fiber in selected foods, the applications of computational fluid dynamics (CFD) in food processing, food safety engineering, food engineering economics, and the systemic approach for curriculum development. Part II has two comprehensive overviews, one on advanced thermal processing and the other on nonthermal processing, as well as chapters dealing with the optimization of thermal processes, the sterilization of foodstuff by pressure-assisted thermal processing (PATS), and the extraction of essential oils and nutraceuticals by supercritical fluid extraction. Part III has a very good selection of chapters, including an update on glass transition in foods, caking in food powders, the rehydration modeling of food particulate systems, and the identification of drying zones in a laboratory spray-dryer. Part IV includes a chapter that envisions how food microstructure studies will help the development of healthy foods that promote well-being and pleasure, as well as a chapter that deals with the analysis of food microstructures by synchrotron X-ray-computed tomography. Finally, Part V covers, among other topics, the utilization of edible coatings as food safety

and quality enhancers, physical properties of gel-based edible films, and packaging materials based on renewable resources.

We truly hope that this book, with its visionary approach, will be a valuable addition to the food engineering literature and will promote interest in food engineering research, development, and implementation.

José M. Aguilera
Gustavo V. Barbosa-Cánovas
Ricardo Simpson
Jorge Welti-Chanes
Daniela Bermúdez-Aguirre

Acknowledgments

The editors would like to express their gratitude and appreciation to Sharon Himsl, Publication Coordinator, Center for Nonthermal Processing of Food, Washington State University, for her professionalism and dedication in facilitating the steps needed to complete this challenging project. She kept track of all the manuscripts and had them copyedited and effectively interacted with the editors, authors, and the staff at Springer.

Contents

Contributors

Alik Abakarov Departamento de Ingeniería Química y Ambiental, Universidad Técnica Federico Santa María, P.O. Box 110-V, Valparaíso, Chile

José Miguel Aguilera Department of Chemical and Bioprocess Engineering, Pontificia Universidad Católica de Chile, Santiago, Chile

Liliana Alamilla-Beltrán Departamento de Graduados e Investigación en Alimentos, Escuela Nacional de Ciencias Biológicas, Instituto Politécnico Nacional, Carpio y Plan de Ayala, s/n CP, 11340 México, DF, Mexico

Yves Arcand Agriculture and Agri-Food Canada's Food Research and Development Centre, 3600 Casavant Blud West, St. Hyacinthe, Quebec, Canada

Gustavo V. Barbosa-Cánovas Center for Nonthermal Processing of Food, Washington State University, Pullman, WA, USA

Daniela Bermúdez-Aguirre Center for Nonthermal Processing of Food, Washington State University, Pullman, WA, USA

Gerd Brunner Thermische Verfahrenstechnik, Technische Universität Hamburg-Harburg (TUHH), Harburg, Germany

Roman Buckow CSIRO Food and Nutritional Sciences, 671 Sneydes Road, VIC-3030 Werribee, Australia

Branko Bugarski Department of Chemical Engineering, University of Belgrade, Karnegijeva 4, 11000 Belgrade, Serbia

Osvaldo Campanella Agricultural and Biological Engineering Department, Purdue University, 47907 West Lafayette, IN, USA

Rosemary A. Carvalho Department of Food Engineering, University of São Paulo, Pirassununga (SP), Brazil

Jose Jorge Chanona-Pérez Departamento de Graduados e Investigación en Alimentos, Escuela Nacional de Ciencias Biológicas, Instituto Politécnico Nacional, Carpio y Plan de Ayala, s/n CP, 11340 México, DF, Mexico

Peter Cloetens European Synchrotron Radiation Facility, 6 Rue Jules Horowitz, BP 220, 38043 Grenoble Cedex, France

Valerie Davidson School of Engineering, University of Guelph, N1G 2W1 Guelph, Ontario, Canada

Juan C. de la Fuente Departamento de Procesos Químicos, Biotecnológicos y Ambientales, Universidad Técnica Federico Santa María, Valparaíso, Chile

Adriana Delgado FRCFT Group, Biosystems Engineering, UCD Agriculture & Food Science Centre, University College Dublin, Belfield, Dublin 4, Ireland

José M. del Valle Departamento de Ingeniería Química y Bioprocesos, Pontificia Universidad Católica (PUC) de Chile, Santiago, Chile

Carlos Daza Donoso School of Engineering, University of Guelph, N1G 2W1 Guelph, Ontario, Canada

Inés Ecima Ingeniería de Producción Agroindustrial, La Sabana University, Bogotá, Colombia

Carmen S. Fávaro-Trindade Department of Food Engineering, University of São Paulo, Pirassununga (SP), Brazil

Nathalie Gontard Joint Research Unit, Agropolymers Engineering and Emerging Technologies, Montpellier SupAgro, INRA, UM II, CIRAD, 34060 Montpellier, France

Gloria González-Mariño Biosciences Doctoral Program, La Sabana University, Bogotá, Colombia

Stéphane Guilbert Joint Research Unit, Agropolymers Engineering and Emerging Technologies, Montpellier SupAgro, INRA, UM II, CIRAD, 34060 Montpellier, France

Carole Guillaume Joint Research Unit, Agropolymers Engineering and Emerging Technologies, Montpellier SupAgro, INRA, UM II, CIRAD, 34060 Montpellier, France

Gustavo Fidel Gutiérrez-López Departamento de Graduados e Investigación en Alimentos, Escuela Nacional de Ciencias Biológicas, Instituto Politécnico Nacional, Carpio y Plan de Ayala, s/n CP, 11340 México, DF, Mexico

Bruce Hamaker Department of Food Science, Purdue University, 47907 West Lafayette, IN, USA

Volker Heinz German Institute of Food Technology, Prof.-von-Klitzing-Str. 7, D-49601 Quakenbrueck, Germany

Dennis Heldman Heldman Associates, 5224 Kings Mills Rd; #314, 45040 Mason, OH, USA

Humberto Hernández-Sánchez Departamento de Graduados e Investigación en Alimentos, Escuela Nacional de Ciencias Biológicas, Instituto Politécnico Nacional, Carpio y Plan de Ayala, s/n CP, 11340 México, DF, Mexico

Els Herremans Division BIOSYST-MeBioS, K.U.Leuven, W. de Croylaan 42, Box 2428, BE-3001 Leuven, Belgium

Quang Tri Ho Division BIOSYST-MeBioS, K.U.Leuven, W. de Croylaan 42, Box 2428, BE-3001 Leuven, Belgium

Antonio Ruperto Jiménez-Aparicio Centro de Desarrollo de Productos Bióticos del Instituto Politécnico Nacional, CEPROBI-IPN, Yautepec, Morelos, Mexico

Madhuvanti Kale Department of Food Science, Purdue University, 47907 West Lafayette, IN, USA

Greet Kerckhofs Research group of Materials Performance and Non-destructive Evaluation, Katholieke Universiteit Leuven, Kasteelpark Arenberg 44, BE-3001 Leuven, Belgium

Dietrich Knorr Department of Food Biotechnology and Food Process Engineering, Berlin University of Technology, Koenigin-Luise-Str. 22, D-14195 Berlin, Germany

Jozef L. Kokini Department of Food Science and Human Nutrition 2 College of ACES, University of Illinois at Urbana Champaign, 61801 Urbana, IL, USA

Denyse Landry Agriculture and Agri-Food Canada Head Quarter, 1341 Baseline Road, Tower 5, Floor 2, Room 126, Ottawa, ON, K1A OC5, Canada

Daryl B. Lund Department of Food Science, University of Wisconsin-Madison. 1605 Linden Dr., 53706 Madison, WI, USA

Verica Manojlović Department of Chemical Engineering, University of Belgrade, Karnegijeva 4, 11000 Belgrade, Serbia

Alejandro Marabí Institute of Biochemistry, Food Science and Nutrition, Robert H. Smith Faculty of Agricultural, Food and Environment, The Hebrew University of Jerusalem, P.O. Box 12, 76100 Rehovot, Israel

Michèle Marcotte Agriculture and Agri-Food Canada's Eastern Cereal and Oilseed Research Centre, 960 Carling Avenue, KW Neatby, Room 1093, Ottawa, ON, k1A OC6, Canada

Zacharias Maroulis School of Chemical Engineering, National Technical University of Athens, 15780 Athens, Greece

Alexander Mathys Department of Food Biotechnology and Food Process Engineering, Berlin University of Technology, Koenigin-Luise-Str. 22, D-14195 Berlin, Germany

Dominique Maxime Agriculture and Agri-Food Canada's Food Research and Development Centre, 3600 Casavant Blud West, St. Hyacinthe, Quebec, Canada

Hibru Kelemu Mebatsion Division BIOSYST-MeBioS, K.U.Leuven, W. de Croylaan 42, Box 2428, BE-3001 Leuven, Belgium

Fernando Mendoza FRCFT Group, Biosystems Engineering, UCD Agriculture & Food Science Centre, University College Dublin, D4 Belfield, Dublin, Ireland

Ulises Ramón Morales-Durán Departamento de Graduados e Investigación en Alimentos, Escuela Nacional de Ciencias Biológicas, Instituto Politécnico Nacional, Carpio y Plan de Ayala, s/n CP, 11340 México, DF, Mexico

Viktor A. Nedović Department of Food Technology and Biochemistry, University of Belgrade, Nemanjina 6, P.O. Box 127, 11081 Belgrade-Zemun, Serbia

Bart Nicolaï Division BIOSYST-MeBioS, K.U.Leuven, W. de Croylaan 42, Box 2428, BE-3001 Leuven, Belgium

Tomás Norton Food Refrigeration and Computerised Food Technology (FRCFT), University College Dublin, National University of Ireland, Agriculture & Food Science Centre, Belfield, Dublin 4, Ireland

Dhananjay Pai Whistler Center for Carbohydrate Research, Purdue University, 47907 West Lafayette, IN, USA

Stefan Palzer Nestlé Research Centre Lausanne, Vers-Chez-Les-Blanc, 1000 Lausanne 26, Switzerland

Maurcio Pardo Ingeniería de Producción Agroindustrial, La Sabana University, Bogotá, Colombia

María del Pilar Buera Departamentos de Industrias y de Química Orgánica, Facultad de Ciencias Exactas y Naturales, 1428 Ciudad de Buenos Aires, Argentina

Hosahalli Ramaswamy Department of Food Science, McGill University, Ste Anne de Bellevue, Montreal, Quebec, Canada

Kai Reineke Department of Food Biotechnology and Food Process Engineering, Berlin University of Technology, Koenigin-Luise-Str. 22, D-14195 Berlin, Germany

Yrjö H. Roos Department of Food and Nutritional Sciences, University College Cork, Cork, Ireland

Juliana Ruzante Joint Institute for Food Safety and Applied Nutrition, University of Maryland, 20742 College Park, MD, USA

I. Sam Saguy Institute of Biochemistry, Food Science and Nutrition, Robert H. Smith Faculty of Agricultural, Food and Environment, The Hebrew University of Jerusalem, POB 12, 76100 Rehovot, Israel

George Saravacos School of Chemical Engineering, National Technical University of Athens, 15780 Athens, Greece

Bernhard Seifried Department of Agricultural, Food and Nutritional Science, University of Alberta, T6G 2P5 Edmonton, Alberta, Canada

Nattiga Silalai Department of Food and Nutritional Sciences, University College Cork, Cork, Ireland

Ricardo Simpson Departamento de Ingeniería Química y Ambiental, Universidad Técnica Federico Santa María, P.O. Box 110-V, Valparaíso, Chile

R. Paul Singh Department of Biological and Agricultural Engineering, University of California, 95616 Davis, CA, USA

Samrendra Singh Department of Biological and Agricultural Engineering, University of California, 95616 Davis, CA, USA

Paulo J.A. Sobral Department of Food Engineering, University of São Paulo, Pirassununga (SP), Brazil

Karl Sommer Department of Process Engineering of Disperse Systems, Technical University of Munich, Am Forum 2, 85354 Freising, Germany

Da-Wen Sun Food Refrigeration and Computerised Food Technology (FRCFT), University College Dublin, National University of Ireland, Agriculture & Food Science Centre, Belfield, Dublin 4, Ireland

Arthur Teixeira Agricultural and Biological Engineering Department, University of Florida, 32611-0570 Gainesville, FL, USA

Feral Temelli Department of Agricultural, Food and Nutritional Science, University of Alberta, T6G 2P5 Edmonton, Alberta, Canada

Oranit Troygot Institute of Biochemistry, Food Science and Nutrition, Robert H. Smith Faculty of Agricultural, Food and Environment, The Hebrew University of Jerusalem, P.O. Box 12, 76100 Rehovot, Israel

Edgar Uquiche Departamento de Ingeniería Química, Universidad de La Frontera, Temuco, Chile

Nektarios Valous FRCFT Group, Biosystems Engineering, UCD Agriculture & Food Science Centre, University College Dublin, Belfield, Dublin 4, Ireland

Pieter Verboven Division BIOSYST-MeBioS, K.U.Leuven, W. de Croylaan 42, Box 2428, BE-3001 Leuven, Belgium

Kiran V. Vyakaranam Department of Food Science, Rutgers University, 08901 New Brunswick, NJ, USA

Rony Wallach Department of Soil and Water Sciences, Robert H. Smith Faculty of Agricultural, Food and Environment, The Hebrew University of Jerusalem, P.O. Box 12, 76100 Rehovot, Israel

Martine Wevers Research group of Materials Performance and Non-destructive Evaluation, Katholieke Universiteit Leuven, Kasteelpark Arenberg 44, BE-3001 Leuven, Belgium

Ronnie Willaert Structural Biology Brussels, Vrije Universiteit Brussel, Flanders Institute for Biotechnology, Pleinlaan 2, B-1050 Brussels, Belgium

Noemí Zaritzky Centro de Investigación y Desarrollo en Criotecnología de Alimentos (CIDCA), Universidad Nacional de La Plata (UNLP) – CONICET La Plata and Depto de Ingeniería Química, UNLP, La Plata, Argentina

Carsten Zetzl Thermische Verfahrenstechnik, Technische Universität Hamburg-Harburg (TUHH), Harburg, Germany

Part I
Selected Topics in Food Engineering

Chapter 1
The Beginning, Current, and Future of Food Engineering: A Perspective

Dennis R. Heldman and Daryl B. Lund

1.1 Introduction

Food engineering is a field of study that has emerged in rather recent history, but is based on concepts that have evolved over a significant period of time. In general, food engineering is the interpretation and application of engineering principles and concepts to any aspect of food manufacturing and operations, including the construction of the facilities for these operations. With this broad interpretation, almost any of the more traditional fields of engineering (electrical, mechanical, civil, chemical, industrial, and agricultural) would contribute to the successful operation of the facilities and processes dealing with food. Recent focus in food engineering has been on processes occurring within manufacturing operations, specifically on the influence of unique characteristics and properties of foods and ingredients in these processes.

The purpose of this paper is to review the history and current status of food engineering, and to provide a framework for discussion about its future. In addition to identifying some of the founding fathers and giants in food engineering, this review will include the development of educational programs and the role of food engineering within those programs. Attention will be given to evolution of research and the potential of food engineering research in the future. Finally, there will be an attempt to evaluate the impact of public sector research on research conducted within the food industry, as well as applications of research within the industrial sector.

D.R. Heldman (✉)
Heldman Associates, 5224 Kings Mills Rd; #314, 45040 Mason, OH, USA
e-mail: drheldman@earthlink.net

D.B. Lund
Department of Food Science, University of Wisconsin-Madison. 1605 Linden Dr., 53706 Madison, WI, USA
e-mail: dlund@cals.wisc.edu

J.M. Aguilera et al. (eds.), *Food Engineering Interfaces*, Food Engineering Series,
DOI 10.1007/978-1-4419-7475-4_1,

1.2 Scope of Food Engineering

As suggested, the term "food engineering" has many interpretations and the scope of this term has evolved over time. In addition, there are varied interpretations and meanings in different regions of the world. It is likely our attempt at a definition will fall short and not capture all of the various interpretations. However, the broadest interpretation of food engineering occurs in the industrial sector, where it is generally accepted on a global basis. This general interpretation includes applications of engineering in any aspect of production, handling, storage, processing, packaging, and distribution of food. This is certainly the interpretation accepted by the founding fathers of the International Congress of Engineering and Food (ICEF), who did not use "food engineering" in the title of the congress. Obviously, this broad interpretation is inclusive of the expertise associated with most of the engineering fields.

In development of food engineering curricula, a more narrow interpretation of food engineering has been applied within education institutions, so as to define the uniqueness of the discipline in teaching and research. As might be expected, these interpretations focus more on basic concepts and principles, and the impact of the product being handled on the application of engineering principles, with special emphasis on the word "food."

Undergraduate food engineering teaching programs incorporate both basic engineering principles and the unique chemical and microbiological characteristics of foods. These programs tend to integrate basic engineering, chemistry, and microbiology into process designs. It is clear that in most regions of the world, these programs have evolved at the interface between science and engineering. In the United States, two types of programs have developed in parallel: some with a clear alignment with engineering curricula (usually in chemical or agricultural engineering), and many with food science programs (associated with colleges of agricultural sciences). Graduate programs and research in food engineering have evolved with an evident focus on basic principles, mathematical models, and process simulations.

In summary, food engineering provides an essential link between engineering and the food sciences. The dimensions of this interface present unique challenges in education, research, and applications, and will continue to provide professionals associated with food engineering with opportunities in the future and a continuing evolution of scope.

1.3 Definitions of Food Engineering

There are many definitions of food engineering, and not one is universally accepted. One of the early definitions appears in the preface of the book *Elements of Food Engineering* (1952) by Parker, Harvey, and Stateler. Parker proposed that "Food Engineering is concerned with the design, construction, and operation of industrial processes and plants in which intentional and controlled changes in food materials

are performed with due consideration to all economic aspects considered." Later in 1963, Charm suggested that the purpose of food engineering is "to illustrate the common relationship between basic engineering principles and the fundamentals of food processing." Finally, in 1966, Earle defined food engineering as "the study of the processes that transform raw materials into finished products, or preserves foods so they can be kept for longer periods." There are obvious similarities and differences in these early definitions. All three indicate that food engineering is the application of engineering to manufacturing and preservation of foods, but there are distinct differences, from more emphasis on basic principles to greater emphasis on applications of engineering in practice.

A more current definition of food engineering has been posted online (Wikipedia 2010; http://en.wikipedia.org/wiki/Food_engineering) as follows: "Food engineering refers to the engineering aspects of food production and processing. Food engineering includes, but is not limited to, the application of agricultural engineering and chemical engineering principles to food materials." However, given the evolution of research and industrial applications, the following definition should also apply, now and in the near future: Food engineering is both the identification and creation of the physical principles associated with foods and ingredients, and the applications of the principles to the handling, storage, processing, packaging and distribution of consumer food products. This definition attempts to include both the interests associated with engineering research and the applications of outcomes from research to ultimate applications in processes associated with the food industry. Undoubtedly, a better appreciation of the diversity of this unique field of study solicits more discussion of the subject.

1.4 Origins of Food Engineering

There are clear relationships between the origins of food engineering and food preservation processes. Design and prediction of the effect of preservation properties on food requires quantification and modeling. One of the most visible applications can be found in the book *Sterilization in Food Technology* by Ball and Olson (1957). This book provides numerous examples of applications of mathematics to heat transfer to foods in containers and the description of the kinetics of microbial destruction. Historically, food preservation evolved from an art to a science. Early preservation techniques (drying, salting, fermentation, and cooling) were based on "trial and error." Later, technologies such as canning and freezing were based on observations that provided the basis for science-based improvements in the processes. Many of these early scientific findings occurred in the basic sciences of chemistry, biology, and physics. One of the more significant outcomes from Louis Pasteur (1860) in response to food spoilage challenges was to provide the foundation for bacteriology and microbiology. Other contributions from basic science and mathematics were significant, such as the influence of temperature on reactions (Arrhenius 1889) and modeling heat and mass transfer (Carslaw and Jaeger 1946; Crank 1956).

There are several other early and significant contributions that have become the foundation of food engineering. The role of Nicholas Appert in demonstrating thermal processing of foods in the early 1800s is recognized as the basis for many current shelf-stable foods. The invention and development of mechanical refrigeration by von Linde (1896) was significant, followed by Birdseye (1930) who established the basis of the modern frozen food industry. Although dehydration has been recognized as a food preservation process for centuries, the contributions of von Loesecke (1943) advanced the process in a quantitative manner. These three processes (thermal processing, food cooling and freezing, and food dehydration) continue to be the most visible processes in the research literature on food engineering.

1.5 Evolution of Food Engineering

In general, food engineering was started by engineers who happened to have some acquaintance with the food industry. However, there were other engineers and scientists who appreciated the application of engineering principles to something as complex as food. At the risk of omission, here are some of the giants in food engineering and others who have made significant contributions to food engineering (in no particular order): Bird, Stewart and Lightfoot, Kessler, Thijssen, Leniger, Cheftel, King, Karel, Plank, Kuprianoff, Diendorfer, Humphrey, Hallstrom, Heldman, Labuza, Berk, Mizrahi, Morgan, Pflug, Earle, Goldblith, Proctor, Hayakawa, Ball, Zahradnick, Saravacos, Brody, Duckworth, Cheftel (J.C.), Loncin, Saguy, Ohlsson, Pham, Teixeira, Sastry, Hall, Farrall, Harper (J.C.), Nickerson, Mannheim, Harper (J.M.), Merson, Lund, Knorr, Singh (R.P.), Schluender, Schwartzberg, Bimbenet, and Lovric.

In addition to people, there are several events and developments that have contributed to the evolution of food engineering in the past 50 years. For professionals involved in teaching, there are several textbooks, including the following key books:

1952 – *Elements of Food Engineering* by Milton E. Parker, Ellery H. Harvey, and E. S. Stateler
1963 – *Fundamentals of Food Engineering* by Stanley E. Charm
1966 – *Unit Operations in Food Processing* by Richard Earle
1975 – *Food Process Engineering* by H.A. Leniger and W.A. Beverloo
1975 – *Food Process Engineering* by Dennis R. Heldman
1976 – *Elements of Food Engineering* by John C. Harper
1979 – *Food Engineering; Principles and Selected Applications* by Marcel Loncin and Larry Merson
1980 – *Fundamentals of Food Process Engineering* by Romeo Toledo
1984 – *Introduction to Food Engineering* by R. Paul Singh and Dennis R. Heldman

Although other textbooks have been published in this recent time period, these nine demonstrate the evolution of food engineering as a field of study. Parker et al.

(1952) placed significant emphasis on the description of manufacturing operations and the role of engineering in all aspects of the manufacturing facility. Charm (1963) introduced mathematics and an emphasis on process design and unit operations. Earle's book (1966) was ideal for undergraduate students pursuing a degree in food science, and the objectives in Harper's book (1976) were similar. Books by Leninger and Beverloo (1975) and Heldman (1975) were designed for students with a significant background in engineering concepts, and emphasized advanced analysis of unit operations. The book by Loncin and Merson (1979) provided even more emphasis on mathematical analysis of unit operations, and was suited to introductory graduate students in some dimension of food engineering. Both Toledo (1980) and Singh and Heldman (1984) developed textbooks for undergraduate students in food science with specific attention to topics identified in guidelines for food science curricula recommended by the Institute of Food Technologists.

During the past 25 years, several of these pioneering textbooks have been published in later editions. In most cases, emphasis has been on new information and technologies, as well as on advancement in tools available for conducting analysis. There has been a continuous trend toward more mathematical description of processes, and computer simulation of operations within the food industry. Further, there has been an obvious emphasis on the impact of processes on product quality attributes, including nutrients, as well as changes in process design to enhance the efficiency of processes.

Another measure of the evolution and development of food engineering as a field of study and research is the holding of national and international meetings that focus on food engineering. Some of the key meetings and events that have occurred during the last 50 years include:

1972 – *Food Engineering Conference*; organized by H.A. Leninger and Hans Thijssen, hosted at Agricultural University, Wageningen, The Netherlands.

1976 – *International Congress on Engineering and Food (ICEF1)*; 1st Congress was chaired by Dr. Joe Clayton, held in Boston, Massachusetts. The 11th Congress will be hosted in Athens, Greece on May 22–26, 2011.

1976 – *Food Engineering Division of IFT*; a petition signed by several food engineering members of IFT was approved by the Executive Committee; the Division continues to organize symposia and research programming at annual IFT meetings.

1981 – *International Conference in Fouling and Cleaning*; conference was organized by Bengt Hallstom, Lund University, and Daryl Lund, University of Wisconsin; subsequent conferences were held in 1985 (USA) and 1989 (Germany); now part of ICEF.

1991 – *Conference of Food Engineering (CoFE)*; first of nine conferences organized by Dr. Martin Okos, held in Chicago. The 11th conference is being planned for 2011.

1996 – *CIBIA*; 1st Congreso IberoAmericano de Ingenieria de Alimentos (CIBIA) was hosted in Campinas, Brazil. The 6th Congreso was hosted in Bogata, Columbia, in 2009.

2007 – *European Workshop on Food Engineering and Technology*; first of series of workshops held with focus on applications of food engineering research.

Although many other meetings related to food engineering have occurred, the above list illustrates the continuing development of research programs in the past 35 years.

The historical evolution of food engineering can also be illustrated by the publication of research literature. Specific journals for publication of current food engineering research have been created with some of the more visible journals and reference books, such as:

1970 – *Journal of Food Science*; first issue published, which included a section titled "Applied Science and Engineering by the Institute of Food Technologists."
1976 – *Journal of Food Process Engineering*; first issue published by Food & Nutrition, Press.
1982 – *Journal of Food Engineering*; first issue published by Academic Press, Inc.
1992 – *Handbook of Food Engineering*; first edition published by Marcel Dekker, Inc.
1997 – *Handbook of Food Engineering Practice*; published by Academic Press, Inc.
2003 – *Encyclopedia of Agriculture, Food and Biological Engineering*; first edition published by Marcel Dekker, Inc.

Information about food engineering has been published in many other journals and references, but the above list illustrates the evolution within a relatively short time period.

All of the developments described have occurred during a period of significant change in the food industry and related industries. Bruin and Jongen (2001) suggested the following categories of significant change:

1. Mergers and acquisitions of companies in the food and related industries. These changes have caused significant reorganization within all companies, impacting the role of food engineers in the industry.
2. Expectations for innovation. Changes in consumer expectations have increased in frequency, forcing the identification and implementation of new, innovative processes.
3. Changes in industry expectations. Previously, expectations of the food industry were to deliver an abundant and safe supply of food to consumers. These expectations have evolved to include not only more abundant and safe foods but also foods with greater convenience, and eventually, foods with enhanced influence on health and wellness.
4. Advances in computer technology. These advances have provided the tools to accelerate the responsiveness of engineers to all types of challenges.

These changes have influenced the environment of food engineering activities, and have had an impact on the expectations of food engineers in the industry. Many of these changes also will be incorporated into future educational programs for food

engineers. Thus, a challenge to educators will be to incorporate these changes into food engineering programs.

1.6 Evolution in Food Engineering Research

There have been significant advancements in food engineering research over the past 50 years. Although the research has been conducted over a broad range of applications, the unique focus of research that has evolved is the integration of reaction kinetics with transport phenomenon to accomplish process design. The research model concept is illustrated in Fig. 1.1.

The concept described by the model encourages research in three distinct areas: kinetic parameters, transport phenomenon, and process design. Research on kinetic models has expanded the availability of kinetic parameters and enhanced the investigation of appropriate models used for food products. Transport phenomenon research has improved our understanding of heat and mass transfer in foods, with specific attention to the unique properties of food products and the mathematic models needed to describe the phenomenon in a food system. Process design research integrates the kinetic models with appropriate transport phenomenon models to allow prediction of a parameter to quantify the quality of the food product. In general, the concept is ideal for optimization of the process through maximizing the product quality attributes, while identifying the best combination of process parameters.

1.6.1 Kinetic Models

The development of kinetic models for food systems is still evolving. A typical model used to describe changes in a food component or attribute is expressed as:

$$dA/dt = -kA \tag{1.1}$$

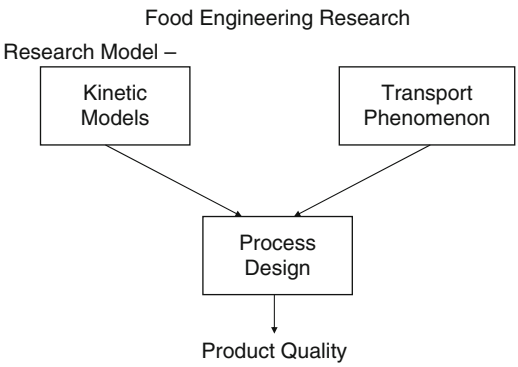

Fig. 1.1 A food process engineering research model

where A = the concentration or intensity of component, and k = the first-order rate constant.

There has been a significant increase in the measurement and publication of rate constants for an array of product component changes as a function of process or storage parameters, as illustrated by Villota and Hawkes (2007). Traditionally, the same model has been used to describe changes in microbial populations during preservation processes; the rate constants have been assembled in several locations, including the IFT Task Force Report (2000). These rate constants are evaluated and expressed as a function of parameters such as temperature, water activity, pressure, pH, etc. The evolution of more complex models has been explored by von Bockel (2008), with specific attention to variations from first-order kinetics.

1.6.2 Transport Phenomenon

Significant attention has been given to the development of models to describe heat, mass, and momentum transfer in food systems, expressed as follows:

$$\partial N/\partial t = \alpha \blacktriangledown^2 N \tag{1.2}$$

where N = intensity of a process parameter, and α = appropriate property of food structure.

Expressions of this type are used to predict distribution histories of the preservation process parameter. Typical parameters include temperature, moisture content, pressure, and other parameters used to accomplish reductions in microbial populations. Over the past 30–40 years, the availability of quantitative physical properties data has increased significantly (Rao et al. 2005). In addition, there has been increased emphasis on the development of prediction models for properties based on product composition.

1.6.3 Process Design

Integration of the appropriate kinetic model with transport phenomenon expressions leads to process design. In general, the outcomes are product quality attributes, predicted as follows:

$$A = \int k(N)\ \mathrm{d}t \tag{1.3}$$

where A = the intensity or concentration of a quality attribute.

The focus of process design is on the product, with impact of the process on reduction of the microbial population and/or the retention of a sensitive product quality attribute. Process design provides the opportunity to consider multiple attributes as long as the kinetic parameters and models are available. An even more important dimension of this approach is the potential for process optimization, which is the identification of the process parameters to achieve maximum retention of product quality attributes, while ensuring the desired reduction in microbial population for safety or shelf-life extension.

1.7 Contributions of Food Engineering Research

The process design approach has contributed to many positive products manufactured by the food industry. These contributions can be expressed in several different ways. In general, process design facilitates the quantitative prediction of process outcomes, while evaluating a range of process parameters without conducting time-consuming and costly experimental trials.

1.7.1 Safe and Wholesome Foods

Process design has had significant impact on the safety and wholesomeness of food products. The development of food canning by Nicholas Appert (1750–1841) took 14 years. Using the current process design approaches, processes can be developed within hours. These approaches ensure microbiological safety of products, along with the capability to maximize the retention of product quality attributes.

A current example of process design is illustrated in Fig. 1.2. Knorr (2006) has demonstrated that through measuring and understanding the kinetics of *Escherichia coli* population reductions at high pressures, the retention of product quality attributes in sausage are evident. These same approaches have been used to ensure maximum retention of nutrients in a food product using high temperatures to ensure microbiological safety and shelf-life of the product.

1.7.2 Affordable Food Supply

Food engineering research has contributed to keeping quantities of food available at a modest cost to the consumer. These contributions have been accomplished through overall improvements in the efficiency of food manufacturing. These improvements have occurred through a focus on specific processes, as well as an analysis of processing operations. Many of the improvements in efficiency have occurred through increased capacity of individual pieces of equipment and

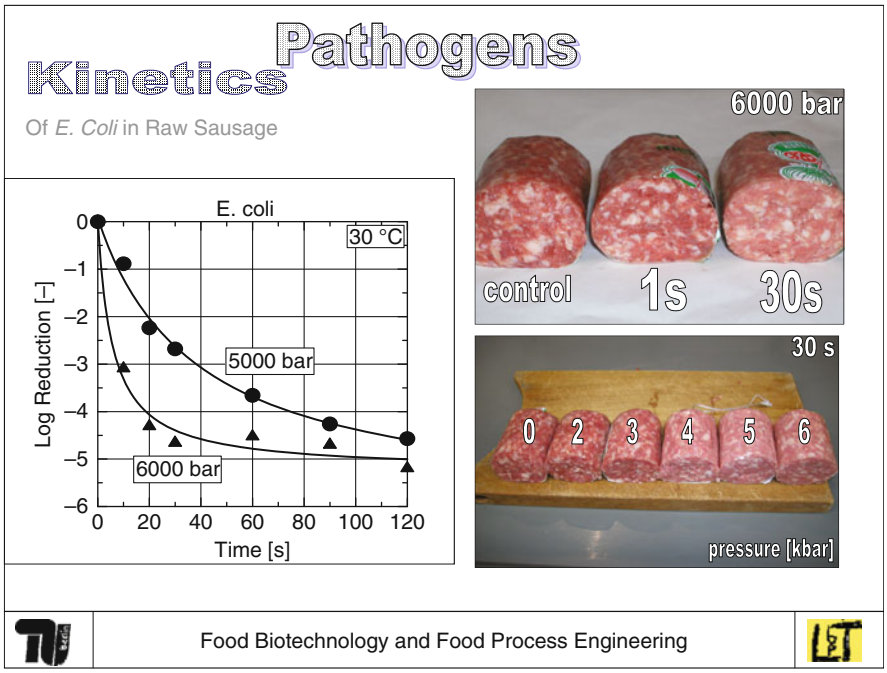

Fig. 1.2 Process design for pathogen reduction of *Escherichia coli* in sausage while retaining product quality attributes (Knorr 2006)

throughput of processing lines. Another contributor to a low-cost food supply has been the development of processes that allow foods to be transported for long distances without noticeable reductions in product quality attributes.

An example of process improvements for shelf-stable foods has been aseptic processing and packaging. This continuous process has been demonstrated as an excellent alternative to the more traditional batch retort process. As illustrated in Fig. 1.3, the process involves continuous processing of both product and packaging, before filling the product into the package. As illustrated by Bruin and Jongen (2001), improvements in the process have continued with capabilities to accomplish thermal processing of food particles within the carrier liquid.

1.7.3 Convenient Food Products

Process design has contributed to the development of convenient foods in a significant way. Examples include products with reduced preparation times, products with improved quality attributes, products with extended shelf-life, and a variety of shelf-stable products.

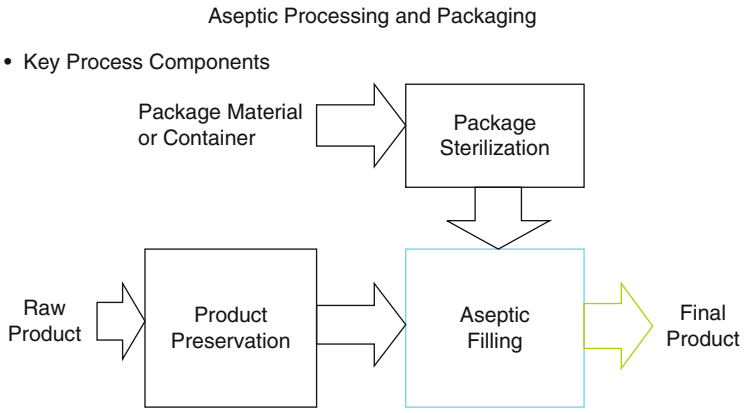

Fig. 1.3 The aseptic processing and packaging concept in an aseptic environment

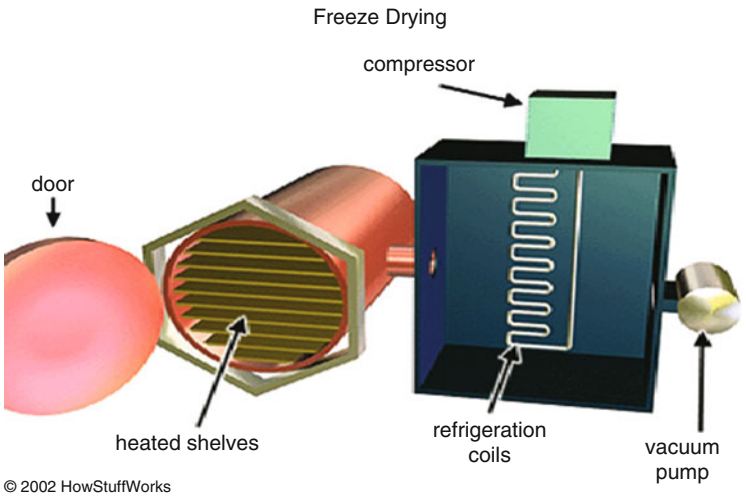

Fig. 1.4 The freeze-drying process

Freeze-dried foods are examples of products convenient for consumers. As illustrated in Fig. 1.4, the freeze-drying process produces high-quality dry foods by removing moisture from the product through sublimation at low temperature, and preserving the product's quality attributes. The freeze-drying process is not a new one, since the first application was to produce freeze-dried coffee in 1938. The process gained significant visibility in the 1960s during development of low-mass foods for space flights. Applications of the process to foods continue as efforts to reduce the costs associated with the process are evaluated.

1.7.4 Product Quality Improvements

Process design has contributed to food quality improvements in many different ways. These improvements have occurred as a result of new and unique ingredients manufactured using new processes created through process design. Product flavors are being enhanced with new technologies to preserve volatile flavors, with specific attention to encapsulation processes. Based on new physical properties knowledge, process design has created an array of new and improved product textures. Many of the recent improvements in food product quality can be traced to the "food stability map" (Fig. 1.5) as suggested by Labuza et al. (1970).

The concept of water activity has provided a unique basis for product and process development. Many new relationships between reaction rates in foods and water activity have guided the development of foods with extended shelf-life and unique quality attributes. These early developments have led to the more recent concepts of glass transition as illustrated in Fig. 1.6 (Roos and Karel 1991). The more sophisticated relationships between temperature and moisture content within a food provide even more opportunities for process development now and in the future. These state diagrams provide the ideal basis for evaluation of new ingredients and their impacts on response of a product to a process, and optimization of product quality attributes as a function of process parameters. These concepts will provide the basis for food engineering research and applications for many years into the future. All of these developments are based on the unique relationships between the process and the ingredients of the food products.

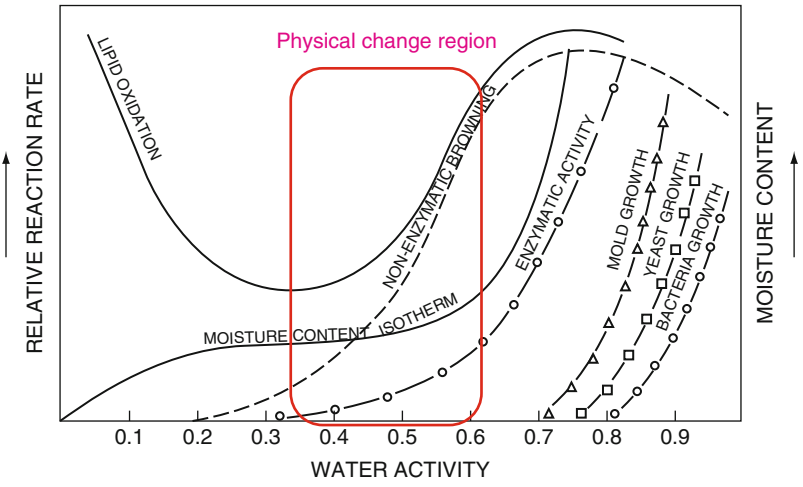

Fig. 1.5 The food stability map (Figure redone by T.P. Labuza based on Labuza et al. 1970)

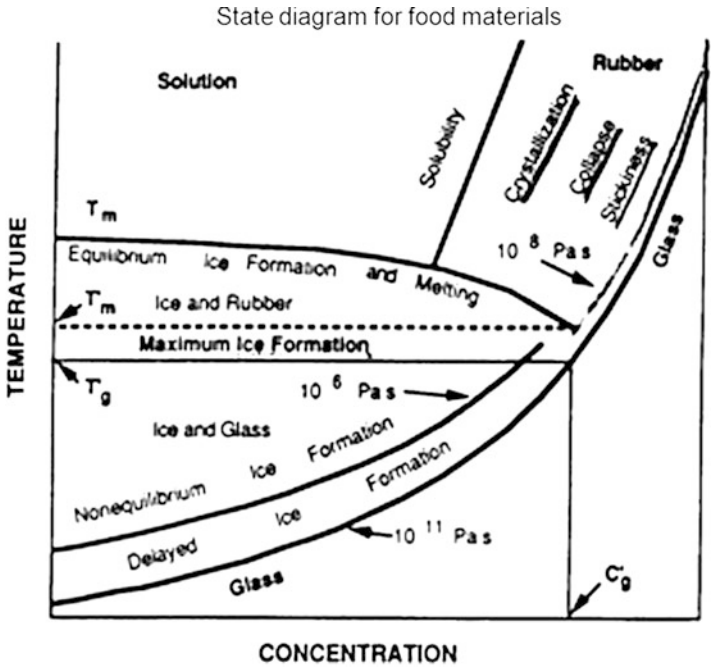

Fig. 1.6 The "state diagram" concept (Roos and Karel 1991)

1.7.5 Innovative Food Products

The development of many innovative new products has resulted from process design. As new process technologies are identified and applied to food manufacturing the opportunities for new and different products evolve. Similar opportunities occur as new packaging and packaging systems are developed. In many situations, these new process technologies are important to the enhancement of product quality.

An excellent example of a process technology with significant impact on food product development is extrusion. Extrusion is a process developed in the polymer industry, but it has been adapted to a range of applications in the food industry. The process combines the parameters of pressure, temperature, and time to produce products with unique characteristics and properties. By considering the significant range for each parameter, and the combinations of parameters for each one, the opportunities for product attributes are nearly unlimited.

The opportunities for future developments in food extrusion are emphasized by Bruin and Jongen (2001). By superimposing a typical cycle during an extrusion process on a state diagram (Fig. 1.7), the depth of understanding achieved from recent process design research is recognized.

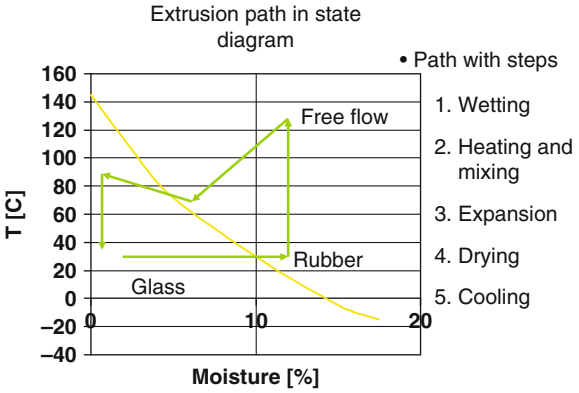

Fig. 1.7 The extrusion process on a state diagram (Bruin and Jongen 2001)

As is evident in Fig. 1.7, the steps associated with the extrusion process shift the product ingredients from a glass state to a rubber state, followed by elevation of temperature before expansion and drying back to a glass state. The final step of cooling returns the product to the same composition and temperature, but the final product has completely different properties and characteristics. Obviously, this understanding of the process and the product creates an unlimited array of opportunities for new and innovative products.

1.8 The Future of Food Engineering

The future of food engineering is very bright. It is evident that food engineering education will continue to evolve for both undergraduate and graduate students. It will continue to be an attractive field of study because of the unique characteristics of foods and ingredients, and the challenges associated with applications of engineering concepts and principles. The education of future students will be driven by the new information created by current and future research.

One of the currently evolving areas of research is nanoscale science and the translation of outcomes into applications in food systems. Bruin and Jongen (2001) have suggested that nanoscale adds another scale of consideration to existing scales that range from molecular scale to supply-chain scale. Although the visible applications are still evolving, there seem to be several potential outcomes. The shelf-life of foods is likely to be increased through a combination of nano-sensors used to detect the onset of product deterioration, followed immediately by intervention to prevent this deterioration. Through the study and understanding of food properties at the nanoscale, the texture of food products can be improved and new product textures are likely to evolve. Many of these improvements are likely to be the result of the creation of nano-structured particles and films. The encapsulation of flavors within

nanoscale particles should ensure that food products retain optimum flavor intensity through processing steps and for longer periods of time during storage and distribution. Similar opportunities seem logical for bioactive compounds. Knowledge about packaging materials at the nano-scale should lead to the development of new and improved packaging materials for food products.

Food engineering will contribute to the goals of improved health and wellness of consumers through development of functional foods. The application of engineering concepts and principles to the metabolism of food will provide insights on the product and process development cycle. The potential for incorporating bioactive compounds into food products in a manner that ensures delivery of the compound to the appropriate site within the body during metabolism of the food is achievable through food engineering research.

An evolving challenge to food manufacturing and distribution is the constraint of sustainability. Food engineering should contribute to sustainability in many different ways. The basic concepts of material and energy balances will become standard tools in evaluation of all scales of operation from the point of raw material production to delivery of the product to the consumer and beyond. The transitions of new information from process design to commercial manufacturing operations will continue to be a significant challenge. These transitions must be accomplished in a more efficient manner.

1.9 Summary

Food engineering has a relatively brief history as a field of study. Educational programs for undergraduate and graduate studies have evolved over the past 50 years, with somewhat different approaches globally. Many engineering impacts on the food industry have a longer history, as indicated by the origin of several preservation processes, such as drying, canning, and refrigeration. More recently, food engineering research has brought a quantitative dimension to both product and process development. The future of food engineering research will continue to focus on technology transfer and attempts to accelerate the transition of new processes from the laboratory bench to operations scale in manufacturing. Future research must be directed toward meeting the expectations of the consumer for safe and convenient foods that will contribute to a healthy lifestyle for extended periods of time.

References

Arrhenius S (1889) Z Phyzik Chem 4:226, Title not available
Ball CO, Olson FCW (1957) Sterilization in food technology. McGraw-Hill, New York
Birdseye C (1930) Production of quick-frozen fish. US Patent #1773070

Bruin S, Jongen RG (2001) Food process engineering: the past 25 years and challenges ahead. The Food Engineering Division Lecture. Institute of Food Technologists Annual Meeting, New Orleans, LA

Carslaw HS, Jaeger JC (1946) Heat of conduction in solids. Oxford University Press, London

Charm SE (1963) The fundamentals of food engineering. The AVI Publishing Co., Westport, CT

Crank J (1956) The mathematics of diffusion. Oxford University Press, London

Earle RL (1966) Unit operations in food processing. Pergamon, London

Harper JC (1976) Elements of food engineering. The AVI Publishing Co., Westport, CT

Heldman DR (1975) Food process engineering. The AVI Publishing Co., Westport, CT

IFT Task Force Report (2000) Kinetics of microbial inactivation for alternative food processing technologies. JFS Special Supplement. pp 1–108

Knorr D (2006) Processing concepts for non-thermal modification of foods. 13th World Food Congress of Food Science & Technology. Nantes, France. Sept. 17–21

Labuza TP, Tannenbaum SR, Karel M (1970) Water content and stability of low moisture and intermediate moisture foods. Food Technol 24:543–550

Leninger HA, Beverloo WA (1975) Food process engineering. Reidel, Dordrecht, The Netherlands

Loncin M, Merson RL (1979) Food engineering. Principles and selected application. Academic, New York

Parker ME, Harvey EH, Stateler ES (1952) Elements of food engineering. Reinhold, New York

Rao MA, Rizvi SSH, Datta AK (2005) Engineering properties of foods, 3rd edn. CRC Press/Taylor & Francis, Boca Raton, FL

Roos YH, Karel M (1991) Applying state diagrams to food processing and development. Food Technol 45(12):68–71, 107

Singh RP, Heldman DR (1984) Introduction to food engineering. Academic, Orlando, FL

Toledo RT (1980) Fundamentals of food process engineering. The AVI Publishing Co., Westport, CT

Villota Ricardo, Hawkes James G (2007) Reaction kinetics in food systems. In: Heldman Dennis R, Lund Daryl B (eds) Handbook of food engineering, 2nd edn. CRC Press/Taylor & Francis, Boca Raton, FL

von Bockel MA (2008) Kinetic modeling of reactions in foods. CRC Press/Taylor & Francis, Boca Raton, FL

von Linde C (1896) Process and apparatus for liquefying gases or gaseous mixtures, and for producing cold, more particularly applicable for separating oxygen from atmospheric air. German Patent # GB189512528

von Loesecke HW (1943) Drying and dehydration of foods. Reinhold, New York

Chapter 2
Advances in 3D Numerical Simulation of Viscous and Viscoelastic Mixing Flows

Kiran V. Vyakaranam and Jozef L. Kokini

2.1 Introduction

Mixing processes in the food industry often involve highly viscous and viscoelastic fluids like wheat flour dough, pastes, batters, and syrups. The design of mixing equipment, whether batch or continuous, is aimed at achieving a well-mixed and blended product with a consistent rheological character. Design of mixing equipment also involves devising guidelines for scale-up of mixing devices and their comparison in terms of mixing efficiency, especially when batch mixers are to be replaced by continuous mixing equipment. A well-designed mixing process could result in the blending of ingredients, improvement of rate of heat transfer, facilitation of chemical reactions, creation of structure, addition of energy to create or break molecular bonds, etc. In order to evaluate the efficiency of a mixer design in performing these operations, a kinematic analysis of the process can be made wherein the mixing mechanisms are characterized as "dispersive" or "non-dispersive" (or extensive) (Wang and Manas-Zloczower 2001). Dispersive mixing is quantified by elongational flow and shear stress, which aid in the breakup of cohesive particles like droplets, bubbles, or solid agglomerates. Non-dispersive mixing includes the spatial separation and rearrangement of an initially cohesive cluster of particles (distributive mixing) or the laminar stretching and folding of the material elements, resulting in a homogeneous distribution (Meijer and Janssen 1994).

Mixing devices currently used in process industries are either batch or continuous. These devices vary in the design of the impellers, kneading blocks, and/or static mixing elements, depending on the material used, the throughput requirements, and the specific aim of the mixing process, for example, the stretching and folding of material or dispersion of ingredients. Examples of batch mixers include

K.V. Vyakaranam
Department of Food Science, Rutgers University, New Brunswick, NJ 08901, USA

J.L. Kokini (✉)
Department of Food Science and Human Nutrition, College of ACES, University of Illinois at Urbana Champaign, Urbana, IL 61801, USA
e-mail: kokini@uiuc.edu

J.M. Aguilera et al. (eds.), *Food Engineering Interfaces*, Food Engineering Series,
DOI 10.1007/978-1-4419-7475-4_2,

the stirred tank reactors with Rushton impellers and dough kneaders like the Brabender farinograph and Banbury mixers, while examples of continuous mixers include the twin-screw/single-screw extruders and static mixers fitted with varying mixing elements (e.g., Kenics mixer). While the evaluation of flow and subsequent mixing parameters can be done using visualization techniques like particle image velocimetry (PIV) and laser doppler anemometry (LDA), it is often not practical to optimize the design of such large mixing devices (i.e., to industrial scale) through experimental trial-and-error analysis. Numerical simulation techniques thus have proven to be a viable, nonintrusive, and cost-effective alternative tool that can optimize the design of complex mixer geometries through analysis of the flow field and mixing parameters.

Research involving numerical simulation of mixing flows has been under steady development, ranging in the beginning from the simplest 2D problems to more realistic 3D mixer geometries. In this chapter we initially discuss the basic ideas behind numerical simulation of mixing flows, using the finite element method (FEM) and the governing equations and theoretical measures of the mixing process. A review is then presented of the recent work done in analyzing flow and mixing of viscous and viscoelastic fluids in various batch and continuous mixing geometries using FEM simulations.

2.2 Theoretical Measures of Mixing

There are several measures used to quantify distributive and dispersive mixing, as well as laminar stretching and folding of the material. During mixing of two components (distributive mixing) the homogeneity of the mixture can be quantified through the scale of segregation, *S(t)*, which is a measure of the binomial distribution of the components and is calculated as

$$S(t) = \int_0^{\zeta} R(r,t)\mathrm{d}r \tag{2.1}$$

where $R(|r|)$ is a correlation coefficient that gives the probability of "M" pairs of material points in the mixer separated by a distance $|r|$ having the same concentration,

$$R(|r|) = \frac{\sum_{j=1}^{M} (c'_j - \bar{c}) \cdot (c''_j - \bar{c})}{MS^2} \tag{2.2}$$

The parameter *S(t)* gives an indication of the average size of the segregated regions but cannot detect local defects in the flow.

When a cluster of material points is distributed, the difference between the actual distribution and the ideal distribution of the material points is called the "pair-wise distribution index" or the "cluster distribution index" ε, and is calculated as

$$\varepsilon = \frac{\int_0^\infty \left[c(r) - c(r)_{\text{ideal}}\right]^2 \mathrm{d}r}{\int_0^\infty \left[c(r)_{\text{ideal}}\right]^2 \mathrm{d}r}, \tag{2.3}$$

where $c(r)$ is the coefficient of the probability density function and the value of index ε varies from 0 (ideal distribution) to 1 (no distribution) (Connelly and Kokini 2007).

The efficiency of a mixing flow to stretch and fold the material can be studied using a kinematic approach wherein the deformation of infinitesimal material lines and surface elements is tracked (Ottino 1989).

If the motion of the fluid is described by $X = \chi(X,\mathrm{t})$, and the deformation of an infinitesimal material line by $d\mathbf{x}=\mathbf{F}\cdot d\mathbf{X}$, then the length of stretch λ can be defined in terms of the strain as

$$\lambda = \lim_{|dx|\to 0} \frac{|d\mathbf{x}|}{|d\mathbf{X}|} \tag{2.4}$$

and a local instantaneous efficiency of mixing given by

$$e_\lambda(\mathbf{X},\mathbf{M},t) = \frac{D \ \ln \ \lambda / Dt}{(\mathbf{D} : \mathbf{D})^{\frac{1}{2}}} \tag{2.5}$$

where $\mathbf{M} = \frac{d\mathbf{x}}{|d\mathbf{X}|}$ and $\mathbf{D}$ represents the rate of strain tensor with a magnitude $(\mathbf{D}:\mathbf{D})^{1/2}$.

If the material is an incompressible Newtonian fluid, the local instantaneous efficiency will be the fraction of dissipated energy used to stretch the material, ranging between -1 and 1. The time averaged efficiency $\langle e_\lambda \rangle$ given in (2.6) provides information on the nature of reorientation (stretching and folding) of the flow. Flows with no reorientation will have $\langle e_\lambda \rangle$ decaying with time as t^{-1}, whereas $\langle e_\lambda \rangle$ tending toward a constant value would indicate a flow with strong reorientation (Ottino 1989).

$$\langle e_\lambda \rangle(\mathbf{X},\mathbf{M},t) = \frac{1}{t}\int_0^t e_\lambda(\mathbf{X},\mathbf{M},t')\mathrm{d}t' \tag{2.6}$$

Similar efficiency in stretching of an infinitesimal area element can also be evaluated. In a chaotic time-periodic flow, the arithmetic and geometric means of the length of stretch, λ, grow exponentially and can be represented as

$$\bar{\lambda} \approx \alpha \cdot e^{\Theta n}, \langle \lambda \rangle \approx \alpha \cdot e^{\Lambda n} \tag{2.7}$$

where n is the number of periods of revolutions and Θ and Λ are the topological entropy exponent and Lyapunov exponent, respectively. While topological entropy is a measure of the mixing rate in chaotic regions of flow, the Lyapunov exponent measures the rate of elongation or stretching (Muzzio et al. 2000; Zalc et al. 2002a).

Dispersive mixing involves breakup of agglomerates and drops in flow, caused by stresses large enough to overcome the cohesive or interfacial forces that tend to keep the agglomerate or the drop intact. The mechanical stress required for breakup depends on the type of flow, with pure elongation or irrotational flows being more effective than flows with a rotational component (Grace 1982; Bentley and Leal 1986). A dispersive "mixing index" λ_{MZ}, which quantifies the relative strength of the pure elongational flow component, can be defined as

$$\lambda_{MZ} = \frac{|\mathbf{D}|}{|\mathbf{D}| + |\Omega|} \tag{2.8}$$

where $\mathbf{D}$ and $\mathbf{\Omega}$ are the rate of deformation and vorticity tensors, respectively (Yang and Manas-Zloczower 1992). λ_{MZ} ranges from 0 for pure rotation to 0.5 for simple shear, and to 1.0 for pure elongation. The Manas-Zloczower mixing index (as defined above) is not frame-invariant. However, several other frame-invariant flow-type indices were found to be computationally difficult to evaluate due to the requirement of higher-mesh densities in the simulation; and provided information similar to that of the non-frame-invariant index (Wang and Manas-Zloczower 2001; Connelly 2004).

2.3 Governing Equations for Calculation of Flow

The velocity and pressure distributions for an incompressible and isothermal fluid flow are calculated from the Navier–Stokes equations of mass and momentum conservation:

$$\nabla \cdot \mathbf{v} = 0 \tag{2.9}$$

$$\nabla \cdot \sigma + \rho \mathbf{f} = \rho \left(\frac{\partial \mathbf{v}}{\partial t} + \mathbf{v}.\nabla \mathbf{v} \right) \tag{2.10}$$

where ρ is the fluid density and $\mathbf{f}$ is the external body force per unit mass.

The stress tensor $\boldsymbol{\sigma}$ given in (2.10) incorporates the isotropic pressure (P) and extra stress tensor ($\mathbf{T}$), defined as

$$\sigma = -P\mathbf{I} + T \tag{2.11}$$

An additional energy conservation equation has to be solved in the case of a non-isothermal flow to obtain the temperature distribution:

$$\rho C(T) \cdot \left(\frac{\partial T}{\partial t} + \mathbf{v} \cdot \nabla T \right) = \mathbf{T} : \nabla \mathbf{v} + \mathbf{r} - \nabla \cdot q \tag{2.12}$$

where *C(T)* is the dependence of heat capacity on temperature, *r* is the volumetric heat source, *q* is the heat flux, and **T**:∇**v** represents the viscous heating.

The extra stress tensor of (2.11) for a generalized Newtonian fluid in an isothermal flow is given by

$$\mathbf{T} = 2\mu \mathbf{D} \tag{2.13}$$

where **D** is the rate of deformation tensor and μ($\dot{\gamma}$) is the viscosity function of the local shear rate, $\dot{\gamma}$, as given in (2.14).

$$\dot{\gamma} = \sqrt{2tr(\mathbf{D^2})} \tag{2.14}$$

The simplest form of the viscosity function is in the case of a Newtonian fluid, when it reduces to a constant value (μ_0) called Newtonian or zero-shear-rate viscosity. Examples of shear-dependent viscosity models used for polymeric liquids include the power-law model and the modified cross model (Prakash 1996); μ can be calculated respectively as

$$\mu = m(\dot{\gamma})^{n-1} \tag{2.15}$$

$$\mu = \mu_0 (1 + k\dot{\gamma})^{n-1} \tag{2.16}$$

For viscoelastic fluids, the extra stress tensor **T** is divided into a viscoelastic part ($\mathbf{T}_1$) and a purely viscous part ($\mathbf{T}_2$), given by

$$A(\mathbf{T_1}, \lambda_t).\mathbf{T_1} + \lambda_t \frac{\delta \mathbf{T_1}}{\delta t} = 2\eta_1 \mathbf{D}, \mathbf{T}_2 = 2\eta_2 \mathbf{D} \tag{2.17}$$

where the relaxation time λ_t, the viscosity factor η_1, and the function A ($\mathbf{T}_1$, λ_t) depend on the specific viscoelastic model used. The common differential viscoelastic models used to describe polymeric food materials are the Oldroyd-B, Maxwell, White-Metzner, Phan-Thien-Tanner, and Giesekus models (Connelly 2004).

2.4 Numerical Methods for Simulation of Mixing Flows

For a given system of fluid and mixing process, the solution of the above set of equations (consisting of conservation of mass and momentum), the energy equation (for non-isothermal problems), and the appropriate constitutive equations can be

obtained by several numerical techniques. The FEM is the most commonly used technique for numerical simulation of viscous mixing flows, even though other methods like the Finite Difference Method and the Finite Volume Method have been used (Dhanasekharan and Kokini 2003; Connelly and Kokini 2003; Heniche and Tanguy 2008).

Simulating a mixing flow using the FEM technique involves three steps:

- Construction of flow volume (or domain of flow problem) into a mesh made up of several finite elements or sub-domains
- Derivation of algebraic equations relating the physical quantities between the element nodes
- Solving whole flow domain: assembling equation parts using continuity and/or balancing the physical quantities across the elements (Reddy 2006)

The mesh generation step requires the construction of the mixing flow domain geometry using a network of linear triangular and quadrilateral elements (2D) or hexahedral, prism, tetrahedron, and wedge elements (3D). Several Computational Fluid Dynamics (CFD) software suites include mesh generation software, for example the Gambit (ANSYS Inc., Lebanon, NH) mesh generator. While maintaining the coarseness of the mesh is important in keeping the computational costs low, a higher density of finer mesh elements is needed in areas involving high gradients of flow properties. Hence, it is important to strike a balance with the coarseness/fineness of the mesh depending on the available computational capabilities. Additionally, for a higher accuracy and quicker convergence of the solution, the transition from coarser to finer mesh element regions has to be smooth and the individual elements as close as possible to ideal shapes, for example square/equilateral shapes (Connelly 2004; Heniche and Tanguy 2008). In the next step, the governing equations of motion are discretized using a weighted residual method and approximation of the flow variables for each element. For a generalized Newtonian fluid, the velocity, pressure, and stress fields (in case of viscoelastic flows) are approximated using the following equations

$$\mathbf{v}^h = \sum \mathrm{V}^{\mathrm{i}} \psi_i \tag{2.18}$$

$$p^h = \sum p^i \pi_i \tag{2.19}$$

$$\mathbf{T}^h = \sum \mathbf{T}^i \phi_i \tag{2.20}$$

where ψ_i, π_I, and φ_i are the finite element basis functions and V_i, p_i, and T_i are the nodal variables.

There are several methods available to discretize the governing equations, for example the Galerkin, the pressure stabilized Petrov-Galerkin, and the Galerkin least-square methods. In the Galerkin method, assuming the inertia terms to be negligible, the set of finite element equations in the flow domain Ω are formulated as

$$\int_{\Omega} \pi_k [\nabla . v^a] \mathrm{d}\Omega = 0 \tag{2.21}$$

$$\int_{\Omega} \left\{ \psi_j \rho \left[\frac{D\mathbf{v}^a}{Dt} - \mathbf{f} \right] + \nabla \psi_j^T . \left[-p^a \mathbf{I} + 2\eta^2 \mathbf{D}^a + \mathbf{T}_1^a \right] \right\} d\Omega = \int_{\Omega} \psi_j \sigma . \mathbf{n} \mathrm{d}s \tag{2.22}$$

$$\int_{\Omega} \phi_i \left[g(\mathbf{T}_1) . \mathbf{T}_1^a + \lambda \frac{\delta \mathbf{T}_1}{\delta t} - 2\eta_1 \mathbf{D}^a \right] \mathrm{d}\Omega = 0 \tag{2.23}$$

For differential viscoelastic models, this system of equations can be solved by using a coupled method where the extra stress tensor is the primary variable along the pressure and velocity fields; the Newton–Raphson technique can be used to solve for the variables. In this method, one usually encounters a large number of unknowns and high computational costs. Another method often used is the decoupled method where the viscoelastic stress tensor is computed separately from the flow kinematics; the method is iterated using the Picard scheme. The accuracy and stability of Galerkin formulations deteriorates in viscoelastic flow problems as the elasticity number increases; thus further stabilization techniques such as streamlined upwind (SU) and elastic-viscous-stress splitting (EVSS) are needed. The reader is directed to literature by Connelly (2004) and references therein for a detailed review of these techniques.

Several commercial FEM simulation packages are available, such as FIDAP (ANSYS, Inc.), AcuSolve (Acusim Software), Polyflow (ANSYS, Inc.), and Poly3D (Rheosoft). In particular, the Polyflow suite, which includes a mesh generator (Gambit), an FEM solver (Polyflow), and a post-processor (Fluent-Post/Fieldview/CFX Post), has been extensively used by our group to simulate viscous and viscoelastic flows in mixers and extruders.

Solving for the flow in a mixing device using a CFD simulation package would include the following steps:

- Building mixer geometry and converting into FEM mesh using a mesh generator (e.g., Gambit)
- Defining flow boundaries, material properties, numerical parameters, and operating conditions
- Solving of velocity profiles using an FEM solver (e.g., Polyflow)
- Calculating various mixing measures from velocity data using a post processor (e.g., Fluent-Post/Fieldview/CFX-Post)

Simulation of mixers with geometry that varies continuously with time, as in the case of moving impellers or screw/paddle elements, requires special meshing techniques. One approach that can be applied to a single impeller or a single screw mixer is the “rotating reference frame technique” in which the impeller/screw becomes the fixed reference frame with the barrel rotating around it. This enables the flow domain mesh to be fixed in time. The velocities are then

transformed back to the inertial reference frame. In asymmetrical mixer geometries, as in the case of an eccentrically placed impeller or a twin screw continuous mixer design, a "mesh superposition technique" (MST) can be used in which the impeller or the screw/paddle elements are meshed separately from the flow domain and then superimposed (Connelly and Kokini 2006a). Here, the equation of motion is modified by the introduction of a penalty term (H) to distinguish the solid (impeller or paddle) mesh elements from the fluid elements:

$$H(\mathbf{v}-\mathbf{v}) + (1-H)(-\nabla P + \nabla.T + \rho\mathbf{g} - \rho\mathbf{a}) = 0 \tag{2.24}$$

The penalty term H is essentially a step function and is set to a value of 1 for all nodes on solid moving parts, and a value of 0 for all nodes in the fluid volume. The continuity equation is also modified with a relative compression factor β to account for conservation of mass in the regions of flow domain covered by the moving solid elements:

$$\nabla.v + \frac{\beta}{\mu}\Delta P = 0 \tag{2.25}$$

2.5 3D Numerical Simulation of Model Mixing Geometries

In this section we present a review of studies evaluating the efficiency of distributive and dispersive mixing in model batch and continuous mixing geometries using numerical simulation techniques. These studies examined the effects of mixer operating parameters like screw design, screw speed, and material rheology on the variations in flow and mixing profiles. Recent studies in the area of numerical simulation and CFD of mixing processes can be broadly classified based on the mixing geometries investigated, for example, stirred tank reactors (Zalc et al. 2001, 2002a; Alvarez-Hernández et al. 2002; Rivera et al. 2004, 2006; Barailler et al. 2006; Iranshahi et al. 2006, 2007), dough kneaders (Jongen 2000; Jongen et al. 2003; Connelly and Kokini 2004, 2006a,b, 2007), static mixers (Rauline et al. 2000; Zalc et al. 2002b, 2003; Heniche et al. 2005), and continuous mixers/extruders (Dhanasekharan and Kokini 2000, 2003; Wang and Manas-Zloczower 2001).

2.5.1 Stirred Tank Reactors/Batch Mixers

Mixing of viscous liquids in stirred tank reactors and impeller-based batch mixers is widely employed in many process industries where effective distribution of additives is of great importance. Impeller design and speed of the impeller (as quantified

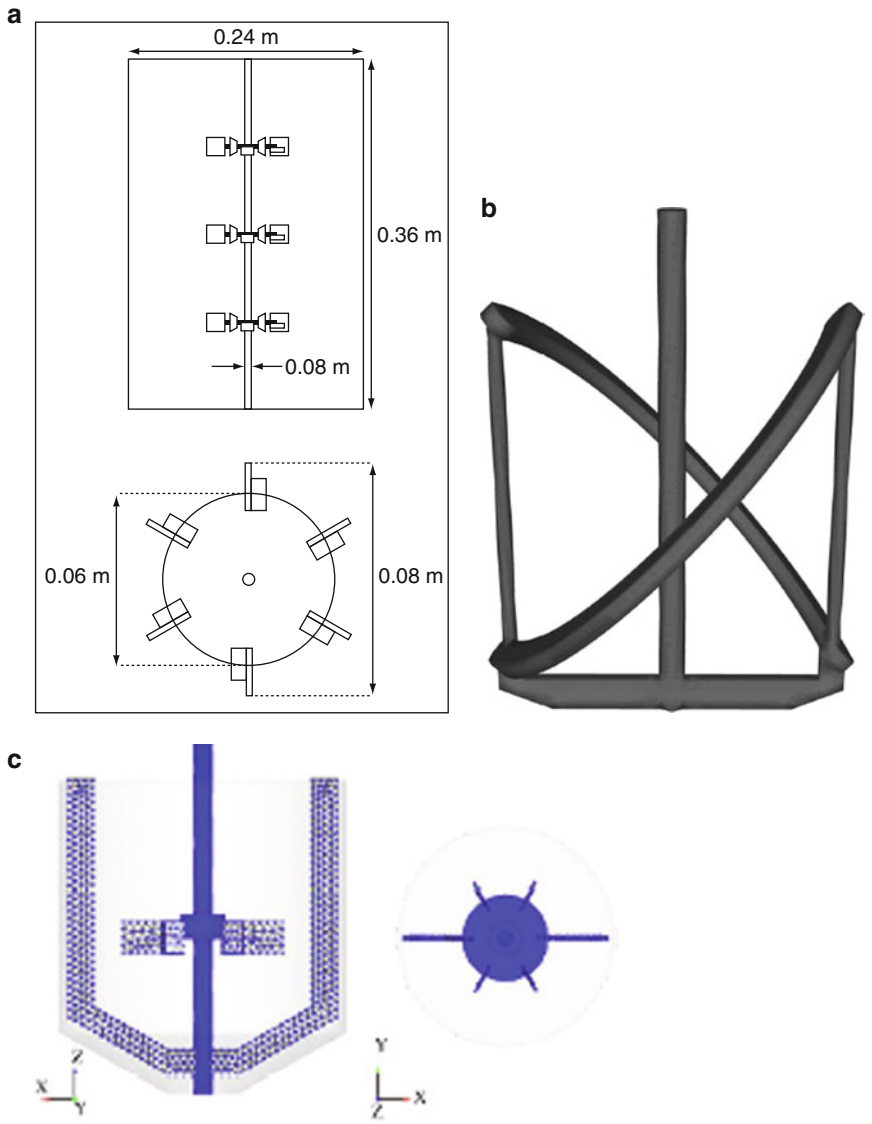

Fig. 2.1 Examples of impeller designs in batch mixers: (**a**) Three-Rushton turbine (Zalc et al. 2001); (**b**) Paravisc impeller (Iranshahi et al. 2006); (**c**) Rushton turbine with coaxial anchor (Rivera et al. 2006)

by Reynold's number, *Re*) are the major operating variables that can be tweaked to attain optimum mixing conditions and power efficiency. Figure 2.1 shows a few of the impeller designs used in stirred tank reactors and impeller-based mixers. The geometrically simple and symmetrical construction of the impellers, coupled with a relatively large flow volume in the reactor/vessel (usually cylindrical), makes these

mixers an excellent choice for use of CFD in the calculation and visualization of the various mixing measures as well as their validation using imaging techniques like the PIV.

Laminar mixing in a three-Rushton turbine stirred tank reactor was studied using the ORAC CFD package (Dantec Dynamics, Mahwah, NJ) (Zalc et al. 2001, 2002a) (Fig. 2.1a). The flow measurements were validated with PIV experiments using planar laser-induced fluorescence. In Fig. 2.2 the simulation results are in excellent agreement with the experiments in revealing the size and location of poorly mixed regions in the mixer. Local mixing efficiency can be quantified and visualized by computing the stretching value (λ). The stretching value λ is calculated from deformation of infinitesimal vectors in the flow, which usually takes place at an exponential rate in chaotic flow regions as compared to a linear rate in non-chaotic flows. The contour maps of the logarithm of stretching shown in Fig. 2.3 reveal the spatial heterogeneity of stretching when mixing at various impeller speeds after 20 revolutions. Knowledge of the distribution patterns of stretching could be valuable in deciding the injection point for additives to achieve optimal distribution (Zalc et al. 2002a).

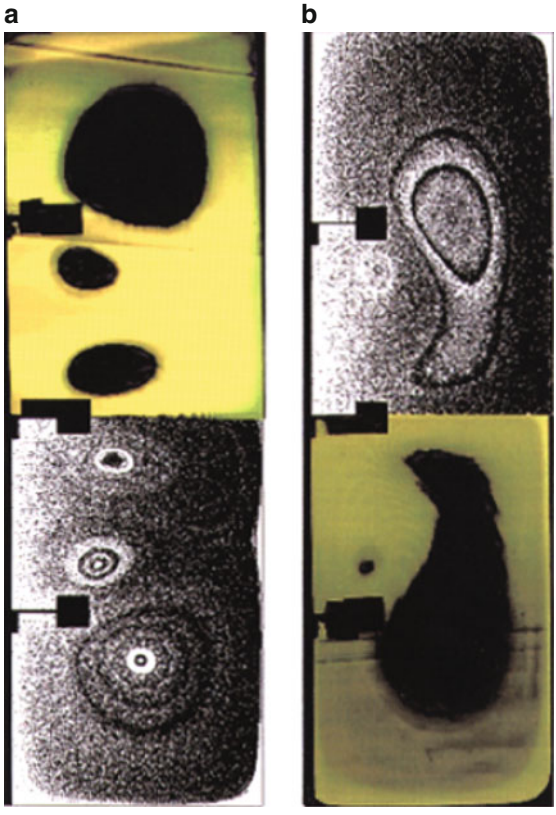

Fig. 2.2 Comparison of experimental and simulated results showing excellent agreement in the mixing patterns in a three-Rushton turbine impeller mixer after 600 revolutions at (**a**) $Re = 20$; and (**b**) $Re = 40$ (Zalc et al. 2002a)

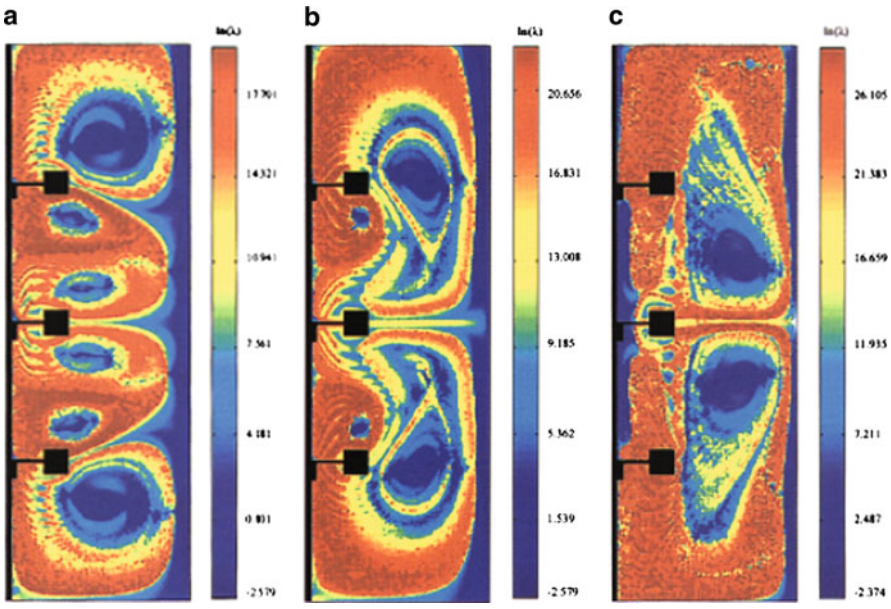

Fig. 2.3 Contour plots of $ln(\lambda)$ reveal the spatial heterogeneity of stretching at various impeller speeds: (**a**) $Re = 20$; (**b**) $Re = 40$; (**c**) $Re = 160$ (Zalc et al. 2002a)

In order for a mixing process to deliver optimum distributive and dispersive mixing, the entire set of operating conditions needs to be considered, that is, the impeller design, impeller speed, fluid rheology, and the injection point for additives. While comparing the mixing performance of an Ekato Paravisc impeller with a Double Helical Ribbon (DHR) impeller (Fig. 2.2b), Iranshahi et al. (2006) showed that the Paravisc impeller was more sensitive to the injection point chosen for a tracer in the effective distribution of the tracer particles in a Newtonian fluid (Fig. 2.4).

An important criterion for many mixing processes is the balance between distributive and dispersive mixing. Rivera et al. (2006) defined a parameter that is a ratio between two dimensionless quantities, the "head number" N_h (representing the shearing ability of the impeller) and the "flow number" N_q (representing the pumping ability of the impeller). The effect of an anchor co-rotating and counter-rotating with a Rushton turbine (Fig. 2.2c) was studied for a Newtonian and a non-Newtonian fluid by simulating the flow and mixing process, using POLY3D^{TM} (Rheosoft, Inc.) finite element software. It can be seen from Table 2.1 that the co-rotating anchor was more effective in combined distribution and dispersion, while the counter-rotating anchor was poor at distribution. The poor distributive mixing with the counter-rotating mode can be visualized in Fig. 2.5, which shows the intensity of segregation of tracer particles (a measure of homogeneity of the mixing) at two different mixing times. Rivera et al. (2006) refer to this figure as "tracer dispersion," whereas the actual process measured by the

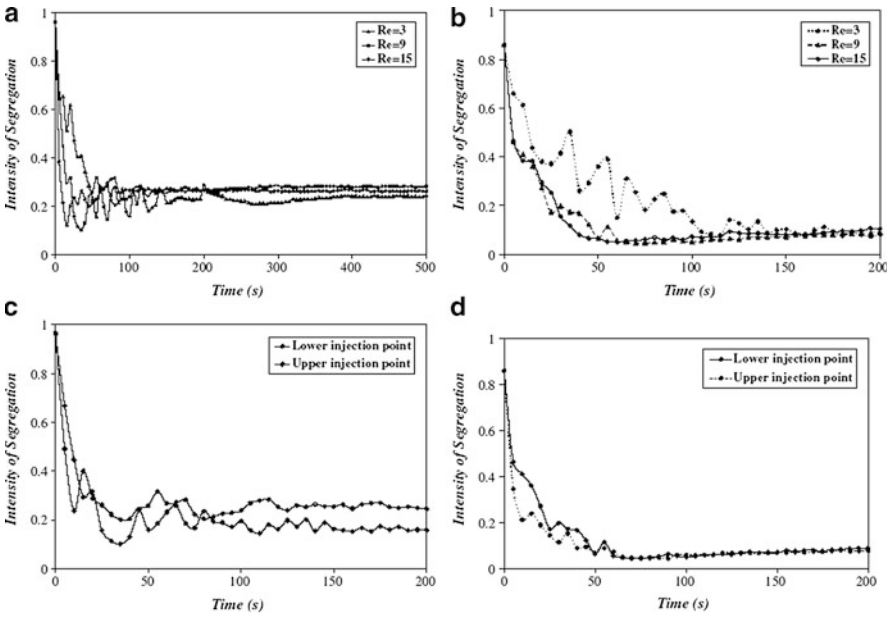

Fig. 2.4 Intensity of segregation vs. time used for different *Re* and points of injection of tracer (Iranshahi et al. 2006)

Table 2.1 Comparison of shearing and pumping abilities of the coaxial mixer for different rotating modes and fluid rheology (Rivera et al. 2006)

Operating conditions	N_q	N_k	N_h/N_q
Co-rotating Newtonian fluid	0.917	1.546	1.685
Rushton impeller only Newtonian fluid	0.658	1.474	2.477
Counter-rotating Newtonian fluid	0.756	1.631	1.948
Co-rotating non-Newtonian fluid	0.761	0.865	1.136
Rushton impeller only non-Newtonian Fluid	0.452	1.082	3.222
Counter-rotating non-Newtonian fluid	0.608	1.457	1.778

intensity of segregation is distributive mixing. Dispersive mixing in our definition relates to the breakup (e.g., of tracer drops) caused by the shearing action of the impellers. The rheology of the fluid also affected the efficiency of the mixing process in that the shear thinning of the viscosity resulted in smaller well-mixed areas.

2.5.2 Dough Mixers and Kneaders

Dough kneaders and mixers are designed for highly viscous doughs and batters that require actions that include pushing portions of the material through other portions, elevating, dropping and rotating the material, and cutting or dividing the material

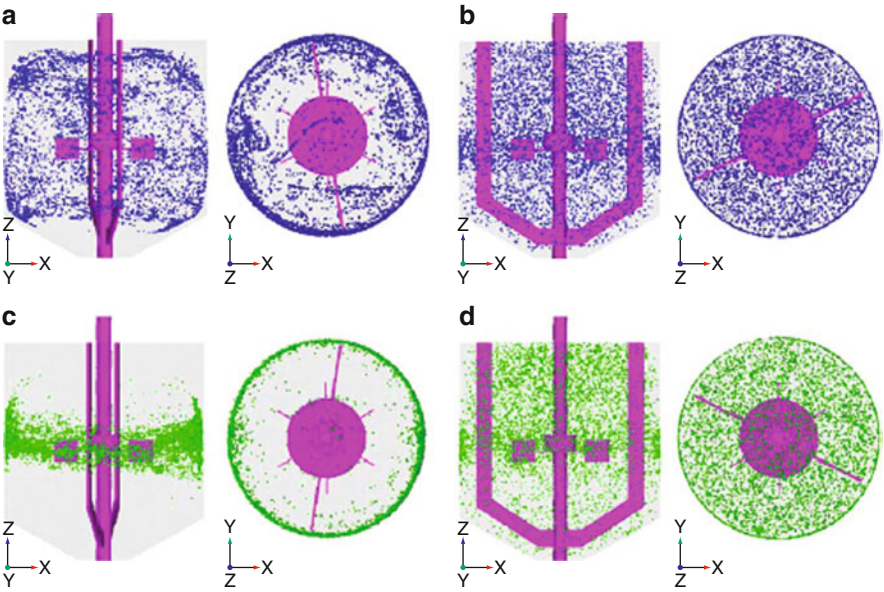

Fig. 2.5 Distributive mixing in a Rushton turbine impeller with a coaxial anchor: (**a**) co-rotating after 15 s; (**b**) co-rotating after 150 s; (**c**) counter-rotating after 15 s; (**d**) counter-rotating after 150 s (Rivera et al. 2006)

(Connelly 2004). Most dough mixers are hence built to operate horizontally, and typically use co-rotating twin blades or arms like roller bars, single and twin sigma blades, open paddle four-way blades, double-arm blades, and spindle geometries. However, several smaller batch dough kneaders with Z blades, sigma blades, or rotating arms are used for empirical dough testing in laboratories. Examples include the plastograph (also called a farinograph) with two counter-rotating but non-intermeshing blades inside a closed cavity; the do-corder with two intermeshing blades co-rotating in a bowl, with limited clearance at the bowl wall; the planetary mixer (or mixograph) with mixing caused by the planetary motion of a rotating arm attached with a pair of vertical pins on either end; and the Eberhart spiral mixer with a spiral rod rotating in a bowl (Jongen et al. 2003) (Fig. 2.6).

Research aimed at optimizing batch kneaders involves experimental methods relating the operating parameters of these mixers to the dough development, rheology, and sensory quality of the product sample. Only a few studies were able to gather specific information on the flow profiles and mixing parameters due to the inherent difficulties with experiments (Prakash et al. 1999; Prakash and Kokini 2000). However, due to the recent advances in the design and simulation capabilities of various CFD software packages, specifically those aimed at viscous and viscoelastic flows, it is now possible to obtain (in a nonintrusive way) detailed information on flow and mixing parameters that includes distribution, dispersion, and laminar stretching in dough mixing.

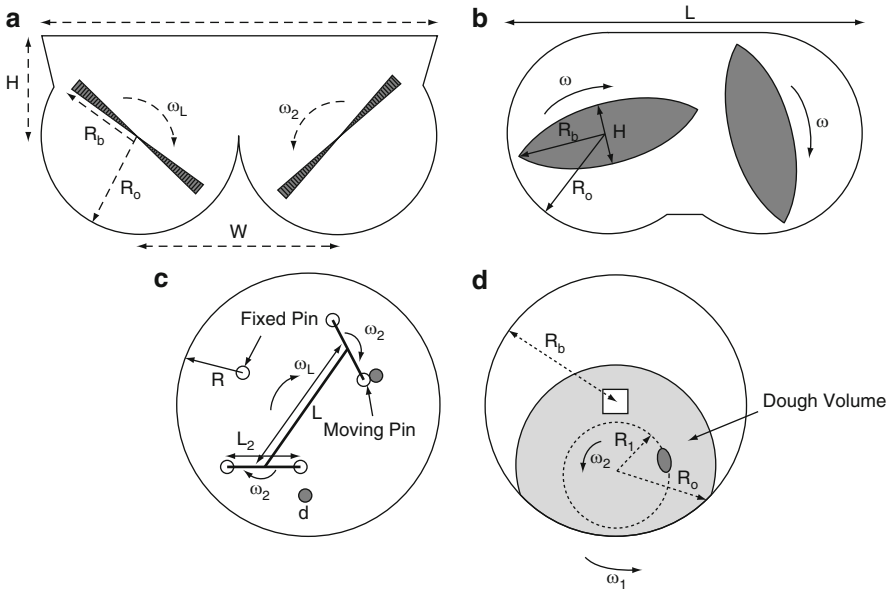

Fig. 2.6 Dough kneaders of various geometries: (**a**) Farinograph; (**b**) Do-corder; (**c**) Mixograph; (**d**) Spiral mixer (Jongen et al. 2003)

Jongen et al. (2003) used a virtual FEM to study the deformation of viscous pastes in four different batch mixing geometries (Fig. 2.6). The technique involved superimposing the moving elements on the flow domain FEM mesh with the FIDAP (Ansys Inc., Lebanon, NH) FEM software. In order to quantify the deformation of the material, a flow parameter R^2 was defined as the ratio of the second invariants of the shear rate and vorticity rate tensors. The normalized value of R^2 was calculated as:

$$D = \frac{1 - R^2}{1 + R^2} \tag{2.26}$$

A comparison of the cumulative time-averaged frequency function for the three types of mixers (Fig. 2.7) showed that the spiral mixer had the most rotational flow; the do-corder the most elongational flow character; and the planetary mixer and plastograph the highest (approximately) shear to the material. An investigation of the same parameter at different operating conditions in the plastograph showed that, while rotational speed of the blades and gap clearance did not affect the type of deformation (value of D), a change in the blade design helped reduce the rotational character of the mixing profile.

A more in-depth and detailed analysis of the 3D flow and mixing profiles in the Brabender® farinograph was performed by Connelly and Kokini (2006a, b) using MST in which the moving sigma blades and the barrel volume were separately meshed and superimposed. An FEM along with the MST was implemented in the

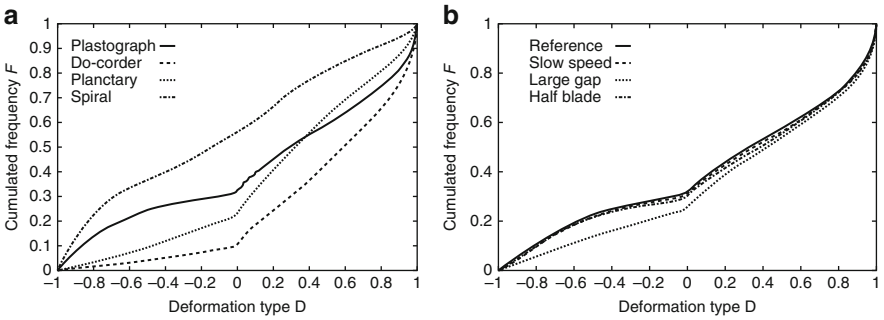

Fig. 2.7 (**a**) Cumulative distribution of mean flow-type parameter *D* for various kneader geometries; (**b**) cumulative distribution of mean flow-type parameter *D* for a farinograph at different blade configurations and speeds (Jongen et al. 2003)

Polyflow® CFD software (ANSYS Inc., Lebanon, NH). Figure 2.8 shows the effect of fluid rheology on the velocity contour maps on the vertical center plane between the two blades. Increased shear thinning of the fluid caused a decrease in the velocity of the fluid right above the blades. The dispersive mixing ability was calculated as defined by (2.8). A histogram of the distribution of the dispersive mixing index in the central planes between the farinograph blades for the three fluids shows a decrease in the elongational flow regions with increasing shear thinning. The paths of material points can be calculated from the velocity profiles, which can then be used to evaluate the distributive and stretching efficiency parameters such as the cluster distribution index, scale of segregation, and the mean length of stretch. The density of probability of the length of stretch experienced by 10,000 infinitesimal material lines in the farinograph (Fig. 2.9) for three blade revolutions showed a gradual and steady increase in the amount of material undergoing effective stretching over time.

Limited work has been done on studying the effect of a fluid's viscoelasticity on flow and mixing profiles. Connelly and Kokini (2003) simulated the flow of a Phan-Thien Tanner fluid model in a 2D single screw mixer using a rotating reference frame technique; they compared different methods of handling the instabilities in dealing with a differential viscoelastic fluid model. It was found that the effect of viscoelasticity (an increase in relaxation times) was to create asymmetry in the velocity and pressure profiles and to reduce the effects of shear thinning on the pressure and stresses (Fig. 2.10).

2.5.3 Continuous Mixers and Extruders

Simulation of continuous mixer geometries requires increased computational costs due to the complexity and lack of symmetry in the geometry. The most common continuous screw-type mixer and extruder design used in the food industry is the

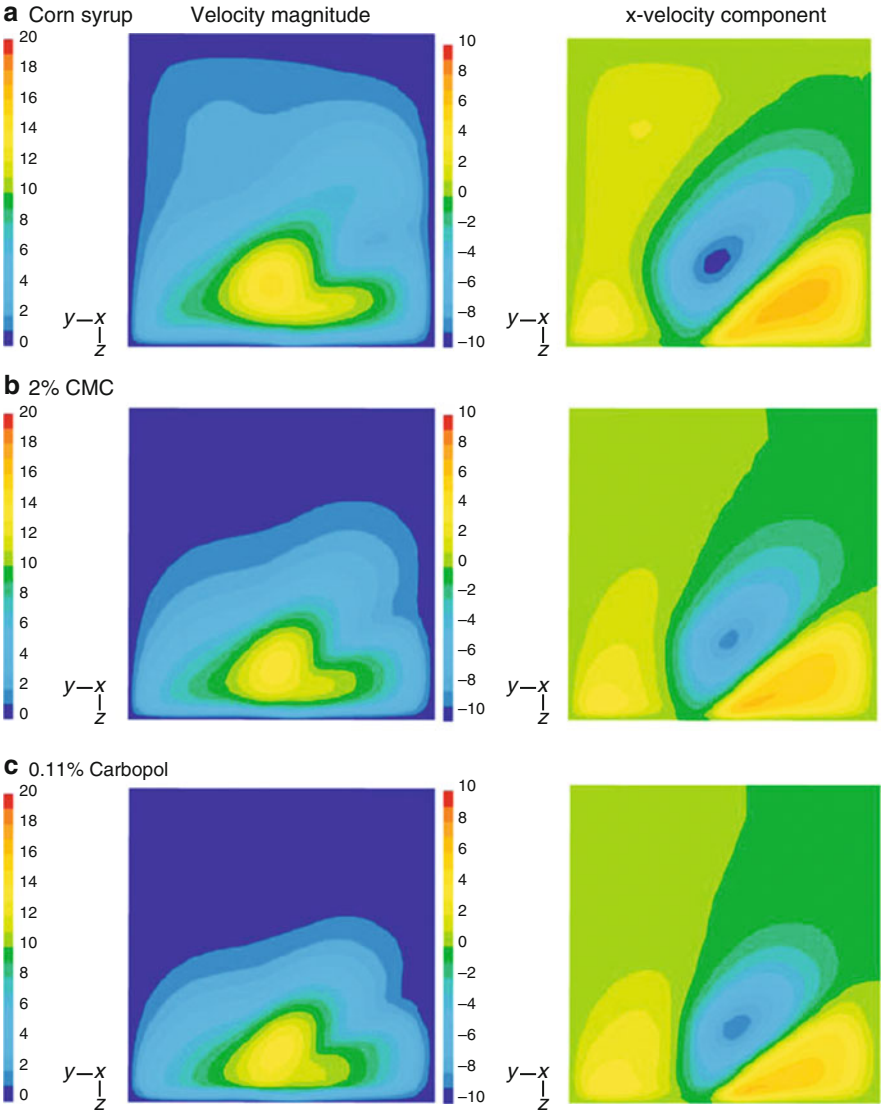

Fig. 2.8 Effect of fluid rheology on the velocity profiles in the vertical center plane of a farinograph (Connelly and Kokini 2006a)

two-lobed twin-screw co-rotating design, for example the Readco® continuous mixer shown in Fig. 2.11. The design consists of a pair of co-rotating shafts fitted with a series of conveying screws, two- or three-lobed kneading blocks that can be staggered followed by discharge screw elements. There have been several analytical, experimental, and numerical studies conducted to decipher the flow and mixing patterns in both the conveying screw regions and the kneading region. As a first step

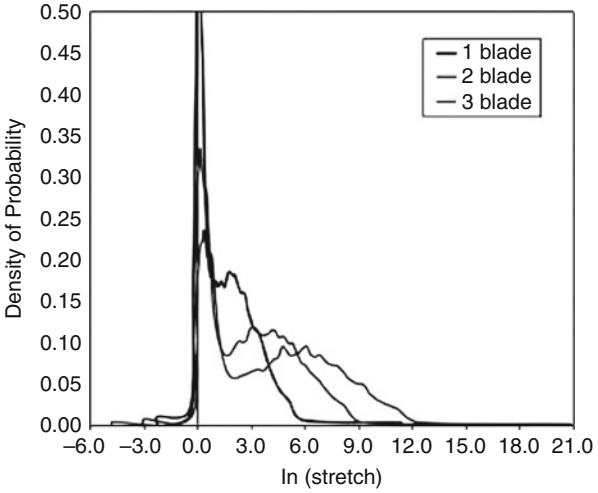

Fig. 2.9 Density of probability for length of stretch *ln(λ)* experienced by 10,000 infinitesimal material lines in a farinograph (Connelly and Kokini 2006b)

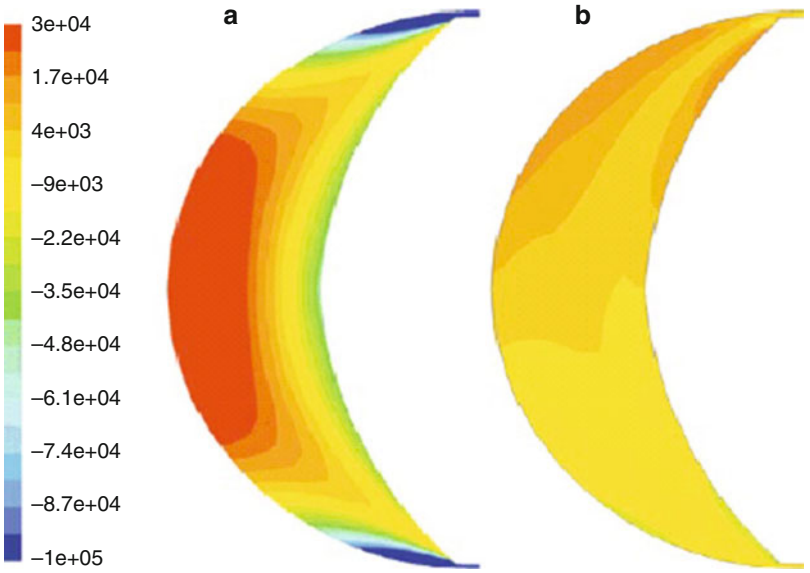

Fig. 2.10 Shear stress (g/cm^2) contour maps for fluid with relaxation times of (**a**) 0 s and (**b**) 100 s in a 2D single-paddle mixer (Connelly and Kokini 2003)

to studying the twin-screw continuous mixer design, Connelly and Kokini (2007) used numerical simulations to compare mixing of a Carreau model fluid in both a 2D single-paddle mixer and a 2D twin-paddle mixer. The presence of a second paddle element in the twin-screw geometry significantly improved both dispersive

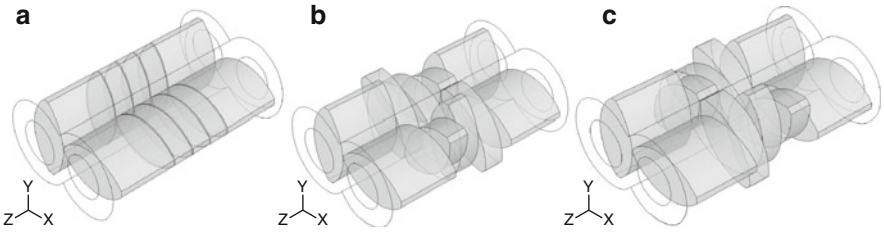

Fig. 2.11 Kneading elements of the Readco® twin-screw processor (Readco Inc., York, PA) arranged in (**a**) FLAT, (**b**) 45F, and (**c**) 45R configurations (Vyakaranam and Kokini 2008)

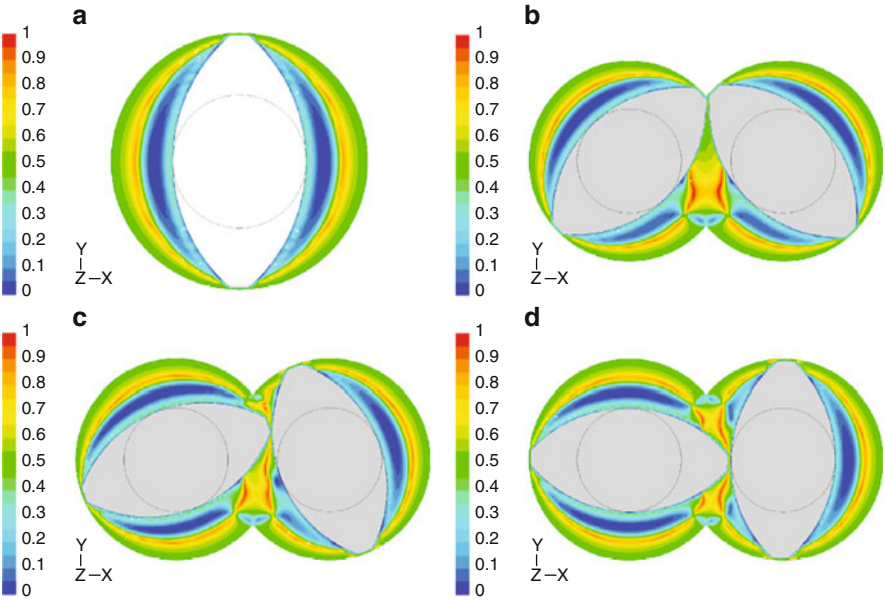

Fig. 2.12 Mixing index (λ_{MZ}) contours for the (**a**) single-screw and twin-screw mixers after rotation of the paddles at (**b**) 45°, (**c**) 67.5°, and (**d**) 90° (Connelly and Kokini 2007)

and distributive mixing. Figures 2.12 and 2.13 shows the dispersive mixing index and the cluster distribution index in both mixers. While the twin-screw geometry shows an increase in the area and magnitude of elongational flow, the single-screw geometry showed a cyclic cluster distribution index, suggesting that the material points were unable to leave the streamlines, leading to poor distributive mixing.

While these simulations were useful in showing the positive effect of a twin-paddle element on the mixing, 3D simulations of the full-length mixer are needed for a realistic simulation of continuous mixing, which involves axial flow. The study of continuous mixers is mainly focused on evaluating the effects of screw speed, stagger angle, and thickness of the paddle elements on the dispersive and distributive mixing measures, and comparing the performance to a batch mixer.

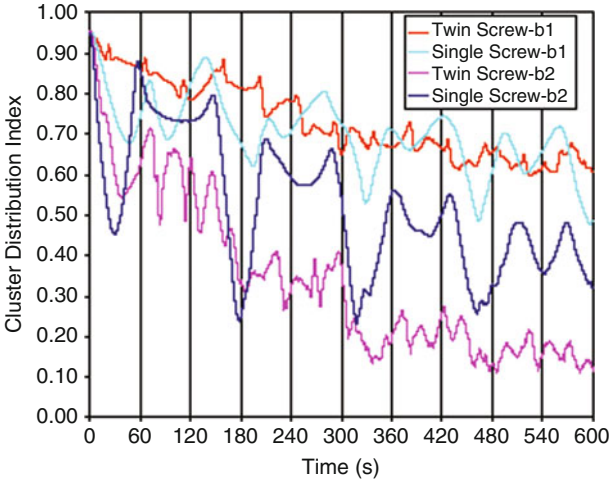

Fig. 2.13 Comparison of cluster distribution index for ten revolutions in the single-screw and twin-screw mixers with different locations for the initial cluster in the flow domain: b1 (center location) and b2 (leftmost location) (Connelly and Kokini 2007)

For example, consider the 3D numerical simulation of the mixing of a generalized Newtonian fluid in a full-length kneading section of the Readco® continuous processor with nine paddle pairs. The flow data were evaluated for every 10° of movement by the paddles for ten rotations at three different screw speeds (1, 50, and 100 RPM); next the various distributive and dispersive mixing measures were evaluated. The paddle elements were staggered forward and reversed at an angle of 45° (Fig. 2.11).

Figure 2.14 shows the effects of screw speed and stagger angle on the time-averaged efficiencies of the three continuous mixer geometries in comparison with the farinograph. The time averaged instantaneous mixing efficiency decreased with increasing screw speed, with highest efficiency at the lowest screw speed of 1 RPM, which has been attributed to higher residence time of the material at lower screw speed resulting in greater stretching and folding of the material. The FLAT (or neutral, with no element stagger) configuration showed the highest efficiency (Ashokan 2008).

Mixing efficiency is also affected by the individual paddle element width and the increase in the number of gaps between the elements, as a result of increasing the number of elements. Figure 2.15 shows the area stretch (as a measure of distributive mixing) of different kneading element widths for two-lobe kneading elements. The smaller the disc width, the better was the area stretch; it was hypothesized that the increase in the number of gaps caused an increase in the area stretch (Ishikawa et al. 2001).

Yoshinaga et al. (2000) studied the isothermal flow of a Carreau model non-Newtonian fluid in the kneading section of a twin-screw extruder using FEM

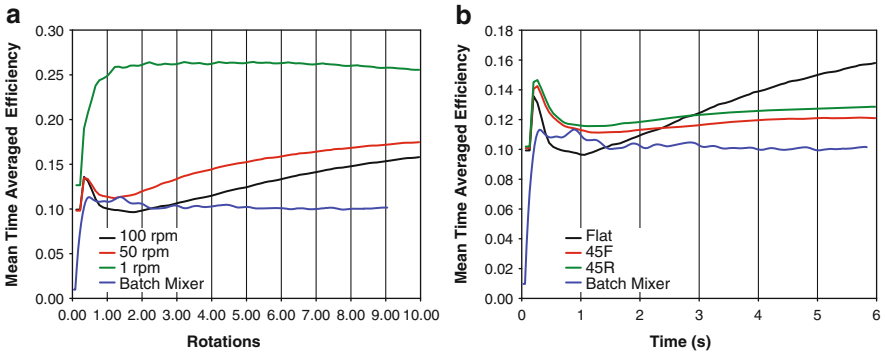

Fig. 2.14 Effect of (**a**) screw speed and (**b**) screw configuration on time-averaged mixing efficiency of the Readco® twin-screw continuous mixer and the farinograph batch mixer (Ashokan 2008)

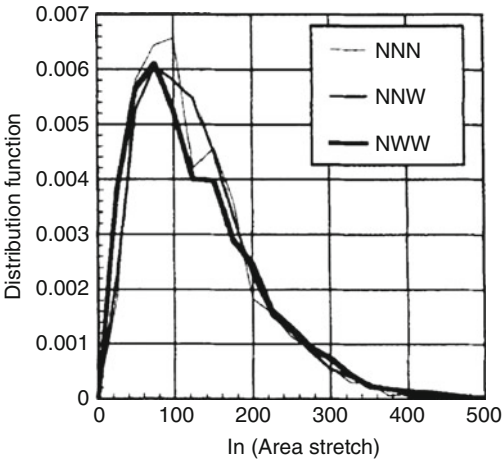

Fig. 2.15 Distribution of the area stretch in mixing region of a co-rotating twin-screw extruder for different kneading disc widths (i.e., NNN, NNW, and NWW) (Ishikawa et al. 2001)

simulations. The shafts were fitted with five pairs of three-lobed mixing elements configured at different stagger angles. Distributive mixing was measured by residence time distributions and the minimum distance between mass-less particle markers after mixing for a given time. The simulations were performed as a quasi-steady state wherein the velocity profiles were calculated for every 3° of rotation of the screw elements. Both the residence time distributions and the mean nearest distance between the markers showed the neutral stagger configuration to be the most beneficial for distributive mixing (Fig. 2.16).

Dispersive mixing can be analyzed by evaluating the dispersive mixing index and corresponding shear stresses (or shear rates, if a Newtonian fluid). Figure 2.17 shows the contour maps of shear rate and mixing index (λ_{MZ}) at the 1st, 4th, and 8th

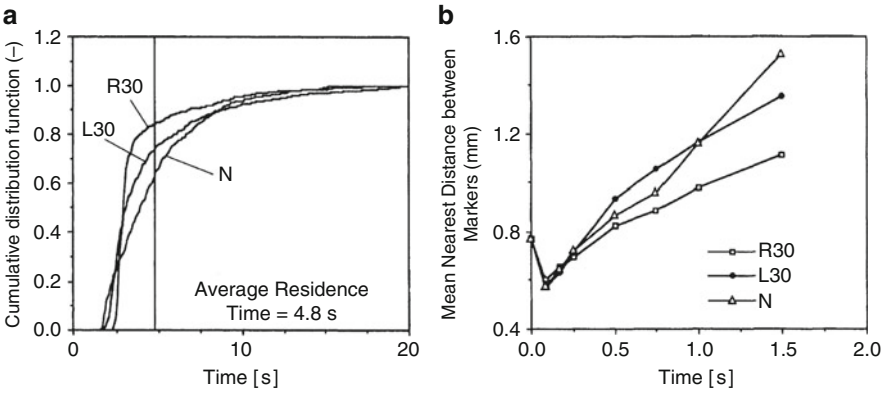

Fig. 2.16 (**a**) Residence time distribution and (**b**) mean nearest distance between markers in mixing region of a co-rotating extruder fitted with three-lobed kneading discs (Yoshinaga et al. 2000)

paddle elements of the FLAT configuration for a Newtonian fluid mixed at 75 RPM. The elongational flow, indicated by the red shade, is the highest in the center region of the mixer (around the 4th paddle element), while highest shear rates are found in the intermeshing regions. The elongational flow is known to cause a breakup of agglomerates and drops in flow; the corresponding shear rate can be made dimensionless by using the capillary number (Ca). The Ca can be defined as the ratio of the viscous forces acting to deform the drop to the interfacial forces resisting deformation and acting to restore its spherical shape. At high enough Ca, the drop deformation becomes unsteady, leading to breakup. The equation for Ca is given as:

$$Ca = \frac{\mu\dot{\gamma}}{\sigma} r \tag{2.27}$$

where μ is the viscosity of the continuous medium (food matrix), $\dot{\gamma}$ is the local shear rate, r is the bubble radius, and σ is the surface tension of the food matrix (Meijer and Janssen 1994; Risso 2000). The effect of paddle element stagger on the distribution of Ca and λ_{MZ} for air bubbles in a Newtonian corn syrup is shown in Fig. 2.18 for the FLAT, 45F (with a 45° forward element stagger), and the 45R (with a 45° reverse element stagger) configurations. It can be seen that the density of points in the mixer with Ca and λ_{MZ}, which are high enough for breakup, decreases with a reverse stagger angle of the paddle elements, suggesting higher breakup in the FLAT configuration. The effects of stagger angle and screw speed on the shear stresses (or Ca) and distribution of flow type give useful information that aids in the design of mixers with better dispersive abilities.

Numerical simulation of the flow of fluids modeled by a viscoelastic constitutive equation in a complex 3D geometry is a nontrivial task. For example, the MST

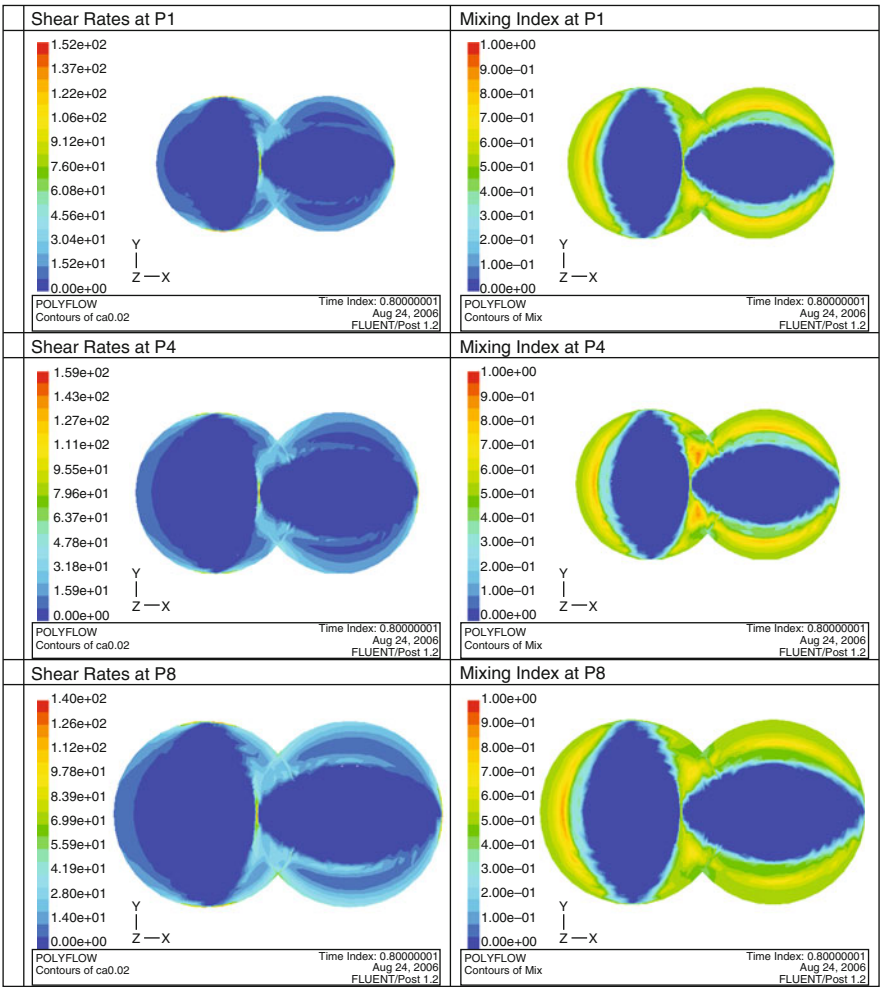

Fig. 2.17 Distribution of shear rate ($\dot{\gamma}$) and mixing index (λ_{MZ}) at different locations in the twin-screw mixer at a screw speed of 75 RPM (Vyakaranam and Kokini 2008)

technique in the POLYFLOW FEM solver does not support the use of a viscoelastic constitutive equation; therefore a new technique is needed to model the fluid flow. One such technique is the Pseudo Steady State (PSS) technique in which the flow is modeled as a steady state with the viscoelastic constitutive equation for a snapshot of the moving geometry; the velocity, pressure, and stress results are then used as the input for successive time steps (Ishikawa et al. 2001). Preliminary demonstration of the technique using a 2D Readco® geometry was successful in obtaining the velocity and shear rate profiles at low Deborah numbers and small rotations of the paddle elements (Ashokan 2008). Further work is needed to extend the simulation

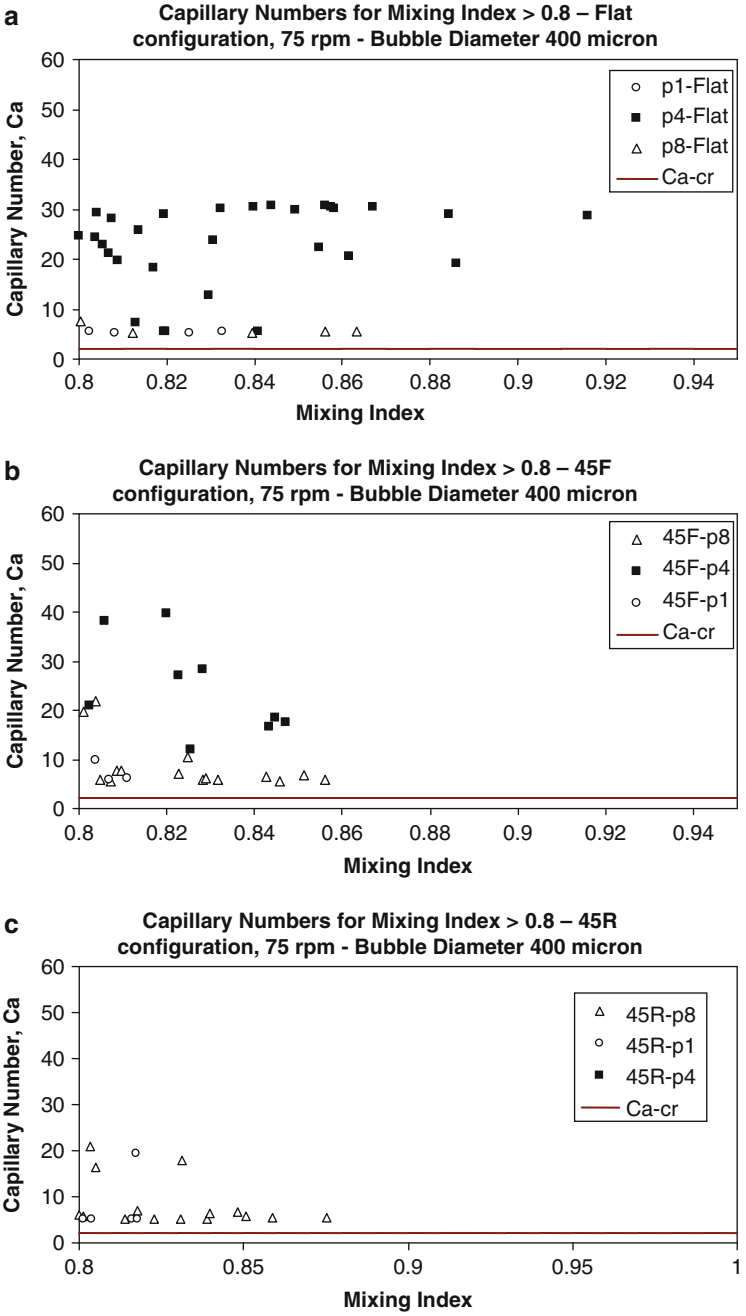

Fig. 2.18 Distribution of Ca and λ_{MZ} values for all calculated points in mixing region of the Readco® twin-screw mixer at different screw configurations (Vyakaranam et al. 2009)

of viscoelastic simulations in full 3D geometry at higher Deborah numbers and larger rotations of the paddles.

2.6 Conclusions

Recent studies in numerical simulation of viscous flow and mixing in the laminar regime have shown the FEM to be a cost-effective and nonintrusive technique for analyzing and visualizing the distributive and dispersive mixing ability in batch and continuous mixing devices of various geometries. A review of recent work analyzing the mixing of viscous and viscoelastic fluids using numerical simulations has been presented. Stirred tank reactors and batch mixers of varying geometries have been successfully employed to demonstrate the use of numerical simulations for visualization and analysis of viscous and viscoelastic mixing in 3D. While the simulation of flow and mixing for fluids of relatively simple rheological character (viscous Newtonian and non-Newtonian) has been done for complex geometries at a 3D level, there is a need for further work in simulating the mixing of more complex viscoelastic fluid models in full-scale continuous mixer geometries.

Acknowledgments The authors would like to thank Dr. Nesli Sozer for help with proofreading the document.

References

Alvarez-Hernández MM, Shinbrot T, Zalc J, Muzzio FJ (2002) Practical chaotic mixing. Chem Eng Sci 57(17):3749–3753

Ashokan BK (2008) Developing methods for design and analysis of continuous mixers through 3D numerical simulation of flow and mixing, Ph.D. thesis. Food Science, Rutgers University

Barailler F, Heniche M, Tanguy PA (2006) CFD analysis of a rotor-stator mixer with viscous fluids. Chem Eng Sci 61(9):2888–2894

Bentley BJ, Leal LG (1986) An experimental investigation of drop deformation in steady, two-dimensional linear flows. J Fluid Mech 167:241–283

Connelly RK (2004) Numerical simulation and validation of the mixing of dough-like materials in model batch and continuous dough mixers, Ph.D. thesis: 430. Food Science, Rutgers University

Connelly RK, Kokini JL (2003) 2-D numerical simulation of differential viscoelastic fluids in a single-screw continuous mixer: application of viscoelastic finite element methods. Adv Polym 22(1):22–41

Connelly RK, Kokini JL (2004) The effect of shear thinning and differential viscoelasticity on mixing in a model 2D mixer as determined using FEM with particle tracking. J Non-Newtonian Fluid Mech 123(1):1–17

Connelly RK, Kokini J (2006a) 3D numerical simulation of the flow of viscous Newtonian and shear thinning fluids in a twin sigma blade mixer. Adv Polym Technol 25(3):182–194

Connelly RK, Kokini J (2006b) Mixing simulation of a viscous Newtonian liquid in a twin sigma blade mixer. AIChE J 52(10):3383–3393

Connelly RK, Kokini JL (2007) Examination of the mixing ability of single and twin screw mixers using 2D finite element method simulation with particle tracking. J Food Eng 79 (3):956–969

Dhanasekharan M, Kokini JL (2000) Viscoelastic flow modeling in the extrusion of a dough-like fluid. J Food Proc Eng 23(3):237–247

Dhanasekharan M, Kokini J (2003) Design and scaling of wheat dough extrusion by numerical simulation of flow and heat transfer. J Food Eng 60(4):421–430

Grace HP (1982) Dispersion phenomena in high viscosity immiscible fluid systems and application of static mixers as dispersion devices in such systems. Chem Eng Commun 14:225

Heniche M, Tanguy PA (2008) Finite element modeling of viscous mixing: a review. Chem Product Process Model 3(1):55

Heniche M, Tanguy PA, Reeder MF, Fasano JB (2005) Numerical investigation of blade shape in static mixing. AIChE J 51(1):44–58

Iranshahi A, Heniche M, Bertrand F, Tanguy PA (2006) Numerical investigation of the mixing efficiency of the Ekato Paravisc impeller. Chem Eng Sci 61(8):2609–2617

Iranshahi A, Devals C, Heniche M, Fradette L, Tanguy PA, Takenaka K (2007) Hydrodynamics characterization of the Maxblend impeller. Chem Eng Sci 62(14):3641–3653

Ishikawa T, Kihara S, Funatsu K (2001) 3-D non-isothermal flow field analysis and mixing performance evaluation of kneading blocks in a co-rotating twin screw extruder. Polym Eng Sci 41(5):840–849

Jongen T (2000) Characterization of batch mixers using numerical flow simulations. AIChE J 46 (11):2140–2150

Jongen TRG, Bruschke MV, Dekker JG (2003) Analysis of dough kneaders using numerical flow simulations. Cereal Chem 80(4):383–389

Meijer MEH, Janssen JMH (1994) Mixing of immiscible liquids. In: Manas-Zloczower I, Tadmor Z (eds) Mixing and compounding of polymers: theory and practice. Carl Hanser Verlag, New York

Muzzio FJ, Alvarez MM, Cerbelli S, Giona M, Adrover A (2000) The intermaterial area density generated by time- and spatially periodic 2D chaotic flows. Chem Eng Sci 55(8):1497–1508

Ottino JM (1989) The kinematics of mixing: stretching, chaos and transport. Press Syndicate of University of Cambridge, Cambridge

Prakash S (1996) Characterization of shear rate distribution in a model mixer using laser doppler anemometry. Ph.D. thesis: 315. Food Science, Rutgers University

Prakash S, Kokini JL (2000) Estimation and prediction of shear rate distribution as a model mixer. J Food Eng 44(3):135–148

Prakash S, Karwe MV, Kokini JL (1999) Measurement of velocity distribution in the Brabender farinograph as a model mixer, using laser-doppler anemometry. J Food Process Eng 22 (6):435–454

Rauline D, Le Blévec JM, Bousquet J, Tanguy PA (2000) A comparative assessment of the performance of the Kenics and SMX static mixers. Chem Eng Res Des 78(3):389–396

Reddy JN (2006) An introduction to the finite element method. Tata McGraw-Hill, New Delhi

Risso F (2000) The mechanisms of deformation and breakup of drops and bubbles. Multiphase Sci Technol 12:1–50

Rivera C, Heniche M, Ascanio G, Tanguy P (2004) A virtual finite element model for centered and eccentric mixer configurations. Comp Chem Eng 28(12):2459–2468

Rivera C, Foucault S, Heniche M, Espinosa-Solares T, Tanguy PA (2006) Mixing analysis in a coaxial mixer. Chem Eng Sci 61(9):2895–2907

Vyakaranam KV, Kokini J (2008) Study of the dynamics and size distributions of air bubbles during mixing in a continuous food mixer. In: Campbell G, Scanlon M, Pyle L (eds) Bubbles in food 2: novelty, health and luxury. AACC, St. Paul

Vyakaranam KV, Evans ME, Ashokan BK, Kokini JL (2009) Evaluation of mixing and air bubble dispersion in viscous liquids using numerical simulations. In: Cullen PJ (ed) Food mixing: principles and applications. Wiley-Blackwell, Oxford

Wang W, Manas-Zloczower I (2001) Temporal distributions: the basis for the development of mixing indexes for scale-up of polymer processing equipment. Polym Eng Sci 41 (6):1068–1077

Yang H-H, Manas-Zloczower I (1992) Flow field analysis of the kneading disc region in a co-rotating twin screw extruder. Polym Eng Sci 32(19):1411–1417

Yoshinaga M, Katsuki S, Miyazaki M, Liu L, Kihara S, Funatsu K (2000) Mixing mechanism of three-tip kneading block in twin screw extruders. Polym Eng Sci 40(1):168–178

Zalc JM, Alvarez MM, Muzzio FJ, Arik BE (2001) Extensive validation of computed laminar flow in a stirred tank with three Rushton turbines. AIChE J 47(10):2144–2154

Zalc JM, Szalai ES, Alvarez MM, Muzzio FJ (2002a) Using CFD to understand chaotic mixing in laminar stirred tanks. AIChE J 48(10):2124–2134

Zalc JM, Szalai ES, Jaffer S, Muzzio FJ (2002b) Characterization of flow and mixing in an SMX static mixer. AIChE J 48(3):427–436

Zalc JM, Szalai ES, Muzzio FJ (2003) Mixing dynamics in the SMX static mixer as a function of injection location and flow ratio. Polym Eng Sci 43(4):875–890

Chapter 3
CFD: An Innovative and Effective Design Tool for the Food Industry

Tomás Norton and Da-Wen Sun

3.1 Introduction

Fluids are ubiquitous in nature. In fact, many if not most industrial food processes require work done on or by a fluid-based system during product development. During the design and optimization of food processes, engineers must regularly tackle problems that involve not only fluids but also complex phenomena such as heat and mass transfer, phase change, and chemical reactions. Forming a comprehensive understanding of food-processing systems is not easy because the above phenomena generally progress as invisible to the eye, and thus often their dynamics cannot be easily realized or quantified. Moreover, when presented with complex flow fields, which are governed by nonlinear dynamics, measurements alone may not be sufficient for accurate analysis, as not only can equipment be intrusive but too many measurement probes may also be required to fully diagnose a problem.

Computational fluid dynamics (CFD) is mainly concerned with the numerical solution of the partial differential equations governing transport of mass, momentum, and energy in moving fluids. However, most importantly, many processes involving the motion of fluids and heat transfer, mass transfer, and chemical reactions can be accurately described with CFD. Currently CFD is being universally used as an effective tool to investigate the spatiotemporal dynamics of many interesting processes used by the food and beverage industry such as mixing, drying, cooking, sterilization, chilling, and cold storage (Sun 2007). As a result, the application and development of CFD for food processing is now proving to play a fundamental role in problem solving for both industry and research, and its use by the scientific community has grown exponentially within the last number of years (Norton and Sun 2007). CFD has many advantages over traditional design and analysis techniques, for example:

T. Norton and D.-W. Sun (✉)
Food Refrigeration and Computerised Food Technology (FRCFT), University College Dublin, National University of Ireland, Agriculture & Food Science Centre, Belfield, Dublin 4, Ireland
e-mail: dawen.sun@ucd.ie

J.M. Aguilera et al. (eds.), *Food Engineering Interfaces*, Food Engineering Series,
DOI 10.1007/978-1-4419-7475-4_3,

- Because food processes can be examined in a virtual environment, designs can be achieved without encountering health and safety concerns or scaling issues associated with physical prototyping, etc.
- Many designs of a single system/process can be explored on the computer with virtual prototypes, thereby reducing wasteful trial and error techniques in industry.
- Parametric studies can be easily completed in order to come up with design solutions for a new geometry at a fraction of the cost of manufacturing the various design options.

The fundamentals of CFD applications, its general applications in the food industry, and the existing limitations and challenges that face current users of this technology have been reviewed by some authors (Xia and Sun 2002; Norton and Sun 2007). In light of this technology's rapid development over the last number of years, and the engineering challenges that face the food industry, this chapter gives a comprehensive account of the latest advances made through successful CFD applications in research. Firstly, the equations governing the physical mechanisms encountered when modeling different processes in the food industry will be discussed, followed by an overview of how they are solved in a CFD environment. An account of CFD modeling studies conducted on emerging food-processing technologies will then be highlighted. Finally, an overview will be given on the challenges still encountered in CFD modeling of food processes.

3.2 Modeling Food Processes: Solving Governing Partial Differential Equations

For all food-processing systems, partial differential equations (PDEs) can describe the intensity and spatiotemporal migration of thermodynamic and fluid-dynamic phenomena. In order to develop and optimize food-processing systems, engineers need to form a complete picture of the various mechanisms working within. Also, to avoid the expense and time associated with physical experimentation, such insight demands solutions to PDEs that describe the system. However, whether or not such solutions are achievable is dependent on the physics involved, the level of precision associated with the analysis tools at hand, and the amount of computing power available to the engineer. In fact, because PDEs are generally by their very nature time-consuming to solve, they require substantial computer resources; therefore adequate solutions have not always been attainable with prevailing computer power. In the past this meant that PDEs needed to be simplified so that they could be manageably solved by hand, and assumptions impacting the quality of a solution could easily be introduced. Furthermore, localized phenomena such as mixing, fouling, cleaning, etc. cannot be accurately determined by simple models; numerical analysis has always been required to establish the distribution of variables, that is, temperature, fluid velocity, and concentration in such systems.

Modern CFD codes have been developed using numerical algorithms that solve the nonlinear PDEs governing fluid flow, heat transfer, and many other physical phenomena. With this myriad of capabilities, CFD techniques can be used to build distributed parameter models that are spatially and temporally representative of food-processing systems, thereby allowing solutions with high levels of physical realism. The accuracy of a CFD simulation is a function of many parameters, including the level of empiricism involved, that is, via turbulence models or additional physical models; the assumptions involved, that is, Boussinesq versus the ideal gas approximation for inclusion of buoyancy effects; the simplification of both geometry and boundary conditions to reduce processing time; and whether processes modifying the physical mechanisms are included, that is, chemical kinetics. As with other modeling techniques, the greater the number of approximations, the less accurate the CFD solution will be (Verboven et al. 2004). However, if used correctly, CFD provides an understanding of the physics of a system in greater detail through nonintrusive flow, thermal, and concentration field predictions. Furthermore, after many years of development, CFD codes can now solve advanced problems related to combined convection, radiation and conduction heat transfer, flows in porous media, multiphase flows, and issues involving chemical kinetics.

Many applications of CFD in modern food processing already exist, such as for ovens, refrigerators, heat exchangers, in-place cleaning operations, spray dryers, biosensors, and pasteurization techniques, among others. CFD simulation has made giant leaps in realism with the yearly experience gained from each specialization in tandem with the continual development of commercial CFD codes. For example, in recent designs of multi-deck chilled cabinets, CFD simulations have been used to visualize the impact of various design constraints without the need for physical prototyping (Foster et al. 2005). Further simulations have revealed the impact of these refrigeration systems on the occupant comfort in retail stores. In the advancement of oven technology, CFD analyses have worked in conjunction with other mathematical models of food quality attributes to optimize variations in the weight loss and crust color of bread products prior to baking (Zhou and Therdthai 2007). Also, in modern operations like air impingement ovens, CFD has been employed so that the interaction of the jet flow pattern with the product can be understood; spatially dependent heat and mass transfer coefficients can be predicted; and equipment design parameters can be optimized (Kocer et al. 2007; Olsson and Trägårdh 2007). In recent times, three-dimensional CFD modeling of plate heat exchangers (PHEs) has allowed the milk fouling process to be simulated based on both hydrodynamic and thermodynamic principles. This fouling model permits assessing the influence of corrugation shapes and orientations on the PHE performance (Jun and Puri 2006). The current standard for CFD modeling of spray dryers has also raised the value of simulations by extending the basic models of flow patterns and particle trajectories to sub-models such as drying models, kinetic models of thermal reactions, sub-models describing product stickiness, and agglomeration models (Straatsma et al. 2007). In other areas, CFD has recently been used to model:

- Pasteurization of intact eggs (Denys et al. 2007); this application formerly had little information concerning temperatures and process times required.
- Application of biosensors in the food industry (Verboven et al. 2007a); this modeling allows the optimization of biosensor design in terms of fluid flow, mass transfer, and chemical kinetics.
- Tea fermentation and infusion (Lian 2007); CFD is used to predict the interplay between the heat transfer and enzymatic reactions during tea fermentation; optimal process conditions for desired flavor generation and functional properties can also be obtained.

All of these applications are good examples of CFD's ability to resolve problems in both novel and conventional food-processing operations, even in systems for which there is little prior knowledge. Also, since CFD can compute variables such as fluid velocity, pressure, and temperature at many thousands of locations within a virtual geometry, the solutions can be comprehensive, both spatially and temporally. The various PDEs that govern the phenomena encountered in food-processing systems are introduced next. The governing equations of fluid flow and heat transfer can be considered as mathematical formulations of the conservation laws of fluid mechanics. When applied to a fluid continuum, these conservation laws relate the rate of change of a desired fluid property to external forces. The following sections describe the governing equations for these various phenomena in Cartesian coordinates.

3.2.1 Conservation of Mass

The mathematical formulation of the law of conservation of mass is also known as the continuity equation. For a fluid element the solution for each requires a separate equation. The conservation of mass states that the net mass flowing through all the surfaces of a fluid element must be equal to the rate of accumulation in the element. For incompressible fluids, which are commonly encountered in the food industry, this means that the quantity of mass entering a fluid element must balance exactly with that leaving

$$\nabla.\vec{v} = 0 \tag{3.1}$$

where $\vec{v}$ consists of components of $\bar{v}_i$.

3.2.2 Conservation of Momentum

The conservation of momentum for a fluid element is also termed Newton's second law of motion, which states that the sum of the external forces acting on the fluid particle is equal to its rate of change of linear momentum:

$$\rho \frac{\partial v_i}{\partial t} + \rho \vec{v}.\nabla \vec{v}_i = -\nabla p + \mu \nabla^2 \vec{v}_i + \rho g \tag{3.2}$$

This mathematical formulation of fluid motion has been used for almost two centuries, since the emergence of three very important scientists in the field of fluid mechanics, namely, Leonhard Euler, Claude-Louis Navier, and George Gabriel Stokes. Leonhard Euler (1707–1783), a Swiss mathematician and physicist, formulated the Euler equations, which describe the motion of an inviscid fluid based on the conservation laws of fluid mechanics. The French engineer and physicist, Claude-Louis Navier (1785–1836), and Irish mathematician and physicist, George Gabriel Stokes (1819–1903), later introduced viscous transport into the Euler equations by relating the stress tensor to fluid motion. The resulting set of equations is now termed the Navier–Stokes equation for Newtonian fluids; it has formed the basis of modern-day CFD.

3.2.3 Conservation of Energy

The mathematical formulation of the conservation of energy is also called the first law of thermodynamics, which states that the rate of change in energy of a fluid particle is equal to the heat addition and the work done on the particle, assuming that the thermophysical properties are not temperature-dependent:

$$\rho c_p \frac{\partial \vec{v}_i}{\partial t} + \vec{v}.\nabla T = \lambda \nabla^2 T + s_T \tag{3.3}$$

As many food-processing operations involve heat transfer, and because the properties of fluids can be temperature-dependent, (3.3) is often coupled with the Navier–Stokes equation. When conjugate heat transfer is under investigation it is important to maintain continuity of thermal exchange across the fluid–solid interface, and the transport of heat in a solid structure should also be considered in CFD simulations (Verboven et al. 2004). The Fourier equation, which governs heat transfer in an isotropic solid, can be written as

$$\rho c_p \frac{\partial \vec{v}_i}{\partial t} = \lambda \nabla^2 T + s_T \tag{3.4}$$

For a conjugate heat transfer situation, where evaporation at the food surface is considered and where the heat transfer coefficient is known, the boundary condition for (3.4) may be written as follows:

$$h\left(T_{bf} - T_s\right) + \varepsilon\sigma\left(T_{bf}^4 - T_s^4\right) = -\lambda \frac{\partial T}{\partial n} \tag{3.5}$$

where ε is the emission factor coefficient and σ is the Stefan–Boltzmann constant. Heat transported by radiation and convection from air to food raises the sample temperature (Aversa et al. 2007). The solution of (3.3) can be used for food surfaces to calculate the local heat transfer coefficients as given below:

$$h = \frac{-\lambda \frac{\partial T}{\partial n}\Big|_{\text{surface}}}{\left(T_{bf} - T_s\right)} \tag{3.6}$$

Equation (3.6) can be used provided the surface temperature is assumed independent of the coefficient during calculations.

3.3 Modeling Properties of Fluids

3.3.1 Density

In many food-processing operations, variables such as temperature, concentration, and fluid velocity are functions of density variations caused by the heating and cooling of fluids. Therefore, the density of the fluid must be accurately represented in CFD computations. Since many fluid flows encountered in food-processing applications can be regarded as incompressible, there are two means of accounting for density variations, namely, the Boussinesq approximation and the ideal gas equation (Ferziger and Peric 2002). The Boussinesq approximation has been used successfully in many CFD applications (Abdul Ghani et al. 2001):

$$\rho = \rho_{\text{ref}}[1 - \beta(T - T_{\text{ref}})] \tag{3.7}$$

The approximation assumes that the density differentials of the flow are only required in the buoyancy term of the momentum equations. In addition, a linear relationship between temperature and density, with all other extensive fluid properties being constant, is also assumed. This relationship only considers a single-component fluid medium; however, by using Taylor's expansion theorem, the density variation for a multicomponent fluid medium can also be derived.

For large temperature differences, the fluid flow becomes compressible with a strong coupling between the continuity, the momentum, and the energy equations through the equation of state; its properties (viscosity, heat conductivity) also vary with the temperature, making the Boussinesq flow approximation inappropriate and inaccurate (Ferziger and Peric 2002). Therefore, in such cases another method of achieving the coupling of the temperature and velocity fields is necessary. This can be done by expressing the density difference by means of the ideal gas equation:

$$\rho = \frac{p_{\text{ref}} M}{RT} \tag{3.8}$$

This method can model density variations in weakly compressible flows, meaning that the density of the fluid is dependent on temperature and composition but small pressure fluctuations have no influence.

3.3.2 Viscosity

Viscosity is an important fluid property that must be accurately represented in a CFD model, as it causes the resistance experienced by a fluid when flowing through any geometry. Viscosity is accurately quantified via the relationship between the shear stress in a fluid to the rate of deformation of the fluid.

Newtonian fluids are those that have a linear relationship between stress and rate of deformation, with the proportionality constant, which is actually viscosity. Any fluid that does not obey the Newtonian relationship between the shear stress and shear rate is called a non-Newtonian fluid. The shear stress in a Newtonian fluid is represented by the second term on the right-hand side of (3.1). Many food-processing media have non-Newtonian characteristics and the shear-thinning or shear-thickening behavior of these fluids greatly affects their thermal–hydraulic performance (Fernandes et al. 2006). In recent years, CFD has provided better understanding of the mixing, heating, cooling, and transport processes of non-Newtonian substances. Of the several constitutive formulas that describe the rheological behavior of substances, which include the Newtonian, power law, Bingham, and Herschel Bulkley models, the power law is the most commonly used model in food engineering applications (Welti-Chanes et al. 2005). However, there are some circumstances where modeling the viscosity can be avoided, as low velocities permit the non-Newtonian fluid to be considered Newtonian, for example, as shown by Abdul Ghani et al. (2001).

3.4 Modeling Particular Flow Regimes

3.4.1 Turbulent Flows

Turbulent flows are often encountered in the food industry owing to high flow rates and heat transfer interactions. Currently, even though the Navier–Stokes equations can be solved directly for laminar flows, it is not possible to solve the exact fluid motion in the Kolmogorov microscales associated with engineering flow regimes; thus turbulence requires modeling. For this reason, turbulence models are being developed yearly, with prediction accuracy undergoing great improvement over the last few years for a great many flow regimes. However, none of the existing turbulence models are complete; that is, their prediction performance is highly reliant on turbulent flow conditions and geometry. Without a complete turbulence

model capable of predicting the average field of all turbulent flows, the present understanding of turbulence phenomena will reduce the generality of solutions. In the following sections, some of the best performing turbulence models are discussed.

3.4.1.1 Large Eddy Simulations

Large eddy simulation (LES) forms a solution given the fact that large turbulent eddies are highly anisotropic and dependent on both the mean velocity gradients and geometry of the flow domain. This is done mathematically by separating the velocity field into a resolved and sub-grid part. The resolved part of the field represents the large eddies, while the sub-grid part of the velocity represents the small scales whose effect on the resolved field is included through the sub-grid scale model. With the advent of more powerful computers, LES offers an accurate means of computing turbulent flow. However, the lengthy time involved in arriving at a solution means that it is an expensive technique, and consequently, applications of LES for CFD calculations of food processing are still uncommon (Turnbull and Thompson 2005).

3.4.1.2 Reynolds Averaged Navier–Stokes

When variables are influenced by turbulence, engineers are generally content with a statistical probability that processing variables within the flow regime (e.g., velocity, temperature, and concentration) will lie within a certain range of values. Therefore, the predictions afforded by the Reynolds-averaged Navier–Stokes equations (RANS), which determine the effect of turbulence on the mean flow field through time averaging, are in many cases sufficient. By averaging in this way, the stochastic properties of turbulent flow are essentially ignored along with six additional stresses (Reynolds stresses) emerging, which need to be modeled by a physically well-posed equation system to obtain an accurate closure of the equation system. The following paragraphs describe the common techniques used.

Reynolds Stress Models

The Reynolds stress closure model (RSM) generally consists of transport equations for the Reynolds stresses – three transport equations for the turbulent fluxes of each scalar property and one transport equation for the dissipation rate of turbulence energy. RSMs have exhibited far superior predictions for flows in confined spaces where adverse pressure gradients occur. Terms accounting for anisotropic turbulence, which are included in the transport equations for the Reynolds stresses, means that these models provide a rigorous approach to solving complex engineering flows. However, storage and execution time can be expensive for three-dimensional flows. Moreover, convergence of the RSMs has been reported to be quite poor in the literature for many flow configurations.

Turbulent Viscosity Models

The turbulent viscosity hypothesis (Boussinesq relationship) states that an increase in turbulence can be represented by an increase in the effective fluid viscosity. The Reynolds stresses are proportional to the mean velocity gradients with the effective viscosity representing the proportionality constant (Ferziger and Peric 2002). For a k–ε type turbulence model turbulence viscosity can be represented as follows:

$$\mu_t = \rho C_\mu \frac{k^2}{\varepsilon} \tag{3.9}$$

For the k–ω type turbulence without the low Reynolds number modifications, the turbulence viscosity can be represented by (Wilcox 1993):

$$\mu_t = \rho \frac{k}{\omega} \tag{3.10}$$

This hypothesis forms the foundation for many of today's most widely used turbulence models, ranging from simple models based on empirical relationships to variants of the two-equation k–ε model, which describes turbulence viscosity through turbulence production and destruction (Versteeg and Malalsekeera 1995). All turbulence viscosity models have relative merit with respect to simulating food-processing operations.

The Standard k–ε Model

The standard k–ε model (Launder and Spalding 1974), which is based on the transport equations for the turbulent kinetic energy k and its dissipation rate ε, is semi-empirical and assumes isotropic turbulence. Although it has been successful in numerous applications and is still considered an industrial standard, the standard k–ε model is limited in some respects. A major weakness of this model is that it assumes an equilibrium condition for turbulence, that is, the turbulent energy generated by the large eddies is distributed equally throughout the energy spectrum. However, energy transfer in turbulent regimes is not automatic and a considerable length of time may exist between the production and the dissipation of turbulence.

The RNG k–ε Model

The renormalization group (RNG) k–ε model (Choundhury 1993) is similar in form to the standard k–ε model, but owing to the RNG methods from which it has been analytically derived, it includes additional terms for dissipation rate development and different constants from those in the standard k–ε model. As a result, the solution accuracy of highly strained flows has been significantly improved. The

calculation of the turbulent viscosity also takes into account the low Reynolds number if such a condition is encountered in a simulation. The effect of swirl on turbulence is included in the k–ε RNG model, thereby enhancing accuracy for recirculating flows.

The Realizable k–ε Model

In the realizable k–ε model (Shih et al. 1995) C_μ is expressed as a function of mean flow and turbulence properties, instead of being assumed constant, as in the case with the standard k–ε model. As a result, it satisfies certain mathematical constraints on the Reynolds stress tensor that are consistent with the physics of turbulent flows (e.g., normal Reynolds stress terms must always be positive). Also, a new model for the dissipation rate is used.

The k–ω Model

The k–ω model is based on modeled transport equations, which are solved for the turbulent kinetic energy k and the specific dissipation rate ω, that is, the dissipation rate per unit turbulent kinetic. An advantage that the k–ω model has over the k–ε model is that its performance is improved for boundary layers under adverse pressure gradients, as the model can be applied to the wall boundary, without using empirical log-law wall functions. A modification was then made to the linear constitutive equation of the k–ω model to account for the principal turbulence shear stress. This model is called the shear-stress transport (SST) k–ω model; it provides enhanced resolution of the boundary layer in viscous flows (Menter 1994).

3.4.2 Flows Containing Different Phases

Multicomponent flows occur where the species are mixed at molecular level, that is, they share the same pressure, velocity, and temperature fields. Alongside global mass continuity the transport equation for the species provides the means for updating the field of mass fractions, defining the mixture composition, via the following equation:

$$\frac{\partial eX_k}{\partial t} + \nabla \cdot (e\vec{v}_i X_k) = \nabla \cdot (D_k \nabla X_k) + S_k \tag{3.11}$$

However, as the relative size of the species becomes bigger there is deviation from the uniform flow field, and hence multiphase modeling must take over the multicomponent modeling. In multiphase flows more than one immiscible fluid is present in the flow. In CFD modeling, the term multiphase denotes a fluid system

that contains fluids of different physical properties, and does not necessarily refer to the state of matter, that is, whether it is solid, liquid, or gas. In multiphase systems, multiple fluids are mixed at a macroscopic level, where the mixing scale is larger than the molecular scale. In general, two-phase fluid systems are encountered in the food industry; however, the same concepts for their modeling apply to systems having many more phases. Multiphase flows can be broadly placed into the following categories:

1. Continuous; all the fluids involved in the flow are continuous such as liquid–liquid or liquid–gas flows where a free and distinct interface exists between fluids, for example, bubbly fluids or immiscible fluids.
2. Continuous–dispersed; namely, liquid–solid flows that contain a dispersed phase within a primary continuous phase, for example, particle-laden flows such as chunky soups, spray dryers, and fluidized beds.

In multiphase flows, each phase competes for the same volume, resulting in interactions between phases due to their proximity. Owing to the abrupt difference between the properties of the various phases, mass, momentum, and energy are exchanged between the phases. Such exchanges need to be accounted for in a CFD model, and in many cases these interactions are complex and specific to the type of flow being modeled.

Multiphase modeling has to provide models for tracking phases and/or predicting their distribution in space and time. Three approaches are generally used: the volume of fluid model (VOF), Eulerian–Eulerian model, and Lagrangian-Eulerian model, and are briefly discussed in the following sections.

3.4.2.1 Volume of Fluid Model

This simple multiphase model is well suited to simulate flows of immiscible fluids on numerical meshes that are capable of solving the interface between the mixture's phases. In other words, the VOF is a volume fraction tracking technique, which is highly effective when the shape of the interface between phases is important. Moreover, by using the VOF technique no additional modeling of interphase interactions is required, as all phases are assumed to share the same velocity, pressure, and temperature fields. The VOF model can calculate large-scale breakups and agglomerations such as sloshing effects caused by a moving water tank. If the breakup is too small to calculate, that is, during the formation of air bubbles in water or water droplets in air, then very high mesh refinement is required for accurate predictions.

3.4.2.2 Eulerian–Eulerian Model

Models simulating the distribution of phases via the Eulerian–Eulerian concept look at the presence and transport of phases in space, rather than tracking individual

particles of phases. In the Eulerian approach, the phases are treated as interacting and interpenetrating continua (Nijdam et al. 2006). The phases share the same volume, penetrate each other in space, and exchange mass, momentum, and energy with each other. Each phase is described by its distinctive physical properties and has its own velocity, pressure, concentration, and temperature field. Coupling of the phases is achieved through pressure and interphase exchange coefficients.

The Eulerian–Eulerian model is applicable for continuous–dispersed as well as continuous–continuous systems. For continuous–dispersed systems, the velocity of each phase is computed using the Navier–Stokes equations. The dispersed phase may be in the form of particles, drops, or bubbles. The forces acting on the dispersed phase are modeled using empirical correlations and included as part of the interphase transfer terms. Drag, lift, gravity, buoyancy, and virtual mass effects are some of the forces that may be acting on the dispersed phase. These forces are computed for an individual particle and then scaled by the local volume fraction to account for multiple particles.

3.4.2.3 Lagrangian–Eulerian Model

This model is applicable to modeling continuous–dispersed systems and is very often referred to as a discrete particle model or particle transport model. The primary phase is continuous, whereas the secondary phase is discrete and may be composed of particles, drops, or bubbles. The continuous phase flow is computed by solving the Navier–Stokes equations, and using their solutions in the flow trajectories, as well as the heat and mass transfer to and from the discrete phase, which is computed by solving the appropriate ordinary differential equations. The dispersed phase is represented by tracking a small number of representative particle streams; coupling between the continuous and discrete phases is achieved by including appropriate interaction terms in the equation set. Lagrangian–Eulerian modeling works best when the motion of particles is dominated by their interaction with the continuous phase rather than with each other, that is, when the dispersed phases are dilute. Moreover, this model is mainly applicable for low volume fractions of the dispersed phase, as the volume displacement caused by the discrete phase is not taken into account.

3.4.3 Modeling Flows through Porous Media

Many large-scale processes in the food industry may have the potential to be grid point demanding in CFD models owing to the complex geometry of the modeled structures. For example, to predict the detailed transfer processes within a cold store containing stacked foods one must mesh all associated geometry with a complex unstructured or body-fitted system, which is a highly arduous, and in many cases, inaccessible task. In any case, both computational power and CFD

algorithms have not yet reached such levels of maturity wherein these types of computations can be achieved. Therefore, other methods must be used to exploit the physical relationships that exist on a macroscopic level and sufficiently represent the dynamic flow effects representative of the modeled material. The porous media assumption relates the effects of particle size and shape, alignment with airflow, and void fraction to the pressure drop over the modeled products. This method basically applies Darcy's law to a porous media by relating the velocity drop through the pores to the pressure drop over the material. An extension of this law to account for most commonly encountered nonlinear relationships between pressure drop and velocity is represented by the Darcy–Forcheimer equation:

$$\frac{\partial p}{\partial x} = -\frac{\mu}{K}v + \rho C_2 v^2 \tag{3.12}$$

Equation (3.12) represents the most common relationship used to describe pressure drop across packed beds. In the CFD model this equation is added as an additional sink term to the momentum equation. The general relationships employed to determine both the permeability and inertial loss coefficient can be obtained by inference from the Ergun equation. However, considerable information regarding the detailed flow and transfer processes taking place within the stacked material is lost in this type of modeling strategy. Therefore, before modeling a porous media one must ensure that the parameters in the momentum source terms represent the physical media as closely as possible.

3.5 Numerical Methods Used by CFD Code Developers

CFD code developers have a choice of many different numerical techniques to discretize the transport equations. The most important of these include finite difference, finite elements, and finite volume. The finite difference technique is the oldest one used, and many examples of its application in the food industry exist. However, due to difficulties in coping with irregular geometry, finite difference is not commercially implemented. Furthermore, the current trend of commercial CFD coding is aimed toward developing unstructured meshing technology capable of handling the complex three-dimensional geometries encountered in industry. Therefore, the prospects of finite difference being used in industrial CFD applications seem limited.

Finite element methods have historically been used in structural analysis where the equilibrium of the solution must be satisfied at the node of each element. Nicolaï et al. (2001) provided a short introduction on using the finite elements method in conduction heat transfer modeling, but it will not be discussed here. It is sufficient to say that as a result of the weighting functions used in this method, obtaining a three-dimensional CFD solution with a large number of cells is impractical at

present. Therefore, finite elements are not generally used by commercial CFD developers, especially since many of these CFD codes are marketed toward solving aerodynamic problems. Nonetheless, finite elements methods have been used in the modeling of electromagnetic heating in microwave ovens (Verboven et al. 2007b); vacuum microwave drying (Ressing et al. 2007); radio frequency heating of food; and conduction and mass transport during drying (Aversa et al. 2007). Therefore, it would seem the finite elements method is amenable to the modeling of novel thermal processes if the details of fluid flow do not need explicit quantification.

With finite volume techniques the integral transport equations governing the physical process are expressed in conservation form (divergence of fluxes); the volume integrals are then converted to surface integrals using Gauss's divergence theorem. This is a direct extension of the control volume analysis that many engineers use in thermodynamics and heat transfer applications, etc., so it can be easily interpreted. Thus, expressing the equation system through finite volumes forms a physically intuitive method of achieving a systematic account of the changes in mass, momentum, and energy, as fluid crosses the boundaries of discrete spatial volumes within the computational domain. Also, finite volume techniques yield algebraic equations that promote solver robustness, adding further reasons to why many commercial developers implement this technique.

3.6 Applications of CFD in Food Industry

3.6.1 Sterilization

3.6.1.1 Canned Foods

Sterilization is a conventional thermal process that can be modeled with CFD. In this process rapid and uniform heating is desirable to achieve a predetermined level of sterility with minimum destruction in the color, texture, and nutrients of food products (Tattiyakul et al. 2001). Siriwattanayotin et al. (2006) used CFD to investigate sterilization value (F_0) calculation methods, and concluded that when F_0 was determined using the "Thermal Death Time" (TDT) approach, the process time to achieve the desired temperature in a sugar solution was underestimated if the surrounding temperature was lower than the reference value.

Canned viscous liquid foods such as soup, carboxyl-methyl cellulose (CMC), or corn starch undergoing sterilization have been simulated with CFD. In most cases where natural convection occurs, fluid velocities and shear rates are rather low and thus non-Newtonian fluids can be assumed as Newtonian (Abdul Ghani et al. 2003). Neglecting heat generation due to viscous dissipation is another assumption that is generally made. In such simulations, CFD has shown the transient nature of the slowest heated zone (SHZ), and has illustrated the large amount of time needed for

heat to be transferred throughout food, as well as the sharp heterogeneity in the temperature profile when the process is static.

CFD has also been used to study the effect of container shape on the efficiency of the sterilization process (Varma and Kannan 2005, 2006). Conical vessels pointing upward were found to reach appropriate sterilization temperature the quickest (Varma and Kannan 2005). Full cylindrical geometries performed best when sterilized in a horizontal position (Varma and Kannan 2006).

3.6.1.2 Pouched Foods

In recent years, CFD has provided a rigorous analysis of the sterilization of three-dimensional pouches containing liquid foods (Abdul Ghani et al. 2002; Abdul Ghani and Farid 2006). Coupling first-order bacteria and vitamin inactivation models with the fluid flow has allowed prediction of the transient temperature, velocity, and concentration profiles of both the bacteria and ascorbic acid during natural convection. The concentrations of bacteria and ascorbic acid after heat treatment of pouches filled with the liquid food were measured, and close agreement was found with the numerical predictions. The SHZ was found to migrate during sterilization until eventually resting in a position at a distance about 30% from the top of the pouch. As expected, the bacterial and ascorbic acid destruction was seen to depend on both the temperature distribution and flow pattern.

3.6.2 Pasteurization

CFD has been used to predict the transient temperature and velocity profiles during pasteurization of intact eggs (Denys et al. 2007). Owing to its ability to account for complex geometries, heterogeneous initial temperature distributions, transient boundary conditions, and nonlinear thermophysical properties, CFD has permitted a comprehensive understanding of this thermal process. Such analysis has allowed the gap in knowledge of this area to be filled, because up to recently little information was available on the correct processing temperatures and times for safe pasteurization, without loss of functional properties. In the series of studies published on this topic by Denys et al. (2007), a procedure to determine the surface heat transfer coefficient using CFD simulations of eggs filled with a conductive material of known thermal properties was first developed, after which conductive and convective heating processes in the egg were modeled (Denys et al. 2007). This revealed that, similar to the phenomena noted by Abdul Ghani et al. (1999) for canned foods, the cold spot moved during the process toward the bottom of the egg. The location of the cold zone in the yolk was predicted to lie below its geometrical center, even when the yolk was positioned at the top of the egg. It was concluded that no convective heating takes place in the egg yolk during processing.

3.6.3 Aseptic Processing

3.6.3.1 Plate Heat Exchangers for Milk Processing

In the dairy industry it is essential to heat-treat milk products in a continuous process, as on the one hand, it is necessary to promote microbial safety and increase the shelf life of milk. However, on the other hand, efficient plant processes are also desirable, but the adverse influences of heat on the sensory and nutritional properties of the final milk product act as a hindrance to efficient thermal processing.

Many CFD studies of PHEs exist, and have presented different techniques for geometry optimization, for example, corrugation shape or the optimization of other process parameters such as inlet and outlet positions and PHE–product temperature differences (Grijspeerdt et al. 2007; Jun and Puri 2005). Grijspeerdt et al. (2007) investigated the effect of large temperature differences between the product and PHE, and noted that the larger the difference, the greater is the opportunity for fouling. While fouling has been studied by the same group of authors, Jun and Puri (2005) were the first to couple a fouling model with a three-dimensional thermal–hydraulic model with CFD simulations. In this study, Jun and Puri investigated the influence of various PHE designs on fouling rates, comparing those typically used in the dairy industry with those used in the automobile industry.

3.6.3.2 Plate Heat Exchangers for Yoghurt Processing

Fernandes et al. (2005, 2006) studied the cooling of stirred yoghurt in PHEs with CFD simulations in order to investigate the thermal–hydraulic phenomena. They modeled the rheological behavior of yoghurt via a Herschel–Bulkley model. In addition to accounting for this rheological behavior, they also provided a high level of precision in the PHE geometrical design and the imposed boundary conditions. During the course of these studies, it was found that due to the higher Prandtl numbers and shear thinning effects of the yoghurt, the Nusselt numbers of the fully developed flows were more than ten times higher than those of water. This result presented a substantial thermal–hydraulic performance enhancement in comparison with that from Newtonian fluids. Furthermore, it was shown that PHEs with high corrugation angles may provide better opportunities for the gel structure breakdown desired during the production stage of stirred yoghurt.

3.6.4 Drying

3.6.4.1 Fluidized Beds

Because of the complex interactions that occur during fluidized bed drying, empirical correlations are only valid for a certain range of conditions, and CFD simulations have been the only means of providing accurate information on the flow

phenomena. However, similar to other drying applications, difficulties exist in modeling the interactions between the solid and liquid phases, as well as limitations in computing power, and consequently only a limited number of CFD simulations exist.

The Eulerian–Eulerian approach offers the most efficient way of representing the two phases in this type of system, considering the present level of computer power available and the large number of granules (grain) in a typical system; consequentially its use has been preferred over discrete methods by some researchers. Szafran and Kmiec (2004), via the multi-fluid granular kinetic model of Gidaspow et al. (1992) and the k–ε model, used this approach in their CFD simulations of the transport mechanisms in the spouted bed.

A major difficulty encountered in modeling spouted bed dryers has been the excessive computing times required to simulate only a fraction of the drying process. For example, owing to the small time steps required to resolve the instabilities in the flow regime, it would take a two-dimensional CFD simulation almost 1 year to simulate 1 h of drying (Szafran and Kmiec 2004). Thus, at present CFD can only be used as a tool that permits a deeper understanding of the flow patterns and their effects on the drying kinetics rather than for design and optimization.

3.6.4.2 Spray Drying

Spray drying is another traditional drying technique and is used to derive powders from products, with its main objective being to create a product that is easy to store, handle, and transport. CFD has been a necessary requisite for accurate spray dryer modeling, and has been employed for over 10 years now (Langrish and Fletcher 2003).

One of the big difficulties when using CFD software packages in spray dryer modeling is that owing to the presence of both solid and fluid, the mass transport limitations within a droplet cannot be easily taken into account, and therefore sub-models must be included to do so; for accurate solutions these must be used alongside many other sub-models that account for other phenomenological aspects (Straatsma et al. 2007). In a recent study by Straatsma et al. (2007), sub-models for mass transport, inter-particle collision, agglomeration, thermal reactions, and stickiness were implemented with an Lagrangian-Eulerian model of an industrial dryer. The CFD simulations allowed the authors (Straatsma et al. 2007) to assess the agglomeration size of the particles and the stickiness of the particles colliding with each other and the wall, and as a consequence allowed the fouling liability of the dryer to be evaluated.

3.6.4.3 Forced Convection Drying

Because of the complex geometry usually encountered in drying applications, theoretical studies are often not applicable; to obtain the spatial distribution of transfer coefficients with reasonable accuracy it is necessary to solve the

Navier–Stokes equations in the product surroundings. From the distribution of transfer coefficients the correct temperature and moisture profiles within the product can be predicted, so that the drying process can be optimized. Kaya et al. (2007) used this approach with CFD to determine the transfer coefficients; then the heat and mass transfer within the food was simulated with an external program. However, it is also possible to do this within the CFD package by determining the heat transfer coefficient, and the mass transfer with the Lewis relation, once a transient solution is performed.

3.6.5 Cooking

3.6.5.1 Natural Convection Ovens

Electric ovens are commonly used household appliances that rely on conjugate thermal exchange to produce the desired cooking effect in a foodstuff. For that reason, CFD is an appropriate tool to quantify the internal thermal field. A thorough investigation into the thermal profile of an electrical oven, operated under both broil and bake modes, was completed by Mistry et al. (2006). The solution first obtained from the steady-state analysis yielded a flow field, which opposed that evident from experimental observation. This was addressed by imposing an artificial, that is, a "numerical," vent suction pressure, the value of which was tweaked until thermal field predictions corresponded with experimental measurements. Full cycling times, employing intermittent ON/OFF operation of heaters, were also simulated for both the broil and bake cycles. From the comparison of predictions, the broil cycle was confirmed to be less efficient, with a notable heterogeneity in temperature profile, owing to temperature stratification; this underscored the fact that the main thermal exchange in this cycle was due to radiation.

3.6.5.2 Forced Convection Ovens

Application of CFD in jet impingement oven systems provides detailed understanding of the effect of different oven geometries as well as object geometries on the system performance. A full three-dimensional CFD model of a multiple jet impingement oven was developed by Kocer et al. (2007). Convection and conduction heat transfers were coupled. However, as the thermal exchange was a result of jet impingement only, radiation was ignored with a small compromise in accuracy. Moisture transfer was not considered. Kocer et al. (2007) then determined a correlation for the average Nusselt number in terms of Reynolds number for multiple jets impinging on the surface of a cylindrical model cookie, which indicated the strong dependence of surface heat transfer coefficient on velocity of the jet.

3.6.5.3 Baking Ovens

Recent CFD modeling studies of the bread-baking process have looked at the two-dimensional physical representation, coupling convection, and radiative heat transfer via the discrete ordinate (DO) model (Wong et al. 2007a). Moreover, the density, heat capacity, and thermal conductivity were allowed to vary with temperature. However, some discrepancies between predictions and measurements of the actual baking process were found, especially for those comparisons made at the dough center, which were probably caused by no modeling of the moisture transport in the dough and evaporation kinetics. Moreover, the confining effect afforded by the two-dimensional model was seen to cause lack of correspondence in the validation study.

3.7 Challenges in Use of CFD in the Food Industry

3.7.1 Improving the Efficiency of the Solution Process

Insight into the numerical abilities of CFD packages is important if one needs to solve the problems of excessive computing times. Taking the parallelization features of commercial CFD codes as an example, these can allow a solution to be formed quicker, via domain decomposition, as long as the computing power is available and Lagrangian particle tracking is not employed. Alongside this, the solving techniques employed in commercial CFD codes have also been found to play a major role in efficiency. Fletcher et al. (2006) noted how segregated solvers and coupled solvers can bring different attributes to solution progression, and found that owing to the reduced levels of "random noise" introduced, the coupled solver permitted a high level of control over the solution process, allowing efficient and accurate predictions of the transient evolution of the flow instability in a spray dryer, when compared to the segregated solver.

Simplifying the geometrical representation of CFD models can also cut down on both pre-processing and solving time. The two-dimensional modeling technique assumes that the length of a system is much greater than its other two dimensions, and that the process flow is normal up to this length. As the effects of the confining geometry are essentially disregarded, accurate judgment of whether the process is amenable to the two-dimensional assumption is required.

3.7.2 CFD to Control Food Processes

All processes in the food industry are performed under controlled conditions. Unfortunately, due to the nonlinearity of the transport phenomena, CFD techniques are not yet amenable to the online control of thermal processes; reduced order

models, which use statistical data to manipulate the process variables via controlled inputs, are more appropriate. However, this does not mean that the actions of a control system cannot be modeled by CFD. Wong et al. (2007b) were the first to implement a control system within a CFD model to simulate its performance. Such abilities undoubtedly provide benefits during the pre-design or optimization stages of system development.

3.7.3 Turbulence

One of the main issues facing the food industry over the last two decades is the fact that most turbulence models have been shown to be application-specific. At the present time, there are many turbulence models available; however, until a complete turbulence model capable of predicting the average field of all turbulent flows is developed the CFD optimization of many thermal processes will be hampered. The reason is that in every application many different turbulence models must be applied until the one that gives the best predictions is found. The closest to the complete turbulence model thus far is the LES, which uses the instantaneous Navier–Stokes equations to model large-scale eddies, with smaller scales solved with a sub-grid model. However, using the LES model demands large amounts of computer resources, which may not be presently achievable.

3.7.4 Need for Sensitivity Analysis

In CFD simulations, the boundary conditions must be adequately matched to the physical parameters of the process, with the precision of similarity being conditioned by the mechanism under study and the level of accuracy required. Even when this is done, the CFD solution still may not be a correct physical representation of the physical system. This was shown by Mistry et al. (2006), who found that an artificial pressure differential was required to predict the correct flow patterns in an oven heated by natural convection. Such results suggest the importance of sensitivity analysis studies alongside experimental measurements in the early stages of model development. Sensitivity analyses are also necessary for turbulence model specification, or turbulence model tuning via inlet conditions, and for CFD model simplification.

3.8 Conclusions

CFD has played an active part in the design of food operation processes for over a decade now. In recent years simulations have reached higher levels of sophistication, as application-specific models can be incorporated into the software with ease

via user-defined files. The importance of maintaining a high level of accuracy via circumspect choices made during model development is evident from the reviewed studies, as many of these studies provide detailed validation exercises. Undoubtedly, with current computing power progressing unrelentingly, it is conceivable that CFD will continue to provide explanations for transport phenomena, leading to better design of processes in the food industry.

3.9 Nomenclature

C_μ	Empirical turbulence model constant
c_p	Specific heat capacity (W kg^{-1} K^{-1})
D	Diffusion coefficient
E	Mole fraction
g	Acceleration due to gravity (m s^{-2})
K	von Karman constant
M	Molecular weight (kg $kmol^{-1}$)
Nu	Nusselt number
p	Pressure (Pa)
R	Gas constant (J $kmol^{-1}$ K^{-1})
Re	Reynolds number
K	Turbulent kinetic energy (m^2 s^{-2})
s_T	Thermal sink or source (W m^{-3})
s_c	Concentration sink or source (mol m^{-3})
T	Temperature (K)
Tu	Turbulence intensity (%)
t	Time (s)
U	Velocity component (m s^{-1})
$\vec{v_i}$	Velocity component (m s^{-1})
x	Cartesian coordinates (m)
X_k	Volume fraction of k

3.9.1 Greek Letters

ρ	Density (kg m^{-3})
μ	Dynamic viscosity (kg m^{-1} s^{-1})
β	Thermal expansion coefficient (K^{-1})
λ	Thermal conductivity (W m^{-1} K^{-1})
ε	Turbulent dissipation rate (m^2 s^{-3})
φ	Transported quantity
Γ	Diffusion coefficient of transported variable

ϑ Diffusivity of the mass component in the fluid ($m^2\ s^{-1}$)
ω Specific dissipation (s^{-1})
μ_t Turbulent viscosity (kg $m^{-1}\ s^{-1}$)

3.9.2 Subscripts

i Cartesian coordinate index
bf Bulk fluid
s Surface
V Mesh element volume
A Area of mesh element
m Mean
t Turbulent
k *k*th phase

References

Abdul Ghani AG, Farid MM (2006) Using the computational fluid dynamics to analyze the thermal sterilization of solid–liquid food mixture in cans. Innovative Food Science & Emerging Technologies 7(1–2):55–61

Abdul Ghani AG, Farid MM, Chen XD (2002) Theoretical and experimental investigation of the thermal inactivation of *Bacillus stearothermophilus* in food pouches. J Food Eng 51(3):221–228

Abdul Ghani AG, Farid MM, Chen XD, Richards P (1999) An investigation of deactivation of bacteria in a canned liquid food during sterilization using computational fluid dynamics (CFD). J Food Eng 42:207–214

Abdul Ghani AG, Farid MM, Chen XD, Richards P (2001) Thermal sterilization of canned food in a 3-D pouch using computational fluid dynamics. J Food Eng 48:147–156

Abdul Ghani AG, Farid MM, Zarrouk SJ (2003) The effect of can rotation on sterilization of liquid food using computational fluid dynamics. J Food Eng 57:9–16

Aversa M, Curcio S, Calabro V, Iorio G (2007) An analysis of the transport phenomena occurring during food drying process. J Food Eng 78(3):922–932

Choundhury D (1993) Introduction to the renormalization group method and turbulence modelling. Fluent Inc. Technical Memorandum TM-107

Denys S, Pieters J, Dewettinck K (2007) CFD analysis of thermal processing of eggs, chapter 14. In: Da-Wen Sun (ed) Computational fluid dynamics in food processing. CRC Press, Boca Raton, FL, pp 347–381

Fernandes CS, Dias R, Nóbrega JM, Afonso IM, Melo LF, Maia JM (2005) Simulation of stirred yoghurt processing in plate heat exchangers. J Food Eng 69:281–290

Fernandes CS, Dias RP, Nobrega JM, Afonso IM, Melo LF, Maia JM (2006) Thermal behaviour of stirred yoghurt during cooling in plate heat exchangers. J Food Eng 69:281–290

Ferziger JH, Peric M (2002) Computational methods for fluid dynamics. Springer-Verlag, Berlin/Heidleberg, pp 1–100

Fletcher DF, Guo B, Harvie DJE, Langrish TAG, Nijdam JJ, Williams J (2006) What is important in the simulation of spray dryer performance and how do current CFD models perform? Appl Math Model 30(11):1281–1292

Foster AM, Madge M, Evans JA (2005) The use of CFD to improve the performance of a chilled multideck retail display cabinet. Int J Refrig 28:698–705

Gidaspow D, Bezburuah R, Ding J (1992) Hydrodynamics of circulating fluidized beds, kinetic theory approach. Fluidization VII, Proceedings of the 7th Engineering foundation conference on fluidization, Brisbane, Australia, pp 75–82

Grijspeerdt K, Vucinic D, Lacor C (2007) CFD modelling of the hydrodynamics of plate heat exchangers for milk processing, chapter 19. In: Da-Wen Sun (ed) Computational fluid dynamics in food processing. CRC Press, Boca Raton, FL, pp 403–417

Jun S, Puri VM (2005) 3D milk-fouling model of plate heat exchangers using computational fluid dynamics. Int J Dairy Technol 58(4):214–224

Jun S, Puri VM (2006) A 2D dynamic model for fouling performance of plate heat exchangers. J Food Eng 75(3):364–374

Kaya A, Aydin O, Dincer I (2007) Numerical modeling of forced-convection drying of cylindrical moist objects. Numer Heat Transf A-Appl 51(9):843–854

Kocer D, Nitin N, Karwe MV (2007) Applications of CFD in Jet impingement oven, chapter 19. In: Da-Wen Sun (ed) Computational fluid dynamics in food processing. CRC Press, Boca Raton, FL, pp 469–487

Langrish TAG, Fletcher DF (2003) Prospects for the modelling and design of spray dryers in the 21st century. Drying Technol 21(2):197–215

Launder BE, Spalding DB (1974) The numerical computation of turbulent flows. Comput Meth Appl Mech Eng 3:269–289

Lian G (2007) CFD simulation of multi-physical multi-(bio) chemical interactions of tea fermentation and infusion, chapter 24. In: Da-Wen Sun (ed) Computational fluid dynamics in food processing. CRC Press, Boca Raton, FL, pp 478–505

Menter FR (1994) Two-equation eddy-viscosity turbulence models for engineering applications. AIAA J 32(8):1598–1604

Mistry H, Ganapathi-subbu, Dey S, Bishnoi P, Castillo JL (2006) Modeling of transient natural convection heat transfer in electric ovens. Appl Therm Eng 26(17–18):2448–2456

Nicolaï BM, Verboven P, Scheerlinck N (2001) Modelling and simulation of thermal processes, Chapter 6. In: Philip Richardson (ed) Thermal technologies in food processing. Woodhead Publishing, Cambridge/England, pp 91–109

Nijdam JJ, Guo BY, Fletcher DF, Langrish TAG (2006) Lagrangian and Eulerian models for simulating turbulent dispersion and coalescence of droplets within a spray. Appl Math Model 30(11):1196–1211

Norton T, Sun D-W (2007) An overview of CFD applications in the food industry, chapter 1. In: Da-Wen Sun (ed) Computational fluid dynamics in food processing. CRC Press, Boca Raton, FL, pp 1–43

Olsson E, Trägårdh C (2007) CFD modelling of jet impingement during heating and cooling of foods, chapter 20. In: Da-Wen Sun (ed) Computational fluid dynamics in food processing. CRC Press, Boca Raton, FL, pp 478–505

Ressing H, Ressing M, Durance T (2007) Modelling the mechanisms of dough puffing during vacuum microwave drying using the finite element method. J Food Eng 82(4):498–508

Shih TH, Liou WW, Shabbir A, Zhu J (1995) A new k–ε eddy viscosity model for high Reynolds number turbulent flows—model development and validation. Comput Fluids 24(3):227–238

Siriwattanayotin S, Yoovidhya T, Meepadung T, Ruenglertpanyakul W (2006) Simulation of sterilization of canned liquid food using sucrose degradation as an indicator. J Food Eng 73:307–312

Straatsma J, Verdurmen REM, Verscheuren M, Gunsing M, de Jong P (2007) CFD simulation of spray drying of food products, Chapter 10. In: Da-Wen Sun (ed) Computational fluid dynamics in food processing. CRC Press, Boca Raton, FL, pp 249–287

Sun D-W (ed) (2007) Computational fluid dynamics in food processing. CRC Press, Boca Raton, FL

Szafran RG, Kmiec A (2004) CFD modeling of heat and mass transfer in a spouted bed dryer. Ind Eng Chem Res 43(4):1113–1124

Tattiyakul J, Rao MA, Datta AK (2001) Simulation of heat transfer to a canned corn starch dispersion subjected to axial rotation. Chem Eng Process 40:391–399
Turnbull J, Thompson CP (2005) Transient averaging to combine large eddy simulation with Reynolds averaged Navier-Stokes simulations. Comput Chem Eng 29:379–392
Varma MN, Kannan A (2005) Enhanced food sterilization through inclination of the container walls and geometry modifications. Int J Heat Mass Transfer 48:3753–3762
Varma MN, Kannan A (2006) CFD studies on natural convective heating of canned food in conical and cylindrical containers. J Food Eng 77(4):1027–1036
Verboven P, Atalay YT, Vermeir SE, Nicolaï BM, Lammertyn J (2007a) CFD design and optimization of biosensors for the food industry, chapter 26. In: Da-Wen Sun (ed) Computational fluid dynamics in food processing. CRC Press, Boca Raton, FL, pp 478–505
Verboven P, de Baerdemaeker J, Nicolaï BM (2004) Using computational fluid dynamics to optimise thermal processes, chapter 4. In: Philip Richardson (ed) Improving the thermal processing of foods. Woodhead Publishing, Cambridge/England, pp 82–102
Verboven P, Datta AK, Nicolaï BM (2007b) Computation of airflow effects in microwave and combination heating, Chapter 12. In: Da-Wen Sun (ed) Computational fluid dynamics in food processing. CRC Press, Boca Raton, FL, pp 313–331
Versteeg HK, Malalsekeera W (1995) An introduction to computational fluid dynamics. Longman, Harlow, UK, pp 1–100
Welti-Chanes J, Vergara-Balderas F, Bermúdez-Aguirre D (2005) Transport phenomena in food engineering: basic concepts and advances. J Food Eng 67:113–128
Wilcox DC (1993) Comparison of 2-equation turbulence models for boundary-layer flows with pressure gradient. AIAA J 31(8):1414–1421
Wong SY, Zhou WB, Hua JS (2007a) CFD modeling of an industrial continuous bread-baking process involving U-movement. J Food Eng 78(3):888–896
Wong SY, Zhou WB, Hua JS (2007b) Designing process controller for a continuous bread baking process based on CFD modelling. J Food Eng 81(3):523–534
Xia B, Sun D-W (2002) Applications of computational fluid dynamics (CFD) in the food industry: a review. Comput Electron Agric 34:5–24
Zhou W, Therdthai N (2007) Three-dimensional CFD modelling of a continuous baking process, chapter 11. In: Da-Wen Sun (ed) Computational fluid dynamics in food processing. CRC Press, Boca Raton, FL, pp 287–213

Chapter 4
Incorporation of Fibers in Foods: A Food Engineering Challenge

Madhuvanti Kale, Dhananjay Pai, Bruce Hamaker, and Osvaldo Campanella

4.1 Introduction

Dietary fiber is an essential part of the human diet. It performs several functions in the body, such as water binding, cholesterol and fat binding, attenuation of blood glucose levels, preventing constipation, and facilitating good colonic health. However, dietary fiber often plays a poor functional role in processed foods, impairing processing operations and greatly compromising the sensory quality of the food. As a result, processed foods are typically made from ingredients having low fiber content, such as refined flours. Diets that predominantly consist of such processed foods are therefore seriously lacking in this valuable nutritional constituent. The alarming growth in the prevalence of diseases such as obesity, coronary heart disease, diverticular disease, and colorectal cancer has been associated at least in part with low fiber intake. This conclusion calls for urgent action by the food industry to produce fiber-enriched processed foods that will be a good source of fiber, while at the same time being acceptable to the consumer.

The importance of dietary fiber and potential fiber sources as well as food vehicles for fortification will be briefly discussed in this chapter. Emphasis will be given to corn bran as a fiber source, as it is a cheap and abundant by-product of the corn milling industry. The food processing and product quality problems associated with the addition of corn bran in convenience foods such as extruded breakfast cereals and snacks will be discussed, with some strategies for fiber modification to overcome these problems. In addition, some analytical techniques

M. Kale and B. Hamaker,
Department of Food Science, Purdue University, West Lafayette, IN, USA
and
Whistler Center for Carbohydrate Research, Purdue University, West Lafayette, IN, USA

D. Pai and O. Campanella (✉)
Whistler Center for Carbohydrate Research, Purdue University, West Lafayette, IN, USA
and
Agricultural and Biological Engineering Department, Purdue University, West Lafayette, IN, USA
e-mail: campa@purdue.edu.

J.M. Aguilera et al. (eds.), *Food Engineering Interfaces*, Food Engineering Series,
DOI 10.1007/978-1-4419-7475-4_4,

to assess fiber functionality will be described. Finally, a process dealing with alkali treatment of corn bran to improve fiber functionality during extrusion processing will be presented as a case for fiber incorporation in extruded foods. The rheological behavior of fiber-enriched foods and its role in the extrusion process will also be discussed.

4.1.1 Dietary Fiber

Dietary fiber typically refers to those carbohydrates from plant foods that are not digested by enzymes in the small intestine, including non-starch polysaccharides and lignin (USDA 2005), and also resistant starch. Dietary fiber can be soluble or insoluble. Soluble fiber typically undergoes fermentation by colonic microorganisms, whereas insoluble dietary fiber passes through the body largely unchanged. Incorporation of insoluble fiber at high levels into processed foods often causes problems due to poor functional properties, such as severe reduction of expansion in extruded foods (Breen et al. 1977; Mottur and Glass 1985; Hseih et al. 1989, 1991; Lue et al. 1991; Onwulata et al. 2001; Moraru and Kokini 2003). Soluble fiber, on the other hand, tends to compromise the sensory quality of the food, and may hamper functionality as well (Colliopoulos 1991; Ringe and Stoll 1991; Foehse et al. 1992; van Lengerich and Larson 2000).

4.1.2 Importance of Dietary Fiber

The Food and Nutrition Board of the Institute of Medicine (National Academy of Sciences 2002) has set recommendations for fiber intake at 38 and 25 g/day (14 g/1,000 kcal) for men and women, respectively. These levels are based on the minimum intake required to reduce the risk of coronary heart disease and colon cancer, prevent constipation and diverticular disease, provide energy for colonic bacteria, attenuate blood glucose and lipid levels, and provide foods that may contribute to satiety. On average, people consume about one half of these recommended levels. Thus, there is an obvious need to increase dietary fiber consumption among the general public. One way to achieve this goal is through fiber incorporation in commonly consumed foods, for instance, breakfast cereals, ready-to-eat (RTE) puffed snacks, yogurt, and baked products.

4.1.3 Sources of Fiber

Most plant foods contain some amount of dietary fiber. However, much of this fiber is removed during processing and pre-processing operations. A common example

of pre-processing is the refining of cereal flour to remove bran, which improves the functionality of the flour, while producing a fiber-rich by-product which can be a potentially valuable source of fiber for fortification. There are other soluble fiber sources, such as psyllium and inulin, which in fact show good processing functionality in extruded foods because they do not reduce their expansion (Foehse et al. 1992). However, their significantly higher cost and tendency to dissolve rapidly in water, saliva, or milk and to produce gummy or slimy texture limit the level at which they can actually be utilized in these products.

Cereal brans represent a valuable class of by-products of the milling industry that can serve as a source of dietary fiber. Many countries are major producers and processors of corn and, consequently, corn bran is one of the most abundant and cheap resources for fiber fortification. Therefore, the focus of this chapter will be on corn bran as a source of fiber. The discussion will apply, in the most part, to other fiber sources as well.

4.1.4 Fortification of Foods with Fiber

The level of added fiber and the amount of fiber per serving are technologically and nutritionally significant quantities to be decided by the food manufacturer. From a practical standpoint, the level of addition is dictated by the occurrence and extent of processing difficulties and the effect of the fiber on the sensory qualities of fiber-enriched products, while the amount of fiber per serving decides the kind of labeling declaration that can be made, more specifically if it can be labeled as a "good," "very good," or "excellent" source of dietary fiber.

Several foods can be considered as candidates for fortification with fiber, the notable categories being extruded foods, baked foods, beverages, and dairy products such as yogurts; the latest reports even suggest the development of high-fiber drinks (Decker 2007). This chapter focuses on fiber processing and fiber functionality enhancement for extrusion processing, as incorporation of high levels of fiber is arguably most challenging in extruded foods.

4.2 Processing and Chemical Evaluation of Fiber-Enriched Foods and Corn Fibers

4.2.1 Extrusion Processing

Extrusion is a processing tool that can be used to incorporate fibers in highly consumed foods like breakfast cereals and snacks. Extrusion technology has had an important role in the food industry development as it is an efficient and cost-effective manufacturing process. In a way, it can be considered as a process

intensification tool, a term used to categorize processes that result in better products and processes that are safer, cleaner, smaller, and cheaper. Extrusion cooking technologies are used for cereal and protein processing in the food, pet food, and feed sectors. Raw material properties are critical in determining the magnitude of variables used in the process such as pressure, temperature, moisture, feed, as well as providing structure to the final product (Guy 2001). The most commonly used materials are corn and wheat flours or meals. Other starch sources such as rice, potato, rye, and barley flours are also used for extrusion purposes, as well as globular proteins such as those present in soybean, which provide structure to the food product when used at high concentrations larger than 40% (Guy 2001; Moraru and Kokini 2003). While proteins denature at the high temperature existing in the extruders, fibers were reported to be unaffected by the heat and shear applied during extrusion processing (Guy 2001).

Moraru and Kokini (2003) have extensively described the mechanism of extrudate expansion. During expansion, there is a rapid decrease in the moisture and temperature of the product, which causes a dramatic change in the extrudate rheology and transport properties (Fan et al. 1994). Several researchers (Lai and Kokini 1990; Kokini et al. 1992; Fan et al. 1994; Della Valle et al. 1996, Li et al. 2004) have hypothesized that the rheological properties of the polymeric matrix just before exiting the extruder (known as melt) have an important role in expansion, since they determine the resistance to the growth of the air bubbles due to the pressure difference between the inside and the outside of the bubble.

Both raw material properties and operating parameters affect the rheological properties of the melt, and have a large influence on the product expansion. The film of biopolymers surrounding the bubbles must flow easily in the bubble walls to allow the bubbles to expand, as the superheated water is released very quickly at atmospheric pressure once the product exits the extruder die. The resistance to this flow is governed by the shear viscosity. Expansion seems to be favored at certain optimum shear viscosities depending on the material, since it has been observed that excessively high or low viscosities impede expansion (Fan et al. 1994; Della Valle et al. 1996; Li et al. 2004; Moraru and Kokini 2003; Kokini et al. 1992). Melt shear viscosity is affected by biopolymer structure, die dimensions (L/D), screw speed, temperature, and moisture. Concerning the biomolecular structure, several researchers have reported differences in extrusion expansion and melt rheology due to differences in amylose/amylopectin content (Guy 2001; Chinnaswamy and Hanna 1988; Della Valle et al. 1996; Kokini et al. 1992; Lai and Kokini 1990; Li et al. 2004).

The mechanism of the expansion process can be described as consisting of several stages starting from a nucleation stage, which generates a two phase structure, where tiny gas bubbles are surrounded by polymeric films (bubble wall). As bubbles grow, these films are stretched to a point where they are no longer able to withstand the stretching forces (Gendron and Daigneault 2000; Guy 2001). When the film becomes thin, shear effects become less important and the deformation flow of relevance is that of an extensional flow. Consequently, extensional properties of the melt, which measure the resistance of the film to the

stretching deformation, become the control for the extent of bubble growth. Even though the relevance of extensional properties and biaxial stretching have been recognized as one of the main modes of deformation in food extrusion (foam extrusion), few rheological studies using this type of flow have been performed, mainly due to the difficulty of finding reliable techniques to measure biaxial extensional properties of extruded melts.

One aspect that has been investigated in the area of plastic extrusion, but not in foods, is the effect of the material molecular structure on expansion and extensional properties of the melt. For plastics it has been recognized that extensional properties of the melt are very sensitive to macromolecular structural differences (Hingmann and Marczinke 1994; Gendron and Daigneault 2000). In this sense, structural aspects of food polysaccharides and their potential effects on melt rheology are discussed in this chapter.

4.2.2 Challenges in Corn Fiber Processing

It has been reported that the presence of a high proportion of fiber in product formulation results in the reduction of expansion during extrusion, which in turn yields products that are dense, tough, and non-crispy (Lue et al. 1991). Mendonca et al. (2000) reported that co-extrusion of corn bran and cornmeal resulted in less radial expansion and products with undesirable textural characteristics when the amount of corn bran was increased. Garber et al. (1997) investigated the influence of corn bran particle size on extrusion expansion and found that radial expansion decreased with increasing particle size, producing very hard extrudates of poor textural properties.

Moraru and Kokini (2003) hypothesized that above a critical concentration, fibers may disrupt the continuous structure of the melt, thus impeding its elastic deformation during expansion. Since fibers are not much affected by the harsh environment existing inside the extruder and largely retain their macrostructure (Guy 2001), their physical presence in the extrudate bubble walls will tend to reduce the expansion because they disrupt the bubble wall film when their structures penetrate it. In addition, it has been hypothesized that, even at small concentrations, the structural anisotropy caused by the aligning of long and stiff fiber molecules in the extruder flow direction increases the extensional viscosity of the melt film, thus lowering the radial expansion of the product.

4.2.3 Chemistry of Corn Fiber

Corn bran, like any other food material, is a complex system. It consists of thick-walled cells of pericarp, germ and aleurone layer, and a residual endosperm tissue of the corn kernel (Saulnier et al. 1995). Corn bran contains about 80–90% dietary

fiber (Shelton and Lee 2000). The major polysaccharides present in cereal brans are cellulose and hemicelluloses. Cellulose is a polymer made of β (1 → 4)-linked glucose units. Hemicelluloses are classically defined as polysaccharides that are extractable from higher plants by aqueous alkaline solutions (Schulze 1891). It is now known that there are at least four major types of hemicelluloses, namely xylans, mannans, mixed linkage glucans, and xyloglucans (Ebringerova et al. 2005). In addition to cellulose and heteroxylans, primary cell walls of cereals consist of certain β-D-glucans, xyloglucans, aromatic substances (such as phenolic acids), and structural proteins are also present (Saulnier et al. 1995; Carpita 1996). The major heteroxylans in cereals are arabinoxylans, with some amount of glucuronic acid present. Corn bran arabinoxylans, for instance, comprise about 60% of total bran weight and contain some glucuronic acid and trace amounts of D- and L-galactose that are extracted from crude corn fiber under alkaline conditions. Wheat bran contains approximately 45% total dietary fiber that is composed of 44% hemicellulose, 32% cellulose, 5% lignin, and 4% insoluble pectins (Claye et al. 1996). Saulnier and Thibault (1999) suggested, based on their studies on corn bran, that the corn cell wall is a three-dimensional network of cellulose bundles embedded in a network of highly cross-linked arabinoxylans (Fig. 4.1).

Arabinoxylans are composed of a β (1 → 4)-linked xylan backbone, with arabinosyl residues attached as short branches. Some of the arabinosyl residues are esterified with ferulic acid, which is a phenolic acid (Doner and Hicks 1997). Figure 4.2a shows a schematic structure of a feruloylated arabinoxylan. Cross-linking of arabinoxylan chains through diferulic acid bridges has been identified (Saulnier et al. 1995). This is shown in the schematic Fig. 4.1, and in closer detail in Fig. 4.2b. Each corn bran heteroxylan contains about 75 ferulic acid esters and is connected by about 30 diferulic cross-links (Saulnier and Thibault 1999).

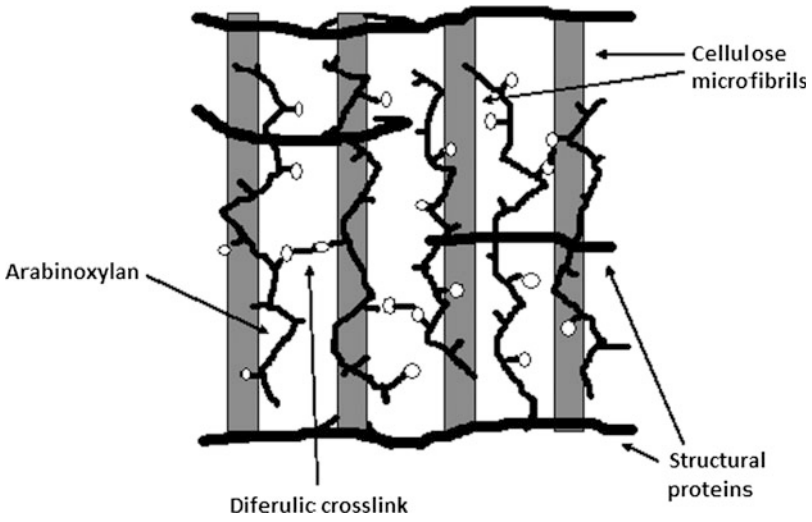

Fig. 4.1 Schematic of cereal cell wall structure (Adapted from Saulnier and Thibault 1999)

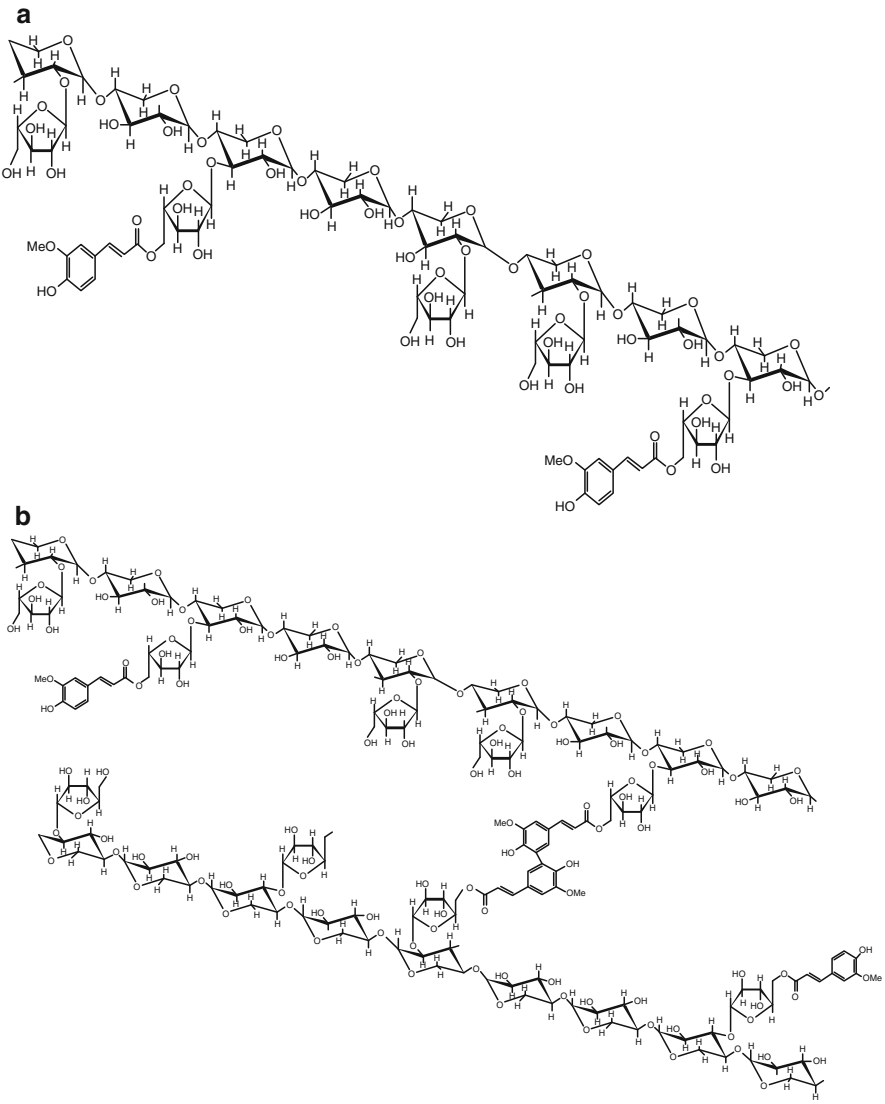

Fig. 4.2 (**a**) Schematic of feruloylated arabinoxylan molecule. (**b**) Schematic of two arabinoxylan chains cross-linked by diferulate bridges

The presence of these diferulic bridges and the cross-linking of arabinoxylan chains severely impair the functionality of corn fiber. Also, the presence of crystalline cellulose microfibrils greatly compromises functionality. Thus, strategies for improving the functionality of bran should be essentially aimed at breaking apart this network of cross-links to aid the dispersion of the fiber material in the food system. Some strategies for modification of fibers to be able to incorporate them in large quantities into processed foods are discussed below.

4.2.4 Strategies for Modification of Corn Fiber

Fiber modification strategies generally fall into three categories: chemical, physical, and enzymatic. The ultimate aim of all of these methods is to alter the molecular and/or supramolecular structure of the fiber so that its functionality can be improved.

4.2.4.1 Chemical Modification

The chemical modifications of interest here are those intended to increase functionality through the selective breakage of ferulic acid cross-links, as well as other hydrolysis reactions to reduce molecular size. Ferulic acid cross-link removal and other main chain hydrolysis effects are achieved by the addition of either an acid or a base. This aids in the dispersal of bran polysaccharides, can decrease polymer chain length, and may open up junction zones to increase water-binding sites and solubility. These treatments additionally allow for greater functionality because they loosen the tightly packed fiber polymeric chains. Treatment with hydrogen peroxide has also been used to remove lignin (Gelroth and Ranhotra 2001) and to bleach the undesirable brown color (Doner and Johnston 2001).

4.2.4.2 Physical Modification

Physical treatments involve high shear, high temperature, extrusion, and corn bran grinding. Particle size reduction has been studied as a possible method for fiber incorporation into an extruded corn-based product (Blake 2006). However, it was found that in the range studied, particle size does not have much effect on the properties of the extrudate, notably expansion.

High shear may decrease polymer chain length and increases the ability of a fiber to associate with other food components. Shear has been used to create a patented dietary fiber (Z-Trim^{TM}) in USDA laboratories that is used as fat mimetics. On the other hand, high temperature processing results in swelling of the cell wall material and improvement in solubilization of hemicellulose and insoluble pectins (Ng et al. 1999).

The use of extrusion as a processing tool for physical pretreatment offers advantages involving a combination of both shear and high temperature, which results in dispersion of the dietary fiber produced by the depolymerization and disruption of its crystalline structure within the cell wall (Ning et al. 1991; Ralet et al. 1993).

4.2.4.3 Enzymatic Modification

A review on enzymatic modification of dietary fibers (Arrigoni 2001) describes two approaches to dietary fiber modification by enzymatic means. The first is to increase

dietary fiber content in a food by removing digestible compounds; the second is to use enzymes to alter the fiber fraction itself. The second approach, which is more pertinent to fiber fortification of foods, is aimed at the modification of the fiber. This approach requires a mixture of cellulose, hemicellulose, and pectinases. Enzymes can also be used to modify purified fiber fractions, such as to hydrolyze polysaccharides in order reduce molecular weight and possibly improve functionality.

4.3 Techniques to Assess Fiber Chemistry and Fiber-Enriched Foods

4.3.1 Rheological Characterization

The rheological properties of fiber directly affect its behavior in a processing system. This brief discussion focuses on the assessment of these rheological properties, using instruments that may either simulate the actual processing conditions or measure properties that will affect flow behavior during processing.

4.3.1.1 Solution Rheology

Polysaccharides produce solutions of high viscosity at low concentrations. The viscosity can be measured using a rotational rheometer. These data may provide qualitative information about the molecular weight and branching of the fiber molecules.

4.3.1.2 Capillary Rheometry

A capillary rheometer is a pressure-driven rheometer. Gravity, compressed gas, or a motor-driven piston can be used to generate pressure on the test fluid in a reservoir (Macosko 1994). The fluid flows through a capillary die of radius R and length L. Pressure drop and flow rate through this die are used to determine apparent viscosity of the fluid (Malkin and Isayev 2006; Macosko 1994).

Irrespective of the type of fluid, for a cylindrical capillary, the wall shear stress is given by

$$\sigma_w = \frac{\Delta P R}{2L} \tag{4.1}$$

where ΔP is the pressure causing the flow, and R and L are the radius and length of the capillary die, respectively. Foods undergoing extrusion are generally

biopolymers that exhibit non-Newtonian behavior. The wall shear rate in a cylindrical capillary is calculated by Malkin and Isayev (2006) as

$$\dot{\gamma}_w = \dot{\gamma}_0 \left[3 + \frac{d\log\dot{\gamma}_0}{d\log\sigma_w}\right] \tag{4.2}$$

The bracketed term in the above equation is the correction for non-Newtonian fluid and $\dot{\gamma}_0$ is the average shear rate in the capillary, and is given by

$$\dot{\gamma}_0 = \frac{Q}{\pi R^3} \tag{4.3}$$

where Q is the flow rate through the capillary. The flow curves obtained from the test can be used to measure the apparent viscosities at different shear rates and thus calculate the rheological parameters (i.e., power law) of non-Newtonian fluids.

The advantages in using a capillary rheometer is that it is relatively inexpensive to build and simple to operate. For viscous polymeric melts, capillary rheometry appears to be one of the few satisfactory means of obtaining data at shear rates greater than 10 s^{-1} (Macosko 1994). Capillary rheometers can also reduce solvent evaporation more efficiently than rotational geometry instruments, which have larger exposed free surfaces. These instruments are also one of the simplest extrusions and die flow simulators (Macosko 1994). The disadvantages are that a large amount of sample is needed for the test and the instrument can measure only steady shear properties. The reader is encouraged to refer to Malkin and Isayev (2006) and Macosko (1994) for details on working principles and different tests that can be conducted using capillary rheometry.

4.3.1.3 Lubricated Squeezing Flow

Entrance pressure drop measured from the flow into a converging die has been used to evaluate the extensional viscosity of cornmeal dough (Bhattacharya et al. 1994; Padmanabhan and Bhattacharya 1993; Seethamraju and Bhattacharya 1994). Although this may be the best method for approximating extrusion conditions, the amount of sample needed for each trial is very high.

The lubricated squeezing flow technique is a simple method to measure extensional viscosity of dough-like samples. The material whose extensional viscosity is to be measured is placed between two lubricated plates and compressed at either a constant velocity or a constant strain rate. The squeezing force is used to calculate the extensional viscosity. If the sample fills the plates completely, i.e., sample and plate radius is the same during the test, then the method is known as the constant area method. If the sample radius is less than the plate radius, it is called constant volume method.

Extensional strain is calculated using the following equation:

$$\varepsilon = \frac{1}{2}\left(\frac{V}{H(t)}\right)t \tag{4.4}$$

For the constant area method and constant crosshead velocity, the extensional viscosity in lubricated squeezing flow is given by the following equation (Campanella and Peleg 2002):

$$\mu_b = \frac{2F(t)H(t)}{\pi R^2 V} \tag{4.5}$$

where μ_b is the extensional viscosity, $F(t)$ is the force at time t after commencement of the experiment, $H(t)$ is the momentary sample height, R is the radius of the sample, which is the same as the radius of the plate (constant area method), and V is the crosshead velocity or velocity of deformation.

At a constant strain rate $\dot{\varepsilon}$, extensional viscosity is given by

$$\mu_b = \frac{2F(t)}{\pi R^2 \dot{\varepsilon}} \tag{4.6}$$

Apart from the simplicity, this method offers a practical way to avoid the extensive structural disruption that occurs at the narrow space of the die. By using lubricated squeezing flow, this damage can be almost completely eliminated and the specimen can be tested as practically intact by carefully placing the material on the lower plate with a wide spatula or spoon (Suwonsichon and Peleg 1999; Corradini et al. 2000). For details and variations of the technique for use in food, please refer to the review by Campanella and Peleg (2002).

4.3.2 Structural Characterization

As described earlier, the molecular and structural characteristics of fiber may play a significant role in its functionality during processing and also in the human body. This discussion will focus on a few techniques commonly used for structural characterization of polysaccharides in general, and arabinoxylans, which are the major polysaccharides in corn fiber, in particular. The specific characteristics that appear to be more significant for fiber functionality are chemical nature, constituent sugars, linkage pattern, molecular weight, molecular size, degree of branching, and branching pattern.

4.3.2.1 Chemical Analysis

The chemical constituents of cereal brans have been discussed in some detail above. The chemical characterization of fiber is a fundamental consideration in its

evaluation for fiber fortification. As mentioned before, cellulose, hemicelluloses, and lignins are the principal constituents of brans. Some structural proteins and phenolic acids which are components of cell walls are also present. Invariably, bran has some starch associated with it. Also, there is some lipid constituent particularly associated to the germ that can be mixed with the bran during the milling operation. Thus, cereal bran represents a complex system of starch and non-starch polysaccharides (arabinoxylans), proteins, and lipids. Fiber modification, particularly chemical modification as discussed before, is often aimed at enriching a particular fraction which has good functionality and nutritional properties. Thus, the chemical analysis of the fiber is arguably one of the most important parts of its characterization. Various techniques available for monosaccharide analysis and to determine the amounts of lipids, protein, and phenolic acids in the fiber can be used to chemically characterize the fibers. A detailed description of each technique is beyond the scope of this chapter and the reader is referred to specific works on each technique for further detail.

Monosaccharide Analysis

The major polysaccharides of cereal cell walls are cellulose, glucuronoarabinoxylans, β-D-glucans and some other glycans such as glucomannans (Carpita 1996). Thus, the various monosaccharides present in the bran are D-glucose, D-xylose, L-arabinose, D-galactose, glucuronic acid, and D-mannose. Monosaccharide analysis is often carried out using chromatography techniques, both gas chromatography (GC) and high-pressure liquid chromatography (HPLC). Trifluoroacetic acid is used to hydrolyze the polysaccharide. This can be followed by HPLC analysis of the monosaccharides. For GC analysis, the monosaccharides have to be derived to make them volatile. A common derivation technique is conversion of the sugars into their alditol acetates (Englyst et al. 1982).

Protein Estimation

Protein content can be measured using the Bradford assay or, more commonly, the bicinchoninic acid (BCA) method, both of which are colorimetric methods. The Kjeldahl and Dumas methods are based on nitrogen content estimation and are less common owing to their tedious nature.

Phenolic Acid Analysis

There are several techniques for identification and quantification of phenolic acids. Ferulic acid, being the major phenolic acid of cereal brans, is of relevance to the

incorporation of fibers in food products. Barberousse et al. (2008) reviewed various techniques for quantification of ferulic acid, including ultraviolet (UV) spectrometry, fluorescence spectroscopy, and HPLC with UV detection.

Lipid Analysis

A normal phase HPLC technique with evaporative light-scattering detection was developed for non-polar lipid analysis by Moreau et al. (1996). This technique was recently used by Yadav et al. (2007) for quantification of non-polar lipids in corn fiber gum extracted from wet-milled corn bran using alkaline hydrogen peroxide.

4.3.2.2 Spectroscopy Techniques

Nuclear magnetic resonance (NMR) and Fourier transform infrared spectroscopy (FT-IR) are the most commonly used techniques to evaluate the fine structure of polysaccharides. ^{13}C-NMR spectroscopy has been widely used to determine the linkage pattern, relative contents of mono- or di-substituted sugar residues, and to elucidate the relative contents of different monosaccharides present (Izydorczyk and Biliaderis 1995). NMR spectroscopy of the polysaccharide itself cannot provide information about the sequence of monosaccharide residues. Instead, breakdown of the chain with site-specific enzymes can be used to degrade the polymer backbone followed by a study of the structures of formed oligomers. Kacurakova et al. (2000) studied the structure of plant cell wall polysaccharides, including pectins and hemicelluloses using FT-IR. They suggest that the FT-IR spectrum in the 1,200–800 cm^{-1} region can be used to identify polysaccharides and report the absorption maxima for the studied polysaccharides. Robert et al. (2005) analyzed the FT-IR spectrum of wheat endosperm arabinoxylans and performed principal component analysis of some model mixtures of polysaccharides to determine the relative proportions of each in the mixture. Kacurakova and Wilson (2001) reviewed FT-IR spectroscopy techniques for various carbohydrates, including cell wall polysaccharides.

4.3.2.3 Thermal Analysis

One thermal property of polysaccharides that is most relevant to its functionality during processing is the glass transition temperature and its variation with moisture content. Thermal decomposition onset temperatures may also be significant, depending on the kind of processing. These properties can be studied using differential scanning calorimetry (DSC), dynamic mechanical analysis (DMA), and thermo gravimetric analysis (TGA) (Abiad et al. 2009).

4.3.2.4 High-Pressure Size Exclusion Chromatography Techniques

High-pressure size exclusion chromatography (HPSEC), also known as gel permeation chromatography, is commonly used to separate polymers based on their size. HPSEC can be used as a method to estimate molecular weight by calibrating the instrument with standards of known molecular weight. The elution time of the sample can therefore be related to its molecular weight. However, this method of estimation may not be accurate for fibers as differences in degree of branching and in size may cause polymers of the same molecular weight to elute at different times. Thus, for absolute characterization of molecular weight, an analysis technique such as light scattering coupled with HPSEC is often required.

4.3.2.5 Light Scattering

Light scattering is a powerful tool for analysis of macromolecules in solution. It has been extensively applied in the world of synthetic polymers for determination of molar mass, size, degree of branching, and calculation of parameters which are very relevant to the functionality of the polymers during processing, such as branching ratio and persistence length of the polymer. Although its potential application to food polymers is equally significant, it could be somewhat complicated by the inherent polydispersity and diverse nature of food macromolecular components. For details regarding the theory of light scattering, the reader is referred to the seminal works of Debye (1944), Zimm (1948a, b, c), and Wyatt (1993).

The results presented below focus on static light scattering for the analysis of polysaccharides. Since static light scattering measures the average molecular weight and size, it is often desirable to fractionate the molecules based on size prior to the light-scattering analysis. This is most commonly established by HPSEC, although other liquid chromatography techniques may also be used.

HPSEC-MALS

HPSEC separates molecules based on their size, with the larger molecules eluting first from the column followed by the smaller molecules. When an MALS instrument is used as an SEC detector, a concentration detector such as a refractive index detector or a UV detector (for molecules which absorb light in the UV range, such as proteins) is often coupled to it. This enables calculation of concentration for each data slice, which makes it possible to calculate the molecular weight (M_w) and the root mean square (rms) radius (also known as radius of gyration of the molecule, r_g) for each individual data slice, as well as the average across a peak.

Conformation Plots and Branching Analysis

Knowing the average molecular weight (M_w) and rms radius/radius of gyration (r_g) across a peak, a log–log plot of r_g versus M_w, called a conformation plot, can be used to obtain information about the conformation of the molecule in solution. For instance, for a solid sphere, the radius is proportional to the cube root of molar mass; thus the conformation plot will have a slope of 0.33 (Wyatt 1993). For rigid rods, the slope will be 1, while random coils should give a slope of 0.5–0.6. In general spherical-like molecules in solution are associated with a large degree of branching. Thus, these plots can be used to compare the degree of branching between different fiber polymers; lower slope of the conformation plot implies a greater degree of branching, which, as discussed, may have an important effect on the expansion of fiber-enriched foods. Another method of determining the degree of branching of a polymer is the use of the radius method described by Zimm and Stockmayer (1949). In this method, the branching ratio of a polymeric molecule is simply defined as the ratio of rms radius of the polymer to that of a linear polymer that has the same composition and molecular weight. This method has been used by Grcev et al. (2004) to find the degree of branching of polyvinyl acetate. Its use for natural polymers such as polysaccharides may be limited due to the difficulty in obtaining linear and branched polymers of the same molecular weight. So, for these cases, the conformation plots serve as a simple method to qualitatively evaluate branching.

Other methods that can be used include spectroscopy techniques such as NMR, mass spectrometry, and indirect techniques such as GC to determine individual sugar residues if the branches and backbone are known to be made of different sugars. Some data showing the use of light scattering to determine molecular weight, size, and degree of branching of alkali-soluble corn arabinoxylans are presented and discussed in a later section.

4.3.2.6 Fermentation Profiling

The fermentation profile of fiber within the colon is also an important aspect to be considered due to the implications of the role of fiber on human health. In particular, the type and amount of short chain fatty acids produced, as well as the completeness and rapidity of fermentation are all important functional parameters to consider. In vitro fermentation has been used to characterize the pH, gas production, and short-chain fatty acid production by the polysaccharide in the colon. Studies point to a desirability for fibers with controlled fermentation to distribute beneficial fermentation products into the distal colon, while providing some bulking effect for regularity (Rose et al. 2007). Adiotomre et al. (1990) suggested in vitro techniques, dialysis, and fermentation to screen polysaccharides for their impact on nutrient absorption, sterol metabolism, bulking, and fermentation.

4.4 Structure and Functionality of Alkali-Treated Corn Arabinoxylans

A chemical method to improve the functionality of corn bran so it may be incorporated at high levels in an extrusion process is described below.

4.4.1 Description of Chemical Treatment

Corn bran was mixed with 5% NaOH in a 1:10 ratio for 2 h at room temperature to hydrolyze ferulic acid ester cross-linkages following the procedure described by Doner et al. (2000). The mixture was then neutralized with hydrochloric acid, and 95% ethanol was added to the neutralized extract in a ratio of 2:1. The precipitate, termed "alkali-treated bran" (ATB), was dried at 50°C, and milled using a Cyclotec™ cyclone mill equipped with a screen of mesh size 40.

Separation of the alkali-soluble bran (ASB) hemicellulosic fraction from the alkaline-insoluble fraction was done by centrifuging the alkaline mixture (before the neutralization step to produce ATB) at 11,159 g for 8 min. The supernatant was neutralized with HCl and 80% ethanol was added to the supernatant in a ratio of 2:1 to obtain the ASB. The precipitate was dried at 50°C and milled using a cyclone mill equipped with a screen of mesh size 40.

After alkali treatment, there was a significant reduction in insoluble fiber, from 79–52%, and an increase in soluble fiber from 1.6–30% (Blake 2006). The main dietary fiber component of the ASB fraction contains 64% of soluble dietary fiber, which is the branched hemicellulose B. Alkali treatment of corn bran disrupts its supramolecular structure producing dietary fiber that can be separated into various components, which are hemicelluloses A, B, and an alkali-insoluble fraction that consists of cellulose and cross-linked hemicellulose (hemicellulose C), and starch.

4.4.2 Rheological Properties and Extrusion Expansion of Modified Fibers Mixed with Cornmeal

4.4.2.1 Extrusion Trials

Each fiber, that is, ATB, ASB, and unmodified bran (UMB), was mixed with cornmeal in a ratio so as to produce a mixture containing 26% total dietary fiber. The details of the process and extrusion equipment used can be found in Pai et al. (2009). Sectional expansion index (SEI) was measured in each case. SEI is defined as the squared ratio of average diameter of the extrudate to that of the die diameter (Alvarez-Martinez et al. 1988). The SEI of each extrudate is listed in Table 4.1 below. The SEI of extrudates containing 26% ASB was equivalent to that of the

Table 4.1 Sectional expansion indices of cornmeal extruded with various fibers

Sample	SEI
Cornmeal	27
Cornmeal + UMB	11
Cornmeal + ATB	21
Cornmeal + ASF	27

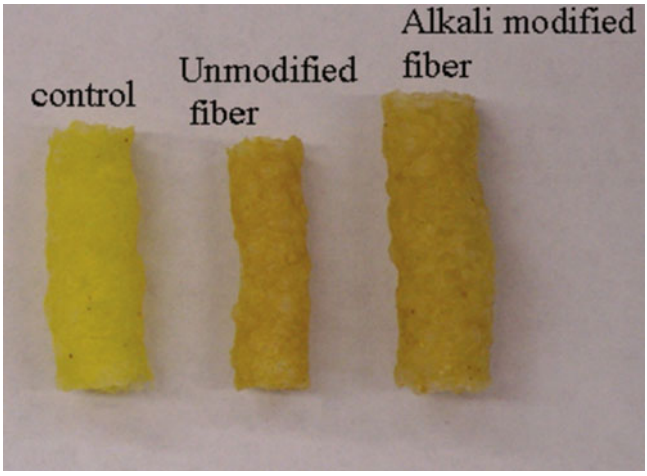

Fig. 4.3 Extrudates obtained from mixing cornmeal with unmodified corn bran and alkali-modified corn fiber

cornmeal with no fiber added. Incorporation of both the modified bran fractions ASB and ATB resulted in much higher radial expansion as compared to the UMB. The difference in expansion is clearly visible in Fig. 4.3, with the alkali modified fiber giving radial expansion similar to that of the control (cornmeal only).

4.4.2.2 Capillary Rheometry

In order to study the effect of incorporation of these fibers on the melt shear rheology, a twin-bore capillary rheometer (Rosand RH 2,000 Capillary Rheometer, Malvern Instruments, Southborough, MA) was used. These experiments were performed to characterize the shear rheology of the melt at conditions similar to those of the extrusion operation. Due to operational limitations of the capillary rheometer, samples with 20% total fiber and 25% moisture were prepared. Shear rates in a range of 20–800s^{-1} for extrusion operations have been reported by several researchers (McMaster et al. 1987; Senouci and Smith 1988; Lai and Kokini 1990; Padmanabhan and Bhattacharya 1993; Seethamraju and Bhattacharya 1994; Della Valle et al. 1996; Drozdek and Faller 2002; Sandoval and Barreiro 2007).

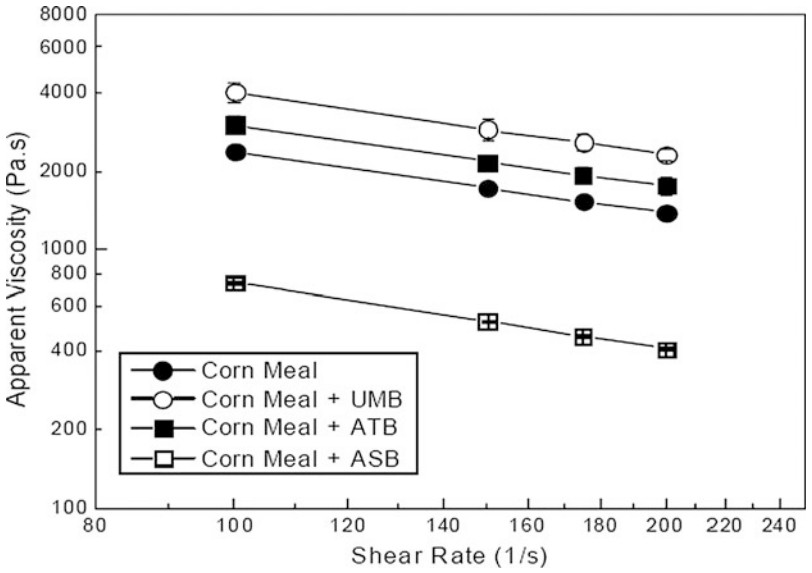

Fig. 4.4 Apparent shear viscosity versus shear rate data from capillary rheometry of cornmeal with various fibers (shear rate range: 100–200 s^{-1})

Steady shear viscosities were measured at shear rates of 100, 150, 175, and 200 s^{-1}. No end correction was applied due to the high sample requirement. A long die was used (L/D = 8) in order to minimize the contribution of the nonlinear portion of the pressure drop (Byler and Kwei 1971).

Addition of ATB at the 20% level resulted in a significant increase in shear viscosity, while a decrease was noted with the addition of ASB. However, by the addition of UMB to the cornmeal, the shear viscosity increased substantially compared to the control. Figure 4.4 shows the differences in melt shear rheology based on addition of fibers. As shown by the linearity of the plot in logarithmic coordinates, all samples showed a pseudoplastic behavior and obeyed the power law model in the experimental shear rate range tested.

4.4.2.3 Extensional Rheology

Lubricated squeezing flow between two plates was chosen to characterize the extensional viscosity of the mixed fiber samples. Huang and Kokini (1993) and Wikström and Bohlin (1999) used this technique for characterizing the extensional viscosity of wheat doughs.

In this work, it was necessary to add gluten at an 8.3% level to produce a cohesive dough. Thus, the mixture of cornmeal and gluten served as a base to observe the effect of the different fiber components on the extensional rheology of the dough. The samples prepared in this way consisted of cornmeal mixed with

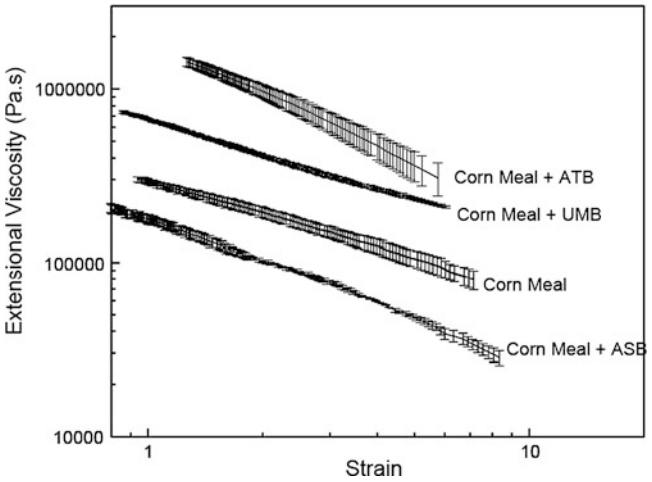

Fig. 4.5 Extensional viscosity versus strain data obtained from lubricated squeezing flow rheometry of cornmeal with various fibers

gluten and each of the fiber components (ATB, ASB, and UMB), with a resultant composition of approximately 20% total dietary fiber, 25% cornmeal, 8.3% gluten, and water making up the rest of the sample. Lubricated squeezing flow experiments were conducted on a Sintech 1/G Universal Testing Machine (MTS, Eden Prairie, MN). Samples of initial height 10 mm were compressed between Teflon plates (25.4 mm in diameter) which were lubricated with silicone oil. Experiments were conducted with the constant area method with crosshead velocities of 10 and 20 mm/min until the point where the force reached a value of 100 lbf. Results showed that the addition of gluten served to improve the squeezing flow testing and its reproducibility without qualitatively changing the behavior of the samples. All samples were shown to exhibit strain thinning behavior. Differences in extensional rheology were observed with the type of fiber used. Cornmeal with ATB showed the highest extensional viscosity, while addition of UMB resulted in an extensional viscosity higher than that for cornmeal with no added fiber, but ASB addition resulted in an extensional viscosity slightly lower than that of the control cornmeal (Fig. 4.5).

4.4.2.4 Effect of Rheology on the Expansion Process

Once bubble growth is initiated, the bubbles have to overcome the resistance created by the shear viscosity in order to grow. After the bubbles have grown sufficiently, the melt film between the bubbles undergoes biaxial extension (Gendron and Daigneault 2000; Steffe 1996). Hence, consideration of extensional viscosity becomes an essential part in the prediction of extrusion expansion from the melt rheology. Once a certain normal stress in the melt film has been exceeded due to

further bubble expansion, the melt film ruptures, causing bubble collapse. For the bubbles to remain intact, the melt should have an extensional viscosity high enough to withstand the extensional stress caused by bubble expansion.

Excluding the sample of cornmeal with ASB, it was observed that shear viscosity increased for cornmeal, cornmeal with ATB, and cornmeal with UMB, whereas extensional viscosity increased for cornmeal, cornmeal with UMB, and cornmeal with ATB. Addition of both UMB and ATB to cornmeal increased shear and extensional viscosities when compared to cornmeal alone, thus increasing overall resistance to expansion during the two stages of bubble growth, that is, when shear and extensional flows, respectively, were the prevalent flows, which caused the observed lower expansion. However, comparing the rheology of cornmeal with UMB to that of cornmeal with ATB, it can be concluded that an increase in extensional and decrease in shear viscosities resulting from alkali treatment resulted in an increased extrusion expansion. This trend suggests that a relatively high extensional viscosity and a low shear viscosity appear to be the rheological parameters that cause good expansion.

Although cornmeal with ASB had a significantly lower shear viscosity compared to cornmeal alone, both samples showed a similar radial and longitudinal expansion, suggesting that the shear viscosity could not be the sole rheological parameter governing the extrudate expansion and that extensional viscosity also has a role to play in expansion. The similarity in expansion can be explained by the effect of rheology on the expansion mechanism. Sun (2004) and Stange and Munstedt (2006) showed that higher shear viscosity causes a slower diffusion of the gas in polymers resulting in better foam expansion, which would explain the better expansion observed on extrudates prepared with cornmeal alone. Although the extensional viscosity of the ASB sample was lower than that for the cornmeal control, the similar expansion probably cannot be explained by the reduced extensional viscosity of the sample with ASB compared to cornmeal alone. In the present study, it was observed that extrudates with bran had a larger number of bubbles compared to the cornmeal control (not shown). The presence of a high amount of bubbles of large sizes may have increased the heat transfer rate of the extrudate containing ASB as compared to cornmeal. This effect would cause a more rapid heat and moisture loss, which could have promoted the attainment of the glass transition sooner than the control sample, thus preventing further bubble growth. The combination of reasons presented above probably explains why cornmeal with ASB has the same expansion as the control samples.

4.4.2.5 Possible Effects of Structure and Composition of Fibers on Rheology

An increase in the soluble arabinoxylan content in the ATB fiber compared to UMB caused a decrease in shear viscosity and an increase in extensional viscosity. On the other hand, ASB (highest soluble fiber content) exhibited both lower shear and extensional viscosities as compared to the control with no fiber. This finding

suggests that the interaction of ASB with starch is different than the interactions of UMB or ATB with starch.

The major component of ASB is hemicellulose B (64%), which is a branched arabinoxylan (Whistler 1993). Due to its high degree of branching, it is postulated that ASB is able to interact with starch differently than the other two fibers. An enhanced functionally that seems to result from the molecular dispersal is produced by the chemical treatment. The favorable interaction between starch and the ASB fraction would in turn result in a rheological behavior of the fiber in the melt similar to that of starch, that is, without disrupting the melt structure and resulting in a melt rheology which favors bubble growth and expansion. A similar phenomenon has been observed during the extrusion of synthetic polymers, where the use of highly branched polymers such as low-density polyethylene (LDPE) results in higher expansion than linear high-density polyethylene (HDPE) (Gendron and Daigneault 2000). Li et al. (2004) reported that higher amylopectin content leads to lower melt shear viscosity, resulting in higher expansion. Thus, the highly branched arabinoxylan fraction of hemicellulose B in the ASB fiber would lead to higher expansion. Conversely, the main components of the water-insoluble portion of the ATB fiber consist of cross-linked insoluble hemicellulose, such as hemicellulose C (15% w/w of bran, linear xylan polysaccharide with few arabinose branches), and cellulose (16% w/w) (Sugawara et al. 1994). UMB is composed of 79% insoluble dietary fiber as compared to ATB, which has 52% (Blake 2006). The high proportion of cross-linked and linear polymers that compose UMB are likely to break the continuity of the melt forming a multiphase melt, whereas ATB may form a melt that is less discontinuous, thus favoring some expansion.

4.4.3 Effect of Branching on Rheology of Alkali-Soluble Corn Arabinoxylans

Physico-chemical characterization and rheological characterization are complementary techniques for assessment of fiber quality. While most of the rheological measurements can be used to simulate actual processing conditions and directly assess the behavior of the fiber under these conditions, there are other rheological methods aimed to be related with structural parameters, which can be used as tools for fiber quality assessment. In order to illustrate the use of both of these techniques, differences in structural and rheological properties of some alkali-soluble corn bran fractions are discussed.

Alkali treatment of bran was carried out as described previously and the alkaline supernatant was separated from the insoluble fraction. The alkaline supernatant was acidified to precipitate the alkali soluble and separate the water-insoluble fraction. Ethanol was then added to this solution so that the solution contained 20% by volume of ethanol. The fraction that precipitated out was separated and freeze-dried and regarded as the 0–20% fraction. The ethanol concentration was then increased

to 40% and the fraction called the 20–40% fraction was isolated. Similarly, the 40–60% and 60–80% fractions were collected. This fractionation was carried out for the purpose of obtaining fractions homogeneous in terms of molecular characteristics of the polysaccharides, with lesser variability in their structures. It was observed that most of the polysaccharides precipitated in the 20–40% and 40–60% fractions. The shear and extensional viscosities in doughs containing these fibers and their solutions in water were measured as follows.

4.4.3.1 Melt Shear Rheology Using Capillary Rheometry

Melt shear rheology was measured using the same methodology as described in the capillary rheometry section. Samples were prepared by mixing cornmeal, fiber, and water such that each sample contained 25% fiber and 50% cornmeal. Steady shear experiments were conducted at 120 °C, which was the extrusion temperature for trials conducted in our laboratory (Blake 2006). Steady shear viscosities were measured at shear rates of 75, 100, 150, 175, and 200 s^{-1}. The variation of shear viscosity with shear rate is shown in Fig. 4.6. It is clear that addition of the fiber fractions 20–40% and 40–60% reduces the shear viscosity of the melt. There is also some difference between the measured shear viscosities. The samples containing the 20–40% fraction show a slightly higher viscosity compared to those with the 40–60% fraction, but addition of both fiber fractions significantly lowers the viscosity compared to cornmeal alone.

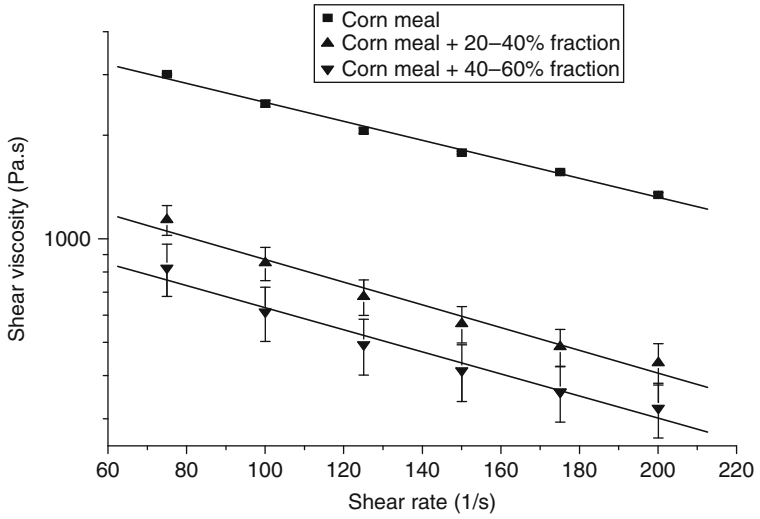

Fig. 4.6 Apparent shear viscosity as a function of shear rate for cornmeal mixed with the 20–40% and 40–60% fractions of ASB (range: 75–200 s^{-1})

4.4.3.2 Extensional Rheology Using Lubricated Squeezing Flow

The effect of individual fiber fractions on extensional viscosity of dough containing these fibers along with the control samples (no fiber) was characterized by the lubricated squeezing flow technique. Samples were prepared with cornmeal mixed with each of the fiber components, that is, 20–40% and 40–60% ASB fractions, resulting in a final fiber composition of 25%.

The constant area method was used at constant biaxial strain rates of 0.1 s^{-1} and 1 s^{-1} until the total biaxial strain reached a value of 90% Cauchy strain. Wei et al. (2007) reported that the dependence of extensional viscosity on strain is probably the result of orientation developed in the polymer molecules as the fluid undergoes extensional deformation. Cornmeal with no fiber showed a higher extensional viscosity compared to samples with added fiber. In order to distinguish the rheological behavior of the two fiber fractions, results for cornmeal are excluded, but its elongational viscosity is slightly higher than the elongational viscosity of the fiber-enriched samples. At a lower strain rate of 0.1 s^{-1} differences in extensional viscosity between the 40–60% and 20–40% fractions are quite significant (Fig. 4.7). This difference is minimal at 1 s^{-1}, which indicated that there could be fine structural differences between the two fractions that were apparent only at low strain rates. Moreover, although the 40–60% fraction samples exhibited a lower extensional viscosity at 0.1 s^{-1}, that is, a lower resistance against deformation, they showed a lower decrease in extensional viscosity when the strain rate was increased from 0.1 to 1 s^{-1}, as compared to samples with 20–40% fraction. It was hypothesized that the likely higher branching of the 40–60% fraction was responsible for this behavior.

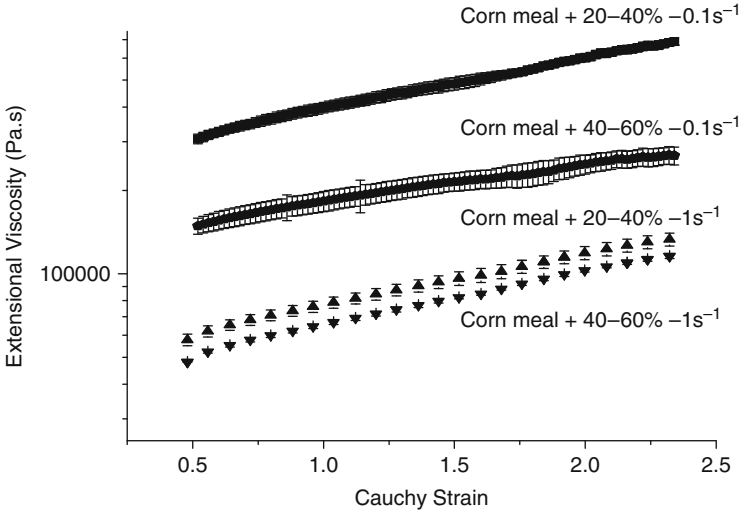

Fig. 4.7 Extensional viscosity as a function of Cauchy strain for cornmeal mixed with 20–40% and 40–60% fractions of ASB

4.4.3.3 Solution Shear Rheology Using Rotational Rheometer

The 20–40% and 40–60% fractions were dissolved in water to make 5% solutions which were placed in concentric cylinder geometry in a rheometer (ARG2 from TA Instruments, Newcastle, DE) and viscosity was determined at shear rates varying from 1 to 200 s^{-1}. Both samples showed shear thinning behavior for shear rates less than 20 s^{-1}. Between 20 and 200 s^{-1} the samples showed a Newtonian behavior (Fig. 4.8).

The 40–60% fraction had a lower solution viscosity compared to the 20–40% fraction, but similar molecular weight distribution profiles (results from HPSEC not shown). This suggests that the 40–60% fraction has a smaller hydrodynamic radius and thus a more highly branched structure. It is thus hypothesized that there are fine structural differences between the two fractions of alkali-soluble corn bran, as seen from the difference in their behavior in these rheological tests.

4.4.3.4 Branching Analysis Using HPSEC-MALS

In order to confirm the existence of structural differences as suggested by rheological properties, the two fractions were analyzed by HPSEC-MALS and conformation plots were made as described above. The slope of the conformation plot for the 40–60% fraction was of 0.39, which is slightly lower than that for the 20–40% fraction (0.44), as can be seen in Fig. 4.9. These results confirm the qualitative

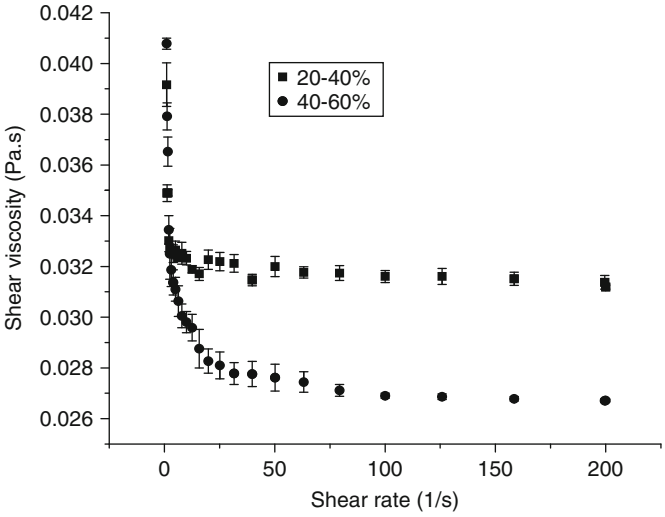

Fig. 4.8 Comparison of solution (5%) shear rheology between 20–40% and 40–60% fractions for shear rates between 1 and 200 s^{-1}

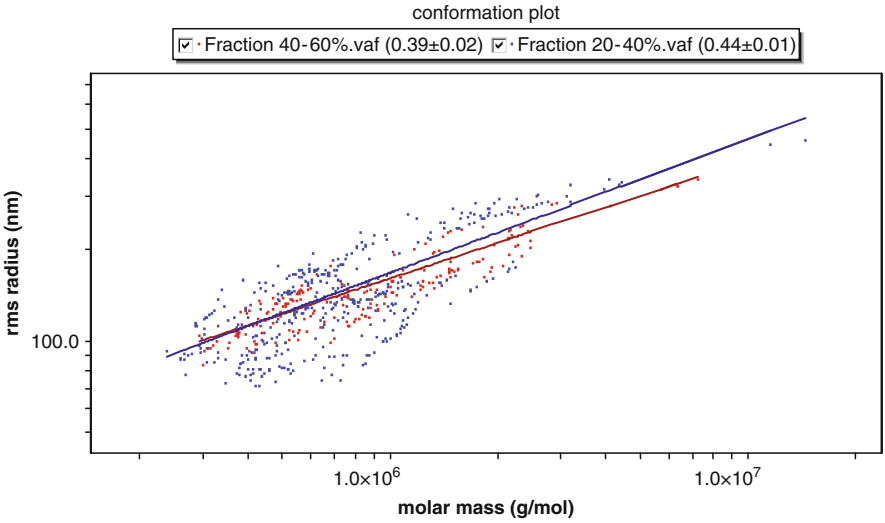

Fig. 4.9 Conformation plots for 20–40% and 40–60% fractions

information obtained from the rheology tests, which indicated that the 40–60% fraction has a more branched structure than the 20–40% fraction. Thus, while rheological characterization can be used to hypothesize about differences in fine structure of the polymers, branching analysis using, for example, HPSEC-MALS must be used to confirm differences in branching pattern between the polysaccharide polymers.

4.4.3.5 Possible Implications in Extrusion

Irrespective of the strain rates, it was found that the control cornmeal with no added fiber exhibited the highest extensional viscosity among these tests. Addition of fibers in all forms decreased shear and extensional viscosities of the cornmeal fiber composites. It was also noted that the presence of modified fibers allowed the sample to be squeezed to extremely high strains without evidence of fracture along the lateral surface of the cylindrical sample. The different behaviors can be observed by comparing Fig. 4.10a (cornmeal) and b (composite of cornmeal and 25% ASB), where the latter showed no fracture and a homogeneous deformation. Homogeneous deformation during extensional flow is a characteristic of branched polymers (Stange and Munstedt 2006). Homogeneous deformation prevents the growth of inhomogeneities that can result in sample breakage or cause the inhomogeneities to grow in a restrained manner. It could very well be expected that these fibers will have a favorable impact on extrusion expansion due to homogeneous deformation.

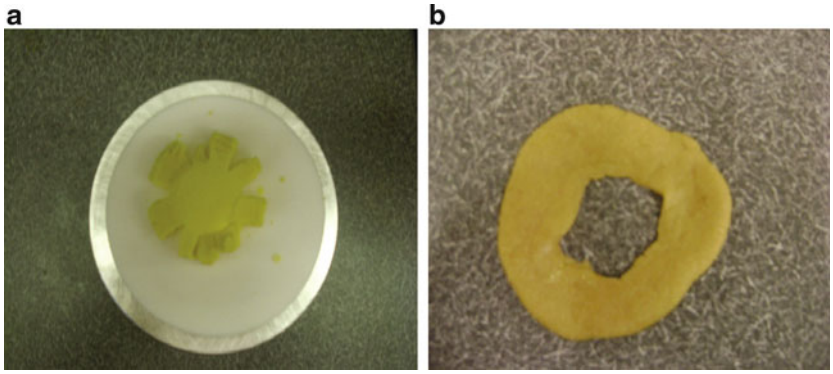

Fig. 4.10 Pictures of samples after lubricated squeezing flow test: (**a**) cornmeal, (**b**) cornmeal with 20–40/40–60% fractions of ASB. Cornmeal shows extensive fracture, while samples with ASB fractions are squeezed without fracture

4.5 Conclusion

Dietary fiber is an important part of the diet, with significant nutritional and physiological benefits. However, poor functionality during processing makes production of high-fiber foods a challenge. Some strategies for fiber modification, including physical, chemical, and enzymatic methods, may be employed to improve this functionality and make addition of high levels of fiber into processed foods possible. Several sources of fiber are available to the food industry, cereal brans being arguably among the cheapest and most abundant. Physico-chemical and rheological characterization techniques can be successfully employed for the assessment of fiber quality for potential incorporation into different foods. Some rheological tests are designed to simulate actual processing conditions, while others give information about the structure of the polymer. Complementary information on these structures can be obtained by physical and chemical techniques such as light scattering and monosaccharide analysis. Together, all of these techniques, along with modification strategies, can be employed to overcome the engineering challenge of fiber incorporation and aid the food industry in producing better products that will help to improve public health.

Acknowledgments The authors wish to acknowledge Midwest Advanced Food Manufacturing Alliance (MAFMA) and Dr. Kevin Schilling of Grain Processing Corporation for his continued support during this research.

References

Abiad MG, Carvajal MT, Campanella OH (2009) Review on methods and theories to describe the glass transition phenomenon: applications in food and pharmaceutical products. Food Eng Rev 1:105–132

Adiotomre J, Eastwood MA, Edwards CA, Brydon WG (1990) Dietary fiber – *in vitro* methods that anticipate nutrition and metabolic-activity in humans. Am J Clin Nutr 52:128–134
Alvarez-Martinez L, Kondury K, Harper J (1988) A general model for expansion of extruded products. J Food Sci 53:609–615
Arrigoni E (2001) Enzymatic modification of dietary fiber sources. In: Cho S, Dreher M (eds) Handbook of dietary fiber. Marcel Dekker, New York, pp 206–208
Barberousse H, Roiseux O, Robert C, Paquot M, Deroanne C, Blecker C (2008) Analytical methodologies for quantification of ferulic acid and its oligomers. J Sci Food Agric 88:1494–1511
Bhattacharya M, Seethamraju K, Padmanabhan M (1994) Entrance pressure-drop studies of cornmeal dough during extrusion-cooking. Polym Eng Sci 34:1187–1195
Blake O (2006) Effect of molecular and supramolecular characteristics of select dietary fibers on extrusion expansion. Ph.D. thesis, Purdue University, Indiana, USA
Breen M, Seyam A, Banasik O (1977) The effect of mill by-products and soy protein on the physical characteristics of expanded snack foods. Cereal Chem 54:728–736
Byler L, Kwei T (1971) Flow behavior of polyethylene melts containing dissolved gases. J Polym Sci 35:165–176
Campanella O, Peleg M (2002) Squeezing flow viscometry for nonelastic semiliquid foods: theory and applications. Crit Rev Food Sci Nutr 42:241–264
Carpita N (1996) Structure and biogenesis of the cell walls of grasses. Annu Rev Plant Phys 47:445–476
Chinnaswamy R, Hanna MA (1988) Relationship between amylose content and extrusion-expansion properties of corn starches. Cereal Chem 65:138–143
Claye S, Idouraine A, Weber C (1996) Extraction and fractionation of insoluble fiber from five fiber sources. Food Chem (UK) 57:305–310
Colliopoulos J (1991) Psyllium mucilloid fiber food products. US Patent 5,009,916
Corradini M, Stern V, Suwonsichon T, Peleg M (2000) Squeezing flow of semi-liquid foods between parallel Teflon® coated plates. Rheol Acta 39:452–460
Debye P (1944) Light scattering in solutions. J Appl Phys 15:338–342
Decker K (2007) Fiber goes with the flow. Food Product Design. http://www.foodproductdesign.com/articles/beverages/7a1applications.html
Della Valle G, Collona P, Patria A, Vergnes B (1996) Influence of amylose content on the viscous behavior of low hydrated molten starches. J Rheol 40:347–362
Doner LW, Hicks KB (1997) Isolation of hemicellulose from corn fiber by alkaline hydrogen peroxide extraction. Cereal Chem 74:176–181
Doner L, Johnston D (2001) Isolation and characterization of cellulose/arabinoxylan residual mixtures from corn fiber gum processes. Cereal Chem 78:200–204
Doner L, Sweeney G, Hicks K (2000) Isolation of hemicellulose from corn fiber. US Patent 6,147,206
Drozdek K, Faller J (2002) Use of a dual orifice die for on-line extruder measurement of flow behavior index in starchy foods. J Food Eng 55:79–88
Ebringerova A, Hromadkova Z, Heinze T (2005) Hemicellulose. Adv Polym Sci 186:1–67
Englyst H, Wiggins HS, Cummings JH (1982) Determination of the non-starch polysaccharides in plant foods by gas-liquid-chromatography of constituent sugars as alditol acetates. Analyst 107:307–318
Fan JT, Mitchell JR, Blanshard JMV (1994) A computer-simulation of the dynamics of bubble-growth and shrinkage during extrudate expansion. J Food Eng 23:337–356
Foehse KB, Efstathiou JD, Stoll JR (1992) High soluble fiber barley expanded cereal and method of preparation. US Patent 5,151,283
Garber BW, Hsieh F, Huff HE (1997) Influence of particle size on the twin-screw extrusion of corn meal. Cereal Chem 74:656–661
Gelroth J, Ranhotra G (2001) Food uses of fiber. In: Cho S, Dreher M (eds) Handbook of dietary fiber. Marcel Decker, New York, pp 435–452

Gendron R, Daigneault L (2000) Rheology of thermoplastic foam extrusion process. In: Lee S (ed) Foam extrusion. Technomic Publishing Co, Lancaster, PA, pp 35–80
Grcev S, Schoenmakers P, Iedema P (2004) Determination of molecular weight and size distribution and branching characteristics of PVAc by means of size exclusion chromatography/multi- angle laser light scattering (SEC/MALLS). Polymer 45:39–48
Guy R (2001) Extrusion cooking. Technologies and applications. Woodhead Publishing Limited, Cambridge/England
Hingmann R, Marczinke BL (1994) Shear and elongational flow properties of polypropylene melts. J Rheol 38:573–587
Hseih F, Mulvaney S, Huff S, Lue S, Brent J (1989) Effect of dietary fiber and screw speed on some extrusion processing and product variables. Lebensmittel-Wissenshaft und-Technologie 22:204–207
Hseih F, Huff H, Lue S, Stringer L (1991) Twin-screw extrusion of sugar beet and corn meal. Lebensmittel-Wissenshaft und-Technologie 24:495–500
Huang H, Kokini J (1993) Measurement of biaxial extensional viscosity of wheat flour doughs. J Rheol 37:879–891
Izydorczyk M, Biliaderis C (1995) Cereal arabinoxylans: advances in structure and physicochemical properties. Carbohydr Polym 28:33–48
Kacurakova M, Wilson R (2001) Developments in mid-infrared FT-IR spectroscopy of selected carbohydrates. Carbohydr Polym 44:291–303
Kacurakova M, Capek P, Sasinkova V, Wellner N, Ebringerova A (2000) FT-IR study of plant cell wall model compounds: pectic polysachharides and hemicelluloses. Carbohydr Polym 43:95–203
Kokini JL, Chang C, Lai L (1992) The role of rheological properties on extrudate expansion. In: Kokini J, Ho C, Karwe M (eds) Food extrusion science and technology. Marcel Dekker, New York, pp 631–653
Lai L, Kokini J (1990) The effect of extrusion operating conditions on the on-line apparent viscosity of 98% amylopectin (Amioca) and 70% amylose (Hylon 7) corn starches during extrusion. J Rheol 34:1245–1266
Li P, Campanella O, Hardacre A (2004) Using an in-line slit-die viscometer to study the effects of extrusion parameters on corn melt rheology. Cereal Chem 81:70–76
Lue S, Hsieh F, Huff H (1991) Extrusion cooking of corn meal and sugar beet fiber: effects on expansion properties, starch gelatinization, and dietary fiber content. Cereal Chem 68:227–234
Macosko C (1994) Shear rheometry: Pressure driven flows. In: Macosko C (ed) Rheology: Principles, measurements and applications. Wiley-VCH, New York, pp 237–283
Malkin A, Isayev A (2006) Rheology: concepts, methods and applications. *ChemTec Publishing*. Online version: http://knovel.com/web/portal/browse/display?_EXT_KNOVEL_DISPLAY_bookid=2189andVerticalID=0
McMaster T, Senouci A, Smith A (1987) Measurement of rheological and ultrasonic properties of food and synthetic polymer melts. Rheologica Acta 26:308–315
Mendonca S, Grossmann MVE, Verhe R (2000) Corn bran as a fiber source in expanded snacks. Lebensmittel-Wissenschaft Und-technologie-Food Sci Technol 33:2–8
Moraru CI, Kokini JL (2003) Nucleation and expansion during extrusion and microwave heating. Comprehensive Reviews in Food Science and Food Safety 2:120–138
Moreau RA, Powell MJ, Hicks KB (1996) Extraction and quantitative analysis of oil from commercial corn fiber. J Agric Food Chem 44:2149–2154
Mottur G, Glass R (1985) Reduced calorie puffed snack food products. US Patent 4,517,204
National Academy of Sciences, Institute of Medicine (2002) Appendix E: dietary intake data from the continuing survey of food intakes by individuals (1994–1996, 1998) In: Dietary reference intakes for energy, carbohydrate, fiber, fat, fatty acids, cholesterol, protein, and amino acids (Macronutrients) pp 801–819. Available at: http://www.nap.edu/books/ 0309085373/html/265.html
Ng A, Lecain S, Parker ML, Smith AC, Waldron KW (1999) Modification of cell-wall polymers of onion waste III. Effect of extrusion-cooking on cell-wall material of outer fleshy tissues. Carbohydr Polym 39:341–349

Ning L, Villota R, Artz W (1991) Modification of corn fiber through chemical treatments in combination with twin-screw extrusion. Cereal Chem 68:632–636
Onwulata C, Konstance R, Smith P, Holsinger V (2001) Co-extrusion of dietary fiber and milk proteins in expanded corn products. Lebensmittel-Wissenshaft und-Technologie 34:424–429
Padmanabhan M, Bhattacharya M (1993) Effect of extrusion processing history on the rheology of cornmeal. J Food Eng 18:335–349
Pai D, Blake O, Hamaker B, Campanella O (2009) Importance of extensional rheological properties on fiber-enriched corn extrudates. J Cereal Sci 50:227–234
Ralet M, Della Valle G, Thibault J (1993) Raw and extruded fibre from pea hulls. I: composition and physico-chemical properties. Carbohydr Polym 20:17–23
Ringe M, Stoll J (1991) R-T-E cereal with psyllium. US Patent 5,026,689
Robert P, Marquis M, Barron C, Guillon F, Saulnier L (2005) FT-IR investigation of cell wall polysaccharides from cereal grains: arabinoxylan infrared assignment. J Agric Food Chem 53:7014–7018
Rose DJ, Demeo MT, Keshavarzian A, Hamaker BR (2007) Influence of dietary fiber on inflammatory bowel disease and colon cancer: importance of fermentation pattern. Nutr Rev 65:51–62
Sandoval A, Barreiro J (2007) Off-line capillary rheometry of corn starch: effects of temperature, moisture content and shear rate. Lebensmittel-Wisenshaft und- Technologie 40:43–48
Saulnier L, Thibault J (1999) Ferulic acid and diferulic acids as components of sugar beet pectins and maize bran heteroxylans. J Sci Food Agric 79:396–402
Saulnier L, Vigouroux J, Thibault J (1995) Isolation and partial characterization of feruloylated oligosaccharides from maize bran. Carbohydr Res 272:241–253
Schulze E (1891) Information regarding chemical composition of plant cell membrane. Ber Dtsch Chem Ges 24:2277–2287
Seethamraju K, Bhattacharya M (1994) Effect of ingredients on the rheological properties of extruded corn meal. J Rheol 38:1029–1044
Senouci A, Smith A (1988) An experimental study of food melt rheology. I. Shear viscosity using a slit die viscometer and a capillary rheometer. Rheologica Acta 27:546–554
Shelton D, Lee W (2000) Cereal carbohydrates. In: Kulp K, Ponte J (eds) Handbook of cereal science and technology. Marcel Dekker, New York, pp 385–416
Stange J, Munstedt H (2006) Rheological properties and foaming behavior of polypropylenes with different molecular structures. J Rheol 50:907–923
Steffe J (1996) Rheological methods in food process engineering, 2nd edn. Freeman Press, East Lansing, MI
Sugawara M, Tetsuya S, Totsuka A, Takeuchi M, Ueki K (1994) Composition of corn hull dietary fiber. Starch-Staerke 46:335–337
Sun S (2004) Physical chemistry of macromolecules: Basic principles and issues, 2nd edn. Wiley, New York
Suwonsichon T, Peleg M (1999) Imperfect squeezing flow viscometry of mustards with suspended particulates. J Food Eng 39:217–226
USDA (2005) Backgrounder 2005 dietary guidelines advisory committee report [Online]. Available at United States Department of Agriculture: http://www.health.gov/dietaryguidelines/dga2005/Backgrounder.html
van Lengerich B, Larson M (2000) Cereal products with inulin and methods of preparation. US Patent 6,149,965
Wei X, Collier J, Petrovan S (2007) Shear and elongational rheology of polyethylenes with different molecular characteristics. II. Elongational rheology. J Appl Polym Sci 104:1184–1194
Whistler R (1993) Hemicelluloses. In: Whistler R, BeMiller J (eds) Industrial gums, 3rd edn. Academic, San Diego, CA
Wikström K, Bohlin L (1999) Extensional flow studies of wheat flour dough. II. Experimental method for measurements in constant extension rate squeezing flow and application to flours varying in breadmaking performance. J Cereal Sci 29:227–234

Wyatt PJ (1993) Light-scattering and the absolute characterization of macromolecules. Anal Chim Acta 272:1–40

Yadav MP, Moreau RA, Hicks KB (2007) Phenolic acids, lipids, and proteins associated with purified corn fiber arabinoxylans. J Agric Food Chem 55:943–947

Zimm BH (1948a) The dependence of the scattering of light on angle and concentration in linear polymer solutions. J Phys Colloid Chem 52:260–267

Zimm BH (1948b) The scattering of light and the radial distribution function of high polymer solutions. J Chem Phys 16:1093–1099

Zimm BH (1948c) Apparatus and methods for measurement and interpretation of the angular variation of light scattering - preliminary results on polystyrene solutions. J Chem Phys 16:1099–1116

Zimm BH, Stockmayer WH (1949) The dimensions of chain molecules containing branches and rings. J Chem Phys 17:1301–1314

Chapter 5
Gastric Digestion of Foods: Mathematical Modeling of Flow Field in a Human Stomach

Samrendra Singh and R. Paul Singh

5.1 Introduction

Knowledge of the disintegration of solid foods in a human stomach is essential to assess the bioavailability of nutrients in the gastrointestinal (GI) tract. Some of the key factors impacting gastric digestion are stomach physiology including composition and rheological properties of gastric contents, stomach wall motility in fed/fasted states, and hydrodynamics and mechanical forces that act on the ingested food. To advance our current understanding of the digestion process, a quantitative description of the flow field in the human stomach is necessary. The overall goal of this study was to develop a mathematical model of the flow field in a human stomach and to use the model to investigate the influence of stomach wall motility on the flow behavior.

5.2 Fluid Flow in a Human Stomach

The human stomach consists of two parts: the proximal stomach, which can be divided into the fundus and the orad corpus (one third of corpus); and the distal stomach, which includes the remaining corpus, the antrum, and the pylorus (Szurszewski 1981) (Fig. 5.1). The stomach plays three major roles in the digestion process: storing of high-density food, mixing, and emptying the chyme (Forte 1996; Schubert and Makhlouf 1992; Soll and Berglindh 1994). The stomach reduces the size of food particles and fat globules and disperses them in the gastric juice. It also controls the pH, viscosity, and density of the gastric content with the help of digestive secretions. After the ingestion of food, powerful contraction waves originating from the mid-stomach move toward the pylorus at a speed of 2.5 mm/s. The depth of the contraction waves is shallow at the origin and increases

S. Singh and R.P. Singh (✉)
Department of Biological and Agricultural Engineering, University of California, Davis, CA 95616, USA
e-mail: rpsingh@ucdavis.edu

J.M. Aguilera et al. (eds.), *Food Engineering Interfaces*, Food Engineering Series,
DOI 10.1007/978-1-4419-7475-4_5,

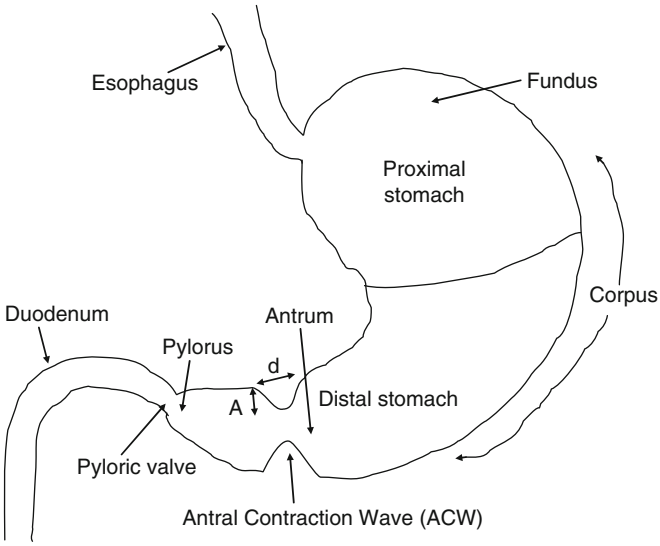

Fig. 5.1 Schematic diagram of a human stomach (*A* wave amplitude, *d* width of wave) (not drawn to scale)

as they approach the pylorus where they end. The occlusion diameter becomes narrower during its travel and at the end the gastric content is squeezed back through the narrow opening creating a retropulsive jet. These antral contraction waves (ACWs) generate forces and fluid motions that break down and mix the gastric content (Horowitz et al. 1994; Kelly 1980; Macagno and Christensen 1981; Pallotta et al. 1998; Indireshkumar et al. 2000; Pal et al. 2004).

The size and shape of the stomach vary from one individual to another. It depends upon many factors including age, food habits, posture, and the interval since eating. The stomach walls are very flexible and the size of the stomach can vary from a few hundred milliliters (when empty) to 2 L. The shape of the stomach, it can be assumed, is somewhat like a "J."

The food has a significant effect on the properties of the contraction waves. The length of propagation, the amplitude of contractions, and the time duration the stomach takes to generate the contraction waves are affected by the volume and chemical and physical properties of the meal (Code and Carlson 1968; Meyer 1991; Mayer 1994; Camilleri and Prather 1993). A large meal volume induces powerful phasic contractions that originate higher up in the stomach as compared to small volumes. A highly viscous food results in shallow contractions and a diluted or aqueous meal generates deep contractions (Carlson et al. 1966). The deforming wall boundaries of the stomach fill with a complex mixture of fluid and the food particulates generate a complex and unsteady flow field. There are some distinctive features of the flow field inside the stomach such as retropulsive jet and recirculating eddy structures.

As the ACW moves closer to the pylorus, the space between the contraction wave and the pyloric valve decreases. The gastric content trapped inside this

decreasing space is pushed back into the proximal part of the stomach, forming a jet-like flow. It is also known as retropulsive jet. Retropulsive jet has been reported by several authors (Carlson et al. 1966; Keinke et al. 1984; Issa et al. 1994; Pallotta et al. 1998; Pal et al. 2004). Retropulsive flow results in an increase in the flow velocity. The interaction of retropulsive jet with a relatively stagnant fluid inside the stomach develops a high shear field at the boundaries of the jet. The food particulates carried along with the retropulsive jet are subjected to this high shear. Issa et al. (1994) visualized the movement of gastric content using a high-speed echo planner magnetic resonance imaging (MRI) technique. They observed the retropulsive motion with an increase in activities in the distal part of the stomach. Pallotta et al. (1998) studied the retropulsive flow with the contraction pattern in the antral region and in the closing and opening of the pyloric valve. They discussed the role of retropulsive jet in mixing and transport of gastric contents. Pal et al. (2004) observed retropulsive flow in their simulation model of the stomach. They also reported the contribution of this motion in the mixing of the gastric content.

Pal et al. (2004) modeled the flow and mixing in human stomach using a two-dimensional numerical model. They assumed that two-dimensional models have the same quantitative behavior as that of three-dimensional models in axisymmetric geometries. They demonstrated two important flow phenomenon taking place inside the stomach and were able to show the retropulsive jet also reported by many researchers earlier. Their simulation showed an increase in flow velocity up to 7.5 mm/s. The retropulsive jet disperses the particles along the longitudinal axis of the stomach. They also observed a second flow pattern (flow eddies) between any two ACWs. These eddies are important for lifting the food particles from the stomach wall and transporting them toward the center of the stomach. Although retropulsive jets have been reported by many researchers, eddies between the contraction waves were reported for the first time by this research group. Nevertheless, the human stomach is not axisymmetric in nature, especially considering the effect of gravitational force on the lower part of the stomach. Therefore, it is necessary to model the stomach as a three-dimensional geometry.

Further, the flow inside a human stomach is peristaltic in nature, driven by deforming boundaries of the stomach muscles. In order to solve the peristaltic flow in a complex system, such as a human stomach, one has to start with the peristaltic flow in simpler geometries. There are several publications dealing with analytical as well as numerical solutions of peristaltic motion in tubular geometry. Burns and Parkes (1967) expanded the stream function as a Fourier series and used wall boundary conditions to evaluate the coefficients of the Fourier series. They were able to obtain a reasonable estimate of the flux through the tube under peristaltic deformation of the walls as described by sinusoidal waves. Shapiro et al. (1969) studied the flow properties of viscous incompressible fluid in a tube with deforming walls. They solved the flow equations to obtain the parabolic velocity profile along the cross section of the tube under the deforming wall according to (5.1):

$$\frac{u}{c} = -1 - \frac{1}{4\mu c}\frac{dP}{dx}\left(h^2 - r^2\right) \tag{5.1}$$

where u is the fluid velocity in the wave frame of reference, dP/dx is the pressure gradient in x direction, and r is the radial position from the axis of the tube. Zien and Ostrach (1970) analyzed peristaltic flow in two-dimensional geometry due to the traveling wave motion of the confining walls. They solved the stream function (ψ) in the form of an expansion with power of (a/λ). Li (1970) applied the analysis carried out by Zien and Ostrach (1970) for an axisymmetric geometry, which represents many of the biological systems in a more realistic way. He obtained the mean values and distribution of fluid velocity and pressure in terms of amplitude, frequency, and wavelength of the sinusoidal wave. Shen (1976) reduced the three-dimensional Navier–Stokes equations to a series of linear boundary value problems with Laplace and biharmonic operators.

Food particulates upon breakdown either dissolve in the gastric juice (polysaccharides) or disperse as a suspension. This contributes to change in viscosity of the gastric fluid. Many food fluids are non-Newtonian in nature with flow characteristics that depend upon the shear rate. Many researchers have reported the viscosity values of the stomach and small intestine digesta, but mostly at one shear rate value as observed by Dikeman and Fahey (2006). Additionally, the flow dynamics of the gastric fluid depends upon its viscosity. Overall, viscosity of the gastric fluid is influenced by the composition of the food material and the secretions through stomach walls after food intake. Moreover, in solid foods the viscosity changes as the food particles disintegrate.

5.3 Procedures in Modeling

5.3.1 Stomach Geometry

We used the geometrical dimensions of a human stomach as defined by Pal et al. (2004). Stomach volume was assumed to be 500 mL. The grids were constructed with the help of GAMBIT, a three-dimensional mesh creation software. The stomach was constructed with a series of circular rings in varying diameters across the length. The rings were used as a base frame and joined together to form the three-dimensional shape of the stomach. To save on computational time, the stomach geometry was split in half along the plane of symmetry (Fig. 5.2b), whereupon only half the stomach was used to compute the flow field. Hexagonal grids were generated using the Hex–Cooper algorithm. A total of 281,602 cells were used to construct the grids of stomach geometry. The centerline of the stomach geometry was represented by a third-order polynomial equation given by (5.2):

$$y = 0.0067x^3 - 0.0624x^2 + 0.3436x - 5.8323 \quad \text{(units in mm)} \tag{5.2}$$

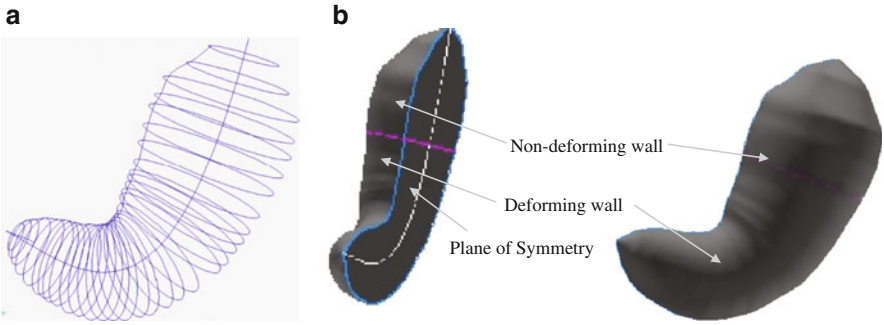

Fig. 5.2 (**a**) Schematic diagram of circular rings constructing stomach geometry; (**b**) boundary conditions used in FLUENT simulation

5.3.2 Deformation of Stomach Using Dynamic Meshing

The grids of the stomach geometry were deformed with every time step to represent a real contracting stomach. An ACW started from near the middle of the stomach (14.4 cm from the pyloric valve) and traveled toward the pylorus at a speed of 2.4 mm/s. The lifetime of an ACW lasted for 60 s. Any two ACWs were separated by a 20 s time gap, making its frequency 3/min. The shape of an ACW was taken as the sixth power of the sinusoidal function. The amplitude of an ACW varied along its travel length from its origin to the pylorus. The occlusion diameter ratio was defined as the ratio of diameter of the contraction ring (ε) to the original diameter of the section before contraction (D). The occlusion diameter ratio (ε/D) decreased linearly from 1.0 to 0.6 during the first 17.5 s and then remained constant at 0.6 for the next 16.0 s. The occlusion diameter ratio decreased linearly from 0.6 to 0.1 for 23.5 s and then increased to 1.0 at the end of the wave's travel. The stomach geometry repeated itself after a 20 s time interval.

An imaginary line was assumed along the center of the stomach, connecting the center of all the circular rings used to construct the stomach geometry. Deformation in the stomach grid was performed by moving the nodes of the grid closer (contraction) or farther (expansion) from the imaginary centerline of the stomach (Fig. 5.3). Radial distance of the nodes (vertices of the computational elements) from the imaginary centerline was increased or decreased to create the desired volumetric deformations. The amount of displacement of a given node (Δr_i) at a given time was the function of its distance from the centerline of the stomach (x_i) and the center of the ACW (x_w) (Fig. 5.4a; (5.3) and (5.4)).

$$\Delta r_i = b\left(\frac{\varepsilon}{D}\right)\left[1 - \sin\left\{\frac{\pi}{2}\left(\frac{d - |x_w - x_i|}{d}\right)\right\}^6\right] \quad \text{if} \quad |x_w - x_i| \le d \tag{5.3}$$

$$\Delta r_i = 0 \quad \text{if} \quad |x_w - x_i| > d \tag{5.4}$$

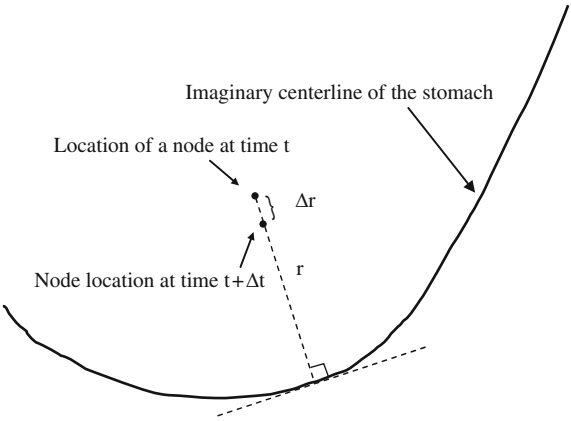

Fig. 5.3 Schematic diagram showing movement of a node during deformation

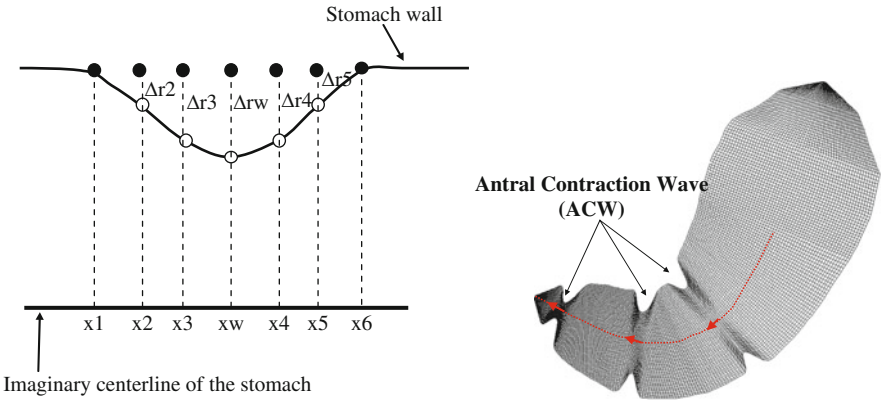

Fig. 5.4 (**a**) Schematic diagram describing sinusoidal deformation procedure along stomach wall; (**b**) grids of stomach geometry with ACW modified by flow time

where Δr_i is the displacement of the *i*th node along the radial distance (m), *b* is the maximum depth (amplitude) of the contraction wave at a given time (m), $\frac{\varepsilon}{D}$ is the occlusion diameter ratio, *d* is half of the width of the contraction wave (m), x_i is the projection of the *i*th node on the imaginary stomach centerline (m), and x_w is the position of the center of the contraction wave (m).

At any given time all ACWs were perpendicular to the imaginary centerline. Grids were denser near the lower (deformation) region and coarser in the upper region of the stomach (Fig. 5.4b). The grid size was selected such that the stomach wall was smooth at the peak of the ACWs. A relatively larger grid size resulted in a non-smooth surface near the ACWs and a smaller grid size increased the computational time. The grid size for this study was taken as 2.0 mm.

Fluid flow in a system is governed by three basic equations: the continuity, conservation of momentum, and conservation of energy equations. Since this model did not involve any heat transfer, only the first two equations were considered:

$$\text{Continuity}: \quad \nabla.U = 0 \tag{5.5}$$

$$\text{Momentum}: \quad \frac{\partial U}{dt} + (U.\Delta)U = -\frac{1}{\rho_f}\Delta p + v_f \nabla^2 U + g \tag{5.6}$$

where U is the velocity component (m/s), p is the pressure (Pa), v_f is the kinematics viscosity of the fluid, and ρ_f is the density of the fluid (kg/m^3).

The above flow equations were solved with the help of a CFD solver (FLUENT 6.3.26). There were a number of assumptions made to simplify the model. The gastric fluid was assumed to behave like a Newtonian fluid at a very low Reynolds number. The stomach did not empty the gastric content for the duration of the simulation. Physical properties of the gastric fluid remained unchanged with time. The chemical reactions between the gastric fluid and food were not accounted for in the model. The temperature of the system remained constant at 37°C.

5.4 Results and Discussions

5.4.1 Validation of a Modeled Flow Field inside a Circular Tube

A flow field inside a tubular geometry was simulated using FLUENT. Dimensions of the tube were taken from that defined by Shapiro et al. (1969). Water was used as the fluid inside the tube. The boundary wall of the tube was deformed as a sinusoidal wave (Fig. 5.5). Flow in a tube is axisymmetric in nature; therefore, it was sufficient to solve the flow field in a two-dimensional plane with a width equal to the radius of the tube. The computational grid was created using GAMBIT.

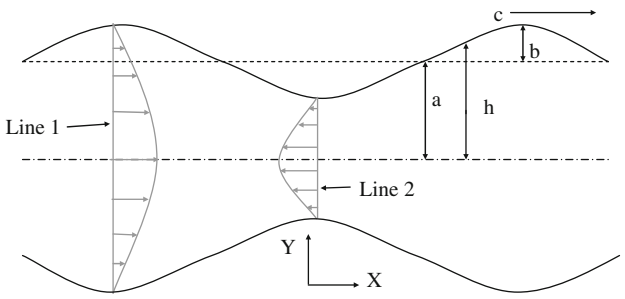

Fig. 5.5 Peristaltic flow in a circular tube

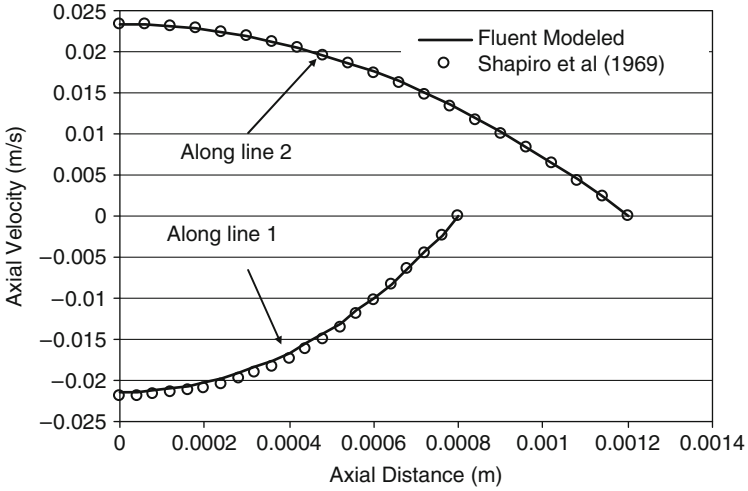

Fig. 5.6 Comparison between velocity profiles obtained by FLUENT simulation and analytical model by Shapiro et al. (1969)

A user-defined function was written in C language to deform the nodes of the computational grid given by (5.7):

$$h = a + b \sin \frac{2\pi}{\lambda}(X - ct) \tag{5.7}$$

Velocity profiles obtained in the simulation were compared to the analytical equation given by Shapiro et al. (1969) along two lines, as shown in Fig. 5.6. There was an excellent agreement between the predicted and the analytical results. This confirmed the capability of this CFD model to handle peristaltic flow with deforming walls. A correlation between the two results showed slopes of 0.996 ($R^2 = 1$) and 0.998 ($R^2 = 0.99$). This validation supports the use of FLUENT software in handling peristaltic types of flow under deforming walls.

5.4.2 Pressure Validation

The pressure field simulated by the stomach model was compared to the data available in literature. For gastric juice viscosity 0.1 (kg/m.s) and density 1,000 kg/m^3, the pressure fields simulated by this stomach model and the model from Pal et al. (2004) are shown in Fig. 5.7. The pressure contours in the antral region are comparable and the maximum pressure is on the order of 0.1 mmHg. However, the pressure between the most distal and the middle ACWs did not agree in two cases. The Pal model showed uniform pressure in this region, whereas our model showed that pressure in the region between the ACWs decreased in steps. The flow

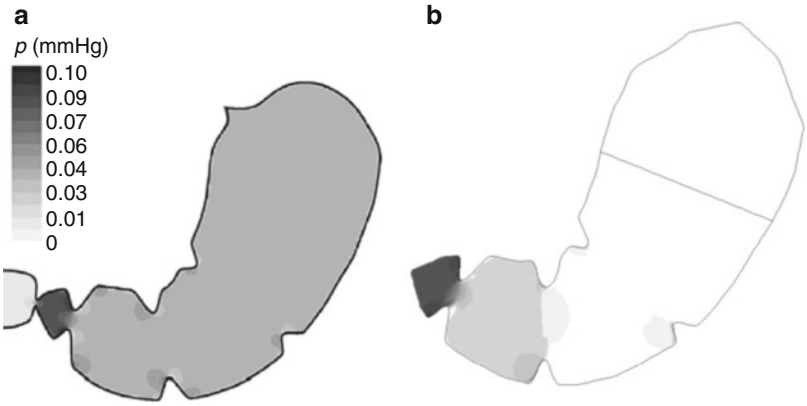

Fig. 5.7 **(a)** Pressure field predicted by Pal et al. (2004); **(b)** pressure field obtained from our model (density = 1,000 kg/m^3, viscosity = 1,000 cP)

inside the stomach was a pressure-driven flow caused by deforming walls and decreasing volumes between the ACWs. Thus, the volume between two consecutive ACWs is constantly decreasing, and therefore, the pressure between two consecutive ACWs always increases with time until the volume completely collapses in the pylorus.

5.4.3 Flow Field Inside the Stomach

Simulated unsteady flow patterns are shown in Fig. 5.9 for fluid density 1,000 kg/m^3, viscosity 1 cP, and ACW lifetime (T_L) of 60 s; these settings were used for most of the results unless otherwise specified. The lifetime of an ACW was defined as the time interval between its creation and end.

The velocity contours shown in Fig. 5.9 represent the flow field beginning at time N.T_L, where *N* is an integer. Most of the flow activity takes place in the distal part of the stomach as compared to the proximal part where flow was minimal. As the ACW travels closer to the pyloric valve, the fluid trapped between the contraction wave and pyloric region is forced behind the enclosure, creating a retropulsive jet. Figure 5.8 shows the volume between the two consecutive ACWs and the cross-sectional area of an ACW as a function of time. The area marked by a circle in Fig. 5.8 corresponds to the time of high intensity of the retropulsive jets. A combination of high rate of volume change (steeper slope) and the small cross-sectional area results in high-intensity retropulsive jets. The jet length increases as the ACW moves closer to the pyloric valve. The maximum fluid velocity is achieved just before the ACW collapses completely near the pyloric valve (Fig. 5.9). The maximum fluid velocity observed was 30 mm/s. Minimum fluid velocity is observed when only two ACWs are present and a third one has just started to grow (Fig. 5.9a, f).

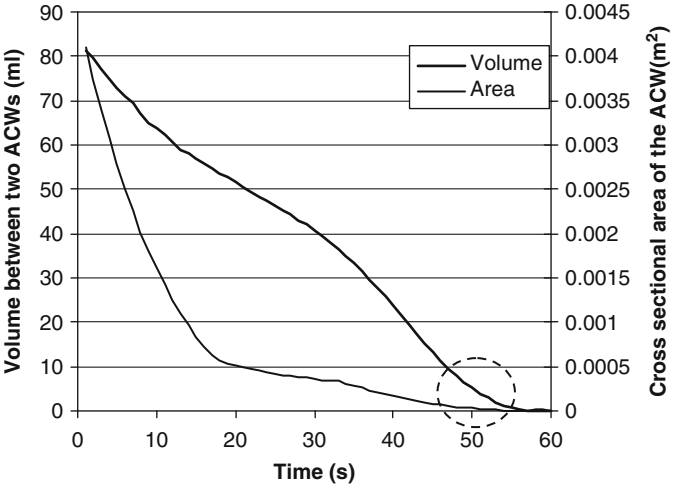

Fig. 5.8 Graph showing change in volume between two successive ACWs and change in cross-sectional area of an ACW with time

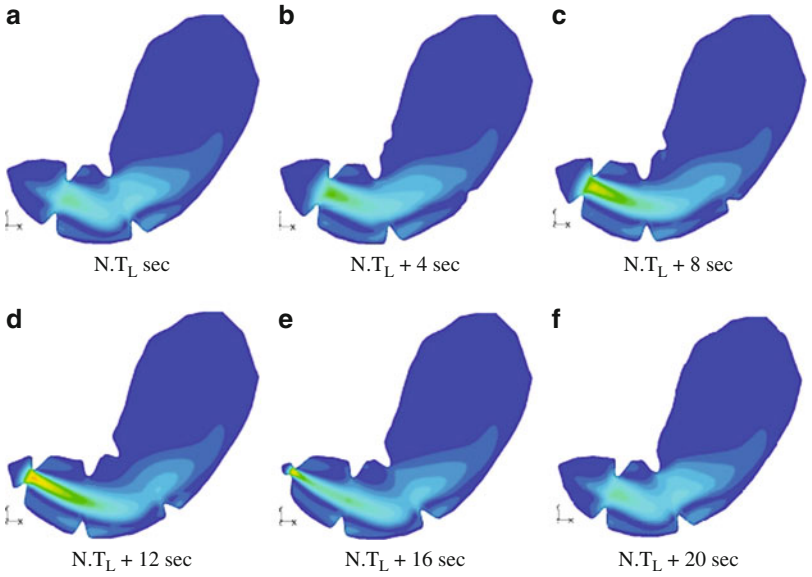

Fig. 5.9 Velocity contours in stomach as ACWs move toward the pylorus

There was an additional flow pattern besides the retropulsive jet, wherein flow recirculation was observed between two ACWs. This recirculation was mainly due to the wall motion of the contraction waves and was assisted by shearing flow of the retrograde jet. The maximum velocity in these eddying flow structures was found to

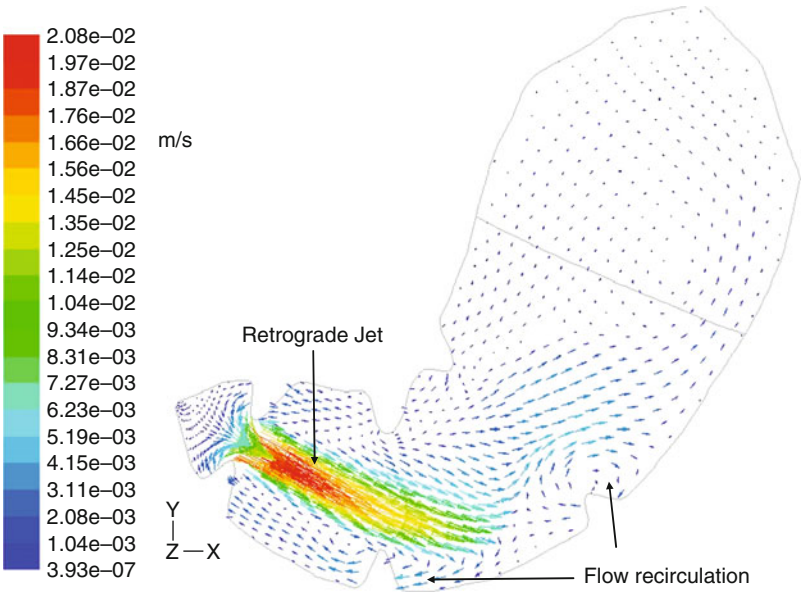

Fig. 5.10 Velocity vectors (m/s) of flow in a human stomach at $T_L(N + 1/3)$ s

be on the order of 7.5 mm/s. The role of these flow recirculation patterns and retropulsive jets in mixing gastric content has been discussed previously by Pal et al. (2004). The recirculating flow scrapes any food particles adhering to the stomach walls and pushes them toward the retropulsive jet region.

In Fig. 5.10 it can be observed that the retrograde jet is the main flow event taking place inside the stomach. Also, the flow direction below the retrograde jet and between two contraction waves is toward the pyloric valve. The flows in this region and the retrograde jet are in opposite directions from each other. The retrograde jet carries the gastric content away from the lower stomach, whereas the flow recirculation moves part of the gastric content back toward the lower stomach region.

5.4.4 The Effect of Viscosity of Gastric Fluid

At the start of the digestion process the gastric fluid is less viscous (close to water). The viscosity of the gastric fluid gradually increases as the food particulates disintegrate and dissolve into the gastric juices. The viscosity plays a significant role in flow dissipation of gastric flow as well as in the drag force on the food particulates. The effect of viscosity on the gastric flow was observed in this study at five levels: 1, 5, 10, 20, and 50 cP.

The length of the retropulsive jet in this study is defined as the distance from the origin of the jet to the point where jet velocity drops to 90% of its original velocity.

It can be observed that the length of the retropulsive jet decreases as the gastric juice becomes increasingly viscous (Figs. 5.11 and 5.12). The energy loss due to viscous dissipation increases with the viscosity of the gastric juice and the jet length becomes shorter. The role of retropulsive jets is mainly for shearing and mixing of the food particulates. Therefore as viscosity increases, mixing of the food particulates is expected to decrease.

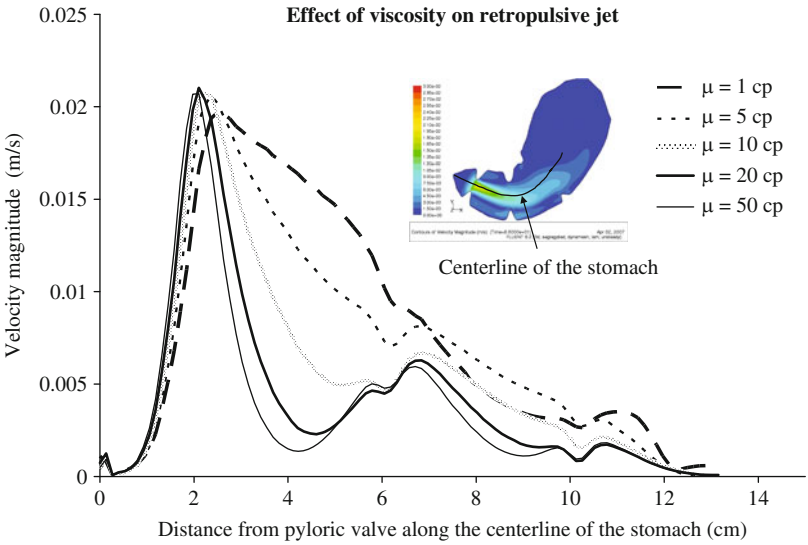

Fig. 5.11 Velocity profiles along centerline of stomach at time $T_L(N + 1/3)$ s. $\rho = 1{,}000$ kg/m^3

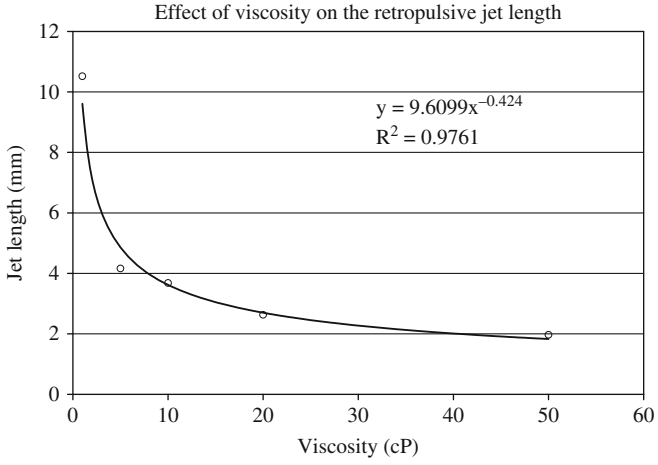

Fig. 5.12 Retropulsive jet length decreases as viscosity of gastric fluid increases. $\rho = 1{,}000$ kg/m^3

5.4.5 The Effect of Density of Gastric Fluid

The effect of density of the gastric fluid was studied at three levels: 1,000, 1,050, and 1,100 kg/m^3. Small differences were noticed near the regions of the contraction waves. Beyond that there was no notable difference in the flow field due to change in the density of gastric fluid (Fig. 5.13). The maximum velocity of the retropulsive jet remained the same for all three densities. Thus, it may be concluded that the density of the gastric fluid does not have any significant effect on the flow field; however, it is likely to play a major role in the flow dynamics of the food particulates. The density difference between the gastric fluid and the food material determines the flow path of a food particulate and the frequency at which the particulate is exposed to the antral grinding. A food particulate that is heavier than the gastric fluid is likely to settle at the bottom of the stomach, whereas a lighter food particulate would float along the surface of the gastric fluid.

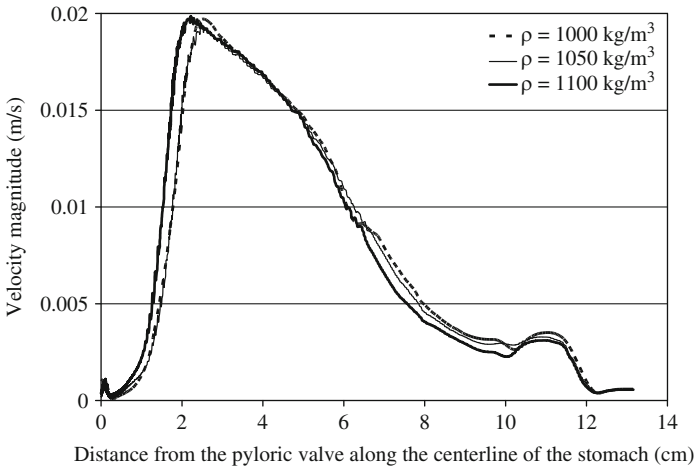

Fig. 5.13 Velocity profiles along centerline of stomach at time t + 10 s for gastric fluid viscosity of 1 cP

5.4.6 The Effect of ACW Speed

Three levels of wave speed (mild, normal, and high) were selected to study their effect on the flow field inside the model stomach. The speed of contraction waves was changed by altering their lifetime. The total lifetime (T_L) of an ACW for a normal speed was 60 s, whereas for mild and high speeds the lifetimes were 66 and 54 s, respectively

The velocity profiles along the centerline of the stomach were compared to assess any changes due to the speed of the ACWs. Figure 5.14 shows velocity

magnitude along the stomach centerline when the most distal (leftmost) ACW was 7.2 cm away from the pyloric valve. The velocity of the gastric fluid increased with the speed of ACW. The maximum velocity magnitude increased by 6.45% (19.7–20.97 mm/s) at a 10% increase in ACW speed (2.4–2.68 mm/s). The length of the retropulsive jet also increased from 10.52 to 11.71 mm (11.3% increment). The flow pattern before the start and near the end of the jet remained similar. The flow recirculation near the ACW also intensified as the ACW traveled faster.

Increasing the wave speed (decreasing T_L) increases the fluid velocity (Figs. 5.14 and 5.15) and the length of the retropulsive jet increases with the wave speed. There was an increase in the size of eddies due to flow recirculation. It was also observed that the relationship between maximum velocity and lifetime of an ACW was linear for the range considered in this study (Fig. 5.16). The retropulsive jets in the stomach are generated by continuously decreasing the

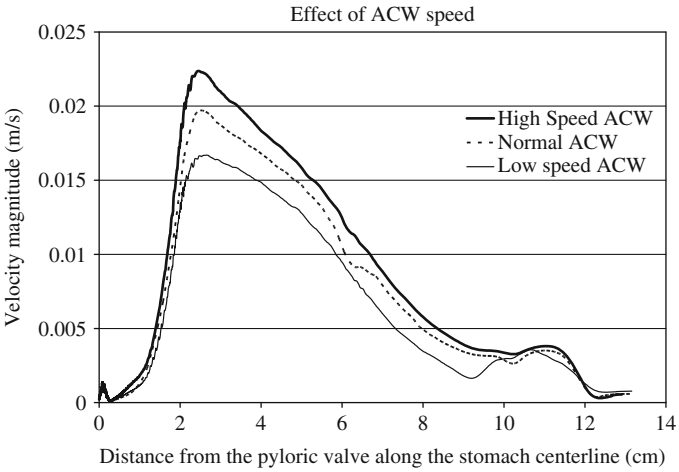

Fig. 5.14 Effect of ACW speed on flow profile along centerline of stomach at time $T_L(N + 1/3)$ s. Density = 1,000 kg/m^3, viscosity = 1 cP, high-intensity ACW

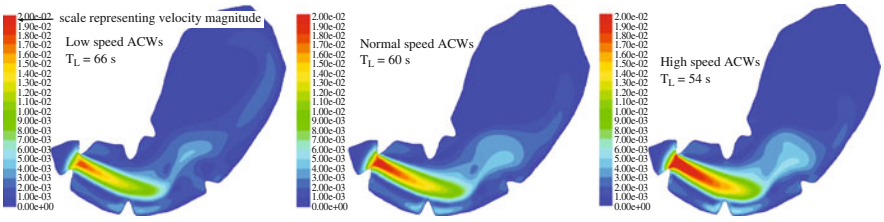

Fig. 5.15 Effect of speed of ACW on flow profile inside stomach at time $T_L(N + 1/3)$ s. Density of gastric juice = 1,000 kg/m3, viscosity = 1 cP

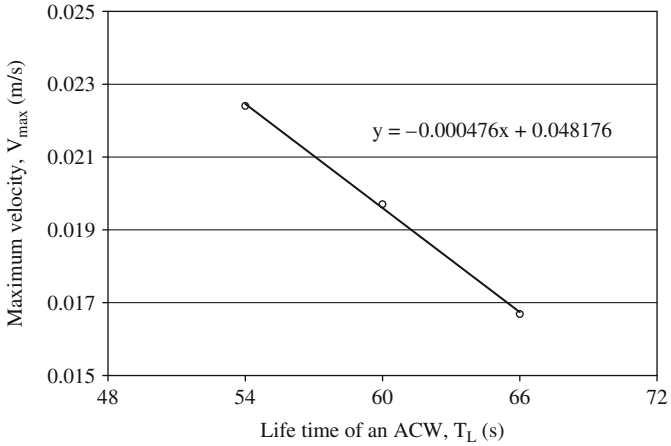

Fig. 5.16 Maximum velocity magnitude in stomach at time $T_L(N + 1/3)$ s, as a function of speed of ACW. Density of gastric juice = 1,000 kg/m^3, viscosity = 1 cP

volume between two ACWs. The rate at which the volume between two ACWs collapses is directly proportional to the speed of the ACWs. Therefore, a higher ACW speed means a faster collapsing volume between two ACWs, which results in stronger retropulsive jets.

5.4.7 The Effect of Depth of Contraction

The initial phase of gastric motility consists of mild contraction waves increasing slowly to high-intensity contraction waves over time. The mild waves represent the initial quiescence phase when the food is entering or has just entered the stomach. After the quiescence period the high-intensity contraction waves emerge, during which time most of the mixing and disintegration activities take place (Coupe et al. 1991). Two contraction profiles of ACWs were used to study the effect of the contraction depth on the flow field. The change in nondimensional occlusion diameter (ε/D) with time was varied, as described by (5.8) (high-intensity waves) and (5.9) (mild waves).

Occlusion diameter ratio profile for high-intensity waves (Pal et al. 2004):

$$\frac{\varepsilon}{D} = \begin{cases} 0.5 + 0.5(17.5)/17.5 & 0.0 \le t \le 17.5 \\ 0.5 & 17.5 \le t \le 33.5 \\ 0.1 + 0.4(57 - t)/23.5 & 33.5 \le t \le 57.0 \\ 0.1 + 0.9(t - 57)/3.0 & 57.0 \le t \le 60. \end{cases} \tag{5.8}$$

Occlusion diameter ratio profile for mild waves (included in this study):

$$\frac{\varepsilon}{D} = \begin{cases} 0.75 + 0.25(17.5 - t)/17.5 & 0.0 \le t \le 17.5 \\ 0.75 & 17.5 \le t \le 33.5 \\ 0.35 + 0.4(57 - t)/23.5 & 33.5 \le t \le 57.0 \\ 0.35 + 0.65(t - 57)/3.0 & 57.0 \le t \le 60.0 \end{cases} \tag{5.9}$$

The maximum velocity of retropulsive jet was higher for the high-intensity waves compared to the mild waves (Figs. 5.17 and 5.18). This was due to the bigger occlusion diameter (larger opening) of the mild waves. For a given flow rate the velocity was inversely proportional to the cross-sectional area of the flow path. Moreover, in the case of mild waves, the rate at which the volume between any two neighboring ACWs decreased was less compared to the high-intensity waves. The flow rate of the gastric fluid was directly related to the rate of change in volume

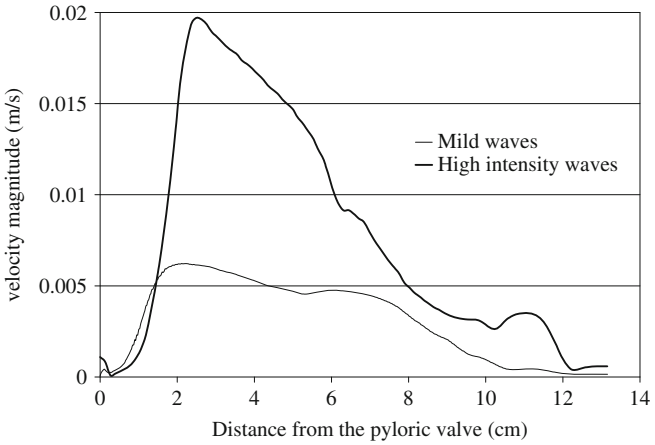

Fig. 5.17 Velocity profiles along centerline of stomach for mild and high-intensity waves at $T_L(N + 1/3)$ s

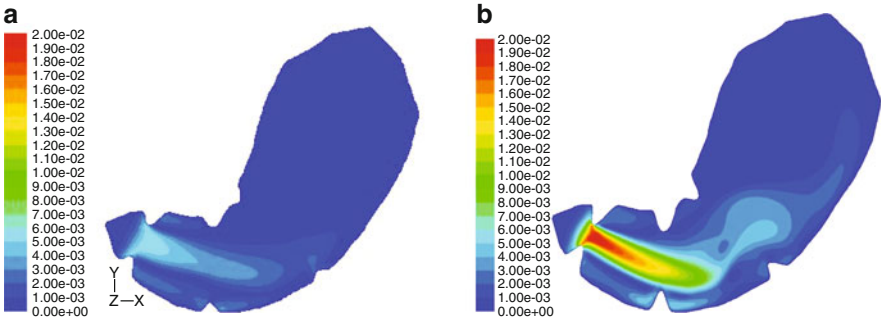

Fig. 5.18 Velocity contour for (**a**) mild and (**b**) high-intensity ACWs at time $T_L(N + 1/3)$ s

between two ACWs. Therefore, the combination of larger occlusion diameter and less flow rate resulted in a drop in the retropulsive jet velocity. The maximum velocity observed for mild ACWs was 5.9 mm/s, which is 70% less than for the high-intensity waves. A lower velocity of retropulsive jet (for mild ACWs) results in poor mixing and shearing, and the retropulsive jet may not be able to carry the larger food particulates for long distances, resulting in poor mixing. Further, the eddy flow near the ACWs becomes milder with contraction depth.

5.5 Conclusions

This study was focused on modeling the flow field and the disintegration kinetics of the food particles inside the human stomach. The effect of the viscosity of gastric juice, density of the juice, speed, and intensity of ACWs on the flow field was studied. Fluid flow inside a human stomach driven by peristaltic deformation of the stomach walls was simulated using FLUENT software, while dynamics meshing was used to model the contracting shape of the stomach. The flow field was solved assuming that the gastric juice follows a laminar flow rather than a non-Newtonian flow at a very low Reynolds number, as found in the stomach. Retropulsive and recirculatory flow structures were observed inside the simulated flow field of the stomach. The size of the retropulsive jet is a function of the viscosity of the gastric juice and characteristics of the ACWs. The length of the retropulsive jet decreased with increasing viscosity or decreasing speed/depth of the ACWs. Recirculatory flow regions were observed near the ACWs.

5.6 Suggestions for Future Work

This model has a number of limitations that can be pursued as future modifications. This research was limited by information available in medical literature on the human stomach, but with advancements in measurement techniques and methods, the model can be modified in the future to predict the flow field and disintegration kinetics more realistically. It was assumed that the flow inside the stomach is Newtonian in nature, but there are many reports suggesting that the gastric content behaves like a non-Newtonian fluid. The non-Newtonian properties of the gastric content can be measured as a function of food properties (size, chemical compositions, etc.) and the fluid's concentration. A physical model of the human stomach can be used for validation purposes, since one of the major limitations of this study was lack of validation methods. In the future the flow field could be validated with this physical model, more closely representing a stomach with peristaltic flow. This physical model should also be capable of simulating food disintegration.

Furthermore, the current model does not consider the gastric emptying during the digestion/disintegration process. The size, shape, and flow field of the stomach

change as the gastric contents are emptied and the stomach becomes increasingly smaller. This model assumes that the depth and speed of the ACWs remain the same throughout the digestion process. Four digestion cycle stages, wherein the properties of the ACWs change, can be added to the model. However, at the current computational power available with computers, it could take an extremely long time to complete such a simulation, but with advancements in computational speed or application of parallel computing simulation, time may become more reasonable.

References

Burns JC, Parkes T (1967) Peristaltic motion. J Fluid Mech 29:731–743

Camilleri M, Prather CM (1993) Gastric motor physiology and motor disorders. In: Feldmann M, Scharschmidt BF, Sleisenger MH (eds) Sleisenger and Fordtran's gastrointestinal and liver disease, 6th edn. W.B. Saunders, Philadelphia, pp 572–86

Carlson HC, Code CF, Nelson RA (1966) Motor action of the canine gastroduodenal junction; a cineradigraphic, pressure and electric study. Am J Dig Dis 11:155–72

Code CF, Carlson HC (1968) Motor activity of the stomach. In: Code CF (ed) Handbook of physiology, alimentary canal, vol IV. American Physiological Society, Washington, DC, pp 1903–1916

Coupe AJ, Davis SS, Wilding IR (1991) Variation in gastrointestinal transit of pharmaceutical dosage forms in healthy subjects. Pharm Res 8:360–364

Dikeman CL, Fahey GC (2006) Viscosity as related to dietary fiber: a review. Crit Rev Food Sci Nutr 46(8):649–63

Forte JC (1996) Gastric function. In: Greger R, Windhorst U (eds) Comprehensive human physiology: from cellular mechanism to integration. Springer-Verlag, Berlin, p 1253

Horowitz M, Dent J, Fraser R, Sun W, Hebbard G (1994) Role and integration of mechanisms controlling gastric emptying. Dig Dis Sci 39(12):7S–13S

Indireshkumar K, Brasseur JG, Faas H (2000) Relative contributions of pressure pump and peristaltic pump to gastric emptying. Am J Physiol Gastrointest Liver Physiol 278:G604–16

Issa B, Freeman A, Boulby P, Wright J, Gowland P, Bowtell R, Spiller R, Mansfield P (1994) Gastric motility by tagged EPI. Magma, magnetic resonance materials in physics. Biol Med 2(3):295–298

Keinke O, Schemann M, Ehrlein HJ (1984) Mechanical factors regulating gastric emptying of viscous nutrient meals in dogs. Q J Exp Physiol 69:781–95

Kelly KA (1980) Review: Gastric emptying of liquids and solids: roles of proximal and distal stomach. Am J Physiol 239:G71–G76

Li C (1970) Peristaltic transport in circular cylindrical tubes. J Biomech 3(5):513–523

Macagno EO, Christensen J (1981) Fluid mechanics of gastrointestinal flow. In: Johnson LR (ed) Physiology of the gastrointestinal tract. Raven, New York, pp 335–58

Mayer EA (1994) The physiology of gastric storage and emptying. In: Johnson L (ed) Physiology of the gastrointestinal tract, 3rd edn. Raven, New York, pp 929–76

Meyer JH (1991) The physiology of gastric motility and gastric emptying. In: Yamada T (ed) Textbook of gastroenterology. J.B. Lippincott, Philadelphia, pp 137–57

Pal A, Indireshkumar K, Schwizer W, Abrahamsson B, Fried M, Brasseur JG (2004) Gastric flow and mixing studied using computer simulation. Proc Roy Soc B: Biol Sci 271 (1557):2587–2594

Pallotta N, Corazziari E, Scopinaro F, Bonino R, Schillaci O, Vignoni A, Mangano M, Torsoli A (1998) Noninvasive estimate of bile flux through the gallbladder in humans. Am J Gastroenterol 93:1877–85

Schubert ML, Makhlouf GM (1992) Neural, hormonal, and paracrine regulation of gastrin and acid secretion. Yale J Biol Med 65(6):553–560

Shapiro AH, Jaffrin MY, Weinberg SL (1969) Peristaltic pumping with long wavelengths at low Reynolds number. J Fluid Mech 37:799–825

Shen MC (1976) Asymptotic theory for peristaltic transport in a tube of arbitrary cross section. Phys Fluids 19(2):213–218

Soll AH, Berglindh T (1994) Receptors regulating acid secretory function. In: Johnson LR, Alpers DH, Christensen J, Jacobson ED, Walsh JH (eds) Physiology of the gastrointestinal tract, 3rd edn. Raven, New York, pp 1139–1158

Szurszewski JH (1981) Electrical basis for gastrointestinal motility. In: Johnson LR (ed) Physiology of the gastrointestinal tract. Raven, New York, pp 1435–1466

Zien TF, Ostrach S (1970) A long wave approximation to peristaltic motion. J Biomech 3(1):63–75

Chapter 6
State of the Art in Immobilized/Encapsulated Cell Technology in Fermentation Processes

Viktor A. Nedović, Verica Manojlović, Branko Bugarski, and Ronnie Willaert

6.1 Introduction

The process of sugar conversion from wort or malt into alcohol, carbon dioxide, and other components catabolized by yeast enzymes is called the alcohol fermentation process. In beverage production, it is of great importance to achieve a particular balance between different secondary metabolites. High productivity is another demand of the beverage industry. Immobilization of cells provides high cell densities leading to higher volumetric productivities, and as a consequence, reduces essential bioreactor sizes (decreased capital costs) and shortens residence times. Immobilized cell technology (ICT) coupled with continuous mode of fermentation offers additional benefits, like ease of biomass separation and recovery, simplification of process design, lower risk of microbial contamination of the pitching yeast population, greater efficiency in utilization of carbohydrates, and better use of equipment and potential savings. However, continuous fermentation processes have not been commercially successful due to many practical problems, such as increased risk of contamination not only during fermentation but also during storage of wort in supplementary holding tanks, which are usually required for batches upstream and downstream fermentation processes; in addition, there are variations in beverage flavor and poor understanding of the fermentation kinetics

V.A. Nedović (✉)
Department of Food Technology and Biochemistry, University of Belgrade, Nemanjina 6, P.O. Box 127, 11081 Belgrade-Zemun, Serbia
e-mail: vnedovic@agrif.bg.ac.rs

V. Manojlović and B. Bugarski
Department of Chemical Engineering, University of Belgrade, Karnegijeva 4, 11000 Belgrade, Serbia
e-mail: vmanojlovic@tmf.bg.ac.rs; branko@tmf.bg.ac.rs

R. Willaert
Structural Biology Brussels, Vrije Universiteit Brussel, Flanders Institute for Biotechnology, Pleinlaan 2, B-1050 Brussels, Belgium
e-mail: Ronnie.Willaert@vub.ac.be

J.M. Aguilera et al. (eds.), *Food Engineering Interfaces*, Food Engineering Series,
DOI 10.1007/978-1-4419-7475-4_6,

under continuous conditions. Over the last 30 years, ICT for alcoholic beverage production has been extensively investigated and some systems have already reached commercial exploitation. Intensification of a particular fermentation process using ICT can generally be industrialized if the acquired new characteristics result in a more economic system and the new technology can be readily scaled up. ICT processes have been designed for different stages in the beer fermentation process: wort acidification, primary fermentation, and bioflavoring during secondary fermentation; these fermentation processes are used in the production of alcohol-free or low-alcohol beers (Brányik et al. 2005; Nedovic et al. 2005a; Willaert and Nedovic 2006), as well as wine (Divies and Cachon 2005) and cider (Nedovic et al. 2000; Durieux et al. 2005). The most challenging complex application in fermentation processes is the combined main (ethanol fermentation) and secondary fermentation (maturation) processes.

Traditional beer fermentation technology uses freely suspended yeast cells to ferment wort in a non-stirred batch reactor. The traditional primary fermentation for lager beer takes approximately 7 days with a subsequent secondary fermentation (maturation) of several weeks. The resulting beer has a well-balanced flavor profile. Nowadays, large breweries use a selected specific yeast strain and elevated temperatures to accelerate production. This enables the production of finished lager beer in 12–15 days. ICT is able to produce lager beer in a much shorter time period (usually 1–3 days). A major difficulty is to achieve the correct balance of sensory compounds to create an acceptable flavor profile in such a short time frame. ICT for beer production can only be introduced successfully on an industrial scale if the flavor profile can be controlled and fine-tuned.

Cider and wine production also involves complex processes that imply transformation of apple juice in the case of cider, or grape juice in the case of wine, by activity of both yeast and lactic acid bacteria (LAB) to accomplish alcoholic and malolactic fermentations (MLFs). The traditional process consists of natural fermentation via autochthon yeasts and bacteria associated with the fruit or the cellar equipment. This natural process is very unpredictable in terms of desirable flavor compounds formation. The development of starter cultures enabled the use of selected strains and the control of cider production to achieve high and uniform quality, through several successive steps: pretreatment, alcoholic fermentation of sugars into ethanol proceeded by yeast strains, and malolactic fermentation (MLF), that is, bacterial conversion of L-malic into L-lactic acid and carbon dioxide (needed to reduce acidity). Spontaneous MLF of cider begins within a few hours if the temperature of the juice rises above 10°C. This process is usually very slow. It requires 2–3 weeks to accomplish the main fermentation and several months for the maturation. There is a risk of spontaneous fermentation by indigenous microbial flora and it is difficult to control the flavor formation. The initiation of MLF appears to be the main limiting factor in cider and wine production. MLF can occur several weeks after alcoholic fermentation but there is no guarantee it will occur, which is an unfavorable milieu for growth of microorganisms (ethanol $> 10\%$; pH < 3.0–3.5; temperature < 15°C). ICT offers a new alternative to better control of the microbiology that defines the final product. In addition, this new technology

significantly reduces consumption of time, facilitating MLF simultaneously with alcoholic fermentation or at the end of this process.

Key parameters of this technology are the selection of carrier materials and the method of immobilization together with the bioreactor design. Determination of these parameters is directed by operational conditions such as temperature, pH, substrate composition, and fluid dynamics, wherein special attention should be paid to mass transfer properties since limited nutrient supply can result in changes in yeast metabolism, leading to inadequate flavor of the final product.

6.2 Carrier Selection and Design

Cell immobilization can be classified into four categories based on the mechanism of cell localization and the nature of support material: (i) attachment to the support surface, which can be spontaneous or induced by linking agents; (ii) entrapment within a porous matrix; (iii) containment behind or within a barrier; and (iv) self-aggregation, naturally or artificially induced. Various supports and immobilization techniques have been proposed and tested for application in brewing and wine- and cider-making. Those that fulfill the following prerequisites are preferable:

- High surface-to-volume ratio of the immobilization support to achieve high cell loading capacity
- Simple procedure and non-harsh conditions under way during immobilization
- Mechanical stability (compression, abrasion) and chemical stability of the immobilization support
- Sterilization capability and regeneration of the immobilization support
- Cost-effectiveness of the support and immobilization process
- Suitability for conventional reactor systems
- Acceptance of immobilization support by consumers and avoidance of negative effects on final product (e.g., off-flavor formations)
- Retention of immobilized cell viability
- Avoidance of negative effects of cell immobilization on biological and metabolic activity of immobilized cells
- Easy separation of carriers with immobilized cells from media
- Wide choice of yeast
- Compounds approved for food applications

Table 6.1 Summarizes most of the carrier materials and bioreactors used in fermentation processes for alcoholic beverages.

6.2.1 Immobilization on Solid Carrier Surfaces

Cell immobilization by adsorption to a support material is a very popular method, because it is simple, easy to carry out, cheap, and fast. Microorganisms adsorb

Table 6.1 Carrier materials and reactor types for selected fermentation processes using immobilized cells

Carrier material	Reactor type	Type of fermentation	Product	Reference
Apple pieces	Fixed-bed	AF	Wine	Kourkoutas et al. 2001, 2002
γ-Alumina	Fixed-bed	AF	Wine	Bakoyianis et al. 1997; Loukatos et al. 2000
Ca-alginate beads	Fixed-bed	AF	Beer	Ryder and Masschelein 1985; White and Portno 1979; Onaka et al. 1985; Ryder and Masschelein 1985;
Ca-alginate beads	Gas-lift	AF	Beer	Nedovic et al. 1993, 1996, 2004, 2005a
Ca-alginate beads		AF	Sparkling wine	Fumi et al. 1987; Fumi et al. 1988
Ca-alginate beads	Fixed-bed	AF	Wine	Ferraro et al. 2000
Ca-alginate beads	Fixed-bed	AF and MLF	Cider	Simon et al. 1996
Ca-alginate beads	Fixed-bed	MLF	Cider	Cabranes et al. 1998
Ca-alginate beads	Fixed-bed	AF and MLF	Cider	Nedovic et al. 2000
Ca-alginate beads	Shaken flasks	MLF	Cider	Herrero et al. 2001
Ca-alginate beads	Fixed-bed	Maturation	Beer	Shindo et al. 1994
Ca-alginate beads	Gas-lift	AF	Beer	Smogrovicová et al. 1997; Smogrovicová and Dömény 1999
Ca-alginate beads	Shaken flasks	MLF	Wine	Kosseva et al. 1998
Ca-alginate beads	Shaken flasks	MLF	Wine	Kosseva and Kennedy 2004
κ-Carrageenan beads	Gas-lift	AF	Beer	Mensour et al. 1996, Mensour et al. 1997; Decamps et al. 2004
Ceramic beads	Fixed-bed	AF	Beer	Inoue 1995
Corncobs	Gas-lift	AF	Beer	Brányik et al. 2006
Chitosan	Shaken flasks	MLF	Wine	Kosseva et al. 1998
Chitosan	Fluidized-bed	AF	Beer	Unemoto et al. 1998; Maeba et al. 2000
DEAE-cellulose	Fixed-bed	AF	Beer	Kronlöf et al. 1989; Andersen et al. 1999
DEAE-cellulose	Fixed-bed	Maturation	Beer	Pajunen and Grönqvist 1994
DEAE-cellulose	Fixed-bed		Acidified wort	Pittner et al. 1993
DEAE-cellulose	Fixed-bed	MLF	Wine	Maicas, Pardo, and Ferrer 2001
DEAE-cellulose	Fixed-bed		Alcohol-free beer	Collin et al. 1991; Lommi 1990
Delignified cellulosic material	Fixed-bed	AF	Wine	Bardi and Koutinas 1994; Iconomou et al. 1996; Iconomopoulou et al. 2003
Delignified cellulosic material	Fixed-bed	MLF	Wine	Agouridis et al. 2005
Gluten pellets	Fixed-bed	AF	Beer	Bardi et al. 1997
Gluten pellets	Gas-lift (external-loop)	AF	Beer	Manojlovic et al. 2008
Gluten pellets	Fixed-bed	AF	Wine	Bardi et al. 1996; Iconomopoulou et al. 2002
Gluten pellets	Fixed-bed and MFBT	AF	Wine	Sipsas et al. 2009
Kieselguhr (diatomaceous earth)	Fixed-bed	AF	Beer	Narziss and Hellich 1971; Moll et al. 1973; Virkajärvi and Pohjala 2000
Kissiris	Fixed-bed	AF	Wine	Bakoyianis et al. 1992
	"in the bottle"	Maturation	Beer	Lemonnier and Duteurtre 1989;

(*continued*)

Table 6.1 (continued)

Carrier material	Reactor type	Type of fermentation	Product	Reference
Microfiltration membranes				
Microfiltration ceramic membranes	Membrane reactor	MLF	Cider	Lovitt et al. 2006
Orange pieces	Fixed-bed	AF	Wine	Plessas et al. 2007
Pear pieces	Fixed-bed	AF	Wine	Mallios et al. 2004
PVA beads	Gas-lift	AF	Beer	Smogrovicová et al. 2001
PVA beads	Fixed-bed	Maturation	Beer	Smogrovicová et al. 2001
PVA beads	Champagne bottles	AF	Champagne	Martynenko et al. 2004
PVA/alginate beads	MFBT	AF	Beer	Manojlovic et al. 2007
PVA Lentikats®	Gas-lift	AF	Beer	Smogrovicová et al. 2001; Bezbradica et al. 2007
Polyvinyl chloride granules	Fixed-bed	AF	Beer	Moll et al. 1973
Porous glass beads	Fixed-bed	AF	Beer	Virkajärvi and Krönlof 1998; Virkajärvi and Pohjala 2000
Porous glass beads	Fixed-bed	Maturation	Beer	Linko et al. 1993; Aivasidis 1996
Porous glass beads	Fixed-bed		Alcohol-free beer	Aivasidis et al. 1991
Quince pieces	Fixed-bed	AF	Wine	Kourkoutas et al. 2003
Raisin berries	Fixed-bed	AF	Wine	Tsakiris et al. 2004a, 2004b
Self-aggregation using super-flocculent yeast	Stirred-tank reactors	AF	Beer	Coutts 1957; Linko et al. 1997
Self-aggregation using yeast biocapsules	Erlenmeyer flasks	AF	Wine	Peinado et al. 2006; Peinado et al. 2005
Silicon carbide rods	Monolith reactor	AF	Beer	Van De Winkel et al. 1993; Andries et al. 1996
Silicon carbide rods	Monolith reactor		Alcohol-free beer	Van De Winkel et al. 1991
Spent grains	Gas-lift	AF	Beer	Brányik et al. 2002, 2004
Spent grains	Fixed-bed	AF	Beer	Kopsahelis et al. 2007
Spent grains	Fixed-bed	AF	Wine	Mallouchos et al. 2007
Sponge-like material	Fixed-bed	AF and MLF	Cider	Scott and O'Reilly 1996
Stainless-steel fiber cloth	Gas-lift	AF	Beer	Verbelen et al. 2006
Stainless-steel wire spheres	Fluidized-bed	AF	Beer	Cross and Mavituna 1987
Wood chips (Aspen)	Fixed-bed	AF	Beer	Pajunen et al. 2001
Wood chips (Beech)	Fixed-bed	AF	Beer	Linko et al. 1997; Kronlöf and Virkajärvi 1999
Watermelon pieces	Fixed-bed	AF	Wine	Veeranjaneya Reddy et al. 2008

PVA polyvinyl alcohol, *AF* alcoholic fermentation, *MLF* malolactic fermentation, *MFBT* multi-stage fixed-bed tower

spontaneously on a wide variety of organic and inorganic support materials. Binding of cells occurs through interactions such as Van der Waals forces, ionic bonds, hydrogen bridges, or covalent interactions. Microbial cells exhibit a dipolar character and behave as cations or anions depending on the cell type and environmental conditions, such as pH of the solution. The thickness of cell film usually ranges from one layer of cells to 1 mm or more. The strength with which the cells are bonded to the carriers as well as the depth of the biofilm varies from one system to another. Cell detachment and relocation readily occur, followed by establishment of equilibrium between adsorbed and freely suspended cells. Various rigid organic and inorganic support materials have been used in alcohol fermentation processes. Inorganic materials are cheap and abundant. Among the inorganic types, porous glass beads have been used successfully for primary beer fermentation (Tata et al. 1999) and beer maturation (Yamauchi et al. 1995), kissiris (a porous volcanic mineral found in Greece, similar to granite, containing 70% SiO_2,13% Al_2O_3, and other inorganic oxides) for wine (Kana et al. 1989), ethanol production (Bakoyianis et al. 1992), γ-alumina for wine-making (Kana et al. 1989; Loukatos et al. 2000), and stainless-steel wire spheres for ethanol production (Bekers et al. 1999). Various organic materials are suitable for immobilization in beverage production, such as diethylaminoethyl (DEAE) cellulose, delignified cellulosic material, wood, sawdust, delignified sawdust, gluten pellets, and spent grains, aimed at applications in packed-bed reactors. A micrograph of yeast cells immobilized on wood chips is shown in Fig. 6.1. Solid materials like glass and cellulose have been treated with polycations, chitosan, or other chemicals to obtain preformed carriers with enhanced adsorption ability (Norton and D'Amore 1994). In recent years, special attention has been paid to usage of fruit pieces, since they are of food-grade purity, and are easily accepted by consumers. Apple (Kourkoutas et al. 2001, 2002), quince (Kourkoutas et al. 2003), pear (Mallios et al. 2004), raisin berries (Tsakiris et al. 2004a, 2004b), grape skin (Mallouchos et al. 2002), orange (Plessas et al. 2007),

Fig. 6.1 Scanning electron microscope (*SEM*) photo of yeast cells immobilized on wood chips

and watermelon (Veeranjaneya Reddy et al. 2008) have been used so far as support materials for cells involved in fermentation processes.

6.2.2 Entrapment Within Porous Matrix

Entrapment involves containment of living cells within a network, which permits the diffusion of substrates and products, thereby making possible the growth and maintenance of active cells. Natural polysaccharides (e.g., alginate, pectate, carrageenan, chitosan, agar, polygalacturonic acid), synthetic polymers (polyvinyl chloride, polyvinyl alcohol (PVA) lens-shaped Lentikats, polyacrylamide), and proteins (gelatin, collagen) can be gelled into hydrophilic matrices under mild conditions, thus allowing cell entrapment with minimal loss of viability. Very high biomass loadings can be achieved, since gel systems are characterized by very high porosities (95–98%) and the cells are protected from fluid shear. Cell growth in the porous matrix depends on diffusion limitations imposed by the porosity of the matrix and the available interstitial space, which decreases in time with cell propagation and the accumulation of biomass. Available literature shows that the effective oxygen penetration rate varies in the range 0.08–010 mm in carrageenan beads (Huang et al. 1990) and 0.1–0.15 mm in alginate beads (Ogbonna et al. 1991). Cells that are growing can cause stress expressed in volumetric deformation and also partial disintegration of the hydrogel. It opens a new space for cell growth inside the matrix. This particular part of the process causes the mechanical transformation of the network. There are only a few reports on the relaxation effects of hydrogel caused by cell growth (a recent one is from Pajic-Lijakovic et al. 2007). Gels are mostly used in the form of spherical beads with diameters ranging from about 0.3 to 5 mm. Smaller particles show better mass transfer properties of nutrients and metabolic products. Moreover, reduction in bead size lowers the shear forces and may increase their long-term stability. However, small beads have larger surface-to-volume ratio compared to big particles and therefore can be more easily harmed by swelling or by exposure to oppositely charged ions (Strand et al. 2002). In addition, smaller spheres are more fragile to internal stresses caused by cell proliferation and expansion of cell colonies. Numerous techniques for bead production have been developed up to now and are available to achieve the desired size of capsules (Nedovic and Willaert 2004; Prusse et al. 2008). The use of synthetic hydrogels may allow design of a carrier/matrix with preferred characteristics. LentiKats® (specially designed particles made from PVA) have a specific lenticular shape (Fig. 6.2) due to which they combine the advantages of small (good diffusion properties) and large (easy retention and removal) beads. Production of LentiKats® particles is based on the usage of the specially designed LentiKats® Printer in lab and industrial scales. LentiKats® particles with immobilized yeast have been successfully used for beer fermentation performed in a gas-lift bioreactor (Bezbradica et al. 2007) and in cider production (Durieux et al. 2002). The design of synthetic materials that could balance the opposite demands of high open-pore

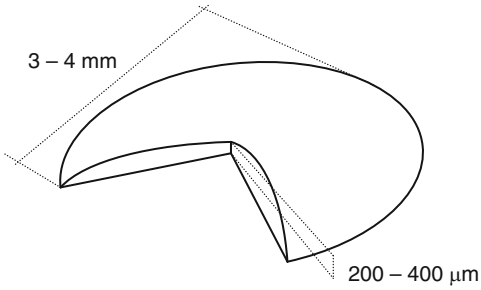

Fig. 6.2 LentiKats® hydrogel particle based on polyvinyl alcohol (*PVA*)

structure, and at the same time, provide good protection to cells against washout is a challenge for researchers involved in polymer science. One such attempt was the design of a synthetic double-layer hydrogel, where the core was made of hydroxyethylcellulose cryogel and then coated with a layer of poly(ethylene oxide) (Manojlovic et al. 2009).

A disadvantage of gels is the limited mechanical stability under conditions of rapid cell growth, excessive CO_2 production, or prolonged exposure to phosphates during the maturation process. Several methods have been proposed for reinforcement of gel structures. For example, alginate gel can be strengthened by reaction with polyethyleneimine, gluteraldehyde cross-linking, addition of silica, genepin, and PVA, or by partial drying of the gel (Willaert and Baron 1996). The major drawback in these systems is mass transfer limitation. However, understanding of mass transfer phenomena within entrapment matrices may allow one to simultaneously provide different conditions at the carrier surface and in the interior, which could be attractive for co-immobilization of different cell types performing consecutive processes. For example, gels with varying degrees of anisotropy, with respect to polymer concentration, can be formed by controlling the kinetics of the gel formation. Simply by adjusting the concentration of alginate and the cross-linking ions, the distribution of the polymer in the gel can be controlled; alginate beads with a capsular structure have been made without adding polycations or any other non-gelling polymer (Thu et al. 2000). Another way is to create an external layer of another polymer around the hydrogel core. Double-layer beads solve the problem of escaping of cells out of beads when the system also contains (besides immobilized cells) free ones. However, microencapsulation is generally too expensive to be used in the beverage industry.

Porous preformed supports can be inoculated directly from the bulk medium. In these systems, cells are not completely separated from the effluent, similarly as in the adsorption method. Cell immobilization occurs by attachment to the internal surfaces, self-aggregation, and retention in dead-end pockets within the material (Baron and Willaert 2004). Ideally, the colonized porous particles should retain some void spaces for flow so that mass transport of substrates and products can be achieved by both molecular diffusion and convection. Consequently, mass transport limitations are less stringent under optimal conditions as compared to gel entrapment methods. However, when high cell densities are reached, convection is no longer possible and the particles behave as dense cell agglomerates with high diffusion limitations.

As compared to gel particles, preformed carriers provide better mechanical properties and higher resistances to compression and disintegration.

6.2.3 Cell Aggregation

Cell immobilization by self-aggregation is based on formation of cell clumps or floccules, which can be naturally occurring as in the case of flocculent yeast strains, or induced by addition of artificial flocculating agents or cross-linkers. It is the simplest and the least expensive immobilization method. However, interactions among cells are not easily controlled and cell aggregates are very sensitive to conditions in fermentors, including pH, dissolved oxygen, and medium composition. The flocculation of *Saccharomyces cerevisiae* is determined by the adhesin protein family. The adhesin proteins are encoded by the genes *FLO1*, *FLO5*, *FLO9*, and *FLO10* (Verstrepen et al. 2003a, 2004). These proteins are called flocculins (Caro et al. 1997) because they promote cell–cell adhesion forming multicellular clumps that settle out of solution. The structure, location, and activity of flocculins are well described in a recent report from Van Mulders et al. (2009). The ethanol productivity achieved by flocculated cells was almost double that of a freely suspended yeast cell system (Xu et al. 2005). It was found that the floc size distribution influenced the effectiveness of glucose uptake and ethanol production (Ge et al. 2006). An interesting approach has been recently proposed by Peinado and coworkers (2005, 2006): a filamentous fungus and a flor yeast under adequate conditions form a cluster that looks like a hollow biocapsule; here mycelium creates walls around the biocapsule and the yeast is entrapped in an inner space. The yeast biocapsules were successfully used in must (wine) fermentation.

6.2.4 Containment Behind a Membrane Barrier

Cell immobilization behind or within a porous barrier includes systems with cells contained in a compartment separated by a preformed membrane such as hollow fiber and flat membrane modules. Micromembrane technology, like microencapsulation, is generally too expensive to be used in beverage production. Moreover, mass transfer limitations are relatively high (Lebeau et al. 1997), and membrane biofouling caused by cell growth often occurs (Gryta 2002).

6.3 Bioreactor Design

Selecting the appropriate reactor type or configuration for an immobilized cell system is related to a number of important factors, such as carrier design, supply and removal of gases and solutes in the liquid phase, as well as removal of excess

biomass formed, investment and operation costs, operation mode, maintaining sterile conditions, heat and mass transfer rates, and others. In fermentors, immobilized cells can be either mixed with suspended carriers or localized on carrier particles/surfaces, which are then fixed or in movement. The operation mode of immobilized cell reactors can be batch, fed-batch, or continuous. Continuous operation eliminates the unproductive time in batch and fed-batch processes associated with filling, emptying, cleaning and disinfection/sterilization, and start-up phase of the fermentation. Therefore, it provides a higher productivity compared to the "old-fashion" batch method of processing. With respect to sterility, reactors that can be directly inoculated with cells or cell-aggregates (e.g., membrane modules or reactors packed with preformed porous carriers) are more desirable compared to reactors that require transfer of a biocatalyst from the immobilization equipment to the reactor (e.g., fermentors using cells entrapped in gel systems). The bioreactor should be designed and the hydrodynamic conditions optimized to provide easy access to nutrient media, optimum mass transfer from flowing media to the support interior, controlled yeast growth, low shear experienced by cells, simple scale-up, controlled oxygenation, complete attenuation and desired flavor profile, consistent product quality, and low risk of contamination.

Most of the studies have been on packed-bed (fixed-bed) bioreactors. Packed-bed bioreactors are characterized by a simple design consisting of a single column packed with biocatalysts. The liquid flow is close to the plug flow regime and causes low shear rates (Obradovic et al. 2004). The main disadvantages of packed-bed fermentors are high mass transfer restrictions, accumulation of carbon dioxide, non-uniform temperature profiles, flow channeling, and stagnant zones. Therefore, the first trials conducted on using a packed-bed configuration for primary beer fermentation on an industrial scale gave unsatisfactory results with respect to product quality. Afterwards, packed-bed reactors were selected for production of alcohol-free or low-alcohol beers and for enhanced flavor maturation using immobilized cells. In these applications, conditions are anaerobic and yeast growth is limited. Immobilization of cells can be by adsorption (e.g., DEAE-cellulose beads) or by a combination of adsorption and entrapment (e.g., porous glass beads). These carrier materials need to be mechanically strong to withstand the high pressures in packed-bed reactors. However, the use of mechanically week materials (e.g., hydrogels) can be limited to lower bed heights and liquid flow rates due to possible compression of beads. In order to eliminate some of the drawbacks of the packed-bed configuration, a modification of a packed-bed fermentor, that is, the "multistage fixed-bed tower" (MFBT), has been proposed for beer production (Manojlovic et al. 2007) and wine-making (Sipsas et al. 2009). It consists of a vertical cylindrical tank with five packed sections containing freeze-dried immobilized cells. A relatively small (5000–10000 L) MFBT bioreactor (Fig. 6.3) (Koutinas et al. 1997; Loukatos et al. 2000) was proposed for industrialization of immobilized cells in wine-making. Handling of the support at this scale could be performed without any problems, and cell immobilization could be carried out in the bioreactor. The application of the MFBT bioreactor on an industrial scale eliminates insufficient mass transfer and enables support

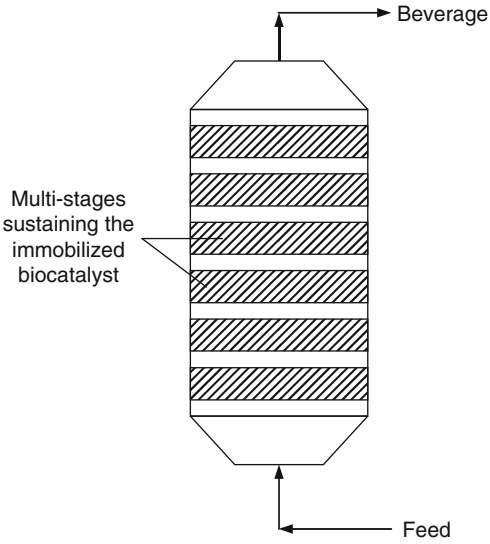

Fig. 6.3 Multistage fixed-bed tower (*MFBT*) bioreactor (Adapted from Sipsas et al. 2009)

division, especially when mechanically unstable supports are used to minimize high pressure effects, which may result in support destruction and reduction of fermentation activity (Kourkoutas et al. 2009). Experiments concerning long-term storage of the immobilized biocatalysts (Kourkoutas et al. 2003) are very promising, since the preparation of new biocatalysts, emptying and filling of the bioreactor, could be avoided when industrial production is halted. Taking into consideration the above discussion of technical problems, the scale-up of the proposed technology seems feasible.

Different approaches for the adaptation of bioreactors containing immobilized cells were investigated in order to correct the final beverage quality. One was to establish biocatalyst movement or circulation for the purpose of speeding up the transfer of nutrients and metabolic products through the fermenting medium, as in fluidized-bed, stirred-tank, and gas-lift bioreactors. In the fluidized-bed bioreactors, particles with immobilized cells are fluidized in the liquid up-flow, while gas can be optionally supplied. As a consequence of particle fluidization, moderate local mixing is established, which provides better mass and heat distribution with more uniform liquid flow throughout the reactor volume, as compared to packed-bed reactors. It is difficult to maintain low-density particles in fluidization and to prevent their washout. Particle movements and collisions in the fluidized state result in moderate shear stresses and abrasion, creating a need for relatively mechanically stable supports (Obradovic et al. 2004). The scaling up of fluidized-bed bioreactors addresses problems due to the difficulties in controlling the bed expansion and may encounter hydrodynamic problems. In stirred tank reactors high aeration resulted in a less balanced aroma profile of the final product. Beers produced in fluidized and stirred-tank fermentors had high concentrations of diacetyl and low concentrations of higher alcohols and esters (Okabe et al. 1992; Mensour et al. 1997).

Gas-lift reactors are especially attractive since they apply pneumatic agitation with no mechanical devices. They are based on liquid circulation, which can be effectively tuned to achieve an adequate flow regime and optimal external mass transfer. This bioreactor concept was introduced in beer fermentation studies by a Serbian group in 1993 (Nedovic et al. 1993). Internal loop configuration (Fig. 6.4) has been investigated in lab- and pilot-scale production mainly for beer fermentation (Nedovic et al. 1993, 2004, 2005a; Mensour et al. 1997), while the external loop design (Fig. 6.5) has been recently tested for alcoholic fermentation in lab-scale beer production (Manojlovic et al. 2008). Efficient mixing and low shear rates make gas-lift reactors suitable for all types of low-density immobilization materials (Mensour et al. 1997; Obradovic et al. 2004).

The design of membrane reactors is relatively complex and expensive, mainly due to the high cost of the membrane material. Membrane reactors provide simultaneous bioconversion and product separation. A special design of a multichannel loop bioreactor has been developed by the Belgian company, Meura (Tournai), for production of lager, ale, and acidified wort (Masschelein et al. 1994). Yeast cells are

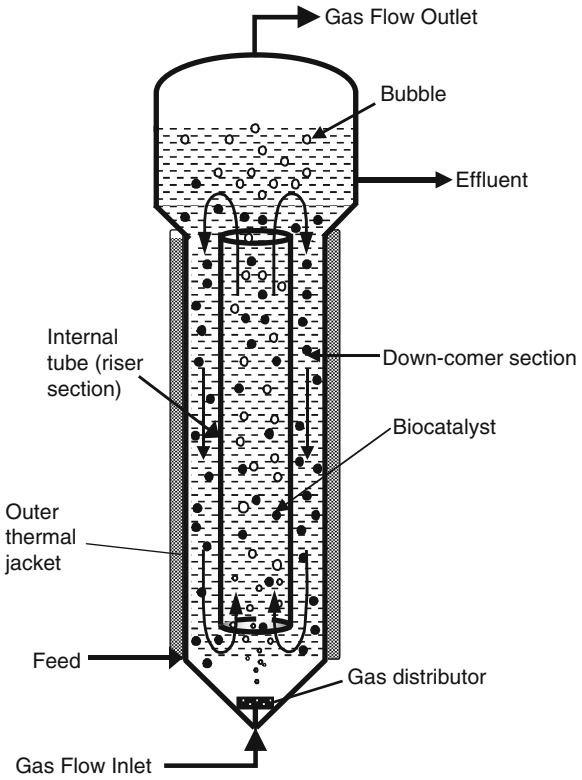

Fig. 6.4 Gas-lift bioreactor internal loop configuration with an immobilized biocatalyst (Adopted from Nedovic et al. 1993)

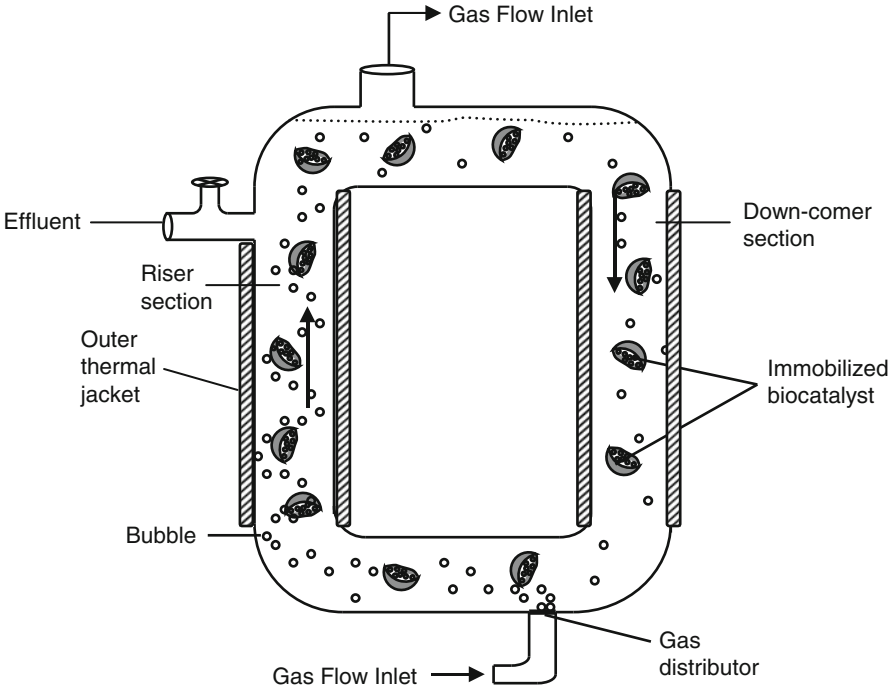

Fig. 6.5 Gas-lift bioreactor external loop configuration with an immobilized biocatalyst (Adapted from Manojlovic et al. 2008)

immobilized in porous sintered silicon carbide rods perforated with 19 or 37 channels for fluid flow. This immobilization method can be regarded as containment behind a preformed barrier, and as entrapment in a porous preformed support. Continuous beer fermentation technology using yeast flocculation and cell recycling has been successfully exploited over almost 40 years by Dominion Breweries in New Zealand (Coutts 1957; Van de Winkel and De Vuyst 1997).

Selected yeasts entrapped in micro-filtration membranes have been developed and used in wine production. On-market available "Millispark" cartridges (Millipore) were used for secondary fermentation of sparkling wine in bottles (Lemonnier and Duteurtre 1989). In dry wine production, a single-vessel membrane bioreactor was found unsuitable for continuous fermentation, as high levels of unfermented sugars were reported (Takaya et al. 2002). However, a double-vessel continuous membrane configuration resulted in a sugar content lower than 4 g/L, which was considered satisfactory for dry wine-making. Additionally, wine productivity was 28 times higher compared to traditional batch systems.

In a recent study, the approach of splitting cell propagation and cell maturation was applied in a pilot-scale membrane bioreactor with ceramic membrane modules to perform MLF of media containing ethanol (Lovitt et al. 2006). Herein, the overall productivity of both process rate and longevity was successfully increased.

6.4 Impact of Immobilization on Flavor Formation

Although ICT offers a number of benefits, it has so far found limited application in the fermentation industry. A major difficulty is to achieve the correct balance of volatile compounds to create an acceptable flavor profile of alcoholic beverages. Immobilized cells appear to have modified physiology compared to the physiology of free cells. The nutrient uptake and synthesis patterns of metabolites such as fusel alcohols, esters, and carbonyl compounds change upon immobilization; the following paragraphs describe the impact of immobilization on flavor formation.

6.4.1 Influence of ICT on Higher Alcohol Production

Higher alcohols (also called "fusel alcohols") are produced by yeast cells and represent the major fraction of the volatile compounds. Higher alcohols can be classified as aliphatic [n-propanol, isobutanol, 2-methyl butanol (or active amyl alcohol), 3-methyl butanol (or isoamyl alcohol)], and aromatic (2-phenyl ethanol, tyrosol, tryptophol). Aliphatic higher alcohols contribute to the "alcoholic" or "solvent" aroma of a beverage, and produce a warm mouthfeel. The aromatic alcohol 2-phenyl ethanol has a sweet scent and is a positive contribution to the aroma, whereas the aroma of tyrosol and tryptophol are undesirable. Higher alcohols are synthesized by yeast during fermentation via the catabolic (Ehrlich) and anabolic pathway (amino acid metabolism) (Ehrlich 1904).

Catabolism of the branched-chain amino acids (leucine, valine, and isoleucine), aromatic amino acids (phenylalanine, tyrosine, and trytophan), and sulfur-containing amino acid (methionine) leads to the formation of fusel acids and fusel alcohols. Firstly, the yeast cells use amino acids from the wort to produce the corresponding α-keto acids via a transamination reaction. The excess oxoacids are subsequently decarboxylated into aldehydes and further reduced (by alcohol dehydrogenase) to higher alcohols. The simplified Ehrlich pathway is shown in Fig. 6.6. The genes encoding each step of the process are quoted in a recent review by Hazelwood et al. (2008).

In the anabolic pathway, the higher alcohols are synthesized from α-keto acids during the synthesis of amino acids from the carbohydrate source. Both pathways may take place during the same fermentation in the traditional batch process with a switch from the degradative route to the biosynthetic route, occurring when the amino acids in the substrate have been metabolized or missed. The pathway choice depends on the individual higher alcohol and on the level of available amino acids. The importance of the anabolic pathway increases during the later stage of a conventional batch fermentation as wort amino acids are depleted, as well as in cider production where the apple juice contains only small amounts of amino acids.

Conditions that promote yeast cell growth – such as high levels of nutrients (amino acids, oxygen, lipids, zinc), increased temperature, and agitation – stimulate

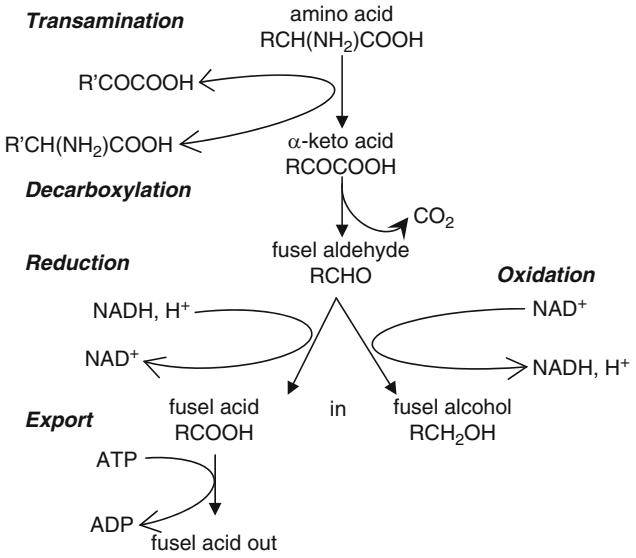

Fig. 6.6 The Ehrlich pathway (Adapted from Hazelwood et al. 2008)

the production of higher alcohols (Landaud et al. 2001). On the other hand, conditions that restrict yeast growth – such as lower temperature and higher (CO_2) pressure – reduce the extent of higher alcohol production (Renger et al. 1992).

In immobilized systems with enhanced or similar free amino nitrogen (FAN) uptake levels, the formation of higher alcohols was higher or equal to batch systems (Shen et al. 2003). A decrease of higher alcohol production in beer upon cell immobilization, compared to free-cell fermentation, has been frequently reported and nicely summarized by Willaert and Nedovic (2006). This decrease has been attributed to the limited cellular growth in immobilized cell systems, leading to poor nitrogen removal. Similarly, in the case of cider production, in a continuous fermentation system with *Saccharomyces bayanus* co-immobilized with *Oenococcus oeni* in alginate beads, production of fusel alcohols was several times lower compared to synthesis during batch fermentation process with suspended cells (Nedovic et al. 2000). The anabolic flux limitation of yeast cells in the pseudo-stationary phase was proposed to justify the lower concentration of fusel alcohols. It was also found that the behavior of cells adsorbed on the carrier surface was similar to that of free cells, but significantly different from entrapped cells (Smogrovicová and Dömeny 1999). New technologies have introduced some new inclusion carriers, with adjusted shape and size to overcome internal mass transfer restrictions, which give similar higher alcohol concentrations, compared to a conventional process (Nedovic et al. 2005b).

It has been demonstrated that mass (i.e., amino acids) transfer rates in the fermenting medium or, in other words, the external mass transfer properties, also

influence higher alcohol synthesis. Thus, in fluidized-bed and gas-lift bioreactors the rate of amino acid uptake increased with the superficial velocity of the fluid (Cop et al. 1989; Masschelein et al. 1994; Nedovic et al. 1996; Aivasidis et al. 1991).

6.4.2 Ester Production in ICT Systems

Esters constitute a major group of desirable flavor compounds. Among the esters formed, the most significant in fermented beverages are ethyl acetate (fruity, solvent-like), isoamyl acetate (pear drops), isobutyl acetate (banana-like), ethyl hexanoate (apple-like), and 2-phenyl acetate (honey, fruity, flowery). They are formed by yeast during fermentation in a reaction between the alcohols, fatty acids, co-enzyme A (CoASH), and an ester synthesizing enzyme. Actually, the formation of esters occurs in two steps: (1) fatty acids that have undergone a previous activation by CoASH form acyl-CoA and (2) alcohols become esterified by reacting with acyl-CoA to the corresponding ester under the action of alcohol acetyl transferase (Peddie 1990). Because ethanol is the dominant alcohol in fermenting beverages, ethyl acetate (produced from acetyl-CoA and ethanol) is the dominant ester. It has been shown that the main factor controlling ester biosynthesis is the expression level of the *ATF1* gene, which encodes alcohol acetyl transferase I (Lilly et al. 2000; Verstrepen et al. 2003b). *ATF1* gene expression is repressed by oxygen and unsaturated fatty acids (Fujii et al. 1997; Fujiwara et al. 1998). The ester production rate is influenced by many factors, such as temperature, specific growth rate, pitching rate, top pressure, oxygen availability, as well as fermenting medium composition (Willaert and Nedovic 2006; Verbelen et al. 2009).

In some immobilized processes low ester concentrations are found, while in others ester synthesis is increased upon cell immobilization. Low ester content is related to the low cellular metabolic activities in these systems. In a study of continuous fermentation in cider, concentration of isoamylacetate was two times lower compared to concentration achieved in a control batch fermentation process with suspended cells, as a result of isoamylalcohol availability (Nedovic et al. 2000). On the other hand, due to mass transfer limitations, oxygen concentration in an immobilization matrix is low, causing reduced cellular growth, so that the cellular acetyl-CoA pool is more available for ester synthesis instead of channeling for fatty acid biosynthesis. Thus, the anaerobic conditions and the absence of substantial levels of unsaturated fatty acids limit cell growth during production and stimulate formation of acetate esters. For example, this occurred during the production of alcohol-free beer in a packed-bed reactor with surface-attached cells on DEAE-cellulose beads (Van Iersel et al. 1999). In another study, a 22% increase in ester concentration upon cell immobilization on stainless-steel fiber cloth was explained by a significant rise in the expression level of *AFT1* in the immobilized cells, leading to enhanced ester concentrations in the final fermented product (Shen et al. 2003).

6.4.3 Carbonyl Compounds Production in ICT Systems

The most important carbonyl compounds formed in beverage fermentation are acetaldehydes, diacetyl, and 2,3-pentanedione. Aldehydes, having very low flavor thresholds, tend to be considered as off-flavors (e.g., acetaldehyde causes a green leaf-like flavor in beer). As intermediates in the formation of ethanol and higher alcohols from amino acids and sugar, the conditions favoring alcohol production also generate the formation of small quantities of aldehydes. These may be excreted but can be reabsorbed and reduced by yeast to the corresponding alcohol during the later stages of fermentation (acetaldehyde is normally reduced to ethanol). The most extensively studied carbonyl compound is diacetyl, which makes an important contribution to the flavor of cider, red wine, beer, and some distilled products such as whisky and rum. Although its presence may contribute to the correct flavor, especially in cider and red wine, excessive production can lead to off-flavors, particularly in the case of beer. Diacetyl and 2,3-pentanedione are side products of amino acid synthesis in yeast. They are produced by the spontaneous oxidative decarboxylation of the corresponding acetohydroxy acids, α-acetolactate, and α-acetohydroxybutyrate, which are metabolite intermediates of the common biosynthetic pathways of valine and isoleucine. Acetohydroxy acids are firstly excreted from the yeast cells to the surrounding medium where they are transformed chemically into diacetyl and 2,3-pentanedione. The formation and subsequent reassimilation of actohydroxy acids by the yeast and degradation of diacetyl are shown schematically in Fig. 6.7. Due to the coupling of acetohydroxy acids with the anabolic metabolism of yeast, they are produced only in the earlier phases of batch fermentation. In the later stages of fermentation, actively metabolizing yeast cells are able to reduce diacetyl and 2,3-pentanedione to acetoin and butane-2,3-dione, and 2,3-butanediol, respectively. Hence, the balance between rate of formation and rate of degradation determines the final concentrations of diacetyl and 2,3-pentanedione in beverages. In cider, in addition to the formation of vicinal diketones by yeast, a part of diacetyl present is also produced by bacteria from pyruvic acid. Thus, *Oenococcus oeni* is able to produce diacetyl directly by the activity of the diacetyl synthetase without any excretion of precursors in the fermenting medium.

In the case of diacetyl content in beer, different phenomena upon immobilization have been reported. In most cases, the production of diacetyl by immobilized cells is much higher than for free cells. In addition, the production of vicinal diketones can be controlled by the initial yeast cell concentration in Ca-alginate beads (Shindo et al. 1994). This has been explained by an increased expression of the acetohydroxy acid synthetase gene during the growth of the yeast cells in the carrier (Shindo et al. 1994). In a recirculation bioreactor system with continuous sugar feed, the concentration of 2,3-pentanedione was two to four times larger than the diacetyl concentration due to a more intensive pentanedione pathway (Pajunen et al. 2001). In an air-lift reactor with spent grains as the immobilization matrix, the total diacetyl concentration largely varied depending on the operational conditions and decreased with increasing aeration and temperature (Brányik et al. 2004).

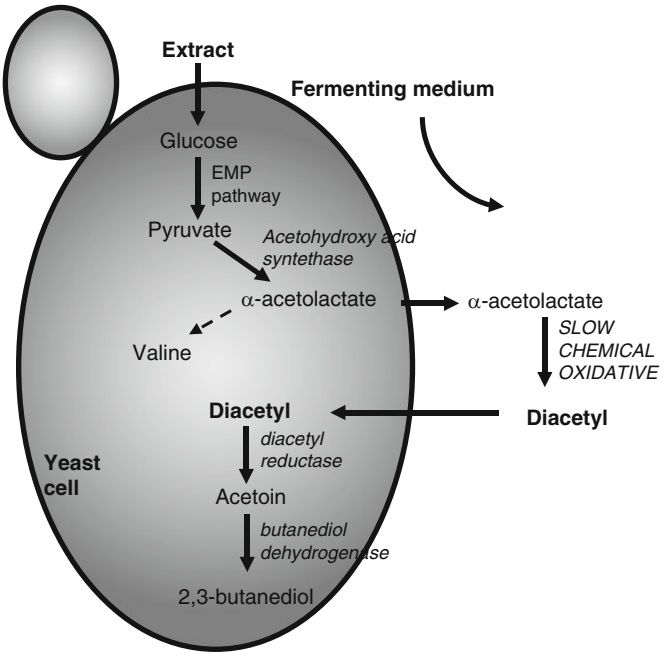

Fig. 6.7 Schematic presentation showing diacetyl formation, reassimilation, and removal (Adapted from Willaert and Nedovic 2006)

After a maturation period of 10 days at 4°C, the concentration of diacetyl was reduced below its flavor threshold (Brányik et al. 2002). The concentrations of vicinal diketones were around 20 times higher in a continuous fermentation of cider with yeast immobilized in Lentikats at a sugar attenuation of 95% compared with those obtained in a batch process (Durieux et al. 2002). In another study with alginate beads used for cider production in the same continuous system, diacetyl concentration was increased two times compared to concentration achieved in a fermentation process with suspended cells (Nedovic et al. 2000). The larger concentration of diacetyl in the immobilized systems was explained by the diffusion mass transfer effect that prevents transfer of diacetyl from the medium to the immobilized yeast after chemical oxidative decarboxylation of α-acetolactate in the medium. Addition of the missing enzyme α-acetolactate decarboxylase (commercially available) to the wort may also lead to increased formation of diacetyl (Hanneman 2002).

The drawback in using alginate is biomass leakage due to local overpressure in the beads generated by carbon dioxide production. Nedovic and coworkers (2004, 2005a) suggested that free yeast issued from the continuous reactor could be used for diacetyl uptake in a maturation tank. Optimization of the operational parameters in a gas-lift bioreactor with alginate microbeads as yeast carriers can provide low concentrations of diacetyl. One way to decrease the diacetyl level in a continuous

system is to prolong the residence time during fermentation and/or maturation process (Andersen et al. 1999; Nedovic et al. 2000). Also the use of genetically modified yeast enables reduction of the diacetyl level (Hammond 1995).

6.4.4 *Secondary Fermentation Using ICT*

The maturation of green beer is needed primarily to reduce the level of diacetyl (an unwanted aroma compound in beer). This vicinal diketone has a very low threshold (0.08–0.15 ppm) in beer (Wainwright 1973). The traditional maturation process lasts for 3–4 weeks at a low temperature and low yeast concentration. However, using ICT, this period could be reduced to 2 h. So far, two continuous maturation systems have been implemented industrially. The first one is a packed-bed bioreactor with DEAE-cellulose granules (later replaced by cheaper aspen wood chips) used at Sinebrychoff Brewery (Finland); it has a capacity of 1 million hectoliters/year (Yamauchi et al. 1995; Virkajärvi 2002). Another system was developed by Alfa Laval and Schott Engineering (Mensour et al. 1997) based on porous glass beads (Dillenhofer and Ronn 1996). The Alfa Laval system for secondary fermentation of beer is shown in Fig. 6.8. This system has been implemented in several breweries in Finland, Belgium, and Germany. The German company Brau & Brunnen purchased and installed a 30,000 hL/year pilot-scale Alfa Laval

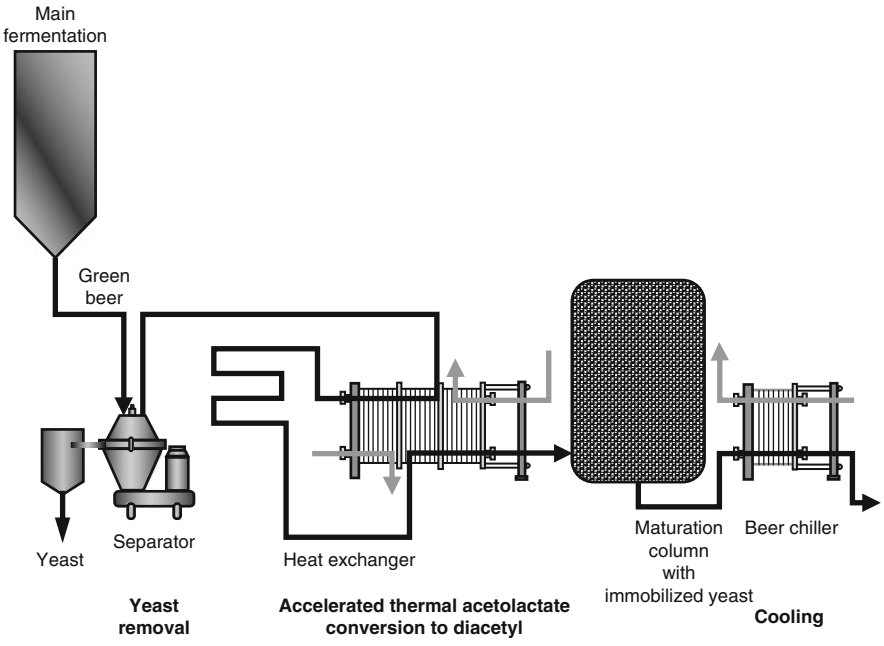

Fig. 6.8 Process flow sheet for secondary fermentation of beer using the Alfa Laval system

maturation system in 1996 (Mensour et al. 1997). The same system was implemented in a medium-sized German brewery as well (Schäff/Treuchtlingen) (Back et al. 1998). The beers obtained overall yielded good analytical and sensorial results.

6.4.5 Malolactic Fermentation in ICT Systems

MLF is a very important process in the maturation of alcoholic beverages, particularly wines and ciders. The fermentation is catalyzed by a number of LAB that can gain a competitive advantage by metabolizing malic acid to lactic acid. MLF is generally recognized as an important manufacturing step: (1) it reduces the acidity of wine or cider, (2) it stabilizes the product with respect to microbial spoilages through the bacteriostatic effect of the lactic acid produced and consumption of residual substrates, and (3) it contributes to the flavor complexity of wine/cider by producing compounds such as acetaldehyde, acetic acid, ethyl acetate, ethyl lactate, diacetyl, acetoin, and 2,3-butanediol. The MLF process, therefore, not only affects the flavor of the beverage, but also stimulates growth or enhances resistance to the extreme environment found in wines and ciders, for example, low pH and high alcohol concentration. Whether MLF should be encouraged or discouraged in wine-making depends on the quality of ripe grapes and the desired level of certain flavorful by-products.

The growth of LAB, that is, *O. oeni* and *Lactobacillis brevis*, has been investigated in this context. The initiation of MLF appears to be the main limiting factor in cider and wine production. Several strategies have been suggested to sustain and accomplish MLF in wine and cider: the use of enzymatic reactors, recombinant yeast strains, and cell-recycle bioreactors (Durieux et al. 2005). The immobilization of LAB for controlling MLF provides increased tolerance of malolactic bacteria and acceleration of the MLF process. Different immobilization supports have been used so far to immobilize *O. oeni*, such as calcium alginate, kappa-carrageenan, cellulose sponge, and polyacrylamide (reviewed by Kourkoutas et al. 2009).

The immobilization of *O. oeni* enabled accomplishment of MLF simultaneously with the alcoholic fermentation or at the end of this fermentation. The alcoholic fermentation was preceded either by free (Cabranes et al. 1998) or co-immobilized yeast cells in batch (Scott and O'Reilly 1996) and continuous (Nedovic et al. 2000) bioreactor systems. Yeast growth and ethanol production were not affected by the presence of immobilized *O. oeni*. The final organoleptic profile of cider depended on the fermentation temperature and the carrier used.

Thus, in the case of alginate beads, malic acid was fully metabolized at 18°C, while a residual amount of this acid was detected at 12°C (Cabranes et al. 1998). Acetic acid produced at the end of fermentation at 18°C was doubled compared to that obtained by free *O. oeni*. In another study, using Lentikats as an alternative to alginate beads in a continuous system, the largest malic acid attenuation was achieved at temperatures between 25°C and 30°C (Durieux et al. 2000). Surprisingly,

the malic acid conversion was possible even at very acidic pH (down to pH 2.3), while with free cells the MLF did not occur below 3.9. A modification of the cell physiology and the immobilized cell microenvironment, characterized by pH gradient inside the matrix, was proposed to explain the improved performance of *O. oeni* at acidic pH by respectively allowing generation of enough adenosine triphosphate (ATP) to maintain cytoplasmic pH without any perturbation of the MLF and by restoring favorable pH in the direct environment of the cells. In continuous systems, deacidification levels can be easily adjusted as a function of the residence time (Nedovic et al. 2000). In those systems, the production of soft or dry cider is possible by controlling the feeding flow rates.

6.5 Conclusion

In this chapter, an overview of ICT applications in fermentation processes aimed at alcoholic beverage production was presented. The objective was to analyze and assess data on the impact of immobilization technologies on viable microbial cells in the alcoholic and malolactic fermentation of beer, wine, and cider. ICT is well established for flavor maturation and the production of alcohol-free and low-alcohol beer on an industrial scale. In addition, several primary beer and wine fermentation processes based on ICT have been developed on a pilot and an industrial scale. However, the issues of mass transfer limitations and process control still need to be resolved in order to obtain a beverage of consistent quality. Selecting a suitable carrier and bioreactor system is a challenge and many issues should be taken into account, such as maintenance of cell viability during production, product quality, safety and stability during processing and storage, and investment and operating costs. In particular, assessment of industrial feasibility of the immobilization fermentation technology is mandatory for cost-effective, large-scale applications.

References

Agouridis N, Bekatorou A, Nigam P, Kanellaki M (2005) Malolactic fermentation in wine with *Lactobacillus casei* cells immobilized on delignified cellulosic material. J Agric Food Chem 53(7):2546–2551

Aivasidis A (1996) Another look at immobilized yeast systems. Cerevisia 21(1):27–32

Aivasidis A, Wandrey C, Eils HG, Katzke M (1991). Continuous fermentation of alcohol-free beer with immobilized yeast cells in fluidized bed reactors. Proc. 23rd EBC Cong., pp 569–576

Andersen K, Bergin J, Ranta B, Viljava T (1999). New process for the continuous fermentation of beer. Proc. 27th Eur. Brew. Conv. Cong. EBC, pp 771–778

Andries M, Van Beveren PC, Goffin O, Masschelein CA (1996) Design and application of an immobilized loop bioreactor for continuous beer fermentation. In: Wijffels RH, Buitelaar RM, Bucke C, Tramper J (eds) Immobilized cells: basics and applications. Elsevier, Amsterdam, pp 672–678

Back W, Krottenthaler M, Braun T (1998) Investigations into continuous beer maturation. Brauwelt International 3:222–226

Bakoyianis V, Kanellaki M, Kaliafas A, Koutinas AA (1992) Low temperature wine making by immobilized cells on mineral kissiris. J Agric Food Chem 40:1293–1296

Bakoyianis V, Koutinas AA, Agelopoulos K, Kanellaki M (1997) Comparative study of kissiris, γ-alumina, and calcium alginate as supports of cells for batch and continuous wine-making at low temperatures. J Agric Food Chem 45:4884–4888

Bardi EP, Bakoyianis V, Koutinas AA, Kanellaki M (1996) Room temperature and low temperature wine making using yeast immobilized on gluten pellets. Process Biochem 31:425–430

Bardi EP, Koutinas AA (1994) Immobilization of yeast on delignified cellulosic material for room temperature and low-temperature wine making. J Agric Food Chem 42:221–226

Bardi E, Koutinas AA, Kanellaki M (1997) Room and low temperature brewing with yeast immobilized on gluten pellets. Process Biochem 32:691–696

Baron GV, Willaert RG (2004) Cell immobilisation in pre-formed porous matrices. In: Nedovic V, Willaert R (eds) Fundamentals of cell immobilisation biotechnology. Springer, Dordrecht, The Netherlands, pp 229–244

Bekers M, Ventina E, Karsakevich A, Vina A, Rapoport A, Upite D, Kaminska E, Linda R (1999) Attachment of yeast to modified stainless steel wire spheres, growth of cells and ethanol production. Process Biochem 35:523–530

Bezbradica D, Obradovic B, Leskosek-Cukalovic I, Bugarski B, Nedovic V (2007) Immobilization of yeast cells in PVA particles for beer fermentation. Process Biochem 42 (9):1348–1351

Bránýik T, Silva DP, Vicente AA, Lehnert R, Almeida e Silva JB, Dostálek P, Teixeira JA (2006) Continuous immobilized yeast reactor system for complete beer fermentation using spent grains and corncobs as carrier materials. J Ind Microbiol Biotechnol 33:1010–1018

Bránýik T, Vicente AA, Cruz JMM, Teixeira JA (2002) Continuous primary beer fermentation with brewing yeast immobilized on spent grains. J Inst Brew 108:410–415

Bránýik T, Vicente AA, Cruz JMM, Teixeira JA (2004) Continuous primary fermentation of beer with yeast immobilized on spent grains – the effect of operational conditions. J Am Soc Brew Chem 62:29–34

Bránýik T, Vicente AA, Dostálek P, Teixeira JA (2005) Continuous beer fermentation using immobilized yeast cell bioreactor systems. Biotechnol Prog 21(3):653–663

Cabranes C, Moreno J, Mangas JJ (1998) Cider production with immobilized *Leuconostoc oenos*. J Inst Brew 104:127–130

Caro LH, Tettelin H, Vossen JH, Ram AF, van den Ende H, Klis FM (1997) In silicio identification of glycosyl-phosphatidylinositol-anchored plasma-membrane and cell wall proteins of *Saccharomyces cerevisiae*. Yeast 13:1477–1489

Collin S, Montesinos M, Meersman E, Swinkels W, Dufour JP (1991) Yeast dehydrogenase activities in relation to carbonyl compounds removal from wort and beer. Proc. Eur. Brew. Conv. Cong., pp 409–416

Cop J, Dyon D, Iserentant D, Masschelein CA (1989). Reactor design optimization with a view to the improvement of amino acid utilization and flavor development of calcium alginate entrapped brewing yeast fermentations. Proc. 22nd EBC Cong., pp 315–322

Coutts MW (1957) A continuous process for the production of beer. UK Patent 872,391400

Cross PA, Mavituna F (1987) Yeast retention fermentors for beer production. Proc. 4th Eur. Cong. Biotechnol. Amsterdam, pp 199–200

Decamps C, Norton S, Poncelet D, Neufeld RJ (2004) Continuous pilot plant-scale immobilization of yeast in κ-carrageenan gel beads. AlChE J 50:1599–1605

Dillenhofer W, Ronn D (1996) Secondary fermentation of beer with immobilized yeast. Brauwelt International 14:344–346

Divies C, Cachon R (2005) Wine production by immobilized cell systems. In: Willaert R, Nedovic V (eds) Applications of cell immobilisation biotechnology. Springer, Dordrecht, The Netherlands, pp 285–293

Durieux A, Bodo E, Nedovic V, Simon JP (2002) Effect of yeast and *Oenococcus oeni* immobilisation on the formation of flavour components for cider production. Proc. International workshop bioencapsulation X: cell physiology and interactions of biomaterials and matrices. Prague, Czech Republic, pp 54–57

Durieux A, Nikolay X, Simon JP (2000) Continuous malolactic fermentation by *Oeconoccocus oeni* entrapped in Lentikats. Biotechnol Lett 22:1679–1684

Durieux A, Nicolay X, Simon J-P (2005) Application of immobilisation technology to cider production: a review. In: Willaert R, Nedovic V (eds) Applications of cell immobilisation biotechnology. Springer, Dordrecht, The Netherlands, pp 275–284

Ehrlich F (1904) Uber das natürliche isomere des leucins. Berichte der Deutschen Chemisten Gesellschaft 37:1809–1840

Ferraro L, Fatichenti F, Ciani M (2000) Pilot scale vinification process using immobilized *Candida stellata* cells and *Saccharomyces cerevisiae*. Process Biochem 35:1125–1129

Fujii T, Kobayashi O, Yoshimoto H, Furukawa S, Tamai Y (1997) Effect of aeration and unsaturated fatty acids on expression of *Saccharomyces cerevisiae* alcohol acetyltransferase gene. Appl Environ Microbiol 63:910–915

Fujiwara D, Yoshimoto H, Sone H, Harashima S, Tamai Y (1998) Transcriptional co-regulation of *Saccharomyces cerevisiae* alcohol acetyltransferase gene *ATF1* and D-9 fatty acid desaturase gene, *OLE1* by unsaturated fatty acids. Yeast 14:711–721

Fumi MD, Trioli G, Colagrande O (1987) Immobilization of *Saccharomyces cerevisiae* in calcium alginate for sparkling wine processes. Biotechnol Lett 9:339–342

Fumi MD, Trioli G, Colombi MG, Colagrande O (1988) Immobilization of *Saccharomyces cerevisiae* in calcium alginate gel and its application to bottle-fermented sparkling wine production. Am J Enol Viticult 39:267–272

Ge XM, Zhang L, Bai FW (2006) Impacts of yeast floc size distributions on their observed rates for substrate uptake and product formation. Enzyme Microb Technol 39:289–295

Gryta M (2002) The assessment of microorganism growth in the membrane distillation system. Desalination 142:79–88

Hammond JRM (1995) Genetically-modified brewing yeast for the 21st century. Progress to date. Yeast 11:1613–1627

Hanneman W (2002) Reducing beer maturation time and retaining quality. Mast Brew Assoc Am Techn Quart 39(3):149–155

Hazelwood LA, Daran J-M, van Maris AJA, Pronk JT, Dickinson JR (2008) The Ehrlich pathway for fusel alcohol production: a century of research on *Saccharomyces cerevisiae* metabolism. Appl Environ Microbiol 74(8):2259–2266

Herrero M, Laca A, Garcia LA, Díaz M (2001) Controlled malolactic fermentation in cider using *Oenococcus oeni* immobilized in alginate beads and comparison with free cell fermentation. Enzyme Microb Technol 28:35–41

Huang J, Hooijmans CM, Briasco CA, Geraats SGM, Luyben KCAM, Thomas D, Barbotin JN (1990) Effect of free-cell growth parameters on oxygen concentration profiles in gel-immobilized recombinant *Escherichia coli*. Appl Microbiol Biotechnol 33:619–623

Iconomopoulou M, Kanellaki M, Soupioni M, Koutinas AA (2003) Effect of freeze-dried cells on delignified cellulosic material in low-temperature wine making. Appl Biochem Biotechnol 104:23–36

Iconomopoulou M, Psarianos K, Kanellaki M, Koutinas AA (2002) Low temperature and ambient temperature wine making using freeze-dried immobilized cells on gluten pellets. Process Biochem 37:707–717

Iconomou L, Kanellaki M, Voliotis S, Agelopoulos K, Koutinas AA (1996) Continuous wine making by delignified cellulosic materials supported biocatalyst. An attractive process for industrial applications. Appl Biochem Biotechnol 60:303–313

Inoue T (1995) Development of a two-stage immobilized yeast fermentation system for continuous beer brewing. Proc. Eur. Brew. Conv. Cong., pp 25–36

Kana K, Kanellaki M, Papadimitriou A, Psarianos C, Koutinas AA (1989) Immobilization of *Saccharomyces cerevisiae* on γ-alumina pellets and its ethanol production in glucose and raisin extract fermentation. J Ferment Bioeng 68:213–215

Kopsahelis N, Kanellaki M, Bekatorou A (2007) Low temperature brewing using cells immobilized on brewer's spent grains. Food Chem 104(2):480–488

Kosseva M, Beschkov V, Kennedy JF, Lloyd LL (1998) Malolactic fermentation in Chardonnay wine by immobilized *Lactobacillus casei* cells. Process Biochem 33:793–797

Kosseva MR, Kennedy JF (2004) Encapsulated lactic acid bacteria for control of malolactic fermentation in wine. Artif Cells Blood Substit Immobil Biotechnol 32:55–65

Kourkoutas Y, Koutinas AA, Kanellaki M, Banat IM, Marchant R (2002) Continuous wine fermentation using a psychrophilic yeast immobilized on apple cuts at different temperatures. Food Microbiol 19:127–134

Kourkoutas Y, Komaitis M, Koutinas AA, Kaliafas A, Kanellaki M, Marchant R, Banat IM (2003) Wine production using yeast immobilized on quince biocatalyst at temperatures between 30 and 0°C. Food Chem 82:353–360

Kourkoutas Y, Komaitis M, Koutinas AA, Kanellaki M (2001) Wine production using yeast immobilized on apple pieces at low and room temperatures. J Agric Food Chem 49:1417–1425

Kourkoutas Y, Manojlovic V, Nedovic V (2009) Immobilisation of microbial cells for alcoholic and malolactic fermentation of wine and cider. In: Zuidam N-J, Nedovic VA (eds) Encapsulation technologies for food active ingredients and food processing. Springer, Dordrecht, The Netherlands, pp 327–345

Koutinas AA, Bakoyianis V, Argiriou T, Kanellaki M, Voliotis S (1997) A qualitative outline to industrialize alcohol production by catalytic multistage fixed bed tower (MFBT) bioreactor. Appl Biochem Biotechnol 66:121–131

Kronlöf J, Härkönen T, Hartwall P, Home S, Linko M (1989) Main fermentation with immobilized yeast. Proc. 22nd Eur. Brew. Conv., Zurich, pp 355–362

Kronlöf J, Virkajärvi I (1999). Primary fermentation with immobilized yeast. Proc. Eur. Brew. Conv. Cong., pp 761–770

Landaud S, Latrille E, Corrieu G (2001) Top pressure and temperature control the fusel alcohol/ester ratio through yeast growth in beer fermentation. J Inst Brew 107:107–117

Lebeau T, Jouenne T, Junter GA (1997) Simultaneous fermentation of glucose and xylose by pure and mixed cultures of *Saccharomyces cerevisiae* and *Candida shehatae* immobilized in a two-chambered bioreactor. Enzyme Microb Technol 21:265–272

Lemonnier J, Duteurtre B (1989) Un progress important pour le champagne et lens vins "methode traditionnelle". Rev Fr Cenol 121:15–26

Lilly M, Lambrechts MG, Pretorius IS (2000) Effect of increased yeast alcohol acetyltransferase activity on flavor profiles of wine and distillates. Appl Environ Microbiol 66:744–753

Linko M, Suihko M-L, Kronlöf J, Home S (1993) Use of brewer's yeast expressing α-acetolactate decarboxylase in conventional and immobilized fermentations. Mast Brew Assoc Am Techn Quart 30:93–97

Linko M, Virkajärvi I, Pohjala N, Lindborg K, Kronlöf J, Pajunen E (1997) Main fermentation with immobilized yeast – a breakthrough? Proc. 26th Eur. Brew. Conv. Maastricht, pp 385–394

Lommi H (1990) Immobilized yeast for maturation and alcohol-free beer. Brew Dist Int 5:22–23

Loukatos P, Kiaris M, Ligas I, Bourgos G, Kanellaki M, Komaitis M, Koutinas AA (2000) Continuous wine making by γ-alumina-supported biocatalyst. Quality of the wine and distillates. Appl Biochem Biotechnol 89:1–13

Lovitt R, Jung I, Jones M (2006) The performance of the membrane bioreactor for the malolactic fermentation of media containing ethanol. Desalination 199:435–437

Maeba H, Unemoto S, Sato M, Shinotsuka K (2000) Primary fermentation with immobilized yeast in porous chitosan beads. Pilot scale trial. Proc. 26th Conv. Inst. Brew. Aus. N.Z. Sec. Singapore, pp 82–86

Maicas S, Pardo I, Ferrer S (2001) The potential of positively charged cellulose sponge for malolactic fermentation of wine using *Oenococcus oeni*. Enzyme Microb Technol 28:415–419

Mallios P, Kourkoutas Y, Iconomopoulou M, Koutinas AA, Psarianos C, Marchant R, Banat IM (2004) Low temperature wine-making using yeast immobilized on pear pieces. J Sci Food Agric 84:1615–1623

Mallouchos A, Loukatos P, Bekatorou A, Koutinas A, Komaitis M (2007) Ambient and low temperature wine-making by immobilized cells on brewer's spent grains: Effect on volatile composition. Food Chem 104(3):918–927

Mallouchos A, Reppa P, Aggelis G, Koutinas AA, Kanellaki M, Komaitis M (2002) Grape skins as a natural support for yeast immobilization. Biotechnol Lett 24:1331–1335

Manojlovic V, Agouridis N, Kopsahelis N, Kanellaki M, Bugarski B, Nedovic V (2008) Brewing by immobilized freeze dried cells in a novel gas flow bioreactor. Proc. 2008 Joint Central Europ. Cong. Food, 6th Croat. Cong. Food Technol. Biotechnol. Nutrit. Cavtat, Croatia 2, pp 327–334

Manojlovic V, Nedovic V, Bugarski B, Winkelhausen E, Velickova E, Petrov P, Ivan B, and Tsvetanov C (2009). Immobilized yeast cells in double-layer hydrogel carriers for beer production. Proc. COST Spring workshop on bioencapsulation, Luxembourg, p 112

Manojlovic V, Sipsas V, Agouridis N, Bugarski B, Leskosek-Cukalovic I, Kanellaki M, and Nedovic V (2007). Beer fermentation by immobilized yeast in PVA/alginate beads using a catalytic multistage fixed bed tower bioreactor. Proc. 5th Int. Cong. Food Technol. Thessaloniki, Greece, pp 219–222

Martynenko NN, Gracheva IM, Sarishvili NG, Zubov AL, El'Registan GI, Lozinsky VI (2004) Immobilization of champagne yeasts by inclusion into cryogels of polyvinyl alcohol: Means of preventing cell release from the carrier matrix. Appl Biochem Microbiol 40:158–164

Masschelein CA, Ryder DS, Simon J-P (1994) Immobilized cell technology in beer production. Crit Rev Biotechnol 14:155–177

Mensour N, Margaritis A, Briens CL, Pilkington H, Russell I (1996) Applications of immobilized yeast cells in the brewing industry. In: Wijffels RH, Buitelaar RM, Bucke C, Tramper J (eds) Immobilized cells: basics and applications. Elsevier, Amsterdam, pp 661–671

Mensour N, Margaritis A, Briens CL, Pilkington H, Russell I (1997) New developments in the brewing industry using immobilised yeast cell bioreactor systems. J Inst Brew 103:363–370

Moll M, Durand G, Blachere H (1973) Continuous production of fermented liquids. French Patent 73/23397. US Patent 4009286

Narziss L, Hellich P (1971) Ein Beitrag zur wesentlichen Beschleunigung der Gärung und Reifung des Bieres. Brauwelt 111:1491–1500

Nedovic V, Bezbradica D, Obradovic B, Leskosek-Cukalovic I, Bugarski B (2004). Primary beer fermentation by PVA-immobilized brewing yeast in a gas-lift bioreactor. World Brew. Cong. 2004 CD Rom Proc. San Diego CA, pp O-63

Nedovic V, Cukalovic IL, Bezbradica D, Obradovic B, Bugarski B (2005b) New porous matrices and procedures for yeast cell immobilisation for primary beer fermentation. Proc. 30th Eur. Brew. Conv. Prague, pp 401–413

Nedovic V, Durieux A, Van Nederveide L, Rosseels P, Vandegans J, Plaisant AM, Simon J-P (2000) Continuous cider fermentation with co-immobilized yeast and *Leuconostoc oenos* cells. Enzyme Microb Technol 26:834–839

Nedovic V, Obradovic B, Vunjak-Novakovic G, Leskosek-Cukalovic I (1993) Kinetics of beer fermentation with immobilized yeast cells in an internal-loop air-lift bioreactor. Chem Indus 47:168–172

Nedovic V, Vunjak-Novakovic G, Leskosek-Cukalovic I, Cutkovic M (1996) A study on considerable accelerated fermentation of beer using an airlift bioreactor with calcium alginate entrapped yeast cells. Proc 5th World Cong Chem Eng 2:474–479

Nedovic V, Willaert R (eds) (2004) Fundamentals of cell immobilisation biotechnology. Kluwer, Dordrecht, The Netherlands

Nedovic V, Willaert R, Leskosek-Cukalovic I, Obradovic B, Bugarski B (2005b) Beer production using immobilized cells. In: Nedovic V, Willaert R (eds) Applications of cell immobilisation biotechnology. Springer, Dordrecht, The Netherlands, pp 259–273

Norton S, D'Amore T (1994) Physiological effects of yeast cell immobilization applications for brewing. Enzyme Microb Technol 16:365–375

Obradovic B, Nedovic V, Bugarski B, Willaert RG, Vunjak-Novakovic G (2004) In: Nedovic V, Willaert RG (eds) Fundamentals of cell immobilisation biotechnology, vol 8a, Focus on biotechnology. Kluwer, Dordrecht, pp 411–436

Ogbonna JC, Matsumura M, Kataoka H (1991) Effective oxygenation of immobilized cells through reduction in bead diameters: a review. Process Biochem 26:109–121

Okabe M, Katoh M, Furugoori F, Yoshida M, Mitsui S (1992) Growth and fermentation characteristics of bottom brewer's yeast under mechanical stirring. J Ferment Bioeng 73 (2):148–152

Onaka T, Nakanishi K, Inoue T, Kubo S (1985) Beer brewing with immobilized yeast. Nat Bio/ Technol 3:467–470

Pajic-Lijakovic I, Plavsic M, Nedovic V, Bugarski B (2007) Ca-alginate hydrogel mechanical transformations – the influence of yeast cell growth dynamics. J Microencapsul 24(5):410–429

Pajunen E, Grönqvist A (1994) Immobilized yeast fermenters for continuous lager beer maturation. Proc. 23rd Conv. Inst. Brew. Aus. N.Z. Sec., Sydney, pp 101–103

Pajunen E, Tapani K, Berg H, Ranta B, Bergin J, Lommi H, Viljava T (2001) Controlled beer fermentation with continuous on-stage immobilized yeast reactor. Proc 28th EBC Cong 49:1–12

Peddie HAB (1990) Ester formation in brewery fermentations. J Inst Brew 96:327–331

Peinado RA, Moreno JJ, Maestre O, Mauricio JC (2005) Use of a novel immobilization yeast system for winemaking. Biotechnol Lett 27:1421–1424

Peinado RA, Moreno JJ, Villalba JM, González-Reyes JA, Ortega JM, Mauricio JC (2006) Yeast biocapsules: a new immobilization method and their applications. Enzyme Microb Technol 40:79–84

Pittner H, Back W, Swinkels W, Meersman E, Van Dieren B, Lomni H (1993) Continuous production of acidified wort for alcohol-free-beer with immobilized lactic acid bacteria. Proc. Eur. Brew. Conv. Cong., pp 323–329

Plessas S, Bekatorou A, Koutinas AA, Soupioni M, Banat IM, Marchant R (2007) Use of *Saccharomyces cerevisiae* cells immobilized on orange peel as biocatalyst for alcoholic fermentation. Bioresour Technol 98(4):860–865

Prusse U, Bilancetti L, Bučko M, Bugarski B, Bukowski J, Gemeiner P, Lewinska D, Manojlovic V, Massart B, Nastruzzi C, Nedovic V, Poncelet D, Siebenhaar S, Tobler L, Tosi A, Vikartovská A, Vorlop K-D (2008) Comparison of different technologies for alginate beads production. Chem Pap 62(4):364–374

Renger RS, Vanhateren SH, Luyben K (1992) The formation of esters and higher alcohols during brewery fermentation – the effect of carbon-dioxide pressure. J Inst Brew 98:509–513

Ryder DS, Masschelein CA (1985) The growth process of brewing yeast and the biotechnological challenge. J Am Soc Brew Chem 43(2):66–75

Scott JA, O'Reilly AM (1996) Co-immobilization of selected yeast and bacteria for controlled flavour development in an alcoholic cider beverage. Process Biochem 31(2):111–117

Shen H-Y, Moonjai N, Verstrepen KJ, Delvaux FR (2003) Impact of attachment immobilization on yeast physiology and fermentation performance. J Am Soc Brew Chem 61(2):79–87

Shindo S, Sahara H, Koshino S (1994) Suppression of α-acetolactate formation in brewing with immobilized yeast. J Inst Brew 100:69–72

Simon JP, Durieux A, Pinnel V, Garré V, Vandegans J, Rosseels P, Godan N, Plaisant AM, Defroyennes J-P, Foroni G (1996) Organoleptic profiles of different ciders after continuous fermentation (encapsulated living cells) versus batch fermentation (free cells). In: Wijffels RH, Buitelaar RH, Bucke C, Tramper J (eds) Immobilized cells: basics and applications. Elsevier, Amsterdam, pp 615–621

Sipsas V, Kolokythas G, Kourkoutas Y, Plessas S, Nedovic VA, Kanellaki M (2009) Comparative study of batch and continuous multi-stage fixed-bed tower (MFBT) bioreactor during wine-making using freeze-dried immobilized cells. J Food Eng 90:495–503

Smogrovicová D, Dömény Z (1999) Beer volatile by-product formation at different fermentation temperature using immobilized yeasts. Process Biochem 34:785–794

Smogrovicová D, Dömény Z, Gemeiner P, Malovíková A, Sturdík E (1997) Reactors for the continuous primary beer fermentation using immobilised yeast. Biotechnol Tech 11:261–264

Smogrovicová D, Dömeny Z (1999) Beer volatile by-product formation at different fermentation temperature using immobilized yeasts. Process Biochem 34:785–794

Smogrovicová D, Dömény Z, Navrátil M, Dvorák P (2001) Continuous beer fermentation using polyvinyl alcohol entrapped yeast. Proc Eur Brew Conv Cong 50:1–9

Strand BL, Gaserod B, Kulseng B, Espevik T, Skjak-Braek GJ (2002) Alginate-polylysine-alginate microcapsules: effect of size-reduction on capsule properties. J Microencapsul 19:615–630

Takaya M, Matsumoto N, Yanase H (2002) Characterization of membrane bioreactor for dry wine production. J Biosci Bioeng 93:240–244

Tata M, Bower P, Bromberg S, Duncombe D, Fehring J, Lau V, Ryder D, Stassi P (1999) Immobilized yeast bioreactor systems for continuous beer fermentation. Biotechnol Prog 15:105–113

Thu B, Gaserod O, Paus D, Mikkelsen A, Skjak-Braek G, Toffanin R, Vittur F, Rizzo R (2000) Inhomogeneous alginate gel spheres: An assessment of the polymer gradients by synchrotron radiation-induced x-ray emission, magnetic resonance microimaging, and mathematical modeling Biopolymers 53:60–71

Tsakiris A, Bekatorou A, Psarianos C, Koutinas AA, Marchant R, Banat IM (2004a) Immobilization of yeast on dried raisin berries for use in dry white wine-making. Food Chem 87:11–15

Tsakiris A, Sipsas V, Bekatorou A, Mallouchos A, Koutinas AA (2004b) Red wine making by immobilized cells and influence on volatile composition. J Agric Food Chem 53:1357–1363

Unemoto S, Mitani Y, Shinotsuka K (1998) Primary fermentation with immobilized yeast in a fluidized bed reactor. Mast Brew Assoc Am Techn Quart 35:58–61

Van De Winkel L, De Vuyst L (1997) Immobilized yeast cell systems in today's breweries and tomorrow's. Cerevisia 22(1):27–31

Van De Winkel L, Van Beveren PC, Borremans E, Goossens E, Masschelein CA (1993) High performance immobilized yeast reactor design for continuous beer fermentation. Proc. 24th Eur. Brew. Conv. Congr., pp 307–314

Van De Winkel L, Van Beveren PC, Masschelein CA (1991) The application of an immobilized yeast loop reactor to the continuous production of alcohol-free beer. Proc. Eur. Brew. Conv. Cong., pp 307–314

Van Iersel MFM, Van Dieren B, Rombouts FM, Abee T (1999) Flavor formation and cell physiology during the production of alcohol-free beer with immobilized *Saccharomyces cerevisiae*. Enzyme Microb Technol 24:407–411

Van Mulders SE, Christianen E, Saerens SM, Daenen L, Verbelen PJ, Willaert R, Verstrepen KJ, Delvaux FR (2009) Phenotypic diversity of Flo protein family-mediated adhesion in *Saccharomyces cerevisiae*. FEMS Yeast Res 9(2):178–190

Veeranjaneya Reddy L, Harish Kumar Raddy Y, Prasanna Anjaneya Reddy L, Vijaya Sarathy Reddy O (2008) Wine production by novel yeast biocatalyst prepared by immobilization on watermelon (*Citrullus vulgaris*) ring pieces and characterization of volatile compounds. Process Biochem 43:748–752

Verbelen PJ, De Schutter DP, Delvaux F, Verstrepen KJ, Delvaux FR (2006) Immobilized yeast cell systems for continuous fermentation applications. Biotechnol Lett 28:1515–1525

Verbelen P, Nedovic VA, Manojlovic V, Delvaux F, Leskosek-Cukalovic I, Bugarski B, Willaert R (2009) Bioprocess intensification of beer fermentation using immobilised cells. In: Zuidam

N-J, Nedovic VA (eds) Encapsulation technologies for food active ingredients and food processing. Springer, Dordrecht, The Netherlands, pp 303–327
Verstrepen K, Derdelinckx G, Verachtert H, Delvaux FR (2003a) Yeast flocculation: what brewers should know. Appl Microbiol Biotechnol 61:197–203
Verstrepen KJ, Moonjai N, Derdelinckx G, Dufour J-P, Winderickx J, Thevelein JM, Pretorius IS, Delvaux FR (2003b) Genetic regulation of ester synthesis in brewer's yeast: new facts, insights and implications for the brewer. In: Brewing yeast fermentation performance, vol 2, 2nd edn. Blackwell Science, Oxford, pp 234–248
Verstrepen KJ, Reynolds TB, Fink GR (2004) Origins of variation in the fungal cell surface. Nat Rev Microbiol 2:533–540
Virkajärvi I, Krönlof J (1998) Long-term stability of immobilized yeast columns in primary fermentation. J Am Soc Brew Chem 56:70–75
Virkajärvi I, Pohjala N (2000) Primary fermentation with immobilized yeast: effects of carrier materials on the flavour of the beer. J Inst Brew 106:311–318
Virkajärvi I, Vainikka M, Virtanen H, Home S (2002) Productivity of immobilized yeast reactors with very-high-gravity worts. J Am Soc Brew Chem 60(4):188–197
Wainwright T (1973) Diacetyl - a review. J Inst Brew 79:451–470
White FH, Portno AD (1979). The influence of wort composition on beer ester levels. Proc. Eur. Brew. Conv. Cong., pp 447–460
Willaert R, Baron GV (1996) Gel entrapment and micro-encapsulation: methods, applications and engineering principles. Rev Chem Eng 12:1–205
Willaert R, Nedovic V (2006) Primary beer fermentation by immobilised yeast – a review in flavour formation and control strategies. J Chem Technol Biotechnol 81:1353–1367
Xu TJ, Zhao XQ, Bai FW (2005) Continuous ethanol production using self-flocculating yeast in a cascade of fermentors. Enzyme Microb Technol 37:634–640
Yamauchi Y, Okamoto T, Murayama H, Kajino K, Amikura T, Hiratsu H, Nagara A, Kamiya T, Inoue T (1995) Rapid maturation of beer using an immobilized yeast bioreactor. 1. Heat conversion of α-acetolactate. J Biotechnol 38:101–108

Chapter 7
Multifactorial Assessment of Microbial Risks in Foods: Merging Engineering, Science, and Social Dimensions

Valerie Davidson, Juliana Ruzante, and Carlos Daza Donoso

7.1 Introduction and Context

The tenth International Congress on Engineering and Food (ICEF 10, Viña del Mar, Chile, April 2008) broadly explored "the new agenda of innovation and achievement in food and engineering." A common theme across many presentations was the need for food engineers to work across interfaces between engineering and science disciplines. Martin Cole, Director of the National Center for Food Safety and Technology (USA), recognized this as a "crucial role" for food engineers in his plenary lecture on emerging challenges in food safety. He pointed out that to be successful in the current global food environment, "it will be necessary for the food engineer to move deeper into the basic sciences," and that in the area of food safety, the food engineer will need "to use risk-driven studies to develop, improve and optimize food products and processes" (Cole and Rodriguez 2008).

Under the ICEF 10 conference theme of "Food Processing" our research group presented a body of work titled "Multifactorial Risk Prioritization Framework for Food-borne Pathogens" (Davidson et al. 2008). This framework systematically compiles information and characterizes risks due to microbial hazards in foods based on four factors: public health, market value, consumer perceptions of risk, and social concerns. The framework includes specific tools to assist risk managers in comparing and ranking risks as a basis for setting priorities and strategic allocation of resources for risk assessment needs and interventions to mitigate risks. The Multifactorial Risk Prioritization Framework is positioned at the interface between risk management and risk assessment and serves as an important connection between these essential elements of food safety.

V. Davidson (✉) and C.D. Donoso
School of Engineering, University of Guelph, Guelph, ON N1G 2W1, Canada
e-mail: vdavidso@uoguelph.ca

J. Ruzante
Joint Institute for Food Safety and Applied Nutrition, University of Maryland, College Park, MD 20742, USA

J.M. Aguilera et al. (eds.), *Food Engineering Interfaces*, Food Engineering Series,
DOI 10.1007/978-1-4419-7475-4_7,

In this chapter, we outline the components of the multifactorial framework and the tools to assist risk managers. The discussion highlights the multidisciplinary nature of the risk framework and the ways that food engineers can contribute to the development and implementation of food safety strategies. We also offer some thoughts on the challenges of multidisciplinary research as well as the implications for training food engineers.

7.2 Risk Management Frameworks for Food Safety

A generic representation of a risk management cycle, fully integrated with risk assessment, is shown in Fig. 7.1. Risk management is an iterative process, beginning with the need to evaluate and rank risks within an appropriate context (Block A). Typically, microbial risk assessment (Block B) is focused on public health and carried out by experts who have specialized scientific and technical knowledge and are at an arm's-length from the risk management process. Their knowledge is derived from observations, forecasts, and expert judgments. These various inputs need to be summarized in formats that allow decision-makers to compare risks across multiple dimensions, with an understanding of any limitations, including

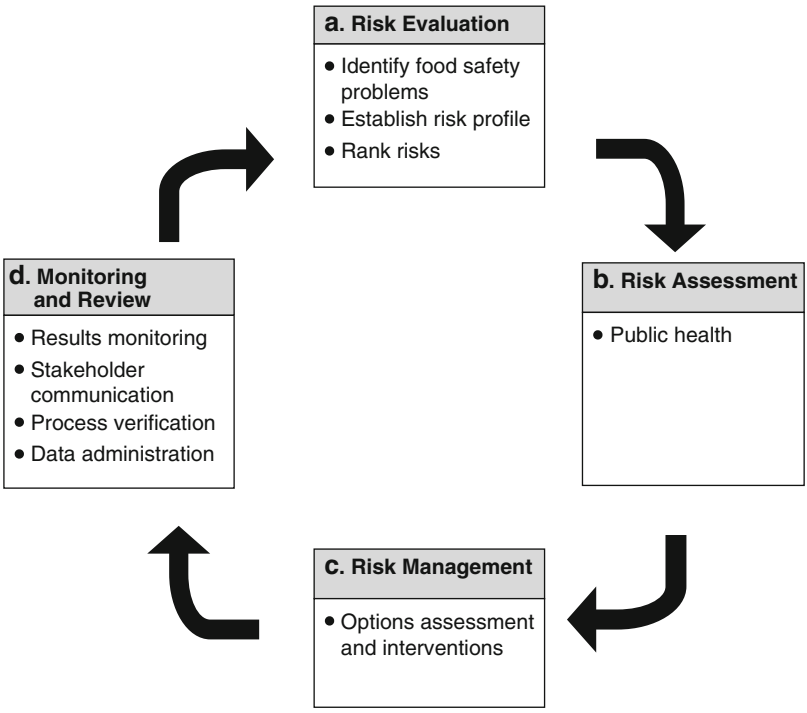

Fig. 7.1 Generic risk management cycle

uncertainty and variability, in the data and opinions. Based on scientifically sound risk assessment, risk managers make decisions regarding allocation of resources to implement interventions and mitigate serious risks (Block C). The final step includes routine surveillance and data gathering (Block D) in order to review specific interventions.

The joint FAO/WHO report, "Principles and guidelines for incorporating microbiological risk assessment in the development of food safety standards" (Food and Agriculture Organization of the United Nations and the World Health Organization 2002), defines a comprehensive context for risk management related to food safety. It recognizes that risk management must rest on the foundations of scientifically sound risk assessment and should consider areas of health impact (e.g., adverse health effects, duration of illness, severity and impairment of life quality), economic and market impact (e.g., economic burden and facilitation of fair trade), impact on consumer behavior, and social/ethical concerns (susceptibility of exposed population, nutritional status, social status).

A comprehensive review (Henson et al. 2007) identified a number of frameworks for prioritization of food-borne microbial risks. Impact on human health was the primary basis for ranking risks but some frameworks attempted to incorporate additional risk factors. In the United States, the Food Safety Research Consortium developed the Food-borne Illness Risk Ranking Model (FIRRM), which evaluates multiple aspects of public health, including incidence of illness, outcome severities, monetary (e.g., cost of illness) and non-monetary factors (quality-adjusted life years) (Batz et al. 2004). New Zealand's risk ranking tool includes public health measures that are weighted by severity in the general public and subpopulations; it acknowledges the economic implications of food-borne pathogens on trade (New Zealand Food Safety Authority 2008). A recent FAO/WHO expert meeting defined six criteria for ranking microbial risks in fresh fruits and vegetables and three criteria are associated with market and economic factors: size of production in a global context, diversity and complexity of the production chain and industry, and extent of international trade and economic impact (Food and Agriculture Organization of the United Nations and the World Health Organization 2008). Finally, the European Commission (EC) has put forward an integrated framework that highlights the importance of balancing the scientific, economic, social, and cultural aspects of risks and benefits as well as risk–benefit distribution within society (European Commission 2002). The EC framework is intended to provide guidelines for harmonizing risk management strategies in the European Union.

7.3 Multifactorial Risk Prioritization Framework

The Multifactorial Risk Prioritization Framework recognizes the need to evaluate multiple risk factors in an integrated format so that risk managers can compare and rank risks – at the level of pathogen–food pairs, across pathogens, and across food

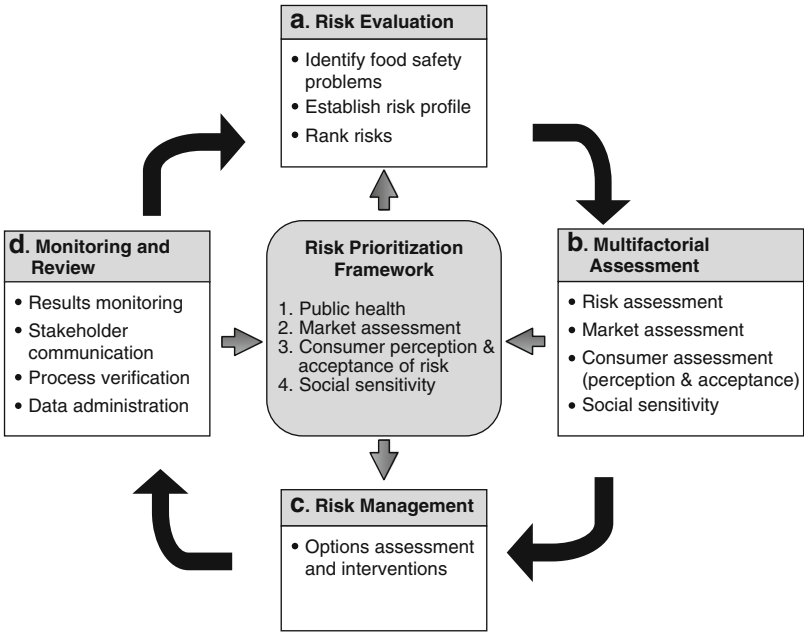

Fig. 7.2 Multifactorial risk prioritization framework

categories. Figure 7.2 shows the integration of the Multifactorial Risk Prioritization Framework within a risk management cycle. The framework is intended to assist risk managers and provide tools to support decision-making. Risk prioritization or ranking at the evaluation stage (Block A) is based on multifactor risk profiles extracted from the framework knowledge base; this ranking is the basis for allocating resources for development of adequate knowledge, which is carried out through multidimensional assessments of high-priority hazards (Block B). Ranking is also a key component in selecting appropriate interventions (Block C). As shown in Fig. 7.2, the framework addresses the need for an integrated information system that provides inputs for evaluation and assessment of interventions, and can be updated by knowledge developed through risk assessments, consumer behavior, market-level studies, and surveillance systems.

Given the nature and complexity of risk associated with microbial hazards in foods, one of the first challenges in developing a framework is to establish an appropriate context for comparing different pathogens and food sources. The Multifactorial Risk Prioritization Framework integrates information from four major areas identified in the FAO/WHO guidelines: public health, market-level, consumer behavior, and social factor assessments. Risk assessments for each area are complex and multidimensional. A detailed discussion of possible risk measures for each factor in the framework is presented in Henson et al. (2007) and the rationale for choosing particular risk measures is given in Ruzante et al. (2009). In the discussion that follows, the multifactor risk measures are outlined in terms of

underlying models, data requirements, and engineering analysis; decision tools are also demonstrated with examples of risk profiles based on Canadian data.

7.3.1 Defining Risk Factors

7.3.1.1 Public Health Assessment

Clearly public health impact is a primary consideration for risk management decisions related to food safety. Potential outcomes include morbidity (immediate illness with varying degrees of severity and longer-term sequelae) and mortality (fatalities). Since health outcomes vary for different food-borne pathogens, a number of aggregate measures are used to summarize burden and cost of illness. In the current framework, we use two dimensions to characterize public health impact: cost of illness and disability-adjusted life years. Cost of illness (COI) reflects medical care costs, productivity costs due to time lost from paid employment, and economic value of premature death. Disability-adjusted life years (DALY) is a summary measure of population health and combines morbidity and mortality measurements in a single parameter, as shown in the following equations:

$$\text{DALY} = \text{Years of life loss}(\text{YLL}) + \text{Years lived with disability}(\text{YLD}),$$

where

$$\text{YLL} = \sum_{j=1}^{9} d_j e_j \ (\text{j} = \text{age group},\ \text{d} = \#\ \text{deaths},\ \text{e} = \text{expected lifespan}),$$

and

$$\text{YLD} = \sum_{l} n_l t_l w_l \ (\text{l} = \text{health outcome},\ \text{n} = \#\ \text{of cases},$$
$$\text{t} = \text{duration of the illness}, \text{w} = \text{diability/severity weight}).$$

The COI approach can mask differential effects across subpopulations since it does not consider productivity costs outside the paid labor force (e.g., young children and the elderly are not included). Although DALY is used by the WHO in global assessments of the burden of disease, the disability weights are subjective valuations of the time lived in nonfatal health status (Murray 1994; Murray and Acharya 1997). Since both COI and DALY have strengths and weaknesses, we include both measures in the framework to provide complementary depictions of the public health impact.

The underlying models for COI and DALY are developed by economists and scientists with specialized knowledge of public health. However, implementation

requires careful systems analysis to ensure consistency of data and analysis across diverse health outcomes, and to define limitations in the calculated values due to uncertainty and variability in model inputs. As food engineers, we work with economists, epidemiologists, microbiologists, veterinarians and food scientists to understand the issues related to underreporting of food-borne illness, attribution of illness to particular food categories, and other challenges in building credible models. At present, we are using existing knowledge of uncertainty and variability in model parameters to estimate uncertainty intervals for DALY and COI values in the framework. We are also working to develop better knowledge for the Canadian context in areas such as attribution of illness to particular food categories.

7.3.1.2 Market-Level Assessment

The economic losses arising from food-borne pathogen incidence and prominent outbreaks can be large – for individual groups or firms and, in some cases, for an entire industry sector. Recently a Canadian food processor agreed to pay up to $27 million to settle class action lawsuits initiated after a national listeriosis outbreak linked to 20 deaths (Canadian Broadcasting Corporation 2008). Another recent outbreak of *Salmonella saitpaul* associated with tomatoes and peppers caused losses of approximately $100 million for the US tomato industry due to lower prices and reduced demand (Western Farm Press 2008). These examples underscore the importance of considering economic impacts that could arise from food-borne pathogen outbreaks or unacceptable levels of incidence in the risk management process. The goal of the market-level dimension is to review a priori the potential economic impacts of pathogen incidence or outbreaks at an overall market level. At this point, we do not attempt to estimate the likelihood of an economically significant outbreak or unacceptable incidence levels; however, we recognize the value of developing estimates of likelihood for the framework in the future.

Henson et al. (2007) presented a comprehensive list of market-level intelligence that would be helpful in evaluating economic impacts; this list is summarized in Table 7.1. This broad set of inputs spanning the entire food supply chain, from production to retail, accounts for the economic value of imports and exports. In developing some of this information for the Canadian context, we encountered challenges in obtaining complete information for particular food groups and industry subsectors. For example, information on wages and number of employees by sectors was not available in Canada. Also, public information on the value of sales is generally limited to cash receipts at the farm gate and comparable information for processed foods is only available through special reports (e.g., reports produced by government agencies such as Statistics Canada and Agriculture and Agri-food Canada) or market surveys prepared by market consultants.

Figure 7.3 shows an example of market-level information extracted from the framework database for Canadian chicken products. The market summary includes descriptive and quantitative information that provides context and consistent measures for decision-makers to use in comparing risks across pathogen–food combinations.

Table 7.1 Suggested elements for market-level assessment (Henson et al. 2007)

Subsector	Domestic market	International market
Retail level	• Value of sales ($)	• Value of trade ($ and % of value of domestic production)
	• Volume of sales (#)	• Volume of trade (#)
	• Employment (#)	• Change in consumption (%)
	• Wages ($)	• Impact on market access (index)
	• Change in consumption (%)	• Export competitiveness (index)
		• Size of global market (% of global production)
		• Number of trade partners (#)
		• Trade concentration ratio (index)
Processing–distributing–wholesaling level	• Value of sales ($)	• Value of trade ($ and % of value of domestic production)
	• Volume of sales (#)	• Volume of trade (#)
	• Employment (#)	• Change in consumption (%)
	• Wages ($)	• Impact on market access (index)
	• Change in consumption (%)	• Export competitiveness (index)
		• Size of global market (% of global production)
		• Number of trade partners (#)
		• Trade concentration ratio (index)
Farm level	• Value of sales ($)	• Value of trade ($ and % of value of domestic production)
	• Volume of sales (#)	• Volume of trade (#)
	• Employment (#)	• Change in consumption (%)
	• Wages ($)	• Impact on market access (index)
	• Change in consumption (%)	• Export competitiveness (index)
		• Size of global market (% of global production)
		• Number of trade partners (#)
		• Trade concentration ratio (index)

At present we use a simple aggregate measure as a basis to compare market risk across different food categories. This is an estimate of the economic importance of domestic market activities (on an annual basis) calculated as the total value at retail plus the value of exports minus the value of imports. This measure captures the size of economic activity in the domestic market that is potentially at risk due to incidence and outbreaks.

The market-level analysis is a critical component of the risk context and must be integrated into the food safety framework. As mentioned, we would like to include estimates of the likelihood of outbreaks in a future version of this framework. This will require a multidisciplinary approach, and food engineers' knowledge of processing operations and systems-based failure analysis will be important contributions to this enhancement of the framework.

7.3.1.3 Consumer Assessment

The consumer behavior dimension of the multifactorial risk framework recognizes that consumers may well be willing to accept a food-safety risk if the perceived risk

Salmonellosis associated with chicken consumption

MARKET IMPACT

Chicken consumption in Canada has been steadily increasing over the last 3 decades. The demand for chicken rose by 136% from 1975 to 2005. Since 1979, the Canadian production of chicken has been regulated under a supply management system. The intention of the supply management system is to match demand with domestic supply and to guarantee a predetermined price to producers. For the most part Canadian producers meet domestic demand and world-wide Canada is ranked 15th as a chicken exporter. Chicken production is mainly concentrated in ON, QC and BC.

Data was obtained from Agriculture Economic Statistics (May 2007), CANSIM II (Statistics Canada) and Agriculture and Agri-Food Canada. Averages were calculated based on the most recent 3 years including 2006. The following market characteristics provide an overview of the commodity market and points of comparison to the other commodities.

✓ Industry size is depicted by farm cash receipts, which is the total revenue to farms in an agricultural sub-sector. It is comprised of agricultural commodity sales and program payments.

✓ The importance of the commodity at the consumer level is represented by the total value at retail, which is the amount of the final consumer good purchased, multiplied by the average price per unit weight.

✓ The value of exports and imports is the quantity of the exported and imported commodity multiplied by the repspective values.

✓ To depict the economic significance of the commodity market in the domestic market, the following formula applies: Total value at retail + value of exports – value of imports.

✓ The proportion of the domestic consumption of the commodity that is domestically produced is calculated by the domestic consumption divided by the domestic production.

✓ The key import/export market values depict the importance of imports and exports of the commodity. For the import market, the key import market number is calculated by the value of all imports of a specific commodity divided by the value of the total agri-food imports.

Market Information ($1,000)	2006	Annual average (2004-2006)
Size of Industry (farm gate) farm cash receipts	$1,545,000	$1,580,000
Total Value at retail	$5,791,000	$5,664,000
Value of exports	$223,000	$223,000
Value of imports	$396,000	$415,000
Economic importance of the domestic market	$5,619,000	$5,472,000
% domestic consumption/domestic production	108.9%	107.6%
Key export market	0.80%	0.83%
Key import market	1.72%	1.94%

2

Fig. 7.3 Summary of market-level information for *Salmonellosis* – chicken

is low or if the perceived benefits arising from the consumption of a particular food offset perceptions of ill consequences. The consumers' perception and acceptance of risk arising from food-borne pathogens can translate into shifts in market demand for particular food products. For example, the Guelph Food panel (a large-scale panel of consumers dedicated to food research) reported the following changes in consumer behavior after a recent listeriosis outbreak in Canada (University of Guelph 2008):

- Thirty-nine percent would not consume ready-to-eat meats at home (up from 6% reported before recall).
- Fifty-six percent would not consume ready-to-eat meat products in fast-food outlets or restaurants (up from 9% reported before recall).
- Thirty percent stopped buying ready-to-eat meats from Canada.

Consumers may switch from certain products perceived as "less safe" to those perceived as "more safe," although such perceptions may bear only a loose relationship with scientific assessments of risks to human health. Furthermore, consumer perceptions of risks associated with food are an important determinant in the confidence the general public has in the security of food systems and in related systems of public regulation and oversight. Relatively small but highly visible outbreaks of disease can have a profound impact on the trust that consumers have in food producers, manufacturers and distributors, or government regulators.

Measurement of risk acceptability and perception is complex. There is a considerable amount of literature and survey-based research on how consumers rank different risks (Fife-Schaw and Rowe 1996; Fischoff et al. 1978; Frewer et al. 1994, 1997, 1998a, 1998b). However, as Frewer et al. (1998a) point out, food is not something to be avoided. Thus, consumers may view food-related risks differently from avoidable risks.

In the current framework, we use five scales to assess consumers' perception and acceptance of risks associated with a food–pathogen combination:

1. Degree to which risk is perceived as uncontrollable by consumers
2. Degree to which risk is perceived as unknown to the individual
3. Degree to which risk is perceived as unknown to scientists
4. Degree to which risk is perceived as involuntary
5. Degree to which consumers perceive health outcome as severe

Each criterion is scored on a three-level nominal scale (low, medium, high) by a consumer panel. To date, a small Delphi panel has provided opinions for the six case studies based on their knowledge of consumer behavior. The overall measure used to represent consumers is the sum of the average scores for each criterion, normalized on a 0–1 scale (i.e., sum is divided by 5).

Some of the researchers in our team recently conducted a consumer survey to explore perceptions and acceptance of risks related to pathogen–food combinations. Preliminary results need to be validated with a follow-up survey; however, initial results showed that consumers are concerned about risks perceived as uncontrollable (e.g., through their own preparations prior to consumption, by process steps in

manufacturing) and where the outcome is severe (e.g., chronic health effects, death). There is also concern about risks in foods given to young children or other vulnerable groups.

7.3.1.4 Social Factor Assessment

As noted by Caswell (2005), there needs to be "a recognition that risk analysis, especially risk assessment, are tools for making decisions that better reflect society's values." Impacts on vulnerable groups such as young children and the elderly are given careful consideration in risk management decisions because society feels an obligation to protect these groups. We have incorporated a social sensitivity factor into the risk prioritization framework to account for the potential of wider social consequences, beyond what is accounted for in public health and market-level dimensions. The social sensitivity factor is based on two sub-criteria: consumers (e.g., subpopulations such as pregnant women) and firms (e.g., niche industries unique to certain regions).

At the consumer level, the sensitivity measure does not relate to the potentially greater individual risk that consumer subgroups may face from a particular pathogen–food combination, since this is incorporated into the public health factor. Societal concerns may relate, for example, to the more limited ability of some individuals to take self-protective actions or may be based in altruism. Similarly, on the food supply side, such concerns do not reflect the unfavorable economic impact on individual firms or an industry per se because this is included in the market-level factor. Instead this measure reflects sensitivity to the role that such enterprises play in rural or economically vulnerable areas and their contribution to the historical and/or social fabric of society. The social sensitivity factor is perhaps more controversial than the other factors since it is dependent upon individual views and ethical positions. However, these considerations need to be incorporated in an explicit rather than ad hoc manner. At this point, the social sensitivity factor is a binary flag (0 = no concern; 1 = concern) for each of the two sub-criteria.

7.3.2 Information Cards

The first tool that has been developed in the Multifactorial Risk Prioritization Framework is a set of concise summaries or information cards for each of the four risk factors. For example, the information card in Fig. 7.4 shows the public health impact for a specific food–pathogen combination: *Salmonellosis* in chicken. These information cards provide contextual information, such as health outcomes and market characteristics (Fig. 7.3), as well as quantitative indicators. The data required to calculate the measures for each of the four risk factors are stored in electronic format and are updated at intervals appropriate for the information source. For example, Statistics Canada data are available on an annual basis but

Salmonellosis associated with chicken consumption

PUBLIC HEALTH IMPACT

SALMONELLOSIS

Salmonellosis is an illness which attacks the digestive system. It is caused by bacteria belonging to the family of *Salmonella*. Two types are most commonly associated with illness, *Salmonella typhimurium*, and *Salmonella enteritidis*. Most types of *Salmonella* live in the intestines of animals and birds. Infection is acquired by the ingestion of organisms in food contaminated by the stool of an infected animal or person. Symptoms include fever, abdominal cramps and diarrhea about 12-72 hours after eating contaminated food or beverages. Epidemics have implicated foods such as meat, poultry, uncooked or lightly cooked eggs and egg products, raw milk and dairy products. Pets are another common source of infection. The bacteria can be carried by iguanas, turtles, tortoises, chicks, and sometimes cats and dogs.

DATA

Data was collected for the period from 1994 to 2004. Disease incidence data was obtained from Notifiable Diseases On-line (Public Health Agency of Canada website) and population estimates were obtained from Statistics Canada. An underreporting factor of 25 was used to estimate total illness.
Cost-of-illness was calculated based on the medical costs, loss of productivity and loss of life. OHIP costs were considered for doctor's visit, emergency services and hospitalization. The years of life loss and the years lived with disability were calculated to determine Disability Adjusted Life Years (DALY).

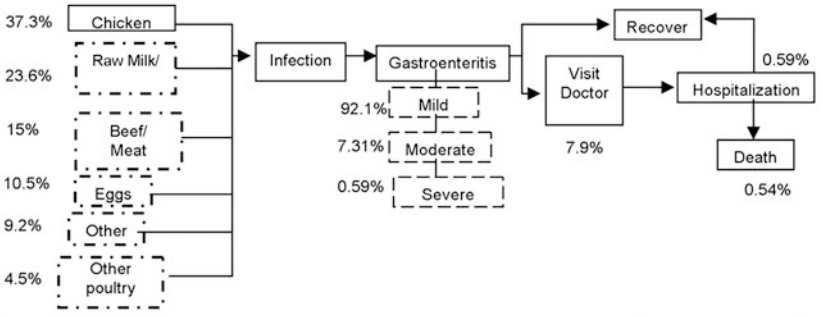

Public Health Information (associated with **chicken** consumption)	2004		Annual average (2002-2004)	
		#cases		#cases
Incidence of Salmonellosis	120*	38,086	128*	40,222
Case-fatality of Salmonellosis	0.022%	8	0.022%	9
Cost-of-Illness (COI)	$75,140,000		$79,400,000	
Disability Adjusted Life Years DALYs)	431		449	

*Per 100,000

1

Fig. 7.4 Summary of public health information for *Salmonellosis* – chicken

information from the scientific literature may not be revised as frequently. In cases where data are updated on an annual basis, values are shown for the most recent year as well as a 3-year average based on annual values to reduce the effect of unusual events on decisions. At this point, the values for all risk factors are shown as single values or point estimates, without explanation of uncertainty. We recognize the need to quantify the uncertainty due to variability and, in some cases, limited knowledge or data in each of the risk measures. This analysis is in progress.

7.3.3 Multifactorial Risk Prioritization

As outlined in the preceding sections, one or two aggregate measures are defined for each of the four areas of risk assessment: public health (DALY and COI values), market-level (economic value of domestic market activities), consumer (aggregate measure of perception and acceptance of risk), and social sensitivity (consumer and firm). While we recognize that other measures could be used, we consider these six measures to be comprehensive and consistent with the principles outlined by FAO/WHO. Using our framework, multidimensional risk profiles can be created for pathogen–food combinations, food categories, and different pathogens. In all cases, a ranking process must be able to compare each one on the basis of multiple criteria.

Multi-criteria decision analysis (MCDA) techniques are structured, consistent, and transparent, and therefore helpful in dealing with large amounts of complex information. We have explored a number of MCDA tools for use in the prioritization framework (Daza Donoso 2008; Ruzante et al. 2009). Daza Donoso (2008) compared a number of MCDA techniques on the basis of their expandability, ability to incorporate uncertainty and variability, and interactions with decision-makers (e.g., level of knowledge, inputs and time requirements, analytical skills). On this basis, outranking methods had definite advantages over techniques such as the multi-attribute utility theory and the analytic hierarchy process. Outranking methods are based on pair-wise comparisons of alternatives. For each criterion, alternative "a_2" is compared to alternative "a_1" using a preference or outranking relation defined in an appropriate scale for the criterion. This permits the use of ordinal scales and binary values for risk criteria. Furthermore, the outranking relations can be constructed to reflect uncertainty and varying degrees of preference (weak to strong) or higher ranking. Figure 7.5 shows an outranking relation for the criterion related to consumer risk perception and acceptance of risk. Two discrimination thresholds are defined: indifference (r) and strict preference (s). When two alternatives (a_1 and a_2) are compared, there is insufficient evidence to rank a_2 higher when the difference in the criterion scores is less than 0.05 (indifference threshold r). This threshold value is defined specifically for the criterion related to consumer perception and acceptance of risk; it is based on our estimate of the consistency in opinions from our Delphi panel. For score differences in the interval between 0.05 and 0.33, there is weak but increasing preference (or higher priority) for a_2; above 0.33 (strict preference threshold s)

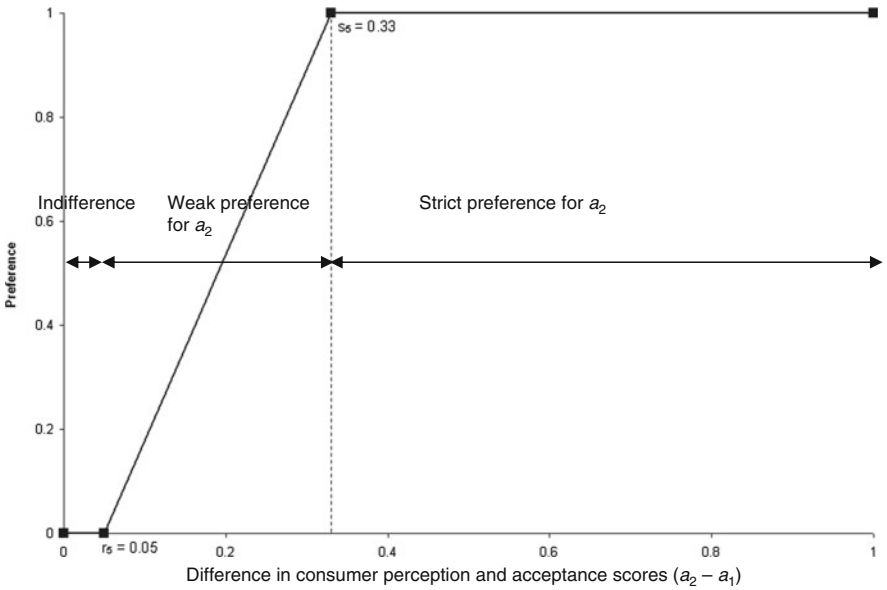

Fig. 7.5 Outranking relation for consumer perception and acceptance of risk criterion

a_2 clearly ranks as a higher risk than a_1. The characteristics of the outranking relations (thresholds and transitions between thresholds) can be used to reflect some aspects of uncertainty and variability in the risk measures.

Daza Donoso et al. (2008) used two outranking methods, ELECTRE III (Elimination et Choix Traduisant la Réalité) and PROMETHEE (Preference Ranking Organization Method for Enrichment Evaluations) to rank six pathogen–food combinations. The multidimensional risk profiles for the six examples are summarized in Table 7.2. The ELECTRE III method developed by Roy (1978) is available in *Windows*-compatible software from the LAMSADE research group (Laboratoire d'analyse et modélisation pour l'aide à décision 1994). PROMETHEE is an outranking method developed by Brans and colleagues (Brans and Vincke 1985; Brans et al. 1986) and implemented in Decision Lab software (Visual Decision Inc., Montreal, QC, Canada). The same discrimination thresholds were defined for PROMETHEE and ELECTRE III ranking relations as shown in Table 7.3. Although the ELECTRE III method allowed for a "veto" effect, this component was not used in ranking the six pathogen–food combinations since it was assumed that all six pairs posed risk, regardless of how much lower its performance in any one criterion may be. The final rankings were based on the equal weightings for the four risk factors (Table 7.2).

As shown in Table 7.4, *Escherichia coli* O157 in beef is ranked as the highest priority in both outranking methods. At the number two rank, there are differences depending on the ranking method. In ELECTRE III, two pathogen–food

Table 7.2 Risk profiles for six pathogen–food combinations (Canadian data)

Pathogen–food combination	Public health		Market	Consumer perception and acceptance of risk	Social sensitivity	
	DALY[a]	COI[b]	Domestic size[c]		Consumer	Firm
	(years)	(CAN $ 10^6)	(CAN$ 10^6)	Normalized average	Flag	Flag
Campylobacter/chicken	808	79.8	5472	0.3	0	0
Salmonella/chicken	449	79.4	5472	0.25	0	0
Salmonella/spinach	1	0.2	118	0.5	0	0
Escherichia coli O157/spinach	3	0.5	118	0.8	1	0
E. coli O157/beef	260	40.2	5264	0.6	1	0
Listeria monocytogenes/ready-to-eat meats	58	12.7	974	0.6	1	1
Criterion weights	0.125	0.125	0.25	0.25	0.125	0.125

[a]DALY – Disability-adjusted life years
[b]COI – Cost of illness
[c]Domestic market size (annual basis) = value of retail sales + value of exports – value of imports

Table 7.3 Characteristics of outranking relations in ELECTRE III and PROMETHEE analysis

Criterion	Discrimination thresholds		Transition between thresholds
	Indifference	Strict preference	
DALY (years)	10	78	Linear
COI (CAN$ 10^6)	0.1	9	Linear
Economic value of domestic market activities (CAN$ 10^6)	100	1000	Linear
Consumer risk perception and acceptance of risk	0.05	0.33	Linear
Social sensitivity – consumer	0	1	Not applicable
Social sensitivity – firm	0	1	Not applicable

Table 7.4 Ranking of six pathogen–food combinations

Rank position	ELECTRE III	PROMETHEE I Partial ranking	PROMETHEE II Complete ranking
1	*Escherichia coli* O157/beef	*E. coli* O157/beef	*E. coli* O157/beef
2	*Campylobacter*/chicken *L. monocytogenes*/RTEm	*Campylobacter*/chicken *L. monocytogenes*/RTEm	*Listeria monocytogenes*/RTEm
3	*Salmonella*/chicken *E. coli* O157/spinach	*Salmonella*/chicken	*Campylobacter*/chicken
4	*Salmonella*/spinach	*E. coli* O157/spinach	*Salmonella*/chicken
5		*Salmonella*/spinach	*E. coli* O157/spinach
6			*Salmonella*/spinach

combinations – *Campylobacter* in chicken and *Listeria monocytogenes* in ready-to-eat meats – are considered to be of equivalent risk priority but are actually incomparable. The basis for this "incomparability" can be understood by comparing the risk profiles in Table 7.2. *Campylobacter* in chicken has high scores in the factors related to public health and market-level impact but much lower scores (relative to the other five pairs) in consumer perception and acceptance of risk and social sensitivity. *L. monocytogenes* in ready-to-eat meats is the highest risk case in terms of social sensitivity factors and higher than *Campylobacter* in chicken in terms of consumer perception and acceptance of risk. The PROMETHEE I ranking is referred to as a partial ranking and positions the same two pathogen–food combinations at number two. In the partial ranking procedure, the six pairs are ordered based on the degree to which each pair outranks the other pairs (positive preference flows) as well as the degree to which each pair is outranked by the others (negative preference flows). Incomparability in PROMETHEE I arises when there is an inconsistency in the ordering based on the two analyses – the two pairs change positions in the positive and negative preference orders. The PROMETHEE II ranking is referred to as a complete ranking and is based on the net preference flow (positive preference flow – negative preference flow). It may be easier to interpret because there are no incomparable cases. However, the complete rankings can mask diversity in the risk profiles that should be appreciated by risk managers in making their decisions.

Overall, this is a limited data set but it is useful in demonstrating some of the limitations and the value of MCDA methods in ranking microbial risks in the food system. Future work includes refinement of ranked lists to reflect uncertainty in ranking and feasibility of interventions to reduce risks.

7.4 Food Engineering at Risk Management/Risk Assessment Interface: Challenges and Implications for Training

As noted in the introduction, the Multifactorial Risk Prioritization Framework has been developed by a multidisciplinary research group. The members of the group as well as their primary discipline areas and affiliations are listed below:

Sven Anders	Agricultural Economics	University of Alberta
Julie Caswell	Agricultural Economics	University of Massachusetts – Amherst
John Cranfield	Agricultural Economics	University of Guelph
Valerie Davidson	Food Science/Engineering	University of Guelph
Carlos Daza Donoso	Food Science/Engineering	University of Guelph
Jeff Farber	Food Microbiology	Health Canada
Aamir Fazil	Risk Assessment	Public Health Agency of Canada
Spencer Henson	Agricultural Economics	University of Guelph
Shannon Majowicz	Epidemiology	Public Health Agency of Canada
Juliana Ruzante	Veterinary Medicine	University of Maryland
Claudia Schmidt	Agricultural Economics	University of Guelph

In addition, we have consulted widely to address specific data areas (e.g., food attribution and market information) and to gather expert knowledge needed for health outcome and economic models. Not surprisingly there have been challenges as well as rewards. In keeping with the overall theme of "Food Engineering at the Interfaces" we have included a short reflection on our experiences in multidisciplinary research.

Food safety efforts at the interface of risk management and risk assessment clearly must rely on science- and systems-based analyses. Many disciplines (e.g., epidemiology, microbiology, food science, economics, food engineering) bring important but specialized knowledge to this interface. It is our observation that language is one of the first challenges in a multidisciplinary group. Each discipline has its own unique vocabulary and terms, but it is the deeper use of language – the way we develop our ideas, frame research questions, and present analysis – that is probably more challenging. Key to success is the willingness of the experts to communicate and explain their knowledge at an appropriate level as well as the willingness of "outsiders" to admit any incomplete understanding and to ask questions. In other words, everyone must reach a point of humility and this is not necessarily easy for researchers in any discipline.

Another challenge is the range of methods required in this research. Food engineers are trained in quantitative analysis and predictive modeling but are less familiar with qualitative methods and survey tools. These are important techniques in areas related to consumer behavior as well as in some data gathering. Some information cannot be obtained by direct observation and must be developed by soliciting experts' opinions. Food engineers need to recognize the need for additional research tools and to value the contributions of all research methods equally. Adjectives like "hard" and "soft" should be avoided when discussing methods and results, because they are often used erroneously to convey perceptions that certain methods lack scientific rigor.

Finally, we were fortunate that there was a funding opportunity through the Natural Sciences and Engineering Research Council (NSERC), a national funding agency for science and engineering research in Canada, which established food safety as a priority area in the Strategic Grants Program. The NSERC funding was critical in moving the framework from a conceptual stage to the concrete measures and six case studies presented here. The funding was a unique opportunity to bring this multidisciplinary research group together. Several components of the work (e.g., economics, consumer behavior) fall under the jurisdiction of the Social Sciences and Humanities Research Council and there are very few programs to support research at the interface of two research councils.

Multidisciplinary research is an excellent training experience for graduate students. A number of graduate students in engineering are currently involved in developing different aspects of the framework (knowledge base, multi-criteria decision, analysis tools). Their knowledge and skills are important contributions to the framework; they are also learning new areas of public health, risk management, and operations research.

7.5 Concluding Statements

The Multifactorial Risk Prioritization Framework addresses the need to base risk management decisions on scientific analysis across a comprehensive set of criteria, and to communicate such decisions among varied stakeholders in a clear and transparent way. It is not intended to replace risk managers but to provide context and tools for strategic planning of research needs and interventions that reduce risk.

The Multifactorial Risk Prioritization Framework has been developed and implemented by a multidisciplinary group that includes food engineers. Systems analysis, modeling, and quantitative methods are necessary components of risk analysis, but they are not sufficient on their own. Food engineers must work collaboratively with scientists (e.g., economists, epidemiologists, microbiologists, risk analysts) as well as decision-makers (e.g., risk managers, policy makers) to develop effective strategies for setting food-safety priorities. The present framework is an excellent example of the potential to develop a more comprehensive solution by working together rather than in isolated disciplines.

Acknowledgments The financial support of the Natural Sciences and Engineering Research Council to carry out this work is gratefully acknowledged.

References

Batz MB, Hoffmann S, Krupnick AJ, Morris JG, Sherman DM, Taylor MR, Tick JS (2004) Identifying the most significant microbiological food-born hazards to public health: a new risk ranking model. Food Safety Research Consortium Discussion Paper Series No. 1. Available at: http://www.thefsrc.org/Discussion%20Papers/FRSC-DP-01.pdf (accessed January 30, 2009)

Brans JP, Vincke P (1985) A preference ranking organization method: the PROMETHEE method for MCDM. Manage Sci 31(6):647–656

Brans JP, Vincke P, Mareschal B (1986) How to select and how to rank projects: The PROMETHEE Method. Eur J Oper Res 24:228–238

Canadian Broadcasting Corporation (2008) Maple Leaf settles class action listeriosis lawsuits for $27 M. Available at: www.cbc.ca/canada/story/2008/12/18/listeriosis-settlement.html?ref = rss (accessed January 29, 2009)

Caswell JA (2005) Opportunities for Risk Reduction: An Economist's Perspective. In: Hoffmann SA, Taylor MR (eds) Toward Safer Food Perspectives on Risk and Priority Setting. RFF Press, Washington, DC, p 276

Cole M, Rodriguez A (2008) Emerging Challenges in Food Safety and the Role of Food Engineers, Plenary Lecture at 10th International Congress on Engineering and Food, Viña del Mar, Chile, April 20–24

Davidson VJ, Ruzante J, Fazil A, Caswell J, Cranfield J, Henson S (2008) Multifactorial risk prioritization framework for food-borne pathogens. 10th International Congress on Engineering and Food, Viña del Mar, Chile, April 20–24

Daza Donoso CA (2008) Application of multicriteria decision analysis tools to the prioritization of microbial hazards in food systems. M.Sc. thesis, Faculty of Graduate Studies, University of Guelph

Daza Donoso CA, Davidson VJ, Ruzante JM, Fazil A (2008) Prioritization of microbial risks in foods using multi-criteria decision analysis tools, Canadian Society of Chemical Engineering Conference, October 19–22, Ottawa, Ontario

European Commission (2002) Risk assessment of foodborne bacterial pathogens: quantitative methodology relevant for human exposure assessment. Health and Consumer Protection Directorate-General Directorate C – Scientific Opinions, C1 – Follow-Up and Dissemination of Scientific Opinions, Preliminary Report. Available at: http://europa.eu.int/comm/food/fs/sc/ssc/out252_en.pdf (accessed January 30, 2009)

Fife-Schaw CR, Rowe G (1996) Public perceptions of everyday food hazards: a psychometric study. Risk Anal 16(4):487–500

Fischoff B, Slovic P, Lichtenstein S, Read S, Combs B (1978) How safe is safe enough? A psychometric study of attitudes towards technological risks and benefits. Policy Sci 9(2):127–152

Food and Agriculture Organization of the United Nations and World Health Organization (2002) Principles and guidelines for incorporating microbiological risk assessment in the development of food safety standards and related texts. Kiel, Germany. Report of a Joint FAO/WHO consultation, March 18-xx Available at: http://www.fao.org/docrep/006/y4302e/y4302e00.HTM (accessed January 31, 2009)

Food and Agriculture Organization of the United Nations (FAO) and World Health Organization (WHO) (2008) Microbial hazards in fresh fruits and vegetables (pre-publication version). Available at: http://www.fao.org/ag/agn/agns/files/ffv_2007_Final.pdf (accessed January 30, 2009)

Frewer LJ, Howard C, Shepherd R (1997) Public concerns about general and specific applications of genetic engineering: risk, benefit and ethics. Sci Technol Hum Values 22:98–124

Frewer LJ, Howard C, Hedderley D, Shepherd R (1998a) Methodological approaches to assessing risk perceptions associated with food-related hazards. Risk Anal 18:95–102

Frewer LJ, Howard C, Shepherd R (1998b) Understanding public attitudes to technology. J Risk Res 1(3):221–235

Frewer LJ, Shepherd R, Sparks P (1994) Biotechnology and food production: knowledge and perceived risk. Br Food J 96:26–32

Henson S, Caswell J, Cranfield J, Fazil A, Davidson VJ, Anders S, Schmidt C (2007) A multi-factorial risk prioritization framework for food-borne pathogens. Available at: Social Science Research Network: http://ssrn.com/abstract = 989768

Laboratoire d'analyse et modélisation pour l'aide à décision (LAMSADE) (1994) ELECTRE III/IV Software, Université Paris-Dauphine, PARIS CEDEX 16, France

Murray CJL (1994) Quantifying the burden of disease: the technical basis for disability-adjusted life years. Bull World Health Organ 72(3):429–445

Murray CJL, Acharya AK (1997) Understanding DALYs. J Health Econ 16:703–730

New Zealand Food Safety Authority (2008) Food safety in New Zealand: application of a risk management framework. Available at: http://www.nzfsa.govt.nz/about-us/risk-management-framework/page-03.htm (accessed January 30, 2009)

Roy B (1978) ELECTRE III: Un algorithme de classements fondé sur une représentation floue des préférences en présence de critères multiples. Cahiers du Centre d'Etudes de Recherche Opérationnelle 20(1):3–24

Ruzante JM, Davidson VJ, Fazil A, Cranfield JAL, Henson SJ, Caswell JA, Anders SM, Schmidt C, Farber J (2009) A Multifactorial risk prioritization framework for foodborne pathogens, accepted risk analysis, July. doi:10.1111/j.1539–6924.2009.01278.x

University of Guelph (2008) Consumers changed habits following listeriosis outbreak, Study finds, December 03 news release. Available at: http://www.uoguelph.ca/news/2008/12/post_157.html (accessed November 18, 2009)

Western Farm Press (2008) Fresh tomato industry shaken by FDA salmonella links, seeks answers. Available at: http://westernfarmpress.com/vegetables/fresh-tomato-0821/

Chapter 8
Development of Eco-efficiency Indicators to Assess the Environmental Performance of the Canadian Food and Beverage Industry

Michèle Marcotte, Yves Arcand, Dominique Maxime, and Denyse Landry

8.1 Introduction

Agriculture and Agri-Food Canada (AAFC) is committed to adopting sustainability as a key principle and has been working on the development of agri-environmental indicators (AEI) to assist the agricultural sector in assessing its impact on environmental health. Since 2003 and for a period of 5 years, through the implementation of the Agriculture Policy Framework (APF) (Agriculture and Agri-Food Canada 2004), agri-environmental indicators have been developed specifically addressing environmental issues at the Canadian Food and Beverage Industry (FBI) level to provide a more comprehensive assessment of the impact of the whole food value chain on the environment (NAHARP 2004). This chapter presents the general approach being used in the development of science-based agri-environment indicators specific to the Canadian Food and Beverage Industry, their calculation using statistical survey data, and a first report on the results.

8.2 Overview of the Canadian FBI

The Canadian food and beverage industry (FBI) consists of approximately 6,700 establishments involved in the transformation of raw agricultural commodities into semi-prepared and consumer-ready food and beverage products. The FBI is important

M. Marcotte (✉)
Agriculture and Agri-Food Canada's Eastern Cereal and Oilseed Research Centre, 960 Carling Avenue, KW Neatby, Room 1093, Ottawa, ON, K1A 0C6, Canada
e-mail: Michele.marcotte@agr.gc.ca

Y. Arcand and D. Maxime
Agriculture and Agri-Food Canada's Food Research and Development Centre, 3600 Casavant Blud West, St. Hyacinthe, QC, Canada

D. Landry
Agriculture and Agri-Food Canada Head Quarter, 1341 Baseline Road, Touer 5, Floor 2, Room 126 Ottawa, ON, K1A OC5, Canada

J.M. Aguilera et al. (eds.), *Food Engineering Interfaces*, Food Engineering Series,
DOI 10.1007/978-1-4419-7475-4_8,

to the Canadian economy, being the largest manufacturing employer (296,000 Canadians), especially in many rural and agricultural areas across Canada. Over 90% of FBI establishments have fewer than 100 employees – 45% have fewer than five employees. It is the second largest manufacturing industry in Canada and accounts for 14% of total manufacturing shipments and 2% of the national Gross Domestic Product (GDP). The FBI produces shipments worth $87 billion. Furthermore, it supplies approximately 77% of all processed food and beverage products available in Canada.

The food and beverage processing industry (FBI), which is classified as a manufacturing industry, is a major intermediary in the food chain. The FBI is the critical link in the "farm to fork" value chain that transforms agricultural products for consumers. It is the pathway of almost half of Canada's raw primary agricultural output, and around 70% of FBI's inputs come directly or indirectly from agricultural production or fisheries. These inputs are processed into a wide range of food products prior to shipping to domestic (78%) or international consumers (22%). It is an important industry in all provinces and generally ranks among the top three manufacturing sectors in terms of shipments and jobs. Figure 8.1 shows the distribution of food and beverage manufacturing establishments in each province. Establishments in Ontario and Quebec accounted for 56% of the total number of establishments. Ontario accounts for 40% of shipments, Quebec for 22% and Alberta for 13%.

According to the North American Industry Classification System (NAICS) (Statistics Canada 2004), the FBI is divided into sub-sectors according to similarities in their input materials and the production processes involved. The food processing sub-sectors are: animal food, grain and oilseed, sugar and confectionery, fruit, vegetable and specialty food, dairy products, meat products, seafood products, bakeries and tortilla, and other food. Beverage processing sub-sectors are: soft drink and ice manufacturing, breweries, wineries, and distilleries.

The food and beverage industry uses a wide range of technologies to achieve two primary objectives: (1) to carry out the desired processing (e.g., bread

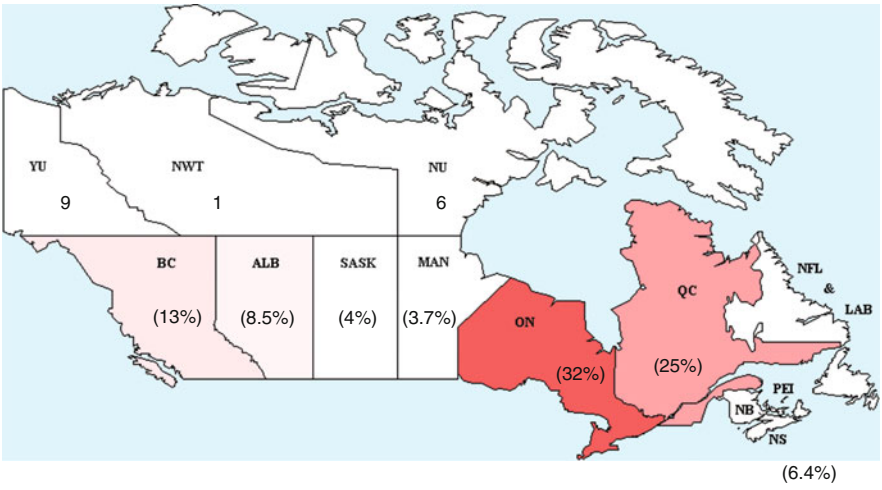

Fig. 8.1 Distribution of the Canadian food and beverage industry (Statistics Canada 2002a)

production) and (2) to stabilize foods and beverages so they will have a longer shelf life (e.g., milk pasteurization). The manufacturing steps and processes for most foods and beverages are well known and usually fall into the following categories:

- Preparing raw materials (washing, cutting, mixing, homogenization)
- Utilizing heat (sterilization, pasteurization)
- Utilizing cold (refrigeration, freezing)
- Removing water (drying, evaporation, pressing, filtration)
- Modulating product composition (pH, salts, sugars, preservatives, smoking fermentation)
- Modulating product environment (dissolved oxygen, modified or controlled atmosphere, active packaging)
- Separating/concentrating the components of agricultural products (extraction, membrane, distillation)

As in all other sectors, food and beverage processing plants are required to meet various environmental performance standards, which may be critical for competing on the world market. In manufacturing food products, the food and beverage industry uses a significant amount of resources (raw agricultural products or ingredients, energy, water). It also generates gaseous emissions, liquid wastes and solid organic residues. While most packaging waste is generated at the consumption level, almost all of it enters the system at the processing stage. Five issues (or environmental loads) have been identified for the development of eco-efficiency indicators in the food and beverage processing industry:

- Energy use
- Greenhouse gas (GHG) generation
- Water use
- Waste water production (e.g., effluents)
- Packaging waste generation

The indicators are based on the concept of eco-efficiency, which is a widely recognized concept in the manufacturing industry and is often used to help companies characterize and meet both environmental and economic objectives (Verfaillie and Bidwell 2000) Eco-efficiency is defined as a process during which goods or services of greater value or greater quantity are produced using fewer raw materials, and less water and energy, thereby reducing natural resource depletion and pollution (NRTEE 2001). The indicators essentially compare the environmental factors or "loads" to the quantity of products manufactured. While this actually provides an intensity rating (which is the inverse of efficiency), the use of a common denominator (physical production unit or value) facilitates a comparison within each sub-sector for each of the five issues of interest. The indicator concepts are evaluated and validated using data from past surveys (e.g., Annual Survey of Manufactures for 2002; Statistics Canada 2002a), and the Annual Industrial Consumption of Energy Survey for 2002 (Statistics Canada 2002b) and Industrial Water Use Survey (Statistics Canada 2008d).

8.3 Energy Consumption and Greenhouse Gas Emissions

The food and beverage industries (FBI) consume a significant amount of energy for processing most of what Canadians eat and drink. This energy consumption has a significant impact on the environment, whether direct (impacts generated onsite) or indirect (impacts generated during energy production, and its conversion and transportation to site where consumed). For example, a direct impact would be when natural gas is burnt onsite in an industrial oven, or in the case of an indirect impact, when the company uses an electric oven with electricity coming from a coal burning power plant. The burning of fossil fuels results in the emission of greenhouse gases (GHG) and other residues.

According to statistics on energy consumption in the Canadian industry, published by the Canadian Industrial Energy End-use Data and Analysis Centre[1] (CIEEDAC 2008), the Canadian FBI consumed around 100,700 TJ (terajoules or millions of megajoules) in 2002, which is about 4% of the energy consumption of all Canadian manufacturing sectors. This is enough energy to power approximately 2.5 million Canadian households for 1 full year. The left side of Table 8.1 presents

Table 8.1 Energy use and greenhouse gas emissions from manufacturing industries and agriculture in Canada in 2002

	Energy use		GHG emissions	
	Terajoules	%[a]	Thousands/tons CO_2 equivalent	%[a]
Food manufacturing[b]	88,765	3.5	3,477	3.3
Beverage manufacturing[b]	11,975	0.5	517	0.5
Total, Food and Beverage manufacturing (FBI)[b]	100,740	4	3,994	3.8
Pulp and paper manufacturing[b]	830,779	33	9,888	9.5
Total, manufacturing industries[b]	2,515,928	100	103,911	100
Agriculture[c]	205,655	–	52,000	–
Canada[c, d]	9,669,768	–	720,000	–

[a]Since data sources and accounting methods differ, precise comparisons are not recommended between manufacturing and other data, and are presented for information only. CIEEDAC data is deemed more comprehensive and includes energy and GHG emissions from waste, biomass, etc., which can influence significantly total energy use in some manufacturing sectors

[b]Manufacturing data from CIEEDAC (2008), both for energy and GHG

[c]Energy use data (Statistics Canada 2003, 2004, 2007); GHG emission data from Environment Canada's GHG national inventory reports (Environment Canada 2007; Environment Canada 2004) GHG for Agriculture *excludes* combustion-related emissions, which are a small percentage of total agriculture emissions

[d]Canada energy use is the total net energy supply in Canada

[1]CIEEDAC has developed and maintains a comprehensive database on energy, and GHG from information supplied by Natural Resources Canada, and is produced by Statistics Canada, among others. It should be noted there are some discrepancies in official publications by Statistics Canada or Environment Canada (for more information on issues concerning energy accounting and GHG calculations, see Nyboer 2008a, b).

details on energy use in the FBI as compared to other manufacturing industries, as well as energy used by the agricultural sector and the total net energy supplied in Canada.

In 2002, around two thirds of FBI energy needs were supplied by natural gas, a non-renewable, fossil fuel resource, and more than 20% by electricity (CIEEDAC 2008), although this figure may vary significantly depending on the activity sector within the FBI. The FBI sub-sectors can be distinguished by the raw materials they process into food products; the FBI is a very diverse industry, manufacturing a broad range of different products using specific processes and technologies with various energy needs.

Energy is an important input cost for the FBI, typically ranking third after raw materials and labor costs. Energy accounts for a significant share of FBI production costs, up to 16% for the corn milling industry, around 10% for rendering and meat processing, rice and malt processing, distillery and brewery sub-sectors (Navarri et al. 2001). Furthermore, it is estimated that 40% of the value of processed food is added through energy-intensive manufacturing (US Environmental Protection Agency 2007), such as process heating and cooling systems. Figure 8.2 shows the typical energy uses in a FBI plant. It is important to note that most of the energy demand is necessary to maintain food safety. Thus, FBI is very sensitive to rises in energy prices, especially since profit margins are often low, and increased energy

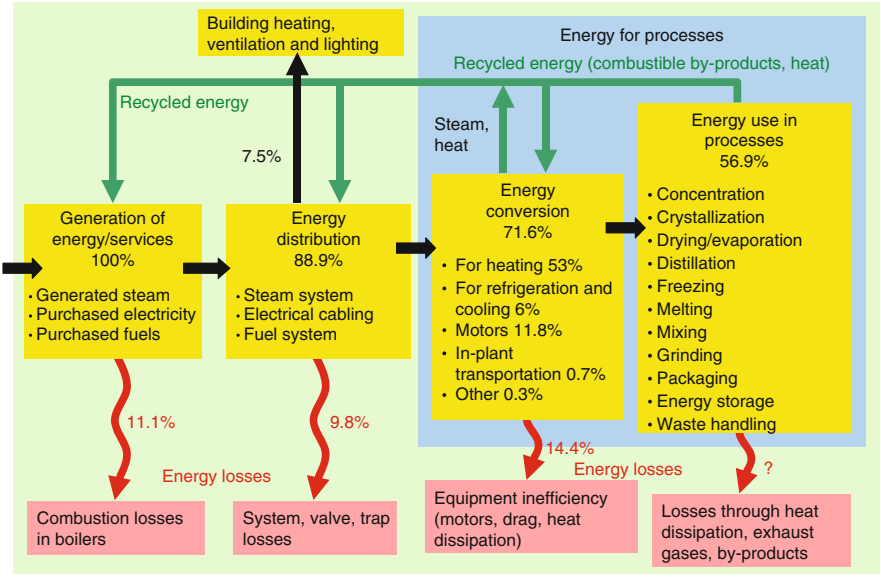

Fig. 8.2 Diagram of typical energy flows in a food manufacturing plant (Adapted from US Department of energy 2004)

efficiency, rather than just energy reduction, is the main pathway to a sustainable food industry.

Energy sources are numerous but most are of the non-renewable type, whether they are fossil fuels or electricity produced using coal, heavy fuel or nuclear sources. Apart from the fact that the price of all fossil fuels is skyrocketing and its extraction and refining generate different types of pollution, one of the most concerning side effects of using energy coming directly or indirectly from fossil fuels is the generation of greenhouse gases (GHG) that contribute to global warming.

There are typically three main sources of direct – onsite – GHG emissions in the FBI.[2] Fossil fuel combustion (e.g., in boilers and ovens) is the major source, accounting for up to 90% of total emissions in a plant heavily relying on these types of energy, emitting mainly CO_2 (and other pollutants contributing to GHG, such as N_2O; or not contributing, such as soot particles). Another source is refrigeration and freezing units using hydrofluorocarbons (HFCs), which can leak during a system's lifespan. Despite the low volume of such leaks, their global warming potential (GWP) is a hundred to a thousand times higher than that of CO_2, meaning the release into the atmosphere of a few kilograms of most refrigerants may have a similar contribution to global warming as a ton of CO_2. Thus, they may account for a significant share of total GHG emissions in plants with large needs for cold processing or storage (e.g., frozen foods, dairy products, meat, and seafood). A third source of emissions is closely related to biomass and organic wastes, and can be either solid or liquid. A plant's wastewater treatment system using anaerobic digestion emits methane, which should be inventoried as a GHG (because 1 kg of methane has a similar effect as 21 kg of CO_2), if not captured to fire in a boiler (methane when burned is chemically transformed into CO_2 with a GWP of 1). In addition, solid biomass (e.g., spent grains from distilleries, breweries residues, agriculture wastes) may be land filled, composted (onsite or offsite) or burned by some FBI plants for energy valorization, all of these emitting various levels of GHG.[3]

Unfortunately, the two latter sources of emissions (refrigerants and organic wastes) are still difficult to estimate accurately at the sectoral or FBI level, as reliable statistics, indeed aggregate, are available only for fossil fuel related GHG emissions. At FBI production sites in 2002 and 2005, there were 3,994 and 4,020 kt of CO_2-equivalent GHG produced, respectively (CIEEDAC 2008), that is, 3.7% of total Canadian industry emissions.

Demand for energy in the FBI is expected to grow due to increased demand for shelf-stable products, individual ready-to-serve or quick-to-prepare meals, and processed fresh food. This makes energy a particularly complex challenge for the FBI given that the industry is often reluctant to changes because of its desire to

[2]Note that the consumption of electricity does not emit GHG directly.

[3]According to GHG inventory and reporting standards from the Intergovernmental Panel on Climate Change, GHGs from biomass combustion do not have to be reported in national inventory since the biomass is *carbon neutral*, *provided it is consumed in a sustainable way* (i.e., at a rate not higher than one needed for its renewal).

maintain high product quality and its obligation to ensure product safety. The underlying intent of the following eco-efficiency indicators is to provide more comprehensive – disaggregated – insight on energy use and consequent GHG emissions *through reporting of sub-sector and regional specificities related to activity levels*. They also aim to follow over time energy efficiency improvements, as well as shifts to energy sources emitting less GHG.

The two indicators were developed as a way to provide establishments with a measure of their "environmental impact" on the quantity of energy used (ECI), as well as a measure of the effect of their GHG management practices (GHGEI). By comparing with different agreed to targets (which should be related to the sustainable capacity of the natural habitat), these indicators could also give local, provincial, and national authorities a more adequate picture of the total energy demand/GHG generation as well as the relative impact of each stakeholder, helping governments take appropriate actions to sustain human and economic growth.

8.3.1 The Indicators: Energy Consumption Intensity and Greenhouse Gas Emission Intensity

In order to provide information about these environmental concerns, two indicators have been developed: the energy consumption intensity (ECI) indicator and the greenhouse gas emission intensity (GHGEI) indicator, the former expressing the ratio of the amount of energy used per dollar of manufactured goods produced[4] (MJ/$) and the latter expressing the ratio of the amount of GHG emitted (expressed in CO_2-equivalent) per dollar of manufactured goods produced (kg CO_2-e/$), respectively:

$$\text{ECI} = \frac{\text{Total energy consumed}}{\text{Value of production}} \quad \text{GHGEI} = \frac{\text{Total GHG emissions}}{\text{Value of production}}$$

These intensity indicators reflect how much energy is used (ECI) and the volume of GHG emissions produced (GHGEI) per dollar of product sold, and are inversely proportional to efficiency performances: the larger the indicator, the lower the efficiency and the environmental performance.

Since the FBI manufactures a broad range of highly diversified products (often tightly linked to regional agricultural production characteristics), and because the industry involves various scales of production (from small facilities to very large

[4]As defined by Statistics Canada in the Annual Survey of Manufactures (ASM) protocol: "The production is measured by the value of shipments of goods of own manufacture, that is the selling value of goods made by reporting establishments, excluding transfers into inventory and consignment sales, shipping charges by common or contract carriers, discounts and returns, federal and provincial sales taxes and excise duties and taxes, sales of goods purchased for resale."

processing plants), the indicators should reflect these peculiarities. Therefore, in order to maintain consistency within food industry sectors and to make valid regional comparisons, establishments were grouped according to similar characteristics: same sector of activity, same region, and same size as determined by number of employees. Table 8.2 details these characteristics.

Both indicators use data from the Statistics Canada 2002a Annual Survey of Manufactures (*ASM*[5]). For each establishment included in the calculations, the value of production (i.e., value of products sold) and the purchase cost of each form of energy used are needed. The amount of each form of energy used is calculated, using appropriate regional energy prices, and converted into a common unit of energy (megajoule, MJ) using Statistics Canada's 2002 energy conversion factors (2004). GHG emissions (CO_2, CH_4, and N_2O) in CO_2 equivalents are also calculated for each form of energy consumed, using Environment Canada (2004a) GHG emission factors and the Intergovernmental Panel on Climate Change (IPCC 1996) global warming potentials (GWP). HFCs were not included here, as the *ASM* does not provide sufficient data to quantify these refrigerants.

The ECI (or GHGEI) indicator is calculated for each group according to two complementary methods (Fig. 8.3):

- The first method calculates a *global indicator* value for the group, using the sum of all energy used by all establishments included in the group divided by the total sales value of the whole group. This process gives a good picture of the group as a whole (i.e., considers the group as one unique establishment). Unfortunately, this method does not provide information on the performance of any individual plant compared to the group.
- The second method calculates a *median indicator range* for the group. First, a single indicator is calculated for all establishments, which are then ranked by increasing value. Forty percent of the establishments with the lowest values are tagged as "better than average," while 40% with the highest values are tagged as "worse than average." The remaining values are tagged as "on average," and the lowest and highest values of this "on average" group represent *the median indicator range*. This second method provides an indication of the range of efficiencies within the groupings and is useful for comparison to the global indicator, because each establishment has the same importance in the calculation regardless of size. It also involves calculations particularly suited to the presence of outliers in the groups (e.g., invalid or unrepresentative single indicators). Lastly, the median is a more robust statistic than the mean in the case of small groups.

[5]More details about *ASM* method can be found at Statistics Canada Web site. http://www.statcan.ca/cgi-bin/imdb/p2SV.pl?Function = getSurvey&SDDS = 2103&lang = fr&db = imdb&dbg = f&adm = 8&dis = 2

Table 8.2 Parameters for plant grouping and indicator reporting for energy and greenhouse gas indicators

Sector (o) and sub-sector (•) short name	Activity sector (o) and sub-sector (•) definition and NAICS[a] code
○ Grain and oilseed	○ Grain and oilseed milling (3112)
• Flour	• Flour milling (311211)
• Malt	• Rice milling and malt manufacturing (311214)
• Oilseed	• Oilseed processing (311224)
• Breakfast	• Breakfast cereal manufacturing (311230)
○ Sugar and conf.	○ Sugar and confectionery product manufacturing (3113)
• Sugar	• Sugar manufacturing (311310)
• Cacao conf.	• Chocolate and confectionery manufacturing from cacao beans (311320)
• Chocolate conf.	• Confectionery manufacturing from purchased chocolate (311330)
• Candy conf.	• Non-chocolate confectionery (311340)
○ F&V	○ Fruit and vegetable preserving (3114)
• Frozen F&V	• Frozen food (311410)
• Other F&V	• Fruit and vegetable canning, pickling and drying (311420)
○ Dairy	○ Dairy product manufacturing (3115)
• Milk	• Fluid milk (311511)
• Other dairy	• Butter, cheese and dry and condensed dairy product manufacturing (311515)
• Ice cream	• Ice cream and frozen dessert manufacturing (311520)
○ Meat	○ Meat product manufacturing (3116)
• Red meat slaughter	• Animal (except poultry) slaughter (311611)
• Red meat	• Rendering and meat processing from carcasses (311614)
• Poultry	• Poultry processing (311615)
○ Seafood	○ Seafood product preparation and packaging (3117)
○ Bakeries	○ Bakeries and tortilla manufacturing (3118)
• Retail bakeries	• Retail bakeries (311811)
• Com. bakeries	• Commercial bakeries and frozen bakery product manufacturing (311814)
• Cookies	• Cookie and cracker manufacturing (311821)
• Flour mixes	• Flour mix and dough manufacturing from purchased flour (311822)
• Pasta	• Dry pasta manufacturing (311823)
○ Beverage	○ Beverage manufacturing (3121)
• Soft drinks	• Soft drink and ice manufacturing (312110)
• Breweries	• Breweries (312120)
• Wineries	• Wineries (312130)
• Distilleries	• Distilleries (312140)
Region short name	**Geographical region**
○ CA	○ Canada
• AT	• Atlantic (Newfoundland and Labrador, Nova Scotia, Prince Edward Island, New Brunswick)
• QC	• Quebec
• ON	• Ontario
• PR	• Prairies (Manitoba, Saskatchewan, Alberta)
• BC	• British Columbia
Size short name	**Establishment size category**
○ All	○ All sizes
• Small	• Up to 49 employees
• Medium	• 50–99 employees
• Large	• 100–199 employees
• Very large	• 200 or more employees

[a]North American Industry Classification System

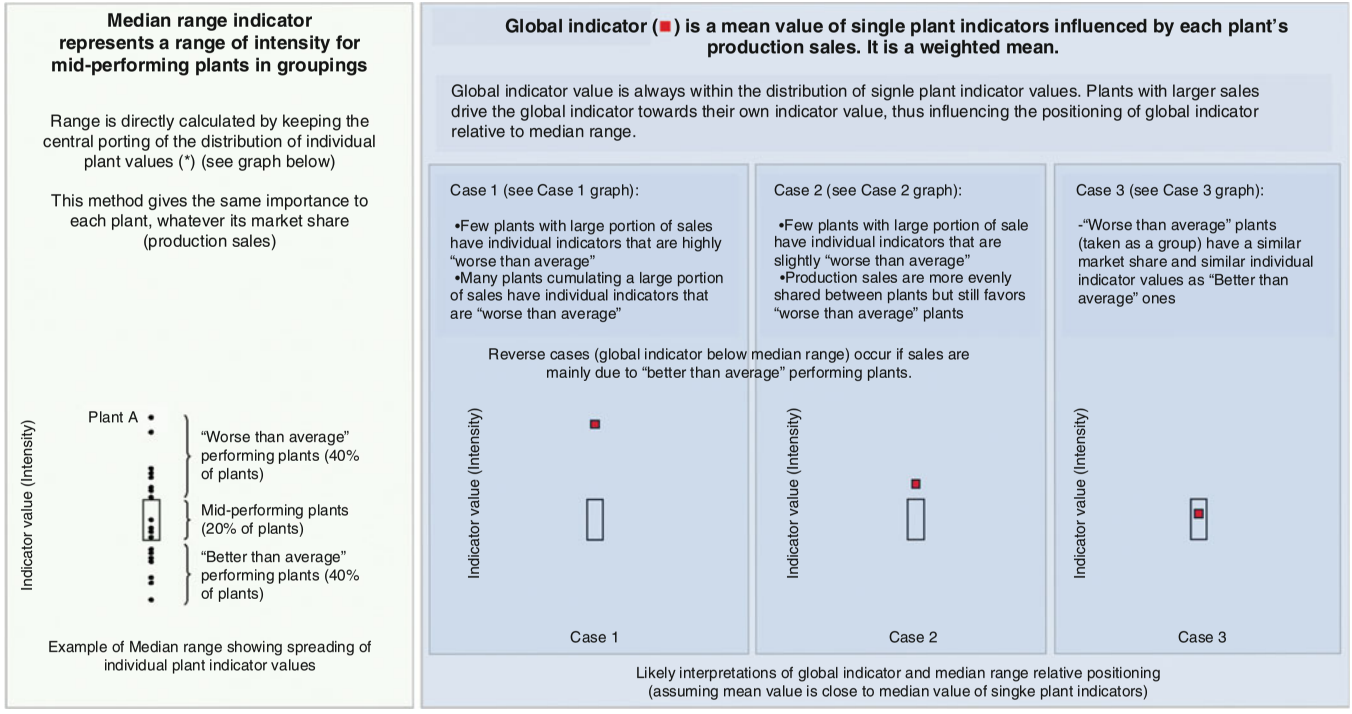

Fig. 8.3 How to read and interpret indicators data

8.3.2 Results and Interpretation: ECI and GHGEI

This report provides the national and provincial results of both indicators for the year 2002 for various manufacturing sectors of the FBI. The main objective of reporting these indicators is to follow *over time* how a given sector is increasing or reducing its intensity (i.e., increasing or reducing its pressure on resource depletion or GHG production). Consequently, the present report does not discuss any timeline trend but sets the baseline. Thus, the following discussion aims rather at interpreting these 2002 indicator results by focusing on the inter-sectoral and inter-regional distinctiveness of the Canadian FBI, while avoiding as much as possible direct comparisons of the indicators. The main goal here is to provide objective information that enlightens future interpretation of indicator trends.

Results will first present the effect of different employee sizes on each sector for ECI and GHGEI at the national level. Second, the difference between sub-sectors will be presented at the national level. Finally, sectors will be compared per region. All graphs will present the different groupings on the X-axis and the value of the indicator on the Y-axis. Additional comparisons at the regional level will be possible by using Figs. 8.4 and 8.5, respectively, to present the importance of each sector (in terms of sales) in each province and the proportion of each energy source used in each region.

Unless otherwise indicated, the ECI indicator is expressed in megajoules per dollar in 2002 (MJ/$), and the GHGEI indicator in kilograms of CO_2 equivalent per dollar in 2002 (kg CO_2e/$). Establishments' groupings are reported using the short

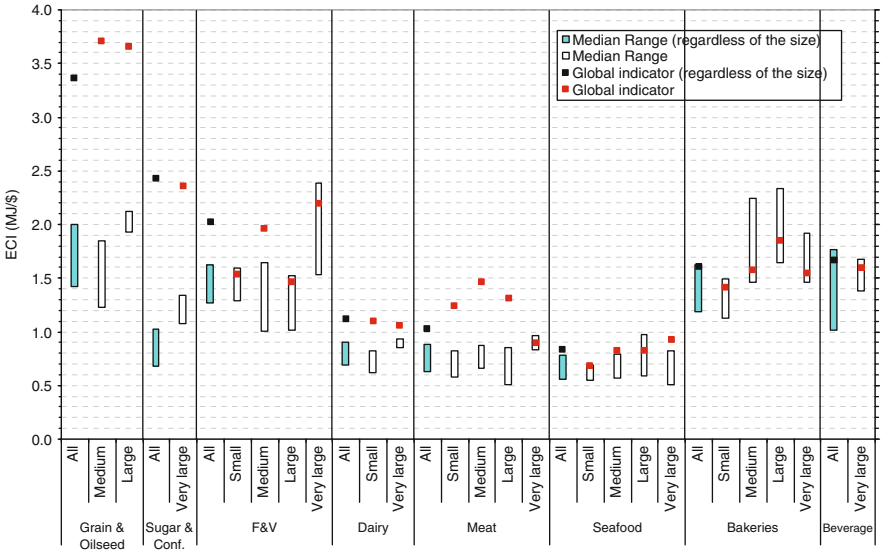

Fig. 8.4 Energy consumption intensity (*ECI*) as a function of activity sector and size calculated for year 2002

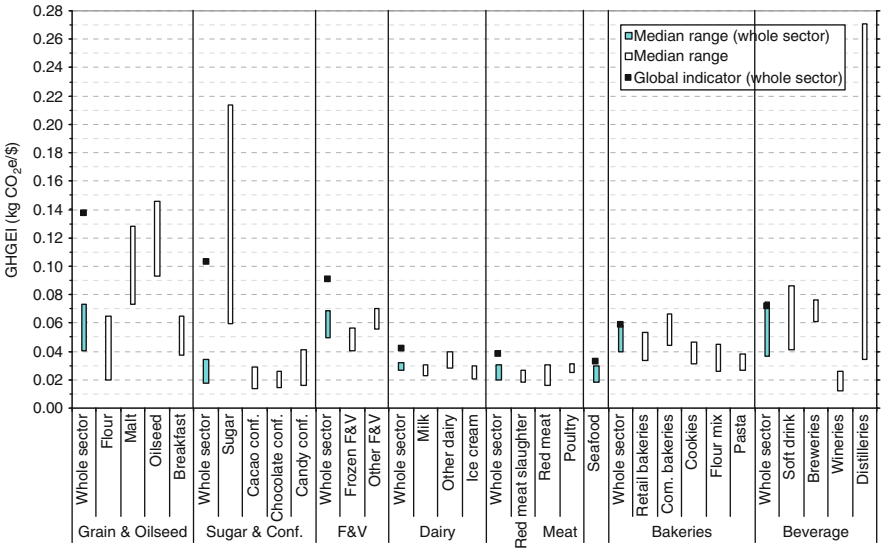

Fig. 8.5 Greenhouse gas emissions intensity (*GHGEI*) as a function of activity sector and sub-sector calculated for year 2002. There is no sub-sector in the seafood sector

names listed in Table 8.2. Data from some sub-sectors and some plant sizes could not be published due to confidentiality, while the "animal food" sector and "other food" manufacturing sectors are not covered within this indicator set. In the following, the median range indicator will be referred to as *median range*, *median*, or *typical representative plant indicator*.

8.3.2.1 National Results and Interpretation: ECI and GHGEI

Figure 8.4 provides an overall picture of ECI indicator values across Canada for all sectors reported, with or without regard to size of establishments.

ECI, Sectoral Features Regardless of Size of Establishments

Looking first at the median range indicators without regard to size of establishments ("blue-filled bars" in Fig. 8.4), two sets of sectors stand out when it comes to energy eco-efficiency. In the sugar and confectionery, dairy, meat, and seafood sectors a typical representative plant shows an ECI of around 0.75 MJ/$, while other sectors have a median range ECI of around 1.5 MJ/$. The higher values for grain and oilseed, fruit and vegetable (F&V), bakeries, and beverage sectors are hardly

surprising, given that energy makes up a high proportion of the production cost in these sectors, which generally make extensive use of energy-intensive operations, such as evaporation, concentration and drying, cooking and baking, and process heating and freezing for the fruit and vegetable sector.

Looking now at sector global indicators ("black dots" in Fig. 8.4), the observed values reveal that the grain and oilseed, and sugar and confectionery sectors, and to a lesser extent the fruit and vegetable sector, have far higher global intensity (two to four times higher than those of dairy, meat and seafood sectors). Comparing global with median range calculation methods for all three sectors (i.e., grain and oilseed, sugar and confectionary, and fruit and vegetable) shows that global intensity is significantly higher than each sector's own median range intensity, especially for sugar and confectionery (global intensity is 136% higher than upper boundary of median range) and grain and oilseed (64% higher).

The situation described above highlights the fact that the biggest players (in terms of sales) within these sectors are energy-intensive plants, although not enough to shift up the median range of the whole sector. This particular situation reveals that within a group the "worse than average" category is accountable for a lot more than 40% of sales (even though it accounts for exactly 40% of plants), thus shifting the global indicator far above the median range indicator. Conversely, if most sales are made by "better than average" plants, the global indicator will then be shifted below the median range indicator. Moreover, if the proportion of "better than average" and "worse than average" sales are approximately equal, then the global indicator will stand very close to, if not within, the median range indicator. The situation where the global indicator is far above the median range reveals a *potential* gain in energy efficiency for the major players of these sectors.

It is worth noting, however, that this may be due to a number of reasons. First, larger plants (in term of sales) within a sector are generally more automated than smaller plants and therefore may require more energy to operate their higher capital intensity operations, be it for production (machine feeding, conveyors, etc.) or sanitization/food safety and quality standards to satisfy stringent buyer requirements. Second, larger plants often sell products that are more commoditized, less differentiated, and therefore of lower value per volume sold. For example, consumers are often willing to pay a premium for hand-made specialty bread from a local bakery instead of "industrial" bread from one of the big Canadian bakeries. The fact this bread is hand-made may surprisingly reduce the quantity of energy used in production since some operations (e.g., machine feeding, emptying and cleaning, packaging, etc.) are not automated, whereas specialty bread would bring up the price, tending to reduce ECI value of the local bakery.

The evidence of few plants having low energy efficiency within a sector, while representing a high share of sales, is also observed to a lower extent in the fruit and vegetable sector, and to a much lower extent in the dairy and meat sectors. This is not the case however in the seafood, bakery or beverage sectors. However, it is worth noting there is no sector where the major players (in terms of production) have a "better than average" ECI, which would have shifted the global indicator below the median range.

ECI, Sectoral Features with Regard to Establishment Size

The effect of establishment size is also reported for all FBI sectors (white bars and red dots, Fig. 8.4). This graph allows easy identification of employment size categories where significant improvements can be achieved, at least by some of the larger selling processors within most size groups. For instance, in the fruit and vegetable sector, the median range ECI is similar for "small," "medium" and "large" plants but significantly higher for "very large" ones. However, this trend is not confirmed by the corresponding global indicator because of the medium size category, which is the only one in the sector to show a global ECI (red dot) higher than the median range (white bar). Consequently, the big sellers of medium size plants should be investigated to see why they are using more energy than their peers. Furthermore, any plant in the very large category should also be investigated for energy efficiency improvements in order to achieve a typical intensity in line with other categories (i.e., between 1.0 and 1.6 MJ/$, a kind of "average" benchmark).

Within the meat sector, the median range is not dependent on plant size and has a value close to 0.75 MJ/$. However, all but the very large size categories include plants with potential energy efficiency improvements because the biggest sellers in each group size have global indicators significantly above their respective median range. Similar behavior of the median range indicator prevails in the seafood sector. As for the global indicator, the very large category only depicts this situation, though a slight gain only in efficiency seems achievable. Thus, very similar values for all median ranges in this sector, together with several global indicators ranking inside – or very close to – the median range, might depict a situation where similar performance is already achieved within most of the sector, probably because similar best practices have been globally deployed. This situation is also observed within the beverage sector (although only one size category is provided), and partly within the fruit and vegetable sector. The dairy sector, as well as the grain and oilseed, and sugar and confectionery sectors, show that some plants could achieve improvements whatever the size category reported.

The case of the bakeries sector is singular in this study, in the sense that it is the only sector to display a similar trend for both median range and global calculation methods. Both methods show that smaller plants are more efficient energy users (excluding the very large category). But a finer analysis shows a tendency towards medium to very large establishments with a high share of sales to a downward shift of global ECI towards the lower boundary of the median range. This means that these plants tend to perform better than a typical plant in the category; and that they could have implemented eco-efficiency measures or better management practices.

Lastly, the commonly held belief is undermined in that the biggest establishments are more eco-efficient because of their capacity (financial resources, know-how) to be proactive in environmental management. Indeed, whatever the sectors displayed in Fig. 8.4, the ECI of a typical representative plant does not decrease clearly or significantly for those with more employees. At least this can be observed through the global ECI trend (e.g., meat sector from large plants, and bakeries

sector from very large plants), but as already explained only a few plants in the size category are included.

ECI, Sub-sectoral Features Regardless of the Size of Establishments

A study of the effect of sub-sectors on ECI was done and the following conclusions surfaced.[6] Within three of the eight sectors studied (grain and oilseed, sugar and confectionary, and beverage sectors), there are significant differences between sub-sector ECI values. This may have an impact on large data spreading in a sector and influence sector conclusions. The malt and the oilseed sub-sectors have the highest ECIs within the grain and oilseed sector,[7] about twice as high as that of flour and breakfast sub-sectors. Sugar refining plants are the driver of the whole sugar and confectionery sector's energy intensity; whereas cacao and chocolate confectionery sub-sectors show a very low intensity (as low as a typical dairy, meat, or seafood plant). There are few differences within the dairy sector, as well as the meat sector. Retail and commercial bakeries are slightly more energy-intensive than cookie and cracker manufacturing, flour mix and dough manufacturing, and dry pasta manufacturing sub-sectors within the bakeries sector. Within the beverage sector, winery and distillery sub-sectors clearly stand out, the first being the sector's least intensive energy user, and the second posting a very large median range, which may be explained by a large spreading of single plant ECIs.

Greenhouse Gas Emission Intensity

The total amount of GHG a plant can emit depends on the quantity of energy it consumes as well as on the type(s) of energy used. Obviously, some energy types are cleaner than others: consumption of electricity does not emit GHG at all, while some fossil fuels emit less GHG during combustion than others to provide the same amount of useful energy (e.g., natural gas emits around 1.5 times less GHG than light fuel oil to provide 1 MJ of steam in a boiler). Thus, for a given quantity of total energy consumed, the mix of energy types involved will influence the amount of GHG emitted.

Figure 8.5 provides Canada-wide details on the GHGEI median range indicator at the sub-sector level, as well as global and median range indicator at the sector level (global indicator at sub-sector level could not be published for confidentiality reasons). With regard to national GHGEI results at sector level (Fig. 8.5), displayed patterns are fairly similar to those of ECIs (Fig. 8.4). It means that the amount of

[6]See technical supplement for detailed results.

[7]Data on two other subsectors of the grain and oilseed sector, i.e., wet corn milling (or 'corn milling') and fat and oil refining and blending, cannot be published because of confidentiality.

GHG produced per quantity of energy used was not very different from one FBI sector to another in 2002. Hence, analysis and arguments provided above for ECIs should hold true for GHGEIs, and therefore will not be repeated here.

As an adjunct to the GHGEI indicator, calculation of sector ratio GHGEI/ECI for the global indicator (amount of GHG emitted for each MJ of energy consumed) provides useful information complementary to the whole sector GHGEI indicator (Fig. 8.5), allowing sector comparisons independent of the dollar value of sales. Furthermore, it provides an indicator on how clean the energy consumed within a sector is, or how much effort this sector is putting to reduce GHG emissions once energy needs have been optimized. Improvements are mainly technological and can be looked for in different areas, for example, process changes in electric technologies, and shifts in energy supply toward cleaner energy or energy mix, etc. Sector results of this calculation are as follows, in increasing order of GHG emitted per unit of energy consumed (g CO_2e/MJ): bakeries (36.7), dairy (37.6), meat (37.7), seafood (39.6), grain and oilseed (40.8), sugar and confectionery (42.5), beverage (43.1), and fruit and vegetable (45.0).

It is worth noting that differences between sectors are slight; bakeries compared to fruits and vegetables show both a 10% difference with respect to mean of dataset ($41 \pm 10\%$). Thus, no sector clearly distinguishes itself, whether as a "cleaner energy" user or not. This is somewhat surprising since one would have expected sectors heavily using electric processes (e.g., cooling, refrigeration, and freezing) to clearly stand out. Several factors are responsible for these similar results. First, the expected difference is likely to stand out more clearly at the sub-sector level (e.g., frozen food requires mostly electricity while fruit and vegetable canning uses more fossil fuel, yet both are in same sector). Second, any sector has to comply with food safety standardized procedures requiring pasteurization or sterilization processes and/or strict sanitation processes that might involve a significant amount of thermal energy from fossil fuels. Third, plants relying on one unique energy source – be it clean or not – are now scarce. Fourth, regional distribution of the sector displayed in Fig. 8.6 reveals that Alberta, Ontario and Quebec are each contributing approximately 30% to national production. Figure 8.7 shows that their respective energy grid is very different. This tends to level out the national ratio. Lastly, it should be noted, specifically for the seafood sector, that fuel consumed by fishing vessels is often accounted for in the manufacturing process because fish processing generally starts on board.[8] It tends to counterbalance the electric process energy used at the processing plant for refrigeration and freezing operations.

The seafood sector, while the most GHG-efficient of sectors, is not the cleanest energy user, which is due to particularly marked regional discrepancies related to both the kind of seafood processed and energy source availability.

[8]National data on energy consumption and GHG emission from seafood sector in 2002 are available from CIEEDAC and give a ratio of 20.2 g CO_2e/MJ, well below the value calculated here, whereas other available sector ratios are in accordance. It is likely that CIEEDAC raw data does not account for fishing vessel fuel consumed.

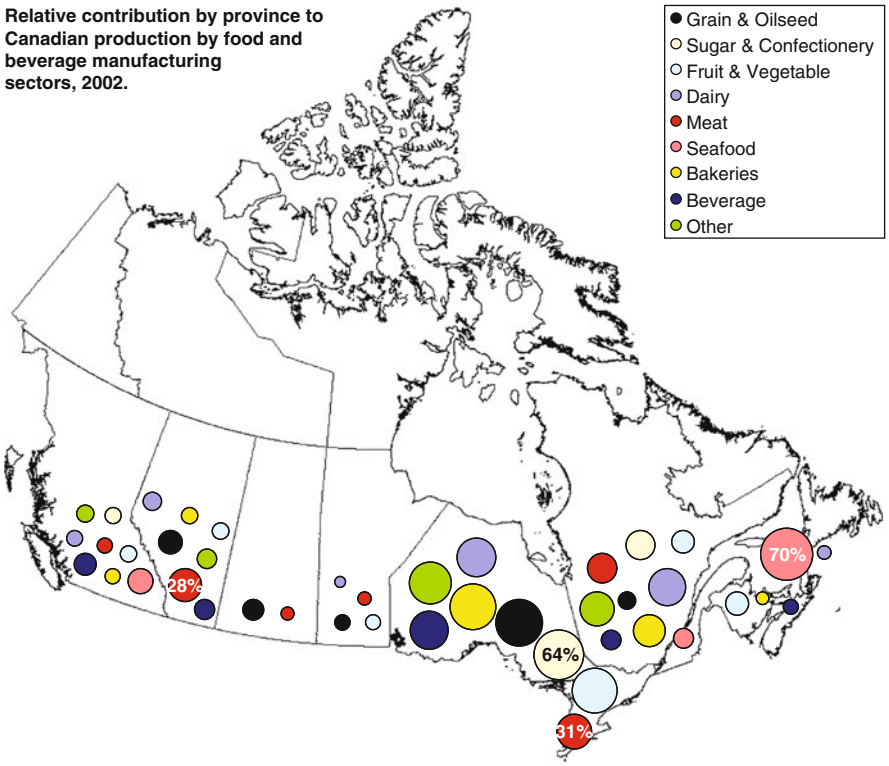

Fig. 8.6 Overview of provincial characteristics of Canadian food and beverage industry production (Statistics Canada, *Annual Survey of Manufactures 2002a*). Contribution is measured in terms of sales. Each sector representation is not necessarily equal to 100% across Canada due to confidentiality of data in certain provinces; data below 4% is not represented. Atlantic Provinces data is grouped together. It excludes animal feed. "Other" stands for snack foods, coffee and tea, flavoring syrup and concentrate and all other manufacturing sectors

The fruit and vegetable sector is the worst performer; the sugar and confectionery sector and the beverage sector are both high ranking, which is less of a surprise given the high GHGEIs that can be reached in the sugar sub-sector and the distilleries sub-sector, respectively. As noted, regional particularities (also discussed later) induce these results.

The grain and oilseed sector, while the least GHG-efficient (and least energy-efficient) of sectors, is mid-ranking in the GHGEI/ECI ratio. This may be explained by a significant amount of energy consumed by the sector in flour milling and breakfast cereal manufacturing sub-sectors in the form of electricity or low-emitting process energy, as in the bakeries sector. The bakeries sector, which as mentioned is an intensive energy user and GHG emitter sector, shows the lowest GHGEI/ECI ratio of the FBI. Energy in this sector is mainly required for baking processes in well-controlled gas or combined-energy ovens, which emit lower quantities of GHG. The bakeries sector is a rather "dry" sector and uses only a small amount

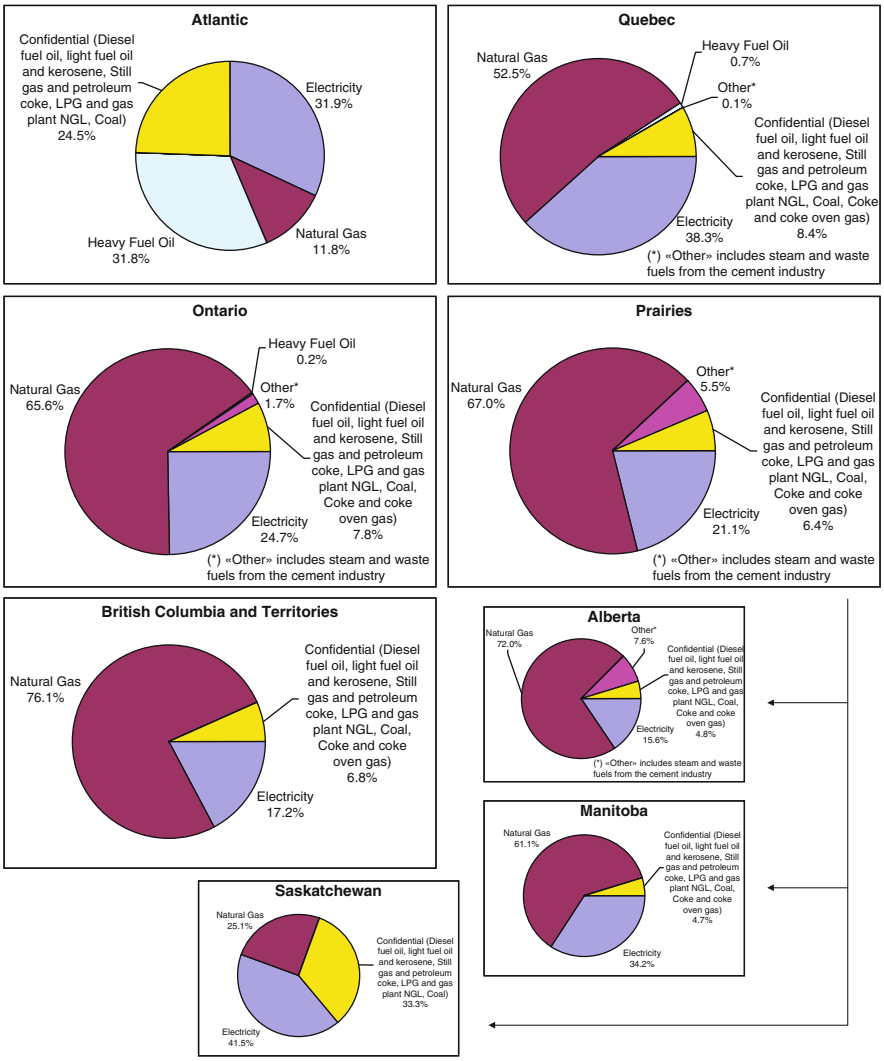

Fig. 8.7 Share in each region and province of energy sources used in 2002 by manufacturing industries in the category, "other manufacturing" (Natural Resources Canada 2007)

of steam; other energy usages in this sector are supplied by electricity, which is not directly emitting GHG.

8.3.2.2 Provincial Results and Interpretation: ECI and GHGEI

Provincial indicators are available at the sector level only and cannot be broken down by size of employment. Not all sectors are necessarily reported for each region, because of a very low number of plants within a specific sector in a given

region (e.g., seafood sector in Prairie Provinces) and/or to respect the confidentiality of responding plants under the *Statistics Act* (e.g., fruit and vegetable sector in the Atlantic region).

Energy Consumption Intensity

Figure 8.8 illustrates the regional effect on the global and median ECI indicators. The main regional features are presented, often with reference to national results available.

The global ECI peak of 3.8 MJ/$ for the sugar and confectionery sector in British Columbia (red dot) is twice as high as the sector scores in Ontario. This result is symptomatic of a sector with very energy-intensive activities and is delivered by only a few big plants. As already mentioned, the sugar refinery sub-sector is responsible for a high global ECI within this sector: a typical Canadian sugar refinery can display intensity as high as 4.2 MJ/$, whereas typical confectionery Canadian plant intensity does not exceed 1.2 MJ/$ (data not shown). However, it should be noted that a typical British Columbian plant within the sugar and confectionery sector (white bar) displays the lowest Canadian ECI in this sector.

Moreover, the British Columbian global ECI indicator in the meat sector is the highest in Canada. It indicates that energy efficiency improvements could be achieved by local meat plants with a large share of sales, reaching values close to – or below – 1 MJ/$. These plants are not numerous because the provincial median

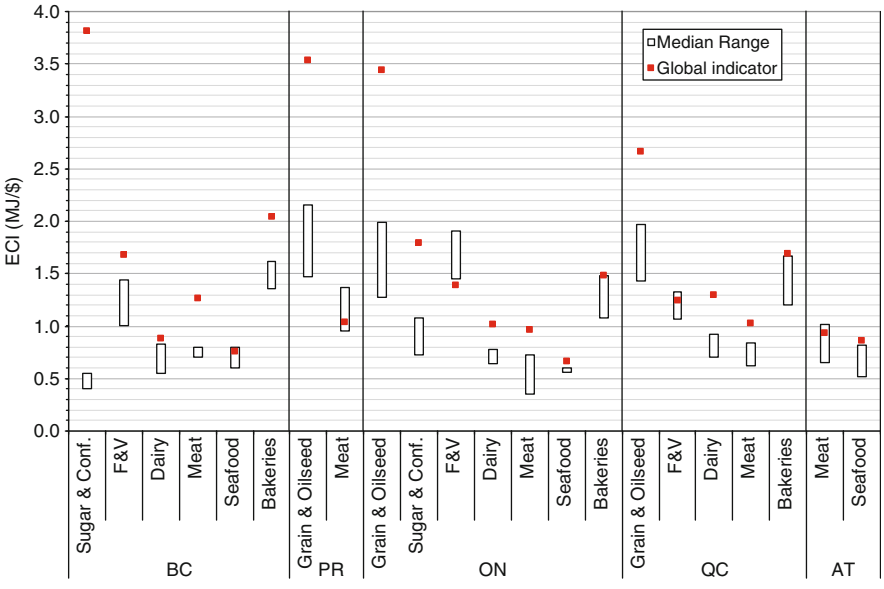

Fig. 8.8 Energy consumption intensity (*ECI*) as a function of regions and activity sector calculated for year 2002

range ECI is typical of the national values. The same conclusions prevail for the bakeries sector as well as the fruit and vegetable sector, compared to provinces like Ontario and Quebec, even though the latter sector is well performing compared to the national values. Lastly, the dairy sector and the seafood sector are both well performing in British Columbia.

The Prairies' grain and oilseed sector's performance is at a level similar to that of Ontario and Quebec, and of Canada as a whole. The meat sector in the Prairies is one of the main food sectors in these provinces; Alberta is one of Canada's leaders in red meat processing. However, the Prairies' meat sector displays the highest typical plant ECI across Canada, twice as high as that of Ontario, despite a more energy efficient production by some of the largest processors (in terms of sales); this is illustrated by the global ECI as close to the median range bottom boundary.

The good performance of the Ontario sugar and confectionery sector (global indicator), as compared to British Columbia level, is explained by a higher diversification of the sector, with a larger share of low energy-intensive activities such as confectionery manufacturing. Establishments in the fruit and vegetable sector typically reflect higher intensity in Ontario than in British Columbia or Quebec. The global ECI of the sector is nevertheless lower than the median range (though close to), which means that a major part of the fruit and vegetable processing in Ontario is performed by plants slightly more energy-efficient than a typical representative one. Lastly, this province is among the most eco-efficient regarding energy use in the meat (lowest median range across Canada), seafood, and bakeries sectors.

Quebec performs relatively well in the grain and oilseed and the fruit and vegetable sectors since the province shows the lowest global ECI across Canada for both sectors.[9] For the former though, some higher intensity plants could still make improvements, whereas the fruit and vegetable sector reveals no "atypical" eco-efficiency plant (global ECI stands within the median range). Quebec's energy intensity (either global or typical) in the meat sector stands at the national level, quite similar to Ontario and Atlantic Provinces. Lastly, the dairy sector in Quebec shows the highest global ECI across Canada, significantly above the intensity achieved by a typical representative plant of the sector in the province, or in Ontario or British Columbia, or Canada as a whole.

The Atlantic Provinces' food industry is highly oriented towards seafood, fruit and vegetable processing, confectionery, and beverage. Most of Canadian seafood production and processors are located in these provinces (Fig. 8.6), which consequently "shape" the Canadian seafood sector indicators. British Columbia and the Atlantic region show quite similar values, a bit higher than that of Ontario, although this latter is hardly comparable since, as a non-coastal province, its processing activities are limited.

[9]Global ECI at national level for fruit and vegetable sector (2 MJ/$) is higher than any provincial value of the sector, which means at least one of the non-reported provincial global ECIs (i.e., from Prairies or Atlantic Provinces) is at least worth 2 MJ/$.

Lastly, it is worth noting that the peculiarity of the large spreading of the ECI median range in the distilleries sub-sector in Canada as a whole (data not shown, but relative spreading is similar to that of GHGEI shown in Fig. 8.4) is not observed in Ontario (data not shown). Ontario's median range ECI stands between 0.56 and 1.09 MJ/$. It is likely that the cause of this observed national spreading comes from another province or region.

Greenhouse Gas Emission Intensity

As explained earlier, the energy mix (i.e., proportion of each energy type) influences the total amount of GHG a plant will emit. Even though each establishment is free to choose the energy type(s) to use, it still depends on the local availability and price from suppliers. Figure 8.6 shows the different provincial energy mixes consumed in 2002 for an aggregate group of manufacturing industries, including the FBI. Consequently, the GHGEI indicator can be discussed more easily and in more detail using this regional analysis.

Figure 8.9 illustrates the regional GHGEI indicator results per sector. This figure shows a computation of the regional global indicator ratio GHGEI/ECI – the amount of GHG emitted for each MJ of energy consumed – to provide insight on "how clean" the energy consumed is and the effort made to shift to technologies or processes using electricity or low GHG-emitting energies.

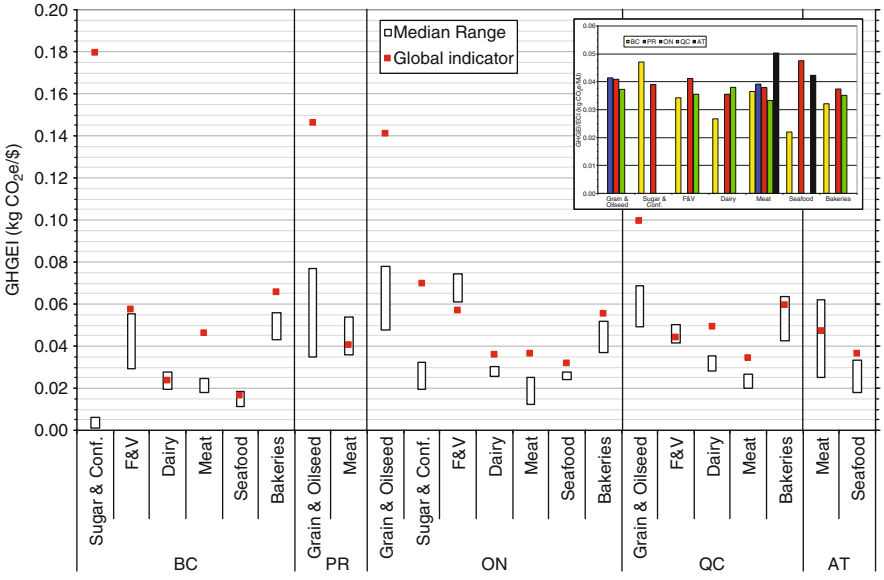

Fig. 8.9 Greenhouse gas emissions intensity (*GHGEI*) as a function of region and activity sector calculated for year 2002. Global indicators' ratio GHGEI/ECI (kg CO_2 equivalent of GHG emitted per MJ of energy consumed) as a function of region

British Columbia seems to have adopted cleaner energy mixes or processes in the fruit and vegetable, dairy, seafood, and bakeries sectors, as shown by its lower GHGEI/ECI ratio in these sectors as compared to other provinces. This is not due to the availability of a particular energy type, as in Fig. 8.6 showing the Prairies, Ontario and Quebec to have similar or cleaner energy mixes. Plants in British Columbia from the above-mentioned sectors have probably been proactive in choosing lower emission energy mixes. Such a shift is not always possible, especially in older plants where the production and processes are not easily modified to take a different energy source. This is the case obviously in the sugar and confectionery sector, for which British Columbia displays a high GHGEI/ECI ratio (along with a huge ECI). In fact, with 47 g of CO_2-equivalent emitted per MJ used, it is the highest value of the province and the third highest value nationwide. Comparison of the global and median range calculating methods reveals that a few large plants are responsible for these "below average" performances, especially when pointing out that the median range of both ECI and GHGEI are among the lowest sector values attained in Canada. It is very likely a large part of British Columbia's activity in this sector is oriented towards sugar manufacturing, which needs extensive amounts of fossil fuel energy for process operations that cannot be handled economically by electricity. On the other hand, a very small part of activity in this sector comes from other sub-sectors (e.g., confectionery manufacturing activities) that are very efficient users of "cleaner" energy sources.

The Atlantic Provinces emit around 30% more GHGs per unit of energy consumed than any other province in the meat sector and twice as much as British Columbia in the seafood sector. The marked dependence of this region on GHG-intensive sources of energy, such as heavy fuel oil and refined petroleum products, is the reason for such difference. As a result, the Atlantic region, which ranked first in terms of energy-related eco-efficiency (ECI), is last when it comes to GHG emissions. In the seafood sector, however, Ontario cannot directly compare because of its activities mainly orientated towards secondary processing operations involving more fossil fuel thermal energy.

Between the extreme positions of the Atlantic region and British Columbia, with regard to the GHGEI/ECI ratio, the Prairies, Ontario and Quebec globally rank in the order of decreasing GHG emission per unit of energy consumed. One exception is Quebec being over Ontario in the dairy sector, also showing a higher median range GHGEI. This is likely due to the more diversified and structurally different dairy industry in Quebec, with more small factories and more atypical processes (e.g., cheese specialties), implying less rationalized operations (e.g., cleaning and disinfection), which tends to emit more GHG. The difference observed between Quebec and Ontario for ECI in the fruit and vegetable sector, Quebec being more energy-efficient, is still larger when it comes to the GHGEI. This holds true also for the grain and oilseed sectors in the same two provinces.

Although data cannot be released, the fruit and vegetable sector has significant activities in all Canadian regions (Fig. 8.6). Given the national GHGEI/ECI ratio of 45 g CO_2e/MJ (data not shown), it is likely that the Prairies' and/or the Atlantic region's GHGEI/ECI values are significantly above the national average.

Limitations: ECI and GHGEI

The proposed indicators have several limitations, most resulting from the desire to provide indicators that report sub-sector, regional and size specificities. First, both indicators are calculated per *value* of product manufactured, instead of per *volume* as initially intended (Marcotte et al. 2005) due to the limited amount of volume data in the Statistics Canada ASM database. Second, these new indicators from the Agriculture and Agri-Food Canada's series of agri-environmental indicators were computed for a single benchmark year, 2002, which does not allow for year-to-year comparison.

8.3.3 Response Options: ECI and GHGEI

As this series of energy and GHG indicators for the FBI is the first of its kind, there are no benchmark values to compare the indicators with a previous situation or to assess the effectiveness of any measures already implemented by the FBI or various governmental institutions. However, the fact remains that measures to improve energy efficiency and the on-site production of secondary energy (such as steam) will help reduce both energy consumption intensity and GHG emissions. The challenge the FBI faces is to reduce its current demand for energy by improving its efficiency through the adoption of best practices[10] without, however, compromising hygiene or food safety procedures. Improved efficiency would result in a reduction in the intensity indicators measured here. Companies can take a large variety of possible measures, the costs of which vary. Low-cost measures, first and foremost the measurement of consumption and heat flows, and management of the procedures that require most energy will allow companies to react swiftly to any problems and to avoid waste. As seen in Fig. 8.2, energy losses are at all operational stages and account for a large share of the initial energy used, although some of these losses are physically unavoidable. A more comprehensive analysis of operational procedures may reveal opportunities requiring varying levels of investment. By using the process integration approach, for example, a plant's energy and water flows can be studied jointly, which is particularly relevant to the FBI, where these two resources are often closely linked. For example, in the dairy products group, 60% of the water consumed is used for energy-related operations (e.g., to cool or generate steam). The results of a process integration analysis generally provide a series of options for optimizing the flow of heat and water in a plant, as a result of which the best ways to recycle and save energy and water can be identified. Such an analysis may, for example, confirm the benefits of using an energy cogeneration system to simultaneously produce mechanical – usually transformed into electricity – and thermal energy (cogeneration), and also cooling energy (trigeneration).

[10]Energetics Inc. and E3M Inc. (2004).

8.4 Water Intake and Water Discharge

The FBI is known for its need for exceptionally large amounts of water, in both volume and quality, as it uses water both as an ingredient and to carry out numerous processing operations. Indeed, water is used at almost all stages of processing: as a heat transfer medium (e.g., as hot water for blanching or steam for heating), as a carrier (e.g., for transportation of fragile products on a production line), or for washing, rinsing, cleaning and sanitizing operations. However, water needs vary significantly in both quality and quantity depending on the kind of products manufactured and on the process implemented to achieve the desired transformation. Water quality is of paramount importance for meeting food hygiene and safety standards when there is a chance of direct or indirect contact with food (Maxime et al. 2005).

It is estimated that in Canada the FBI withdrew 1,500 million m^3 of water in 2005, i.e., almost 20% of the total amount withdrawn by Canada's manufacturing industries (Fig. 8.10) and close to 3% of total water intake in Canada (Environment Canada 2008a), which is equivalent to 600,000 Olympic pools. Establishments obtained half of their water requirements from public water suppliers and supplied the other half themselves from surface water systems (e.g., lakes, rivers), ground water systems (e.g., wells, springs) or even tide water bodies (e.g., estuaries, bays, oceans), each source needing its own water treatment according to the quality

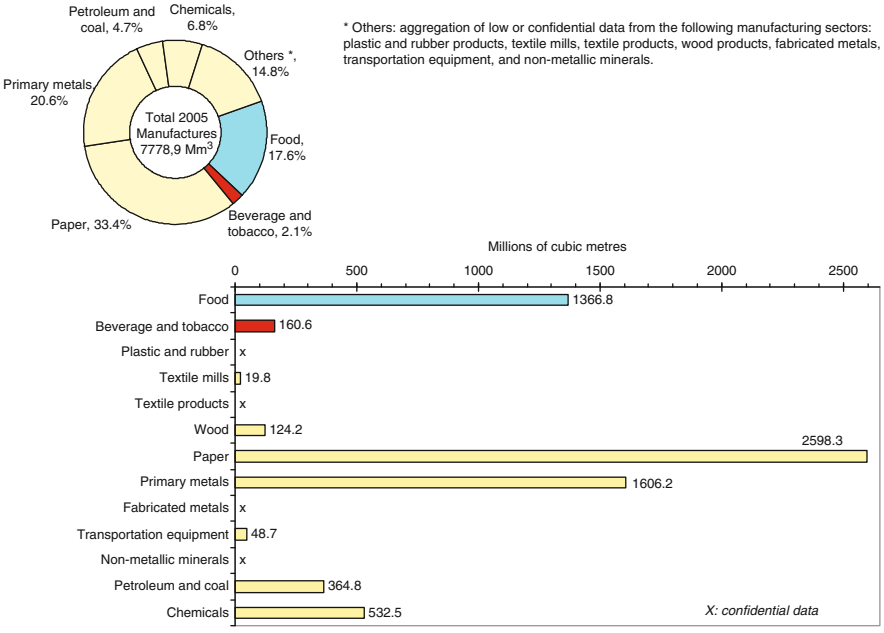

Fig. 8.10 Water intake volumes by the main manufacturing sectors in Canada and share of total manufactures' intake calculated for year 2005

of the water withdrawn and based on the required quality standards at each stage of the process. Of the FBI's intake volume, 4% was recirculated or reused in process or cooling systems and 77% was discharged after use as wastewater, either to public utilities or directly back to the environment, generally after onsite treatment. The remaining 19% was either incorporated into finished products, evaporated during processing operations, or processed as part of wastewater sludge and solid wastes.

The main pollutants of the FBI industry are biodegradable materials and residuals from cleaning agents with no hazardous or acute human toxic pollutants, although ecotoxicity of some effluents might be of concern in fragile environments (e.g., a bay or an estuary receiving effluents from fish processing plants [Environment Canada 2008b]). Prior to discharging wastewater directly to the environment or to a public sewer, the raw wastewater must be treated to convert these pollutants into non-polluting chemicals or to abate their load according to regulations. Some large plants operate their own wastewater treatment system (Fig. 8.11). However, the build-up of some pollutants and the wastewater treatment plant's capacity to properly treat the pollutant loads of the effluents received, particularly during pollution peaks, may pose ecological concerns in the receiving waters. Chlorides (e.g., discharged from food salting processes and water softener regeneration) become toxic to aquatic life at high concentrations; phosphorus and nitrogen compounds (e.g., from sanitation chemicals) induce the aquatic system's eutrophication. A wide unknown also exists regarding the build-up and toxicity in the environment of residual pesticides (e.g., from fruit and vegetable sector), antibiotics, growth hormones, and pathogenic organisms (e.g., from meat and seafood sectors). It is also worth mentioning that processors often overuse or overdose sanitation chemicals to ascertain their food safety security margin, thus increasing the toxicity level of chemicals in wastewater.

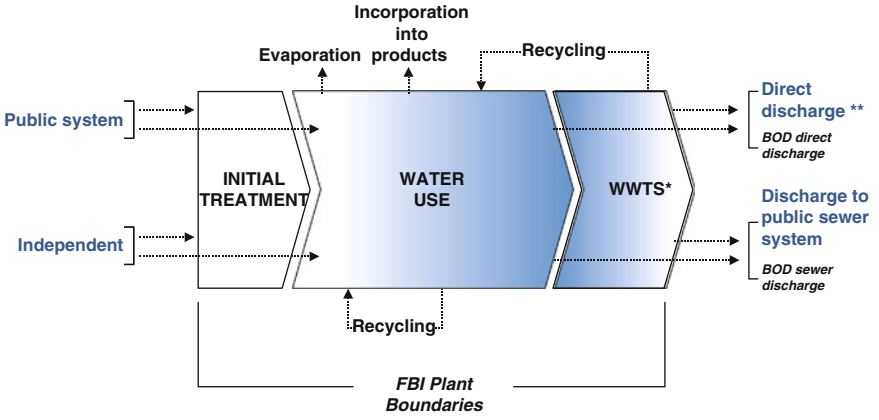

Fig. 8.11 Primary water and wastewater flow in a food processing plant

The FBI significantly depends on – and therefore contributes to – demand for water resources, which can have direct and indirect impacts on their availability and quality, as well as on the ecosystems and economies that depend on them. In fact, depletion of high-quality water reserves in some parts of the country has already pushed up industrial water supply costs and placed additional pressure on public water utilities to find new supply sources (Environment Canada 2004b). The geographic concentration of FBI groups and, for some sectors, the marked seasonality of their withdrawals (e.g., fruit and vegetable processing reaches a peak just after the harvest season) increase pressure on the environment locally and seasonally. Part of the problem with the food-processing industry's use and discharge of large amounts of water is that it is often located in rural areas in which the municipal water treatment systems (i.e., drinking and wastewater systems) are designed to serve small populations. As a result, one medium-sized plant can have a major effect on local water supply and surface water quality. A large food processing plant will typically use more than 4,000 $m^3$of drinking water per day, which is the equivalent of supplying 12,000 residents.

8.4.1 The Indicators: Water Intake Intensity and Water Discharge Intensity

Two indicators were developed: water intake intensity (WII) indicator and water discharge intensity (WDI) indicator, the former expressing the ratio of the amount of water used by the plant per dollar of manufactured goods produced[11] and the latter expressing the ratio of the amount of water discharged per dollar of manufactured goods produced (both in L/$):

$$\text{WII} = \frac{\text{Volume of water withdrawn}}{\text{Value of production}} \qquad \text{WDI} = \frac{\text{Volume of water discharged}}{\text{Value of production}}$$

The WII indicator measures the volume of water withdrawn from the environment to meet the production needs of the FBI plant, while the WDI indicator measures the volume of water returned to the environment through the plant's different liquid waste streams. Theoretically, the WDI reflects the maximum amount of water withdrawn in excess. Moreover, this "auxiliary" indicator is a mandatory step in quantifying the pollution load emitted from the FBI into the

[11]The production is measured by the value of shipments of goods of own manufacture, that is, the selling value of goods made by reporting establishments, excluding transfers into inventory and consignment sales, shipping charges by common or contract carriers, discounts and returns, federal and provincial sales taxes and excise duties and taxes, sales of goods purchased for resale.

public sewage system or directly into the environment (these pollution load indicators will be released in the next report). These intensity indicators are inversely proportional to efficiency performances: the larger the indicator, the lower the efficiency and the environmental performance.

The two indicators were developed as a way to provide establishments with a measure of their "environmental impact" on the water resource as well as a measure of the effect of their water management practices on the sustainable capacity of the natural habitat; these indicators could also give local, provincial, and national authorities a more adequate picture of the total demand/impact on the water resource as well as on the relative impact of each stakeholder. These indicators could also be used to foresee the capacity of a region to accept more development, helping governments take appropriate actions to sustain human and economic growth.

Since the FBI manufactures a broad range of highly diversified products (often tightly linked to regional agricultural production characteristics), the indicators should reflect these peculiarities. Therefore, in order to maintain consistency within food industry sectors and to make valid regional comparisons, establishments were stratified into groups having similar characteristics: same sector of activity and same region. Table 8.3 details these characteristics.

The method employed to calculate both indicators uses data gathered from two Statistics Canada surveys, the 2005 Industrial Water Survey[12] and the Annual Survey of Manufactures and Logging (*ASML*).[13] Both indicators are calculated for each grouping by dividing the total of all water withdrawn (or discharged, respectively) by the sum of the sales value for the whole group. This process gives a good picture of the group as a whole (considering the group as one unique establishment) but does not provide information on the performance of any individual plant compared to the group.

The proposed indicators have several limitations, most of them resulting from the desire to provide indicators that report sub-sector and regional specificities. First, both indicators are calculated per *value* of product manufactured, instead of per *amount* of product manufactured, which would have been a better eco-efficiency indicator (Marcotte et al. 2005) since there were too few available and reliable data in the Statistics Canada ASML database. Second, these new indicators (from Agriculture and Agri-Food Canada's series of agri-environmental indicators) were computed for a single benchmark year, 2005, which does not allow for year to year comparison.

[12]For more details on the survey, go to http://www.statcan.ca/cgi-bin/imdb/p2SV.pl?Function = getSurvey&SDDS = 5120&lang = fr&db = IMDB&dbg = f&adm = 8&dis = 2

[13]For more details on the survey, go to http://www.statcan.ca/cgi-bin/imdb/p2SV.pl?Function = getSurvey&SDDS = 2103&lang = fr&db = IMDB&dbg = f&adm = 8&dis = 2

Table 8.3 Parameters for plant grouping and indicator reporting for water indicators

Sector (o) and sub-sector (•) short name	Activity sector (o) and sub-sector (•) definition and NAICS[a] code
○ Grain and Oilseed	○ Grain and oilseed milling (3112)
• Flour	• Flour milling (311211)
• Malt	• Rice milling and malt manufacturing (311214)
• Oilseed	• Oilseed processing (311224)
• Breakfast	• Breakfast cereal manufacturing (311230)
○ Sugar and Conf.	○ Sugar and confectionery product manufacturing (3113)
• Sugar	• Sugar manufacturing (311310)
• Cacao conf.	• Chocolate and confectionery manufacturing from cacao beans (311320)
• Chocolate conf.	• Confectionery manufacturing from purchased chocolate (311330)
• Candy conf.	• Non-chocolate confectionery (311340)
○ Dairy	○ Dairy product manufacturing (3115)
• Milk	• Fluid milk (311511)
• Other dairy	• Butter, cheese and dry and condensed dairy product manufacturing (311515)
• Ice cream	• Ice cream and frozen dessert manufacturing (311520)
○ Meat	○ Meat product manufacturing (3116), *made of*
• Red meat slaughter	• Animal (except poultry) slaughter (311611)
• Red meat	• Rendering and meat processing from carcasses (311614)
• Poultry	• Poultry processing (311615)
○ Seafood	○ Seafood product preparation and packaging (3117)
○ Bakeries	○ Bakeries and tortilla manufacturing (3118)
• Retail bakeries	• Retail bakeries (311811)
• Com. bakeries	• Commercial bakeries and frozen bakery product manufacturing (311814)
• Cookies	• Cookie and cracker manufacturing (311821)
• Flour mixes	• Flour mix and dough manufacturing from purchased flour (311822)
• Pasta	• Dry pasta manufacturing (311823)
○ Beverage	○ Beverage manufacturing (3121)
• Soft drink	• Soft drink and ice manufacturing (312110)
• Breweries	• Breweries (312120)
• Wineries	• Wineries (312130)
• Distilleries	• Distilleries (312140)
Region short name	**Geographical region**
○ CA	○ Canada
• AT	• Atlantic (Newfoundland and Labrador, Nova Scotia, Prince Edward Island, New Brunswick)
• QC	• Quebec
• ON	• Ontario
• PR	• Prairies (Manitoba, Saskatchewan, Alberta)
• BC	• British Columbia

[a]North American Industry Classification System

8.4.2 *Results and Interpretation: WII and WDI*

This report presents the national and provincial results of both indicators for the year 2005 for various manufacturing sectors of the FBI. The main objective of these indicators is to follow *over time* how a given sector is increasing or reducing its intensity (i.e., increasing or reducing pressure on resource depletion or, indirectly, on aquatic ecosystem pollution); however, the present report does not discuss any timeline trend but sets the baseline. Thus, the following discussion aims rather at interpreting the results of the 2005 indicators through focusing on the inter-sector and inter-regional distinctiveness of the Canadian FBI, while avoiding as much as possible direct comparisons of the indicators. The main goal here is to provide objective information that enlightens future interpretation of the indicators' trends.

Data from the sugar and confectionery sector (except for Ontario), the fruit and vegetable sector, and partly, the bakeries sector, could not be published due to confidentiality, while the animal food sector and the other food manufacturing sectors were not covered within this indicator set.

8.4.2.1 National Results and Interpretation: WII and WDI

Figure 8.12 provides an overall picture of both indicator values across Canada. The first thing that can be noted is the great variability from one industry group to the next in terms of both intake and discharge intensity. The meat sector and the

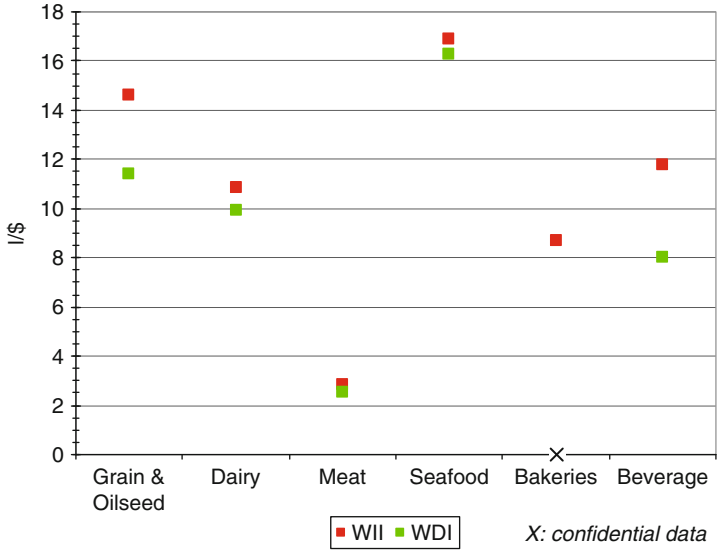

Fig. 8.12 Water intake intensity (*WII*) and Water Discharge Intensity (*WDI*) as a function of FBI sectors calculated for year 2005

seafood sector are at two extremes, with WII national values ranging from 3 to 17 L/$ of product sold, respectively.

Because of the important availability of marine water, the seafood industry has been reputed for its extensive use of water and ice[14] for fish conservation, handling, rinsing and defrosting, and for general hygiene and washing of equipment. However, uncontrolled procedures are still widely used in this sector (Tchoukanova et al. 2003; Fisheries and Oceans Canada 2003; European Commission 2006). Even though a large amount of water is used in this sector for hygiene and process purposes (i.e., WII is high), the potential for improvement is also important (WDI is also high) and could be easily achieved through dry procedures and better water management to save water, especially during fish washing and area clean up, without compromising safety and quality standards. This could beneficially lead to wastewater volume and pollution content reduction, especially because the seafood industry effluents are typically rich in organic matter, suspended solids, nitrogen and phosphorus nutrients, and sanitation chemicals that can affect the health of the receiving environment (Environment Canada 2008b; Gonzalez and Poirier 2003). However, wastewater from processing facilities is generally untreated except for fine screening before discharge from the plant, and dissolved pollutants are thus rejected into the receiving environment (e.g., in harbor's seawater). Moreover, the legislation, whether federal or provincial, remains mainly based on old regulations and guidelines from the 1970s. Since that time, little has been done to assess the impact or to identify suitable emission standards, whereas other FBI sectors have fallen under increasingly strict controls (Tchoukanova et al. 2003; AMEC Earth and Environmental Ltd 2003; Fisheries and Oceans Canada 2003).

The meat sector is rather similar to the seafood sector in the sense that large amounts of water are required for carcass washing and surface cleaning operations. This results in large volumes of wastewater rich in nitrogenous organic matter and suspended solids. However, WII and WDI indicators are much lower for the meat sector than the seafood sector for several reasons. The coastal location of the majority of establishments in the seafood sector are in the Atlantic Provinces and British Columbia, where fewer incentives exist to limit water intake and especially to recycle water as compared to the meat sector in regions where water is less abundant. This relative scarcity has led to more advanced implementation of best management practices in the meat sector (e.g., air instead of water thawing, dry cleaning methods), as well as water recycling opportunities owing to a more widespread use of onsite advanced wastewater treatment systems. The provincial section below discusses these points in greater detail.

Intake intensity is also high in the grain and oilseed sector (15 L/$), as this industry uses a great deal of water and steam during extraction processes (e.g., wet dehulling, wet milling, malt steeping, oil refining, and deodorization). The sector

[14]Seafood sector's plants can use seawater, either directly in some processes where there is no contact with food, or after adequate treatment where contact is possible.

also shows that 22% of water withdrawn is not discharged, the result of (WII-WDI)/WII. Water is actually consumed to some extent through evaporation[15] during dehydration and drying operations in flour processing, malting processes, and breakfast cereal manufacturing.

The dairy products sector, bakeries and tortillas sector, and beverage sector all show intermediate WII values of 11, 9, and 12 L/$, respectively. The bakeries sector includes manufacturing activities requiring that water be mixed with flour or semolina to form dough. This is the main use of water, along with water usage for equipment cleaning. A large amount of added water is evaporated during baking, cooking and drying, and thus it is not discharged as wastewater, which comes mainly from cleaning operations. A very sensible sector regarding microbiological food safety, like the meat and seafood sectors, the dairy sector needs water for cleaning and disinfecting all equipment used in contact with milk or dairy products in the process lines, requiring large quantities of water whatever the dairy product manufactured. Cleaning and disinfection wastewaters are highly concentrated in dissolved organic substances and minerals, such as phosphorus, nitrogen and chloride, which contain cleaning agent residuals as well. As in the meat sector, dairy plants generally treat wastewater onsite to accommodate the contaminant's threshold in public sewage systems. It should be noted however that the dairy sector has long been a fore-runner within the FBI in the area of water management and potential savings through membrane separation and cleaning-in-place technologies development, allowing them to reduce the strength of effluents, to recycle water and chemicals, and to recover valuable milk ingredients.

The beverage sector exhibits different behavior regarding water usage because in this case, water is the main ingredient in most of the finished products. That could explain the large difference between WII and WDI (12 vs 8 L/$, respectively): almost one third of water withdrawn is not discharged, but consumed to some extent through incorporation into products such as bottled water, soft drinks, beer and other alcoholic beverages. Another significant usage of water in this sector is in the cleaning and rinsing of containers and equipment.

The seafood sector's high WII and WDI values signify that it has a higher environmental impact, thus there is far greater potential for improvement in the seafood sector than the meat sector. Or, said differently, for the same quantity of water withdrawn/used, an average meat plant would sell six times more products (in value) than a seafood plant.

[15]Even though evaporation is the obvious main cause for significant water consumption in the sector, this consumption figure is calculated from a volume balance and accounts also for any water loss (leaks, incidental overflows, etc.) and/or water added into finished product. Furthermore, leaks of water are unfortunately endemic to any industrial activity using water, which should be controlled to the extents possible.

8.4.2.2 Provincial Results and Interpretation: WII and WDI

Due to the methodology used to survey establishments and calculate the WII and WDI indicators, it is impossible to report on more regional groupings than those displayed in Fig. 8.13. Thus, missing sectors in the figure does not mean that an industry is not present in the region.

As can be seen, regions can be put in perspective for the seafood sector and meat product sector only. In the seafood sector, for example,[16] there is great variability between British Columbia (WII = 7 L/$), the Atlantic Provinces (WII = 26 L/$) and Ontario (WII = 0.7 L/$), with a difference of a factor of four between the first two regions, and a factor of 40 between the latter two. Actually, the Ontario seafood industry is quite different from that of British Columbia and Atlantic Provinces, where WII and WDI indicators cannot be blindly compared.

Fish landings in Ontario are restricted and limited to freshwater fish, and imports dominate in quantity (Fig. 8.14). It is therefore not a surprise to see lower intensity of water intake and discharge from Ontario establishments since their main activity is essentially secondary processing, such as canning, and they are generally technologically more advanced in streamlining of operations in this respect. In addition (also true for Prairies), it is reasonable to believe that a portion of imports to Ontario

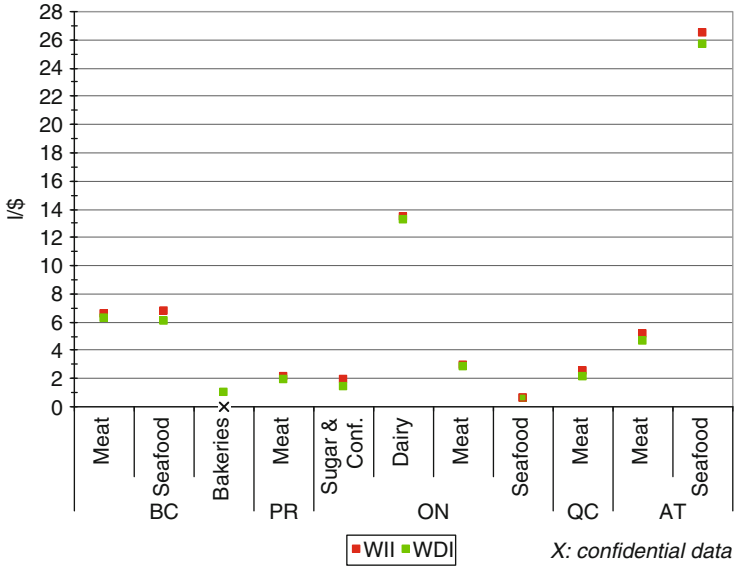

Fig. 8.13 Water intake intensity (*WII*) and Water discharge intensity (*WDI*) as a function of region and sector calculated for year 2005

[16]Aquaculture is not considered a manufacturing group. Any industrial processing activity that might be carried out on an aqua farm is therefore not taken into account in this study.

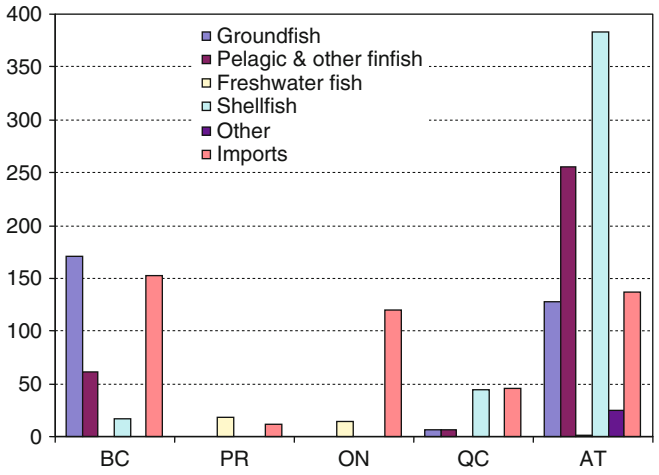

Fig. 8.14 Seafood commercial landings and imports in 2005 (Fisheries and Oceans Canada 2007)

include entirely or partially processed products, leading to lower water intake and discharge intensity indicators. The case of British Columbia is a happy medium between the Atlantic Provinces and Ontario. Since British Columbia and the Atlantic Provinces are the two regions processing significant quantities of landed fish, they remain comparable to some extent. In this respect, the fourfold difference between their indicators suggests that the dominant shellfish activity is the driver of high intensity in the Atlantic region. This activity often involves use of seawater (Fisheries and Oceans Canada 2003) that can be discharged back to the sea (which is not allowed in British Columbia), thus implying the high discharge rate observed in Atlantic region as compared to British Columbia (97.2% vs 89%, respectively). Conversely, British Columbia's seafood product industry focuses on the freezing, canning and secondary processing of salmon, bottom-feeding fish such as halibut, tuna and other fish, and roe (British Columbia Ministry of the Environment 2007). With production ranging from the landing to advanced processing of seafood, all of which require water (brine, canning juices, use of steam during canning operations, etc), it is not surprising that British Columbia has a lower discharge rate, in other words a higher water consumption rate in comparison to the Atlantic region. In contrast, Ontario, which imports most of its production, uses only a few water-intensive operations. Finally, one also needs to be reminded that regarding water and wastewater, local regulatory differences with respect to intake volume, discharge pollution load, and volume are also important drivers of an establishment's behavior, whatever the characteristics of the production.

It should be noted that Canada's average is pushed up significantly by the Atlantic Provinces' intensity indicators since these provinces account for a large share (70%) of seafood production in Canada (Statistics Canada 2006).

The other sector that can be analyzed at the regional level is the meat sector. In this sector, there are two regional groups: British Columbia and Atlantic Provinces

on one side, with WII indicators between 5 and 7 L/$, and Ontario, Prairies and Quebec regions on the other side, with intensity between 2 and 3 L/$, which are two to three times lower than indicators of the first group. The two groups actually differ substantially because of the level of industrialization in industry and their qualitative production differences.

British Columbia and the Atlantic Provinces have numerous small plants processing different products (beef, hog and poultry), which account for only 6% and 3% of national manufacturing shipments, respectively. As a consequence, most of the Canadian meat processing activities are performed in other regions (typically the Prairies, Ontario and Quebec), which have the largest and most specialized facilities. Because of their size, these facilities were historically the first to face local issues concerning very large water usage (and increasing cost), and effluent limits requirements. Onsite wastewater treatment was necessary for most of the facilities, which also had to absorb the associated cost. Consequently, they had to globally implement rationalized procedures aimed at limiting water usage, especially because the generalized implementation of HACCP program[17] tends to require greater use of water for sanitation purposes.

Here, too, Canada's national intensity (2.8 and 2.5 L/$ for WII and WDI, respectively) are similar to the more eco-efficient group (Quebec, Ontario and the Prairies), which can be explained by their share of Canada's meat production (91%) (Statistics Canada 2006).

8.4.3 Response Options: WII and WDI

The challenge FBI faces is to reduce current demand for water by improving its efficiency through adoption of the best practices, without compromising the quality of its products, hygiene or food safety. Improved water use efficiency would result in a reduction of the water intake intensity indicator measured here, and would translate into a decrease of water resource depletion, as well as the cost associated with water utility. Consequently, the volume of water discharged and associated pollution would be reduced, leading to a reduction of the water discharge intensity indicator and discharge cost. Ultimately, each plant should work in "pseudo closed loop," which means withdrawing only water added to the final product and recycling all other

[17]HACCP: Hazard Analysis and Critical Control Point. HACCP is an internationally recognized preventative system designed to detect potential hazards before they occur, and to implement control measures to reduce or eliminate the likelihood of their occurrence at each step in a process, and in all ingredients and packaging. All meat products must have a HACCP plan and if a new meat item is produced it cannot be marketed until a HACCP plan for that production process is developed. Canadian law requires that all federally inspected meat processing facilities (who are eligible to export) develop HACCP systems for their beef product lines. Today, food plants worldwide are using HACCP in a wide range of food manufacturing settings. HACCP is thus not limited to meat products.

water 100%; this includes water discharged in the wastewater, through the chimneys (during baking, cooking or drying) or water lost in solid wastes. Of course, this is not economically feasible but there are a large variety of possible measures that companies can take towards that goal, the cost of which varies greatly (European Commission 2006).

Low cost measures, such as simply measuring discharge and managing procedures that require large quantities of water, will allow companies to react swiftly to any problems and to avoid waste. Optimizing cleaning and disinfection procedures and cycles and using control valves can also be quick cost-effective measures, particularly for those sub-sectors urged by stronger food safety regulations on cleaning efficiency. Furthermore, more advanced technologies for filling and cleaning equipment, albeit more expensive, would allow establishments to win on two fronts: first by simultaneously reducing water requirements and the volume of effluents, and second, making it possible to recover usable raw materials from the latter. A more comprehensive analysis of operational procedures may reveal opportunities requiring varying levels of investment. For example, by using the process integration approach, energy and water flows can be studied simultaneously across the plant. This is particularly relevant to the FBI, where these two resources are often closely linked. A process integration analysis aims to optimize interactions between the different components of the production chain rather than improving each component individually. Given constraints such as water and effluent quality standards, food safety and quality, process and financial options, the best strategy for water (and energy) usage, recycling and discharge within a plant can be identified, leading to savings in both resources and production costs (Gonzalez and Poirier 2003).

8.5 Packaging Use

Food packaging fulfils several functions. It protects products to ensure they are preserved from the moment they are packaged until their consumption, thereby preventing any physical damage, spoilage or sensory attribute degradation during transportation, storage and handling along the supply chain. Packaging is also the conveyor of consumer and manufacturer information and is a marketing tool for the brand owner. Usually one can distinguish between primary, secondary and tertiary packaging as follows. Primary packaging is in direct contact with the food product (e.g., the plastic liner inside a breakfast cereal box, or a glass beer bottle). Secondary packaging exists mainly to facilitate consumer use. It may be, for example, the folding carton of a breakfast cereal box, the boxboard of a case of beer bottles, or the shrink plastic film used in packing water bottles together. Tertiary packaging is for products packaged together as a lot and is used to facilitate their transfer from the manufacturing plant to the warehouse, distribution center, and retail store (e.g., a larger boxboard containing 12 cereal boxes and the pallet containing eight of these boxboards). Thus, primary and secondary packaging is generally discarded by the consumer, while tertiary packaging is managed by wholesalers and/or retailers.

Although very useful, the use of packaging generates important environmental impacts. First in line, the manufacturing of packaging uses important resources such as iron, aluminum and silica (for metal and glass containers), trees (for paper and cardboard), and oil (for plastics) as well as energy for their processing. Secondly, primary and secondary packages become waste at the consumer level, where they must be collected and transported to a site and either eliminated or sorted for reuse or recycling. The same problem exists for tertiary packaging although this is managed at the industry level.

Management of packaging wastes became a major local issue in the late 1980s when it was realized that close to 80% of packaging used in Canada was going to disposal (CCME 1990), and that in 1989 an estimated 30% (by weight) of municipal wastes going to the landfill consisted of disposed packaging (CCME 1996). Hence, the creation of "alternative solutions" to divert packaging from landfills came into being, such as local selective collection, deposit-refund containers, recyclable material sorting plants, waste exchange systems for recycled material, plants dedicated to specific recycled materials (e.g., aluminum, plastics, etc.), new waste reclamation routes (particularly for plastics), and energy recovery through waste incineration. However, these options are still not available everywhere in Canada. For example, EPS (expanded polystyrene), the most voluminous domestic packaging waste, can be recycled (plastic with logo #6) but it is not accepted in blue boxes in most parts of Canada simply because the price of the virgin material is lower than its recycling cost. Valorization of packaging material raises a serious challenge due to the diversity of material (Table 8.4) and the many players and responsibilities involved (by designers, manufacturers, distributors, wholesalers, retailers, consumers, and local authorities), resulting in a large proportion of packaging waste still being land filled or incinerated.

These environmental concerns should be put into perspective along with recent and future societal trends. Canadian households generate more waste than ever (an increase of 11% between 2002 and 2006). Unfortunately, despite all the efforts put into the valorization programs, land filled and incinerated wastes have increased by 5.2% during the same period (Statistics Canada 2008a). Societal trends including decreasing household size, growing demand for products packaged in smaller or individual portions, and the increasingly technical nature of newer packaging (designed to better maintain food quality, safety and marketing appeal) are resulting in increased packaging waste quantity per capita. Figure 8.15 provides a breakdown of household packaging waste generation in Ontario in 2005. Assuming this Ontario figure can be applied to Canada as a whole,[18] it can be estimated that about 2.3 million tons of household packaging waste were generated in the country in 2005. As food packaging accounts for around 60% of total packaging (Dworkin 2006),

[18]National data is extrapolated from Ontario because its data is the most complete within major provinces. With similar data in Quebec (queryRecyc-Québec 2007) and B.C., extrapolation to national values should not be far from the real amount of food waste generated by an average Canadian home.

Table 8.4 Environmental issues and cost of main food packaging materials (Marsh and Bugusu 2007)

Material	Environmental issues		Cost
	Advantages	Disadvantages	
Glass	• Reusable • Recyclable • Often contains recycled content	• Heavy and bulky to transport	• Low cost material but somewhat costly to transport
Aluminum	• Recyclable • Lightweight • Economic incentive to recycle	• No disadvantages in rigid form • Separation difficulties in laminated form	• Relatively expensive but value encourages recycling
Tinplate	• Recyclable • Magnetic, thus easily separated	• Heavier than aluminum	• Cheaper than aluminum
Tin-free steel	• Recyclable • Magnetic, thus easily separated	• Heavier than aluminum	• Cheaper than tinplate
Polyolefins (e.g., polyethylene, polypropylene)	• Recyclable[a] • High energy source for incineration	• Easily recycled in semi-rigid form but identification and separation more difficult for films	• Low cost
Polyesters (PET, PETE, polycarbonates, and polyethylene naphthalates)	• Recyclable[a, b]	• Easily recycled in rigid form but identification and separation more difficult for films	• Inexpensive but higher cost among plastics
Polyvinyl chloride (PVC)	• Recyclable[a]	• Contains chlorine • Requires separating from other waste	• Inexpensive
Polyvinylidene chloride	• Recyclable[a]	• Contains chlorine • Requires separating from other waste	• Inexpensive but higher cost among plastics
Polystyrene (PS)	• Recyclable[a]	• Requires separating from other waste	• Inexpensive
Polyamide	• Recyclable[a]	• Requires separating from other waste	• Inexpensive but higher cost among plastics
Ethylene vinyl alcohol (EVOH)	• Recyclable[a]	• Requires separating from other waste	• Inexpensive when used as thin film
Polylactic acid (PLA)	• Recyclable[a, c]	• Requires separating from other waste	• Relatively expensive
Laminates/ coextrusions (plastic and plastic /or foil or paper)	• Often allows for source reduction	• Layer separation is required	• Relatively expensive but cost- effective for purpose used

(*continued*)

Table 8.4 (continued)

Material	Environmental issues		Cost
	Advantages	Disadvantages	
Paper and paperboard	• Made from renewable resources • Recyclable[b]		• Low cost

[a]All thermoplastics are technically recyclable and can be recycled at production site, contributing to lower cost. As inexpensive materials, post-consumer recycling competes with the ease of separating and cleaning these materials
[b]Recycled extensively for non-food product uses
[c]Can be broken down to monomer level and reprocessed

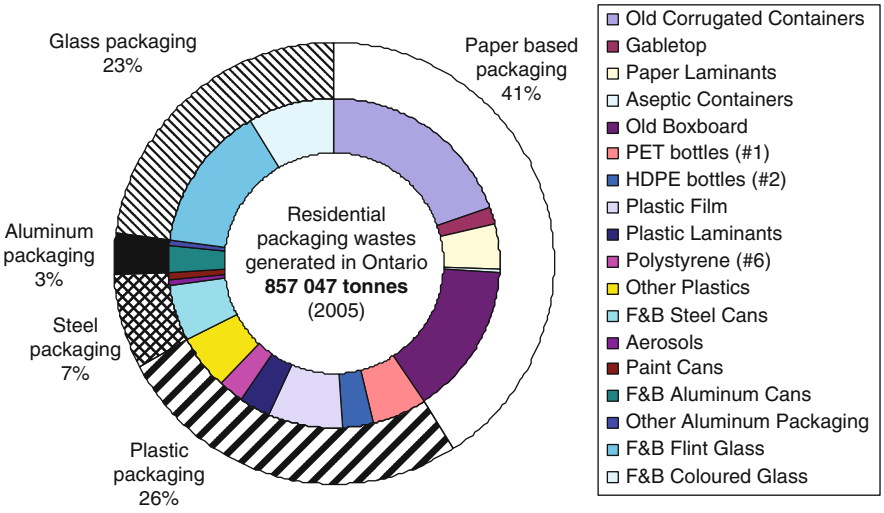

Fig. 8.15 Household packaging waste generation in Ontario for the year 2005 (Stewardship Ontario 2006, 2007)

food packaging waste would tally to approximately 1.4 million tons or 42 kg per inhabitant.[19]

Packaging waste is on the rise. Hence, management costs supported by local governments have increased dramatically in the last decade, especially for collection and transportation (Statistics Canada 2008c). Despite numerous valorization programs, packaging today still accounts for a significant 15% share of materials

[19]However, this value represents only part of the grand total since industrial, commercial and institutional sector waste is not considered here. This latter waste comes from food consumption outside the home, in workplaces and food services and tertiary packaging waste from processors, wholesalers and retailers. For example, in the United States in 1999, 27% of residual beverage containers were generated outside the home (R.W. Beck Inc. 2002).

disposed of in landfills (Downham 2008). Part of the solution lies in the reduction of packaging. With the main objective of decreasing the costs associated with packaging and transportation, while maintaining the quality of products sold, food processors have significantly reduced the amount of material per standard container in the last few decades (Refreshments Canada 2008; Marsh and Bugusu 2007). However, the reduction of FBI packaging waste is a complex issue. Managing packaging-related environmental issues cannot be limited to reducing packaging quantity only, because trying to decrease the latter may lead to food losses, producing a larger negative impact than the gain provided by reduction in packaging (Erlöv et al. 2000). The real challenge lies rather in choosing packaging materials and designs with a smaller environmental impact, taking into account the manufacturing steps of each material, the minimum requirements of the product–packaging–distribution system, and impact that packaging generates once it becomes waste.

8.5.1 The Indicator: PUI

In order to provide information about the packaging materials purchase, to fulfill the production needs of FBI plants, the packaging use intensity indicator (PUI) was developed. The PUI expresses the ratio of the value of packaging and containers purchased per dollar of manufactured goods produced[20] ($/$):

$$\text{PUI} = \frac{\text{Value of packaging and containers purchased}}{\text{Value of production}}$$

The proposed indicator was developed as a way to provide establishments with a measure of their "environmental impact" on the quantity of packaging put on the market. By comparing with different territories (regions/countries), this indicator may also give local, provincial, and national authorities a more adequate picture of the total amount (financial value) of each type of packaging generated, as well as the relative impact of each stakeholder, helping governments take appropriate actions to sustain human and economic growth.

Since the FBI manufactures a broad range of highly diversified products (often tightly linked to regional agricultural production characteristics), and because the industry involves various scales of production (from small facilities to very large processing plants), the indicator should reflect these peculiarities. Therefore, to maintain consistency within food industry sectors and to make valid regional

[20]The production is measured by the value of shipments of goods of own manufacture, that is, the selling value of goods made by reporting establishments, excluding transfers into inventory and consignment sales, shipping charges by common or contract carriers, discounts and returns, federal and provincial sales taxes and excise duties and taxes, and sales of goods purchased for resale.

comparisons, establishments were grouped so as to have similar characteristics (Table 8.2) (i.e., same sector of activity, same region, and same size as determined by number of employees). The PUI is calculated for each group according to two complementary methods, as described earlier for ECI and GHGEI. This indicator uses data from Statistics Canada's 2002 Annual Survey of Manufactures (*ASM*[21]). For each establishment included in calculations, the value of production (i.e., value of products sold) and the purchase cost of each packaging or containers are needed.

8.5.2 Results and Interpretation: PUI

This report presents national and provincial results of the PUI for the year 2002 in various manufacturing sectors of the FBI. The main objective of indicator reporting is to follow *over time* how a given sector is increasing or reducing its intensity (i.e., increasing or reducing its pressure on materials requirement); however, the present report does not discuss any timeline trend but sets the baseline. Thus, the following discussion aims rather at interpreting this 2002 indicator results by focusing on the inter-sector and inter-regional distinctiveness of the Canadian FBI, while avoiding as much as possible direct comparisons of the indicators. The main goal here is to provide objective information that enlightens future interpretation of PUI trends.

Results will first show the difference between sectors and sub-sectors for PUI at the national level. Second, the effect of different employee sizes will be briefly presented for a few sectors and sub-sectors, at the national level. Finally, sectors will be compared per region. All graphs will present the different groupings on the X- axis and the value of the indicator on the Y-axis.

Unless otherwise stated, the indicator is expressed either in dollars per dollar ($/$) or dollars per one hundred dollars ($/$100). Establishment groupings are reported using the short names listed in Table 8.1. Data from some sub-sectors and some plant sizes could not be published due to confidentiality, while the animal food sector and the other food manufacturing sectors are not covered within this indicator set.

8.5.2.1 National Results and Interpretation: PUI

Figure 8.16 provides an overview of PUI values across Canada for all sectors and sub-sectors reported, without regard to size of establishment. Looking first at the indicator's median range at the sector level (blue-filled bars in Fig. 8.16), three sets of industry groups stand out when it comes to "typical plant" intensity: some show

[21]More details about the *ASM* method can be found at the Statistics Canada Web site. http://www.statcan.ca/cgi-bin/imdb/p2SV.pl?Function = getSurvey&SDDS = 2103&lang = fr&db = imdb&dbg = f&adm = 8&dis = 2

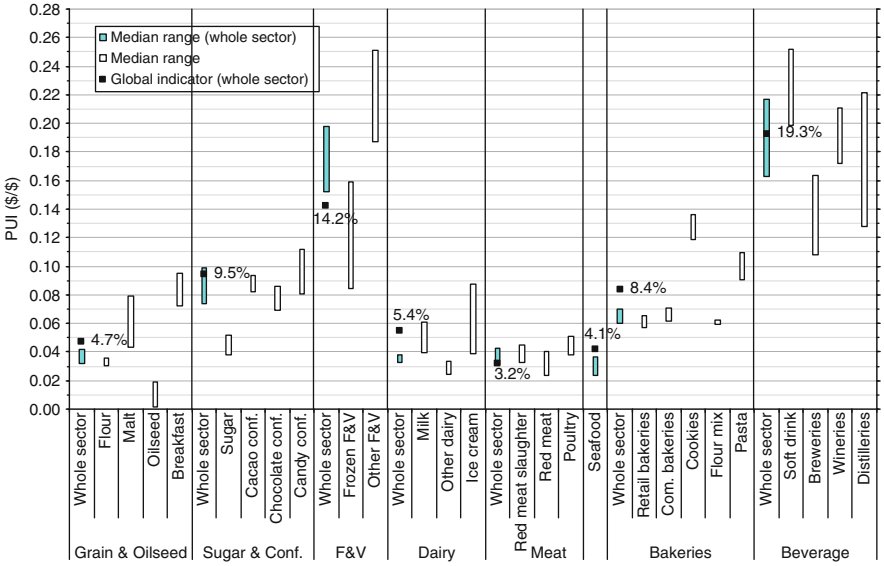

Fig. 8.16 Packaging use intensity (*PUI* in $/$) as a function of activity sector and sub-sector for year 2002. Percentage data expresses PUI global values as $/100$. Global indicator is not available at sub-sector detail

intensity as low as a few percent (less than 5%); some sectors show intensity higher than 15%; "in-between" sectors with PUI from 6 to 10% also exist.

The high values of the fruit and vegetable sector and the beverage sector (up to six or seven times higher than least intense sectors) can be explained on the sole basis of containers usually used in both industry groups. The fruit and vegetable sector uses, for all production of non-frozen products (approximately half of total shipments), mainly metal containers (steel cans) or glass containers, which are costly compared to non complex plastic packaging. Fresh juices from fruits or vegetables, also sold by this group, are often packaged (especially for retail sales, in volumes under 2 L) in sophisticated composite packaging such as multilayered laminated cartons, including aluminum and/or plastic films (gable top and aseptic cartons), whose price compared to the price of the final product is higher than for plastic bottles and jugs. It should be noted here that the fruit and vegetable sector shows the peculiarity of a global PUI below the median range PUI, meaning that few of the larger establishments in terms of production sales spend less for packaging materials than typical plants in the sector.

The beverage manufacturing sector also uses glass (bottles) or metal (aluminum cans, kegs) for all alcoholic beverages, as well as for numerous other beverages not packaged in plastic bottles, thus inducing a share of packaging cost to production cost as high as almost 20%.

A closer look at the sub-sector level within the fruit and vegetable and the beverage sectors (white-filled bars in Fig. 8.15) reveals high intensity in the fruit

and vegetable canning, pickling, and drying sub-sectors (labeled "Other F&V"). This industry uses a lot of cans and glass jars; its indicator is higher than that of the frozen fruit and vegetable industry, for which the primary packaging is mainly flexible plastics or boards. It can be more difficult to interpret the beverage sector results at the sub-sector level due to product-based intrinsic economic differences between non-alcoholic (soft drink) and alcoholic industries (breweries, wineries and distilleries), as well as among alcoholic beverage industries. However, it should be noted that the unit cost of multi-layer and multi-material containers for fruit beverages (gable top and aseptic multi-layered cartons, Table 8.4), may be the driver behind the high intensity of the soft drink industry, together with lower economic value of soft drinks and bottled water as compared to alcoholic beverages. Furthermore, the deposit system implemented in all provinces for reusable glass beer bottles (Comeau 2005) significantly reduces the cost of packaging purchased by breweries.

Among the least intensive sectors, i.e., the grain and oilseed, dairy, meat, and seafood sectors, meat product manufacturing showed little variability within its industries. It is worth pointing out that meat and fish products sold fresh at the retail level (mainly on foam polystyrene trays covered with plastic shrink film) are generally packaged by retailers themselves, and consequently such packaging is not accounted for by the indicator.

The grain and oilseed sector, on the contrary, shows significant variability in the PUI. The oilseed processing sub-sector is the least intensive, eight times less than the breakfast cereal sub-sector. The latter provides the marketplace mainly household retail products packaged in small units, within a plastic liner bag inside a boxboard.

With a typical value (i.e., median range) of packaging, expenses around 3–4% of finished product, the dairy sector as a whole shows a low intensity. However, it is one of the few food sectors (together with the bakeries and tortilla manufacturing sector) for which the global PUI value is significantly higher than the median range (at least +40%). This can be explained by this sector's make up of numerous establishments with large numbers of shipments and high intensity simultaneously. Given the high concentration ratio in this sector, where only a few companies – that is, a limited number of very productive establishments – dominate the market, this indicator shows that these establishments could improve their eco-efficiency and shift intensity down to a lower median level. In industries within the dairy sector, better performance of the other dairy products sub-sector (butter, cheese, and dry and condensed dairy products manufacturing) can be seen. This can be explained by the very high sales value of this kind of processed food compared to that of the fluid milk sub-sector or ice cream and frozen dessert sub-sector, despite the packaging quantities (and cost) involved in the selling of highly diversified products packaged in small units such as yogurts, cream and cheese.

The bakeries sector shows an intermediate intensity level. The cookie and cracker sub-sector stands out from the others with its high intensity (typical plant values are about 13%) without pulling the whole sector up to its level; however, since the median range of the latter still stays between 6% and 7% and the global indicator is slightly higher than 8%. The cookie and cracker sub-sector is quite

similar to the breakfast cereal sub-sector within the grain and oilseed sector. It is mainly a retail products industry, often using multiple packaging (e.g., cookies are packaged in trays and/or individual plastic bags, and over-packed within folding cartons) in comparison with bakery products from commercial or retail bakeries sub-sectors, which use more basic packaging.

The sugar and confectionery sector belongs also to the group of "intermediate-intensity" sectors. All sub-sectors within this industry behave similarly, except for the sugar manufacturing sub-sector. It is not surprising to find the lowest intensity for this latter one, given the simplicity and low cost of packaging materials used for powdered sugar (paper pouches, plastic bags, and paper bags for larger quantities), and sugar syrups, which are essentially wholesale marketed in plastic pails or drums, moreover generally reused. On the contrary, chocolate and confectionery products are mainly shipped individually packaged, involving more advanced costly packaging materials.

There is no clear trend regarding the influence of establishment size (in terms of number of employees) on the PUI. At the sector level, only the dairy sector displays a clear and significant influence, displayed through both global and median range indicators (results available in technical supplement of the report). Surprisingly, the global PUI increases with plant size from 3.5$/100$ for small plants up to 6.8$/100$ for very large plants. This trend does not hold true at the sub-sector level. Other sub-sectors show slight trends but none are significant.

8.5.2.2 Provincial Results and Interpretation

Details by region (province or group of provinces) on the PUI are presented in Fig. 8.17 (FBI regional sub-sector detail is not available due to confidential data).

British Columbia stands among the least intense region for the sugar and confectionery sector, which is explained by the predominance of the sugar manufacturing sub-sector within this industry in this province. Conversely, the province shows a significantly higher PUI than any other region in the seafood sector. The global PUI is 50% higher there than in Quebec, and more than three times higher than in Ontario. Moreover, a typical plant of the sector is at least three times more intensive than a typical plant in any other region. British Columbia's seafood industry activity is largely oriented towards salmon canning, which means that a large amount of its packaging purchases are expensive steel or aluminum cans. The seafood industries in the Atlantic Provinces and in Quebec are mostly focused on shellfish and seafood activities involving more basic and cheaper packaging materials, together with far higher selling prices.

In the beverage sector, British Columbia stands out as the most intensive province. This may be due to the peculiarity of that province to package beer[22]

[22]The breweries subsector accounted for 44% of beverage sector sales of manufactured goods in British Columbia, in 2002 (Statistics Canada 2008b).

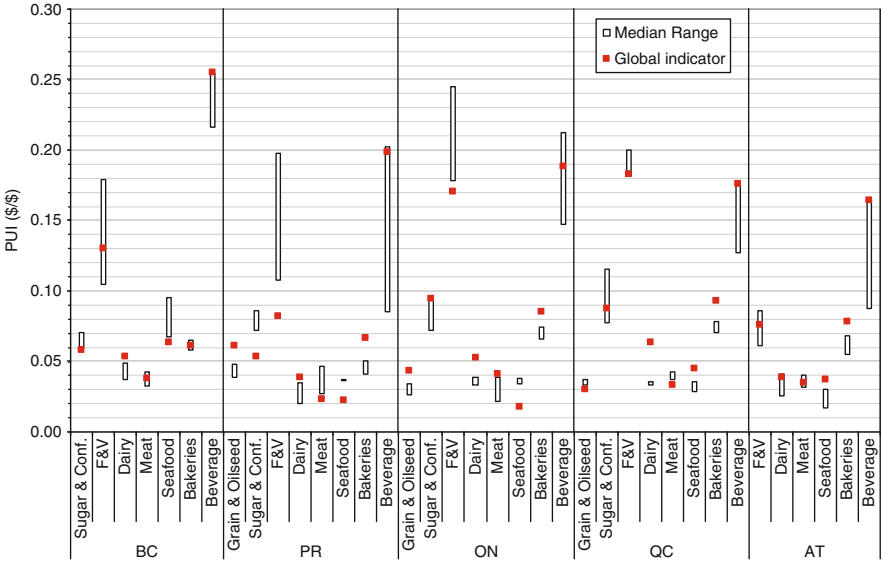

Fig. 8.17 Packaging use intensity (*PUI* in $/$) as a function of activity sector and region calculated for year 2002

mainly in cans or draught kegs instead of refillable glass bottles as other regions do, thus increasing packaging cost.[23] In 2002, use of bottles represented only 26.1% of the beer sold in the province, whereas bottled beer represented 47.5% in the Prairies, 76.9% in the Atlantic Provinces, 77.2% in Ontario, 85.1% in Quebec, and in Canada averaged 68.1% overall (Brewers Association of Canada 2007).

The Prairies, like British Columbia, show a low PUI in the sugar and confectionery sector. It is also the lowest intensive region in the meat sector, one of the main economic drivers of the FBI in the Prairies. This is also true in the fruit and vegetable sector, where the region compares with the Atlantic Provinces in global PUI (8$/100$). However, good economic performance is common to only a few of the larger selling plants since – as revealed through the median range indicator – a typical mid-performing plant should score higher, between 11 and 20$/100$, as in the Prairies' fruit and vegetable sector. It is likely that larger productive plants can benefit from cheaper packaging materials[24]; the same reasoning may hold for the sugar and confectionery, meat, and seafood sectors. The reverse is observed in the grain and oilseed sector, another important FBI

[23]Glass bottles are reused by breweries (no need to buy a new bottle for each portion sold) contrary to aluminum cans, which are recycled (a new can is needed for each portion sold).

[24]The F&V sector in the Prairies is dominated by a few large plants selling uncooked French fries in large plastic bags to restaurants.

sector in the Prairies, where the higher positioning of the global indicator may reveal that few of the largest selling plants are more intensive than other mid-performing plants.

Ontario is a leading province in almost all sectors of Canadian FBI, both in terms of number of establishments and production. It is thus not surprising to see national sector values presented as being close to that of the province, whether for the global or the median range PUI. The main exception is in the seafood sector, for which Ontarian establishments are quite different from processing plants in coastal regions and deal mainly with imported materials for secondary processing. This is true in the Prairies too, where similar PUI values are observed.

Other exceptions, though to a lower extent, are in the meat and the fruit and vegetable sectors where the dominance of Ontario is less marked because of the share in production with other provinces. In the meat sector, the Prairies and Quebec are also big players, and variability among PUIs is slight, although Ontario's larger processors seem to show a higher intensity.

In the fruit and vegetable sector, Ontario (along with Quebec) is the most intensive buyer of packaging materials. Mid-performing plants can spend up to 25$ for packaging per 100$ of production, which is substantial. As seen previously, such a high intensity level is characteristic of the canning and pickling sub-sector, and Ontario's fruit and vegetable industry was mainly engaged (75%) in this sub-sector activity in 2002 (Statistics Canada 2008b). This was also the case for Quebec (78%).

Figure 8.14 also confirms the previous observation of the effect of economic concentration in the dairy sector. It is not surprising to see that the global PUI is higher than the median range, especially for Quebec and Ontario. In 2002, both provinces together accounted for more than 74% of Canadian dairy product manufacturing shipments (Statistics Canada 2006), and almost 60% of all establishments. The concentration effect is particularly marked in this sector, with three companies owning 75% of the market through 15% of all establishments (Agriculture and Agri-Food Canada 2005). These highly productive establishments influence the global PUI as a result. However, this analysis needs to take into account several particularities in Quebec, such as a fluid milk market less oriented than elsewhere to plastic pouches (which are cheaper than milk cartons), and a cheese market open to specialty goods packed in more sophisticated and costly packaging materials (although these products are also more expensive than traditional North American cheeses).

The Atlantic Provinces show the lowest global PUI in the fruit and vegetable sector, slightly below 8$/100$. However, unlike the Prairies, their median range stays in line with this value and displays a narrow range. It is thus likely that all plants in the region behave similarly in this sector concerning packaging requirements, provided their production is qualitatively comparable. This region might also serve as a benchmark for other provinces in this sector, provided production patterns are similar. Unfortunately, the lack of disaggregated data about the relative importance of both fruit and vegetable sub-sectors in the Atlantic Provinces does not allow such inferences.

8.5.3 Limitations: PUI

The proposed indicators have several limitations, most of them resulting from the desire to provide indicators that report sub-sector, regional and size specificities. First, the indicator is calculated per *value* of product manufactured, instead of per *volume* of product manufactured as initially intended, which would have been a better eco-efficiency indicator (Arcand et al. 2005) due to the limited amount of volume data in the Statistics Canada *ASM* database. Second, this new indicator from Agriculture and Agri-Food Canada's series of agri-environmental indicators was computed for a single benchmark year, 2002, which does not allow for year to year comparison. Lastly, another significant limitation of the PUI resides in its environmental significance, since, at this stage of development, it does not report packaging quantities, nor does it weight each type of packaging accounted for, due to an environmental impact factor. As mentioned above, it is through such weighting that the environmental issues of food packaging can truly be addressed, and future enhancements are expected using this approach.

8.5.4 Response Options: PUI

Since this is the first time the PUI has been calculated, we still do not have any references for comparison purposes and are thus unable to assess the benefit of any actions previously implemented, whether by industry or government. The industry has an important role to play in reducing the environmental impact of packaging. The 4R (Reduction, Reuse, Recycling, Recovery) waste management hierarchy is the rule of thumb in any waste minimization strategy.[25] As already mentioned, the industry can act by reducing the quantity of materials needed to pack a given quantity of finished product. However, such a source reduction approach is limited by the minimal protection required by the product and the distribution system, a threshold that cannot be crossed. Another source reduction option is to reduce over-packing (secondary packaging) to the bare minimum by redesigning the packaging. New designs may also offer the opportunity to choose materials with a lower environmental impact: either the same materials with a higher recycled content or those coming from cleaner processes (interaction with the supplier is thus of prime importance), or new materials with a smaller ecological footprint (calculated over whole life cycle, taking into account end-of-life options). The industry may be influenced in this way by downstream market drivers from distributors and consumers who – thanks to their purchasing power – may request low ecological footprints. This phenomenon is already being observed. A significant amount of packaging waste also comes from imported

[25]A short list of generic beneficial operating or management practices is also provided in the appendix section of the Web version of this document.

food products, over which the industry has no influence, unless it is the actual importer who can in this case negotiate with suppliers, e.g., for more environmental-friendly packaging. However, governments can play a role by requiring transparent information about the packaging materials used and their ecological footprint. Governments also should ensure that these materials, once they become waste, are efficiently managed through locally available reuse or recycling channels in order to limit land filling. A principle already implemented in a few provinces, referred to as the extended producer responsibility, is also a policy tool that may raise the food and beverage industry's awareness of packaging. This principle should ideally be based on criteria arising from more thorough life cycle assessments. As a supporting stakeholder, governments could play a more active role in setting up and centralizing Canadian life-cycle databases, to then be made publicly available to assist decision makers in the industry. The industry is not solely responsible and should not be expected to meet all the constraints alone. The consumer is the last decision-maker when purchasing and is also the "local" waste generator. One of the mandates of governments and local authorities is to inform consumers and to support education of the public about packaging wastes. One step further could be to guide the public about alternative consumer choices, through information based on impacts embedded in the packaging of products.

8.6 Conclusions and Recommendations

In summary, the Canadian FBI sector uses a significant amount of energy: close to 4% of the energy used by the Canadian manufacturing industry as a whole. The consumption of this energy is responsible for most of the FBI's greenhouse gas (GHG) emissions. The grain and oilseed milling sector, and the sugar and confectionery products manufacturing sector are among the most energy-intensive users. Indicators also reveal that the largest companies in terms of sales in these groups are, in general, "worse than average" performers, regardless of their location in Canada. Within these sectors, three sub-sectors – rice milling and malt manufacturing, oilseed processing, and sugar manufacturing (particularly in British Columbia) – drive up their respective group's energy intensity values. The same is true of the distilleries within the beverage sector. Least energy-intensive sectors are seafood, meat, and dairy products manufacturing. Greenhouse gas emission intensity indicators are generally consistent with energy consumption. However, regional differences exist in use of petroleum products, the combustion of which emits large quantities of GHGs. In 2005, the FBI was responsible for nearly 20% of the total water used by all Canadian manufacturing industries. Of this water intake (i.e., volume of water withdrawn), the FBI discharges 77% and recirculates 4%. The seafood product preparation and packaging industry is the most intense water withdrawing industry among the FBI in Canada, with a national average value of 17 L of water withdrawn per dollar of product sold, although regional values vary from 1 L/$ in Ontario to 26 L/$ in the Atlantic Provinces. Nevertheless, it is also the sector that discharges the

most water (96% is withdrawal). In contrast, the beverage manufacturing industry group is the most intense "consumer" of water (difference is between withdrawn and discharged water) with discharges accounting for two-thirds of the water withdrawn, most of it being incorporated into finished products. The meat product manufacturing industry group is the least intense water-withdrawing group (3 L/$), withdrawing six times less than the seafood product group and almost four times less than the dairy product manufacturing group (11 L/$). Within the meat sector, geography makes a clear difference, with provinces known for livestock production (the Prairies, Ontario and Quebec) performing much better (below 3 L/$) than British Columbia (7 L/$) and the Atlantic Provinces (5 L/$). The FBI transforms raw agricultural commodities, or ingredients, into semi-prepared and consumer-ready food and beverage products that have to be packaged adequately to ensure they can reach consumers without losing their physical and hygienic integrity and quality attributes, as well as to convey consumer and manufacturer information. The Packaging Use Indicator (PUI) first results reported here are sectorial measures for 2002 and provide a baseline for future reference. The highest PUI values (greater than 15$ of packaging per 100$ of product) are produced by the fruit and vegetable and the beverage manufacturing sectors, which are typically high consumers of such packaging as metal cans (iron and aluminum) and glass containers. Conversely, animal materials processing groups (meat, fish and seafood, and dairy products) show the lowest PUI values for reasons such as the economic value of their production (e.g., highly processed dairy products), the small quantity of packaging required (e.g., unprocessed meat products, fish and seafood), or even geographical characteristics (e.g., fish and seafood in Atlantic region and Quebec).

The indicators proposed here could be optimized to become more robust, have better coverage, represent relevant environmental issues and, lastly, facilitate response options. ECI and GHGEI indicators at the sub-sector level with both global and median range results could be released. The ECI indicator could be calculated by adding a weight for each source of energy used, computing an environmental pressure factor taking into consideration the total direct and indirect impacts of a source and geographic location. This would highlight any shift made to more sustainable energy use, in particular, renewable ones. An ECI indicator calculated to break down the energy consumption according to main uses in a plant would be a significant improvement. Causes of low efficiencies could then more easily be identified, and therefore eco-efficiency measures and best management practices could be more straightforwardly deployed.

Improvements could also include the development of purely physical indicators independent of financial data, for example, L of water used per kg of product sold instead of per $. These indicators would be independent of price fluctuation, from region to region, or from high quality vs. low quality products sold. This raises a delicate issue because the data from ASML does not provide "per kg" data, although the survey is an ideal source of information, because of its frequency and coverage of the FBI. Another source of physical data (i.e., all outputs sold by each establishment expressed in kg per year) is therefore required, unless the ASML

is adapted accordingly, which could serve many other national purposes (e.g., national environment accounts managed by Statistics Canada). One other option is the generation of a tool to gather and aggregate establishments' physical data and to calculate sector and regional indicators, which at the same time could allow establishments to compute their own eco-efficiency indicators. This would allow the measurement of the quality of the water discharged by, for example, quantifying the pollution loads (organic load using biochemical oxygen demand) (BOD), as described by Maxime et al. (2006), as well as measuring nitrogen, phosphorus, specific chemicals, microbial loads, and toxicity among other).

Taking a life cycle approach as a basis for the analysis of environmental issues of packaging is gradually achieving consensus within policies both abroad[26] and in Canada,[27] as well as within the scientific community. From a broader perspective, many urban communities now assess and choose solid waste management plans on the basis of life cycle-based comparison studies. It is well known that such analysis is very time-consuming in the data inventory phase and thus requires a significant investment, but it becomes very cost-effective afterwards and will pay off during subsequent similar analyses. Furthermore, it is not limited to environmental assessments and can also be used for cost analyses of the whole life cycle of a packaged product. The current indicator should eventually be improved to allow for a breakdown by types of packaging. Simultaneously, it should weight every type of packaging material put on the market by an environmental pressure factor embedding the total impacts – direct and indirect – of each type, also taking into account geographical location, as the life cycle approach allows.

Lastly, the adoption of a comprehensive, open approach to environmental pressures and natural resource use along the food chain, from production to final consumption and even to end of life cycle (including waste management and biomass recycling at farms, establishments, and consumer and post-consumer levels), would be another useful research stream to precisely identify the causes and division of responsibilities, as well as the effects and response options (avoiding collateral damages). The national environment accounts mentioned above and life-cycle analyses are in line with this. Additional national research initiatives in these areas would contribute towards achieving a sustainable Canadian agri-food system.

In practice, the food and beverage industry's environmental performance is influenced by an individual plant's business practices, including internal policies, management system and staff awareness, and manufacturing processes. Some of the available business practice options can be grouped under the label "best operating practices" (BOPs), such as those recently described (European Commission 2006). Three criteria are generally used to prioritize and classify these practices: the

[26]For example, in Australia with the National Packaging Covenant (http://www.packagingcovenant.org.au) and Europe (European Union 2004).

[27]For instance, the Canadian Council of Ministers of the Environment's Extended Producer Responsibility Task Group is developing a Canada-wide strategy for sustainable packaging. Aspects and stakeholders involved are considered in the life cycle. (http://www.ccme.ca/ourwork/waste.html)

investment cost to adopt, quantification of the anticipated environmental gains (made apparent by the indicators), and the return-on-investment period. Once calculated, the indicators will shed light on the extent to which the best operating practices are being implemented and, in a sense, will quantify a company's efforts towards environmental sustainability (Richard 2003; Industry Canada 2001)

Acknowledgments The authors would like to thank the Manufacturing, Construction and Energy Statistics Division of Statistics Canada, Ottawa, and in particular Daniel Scott, André Gravelle and Francine Rouleau. Many thanks are addressed to Andy Shinnan, François Soulard, Joe St. Lawrence and Martin Lemire, of the Environment Accounts and Statistics Division, Statistics Canada, Ottawa. Dr. André Talbot of the Aquatic Ecosystem Protection Research Division, Environment Canada, Montreal, is kindly acknowledged for much advice provided. The authors would like to thank Isabelle Vézina, a master student in environment at the Université de Sherbrooke, for her dedicated work at the Food Research and Development Centre – St Hyacinthe, from April to September, 2006. Finally, many thanks are being addressed to Mathieu Guillemette from Éco Entreprises Québec.

References

Agriculture and Agri-Food Canada (AAFC) (2004) Agricultural Policy Framework. http://www.agr.gc.ca/cb/apf/index_e.php. Accessed 12 October 2004

Agriculture and Agri-Food Canada (AAFC) (2005) Canadian Dairy Industry Profile. Ottawa, Ontario: AAFC (August 2005). http://www4.agr.gc.ca/resources/prod/doc/dairy/pdf/dairyprofile.pdf

AMEC Earth & Environmental Ltd. (2003) Management of Wastes from Atlantic Seafood Processing Operations. Final report submitted to the National program of action, Atlantic regional team, Environment Canada Atlantic Region. http://www.dal.ca/aczisc/nparpt.pdf (visited September 12, 2008). Other related documents (including this one) also available online: Canada. Fisheries and Oceans Canada (DFO), Gulf Home; Seafood Plant Effluents – Turning Problems into Profits; http://www.glf.dfo-mpo.gc.ca/os/effluents/index-e.php [last updated January 15, 2007; visited September 12, 2008]

Arcand Y, Maxime D, and Marcotte M (2005) Organic solid residues and packaging wastes, Ch. 30. In: Lefebvre A, Eilers W, Chunn B (eds) Environmental sustainability of Canadian agriculture: agri-environmental indicator report series – report #2 (eds). Agriculture and Agri-food Canada, Ottawa, Ontario, pp 184–187. http://dsp-psd.pwgsc.gc.ca/Collection/A22–201–2005E.pdf

Brewers Association of Canada (2007) 2007 Annual Statistical Bulletin. http://www.brewers.ca/UserFiles/Documents/pdfs/eng/statistics/asb/2007/Brewers_ASB_2007_Eng.pdf

British Columbia Ministry of Environment, Oceans and Marine Fisheries Branch (2007) 2006 British Columbia Seafood Industry Year in Review. October 22, 2007. The Ministry, Victoria, BC. http://www.env.gov.bc.ca/omfd/reports/YIR-2006.pdf [visited November 14, 2007]

CCME (Canadian Council of Ministers of the Environment) (1990) National Packaging Protocol. http://www.ccme.ca/assets/pdf/napp_e.pdf

CCME (Canadian Council of Ministers of the Environment) (1996) National Packaging Survey-The 1996 Results. http://www.ccme.ca/assets/pdf/packaging_srvy_96.pdf

CIEEDAC (Canadian Industrial Energy End-use Data and Analysis Centre) (2008) Data report created online July 30, 2008, from CIEEDAC database, covers annual energy consumption, CO_2, CH_4 and N_2O emissions, cumulative GHG emissions, production data. Simon Fraser University, Burnaby, British Columbia. http://www.cieedac.sfu.ca

Comeau M (2005) La gestion des contenants de boissons au Québec. Évaluation du marché et analyse des options de récupération. Recyc-Québec, Québec, Quebec (La Société québécoise

de récupération et de recyclage), September 1, 2005. http://www.recyc-quebec.gouv.qc.ca/upload/publications/consigne/EtudeContBoissons.pdf; http://oee.nrcan.gc.ca/corporate/statistics/neud/dpa/comprehensive_tables/index.cfm?attr = 0

Downham J (2008) Presentation on packaging issues at the City of Toronto Packaging Waste Reduction Forum, September 10, 2008, Toronto, Ontario. http://www.toronto.ca/garbage/packagingforum/pdf/1_downham_pac_na08_cot_jd_speech_6up.pdf

Dworkin L (2006) Presentation on the packaging industry in Canada, Section 4.2 in Marbek Resource Consultants Ltd., National Extended Producer Responsibility (EPR) Workshop: final report, pp 11–12. Canadian Council of Ministers of the Environment (CCME), Ottawa, Ontario, 2007. (PN 1376) http://www.ccme.ca/assets/pdf/epr_wkshp_rpt_1376_e.pdf

Energetics Inc. and E3M Inc. (2004) Energy use, loss and opportunities analysis: US manufacturing and mining. Prepared by energetics inc. and E3M inc. for US Department of Energy (DOE), energy efficiency and renewable energy industrial technologies program. Columbia, Maryland and North Potomac, Maryland: December 2004. http://www1.eere.energy.gov/industry/energy_systems/pdfs/energy_use_loss_opportunities_analysis.pdf

Environment Canada (2004a) Greenhouse gas division. Canada's greenhouse gas inventory, 1990–2002. Environment Canada, Ottawa, August 2004. http://www.ec.gc.ca/pdb/ghg/inventory_report/1990_02_report/toc_e.cfm; http://www.ec.gc.ca/pdb/ghg/inventory_report/1990_02_report/errata_e.cfm; http://www.ec.gc.ca/pdb/ghg/ghg_home_e.cfm

Environment Canada (2004b) Threats to Water Availability in Canada. National Water Research Institute (NWRI), Scientific Assessment Report Series No. 3 and ACSD Science Assessment Series No. 1. Environment Canada, NWRI, Burlington (Ont.). http://www.nwri.ca/threats2full/intro-e.html

Environment Canada (2007) National inventory report 1990–2005: Greenhouse gas sources and sinks in Canada. Greenhouse gases division, No de cat.: En81–4/2005E. http://www.ec.gc.ca/pdb/ghg/inventory_e.cfmCanada

Environment Canada (2008) Water use in Canada, 2005. http://www.ec.gc.ca/water/en/manage/use/e_wuse.htm [visited September 12, 2008]

Environment Canada, Atlantic Region (2008) Report on the characterization and toxicity testing of fish processing plant effluent in Canada. Toxic Chemicals Updates Newsletter – Atlantic Canada Edition, 10(1), January 2008. ISSN 1206–5455. http://atlantic-web1.ns.ec.gc.ca/epb/newsletters/toxchem/Default.asp?lang = En&n = 3F836B38–1 [visited September 12, 2008]

Erlöv L, Löfgren C, Sörås A (2000) Packaging – a tool for the prevention of environmental impact. Foundation Packforsk, Kista, Sweden, June 2000 (Report No. 194). http://www.stfi-packforsk.se/upload/Gamla_PF-sidor/REPORT_194.PDF

European Commission (2006) Integrated Pollution Prevention and Control – Reference document on best available techniques in the food, drink and milk industries. European Commission, Directorate-General, Joint Research Centre Institute for Prospective Technological Studies (Seville, Spain), European Integrated Pollution Prevention and Control Bureau. http://eippcb.jrc.ec.europa.eu/pages/locatemr2.cfm?file = fdm_bref_0806.pdf&name = Food,%20drink%20and%20milk%20processes&info = info/fdm.htm

European Union (2004) Directive 2004/12/EC of the European parliament and of the council of 11 February 2004 amending directive 94/62/EC on packaging and packaging waste – statement by the council, the commission and the European parliament. official journal of the European Union L 47, 18/02/2004, pp 26–32. Published online edition: http://eur-lex.europa.eu/smartapi/cgi/sga_doc?smartapi!celexplus!prod!DocNumber&lg = en&type_doc = Directive&an_doc = 2004&nu_doc = 12; [see also: ECOLAS – PIRA (2005). Study on the implementation of directive 94/62/EC on packaging and packaging waste and options to strengthen prevention and re-use of packaging. Report 03/07884–AL; http://ec.europa.eu/environment/waste/studies/packaging/050224_final_report.pdf]

Fisheries and Oceans Canada (DFO), Gulf Home (2003) Fish plant effluents: a workshop on sustainability. Canadian industry report of fisheries and aquatic sciences. In: Morry CJ,

Chadwick M, Courtenay S, Mallet P (eds), p 271. http://www.glf.dfo-mpo.gc.ca/os/effluents/workshop-report-e.pdf; other related documents, including this one, available online: Canada. Fisheries and Oceans Canada (DFO), Gulf Home. Seafood plant effluents – turning problems into profits. http://www.glf.dfo-mpo.gc.ca/os/effluents/index-e.php [last updated January 15, 2007; visited September 12, 2008]

Fisheries and Oceans Canada (DFO), Statistical Services Unit (2007) DFO's statistical services. DFO, Ottawa, policy sector, the unit, March 14, 2007. http://www.dfo-mpo.gc.ca/communic/Statistics/main_e.htm [visited November 15, 2007]

Gonzalez M, and Poirier S (2003) Minimiser l'impact environnemental des usines de transformation de produits marins. *Alerte Technologique* 1(1):8–10. Shippagan, Institut de recherche sur les zones côtières Inc., New Brunswick, Canada. http://www.umcs.ca/Institut/AT001.pdf [visited September 12, 2008]

Industry Canada (2001) Three steps to eco-efficiency. Ottawa. http://www.ic.gc.ca/eic/site/ee-ee.nsf/vwapj/finaltool.PDF/$FILE/finaltool.PDF

IPCC (Intergovernmental Panel on Climate Change) (1996) Climate change 1995. The science of climate change. Contribution of working group 1 to the second assessment report of the intergovernmental panel on climate change. In: Houghton JT, Meira Filho LG, Callender BA, Harris N, Kattenberg A, Maskell K (eds) Cambridge University Press, Cambridge, UK. http://www.ipcc.ch/ipccreports/sar/wg_I/ipcc_sar_wg_I_full_report.pdf

Marcotte M, Maxime D, and Arcand Y (2005) Energy use and greenhouse gas emissions, ch. 28. In: Lefebvre A, Eilers W, Chunn B (eds) Environmental sustainability of Canadian agriculture: agri-environmental indicator report series – report #2. Agriculture and Agri-food Canada, Ottawa, pp 176–179

Marsh K, Bugusu B (2007) Food packaging – roles, materials, and environmental issues. J Food Sci 72(3):R39–R55. http://webprod.ift.org/NR/rdonlyres/C3FC4F7C-BE99–4124-BA67-A5-C3A77D1B05/0/FoodPkgEnviron.pdf

Maxime D, Arcand Y, Marcotte M (2005) Water use and effluent generation, ch. 29. In: Lefebvre A, Eilers W, Chunn B (eds) Environmental sustainability of Canadian agriculture: agri-environmental indicator report series – report #2. Agriculture and Agri-food Canada, Ottawa, pp 180–183. http://dsp-psd.pwgsc.gc.ca/Collection/A22–201–2005E.pdf

Maxime D, Marcotte M, Arcand Y (2006) Development of eco-efficiency indicators for the Canadian food and beverage industry. J Cleaner Prod 14(6–7):636–648

NAHARP (National Agri-Environmental Health Analysis and Reporting Program) (2004) Agriculture and agri-food Canada. http://www.agr.gc.ca/env/naharp-pnarsa/index_e.php; see also NAHARP summary at http://www.agr.gc.ca/env/naharppnarsa/pdf/naharp-pnarsa_e.pdf [accessed: 12 October 2004]

Natural resources Canada, office of energy efficiency (2007) Comprehensive energy use database, Table 10: other manufacturing secondary energy use and GHG emissions. Office, Ottawa, December 12, 2007

Navarri P, Legault A, Bédard S (2001) Process integration. Presentation at managing waste and wastewater in the food processing industry seminar, organized by Manitoba Hydro. November 21, 2001, Winnipeg, Manitoba. Varennes, Natural Resources Canada, CANMET energy technology centre, Quebec

NRTEE (National Round Table on the Environment and the Economy) (2001) Eco-efficiency indicators. Workbook. Calculating eco-efficiency indicators. A workbook for industry. Prepared by indeco strategic consulting, inc. & Carole Burnham consulting. Renouf Ltd. Ottawa, ON

Nyboer J (2008a) Development of energy intensity indicators for Canadian industry, 1990–2006. Simon Fraser University, Burnaby BC, Canadian Industrial End-use Energy Data and Analysis Centre (CIEEDAC) [prepared for Canadian industry program for energy conservation and natural resources Canada]. http://www.cieedac.sfu.ca/

Nyboer J (2008b) Development of greenhouse gas intensity indicators for Canadian industry, 1990–2005. Simon Fraser University, Burnaby BC, Canadian Industrial End-use Energy Data and Analysis Centre (CIEEDAC) [prepared for Environment Canada]. http://www.cieedac.sfu.ca/

Recyc-Québec (2007) Bilan 2006 sur la gestion des matières résiduelles au Québec. La Société québécoise de récupération et de recyclage (Recyc-Québec), Québec, Quebec. http://www.recyc-quebec.gouv.qc.ca/upload/Publications/Bilan2006.pdf

Refreshments Canada (2008) Beverages & the environment: about beverage packaging. Refreshments Canada. Online promotional literature from beverage trade association, Toronto, Ontario. Visited December 27, 2008. http://www.refreshments.ca/en/environment/beverages_environment.asp

Richard F (ed) (2003) Waste management guide for small and medium enterprises. Canadian version. Éditions Ruffec and NI environnement, Montreal. http://www.qc.ec.gc.ca/dpe/Anglais/dpe_main_en.asp?innov_guide_mat_residuelles; http://www.qc.ec.gc.ca/dpe//Publication/Mat

RW Beck Inc (2002) Understanding beverage container recycling: a value chain assessment prepared for the multi-stakeholder recovery project. Businesses and Environmentalists Allied for Recycling (BEAR), Santa Monica, California, January 16, 2002. http://www.globalgreen.org/bear/Projects/FinalReport.pdf

Statistics Canada (2002a) Annual survey of manufactures. http://www.statcan.gc.ca

Statistics Canada (2002b) Annual industrial consumption of energy. http://statcan.gc.ca

Statistics Canada (2003) Report on energy supply-demand in Canada, 2002. Statistics Canada, Ottawa, October 2003 (Catalog no. 357–003-XIB, annual publication). http://www.statcan.ca/english/freepub/57–003-XIB/0000257–003-XIB.pdf

Statistics Canada (2004) Report on energy supply-demand in Canada, 2003. Statistics Canada, Ottawa, November 2004 (Catalog no. 57–003-XIB, annual publication). http://www.statcan.ca/english/freepub/57–003-XIB/0000357–003-XIB.pdf

Statistics Canada (2006) CANSIM Table No 301–0006. Principal statistics for manufacturing industries, by North American Industry Classification System (NAICS), annual. [124134 series]. Statistics Canada, Ottawa, November 30, 2006. http://cansim2.statcan.ca/cgi-win/cnsmcgi.exe?Lang = E&RootDir = CII/&ResultTemplate = CII/CII___&Array_Pick = 1&ArrayId = 3010006 [visited December 10, 2007]

Statistics Canada (2007) Report on energy supply-demand in Canada, 2005. Statistics Canada, Ottawa, June 2007 (Catalog no. 57–003-XIE, annual publication). http://www.statcan.ca/bsolc/english/bsolc?catno = 57–003-X; http://www.statcan.ca/english/freepub/57–003-XIE/57–003-XIE2005000.htm; http://www.statcan.ca/english/freepub/57–003-XIE/57–003-XIE2005000.pdf

Statistics Canada (2008a) EnviroStats, 2(3):18 (Table 3) (Catalog no. 16–002-X). http://www.statcan.ca/english/freepub/16–002-XIE/16–002-XIE2008003.pdf

Statistics Canada (2008b) CANSIM Table #301–0003: annual survey of manufactures (ASM), principal statistics by North American Industry Classification System (NAICS). Statistics Canada, Ottawa, Ontario. http://cansim2.statcan.ca/cgi-win/cnsmcgi.exe?Lang = E&RootDir = CII/&ResultTemplate = CII/CII___&Array_Pick = 1&ArrayId = 3010003 [last modification Apr. 25, 2008; visited 2008/11/04]

Statistics Canada (2008c) CANSIM Table #153–0045: local government characteristics of the waste management industry. Statistics Canada, Ottawa, Ontario. http://www.statcan.ca [last modification August 14, 2008; visited 2008/11/18]

Statistics Canada (2008d) Industrial water use, 2005 (Catalog no. 16–401-XIE). March 2008, Statistics Canada, Ottawa, Ontario. http://www.statcan.ca/bsolc/english/bsolc?catno = 16–401-X

Stewardship Ontario (2006) Ontario blue box markets overview: 2003/2004 blue box materials generated and municipally marketed, mass balance report. Stewardship Ontario, Toronto, Ontario, March 2006. http://webservices.siriusweblabs.com/dotconnector/files/domain4116/2003–2004%20Mass%20Balance%20Report%20-%20final.pdf

Stewardship Ontario (2007) Ontario generation and recovery of blue box materials by demographic type (based on waste composition study results). Stewardship Ontario, Toronto, Ontario. http://www.stewardshipontario.ca/pdf/eefund/gen_and_rec_rates.pdf

Tchoukanova N, Gonzalez M, Poirier S (2003) Best management practices: marine products processing. Prepared for fisheries and oceans Canada – Gulf region. Fisheries and Marine

Products Division of the Coastal Zones Research Institute inc., Shippagan, New Brunswick, Canada. http://www.glf.dfo-mpo.gc.ca/os/effluents/bmp-e.pdf. Also available in html (revised version) at: http://www.glf.dfo-mpo.gc.ca/os/effluents/bmp-e.php.

US Department of energy (2004) Energy efficiency and renewable energy. Industrial technologies program, industrial energy systems: food and beverage energy footprint. http://www.eere.energy.gov/industry/energy_systems/footprints.html [content updated 18 August 2004; accessed 17 September 2004]

US Environmental Protection Agency (2007) Energy trends in selected manufacturing sectors: opportunities and challenges for environmentally preferable energy outcomes, final report. Prepared by ICF international for US Environmental Protection Agency (EPA)'s office of policy, economics, and innovation, sector strategic division, Washington, DC. March 2007. http://www.epa.gov/sectors/energy/index.html; http://www.epa.gov/sectors/pdf/energy/report.pdf

Verfaillie HA, Bidwell R (2000) Measuring eco-efficiency. A guide to reporting company performance. World Business Council for Sustainable Development (WBCSD), Geneva, Switzerland. 38 pp. http://www.wbcsd.org

Chapter 9
Food Process Economics

George Saravacos and Zacharias Maroulis

9.1 Importance of Economics in Food Processing

Food processing is a large industry consisting of several small or medium size plants and a few large installations. It produces a variety of food products that satisfy the nutritional and sensory needs of consumers. Economics plays a very important role in the efficient design of food processes and the production of sufficient quantities of food products for an ever expanding world population (Maroulis and Saravacos 2007).

The design and optimization of food processes is based on the principles of food science and the established techniques of chemical process design, and simplified computer spreadsheet techniques have been applied to the design of various food processes (Maroulis and Saravacos 2003). For example, heat and mass transfer food processes, such as heating, cooling, freezing, evaporation, dehydration, extraction, and membrane separations, can be designed and optimized using transport properties and other engineering data of foods, as published in the literature (Saravacos and Maroulis 2001; Rao et al. 2005; Rahman 1995). On the other hand, mechanical processes involving solid and semi-solid food materials, such as grinding, mixing, and mechanical separations or forming, are designed empirically using specialized processing equipment provided by equipment manufacturers and suppliers (Saravacos and Kostaropoulos 2002).

Food plant design is the integration of process design and process engineering economics (Lopez-Gomez and Barbosa-Cánovas 2005). Food processing plants are characterized by strict hygienic (sanitary) and food safety requirements, which should be satisfied in any economic analysis. However, recent worldwide demand for fresh processed foods at affordable prices stresses the importance of process economics.

G. Saravacos (✉) and Z. Maroulis
School of Chemical Engineering, National Technical University of Athens, 15780 Athens, Greece
e-mail: gsaravac@otenet.gr, maroulis@mail.ntua.gr

J.M. Aguilera et al. (eds.), *Food Engineering Interfaces*, Food Engineering Series,
DOI 10.1007/978-1-4419-7475-4_9,

9.2 Process Engineering Economics

Process engineering economics is based on the estimation of capital and operating costs, on which plant profitability can be estimated. It is applied in designing new processing plants, and in process and product improvement of existing installations (Clark 1997; Holland et al. 1997; Peters et al. 2003; Couper 2003). Safety and environmental requirements of the process should be considered.

9.2.1 Capital Cost

The capital cost is based on the equipment cost (C_{eq}), which is estimated from material and energy balances on the process flowsheet. Cost of food processing equipment is estimated from equipment size (surface area, volume, weight) using empirical correlations or the suppliers' data (Maroulis and Saravacos 2007). Sizing of food processing equipment is based on material and energy balances of the process flowsheet, using simplified design equations and engineering property data (Saravacos and Kostaropoulos 2002). Empirical correlations (diagrams) of cost versus equipment size (Guthrie charts) can be used for engineering calculations. Cost quotations of specialized food processing equipment can be obtained from equipment suppliers.

Typical cost: capacity diagrams of food processing equipment include fluid transport-power (kW); vessel-volume (m^3); conveyor belts-surface area (m^2); heat exchanger-surface area (m^2); dryers-surface area (m^2); filters-surface area (m^2); size reduction-capacity (kg/s); mechanical processing-capacity (kg/s); and utilities-kW (Maroulis and Saravacos 2007). Increases in cost of processing equipment (inflation) over the years are taken into account using the Marshall and Swift (M&S) cost index, published periodically in the journal *Chemical Engineering,* e.g., M&S Index: (1990) = 915, (2005) = 1,261.

9.2.2 Operating Cost

The operating cost includes the direct cost of raw and packaging materials, labor, and utilities, and various indirect costs such as maintenance, quality assurance, and office personnel.

9.2.2.1 Raw Food Materials and Packaging Materials

The cost of raw food materials is estimated with data obtained from US government organizations such as the Bureau of Labor Statistics (http://www.bls.gov) and the

National Agricultural Statistics Services (http://www.nass.usda.gov). Typical farm prices in the US (2003) for food materials are ($/kg): wheat 0.13, corn 0.09, potatoes 0.14, milk 0.27, beef 1.61, chicken 0.72, hogs 0.78, store-bought fresh tomatoes 0.76, tomatoes for processing 0.10, oranges 0.10, grapes 0.40, peaches 0.40, and apricots 0.65. Both retail and farm prices, or retail to farm price ratios (r), should be considered. Typical (r) values in the US are: eggs 1.7, milk 4, sugar 5, wheat flour 5.5, margarine 10, potato chips 15, bread 25, corn flakes 28, and corn syrup 35.

The cost of packaging materials may run from relatively low in bulk packing of fruit products in plastic-lined drums to very high in plastic cups for dairy products (Maroulis and Saravacos 2007). Intermediate costs include using metallic cans, glass bottles, and paper/plastic bags. The packaging cost per unit mass of food products ($/kg) increases substantially as the package size is reduced (e.g., plastic cups 0.80, glass bottles 0.20, metallic cans 0.12, plastic bags 0.10, and 208 L plastic drums 0.09).

9.2.2.2 Labor

Labor requirements include production and nonproduction workers, and amount to about 20% of the manufacturing cost. The process labor required can be estimated from the process flowsheet and the material and energy balances. The supporting labor is usually estimated using empirical correction factors and the total personnel is approximately equal to three times the process labor. A labor cost model (as in following example) has been proposed for estimating the total labor cost, using correction factors for the country (i.e., cultural) effect, skilled personnel, supervision, social benefits, and overtime work.

The annual operating time (hours) is estimated as the product of (hours per shift) × (shifts per day) × (days per week) × (weeks per year). Food plants can be operated for one or more seasons. The annual operating time for one season can vary from 500 to 2,100 h, with workers employed 12.5 weeks a year and 5–7 days a week, 1–3 shifts a day. A two-season operation (25 weeks) amounts to 1,000–4,200 h a year, while an all-year operation (50 weeks) amounts to 2,000–8,400 h a year. Food preservation plants usually operate 2–4 months per year, due to seasonal availability of agricultural raw materials. Some food manufacturing plants may operate 12 months a year, e.g., bakeries. Food ingredients plants may operate several months a year, depending on the availability of raw materials. Bulk storage of large volumes of raw materials (e.g., wheat, corn, and oilseeds) near a food plant can extend its operating time substantially.

The manpower requirements of a food processing plant can be estimated analytically by summation of the requirements for each processing equipment or operation (Maroulis and Saravacos 2007). Approximate personnel requirements for various food processing plants can also be estimated from the following empirical equation developed by regression analysis from published data (Bartholomai 1987).

$$M = 10F^{2/3} \tag{9.1}$$

where M is the manpower (number of personnel) and F is the plant product capacity (t/h).

The cost of labor primarily depends on the country and the degree of specialization. Labor rates are found in government publications such as the US Bureau of Labor Statistics. The average hourly rate for production workers in the US was $15 in 2008. Higher rates are found in some European countries, such as Germany and Norway, but substantially lower rates are observed in the rest of the world, with very low rates in underdeveloped countries. The cost of skilled operators, mechanics, technicians, foremen, and plant managers is normally estimated as 2, 3, 3.5, 4, and 5 times, respectively, the cost of unskilled labor.

9.2.2.3 Utilities

The main public utilities used in food processing plants are energy and water. Energy includes fuel (oil, gas) and electricity, and it is conveniently expressed in kWh/kg product (1 kWh = 3.6 MJ). Water is used as process water, and in cleaning operations, cooling, refrigeration, and steam generation; it is also involved in wastewater effluents. The cost of fuel ($/kWh) is a function of the cost of crude oil ($/barrel (bbl) = 159 L oil). The cost of crude oil is affected strongly by international political crises and wars (e.g., increasing from $60 to $100/bbl between the years 2007 and 2009). An empirical model was developed for the estimation of various energy forms from the price of crude oil (Maroulis and Saravacos 2007). Typical diagrams of energy cost of crude oil at $100/bbl and $60/bbl are shown in Figs. 9.1 and 9.2.

Typical energy cost (US 2008) follows: electricity – $0.10/kWh; steam – 10 bar $08/kWh ($40/t); fuel oil – $1.30/L; and natural gas – $0.80/m^3. The cost of food processing water (cleaning of or adding to food products) is about $0.50/m^3, while boiler water is more expensive ($2.50/m^3) due to its pretreatment. Waste disposal costs are about $50/t, while wastewater treatment (primary and secondary) costs about $1.00/t.

9.2.3 Process Profitability

9.2.3.1 Capital Cost

The total capital cost C_T is covered partly by the investor's own capital C_O and partly by a bank loan C_L:

$$C_T = C_O + C_L \tag{9.2}$$

The loan is expressed as a fraction (leverage, λ) of the total capital ($\lambda = C_L/C_T$). A typical leverage in food processing is $\lambda = 0.50$. The total capital cost C_T invested

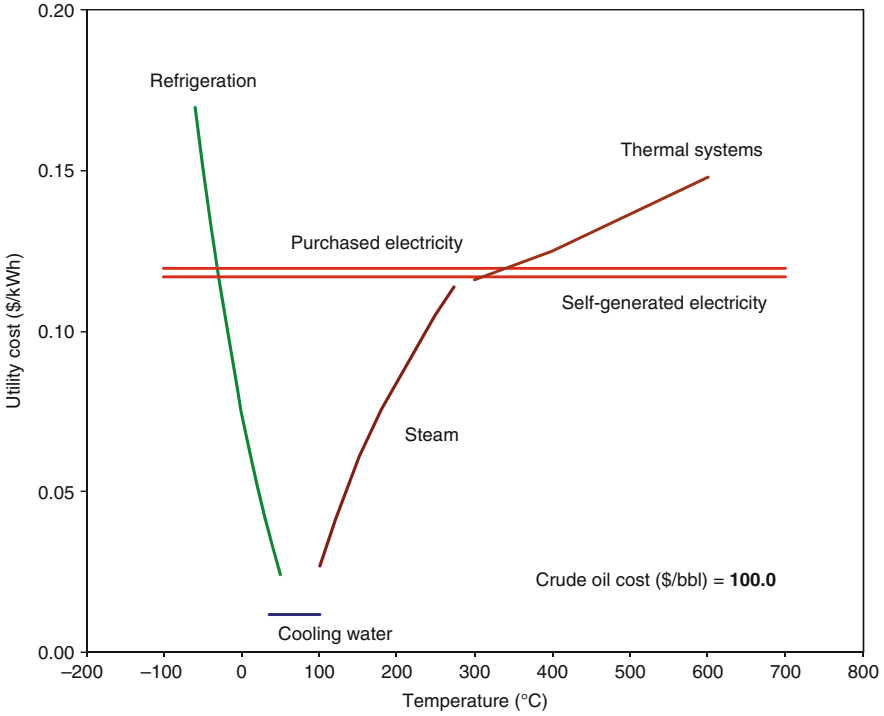

Utility	Description	$/kWh	$/Common unit
Electricity	Purchased	0.117	
	Self-generated	0.120	
Crude			100.0 $/bbl
Fuels	Fueloil	0.096	0.96 $/L
	Natural gas		0.64 $/m3
	Coal		65.0 $/t
Thermal systems	300°C	0.116	
	400°C	0.125	
	600°C	0.148	
Steam	40 bar	0.105	52.5 $/t
	10 bar	0.076	37.8 $/t
	5 bar	0.061	30.4 $/t
	1 bar	0.027	13.3 $/t
Cooling water	tower	0.012	0.271 $/m3
	river or sea		0.231 $/m3
	well		0.312 $/m3
Refrigeration	5°C	0.081	
	–20°C	0.102	
	–50°C	0.150	

Fig. 9.1 Energy cost of oil priced at $100/bbl

in a processing plant consists primarily of the fixed capital cost C_F and, secondly, the working capital C_w:

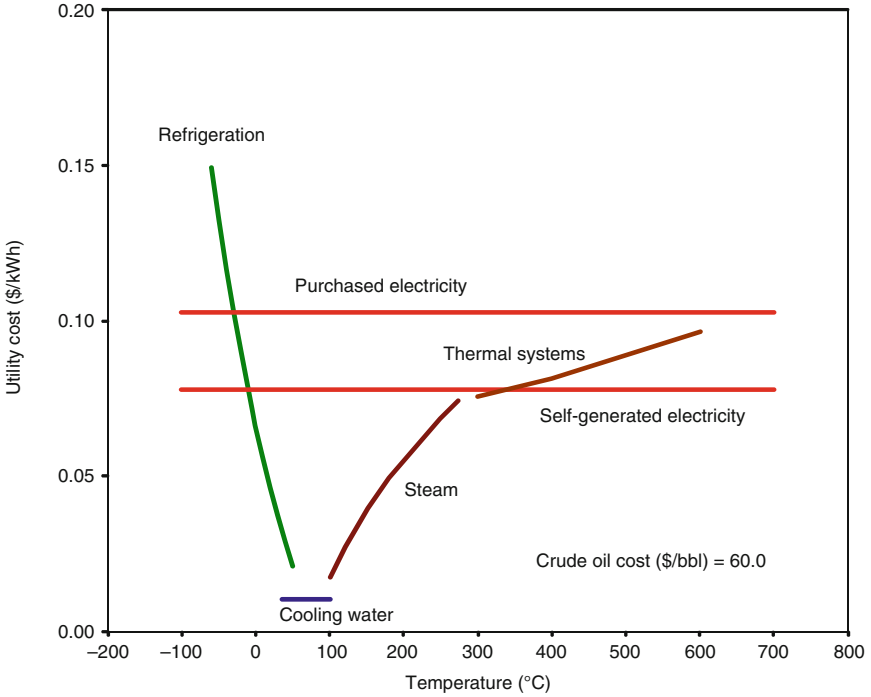

Utility	Description	$/kWh	$/Common unit
Electricity	Purchased	0.103	
	Self-generated	0.078	
Crude			60.0 $/bbl
Fuels	Fuel oil	0.062	0.63 $/L
	Natural gas		0.42 $/m³
	Coal		65.0 $/t
Thermal systems	300°C	0.076	
	400°C	0.081	
	600°C	0.096	
Steam	40 bar	0.068	34.2 $/t
	10 bar	0.049	24.6 $/t
	5 bar	0.040	19.8 $/t
	1 bar	0.017	8.7 $/t
Cooling water	tower	0.010	0.238 $/m³
	river or sea		0.203 $/m³
	well		0.274 $/m³
Refrigeration	5°C	0.072	
	–20°C	0.089	
	–50°C	0.132	

Fig. 9.2 Energy cost of oil priced at $ 60/bbl

$$C_T = C_F + C_w \tag{9.3}$$

The fixed capital cost C_F includes the cost of processing equipment C_{eq}, installation, piping, instrumentation and control, electrical installations, buildings, land and site improvements, office facilities, engineering, and contingency. The working capital C_w consists of the total amount of money invested in raw materials and supplies in stock, finished and semi-finished products, accounts receivable and payable, and cash kept on hand. The working capital amounts to 15–50% of the total cost. In general, food manufacturing plants require higher proportions of working capital than food preservation operations. The fixed cost C_F is estimated from the equipment cost, using the empirical equation,

$$C_F = f_L C_{eq} \tag{9.4}$$

where f_L is the Lang factor. The empirical Lang factor f_L in older plants (Bartholomai, 1987) is approximately $f_L = 2$, but in recent installations, using more instrumentation, process control and computers, values are $f_L = 3$ for main plants and $f_L = 4$ for grassroots plants (including off-site facilities) (Maroulis and Saravacos 2007).

9.2.3.2 Manufacturing Cost

The manufacturing cost C_M of a processing plant consists primarily of the variable cost of raw and packaging materials, labor, and utilities. It also includes the fixed cost of maintenance, insurance, taxes and royalties, and the indirect cost of sales and general expenses. The total manufacturing cost C_{MT} or total annualized cost *TAC* includes the effect of capital cost, as given by the following equation:

$$C_{MT} = C_M + eC_T \tag{9.5}$$

where C_T is the total capital cost, and e is the capital recovery factor, as calculated from the following equation:

$$e = i \Big/ \left[1 - (1+i)^{-N}\right] = i(1+i)^N \Big/ \left[(1+i)^N - 1\right] \tag{9.6}$$

The capital recovery factor is a function of the discount (interest), rate i, and the lifetime of the investment N (years).

9.2.3.3 Discounted Cash Flow

The annual gross profit before taxes P_G is the sales income S minus the manufacturing cost C_M:

$$P_G = S - C_M \tag{9.7}$$

The cumulated cash flow (*CCF*) or annual cash flow is defined by the simplified equation,

$$CCF = -C_O + N\,P \tag{9.8}$$

where C_O is personal capital and P the annual profit after taxes and loan payment, assumed to be constant over the operating time N (years). The investor's own capital is the total capital minus the bank loan. The discounted cash flow or the net present value (*NPV*) is lower than the *CCF*, because it includes the interest rate i of the money:

$$NPV = -C_O + P/e \tag{9.9}$$

where e is the capital recovery factor, defined in (9.5). In the simplified (9.7) and (9.8), the annual profit after taxes and loan payment P is assumed to be constant over the years. When P varies over time, the following summation equations, similar to (9.8) and (9.9), are used to estimate *CCF* and *NPV*:

$$CCF = -C_O + \sum_{n=1}^{N} P_n \tag{9.10}$$

$$NPV = -C_O + \sum_{n=1}^{N} \frac{P_n}{(1+i)^n} \tag{9.11}$$

9.2.3.4 Measures of Plant Profitability

The following measures are used to evaluate plant profitability:

(a) Cash: *CCF* (non-discounted) and *NPV* (discounted)
(b) Time: simple payback period, $SPB = C_T/P$ (non-discounted)
Discounted payback period, $DPB = ln((1 - iSPB)^{-1})/ln(1 + i)$
(c) Rate: return on investment, $ROI = 1/SPB = P/C_T$ (non-discounted)

Internal rate of return, IRR: $ROI = IRR/(1 - (1 + IRR)^{-N})$ (discounted)

The results of profitability analysis are presented in diagrams of *CCF* and *NPV* versus time (years), and break-even analysis of (annual income or sales) and (manufacturing cost or expenses) versus annual operating time. The latter diagram shows the optimum operating time for maximum profit for the specific food plant (Maroulis and Saravacos 2007). The values of *SPB* and *DPB* can be estimated from the cash flow diagrams as the intersection of the *CCF* and *NPV* curves with the time axis, respectively.

9.3 Food Processing Plants

For the purpose of economic analysis, food processing plants can be categorized as follows: food preservation, food manufacturing, and food ingredients plants. Food engineering is mainly concerned with food preservation and food manufacturing plants, while food ingredients plants are more related to chemical engineering. Application examples of some typical plants are presented in this section from process data in the literature (Maroulis and Saravacos 2007).

9.3.1 Food Preservation Plants

Food preservation processes include concentration, dehydration, freezing, and thermal processing (pasteurization, canning). Most plants are located near the production of raw materials (fruits and vegetables, animal products) and usually operate only for one season (e.g., 2–3 months a year). Application examples of two typical food plants are presented in this section, from process data in the literature (Maroulis and Saravacos 2007).

The economics of an orange juice concentrate (*OJC*) is summarized here as an application example. Figure 9.3 shows a block diagram of the process with material and energy balances based on 1 kg of 65% *TS* (total solids) *OJC*, using literature data on fruit composition and process technology. The requirement for raw material is 10.35 kg oranges of 13.6% *TS*. Figure 9.3 shows the material and energy balances of the orange juice concentrate *OJC* processing plant.

The extracted juice is concentrated from 12% to 65% TS, using a four-effect falling film evaporator. The *OJC* is packed in plastic drums and stored at 0°C. The orange peels are used to produce press oil and then dehydrated in an air dryer to produce animal feed with 10% moisture. The theoretical energy requirements for the process are 8 MJ/kg of product. Assuming a thermal efficiency of 75%, the actual energy requirement is about 10.7 MJ/kg or 3 kWh/kg of product.

The plant operates seasonally when ripe oranges are available for processing, which is 16 weeks (or about 4 months) a year. The annual operating time is assumed to be 1,280 h/y and the annual production 1,280 t/year OJC (16 weeks/year $\times$ 5 days/week $\times$ 2 shifts/day $\times$ 8 h/shift). Table 9.1 shows the annual material balances for the orange juice concentrate plant based on a production rate of 1 t/h *OJC*.

The *OJC* product is packed in 5,565 plastic drums of 230 kg capacity, amounting to 5,565 $\times$ 0.23 = 1,280 t/year OJC. The required processing equipment, including cleaning of oranges, juice extraction and finishing, juice evaporation, aseptic packing, and peel drying, were sized and priced following simplified engineering procedures (Saravacos and Kostaropoulos 2002). The equipment cost was $1.62 million. Table 9.2 shows the capital cost components of the *OJC* plant. The working capital is assumed to be 25% of the fixed.

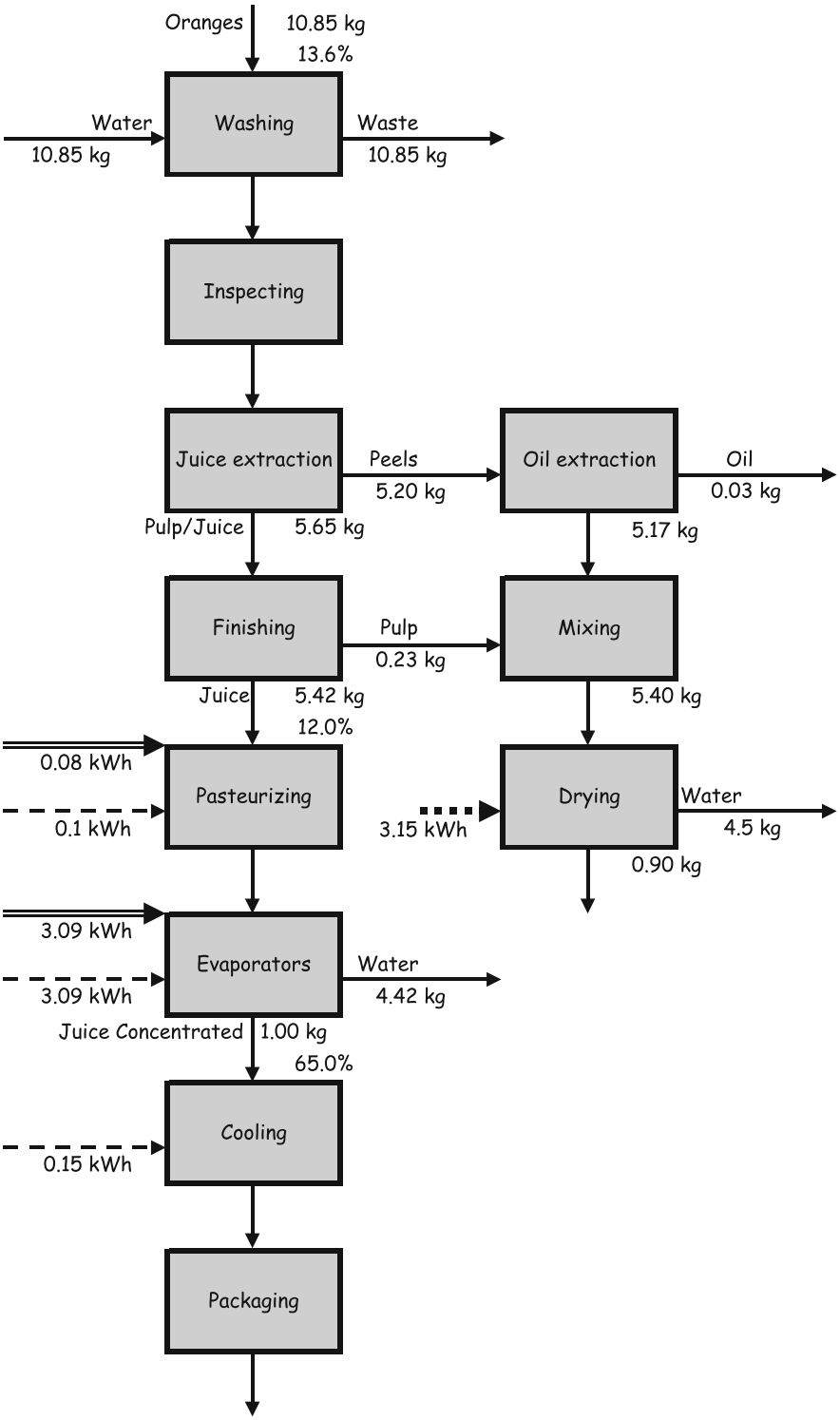

Fig. 9.3 Block process diagram of the *OJC* plant

Table 9.1 Annual material balances of the *OJC* plant

Oranges	13,890 t/year
OJC	1,280 t/year
Dried peels	1,150 t/year
Peel oil	38 t/year

Table 9.2 Capital cost of the OJC plant

Process equipment, C_{eq}	1.62 M$
Lang factor, f_L	3
Fixed capital, C_F	4.86 M$
Working capital, C_W	1.21 M$
Total capital, C_T	6.07 M$

Table 9.3 Annual operating cost of the *OJC* plant

Raw materials (0.12$/kg oranges)	1.67 M$
Labor	0.72 M$
Packaging materials (20$/drum)	0.11 M$
Utilities	0.65 M$
Waste treatment	0.07 M$
Variable manufacturing, C_{MV}	3.22 M$
Fixed manufacturing, C_{MF}	0.49 M$
Overheads, C_{over}	0.23 M$
Manufacturing cost, C_M	3.94 M$
Capital recovery factor, e	0.083 ($i = 0.07$, $N = 27$)
Capital charge, eC_T	0.50 M$
Total annualized cost, $C_M + eC_T$	4.44 M$

The annual operating cost of the *OJC* plant was calculated from material balances, cost data, and empirical correlations, as shown in Table 9.3 (2006 prices). It is assumed that the discount (interest) rate is $i = 0.07$ and the lifetime of the plant is $N = 7$ years.

Table 9.4 summarizes the plant profitability data for the *OJC* plant. The investor's own capital C_0 is assumed to be 50% of the total C_T. The capital return ratio is defined as $CRR = NPV/C_0$.

The annual sales income is based on an *OJC* product price of $3.60/kg, which it is assumed includes the income from the dried peels and peel oil. Figure 9.4 shows the cost components of the orange juice concentrate. The raw material (oranges) is the main cost item (36%), followed by labor (20%) and utilities (15%). Food manufacturing (equipment) cost is about 19% of the total, while bulk packaging in large containers is a relatively low cost. Overheads and capital charge amount to 18% of the total cost.

The relatively high cost of utilities in the *OJC* plant is due to the removal of large amounts of water by evaporation and dehydration, requiring large amounts of steam and fuel gas. Figure 9.5 shows the cash flow, the cumulative cash flow (*CCF*), and the net present value (*NPV*) of the *OJC* plant as a function of operating time N (years). The values of depreciation period ($N_D = 7$ years), loan period ($N_L = 15$ years), salvage period ($N_S = 20$ years), and project lifetime ($N_E = 27$ years) are also shown. The *ROI* value is estimated from the relation $ROI = 1/SPB$.

Table 9.4 Plant profitability of the *OJC* plant

Annual sales income, S	4.61 M$/year
Manufacturing cost, C_M	3.93 M$/year
Gross profit, P_G	0.68 M$/year
Net present value, *NPV*	1.30 M$
Own capital cost, C_0	3.01 M$
Capital return ratio, *CRR*	0.43
Internal Rate of Return, *IRR*	0.12
Return On Investment, *ROI*	0.16
Simple payback period, *SPB*	6.3 years
Discounted payback period, *DPB*	10 years

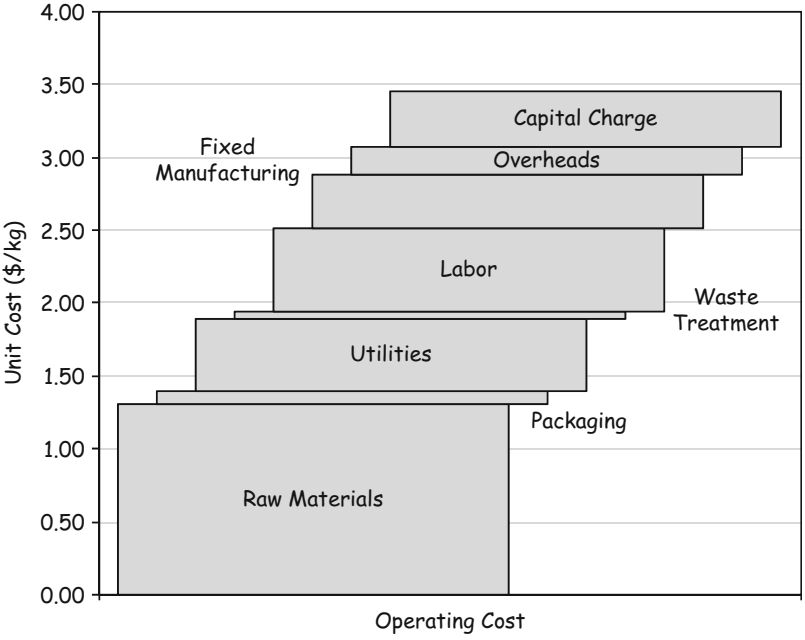

Fig. 9.4 Operating cost of the *OJC* plant

Figure 9.6 shows a break-even analysis of the *OJC* plant. For the process system analyzed here, the optimum operating time (maximum annual profit) is about 1,000 h/year.

9.3.2 Food Manufacturing Plants

Food manufacturing plants typically produce several food products packaged in small consumer units, using agricultural raw materials or semi-finished food

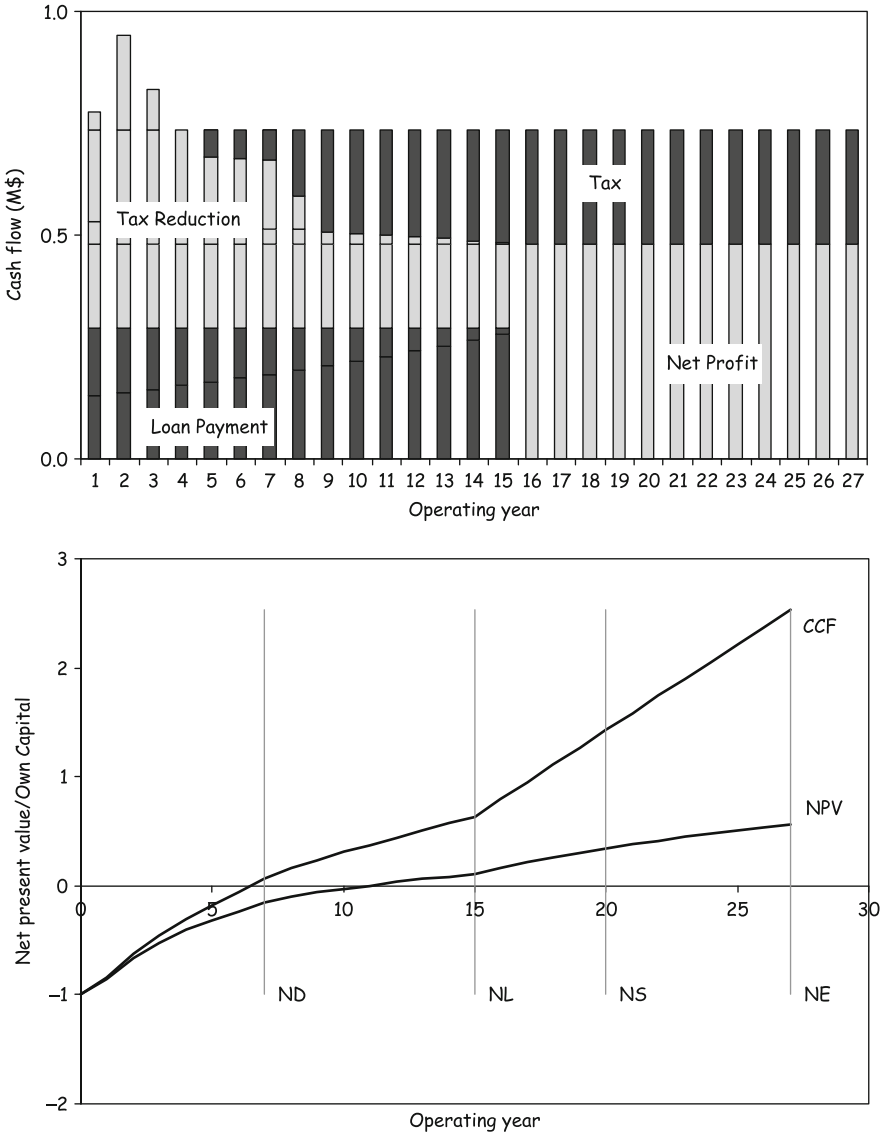

Fig. 9.5 Cash flow and *NPV* of the *OJC* plant

materials and food ingredients. The plants are preferably located close to large consumer centers, operate several months a year, and require more labor and packaging materials than food preservation plants. Food manufacturing plants are characterized by strict hygienic and food safety regulations, due to the sensitivity of food products to microbial and chemical spoilage. Thus, they require special quality control and compliance with government and international regulations. Products

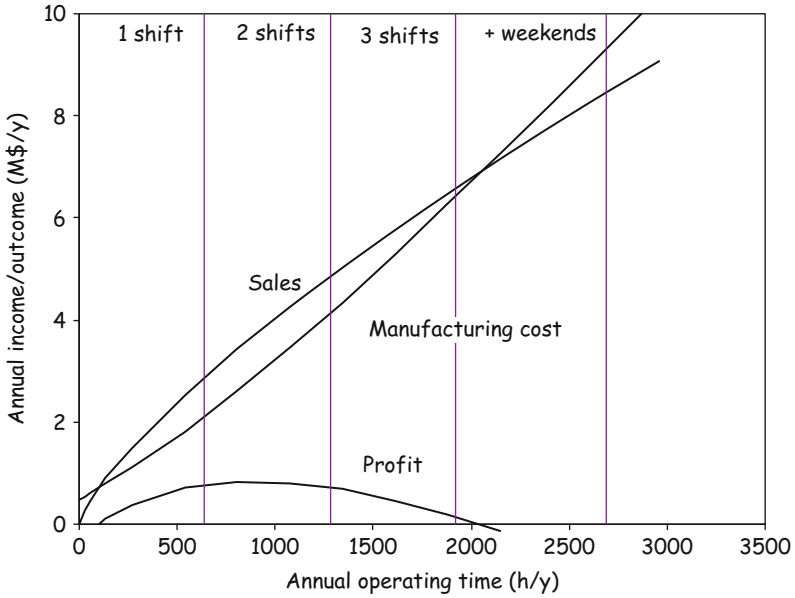

Fig. 9.6 Beak-even analysis of the *OJC* plan

produced in food manufacturing plants include cereal, dairy, fruit and vegetable, animal, and prepared food products. It should be noted that these plants may use some food preservation technology during processing and storage.

As a typical application example, the economics of yogurt manufacture in producing consumer packages is discussed in this section. Figure 9.7 shows the process block diagram and the material and energy balances for the manufacture of dairy yogurt.

The material and energy balances in this example are based on the raw materials, 1,000 kg of milk and 40 kg of nonfat dry milk (*NFDM*). The yogurt plant operates 48 weeks a year, 5 days a week, with two shifts per day and 8-h shifts, amounting to 3,840 h/year. Table 9.5 shows the annual material balances for the yogurt manufacturing plant, producing 4,000 t/year yogurt.

The yogurt product is packaged in plastic cups of 0.250 kg capacity, resulting in 15,976,000 cups/year. The theoretical energy requirement for the process is 0.73 MJ/kg product. Assuming a thermal efficiency of 75%, the actual energy requirement is about 1 MJ/kg or 0.3 kWh/kg product. The required processing equipment, including for milk storage, mixing, homogenization, heat treatment, culture inoculation, and aseptic packaging, was sized and priced, following simplified engineering procedures (Saravacos and Kostaropoulos 2002). The equipment cost was $2.49 million. Table 9.6 shows the capital cost components of the yogurt plant. The working capital is assumed to be 25% of the sales.

The annual operating cost of the yogurt plant was calculated from material balances, cost data, and empirical correlations, as shown in Table 9.7 (2006 prices).

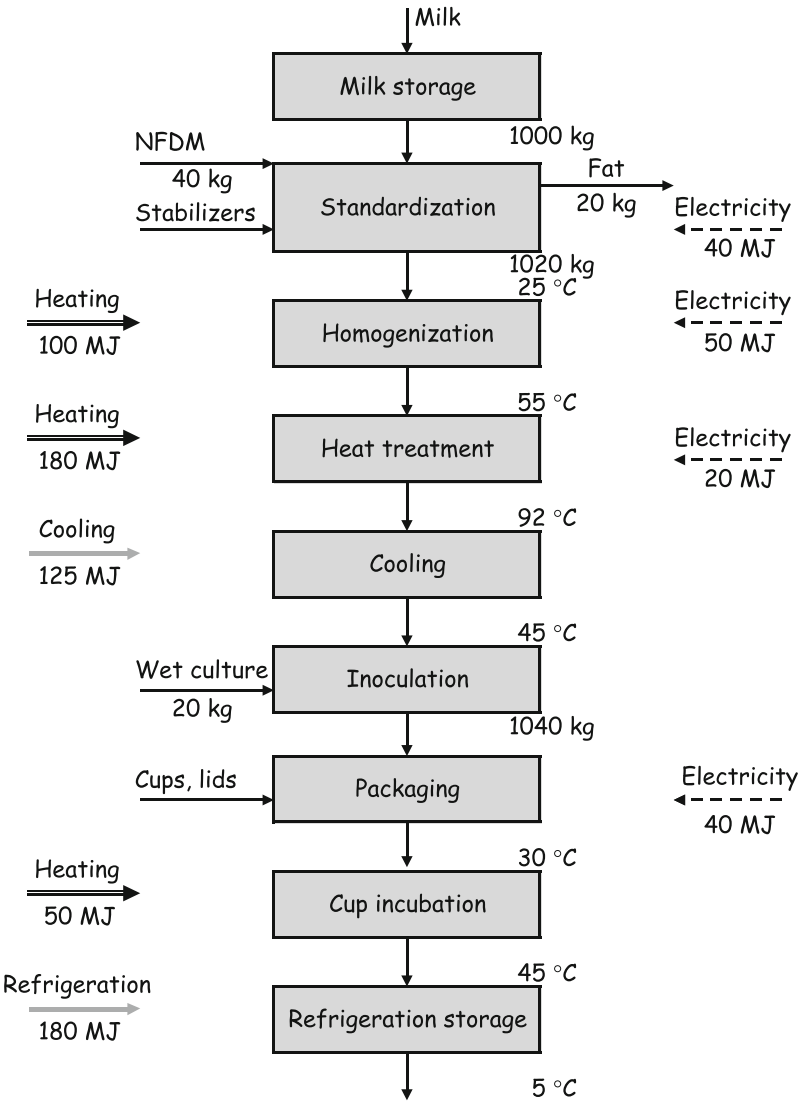

Fig. 9.7 Process block diagram of the yogurt manufacturing plant

Table 9.5 Annual material balances of the yogurt manufacturing plant

Material product rate	t/year
Milk	3,840
NFDM	156.3
Stabilizer	76.8
Fat removed	76.8
Yogurt	3,994

Table 9.6 Capital cost of the yogurt manufacturing plant

Process equipment, C_{eq}	2.49 M$
Lang factor, f_L	3
Fixed capital, C_F	7.47 M$
Working capital, C_W	5.05 M$
Total capital, C_T	12.52 M$

Table 9.7 Annual operating cost of the yogurt manufacturing plant

Raw materials (0.35 $/kg milk)	7.68 M$
Labor	3.24 M$
Packaging materials	(0.04$/piece) 3.84 M$
Utilities	0.32 M$
Variable manufacturing, C_{MV}	15.09 M$
Fixed manufacturing, C_{MF}	0.75 M$
Overheads, C_{over}	1.01 M$
Manufacturing, cost C_M	16.85 M$
Capital recovery factor, e	0.083 ($i = 07$, $N = 27$)
Capital charge, eC_T	1.04 M$
Total annualized cost $C_M + eC_T$	17.89 M$

Table 9.8 Plant profitability of the yogurt manufacturing plant

Annual sales income, S	20.18 M$/year
Manufacturing cost, C_M	16.84 M$/year
Gross profit, P_G	3.34 M$/year
Net present value, *NPV*	16.99 M$
Own capital cost, C_0	6.26 M$
Capital return ratio, *CRR*	2.72
Internal Rate of Return, *IRR*	0.32
Return On investment, *ROI*	0.40
Simple payback period, *SPB*	2.5 years
Discounted payback period, *DPB*	3 years

It is assumed that the discount (interest) rate is $i = 0.07$ and the lifetime of the plant is $N = 27$ years.

Table 9.8 summarizes the plant profitability data for the yogurt plant. The investor's own capital C_0 is assumed to be 50% of the total C_T.

The annual sales income is based on a yogurt product price of $1.25/kg. Figure 9.8 shows the cost components of the yogurt manufacturing plant. The raw material (milk) is the major cost item (43%), followed by packaging materials (23%), labor (18%), and processing equipment (5%). Utilities, overheads, and capital charge amount to about 11% of the total cost.

The cumulative cash flow (*CCF*) and the net present value (*NPV*) plots of the yogurt plant are similar to the diagrams of the *OJC* plant. Break-even analysis of the yogurt plant resulted in a diagram similar to Fig. 9.6, indicating a higher optimum operation time (maximum annual profit) of about 2,500 h/year.

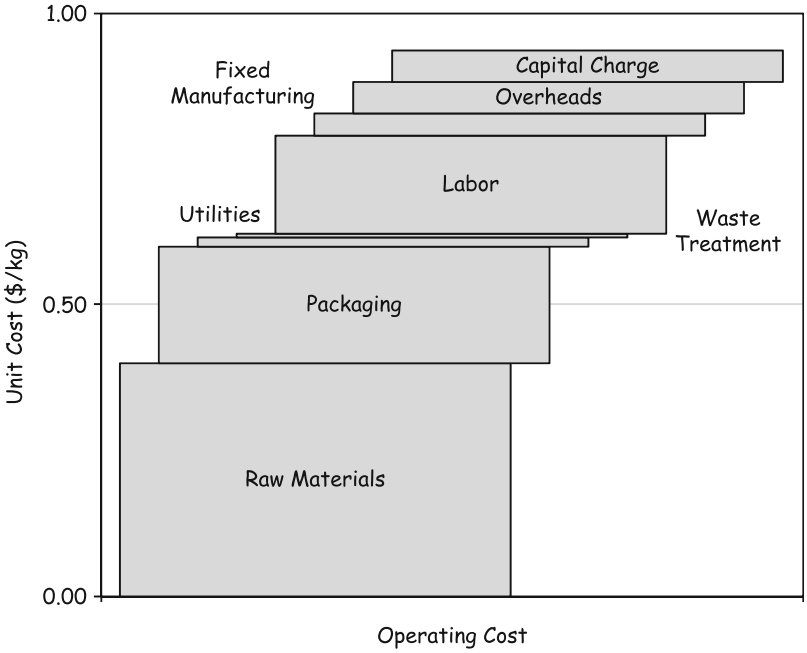

Fig. 9.8 Operating cost of the yogurt manufacturing plant

9.3.3 Food Ingredients Plants

Food ingredients plants utilize agricultural and natural raw materials to recover valuable components, which are then used in food manufacturing. Typical products are wheat flour, vegetable oils, starch, pectin, sugar, and proteins. Special food components used in smaller quantities include flavorings, vitamins, coloring materials, sweeteners, preservatives, and antioxidants.

9.4 Conclusions

Applying the principles of process economics to food processing can lead to useful information on the economics of food processes. Simplified procedures based on material and energy balances, sizing of process equipment, and cost data on raw materials, labor, and utilities result in new food process designs and economic evaluation of existing processing operations. Raw materials, followed by labor, are the major cost items in most food production processes. Packaging cost also may be important for some food manufactured products. Food products manufactured from raw food materials and food ingredients are generally more profitable than products of food preservation plants.

References

Bartholomai A (1987) Food factories – processes, equipment, costs. VCH Publishers, Weinheim
Clark JP (1997) Cost and profitability estimation. In: Valentas KL, Rotstein E, Singh RP (eds) Handbook of food engineering practice. CRC Press, New York, pp 537–557
Couper JR (2003) Process engineering economics. Marcel Dekker, New York
Holland FA, Wilkinson JK (1997) Perry's chemical engineers' handbook. In: Perry RH, Green DW, Maloney JO (eds) Process economics, 7th edn. McGraw-Hill, New York, pp 9.1–9.63
Lopez-Gomez A, Barbosa-Cánovas G (2005) Food plant design. Taylor & Francis, New York
Maroulis ZB, Saravacos GD (2003) Food process design. Marcel Dekker, New York
Maroulis ZB, Saravacos GD (2007) Food plant economics. CRC Press, Boca Raton, FL
Peters SM, Timmerhaus KD, West RE (2003) Plant design and economics for chemical engineers, 5th edn. McGraw-Hill, New York
Rahman S (1995) Food properties handbook. CRC Press, New York
Rao MA, Rizvi SSH, Datta AK (2005) Engineering properties of foods, 3rd edn. Taylor & Francis, New York
Saravacos GD, Maroulis ZB (2001) Transport properties of foods. Marcel Dekker, New York
Saravacos GD, Kostaropoulos AE (2002) Handbook of food processing equipment. Kluwer/ Plenum, New York

Chapter 10
Systemic Approach to Curriculum Design and Development

Inés Ecima, Maurcio Pardo, and Gloria González-Mariño

10.1 Introduction

Engineering leaders and educators consider innovation to be an important topic in any program related to the training of engineers (Apelian 2007; National Academy of Engineering 2004). The development of traditional skills and knowledge are not the most important goals of an engineering curriculum nowadays, and due to the influence of technology and globalization, traditional engineering skills are now considered a commodity. Identifying this trend, Thomas Friedman (2005) described the modern world as "flat," trying to illustrate the great impact of technology and globalization on the economy of modern society. To make matters worse for new engineering graduates, today's computers are capable of doing almost everything engineers have done up until now. As a consequence, it is important to reorient engineering education in such a way that engineers are prepared to understand the societal context of their work from both a local and global perspective. Innovation and creativity also should be coupled with the engineer's ability to gather information, analyze it, make decisions, and take the right course of action.

Food engineering is a branch of engineering education that has inadvertently addressed the need for innovation in meeting the demands of technological and scientific advances in the new century. There are many challenges involved during processing in how to preserve the original quality of food and its active ingredients, which are considered good for humans. As a result, customization of food products is actually one of the strongest trends in the food industry today (Higgins 2007; Coulston et al. 2003). Thus, collaboration among food engineers, nutritionists, medical doctors, microbiologists and microelectronic engineers, together with other experts, has become an essential element in dealing with these challenges.

I. Ecima and M. Pardo
Ingeniería de Producción Agroindustrial, La Sabana University, Bogotá, Colombia

G. González-Mariño (✉)
Biosciences Doctoral Program, La Sabana University, Bogotá, Colombia
e-mail: gloria.gonzalez@unisabana.edu.co

J.M. Aguilera et al. (eds.), *Food Engineering Interfaces*, Food Engineering Series,
DOI 10.1007/978-1-4419-7475-4_10,

For one, it is necessary that engineers be capable of producing and offering customized products at fair prices to the market. This customization should not only attend to fair pricing and the consumers' tastes but to their health needs as well. Food engineers must be able to integrate new technologies into traditional processing lines in order to offer products nearer to consumer needs. They must also have an ample view of the food sector and be capable of relating people and procedures that affect the production and quality of food, by undertaking joint actions, making faster decisions, and sharing their knowledge and experience with conforming professional communities and peers located around the world.

To achieve this goal, engineering students should have flexible educational programs that encourage a systemic approach to the food industry, programs that allow them to travel the world and remain in permanent contact with their colleagues. These programs must also be developed according to international standards so students are allowed to travel without interrupting their studies. Nowadays the trend is to solve problems and make decisions from a broad perspective instead of concentrating on a specific discipline. Generally, however, this does not mean that the depth of understanding a specific scientific field is lost; rather it means that the engineering professional is able to decide which basic science principles are actually needed to solve a particular problem.

10.2 Systems Theory and Thinking

Systemic or systems theory has been taken into account by numerous scientific fields including the field of education (Cabrera and Colosi 2008; Kim and Senge 1994; Ison 2008; Senge 1990). Although there are many conflicting claims that need to be reconciled around this topic, such discussion is out of the scope of this chapter. Therefore the classical definition proposed by Ludwig von Bertalanffy in 1968 is being used as reference:

> Classical sciences tried to isolate the elements of the observed universe… Now we have learned that for an understanding of not only the elements, but their interrelations as well are required… It is necessary to study not only [the] parts and processes in isolation, but also to solve the problems [organization and order] resulting from dynamic interaction of parts, and making the behavior of the parts different when studied in isolation or within the whole… General system theory, therefore, is a general science of wholeness… The meaning of the somewhat mystical expression 'The whole is more than the sum of its parts' is simply that constitutive characteristics are not explainable from the characteristics of the isolated parts. The characteristics of the complex, therefore, appear as 'new' or 'emergent'….

Additionally, a system can be defined as a dynamic and complex whole interacting as a unit, located within an environment in which energy, material, and information flow between the different elements that compose the system and between the elements and their surrounding environments. If the set of courses, methods, people, and tools involved in a learning-teaching interaction are considered as a system, they will show certain characteristics as summarized in Table 10.1.

Table 10.1 Comparison between the characteristics of a basic system and those of the curriculum as a system

System	Curriculum
Dynamic and complex **whole** interacting as a unit	Dynamic and complex academic, social, technical, scientific and empiric **knowledge** interacting as a unit
Energy, material, and information **flowing** between the different elements that compose the system	Topics, issues, theories, information, people, feelings, perceptions, sciences, personal skills, and hidden things **flowing** between students, teachers, parents, industry, among others
Community located within an environment	Academic **community** immersed in a context
Energy, material, and information **flowing** from and to the surrounding environment	Knowledge and agents **interacting** within the academic community and national and international peer communities
Seeks **equilibrium** but can exhibit oscillating, chaotic or exponential behavior	Seeks **articulation** but has to be flexible. Loop planning and developing-assessing changes in every course

According to O'Connor and McDermott (1998), systems thinking (i.e., the practice of systems theory) comprises the whole and the parts as well as the links among parts. Furthermore, it studies the whole in order to understand the parts. It is a pattern of thinking that is not disciplinary in scope and can act as a bridge between the physical, natural, and social sciences. Four universal conceptual patterns have been observed in every system and can be used as tools to apply systems thinking in any situation, as proposed by Cabrera et al. (2008):

1. System definition
2. Distinction from others
3. Perspective or frame of reference
4. Relationships between systems and parts

10.2.1 Designing Curriculum Using Systems Thinking

If the four universal principles just described are followed in the design of a curriculum, the first step should be to define the framework and the system, its parts and its limits. Therefore, a definition of the curriculum from the point of view of the institution is needed. Additionally, the boundaries of this system should be identified to differentiate it from others. Finally, relationships should be identified.

Table 10.2 describes the different aspects that should be taken into account in defining the curriculum. Readers should note that even though Table 10.2 depicts a step by step methodology this is far from a real procedure. Many steps need to be carried out in parallel and many others will require revision after defining the whole curriculum. Figure 10.1 gives a closer visual description of the methodology used for systems thinking.

Table 10.2 Some steps taken into account during curriculum design

Activity	Systems thinking principles used
Define program (field and duration) and level (undergraduate or postgraduate)	Perspective, System definition, and distinction
Find similar programs (locally and abroad)	System distinction
Identify educational trends nationally and internationally	System distinction
Identify skills of student entering the program	Relationships (between system and environment)
Identify skills and competencies demanded by society	Relationships (between system and environment)
Identify institution's educational purposes	Perspective and system definition (parts)
Define problematic and nuclear topics to be taught	System definition (parts)
Define courses	System definition (parts) Relationships (between parts of system)
Define learning-teaching strategy	System definition (parts) Relationships (between parts of system)
Identify institutional capacities (teachers, buildings, equipment, software)	System definition (parts)
Define assessment strategy	System definition (parts) Relationships (between parts of system)

10.2.2 Designing Curriculum for Undergraduate Courses

Educational institutions are guided by educational goals, so the first step in designing a curriculum is to establish the goals. At the School of Engineering at Universidad de La Sabana, the main educational goal at the undergraduate level is to teach students how to design and manage their own projects when they become professionals.

To achieve this goal, an interdisciplinary curriculum is designed that takes into account the basic sciences, such as physics, chemistry, and biology, with mathematics as the common language, which allows the engineers to represent different phenomena. Study of the basic sciences should include the following objectives:

- Describe and study a phenomenon from the perspective of each basic science using mathematical language
- Identify the principles, laws, and theories that explain the natural phenomenon
- Understand the phenomenon as a whole from different points of view

Additionally, graduates are expected to have the following competencies as a result of their educational program. They should be able to:

- Adopt systems thinking as an attitude
- Identify food systems and their parts at different levels, such as tissues, processed products, and supply chains

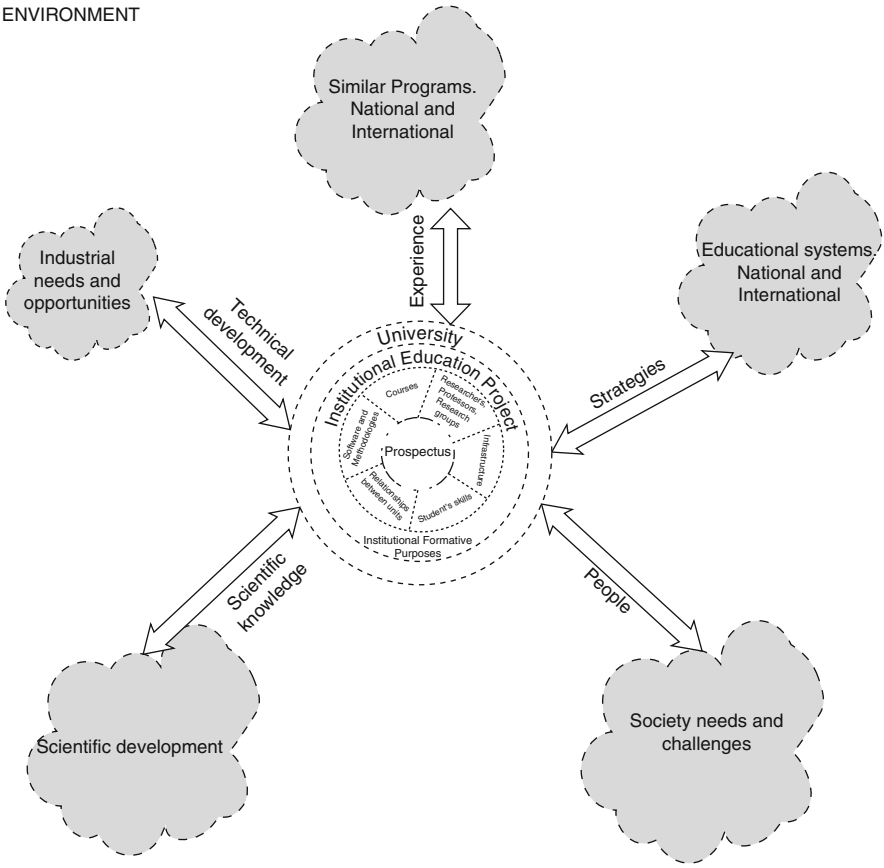

Fig. 10.1 Closer visual description used for curriculum design under systems thinking methodology

- Design processes taking into account the interactions between food materials and other components of the food chain
- Manage food handling and processing projects by considering all factors of the network

During this learning – teaching period, the educator should also assist students in finding the linkages between the concepts and reality.

10.2.3 Designing Curriculum for a Master's Degree Program

At this level the educational goal is to train students to be professionals, as capable of solving an industrial problem in an innovative way. To innovate means to perform a creative solution in order to obtain a new product. In the end, these

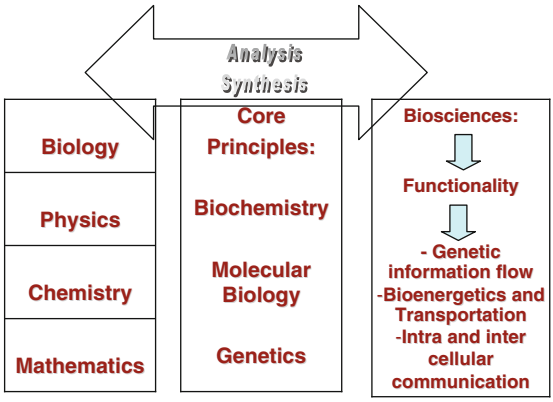

Fig. 10.2 Biosciences curriculum development

professionals who come from different disciplines should have in common their capacity to solve problems using systems thinking and integrating the different sciences. The training process has the following purposes:

- Develop the student's ability to solve problems using an integration of sciences approach.
- Develop the student's creativity and design capacity.
- Develop the student's ability in mathematical modeling.

In the case of the Master's program in Process Design and Management, the former training purposes are not only competencies to develop but are also specific courses wherein students can find practical situations to develop these skills.

10.2.4 Designing Curriculum for a Doctoral Program

At the doctoral level, the educational goal is to train researchers via different disciplines. For example, in the biosciences program, the goal is to guide students during the study of biological elements (molecules) and their vital functions, in such a way, that they are able to discover new and different uses for these molecules. To achieve this goal, the biosciences course uses a systems thinking approach to review different functions such as transport, signaling, and reproduction in cells. This systems thinking approach is supported by a permanent analysis-synthesis activity using concepts from molecular biology, biochemistry, and genetics (Fig. 10.2).

10.3 Conclusion

The four universal principles of systems thinking have been used at Universidad de la Sabana in curriculum design for both undergraduate and postgraduate levels. Additionally, systems thinking has been introduced as an educational goal in order

to give engineers more skills in defining systems (their parts and interactions), which will serve as a tool in problem solving and decision taking.

References

Apelian D (2007) The engineering profession in the 21st century – educational needs and societal challenges facing the profession. AFS Hoyt Memorial Lecture. American Foundry Society. International Journal of Metalcasting Fall 07

Bertalanffy L von (1968) General system theory: foundations, development, applications. Braziller, New York

Cabrera D, Colosi L (2008) Distinctions, systems, relationships, and perspectives (DSRP): a theory of thinking and of things. Eval Program Plann 31:311–334

Cabrera D, Colosi L, Lobdell C (2008) Systems Thinking. J Eval Prog Plan 31:299–310

Coulston AM, Feeney MJ, Hoolihan LE (2003) The challenge to customize. J Am Diet Assoc 103(4):443–444

Friedman TL (2005) The world is flat: a brief history of the twenty-first century. Farrar, Straus & Giroux, New York

Higgins KT (2007) Meeting the challenges of customized manufacturing. BNP Media. *Food Engineering* online magazine: http://www.foodengineeringmag.com/

Ison RL (2008) Systems thinking and practice for action research. In: Reason P, Bradbury H (eds) The Sage handbook of action research participative inquiry and practice. Sage, London, pp 139–158. ISBN 1-4129-2029-9, 978-1-4129-2029-2

Kim DH, Senge P (1994) Putting Systems thinking into practice. Syst Dyn Rev 10(2–3):277–290

National Academy of Engineering (2004) Educating the engineer of 2020: Adapting engineering. Education to the New Century. Available for free online: http://fermat.nap.edu/catalog/11338.html

O'Connor J, McDermott I (1998) The art of systems thinking. Thorson, London

Senge P (1990) The fifth discipline. Doubleday Dell Publishing, New York

Part II
Advances in Food Process Engineering

Chapter 11
Innovations in Thermal Treatment of Food

Arthur Teixeira

11.1 Introduction

Thermal processing (heat treatment) for sterilization of shelf-stable foods has been one of the most widely used methods of food preservation during the twentieth century, and has contributed significantly to the nutritional well-being of much of the world's population. For most solid and semi-solid foods, thermal processing is accomplished after the product has been filled and hermetically sealed in airtight containers. Thermal processing consists of heating food containers in pressurized retorts at specified temperatures for prescribed lengths of time. These process times are calculated on the basis of achieving sufficient bacterial inactivation in each container to comply with public health standards and to ensure that the probability of spoilage will be less than some minimum. Many liquid food products, such as milk or fruit juices, are pasteurized or sterilized by heat treatments applied before filling and sealing into packages. These heat treatments are accomplished by pumping the liquid product through a series of heat exchangers and hold tubes that deliver a high temperature-short time (HTST) heat treatment for pasteurization, or an ultra-high temperature (UHT) short time treatment for sterilization.

This chapter presents a review of recent innovations that have been made in the field of thermal processing for food preservation, and attempts to foresee the impact these innovations may have on the marketplace. Three categories of innovation are addressed: (i) improved methods in estimating kinetic parameters for establishing optimum process conditions, (ii) a review of new equipment systems for retorting and materials handling to improve cookroom operations, and (iii) new and novel packaging systems, and their potential impact on markets for shelf-stable foods.

A. Teixeira
Agricultural and Biological Engineering Department, University of Florida, Gainesville, FL 32611–0570, USA
e-mail: atex@ufl.edu

J.M. Aguilera et al. (eds.), *Food Engineering Interfaces*, Food Engineering Series,
DOI 10.1007/978-1-4419-7475-4_11,

11.2 Microbial Kinetics for Process Calculations

The manner in which populations of microorganisms decrease in response to lethal heat treatments is fundamental to the engineering design of thermal inactivation processes (pasteurization and sterilization) and important in the food, pharmaceutical, and bioprocess industries. In order to determine the optimum process conditions needed to achieve desired results, the effect of these conditions on rates (kinetics) of population decrease needs to be characterized and modeled mathematically. This chapter section will focus on the use of new methods for estimating kinetic parameters more accurately. Use of more accurate parameters in appropriate mathematical models will enhance the accuracy of these models. When properly developed and validated, these models can predict the extent to which a population of viable spores will be reduced in response to a lethal heat treatment at specified temperature and time. These models are essential tools in establishing process conditions, i.e., time and temperature, needed to achieve a specified level of bacterial lethality.

Thermal inactivation of bacteria generally follows first-order kinetics; it can be described by logarithmic reduction in the number of bacterial spores with time during exposure to a constant lethal temperature. The logarithm of number of bacterial spores when plotted against time normally produces a straight line known as a survivor curve. The slope of this curve will give the first order rate constant at this temperature. Alternatively, the reciprocal of this rate, known as decimal reduction time, D, is expressed as time in minutes to achieve one log cycle reduction in spore population when subjected to a specified constant lethal temperature.

The temperature dependency of the rate constant is also an exponential function that can be described by the Arrhenius equation. This is the equation used for a straight line on a semi-log plot when the natural log of the rate constant is plotted against the reciprocal of absolute temperature. Likewise, the temperature dependency of the decimal reduction time, D, is also logarithmic (straight line on a semi-log plot of D versus temperature within the lethal range), and can be expressed as the temperature difference, Z, required for the curve to transverse one log cycle. Thermal death-time kinetic parameters "D" and "Z" are widely used in the food science community, while the first order rate constant and the Arrhenius relationship are most often used in the chemical and biochemical communities. In either case, these parameters must be estimated as accurately as possible to calculate optimum thermal process conditions that ensure public safety with maximum product quality.

Traditional methods for estimating these kinetic parameters consist of plotting a series of survivor curves at different lethal temperatures, and measuring the slope or D-value from each curve. Data for these curves are obtained from carefully executed microbiology laboratory procedures. Typically, a series of small glass vials containing a known high concentration of viable spores are immersed simultaneously into a heated oil bath maintained at a known constant lethal temperature. At predetermined time intervals one of the vials is quickly removed and immediately cooled until all vials have been removed. Thus, each vial contains spores exposed to a lethal

temperature for a different length of time. The contents of each vial are plated onto appropriate growth media and incubated for subsequent enumeration of survivors. The logarithm of number of survivors from each vial is plotted against time to produce the log-linear survivor curve, and the *D*-value at that temperature is taken from the slope of that curve.

The same experiment is repeated at different constant lethal temperatures in order to obtain *D*-values at different temperatures, from which the temperature dependency factor, *Z*-value, can be determined. These methods are prone to error because of heat transfer limitations causing thermal lag in the temperature response in each vial. The spores themselves do not rise instantly to the oil bath temperature, nor do they cool instantly in response to the quenching temperature. In those cases where the kinetics are needed for mesophylic spores in a liquid product, errors can be minimized by use of a three-neck flask containing the liquid product heated to a known constant lethal temperature. One neck is used to accommodate a thermometer for temperature measurement, a second neck holds an inoculation needle through a rubber stopper, and the third neck holds a number of extraction needles for removing and quenching samples of spore suspension at predetermined time intervals (Rodriguez et al 1988). Although this method minimizes errors from lag in thermal response, it is still prone to errors in timing, particularly when samples must be extracted within a few seconds of each other at higher temperatures where the lethal rate is very high.

An entirely new and different experimental approach for estimating kinetic parameters in liquid products was first developed by Swartzel (1984) and called the Equivalent Point Method (EQM). It was later modified by Welt et al (1997), and called the Paired Equivalent Isothermal Exposure (PEIE) method. These methods do away completely with the use of constant temperature baths (isothermal experiments). Instead, a batch of liquid product inoculated to a known high initial concentration of spores is "processed" through an HTST or a UHT heat exchanger-hold tube system that delivers a precisely known dynamic temperature-time profile experienced by the inoculated product. Samples of the "processed" product are plated, incubated, and enumerated to determine the number of survivors, thus giving the extent of reaction accomplished. By knowing the extent of reaction from two different sets of process conditions and the precise dynamic temperature-time profiles of each, a nearly "true" estimate of kinetic parameters can be determined.

This was confirmed by work carried out at the University of Florida, in which kinetic parameters for thermal inactivation of *Escherichia coli* in orange juice were estimated using the new PEIE method with a Microthermics® HTST Lab 25 pasteurizer, as well as the traditional isothermal bath method with the three-neck flask (Moody 2003). *D*-values obtained from both methods at different temperatures are shown in Table 11.1. For the two temperatures used in common by both methods (58 and 60°C), *D*-values estimated by the new PEIE method were lower than those estimated by the traditional isothermal bath method. Lower *D*-values mean faster kinetics and would justify shorter process times if known to be true. In order to determine which method produced estimates closest to the "truth," inoculated samples of orange juice were processed through the HTST pasteurizer at temperatures

Table 11.1 Comparison of kinetic parameters (*D*- and *Z*-values), estimated using traditional isothermal and new PEIE methods (Reproduced from Moody 2003. With permission)

Temperature (C)	Isothermal (Three-neck flask)		Dynamic (PEIE)	
	D-value (s)	Standard Deviation	D-value (s)	Standard Deviation
52	353	39.08		
55	148	2.18		
58	34.7	2.27	29.8	3.3
60	18	1.52	13.27	1.54
62			6.93	0.47
z-value (C)	5.99		6.16	

Table 11.2 Results of validation experiments comparing the number of survivors measured experimentally with those predicted using traditional and new PEIE methods (Reproduced from Moody 2003. With permission)

Experiment	Hold Tube				Survivors (cfu)	
	Time (sec)	Temp. (C)	Initial (cfu)	PEIE Predicted	Isothermal Predicted	Experimental
I	15	65	5.4×10^8	3.5×10^3	5.0×10^4	5.2×10^3 2.8×10^3
II	10	65	5.4×10^8	2.0×10^3	8.6×10^4	1.0×10^3 1.3×10^3

above the range used to estimate the parameters (65°C). Two different processes were used, one with a hold tube residence time of 15 s, and 10 s for the other, in order to obtain distinctly different numbers of survivors from each process. Processed samples were plated, incubated, and enumerated to determine the number of survivors from each process. These experimental results were compared with numbers of survivors predicted by the mathematical model using both sets of parameters.

Model-predicted results using parameters estimated by the new PEIE and traditional isothermal bath method are compared with experimental results in Table 11.2. The number of survivors predicted by the model, using parameters estimated by the PEIE method, agrees very closely with those measured experimentally (within a fraction of one log cycle). In contrast, the number predicted by the model using parameters estimated by the traditional isothermal bath method differed from those measured experimentally by one and two log cycles for processes I and II, respectively. The significance of these differences can best be appreciated when the two sets of parameters are used to calculate the process time needed to accomplish a 6-log cycle reduction in the *E. coli* population in orange juice at a typical pasteurization temperature of 65°C. At this temperature, the *D*-value estimated by the traditional isothermal bath method would be 1.8 s leading to a hold tube residence time of 1.8 (6) = 11 s. In contrast, the *D*-value estimated by the new PEIE method would be 1.3 s leading to a hold tube residence time of 1.3 (6) = 8 s. This 30% reduction in process time is made possible by adopting better methods for estimating kinetic parameters more accurately.

11.3 Retort Equipment Systems in Cookroom Operations

The preponderance of thermally processed shelf-stable foods in the marketplace today continues with products processed in batch retorts that must be repeatedly loaded and unloaded between each process cycle throughout the workday. In years past, this was performed by teams of workers with the help of chain hoists and rail carts moving from retort to retort around the cookroom floor, while retort operators kept vigilance as time keepers, temperature monitors and record keepers. Recent innovations in retort control and materials handling systems have essentially revolutionized traditional cookroom operations. Today's modern retorts such as that shown in Fig. 11.1 are equipped with sophisticated computerized electronic control systems that can be remotely monitored from a control room by a single operator who may be responsible for an entire battery of retorts. These control systems are capable of operating each retort through its entire process cycle, while controlling and recording temperatures and pressures, as well as monitoring process conditions at all critical control points. At the end of each process cycle, a complete set of batch records is provided for compliance with record keeping requirements of the FDA Low-acid Canned Food regulations.

The introduction of automation and robotics for the materials handling operations on the cookroom floor has perhaps had the greatest impact in reducing the cost of manufacturing thermally processed products. An automated batch retort system in a modern cookroom today consists of a battery of retorts laid out in a row on the cookroom floor to accommodate automated loading and unloading (Fig. 11.2). Both track-guided and trackless systems are available for this purpose. In track-guided

Fig. 11.1 Modern Retort with pressure vessel, field devices, and process control system (Photo courtesy of JBT FoodTech, formerly FMC FoodTech, Madera, CA)

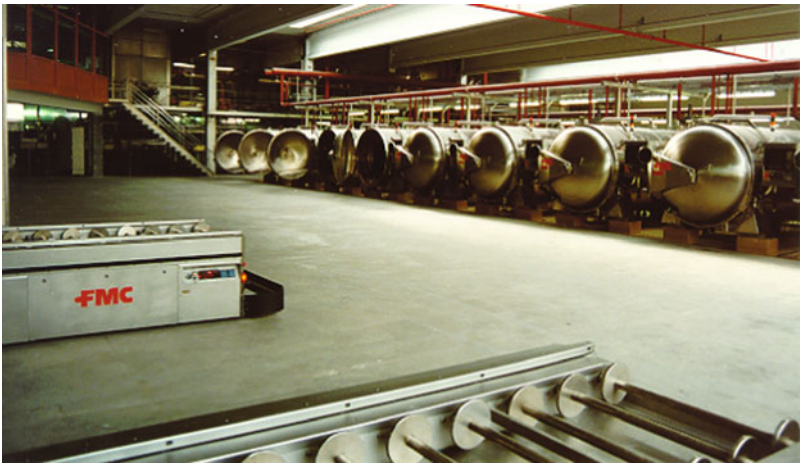

Fig. 11.2 Modern cook room showing battery of retorts arranged for automated loading and unloading (Photo courtesy of JBT FoodTech, formerly FMC FoodTech Madera, CA)

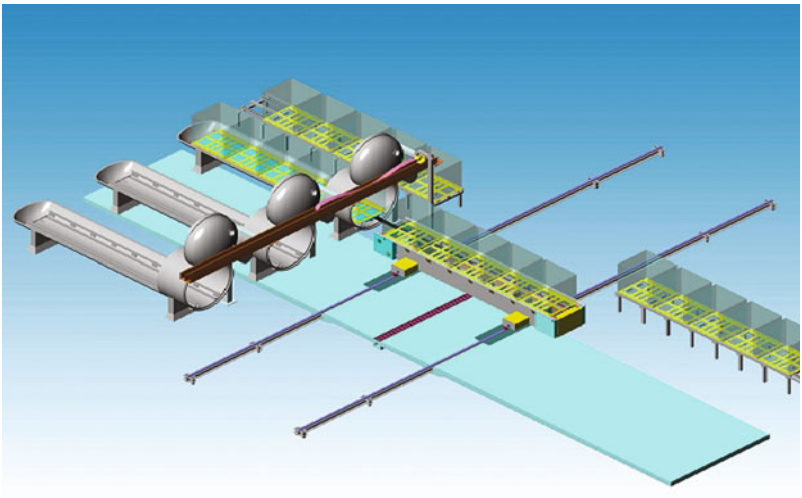

Fig. 11.3 Track-guided automated batch retort system (ABRS) (Courtesy of Allpax Products, Inc., Covington, LA)

systems, a rail cart transfers crates or baskets of products from the loading stations to the retorts, and from the retorts to the unloading stations automatically on a rail track that allows the cart to move in a transverse direction along the cookroom floor until it is aligned with the target retort (Fig. 11.3). Once the cart is aligned with the retort, the loaded baskets or crates are automatically transferred from the cart into the retort for loading operations, or from the retort onto the cart for unloading operations. Trackless systems such as that illustrated in Fig. 11.4 work much the

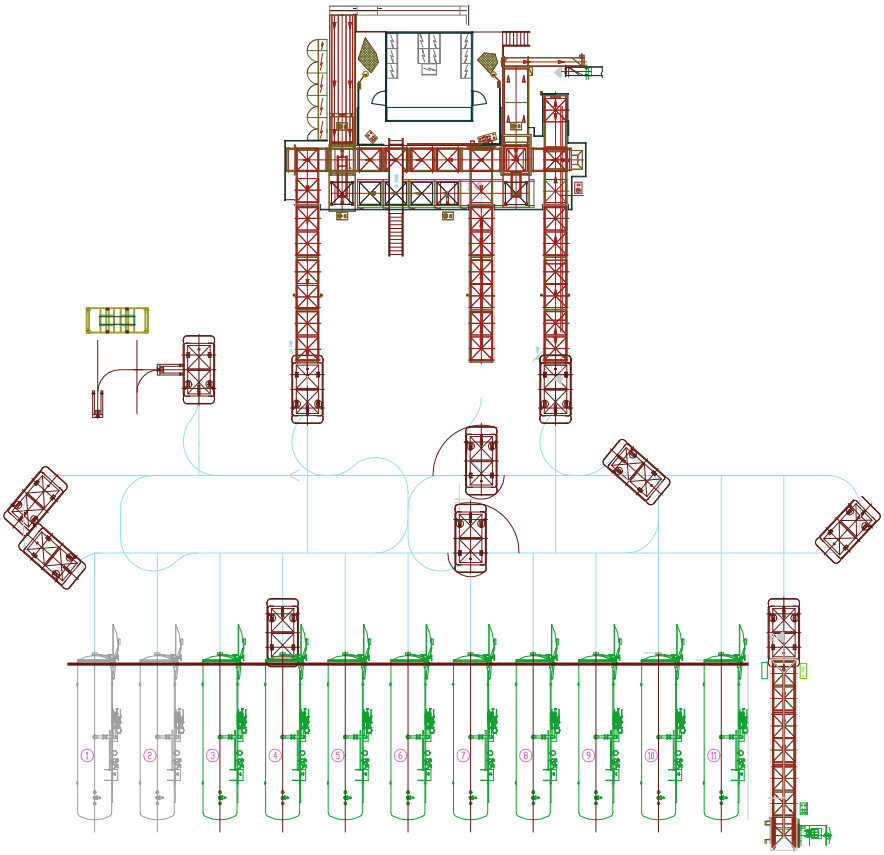

Fig. 11.4 Trackless system layout for automated guided vehicles (AGV) (Photo courtesy of JBT FoodTech, formerly FMC FoodTech, Madera, CA)

same way, except that the rails and rail carts are replaced by automated guided vehicles (AGV) that move about the cookroom floor controlled by electronic guidance systems. These systems offer the advantage of keeping the cookroom floor free of rails or tracks that could impede safe movement of workers on the floor. A close-up view of an AGV that has just been loaded or is about to unload a retort is shown in Fig. 11.5, and an automated materials handling system for retort basket, rack, or tray loading is shown in Fig. 11.6.

11.4 Flexible Retortable Packages

Perhaps the most intriguing innovation in thermal processing in recent years has been the introduction of flexible retortable pouches and semi-rigid trays and bowls in the marketplace for shelf-stable canned foods (Fig. 11.7). The relatively thin profiles

Fig. 11.5 Automated Guided Vehicle in process of retort loading/unloading (Photo courtesy of JBT FoodTech, formerly FMC FoodTech, Madera, CA)

Fig. 11.6 Automated materials handling system for retort basket, rack, or tray loading (Courtesy of Allpax Products, Inc., Covington, LA)

Fig. 11.7 New flexible and semi-rigid retortable packaging systems

offered by these flexible packages allows them to be heated more rapidly than metal cans or glass jar counterparts, often resulting in better product quality. Moreover, they offer the consumer a variety of convenient features. Flexible pouches carry less weight, occupy less space, and are easy to open with a simple pair of scissors. Semi-rigid trays and bowls can be fashioned as attractive serving dishes that are microwaveable, and can be placed on the dinner table ready to serve directly from the microwave oven. However, the flexible and semi-rigid properties that make these attractive features possible pose technical challenges in the retort processing of such packages. These flexible packages lack the strength of traditional metal cans and glass jars, and are incapable of withstanding the pressure gradients normally experienced by cans and jars during typical retort process cycles.

Successful retorting of such flexible or semi-rigid packages requires that they be processed under carefully controlled dynamic pressure excursions (profiles) to prevent package expansion during processing. When not controlled properly, this expansion can result in permanent distortion or deformation of the final package after retorting. Design and control of these complex pressure profiles is accomplished with the simultaneous use of both pressure and deflection detectors during a heat penetration test. The electronic deflection detectors continuously monitor the package expansion or contraction, sending a signal to the on-line retort control system, which adjusts overriding air pressure as needed to counter the detected expansion or contraction, thus resulting in a dynamic pressure profile ideally suited for that product.

The need for these dynamic pressure excursions during processing requires that retort pressure be controlled independently from temperature. This means that pure

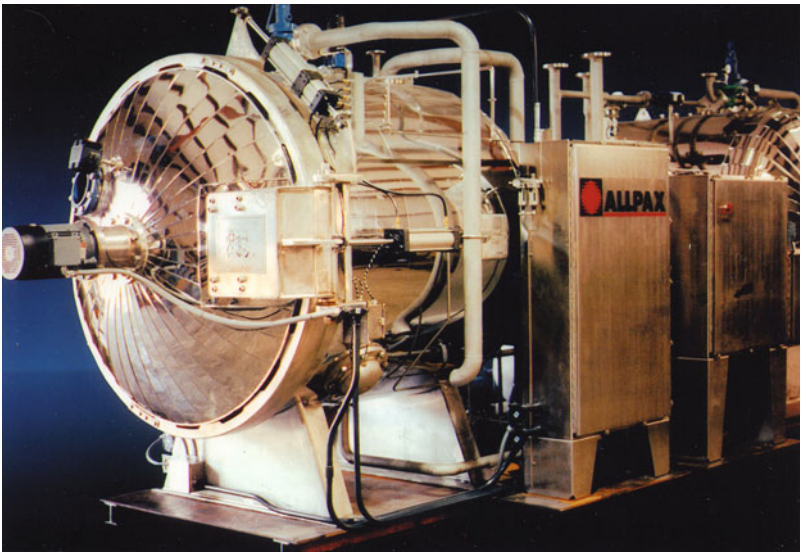

Fig. 11.8 Modern steam–air mixture retort with programmable pressure control (Courtesy of Allpax Products, Inc., Covington, LA)

saturated steam can no longer be used alone as the heating medium in the retort and that controllable overriding air pressure must be included during heating. However, the introduction of air into the retort during heating with steam poses the risk of insulating air pockets forming around packages, which could leave them under-processed. The desire to meet the processing needs of these flexible packaging systems has created a market for new retort designs and control systems that are capable of delivering these complex process conditions. Essentially, all designs accomplish the dynamic pressure profiles with overriding air pressure, but they eliminate the problem of insulating air pockets in different ways. Some retorts heat with steam–air mixtures that are kept well mixed with the use of strong fans within the retort (Fig. 11.8). Other retort designs feature water immersion, water spray, or water cascade as a means of contacting the packages with the heat exchange medium during processing. In addition to independent pressure control for these flexible packages, their lack of strength and rigidity also requires special racking designs and systems in the materials handling of these packages to safely support them within the retort (Fig. 11.9).

11.5 Market Implications

Prepared foods in microwavable retortable dinner trays and lunch bowls have been gaining in popularity because of their convenience, attractiveness, and quality relative to their traditional “canned” food counterparts in metal cans and

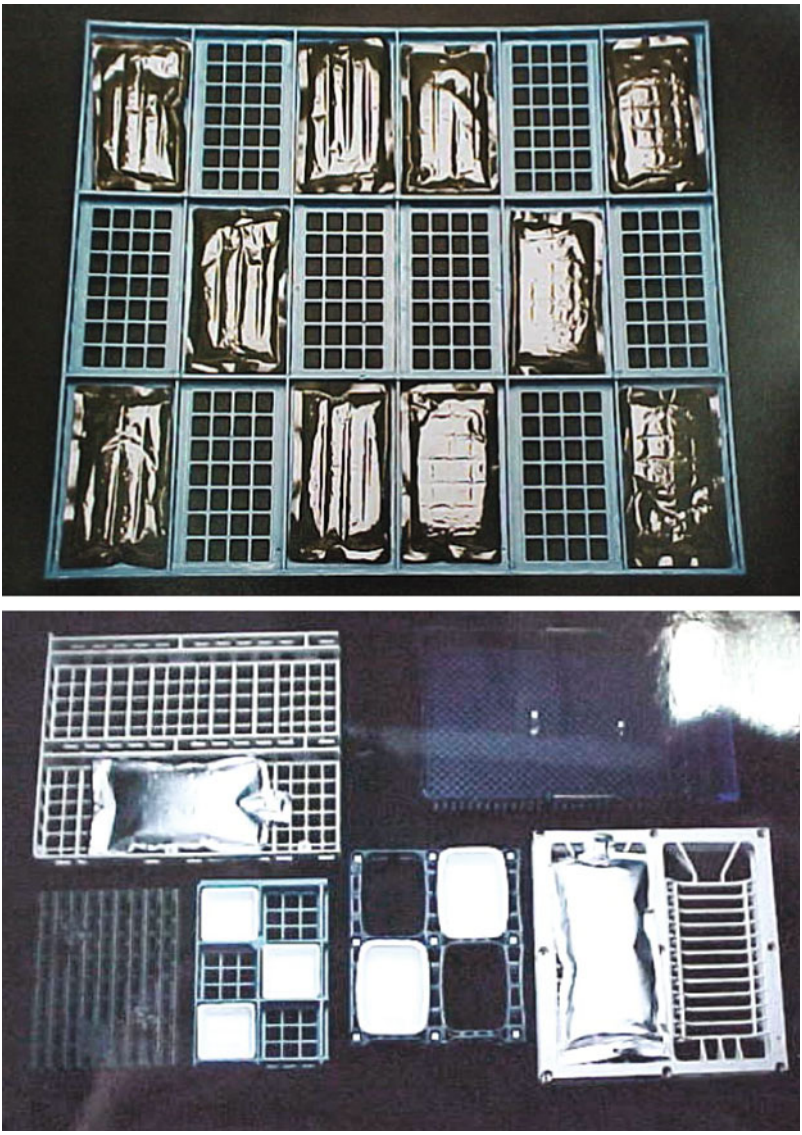

Fig. 11.9 Custom-designed racking systems for retortable flexible pouches (Courtesy of Allpax Products, Inc., Covington, LA)

glass jars. These novel packages were made possible by the development of food-grade polymer films with high oxygen-barrier properties capable of withstanding the high temperatures and pressures during the necessary heat sterilization process in pressurized retorts. The attractiveness of these packages and the fact that they are microwavable make them well suited for ready-to-eat dinner menu items. These packages have gained particular interest with those wishing to market

Fig. 11.10 Prototype of shelf-stable prepared meal ready-to-eat in retortable microwavable semi-rigid tray with transparent lid stock (Reproduced from Rich 2007 with permission)

shelf-stable prepared foods that can be featured as natural, organic, ethnic, vegetarian, or cultural such as "Ayurvedic." Ethnic food dishes typical of Latino, Mediterranean, Arabic, Indian, and Oriental cultures are becoming increasingly popular worldwide.

Research at the University of Florida has been underway to assist a small start-up company in developing a line of ethnic menu items in retortable semi-rigid trays (Rich 2007). The company has been operating restaurants featuring authentic cultural food dishes appropriate for strict vegetarian diets and the Ayurvedic life styles in India and Southeast Asia. It now wishes to distribute these menu items in retail markets as pre-packaged, shelf-stable, ready-to-eat meals so consumers can enjoy them conveniently in their homes (Fig. 11.10). This technology will enable manufacturers of shelf-stable food products to introduce into the marketplace a wider variety of fully-prepared ready-to-eat convenience food items.

References

Moody V (2003) Thermal inactivation kinetics of *Escherichia coli* and *Alicyclobacillus acidoterrestris* in orange juice. Dissertation, Agricultural and Biological Engineering Department, presented to Graduate School of University of Florida

Rich EC (2007) Heat penetration studies on shelf-stable ethnic foods in retortable trays. Project report toward Engineering degree, Agricultural and Biological Engineering Department, Institute of Food and Agricultural Sciences (IFAS), University of Florida

Rodriguez AC, Teixeira AA, Smerage GH, Busta FF (1988) Kinetic effects of lethal temperatures on population dynamics of bacterial spores. T ASAE 31(5):1594–1601, 1606

Swartzel KR (1984) A continuous flow procedure for reaction kinetic data generation. J food sci 49 (3):803–806

Welt BA, Teixeira AA, Balaban MO, Smerage GH (1997) Iterative method for kinetic parameter estimation from dynamic thermal treatments. J Food Sci 62(1):8–14

Chapter 12
Optimization of Food Thermal Processing: Sterilization Stage and Plant Production Scheduling

Ricardo Simpson and Alik Abakarov

12.1 Introduction

A large number of real-life, decision-making problems in food sciences and engineering can be formulated as a problem of optimization of various real-valued functions (objective functions) with real-valued or discrete decision variables with specific constraints, where the global optimum corresponds to the best solution of the initial problem. Depending on the features of the decision variables, optimization problems can be continuous, integer (discrete) or mixed; and depending on the features of the objective functions and constraints, they can be linear or nonlinear with many local solutions. Thus, each optimization problem can require any number of optimization techniques, which could guarantee finding an optimal solution.

Two optimization problems in thermal process calculation are considered in this chapter. First, there is the problem of thermal process calculations where process times at specified retort temperatures are calculated to achieve safe levels of microbial inactivation (lethality). Therefore, the accuracy of methods used for this purpose is important to food science and engineering professionals working

R. Simpson (✉)
Departamento de Ingeniería Química y Ambiental, Universidad Técnica Federico Santa María, P.O. Box 110-V, Valparaíso, Chile
and
Centro Regional de Estudios en Alimentos Saludables, Blanco 1623 Room 1402, Valparaíso, Chile
e-mail: ricardo.simpson@usm.cl

A. Abakarov
Departamento de Ingeniería Química y Ambiental, Universidad Técnica Federico Santa María, P.O. Box 110-V, Valparaíso, Chile
e-mail: alik.abakarov@usm.cl

J.M. Aguilera et al. (eds.), *Food Engineering Interfaces*, Food Engineering Series,
DOI 10.1007/978-1-4419-7475-4_12,

in the field (Holdsworth 1997). The second problem consists of determining an optimized scheduling at a food cannery using several autoclaves of different capacities to sterilize given amounts of different canned food products with specific quality requirements.

12.1.1 Thermal Process Calculation

Optimization of thermal sterilization is an optimal control problem, the solution to which requires searching for the best retort temperature as a function of process time. Banga et al. (1991) showed that the optimal control problem can be transformed into a nonlinear programming (NLP) problem, and in most cases the NLP problem becomes a multi-modal optimization problem with several types of constraints. These types of optimization problems make use of classical deterministic optimization methods within a local search domain, such as Hooke-Jeeves, Nelder-Mead, and Quasi-Newton methods (Himmelblau 1972), and are frequently limited in their effectiveness. To ensure a global solution to these problems, it would be more suitable to use global optimization methods. Considerable work has been reported in the literature showing that variable retort temperature (VRT) processing can be used to marginally improve the quality of canned food, and alternatively, to reduce the sterilization process time, in comparison to traditional constant retort temperature (CRT) processing (Banga et al. 1991; Banga and Alonso 2003; Teixeria et al. 1975; Almonacid-Merino et al. 1993; Simpson et al. 2008; Abakarov et al. 2009).

The usefulness and advantages of some global optimization algorithms based on the utilization of Gaussian probability distribution for VRT thermal processing optimization were presented by Banga and Casares (1987), Banga et al. (1991, 2003, 2005), Banga and Seider (1996), Simpson et al. (2008), and Abakarov et al. (2009).

Other global optimization algorithms, such as genetic algorithms (GA), were also successfully implemented for VRT thermal processing by Chen and Ramaswamy (2002). This chapter explains the implementation of a global stochastic method, an adaptive random search based on logistic curve utilization for finding the optimum VRT in thermal processing of conduction heated canned food. The specific objectives were the following:

- Explore the use of a cubic spline approximation for optimum dynamic temperature profiles to simplify the problem by reducing the number of variables (dimensional space of random search)
- Search for the optimum variable retort temperature profile to maximize retention of a specified quality factor (thiamine) within the constraint of assuring minimum required target lethality
- Search for the optimum variable retort temperature profile to minimize process time within the constraints of assuring both minimum required target lethality and quality retention

12.1.2 Optimal Scheduling for Food Canneries

In the majority of small- to medium-sized food canneries, retorting is carried out in a battery of retorts as a batch process (Norback and Rattunde 1991). In such canneries, the unloading and reloading operations for each retort are also labor-intensive. Therefore, a well-designed and -managed plant should be utilized to optimize the whole sterilization process. In other words, it is necessary to develop a suitable mathematical model for operation of the whole plant and to find the optimal values of the decision variables. The result of such a model involves the quantities of each product to be loaded into the autoclaves in each batch, and the optimal solution that gives optimum scheduling. One interesting and practical objective function is to find out the minimum plant operation time for specific amounts of different products (Simpson and Abakarov 2009).

In general, "scheduling" is understood as the process of managing given resources across a variety of possible tasks in order to optimize the objective function (criterion). Many scheduling models can be mathematically described by mixed-integer linear programming (MILP). Examples of sequential MILP short-term scheduling models can be found in Méndez and Cerda (2000, 2002), Harjunkoski and Grossmann (2002), and Castro and Grossmann (2006). The following researchers have presented sequence-based MILP models for multiproduct batch plants: Jung et al. (1994), Moon et al. (1996), Castro and Grossmann (2005), Floudas and Lin (2004), Gupta and Karimi (2003), Maravelias (2006), Mendez et al. (2001), (2006), Ha et al. (2006), and Liu and Karimi (2008). An interesting application of MILP planning for a petrochemical plant was described by Hui and Natori (1996). Erdirik-Dogan and Grossmann (2007) presented a multi-period mixed-integer linear programming model for the simultaneous planning and scheduling of a single-stage, multi-product, continuous plant with parallel units. In research by Doganis and Sarimveis (2007, 2009), the MILP model was developed to target optimal production scheduling for a single yogurt production line. This model took into account all standard constraints encountered in production scheduling (material balances, inventory limitations, machinery capacity, labor shifts, and manpower restrictions). Simpson and Abakarov (2009) proposed a particular MILP model for optimal scheduling of food canneries, addressing the problem of sterilizing given quantities of different canned food products within a minimum plant operation time, with specific quality requirements, in a set number of autoclaves of the same capacity. However, the model although relevant, cannot be implemented in most canning plants because the autoclaves are of different capacities.

In this chapter, a mathematical model for thermal process scheduling at food canneries with autoclaves of different capacities is described. The resulting model is based on mixed-integer linear programming and simultaneous sterilization. Since the initial version of the model developed here was non-linear due to its non-linear *(minimax)* objective function, the necessary modifications were made to transform it into a MILP model.

12.2 Methodology

12.2.1 Sterilization Stage Optimization

In this example, a cylindrical container with radius R and height $2L$ was used. The mathematical model describing heat conduction in this particular case is a mixed boundary problem (Teixeira et al. 1969), as follows:

$$\frac{\partial T}{\partial t} = \alpha\left(\frac{\partial^2 T}{\partial r^2} + \frac{1}{r}\frac{\partial T}{\partial r} + \frac{\partial^2 T}{\partial z^2}\right) \tag{12.1}$$

where T is temperature, t is time, r and z are radial and vertical locations within the container, and alpha (α) is thermal diffusivity of the product.

There were the following initial and boundary conditions (according to symmetry):

$$T(R, z, t) = T_{rt}(t)$$

$$T(r, L, t) = T_{rt}(t)$$

$$\frac{\partial T}{\partial r}(0, z, t) = 0$$

$$\frac{\partial T}{\partial z}(r, 0, t) = 0$$

$$T(r, z, 0) = T_{\text{in}}$$

where $T_{rt}(t)$, $t \in (0 : t_f)$ is retort temperature as a function of time, and T_{in} is initial temperature at $t = 0$.

The first objective was to find the retort function for Problem 1: $T_{rt}(t)$, $T_{\text{low}} \leq T_{rt}(t) \leq T_{\text{high}}$, where the final quality retention $\overline{C(t)}$ is maximized, while the final process lethality F_0^d is held to a specified minimum. A second objective was also to find the retort function for Problem 1: $T_{rt}(t)$, $T_{\text{low}} \leq T_{rt}(t) \leq T_{\text{high}}$, but where the final process time t_f is minimized subject to the same lethality requirement above, while the quality retention must not fall beneath some specified minimum.

The lethality constraint can be specified as follows:

1. $F_0(t_f) \geq F_0^d$, where F_0^d is the final required lethality, and is calculated as a function of time and temperature at the critical point (cold spot) according to the following equation:

$$F_0(t) = \int_0^t 10^{\frac{(T - T_{\text{ref}})}{z}} \mathrm{d}t \tag{12.2}$$

where T is temperature at the critical point or cold spot, normally at the geometric center of the container (in the case of conduction-heated canned foods).
Quality retention, on the other hand, is greatly affected by the non-uniform temperature distribution existing at any point in time from the heated boundary to the cool center cold spot, and must be integrated in space over the volume of the container, as well as over time. To accomplish this integration over both space and time, the following approach was used:

2. $\overline{C(t_f)} \geq C^d$, where C^d is the desired volume-average final quality retention value and calculated as follows:

$$\overline{C(t)} = C_0 \frac{2}{LR^2} \int_0^L \int_0^R \exp\left[-\frac{\ln 10}{D_{\text{ref}}} \int_0^t 10^{\frac{(T-T_{ref})}{z}} \right] \mathrm{d}r \, \mathrm{d}z \tag{12.3}$$

12.2.1.1 Penalty Functions

To handle constraints 1 and 2, the following penalty functions were used:

$$P_1 = \sum_{t=0}^{t_f} A \times \left({F_0}^d - F_0(t) + |{F_0}^d - F_0(t)| \right)$$

$$P_2 = \sum_{t=0}^{t_f} A \times \left(C^d - \overline{C(t)} + |C^d - \overline{C(t)}| \right)$$

where A is a sufficiently large number. Use of this kind of penalty function will lead very quickly to finding $X' \subseteq X$, where all given constraints are satisfied when the random search is implemented.

12.2.1.2 Process Optimization and Computer Simulation

In general, function $T_{rt}(t)$ over $t \in (0 : t_f)$ can be parameterized using N_p points; during each time interval $t'_k = (t_k, t_{k+1}), k \in 0 : (N_p - 1)$ the value of $T_{rt}(t'_k)$ remains constant (u_k) (Teixeria et al. 1975; Banga et al. 1991, 2003, 2005). However in this case, the use of cubic spline in approaching global optimization problems with random search techniques can produce superior results over discrete step-wise functions (Simpson et al. 2008), mainly because the cubic spline approximation allows reducing significantly the number of decision variables and therefore the random search.

Natural cubic splines are used for creating a smooth function that can fill in the gaps between data points in a step-wise discrete function to approximate a smooth trend. The philosophy in splining is to use low order polynomials to interpolate from grid point to grid point. This is ideally suited when one has control of the grid locations and the values of data being interpolated, as in the work presented here.

Therefore, approximation by the cubic spline was only utilized in this work to obtain optimal VRT profiles.

The following penalty function was used simultaneously with the cubic spline approximation in the search process in order to hold the autoclave temperature profile $T_{rt}(t)$ in the given range $\left[T_{\text{low}}, T_{\text{high}}\right]$:

$$P_3 = \sum_{t=0}^{t_f} A \times \left(|T_{\text{low}} - T_{rt}(t)| + |T_{\text{high}} - T_{rt}(t)| - (T_{\text{low}} - T_{rt}(t))\right)$$

where A is a sufficiently large number.

In general, the objective function used by the search procedure can be presented as:

$$\Phi(u_1, u_2, \ldots, u_{N_p-1}, t_f) = t_f + P_1 + P_2 + P_3, \quad t_f \in \left[t_{\text{left}}, t_{\text{right}}\right]$$

where $u_i,\ i \in 1 : (N_p - 1)$ are the control variables, and t_{left} and t_{right} could be obtained from the following expressions:

$$F_0^d = \int_0^{t_{\text{right}}} 10^{\frac{(T_{\text{low}} - T_{\text{ref}})}{z}} \mathrm{d}t \tag{12.4}$$

$$F_0^d = \int_0^{t_{\text{left}}} 10^{\frac{(T_{\text{high}} - T_{\text{ref}})}{z}} \mathrm{d}t \tag{12.5}$$

12.2.1.3 Adaptive Random Search Method

In this method, let $I_i \subset X$ be a perspective interval for variable $x_i,\ i \in 1 : n$, and let $2q$ be the width of each perspective interval. Let I be a Cartesian product of sets, $I_i,\ i \in 1 : n$, and for the random search, let I be a perspective sub-domain with center point $x_i^0,\ i \in 1 : n$.

The pedestal distribution is utilized in the adaptive random search as a probability distribution $P_s(x^{s-1})$. After each calculation of objective function the pedestal distribution of $x = \langle x_1, x_2, \ldots, x_n \rangle$ is modified so that the probability of finding the optimal value of the objective function is increased.

The example in Fig. 12.1 (a, b, c) shows a two-dimensional pedestal frequency distribution transformation during the whole random search process. Figure 12.1a shows the pedestal frequency distribution used for the first algorithms iteration. Because there is no information about the optimization problem being solved, any point of the domain X could be chosen with the same probability.

During the search process, the random search generates random vector values of $x^0,\ x^1,\ \ldots, x^s$, calculates objective function, accumulates information about the solved problem, and transforms the pedestal frequency distribution according to the computations done. Transformations consist of reducing the deviation of the pedestal

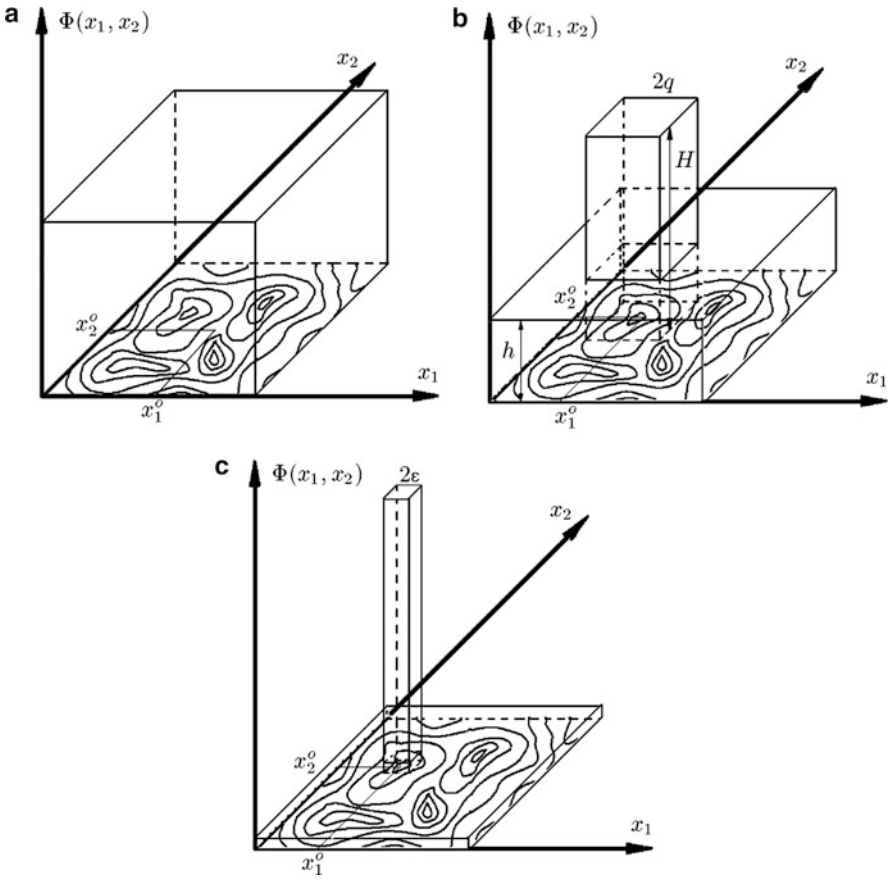

Fig. 12.1 Two-dimensional pedestal frequency distribution transformations occurring during the whole random search process

distribution (or perspective sub-domain $I \subseteq X$) around the mean (or center point, $x_i^0,\ i \in 1:n$), which is the current best solution: $x^0 \in X,\ f(x^0) < f(x^j),\ \forall j \in 1:s$. Figure 12.1b shows that the pedestal frequency distribution could be obtained in the middle of the search process, and now the points of domain X (in terms of probability density) can be divided into two non-overlapping subsets; h and H are the probability densities of the non-perspective and the perspective sub-domains, correspondingly. Figure 12.1c shows the pedestal frequency distribution for the final algorithm iteration, transformed into the $\delta - function,$ and it is assumed for any point x' of the final perspective domain I, the following condition holds: $|f[x\prime] - f([x^*])| \leq \varepsilon$.

The adaptive random method procedure could be described as follows:

1. Set the total number of random search iteration N_s; set the center point $x_i^0,\ i \in 1:n$ as the center point of initial perspective sub-domain I; and set iteration counter $s = 1$.

2. Generate a new vector $x^j \in X$ from the current pedestal probability distribution: $P_j(x^{j-1}, x^0)$
3. Compute the value of objective function $\Phi^j = \Phi(x^j)$, and by using the formula:

$$\Phi^j_{\min} = \min\left\{\Phi^j, \Phi^j_{\min}\right\}$$

Calculate a minimal value of objective function in step: j, $j \in 1 : N_s$.
4. If $\Phi^j_{\min} < \Phi^{j-1}_{\min}$, set the center point $x^0 = x^j$.
5. If $j < N_s$, then go to step 2.

To modify the pedestal probability distribution (step 2), the following formulas are used:

- Calculate the probability density h^j for step j, $j \in 1 : N_s$ as follows:

$$h^j = \frac{1 - p^j}{1 - v^j}$$

where v^j is volume of the perspective domain of random search, which is in step j ($v^0 = 1$), and p^j is the assumed in step j probability, where the optimal point belongs to the current perspective domain I.
- To calculate current volume v^j and assumed probability p^j, the basic random search method uses the following expressions:

$$q^0 = \frac{1}{2}$$

$$q^{j+1} = q^j (2\varepsilon)^{\frac{1}{N_s}}$$

$$v^j = \left(2q^j\right)^n, \tag{12.6}$$

where ε is given accuracy;

$$p^j = \begin{cases} \dfrac{s^j(p_{\min} - 1)}{s_{\min}} + 1, & \text{if } 0 \le v^j \le v_{\min,} \\ \dfrac{v^j(1 - p_{\min})}{1 - v_{\min}} + \dfrac{p_{\min} - v_{\min}}{1 - v_{\min}}, & \text{if } v_{\min} \le v^j \le 1 \end{cases}$$

where $p_{\min}$ and $q_{\min}(v_{\min} = (q_{\min})^n)$ are two heuristic parameters of adaptive random search, which allow tuning the algorithm to different types of problems as well as humans can.

In this chapter, a modification of the adaptive random search was used for thermal process calculation. The proposed modification utilizes the logistic curve as a law to reduce the q value during the whole search process, in other words, as a law to reduce the volume of perspective sub-domain I from $v^0 = 1$ to $v^{N_s} = (2\varepsilon)^n$.

The logistic equation was first published by Verhulst (1845) as a model of population growth. The continuous version of a logistic model is as follows:

$$\frac{\mathrm{d}x}{\mathrm{d}t} = \mu x(1 - x) \tag{12.7}$$

where μ is the Malthusian parameter (rate of maximum population growth). The solution of (12.7) could be written as:

$$x(t) = \frac{1}{1 + \alpha\, \mathrm{e}^{-\mu t}}, \tag{12.8}$$

where α and μ are the parameters of the logistic curve. The function of $x(t)$ is also called the sigmoid function (Krose 1993).

Figure 12.2 displays two curves; the interrupted curve (dashed line) shows a relationship between volume v^j and iteration number j in a basic version of the random search, and is obtained with (12.6); the solid curve is the possible logistic curve, utilized as the same relationship in the proposed modification and obtained in (12.8).

A wide set of experiments and practice implementations of the basic random search algorithm have been conducted, to show the effectiveness of the adaptive algorithm and to make recommendations for choosing heuristic parameter values (Abakarov and Sushkov 2002, 2005; Simpson et al. 2008). However, we propose the following:

- Reduce the local nature of the basic random search algorithm, because after 25% iterations, volume of the perspective sub-domain was reduced by more than 50%, which is not well-grounded in the case of multimodal optimization (Fig. 12.2).

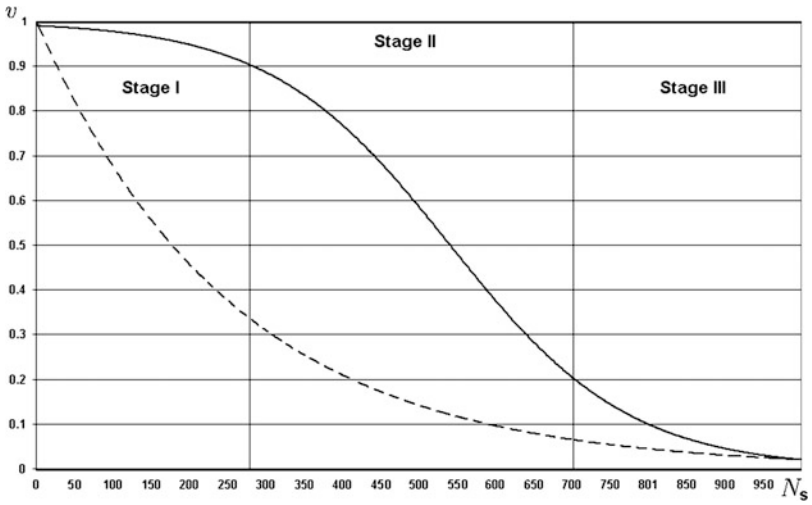

Fig. 12.2 Curves showing the relationship between volume $v^j$and iteration number j for the basic version of adaptive random search, obtained by (12.6), and for the modified version, (12.8)

- The nature of the logistic curve as a law of perspective sub-domain is reduced, as it is soundly related to behavior of the random search seemingly needed in general, namely, in the case of any a priori information about optimization problem, which is not available.

The whole random search process based on logistic curve utilization can be divided into three stages (Fig. 12.2) and interpreted as follows:

Stage I. There is no *apriori* information about the solved problem, so the slow reduction of volume of the perspective sub-domain is preferable at the beginning of the search process, which allows accumulating primary information about the location of the global solution inside domain X.

Stage II. Based on primary information accumulated in Stage I, we can assume the global solution belongs to the perspective sub-domain and accelerates the volume reduction process of the perspective sub-domain around its center point.

Stage III. To ensure the global solution is computed with accuracy ε, the process of reducing the volume of the perspective sub-domain should be slowed-down.

12.2.2 Canning Plant Scheduling

The simultaneous sterilization approach was developed especially for small canneries with few retorts, as they frequently process small batches of different products in various container sizes that require different process times and retort temperatures (Simpson 2005). The proposed approach takes advantage of the fact that, for any given product and container size, there exist many alternative combinations of retort temperatures (above the lethal range) and corresponding processing times that deliver necessary lethality (F_0value). In practice, the following two F_0 values are considered for each product sterilized: $F_0^{\min}$ and $F_0^{\max}$. These values are product-related, but in general the value $F_0^{\min}$ is chosen according to safety criterion and $F_0^{\max}$ according to quality criterion (resulting in a safe product with required quality). All combinations of retort temperature and processing time correspond to the same F_0 value and are called isolethal or equivalent lethality processes (Holdsworth and Simpson 2007). Figure 12.3 shows two equivalent lethality curves corresponding to the values $F_0^{\min}$ and $F_0^{\max}$. The region R' between the two curves contains all combinations of retort temperatures and processing times sufficient for sterilization of a selected product. We will call this region the "permissible region."

One important aspect of the simultaneous sterilization approach is that the difference in the absolute level of quality retention is relatively small over a practical range of isolethal process conditions. The relative insensitivity of quality over a range of different isolethal process conditions opens the door to maximizing output from a fixed number of retorts for different product and container sizes. The following procedure (I) can be utilized to obtain equivalent lethality processes (in permissible region) for a given product and its container size:

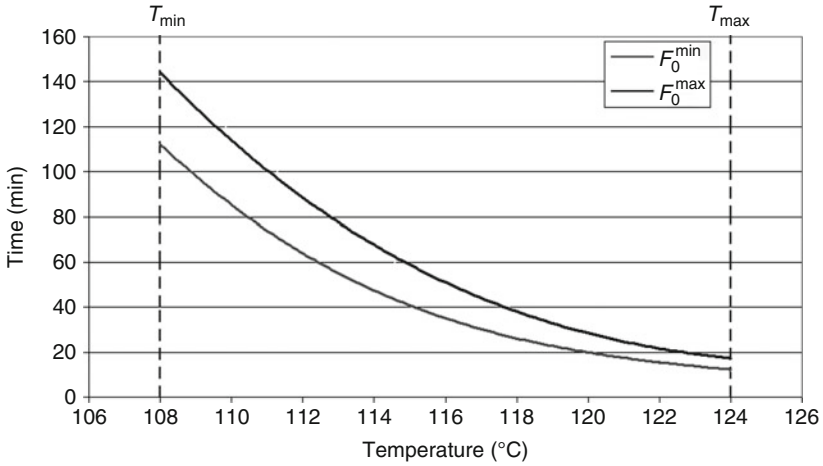

Fig. 12.3 Two equivalent lethality curves corresponding to values $F_0^{\min}$ and $F_0^{\max}$. The region R' between the curves contains all combinations of retort temperatures and processing times sufficient for sterilization of a selected product

Procedure (I):

1. For a given product and its can size, choose $F_0^{\min}$ and $F_0^{\max}$ values.
2. Choose an interval $[T_{\min}, T_{\max}]$, where $T_{\min}$ and $T_{\max}$ are the minimum and maximum retort temperatures, respectively.
3. Choose the discretization points $T_i,\ i \in 1:N$, in $[T_{\min}, T_{\max}]$.
4. For each discretization point, $T_i,\ i \in 1:N$, and lethality values, $F_0^{\min}$ and $F_0^{\max}$, obtain isolethal processes. (Heat penetration tests can be conducted on each product or computer simulations to establish processing times $t_i,\ i \in 1:N$, at retort temperatures $T_i,\ i \in 1:N$, to achieve the necessary target lethality values).
5. To obtain a set of two continuous curves per product, fit the discrete values $t_i,\ i \in 1:N$, using the cubic spline procedure. The region restricted by the two continuous curves, and by the left and right bounds of retort temperatures $T_{\min}$ and $T_{\max}$, is the permissible region for the given product (Fig. 12.3). Thus, the two strictly decreasing continuous functions, which are iso-lethality curves, are obtained for the product (Fig. 12.3) as follows:

$$m, M : [T_{\min}, T_{\max}] \rightarrow (0, +\infty)$$

where $m(T) \leq M(T)$ for each $T \in [T_{\min}, T_{\max}]$ and the minimum and maximum times needed to process the product at temperature T are denoted by $m(T)$ and $M(T)$, respectively.

Figure 12.4 shows the results of utilizing procedure (I) for three different products: A, B and C. (The permissible regions for each product, R_A, R_B and R_C, were obtained). The intersection R_{ABC} of the permissible regions R_A, R_B and R_C indicates processes that are sufficient for simultaneous sterilization of products A, B, and C.

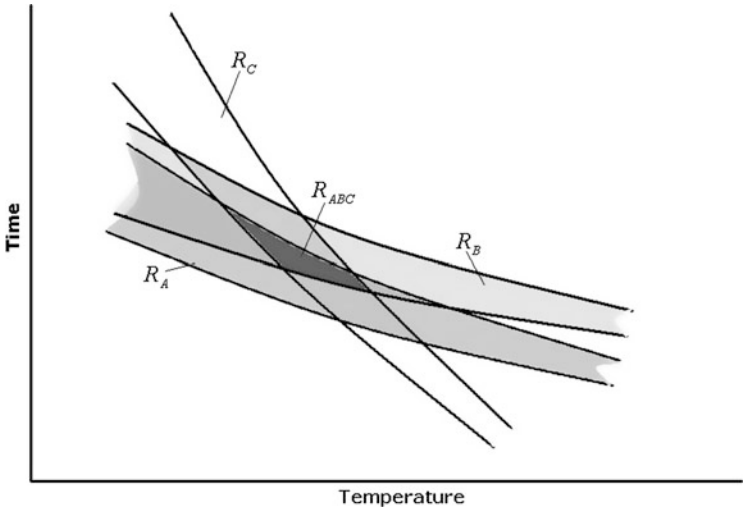

Fig. 12.4 The intersection R_{ABC} of the permissible regions R_A, R_B and R_C indicates processes that are sufficient for simultaneous sterilization of products A, B and C

Any simultaneous sterilization possibility can be presented as the following:

$$\langle v, t, T \rangle$$

where $v = (v_1, v_2, \ldots, v_n)$ is a simultaneous sterilization vector, $v_k \in \{0, 1\}$, $k \in 1 : n$, and

$$v_k = \begin{cases} 1, & \textit{if product k can be sterilized} \\ 0, & \textit{otherwise} \end{cases}$$

and t, T are the necessary time and retort temperature, respectively, used to process a subset of products determined by vector v.

It can be assumed the simultaneous sterilization vector v^1 is dominated by the other simultaneous sterilization vector v^2 if the following two conditions hold:

$$\forall j \in 1 : n\big(v^1[j] = 1 \;\Rightarrow\; v^2[j] = 1\big)$$

$$t^1 \leqslant t^2$$

where t^1 and t^2 are the times necessary to process the subsets of the products determined by the vectors v^1 and v^2, respectively.

This fact can be denoted as $v^1 > v^2$. Obviously, only non-dominated vectors should be used in the sterilization process; otherwise, a sterilization vector exists that could be replaced by another vector, which would mean it is possible to sterilize at least the same subset of products in reduced process time.

12.2.2.1 Problem Definition

The optimization problem in this research consists of finding a given quantity of each product, $a_j, j \in 1:n$, a subset of simultaneous sterilization vectors, $V^{\text{opt}} \subseteq V_A$, and its assignment among a given number of autoclaves of different capacities, c_k, $k \in 1:s$, such that each product is sterilized completely within the minimum plant operation time.

To solve the optimization problem in the present research, the following data was generated:

- Number of sterilization products: n
- Quantity for each product: $a_j,\ j \in 1:n$
- Number of sterilization vectors: m
- Set of non-dominated sterilization vectors: $V_A = \{v^i\},\ v_j^i \in \{0,1\},\ i \in 1:m,\ j \in 1:n$
- Set of sterilization times: $T_A = \{t_i\},\ i \in 1:m$
- Number of autoclaves: s
- Capacity of autoclave: $c_k, k \in 1:s$

12.2.2.2 Mathematical Model Description

Two types of decision variables were used in the mathematical model:

- Integer decision variables:

$$u_i^k = \begin{cases} 1, & \textit{if vector } v^i \in V \textit{ is used for sterilization process in the autoclaves}, \\ 0, & \textit{otherwise} \end{cases}$$

- Continuous decision variables: $x_{ij}^k,\ i \in 1:m,\ j \in 1:n,\ k \in 1:s$, corresponding to the quantity of product P_j loaded into autoclave k utilizing sterilization vector i

The objective function to minimize plant operation time can be written as follows:

$$\max_k \left\{ \sum_{i=1}^{m} u_i^k t_i \right\} \rightarrow \min_u \tag{12.9}$$

where the goal is to minimize the maximum time $\left(\max_k \left\{ \sum_{i=1}^{m} u_i^k t_i \right\} \right)$ spent by one of the autoclaves $k$in processing its part of the product and thus minimizing plant operation time.

Given all products must be completely sterilized, the following constraints should be considered:

$$\sum_{k=1}^{s}\sum_{i=1}^{m} x_{ij}^{k} = a_j, \quad \forall j \in 1:n \tag{12.10}$$

For all chosen simultaneous sterilization vectors v^i, $i \in 1:M$, and all given autoclave capacities, c_k, $k \in 1:s$, the amount of product in each batch loaded into autoclave k should be less than its capacity c_k. These constraints can be written as:

$$\sum_{j=1}^{N} x_{ij}^{k} \le u_i^k c_k, \quad \forall i \in 1:m,\ \forall k \in 1:s \tag{12.11}$$

Since the above mathematical model is non-linear, due to its non-linear (minimax) objective function, the following modifications were made in order to transform it into an equivalent MILP model. The objective function (2) was replaced by the following objective function:

$$MinMax \rightarrow \min$$

where $MinMax \in (0, +\infty)$, and the following constraints for each of the given autoclaves $k \in 1:s$, were added to constraints in (12.10) and (12.11):

$$\sum_{i=1}^{m} u_i^k t_i \le MinMax, \quad k \in 1:s$$

Thus, the minimization of plant operation time by MILP can be written in terms of an objective function:

$$MinMax \rightarrow \min$$

subject to:

$$\sum_{i=1}^{m} u_i^k t_i \le MinMax, \quad k \in 1:s$$

$$\sum_{k=1}^{s}\sum_{i=1}^{m} x_{ij}^{k} = a_j, \quad \forall j \in 1:n$$

$$\sum_{j=1}^{N} x_{ij}^{k} \le u_i^k c_k, \quad \forall i \in 1:m,\ \forall k \in 1:s$$

The obtained MILP model is the preferred choice over the model with a non-linear objective function, for two reasons. First, there are algorithms, which guarantee finding a global solution to the linear programming problems (Taha 2006). Second, efficient computer tools have been developed based on such algorithms (Robert Fourer, "Software Survey: Linear Programming" 2009).

12.3 Results and Discussion

12.3.1 Thermal Process Calculation

The following data in Table 12.1 was used in the optimization of the thermal processing of canned foods.

12.3.1.1 Maximizing Quality Retention Problem

The next numerical experiment consists of searching for the optimum variable retort temperature profile, to maximize retention of a specified quality factor (thiamine) within the constraint of assuring minimum required target lethality and by variable retort temperature profile utilization, within the upper and lower limits of retort temperature in the range of this study (110–140°C). In this example, a final target lethality of $F_0^d = 8$ min was chosen (typical for many canned foods).

The results obtained from a basic random search algorithm, and its modification, are shown in Fig. 12.5 (Simpson et al. 2008) and Fig. 12.6, respectively. Utilizing the proposed modification, the optimal solution computed before was improved in terms of process time (89 against 91 min) and number of objective function computations (600 against 1,000 calculations). The final lethality F_0 was equal to 8.001.

12.3.1.2 Minimization Process Time Problem

This numerical experiment deals with searching for the optimum variable retort temperature profile to minimize process time within the constraints of assuring both minimum required target lethality and quality retention. In this case, the search routine was restricted in two ways, first to satisfy the lethality constraint of $F_0^d = 8\text{min}$, as before, and second, that the quality constraint thiamine retention could not fall below 50% ($\overline{C(t)} > 0.5$).

Table 12.1 Parameters utilized in thermal process simulation study (From García et al. 2005)

Can radius *(m)*	0.04375
Can height *(m)*	0.1160
Thermal diffusivity α (m^2s^{-1})	1.5443×10^{-7}
T_0 (°C)	71.11
Microorganism	*Bacillus stearothermophilus*
$z_{M,\text{ ref}}$ (°C)	10
$T_{M,\text{ ref}}$ (°C)	121.11
Nutrient	*Thiamine*
$z_{N,\text{ ref}}$ (°C)	25.56
$D_{\text{ref}}\,(s)$	10716.0
$T_{N,\text{ ref}}$ (°C)	121.11

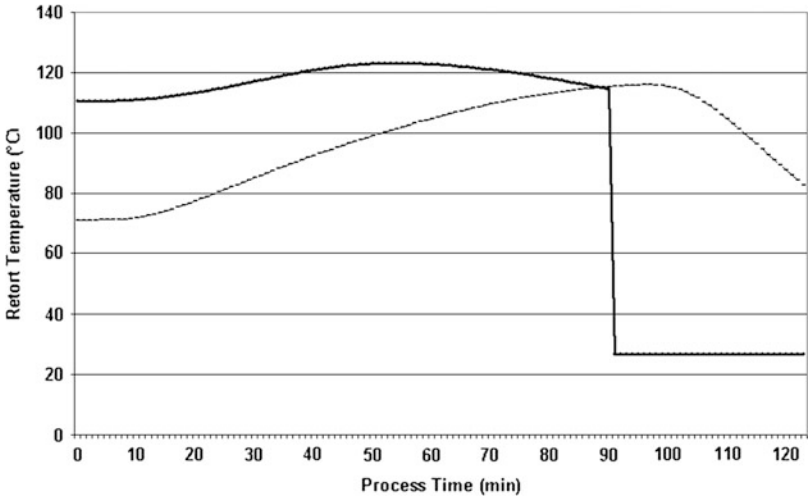

Fig. 12.5 Optimum VRT profile for maximum thiamine retention (55%) from a basic random search algorithm using cubic spline approximation and 1,000 iterations

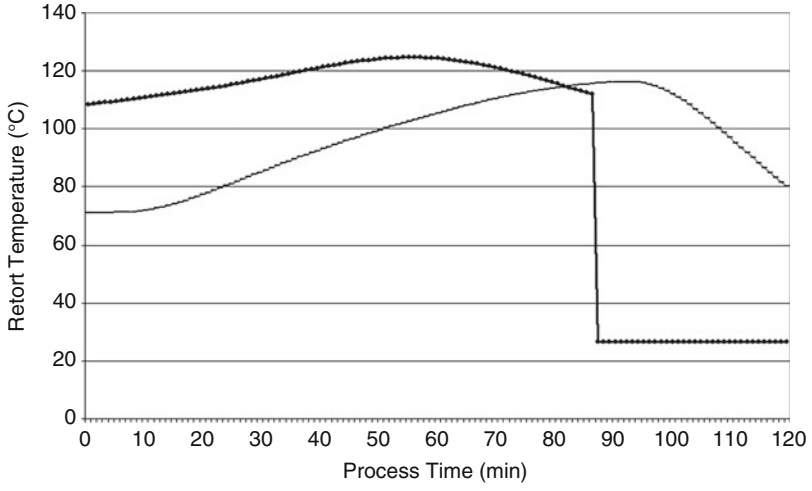

Fig. 12.6 Optimum VRT profile for maximum thiamine retention (55%) from a modified random search algorithm using cubic spline approximation and 600 iterations

The results obtained from a basic random search algorithm, and its modification, are shown in Fig. 12.7 (Simpson et al. 2008) and Fig. 12.8, respectively. Utilizing the proposed modification, the optimal solution computed before was improved in terms of Process Time (67 against 68 min.) and the number of objective function computations (600 against 1,000 calculations). The final thiamine retention $\overline{C(t_f)}$ was equal to 0.503 (50%).

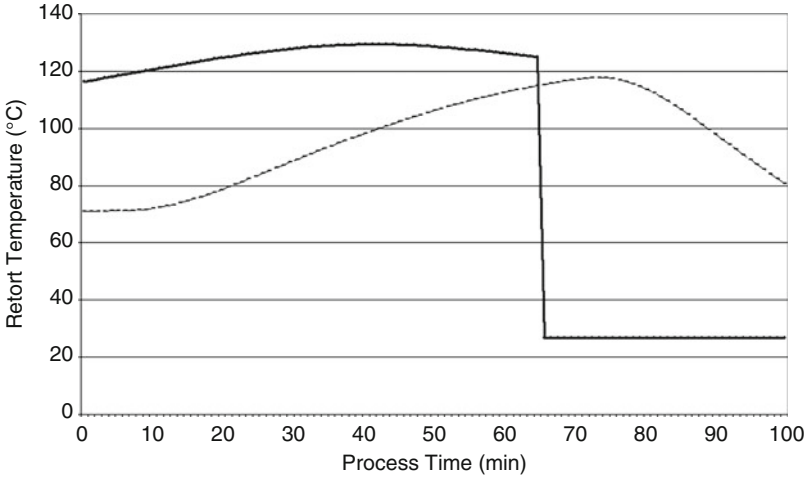

Fig. 12.7 Optimum VRT profile for minimum thiamine retention (50%) from a basic random search algorithm using cubic spline approximation and 1,000 iterations

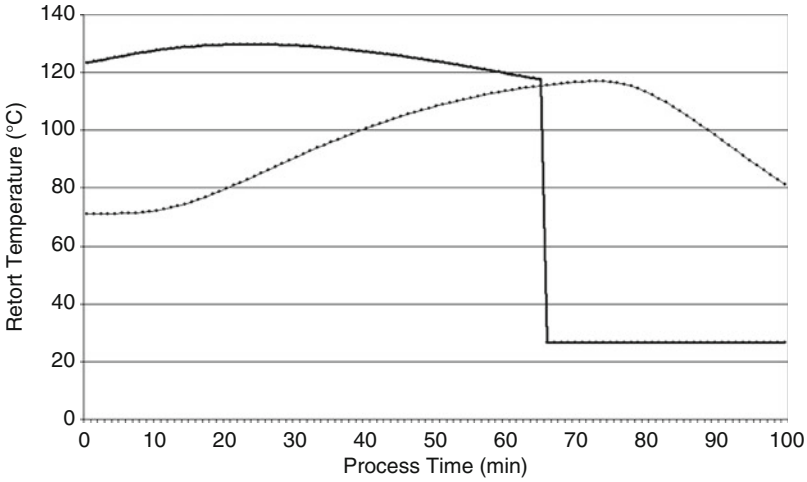

Fig. 12.8 Optimum VRT profile for minimum thiamine retention (50%) from a basic random search algorithm using cubic spline approximation and 600 iterations

12.3.1.3 Canning Plant Optimization

To demonstrate the ability of the proposed approach, several plant production problems were solved. These problems differed according to the capacities of the autoclaves used in the plant. As shown in Table 12.2, 16 combinations of products and can sizes were selected for this study.

A computer program developed by the authors was used to generate a set V'_A of 79 non-dominated simultaneous sterilization vectors and a set of times, T'_A, for temperatures ranging from $T_{\min} = 110°C$ to $T_{\max} = 124°C$. Values 0.1 and 0.5 were used as precision parameters of procedure (II) Δ_t and Δ_T, respectively.

Table 12.3 shows all simultaneous sterilization vectors computed at temperature 112°C utilizing procedure (II). The following common data was used for problems 1–4:

- Number of combinations of products and can sizes: 16
- Quantity for each product: see Table 12.4
- Number of sterilization vectors: 79
- Set of non-dominated sterilization vectors: V'_A
- Set of sterilization time: T'_A

Table 12.2 Combinations of products and can sizes used in this study

	Can size				
Product	211 × 400	300 × 407	307 × 409	307 × 113	401 × 411
	Number of combinations[a]				
Asparagus	1	2	3	4	5
Corn	6	7	8		9
Green beans	10	11	12		13
Peas	14		15		16

[a]Number of product and can size combinations

Table 12.3 Sterilization vectors computed at temperature 112°C

Vector	Products																Time (min)
	1[a]	2	3	4	5	6	7	8	9	10	11	12	13	14	15	16	
1	0	0	1	0	0	0	0	0	0	1	0	0	0	0	0	0	60.06
2	0	0	0	0	1	0	0	0	0	0	0	0	1	0	0	0	97.05
3	0	0	0	0	0	0	0	0	0	0	1	0	1	0	0	0	104.84
4	0	0	1	0	0	1	0	0	0	1	0	0	0	0	1	0	61.99
5	0	0	1	0	0	1	0	1	0	1	0	0	0	0	1	0	62.14
6	1	0	1	0	0	1	0	1	0	1	0	0	0	0	1	0	63.35
7	1	0	1	1	0	1	0	1	0	1	0	0	0	0	1	0	63.54
8	1	0	1	1	0	1	0	1	0	1	0	0	0	1	1	0	65.06
9	1	0	1	1	0	1	0	1	0	1	0	1	0	1	1	0	67.23
10	1	1	1	1	0	1	0	1	0	1	0	1	0	1	1	0	70.81
11	0	1	0	0	1	0	1	0	1	0	0	0	0	0	0	1	86.07
12	0	1	0	0	0	0	1	0	1	0	0	1	0	1	0	1	79.78
13	1	1	1	1	0	1	0	1	0	1	0	1	0	1	1	1	71.25
14	1	1	1	1	0	1	0	1	1	1	0	1	0	1	1	1	73.25

[a]Row refers to the 16 product/can size combinations used in study

Table 12.4 Quantities for the 16 product/can size combinations

	Combinations of products and can sizes															
	1	*2*	*3*	*4*	*5*	*6*	*7*	*8*	*9*	*10*	*11*	*12*	*13*	*14*	*15*	*16*
Quantity[a] (volume in thousands of liters)	7	13	4	16	6	17	18	5	8	11	2	14	10	12	19	9

[a]Product quantities were generated randomly in accordance with uniform probability distribution from interval $[1,\ 20]$

Specific data for Problem 1:
Number of autoclaves: 1
Capacity of autoclave $c_1 = 20,000\,\text{L}$
(Results for Problem 1 are presented in Table 12.5).
Specific data for Problem 2:
Number of autoclaves: 2
Capacity of autoclave $c_1 = 20,000\,\text{L}$
Capacity of autoclave $c_2 = 15,000\,\text{L}$
(Results for Problem 2 are presented in Table 12.6).
Specific data for Problem 3:
Number of autoclaves: 2
Capacity of autoclave $c_1 = 20,000\,\text{L}$
Capacity of autoclave $c_2 = 10,000\,\text{L}$
(Results for Problem 3 are presented in Table 12.7).
Specific data for Problem 4:
Number of autoclaves: 3
Capacity of autoclave $c_1 = 20,000\,\text{L}$
Capacity of autoclave $c_2 = 15,000\,\text{L}$
Capacity of autoclave $c_3 = 10,000\,\text{L}$
(Results for Problem 4 are presented in Table 12.8).

The MILP model proposed in this research always gave plant operation times lower than or equal to those of the non-simultaneous sterilization operation, but the difference between the schedules depended on given data, including the

Table 12.5 Results obtained for Problem 1

Optimal plant operation time
Non-simultaneous sterilization case: 332.5 min
Simultaneous sterilization case: 251.42 min
Optimal solution: simultaneous sterilization case

Autoclave $c_1 = 20000$L	Simultaneous sterilization vectors utilized $v^{29}, v^{44}, v^{50}, v^{51}, v^{54}, v^{55}, v^{59}, v^{68}, v^{70}, v^{78}$

Number of vector	Quantities for each can size and product combination loaded into autoclave (volume in thousands of liters)																Time (min)
	1[a]	2	3	4	5	6	7	8	9	10	11	12	13	14	15	16	
v^{29}	0	0	0	0	0	0	0	0	0	0	2	0	10	0	0	0	69.18
v^{44}	0	0	4	0	0	0	0	5	0	11	0	0	0	0	0	0	18.13
v^{50}	0	1	0	0	0	0	0	0	0	0	0	10	0	0	0	9	23.76
v^{51}	0	0	0	0	0	0	0	0	0	0	0	4	0	12	0	0	20.14
v^{54}	7	0	0	13	0	0	0	0	0	0	0	0	0	0	0	0	16.44
v^{55}	0	12	0	0	0	0	0	0	8	0	0	0	0	0	0	0	21.63
v^{59}	0	0	0	3	0	17	0	0	0	0	0	0	0	0	0	0	16.14
v^{68}	0	0	0	0	6	0	0	0	0	0	0	0	0	0	0	0	30.0
v^{70}	0	0	0	0	0	0	18	0	0	0	0	0	0	0	0	0	22.0
v^{78}	0	0	0	0	0	0	0	0	0	0	0	0	0	0	19	0	14.0

[a]Row refers to the 16 product/can size combinations used in study

Table 12.6 Results obtained for Problem 2

Optimal plant operation time
Non-simultaneous sterilization case: 166.5 min
Simultaneous sterilization case: 129.83 min
Optimal solution: simultaneous sterilization case

Autoclave	Simultaneous sterilization vectors utilized
$c_1 = 20000$L	$v^{56}, v^{58}, v^{59}, v^{61}, v^{68}, v^{69}, v^{70}$
$c_2 = 15000$L	$v^{29}, v^{55}, v^{62}, v^{75}$

Number of vector	Quantities for each can size and product combination loaded into autoclave (volume in thousands of liters)																Time (min)
	1[a]	2	3	4	5	6	7	8	9	10	11	12	13	14	15	16	
v^{29}	0	0	0	0	0	0	0	0	0	0	2	0	10	0	0	0	69.18
v^{55}	0	7	0	0	0	0	0	0	8	0	0	0	0	0	0	0	21.63
v^{56}	0	0	4	0	0	0	0	0	0	11	0	0	0	0	0	0	13.62
v^{58}	7	0	0	1	0	0	0	0	0	0	0	0	0	12	0	0	17.14
v^{59}	0	0	0	15	0	0	0	0	0	0	0	0	0	0	5	0	16.14
v^{61}	0	0	0	0	0	1	0	5	0	0	0	0	0	0	14	0	15.6
v^{62}	0	6	0	0	0	0	0	0	0	0	0	0	0	0	0	9	21.02
v^{68}	0	0	0	0	6	0	0	0	0	0	0	0	0	0	0	0	30.0
v^{69}	0	0	0	0	0	16	0	0	0	0	0	0	0	0	0	0	15.0
v^{70}	0	0	0	0	0	0	18	0	0	0	0	0	0	0	0	0	22.0
v^{75}	0	0	0	0	0	0	0	0	0	0	0	14	0	0	0	0	18.0

[a]Row refers to the 16 product/can size combinations used in study

Table 12.7 Results obtained for Problem 3

Optimal plant operation time
Non-simultaneous sterilization case: 166.5 min
Simultaneous sterilization case: 138.13 min
Optimal solution: simultaneous sterilization case

Autoclave	Simultaneous sterilization vectors utilized
$c_1 = 20000$L	$v^{55}, v^{56}, v^{58}, v^{59}, v^{61}, v^{70}, v^{75}, v^{78}$
$c_2 = 10000$L	$v^{62}, v^{68}, v^{74}, v^{76}$

Number of vector	Quantities for each can size and product combination loaded into autoclave (volume in thousands of liters)																Time (min)
	1[a]	2	3	4	5	6	7	8	9	10	11	12	13	14	15	16	
v^{55}	0	12	0	0	0	0	0	0	8	0	0	0	0	0	0	0	21.63
v^{56}	0	0	4	0	0	0	0	0	0	11	0	0	0	0	0	0	13.62
v^{58}	7	0	0	0	0	0	0	0	0	0	0	0	0	12	0	0	17.14
v^{59}	0	0	0	16	0	2	0	0	0	0	0	0	0	0	0	0	16.14
v^{61}	0	0	0	0	0	15	0	5	0	0	0	0	0	0	0	0	15.6
v^{62}	0	1	0	0	0	0	0	0	0	0	0	0	0	0	0	9	21.02
v^{68}	0	0	0	0	6	0	0	0	0	0	0	0	0	0	0	0	30.0
v^{70}	0	0	0	0	0	0	18	0	0	0	0	0	0	0	0	0	22.0
v^{74}	0	0	0	0	0	0	0	0	0	0	2	0	0	0	0	0	48.0
v^{75}	0	0	0	0	0	0	0	0	0	0	0	14	0	0	0	0	18.0
v^{76}	0	0	0	0	0	0	0	0	0	0	0	0	10	0	0	0	39.0
v^{78}	0	0	0	0	0	0	0	0	0	0	0	0	0	0	19	0	14.0

[a]Row refers to the 16 product/can size combinations used in study

Table 12.8 Results obtained for Problem 4

Optimal plant operation time
Non-simultaneous sterilization case: 111.0 min
Simultaneous sterilization case: 92.87 min
Optimal solution: simultaneous sterilization case

Autoclave	Simultaneous sterilization vectors
$c_1 = 20000$L	$v^{54}, v^{55}, v^{58}, v^{61}, v^{70}$
$c_2 = 15000$L	v^{29}, v^{51}
$c_3 = 10000$L	$v^{56}, v^{57}, v^{62}, v^{68}, v^{78}$

Number of vector	Quantities for each can size and product combination loaded into autoclave (volume in thousands of liters)																Time (min)
	1[a]	2	3	4	5	6	7	8	9	10	11	12	13	14	15	16	
v^{29}	0	0	0	0	0	0	0	0	0	0	2	0	10	0	0	0	69.18
v^{51}	0	0	0	0	0	0	0	0	0	0	0	14	0	1	0	0	20.14
v^{54}	7	0	0	7	0	6	0	0	0	0	0	0	0	0	0	0	16.44
v^{55}	0	12	0	0	0	0	0	0	8	0	0	0	0	0	0	0	21.63
v^{56}	0	0	4	0	0	0	0	0	0	6	0	0	0	0	0	0	13.62
v^{57}	0	0	0	0	0	0	0	5	0	5	0	0	0	0	0	0	14.23
v^{58}	0	0	0	9	0	0	0	0	0	0	0	0	0	11	0	0	17.14
v^{61}	0	0	0	0	0	11	0	0	0	0	0	0	0	0	9	0	15.6
v^{62}	0	1	0	0	0	0	0	0	0	0	0	0	0	0	0	9	21.02
v^{68}	0	0	0	0	6	0	0	0	0	0	0	0	0	0	0	0	30.0
v^{70}	0	0	0	0	0	0	18	0	0	0	0	0	0	0	0	0	22.0
v^{78}	0	0	0	0	0	0	0	0	0	0	0	0	0	0	10	0	14.0

[a]Row refers to the 16 product/can size combinations used in the study

simultaneous sterilization vectors, quantity of products considered, and capacity of autoclaves. According to the test problems (1–4), reduction in plant operation time between simultaneous and non-simultaneous operations was in the range 20–25%. In addition, this reduction was linked to the number of autoclaves; a larger number resulted in less reduction in plant operation time.

All numerical results for problems 1–4 were obtained with online mixed-integer linear programming solvers of COIN-OR (Computational Infrastructure for Operations Research, http://www.coin-or.org) using AMPL (a modeling language for mathematical programming, http://www.ampl.com) input.

12.4 Conclusions

Two optimization problems in thermal process calculation were solved in this chapter. The results drawn from this work are as follows:

1. Global optimization using random search techniques can be used effectively to search for optimum variable retort temperature processes that will either:
   - Maximize quality retention subject to achieving minimum target lethality, or
   - Minimize process time to reach target lethality subject to holding quality retention to a specified minimum.

2. Use of cubic spline in approaching global optimization problems via random search techniques can produce superior results over discrete step-wise functions in cases where optimal VRT profiles are expected to be a smooth curve; so in other words the optimal VRT profile can be better approximated by implementation of cubic spline as opposed to increasing the number of discretization points in the domain $[t_0, t_f]$.

Also, this research proposed a mathematical model for optimized scheduling at food canning plants where autoclaves of different capacities are used to sterilize given amounts of various canned food products with specific quality requirements. This approach is of special relevance to small- and medium-sized canneries, which normally work with many products at the same time. Depending on the situation, the proposed methodology for developing the MILP model may be used to address other types of optimization problems arising in food processing plants.

Acknowledgements The authors Ricardo Simpson and Alik Abakarov are grateful for the financial support provided by CONICYT through the FONDECYT project number 1090628.

References

Abakarov A, Sushkov Yu (2002) The statistical research of random search. Mathematical models. Theory and application. Saint-Petersburg State University, Saint-Petersburg, pp 70–101

Abakarov A, Sushkov Y (2005) The algorithm of adaptive random search for discrete-continuous optimization. In: Proceedings of the 5th Saint Petersburg Workshop on Simulation, St. Petersburg State University, St. Petersburg, June 26–July 2, 2005, pp 11–17

Abakarov A, Sushkov Yu, Almonacid S, Simpson R (2009) Thermal processing optimization through a modified adaptive random search. J Food Eng

Almonacid-Merino SF, Simpson R, Torres JA (1993) Time variable retort temperature profiles for cylindrical cans: batch process time, energy consumption, and quality retention model. J Food Process Eng 16(4):171–187

Banga JR, Casares JJ (1987) ICRS: application to a wastewater treatment plant model. In: The Institution of Chemical Engineers (ed) Process optimisation (IChemE Symposium Series No. 100). Pergamon, Oxford, pp 183–192

Banga JR, Seider WD (1996) Global optimization of chemical processes using stochastic algorithms. In: Floudas CA, Pardalos PM (eds) State of the art in global optimization: computational methods and applications. Kluwer, Dordrecht, The Netherlands, pp 563–583

Banga JR, Perez-Martin RI, Gallardo JM, Casares JJ (1991) Optimization of thermal processing of conduction-heated canned foods: study of several objective functions. J Food Eng 14:25–51

Banga JR, Balsa-Canto E, Moles CG, Alonso AA (2003) Improving food processing using modern optimization methods. Trends Food Sci Technol 14(4):131–144

Banga JR, Balsa-Canto E, Moles CG, Alonso AA (2005) Dynamic optimization of bioprocesses: efficient and robust numerical strategies. J Biotechnol 117(4):407–419

Castro PM, Grossmann IE (2005) New continuous-time MILP model for the short-term scheduling of multi-stage batch plants. Ind Eng Chem Res 44(24):9175–9190

Castro PM, Grossmann IE (2006) An efficient MILP model for the short-term scheduling of single stage batch plants. Comput Chem Eng 30:1003–1018

Chen CR, Ramaswamy HS (2002) Modeling and optimization of variable retort temperature (VRT) thermal processing using coupled neural networks and genetic algorithms. J Food Eng 53(3):209–220

Doganis P, Sarimveis H (2007) Optimal scheduling in a yogurt production line based on mixed integer linear programming. J Food Eng 80:445–453

Doganis P, Sarimveis H (2009) Mixed integer linear programming scheduling in the food industry. In: Ferruh E (ed) Optimization in food engineering. CRC Press, Boca Raton, FL, p 800

Erdirik-Dogan M, Grossmann I (2007) Simultaneous planning and scheduling of single-stage multi-product continuous plants with parallel lines. Comput Chem Eng 32(11):2626–2642

Floudas CA, Lin X (2004) Continuous-time versus discrete-time approaches for scheduling of chemical processes: a review. Comput Chem Eng 28(11):2109–2129

Fourer R (2009) Software Survey: Linear Programming. OR/MS Today 36(3):46–55

García MSG, Balsa-Canto E, Alonso AA, Banga JR (2005) Computing optimal operating policies for the food industry. J Food Eng 74(1):13–23

Gupta S, Karimi IA (2003) Animproved MILP formulation for scheduling multi-product, multi-stage batch plants. Ind Eng Chem Res 42(11):2365–2380

Ha JH, Chang HK, Lee ES, Lee IB, Lee BS, Yi G (2006) Inter-stage storage tank operation strategies in the production scheduling of multi-product batch processes. Comput Chem Eng 24:1633–1640

Harjunkoski I, Grossmann IE (2002) Decomposition techniques for multistage scheduling problems using mixed-integer and constraint programming methods. Comput Chem Eng 26:1533

Himmelblau DM (1972) Applied nonlinear programming. McGraw-Hill, New York

Holdsworth SD (1997) Thermal processing of packaged foods. Blackie Academic & Professional, London

Holdsworth SD, Simpson R (2007) Thermal processing of packaged foods, 2nd edn. Springer, New York, p 412

Hui C-W, Natori Y (1996) An industrial application using mixed-integer programming technique: a multi-period utility system model. Comput Chem Eng S20:S1577–S1582

Jung JH, Lee HK, Lee IB (1994) Completion times and optimal scheduling for serial multi-product processes with transfer and set-up times in zero-wait policy. Comput Chem Eng 18:537–544

Krose Ben JA (1993) Fundamentals. In: Patrick van der Smagt (ed). An introduction to networks neural, 5th edn. The University of Amsterdam, Amsterdam, The Netherlands

Liu Y, Karimi I (2008) Scheduling multistage batch plants with parallel units and no interstage storage. Comput Chem Eng 32:671–693

Maravelias CT (2006) A decomposition framework for the scheduling of single- and multi-stage processes. Comput Chem Eng 30:407–420

Méndez C, Cerda J (2000) Optimal scheduling of a resource-constrained multiproduct batch plant supplying intermediates to nearby end-product facilities. Comput Chem Eng 24:369

Méndez C, Cerda J (2002) An efficient MILP continuous-time formulation for short-term scheduling of multiproduct continuous facilities. Comput Chem Eng 26:687

Mendez CA, Henning GP, Cerda J (2001) An MILP continuous time approach to short-term scheduling of resource-constrained multi-stage flowshop batch facilities. Comput Chem Eng 25:701–711

Mendez CA, Cerda J, Grossmann IE, Harjunkoski I, Fahl M (2006) State-of-the-art review of optimization methods for short-term scheduling of batch processes. Comput Chem Eng 30 (6–7):913–946

Moon S, Park S, Lee WK (1996) New MILP models for scheduling of multi-product batch plants under Zero-Wait policy. Ind Eng Chem Res 35:3458–3469

Norback J, Rattunde M (1991) Production planning when batching is part of the manufacturing sequence. J Food Proc Eng 14:107–123

Simpson R (2005) Generation of isolethal processes and implementation of simultaneous sterilization utilizing the revisited general method. J Food Eng 67(1–2):71–79

Simpson R, Abakarov A (2009) Optimal scheduling of canned food plants including simultaneous sterilization. J Food Eng 90:53–59

Simpson R, Abakarov A, Teixeira A (2008) Variable retort temperature optimization using adaptive random search techniques. J Food Control 19(11):1023–1032

Taha H (2006) Operations research: an introduction, 8th edn. Prentice Hall, New Jersey (USA)

Teixeira AA, Dixon JR, Zahradnik JW, Zinsmeister GE (1969) Computer optimization of nutrient retention in thermal processing of conduction heated foods. Food Technol 23(6):137–142

Teixeria AA, Zinsmeister GE, Zahradnik JW (1975) Computer simulation of variable retort control and container geometry as a possible means of improving thiamine retention in thermally-processed foods. J Food Sci 40(3):656–659

Verhulst P-F (1845) Recherches mathématiques sur la loi d'accroissement de la population. Nouv Mém de l'Academie Royale des Sci Et Belles-Lettres de Bruxelles 18:1–41

Chapter 13
Recent Advances in Emerging Nonthermal Technologies

Daniela Bermúdez-Aguirre and Gustavo V. Barbosa-Cánovas

13.1 Introduction

Thermal treatment and reduction of water activity in food have been two of the most used techniques to process and preserve food. Pasteurization and sterilization, the main thermal processes used around the world to inactivate pathogenic bacteria, reduce spoilage microorganisms and enzyme activity, inactivate spores (using sterilization), and extend the shelf life of the product. Drying is one of the most effective techniques used to reduce the water activity in the product and as a result the growth of microorganisms is retarded. However, the use of high temperature in these processes has an undesirable effect on the quality of the final product. While heat is responsible for achieving microbial and enzyme inactivation in the product, heat also affects the sensorial quality (color, taste, texture, flavor) and nutrient content of the product and promotes undesirable chemical reactions. In addition to using heat, for some products chemical compounds can be added to preserve the product and provide better stability during storage, such as artificial colorants and preservatives. Most of the time, the final product does not represent the original characteristics of the fresh product because of the changes in its properties during processing. Thus, the search for new alternatives in food processing and preservation has become a priority of food scientists, not only to provide a better quality product, but also to satisfy the needs and preferences of the consumer, and further to fulfill regulations regarding food safety and to offer new alternatives in the food market. These new alternatives include the use of other preservation factors, as opposed to heat, that are able to inactivate microorganisms and enzymes and provide better stability to the product with only minor changes in the overall quality of the food.

D. Bermúdez-Aguirre (✉) and G.V. Barbosa-Cánovas
Center for Nonthermal Processing of Food, Washington State University, Pullman, WA, USA
e-mail: daniela@wsu.edu; barbosa@wsu.edu

J.M. Aguilera et al. (eds.), *Food Engineering Interfaces*, Food Engineering Series,
DOI 10.1007/978-1-4419-7475-4_13,

13.1.1 Consumer Trends

Consumers are becoming more demanding about what to expect after paying for a food product. In the past, consumers would buy a food product simply to satisfy a primary need, i.e., to satisfy their hunger. Today, consumers expect additional benefits from the same products, and some of these benefits include (among others) fortification with extra nutrients, enhancement of characteristics like flavor and texture, food free of chemicals or preservatives, and appealing product appearance; in other words, consumers want to eat fresh-like products but also want extended shelf life. The trend toward "clean" labels (with or without chemicals) is one of the most cited around the world (Clark 2002); from 2008 to 2009 alone there was an increase in the percentage of consumers who considered the absence of chemical additives and preservatives in products to be a very important characteristic, products free of chemical additives (from 37% in 2008 to 44% in 2009) and those free of preservatives (from 28% in 2008 to 34% in 2009), according to the latest survey (Sloan 2010). However, consumers have also developed preferences regarding the technology used to process foods, as well as the origin and possible modification of products (e.g., genetically modified foods); sometimes the consumer does not easily accept novel technologies for processing food (Nielsen et al. 2009). For example, irradiated food is not well accepted in specific regions of the world, where some consumers believe that food becomes radioactive with this processing technology; in some countries the term "irradiation" has been changed to "electric pasteurization."

To gain acceptance of a new technology, food scientists must provide consumers with enough information about its benefits. Sometimes the educational background of consumers is important in achieving a full understanding of the technology; other factors to consider are age, gender and geographical region (Nielsen et al. 2009).

Generally, when higher quality is offered to consumers they are willing to pay a higher price if the product is attractive to them (Lelieveld 2005). One interesting study on the consumer's acceptance level in the use of two novel nonthermal technologies, high hydrostatic pressure and pulsed electric fields (PEF), provided some facts on what consumers think is positive or negative about these technologies. Consumers preferred both nonthermal technologies because of the products' high quality attributes (taste, nutritional content); on a negative note, they did not like the higher price, the lack of information about the technology, and the extended shelf life of products (Nielsen et al. 2009). This last point is really interesting because these particular consumers are looking for food products with fresh-like characteristics but also believe that if a product has a longer shelf life than conventionally treated ones, the product will have lower quality. That fact is opposite to the goal set for specific foods such as military and space rations in which the basic requirement is a food with at least a 3-year shelf life. Maybe the consumer's lack of information is what leads to rejection of the novel technologies, since high pressure and pulsed electric fields can produce safe products with long

shelf life while maintaining fresh-like characteristics during storage. On the hand, participants in the study were positive towards these new technologies to some degree because both are environmentally friendly and no preservatives are added to the food during processing (Nielsen et al. 2009).

13.2 Emerging Technologies

It has been shown that there has been an important increase in the research of novel technologies, due to a joint effort by academia, industry and government (Clark 2008). The area commonly referred to as emerging technologies is very wide-ranging with two main trends in research, that of thermal and nonthermal novel technologies.

Although novel thermal technologies such as microwave, ohmic heating, radio frequency and inductive heating use heat as an inactivation tool, the application and generation of heat is different from conventional thermal treatment. Processing times in these thermal technologies are very short, and lower temperatures are used, which allows having a safe product but with minimal change in quality. Another important development in the thermal processing area is the use of pouches instead of cans. Layers of polyethylene or polypropylene, adhesive, aluminum foil, polyester and nylon are constructed together to contain and sterilize the food product (Clark 2002). These pouches are convenient because of better heat penetration in food, lighter weight, feasibility to label them directly on the surface and higher production rate. In the last several years, use of polymeric trays for thermal processing (conventional or novel processes) has become more common.

13.2.1 Nonthermal Technologies

Several nonthermal technologies have been explored recently, from high hydrostatic pressure to cold plasma. Some physical and chemical preservation factors have been combined in an intelligent way to successfully inactivate bacteria and extend the shelf life of the product, as shown in Table 13.1. During research of these novel technologies, knowledge about changes in the product, such as protein modification, delivered new ingredients for novel food products. The novel nonthermal technologies offer not only opportunities to explore other inactivation effects on microorganisms, but also to develop new processes and products through specific modification of certain food components, as shown in Table 13.2. In some of these technologies, the use of mild thermal treatment has been useful to enhance the effects of the technology by providing better characteristics in the final product; however, the name “nonthermal” is used because the main effects in the product and microorganisms are the result of pressure, electricity, light or sound, among

Table 13.1 Examples of microbial inactivation using selected nonthermal technologies

Microorganism	Technology	Food product	Tested conditions	Results	Reference
Listeria monocytogenes LM 54004	High hydrostatic pressure	Food matrix (soybean protein, sucrose and bean oil)	448 MPa, 41°C, 11 min	6 log reduction; soybean protein, sucrose and pH had significant effect on reduction	Gao et al. 2007
Escherichia coli ATCC 25922	Pulsed electric fields	Simulated milk ultra filtrated	9.5–43 kV/cm, 26.4 μs, 25°C	Up to 1.2 log reduction	Alkhafaji and Farid 2008
Escherichia coli ATCC 25922	Ultrasound	Broth, model orange juice, model apple juice	37.5 μm,20 kHz, 30°C, 15 min	Up to 6 log reduction; higher inactivation when cells were exposed to previous acid stress conditions	Patil et al. 2009
Hiochi bacteria (*Lactobacillus* species)	Bacteriocin	Raw sake	Bacteriocin from *Lactococcus lactis* subsp. *lactis* C 101910 and NBRC 12007, pH 4.5, 4°C, 24 h	3 log reduction using 18–35 U/ml of C101910 and 5.6 U/ml of NBRC 12007	Taniguchi et al. 2009
Escherichia coli type 1	Cold plasma	Pericarp of mango	16 kV, 30 kHz	3 log reduction	Perni et al. 2008b
Pseudomonas aeruginosa, Aeromonas hydrophila, Salmonella enteritidis, Salmonella typhimurium, Yersinia enterocolitica, Escherichia coli, Staphylococcus aureus, Listeria monocytogenes	High pressure Carbon dioxide	Microbiological media	35°C, 10 MPa, 1 min	6 log reduction	Furukawa et al. 2009

Table 13.2 Examples of changes or improvements in food quality/characteristics using nonthermal technologies

Characteristic	Technology	Food product	Tested conditions	Results	Reference
Activity of bovine cathepsin D (meat tenderization)	High hydrostatic Pressure	Bovine meat	0.1–650 MPa, 20–75°C	More than 50% reduction of enzymatic activity using 100–400 MPa	Buckow et al. 2010
Peroxidase (POD) and polyphenoloxidase (PPO) activity	Pulsed electric fields	Apple juice	40 kV/cm, 100 μs, 50°C	Reduction of 71% PPO and 68% POD	Riener et al. 2008
Tartaric esters extraction	Ultrasound assisted extraction (UAE)	Red grape marc	Not mentioned	Yield increased 16–23% using ultrasound	Vilkhu et al. 2008
Chlorophylls	Pulsed electric fields	Spinach puree	60 kV/cm	Increased green color because of microbial and enzymatic inactivation	Soliva-Fortuny et al. 2009
Texture	Pressure assisted thermal processing	Carrot, zucchini, apricot, red radish and jicama	600 MPa, 105°C	Better texture and retained color compared to using only high pressure or thermal treatment	Nguyen et al. 2010

other. In this chapter, some of the most known nonthermal technologies such as high hydrostatic pressure and pulsed electric fields, and some of the newest technologies such as cold plasma will be addressed.

13.3 High Hydrostatic Pressure

Even though high hydrostatic pressure is currently used in the food industry to process and preserve specific food items, there is still important research being conducted. Because of the benefits observed in food products using high pressure, in addition to microbial inactivation and enzymatic stability, many researchers are devoted to studying other effects of high hydrostatic pressure on foods. To mention just one example, when pressurized products were offered to panelists along with untreated samples, the panelists could not distinguish between the treated and untreated samples (Torres and Velazquez 2005). Also, research in the development of new products using the particular characteristics of pressure in treating some food components is a new and fascinating area that is being explored around the world. Many products have been tested under high pressure conditions, such as dairy (milk, yogurt, cheese, ice cream); fruits and vegetables in different presentations such as purée, juices, jams or chunks; meat (turkey, beef, pork, poultry), seafood; grains; eggs; ethnic products; and specific food components such as starch or protein, to mention just a few examples.

13.3.1 Effects on Microorganisms, Enzymes and Food Components

Although high pressure technology was used to inactivate microorganisms in milk in 1899 by Hite, it was not until 1990 when Japanese researchers looked again at this technology and started to use it in food processing. The first commercial pressurized food products were launched into the market in 1990 using high pressure as a microbial and enzymatic inactivation tool (Rastogi et al. 2007). Today the number of pressurized food products extends around the world, including a number of vegetable and animal food products; in some of these products more preservation factors, in addition to pressure, are included.

Figure 13.1 provides examples of specific food products treated with high pressure, demonstrating how this technology achieves better quality and longer storage. For example, Fig. 13.2a shows the extension of shelf life for macaroni salad with vegetables, a product currently sold at the deli counter of supermarkets. After pressurizing the product, the growth of mesophiles and lactic acid bacteria was delayed considerably, resulting in a stable product for more than 50 days. Similar cases have been shown in other products such as artichoke dip, guacamole,

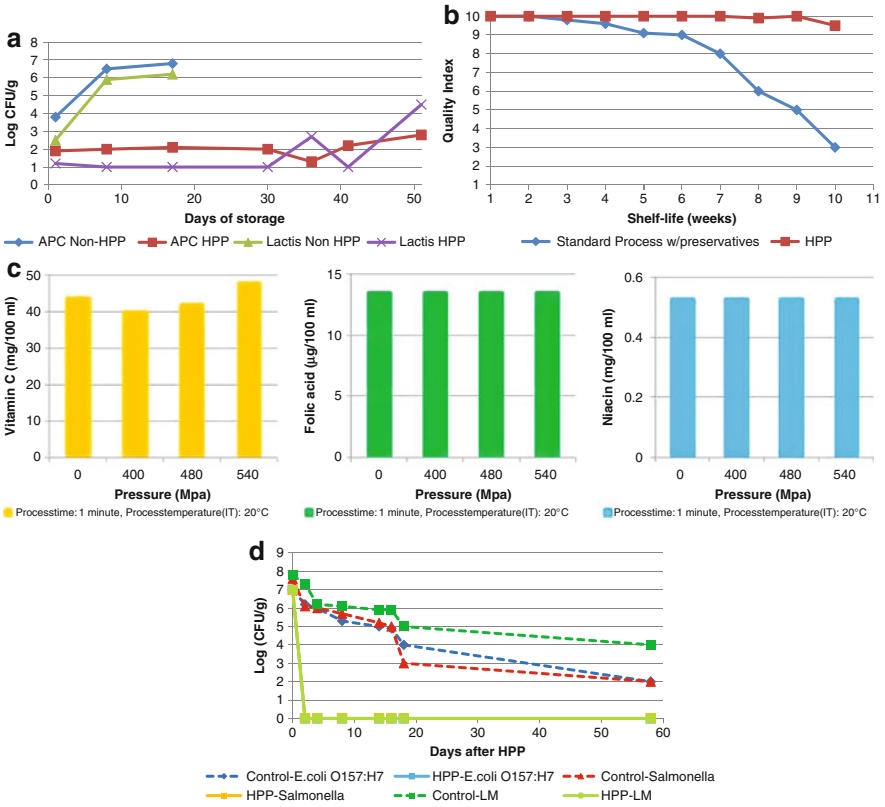

Fig. 13.1 Examples of the use of high pressure for some food products: (**a**) Shelf life extension of macaroni salad with vegetables (pH 4.83); (**b**) quality extension (texture, color and nutritional content) of RTE meats (sliced cooked ham); (**c**) nutrient retention (vitamin C, folic acid and niacin) in fresh orange juice processed with high pressure; (**d**) inactivation of pathogenic microorganisms in strawberry and banana smoothie (Adapted from Avure Technologies, Inc. 2010)

hummus, dips and salsas. In Fig. 13.1b, the graph shows how the quality index of some RTE meats is kept almost constant during storage after pressurization. This example shows that the overall quality (texture, color and nutritional content) of sliced cooked ham after 10 weeks of storage; the quality of the pressurized product is the same as ham just after processing. The comparison in the plot of the common and traditional ham processed with chemicals and additives shows the advantages of pressurizing the product in addition to having a preservative-free product. Figure 13.1c shows the nutrient content in orange juice after pressurizing the juice at room temperature (20°C) and inactivating the microorganisms in the product; the content of vitamin C, folic acid and niacin remained the same as that in the fresh product even when using the highest pressure (540 MPa) for only 1 min. Finally, in Fig. 13.1d, the inactivation of pathogenic bacteria such as *Escherichia coli*, *Salmonella* and *Listeria monocytogenes* is shown in a popular beverage

a

Model QFP 2L-700
Characteristics:
- Lab scale
- 2 liters
- Maximum pressure vessel: 100000 psi (689 MPa)
- Maximum temperature: 90˚C

b

Model QFP 35L-600
Characteristics:
- Suitable for food product development
- 35 liters
- Maximum pressure vessel: 87000 psi (600 MPa)
- Maximum temperature: 50˚C

c

Model QFP 320L-400
Characteristics:
- Suitable for seafood processing
- 320 liters
- Maximum pressure vessel: 22000–58000 psi (150 - 400 MPa)
- Temperature range: 4-35˚C

d

Model QFP 350L-600
Characteristics:
- World's most successful horizontal HPP system
- Highest throughput worldwide
- 350 liters
- Maximum pressure vessel: 87000 psi (600 MPa)
- Maximum temperature: 50˚C

Model QFP 100L–600
Charateristics:
- **Highest available throughput for small, medium and specialty food processors**
- **100 liters**
- Maximum pressure vessel: 87000 psi (600 Mpa)
- Maximum temperature: 50˚C

Fig. 13.2 Examples of current high pressure processing equipment (Avure Technologies, Inc. 2010)

(strawberry and banana smoothie). Bacteria were successfully inactivated using high pressure and after more than 50 days there was no recovery of any bacteria (Avure Technologies, Inc. 2010).

After many studies on microbial inactivation using high pressure, sometimes in combination with temperature, new preservation factors are now being tested in combination to achieve higher inactivation and/or to preserve the original composition of some food products. An interesting example is the use of food additives commonly used in some processed food items that were used in a combination with high pressure treatments to explore the inactivation of *Salmonella enteritidis*. Around 30 food additives were tested in combination with pressure ranging from 100 to 400 MPa, at 25°C, and holding times from 30 to 180 min. All the additives had important synergistic effects on inactivation at 1% concentration; however, citric acid, adipic acid, C8-sugarester, C10-sugarester, tannin, nisin, wasabi extract, ε-polylysine and protamine showed the strongest inactivation of cells (Ogihara et al. 2009). However, the number of preservation factors used in combination with high pressure is not limited; Rastogi et al. (2007) mention some other nonthermal technologies used in combination with pressure with positive results, such as gamma irradiation, alternating current, ultrasound, carbon dioxide, and argon and microbial peptides or bacteriocins.

The effect of high pressure on some components of foods such as proteins has been used to improve quality parameters in target food products. For example, the use of high pressure on meat can extend the shelf life of the product and tenderize and soften its texture, producing a higher quality food because of the modification of myofibrillar proteins and enzymatic (mainly proteolytic) systems (Buckow et al. 2010). Also, these changes in proteins have been used successfully in fish meat; in *carpaccio* and *carpaccio*-like products, high pressure offers an alternative to "processing" the product but still maintains its raw appearance. However, because of the high pressure processing, these fish products have better texture, they are microbiologically safer and have a longer shelf life. Gómez-Estaca et al. (2009) showed results in these fish products using certain fish varieties such as salmon, tuna and cod, with positive important results during the sensorial evaluation.

Another example of the use of high pressure in product development is the production of high energy density (HED) foods. High pressure is responsible for the modification of proteins as mentioned above, but also for the gelatinization of starch. One of the main requirements in producing food for young children is to meet the nutritional requirements of this age group to permit correct growth and development. Sometimes the food offered at home does not contain enough nutrients or adequate consistency. However, the use of amylolytic lactic acid bacteria such as *Lactobacillus plantarum* A6, can change the rheological properties of cereal-based children's foods when using a pretreatment such as high pressure homogenization, which gelatinizes starch, with further fermentation produced by lactobacillus. This combination of processes offers an HED product that is suitable for young children's consumption (Nguyen et al. 2007).

An extensive research program on the quality of fruits and vegetables treated by high pressure has been explored in the last few years. Currently, microbial quality is

not the only important parameter to consider during processing. More quality parameters are under consideration during experimentation in addition to using novel food products. For example, an apple-broccoli juice functional food was tested at 500 MPa and 10 min; in addition to showing excellent microbial quality for more than 30 days of refrigerated conditions (no presence of coliforms, yeasts, molds, or salmonella), this product also showed similar concentration of sulforaphane (a nutritional component), anti-mutagenic activity, and sensorial quality as a frozen juice (Houŝka et al. 2006).

One market that has been explored with successful results in high pressure processing is the seafood product market. High pressure by itself has been important in improving the quality of some seafood products such as surimi, for which there have been interesting reported results (Tabilo-Munizaga and Barbosa-Cánovas 2004, 2005). One of the most important discoveries using this technology was in the processing of shelled seafood; high pressure can open the shells, "extract" the meat and increase the yielding of the process, in addition to inactivating microorganisms. All of these benefits in addition to the reduction of labor costs and increase of product shelf life have been reported, not only for oysters (as shown in the past), but also as shown in current studies for lobsters, clams and other fresh products (Avure Technologies, Inc. 2010).

13.3.2 Advances in High Pressure Processing

In the last few years, high hydrostatic pressure has shown important advances. The fact that it is one of the few nonthermal technologies commercially available today is because of the extensive research that has provided information on this technology. Although the number of commercial products treated with high pressure was small in the beginning, the demand for these products has increased considerably. The most known case is with Avomex Inc. This company started in 1996 as a small facility processing avocado paste (guacamole), which under pressure keeps its freshness (Torres and Velazquez 2005). Worldwide, the number of facilities has increased in addition to the number of products processed by high pressure, not only those processed by Avomex.

Several facts have been noticed during the processing of foods using this technology, such as compression heating. Although high pressure is considered a nonthermal technology, in recent years there has been much research devoted to studying the effect of temperature during the compression taking place in the high pressure process. This change in temperature is reversible and after completion of pressurization, the temperature returns to the starting temperature. The increase of temperature depends on certain factors such as pressure medium and vessel, pressurization rate, initial temperature and food composition (e.g., higher fat content and higher temperature increase) (Patazca et al. 2007). Considering the pressure medium, some studies have shown that three of the most common pressure transmitting fluids used in high pressure processing have different compression

heating values, the highest being for ethanol, followed by ethylene glycol and the last being water. Also, an important fact is that when the initial temperature is high, the compression heating is increased (Buzrul et al. 2008). This last fact is important, for example in microbial inactivation, because in some cases preheating of the food is required to kill target bacteria in the product; thus, increase in temperature because of compression during pressurization can enhance the inactivation treatment (Wilson et al. 2008).

With regard to equipment, currently there are a good number of high pressure systems available worldwide, not only at lab scale, but also for commercial applications. Figure 13.3 presents a few examples of the high pressure systems available at Avure Technologies, Inc. (2010), which offers options to the food processor, such as the first unit (a) for lab research that has a volume capacity of only 2 L and has been designed to research very high pressures (690 MPa) and high temperatures (90°C). The second option (b) is more suitable for pilot plant scale or product development and has a larger capacity (35 L). The third option (c) represents one of the most innovative systems in food processing in the last few years; this equipment is being used in the food industry to open the shells of seafood to release the meat. This unit (Fig. 13.3c) shows the smallest equipment available for this purpose (320 L) and can process up to 2,300 kg of seafood/h with a processing time of 3.5 min. The biggest unit for this purpose (not shown here) has a volume of up to 687 L, which represents a production of 500 kg per cycle, and each pressure cycle takes approximately 3.7 min. Finally, in Fig. 13.3d the largest high pressure equipment is shown; this device has a volume of 350 L, operates at 600 MPa, and can be used for different applications such as the pasteurization of avocado sauce, salsa, and ready-to-eat meat, among others (Avure Technologies, Inc. 2010). Other companies around the world that manufacture high pressure systems for food processing are Hyperbaric NC (Spain), Engineered Pressure Systems International (EPSI) (Belgium), Kobe Steel (Japan), Stansted Fluid Power, Ltd. (UK), Resato International (The Netherlands), UNIPRESS (Poland), ACB Pressure System-Alstom Hyperbar (France), and UHDE (Germany).

13.3.3 Pressure Assisted Thermal Sterilization (PATS)

One of the most significant advances in high pressure technology is the approval by the Food and Drug Administration of the process called pressure assisted thermal sterilization (PATS), which is basically the combination of pressure (600 MPa) and selected temperature to achieve sterilization patterns in low-acid food products (NCFST 2009). This approval, released in February 2009, opens a world of opportunities in the development of other food products using high hydrostatic pressure and also in transporting food products to remote places and storage for longer periods of time. Just a few years ago, inactivation of spores seemed to be a challenge for the technology, and researchers even were planning to use extremely high pressure (GPa) to achieve inactivation, which was not feasible from the

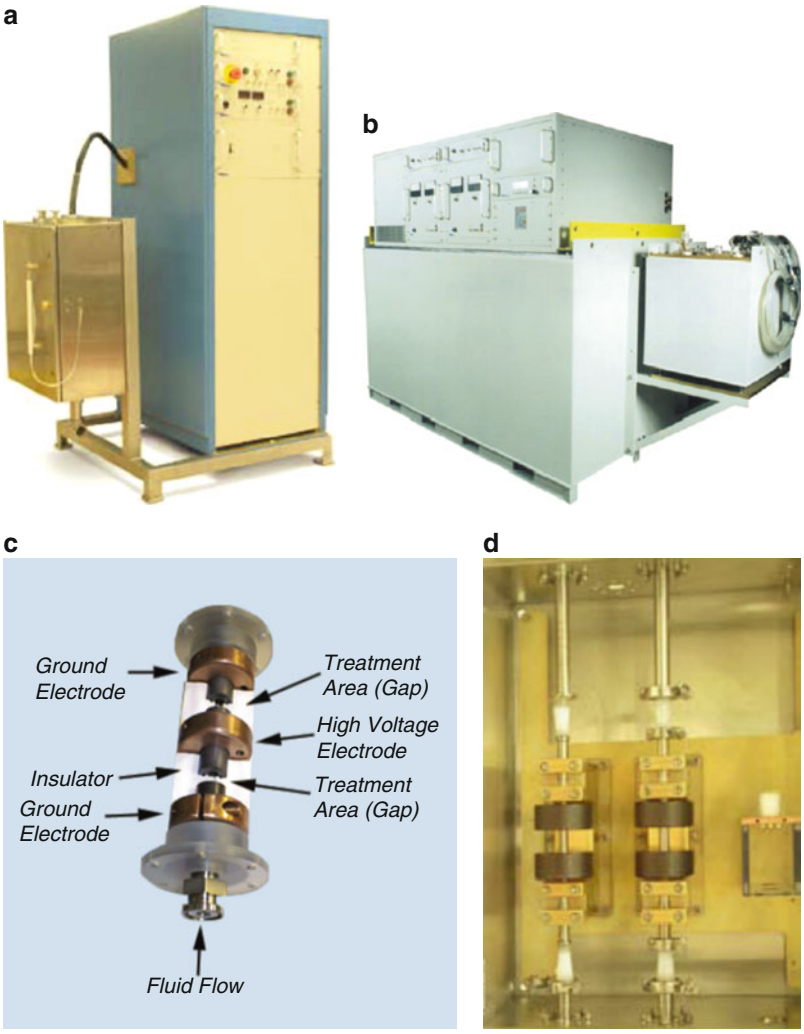

Fig. 13.3 Examples of pulsed electric field devices: (**a**) PEF 25 kW PowerMod®; (**b**) PEF industrial system to process 1,000–5,000 L/h; (**c**) layout of PEF treatment chamber; (**d**) set up of two PEF treatment chambers connected together (DTI 2010)

economic point of view (Torres and Velazquez 2005). Today, it is possible to achieve inactivation of spores using the intelligent combination of pressure, temperature and time without exceeding the values of those parameters. For example, the combination of pressure (0.1–1,400 MPa), temperature (70–120°C) and holding times (less than 8 min) were required to achieve a good degree of inactivation (almost 6 log) of endospores of *Clostridium botulinum* and *Bacillus amyloliquefaciens* using a buffer solution as the medium of treatment; however, in some samples

there was a minor number of remaining spores (Margosch et al. 2006). Spores are very resistant organisms to most of the tested inactivation factors, such as heat, mainly because of their composition. *Clostridium botulinum* spores have been inactivated in some food matrixes using high pressure and high temperature, but the mechanism of inactivation is not fully understood; meanwhile, for *Bacillus* spores there are two possible theories about inactivation using high pressure, such as the release of Ca-DPA (dipicolinic acid), related to germination processes or the formation of pores in the membranes. Also, there is evidence that the presence of minerals and increase of temperature weaken spore resistance to high pressure treatment (Wilson et al. 2008).

13.3.4 Future of High Hydrostatic Pressure

High pressure has shown important results in the last few years, and with the approval of PATS a new huge market is now available to commercialize new products. These products will change the marketing of low acid foods indeed, not only with the feasibility of having a better quality product with longer shelf life, but also because of the kind of packaging used for these products. Commercialization of PATS treated products could be achieved around the world, allowing the free interchange of ethnic food products to remote places on the planet. Also, these PATS food items can be used for the military, space missions, and humanitarian purposes. Development of equipment is growing, together with the development of products in different parts of the world, and there are increasingly more companies offering several options for food processing. Food scientists must now focus on the development of novel, innovative and safe products using this technology, which holds promise for an exciting future.

13.4 Pulsed Electric Fields

Another nonthermal technology that has shown more advances in research and could be the next window for commercial application is pulsed electric fields (PEF) technology. This nonthermal technology, which involves the application of an electric field applied in a pulsed way into a food placed between two electrodes, has been extensively researched around the world. PEF technology was first used to process liquid foods such as in model systems of juices and milk, followed by further applications to real food items. Currently, another area of PEF research is dedicated to studying the application of this technology to solid food products, which has shown important benefits. Some advances in this technology are presented in the next paragraphs, showing the advantages of processing foods with electric fields, as well as developments in the manufacturing of treatment chambers and some of the innovative products treated with PEF.

13.4.1 Effects on Microorganisms, Enzymes and Food Components

As in the case of high hydrostatic pressure, pulsed electric fields technology is being widely explored in the juice industry. Most of the research conducted in the last few years has been related to the application of PEF for microbial and enzymatic inactivation in fruit and vegetable juices (Riener et al. 2008; Aguiló-Aguayo et al. 2008a, b, 2009a, b; Evrendilek et al. 2008; Odriozola-Serrano et al. 2008; Oms-Oliu et al. 2009; Odriozola-Serrano et al. 2009; Martínez-Viedma et al. 2009).

First, the inactivation of microorganisms continues to be studied under PEF treatments using different approaches to confirm the cell death. Spores of *Penicillium expansum* were studied after processing cherry juice, peach and apricot nectars under PEF treatment from very low strengths (13 kV/cm) to higher strengths (34 kV/cm) using 218 μs as the longest processing time. Results showed positively that as the electric fields and treatment times were increased, spore germination was completely inhibited (Evrendilek et al. 2008).

Important results have been observed in enzymatic inactivation of juices; some enzymes that are resistant to thermal pasteurization and responsible for the reduction of quality have been successfully inactivated using PEF. For example, in strawberry juice, lipoxygenase (LOX) was inactivated after processing the juice at 35 kV/cm by 1,000 μs, showing a residual activity of 65% and 70% depending on the mode of PEF operation (monopolar or bipolar). Meanwhile, a monopolar mode was more effective than bipolar for reduction in the activity of another important enzyme in strawberry juice, β-glucosidase (73.2%), making it possible to achieve a more stable juice during storage (Aguiló-Aguayo et al. 2008a). PEF strawberry treated juice also showed flavor stability during storage because of the slow development of unpleasant compounds, compared to the thermal treated samples (Aguiló-Aguayo et al. 2009a). Similar studies using PEF showed that the color and concentration of 5-hydroxymethyl furfural (HMF) in strawberry juice, which is responsible for the development of browning, were positively affected after processing (Aguiló-Aguayo et al. 2009b). Few changes in color were observed for strawberry, tomato and watermelon juices after processing at 35 kV/cm, 40°C and 1,000 μs, and lower concentration of HMF was detected after PEF processing. In the case of watermelon juice treated under PEF, lycopene, vitamin C and antioxidant capacity were evaluated after processing. Lycopene retention and antioxidants in watermelon juice capacity showed the best results after processing with PEF; however, for vitamin C, when the same treatment was applied, a reduction in vitamin C content up to 72% was shown (Oms-Oliu et al. 2009).

Tomato juice is another food product that is of high importance in the food industry. After processing with thermal treatment it shows an important decrease in quality attributes. The search for new alternatives to process this product has led food scientists to explore the use of PEF for tomato juice. One of the most important enzymes in tomato juice is peroxidase (POD), which generates some quality problems during storage. This enzyme was totally inactivated in the juice using 35 kV/cm,

2,000 μs (7 μs bipolar pulses) at 200 Hz; very low residual activities (around 8%) were found under similar processing conditions (Aguiló-Aguayo et al. 2008b). In addition, after treatment, tomato juice showed an enhancement of some carotenoids such as lycopene, β-carotene and phytofluene, in making the color of the juice very red. Also, the evaluation of phenolic compounds, pH and soluble solids remained similar to the fresh product. Only a minor decrease in the health-related compounds was observed after processing, but important losses were observed during storage, with the exception of b-carotene, phytoene and caffeic acid (Odriozola-Serrano et al. 2009).

Furthermore, the combination of PEF with other preservation factors such as bacteriocins has been used recently to inactivate target microorganisms such as lactic acid bacteria. Martínez Viedma et al. (2009) successfully studied the combination of PEF treatment at 35 kV/cm, 1,000 μs and enterocin AS-48 (2 μg/mL) in apple juice to inactivate *Lactobacillus diolivorans* 29. The juice was stable for 15 days at refrigerated and room temperature without the presence of this microorganism.

13.4.2 Recent Advances in PEF Processing

Since the first experiments conducted with PEF, the treatment chamber has been the key part of the system, in which inactivation of microorganisms and enzymes takes place when the liquid is passed through the chamber containing the electrodes. Treatment chambers can be classified in accordance with the operation mode, in static and continuous. Among the first chambers, some of those that have been used for food processing are the U-shaped, parallel plate, disk-shaped, wire cylinder, rod-rod and the sealed static treatment chamber. For continuous processing, the most common devices include the co-axial and co-field treatment chambers (Huang and Wang 2009). In Fig. 13.2, images of current PEF systems, which now have a more compact design than previous older units, are presented. Figure 13.2 a shows the PEF PowerMod 25 kW system, which is suitable for use in pilot plant scale and has the feasibility to work with one or two chambers together (Fig. 13.2d), allowing recirculation of the fluid between each cycle. The maximum output voltage is 35 kV, delivering monopolar pulses, and the maximum flow rate recommended is 10 L/min. In Fig. 13.2c the layout of the co-field treatment chamber is shown, showing that the treatment chamber in Fig. 13.2d and the one installed in the PowerMod 25 kW unit have a gap distance of 0.65 cm and an electrode diameter of 0.5 cm. Finally, Fig. 13.2b presents the first commercial PEF unit; designed by Diversified Technologies, Inc. for use at Ohio State University, it has the capacity to process 1,000–5,000 L/h but can also be scaled-up to process up to 50,000 L/h (DTI 2010).

However, several issues need to be resolved to enhance and optimize the treatment during processing. For example, the possibility of electrical arcing because of the presence of bubbles in the food product is a big problem during PEF processing, although this may have been fixed by using some equipment under vacuum conditions before starting the process or installing sensors in specific parts

of the system to detect bubbles and automatically stop the process. Erosion of electrodes because of strong processing conditions during PEF is another issue that is currently under study and optimization by PEF manufacturers. When an electrical current is discharged into the electrodes and a fluid passes through the chamber, electrochemical reactions take place; as a result some metal particles from the electrodes are released to the medium and particles from the food are deposited onto the electrode surface (Mastwijk 2006). Some available options to minimize the erosion of electrodes include using a specific type of pulse during processing or using stronger and durable material such as platinum, gold and metal oxides; also, the application of conductive polymer coatings onto the electrode can reduce the erosion problems (Góngora-Nieto et al. 2002). Most of the electrodes currently used around the world are made of stainless steel, and some have coatings consisting in part of the strongest materials, such as platinum; however, these coatings are not always strong enough when there are arcing problems during operation, which can erode the electrode surface.

13.4.3 PEF Extraction

Several years ago, PEF technology was recognized as a new processing tool for liquid food products; however, in the last few years PEF has become more important in extraction processes in the food industry and for treatment of solid foods. PEF has been applied, for example, in processing alfalfa mash to extract the juice from the product. Even though other technologies have been applied to maximize the yield of extraction, the juice was never totally extracted. PEF, however, was applied to alfalfa mash with the highest electric field at 2.5 kV/cm and obtained a maximum amount of juice of 13.88 g per 40 g of alfalfa (Gachovska et al. 2009). PEF was able to damage the tissue of alfalfa and extract the juice of the vegetable, although according to the authors, the capacitance of the discharge capacitor should be higher than 1 μF to optimize the process.

Another example is the extraction of betanine extraction from red beet roots, which was faster and with higher yield (90% of extraction) after PEF treatment than the conventional treatment (López et al. 2009a). Also, it is known that for extraction purposes, the intensity of the treatment does not need to be so high; lower electric fields are needed, but longer processing times are required to achieve good extraction levels. For example, for betanine, the electric field was 7 kV/cm, 5 pulses (2 μs) and 300 min (López et al. 2009a); these processing conditions allowed extracting the content from the tissue, but did not support microbial inactivation, which requires electric fields higher than 20 kV/cm in combination with a specific temperature and pulse width conditions. A similar example is the extraction of sucrose from sugar beet, in which an electric field of 7 kV/cm at 40°C and 60 min was able to achieve up to 80% of sucrose extraction (López et al. 2009b). Also, the extraction of anthocyanins and phenols from red grapes has been widely used in the wine industry to reduce the time of maceration and to increase the extraction of

phenolic compounds (Puértolas et al. 2010; López et al. 2008a, b). In addition to these extraction processes for wine making, PEF is also able to inactivate spoilage yeast and bacteria in the wine. *Dekkera anomala, D. bruxellensis, Lactobacillus hilgardii,* and *L. plantarum* are some examples of bacteria that have been successfully inactivated by PEF in must and wine; more than 99.9% of spoilage bacteria in both products can be eliminated (Puértolas et al. 2009).

Some studies using PEF showed an interesting behavior in potato starch after processing. The starch granules were damaged because of the intensity of the electric field. Pieces of the granules after processing showed some structures that were similar to gel and a decrease in the gelatinization temperatures as the PEF treatment became more intense (Han et al. 2009).

13.4.4 Future of Pulsed Electric Fields

Indeed, the next technology to be launched in the market of nonthermal processing will be pulsed electric fields. The number of patents using pulsed electric fields technology has increased in the last few years, from very basic treatment chambers to more complex systems (Barbosa-Cánovas and Sepúlveda 2005). In 2007, Genesis, the first company in the United States to use pulsed electric fields to process fruit juice in the Pacific Northwest, offered PEF treated juices of outstanding quality. (Because of issues not related to the technology, this company is no longer using PEF). The price of a PEF treated product compared with a conventional thermal treated product is not too different; when Genesis products were in the market, the price of their juice was comparable to that of fortified juices using botanical ingredients, extra nutrient content, and similar characteristics in other novel products. Lelieveld (2005) agreed with the idea that the relative cost of PEF is not high and there is an interesting comparison in cost between thermal processing and PEF processing starting from the initial investment. Hoogland and de Haan (2007) presented a study in which there is an increase in cost in the initial investment (0.8 Eurocent/L) and energy (0.2 Eurocents/L) of a PEF system compared with traditional thermal processing equipment, but there is a reduction in cost of cleaning (−0.05 Eurocents/L), maintenance (−0.05 Eurocent/L), and downtime (−2.5 Eurocent/L), having a final balance of −1.5 Eurocent/L favorable to PEF equipment.

Furthermore, in 2010, at least two important companies reportedly will start processing food products with PEF in Europe (Kempkes 2009). Some of the European food companies currently researching and working with PEF are in The Netherlands, Switzerland and France; the basis of their research is mainly focused on milk. Most of the work to scale-up the PEF system has been completed, and now some minor issues remain before pursuing the industrial use of the technology. Although right now the technology in Europe is being used for pasteurization of products such as juice or milk, its use could be extended in the coming years to a number of products, not only liquids. PEF is now under research to treat some solid

food products to improve their quality for extraction purposes or microbial inactivation. However, most of this information is still under research and to date few results have been published. Nevertheless, use of pulsed electric fields has a promising future in Europe and could be approved by regulatory agencies soon.

13.5 Ultrasound

Ultrasound is another nonthermal technology under research in the last few years, as a possible tool to inactivate microorganisms and enzymes. While the lethal effects of ultrasound in microorganisms have long been known, in the last 2 decades there has been a strong research emphasis at several universities and research centers around the world regarding the use of ultrasound for bacteria inactivation. Positive results have been found when ultrasound is used in combination with temperature (thermo-sonication) or pressure (mano-sonication) or even both (mano-thermo-sonication) in the inactivation of pathogenic bacteria and spoilage microorganisms. Also, the use of temperature and ultrasound together have been successfully used to reduce the enzymatic activity in some target products such as juices, providing better stability during storage. One of the most explored products in the last 5 years has been milk under sonication, which shows positive results in pasteurization standards, better homogenization and color, as well as new physical properties for the development of dairy products.

13.5.1 Extraction

Another interesting application of ultrasound is the extraction of components from food matrixes. For example, the extraction of polyphenols is of great interest in the food industry, and these compounds are retained in apple pomace during juice production. Polyphenols are very important as preservatives and antioxidants, in addition to their importance in other industries. Ultrasound was used to study the extraction of these compounds from apple pomace and to improve the typical maceration extraction process (Virot et al. 2009). Results showed that ultrasound increased extraction yield up to 20% and reduced the time considerably. This fact can be attributed to the series of explosions and implosions generated by cavitation during sonication, which produces higher pressure and temperature and disrupts the tissue and vegetable walls of the apple, thus more efficiently extracting the compounds. Similar results were observed in phenolic extraction from citrus peel, in which compounds such as caffeic, *p*-coumaric, ferulic, sinapic, protocatechuic, *p*-hydroxybenzoic and vanillic acid were studied under sonication using 40°C as the highest temperature. Again, the extraction yielding phenolic compounds was higher when time and temperature were increased; however, temperature was an

important factor in the stability of the phenolic compounds and had to be controlled in each particular case (Ma et al. 2009).

Ultrasound, also called ultrasound-assisted extraction (UAE), has been used to extract phospholipids from palm-pressed fiber (Chua et al. 2009). Typical extraction of phospholipids from palm oil takes a considerable amount of time and requires the use of solvents. These phospholipids are currently used in the food industry as emulsifiers and are of great importance in specific products. The need to have a higher yield in extraction in addition to a faster and solvent free method is highly desirable. In the study conducted by Chua et al. (2009), the extraction of phosphatidylethanolamine and phosphatidylcholine was enhanced with the use of ultrasound; a simpler process with a higher yield and shorter processing times was achieved with this nonthermal technology.

Other applications of UAE include the extraction of herbal extracts such as fennel, hops, marigold, mint, geniposide, carnosic acid from rosemary, almond oils, ginseng saponins, ginger, soy protein and soy isoflavones, as well as polyphenols, amino acid and caffeine from green tea and pyrethrines from flowers. Some bioactive compounds such as beta-carotene, other polyphenols, and gingerol have been successfully extracted with UAE from carrots, red grape marc, black tea, apple and ginger (Vilkhu et al. 2008).

13.5.2 Recent Advances in Ultrasound

As mentioned before, ultrasound has been used to inactivate bacteria and enzymes, and some of the most studied products have been fruit juices because of the easy application of ultrasound to these products. Favorable results have been observed in microbial inactivation and stability during storage, and minor changes have been observed; however, there is still a lack of information regarding other components after processing, for example nutritional content in juices. One of the most important components in red grape juices and wines is anthocyanins because of their excellent antioxidant activity; however, most of the anthocyanins are unstable during processing. Ultrasound was used to study anthocyanin content after processing and encouraging results were observed. Higher retention was observed in anthocyanin content after processing; the three major anthocyanins in red grape juice, cyaniding-3-*O*-glocosides, malvanidin-3-*O*-glucosides and delphinidin-3-*O*-glucosides, were retained respectively in the juice 97.5, 48.2 and 80.9% after sonication (Tiwari et al. 2010). Also, non-enzymatic browning and ascorbic acid degradation were studied in sonicated orange juice. Low temperature (5°C) and intermediate amplitudes (42.7 μm, 20 kHz) were the best conditions for achieving less degradation of ascorbic acid and less browning (Valdramidis et al. 2010). These are good examples of the use of ultrasound for juice processing; sonication inactivates bacteria and enzymes, retains higher concentration of nutrient compounds and maintains a product with fresh-like characteristics.

Other potential advances in ultrasound technology are related to extraction processes. Many extraction studies are currently being conducted, but in addition to the extraction process, ultrasound is able to encapsulate the extracted compound through covalent bonding and microsphere formation. This research area, which is very new, mixes different frequencies during operation and uses different compounds to extract and encapsulate target compounds (Vilkhu et al. 2008). Very few experiments have been conducted in this area, but by applying the basic principles of ultrasound and the appropriate combinations of processing parameters, food components and other processing variables, this process has huge potential in food applications and other related industries.

Some research has been started in the last few years related to the sonochemistry in certain foods products to study the reactions that ultrasound generates in food during processing. While some of these reactions could produce toxic compounds, the intelligent selection of frequency and other processing variables could be useful in reducing the amount of toxic compounds (if any) and achieving similar results in terms of inactivation. Also, these chemical reactions can be used to generate new compounds in foods with specific purposes such as modification of proteins (Jambrak et al. 2009), hydroxylation of phenolic compounds to enhance their antioxidant properties, and so on (Ashokkumar et al. 2008).

Ultrasound comprises a very wide area of research that has been explored deeply in the last few years, and currently presents a number of challenges and has raised some other issues that need to be resolved in areas such as equipment manufacturing. Many researchers around the world are now looking at ultrasound not only as a technology to kill bacteria and produce safe products, they are also looking at how to use the properties of this technology to improve the quality of food and to find new alternatives to making a stable product and having new and improved food ingredients. Ultrasound is currently used with many other processes such as emulsification, homogenization, crystallization, dewatering, degassing, defoaming, particle size reduction and viscosity alteration (Patist and Bates 2008). Most ultrasound research equipment is on a lab and pilot plant scale, but further scale-up technology to the industrial level is highly desirable and possibly will occur once the majority of small technical difficulties in lab and pilot plant devices have been solved.

13.6 Cold Plasma

When an electric field is applied to a gas, molecules are ionized and gas plasma is produced. The electrons, which are usually bound to molecules of gas, start to separate from the gas; the resultant ionized gas is known as discharge plasma (Perni et al. 2008b). Some authors consider plasma as a fourth state of matter (Selcuk et al. 2008) and that the mix of free radicals, excited species (atoms and molecules), free electrons and ions are responsible for microbial inactivation. Atomic oxygen has been found in plasma and is considered to be one of the most lethal components for inactivating microorganisms (Perni et al. 2008b). One of the main advantages of plasma in food

applications is that this technology can be used at low temperatures, for example, as low as ambient temperature (Perni et al. 2008a); that allows microbial inactivation because of the generation of free radicals, resulting in a food product free of any residues and that retains the fresh-like characteristics of the food.

13.6.1 Processing Conditions

Studies related to microbial inactivation in food using cold plasma are very scarce and can be considered as a first-generation technology in food research (Niemira and Sites 2008). As a new technology, the interest in this nonthermal option is rising and some attempts to inactivate bacteria are under development. Plasma basically consists of a corona discharge from an electrode; it has been used mainly on food surfaces for disinfection (Perni et al. 2008a). Corona discharge has a very high temperature, on the order of 1,000 K, but the heat located in the electrode is quickly dissipated. In the past the use of vacuum conditions were applied during the generation of plasma to maintain low temperature; today, cold plasma is generated at voltages below those used for corona discharge effects at higher frequencies than those for dielectric-barrier discharge (Perni et al. 2008a). A schematic view of a cold plasma device is shown in Fig. 13.4; the system basically consists of a pair of electrodes, one grounded and the other powered, and a ceramic tube. The gas inlet is set at one of the extremes in the ceramic sheath; once the gas comes into contact with the electric discharge, the plasma is generated on the surface of the sample. Today, cold plasma is tested for disinfection

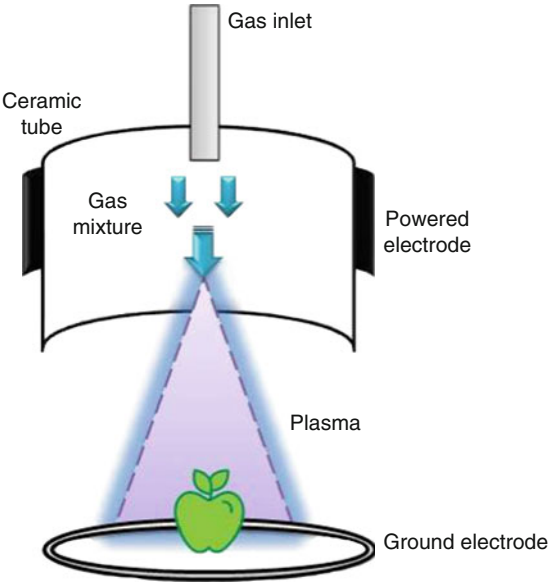

Fig. 13.4 Layout of cold plasma device (Adapted from Perni et al. 2008b; Deng et al. 2006)

of food surfaces only; the microbial inactivation produced is attributed to the formation of free radicals in the plasma environment. Three main categories for plasma generation can be cited: electrode contact, direct treatment and remote treatment (Niemira and Sites 2008). The main difference between these approaches is whether or not the plasma is in contact with the food item.

13.6.2 Effect on Microorganisms

The effect of cold plasma on microorganisms is related mainly to the generation of certain chemical substances and their ability to injure and kill bacteria, yeast, molds and other organisms. These chemicals are dissociated species of oxygen such as ozone, atomic oxygen, hydroxyl, nitric oxide, super oxide radicals and other free radicals (Selcuk et al. 2008).

Some cold plasma studies in food research are related to the inactivation of *Listeria innocua* and *Escherichia coli* in apples, *Salmonella* enteritidis in cantaloupe, *Listeria monocytogenes* in lettuce (Niemira and Sites 2008), and *Aspergillus* spp. and *Penicillum* spp. in several types of seeds (tomato, wheat, bean, chick pea, soy bean, barley, oat, rye, lentil and corn) (Selcuk et al. 2008).

Recent studies in microbial inactivation of *Escherichia coli* cells after plasma treatment show important changes in their structure and breakdown of the cell membrane, with loss of cellular components from the main cell (Critzer et al. 2007). The main lethal effects have been attributed to the presence of oxygen atoms, metastable oxygen molecules, and OH radicals (Yu et al. 2006) because they have high oxidization potential in the cells. One theory about microbial inactivation is related to the oxidation of amino acids and nucleic acids in cells as well as the effects in lipids of the membrane (Critzer et al. 2007).

13.7 Dense Phase Carbon Dioxide

Another nonthermal technology that has been under research in the last 20 years is dense phase carbon dioxide (DPCD), also called high pressure carbon dioxide (HPCD); this technology allows microbial inactivation in foods and has seen a big peak in research in the last 5 years (Garcia-Gonzalez et al. 2007). In this nonthermal technology, carbon dioxide at supercritical conditions (temperature and pressure) is applied to foods in the batch, semi-batch or continuous operation mode (Garcia-Gonzalez et al. 2009); the pressurized CO_2 diffuses through the material, dissolving the cell components, generating microbial inactivation (Ferrentino et al. 2010a). The critical conditions of CO_2 ($T_c = 31\ ^\circ C$, $P_c = 7.35$ MPa, and up) are used for solid and liquid foods. CO_2 has the capability of diffusing throughout solid foods in a gas form and dissolving materials similar to a liquid (Garcia-Gonzalez et al. 2007). The critical conditions of CO_2 are shown in the thermodynamic diagram in Fig. 13.5.

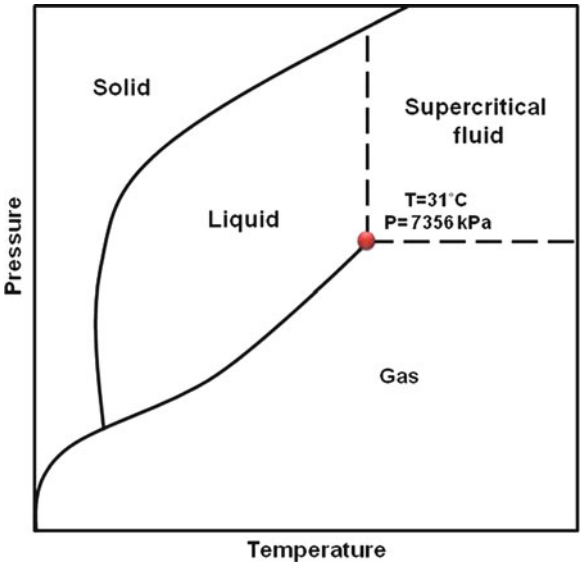

Fig. 13.5 Thermodynamic diagram (temperature–Pressure) for CO_2 showing its critical conditions

As in other novel technologies, the mechanism of inactivation of microorganisms is still unclear, but there are theories suggesting important changes in the pH of the cell with subsequent damage in the cell membrane, and an unbalance of electrolytes in the inner cell content with the final removal of vital components in the cell and membrane (Garcia-Gonzalez et al. 2009).

In a study conducted by Garcia-Gonzalez et al. (2009) with a number of bacteria and selected processing conditions of DPCD, results showed the resistance of microorganisms to this technology, the Gram negative bacteria followed by Gram positive bacteria and yeasts, with spores being the most resistant. To achieve spore inactivation using DPCD, the use of moderate temperatures (60°C and higher) in combination with this technology is required to obtain a good reduction degree (Furukawa et al. 2009; Garcia-Gonzalez et al. 2007). Some of the factors that affect microbial inactivation using DPCD are the pH of the medium and the water activity (a_w). When the pH of the medium is low, the microbial inactivation with DPCD is higher, but with a decrease in a_w the cells become more resistant. According to the type of solute, cells were weakened with the presence of NaCl; meanwhile sucrose and glycerol protected the cells (Garcia-Gonzalez et al. 2009). Other tested microorganisms using DPCD were *Saccharomyces cerevisiae* (Ferrentino et al. 2010b; Parton et al. 2007a), *Pichia awry* (Parton et al. 2007b), *Pseudomonas aeruginosa, Aeromonas hydrophila, Salmonella enteritidis, S. typhimurium, Yersinia enterocolitica, Escherichia coli, Staphylococcus aureus, Listeria monocytogenes* (Furukawa et al. 2009), *Bacillus subtilis* (Parton et al. 2007a), *Leuconostoc dextranicum* (Lin et al. 1993), and *Enterococcus faecalis* (Debs-Louka et al. 1999), among others.

Few studies have been conducted using DPCD to analyze other food properties. Khorshid et al. (2007) used DPCD to precipitate protein from soy. Results of this experiment showed that supercritical CO_2 was useful in isolating pure protein, having a higher recovery than with traditional methods; it also saved energy. Few applications of DPCD for extraction purposes have been reported in food systems and there have been few studies of this novel technology for microbial inactivation in solid foods because of the possibility of altering the sensorial properties (Garcia-Gonzalez et al. 2007).

Indeed, as in other technologies, DPCD is a wide research field with many possibilities to explore. Research currently being conducted is focused on designing the technology and improving the reactions to its use in processing of foods, as well as some studies related to the solubility conditions of CO_2 in water and other complex systems at specific conditions (Parton et al. 2007b, b; Ferrentino et al. 2010b). A number of patents have been produced in the past few years regarding DPCD equipment for pasteurization, especially in the United States, Germany and Japan (Garcia-Gonzalez et al. 2007). Based on the current results of microbial inactivation and quality characteristics of food, processing conditions have been modified to achieve specific objectives.

13.8 Other Novel Nonthermal Technologies for Food Processing

Other nonthermal technologies that have been under research in the last few years are ultraviolet (UV) and the use of certain compounds with antimicrobial activity such as bacteriocins. In the case of ultraviolet technology, most of the applications have been related more to the application of UV light on the surface of fresh cuts of fruits and vegetables than in liquid products. For example, ultraviolet was applied to fresh cuts of watermelon before packaging, followed by evaluation of the characteristics of the fruit, such as CO_2 and C_2H_4 production, microbial counts (mesophilic, psychrophilic and enterobacteria), color parameters, nutrient compounds such as lycopene, polyphenols and ascorbic acid and sensorial attributes. Results showed that ultraviolet treatment can extend the shelf life of cut watermelon with minimal changes in the quality characteristics (Artés-Hernández et al. 2010). Similar studies were conducted with apple slices, using a pretreatment of hot water for blanching and then dipping the slices into solutions with ascorbic acid and calcium chloride. Browning and the growth of bacteria were delayed in samples treated with UV light (Gómez et al. 2009). Other studies included fresh cut fruits such as pineapple, guava, and banana (Alothman et al. 2009), and vegetables such as onion, escarole, carrot and spinach (Selma et al. 2008).

In the field of bacteriocins, probably the most studied microorganism using these compounds is *Listeria* spp., with bacteriocins found in seafood (Pinto et al. 2009); in dairy products using peptide cerein 8A (Bizani et al. 2008); and in soft cheese using *E. faecium* WHE 81 (Izquierdo et al. 2009). Even though a good number of bacteriocins have been isolated and used against specific target microorganisms in other

products, the only bacteriocin that has been approved for use in the food industry (specifically for dairy products) is nisin, in specific concentrations. The use of bacteriocins around the world is different in each country and legislation allows the use of bacteriocins in specific products, which does not permit generalizations regarding concentrations and types of food. However, research in this area is ongoing.

The list of other nonthermal technologies under research is still long; technologies currently being tested in lab facilities include ozone by itself, ozone combined with ultraviolet or electrolyzed water, the use of organic acids, supercritical water, natural antimicrobials derived from species, and a combination of such with most of the well established nonthermal technologies.

13.8.1 Future of Other Novel Technologies

Today, hundreds of food products have been evaluated in relation to at least one nonthermal technology, depending on the product and the objective of the process. Table 13.3 provides a brief summary of some of the tested technologies according to the kind of product and the achievements accomplished for each one. These newest technologies are being researched by food scientists for use in food processing and are indeed showing encouraged results.

Ultrasound was first used in the early 1900s, but interest was lost in the following years; now it is becoming popular again in food processing. This technology has been shown to be important not only for microbial inactivation, but also for reduction of enzymatic activity to provide food products with longer stability. In addition to its inactivation effects, ultrasound is able to reduce processing times considerably because of the two in one effect, for example in milk processing (pasteurization and

Table 13.3 Examples of nonthermal technologies suitable for processing specific foods

Nonthermal technology	Type of product	Examples	Results
High hydrostatic pressure	Liquids	Juices	Pasteurization standards
	Liquid-solids	Eggs	Sterilization
	Gel-like	Jams, jellies	Pasteurization
	Solids	Cheese, meat	Improved quality characteristics (e.g., texture)
Pulsed electric fields	Liquids	Juices, milk	Pasteurization standards
Ultrasound	Liquids	Juices, milk	Pasteurization standards
Dense phase carbon dioxide	Liquids	Juices	Pasteurization standards
Ultraviolet	Liquids	Water, juices	Pasteurization standards
	Solids	Fresh-cuts	Disinfection
Cold plasma	Solids	Nuts, fresh-cuts	Disinfection
Bacteriocin	Liquids and solids	Dairy products	Delay of spoilage degree

homogenization in one step), product development (emulsification and reduction of enzyme activity), cheese-making (increase of yielding, reduction of time for curdling formation, and milk pasteurization), among others. This technology offers many possibilities for use in the food industry. However, more research must be conducted, mainly concerning the toxicological aspects of foods following ultrasound treatment.

As for the technologies ultraviolet light and ozone, both are currently used to some degree in the industry, mainly for drinkable water. The feasibility of ultraviolet radiation being transmitted through transparent water is the main characteristic that allows its use for this product. To the contrary, the limitation of ultraviolet light into opaque fluids such as milk is an issue, because the presence of fat globules and casein micelles in milk prevents the radiation from being transmitted correctly. Ultraviolet light has been tested to disinfect the surface of certain food products with positive results; the main problem is when the product has a very porous surface, since bacteria can hide inside the porous surface and thus cannot be reached by ultraviolet radiation. Nevertheless, ultraviolet light is still being researched for some of these products, and food scientists are trying to combine technologies or find alternatives to process specific foods, such as the case of milk, using turbulent flows to allow better contact between ultraviolet light and the milk.

Although plasma is probably the newest nonthermal technology for food processing, its research is becoming very important. Lately, conferences formerly devoted to the use of plasma in general are now offering specific sessions related to the use of plasma in food processing. Current research being conducted on plasma could possibly be setting up the basic knowledge needed to understand how certain foods react with plasma. This research represents a huge field of opportunities for study not only in the area of microbial inactivation with plasma, but all aspects related to the toxicology of the generated compounds at specific processing conditions, including those generated into the food after processing.

13.9 Modeling of Microbial Inactivation in Nonthermal Technologies

One common denominator in the nonthermal technologies is the inactivation patterns of bacteria, spores and enzymes, which in most of the cases do not follow first order kinetics. Much research has been conducted in the study of inactivation curves after processing samples with high pressure, pulsed electric fields, ultrasound or ultraviolet, to mention just a few. However, there are a number of reasons (or artifacts) explaining why microbial inactivation does not follow a first order kinetics; some of these are related with to experimental procedures, the mix of microorganism strains, clumps of bacteria, protective effects of the media, or a non-homogeneous application of the preservation factor (McKellar and Lu 2004). Some of the most common shapes in microbial inactivation that do not follow first order kinetics include upward or downward concavities and sigmoid curves (Peleg 2000). Most of these concavities

and specific shapes in microbial inactivation are called "shoulders" and "tails" in food engineering and these are shown in Fig. 13.6, representing a typical inactivation curve in nonthermal technologies. Here, the need to find alternative mathematical approaches to fit and model the survivor data is a challenge for food scientists. Survivor data allows a comparison of the inactivation degree under different processing conditions in order to find an equivalent inactivation for thermal processing.

Some of the mathematical models that have been used for fitting the survivor data after using nonthermal technologies are the Weibullian equation, Fermi equation, Gompertz model, Baranyi model, Bigelow model, Peleg's equation and others, as presented in Table 13.4. For example, for pulsed electric fields inactivation the three models used the most to fit the survival curve relating the electric field strength and treatment time are the Huelsheger model, Peleg's model and the Weibull distribution (Fox 2007); all of these models are shown in Table 13.4.

A typical dose–response curve shows the resistance of a specific microorganisms against a lethal agent; this agent can be any preservation factor such as chemicals or nonthermal technologies. When the dose–response curve shows symmetry, one of the options is to fit the data to the Fermi equation (Peleg et al. 1997):

$$S(X) = \frac{1}{\left\{1 + \exp\left[\frac{X - X_c}{a}\right]\right\}} \tag{13.1}$$

where $S(X)$ is the fraction of survivors, X and X_c are the dose of the lethal agent, X_c being the point of the curve when there is an inflection point or when the population becomes 50% of the initial and a is the steepness of $S(X)$ around X_c. It should be noted that in some of the references cited in Table 13.4, where this equation was used to fit the data after different processing technologies, the dose (X) also means the degree of pressure applied, the intensity of the electric field, the concentration of antimicrobial, or the intensity of ultrasound wave, among others.

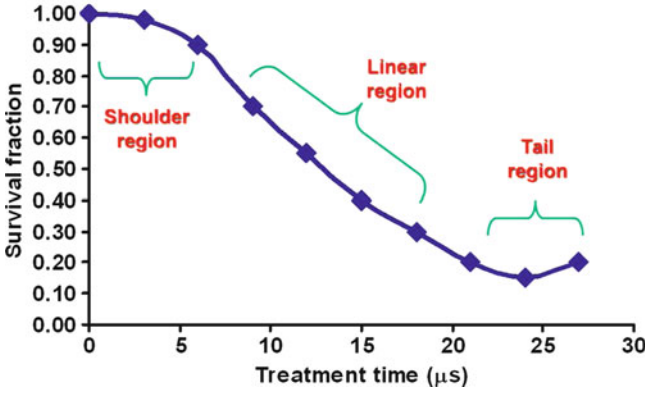

Fig. 13.6 Example of an inactivation curve showing three common regions in nonthermal processing: shoulders, linear region and tails

Table 13.4 Example of mathematical approaches to modeling microbial inactivation using nonthermal technologies

Nonthermal technology	Example of inactivation	Mathematical models	Definition of terms	Reference
Combination of nonthermal hurdles (temperature, pH, sodium chloride)	Inactivation of *Listeria monocytogenes* in model systems, showing significant tailing, perhaps because of mixed population	$\left[\frac{(1-F_1)\left(1+e^{-b_2\times t_L}\right)}{\left(\left(1+e^{b_2(t-t_L)}\right)\right)}\right]$ *Logistic-based equation*	Y: Log_{10} count of bacteria at time t Y_0: Log_{10} at time zero t: time t_L: duration of lag period prior to initiation of inactivation F_1: fraction of initial population in major group b_1: $2.3/D_1$ = inactivation rate for major group b_2: $2.3/D_2$ = inactivation rate for minor group	Buchanan et al. 1994
High pressure	Inactivation of *Listeria innocua* in broth	$\frac{\log N}{N_0} = Ce^{-e^{BM}} - Ce^{-e^{-B(t-M)}}$ *Modified Gompertz equation* $q_B + (1-q_B)e^{-k_{max}(t-B(t))}$ *Baranyi model*	N/N_0 = Survival fraction B: relative death rate C: difference in value between upper and lower asymptote M: maximum death rate time t: treatment time q_B: tailing ratio k_{max}: maximum death rate	Saucedo-Reyes et al. 2009
High pressure thermal sterilization (PATS)	Inactivation curves of endospores of *Clostridium botulinum* and *Bacillus amyloliquefaciens* showing tailing	$\frac{\log N}{N_0} = log\left(1 + k \times N_0^{(n-1)} \times t \times (n-1)\right)^{\frac{1}{1-n}}$ *nth order kinetics model*	N: number of survivors at time *t* N_0: initial spore count t: time k: rate constant n: reaction order	Margosch et al. 2006
High pressure thermal sterilization (PATS)	Inactivation of *Bacillus amyloliquefaciens* in egg patty mince	$\log N/(N_1 0^{\uparrow m}) = [(bt)]^{\uparrow n}$ *Weibull based equation*	N: number of survivors at time *t* N_0: initial spore count t: time b, n: shape factors	Rajan et al. 2006

High pressure in combination with temperature	Inactivation of *Zygosaccharomyces bailii* in juices	$\ln(k) = a_1 + \frac{\beta_1}{T}(P - P_{ref}) + \frac{\gamma_1}{T}(P - P_{ref})^2 - \frac{\delta_1}{T}(T - T_{ref}) - \frac{\varepsilon_1}{T}\left[T\left(\ln\left(\frac{T}{T_{ref}}\right)\right) + T_{ref}\right] + \frac{\mu}{T}(P - P_{ref})(T - T_{ref})$ *Hawley equation* $\ln(k) = \alpha_2 + \beta_2(P - P_{ref}) + \gamma_2(P - P_{ref})^2 + \delta_2(T - T_{ref}) + \varepsilon_2(T - T_{ref})^2 + \mu_2(P - P_{ref})(T - T_{ref})$ *Quadratic equation*	k: kinetic rate constant P: pressure T: temperature α, β, γ, δ, ε, μ: kinetic parameters	Reyns et al. 2000
Pulsed electric fields	Inactivation of *Escherichia coli* in juices following a non-linear trend	$\log(S) = -\frac{t}{D}$ *Bigelow model* $\ln(S) = -b(\ln t - \ln[(t_c)])$ *Hülsheger model* $ls(S) = -\left(\frac{t}{a}\right)^n$ *Weibull distribution function*	S: survival fraction at time *t* D: Decimal reduction time b: regression coefficient *t*: treatment time t_c: critical treatment time a: scale factor n: shape factor	Rodrigo et al. 2003
Pulsed electric fields	Inactivation of *Lactobacillus plantarum* in buffer and apple juice showing concave upward curves	$\mathrm{Log}_{10}\frac{N_t}{N_0} = -\left(\frac{t}{\delta}\right)^p$ *Weibull distribution*	N_t: microbial population at time *t* N_0: microbial population at time zero *t:* treatment time δ: first decimal reduction time p: shape parameter	Gómez et al. 2005
Pulsed electric fields	Inactivation of *Escherichia coli* in buffer	$S(t) = pe^{-k_1 t} + (1 - p)e^{-k_2 t}$ *Exponential based model* $\mathrm{CFU}(t) = \mathrm{CFU}(0) \times \left(1 + e^{\frac{t-m}{s^2}}\right)^{-1}$ *Sigmoidal equation* $\log_{10}S(t) = -\left(\frac{1}{2.303}\right)\left(\frac{t}{b}\right)^n$ *Weibull based model* $\log_{10}S(t) = -aLn(1 + ct)$ *Empirical equation*	S(t): fraction of survivors t: treatment time p: fraction of survivors in population 1 (1-p): fraction of survivors in population 2 k_1: specific death rate of subpopulation 1 k_2: specific death rate of subpopulation2 CFU: concentration of survivors m: peak of PEF resistance	Alvarez et al. 2003

(*continued*)

Table 13.4 (continued)

Nonthermal technology	Example of inactivation	Mathematical models	Definition of terms	Reference
			s: proportional parameter b, n: shape parameters a, c: parameters for characteristics	
Pulsed electric fields	Inactivation of *Escherichia coli* and *Salmonella enteritidis* in egg yolk using temperature and PEF	$S(t) = e^{-k_T(E)\times t}$ $k_T(E) = k_0 \times e^{\frac{-E_a}{RT}}$ *Arrhenius models*	s(t): fraction of survivors t: treatment duration $k_T(E)$: kinetic rate constant T: treatment temperature E_a: activation energy R: gas constant k_0: constant	Amiali et al. 2007
Pulsed electric fields	Inactivation of *Lactobacillus plantarum* in orange-carrot juice	$s = \frac{100}{1+\exp\left[\frac{E-V_c(n)}{k(n)}\right]}$ *Peleg model*	s: percentage of survivors E: field strength $V_c(n)$: critical value of E (survival level 50%) k(n): parameter indicating steepness of curve	Rodrigo et al. 2001
Pulsed electric fields	Dose–response models based on sigmoid curves	$\frac{X_1}{X_0} = \frac{1}{1+e^{\left(\frac{E-E_C}{k'}\right)}}$ *Fermi's equation*	X_1/X_0: survival fraction E: electric field E_C: critical electric field, to reduce population to 50% k': slope of steepest segment of curve	Lado and Yousef 2002
Ultrasound	Inactivation of *Escherichia coli* in apple cider	$\text{Log}\frac{N}{N_0} = -\left(\frac{1}{2.303}\right)\left(\frac{t}{b}\right)^n$ *Weibull based model*	N_t: microbial population at time *t* N_0: microbial population at time zero *t:* treatment time b, n: shape factors	Ugarte-Romero et al. 2006
Ultrasound	Inactivation of *Listeria innocua* in milk showing a non-linear trend	$\log\left(\frac{N_t}{N_0}\right) = -b \times t^n$ *Weibull distribution* $\log\left(\frac{N_t}{N_0}\right) = k_1 t^{n_1 k_2 t^{n_2}}$	N_t: microbial population at time *t* N_0: microbial population at time zero *t:* treatment time	Bermúdez-Aguirre et al. 2009

		Sigmoid or four-parameter model	b: rate parameter n: shape parameter k_1, k_2, n_1, n_2: constants	
Ultrasound	*Listeria monocytogenes* under manosonication and manothermosonication	$\log D_{ms} = \log D_0 - 0.0091 \times (A - 62)$ $\log D_{ms} = \log D_0 - 0.0026 \times p + 2.2x10^{-6} \times p^2$	D_{ms} = decimal reduction time D_0 = control decimal reduction time A: wave amplitude p: static relative pressure	Pagán et al. 1999
Ultrasound	*Escherichia coli* under sonication in water	$\ln N = N_0 + \frac{k}{m+1} t^{m-1}$	N: microbial population at time *t* N_0: microbial population at time zero k: rate coefficient m: empirical constant	Ince and Belen 2001
Ultrasound	*Saccharomyces cerevisiae* inactivated with ultrasound and low weight chitosan in broth	$\log\left[\frac{CFU_t}{CFU_0}\right] = Ce^{-e(A+Bt)} - Ce^{-e(A)}$ Modified Gompertz equation	$Log[CFU_{(t)}/CFU_{(0)}]$: log surviving fraction A, B, C: different regions of curve	Guerrero et al. 2005
Cold plasma	Inactivation of *Escherichia coli* exposed on surface of membrane filters	$N(t) = N_0 e^{-k \max t\left(\frac{1+C_c(0)}{1+C_c(0)e^{-k \max t}}\right)}$	N(t): cell concentration at time *t* $N_{(0)}$: initial cell concentration k_{max}: maximum inactivation constant $C_c(0)$: initial concentration of critical component	Yu et al. 2006
Dense phase carbon dioxide	Inactivation of *Salmonella typhimurium* in carrot juice	$y = A\exp\{-\exp[\frac{-k_{dm} \times e}{A}(\gamma - t) + 1]\}$ *Gompertz equation* $y = \frac{A}{\left\{1+\exp\left[\frac{-4k_{dm}}{A}(\gamma - t)+2\right]\right\}}$ *Modified logistic equation*	$A(N_{min}/N_0)$: lower asymptote value for time approaching infinity k_{dm}: *i*nactivation rate γ: duration of lag phase t: treatment time	Liao et al. 2010
Ultraviolet light and ozone	Inactivation of *Escherichia coli* and *Salmonella enterica* in raspberries and strawberries	$\log_{10}\left(\frac{N}{N_0}\right) = -\frac{1}{2.303}\left(\frac{t}{\alpha}\right)^{\beta}$ *Weibull based equation*	N/N_0: survivors fraction t: treatment time α: characteristic time β: shape parameter	Bialka et al. 2008

Another equation commonly used to fit the survival data is the Weibullian model; this model has been modified in specific cases according to the experimental procedures and results. Basically, the Weibullian equation represents the distribution of the lethal dose applied to the microorganism (Peleg et al. 1997). The most basic form of this mathematical model is:

$$\frac{\log N}{N_0} = -b \times t^n \tag{13.2}$$

where N is the microbial load at a specific time, N_0 is the microbial count at time zero, t is the treatment time and b and n are called shape factors. The parameter b is related to the velocity of inactivation, while n is the parameter that measures and determines the curve's concavity. According to the value of n, it is possible to determine the concavity of the curve. When $n < 1$ indicates an upward concavity, then the shape of the inactivation curve shows the presence of "tailings"; meanwhile, when $n > 1$ there is a downward concavity showing "shoulders" (Bermúdez-Aguirre et al. 2009).

The Weibullian model has been used for isothermal survival curves, but when the temperature or the lethal agent is different during the whole process (i.e., non-isothermal), then each part of the curve becomes a function of the lethal agent. For example, if the inactivation generated with heat and temperature is not constant, then the Weibullian equation needs to be modified to be a function of momentary temperature, i.e., T(t), and transformed into a differential equation (Peleg et al. 2003) as follows:

$$\frac{dLog_{10}S(t)}{dt} = -b[T(t)]n[T(t)]\left\{\frac{-Log_{10}S(t)}{b[T(t)]}\right\}^{\frac{n[\ T(t)\ ]\ -\ 1}{n[\ T(t)\ ]}} \tag{13.3}$$

where $S(t)$ represents the ratio N/N_0.

Other specific cases have been addressed depending on the microorganism, processing conditions and/or technology. For example, some studies have been conducted on spore inactivation, which differs from vegetative cell inactivation because of the intrinsic properties of the spores. It has been shown that when a specific preservation factor is applied to spores, the inactivation is not feasible in the first minutes of treatment, even though an activation of spores or germination has been reported. In this case, the survival curve shows some concavities, which in most cases represents a "shoulder." Corradini and Peleg (2003) studied this specific case and mentioned an "activation shoulder" that can show an upward concavity, linear trend or downward concavity in the first part of the inactivation curve. This "shoulder" generated in the curve because of the spore activation can be described using three mathematical approaches, as suggested by Corradini and Peleg (2003):

$$Y_1(t) = \frac{t}{k_1 + k_2 t} \tag{13.4}$$

where k_1 and k_2 are constants, t is the treatment time and Y_1 the survival fraction

$$Y_2(t) = 1 - ln\{1 + \exp[b(t - t_c)]\}^m \tag{13.5}$$

where b, m and t_c are constants. Combining both equations, the general model can be written as:

$$\log\left(\frac{N(t)}{N_0}\right) = \frac{t[1 - ln\{1 + \exp[b(t - t_c)]\}^m]}{k_1 + k_2 t} \tag{13.6}$$

Other interesting mathematical approaches have been reported by Peleg and Penchina (2000) where the lethal agent against the microorganism shows a variation in intensity during treatment (heating, cooling, oscillating changes in agent, concentration, etc.) and where some of the "artifacts" during processing (and others mentioned above) are shown in the inactivation curve (i.e., mixed population, effects of the medium, processing conditions) and need to be fitted (Peleg and Cole 1998).

13.10 Final Remarks

This chapter has given a brief update on the development of nonthermal technologies under research. Most of these technologies today are showing interesting results not only in microbial inactivation or reduced enzymatic activity, but also in providing food scientists with new input about product development, including some fascinating new tools for specific operations. These discoveries were made by food scientists trying to inactivate bacteria and enzymes in different foods; after comparing the processed product with the control or untreated sample, they observed specific changes in characteristics such as better color, homogeneity, retention of nutrient or aroma compounds, higher efficiency of specific processes or longer stability in microbial and enzymatic activity.

Right now some of these technologies are being used in combination to enhance specific effects and to provide foods with outstanding quality. Also, consumers are becoming more aware of what foods they are buying at the time of purchase and of the benefits these novel technologies and novel products can offer.

The current challenge of food scientists is to keep searching within these technologies for the solutions to food problems related to spoilage, nutrient degradation and damage to sensorial attributes after processing, but also to explore these new tools in order to offer the consumer new and high quality products at an affordable price, as well as to extend the shelf-life of products to allow interchange around the world. Furthermore, the perception of the consumer regarding long shelf life and freshness of the product could be improved by providing complete information about these technologies.

References

Aguiló-Aguayo I, Oms-Oliu G, Soliva-Fortuny R, Martín-Belloso O (2009a) Flavour retention and related enzyme activities during storage of strawberry juices processed by high-intensity pulsed electric fields or heat. Food Chem 116:59–65

Aguiló-Aguayo I, Soliva-Fortuny R, Martín-Belloso O (2009b) Avoiding non-enzymatic browning by high-intensity pulsed electric fields in strawberry, tomato and watermelon juices. J Food Eng 92:37–43

Aguiló-Aguayo I, Sobrino-López A, Soliva-Fortuny R, Martín-Belloso O (2008a) Influence of high intensity pulsed electric field processing on lipoxygenase and β-glucosidase activities in strawberry juice. Innov Food Sci Emerg Technol 9:455–462

Aguiló-Aguayo I, Odriozola-Serrano I, Quintão-Teixeira J, Martín-Belloso O (2008b) Inactivation of tomato juice peroxidase by high-intensity pulsed electric fields as affected by process conditions. Food Chem 107:949–955

Alkhafaji S, Farid M (2008) Modeling the inactivation of *Escherichia coli* ATCC 25922 using pulsed electric field. Innov Food Sci Emerg Technol 9:448–454

Alothman M, Bhat R, Karim AA (2009) UV-radiation induced changes of antioxidant capacity of fresh-cut tropical fruits. Innov Food Sci emerg Technol 10:512–516

Alvarez I, Virto R, Raso J, Condón S (2003) Comparing predicting models for the *Escherichia coli* inactivation by pulsed electric fields. Innov Food Sci Emerg Technol 4:195–202

Amiali M, Ngadi MO, Smith JP, Raghavan GSV (2007) Synergistic effect of temperature and pulsed electric field on inactivation of *Escherichia coli* O157:H7 and *Salmonella enteritidis* in liquid egg yolk. J Food Eng 79:689–694

Artés-Hernández F, Robles PA, Gómez PA, Tomas-Callejas A, Artés F (2010) Low UV-C illumination for keeping overall quality of fresh cut watermelon. Postharvest Biol Technol 55:114–120

Ashokkumar M, Sunartio D, Kentish S, Mawson R, Simons L, Vilkhu K, Versteeg C (2008) Modification of food ingredients by ultrasound to improve functionality: a preliminary study on a model system. Innov Food Sci Emerg Technol 9:155–160

Avure Technologies. Inc (2010) Kent, WA (Personal communication)

Barbosa-Cánovas GV, Sepúlveda D (2005) Present status and the future of PEF technology. In: Barbosa-Cánovas GV, Tapia MS, Cano MP (eds) Novel food processing technologies. CRC Press, Boca Raton, FL, pp 1–44

Bermúdez-Aguirre D, Corradini MG, Mawson R, Barbosa-Cánovas GV (2009) Modeling the inactivation of *Listeria innocua* in raw whole milk treated under thermo-sonication. Innov Food Sci Emerg Technol 10:172–178

Bialka KL, Demirci A, Puri VM (2008) Modeling the inactivation of *Escherichia coli* O157:H7 and *Salmonella enterica* on raspberries and strawberries resulting from exposure to ozone or pulsed UV-light. J Food Eng 85:444–449

Bizani D, Morrissy JAC, Dominguez APM, Brandelli A (2008) Inhibition of *Listeria monocytogenes* in dairy products using the bacteriocin-like peptide cerein 8A. Int J Food Microbiol 121:229–233

Buchanan RL, Golden MH, Whiting RC, Phillips JG, Smith JL (1994) Non-thermal inactivation models for Listeria monocytogenes. J Food Sci 59(1):179–188

Buckow R, Truong BQ, Versteeg C (2010) Bovine cathepsin D activity under high pressure. Food Chem 120:474–481

Buzrul S, Alpas H, Largeteau A, Bozoglu F, Demazeau G (2008) Compression heating of selected pressure transmitting fluids and liquid foods during high hydrostatic pressure treatment. J Food Eng 85:466–472

Chua SC, Tan CP, Mirhosseini H, Lai OM, Long K, Baharin BS (2009) Optimization of ultrasound extraction condition of phospholipids from palm-pressed fiber. J Food Eng 92:403–409

Clark JP (2002) Thermal and nonthermal processing. Food Technol 56(12):63–64

Clark JP (2008) Variety, novelty characterize processing and nonthermal papers. Food Technol 62(5):116–121
Corradini MG, Peleg M (2003) A theoretical note on estimating the number of recoverable spores from survival curves having an "activation shoulder". Food Res Int 36:1007–1013
Critzer FJ, Kelly-Wintenberg K, South SL, Golden DA (2007) Atmospheric plasma inactivation of foodborne pathogens on fresh produce surfaces. J Food Protect 70:2290–2296
Debs-Louka E, Louka N, Abraham G, Chabot V, Allaf K (1999) Effect of compressed carbon dioxide on microbial cell viability. Appl Environ Microbiol 65:626–631
Deng X, Shi J, Kong MG (2006) Physical mechanisms of inactivation of *Bacillus subtilis* spores using cold atmospheric plasmas. IEEE Trans Plasma Sci 34(4):1310–1316
DTI (2010) Diversified Technologies, Inc. Bedford, Massachusetts (Personal communication)
Evrendilek GA, Tok FM, Soylu EM, Soylu S (2008) Inactivation of *Penicillum expansum* in sour cherry juice, peach and apricot nectars by pulsed electric fields. Food Microbiol 25:662–667
Ferrentino G, Balaban MO, Ferrari G, Poletto M (2010a) Food treatment with high pressure carbon dioxide: *Saccharomyces cerevisiae* inactivation kinetics expressed as a function of CO_2 solubility. J Supercrit Fluid 52(1):151–160
Ferrentino G, Barletta D, Balaban MO, Ferrari G, Poletto M (2010b) Measurement and prediction of CO_2 solubility in sodium phosphate monobasic solutions for food treatment with high pressure carbon dioxide. J Supercrit Fluid 52(1):142–150
Fox MB (2007) Microbial inactivation kinetics of pulsed electric field treatment. In: Lelieveld HLM, Notermans S, de Haan SWH (eds) Food preservation by pulsed electric fields. Woodhead Publishing Limited, Cambridge, England, pp 127–137
Furukawa S, Watanabe T, Koyama T, Hirata J, Narisawa N, Ogihara H, Yamasaki M (2009) Inactivation of food poisoning bacteria and *Geobacillus stearothermophilus* spores by high pressure carbon dioxide treatment. Food Control 20:53–58
Gachovska TK, Adedeji AA, Ngadi MO (2009) Influence of pulsed electric field energy on the damage degree in alfalfa tissue. J Food Eng 95:558–563
Gao YL, Ju XR, Ding W (2007) A predictive model for the influence of food components on survival of *Listeria monocytogenes* LM 54004 under high hydrostatic pressure and mild heat conditions. Int J Food Microbiol 117:287–294
Garcia-Gonzalez L, Geeraerd AH, Elst K, Van Ginneken L, Van Impe JF, Devlieghere F (2009) Influence of type of microorganism, food ingredients and food properties on high-pressure carbon dioxide inactivation of microorganisms. Int J Food Microbiol 129:253–263
Garcia-Gonzalez L, Geeraerd AH, Spilimbergo S, Elst K, Van Ginneken L, Debevere J, Van Impe JF, Devlieghere F (2007) High pressure carbon dioxide inactivation of microorganisms in foods: the past, the present and the future. Int J Food Microbiol 117:1–28
Gómez N, García D, Alvarez I, Raso J, Condón S (2005) A model describing the kinetics of inactivation of *Lactobacillus plantarum* in a buffer system of different pH and in orange and apple juice. J Food Eng 70:7–14
Gómez PL, Alzamora SM, Castro MA, Salvatori DM (2009) Effect of ultraviolet-C light dose on quality of cut apple: microorganism, color and compression behavior. J Food Eng. doi:10.1016/j.jfoodeng.2009.12.008
Gómez-Estaca J, López-Caballero ME, Gómez-Guillén MC, López de Lacey A, Montero P (2009) High pressure technology as a tool to obtain high quality *carpaccio* and *carpaccio*-like products from fish. Innov Food Sci Emerg Technol 10:148–154
Góngora-Nieto M, Sepúlveda DR, Pedrow P, Barbosa-Cánovas GV, Swanson BG (2002) Food processing by pulsed electric fields: treatment delivery, inactivation level, and regulatory aspects. Lebensm-WissTechnol 35:375–388
Guerrero S, Tognon M, Alzamora SM (2005) Response of *Saccharomyces cerevisiae* to the combined action of ultrasound and low weight chitosan. Food Control 16:131–139
Han Z, Zeng XA, Yu SJ, Zhang BS, Chen XD (2009) Effects of pulsed electric fields (PEF) treatment on physicochemical properties of potato starch. Innov Food Sci Emerg Technol 10:481–485

Hoogland H, de Haan W (2007) Economic aspects of pulsed electric field treatment of food. In: Lelieveld HLM, Notermans S, de Haan SWH (eds) Food preservation by pulsed electric fields. Woodhead Publishing Limited, Cambridge/England, pp 257–265

Houŝka M, Strohalm J, Kocurová K, Totuŝek J, Lefnerová D, Tříska J, Vrchotová N, Fiedlerová V, Holasova M, Gabrovská D, Paulíčková I (2006) High pressure and foods-fruit and vegetables juices. J Food Eng 77:386–398

Huang K, Wang J (2009) Designs of pulsed electric fields treatment chambers for liquid foods pasteurization process: a review. J Food Eng 95:227–239

Ince NH, Belen R (2001) Aqueous phase disinfection with power ultrasound: process kinetics and effect of solid catalysts. Environ Sci Technol 35(9):1885–1888

Izquierdo E, Marchioni E, Aoude-Werner D, Hasselmann C, Ennahar S (2009) Smearing of soft cheese with Enteroccus faecium WHE 81. A multi-bacteriocin producer against *Listeria monocytogenes*. Food Microbiol 26:16–20

Jambrak AR, Lelas V, Mason TJ, Krešič G, Badanjak M (2009) Physical properties of ultrasound treated soy proteins. J Food Eng 93:386–393

Kempkes M (2009) Personal communication. Pullman, Washington

Khorshid N, Hossain MdM, Farid MM (2007) Precipitation of food protein using high pressure carbon dioxide. J Food Eng 79:1214–1220

Lado BH, Yousef AE (2002) Alternative food-preservation technologies: efficacy and mechanisms. Microb Infect 4:433–440

Lelieveld H (2005) PEF–A Food Industry's View. In: Barbosa-Cánovas GV, Tapia MS, Cano MP (eds) Novel food processing technologies. CRC Press, Boca Raton, FL, pp 145–156

Liao H, Kong X, Zhang Z, Liao X, Hu X (2010) Modeling the inactivation of *Salmonella typhimurium* by dense phase carbon dioxide in carrot juice. Food Microbiol 27:94–100

Lin HM, Yang ZY, Chen LF (1993) Inactivation of *Leuconostoc dextranicum* with carbon dioxide under pressure. Chem Eng J Biochem Eng J 52:B29–B34

López N, Puértolas E, Condón S, Álvarez I, Raso J (2008a) Application of pulsed electric fields for improving the maceration process during vinification of red wine: influence of grape variety. Eur Food Res Technol 227:1099–1107

López N, Puértolas E, Condón S, Álvarez I, Raso J (2008b) Effects of pulsed electric fields on the extraction of phenolic compounds during the fermentation of most of Tempranillo grapes. Innov Food Sci Emerg Technol 9:477–482

López N, Puértolas E, Condón S, Raso J, Alvarez I (2009a) Enhancement of the extraction of betanine from red beetroot by pulsed electric fields. J Food Eng 90:60–66

López N, Puértolas E, Condón S, Raso J, Alvarez I (2009b) Enhancement of the solid-liquid extraction of sucrose from sugar beet (*Beta vulgaris*) by pulsed electric fields. LWT–Food Sci Technol 42:1674–1680

Ma YQ, Chen JC, Liu DH, Ye XQ (2009) Simultaneous extraction of phenolic compounds of citrus peel extracts: effect of ultrasound. Ultrason Sonochem 16:57–62

Margosch D, Ehrmann MA, Buckow R, Heinz V, Vogel RF, Gänzle MG (2006) High-pressure-mediated survival of Clostridium botulinum and Bacillus amyloliquefaciens endospores at high temperature. Appl Environ Microbiol 72:3476–3481

Martínez Viedma P, Abriouel H, Sobrino-López A, Ben Omar N, Lucas López R, Valdivia E, Martín-Belloso O, Gálvez A (2009) Effect of enterocin AS-48 in combination with high-intensity pulsed electric field treatment against the spoilage bacterium *Lactobacillus diolivorans* in apple juice. Food Microbiol 26:491–496

Mastwijk H (2006) Pulsed power systems for application of pulsed electric fields in the food industry. In: Raso J, Heinz V (eds) Pulsed electric fields technology for the food industry. Springer, New York, pp 223–238

McKellar RC, Lu X (2004) Primary models. In: McKellar RC, Lu X (eds) Modeling microbial responses in food. CRC Press, Boca Raton, FL, pp 21–62

National Center for Food Safety and Technology (2009) NFSCT receives regulatory acceptance of novel food sterilization process. Press release, February 27, 2009. Summit-Argo, IL

Nguyen LT, Tay A, Balasubramaniam VM, Legan JD, Turek EJ, Gupta R (2010) Evaluating the impact of thermal and pressure treatment in preserving textural quality of selected foods. LWT–Food Sci Technol 43:525–534

Nguyen TTT, Guyot JP, Icard-Vernière C, Rochette I, Loiseau G (2007) Effect of high pressure homogenization on the capacity of *Lactobacillus plantarum* A6 to ferment rice/soybean slurries to prepare high energy density complementary food. Food Chem 102:1288–1295

Nielsen HB, Sonne AM, Grunert KG, Banati D, Pollák-Tóth A, Lakner Z, Olsen NV, Žontar TP, Peterman M (2009) Consumer perception of the use of high-pressure processing and pulsed electric field technologies in food production. Appetite 52:115–126

Niemira BA, Sites J (2008) Cold plasma inactivates *Salmonella* Stanley and *Escherichia coli* O157:H7 inoculated on golden delicious apples. J Food Protect 71(7):1357–1365

Odriozola-Serrano I, Soliva-Fortuny R, Gimeno-Añó V, Martín-Belloso O (2008) Modeling changes in health-related compounds of tomato juice treated by high-intensity pulsed electric fields. J Food Eng 89:210–216

Odriozola-Serrano I, Soliva-Fortuny R, Hernández-Jover T, Martín-Belloso O (2009) Carotenoid and phenolic profile of tomato juices processed by high intensity pulsed electric fields compared with conventional thermal treatments. Food Chem 112:258–266

Ogihara H, Yatuzuka M, Horie N, Furukawa S, Yamasaki M (2009) Synergistic effect of high hydrostatic pressure treatment and food additives on the inactivation of *Salmonella* enteritidis. Food Control 20:963–966

Oms-Oliu G, Odriozola-Serrano I, Soliva-Fortuny R, Martín-Belloso O (2009) Effects of high-intensity pulsed electric field processing conditions on lycopene, vitamin C and antioxidant capacity of watermelon juice. Food Chem 115:1312–1319

Pagán R, Mañas P, Raso J, Condón S (1999) Bacterial resistance to ultrasonic waves under pressure (manosonication) and lethal (manothermosonication) temperatures. Appl Environ Microbiol 65(1):297–300

Parton T, Bertucco A, Elvassore N, Grimolizzi L (2007a) A continuous plant for food preservation by high pressure CO_2. J Food Eng 79:1410–1417

Parton T, Elvassore N, Bertucco A, Bertoloni G (2007b) High pressure CO_2 inactivation of food: a multi-batch reactor system for inactivation kinetic determination. J Supercrit Fluid 40:490–496

Patazca E, Koutchma T, Balasubramaniam VM (2007) Quasi-adiabatic temperature increase during high pressure processing of selected foods. J Food Eng 80:199–205

Patil S, Bourke P, Kelly B, Frías JM, Cullen PJ (2009) The effects of acid adaptation on *Escherichia coli* inactivation using power ultrasound. Innov Food Sci Emerg Technol 10:486–490

Patist A, Bates D (2008) Ultrasonic innovations in the food industry: from the laboratory to commercial applications. Innov Food Sci Emerg Technol 9:147–154

Peleg M (2000) Microbial survival curves – the reality of flat "shoulders" and absolute thermal death times. Food Res Int 33:531–538

Peleg M, Cole M (1998) Reinterpretation of microbial survival curves. Crit Rev Food Sci 38(5):353–380

Peleg, M., Normand, M.D., and Campanella, O.H (2003) Estimating microbial inactivation parameters from survival curves obtained under varying conditions – the linear case. Bull Math Biol 65:219–234

Peleg M, Normand MD, Damrau E (1997) Mathematical interpretation of dose-response curves. Bull Math Biol 59(4):747–761

Peleg M, Penchina CM (2000) Modeling microbial survival during exposure to a lethal agent with varying intensity. Crit Rev Food Sci 40(2):159–172

Perni S, Liu DW, Shama G, Kong MG (2008a) Cold atmospheric plasma decontamination of the pericarps of fruit. J Food Protect 71(2):302–308

Perni S, Shama G, Kong MG (2008b) Cold atmospheric plasma disinfection of cut fruit surfaces contaminated with migrating microorganisms. J Food Protect 71(8):1619–1625

Pinto AL, Fernandes M, Pinto C, Albano H, Castilho F, Teixeira P, Gibbs P (2009) Characterization of anti-Listeria bactericoins isolated from shellfish: potential antimicrobials to control non-fermented seafood. Int J Food Microbiol 129:50–58

Puértolas E, López N, Condón S, Raso J, Alvarez I (2009) Pulsed electric fields inactivation of wine spoilage yeast and bacteria. Int J Food Microbiol 130:49–55

Puértolas E, López N, Saldaña G, Alvarez I, Raso J (2010) Evaluation of phenolic extraction during fermentation of red grapes treated by a continuous pulsed electric fields process at pilot-plant scale. J Food Eng. doi:10.1016/j.foodeng.2009.12.017

Rajan S, Ahn J, Balasubramaniam VM, Yousef AE (2006) Combined pressure-thermal inactivation kinetics of *Bacillus amyloliquefaciens* spores in egg patty mince. J Food Protect 69(4):853–860

Rastogi NK, Raghavarao SMS, Balasubramaniam VM, Niranjan K, Knorr D (2007) Opportunities and challenges in high pressure processing of foods. Crit Rev Food Sci 47:69–112

Reyns KMFA, Soontjens CCF, Cornelis K, Weemaes CA, Hendrickx ME, Michiels CW (2000) Kinetic analysis and modeling of combined high-pressure-temperature inactivation of the yeast *Zygosaccharomyces bailii*. Int J Food Microbiol 56:199–210

Riener J, Noci F, Cronin DA, Morgan DJ, Lyng JG (2008) Combined effect of temperature and pulsed electric fields on apple juice peroxidase and polyphenoloxidase inactivation. Food Chem 109:402–407

Rodrigo D, Barbosa-Cánovas GV, Martínez A, Rodrigo M (2003) Weibull distribution function on an empirical mathematical model for inactivation of *Escherichia coli* by Pulsed electric fields. J Food Protect 66(6):1007–1012

Rodrigo D, Martínez A, Harte F, Barbosa-Cánovas GV, Rodrigo M (2001) Study of inactivation of *Lactobacillus plantarum* in orange-carrot juice by means of pulse electric fields: comparison of inactivation kinetics models. J Food Protect 64(2):259–263

Saucedo-Reyes D, Marco-Celdrán A, Pina-Pérez MC, Rodrigo D, Martínez-López A (2009) Modeling survival of High Hydrostatic Pressure treated stationary- and exponential- phase *Listeria innocua* cells. Innov Food Sci Emerg Technol 10:135–141

Selcuk M, Oksuz L, Basaran P (2008) Decontamination of grains and legumes infected with *Aspergillus* spp. and *Penicillum* spp. by cold plasma treatment. Bioresource Technol 99:5104–5109

Selma MV, Allende A, López-Gálvez F, Conesa MA, Gil MI (2008) Disinfection potential of ozone, ultraviolet-C and their combination in wash water for the fresh cut vegetable industry. Food Microbiol 25:809–814

Sloan E (2010) What, when, and where America Eats. Food Technol 64(1):34–40

Soliva-Fortuny R, Balasa A, Knorr D, Martín-Belloso O (2009) Effects of pulsed electric fields on bioactive compounds in foods: a review. Trends Food Sci Technol 20:544–556

Tabilo-Munizaga G, Barbosa-Cánovas GV (2004) Color and textural parameters of pressurized and heat-treated surimi gels as affected by potato starch and egg white. Food Res Int 37(8):767–775

Tabilo-Munizaga G, Barbosa-Cánovas GV (2005) Pressurized and heat-treated surimi gels as affected by potato starch and egg white:microstructure and water-holding capacity. LebensmWissTechnol 38(1):47–57

Taniguchi M, Ishiyama Y, Takata T, Nakanishi T, Kaneoke M, Watanabe K, Yanagida F, Chen Y, Kouya T, Tanaka T (2009) Growth-inhibition of hiochi bacteria in namazake (raw sake) by bacteriocins from lactic acid bacteria. J Biosci Bioeng. doi:10.1016/j.jbiosc.2009.11.015

Tiwari BK, Patras A, Brunton N, Cullen PJ, ÓDonell CP (2010) Effect of ultrasound processing in anthocyanins and color or red grape juice. Ultrason Sonochem 17:598–604

Torres JA, Velazquez G (2005) Commercial opportunities and research challenges in the high pressure processing of foods. J Food Eng 67:95–112

Ugarte-Romero E, Feng H, Martin SE, Cadwallader KR, Robinson SJ (2006) Inactivation of *Escherichia coli* with power ultrasound in apple cider. J Food Sci 71(2):E102–E108

Valdramidis VP, Cullen PJ, Tiwari BK, ÓDonnell CP (2010) Quantitative modeling approaches for ascorbic acid degradation and non-enzymatic browning of orange juice during ultrasound processing. J Food Eng 96:449–454

Vilkhu K, Mawson R, Simons L, Bates D (2008) Applications and opportunities for ultrasound assisted extraction in the food industry – a review. Innov Food Sci Emerg Technol 9:161–169

Virot M, Tomao V, Le Bourvellec C, Renard CMCG, Chemat F (2009) Towards the industrial production of antioxidants from food processing by-products with ultrasound-assisted extraction. Ultrason Sonochem. doi:10.1016/j.ultsonch.2009.10.015

Wilson DR, Dabrowski L, Stringer S, Moezelaar R, Brocklehurst TF (2008) High pressure in combination with elevated temperature as a method for the sterilization of food. Trends Food Sci Technol 19:289–299

Yu H, Perni S, Shi JJ, Wang DZ, Kong MG, Shama G (2006) Effects of cell surface loading and phase of growth in cold atmospheric gas plasma inactivation of *Escherichia coli* K12. J Appl Microbiol 101:1323–1330

Chapter 14
High-Pressure-Induced Effects on Bacterial Spores, Vegetative Microorganisms, and Enzymes

Dietrich Knorr, Kai Reineke, Alexander Mathys, Volker Heinz, and Roman Buckow

14.1 Introduction

Pressures currently used in the food industry range from tens of MPa in common homogenizers or supercritical fluid extractors to up to 400 or 800 MPa in ultra high pressure homogenizers or high pressure (HP) pasteurization units, respectively. Laboratory sized HP research units can reach up to 1,400 MPa and temperatures up to 200°C (Reineke et al. 2008). These HP units are principally used for the inactivation of vegetative microorganisms to extend shelf life of the treated food. However, there are numerous other interesting food applications for HP such as food structure engineering (Knorr 2002; Rumpold 2005; Diels and Michiels 2006; Knorr et al. 2006; Sharma and Yadav 2008), enhanced food quality (Ludikhuyze et al. 2002b; Trejo Araya et al. 2007), stress response utilization (Ananta and Knorr 2004; Bothun et al. 2004; Kato et al. 2007; Pavlovic et al. 2008), or control of bioconversion reactions (Knorr et al. 2006; Picard et al. 2006).

D. Knorr (✉) and K. Reineke
Department of Food Biotechnology and Food Process Engineering, Berlin University of Technology, Koenigin-Luise-Str. 22, D-14195 Berlin, Germany
e-mail: dietrich.knorr@tu-berlin.de, k.reineke@tu-berlin.de

A. Mathys
Department of Food Biotechnology and Food Process Engineering, Berlin University of Technology, Koenigin-Luise-Str. 22, D-14195 Berlin, Germany
and
Nestlé Research Center, Food Science and Technology Department, Vers-chez-les-Blanc, P.O. Box 44, CH-1000 Lausanne 26, Switzerland
e-mail: Alexander.Mathys@rdls.nestle.com

V. Heinz
German Institute of Food Technology, Prof.-von-Klitzing-Str. 7, D-49601 Quakenbrueck, Germany
e-mail: V.Heinz@dil-ev.de

R. Buckow
CSIRO Food and Nutritional Sciences, 671 Sneydes Road, Werribee VIC-3030, Australia
e-mail: Roman.Buckow@csiro.au

J.M. Aguilera et al. (eds.), *Food Engineering Interfaces*, Food Engineering Series,
DOI 10.1007/978-1-4419-7475-4_14,

The majority of isostatic HP application in the food industry is the pasteurization of foods at ambient temperature. This principle was first reported by Hite (1899), who achieved an extended shelf life of bovine milk after HP treatment. Furthermore, Bridgman (1914) reported that HP could coagulate egg albumin producing gels different from those obtained by heat coagulation. In addition, he presented an extensive dataset for the phase diagram of pure water under pressure (Bridgman 1912). Since the early 1980s, growing consumer demand for minimally processed, fresh-like, safe, and high quality food products has triggered research efforts in the field of alternative food processing technologies (Hendrickx and Knorr 2002). The application of HP has been evaluated as a promising food processing alternative to classical heat treatment technologies in several studies (Heinz and Knorr 1998) and consequently, a first industrial HP application for the commercial preservation of food was installed in Japan in 1991 (Yaldagard et al. 2008). Because of further extensive research, HP technology was extended to a broad range of products and the number of industrial HP systems for food pasteurization has steadily increased during the past 10 years.

At present, there are more than 156 industrial scale installations with a maximum volume of 687 L in use worldwide with an annual production of 300,000 t pasteurized products (Tonello Samson 2010, NC Hyperbaric, Spain, personal communication).

In order to inactivate bacterial and fungal spores, a combination of HP and elevated initial temperature ($>80°C$) seems to be a promising improvement to traditional heat sterilization. Combined HP and heat treatments can result in a sterilized food product with reduced thermal load and consequently higher nutritional quality and functionalities (Heinz and Knorr 2002).

Extensive research in this field was carried out during the last decade by various research institutes such as the University of Connecticut, the Technische Universität Berlin, the University of Delaware, CSIRO Food and Nutritional Science Australia, the Ohio State University, and the National Center for Food Safety and Technology. These research efforts enabled the Food and Drug Administration (FDA) of the United States to certify a pressure assisted thermal sterilization (PATS) process in February 2009. However, this promising sterilization technology has not been implemented on an industrial scale, yet.

14.2 High Pressure Thermal Sterilization

The advantage of isostatic HP is the instantaneous and uniform application of pressure to the product without any delay. During pressure build-up, adiabatic heating triggers a thermo-physical effect leading to a temperature increase of the pressure transmitting medium and the product. Ambient preheating combined with the compression heating during pressure build-up allows the food to reach sterilization conditions within a short time. During the dwell time, the denaturation of proteins (e.g., enzymes) and a significant reduction of microorganisms were observed, without affecting molecular bonds or inhibiting some chemical reactions. For example, Maillard reactions, which

can produce off-flavors or the destruction of vitamins can be reduced under HP conditions (Heremans 2002; Indrawati et al. 2005).

In addition to enhanced product quality and functionality, the HP sterilization process needs to ensure the microbial safety. Currently, the commercial sterility of low-acid (pH $>$ 4.5) canned foods is often realized by conventional heat processing, in order to achieve a non-refrigerated, shelf-stable product. Sterilization of food products includes the inactivation of yeasts, fungi, viruses, vegetative microbial cells, and spores. Bacterial endospores require special attention, because of their high resistance to wet and dry heat, freezing and thawing, chemical agents, disinfectants, irradiation, and pressure (Setlow 2003). This high resistance is attributed to a number of unique features of the dormant spore: the low spore core water content, in which water is supposed to be free but highly viscous and incorporated into a three-dimensional molecular matrix in dormant spores (De Vries 2006); the thick peptidoglycan layer called the cortex; the low permeability of the inner spore membrane to hydrophilic molecules; the high level of dipicolinic acid (DPA) as well as high levels of minerals (e.g., Ca^{2+}) (Setlow 2003).

Long treatment times required to achieve "commercial" sterility cause unwanted chemical and physical changes of the food. Consequently, intensive research on the HP-combined thermal inactivation of microbial spores has been carried out in the past. During the last several decades, two different approaches for the inactivation of bacterial spores were investigated. One is the pressure-induced (150 MPa $< p <$ 400 MPa) germination of bacterial endospores (Gould and Sale 1970) at ambient temperature, with a subsequent mild thermal treatment to inactivate the germinated and hence temperature sensitive spores (Heinz and Knorr 1998; Wuytack et al. 1998; Paidhungat et al. 2002). A disadvantage of this procedure is, that spores in the super dormant state are not activated by pressure (Margosch et al. 2004) and even repeated cycles of pressure and heat treatment were applied (Hayakawa et al. 1994b; Meyer 2000), but failed to achieve commercial food sterility. Another approach to HP food sterilization is the combination of HP with high temperatures. This combination of HP at elevated temperatures (70–100°C) inactivates most of the spores that normally survive heat pasteurization processes (Ananta et al. 2001; Ardia et al. 2004b; Margosch et al. 2006; Mathys et al. 2009).

14.2.1 Development and Application of Temperature Controlled Spore Inactivation

In contrast to conventional heat processing, where convective heating causes significant temperature gradients in the product, all volume elements in an HP vessel are subjected to the same pressure at the same time due to the isostatic principle of pressure transmission (Ting et al. 2002; Rastogi et al. 2007; Heinz et al. 2009).

Since pressure and temperature are closely connected physical parameters, the thermodynamic effect of the adiabatic heating, which occurs during the compression and decompression of the treated food and the pressure transmitting media,

has to be taken into account. Following the first and the second law of thermodynamics and a rearrangement of the Maxwell equations, heating during the compression and cooling during the decompression can be described as a function of thermo-physical properties of the compressible product (Perry 1984; Ardia et al. 2004; Reineke et al. 2008). This quasi adiabatic heating or cooling occurs instantly. Hence, pressure-induced temperature changes are predictable and relatively uniform within the food product. Thus, compression heating and decompression cooling may be utilized to achieve a rapid and uniform heating and cooling of the product. Typically, an ideal adiabatic process does not occur in practical applications, but the extent of temperature increase could be estimated within 3–9°C per 100 MPa depending on the thermo-physical properties of the food (Ting et al. 2002). Based on the assumption that the heat resistance of bacterial spores under HP conditions is similar to or lower than at atmospheric pressure, the adiabatic heat of compression could be used to reduce the heating and cooling times of a thermal sterilization process (De Heij et al. 2003).

High pressure thermal sterilization (HPTS) has not yet been successfully applied in the food industry, possibly because of the lack of knowledge on the involved inactivation mechanisms of bacterial spores. Hence, new methodologies for a detailed investigation of the heat and pressure effects on bacterial spores are required. Reineke et al. (2008) described an innovative micro HP unit that is capable of reaching isothermal and isobaric conditions in the range of 50–130°C and up to 1,400 MPa within a few seconds (Fig. 14.1). This is advantageous for the investigation of inactivation kinetics, e.g., of bacterial spores or enzymes, under isothermal/isobaric conditions, which could possibly allow a deeper insight into the underlying inactivation mechanisms. The high compression rates were achieved by

Fig. 14.1 Stansted Mini Foodlab *FBG* 5620 high pressure unit with heating/cooling system

combining a gas-filled pressure accumulator and an internal intensifier, which enabled a maximum compression rate of 250 MPa s^{-1}. The installed heating/cooling system allowed a maximum heating rate of 6 K s^{-1} and was controlled by a proportional-integral-derivate (PID) controller, which was implemented into the control software. The control software facilitated a nearly ideal adiabatic pressure build-up phase and isothermal dwell times by calculation of the adiabatic heating of water at the corresponding pressure and preheating conditions. Inactivation kinetics of *Geobacillus stearothermophilus* spores, a commercial sterilization indicator, were investigated in the pressure-temperature range of 600–1200 MPa and 90–120°C in a pressure stable ACES-buffer solution (pH 7) (Mathys 2008). Under dynamic pressure-temperature conditions during the compression and decompression phase (1 s dwell time), a 1–3 $\log_{10}$ reduction of viable spores was observed. During isothermal and isobaric dwell times, microbial inactivation followed a nearly linear $\log_{10}$-inactivation behavior. This dataset covers the combined effects of pressure and temperature on the inactivation of *Geobacillus stearothermophilus* spores and provides the basis for generating a p-T diagram for spore inactivation with isorate lines for a fixed spore inactivation. The n^{th}-order approach has proven to be suitable to describe inactivation kinetics with tailing, which is often found for the inactivation of vegetative microorganisms, bacterial spores, and enzymes during HP treatment.

Based on data obtained for isobaric and isothermal treatment conditions, an empirical model, which is an analog to the n^{th}-order approach for chemical degradation reactions, was used:

$$\log\frac{N}{N_0} = \frac{1}{1-n}\log\left(1 + k \cdot N_0^{(n-1)} \cdot t \cdot (n-1)\right) \tag{14.1}$$

where N and N_0 denotes the spore counts (CFU mL^{-1}) at time t and t_0, respectively; t = time, k = inactivation rate constant, and n = reaction order. Analysis of the inactivation kinetics revealed that all experimental data could be fitted best with a fixed reaction order of $n = 1.05$.

To obtain a functional relationship of the rate constant k with pressure and temperature, empirical equations (e.g., Eq. 14.2) have often been suggested for bacterial spore inactivation data (Ardia et al. 2004; Margosch et al. 2006):

$$\begin{aligned}\ln(k) = {} & A + B(p-p_0) + C(T-T_0) + D(p-p_0)^2 + E(T-T_0)^2 \\ & + F(p-p_0)(T-T_0) + \text{higher order terms}\end{aligned} \tag{14.2}$$

Values for the parameters A-J for *Geobacillus stearothermophilus* spores (Mathys 2008) were estimated as:

$$\mathrm{A} = -96.71, \mathrm{B} = -0.02,\ \mathrm{C} = 2.65,\ \mathrm{D} = -2.92, \mathrm{E} = -0.02,\ \mathrm{F} = 9.45 \times 10^{-4},$$
$$\mathrm{G} = 1.25 \times 10^{-8}, \mathrm{H} = 9.33 \times 10^{-5}, \mathrm{I} = -3.87 \times 10^{-6}, \mathrm{J} = -6.52 \times 10^{-8}$$

Using Eq. (14.2), pressure-temperature isorate lines of spore inactivation can be calculated for any pressure dwell time and facilitate the presentation of the survival data in a pressure and temperature diagram. Based on the assumption of a nearly linear $\log_{10}$ reduction under isothermal/isobaric conditions, in addition to the nth order ($n = 1.05$), a traditional first-order inactivation ($n = 1$) was modeled in the *p-T* landscape (Fig. 14.2a). This first order p-T diagram allows the calculation of increased $\log_{10}$ reduction, just by multiplying the isorate lines by the same value. Inactivation studies showed the highest heat sensitivity of *G. stearothermophilus* spores at approximately 700 MPa, whereas higher pressures caused a stabilization of the spores against inactivation at the same treatment temperature (Fig. 14.2a). Similar results were found for *Bacillus amyloliquefaciens* (Margosch et al. 2006; Rajan et al. 2006) and other strains of *G. stearothermophilus* spores (Ardia 2004).

Ardia (2004) investigated the impact of the dissociation equilibrium shift in ACES and PBS buffer on the inactivation of bacterial spores and concluded that the equilibrium shift is not the main source of the observed heat stabilization of *G. stearothermophilus* spores under pressure. The author compared the behavior of cortex lytic enzymes (CLEs) in the spore coat under HP with the behavior of bacterial spores. CLEs catalyze the cortex break down and therefore are responsible for the access of water to the spore core. It was assumed, that the CLEs are inactivated in a certain range of pressure-temperature conditions. At this stage, only a further temperature increase accelerates spore inactivation, and consequently a further pressure increase would have no effect. With inactive CLEs, the spore cortex can only be rehydrated by ultra high pressure, and hence pressures higher than 800 MPa could squeeze water inside of the spore cortex (Ardia 2004) causing an pressure generated increased heat sensitivity of the spore. On the contrary, Margosch et al. (2006) proposed that bacterial spores are very complex, and that

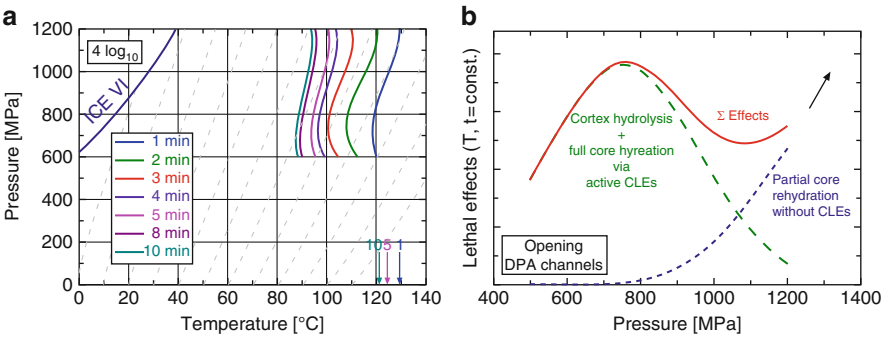

Fig. 14.2 (**a**) Isorate lines for a 4 $\log_{10}$ inactivation of *Geobacillus stearothermophilus* spores in pressure stable 0.05 M *ACES* buffer (pH 7) after 1–10 min treatment at isothermal/isobaric conditions with N (1 s) as initial population N_0. Data for thermal inactivation are shown as arrows with holding times in minutes. Dashed lines indicate the adiabatic heating of water. (**b**) Suggested summed lethal effects at different pressure levels with two generated lethal effect distributions, A (*green dashes*) and B (*blue dots*), showing different germination reactions at given process intensity. All lethal effects resulted in the cumulative distribution ($\sum$ Effects) with a sensitive and stabilized zone (Mathys et al. 2009)

a single protein or enzyme can only be responsible for stabilization under pressure, if it is required for a vital function of the vegetative cell (e.g., as a structural or protective component).

Based on Setlow's (2003) germination model for *Bacillus subtilis* spores, an extended inactivation mechanism of *G. stearothermophilus* spores at different pressure-temperature conditions was proposed by Mathys et al. (2009). The mechanism includes a stable and sensitive domain for the spores in the pressure and temperature landscape (Fig. 14.2). The germination mechanism is initiated by an opening of the dipicolinic acid (DPA) channels at pressures higher than 500 MPa, which enables spore germination in the absence of nutrients (Paidhungat et al. 2002). At these HP conditions, the spore germination is limited in buffer solutions. The key factor for full cortex hydrolysis and core hydration is the activation of the main CLEs. These enzymes probably show different activities or stabilities under specific pressure and temperature conditions, generating different pathways of inactivation. Heinz and Knorr (1998) assumed that pressure and temperature initially triggers the CLEs, but inactivates the same enzymes at a later stage. Hence, the CLE activity is dependent on pressure, temperature, and time. At ultra HPs a partial core rehydration without any CLE activity could induce an additional lethal effect (Setlow 2003). Summarizing all competing reactions, a cumulative lethal effect distribution as a function of the applied pressure level can be generated ($\sum$ Effects, Fig. 14.2b). However, the mechanisms of spore inactivation at HPTS are still not fully understood, and further research is needed to identify the components in bacterial endospores, that are most pressure sensitive and hence provide a fast and complete inactivation by HPTS.

14.2.2 Industrial Relevance and Applications

Currently, industrial HPTS equipment exists with volumes up to 150 L, 700 MPa maximum working pressure, and initial temperatures of up to 95°C (Heinz 2010). The industrial relevance of this study can be exemplified by implementing the generated data into process charts of an industrial scale HPTS unit (Fig. 14.3). One of the few existing pilot systems is the Flow Pressure Systems QUINTUS (Food Press Type; 35 L, 600 MPa) sterilization machine (Avure Technologies, Kent, WA, USA), which is described elsewhere in the literature (Knoerzer et al. 2007). In Fig. 14.3a and 14.3b (location two is near top closure; Knoerzer et al. 2007), two different pressure and temperature profiles from an HPTS process with (10 L) and without (35 L) a polytetrafluoroethylene (PTFE) carrier are shown. Temperature decrease and inhomogeneities during the dwell time can be reduced, when an insulating carrier is used (Juliano et al. 2009). Alternative possibilities to ensure a homogenous temperature during dwell time would be the application of an internal heater or heating of the vessel wall to an appropriate temperature level, that minimizes the temperature gradient between pressure vessel and treated product (Ardia 2004). In Fig. 14.3b the target inactivation level of -4 $\log_{10}$ can be varied,

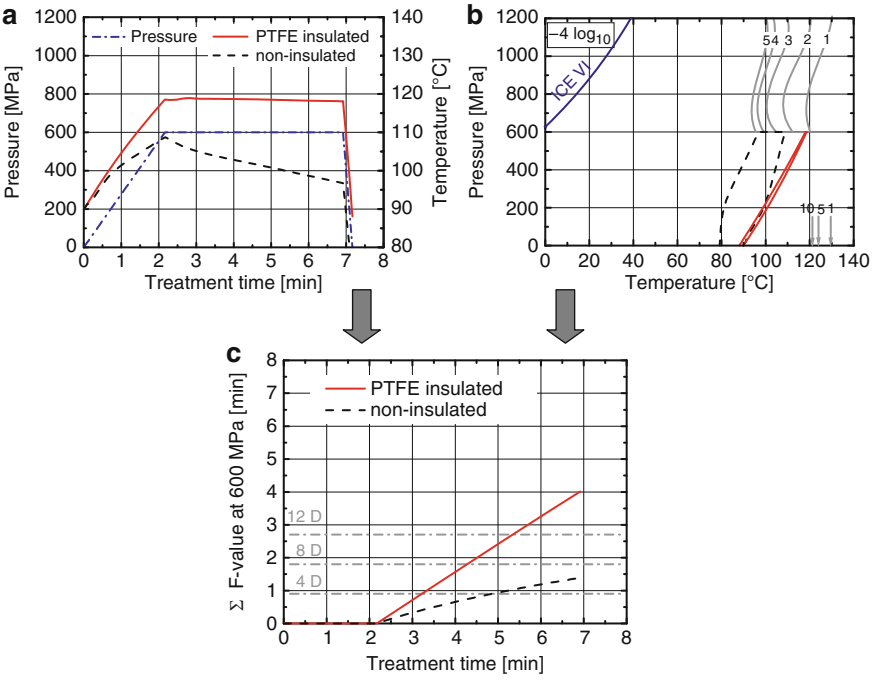

Fig. 14.3 Industrial process analysis of a vertical 35 L vessel (--, black) and with a 10 L insulated carrier (–, red), using an F-value (**c**) (14.3), $T_{\text{ref}} = 121.1°\text{C}$, $z_{600\text{MPa}} = 35.36°\text{C}$, $D_{121.1°\text{C}} = 13.52$ s at 600 MPa in 0.05 M ACES buffer (pH 7), and pressure holding times $T(t)_p$. Pressure and temperature profiles (**a**) were taken from the literature (Knoerzer et al. 2007). The desired inactivation level of (**b**) can be varied by multiplying the dwell times of the isorate lines with the same value (Mathys et al. 2009)

because of a first-order kinetic approach. Process conditions were as follows: 90°C initial temperature, 600 MPa final process pressure, and 285 s dwell time with water as pressure transmitting medium (Knoerzer et al. 2007). Using a modified $F_{121.1°\text{C}}$-value concept for the thermal inactivation of *G. stearothermophilus* spores (Eq. 14.3) in Fig. 14.3c,

$$F = \int_0^t 10^{\frac{T(t)_p - T_{ref}}{Z_{600MPa}}} \mathrm{d}t = D_{ref} \log_{10}\left(\frac{N}{N_0}\right) \tag{14.3}$$

where reference temperature T_{ref} is 121.1°C, $T(t)_p$ is the dwell time; $z_{600\text{MPa}} = 35.36°\text{C}$, $D_{121.1°\text{C}} = 13.52$ s at 600 MPa; N_0 is the initial count, and N is the survival count. Both processes, with or without insulating carrier, can be adequately analyzed and compared.

In thermal processes the F-value is the accumulated lethality expressed as an equivalent time at a specific reference temperature (T_{ref}) with a specific z-value.

The F_0 concept is accepted for the thermal sterilization in the food industry for the case where T_{ref} is 121.1°C, the $D_{121.1°C}$ – value is 13.8 s (for *Clostridium botulinum*), and z-value is approximately 10°C (Stone et al. 2009). In contrast to conventional thermal processes at ambient pressure with an expected $z_{0.1MPa} = 10°C$ for spore inactivation, the z-value at 600 MPa (z_{600MPa}= 35.36°C for *G. sterothermophilus*) was higher (Mathys et al. 2009), resulting in a lower temperature dependence of the inactivation reaction rate. Because of the pressure dependence of the z-value, preheating as well as compression and decompression phases could not be included in the calculation of the spore inactivation level of *G. sterothermophilus*. However, the additional processing time can be considered a safety factor. Using a PTFE carrier, commercial sterility (>12 D) could be achieved within 3 min dwell time at 600 MPa and 90°C initial temperature (Mathys 2008). An alternative process for a HPTS unit with a 55 L horizontal vessel, 700 MPa working pressure, and 95°C initial temperature was also calculated by Mathys et al. (2008) (data not shown). He concluded that more than 12 $\log_{10}$ inactivation of *G. stearothermophilus* spores can be achieved in this machine without any insulation within 3 min at 700 MPa.

14.3 HP Effects on Vegetative Microorganisms and Enzymes

The specific effects of pressure on vegetative microorganisms are complex and cannot be evaluated separate from simultaneous occurring heat effects. Primarily, the lethal effects of HP on vegetative microorganisms are attributed to the inactivation of essential cell enzymes and the rupture of the cell membrane (Ardia 2004; Ananta 2005). In the course of identifying mechanisms behind this pressure-induced inactivation, it was found that flow cytometry is a powerful tool to gain insight into the states and mechanisms of cell damage of pressurized vegetative microorganisms and bacterial spores (Ananta 2005; Black et al. 2006; Mathys et al. 2007). However, pressure treatments do not necessarily weaken biological cells. At low pressure levels, stabilization of microbial cells was observed; for example, pressure-induced thermo-tolerance of lactic acid bacteria occurs after HP treatment between 100 and 200 MPa (Ananta and Knorr 2003). As a result of this phenomenon, pressure-induced stress response was regarded as a promising processing option, such as pretreatment of bacteria before spray drying or freezing for the purpose of starter culture production.

Microbial inactivation of more than five log cycles in food products has been reported by several authors to occur at pressures between 300 and 800 MPa (Henrickx and Knorr 2002; Ananta et al. 2005; Lori et al. 2007). The special shape of isorate lines in the HP-temperature landscape (Fig. 14.4), especially for the inactivation of microorganisms, shows synergisms between pressure and temperature. This behavior is typical for vegetative cells, but was also observed for bacterial spores (Heinz and Knorr 2002; Ardia 2004; Margosch et al. 2006), viruses (Isbarn et al. 2007; Buckow et al. 2008), and proteins (Heinz and Kortschack 2002; Smeller 2002) (Fig. 14.4). Increasing the process temperature allows the decrease

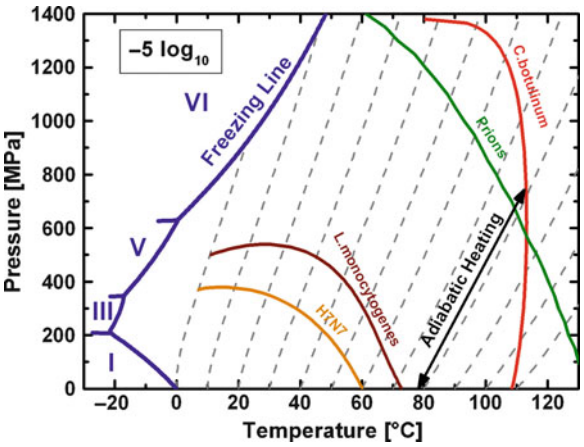

Fig. 14.4 Pressure-temperature isorate diagram showing a 5 $\log_{10}$ reduction of microorganisms, prions, and viruses after a 4 min isothermal/isobaric treatment, with dashed lines (--) indicating adiabatic heating of water; for H7N7, surrogate for bird flu virus H5N1 (in chicken meat slurry) (Isbarn et al. 2007), *Listeria monocytogenes* 75903 (in ham slurry) (Lori 2008), prions-PrP^{SC} (in raw meat) (Heinz and Kortschack 2002), and *Clostridium botulinum* spores (in TRIS buffer pH 5.15) (Margosch et al. 2006). The blue line represents the freezing line between liquid water and the different pressure-dependent ice modifications

of the applied pressure to achieve similar inactivation rates. However, unwanted reactions also occur at moderate temperatures and elevated pressures, for example the activation or insufficient inactivation of quality degrading enzymes, have to be taken into account in these cases.

According to Smelt et al. (2001), the HP induced effects, resulting in the death of vegetative cells, can be summarized as follows:

- *Proteins and enzymes:* HP induces unfolding of globular proteins. It is assumed that the combined, complete or partial inactivation of numerous enzymes and metabolic pathways leads to the inability to proliferate or cell death, respectively (Bunthof 2002).
- *Membranes:* Membrane damage is considered as one of the key events related to microbial cell death. Membranes undergo phase transitions and solidify under pressure and perturbations are promoted (Schlueter et al. 2004). In addition, pressure can lead to the detachment or inactivation of membrane proteins (Ulmer et al. 2002).
- *Ribosomes:* The disintegration of ribosomes in their subunits is promoted by pressure and may cause cell death (Niven et al. 1999).
- *pH:* The maintenance of intracellular pH is crucial for the survival of microbial cells. Some authors attribute cell death predominantly to intracellular pH changes, which are related to the inactivation of enzymes controlling the cell acidity (Molina-Gutierrez et al. 2002).

Given that HP is regarded as a mild process, the primary structure of proteins is not affected. However, pressure can have a deep impact on hydrophobic interactions, which stabilize the quaternary, tertiary, and secondary structure through reversible or irreversible unfolding, respectively. Generally, pressure induces reversible changes in proteins and enzymes between 100 and 300 MPa near room temperature, whereas pressure above 400 MPa can lead to an irreversible unfolding of a protein and thus an inactivation of enzymes. Pressure also favors the unfolding of protein chains as well as a dissociation of oligomeric proteins (Tauscher 1995; Buckow 2006).

Due to conformational changes, unfolding of an enzyme can alter its functionality, resulting in a decreased or increased catalytic activity or change in substrate specificity (Ludikhuyze et al. 2002a; Buckow and Heinz 2008). The pressure stability of enzymes can vary drastically, ranging from pressure sensitive enzymes, such as phosphohexoseisomerase from bovine milk ($p < 400$ MPa) (Rademacher and Hinrichs 2006), to extreme pressure resistant enzymes like, peroxidise from horseradish (Smeller 2002). However, categorization of enzymes as a result of their pressure stability is not appropriate, since there is a structural manifoldness among enzymes catalyzing the same reaction (Buckow and Heinz 2008).

Figure 14.5a depicts the inactivation of 90% of different polyphenol oxidases (PPO) after 10 min isothermal/isobaric treatment. The pressure-temperature resistance of enzymes show a significant dependency on matrix conditions, such as the pH-value (Zipp and Kauzmann 1973; Weemaes et al. 1997; Riahi and Ramaswamy 2004) or the presence of different ions (Buckow et al. 2007a). Furthermore, even

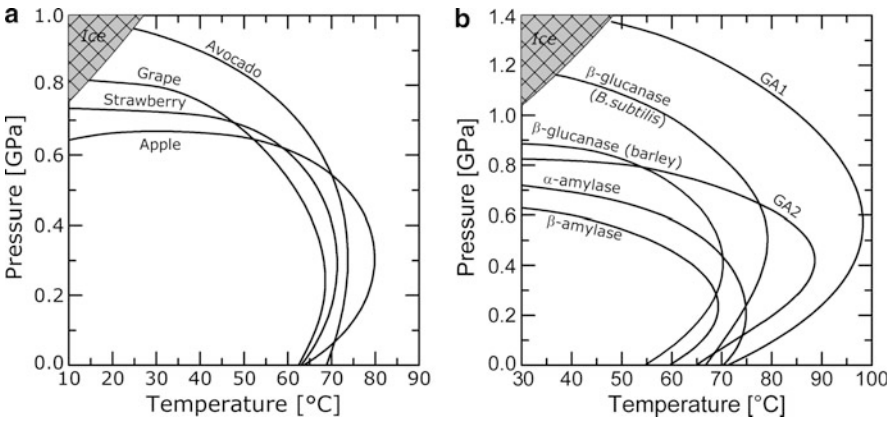

Fig. 14.5 Pressure-temperature isorate diagram for: (**a**) 90% inactivation of apple polyphenol oxidase after 10-min isothermal/isobaric treatment (Buckow et al. 2009), avocado (Weemaes et al. 1998), white grapes (Rapeanu et al. 2005), and strawberry (Dalmadi et al. 2006); (**b**) 95% inactivation of β-amylase (Heinz et al. 2005), β-glucanase (barley malt) (Buckow et al. 2005b), and β-glucanase (*B. subtilis*) (Buckow et al. 2007b) in ACES buffer (pH 5.6; 0.1 M), α-amylase in ACES buffer (pH 5.6; 0.1 M, containing 90 mM NaCl and 3.8 mM $CaCl_2$) (Buckow et al. 2007a), and glucoamylase isoenzymes GA1 and GA2 in ACES buffer (pH 4.5; 0.1 M) (Buckow et al. 2005a) after 30-min isothermal/isobaric treatment

isoforms of an enzyme from the same origin (e.g., glucoamlyse GA1 and GA2, as shown in Fig. 14.5b) can vary in their physical stability up to several hundred MPa (Buckow et al. 2005a; Buckow 2006; Rodrigo et al. 2006).

Pressure and temperature often act antagonistically on protein systems in the high temperature domain (Fig. 14.5), which can result in an enhanced thermostability of enzymes at specific pressures (Heremans and Smeller 1998; Lori et al. 2007). Such stabilization of enzymes occurs when the volume difference between the folded and unfolded state of the protein is positive, which might be due to the promoted formation of non-covalent bonds under pressure conditions.

14.4 Outlook, Needs, and Challenges

The continuously increasing HP research of the last decades has already generated an impressive number of commercially available HP processed, high quality products. Besides the "cold" pasteurization, which mainly inactivates vegetative microorganisms, there is still a lack of knowledge regarding the process conditions that are necessary to inactivate pressure-resistant bacterial endospores. Stable matrix (e.g., pressure stable buffer solutions) as well as defined treatment conditions (e.g., isothermal and isobaric conditions during dwell time) are essential, to generate reliable models, that predict microbial and enzyme inactivation and to obtain a better understanding of the underlying mechanisms (Mathys et al. 2009). This approach, in combination with a suitable pressure and temperature resistant surrogate, will allow a clearer insight into the mechanisms leading to spore inactivation under pressure and would consequently be the next step to successfully introduce HPTS in the food industry. The reduction of relatively high processing costs of HPTS; the investigation of the temperature evolution and distribution in the pressure chamber during a pressure cycle; and the simulation of the behavior of HP-treated biomaterials will be the research challenges of the near future (Delgado et al. 2008).

Isostatic HP can also be used to generate new functional features, such as specific textures or health promoting properties to develop tailor-made foods. A very promising field for future research is the use of HP to modulate microbial fermentations or enzymatic bioconversions. HP might also influence the biosynthetic pathways of foods from plant or animal origin as well as of food-related microorganisms, which could lead to the formation of product variations with unique properties (Aertsen et al. 2009). A better understanding of the mechanisms underlying pressure and temperature stability could also enable the development of HP-resistant enzymes. Despite extensive research in the HP area, there is still a lack of data regarding the behavior of nutrients, flavors, and allergens during the storage of HP-treated foods.

Acknowledgment The authors Dietrich Knorr and Volker Heinz acknowledge the support of part of their work through the Marcel Loncin Research Prize.

References

Aertsen A, Meersman F, Hendrickx M, Michiels C (2009) Biotechnology under high pressure: applications and implications. Trends Biotechnol 27(7):434–441

Ananta E (2005) Impact of environmental factors on vitality and stability and high pressure pretreatment on stress tolerance of *Lactobacillus rhamnosus* GG (ATCC 53103) during spray drying. Thesis, Technische Universität Berlin, Berlin

Ananta E, Heinz V, Knorr D (2005) Assessment of high pressure induced damage on *Lactobacillus rhamnosus* GG by flow cytometry. Food Microbiol 21(5):567–577

Ananta E, Heinz V, Schlüter O, Knorr D (2001) Kinetic studies on high-pressure inactivation of *Bacillus stearothermophilus* spores suspended in food matrices. Innovative Food Sci Emerg Technol 2:261–272

Ananta E, Knorr D (2003) Pressure-induced thermotolerance of *Lactobacillus rhamnosus* GG. Food Res Int 36(9–10):991–997

Ananta E, Knorr D (2004) Evidence on the role of protein biosynthesis in the induction of heat tolerance of *Lactobacillus rhamnosus* GG by pressure pre-treatment. Int J Food Microbiol 96:307–313

Ardia A (2004) Process considerations on the application of high pressure treatment at elevated temperature levels for food preservation. Ph.D. thesis, Berlin University of Technology, Berlin, p 94

Ardia A, Knorr D, Heinz V (2004a) Adiabatic heat modelling for pressure build-up during high-pressure treatment in liquid-food processing. Food Bioprod Process 82(C1):89–95

Ardia A, Knorr D, Ferrari G, Heinz V (2004b) Kinetic studies on combined high-pressure and temperature inactivation of *Alicyclobacillus acidoterrestris* spores in orange juice. Appl Biotechnol Food Sci Policy 1(3):169–173

Black EP, Wei J, Atluri S, Cortezzo D, Koziol-Dube K, Hoover D, Setlow P (2006) Analysis of factors influencing the rate of germination of spores of *Bacillus subtilis* by very high pressure. J Appl Microbiol 102(1):65–76

Bothun GD, Knutson BL, Berberich JA, Strobel H, Nokes S (2004) Metabolic selectivity and growth of *Clostridium thermocellum* in continuous culture under elevated hydrostatic pressure. Appl Microbiol Biotechnol 65(2):149–157

Bridgman PS (1914) The coagulation of albumen by pressure. J Biol Chem 19:511–512

Bridgman PW (1912) Water, in the liquid and five solid forms, under pressure. Proc Am Acad Arts Sci 47:441–558

Buckow R (2006) Pressure and temperature effects on the enzymatic conversion of biopolymers. Thesis, Technsiche Universität Berlin, Berlin

Buckow R, Heinz V (2008) High pressure processing – a database of kinetic information. Chem Ing Tech 80(8):1081–1095

Buckow R, Heinz V, Knorr D (2005a) Two fractional model for evaluating the activity of glucoamylase from *Aspergillus niger* under combined pressure and temperature conditions. Food Bioprod Process 83(C3):220–228

Buckow R, Heinz V, Knorr D (2005b) Effect of high hydrostatic pressure-temperature combinations on the activity of β-glucanase from barley malt. J Inst Brew 111(3):282–289

Buckow R, Isbarn S, Knorr D, Heinz V, Lehmacher A (2008) Predictive model for inactivation of feline calicivirus, a norovirus surrogate, by heat and high hydrostatic pressure. Appl Environ Microbiol 74:1030–1038

Buckow R, Weiss U, Heinz V, Knorr D (2007a) Stability and catalytic activity of a-amylase from barley malt at different pressure-temperature conditions. Biotechnol Bioeng 97:1–11

Buckow R, Weiss U, Knorr D (2007b) Combined pressure and temperature effects on the catalytic activity of cellulase from *Bacillus subtilis*. In: Proceedings of the 4th International Conference on High Pressure Bioscience and Biotechnology, Tsukuba, Japan

Buckow R, Weiss U, Knorr D (2009) Inactivation kinetics of apple polyphenol oxidase in different pressure-temperature domains. Innovative Food Sci Emerg Technol 10(4):441–448

Bunthof CJ (2002) Flow cytometry, fluorescent probes, and flashing bacteria. Ph.D. thesis, Wageningen University, Wageningen, The Netherlands, p 160

Dalmadi I, Rapeanu G, Van Loey A, Smout C, Hendrickx M (2006) Characterization and inactivation by thermal and pressure processing of strawberry (*fragaria ananassa*) polyphenol oxidase: a kinetic study. J Food Biochem 30(1):56–76

De Heij W, van Schepdael L, Moezelaar R, Hoogland H, Matser A, Van den Berg R (2003) High pressure sterilization: maximizing the benefits of adiabatic heating. Food Technol 57:37–41

De Vries Y (2006) *Bacillus cereus* spore formation, structure, and germination. Ph.D. thesis, Wageningen Universiteit, Wageningen

Delgado A, Rauh C, Kowalczyk W, Baars A (2008) Review of modeling and simulation of high pressure treatment of materials of biological origin. Trends Food Sci Technol 19: 329–336

Diels AMJ, Michiels CW (2006) High-pressure homogenization as a non-thermal technique for the inactivation of microorganisms. Crit Rev Microbiol 32(4):201–216

Gould GW, Sale AJH (1970) Initiation of germination of bacterial spores by hydrostatic pressure. J Gen Microbiol 60:335

Hayakawa K, Kanno T, Yoshiyama K, Fujio Y (1994) Oscillatory compared with continuous high pressure sterilization of *Bacillus stearothermophilus* spores. J Food Sci 59:164–167

Heinz (2010) German Institute of Food Technology, Quakenbrueck, Germany (personal communication)

Heinz V, Buckow R, Knorr D (2005) Catalytic activity of β-amylase from barley in different pressure/temperature domains. Biotechnol Prog 21:1632–1638

Heinz V, Knoch A, Lickert T (2009) Product innovation by high pressure processing. New Food 2:43–44

Heinz V, Knorr D (1998) High pressure germination and inactivation kinetics of bacterial spores. In: Isaacs NS (ed) High pressure food science, bioscience and chemistry. The Royal Society of Chemistry, Cambridge, pp 435–441

Heinz V, Knorr D (2002) Effects of high pressure on spores. In: Hendrickx MEG, Knorr D (eds) Ultra high pressure treatments of foods. Kluwer/Plenum, New York, pp 77–114

Heinz V, Kortschack F (2002) Method for modifying the protein structure of PrPsc in a targeted manner. Germany, patent, (WO 02/49460). In: Hendrickx M, Knorr D (eds) Ultra high pressure treatment of foods. Kluwer/Plenum, New York

Heremans K (2002) The effects of high pressure on biomaterials. In: Hendrickx M, Knorr D (eds) Ultra high pressure treatments of foods. Kluwer/Plenum, New York, pp 23–52

Heremans K, Smeller L (1998) Protein structure and dynamics at high pressure. Biochim Biophys Acta 1386:353–370

Hite BH (1899) The effect of pressure in the preservation of milk – a preliminary report. West Virginia Agr Exp Stat Bull 58:15–35

Indrawati I, Van Loey A, Hendrickx M (2005) Pressure and temperature stability of 5-methyltetrahydrofolic acid: a kinetic study. J Agric Food Chem 53(8):3081–3087

Isbarn S, Buckow R, Himmelreich A, Lehmacher A, Heinz V (2007) Inactivation of avian influenza virus by heat and high hydrostatic pressure. J Food Prot 70(3):667–673

Juliano P, Knoerzer K, Fryer PJ, Versteeg C (2009) *C. botulinum* inactivation kinetics implemented in a computational model of a high-pressure sterilization process. Biotechnol Prog 25(1):163–175

Kato N, Sato T, Kato C, Yajima M, Sugiyama J, Kanda T, Mizuno M, Nozaki K, Yamanaka S, Amano Y (2007) Viability and cellulose synthesizing ability of *Gluconacetobacter xylinus* cells under high-hydrostatic pressure. Extremophiles 11(5):693–698

Knoerzer K, Juliano P, Gladman S, Versteeg C (2007) A computational model for temperature and sterility distributions in a pilot-scale high pressure high-temperature process. AlChE J 53:2996–3010

Knorr D (2002) High pressure processing for preservation, modification and transformation of foods. High Pressure Res 22:595–599

Knorr D, Heinz V, Buckow R (2006) High pressure application for food biopolymers. Biochim Biophys Acta 1764:619–631

Lori S (2008) Untersuchungen zur Eignung der nicht-thermischen Druckinaktivierung pathogener Bakterien in Lebensmitteln. Thesis, Hamburg University, Hamburg

Lori S, Buckow R, Heinz V, Lehmacher A (2007) Predictive model for inactivation of *Campylobacter spp*. by heat and high hydrostatic pressure. J Food Prot 70(9):2023–2029

Ludikhuyze L, Van Loey A, Indrawati, Denys S, Hendrickx M (2002a) Effects of high pressure on enzymes related to food quality. In: Hendrickx M, Knorr D (eds) Ultra high pressure treatments of food. Kluwer/Plenum, New York, pp 115–166

Ludikhuyze L, Van Loey A, Indrawati, Hendrickx M (2002b) High pressure processing of fruit and vegetables. In: Jongen W (ed) Fruit and vegetable processing: improving quality. Woodhead Publishing, Cambridge, pp 346–362

Margosch D, Ehrmann MA, Buckow R, Heinz V, Vogel R, Gänzle M (2006) High-pressure-mediated survival of *Clostridium botulinum* and *Bacillus amyloliquefaciens* endospores at high temperature. Appl Environ Microbiol 72(5):3476–3481

Margosch D, Gänzle MG, Ehrmann MA, Vogel RF (2004) Pressure inactivation of Bacillus endospores. Appl Environ Microbiol 70(12):7321–7328

Mathys A (2008) Inactivation mechanisms of *Geobacillus* and *Bacillus* spores during high pressure thermal sterilization. Ph.D. thesis, Technische Universität Berlin, Berlin

Mathys A, Chapman B, Bull M, Heinz V, Knorr D (2007) Flow cytometric assessment of *Bacillus* spore response to high pressure and heat. Innovative Food Sci Emerg Technol 8:519–527

Mathys A, Kallmeyer R, Heinz V, Knorr D (2008) Impact of dissociation equilibrium shift on bacterial spore inactivation by heat and pressure. Food Control 19(12):1165–1173

Mathys A, Reineke K, Heinz V, Knorr D (2009) High pressure sterilization - development and application of temperature controlled spore inactivation studies. High Pressure Res 29(1):3–7

Meyer RS (2000) Ultra high pressure, high temperature food preservation process. US patent 6,017,572

Molina-Gutierrez A, Stippl V, Delgado A, Gänzle M, Vogel R (2002) *In Situ* determination of the intracellular pH of *Lactococcus lactis* and *Lactobacillus plantarum* during pressure treatment. Appl Environ Microbiol 68(9):4399–4406

Niven GW, Miles CA, Mackey BM (1999) The effects of hydrostatic pressure on ribosome conformation in *Escherichia coli*: an *In vivo* study using differential scanning calorimetry. Microbiology 145(2):419–425

Paidhungat M, Setlow B, Daniels W, Hoover D, Papafragkou E, Setlow P (2002) Mechanisms of induction of germination of *Bacillus subtilis* spores by high pressure. Appl Environ Microbiol 68(6):3172–3175

Pavlovic M, Hoermann S, Vogel R, Ehrmann MA (2008) Characterisation of a Piezotolerant Mutant of *Lactobacillus sanfranciscensis*. Z Naturforsch 63b:791–797

Perry RH (1984) Perry´s chemical engineers' handbook. McGraw-Hill, New York

Picard A, Daniel I, Montagnac G, Oger P (2006) *In situ* monitoring by quantitative Raman spectroscopy of alcoholic fermentation by *Saccharomyces cerevisiae* under high pressure. Extremophiles 11(3):445–452

Rademacher B, Hinrichs J (2006) Effects of high pressure treatment on indigenous enzymes in bovine milk: reaction kinetics, inactivation and potential application. Int Dairy J 16(6):655–661

Rajan S, Ahn J, Balasubramaniam VM, Yousef AE (2006) Combined pressure-thermal inactivation kinetics of *Bacillus amyloliquefaciens* spores in egg patty mince. J Food Prot 69(4): 853–860

Rapeanu G, Van Loey A, Smout C, Hendrickx M (2005) Thermal and high-pressure inactivation kinetics of polyphenol oxidase in victoria grape must. J Agric Food Chem 58(8):2988–2994

Rastogi NK, Raghavarao KSM, Balasubramaniam VM, Niranjan K, Knorr D (2007) Opportunities and challenges in high pressure processing of foods. Crit Rev Food Sci Nutr 47:1–44

Reineke K, Mathys A, Knorr D (2008) Temperature control for high pressure processes up to 1400 MPa. J Phys Conf Ser 121:142012–142016

Riahi E, Ramaswamy HS (2004) High pressure inactivation kinetics of amylase in apple juice. J Food Eng 64:151–160

Rodrigo D, Cortés C, Clynen C, Schoofs L, Van Loey A, Hendrickx M (2006) Thermal and high-pressure stability of purified polygalacturonase and pectinmethylesterase from four different tomato processing varieties. Food Res Int 39(4):440–448

Rumpold BA (2005) Impact of high hydrostatic pressure on wheat, tapioca, and potato starches. Thesis, Berlin Technical University, Berlin, p 120

Schlueter O, Benet GU, Heinz V, Knorr D (2004) Metastable states of water and ice during pressure supported freezing of potato tissue. Biotechnol Prog 20:799–810

Setlow P (2003) Spore germination. Curr Opin Microbiol 6:550–556

Sharma A, Yadav BS (2008) Resistant starch: physiological roles and food applications. Food Rev Int 24(2):193–234

Smeller L (2002) Pressure-temperature phase diagram of biomolecules. Biochim Biophys Acta 1595:11–29

Smelt JP, Hellemons JC, Patterson M (2001) Effects of high pressure on vegetative microorganisms. In: Hendrickx M, Knorr D (eds) Ultra high pressure treatments of foods. Kluwer, New York, pp 55–76

Stone G, Chapman B, Lovell D (2009) Development of a log-quadratic model to describe microbial inactivation, illustrated by thermal inactivation of *Clostridium botulinum*. Appl Environ Microbiol 75(22):6998–7005

Tauscher B (1995) Pasteurization of food by hydrostatic high pressure: chemical aspects. Lebensm Unters Forsch 200:3–13

Ting E, Balasubramaniam VM, Raghubeer E (2002) Determining thermal effects in high pressure processing. J Food Technol 56(2):31–35

Trejo Araya XI, Hendrickx M, Verlinden BE, Van Buggenhout S, Smale N, Stewart C, Mawson A (2007) Understanding texture changes of high pressure processed fresh carrots: a microstructural and biochemical approach. J Food Eng 80(3):873–884

Ulmer HM, Herberhold H, Fahsel S, Gänzle M, Winter R, Vogel R (2002) Effects of pressure-induced membrane phase transitions on inactivation of HorA, an ATP-dependent multidrug resistance transporter, in *Lactobacillus plantarum*. Appl Environ Microbiol 68:1088–1095

Weemaes CA, De Cordt SV, Ludikhuyze LR, Van den Brock I, Hendrickx M, Tobbuck P (1997) Influence of pH, benzoic acid, EDTA, and glutathione on the pressure and/or temperature inactivation kinetics of mushroom polyphenoloxidase. Biotechnol Prog 13:25–32

Weemaes CA, Ludikhuyze L, Van den Broeck I, Hendrickx M (1998) Effect of pH on pressure and thermal inactivation of Avocado polyphenol oxidase: a kinetic study. J Agric Food Chem 46(7):2785–2792

Wuytack EY, Boven S, Michiels CW (1998) Comparative study of pressure-induced germination of *Bacillus subtilis* spores at low and high pressures. Appl Environ Microbiol 64(9):3220–3224

Yaldagard M, Mortazavi SA, Tabatabaie F (2008) The principles of ultra high pressure technology and its application in food processing/preservation: a review of microbiological and quality aspects. Afr J Biotechnol 7:2739–2767

Zipp A, Kauzmann W (1973) Pressure denaturation of metmyoglobin. Biochemistry 12(21): 4217–4228

Chapter 15
High Pressure Sterilization of Foods

Hosahalli Ramaswamy

15.1 Introduction

Thermal processing for achieving commercial sterilization involves heating of foods in hermetically sealed containers for specified time-temperature combinations to eliminate the microbial pathogens that endanger public health, along with microorganisms and enzymes that deteriorate food during storage. As originally formulated, the aim of thermal processing was to produce a safe and shelf-stable food product. Today, however, the consumer demands food products that are more fresh-like with high-quality, high nutritive value, and end use convenience. In addition, food processors look for more energy-efficient, cost-effective, and high-capacity processing technologies. Many processing alternatives including high temperature-short time (HTST) processing, aseptic processing and packaging, thin profile packaging and processing, and agitation processing, have primarily evolved to minimize the severity of heat treatment and promote product quality. Aseptic processing, microwave, radio frequency, and ohmic heating techniques have gained attention as alternative and nonconventional rapid processing techniques.

To meet consumer demands, there has been an increasing interest in the use of high hydrostatic pressure processing as a nonthermal food preservation technique. High pressure processing (HPP) is a method of food processing where food is subjected to elevated pressures (often in excess, 80,000 lb/in.^{2} or approximately 5,500 atm or 550 MPa), with or without the addition of heat, to achieve microbial inactivation or to alter the food quality attributes. It is also referred by various similar names: high pressure (HP), ultra-high pressure (UHP), high hydrostatic pressure (HHP) processing, etc. Most vegetative bacteria can be killed at pressures at or around 550 MPa. Microbial spores, however, are more resistant and require much higher pressures as well as higher processing temperatures. HPP retains food quality, maintains natural freshness, and extends microbiological shelf life.

H. Ramaswamy
Department of Food Science, McGill University, Ste Anne de Bellevue, Quebec, Canada
e-mail: hosahalli.ramaswamy@mcgill.ca

J.M. Aguilera et al. (eds.), *Food Engineering Interfaces*, Food Engineering Series,
DOI 10.1007/978-1-4419-7475-4_15,

Over the past decades, high pressure processing has emerged as a commercial alternative to traditional thermal processing methods for many foods, e.g., jams, fruit juices, guacamole, oysters, ready to eat meats, etc. Its primary advantage is that it can inactivate microorganisms and enzymes at substantially lower treatment temperatures (as compared to conventional thermal processing) that results in processed foods possessing sensory and nutrient qualities closely resembling the original, fresh, or raw product. Generally, high pressure processing as a nonthermal food processing technique is widely applied in pasteurization of food to extend food shelf life and preserve high qualities, such as natural color, flavor, and nutrients. However, several resistant microorganisms, especially spores, and some enzymes can survive during HP pasteurization. Therefore, HP processed foods should be kept at refrigerated conditions to prevent spoilage and quality change (Patterson 2005).

HPP has already become a commercially implemented technology worldwide, spreading from its origins in Japan, followed by USA, Mexico, Europe, and now Canada, with worldwide take-up increasing almost exponentially since 2000 (Norton and Sun 2008). High pressure research and development in different disciplines within the food industry has been reviewed by several researchers (Norton and Sun 2008; Rastogi et al. 2007; Toepfl et al. 2006; Torres and Velazquez 2005; San Martin-Gonzalez et al. 2002).

15.2 High Pressure Pasteurization

High pressure processing has been commercialized for a variety of acid and acidified food products. For low acid foods, however, it has been used only as a temporary measure of extending shelf-life under refrigerated storage conditions. It has also been used for several other purposes including control of some pathogens and viruses, for inducing functional changes, as well as improving the nutritional and sensory quality of foods. Novelties in freezing and thawing application have been achieved through the use of pressure shift freezing and thawing.

Pasteurization by HPP can be carried out at pressures in the range 400–600 MPa at relatively moderate (20–50°C) or even at refrigerated temperatures. Under such conditions, HPP can be effective in inactivating most vegetative pathogens and spoilage microorganisms. High pressure processing is, as yet, considered to be a novel process for the production of low acid foods with regulatory bodies.

Extensive research has been carried out in the author's laboratory on HP processing of several foods for pasteurization purposes: milk, meat, pork, fish, orange juice, mango juice, apple juice, etc. (Mussa et al. 1999a, b; Basak et al. 2002; Riahi et al. 2003; Ramaswamy et al. 2003, 2008, 2009; Shao et al. 2006; Gill and Ramaswamy 2008). These studies have aimed at generating the necessary kinetic data useful in establishing HP processes for different foods, and then verifying their validity through inoculated pack/challenge studies with pathogens. Typically, these studies have shown a dual phase destruction kinetics for most

pathogens. The first phase was generally characterized as pulse effect (PE), indicating the destruction to be essentially a pressurization-depressurization effect with no hold time (depends on the pressure level) because the pressure is released immediately after the pressurization process. While pressure come-up and release duration and profiles would undoubtedly contribute to some destruction based on the pressure destruction rates, the measured PE were found to be significantly higher than those that could be computed from the accumulated destruction during come-up and come-down periods (based on the D and z values). Following the PE, the destruction patterns in these studies have generally been found to be well described by the log-linear model following the first order rate kinetics. Typical values of PE and the HP destruction kinetic parameters, D and z for selected microbial pathogens in different food media are shown in Tables 15.1 and 15.2.

Table 15.1 Pressure pulse effect (no-holding time) for selected pathogens in different foods

Microorganism	Food base	Pulse effect (log value)	References
Escherichia coli (O17:H7)	Apple juice (pH 3.5)	3.95 at 30°C, 400 MPa	Riahi et al. (2003)
E. coli (O157:H7)	Cheese	0.3 (400 MPa)	Shao et al. (2006)
Listeria monocytogenes	Cheese	0.25 (400 MPa)	Shao et al. (2006)
L. monocytogenes	Milk	1.3 (400 MPa)	Mussa et al. (1999a)
L. monocytogenes	Pork	1.5 (400 MPa)	Mussa et al. (1999b)

Table 15.2 High pressure destruction kinetics in the context of pasteurization

Name	D value (min) (MPa)	*Z* value	References
Escherichia coli O157:H7 in			
Apple juice	14.3 (10°C, 400 MPa)	654	Riahi et al. (2003)
	3.22 (35°C, 400 MPa)	137	Riahi et al. (2003)
Fish slurry	3.19 (400 MPa)	185	Ramaswamy et al. (2008)
Cheese	2.0 (400 MPa)	128	Shao et al. (2006)
Listeria monocytogenes in			
Milk	10.1 at 350 MPa	266	Mussa et al. (1999a)
Pork	3.52 at 400 MPa	163	Mussa et al. (1999b)
Fish	49 at 400 MPa	103	Ramaswamy et al. (2008)
Cheese	1.4 at 350 MPa	82	Shao et al. (2006)

15.3 High Pressure Sterilization

HPP for producing shelf-stable low acid foods is still a topic of considerable controversy. Processors worldwide are waiting for the full regulatory approval of HP sterilization of low acid foods. HPP has the potential to produce better quality foods than possible from the use of processing novelties such as microwave, RF, or Ohmic heating techniques in combination with aseptic processing. This is because

HPP allows the product temperature to be increased very rapidly (due to adiabatic heating) from around 90–100°C to the sterilization zone (120–130°C) (come-up time) and bringing it back to nearly the same state almost instantaneously by depressurization. The process can be formulated either as a pressure-assisted thermal sterilization (PATS) or temperature-assisted pressure sterilization (TAPS). Either way, it represents a considerable deviation from conventional thermal processing because of lack of kinetic data on destruction of spoilage and pathogenic microorganisms under processing conditions. A better understanding of the inactivation kinetics of pathogens and/or their surrogates under high temperature high pressure processing conditions is the key for the success of HPP and for FDA approval. The critical factors in HPP include pressure, pressure holding time, time to achieve treatment pressure, depressurization time, treatment temperature (including adiabatic heating), product initial temperature, vessel temperature distribution during the pressure treatment, product pH, product composition, product water activity, packaging material integrity, and any concurrent processing aids. Although HP processing-related research work has increased tremendously in the last decade, there is still a serious lack of specific data in this area to permit establishment of a reliable process.

As described earlier, HPP of low acid foods can either be treated as a PATS or TAPS process. For PATS, achieving designated process lethality for commercial sterilization becomes the main issue, which can be easily achieved, and such a process would most likely meet the regulatory approval standards. The process would rely on the effective use of compression heating of the food achieved during the pressurization process. Starting at an appropriate preset initial temperature, process temperatures can easily be brought to levels used for HTST levels practiced in commercial sterilization applications. Thus, holding the product at such pressures for a specified time would easily result in the accumulation of the desired target process lethality. The process generally involves a come-up time during which pressure and temperature continuously increase to set levels. During the hold, pressure generally remains constant, while the temperature could drop due to heat loss from the product to equipment structure. It is necessary to address this issue in order to provide appropriate insulation for the product to prevent large temperature drop and to appropriately take the temperature drop in to consideration in establishing the process. In the second approach (TAPS), additional destruction caused by the pressure at the elevated temperatures is taken into account. It is recognized that unless the process pressure is 600–800 MPa range along with elevated process temperatures in the 80–120°C range, it is not possible to kill the microbial spores and hence not possible to achieve commercial sterility. However, at such pressure levels, microbial destruction at the process temperatures could occur much more rapidly than at the same temperature under conventional retort processing conditions. Thus, the TAPS process could benefit from accelerated destruction kinetics and could potentially result in an effective short time process providing similar quality advantages as the PATS process. However, this process would generally be considered a "novel" process and would need additional data on pressure destruction kinetics on both spoilage and pathogenic microbial spores at

the prevailing processing conditions. While the PATS process could be more easily cleared by regulatory agencies along the guidelines used for traditional thermal processing, the TAPS process would require demonstration of accelerated spore destruction kinetics of pathogenic and spoilage bacterial spores.

15.4 Compression Heating

Compression heating is an unavoidable consequence in high pressure processing. When the food and medium are subjected to HP processing, their volume is reduced and pressure is simultaneously elevated, both of which contribute to an increase in temperature of the food and pressurization medium as a result of the adiabatic compression. The temperature rise depends on the nature of the food and the medium, and is also dependent on the initial temperature and pressure levels involved. Extensive research has been carried out in this area and data have been compiled on the compression heating behavior of various foods and pressurization media. It is necessary to use such data to determine the temperatures of both the medium and the product following pressurization.

Only the pressurization medium and the packaged food (including the packaging material) are subjected to such compression heating. The material used for making the pressure vessel will not undergo such adiabatic compression and will not be subjected to such temperature increases. Thus, the steel chamber acts as a heat sink for the temperature elevated food product and pressurization medium unless compensated by an internal temperature heating system or adequate insulation at the contact surface. Typical changes in the temperature of the product in insulated and uninsulated products are shown in Fig. 15.1.

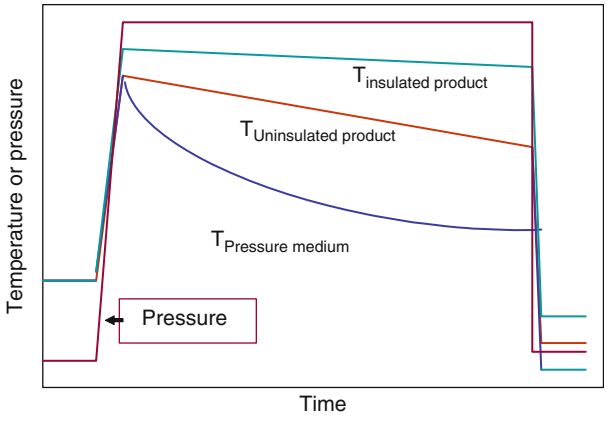

Fig. 15.1 Typical compression heating temperature rise in the pressurization medium and product, and the subsequent heat loss during pressure hold time

It is necessary to evaluate the related time-temperature distribution and compute the process time based on the cold spot location of the product. The holding time needs to be adjusted to bring the accumulated lethality at the coldest point in the product to the target levels (e.g., Fo value of 5 min). This process development would normally follow the guidelines for thermal process establishments which may include temperature distribution in the pressure vessel and heat penetration data gathering. In the TAPS process temperature stability is equally important, since it can affect the spore inactivation kinetics. This aspect is discussed in the next section.

The compression heating or the adiabatic temperature rise is dependent on the type of pressurization liquid and food components since the pressure compressibility of each material or constituent is different. Further, it also depends on the pressure level and initial temperature, generally increasing with an increase in both initial temperature and pressure, and often demonstrating a synergy between the two. Some typical values of adiabatic temperature that rise per 100 MPa pressure rise at an initial temperature of 25°C are given below (Rasanayagam et al. 2003):

Orange juice, tomato salsa, skim milk, salmon fish: 2.6–3.0°C
Carbohydrates: 2.6–3.6°C
Proteins: 2.7–3.3°C
Mayonnaise: 5.0–7.2°C
Extracted beef fat: 6.2–8.3°C
Soybean oil: 6.2–9.1°C
Olive oil: 6.3–8.7°C

Shao et al. (2010) expressed the adiabatic temperature rise (ΔT_P) as a quadratic function of pressure and initial temperature:

$$\Delta T_P = -3.06 + 0.0224T_i + 0.0423P + 4.49 \times 10^{-4}{T_i}^2 + 1.31 \times 10^{-4}T_iP - 1.24 \times 10^{-5}P^2 \quad (15.1)$$

($R^2 = 0.999$, $n = 50$, SE = 0.20°C, $P < 0.05$ for all items) or a function of pressure and a desired HP treatment temperature:

$$\Delta T_P = -2.21 + 0.0328T_P + 0.0381P + 2.82 \times 10^{-4}{T_P}^2 + 8.64 \times 10^{-5}T_PP - 1.25 \times 10^{-5}P^2 \quad (15.2)$$

($R^2 = 0.999$, $n = 50$, SE = 0.18°C, P-value <0.05 for all items).

15.5 Spore Inactivation Studies

Commercially sterile low-acid food (LCAF) products are commonly produced by thermal processing, and they are based on a process which should be able to achieve a 12 decimal reduction (D value) in a *Clostridium botulinum* spore population.

Once the degree of sterility is achieved, the process needs to be fine-tuned with respect to spoilage causing bacterial spores so that shelf stability can be assured. High pressure processing when combined with moderately elevated temperatures can inactivate highly resistant bacterial spores. Traditionally, bacterial spores such as *C. sporogenes, B. sterothermophilus, C. liquifaciencs*, etc., with high heat resistance, have been used for establishing the process for spoilage control and for testing the efficacy of the commercial sterilization. The obvious choices for HP research were to test if these were more pressure resistant as well. Hence, much of the work on bacterial spores has been concentrated on the pressure destruction kinetics of such spores in various food matrices (Patazca et al. 2006; Shao et al. 2010; Zhu et al. 2008).

There have been several reports on the pressure destruction of bacterial spores. Rovere et al. (1996) reported D values of 3.5, 3.2 min for 600, and 700 MPa at 100°C, respectively, for *C. sporogenes* 7,955 spores in meat broth. Mills et al. (1998) found that there is no inactivation of *C. sporogenes* spores with HP treatments at even 600 MPa for 30 min when tested at 20°C and concluded that these spores could not be inactivated by pressure alone. Meyer et al. (2000) reported that a two-cycle treatment with initial temperature of 90°C combined with 690 MPa for 1 min achieved sterility in macaroni and cheese with 10^6/g of *C. sporogenes* spores. Reddy et al. (1999, 2003, 2006) studied the effect of HP treatment on spores of *C. botulinum* type A, B, and E at moderately elevated temperatures and found the Type A spores to be more resistant. They reported that only 3 log cycle reductions were achieved at 827 MPa and 75°C pressure conditions. Margosch et al. (2004a, b, 2006) reported that proteolytic TMW 2.357 (*C. botulinum* Type B) and TMW 2.479 (*Bacillus amyloliquefaciens*) exhibited a greater resistance to pressure than other bacterial spores (*Bacillus* spp. and *C. botulinum* spp.). Koutchma et al. (2005), in their pressure destruction kinetic study of *C. sporogenes* PA3679 spore in phosphate buffer, reported pressure (Z_P) and temperature sensitivity (Z_T) values of 23.7°C and 1,500 MPa, respectively. Ahn and Balasubramaniam (2007b)) observed pressure-assisted thermal processing (PATP) at 700 MPa and 121°C for 1 min inactivated up to 7–8 log reduction for *C. sporogenes* spores. In another paper (Ahn et al. 2007a), it was reported that spore clumps formed during the PATP may lead to an increase in pressure-thermal resistance, and that multiple-pulsed pressurization can be more effective in inactivating bacterial spores. These studies in general suggest that spore inactivation kinetics is likely to depend on the type of substrate (food medium or matrix) in which they are pressure treated.

Recent studies at McGill (Shao 2008) have concentrated on spore (surrogate and pathogenic) inactivation kinetics using high pressure. Destruction kinetics tests were carried out with two strains of *C. sporogenes* (11437, 7955) and *Geobacillus stearothermophilus* 10,149 spores suspended in milk at 700–900 MPa and 70–100°C. The survival counts were found to well fit the first order linear models. The D values of *C. sporogenes* 11,437 varied from 0.73 min at 900 MPa/100°C to 17.0 min at 700 MPa/80°C, while they ranged from 6.0 to 833 min at 80–100°C under thermal processing conditions. The D values associated with *C. sporogenes* 7,955 spores were higher than for *C. sporogenes* 11437 and

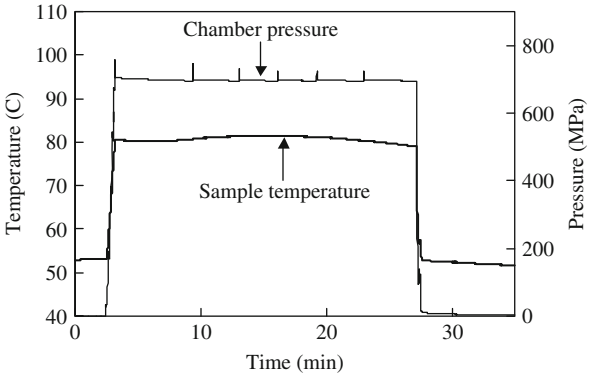

Fig. 15.2 Typical pressure and sample temperature profiles during *HP* treatment at 700 MPa and 80°C for 24 min

varied from 1.3 min at 900 MPa/100°C to 38.2 min at 700 MPa/80°C treatments, and from 12.1 to 156 min at 80–100°C during thermal treatments. Typical temperature stability of test samples during the pressure treatment is shown in Fig. 15.2. The D values of *G. stearothermophilus* 10149 spores varied from 0.6 min at 900 MPa/90°C to 20.9 min at 500 MPa/70°C treatments with 6.3 to 49.4 min for thermal treatments at 110–120°C. Hence, *C. sporogenes* 7955 spores were the most resistant among those studied. The HP destruction kinetics of *C. sporogenes* 7955 spores were also studied in salmon and were lower than in milk (Shao 2008).

15.5.1 Clostridum botulinum Studies

C. botulinum is an anaerobic, mesophilic, spore-forming pathogen that poses public health risk in low acid foods. Most commercial processes for LACF are based on giving a process lethality of least 5 min or longer (which is $>$ 20D of the target *C. botulinum* spores). *C. botulinum* is a pathogen capable of producing severe neurotoxins, and therefore is rarely used in process development studies. Instead, surrogate spores of similar resistance are often employed. *C. sporogenes*, a typical thermally resistant, mesophilic spore-former, is commonly used when inoculated pack verification of thermal processes are warranted. While destruction kinetics of bacterial spores have been widely studied under thermal processing conditions for almost 200 years, similar work in the area of HP processing are in their infancy.

In the most recent studies at McGill (Shao 2008), 12 *C. botulinum* Group I strains (62A IB1-B, CK2-A, MRB, Langeland, A6, GA0108BEC, PA9508B, 13983B, H461297F, GA0101AJO, HO9504A) were subjected to combinations of high pressures (800 and 900 MPa) and elevated temperatures (90 and 100°C). The treatment holding time varied from 0.5 to 15 min. Sample tubes were kept in a POM plastic thick wall insulator, preheated to initial temperature, and placed into a pressure chamber prior to HP treatments for controlling process temperature at

the desired condition. The survival counts showed that higher pressure and temperature combinations always accelerated the inactivation of the spores. Strain 62A was completely inactivated by these combinations. Strains PA9608B, HO9504A, and CK2-A were found to be of higher pressure resistance than the rest 12 strains. The log reductions of these three strains were 1.63, 3.33, and 4.48 log units for 900 MPa/100°C/3 min and the estimated D values were 1.8, 0.88, and 0.66 min, respectively, at 900 MPa/100°C treatment. The strain PA9805B produced the most pressure-resistant spores. By studying pressure destruction effects in milk and buffer (substrate) on spore resistance under high pressure (700–900 MPa, 100–110°C) it was found that PA9508B spores had a higher resistance in milk than in the buffer. In further studies, more detailed evaluation of pressure destruction of the PA9805B strain of *C. botulinum* spores were evaluated in milk. At 900 MPa, the associated D values were 14.5, 1.8, and 0.35 min at 90, 100, and 110°C, respectively. The Z_T values were 11.2, 12.3, 12.4°C at 700, 800, 900 MPa, respectively, increasing with pressure and with higher value than the thermal *z* value 7.8°C. The Z_P values were 470, 630, and 800 MPa at 90, 100, and 110°C, respectively, increasing with temperature. By comparison of the Z_P and Z_T, it appeared that the spore was relatively more sensitive to temperature than to pressure. *D* value trends demonstrated that the pressure inactivation effect steadily decreased as the temperature increased and that at temperatures beyond 115°C, heat was essentially the principle mode of spore destruction.

Overall, spore inactivation studies have demonstrated several important findings. The nonpathogenic *C. sporogenes* 7955 spore was the most resistant surrogate, but the pathogenic *C. botulinum* PA9508B spore was even more resistant. D values associated with HP at elevated temperatures were higher than under conventional thermal treatments, and hence provide accelerated destruction kinetics at least for the nonpathogenic spores and better spoilage control. However, from a safety point of view, conventional thermal sterility requirements would still persist even under HP processing conditions. Milk, as a low acid food medium, provided more resistance for HP destruction than fish.

References

Ahn J, Balasubramaniam V, Yousef A (2007) Inactivation kinetics of selected aerobic and anaerobic bacterial spores by pressure-assisted thermal processing. Int J Food Microbiol 113:321–329

Ahn J, Balasubramaniam V (2007) Effects of inoculum level and pressure pulse on the inactivation of *Clostridium sporogenes* spores by pressure-assisted thermal processing. J Microbiol Biotechnol 17(4):616–623

Basak S, Ramaswamy H, Piette G (2002) High pressure destruction kinetics of *Leucononostoc mesenteroides* and *Sachharomyces cerevisiae* in single strength and concentrated orange juice. Innovative Food Sci Emerg Technol 3(Sept):223–245

Gill A, Ramaswamy H (2008) Application of high pressure processing to kill *Escherichia coli* O157 in ready-to-eat Meats. J Food Prot 71(11):2182–2189

Koutchma T, Guo B, Patazca E, Parisi B (2005) High pressure-high temperature sterilization: from kinetic to analysis to process verification. J Food Process Eng 28:610–629

Margosh D, Ehrmann M, Buckow R, Heinz V, Vogel R, Ganzle M (2006) High-pressure-mediated survival of *Clostridium botulinum* and *Bacillus amyloliquefaciens* endospores at high temperature. Appl Environ Microbiol 72:3476–3481

Margosh D, Ehrmann M, Ganzle M, Vogel R (2004a) Comparison of pressure and heat resistance of *Clostridium botulinum* and other endospores in mashed carrots. J Food Prot 67 (11):2530–2537

Margosh D, Ganzle M, Ehrmann M, Vogel R (2004b) Pressure inactivation of *Bacillus* endospores. Appl Environ Microbiol 70(12):7321–7328

Meyer R, Cooper K, Knorr D, Lelieveld H (2000) High-pressure sterilization of foods. Food Technol 54(11):67–72

Mills G, Earnshaw R, Patterson M (1998) Effects of high hydrostatic pressure on *Clostridium sporogenes* spores. Lett Appl Microbiol 26:227–230

Mussa D, Ramaswamy H, Smith J (1999a) High pressure destruction kinetics of *Listeria monocytogenes* in milk. Food Res Int 31(5):343–350

Mussa D, Ramaswamy H, Smith J (1999b) Ultra high pressure destruction kinetics of *Listeria monocytogenes* in pork. J Food Protect 62(1):165–170

Norton T, Sun D-W (2008) Recent advances in the use of high pressure as an effective processing technique in the food industry. Food Bioprocess Technol 1:2–34

Patazca E, Koutchma T, Ramaswamy H (2006) Inactivation kinetics of *Geobacillus stearothermophilus* spores in water using high-pressure processing at elevated temperatures. J Food Sci 71(3):M110–M116

Patterson M (2005) A review: microbiology of pressure-treated foods. J Appl Microbiol 98:1400–1409

Ramaswamy H, Jin H, Zhu S (2009) Effects of fat, casein and lactose on high-pressure destruction of *Escherichia coli K12* (ATCC-29055) in milk. Food Bioprod Process 87(C1):1–6

Ramaswamy H, Riahi E, Idziak E (2003) High-pressure destruction kinetics of *E-coli* (29055) in apple juice. J Food Sci 68(5):1750–1756

Ramaswamy H, Zaman S, Smith J (2008) High pressure destruction kinetics of *Escherichia coli* (O157:H7) and *Listeria monocytogenes* (Scott A) in a fish slurry. J Food Eng 87(1):99–106

Rasanayagam V, Balasubramaniam V, Ting E, Sizer C, Anderson C, Bush C (2003) Compression heating of selected fatty food substances during high pressure processing. J Food Sci 68(1):254–259

Rastogi N, Raghavarao K, Balasubramaniam V, Niranjan K, Knorr D (2007) Opportunities and challenges in high pressure processing of foods. Crit Rev Food Sci Nutr 47(1):69–112

Reddy N, Solomon H, Fingerhut G, Balasubramaniam V, Rhodehamel E (1999) Inactivation of *Clostridium botulinum types A and B* spores by high-pressure processing. IFT Annual Meeting: Book of Abstracts

Reddy N, Solomon H, Tetzloff R, Rhodehamel E (2003) Inactivation of *Clostridium botulinum* type A spores by high pressure processing at elevated temperatures. J Food Prot 66 (8):1402–1407

Reddy N, Tetzloff R, Solomon H, Larkin J (2006) Inactivation of *Clostridium botulinum* nonproteolytic type B spores by high pressure processing at moderate to elevated high temperature. Innovative Food Sci Emerg Technol 7:169–175

Riahi E, Ramaswamy H, Smith J (2003) High pressure destruction kinetics of *E. coli* (O157:H7) in apple juice. 2003 CSAE/SCGR Meeting, Macdonald Campus of McGill University Ste, Anne de Bellevue, Quebec, 6–9 July 2003

Rovere P, Carpi G, Dall'Aglio G, Gola S, Maggi A, Miglioli L, Scaramuzza N (1996) High-pressure heat treatments: evaluation of the sterilizing effect and of thermal damage. Ind Conserve 71:473–483

San Martin M, Barbosa-Canovas G, Swanson B (2002) Food processing by high hydrostatic pressure. Crit Rev Food Sci Nutr 42(6):627–645

Shao Y (2008) High pressure destruction kinetics of bacterial spores in low acid foods. Ph.D. thesis, McGill University

Shao Y, Ramaswamy H, Zhu S (2006) High pressure destruction kinetics of spoilage and pathogenic bacteria in raw milk cheese. J Food Process Eng 30(3):357–374

Shao Y, Zhu S, Ramaswamy H, Marcotte M (2010) Compression heating and temperature control for high pressure destruction of bacterial spores: an experimental method for kinetics evaluation. Food Bioprocess Technol 3:71–78. doi:10.1007/s11947-008-0057-y

Toepfl S, Mathys A, Heinz V, Knorr D (2006) Potential of high hydrostatic pressure and pulsed electric fields for energy efficient and environmentally friendly food processing. Food Rev Int 22(4):405–423

Torres J, Velazquez G (2005) Commercial opportunities and research challenges in the high pressure processing of foods. J Food Eng 67(1–2):95–112

Zhu S, Naim F, Marcotte M, Ramaswamy H, Shao Y (2008) High-pressure destruction kinetics of *Clostridium sporogenes* spores in ground beef at elevated temperatures. Int J Food Microbiol 126(1–2):86–92

Chapter 16
Bioseparation of Nutraceuticals Using Supercritical Carbon Dioxide

Feral Temelli and Bernhard Seifried

16.1 Introduction

The use of supercritical carbon dioxide for bioseparation of nutraceuticals has been growing rapidly over the past decade in response to increasing consumer demand for "natural" products in the functional foods and nutraceuticals markets. Carbon dioxide at temperature and pressure conditions above its critical point (31.1°C, 74 bar) is referred to as supercritical carbon dioxide (SC–CO_2), which is a dense fluid with physical properties in between those of a gas and a liquid. Thus, SC–CO_2 can be used as a solvent similar to other organic solvents for the extraction of nutraceuticals. The main distinction is that upon depressurization following extraction SC–CO_2 becomes a gas and separates readily from the extract, eliminating the need for extra heat treatment, which is necessary for the removal of organic solvents from the extracts. As well, processing can be carried out at just above ambient temperatures, minimizing degradation of heat labile bioactive compounds. Furthermore, CO_2, being the second least expensive solvent after water, is nontoxic, nonflammable, readily available, inexpensive, and can be recycled relatively easily. Thus, CO_2 has been the solvent of choice for the processing of nutraceuticals. In addition, in the CO_2 environment, undesirable oxidation reactions are minimized in the absence of oxygen, maintaining the integrity of bioactives. Based on all these advantages, SC–CO_2 processing of nutraceuticals has reached commercialization and numerous plants have been built around the world over the last decade. Other fluids, such as propane, dimethylether, and others are being investigated for the extraction and fractionation of biomaterials; however, this chapter will focus mainly on CO_2 due to the advantages listed above.

Because of the nonpolar nature of CO_2 it is selected for nonpolar solutes and requires the addition of a polar co-solvent such as ethanol to solubilize polar solutes. In terms of nutraceuticals, protein- and carbohydrate-based bioactives are

F. Temelli (✉) and B. Seifried
Department of Agricultural, Food and Nutritional Science, University of Alberta, Edmonton, AB, Canada T6G 2P5
e-mail: feral.temelli@ualberta.ca

J.M. Aguilera et al. (eds.), *Food Engineering Interfaces*, Food Engineering Series,
DOI 10.1007/978-1-4419-7475-4_16,

not soluble in SC–CO_2 to any appreciable extent; therefore, this chapter will focus on lipid-based nutraceuticals as well as on minor components or phytochemicals. Even though SC–CO_2 extraction has become more mainstream further processing in terms of fractionation requires additional development. Natural materials are very complex and each matrix needs to be studied separately to optimize various processing parameters on a case-by-case basis. Fundamental data needed for process design and optimization are missing in many cases. Therefore, our understanding of the fundamentals of various separation processes is limited. The objective of this chapter is to provide a review of the fundamentals and separation processes, especially the extraction and fractionation of major classes of nutraceuticals that are typically processed by SC–CO_2 (i.e., lipid-based nutraceuticals, carotenoids, and phytochemicals), and to highlight the challenges and provide some insight into the future outlook of such processes.

16.2 Fundamentals

A pure component when heated above its critical temperature (T_c) and pressurized above its critical pressure (P_c) is called a supercritical fluid. In the supercritical fluid region the phase boundary between the liquid and vapor phases disappears, thus, the two phases having identical density become indistinguishable and form what is often referred to as "dense gas" (Brunner 1994). Above the critical temperature a pure gas cannot be liquefied even at very high pressures, as illustrated in Fig. 16.1 for CO_2. Depending on molecular size, polarity, and intermolecular hydrogen bonding, the critical temperatures of pure substances vary over a wide range, with water having a particularly high critical temperature ($T_c = 374.2°C$) and pressure ($P_c = 220$ bar), while that for SC–CO_2 is considered to be moderate ($T_c = 31.1°C$, $P_c = 74$ bar) (McHugh and Krukonis 1986).

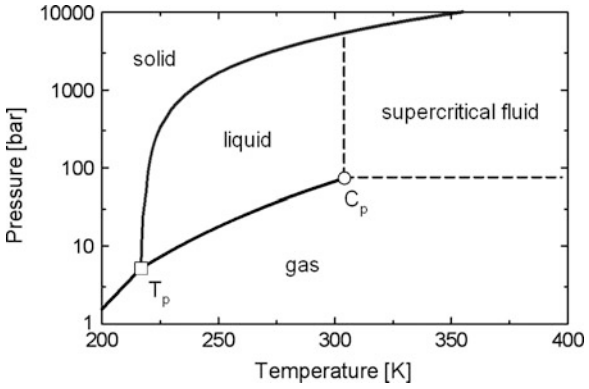

Fig. 16.1 Schematic phase diagram for pure carbon dioxide showing solid, liquid, gas and supercritical fluid regions, triple point (T_p), and critical point (C_p)

16.2.1 Physical and Transport Properties

In Fig. 16.1, there is no sudden change in component properties when crossing the "dashed lines" from the liquid or gas region into the supercritical fluid region. With the exception of the critical point, the variation in fluid properties is monotonous. The values for density, viscosity, and diffusivity of supercritical fluids are between those of gases and liquids (Table 16.1). However, at the critical point, some physical properties such as heat capacity and thermal conductivity exhibit a maximum. Gas-like diffusivity and viscosity, low surface tension, and liquid-like density, together with the tunable solvent power of supercritical fluids, are particularly advantageous for processes involving mass transfer, such as extraction and fractionation. Close to the critical point the density of supercritical fluids is highly dependent on pressure and temperature, where the isothermal compressibility of CO_2 tends to infinity, whereas at higher pressures the influence of temperature is less pronounced. The pressure dependence of density is illustrated in Fig. 16.2, where the slope of the isotherms close to the critical point located in the supercritical region is steeper than at higher pressures and temperatures. Therefore, the density and subsequently the solvent strength of a supercritical fluid are adjustable by modest changes in pressure and temperature, which are utilized in solubility-based separation processes. Additionally, the knowledge of transport properties is crucial for optimal design of separation processes. Transport properties of

Table 16.1 Physical properties of supercritical fluids (SCF)

Physical property	Gas	SCF	Liquid
Density (g/cm^3)	0.001	0.2–1.0	0.6–1.6
Viscosity (mPa.s)	0.0001	0.001	0.01
Diffusivity (cm^2/s)	0.1	0.001	0.00001

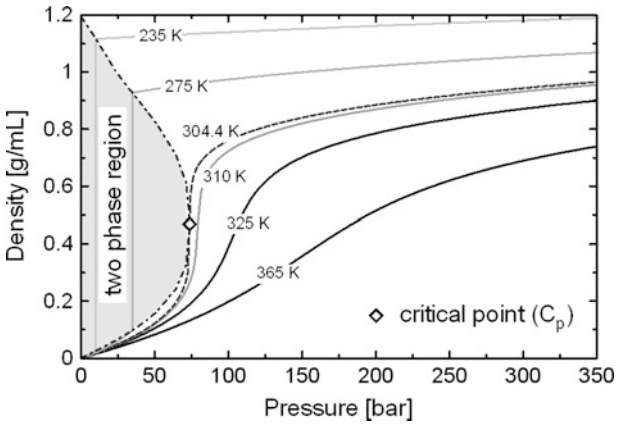

Fig. 16.2 Density versus pressure at various temperatures for carbon dioxide (Data from NIST 2009)

supercritical fluids, such as viscosity, diffusivity, and thermal conductivity are influenced by pressure, temperature, and concentrations of solute or co-solvent.

The dynamic viscosity of neat CO_2 increases with pressure and decreases with temperature, as illustrated in Fig. 16.3 (Fenghour et al. 1998; NIST 2009). It is challenging to measure the viscosity of supercritical fluids close to the critical point due to the highly compressible nature of the fluid phase. Therefore, there are discrepancies between results obtained by different experimental methods (Fenghour et al. 1998). For example, experimental data for the dynamic viscosity of SC–CO_2 determined using a capillary instrument, suggesting that the viscosity increased substantially along isotherms in the vicinity of the critical point (Michels et al. 1957), were found to be inaccurate when compared to other methods (Kestin et al. 1964). It has been shown in later measurements carried out using an oscillating disc viscometer that there is only a mild divergence (<1%) of the viscosity isotherms in the vicinity of the critical point (Kestin et al. 1964). The oscillating disc viscometer is better suited for measurements close to the critical point, whereas compressibility of SC–CO_2 with capillary instruments can lead to errors since such instruments require an appreciable pressure drop across the capillary. The viscosity of binary or multicomponent mixtures of SC–CO_2 involving solute and cosolvent mixtures is even more complex to measure and only limited data are available in the literature (Yener et al. 1998; Tuan et al. 1999). Using a capillary viscometer, Yener et al. (1998) found that the viscosity of SC–CO_2 saturated with methyl oleate at maximum concentrations of 4–5 wt% increased by 15–20%, compared to neat SC–CO_2 at 137 bar and 50°C. The viscosity increase for SC–CO_2 mixed with lipids was found to be linear with increasing lipid concentration. The mixture viscosity of SC–CO_2 with various cosolvents at concentrations ranging from 1 to 5 mol% was measured using a falling weight viscometer, indicating that the fluid viscosity was increased by the cosolvent addition, depending on the size, polarity, and concentration of cosolvent molecules (Tilly et al. 1994). Therefore, during separation processes, changes in the concentration of solutes or cosolvent can have a pronounced effect on the viscosity of the supercritical phase, thereby impacting fluid flow, diffusivity, thickness of boundary layer and, finally, the mass transfer rate.

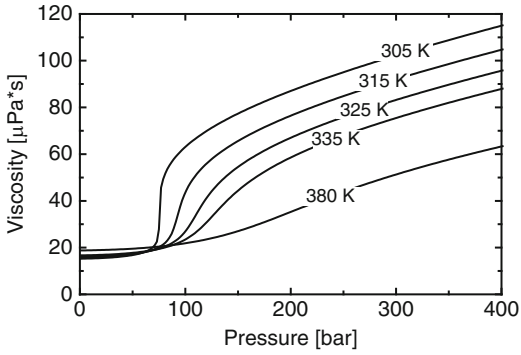

Fig. 16.3 Viscosity versus pressure at various temperatures for carbon dioxide (Data from NIST 2009)

The diffusion coefficient being influenced by viscosity is equally important for separation processes involving mass transfer. Diffusion in supercritical fluids was reviewed by Liong et al. (1991), including a description of experimental methods and a discussion of various factors influencing diffusion coefficients. Diffusion coefficients of solutes in supercritical fluids are affected by numerous factors, such as temperature, pressure, solute and cosolvent concentrations, density, viscosity, as well as molar volume, molecular weight, structure, and polarity of the solute. Similar to viscosity, interactions between solute, solvent, and cosolvent can affect the diffusion coefficient. An excellent review of binary diffusion coefficients at infinite dilution in supercritical fluids, as well as graphical correlations and trends, are given by Suárez et al. (1998). The following general trends can be observed: diffusion coefficients in supercritical fluids increase with increasing temperature and decreasing pressure, due to reduced density and viscosity, leading to decreased collisions and increased mean free paths of the solute. Additionally, smaller molecules diffuse faster than larger ones and diffusion coefficients of polar solutes seem to be more affected by temperature changes than those of nonpolar or low polarity substances, indicating that interactions between solute and solvent need to be considered.

Majority of the data available in the literature regarding diffusion coefficients of solutes in SC–CO_2 has been reported for infinite dilution. However, the reality in some separation processes is far from that, and thus diffusion coefficients determined at infinite dilution have limited applicability and the concentration dependence of diffusion coefficients has to be taken into account (Raspo et al. 2008). Likewise, since most experimental data have been determined for infinite dilution, most of the subsequent correlations and models developed to predict diffusion coefficients are also valid for infinite dilution. For some nutraceutical solutes of very low solubility, such as β-carotene, the diffusion coefficient at infinite dilution may be applicable. However, for cases where solubility is high the influence of concentration has to be taken into account. This can be accomplished by using a modified form of the Darken equation (Darken 1948), which takes into account the solute concentration and a thermodynamic factor that can be predicted by an equation of state approach (Higashi et al. 1999).

Diffusion coefficients of unsaturated fatty acid methyl esters (FAME) with carbon chain lengths ranging from C_{16} to C_{24} in SC–CO_2 were reported by Funazukuri et al. (1991). Additionally, the authors tested several correlations for calculating the binary diffusion coefficient and proposed a new correlation based on the Schmidt number. Diffusion coefficients of lipids, including oleic, linoleic and linolenic acids, methyl and ethyl oleate and di- and trilinolein, were determined by Rezaei and Temelli (2000) based on the peak broadening technique using supercritical fluid chromatography; the diffusion coefficients decreased in the following order: fatty acid esters > fatty acid > triglycerides, indicating that both size and polarity play a role. The effects of molecular weight and degree of unsaturation of lipids on infinite dilution binary diffusion coefficients in SC–CO_2 were assessed by Funazukuri et al. (2004a), showing that for C_{18} fatty acids with increasing number of double bonds, the diffusion coefficient decreased moderately in the case of methyl

and ethyl esters as well as triglycerides. However, for free fatty acids (C_{18} and C_{20}) the trend was the opposite, which may be explained by a stronger effect of the carboxyl group on diffusivity than that of double bonds. A relatively simple hydrodynamic equation relating the binary diffusion coefficient at infinite dilution to viscosity and temperature of the supercritical fluid, together with two solute dependant parameters fitted to experimental data, was successfully applied to lipids and other solutes, including docosahexaenoic acid, eicosapentaenoic acid, α-tocopherol, and β-carotene (Funazukuri et al. 2004b). Under conditions away from the binary mixture critical point, where diffusion coefficients tend to zero, a correlation for calculating the binary diffusion coefficient of various biomaterials, such as tocopherols and triglycerides, can be used with average deviations of ±10% compared to literature data (Catchpole and King 1994). The correlation requires the solvent molecular weight, reduced temperature, density, solute molecular weight, and an estimate of the solute critical volume as input data.

Knowledge of thermal conductivity of the supercritical fluid phase is important for separation processes involving heat transfer, where separation is brought about by a change in temperature, thereby affecting density and solubility. Thermal conductivity for pure CO_2 as a function of pressure and temperature is illustrated in Fig. 16.4 (Vesovic et al. 1990; NIST 2009).

Data on transport properties of supercritical fluid systems are essential for designing processing equipment. However, they are challenging to measure and quantify accurately, to reflect real processing situations, where often multicomponent mixtures at considerable concentrations are encountered rather than dilute binary mixtures. Numerous attempts have been made to develop models and correlations to accurately predict transport properties. However, the accuracy of experimental data still outperforms most correlations and models, which indicates that more research is needed to fully understand all factors impacting transport properties.

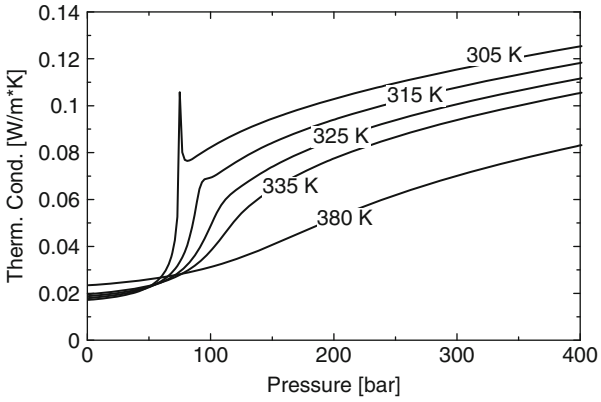

Fig. 16.4 Thermal conductivity versus pressure at various temperatures for carbon dioxide (Data from NIST 2009)

16.2.2 Solubility Behavior

Solubility describes the equilibrium between a solute and a solvent and is a key aspect of separations involving supercritical fluids, similar to conventional solvent processing. Solubility is the maximum amount of a solute that can be solubilized in a solvent at a given temperature and pressure, and is typically reported in terms of mole fraction (i.e., moles of solute per mole of solvent).

16.2.2.1 Factors Affecting Solubility in Supercritical Fluids

Solubility of a solute in SC–CO_2 is highly dependent on temperature and pressure, which influence CO_2 density and subsequently solvent power. The solubility of a substance in a supercritical fluid depends on the interactions between the solute and solvent. Increasing the pressure leads to liquid-like density of the supercritical fluid, thus increasing the probability of interactions between the solute and solvent, including dispersion, polar and hydrogen-bonding (McHugh and Krukonis 1986). Consequently, solubility increases dramatically with pressure. Increasing temperature leads to a decrease in density, which is more pronounced at pressure levels close to the critical point. However, temperature not only affects density of the solvent but it also leads to an increase in the vapor or sublimation pressure of the solute. Therefore, the impact of temperature on solubility depends on both effects. A temperature increase usually leads to a decrease in solubility at low pressures due to the stronger effect on density, whereas at higher pressures an increase in temperature leads to increased solubility. This results in the well-known crossover phenomenon for solubility isotherms. The pressure, above which the effect of temperature on vapor or sublimation pressure prevails, is called crossover pressure. The solubility isotherms converge with increasing pressure and intersect at the crossover pressure, as illustrated in Fig. 16.5 for caffeine (Li et al. 1991), which is a key ingredient of energy drinks, a product of increasing popularity. Separation of solutes can be realized in processes taking advantage of the crossover pressure, which in most cases is a pressure region rather than a specific pressure (Chimowitz and Pennisi 1986). Below the crossover pressure, a solute can be precipitated by increasing the temperature at isobaric conditions. This behavior, where solubility decreases with increasing temperature is also referred to as retrograde condensation, which can be of advantage for certain separation processes. In terms of nutraceuticals, heat sensitivity of the target compound would dictate how much temperature can be increased to achieve retrograde condensation.

Solute properties, especially molecular weight, polarity, and vapor (or sublimation) pressure, also influence solubility in SC–CO_2. The solubility of substances in SC–CO_2 is affected by solute-solvent as well as solute-solute interactions, such as hydrogen bonding. Because of the nonpolar nature of CO_2, the solubility of nonpolar components is usually higher than that for polar components with a similar molecular weight. An increase in the molecular size of a solute decreases

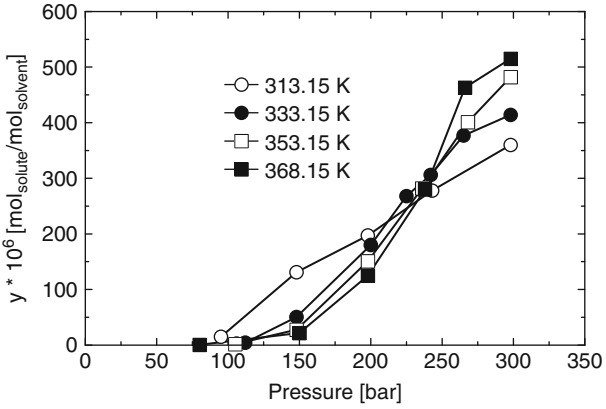

Fig. 16.5 Solubility isotherms and crossover pressure for caffeine (Solubility data from Li et al. 1991)

the solubility in the supercritical fluid. Therefore, nonpolar solutes of low molecular weight and high vapor pressure are preferentially solubilized in SC–CO_2 at relatively low density conditions, and higher density conditions are needed for larger, slightly polar and less volatile solutes. Thus, a few rules of thumb were established for extractability of natural substances by Stahl and coworkers (Stahl and Schilz 1976; Stahl and Quirin 1983):

> "1) hydrocarbons and other lipophilic organic compounds of relatively low molecular mass and polarity are easily extractable;
> 2) the introduction of polar functional groups, hydroxyl or carboxyl groups render the extraction more difficult or impossible;
> 3) sugars and amino acids cannot be extracted up to 500 bar;
> 4) fractionation effects are possible if there are marked differences in mass, vapor pressure, or polarity of the constituents of a mixture."

Besides temperature and pressure, the solvent power of a supercritical fluid can be adjusted by adding a cosolvent exhibiting interaction, such as hydrogen bonding, charge transfer complex formation, and dipole-dipole coupling between solute and cosolvent molecules (Ekart et al. 1993). A cosolvent can also interact with the supercritical solvent, which can in turn affect the solubility of a solute (Ekart et al. 1993). Density of a supercritical fluid solution is increased by the addition of a cosolvent, thereby affecting the solubility of a solute beneficially. In this context, it is noteworthy to mention the so-called cosolvent effect (also referred to as the entrainer effect) (Walsh et al. 1987), which refers to the dramatic increase in both solubility and selectivity when certain cosolvents are added to a supercritical fluid (Brunner and Peter 1982; Brunner 1983; Van Alsten and Eckert 1993; Ruckenstein and Shulgin 2001; Ruckenstein and Shulgin 2002). The cosolvent effect can lead to an increase in the solubility of a solute in a supercritical fluid by up to several hundred percent (Schmitt and Reid 1986), which for some systems is more than what can be achieved by a pressure increase of several hundred bars (Dobbs et al. 1986).

However, interactions between different solutes in a mixture can also cause a decrease in solubility, as observed for the solubility of capsaicin, which was lower in the presence of β-carotene (Skerget and Knez 1997). Recently, Nobre et al. (2009) reported the solubility of a mixture of bixin and β-carotene (1:1, w:w) in SC–CO_2 at 40 and 60°C and pressures of up to 350 bar and showed a substantial solubility enhancement of up to about 265% for bixin in the presence of β-carotene. Solubilities of solid mixtures in SC–CO_2, including a discussion of the observed increase and decrease of solubility, are reviewed by Lucien and Foster (2000). A beneficial cosolvent effect can be exploited for improving separation processes.

The proper selection of a cosolvent can aid in separation processes by improving selectivity and solubility. For example, the addition of up to 10% (vol%) ethanol increased the solubility of gallic acid from 0.005 mg/kg_{CO2} in pure CO_2 to 7.48 mg/kg_{CO2} at 200 bar and 40°C (Murga et al. 2000). Furthermore, the solubility behavior of ternary systems of lipids, cosolvents, and SC–CO_2 is affected by cosolvent addition (Güçlü-Üstündag and Temelli 2005; Güçlü-Üstündag and Temelli 2006). The addition of cosolvents can increase as well as decrease selectivity in fractionation processes of lipids using SC–CO_2, if there are specific interactions between the solutes of interest and cosolvent. For example, the addition of ethanol can improve the deacidification of oils, as demonstrated for the separation of free fatty acids (FFA) from palm oil (Ooi et al. 1996) or FFA and peroxides from Orange Roughy fish oil (Catchpole et al. 2000). However, there are cases where selectivity decreases upon the addition of a cosolvent, such as in the fractionation of shark liver oil, where the separation of squalene from di- and triglycerides decreased with increasing ethanol content (Catchpole et al. 2000).

16.2.2.2 Solubility Determination and Correlation

Methods to determine the phase equilibrium or solubility of a solute in a supercritical fluid can be divided into two classes depending on how the concentration in the phases is determined, namely analytical (direct sampling methods) and synthetic (indirect methods) (Dohrn and Brunner 1995). Several reviews discussing the pros and cons of the various experimental methods can be found elsewhere (Deiters and Schneider 1986; Dohrn and Brunner 1995; Nagahama 1996). However, some challenges that can be encountered when measuring solubilities are highlighted here and discussed briefly, using the case of β-carotene as an example. The literature data for the solubility of β-carotene in SC–CO_2 are very scattered with differences ranging over more than an order of magnitude (Güçlü-Üstündag and Temelli 2004; de la Fuente et al. 2006). These discrepancies can be attributed to differences in the purity of the solutes as well as the limitations of the experimental techniques used. Impurities in the sample can enhance or reduce the solubility of a solute (Güçlü-Üstündag and Temelli 2000), due to impurities acting like a cosolvent. Furthermore, β-carotene can oxidize and isomerize easily during experiments or when exposed to air, which requires special precautions during sample preparation and measurements (Cocero et al. 2000). The crystalline nature of β-carotene affects solubility; as shown by

Sakaki (1992), the solubility of crystalline β-carotene was lower compared to that of amorphous β-carotene, which may be expected due to the higher heat of fusion for crystalline β-carotene. In addition to issues related to purity or cystallinity of β-carotene, the different experimental methods applied for solubility determination come with certain limitations and can lead to errors as well. For example, in systems using a dynamic method reaching true equilibrium may be challenging. In static systems or recirculation systems, attainment of equilibrium may be monitored by adequate sensors to ascertain changes in the solute-SC–CO_2 mixture over time. After ensuring proper equilibration one has to watch out for another source of error caused by the sampling/quantification of the solute in the supercritical phase. During off-line sampling from a static equilibrium cell a small volume of equilibrated fluid phase is removed, which can lead to changes in pressure and/or temperature, thereby disturbing equilibrium. Furthermore, loss of solute by precipitation in the valves or sampling lines can occur. To minimize disturbance of the equilibrium inside a static equilibrium cell, variable volume cells have been developed, which compensate for the sample volume removed. On-line sampling allows solute quantification prior to the depressurization step by means of chromatographic or spectrophotometric systems attached to the extraction cell. However, the use of UV detectors can lead to errors due to the potential saturation of the sensor (Mendes et al. 1999). Another method based on a quartz crystal microbalance (QCM) was used by Saldaña et al. (2006) to measure the solubility of β-carotene *in situ*, which eliminates the need for sampling. However, the QCM technique is very sensitive to environmental factors and loading the crystal uniformly can be challenging. In summary, solubility measurements of unstable substances having a relatively low solubility such as carotenoids in SC–CO_2 are challenging and great care must be taken to avoid the aforementioned errors and pitfalls.

There are also numerous studies where solubility for a component is reported based on dynamic extraction of a complex plant matrix. In this case, the "apparent solubility" is not only based on thermodynamic solubility but also on the interactions of the solute with the solid matrix, as well as the potential cosolvent effects of the other components present. This approach may be more representative of the complex multicomponent systems under consideration for process development purposes; however, care must be taken to ensure equilibrium criteria are met. These include having sufficient solute present to saturate the CO_2, using low enough flow rates to allow sufficient residence time, and evaluating the slope of the initial linear portion of the extraction curve, which corresponds to the solubility-controlled region, rather than reporting the yield obtained on a single point on the extraction curve. Comparison of β-carotene solubility in the binary system of pure β-carotene + SC–CO_2 to the apparent solubility obtained in the multicomponent carrot system revealed a 5–10 fold reduction in the multicomponent system under similar temperature and pressure conditions mainly due to interactions of β-carotene with the solid matrix (Saldaña et al. 2006).

Bibliographic summaries covering high pressure phase equilibrium data published up to 2002 are available in the literature (Hicks 1978; Knapp et al. 1981; Fornari et al. 1990; Dohrn and Brunner 1995; Christov and Dohrn 2002).

Furthermore, solubility data as well as correlations for numerous less volatile substances and high boiling substances can be found (Bartle et al. 1991; Higashi et al. 2001). An excellent collection of solubility data for more than 780 solutes including liquids, solids, polymers, foods, drugs, nutraceuticals, dyes, pesticides, and metal complexes has been compiled by Gupta and Shim (2007). Solubility of numerous nutraceutical compounds in SC–CO_2 has been investigated using pure components and mostly employing static methods. Diaz-Reinoso et al. (2006) compiled a list of pure phenolic components with antioxidant activity for which solubility has been reported.

Accuracy and precision of measured solubility data are believed to be superior to data predicted by correlations or models based on group contribution methods or equations of state (EoS) in many cases. For example, the performance of six different cubic EoS to predict the solubility of cholesterol and β-carotene in SC–CO_2 and ethane was assessed by Hartono et al. (2001). The study revealed deviations by several orders of magnitude between the experimental data and predicted solubility values in cases of the Van der Waals and Redlich Kwong EoS, whereas the Mohsen-Nia–Moddaress–Mansoori EoS delivered acceptable results (Hartono et al. 2001). However, the use of EoS requires the knowledge of parameters, which in many cases are not experimentally accessible, such as critical pressure and temperature. Since those parameters cannot be measured experimentally due to decomposition of the solute, as in the case of cholesterol and β-carotene, the critical parameters need to be estimated by group contribution methods, which add uncertainty to the calculations (Somayajulu 1989). Furthermore, experimental data are needed to adjust interaction parameters in those EoS models. The solubility of a mixture of bixin and β-carotene in SC–CO_2, taking into account the interaction between the solutes, was described reasonably well with a model based on the Peng-Robinson EoS, with deviations from experimental data of about 18.2 and 44.6% for β-carotene and bixin, respectively (Nobre et al. 2009). Nevertheless, empirical, semi-empirical, and theoretical correlations to model solubility data for binary supercritical fluid systems (Chrastil 1982; Ziger and Eckert 1983; Schmitt and Reid 1985) can be used in certain cases to predict solubility data based on available experimental data. Unlike approaches utilizing EoS, which require properties of solutes, such as critical properties, that are often difficult or impossible to determine experimentally, these empirical, semi-empirical, and theoretical correlations are mostly based on accessible density and solubility data. If the properties required for modeling are not available, the application of property estimation methods is required, leading to uncertainties in the prediction of solubility data. A well known density-based correlation for solubility data was developed by Chrastil (1982) that relates the solubility S [g/L] of a solute to the solvent density ρ [g/L] and temperature T [K]:

$$S = \rho^k e^{(a/T+b)} \tag{16.1}$$

where k is the association constant, and a and b are defined as

$$a = \frac{\Delta H}{R} \tag{16.2}$$

$$b = -\ln\left(\frac{M_G^k}{M_A + k^* M_G}\right) + q \tag{16.3}$$

with the ideal gas constant R, the sum of heat of solvation and vaporization ΔH, a constant q, and the molecular weights of solute M_A, and solvent M_G. Chrastil's model is based on the assumption that a solute molecule (A) associates with k molecules of the supercritical solvent (G) forming a solvate complex (AG_k), which is in equilibrium with the supercritical fluid. Plotting ln(S) versus ln(ρ) results in a straight line with a slope of k and intercept of $(a/T + b)$. For solutes with a low solubility, the solubility S can be converted from [g/L] into a mol fraction y in [$mol_{solute}/mol_{solvent}$] by multiplying equation (1) with $\rho^* M_A/M_G$, which leads to:

$$y = \rho^{k+1} \frac{M_A}{M_G} e^{(a/T+b)} \tag{16.4}$$

Plotting ln(y) versus ln(ρ) also results in a straight line, now with a slope of (k + 1), as illustrated in Fig. 16.6 for the solubility data of caffeine in SC–CO_2 (Li et al. 1991).

The density-based correlation methods for solubility data work reasonably well for nonpolar solutes and to a lesser extent for polar solutes at pressure levels corresponding to high supercritical fluid densities (Gurdial et al. 1989). However, when applied over the entire supercritical fluid density range to systems with higher concentrations or polar solutes, simple relationships between the solute solubility and solvent density exhibit a weakness, because the complex nature of solute-solvent and solute-solute interactions cannot be described by these correlations.

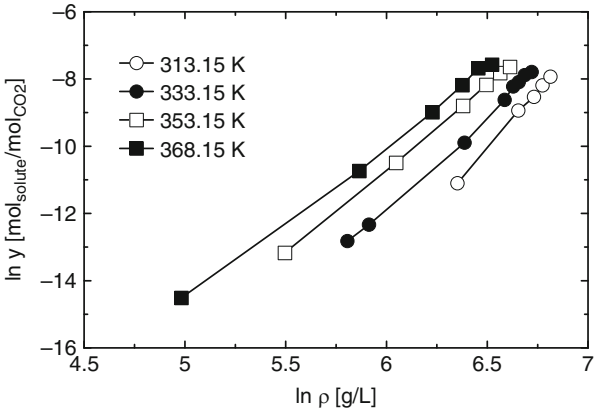

Fig. 16.6 Logarithmic plot of caffeine solubility y [mol_{solute}/mol_{CO2}] versus CO_2 density [g/L] (Solubility data from Li et al. 1991)

Chrastil's model was applied to correlate literature data for solubility of lipids, such as fatty acids, mono-, di-, and triglycerides, and fatty acid esters as well as minor lipid components, such as β-carotene, α-tocopherol, stigmasterol, and squalene in SC–CO_2 (Güçlü-Üstündag and Temelli 2000; Güçlü-Üstündag and Temelli 2004). Solubility data of oleic acid, β-carotene, and capsaicin in SC–CO_2 were also correlated using Chrastil's model (Skerget et al. 1995), resulting in deviations between experimental and correlated solubility values of up to about 30% for both oleic acid and β-carotene. Furthermore, the authors found that the association constant k differs between liquid CO_2 and SC–CO_2, which indicates that the same model constants cannot be used for both cases.

16.3 Separation Processes

16.3.1 Extraction

Over the years, SC–CO_2 extraction of a very large number of plant materials from all over the world has been reported. Even though there are similarities regarding the standard extraction parameters, every system is unique in terms of the specific chemical composition and the interactions between the components. The discussion here focuses on the extraction of lipid-based nutraceuticals (especially specialty oils and carotenoids) and phytochemicals.

Similar to conventional extraction techniques, SC–CO_2 extraction of targeted components from a plant matrix is dictated by several parameters, including pretreatment of plant material, particle size, temperature, pressure, time, solvent flow rate, and solvent-to-feed ratio. These parameters impact the efficiency of extraction, which is determined in terms of yield and recovery of the targeted components. Yield is the amount of total extract obtained per unit mass of starting feed material (i.e., g extract/g feed), whereas recovery is the percentage of targeted component originally present in the feed material recovered in the extract (i.e., [g target compound in extract/g target compound in feed]*100). Unfortunately, there is confusion in a number of reports presented in the literature where these basic parameters are not reported properly.

Pretreatment of plant material may involve drying and/or grinding. Some practical considerations for SC–CO_2 extraction of plant materials with respect to sample preparation, selection of modifiers, collection methods, on-line coupling techniques, means for avoiding mechanical problems, and approaches to optimization of supercritical fluid extraction (SFE) conditions are summarized in a review by Lang and Wai (2001). In general, plant matrices have a high moisture content, which may be a detriment if the targeted components are nonpolar such as lipids. Since CO_2 is a nonpolar solvent, the presence of high levels of moisture can act as a barrier for CO_2 and lipids to diffuse through the solid matrix. On the other hand, if the targeted components are polar, such as phenolics, then water can act as a cosolvent

and enhance the recovery of these compounds. Selectivity of SC–CO_2 extraction is influenced by the moisture content of the plant matrix as well. For example, presoaking the feed material with water is beneficial for the selective extraction of alkaloids, such as caffeine from coffee beans (Peker et al. 1992). Furthermore, some polar components of essential oils, such as thymol, linalool, and terpinene are better solubilized in SC–CO_2, when the moisture level of the samples is increased (Stahl and Gerard 1985; Leeke et al. 2002). As well, the presence of some water may be beneficial in terms of maintaining the permeability of cell membranes. Therefore, there is an optimal level of moisture depending on the plant matrix and the targeted bioactives. It should not be overlooked that water is also solubilized by SC–CO_2, despite at low levels (about 0.0067 mole fraction at 200 bar and 50°C) (Wiebe 1941; King et al. 1992), and will be coextracted. A high level of water in extracted lipids is not desirable since it will impact product quality negatively, necessitating additional fractionation of the extract to remove water. Moisture level of the feed material can be adjusted by various drying techniques such as air drying, vacuum drying, sun drying, and freeze drying; however, care must be taken to minimize any degradation of the bioactives due to exposure to high temperatures over extended periods of time. Needless to say, cost is another consideration and expensive techniques like freeze drying may not be feasible as a pretreatment prior to SC–CO_2 extraction.

It is important to understand the cellular structure of the raw material and the location of the targeted components prior to use in extraction. For example, oil in nuts is easily accessible by diffusion into the cellulosic structure, whereas oil in whole seeds is not accessible due to the presence of an almost impermeable seed coat (Sovova et al. 1994; Reverchon et al. 2000). Therefore, grinding of the plant material to the optimal particle size to break up impermeable structures and to expose the solute to solvent is essential for enhanced extraction efficiency. Depending on the grinding equipment used, again it is critical to avoid overheating of the plant material and to minimize degradation of bioactives during grinding. Smaller particle size is desirable to increase contact surface area with the solvent and to minimize the path length that bioactives have to diffuse through to reach the bulk phase. However, too small particles may lead to bed compaction and channeling effects, which are not desirable.

Extraction temperature and pressure are critical parameters for optimal yield since they dictate the solubility of bioactives in SC–CO_2 as discussed above. Good understanding of the solubility behavior of the targeted bioactive in SC–CO_2 is essential to optimize temperature and pressure for maximum solubility during extraction.

Extraction time, solvent flow rate, and solvent-to-feed ratio are the other parameters that have to be optimized. Solvent-to-feed ratio and extraction time need to be minimized for cost savings; however, sufficient residence time and amount of solvent have to be provided to maximize bioactive recovery. The extraction kinetics proceed through constant-rate and declining-rate periods. The freely available solute on the particle surface is solubilized rapidly during the constant-rate or fast extraction period, where the extraction rate is limited by equilibrium solubility.

This is represented by the initial linear portion of a typical extraction curve. Once the solute on the particle surface is depleted, the extraction rate declines or the slow extraction period begins, where SC–CO_2 has to diffuse into the particles, solubilize the solute, and SC–CO_2 + solute has to diffuse out to the bulk phase. This is a slow process driven by the concentration gradient of the solute, and thus the extraction curve approaches a constant value asymptotically. The extraction time should be optimized to ensure the constant-rate period is completed since the yield increases only marginally during the declining-rate period. The duration of constant-rate period is shorter for smaller particle size due to increased contact surface area as well as for temperature and pressure conditions corresponding to high solubility.

16.3.1.1 Lipid-Based Nutraceuticals

Specialty oils. Specialty oils have received growing interest over the past decade mainly because of the high concentrations of polyunsaturated fatty acids (PUFA) within their fatty acid profile, as well as the fat-soluble bioactive minor components they contain, such as tocols (tocopherols and tocotrienols), carotenoids, sterols, and squalene. Extensive research has demonstrated the health benefits of these components, including beneficial effects against heart disease, cancer, and other degenerative diseases, as highlighted by Temelli et al. (2008) recently.

Specialty oils include nut oils (almond, hazelnut, peanut, pecan, pistachio, and walnut), seed oils (borage, flax, evening primrose, grape, pumpkin, and rosehip), cereal oils (amaranth, rice bran, oat, and wheat germ), and fruit and vegetable oils (buriti fruit, carrot, olive, and tomato). Conventional methods of extracting these oils involve mechanical pressing and/or solvent extraction. Mechanical pressing at temperatures below 60°C (also referred to as cold pressing) is used extensively; however, this technique suffers from the fact that residual oil in the press cake is quite high (~5%), leading to low oil recoveries. Solvent extraction is followed by heat treatment for solvent recovery, which compromise oil quality. Therefore, SC–CO_2 extraction of specialty oils gives a superior product with high efficiencies. An extensive review of the subject by Temelli et al. (2008) gave a detailed discussion of the effect of different extraction parameters on recovery as well as the composition and quality of the extracted oils from nuts, cereals, seeds, and fruits and vegetables in comparison to those obtained using traditional techniques.

In general, temperatures of 35–80°C and pressures of up to 690 bar have been used for SC–CO_2 extraction of specialty oils, resulting in oil recoveries of greater than 95%, as in the case of hazelnut (Bernardo-Gil et al. 2002), peanut (Goodrum and Kilgo 1987), walnut (Oliveira et al. 2002), evening primrose (Favati et al. 1991), grape seed (Cao and Ito 2003), rice bran (Shen et al. 1996), and wheat germ (Taniguchi et al. 1985) oils. The color of the extracted oils varied with extraction conditions, depending on the extent of extraction of pigments (Palazoglu and Balaban 1998). Compositional analysis of all the specialty oils demonstrated very high levels of oleic (C18:1), linoleic (C18:2), and linolenic (C18:3) acids,

accounting for more than 90% of the total fatty acids for the seed oils (Temelli et al. 2008). The tocopherol contents of walnut (Oliveira et al. 2002) and wheat germ (Gomez and de la Ossa 2000) oils extracted with SC–CO_2 were higher than those extracted with hexane. The SC–CO_2-extracted oil was clearer, thus requiring less refining compared to hexane-extracted oil (Bernardo-Gil et al. 2002; Oliveira et al. 2002; Lopes and Bernardo-Gil 2005). Squalene was recovered from rice bran (Kim et al. 1999), and *Amaranthus* grain (He et al. 2003) using SC–CO_2 but to a much lesser extent compared to that obtained by using solvent extraction.

Even though the majority of the studies used neat SC–CO_2, several researchers added ethanol (up to 10%, wt%, or mol%) as a cosolvent into SC–CO_2 and achieved higher yields. For example, the extraction yields of pistachio (Palazoglu and Balaban 1998) and sesame (Odabasi and Balaban 2002) oils increased substantially upon ethanol addition over that obtained by neat SC–CO_2. On the other hand, the phosphorus content of oat oil increased to 80 ppm, probably due to the extraction of polar phospholipids in the presence of ethanol (Fors and Eriksson 1990). Although ethanol addition may offer some advantages in terms of increased yield, it negates the major advantage of SC–CO_2 extraction of avoiding the use of organic solvents and heat treatments since ethanol removal from the extract and the residual meal requires the use of heat. Unfortunately, this aspect is usually overlooked in many studies.

Carotenoids. Carotenoid pigments responsible for the bright yellow, orange, and red colors of various plant materials are comprised of two main classes, carotenes and xanthophylls, which are C_{40} polyunsaturated hydrocarbons and their oxygenated derivatives, respectively. Because of the provitamin A activity of β-carotene and the potent antioxidant activity of lycopene associated with reducing the risk of prostate cancer (FDA 2005), numerous studies have focused on their extraction from carrots and tomatoes, respectively, using SC–CO_2. Use of by-products of conventional processing industries (i.e., carrot cubes, carrot juice, tomato juice, tomato paste, etc.) as the raw material for the recovery of these valuable carotenoids is very attractive. In addition, other sources such as marigold and algae are also receiving increasing attention as raw materials for carotenoids. Extraction of carotenoids as well as oleoresins and capsaicinoids using SC–CO_2 from various sources is summarized in Table 16.2.

It is necessary to dry carrots and tomatoes prior to extraction due to their high moisture content (80% and 95%, respectively) and samples are mostly freeze dried for research purposes. The SC–CO_2 extraction yields of α- and β-carotene increased with decreasing moisture content of carrot feed material, whereas the yield for lutein was higher at higher moisture levels since water can act as a cosolvent for the relatively polar oxygenated lutein (Sun and Temelli 2006). From tomatoes containing 50–60% moisture, only trace levels of lycopene were extracted (Vasapollo et al. 2004).

As expected, lycopene extraction yield increased with pressure at 66°C and with temperature at a pressure level of 450 bar, which is above the crossover pressure of isotherms (Vasapollo et al. 2004). Lycopene recovery from tomato skin reached 96% at 110°C in 40 min (Ollanketo et al. 2001); however, caution

Table 16.2 Extraction of carotenoids and other compounds from tomato, carrot, paprika, apricot, marigold, and algae

Feed material/characteristics	Pressure (bar)	Temperature (°C)	Co-solvent	Yield[a]/Recovery[b] of target compound		Reference
Tomato				Lycopene	β-Carotene	
Skin + seed	138–483	32–86	No	61[b]		(Rozzi et al. 2002)
Skin + seed	250, 300	60, 80	No	80[b*]	88[b*]	(Sabio et al. 2003)
Skin + pulp	77–281	40	No	42[b]	98[b]	(Gomez-Prieto et al. 2003)
Skin	200–500	40–100	No	94[b]		(Topal et al. 2006)
Skin + seed	460	80	No	31.4[a]		(Vagi et al. 2007)
Dried powdered skin	400	60–110	Acetone, dichloromethane, hexane, methanol, ethanol, water; added to sample	n/a highest recovery with acetone as co-solvent		(Ollanketo et al. 2001)
Skin + seed	172–276	40–80	Chloroform, hexane (1 mL); added to sample	64[a**], 84[b**]	35[a**], 93[b**]	(Cadoni et al. 1999)
Saponified tomato powder	370–530	47–63	EtOH (16%)	27.4[a]		(Huang et al. 2008)
Skin + seed	250–350	45–75	EtOH, water, olive oil as single, binary, ternary modifier: 0, 5 or 10% added to sample	73.3[b] (10% EtOH + 10% olive oil)		(Shi et al. 2009)
Dried paste	200–300	35–65	No	20[b]	40[b]	(Baysal et al. 2000)
			EtOH; 5, 10, 15% with SC–CO_2	50[b] (5% EtOH)	50[b] (5% EtOH)	

(*continued*)

Table 16.2 (continued)

Feed material/characteristics	Pressure (bar)	Temperature (°C)	Co-solvent	Yield[a]/Recovery[b] of target compound		Reference
Dried tomato	335, 450	45, 66	No	10[b]		(Vasapollo et al. 2004)
	450	66	Hazelnut oil 10% w/w added to sample	30[b]		
Carrot					β-Carotene	
Freeze dried	120–327	40, 50	No		47.8[b]	(Saldaña et al. 2006)
Pulp press cake	207, 276, 345	40, 55, 70	EtOH; 0, 5, 10% w/w with SC–CO_2		99.5[b]	(Vega et al. 1996)
Particles	276–551	40, 55, 70	No		63[b*]	(Sun and Temelli 2006)
Moisture: 0.8–85% Particle sizes: 0.25–2 mm			Canola oil; 2.5, 5% w/w with SC–CO_2		147[b* **]	
Paprika/red pepper				Carotenoids	Oleoresin (capsaicin)	
Dried powder *Capsicum annuum*	300–500	60–80	No	62[b] linear stage: β-carotene + free xanthophylls nonlinear stage: xanthophyll esters		(Ambrogi et al. 2002)
red pepper *Capsicum frutescens*	150–230	40	No		5200[a] (oleoresin) 252[a] (capsaicinoids)	(Duarte et al. 2004)
Paprika ground *Capsicum annuum* Moisture: 5–30% Oil cont. 5–27% w/w	450	50	No		90[b]	(Nagy and Simandi 2008)

(*continued*)

Table 16.2 (continued)

Feed material/characteristics	Pressure (bar)	Temperature (°C)	Co-solvent	Yield[a]/Recovery[b] of target compound		Reference
Chili powder *Capsicum frutescens* Paprika powder *Capsicum annuum*	CO_2 Density: 0.75–0.9 g/mL	45–75	Methanol, acetic acid and water; 20 μL added to 70 and 250 mg sample		76[a] (capsaicinoids) (co-solvent water)	(Peusch et al. 1997)
Red pepper *Capsicum annuum* Pelletized flakes moisture: 4% w/w	320–540	40	No	Red pigments: 88[b] Yellow pigments: 55[b]		(Uquiche et al. 2004)
Apricot				β-Carotene		
Pomace	133–473	43–77	EtOH; 2–28% v/v with SC–CO_2	9.8[a]		(Sanal et al. 2005)
Marigold				Terpene/Carotenoid	Oleoresin	
Dried flowers	120, 150, 200	26, 30, 40	No		2,100[a]	(Campos et al. 2005)
Flowers	120–200	20–40	No		3,540[a]	(Danielski et al. 2007)
Dried flowers	300, 500, 689	50	EtOH; 0–20% v/v with SC–CO_2	Faradiol esters 650[a]	8,300[a]	(Baumann et al. 2004)
Dried petals	145–455	33.2–71.8	soybean oil; 0–12.1% w/w with SC–CO_2	lutein 96,200[a]		(Ma et al. 2008)
Algae				Total Carotenoids	Astaxanthin[c] Canthaxanthin[d]	
Dried powder *Haematococcus pluvialis*	300–500	40–80	no		22,800[ac]	(Thana et al. 2008)
Freeze dried powder	200–500	40, 50, 60	EtOH; 5% mol	963[a] *(D. salina)*		

(*continued*)

Table 16.2 (continued)

Feed material/characteristics	Pressure (bar)	Temperature (°C)	Co-solvent	Yield[a]/Recovery[b] of target compound	Reference
Nannochloropsis gaditana *Synechococcus sp.* *Dunaliella Salina*				186[a] *(Synechococcus)* 289[a] *(Nannochloropsis)*	(Macias-Sanchez et al. 2008)
Freeze dried, crushed *Chlorella vulgaris*	150–350	40, 55	No	6[ac] 24[ad]	(Mendes et al. 1995)
Dried powder *Haematococcus pluvialis*	300–500	50–80	Soybean oil, olive oil, EtOH; 0–12% v/v	25[bc] (pure CO_2) 36[bc] (soybean oil) 51[bc] (olive oil)	(Krichnavaruk et al. 2008)

d.m. dry matter
*Skin only
**No cosolvent
***Compared to soxhlet
[a]Yield (mg/100 g feed)
[b]Recovery (%) [100 × (g solute in extract/g solute in feed)]
[c]Astaxanthin
[d]Canthaxanthin

should be exercised in processing at such high temperatures to avoid any degradation of lycopene.

Because of the very low solubilities of β-carotene and lycopene in SC–CO_2, cosolvents have been incorporated in an attempt to increase extraction yields of these carotenoids. Several of the studies mixed the cosolvent with the feed material prior to extraction (Ollanketo et al. 2001; Vasapollo et al. 2004; Shi et al. 2009). The problem with this approach is that the cosolvent concentration would change throughout the extraction period as SC–CO_2 flows through the extraction cell and solubilizes the cosolvent together with the carotenoids. Therefore, it is desirable to mix the cosolvent continuously into SC–CO_2 to maintain a constant concentration. On the other hand, Ollanketo et al. (2001) tested cosolvents like acetone, ethanol, methanol, hexane, dichloromethane, and water and all except water increased lycopene recovery. Even though such cosolvents can be used for analytical purposes, they would not be acceptable for large-scale processing due to the demand for "natural" products, especially in the nutraceutical market. Since carotenoids are fat-soluble pigments, vegetable oils were also used as a cosolvent in SC–CO_2 by mixing the oil with feed material (Vasapollo et al. 2004; Shi et al. 2009) and by continuous addition to SC–CO_2 (Sun and Temelli 2006). Vasapollo et al. (2004) used hazelnut oil for lycopene extraction and achieved a lycopene recovery of 30% in 8 h. Upon continuous addition of canola oil into SC–CO_2 for the extraction of carotenoids from carrots, Sun and Temelli (2006) obtained more than a two-fold increase in yield at 288.0–846.7 μg/g and 333.8–900.0 μg/g feed for α- and β-carotene, respectively. The major advantage of using vegetable oil as a cosolvent is the elimination of organic solvents and the fact that vegetable oil enriched in carotenoids can be used in a variety of applications without further treatment.

16.3.1.2 Phytochemicals

Research outcomes demonstrating the health benefits associated with various phytochemicals have triggered the growing demand for "natural" antioxidants and other plant extracts of different bioactivities, which in turn resulted in a tremendous level of research activity focusing on the extraction, characterization, and functionality determination for a range of plant materials from all over the world. A comprehensive compilation of such works is beyond the scope of this chapter; however, Diaz-Reinoso et al. (2006) have done an excellent job in such an attempt.

Plant extracts are complex mixtures comprised of different classes of compounds, including essential oils, esters, terpenes, fatty acids, waxes, resins, pigments, phenolics, etc. In general, these compounds are present in relatively low concentrations, where the total extract yield may be <5% (Diaz-Reinoso et al. 2006). Essential oils in general are more volatile and can be easily extracted at relatively low pressures of less than 150 bar at temperatures of 40–50°C using SC–CO_2 (Reverchon 1997). However, obtaining a total extract would require the use of higher pressures (up to 550–600 bar). Selective extraction of different groups of compounds can be

achieved by proper optimization of extraction conditions as well as the separation conditions as discussed later.

The plant materials used for SC–CO_2 extractions encompass herbs, spices, aromatic, and medicinal plants. These plants are especially rich in bioactives with antioxidant activities as well as other physiological benefits including antimicrobial, antiviral, anti-inflammatory and antimutagenic activities (Moure et al. 2001; Sacchetti et al. 2005; Srinivasan 2005). Previous reviews focused on the SC–CO_2 extraction of bioactives from traditional Chinese medicinal plants (Li 2008), Latin American plants (Meireles 2008), and a variety of spices (Mukhopadhyay 2008). In addition, by-products of the conventional processing industries are receiving growing attention for the recovery of such bioactives as reviewed by Herrero et al. (2006). For example, grape seeds and skins as by-products of the juice and wine industries are being used for the recovery of catechins and other phenolics for their antioxidant activity (Palma et al. 1999; Murga et al. 2000). Supercritical fluid extraction (SFE) of plant materials using SC–CO_2 is advantageous compared to conventional methods, such as hydrodistillation or organic solvent extraction using acetone, methanol, ethanol, hexane or others because generally the extracts obtained with SC–CO_2 are more potent. For example, SC–CO_2 extracts of marjoram were more potent in inhibiting the growth of fungi and bacteria than those obtained using ethanol (Vagi et al. 2005).

16.3.2 Fractionation

It may be desirable to further fractionate an extract in order to obtain the targeted bioactives in a more concentrated form. The supercritical technology offers flexibility in this regard as different fractionation protocols can be employed. Such protocols can be categorized into three approaches requiring different types of equipment.

1. Fractional extraction: Fractions can be collected as a function of time throughout an extraction. In addition, extraction conditions can be programmed to change over time. For example, pressure can be kept low initially to extract low molecular weight compounds, and increased to a higher level once the low molecular weight compounds are depleted to extract the higher molecular weight compounds. As well, neat CO_2 can be used first to extract neutral compounds, followed by the injection of a polar cosolvent to recover more polar components in the second fraction. One extractor and one separator are sufficient for fractional extraction.
2. Fractional separation: In this case, multiple separators are necessary to collect different fractions of an extract. Temperature and pressure conditions corresponding to a very high solvent density are used to recover a total extract followed by adjusting the temperature/pressure conditions in the separators for a stage-wise drop of solvent density so that the highest molecular weight/lowest

volatility fraction falls out of solution first and is collected in the first separator, followed by collection of lower molecular weight/higher volatility fractions in the subsequent separators with a further drop in density in each separator.

3. Column separation: continuous feed of a liquid mixture is what distinguishes a column operation from the first two cases, wherein a batch of solid material is used as the feed. These are usually packed columns with independently heated and controlled sections, designed to create a thermal gradient along the column to take advantage of retrograde condensation so that an internal reflux can be generated for increased efficiency of separation. Countercurrent contacting of the liquid feed with SC–CO_2 results in the separation of the liquid feed into extract and raffinate streams coming out of the top and the bottom of the column, respectively. Brunner (2009) provided an overview of the design considerations for such systems. The following sections will focus on the different applications of these three approaches to various nutraceuticals.

There are additional recent developments in the area of coupling membrane technologies with supercritical technology, which may be the fourth approach in fractionation to achieve difficult separations. It may be possible to separate those components with similar solubilities in SC–CO_2 by attaching a membrane unit after an extraction or a fractionation unit. For example, squalene, which is receiving increasing attention as a nutraceutical, and oleic acid have similar solubilities in SC–CO_2 due to the nonpolar nature of squalene, although squalene (C_{30}) is a much larger molecule than oleic acid (C_{18}) (Güçlü-Üstündag and Temelli 2004). However, such a large molecular weight difference can be an advantage for membrane separation. With the use of an appropriate membrane these two lipids solubilized in SC–CO_2 can be separated under supercritical conditions (Ruivo et al. 2008).

16.3.2.1 Lipid-Based Nutraceuticals

Polyunsaturated fatty acids. Fractionation of polyunsaturated fatty acids (PUFA) obtained from marine sources is the main focus of this section even though processing of specialty oils containing γ-linolenic acid (GLA or C18:3ω6) or α-linolenic acid (ALA or C18:3ω3) using near critical fluids, such as CO_2, propane, and dimethylether, has also been investigated (Catchpole et al. 2009). Processing of fish oils using supercritical fluids has been reviewed recently (Eltringham and Catchpole 2008).

Ever since the early epidemiological studies showing a correlation between high fish consumption and decreased fatal heart attacks (Strøm and Jensen 1951) and heart diseases (Dyerberg et al. 1975), there has been growing interest in fish oils and additional research has demonstrated the importance of long chain polyunsaturated fatty acids (LC-PUFA) in terms of the health benefits of fish oil (Horrocks and Yeo 1999). The two most important LC-PUFA in fish oil, namely eicosapentaenoic acid (C20:5ω3, EPA) and docosahexaenoic acid (C22:6ω3, DHA) belong to the family of omega-3 fatty acids, where the first double bond begins with the third carbon

atom from the methyl end of the molecule. Noteworthy, omega-3 fatty acids such as EPA and DHA obtained from fish oils seem to be superior in reducing the rates of all-cause mortality, cardiac, and sudden death, and possibly stroke compared to ALA found in vegetable oils (Sanderson et al. 2002; Wang et al. 2006). Omega-3 PUFA obtained from marine sources is mainly consumed in the form of either triglycerides (TG) or fatty acid ethyl esters (FAEE). However, there are controversial results in studies concerning the absorption of EPA in these two forms. Early studies claimed that absorption of EPA and DHA when ingested as FAEE was lower than that as TG (El Boustani et al. 1987; Lawson and Hughes 1988), whereas in later studies the absorption levels were found to be similar (Nordoy et al. 1991; Krokan et al. 1993). Alternative sources for EPA and DHA besides fish oil include microbial or single cell oil, with some microbial strains (*Crypthecodinium cohnii*) producing oils containing up to 50% DHA of the total fatty acids (Ratledge 2004; Ward and Singh 2005). The EPA and DHA contents of fish oils depend on numerous factors, such as species, origin, catch season, and feed of the fish, with EPA and DHA levels of up to about 20 and 35%, respectively (Gruger et al. 1964; Özogul and Özogul 2007; Visentainer et al. 2007).

In order to be suitable for human consumption crude fish oil needs to be refined and purified. Refining processes of fish oils aim mainly at removing undesirable compounds such as free fatty acids, off aromas, and peroxides. Additionally, high value compounds such as squalene, diacyl glyceryl ethers (DAGE), vitamin A, and vitamin D are targets of refining processes as well (Eltringham and Catchpole 2008). Fish oils in their TG form with EPA and DHA concentrations of up to 300 mg/g can be obtained by winterization, blending, solvent crystallization, and/or vacuum distillation (Ackman 1988). For applications requiring higher EPA and DHA levels, fish oil TG are hydrolyzed to liberate the fatty acids, which can then be converted into fatty acid ethyl esters (FAEE) or methyl esters (FAME). The esters are subsequently fractionated by various methods to obtain higher concentrates of EPA and DHA (Shahidi and Wanasundara 1998) by means of vacuum or short path distillation (Ackman et al. 1973; Breivik et al. 1997), solvent crystallization (Lee 2003), or urea complexation (Senanayake and Shahidi 2000; Gámez-Meza et al. 2003; Zuta et al. 2003). These conventional methods often require the use of flammable and toxic organic solvents or elevated process temperatures, which can lead to polymerization and degradation of thermally labile PUFA (Staby and Mollerup 1993; Lee and Foglia 2001). Selective enzymatic hydrolysis of fish oil TGs using fatty acid-specific lipases can be used as well for the separation and concentration of EPA and DHA from other fatty acids present in fish oils (Linder et al. 2002; Ramírez Fajardo et al. 2006).

Because of the drawbacks of the various aforementioned conventional techniques, processing of heat sensitive materials containing PUFA using SC–CO_2 offers numerous advantages (Mishra et al. 1993). Fractionation of fish oil FAEE using SC–CO_2 has been investigated by numerous research groups. In an attempt to fractionate fish oil FAEE in semi-continuous equipment, Eisenbach (1984) used a packed column equipped at the top with a “hot finger” held at 90°C to generate a reflux to take advantage of retrograde condensation. This method was suitable for

separating fractions of different carbon lengths but showed limited ability in separating EPA and DHA from other C_{20} and C_{22} fatty acids, respectively. Nilsson et al. (1988) used a packed column equipped with individually controlled heaters to create temperature zones, ranging from room temperature at the bottom of the column up to 100°C at the top. By applying incremental pressure programming to the column, it was possible to reduce the required temperature gradient for the fractionation (Nilsson et al. 1989).

More recently research activities focused mostly on continuous fractionation of fish oil esters using countercurrent columns. Continuous fractionation of fish oil FAEE was studied using a pilot plant countercurrent packed column (Fleck et al. 1998; Riha and Brunner 2000) to separate low molecular-weight components (LMC; C_{14} to C_{18}) from high molecular-weight components (HMC; C_{20} to C_{22}), obtaining concentrations for HMC in the raffinate of greater than 95 wt% at a recovery of HMC of greater than 95%. Continuous fractionation of squalene from shark liver oil in a countercurrent packed column resulted in squalene with up to 99% purity (Catchpole et al. 1997). Semi-continuous separation of a commercial mixture of fish oil FAEE containing 64% EPA + DHA was investigated by Perretti et al. (2007) using a column filled with Raschig rings, employing three temperature zones along the column held at constant temperatures of 40°C, 50°C and 60°C from bottom to top. In this study, 450 g of FAEE mixture were loaded onto the column (L = 3 m, ID = 3 cm) at three different column heights and subsequently fractionated at pressures ranging from 100 to 300 bar and CO_2 flow rates ranging from 2.5 to 10 kg/h over a duration of 2 h. By fractionating the FAEE mixture at 150 bar with a CO_2 flow rate of 5 kg/h, the total content of EPA and DHA esters was increased from 64% in the feed mixture to about 82% in the raffinate (fractions collected from the bottom of the column). However, the yield of raffinate was less than 10% and the EPA/DHA ratio changed from 1.61 for the initial mixture to 0.65 for the raffinate due to EPA being extracted preferentially over DHA from the column.

Simulation of a countercurrent column was carried out by Gironi and Maschietti (2006) after studying the fractionation of a natural mixture of fish oil FAEE by means of a semi-continuous single stage process. The results obtained by the single-stage process showed that in order to achieve the best compromise between selectivity and solubility, the operating conditions resulting in a SC–CO_2 density between 570 and 595 kg/m^3 should be selected at relatively high temperatures. For example, at 70°C and 167 bar, an oil with more than 80% of EPA and DHA ethyl esters was obtained in the process, with a recovery of about 40% in the raffinate. With the results obtained in their semi-continuous fractionation experiments as well as available pilot plant data (Riha and Brunner 2000), Gironi and Maschietti (2006) satisfactorily modeled a continuous fractionation process, which enabled them to study various process parameters, including the number of theoretical stages, reflux ratio, and solvent-to-feed ratio. Based on the simulation of the continuous countercurrent process, it seems feasible to obtain a raffinate with 95% (wt%) of $C_{20} + C_{22}$ FAEE, together with 95% recovery of these valuable compounds, by operating a multistage column (from 11 to 30 stages) with a reflux ratio of 2.5–5.2 and

a solvent-to-feed ratio in the range of 90–150. The results of such simulations based on mass balances and equilibrium calculations are useful to better understand the influence of various parameters on the theoretical performance of a column. However, in order to calculate the required height and diameter of a packed countercurrent column, mass transfer, fluid flow and flooding behavior considerations should be taken into account, thus requiring more sophisticated calculations, involving properties such as density, viscosity, and diffusivity of both the liquid and gaseous phases as well as interfacial tension, which are often challenging to measure or accurately predict (Blaha-Schnabel et al. 1996; Stockfleth and Brunner 2001; Ruivo et al. 2002; Martín and Cocero 2007; Brunner 2009). Therefore, more research is needed, evaluating both the experimental and theoretical aspects in order to obtain reliable data and to develop further the correlations and models used for calculating such complex fractionation processes.

Another novel approach different from the ones described above in order to concentrate EPA and DHA in the form of free fatty acids (FA), or FAEE, is the combination of urea fractionation and supercritical processing. The first steps in the development of the process include the use of urea dissolved in hot ethanol and mixing it with FA or FAEE, thereby forming a complex with their long hydrocarbon chain, which depends on temperature and degree of unsaturation (Eltringham and Catchpole 2008). Then, separation is achieved by cooling until precipitation of urea complexes occurs. However, a potentially better way was suggested, where SC–CO_2 containing fatty acids or esters is passed through a bed of urea, which leads to complexation of the monounsaturated and saturated fatty acids, thereby separating them from the polyunsaturates (Catchpole et al. 2009). Furthermore, the fractionation process was improved by combining urea fractionation as described above using ethanol with supercritical antisolvent fractionation (SAFT) (Catchpole et al. 2002). In the combined process, urea complex formation takes place in ethanol, followed by separation of the urea complex using a filter and feeding the filtrate containing fatty acids or ethyl esters, solvent (ethanol and water), and dissolved urea into a pressurized apparatus together with CO_2. By mixing the solution with CO_2, the antisolvent effect of CO_2 leads to precipitation of urea and water, which are separated in the first separator, while fatty acids and ethanol can be recovered separately in subsequent separators through sequential pressure reduction steps. With this patented method, it seems possible to obtain PUFA concentrates containing over 90% ω-3 FA.

Tocopherols and phytosterols. Tocopherols and tocotrienols, which belong to the family of Vitamin E compounds, have antioxidant activity and are used extensively in the food, cosmetic, and pharmaceutical industries. Deodorizer distillate (DOD), a by-product of the vegetable oil refining process, is rich in tocopherols. Conventional methods to isolate tocopherols by means of vacuum or molecular distillation can lead to degradation of these thermolabile compounds. Supercritical fluids could therefore offer an alternative to conventional methods, by taking advantage of mild processing conditions. Separation of tocopherols using SC–CO_2 was studied in a countercurrent packed column (Fang et al. 2007). The feed material was soybean DOD, which had been subjected to methyl esterification

and methylation to convert all free fatty acids and triglycerides into FAME, thereby improving their solubility in SC–CO_2. This pretreatment step facilitated the removal of most sterols by cooling and crystallization, due to the low solubility of sterols in FAME. The fractionation process consisted of two steps, where the first step was to feed the pretreated DOD into a fractionation column and to extract the FAME, while concentrating the tocopherols in the raffinate. The second step was to increase the pressure to extract the tocopherols from the impurities remaining in the column. To find the optimum conditions for the first step, the pretreated DOD containing about 70 wt% FAME and 10–15 wt% tocopherols was fed continuously into a packed column operated at 140, 160, and 180 bar with a linear temperature gradient along the column ranging from 40°C at the bottom to 75°C at the top. Fang et al. (2007) showed that operating the column at 180 bar resulted in the highest extraction yield for FAME of over 70% requiring the shortest time among all conditions investigated. However, the higher pressure also led to a threefold increase in tocopherols being extracted from the column compared to that at 140 bar, which is clearly a consequence of higher tocopherol solubility at higher pressure. Furthermore, increasing the pressure caused a decrease in the selectivity, which is disadvantageous for the separation. The composition of tocopherols in the fractions obtained from the column was influenced by pressure as well, with mainly α-tocopherol being extracted at the low pressure conditions, whereas at 180 bar all four isomers were found in the fractions in proportions similar to that of the feed material. Thus, a pressure of 160 bar was selected to further optimize the feed location, temperature gradient, and solvent-to-feed ratio. The second step of this patented process was found to work best at a final pressure of 200 bar, which resulted in a high tocopherol content (>50%) and tocopherol recovery (about 80%) (Fang et al. 2007).

Fractionation of canola DOD was investigated by Güçlü-Üstündag and Temelli (2007) to enrich sterols and tocopherols using a packed column in a semi-continuous process. The effects of pressure, temperature, and temperature gradient along the column on the extraction yield and selectivity of the fractionation were studied. Highest extract yields were obtained at the highest pressure (250 bar) and lowest temperature (70°C) studied. However, the tocopherol concentration of the fractions was higher at 250 bar and 100°C, with the content of tocopherol in the fractions collected being lower than that of the feed material. While enrichment of tocopherols in both the collected extract fractions and the column residue was less effective, the sterol content increased by about four-fold from 11% in the feed to 40.4% (determined as % GC area) in the column residue after fractionation of canola DOD using SC–CO_2 at 250 bar and a temperature gradient of 70–100°C along the column (Güçlü-Üstündag and Temelli 2007). In another study, olive pomace, a byproduct of olive oil production, was extracted with SC–CO_2 using a batch extractor operated at 350 bar and 50°C, followed by two depressurization steps into subsequent separators (Ibanez et al. 2000). The first separator in line after the extractor operated at pressures ranging from 100 to 200 bar and various temperatures between 40°C and 60°C contained major proportions of triglycerides, waxes, and sterols, whereas the tocopherols were enriched in the second separator set at 10 bar and 25°C.

Phase equilibria measurements with soy DOD and crude palm oil (CPO) using a static analytical method were carried out to assess the feasibility of fractionation of tocochromanols (tocopherols and tocotrienols), sterols, and squalene by better understanding their distribution coefficients (Gast et al. 2005). The distribution coefficient K_i, describing the ratio of concentrations between the gaseous phase and liquid phase ($K_i = y_i/x_i$), is a measure to assess the feasibility of separation in a fractionation column. A distribution coefficient of $K_i \approx 1$ occurs when the concentrations of a component in liquid and gaseous phases are nearly equal, which means that separation in a fractionation column is impossible. Substances that are enriched in the gaseous phase, as evidenced by a $K_i > 1$, can be collected in the top fraction, whereas substances with a $K_i < 1$ can be withdrawn with the liquid raffinate at the bottom of the column. The distribution coefficients for sterols and tocopherols in soy DOD investigated at 200–260 bar and 80°C were in the range of about 0.35–0.4 and 0.75–1 for sterols and tocopherols, respectively, indicating that the sterols stay preferably in the liquid phase, whereas the separation of tocopherols is more challenging. The distribution coefficient for squalene in soy DOD was above 3.8, indicating that enrichment in the gaseous fractions collected at the top of the fractionation column was feasible. On the other hand, phase equilibrium studies with CPO at 20–300 bar and 67°C revealed distribution coefficients for triglycerides, tocochromanols, and FFA in the range of 0.6–0.8, 2.5–4.5 and 4.5–6.5, respectively. Therefore, FFA and tocochromanols can be separated easily from the CPO triglycerides in a fractionation column. The results obtained in the phase equilibrium studies were reflected in the subsequent column fractionation experiments, where in the case of soy DOD, a top product rich in squalene (18 wt%) and a bottom product enriched in sterols (>50 wt%) were obtained (Gast et al. 2005). In order to assess the feasibility of a separation process, phase equilibrium studies to obtain distribution coefficients are very important and may require investigations on a case by case basis since they depend largely on the nature and composition of the starting feed material. Once distribution coefficients are available for a given system the separation process can be reasonably well described by short-cut methods to calculate the optimum solvent-to-feed ratio, reflux ratio, and the number of theoretical stages.

Carotenoids. Fractional extraction of paprika using SC–CO_2 while monitoring the carotenoid concentration in the supercritical phase by means of a near infrared visible detector was studied to optimize the operating conditions (Ambrogi et al. 2002). The influence of pressure on extraction performance was strong, with extract and carotenoid recovery being faster at 500 bar compared to 300 bar. Additionally, the amount of CO_2 required to recover most of the carotenoids was three times more at low pressure than higher pressure (300 bar). Ambrogi et al. (2002) also compared the extraction performance of the pigments from paprika powder to that from paprika oleoresins, with the powders resulting in a slower extraction due to the effect of the cell structure retaining the pigments. Fractionation of carotenoids was achieved by collecting fractions over time, where two stages of extraction were identified during the experiments, namely the linear and nonlinear stages. In the first stage, the extract was rich in free xanthophylls and β-carotene (about 50% w/w),

whereas in the second stage the concentration of xanthophyll esters was increased in the extract. A further development of the aforementioned fractional extraction process was to use a combined extraction-adsorption process for separating the red pigments (mainly esterified carotenoids) from the yellow pigments (mainly free carotenoids) using silica gel as adsorbent (Ambrogi et al. 2003). The authors noted that β-carotene (free carotenoid) and cryptoxanthin (monoester) were poorly adsorbed onto the silica gel, whereas capsanthin (diester) was efficiently retained. However, recovery of the adsorbed carotenoids from silica gel using SC–CO_2 may be challenging, thus other organic adsorbants such as cyclodextrin or cellulose may be promising candidates for further investigations.

16.3.2.2 Phytochemicals

Phytochemicals such as flavonoids, stilbenoids, essential oils and compounds with antioxidative and antimicrobial activity are often heat-sensitive compounds. Therefore, extraction and subsequent fractionation using SC–CO_2 have been studied for many phytochemicals. One possible pathway for fractionation using SC–CO_2 is the fractional separation, where an extract obtained at high pressures is subsequently depressurized and/or subjected to temperature changes in a cascade of separators to collect various fractions based on solubility. Flavonoids, such as those found in propolis are nearly insoluble in pure SC–CO_2. However, propolis can be readily dissolved in ethanol, to form a tincture that contains up to 40 wt% propolis, which can be further fractionated using SC–CO_2 as both an antisolvent and a solvent (Catchpole et al. 2004). In this process, the propolis tincture is mixed with SC–CO_2, which causes the antisolvent effect to precipitate high molecular mass components and to dissolve ethanol together with soluble components, such as flavonoids. This extract is then further separated in two steps by depressurization in two separators, where a concentrated flavonoid fraction with a concentration of 20–35 wt% is collected as the primary product, and an essential oil/ethanol fraction is produced as a secondary product.

Phytochemicals found in rosemary and sage, including components that have antioxidant activity such as carnosic acid, carnosol, rosmarinic acid, rosmanol, epirosmanol, and isorosmanol, are used as natural ingredients in food, drug, cosmetic, and medicinal applications. Sage herb (*Salvia officinalis L.*) was extracted with SC–CO_2 at 250–350 bar and 100°C using ethanol as cosolvent (Dauksas et al. 2001). The extract was subsequently fractionated in separators by stepwise depressurization and temperature change to obtain fractions of varying antioxidant activity. The antioxidant activity of the fractions depended largely on the pressure and temperature settings in the separators.

Essential oils comprised of hydrocarbon monoterpenes, oxygenated monoterpenes, hydrocarbon sesquiterpenes, and oxygenated sesquiterpenes can be recovered by hydro-distillation from seeds, roots, flowers, herbs, and leaves. However, this simple process suffers from several drawbacks, including thermal degradation, hydrolysis, and loss of water-soluble compounds, which are detrimental to the

quality of the final product. Therefore, extraction of essential oils using SC–CO_2 technology offers great advantages, which also allows relatively simple fractionation of extracts (Reverchon 1997; Reverchon and De Marco 2006). Isolating essential oils using SC–CO_2 involves extraction of plant matter at relatively mild conditions at about 90–100 bar and 40–50°C, where most essential oil components are soluble, followed by fractional separation. When extracting essential oils from plant materials, the cuticular or leaf waxes located at the surface of vegetable matter are coextracted (Reverchon 1992) even though the waxes have a relatively low solubility in SC–CO_2 compared to essential oils. Thus, to separate the essential oil from the waxes, the extraction is carried out at 90 bar and 40°C, followed by a first separation step in which the extract is cooled to 0°C, leading to the precipitation of waxes. The second separation step can then be brought about by depressurization of the remaining extract at 20 bar and by heating to 15°C, thereby recovering the essential oils. Essential oil extraction and fractionation has been successfully performed with basil, rosemary, marjoram, and numerous other plant materials on a laboratory and industrial scale, as reviewed by Reverchon and De Marco (2006). Another approach to fractionate essential oils is fractional extraction, where different fractions are extracted by changing the polarity of the SC–CO_2 throughout an extraction process by adding a cosolvent. In this manner, grape seeds were extracted in a two-step process, in which the seeds were subjected to pure SC–CO_2 extraction first, followed by extraction using SC–CO_2 with added methanol to change the polarity of SC–CO_2 (Palma et al. 1999). The first fraction contained mostly nonpolar compounds, including fatty acids, aliphatic aldehydes, and sterols, whereas the second fraction using the cosolvent had phenolic compounds, mainly catechin, epicatechin, and gallic acid. The first fraction showed strong activity against several human pathogens, which was likely due to the sterols according to Palma et al. (1999).

16.4 Commercialization and Future Outlook

Today's health conscious consumers are increasingly demanding "natural" products when it comes to the functional foods and nutraceuticals marketplace. The use of organic solvents and the safety of residual solvents in the final products are being questioned. Government regulations are becoming stricter concerning the use of organic solvents both from the residual and environmental perspectives. Therefore, SC–CO_2 technology has been experiencing tremendous growth at a commercial scale around the globe, targeting various nutraceutical applications. SC–CO_2-extracted products are being promoted as "natural extract" products with marketing advantages over other products extracted using organic solvents. As well, considering the environmental concerns, "green" technologies like supercritical processing are being evaluated more favorably.

Thermal or oxidative degradation of nutraceutical compounds is minimized throughout SC–CO_2 processing. However, care should be taken to maintain the

high quality during postprocess handling of the products. Further research is needed to show the stability or changes in bioactivity of nutraceuticals during conventional and SC–CO_2 processes to clearly demonstrate the advantages of SC–CO_2 technology for nutraceuticals processing, which then should be communicated to consumers. Another benefit of supercritical technology over conventional solvent extracts is longer shelf life due to inactivation of microorganisms and spores throughout the high pressure treatment and the depressurization step. Such SC–CO_2 treatment is also being looked at as a sterilization technique for various applications, including pharmaceuticals and medical devices (Foster et al. 2003).

Another major advantage of SC–CO_2 technology is its flexibility and the possibility of developing novel processes by coupling different unit operations. For example, extraction operation can be combined with column fractionation or membrane separation such that a crude extract can be obtained and refined or further fractionated to isolate a bioactive component in two steps. Such approaches are opening new opportunities for novel technology development. In addition, there are tremendous developments in the area of particle formation using SC–CO_2 technologies (Jung and Perrut 2001; Weidner 2009), which have opened up new opportunities for the design of delivery systems for bioactive components. Even though some of these approaches have been commercialized for various pharmaceuticals, nutraceutical applications are very limited. These technologies can be classified into three major categories, where CO_2 can be used as: (1) solvent (rapid expansion of supercritical solutions, RESS), (2) gas to saturate a solution (particles from gas-saturated solutions, PGSS), or (3) antisolvent (gas anti-solvent, GAS; supercritical fluid anti-solvent, SAS, and others). Weidner (2009) reviewed such techniques and their food applications. In addition, Weidner (2009) also described a concentrated powder form (CPF), where a liquid ingredient is contacted with a pressurized gas and sprayed through a nozzle onto a solid carrier material. Coupling these techniques with SC–CO_2 extraction/fractionation would allow the recovery of a sensitive bioactive from a plant matrix and encapsulation in a protective coating with minimal degradation. Micro- and nano-sized particles of different morphologies obtained through supercritical techniques can offer functionalities not possible with conventional technologies, such as targeted delivery and controlled release mechanisms; however, more research is needed to understand the relationships between processing parameters and final ingredient functionality.

The feasibility of achieving bioseparations using SC–CO_2 technology has been demonstrated for various nutraceutical applications discussed in this chapter, including extraction of bioactives from a variety of plant materials and fractionation for further concentration of specific compounds. A large number of studies have been carried out in laboratory and pilot plant scale. Some applications have already reached commercial scale, such as extraction of specialty oils and isolation of tocopherols from deodorizer distillate using a fractionation column. As in any process, detailed economic feasibility evaluation is essential for the success of the different approaches discussed for the variety of nutraceutical applications, and cost evaluation should be done on a case by case basis. In general, it is common belief that supercritical fluid technology is expensive and should be restricted to only

high-value end products. This is mainly due to the need for high capital investment for high pressure equipment. However, it has been demonstrated that it is only a matter of scale of operations. At large enough plant capacities, the viability of supercritical processing becomes equivalent to conventional processes even for low-value end products (Perrut 2000; Brunner 2005). Perrut (2000) reported the linear relationship (on a log-log scale) between price index and plant capacity over a range of lab to pilot and production units. Brunner (2009) also demonstrated the substantial drop in cost for continuous supercritical operations and provided cost comparisons for different column operations. The operating cost is generally lower than that for conventional solvent extraction or high vacuum operations. As well, compared to traditional solvent extraction, the overall process becomes simpler because expensive solvent evaporators and meal desolventizers are not needed. Thus, supercritical processing is more favorable especially when the rising cost of energy is taken into account. Rosa and Meireles (2005) developed a rapid method to estimate manufacturing cost by taking into account raw material, operational labor, utilities, waste treatment, and investment. Coupling of supercritical extraction or fractionation with a continuous cross-flow membrane system for the separation of solutes from SC–CO_2 without depressurization shows great promise in terms of substantial savings in energy costs associated with the recompression of CO_2. Considering all the advantages discussed, the future of supercritical technology for separations involving nutraceuticals is bright based on all the know-how gained over the past 2 decades in this field.

Acknowledgements We would like to express our gratitude to the Natural Sciences and Engineering Research Council of Canada for financial support of our research program on supercritical fluid technology and Alberta Ingenuity for scholarship support to B. Seifried.

References

Ackman RG (1988) Oils and fats group international lecture – the year of the fish oils. Chem Ind 7:139–145

Ackman RG, Ke PJ, Jangaard PM (1973) Fractional vacuum distillation of Herring oil methyl-esters. J Am Oil Chem Soc 50:1–8

Ambrogi A, Cardarelli DA, Eggers R (2002) Fractional extraction of paprika using supercritical carbon dioxide and on-line determination of carotenoids. J Food Sci 67:3236–3241

Ambrogi A, Cardarelli DA, Eggers R (2003) Separation of natural colorants using a combined high pressure extraction-adsorption process. Lat Am Appl Res 33:323–326

Bartle KD, Clifford AA, Jafar SA, Shilstone GF (1991) Solubilities of solids and liquids of low volatility in supercritical carbon-dioxide. J Phys Chem Ref Data 20:713–756

Baumann D, Adler S, Grüner S, Otto F, Weinreich B, Hamburger M (2004) Supercritical carbon dioxide extraction of marigold at high pressures: Comparison of analytical and pilot-scale extraction. Phytochem Anal 15:226–230

Baysal T, Ersus S, Starmans DAJ (2000) Supercritical CO_2 extraction of β-carotene and lycopene from tomato paste waste. J Agric Food Chem 48:5507–5511

Bernardo-Gil MG, Grenha J, Santos J, Cardoso P (2002) Supercritical fluid extraction and characterisation of oil from hazelnut. Eur J Lipid Sci Technol 104:402–409

Blaha-Schnabel A, Beyer A, Czech B, Jakob H, Schiemann H, Weidner E, Peter S (1996) Influence of interfacial tension and viscosity on the behavior of a packed column in near-critical fluid extraction. Chem Eng Commun 146:13–31

Breivik H, Haraldsson GG, Kristinsson B (1997) Preparation of highly purified concentrates of eicosapentaenoic acid and docosahexaenoic acid. J Am Oil Chem Soc 74:1425–1429

Brunner G (1983) Selectivity of supercritical compounds and entrainers with respect to model substances. Fluid Phase Equilib 10:289–298

Brunner G (1994) Gas extraction: an introduction to fundamentals of supercritical fluids and the application to separation processes. Springer, New York

Brunner G (2005) Supercritical fluids: technology and application to food processing. J Food Eng 67:21–33

Brunner G (2009) Counter-current separations. J Supercrit Fluids 47:574–582

Brunner G, Peter S (1982) On the solubility of glycerides and fatty acids in compressed gases in the presence of an entrainer. Sep Sci Technol 17:199–214

Cadoni E, Rita De Giorgi M, Medda E, Poma G (1999) Supercritical CO_2 extraction of lycopene and β-carotene from ripe tomatoes. Dyes Pigm 44:27–32

Campos L, Michielin EMZ, Danielski L, Ferreira SR (2005) Experimental data and modeling the supercritical fluid extraction of marigold (*Calendula officinalis*) oleoresin. J Supercrit Fluids 34:163–170

Cao X, Ito Y (2003) Supercritical fluid extraction of grape seed oil and subsequent separation of free fatty acids by high-speed counter-current chromatography. J Chromatogr A 1021:117–124

Catchpole OJ, King MB (1994) Measurement and correlation of binary diffusion coefficients in near critical fluids. Ind Eng Chem Res 33:1828–1837

Catchpole OJ, Von Kamp JC, Grey JB (1997) Extraction of squalene from shark liver oil in a packed column using supercritical carbon dioxide. Ind Eng Chem Res 36:4318–4324

Catchpole OJ, Grey JB, Noermark KA (2000) Fractionation of fish oils using supercritical CO_2 and CO_2 plus ethanol mixtures. J Supercrit Fluids 19:25–37

Catchpole OJ, MacKenzie AN, Grey JB (2002) Improvements in or relating to separation technology. NZ518504, WO03089399

Catchpole OJ, Grey JB, Mitchell KA, Lan JS (2004) Supercritical antisolvent fractionation of propolis tincture. J Supercrit Fluids 29:97–106

Catchpole OJ, Tallon SJ, Eltringham WE, Grey JB, Fenton KA, Vagi EM, Vyssotski MV, MacKenzie AN, Ryan J, Zhu Y (2009) The extraction and fractionation of specialty lipids using near critical fluids. J Supercrit Fluids 47:591–597

Chimowitz EH, Pennisi KJ (1986) Process synthesis concepts for supercritical gas extraction in the crossover region. AlChE J 32:1665–1676

Chrastil J (1982) Solubility of solids and liquids in supercritical gases. J Phys Chem 86:3016–3021

Christov M, Dohrn R (2002) High-pressure fluid phase equilibria: experimental methods and systems investigated (1994–1999). Fluid Phase Equilib 202:153–218

Cocero MJ, González S, Perez S, Alonso E (2000) Supercritical extraction of unsaturated products Degradation of β-carotene in supercritical extraction processes. J Supercrit Fluids 19:39–44

Danielski L, Campos L, Bresciani L, Hense H, Yunes R, Ferreira S (2007) Marigold (*Calendula officinalis L.*) oleoresin: solubility in SC–CO_2 and composition profile. Chem Eng Process 46:99–106

Darken LS (1948) Diffusion, mobility and their interrelation through free energy in binary metallic systems. Trans Am Inst Min Metall Eng 175:184–201

Dauksas E, Venskutonis PR, Povilaityte V, Sivik B (2001) Rapid screening of antioxidant activity of sage (*Salvia officinalis L.*) extracts obtained by supercritical carbon dioxide at different extraction conditions. Nahrung 45:338–341

de la Fuente JC, Oyarzún B, Quezadaa N, del Valle JM (2006) Solubility of carotenoid pigments (lycopene and astaxanthin) in supercritical carbon dioxide. Fluid Phase Equilib 247:90–95

Deiters UK, Schneider GM (1986) High pressure phase equilibria: experimental methods. Fluid Phase Equilib 29:145–160

Diaz-Reinoso B, Moure A, Dominguez H, Parajo J (2006) Supercritical CO_2 extraction and purification of compounds with antioxidant activity. J Agric Food Chem 54:2441–2469

Dobbs JM, Wong JM, Johnston KP (1986) Nonpolar co-solvents for solubility enhancement in supercritical fluid carbon-dioxide. J Chem Eng Data 31:303–308

Dohrn R, Brunner G (1995) High-pressure fluid-phase equilibria: experimental methods and systems investigated (1988–1993). Fluid Phase Equilib 106:213–282

Duarte C, Moldao-Martins M, Gouveia AF, Beirão da Costa S, Leitão AE, Bernardo-Gil MG (2004) Supercritical fluid extraction of red pepper (*Capsicum frutescens L.*). J Supercrit Fluids 30:155–161

Dyerberg J, Bang HO, Hjorne N (1975) Fatty acid composition of the plasma lipids in Greenland Eskimos. Am J Clin Nutr 28:958–966

Eisenbach W (1984) Supercritical fluid extraction: a film demonstration. Phys Chem Chem Phys 88:882–887

Ekart MP, Bennett KL, Ekart SM, Gurdial GS, Liotta CL, Eckert CA (1993) Co-solvent interactions in supercritical fluid solutions. AlChE J 39:235–248

El Boustani S, Colette C, Monnier L, Descomps B, de Paulet AC, Mendy F (1987) Enteral absorption in man of eicosapentaenoic acid in different chemical forms. Lipids 22:711–714

Eltringham W, Catchpole OJ (2008) Processing of fish oils by supercritical fluids. In: Martinez JL (ed) Supercritical fluid extraction of nutraceuticals and bioactive compounds. CRC Press/ Taylor & Francis, Boca Raton, FL

Fang T, Goto M, Wang X, Ding X, Geng J, Sasaki M, Hirose T (2007) Separation of natural tocopherols from soybean oil byproduct with supercritical carbon dioxide. J Supercrit Fluids 40:50–58

Favati F, King JW, Mazzanti M (1991) Supercritical carbon dioxide extraction of evening primrose oil. J Am Oil Chem Soc 68:422–427

FDA (2005) Qualified health claims: letter regarding tomatoes and prostate cancer (Lycopene health claim coalition; Docket no. 2004Q-0201). http://www.fda.gov/food/dietarysupplements/consumerInformation/ucm072767.html.Retrieved 1 June 2009

Fenghour A, Wakeham WA, Vesovic V (1998) The viscosity of carbon dioxide. J Phys Chem Ref Data 27:31–39

Fleck U, Tiegs C, Brunner G (1998) Fractionation of fatty acid ethyl esters by supercritical CO_2: high separation efficiency using an automated countercurrent column. J Supercrit Fluids 14:67–74

Fornari RE, Alessi P, Kikic L (1990) High pressure fluid phase equilibria: experimental methods and systems investigated (1978–1987). Fluid Phase Equilib 57:1–33

Fors SM, Eriksson CE (1990) Characterization of oils extracted from oats by supercritical carbon-dioxide. LWT Food Sci Technol 23:390–395

Foster N, Mammucari R, Dehghani F, Barrett A, Bezanehtak K, Coen E, Combes G, Meure L, Ng A, Regtop HL, Tandya A (2003) Processing pharmaceutical compounds using dense gas technology. Ind Eng Chem Res 42:6476–6493

Funazukuri T, Hachisu S, Wakao N (1991) Measurements of binary diffusion coefficients of C_{16}-C_{24} unsaturated fatty acid methyl esters in supercritical carbon dioxide. Ind Eng Chem Res 30:1323–1329

Funazukuri T, Kong CY, Kagei S (2004a) Effects of molecular weight and degree of unsaturation on binary diffusion coefficients for lipids in supercritical carbon dioxide. Fluid Phase Equilib 219:67–73

Funazukuri T, Kong CY, Kagei S (2004b) Impulse response techniques to measure binary diffusion coefficients under supercritical conditions. J Chromatogr A 1037:411–429

Gámez-Meza N, Noriega-Rodríguez JA, Medina-Juárez LA, Ortega-García J, Monroy-Rivera FJ, Toro-Vázquez HS, García HS, Angulo-Guerrero O (2003) Concentration of eicosapentaenoic acid and docosahexaenoic acid from fish oil by hydrolysis and urea complexation. Food Res Int 36:721–727

Gast K, Jungfer M, Saure C, Brunner G (2005) Purification of tocochromanols from edible oil. J Supercrit Fluids 34:17–25

Gironi F, Maschietti M (2006) Separation of fish oils ethyl esters by means of supercritical carbon dioxide: thermodynamic analysis and process modelling. Chem Eng Sci 61:5114–5126
Gomez AM, de la Ossa EM (2000) Quality of wheat germ oil extracted by liquid and supercritical carbon dioxide. J Am Oil Chem Soc 77:969–974
Gomez-Prieto MS, Caja MM, Herraiz M, Santa-Maria G (2003) Supercritical fluid extraction of all-trans-lycopene from tomato. J Agric Food Chem 51:3–7
Goodrum JW, Kilgo MB (1987) Peanut oil extraction with SC–CO_2 – solubility and kinetic functions. T ASAE 30:1865–1868
Gruger EH, Nelson RW, Stansby ME (1964) Fatty acid composition of oils from 21 species of marine fish, freshwater fish and shellfish. J Am Oil Chem Soc 41:662–667
Güçlü-Üstündag Ö, Temelli F (2000) Correlating the solubility behavior of fatty acids, mono-, di-, and triglycerides, and fatty acid esters in supercritical carbon dioxide. Ind Eng Chem Res 39:4756–4766
Güçlü-Üstündag Ö, Temelli F (2004) Correlating the solubility behavior of minor lipid components in supercritical carbon dioxide. J Supercrit Fluids 31:235–253
Güçlü-Üstündag Ö, Temelli F (2005) Solubility behavior of ternary systems of lipids, co-solvents and supercritical carbon dioxide and processing aspects. J Supercrit Fluids 36:1–15
Güçlü-Üstündag Ö, Temelli F (2006) Solubility behavior of ternary systems of lipids in supercritical carbon dioxide. J Supercrit Fluids 38:275–288
Güçlü-Üstündag Ö, Temelli F (2007) Column fractionation of canola oil deodorizer distillate using supercritical carbon dioxide. J Am Oil Chem Soc 84:953–961
Gupta RB, Shim J-J (2007) Solubility in Supercritical Carbon Dioxide. CRC Press, Boca Raton, FL
Gurdial GS, Wells PA, Foster NR, Chaplin RP (1989) The role of polarity in correlations of solid-supercritical fluid phase systems. J Supercrit Fluids 2:85–96
Hartono R, Mansoori GA, Suwono A (2001) Prediction of solubility of biomolecules in supercritical solvents. Chem Eng Sci 56:6949–6958
He HP, Corke H, Cai JG (2003) Supercritical carbon dioxide extraction of oil and squalene from Amaranthus grain. J Agric Food Chem 51:7921–7925
Herrero M, Cifuentes A, Ibanez E (2006) Sub- and supercritical fluid extraction of functional ingredients from different natural sources: Plants, food-by-products, algae and microalgae – A review. Food Chem 98:136–148
Hicks CP (1978) A bibliography of thermodynamic quantities for binary fluid mixtures. In: McGlashan ML (ed) Chemical thermodynamics. Chemical Society, London
Higashi H, Iwai Y, Nakamura Y, Yamamoto S, Arai Y (1999) Correlation of diffusion coefficients for naphthalene and dimethylnaphthalene isomers in supercritical carbon dioxide. Fluid Phase Equilib 166:101–110
Higashi H, Iwai Y, Arai Y (2001) Solubilities and diffusion coefficients of high boiling compounds in supercritical carbon dioxide. Chem Eng Sci 56:3027–3044
Horrocks LA, Yeo YK (1999) Health benefits of docosahexaenoic acid (DHA). Pharmacol Res 40:211–225
Huang W, Li Z, Niu H, Li D, Zhang J (2008) Optimization of operating parameters for supercritical carbon dioxide extraction of lycopene by response surface methodology. J Food Eng 89:298–302
Ibanez E, Palacios J, Senorans FJ, Santa-Maria G, Tabera J, Reglero G (2000) Isolation and separation of tocopherols from olive by-products with supercritical fluids. J Am Oil Chem Soc 77:187–190
Jung J, Perrut M (2001) Particle design using supercritical fluids: literature and patent survey. J Supercrit Fluids 20:179–219
Kestin J, Zien TF, Whitelaw JH (1964) Viscosity of carbon dioxide in neighbourhood of critical point. Physica 30:161
Kim HJ, Lee SB, Park KA, Hong IK (1999) Characterization of extraction and separation of rice bran oil rich in EFA using SFE process. Sep Purif Technol 15:1–8

King MB, Mubarak A, Kim JD, Bott TR (1992) The mutual solubilities of water with supercritical and liquid carbon dioxides. J Supercrit Fluids 5:296–302

Knapp H, Döring R, Oellrich L, Plöcker U, Prausnitz JM (1981) Vapor-Liquid equilibria for mixtures of low-boiling substances *DECHEMA Chem*. Data series VI

Krichnavaruk, Shotipruk A, Goto M, Pavasant P (2008) Supercritical carbon dioxide extraction of astaxanthin from *Haematococcus pluvialis* with vegetable oils as co-solvent. Bioresour Technol 99:5556–5560

Krokan HE, Bjerve KS, Mørk E (1993) The enteral bioavailability of eicosapentaenoic acid and docosahexaenoic acid is as good from ethyl esters as from glyceryl esters in spite of lower hydrolytic rates by pancreatic lipase in vitro. Biochim Biophys Acta 1168:59–67

Lang Q, Wai CM (2001) Supercritical fluid extraction in herbal and natural product studies – a practical review. Talanta 53:771–782

Lawson LD, Hughes BG (1988) Human absorption of fish oil fatty acids as triacylglycerols, free acids, or ethyl esters. Biochem Biophys Res Commun 152:328–335

Lee SK (2003) Method for isolating high-purified unsaturated fatty acids using crystallization. US Patent 6,664,405

Lee KT, Foglia TA (2001) Fractionation of menhaden oil and partially hydrogenated menhaden oil: characterization of triacylglycerol fractions. J Am Oil Chem Soc 78:297–303

Leeke G, Gaspar F, Santos R (2002) Influence of water on the extraction of essential oils from a model herb using supercritical carbon dioxide. Ind Eng Chem Res 41:2033–2039

Li S (2008) Application of supercritical fluids in traditional Chinese medicines and natural products. In: Martinez JL (ed) Supercritical fluid extraction of nutraceuticals and bioactive compounds. CRC Press/Taylor & Francis, Boca Raton, FL, pp 215–242

Li S, Varadarajan GS, Hartland S (1991) Solubilities of theobromine and caffeine in supercritical carbon dioxide: Correlation with density-based models. Fluid Phase Equilib 68:263–280

Linder M, Matouba E, Fanni J, Parmentier M (2002) Enrichment of salmon oil with n-3 PUFA by lipolysis, filtration and enzymatic re-esterification. Eur J Lipid Sci Technol 104:455–462

Liong KK, Wells PA, Foster NR (1991) Diffusion in supercritical fluids. J Supercrit Fluids 4:91–108

Lopes IMG, Bernardo-Gil MG (2005) Characterisation of acorn oils extracted by hexane and by supercritical carbon dioxide. Eur J Lipid Sci Technol 107:12–19

Lucien FP, Foster NR (2000) Solubilities of solid mixtures in supercritical carbon dioxide: a review. J Supercrit Fluids 17:111–134

Ma Q, Xu X, Gao Y, Wang Q, Zhao J (2008) Optimisation of supercritical carbon dioxide extraction of lutein esters from marigold (*Tagetes erect L.*) with soybean oil as a co-solvent. Int J Food Sci Technol 43:1763–1769

Macias-Sanchez MD, Serrano CM, Rodriguez M, de la Ossa EM, Lubian LM, Montero O (2008) Extraction of carotenoids and chlorophyll from microalgae with supercritical carbon dioxide and ethanol as co-solvent. J Sep Sci 31:1352–1362

Martín A, Cocero MJ (2007) Mathematical modeling of the fractionation of liquids with supercritical CO_2 in a countercurrent packed column. J Supercrit Fluids 39:304–314

McHugh MA, Krukonis VJ (1986) Supercritical fluid extraction: principles and practice. Butterworths, Boston, MA

Meireles MAA (2008) Extraction of bioactive compounds from Latin American plants. In: Martinez JL (ed) Supercritical fluid extraction of nutraceuticals and bioactive compounds. CRC Press/Taylor & Francis, Boca Raton, FL, pp 243–274

Mendes RL, Fernandes HL, Coelho JP, Reis EC, Cabral JMS, Novais JM, Palavra AF (1995) Supercritical CO_2 extraction of carotenoids and other lipids from *Chlorella vulgaris*. Food Chem 53:99–103

Mendes RL, Nobre BP, Coelho JP, Palavra AF (1999) Solubility of β-carotene in supercritical carbon dioxide and ethane. J Supercrit Fluids 16:99–106

Michels A, Botzen A, Schuurman W (1957) The viscosity of carbon dioxide between 0°C and 75°C and at pressures up to 2000 atmospheres. Physica 23:95–102

Mishra VK, Temelli F, Ooraikul B (1993) Extraction and purification of omega-3-fatty-acids with an emphasis on supercritical-fluid extraction – a review. Food Res Int 26:217–226
Moure A, Cruz JM, Franco D, Manuel Domínguez J, Sineiro J, Domínguez H, Núñez MJ, Carlos Parajó J (2001) Natural antioxidants from residual sources. Food Chem 72:145–171
Mukhopadhyay M (2008) Processing spices using supercritical fluids. In: Martinez JL (ed) Supercritical fluid extraction of nutraceuticals and bioactive compounds. CRC Press/Taylor & Francis, Boca Raton, FL, pp 337–366
Murga R, Ruiz R, Beltran S, Cabezas JL (2000) Extraction of natural complex phenols and tannins from grape seeds by using supercritical mixtures of carbon dioxide and alcohol. J Agric Food Chem 48:3408–3412
Nagahama K (1996) VLE measurements at elevated pressures for process development. Fluid Phase Equilib 116:361–372
Nagy B, Simandi B (2008) Effects of particle size distribution, moisture content, and initial oil content on the supercritical fluid extraction of paprika. J Supercrit Fluids 46:293–298
Nilsson WB, Gauglitz EJ Jr, Hudson JK, Stout VF, Spinelli J (1988) Fractionation of menhaden oil ethyl esters using supercritical fluid CO_2. J Am Oil Chem Soc 65:109–117
Nilsson WB, Gauglitz EJ, Hudson JK (1989) Supercritical fluid fractionation of fish oil esters using incremental pressure programming and a temperature gradient. J Am Oil Chem Soc 66:1596–1600
NIST (2009) Isothermal properties for carbon dioxide. http://webbook.nist.gov. Retrieved 10 June 2009
Nobre BP, Mendes RL, Queiroz EM, Pessoa FP, Coelho JP, Palavra AF (2009) Calculation of solubilities for systems containing multiple non-volatile solutes and supercritical carbon dioxide. Ind Eng Chem Res 48:1551–1555
Nordoy A, Barstad L, Connor WE, Hatcher L (1991) Absorption of the n-3 eicosapentaenoic and docosahexaenoic acids as ethyl esters and triglycerides by humans. Am J Clin Nutr 53: 1185–1190
Odabasi AZ, Balaban MO (2002) Supercritical CO_2 extraction of sesame oil from raw seeds. J Food Sci Technol 39:496–501
Oliveira R, Rodrigues MF, Bernardo-Gil MG (2002) Characterization and supercritical carbon dioxide extraction of walnut oil. J Am Oil Chem Soc 79:225–230
Ollanketo M, Hartonen K, Riekkola ML, Holm Y, Hiltunen R (2001) Supercritical carbon dioxide extraction of lycopene in tomato skins. Eur Food Res Technol 212:561–565
Ooi CK, Bhaskar A, Yener MS, Tuan DQ, Hsu J, Rizvi SSH (1996) Continuous supercritical carbon dioxide processing of palm oil. J Am Oil Chem Soc 73:233–237
Özogul Y, Özogul F (2007) Fatty acid profiles of commercially important fish species from the Mediterranean, Aegean and Black Seas. Food Chem 100:1634–1638
Palazoglu TK, Balaban MO (1998) Supercritical CO_2 extraction of lipids from roasted pistachio nuts. T ASAE 41:679–684
Palma M, Taylor LT, Varela RM, Cutler SJ, Cutler HG (1999) Fractional extraction of compounds from grape seeds by supercritical fluid extraction and analysis for antimicrobial and agrochemical activities. J Agric Food Chem 47:5044–5048
Peker H, Srinivasan MP, Smith JM, McCoy BJ (1992) Caffeine extraction rates from coffee beans with supercritical carbon dioxide. AlChE J 38:761–770
Perretti G, Motori A, Bravi E, Favati F, Montanari L, Fantozzi P (2007) Supercritical carbon dioxide fractionation of fish oil fatty acid ethyl esters. J Supercrit Fluids 40:349–353
Perrut M (2000) Supercritical fluid applications: industrial developments and economic issues. Ind Eng Chem Res 39:4531–4535
Peusch M, Müller-Seitz E, Petz M, Müller A, Anklam E (1997) Extraction of capsaicinoids from chillies (*Capsicum frutescens L.*) and paprika (*Capsicum annuum L.*) using supercritical fluids and organic solvents. Z. Lebensm. Unters. Forsch. Eur Food Res Technol 204:351–355

Ramírez Fajardo A, Esteban Cerdán L, Robles Medina A, Muñío Martínez MM, Hita Peña E, Molina Grima E (2006) Concentration of eicosapentaenoic acid by selective esterification using lipases. J Am Oil Chem Soc 83:215–221

Raspo I, Nicolas C, Neau E, Meradji S (2008) Diffusion coefficients of solids in supercritical carbon dioxide: modelling of near critical behaviour. Fluid Phase Equilib 263:214–222

Ratledge C (2004) Fatty acid biosynthesis in microorganisms being used for Single Cell Oil production. Biochimie 86:807–815

Reverchon E (1992) Fractional separation of SCF extracts from marjoram leaves: mass transfer and optimization. J Supercrit Fluids 5:256–261

Reverchon E (1997) Supercritical fluid extraction and fractionation of essential oils and related products. J Supercrit Fluids 10:1–37

Reverchon E, De Marco I (2006) Supercritical fluid extraction and fractionation of natural matter. J Supercrit Fluids 38:146–166

Reverchon E, Kaziunas A, Marrone C (2000) Supercritical CO_2 extraction of hiprose seed oil: experiments and mathematical modelling. Chem Eng Sci 55:2195–2201

Rezaei KA, Temelli F (2000) Using supercritical fluid chromatography to determine diffusion coefficients of lipids in supercritical CO_2. J Supercrit Fluids 17:35–44

Riha V, Brunner G (2000) Separation of fish oil ethyl esters with supercritical carbon dioxide. J Supercrit Fluids 17:55–64

Rosa PTV, Meireles MAA (2005) Rapid estimation of the manufacturing cost of extracts obtained by supercritical fluid extraction. J Food Eng 67:235–240

Rozzi NL, Singh RK, Vierling RA, Watkins BA (2002) Supercritical fluid extraction of lycopene from tomato processing byproducts. J Agric Food Chem 50:2638–2643

Ruckenstein E, Shulgin I (2001) Entrainer effect in supercritical mixtures. Fluid Phase Equilib 180:345–359

Ruckenstein E, Shulgin I (2002) The solubility of solids in mixtures composed of a supercritical fluid and an entrainer. Fluid Phase Equilib 200:53–67

Ruivo R, Cebola MJ, Simoes PC, Nunes da Ponte M (2002) Fractionation of edible oil model mixtures by supercritical carbon dioxide in a packed column. 2. A mass-transfer study. Ind Eng Chem Res 41:2305–2315

Ruivo R, Couto R, SimÃµes PC (2008) Supercritical carbon dioxide fractionation of the model mixture squalene/oleic acid in a membrane contactor. Sep Purif Technol 59:231–237

Sabio E, Lozano M, Montero De Espinosa V, Mendes RL, Pereira AP, Palavra AF, Coelho JA (2003) Lycopene and β-carotene extraction from tomato processing waste using supercritical CO_2. Ind Eng Chem Res 42:6641–6646

Sacchetti G, Maietti S, Muzzoli M, Scaglianti M, Manfredini S, Radice M, Bruni R (2005) Comparative evaluation of 11 essential oils of different origin as functional antioxidants, antiradicals and antimicrobials in foods. Food Chem 91:621–632

Sakaki K (1992) Solubility of β-carotene in dense carbon-dioxide and nitrous-oxide from 308 to 323 K and from 9.6 to 30 MPa. J Chem Eng Data 37:249–251

Saldaña MDA, Sun L, Guigard SE, Temelli F (2006) Comparison of the solubility of β-carotene in supercritical CO_2 based on a binary and a multicomponent complex system. J Supercrit Fluids 37:342–349

Sanal IS, Bayraktar E, Mehmetoglu UU, Calimli A (2005) Determination of optimum conditions for SC-(CO_2 plus ethanol) extraction of β-carotene from apricot pomace using response surface methodology. J Supercrit Fluids 34:331–338

Sanderson P, Finnegan YE, Williams CM, Calder PC, Burdge GC, Wootton SA, Griffin BA, Millward DJ, Pegge NC, Bemelmans WJE (2002) UK Food Standards Agency α-linolenic acid workshop report. Br J Nutr 88:573–579

Schmitt WJ, Reid RC (1985) The influence of the solvent gas on solubility and selectivity in supercritical extraction. In: Penninger JML, Radosz M, McHugh MA, Krukonis VJ (eds) Supercritical Fluid Technology. Elsevier, New York, pp 123–147

Schmitt WJ, Reid RC (1986) The use of entrainers in modifying the solubility of phenanthrene and benzoic acid in supercritical carbon dioxide and ethane. Fluid Phase Equilib 32:77–99
Senanayake S, Shahidi F (2000) Concentration of docosahexaenoic acid (DHA) from algal oil via urea complexation. J Food Lipids 7:51–61
Shahidi F, Wanasundara UN (1998) Omega-3 fatty acid concentrates: nutritional aspects and production technologies. Trends Food Sci Technol 9:230–240
Shen Z, Palmer MV, Ting SST, Fairclough RJ (1996) Pilot scale extraction of rice bran oil with dense carbon dioxide. J Agric Food Chem 44:3033–3039
Shi J, Yi C, Xue SJ, Jiang Y, Ma Y, Li D (2009) Effects of modifiers on the profile of lycopene extracted from tomato skins by supercritical CO_2. J Food Eng 93:431–436
Skerget M, Knez Z (1997) Solubility of binary solid mixture β-carotene-capsaicin in dense CO_2. J Agric Food Chem 45:2066–2069
Skerget M, Knez A, Habulin M (1995) Solubility of β-carotene and oleic acid in dense CO_2 and data correlation by a density based model. Fluid Phase Equilib 109:131–138
Somayajulu GR (1989) Estimation procedures for critical constants. J Chem Eng Data 34:106–120
Sovova H, Kucera J, Jez J (1994) Rate of the vegetable oil extraction with supercritical CO_2. 2. Extraction of grape oil. Chem Eng Sci 49:415–420
Srinivasan K (2005) Spices as influencers of body metabolism: an overview of three decades of research. Food Res Int 38:77–86
Staby A, Mollerup J (1993) Separation of constituents of fish oil using supercritical fluids: a review of experimental solubility, extraction, and chromatographic data. Fluid Phase Equilib 91:349–386
Stahl E, Gerard D (1985) Solubility behaviour and fractionation of essential oils in dense carbon dioxide. Perfum Flavor 10(2):29–30, 32, 34–37
Stahl E, Quirin KW (1983) Dense gas extraction on a laboratory scale: a survey of some recent results. Fluid Phase Equilib 10:269–278
Stahl HCE, Schilz W (1976) Extraktion mit überkritischen Gasen in direkter Kopplung mit der Dünnschicht-Chromatographie Anwendungsmöglichkeiten auf dem Naturstoffgebiet. Chem Ing Tech 48:773–778
Stockfleth R, Brunner G (2001) Holdup, pressure drop, and flooding in packed countercurrent columns for the gas extraction. Ind Eng Chem Res 40:347–356
Strøm A, Jensen RA (1951) Mortality from circulatory diseases in Norway 1940–1945. Lancet 1:126–129
Suárez JJ, Medina I, Bueno JL (1998) Diffusion coefficients in supercritical fluids: available data and graphical correlations. Fluid Phase Equilib 153:167–212
Sun M, Temelli F (2006) Supercritical carbon dioxide extraction of carotenoids from carrot using canola oil as a continuous co-solvent. J Supercrit Fluids 37:397–408
Taniguchi M, Tsuji T, Shibata M, Kobayashi T (1985) Extraction of oils from wheat-germ with supercritical carbon-dioxide. Agric Biol Chem 49:2367–2372
Temelli F, Saldaña MDA, Moquin PHL, Sun M (2008) Supercritical fluid extraction of specialty oils. In: Martinez JL (ed) Supercritical fluid extraction of nutraceuticals and bioactive compounds. CRC Press/Taylor & Francis, Boca Raton, FL, pp 51–101
Thana P, Machmudah S, Goto M, Sasaki M, Pavasant P, Shotipruk A (2008) Response surface methodology to supercritical carbon dioxide extraction of astaxanthin from Haematococcus pluvialis. Bioresour Technol 99:3110–3115
Tilly KD, Foster NR, Macnaughton SJ, Tomasko DL (1994) Viscosity correlations for binary supercritical fluids. Ind Eng Chem Res 33:681–688
Topal U, Sasaki M, Goto M, Hayakawa K (2006) Extraction of lycopene from tomato skin with supercritical carbon dioxide: Effect of operating conditions and solubility analysis. J Agric Food Chem 54:5604–5610
Tuan DQ, Zollweg JA, Harriott P, Rizvi SSH (1999) Measurement and modeling of viscosity of supercritical carbon dioxide/biomaterial(s) mixtures. Ind Eng Chem Res 38:2129–2136

Uquiche E, del Valle JM, Ortiz J (2004) Supercritical carbon dioxide extraction of red pepper (*Capsicum annuum L.*) oleoresin. J Food Eng 65:55–66

Vagi E, Simandi B, Suhajda A, Hethelyi E (2005) Essential oil composition and antimicrobial activity of *Origanum majorana L.* extracts obtained with ethyl alcohol and supercritical carbon dioxide. Food Res Int 38:51–57

Vagi E, Simandi B, Vasarhelyine KP, Daood H, Kery A, Doleschall F, Nagy B (2007) Supercritical carbon dioxide extraction of carotenoids, tocopherols and sitosterols from industrial tomato by-products. J Supercrit Fluids 40:218–226

Van Alsten JG, Eckert CA (1993) Effect of entrainers and of solute size and polarity in supercritical fluid solutions. J Chem Eng Data 38:605–610

Vasapollo G, Longo L, Rescio L, Ciurlia L (2004) Innovative supercritical CO_2 extraction of lycopene from tomato in the presence of vegetable oil as co-solvent. J Supercrit Fluids 29:87–96

Vega PJ, Balaban MO, Sims CA, O'Keefe SF, Cornell JA (1996) Supercritical carbon dioxide extraction efficiency for carotenes from carrots by RSM. J Food Sci 61:757–759

Vesovic V, Wakeham WA, Olchowy GA, Sengers JV, Watson JTR, Millat J (1990) The transport-properties of carbon-dioxide. J Phys Chem Ref Data 19:763–808

Visentainer JV, D'Addio Noffs M, De Oliveira Carvalho P, De Almeida VV, De Oliveira CC, De Souza NE (2007) Lipid content and fatty acid composition of 15 marine fish species from the southeast coast of Brazil. J Am Oil Chem Soc 84:543–547

Walsh JM, Ikonomou GD, Donohue MD (1987) Supercritical phase-behavior – the entrainer effect. Fluid Phase Equilib 33:295–314

Wang C, Harris WS, Chung M, Lichtenstein AH, Balk EM, Kupelnick B, Jordan HS, Lau J (2006) n-3 Fatty acids from fish or fish-oil supplements, but not α-linolenic acid, benefit cardiovascular disease outcomes in primary- and secondary-prevention studies: a systematic review. Am J Clin Nutr 84:5–17

Ward OP, Singh A (2005) Omega-3/6 fatty acids: alternative sources of production. Process Biochem 40:3627–3652

Weidner E (2009) High pressure micronization for food applications. J Supercrit Fluids 47:556–565

Wiebe R (1941) The binary system carbon dioxide-water under pressure. Chem Rev 29:475–481

Yener ME, Kashulines P, Rizvi SSH, Harriott P (1998) Viscosity measurement and modeling of lipid supercritical carbon dioxide mixtures. J Supercrit Fluids 11:151–162

Ziger DH, Eckert CA (1983) Correlation and prediction of solid-supercritical fluid phase equilibria. Ind Eng Chem Process Des Dev 22:582–588

Zuta CP, Simpson BK, Chan HM, Phillips L (2003) Concentrating PUFA from mackerel processing waste. J Am Oil Chem Soc 80:933–936

Chapter 17
Mass Transfer and Equilibrium Parameters on High-Pressure CO_2 Extraction of Plant Essential Oils

José M. del Valle, Juan C. de la Fuente, Edgar Uquiche, Carsten Zetzl, and Gerd Brunner

17.1 Introduction

The production of plant extracts is currently limited by safety and regulatory constraints on the concentration of toxic residues of organic solvents such as *n*-hexane or methanol (Sanders 1993). Carbon dioxide (CO_2) is an excellent alternative to these organic solvents due to its inertness, non-toxicity, non-flammability, and low cost (Brunner 1994; del Valle and Aguilera 1999). The recommended temperature in so-called supercritical fluid (SCF) extraction (SCFE) processes is slightly above the critical temperature (T_c) of the solvent so that a near-environmental temperature is applied when using CO_2 ($T_c = 304.2$ K) in SCFE, thus reducing the requirement of energy for separation as well as the thermal damage of labile bioactive compounds (Brunner 1994). Furthermore, objectionable solvent traces are eliminated from the treated substrate and the extract because, being a gas under normal environmental conditions, CO_2 is easily and fully removed following SCFE.

We would like to dedicate this chapter to the memory of our coauthors and friends Damian Cardarelli (1964–2007) and Miguel Mattea (1955–2007) who died tragically as a result of injuries sustained during a fire accident on December 5, 2007, in the pilot plant of the Facultad de Ingeniería in the Universidad Nacional de Rio Cuarto (Córdoba, Argentina). We met them either briefly (JMdV) or a long time ago (JdlF), but we were touched by their intellectual capacity, perseverance, camaraderie, and warmness.

J.M. del Valle (✉)
Departamento de Ingeniería Química y Bioprocesos, Pontificia Universidad Católica (PUC) de Chile, Avda. Vicuña Mackenna 4860, Macul, Santiago, Chile
e-mail: delvalle@ing.puc.cl

J.C. de la Fuente
Departamento de Procesos Químicos, Biotecnológicos y Ambientales, Universidad Técnica Federico Santa María, Valparaíso, Chile

E. Uquiche
Departamento de Ingeniería Química, Universidad de La Frontera, Temuco, Chile

C. Zetzl and G. Brunner
Thermische Verfahrenstechnik, Technische Universität Hamburg-Harburg (TUHH), Harburg, Germany

J.M. Aguilera et al. (eds.), *Food Engineering Interfaces*, Food Engineering Series,
DOI 10.1007/978-1-4419-7475-4_17,

Because of their high compressibility, particularly in the vicinity of the critical point, SCFs exhibit large variations in physical properties, including near-liquid solvent power and near-gas transport properties, and it is possible to take advantage of these improved properties to devise improved (medium-to-high yield, high selectivity, fast) extraction processes (Brunner 1994; del Valle and Aguilera 1999). These advantages of SCFs extend to near-critical liquids and gases. Thus, in this work the use of both supercritical CO_2 and near-critical CO_2 as extraction solvents will be covered; they will be referred to as high-pressure CO_2. The extraction process with high-pressure CO_2 will be referred as SCFE.

The typical quality fluctuations of vegetable substrates and difficulties in obtaining the standardized information required for designing selective SCFE processes make the industrial application of CO_2 as an extraction solvent for plant materials difficult (Zetzl et al. 2003). In this chapter an attempt is made to bridge the gap between scientific research and industrial application of SCFE for obtaining relevant plant extracts. Specifically, the focus will be on the SCFE of plant essential oils using high-pressure CO_2.

Two well-established SCFE applications in the food industry are the decaffeination of coffee (Lack and Seidlitz 1993) and the recovery of bitter compounds from hops to be used in improved beer-producing processes (Hubert and Vitzthum 1978; Gardner 1993). However, in this work it was felt that, viewed from a broader chemical perspective, the two most important types of components extracted from plant materials using high-pressure CO_2 are fatty oils (triglycerides) and essential oils (del Valle et al. 2005a). In the specific case of plant essential oils, SCFE allows a higher yield to be attained in a shorter time as compared to steam distillation, hydro-distillation, and conventional solvent extraction, while simultaneously avoiding thermal and hydrolytic degradation of labile compounds, as well as toxic solvent residues in the product (Stahl et al. 1988; Moyler 1993; Reverchon 1997; Mukhopadhyay 2000; Reverchon and De Marco 2006, 2008; Quirin and Gerard 2007).

Authors del Valle and de la Fuente (2006) described SCFE of fatty oils from seeds, including relevant mass transfer and equilibrium parameters. Thus, the purpose of this chapter is to provide similar information for the industrially important case of SCFE of plant essential oils. Because the solubility of essential oils in high-pressure CO_2 is great, their selective extraction from a plant requires low-to-medium densities to avoid contamination of the extract with heavier and/or more polar compounds such as, e.g., fatty oils and carotenoids. Thus, for the purpose of this chapter, plant essential oils are defined as those terpenes that can be extracted with high-pressure CO_2 at 15 MPa or less.

17.1.1 Chemistry and Localization of Essential Oils

Essential oils are complex mixtures of many volatile compounds that are responsible for the aroma of herbs and spices. As a group, essential oils do not share

common chemical properties beyond conveying the characteristic aroma of the herb or spice and consequently are used for flavoring foods, drinks, perfumes, cosmetics, incense, and bath and house-cleaning products. For applications in foods, a spice is a seed, fruit, root, bark, or leaf that is dried, ground (usually), and used in small amounts as a preservative against deleterious or harmful microorganisms, or as an additive to impart flavor or color to the food. Herbs differ from spices in that they are leafy, green plant parts that are usually chopped into smaller pieces and used in a fresh (undried) condition as food preservatives or flavor additives.

Brielmann et al. (2006) reviewed the chemistry of plant essential oils. The most volatile components in essential oils are terpenes, which are secondary plant metabolites derived from isoprene (2-methyl-1,3-butadiene), a 5-carbon unsaturated hydrocarbon molecule. Terpenes include the 2-isoprene (or 10-carbon) monoterpene hydrocarbons that typically fit a $C_{10}H_{16}$ molecular formula (e.g., *p*-cymene, limonene, α-pinene), the 3-isoprene (or 15-carbon) sesquiterpene hydrocarbons that typically fit a $C_{15}H_{24}$ molecular formula (e.g., β-caryophyllene, α-humulene), and oxygen-containing derivatives of monoterpene and sesquiterpene hydrocarbons (the so-called oxygenated monoterpenes and oxygenated sesquiterpenes, respectively) such as acetates (e.g., linalyl acetate, farnesyl acetate), alcohols (e.g., β-citronellol, geraniol, farnesol, linalool, menthol, patchoulol, verbenol), aldehydes (e.g., *p*-anisaldehyde, citral), ketones (e.g., camphor, carvone, fenchone), phenols (e.g., carvacrol, eugenol, thymol), and oxides (e.g., artemisinin, 1,8-cineole), among others. Among these compounds the oxygenated monoterpenes are especially important because they are responsible for the characteristic aroma of the herb or spice.

Plant essential oils are encapsulated in specialized secretory structures made of high-molecular-weight nonvolatile waxes (C_nH_{2n+2}) and other fatty compounds that protect them against evaporative losses and deleterious oxidative and/or hydrolytic reactions by atmospheric oxygen and water. Essential oils are secreted into specialized structures that can be located in either the surface (the so-called glandular trichomes or glands) or below the outer surface of the plant material (secretory ducts and secretory cavities) depending on the plant family and species (Denny 1991; Zizovic et al. 2007c; Stamenić et al. 2008). The leaves, terminal shoots, and flowers of aromatic herbs of the *Lamiaceae* family, such as basil (*Ocimum basilicum*), lavender (*Lavandula angustifolia*), marjoram (*Origanum majorama*), oregano (*Origanum vulgare*), pennyroyal (*Mentha pulegium*), peppermint (*Mentha* × *piperita*), rosemary (*Rosmarinus officinalis*), sage (*Salvia officinalis*), spearmint (*Mentha spicata*), thyme (*Thymus vulgaris*), and wild thyme (*Thymus serpyllum*), produce superficial oils that are stored in abundant secretory cells called glandular trichomes or glands (Zizovic et al. 2005, 2007c; Stamenić et al. 2008).

Unlike the aromatic herbs of the *Lamiaceae* family that secrete oils in superficial glands, herbs and spices of the *Apiaceae* and *Asteraceae* families secrete oils into subcutaneous ducts (Zizovic et al. 2007a,b,c; Stamenić et al. 2008). These ducts are elongated cavities that can branch out to create a network of interconnected pores extending from the roots, through the stems, and to the leaves, flowers, and fruits of the plants. In this chapter the *Apiaceae* family is

represented by anise (*Pimpinella anisum*), caraway (*Carum carvi*), celery (*Apium graveolens*), fennel (*Foeniculum vulgare*), and parsley (*Petroselinum crispum*), whereas the *Asteraceae* family is represented by candeia (*Eremanthus erythropappus*), carqueja (*Baccharis trimera*), chamomile (*Matricaria recutita*), and marigold (*Calendula officinalis*).

Other forms of subcutaneous oils are accumulated in secretory cavities, which are spherical structures lined with essential-oil-producing ephitelium cells (Zizovic et al. 2007c; Stamenić et al. 2008). Secretory cavities can be found in both aerial and underground parts of many plants including roots (valerian, *Valeriana officinalis*, *Valerianaceae*), rhizomes (ginger, *Zingiber officinale*, *Zingiberaceae*), leaves (alecrim pimenta, *Lippia sidoides*, *Verbenaceae*; boldo, *Peumus boldus*, *Monimiaceae*; cinnamon of Cunhã, *Croton zehntneri*, *Euphorbiaceae*; eucalyptus, *Eucalyptus globulus*, Myrtaceae; ho-sho, *Cinnamomum camphora*, *Lauraceae*), flower buds (clove, *Syzygium aromaticum*, *Myrtaceae*) and cones (hop, *Humulus lupulus*, *Cannabaceae*), fruit peels (orange, *Citrus sinensis*, *Rutaceae*); black pepper, *Piper nigrum*, *Piperaceae*), and seeds (nutmeg, *Myristica fragrans*, *Myristicaceae*).

17.1.2 Organization of Chapter

Figure 17.1 represents the SCFE of a solid substrate in a packed bed. As will be discussed in Sect. 17.2, the process can be modeled using a differential mass balance equation (Fig. 17.1a) coupled with a mass transfer rate equation. During SCFE of a pre-treated plant material, the partition of solutes between the solid and fluid phases (K), the actual solubility of the solutes in the solvent (C_{sat}), and various resistances to mass transfer play important roles in extraction rates. The effective diffusivity in the solid matrix (D_e), external mass transfer coefficient (k_f), and axial dispersion coefficient (D_{ax}) all influence the concentration gradient-driven mass transfer rates within the solid, the stationary SCF film surrounding each particle, and along the bed, respectively (Fig. 17.1b).

Figure 17.2 presents an integral extraction plot of solute yield versus specific solvent consumption resulting from the SCFE of the solid substrate in a packed bed. Although there might be a positive effect of superficial solvent velocity on extraction rates, integral extraction curves generally collapse to a single line, at least initially, with a slope that represents the so-called operational solubility (C_{fo}) (Fig. 17.2, zone I). Scientific research on SCFE of plant essential oils, aimed at the industrial application of the process, should result in mass transfer (k_f, D_{ax}, D_e) and phase equilibrium or pseudo-equilibrium data (K, C_{sat}, C_{fo}) that can be applied for process design purposes.

In Sect. 17.2, mathematical models are presented and discussed for the SCFE of essential oils from a packed bed of plant material, followed by a presentation of the external (k_f) and internal (D_e) mass transfer parameters that have been fitted in the literature to cumulative extraction plots of essential oil yield versus time or specific

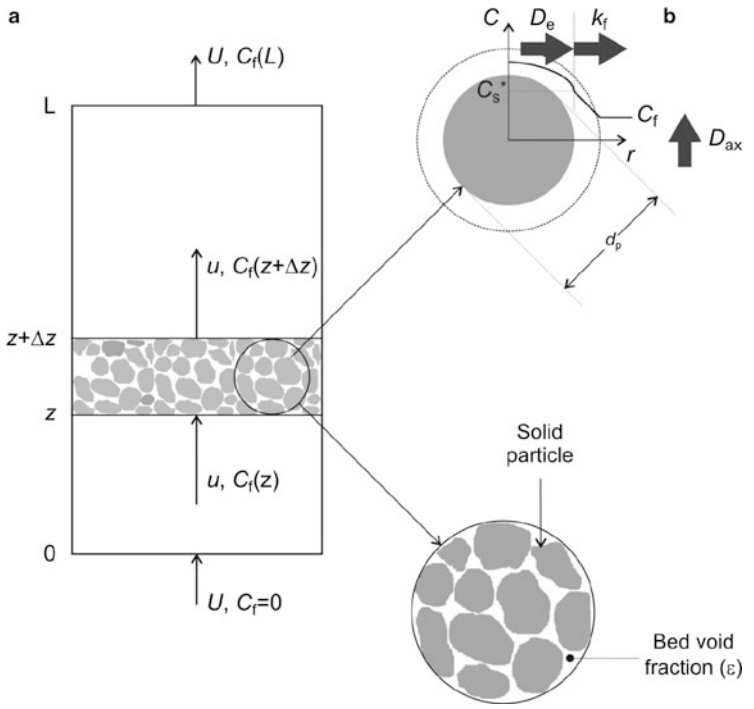

Fig. 17.1 Conceptual model of supercritical fluid extraction of solid substrates in packed beds: (**a**) differential mass balance along packed bed; and (**b**) mass transfer phenomena within solid particle (substrate), between particle and CO_2 (solvent) phase, and in CO_2 phase along bed

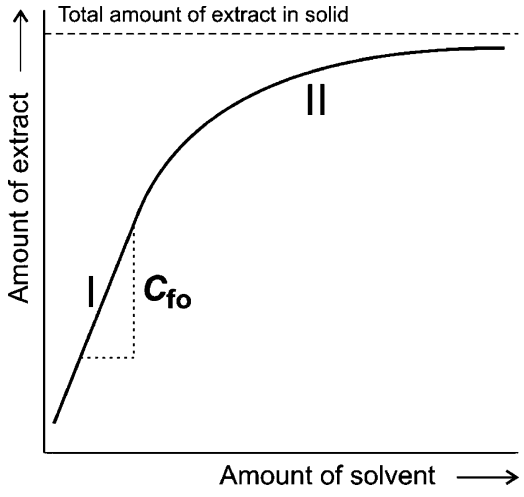

Fig. 17.2 Supercritical fluid extraction curve showing solute yield versus specific solvent consumption. Both the recovered solute and amount of CO_2 passed through the packed bed are expressed in a common base, the amount of substrate loaded into the extraction vessel

solvent consumption (Sect. 17.3). Next, reported "operational" solubility (C_{fo}) values are presented and compared to the "thermodynamic" or true solubility (C_{sat}) values of plant essential oil components in high-pressure CO_2 in binary, ternary, and more complex systems (Sect. 17.4). Some concluding remarks are made in Sect. 17.5.

17.2 Mass Transfer Models

This section presents a mathematical model that can be used as a reference to discuss the effect of mass transfer and equilibrium parameters on the SCFE of plant essential oils using high-pressure CO_2 as the solvent (Sect. 17.2.1). The so-called diffusion model assumes internal mass transfer by diffusion within solid particles, external mass transfer by convection through a static film of SCF next to the particles, and axial dispersion of dissolved solute in the SCF phase along the bed. This reference model also assumes a packed bed of spherical particles, an essential oil that can be treated as a single substance (pseudo-solute), and a constant partition coefficient for this pseudo-solute between the solid substrate and high-pressure CO_2. Discussion follows covering the effect on mass transfer rates of particle shape, localization of the solute in specialized structures within the solid matrix, actual composition of the essential oil, and its partition between the solid matrix and the CO_2 that limit the application of the diffusion model (Sect. 2.2). Finally, this section concludes with a discussion of alternative internal mass transfer mechanisms that can compliment diffusion, thus affecting the rate at which essential oils migrate through the solid substrate (Sect. 2.3).

17.2.1 Diffusion Model

The reference model used in this section will be the diffusion model of Goodarznia and Eikani (1998). The assumptions of this diffusion model are as follows: (1) the substrate particles are spherical (diameter d_p, radius $R = d_p/2$) and homogeneous; (2) the physical properties of the extract (the essential oil) are those of a representative pseudo-solute; (3) the physical properties of the SCF and the substrate remain unchanged during extraction; (4) the extract partitions between the solid and SCF phases according to a constant coefficient (K) that is concentration-independent; and (5) the solute disperses axially in the SCF as a result of irregularities in the packing of the substrate in the bed and concentration-gradient-driven diffusion of the solute along the packed bed. As a result of these assumptions, solute concentration in the solid matrix (C_s) depends on the radial position within the particle (r), the axial position along the bed (z), and the extraction time (t); whereas solute concentration in the SCF (C_f) depends only on z and t. The assumption of constant physical properties is valid when the density and viscosity of the SCF depend only on the

extraction temperature and pressure, and are unaffected by the dissolved pseudo-solute. Because of that, the variations in temperature and pressure should be negligible within the bed, and the concentration of essential oils in the loaded SCF phase should be small (selected process conditions should limit the solubility and/or availability of the solute). On the other hand, the assumption of constant physical properties of the solid phase is valid if the substrate remains unaffected (does not swell or shrink) as a result of CO_2 adsorption and solute removal, and this results in a constant bed porosity (ε) and, consequently, in a constant interstitial velocity of the SCF in the packed bed ($u = U/\varepsilon$). These assumptions are valid in the selective extraction of plant essential oils with high-pressure CO_2 for several reasons. The availability of solute is small because the content of essential oils in a typical herb or spice is limited to a few percent or below. Recommended values of extraction temperature and pressure (e.g., 323 K and 9 MPa) (Reverchon 1997) place a limit on the solubility of the essential oil in high-pressure CO_2, so as to increase the selectivity of the process. A near-environmental extraction temperature is selected to reduce thermal damage of labile compounds as well as energy requirements of the process, which reduces the exchange of heat with the environment and minimizes radial temperature gradients in the extraction vessel. Finally, as for other internally controlled mass transfer processes, small values of superficial solvent velocity ($1 \leq U \leq 5$ mm/s) (Eggers 1996) are recommended to improve economics, and these small velocities reduce losses of energy of the SCF as it passes through the bed of packed substrate, and minimize axial pressures gradients in the extraction vessel.

Equation 17.1 is a differential mass balance for the SCF surrounding the particles of substrate in the packed bed. J, the so-called source-and-transfer term (Zizovic et al. 2007c; Stamenić et al. 2008), is the flux of solute that is transferred from the solid to the SCF, and can be estimated using (17.2). On the other hand, the diffusion of the solute through the solid particles can be estimated using (17.3).

$$\frac{\partial C_\mathrm{f}}{\partial t} + u\frac{\partial C_\mathrm{f}}{\partial z} - D_\mathrm{ax}\frac{\partial^2 C_\mathrm{f}}{\partial z^2} = \frac{6}{d_\mathrm{p}}\frac{(1-\varepsilon)}{\varepsilon}J \tag{17.1}$$

$$J = -D_\mathrm{e}\frac{\partial C_\mathrm{s}}{\partial r}\bigg|_R \tag{17.2}$$

$$\frac{\partial C_\mathrm{s}}{\partial t} = \frac{D_\mathrm{e}}{r^2}\frac{\partial}{\partial r}\left(r^2\frac{\partial C_\mathrm{s}}{\partial r}\right) \tag{17.3}$$

Goodarznia and Eikani (1998) assumed constant solute concentrations in the solid matrix (initial solute content C_so) and the SCF phase (initial solute content C_fo) in the bed initially (17.4a and 17.4b, respectively), a symmetry condition for the removal of solute from the particles (17.4c), continuity in the flux of solute leaving a solid particle and entering the SCF film around it (17.4d), and the Danckwerts conditions for axial dispersion in packed beds (17.4e and 17.4f).

$$C_s = C_{so} \quad (t = 0,\ 0 \le r \le R) \tag{17.4a}$$

$$C_f = C_{fo} \quad (t = 0,\ 0 \le z \le H) \tag{17.4b}$$

$$\left.\frac{\partial C_s}{\partial r}\right|_0 = 0 \quad (t \ge 0,\ 0 \le z \le H) \tag{17.4c}$$

$$-D_e \left.\frac{\partial C_s}{\partial r}\right|_R = k_f \left(\frac{C_s|_R}{K} - C_f\right) \quad (t \ge 0,\ 0 \le z \le H) \tag{17.4d}$$

$$uC_f - D_{ax}\frac{\partial C_f}{\partial z} = 0 \quad (t \ge 0,\ z = 0) \tag{17.4e}$$

$$\frac{\partial C_f}{\partial z} = 0 \quad (t \ge 0,\ z = H) \tag{17.4f}$$

Examination of (17.1)–(17.4) suggests that variations in C_s and C_f as a function of r, z, and t depend on the initial essential oil content in the substrate (C_{so}), the geometry of the packed bed (diameter, D_E; height, H; porosity, ε) and the particles (diameter, d_p), and the conditions of the SCF (interstitial velocity, u; temperature, T; and pressure, P).

A closer examination of (17.1)–(17.4) also suggests that the extraction rate and yield depend on both kinetic (or mass transfer) parameters and equilibrium (or solubility) parameters. The former category includes an internal mass transfer coefficient (the effective diffusivity of the extract in the solid matrix, D_e), an external mass transfer coefficient (the SCF film coefficient, k_f), and an axial dispersion coefficient (D_{ax}) (Fig. 17.1b). Phase equilibrium parameters include the solubility of the essential oils in high-pressure CO_2 at T and P (C_{sat}), and their partition between the solid matrix and the SCF phase (K). Border condition 17.4b implicitly requires extraction to be preceded by a static period (unaccounted for by the model) so as to equilibrate the vessel to the required process temperature and pressure conditions, and to dissolve free solute in the solid phase. The SCF phase becomes saturated (initial solute concentration C_{sat}) only if there is enough free solute in the substrate; when there is less solute, the concentration C_{fo} is determined by the ratio between the total amount of free solute and the total void volume occupied by the SCF in the bed.

Some of the simplifications of the diffusion model applied in the literature include the following (Table 17.1): neglecting the effect of axial dispersion in mass transfer (model Diff/PF of Araus et al. 2009); treating the packed bed as a perfectly mixed extraction vessel (model Diff-Sph/PM of Reverchon et al. 1993a; models Diff-Slab/PM and Diff-Slab/IC of Gaspar et al. 2003; model Diff-Sph/IC of Campos et al. 2005); and neglecting the external resistance to mass transfer (model Diff-Slab/IC of Gaspar et al. 2003; model Diff-Sph/IC of Campos et al. 2005).

The diffusion model adopted in this chapter as the reference model (this section) makes several simplifying assumptions about the particle geometry (spherical), the

Table 17.1 Summary of mathematical models used in the literature for high-pressure CO_2 extraction of plant essential oils in packed beds

Mass transfer model	Substrate particles[a]	Hydrodynamics in packed bed[b]	External mass transfer coefficient[c]	Axial dispersion coefficient[d]	Sorption/ "operational" solubility model[e]
Diffusion (Diff or D) models					
Diff/ADPF (Goodarznia and Eikani 1998)	Sphere	Axially dispersed plug flow	Literature correlation	Literature correlation	Linear isotherm
Diff/PF (Araus et al. 2009; Uquiche et al. submitted)	Infinite slab	Plug flow	Literature correlation	Neglected	Linear isotherm
Diff-Sph/PM (Reverchon et al. 1993a)	Sphere	Perfect mixing	Literature correlation	Neglected	Neglected
Diff-Slab/PM (Gaspar et al. 2003)	Infinite slab	Perfect mixing	Literature correlation	Neglected	Neglected
Diff-Sph/IC (Campos et al. 2005)	Sphere	Perfect mixing	Neglected	Neglected	Neglected
Diff-Slab/IC (Gaspar et al. 2003; Campos et al. 2005)	Infinite slab	Perfect mixing	Neglected	Neglected	Neglected
Shrinking-Core (SC) models					
SC/ADPF (Spricigo et al. 2001; Machmudah et al. 2006)	Porous sphere	Axially dispersed plug flow	Literature correlation	Literature correlation	Limited by saturation
SC/ADPF (Steffani et al. 2006)	Porous sphere	Axially dispersed plug flow	Fitted to data	Literature correlation	Limited by saturation
SC/PF (Akgun et al. 2000; Germain et al. 2005)	Porous sphere	Plug flow	Literature correlation	Neglected	Limited by saturation
SC/PF (Germain et al. 2005)	Porous sphere	Plug flow	Fitted to data	Neglected	Limited by saturation
Desorption-Dissolution-Diffusion (DDD or D^3) models					
DDD/ADPF/BET (Ruetsch et al. 2003)	Porous sphere	Axially dispersed plug flow	Literature correlation	Literature correlation	BET isotherm
DDD/ADPF/Lang (Daghero et al. 2004)	Porous sphere	Axially dispersed plug flow	Literature correlation	Literature correlation	Langmuir isotherm
DDD/ADPF (Salimi et al. 2008)	Porous sphere	Axially dispersed plug flow	Literature correlation	Literature correlation	Several isotherms

(*continued*)

Table 17.1 (continued)

Mass transfer model	Substrate particles[a]	Hydrodynamics in packed bed[b]	External mass transfer coefficient[c]	Axial dispersion coefficient[d]	Sorption/ "operational" solubility model[e]
DDD/PM (Kim and Hong 2002)	Porous sphere	Perfect mixing	Fitted to data	Neglected	Linear isotherm, $K = 1$
Intact-and-Broken-Cell (IBC) models					
IBC-Diff (Kim and Hong 2002)	Sphere	Plug flow	Neglected	Literature correlation	Neglected
IBC/PF/PCPR (Machmudah et al. 2006; Sovová 2005; Langa et al. 2009)	Unaccounted for	Plug flow	Fitted to first stage	Neglected	PCPR isotherm
IBC/PF (Louli et al. 2004)	Unaccounted for	Plug flow	Fitted to first stage	Neglected	Limited by saturation
IBC/PFNA (Sovová et al. 1994a)	Unaccounted for	PF with no accumulation	Fitted to first stage	Neglected	Decreasing solubility
Sovová (Campos et al. 2005;Louli et al. 2004; Mira et al. (1996, 1999); Papamichail et al. 2000; Povh et al. 2001; Ferreira and Meireles 2002; Sousa et al. 2002; Martínez et al. 2003; Rodrigues et al. 2003; Sousa et al. 2005; Vargas et al. 2006; Martínez et al. 2007; Bensebia et al. 2009)	Unaccounted for	PF with no accumulation	Fitted to first stage	Neglected	Limited by saturation
Microscale (μS) models					
μS/SGl (Zizovic et al. 2005; 2007c; Stamenić et al. 2008)	Surface glands	Axially dispersed plug flow	Literature correlation	Literature correlation	Limited by saturation
μS/SDuct (Zizovic et al. 2007b, c; Stamenić et al. 2008)	Secretory ducts	Axially dispersed plug flow	Literature correlation	Literature correlation	Limited by saturation
μS/SCav (Zizovic et al. 2007a, c; Stamenić et al. 2008)	Secretory cavities	Axially dispersed plug flow	Literature correlation	Literature correlation	Limited by saturation

Diffusion models using Linear Driving Force (LDF)					
LDF/ADPF (Reverchon and Marrone 1997)	Unaccounted for	Axially dispersed plug flow	Hidden in k_g	Literature chart	Linear isotherm
LDF/ADPF (Reis-Vasco et al. 2000)	Unaccounted for	Axially dispersed plug flow	Hidden in k_g	Fitted to data	Linear isotherm
LDF/PF/CDIC (Coelho et al. 1997)	Unaccounted for	Plug flow	Hidden in variable k_g	Neglected	Limited by saturation
LDF-Sph/PF (Esquivel et al. 1996)	Sphere	Plug flow	Hidden in k_g	Neglected	Limited by saturation
LDF/PF (Reverchon et al. 1999)	Unaccounted for	Plug flow	Hidden in k_g	Neglected	Linear isotherm
LDF/IMTC (Catchpole et al. 1996b)	Sphere	Plug flow	Neglected	Neglected	Linear isotherm, $K \ll 1$
LDF-Slab/PMMS (Reverchon 1996)	Infinite slab	Perfectly mixed multistages	Hidden in k_g	Neglected	Linear isotherm
LDF/PMMS (Esquivel et al. 1996)	Unaccounted for	Perfectly mixed multistages	Hidden in k_g	Neglected	Linear isotherm
LDF/UENA (Louli et al. 2004; Papamichail et al. 2000)	Sphere	Uniform extraction NA	Hidden in k_g	Neglected	PCPR isotherm
R-SO (Louli et al. 2004; Papamichail et al. 2000; Vargas et al. 2006; Reverchon et al. 1995a; Zekovic et al. 2001; Pfaf-Šovljanski et al. 2005)	Sphere	Uniform extraction NA	Neglected	Neglected	Neglected
DDD models using LDF					
LDF-D^3/DB/BET (Goto et al. 1998)	Infinite slab	Differential bed	Literature correlation	Neglected	BET isotherm
LDF-D^3-Sph/DB (Perakis et al. 2005)	Sphere	Differential bed	Literature correlation	Neglected	Linear isotherm
LDF-D^3-Slab/DB (Sousa et al. 2005; Goto et al. 1993)	Infinite slab	Differential bed	Literature correlation	Neglected	Linear isotherm

(*continued*)

Table 17.1 (continued)

Mass transfer model	Substrate particles[a]	Hydrodynamics in packed bed[b]	External mass transfer coefficient[c]	Axial dispersion coefficient[d]	Sorption/ "operational" solubility model[e]
Equilibrium Desorption (ED), Internal-Mass-Transfer-Control (IMTC), and External-Mass-Transfer-Control (EMTC) models					
ED (Reis-Vasco et al. 2000)	Unaccounted for	Plug flow	Neglected	Fitted to data	Linear isotherm
IMTC (Ferreira et al. 1999)	Sphere	Perfect mixing	Neglected	Neglected	Limited by saturation
EMTC (Ferreira et al. 1999; Kotnik et al. 2007)	Sphere	Simplified diff. mass balance	Fitted to first stage	Neglected	Limited by saturation

[a]The particles were treated as solid or porous spheres (Sph) or infinite slabs (Slab); or else their shape as an inner structure was unaccounted for

[b]Flow conditions in extraction vessel are assumed to be axially dispersed plug flow (ADPF), plug flow (PF), perfect mixing (PM), or perfectly mixed multistages (PMMS). For simplification, the packed bed was treated as a differential bed (DB), and the differential mass balance assumed plug flow with no accumulation (PFNA) or uniform extraction with no accumulation (UENA)

[c]The external mass transfer and was estimated from correlations in the literature, then fitted to data, or neglected. The internal-mass-transfer-control (IMTC) models neglected the external resistance to mass transfer. The external mass transfer coefficient was sometimes hidden in a global mass transfer coefficient (k_g), either implicitly or explicitly; and in some cases (Reis-Vasco et al. 2000; Coelho et al. 1997; Ferreira et al. 1999; Kotnik et al. 2007) k_g was assumed to be an internal mass transfer coefficient (in IMTC models), and in others (Reverchon and Marrone 1997; Ferreira et al. 1999) (external-mass-transfer-control or EMTC models), an external mass transfer coefficient

[d]The axial dispersion coefficient was also estimated from correlations or charts in the literature, fitted to data, or neglected

[e]The equilibrium concentration of essential oils in the SCF phase was assumed to be limited by saturation (solubility), or to depend on the residual concentration of the oils in the solid substrate by a sorption isotherm given by a linear model, BET model, a Langmuir (Lang) model, or Perrut-Clavier-Poletto-Reverchon (PCPR) model of Perrut et al. (1997), among others

solid matrix (homogeneous), the localization of the solute in the solid matrix (homogeneous), the composition of the solute (fully characterized by a pseudo-solute), the partition of the solute between the solid matrix and the CO_2 (constant and independent of solute concentration), and the mass transfer mechanism for the extraction process (diffusion). As discussed in the following sections, some of these simplifying assumptions should be avoided to improve the physical picture of the extraction process.

17.2.2 Limitations of the Diffusion Model

When extracting herbs and spices it is important to consider the geometry of the tissue following application of pretreatments aimed at increasing the speed and/or final yield of the process. Mild pretreatments, such as coarse milling, are typically applied prior to SCFE to take full advantage of the natural barriers within the plant material to selectively extract the essential oils. Coarse milling of leaves and similar plant parts results in large particles having a slab rather than a spherical geometry as assumed in the diffusion model, so that the fitting of mathematical models to the data improves when using the diffusion equation for an infinite slab instead of (17.3) (Goto et al. 1993, 1998; Reverchon 1996; Gaspar et al. 2003; Araus et al. 2009). Stüber et al. (1997) derived analytical solutions for other regular geometries such as disks and cylinders having different aspect ratios by combining the analytic solutions for basic geometries such as infinite cylinders and infinite slabs using superposition theorems. However, the model for spherical particles still can be used to represent mass transfer from particles of various shapes (including disks and cylinders with different aspect ratios) if a characteristic dimension is computed as three times the volume-to-surface area ratio for a representative particle ($d_p/2$, in the case of a sphere) (Ma and Evans 1968).

When extracting herbs and spices it is important to consider the microstructure of the native tissue. Unlike the assumptions in Sect. 17.2.1, herbs and spices are heterogeneous when observed under the microscope. This is important to consider because SCFE of plant materials depends, among other factors, on the location of the solute within the plant tissue, with essential oils being encapsulated in isolated glands, secretory cells, or cavities, or in interconnected pore networks (Zizovic et al. 2007c; Stamenić et al. 2008). Furthermore, the physical properties of the solid may change during extraction as a result of impregnation of CO_2 and removal of essential oils (Eggers 1996).

Also, unlike the assumptions in Sect. 17.2.1, essential oils are not single compounds but mixtures of many different volatile terpenoids. During SCFE of herbs and spices, the waxy constituents of the specialized encapsulating structures of the essential oils are dissolved so that CO_2 extracts also include waxes and other compounds besides terpenoids. Thus, the components of CO_2 extracts of herbs and spices can be grouped as monoterpene hydrocarbons, oxygenated monoterpenes, sesquiterpene hydrocarbons, oxygenated sesquiterpenes, waxes, and other

substrate specific families of compounds such as gingerols in ginger and phenylpropanoids in parsley. In this work, for the purpose of estimating the value of physical properties of CO_2 extracts, the authors selected representative compounds of some of these groups, assigned the properties of representative compounds to whole groups, and represented extracts as pseudo-solutes whose properties were estimated as the weighted average of the properties of the representative compounds in each considered group.

The assumption of a constant coefficient for the partition of the solute (linear sorption isotherm) between the solid substrate and the high-pressure CO_2 is invalid when a fraction of the solute in the substrate, e.g., contained in broken cells or cavities, is freely available to the CO_2, so that its concentration in the fluid phase is determined by availability or solubility constraints. It is also invalid in the final stages of the extraction process, when all remaining solute is strongly bound to the solid substrate (del Valle and de la Fuente 2006). Consequently, Araus et al. (2009) claimed the necessity of relaxing the assumption of a constant partition coefficient of the pseudo-solute between the solid substrate and the CO_2 to improve modeling of SCFE of plant essential oils.

The internal mass transfer mechanism may be different from that stated in Sect. 17.2.1, since solute desorption from the solid, solubilization in the SCF, and/or migration by diffusion through the pores of the solid matrix may control mass transfer in the solid. The subject of the internal mass transfer mechanism is analyzed in the following section.

17.2.3 Alternative Internal Mass Transfer Mechanisms

Considering plant tissue as a multiphase material constituted of interconnected or isolated cells and a network of fully or partially interconnected pores (Zizovic et al. 2007c; Stamenić et al. 2008), and how its microstructure is affected by milling and other pretreatments applied prior to SCFE, alternative mass transfer models picture pretreated herbs and spices as porous solid matrices constituted of intact and broken cells (Sovová 1994, 2005; Zizovic et al. 2007c; Stamenić et al. 2008). del Valle and de la Fuente (2006) reviewed most of these models and others with alternative internal mass transfer mechanisms in detail.

When the solid matrix where mass transfer takes place is assumed to be a network of interconnected pores, two important models that can be applied are the so-called shrinking-core (SC) and desorption-dissolution-diffusion (DDD) models. The shrinking-core hypothesis assumes that the solute is retained in the pores of the solid matrix by mechanical or capillary forces, so that pore space is divided into an inner core filled with condensed solute and an outer region containing a solution of the solute in high-pressure CO_2 that are separated by a moving boundary. Roy et al. (1996) first applied the shrinking-core hypothesis to model SCFE of ginger essential and fatty oils at >15 MPa (data not included), and there are several examples in the literature on this hypothesis to model the extraction of

plant essential oils. Of these models (Table 17.1), that of Machmudah et al. (2006) is different in that they assumed that the extract is a mixture of two pseudo-components, namely the monoterpene and sesquiterpene hydrocarbons, on the one hand, and their oxygenated derivatives (oxygenated monoterpenes and sesquiterpenes), on the other hand (Sect. 17.3.2), that are extracted separately at rates defined by two independent values of D_e. Reverchon (1997) questioned the validity of the shrinking-core hypothesis to model SCFE of substrates containing little solute bound to the solid matrix, as it could be the case for essential oils in most herbs and spices, where the driving force for the extraction depends little on the solubility of the essential oil in high-pressure CO_2 under extraction conditions.

On the other hand, the desorption-dissolution-diffusion hypothesis assumes that the solute is partially adsorbed on the solid matrix within the pores, so that a fraction of the solute is adsorbed on the solid matrix and the rest is dissolved in the SCF phase within the inner pores of the solid, which are related by an equilibrium sorption isotherm (see Table 17.1 for a summary of DDD models applied in literature). Goto et al. (1993) assumed a linear sorption isotherm (or a constant equilibrium-partition coefficient K), Ruetsch et al. (2003) applied a Brunauer-Emmet-Teller (or BET) isotherm, Daghero et al. (2004) applied a Langmuir isotherm for solute concentrations below the saturation concentration in the high-pressure CO_2, and Salimi et al. (2008) compared a linear isotherm with several other sorption models including those of Langmuir, Freundlich, and Langmuir Freunlich. Kim and Hong (2002) did not differentiate between the solute adsorbed on the solid and dissolved in the gas phase within the pores, which implicitly implied a unitary equilibrium-partition coefficient ($K = 1$).

Sovová (1994) proposed the hypothesis of intact and broken cells (IBC), which assumes that as a result of a mild pretreatment such as size reduction, particles of milled plant material have broken cells on the surface, and intact cells in the interior. An external (convective) mass transfer coefficient controls transfer of solute from the broken cells to the SCF in the bed, whereas an internal (diffusive) mass transfer coefficient controls transfer of solute from the intact cells (see Table 17.1 for a summary of IBC models applied in literature). Reverchon et al. (1999) considered the simultaneous extraction of free solute and bound solute using separate coefficients for external mass transfer and internal mass transfer, respectively, and separate equilibrium-partition coefficients for free solute between the broken cells and the SCF in the bed, and between the bound solute in intact cells and the SCF in the bed. The model (LDF/PF) of Reverchon et al. (1999) (Table 17.1) is a simplification of this general IBC model, which they applied SCFE of lipids from milled fennel seeds; the simplifying assumption was that there is no free essential oil in milled fennel seeds and that all was bound to the solid matrix. Unlike Reverchon et al. (1999), Sovová (2005) and Machmudah et al. (2006) assumed that the driving force for the extraction of free essential oil is the difference between an equilibrium concentration of the oil in high-pressure CO_2 that depends on the oil concentration in broken cells according to the so-called PCPR isotherm of Perrut et al. (1997), as described in Sect. 17.4.4, and its concentration in the SCF phase, whereas the driving force for extraction of bound essential oil is the difference in oil

concentration between the intact and broken cells (model IBC/PF/PCPR in Table 17.1).

More advanced models differentiate the effect of the pretreatment on the substrate depending on the localization of the essential oil in specialized structures in the herb or spice, which are ruptured (surface glands or SGl, inner secretory ducts or SDuct, inner secretory cavities or SCav) during milling, or burst (surface glands) as a result of swelling of the glands by dissolution of high-pressure CO_2 in the gland contents (essential oils) (Zizovic et al. 2005, 2007a,b,c; Stamenić et al. 2008). Table 17.1 classifies these so-called Micro-Scale (μS) models, which are further described in Sect. 17.3.3.

Table 17.1 also summarizes several simplifications of the basic mass balance and rate equations of mass transfer models used in the literature to simulate SCFE curves of plant essential oils. Several of these simplifications pertain to the differential mass balance equation. When assuming a so-called differential bed (DB), which is valid if the height of the packed bed is comparable with the inner diameter of the extraction vessel, the second term on the right of the differential mass balance equation (17.1) is replaced by an expression reflecting a linear variation in the concentration of the solute in the SCF with the axial position along the bed (Goto et al. 1993, 1998; Perakis et al. 2005). Alternative simplifications to the differential mass balance equation include assuming that there is no accumulation (NA) of solute in the SCF phase, or neglecting the accumulation or first term on the right of (17.1) (Sovová 1994; Papamichail et al. 2000; Reverchon and Sesti Osséo 1994a); assuming a uniform extraction (UA) along the bed, or replacing the second term on the right of (17.1) by an expression reflecting a linear variation in solute concentration in SCF with the axial position along the bed, which is equivalent to assuming a "differential" bed (Papamichail et al. 2000; Reverchon and Sesti Osséo 1994a); and assuming a plug flow (PF), and/or neglecting the axial dispersion in the SCF phase or the third term on the on the right of (17.1). As summarized in Table 17.1, assuming the axially dispersed plug flow (ADPF) pattern (Reverchon and Marrone 1997; Goodarznia and Eikani 1998; Reis-Vasco et al. 2000; Spricigo et al. 2001; Ruetsch et al. 2003; Daghero et al. 2004; Zizovic et al. 2005, 2007b, c; Machmudah et al. 2006; Steffani et al. 2006; Salimi et al. 2008; Stamenić et al. 2008) that is implicit in the differential mass balance equation (17.1) presented in Sect. 2.1 is more the exception than the norm. Some authors (Reverchon et al. 1993a; Reverchon 1996; Kim and Hong 2002; Gaspar et al. 2003; Campos et al. 2005; Kotnik et al. 2007) circumvent the differential mass balance (17.1) treating the packed bed as a vessel with perfect mixing (PM), and others (Esquivel et al. 1996; Reverchon 1996; Sovová 2005) treating it as perfectly mixed multistages (PMMS) or a series of perfectly agitated mixing vessels. The perfectly mixed vessel or "hot-ball"-type model, so called because of the similitude in the mass transfer process with the cooling of a hot ball of a solid material in a fluid (Reverchon 1997), or Crank model, so called to honor the author of an influential book on diffusion in solids (Crank 1975), fail to account for the effect of the increase in solute concentration in the SCF phase along the bed in decreasing the rate of mass transfer. Models assuming several (n) perfectly mixed vessels in series approach plug flow

as the value of n increases, with the n being an indirect measurement of the axial dispersion along the packed bed; the treatment of a packed bed as a series of discrete stages does not comply with the physical situation but is commonly applied in other separation processes in packed beds such as chromatography (Martin and Synge 1941).

Besides or instead of the differential mass balance equation (17.1), some models listed in Table 17.1 simplify the so-called source-and-transfer J term (17.2) that describes the rate of transfer of essential oil between the herb or spice and the high-pressure CO_2. The linear driving force (LDF) approximation for mass transfer from the substrate to the SCF (see examples of this type of simplifying assumption in Table 17.1), which is valid when the residual solute concentration profile in the partially extracted solid substrate, $C_s(r)$, is approximately parabolic, uses a global driving force and a single global mass transfer coefficient. The global driving force for mass transfer equals the difference between the average residual concentration of solute in the solid, corrected by the equilibrium-partition coefficient $(\bar{C}_s/K)$ and the concentration of solute in the SCF (C_f). The global mass transfer coefficient (k_g, (17.5), Goto et al. 1993), on the other hand, accounts for both the internal resistance to mass transfer (related to an internal mass transfer coefficient, k_i) and external resistance to mass transfer (related to the external mass transfer coefficient, k_f):

$$k_g = \frac{k_f}{1 + \frac{Bi}{\xi}} \tag{17.5}$$

where ξ, a particle-geometry parameter, equals 10 for a sphere and equals 6 for a thin slab (for which the characteristic dimension d_p corresponds to its thickness); Bi is the dimensionless Biot number (17.6):

$$Bi = \frac{k_f d_p}{D_e} \tag{17.6}$$

When both the inner resistance to mass transfer in the plant material and the external resistance in the SCF film surrounding the particles can be neglected, it is unnecessary to include the so-called source and transfer J term in the mass balance and rate equations (17.1–17.4) because under these conditions C_f and $\bar{C}_s$ are related by equilibrium. Reis-Vasco et al. (2000) applied this simplifying assumption to the initial stages of the high-pressure CO_2 extraction of pennyroyal essential oil.

The most simple models in Table 17.1 correspond to simple steady-state approximations that assume the rate of extraction is defined by a single mass transfer controlling resistance, which switches from external control (Ferreira et al. 1999; Kotnik et al. 2007) to internal control (Kotnik et al. 2007) in a given transition time. An alternative way to account for the transition from external control to internal control in a single model is to use a concentration-dependent global mass transfer coefficient when using the linear driving force approximation to mass transfer, as done by Coelho et al. (1997). It is important to point out that some models in

Table 17.1 refer to authors who adopted them for SCFE of plant essential oils instead of the original authors who applied them for alternative SCFE applications. Specifically, these models are the Diff-Sph/IC model of Crank (1975), the EMTC model of Brunner (1984), the IMTC model of Hong et al. (1990), the LDF/PF/CDIC model of Cygnarowicz-Provost (1996), the LDF-Sph/PF model of Catchpole et al. (1994), Sovová's (1994) model, and the LDF-D^3-Sph/DB model of Skerget and Knez (2001).

Selected models that are highlighted in Table 17.1 are widely used because they have relatively simple analytical solutions and are used to best-fit model parameters with ease. The solution of the so-called Reverchon–Sesti Ossèo (R-SO) model was applied by Reverchon and Sesti Osséo (1994a), Reverchon et al. (1995a), Papamichail et al. (2000), Zekovic et al. (2001), Louli et al. (2004), Pfaf-Šovljanski et al. (2005), and Vargas et al. (2006). On the other hand, the solution of Sovová's (1994) model was applied by Mira et al. (1996, 1999), Papamichail et al. (2000), Povh et al. (2001), Ferreira and Meireles (2002), Sousa et al. (2002, 2005), Martínez et al. (2003, 2007), Rodrigues et al. (2003), Louli et al. (2004), Campos et al. (2005), Perakis et al. (2005), Vargas et al. (2006), and Bensebia et al. (2009). Sovová's model (1994) considers SCFE as a two-stage process, where the mass transfer coefficient in the first (convection-controlled) stage is k_f, whereas the mass transfer coefficient in the second (internal-diffusion-controlled) stage decreases proportionally to the difference between the solubility of the essential oil in high-pressure CO_2 and its actual concentration in the SCF phase in the bed. Povh et al. (2001) described a procedure to estimate the parameters of Sovova's model based on the fitting of an integral extraction plot of solute yield versus specific solvent consumption (Fig. 17.2) to a spline with three straight lines representing successively the constant, falling, and diffusion-controlled extraction rate periods. Sovová et al. (1994a) applied an improved version of Sovová's model (model ICB/ADPF in Table 17.1) in two aspects: they did not neglect the accumulation of essential oil in the SCF phase and they considered that the extraction was limited by a decreasing solubility (LDS) or that the saturation solubility of the essential oil in high-pressure CO_2 decreased during extraction due to the progressive enrichment of the oil remaining in the partially extracted substrate in less volatile compounds. Authors using other models include Louli et al. (2004) (LDF/UENA model of Papamichail et al. 2000), Sousa et al. (2005) (LDF-D^3-Slab/DB model of Goto et al. 1993), Campos et al. (2005) (Diff-Slab/IC model of Gaspar et al. 2003), Zizovic et al. (2007c) (μS/SGl model of Zizovic et al. 2005; μS/SCav model of Zizovic et al. 2007a; μS/SDuct model of Zizovic et al. 2007b), Stamenić et al. (2008) (μS/SCav model of Zizovic et al. 2007a; μS/SDuct model of Zizovic et al. 2007b), Langa et al. (2009) (IBC/PF/PCPR model of Sovová 2005), and Uquiche et al. (submitted) (Diff/PF model of Araus et al. 2009).

Although most authors of models in Table 17.1 applied the models to their own data, there are some exceptions. Goodarznia and Eikani (1998) modeled the data of Reverchon et al. (1993a) on SCFE of essential oils from basil, marjoram, and rosemary, as well as the data of Sovová et al. (1994a) on SCFE of caraway essential oil. Germain et al. (2005) also modeled the data of Sovová et al. (1994a) on SCFE

of caraway essential oils. Zizovic et al. (2007b) modeled data of Coelho et al. (2003) on SCFE of fennel fruit oil. Zizovic et al. (2007c) modeled literature data on SCFE of essential oils from orange peel (Mira et al. 1996), ginger rhizome (Roy et al. 1996), clove bud (Reverchon and Marrone 1997), and eucalyptus leaf (Della Porta et al. 1999). Stamenić et al. (2008) modeled the data of Machmudah et al. (2006) on SCFE of nutmeg essential oil. Finally, Araus et al. (2009) modeled literature data on SCFE of essential oils from sage (Reverchon 1996), lavender (Akgun et al. 2000), oregano (Gaspar 2002), pennyroyal (Reis-Vasco et al. 2000), and chamomile (Povh et al. 2001).

17.3 Kinetic Parameters of CO_2 Extraction of Essential Oils

Table 17.2 summarizes the conditions for the experimental studies on kinetics of mass transfer during SCFE of essential oils from herbs and spices reviewed in this chapter. Although most authors in Table 17.2 modeled the results of their own high-pressure CO_2 extraction work, there are some exceptions, including the data of Roy et al. (1996) on extraction of ginger essential oils at 313 K and 10.8 MPa, the data of Della Porta et al. (1999) on extraction of eucalyptus essential oil at 323 K and 9 MPa, the data of Coelho et al. (2003) on extraction of fennel essential oil at 313 K and 9 MPa, and the data of Gaspar (2002) on extraction of oregano essential oil under selected conditions (310 K and 8 MPa or 320 K and 20 MPa).

In this work, analysis required the estimation of the physical properties of the loaded CO_2 phase produced during the extraction of essential oils. For that purpose, the authors neglected the changes in physical properties associated with the dissolution of essential oils in the solvent under the assayed conditions, and estimated the density (ρ) and viscosity (μ) of the loaded high-pressure CO_2 as a function of the extraction temperature and pressure using the NIST (2000) database for pure CO_2 (del Valle and de la Fuente 2006). On the other hand, D_{12} was estimated using the equation of Catchpole and King (1994), which requires reduced temperature ($T_r = T/T_c$) and reduced density ($\rho_r = \rho/\rho_c$, where $\rho_c = 467.6$ kg/m^3 is the critical density of CO_2) of the SCF, and the molecular weight (MW_2) and critical volume (V_{c2}) of the pseudo-solute. As informed in Sect. 17.2.2, for the purpose of estimating MW_2 and V_{c2}, representative compounds in families of compounds were selected, such as monoterpene (MT) hydrocarbons, oxygenated monoterpene (OMT) compounds, sesquiterpene (ST) hydrocarbons, oxygenated sesquiterpene (OST) compounds, waxes, and some plant-specific compounds; properties of representative compounds to whole families were assigned; and extracts were considered as pseudo-solutes whose properties were estimated using Kay's rule as the weighted average of the properties of the representative compounds in each family (Poling et al. 2000). The composition of the essential oils was taken from the literature and was typically determined by gas chromatography analysis of the steam distillate, hydro-distillate, or CO_2-extract of the herb or spice. For calculations in this current work, only those families representing more than 1% of the

Table 17.2 Summary of extraction conditions of selected mass transfer studies on high-pressure CO_2 extraction of plant essential oils in packed beds

Substrate	Particle diameter (d_p, mm)	Temperature (T, K)	Pressure (P, MPa)	Superficial velocity (U, mm/s)	Extractor volume (V, cm^3)	L/D ratio of extractor (–)
Alecrim pimenta (Sousa et al. 2002)	0.38	298	6.7	0.12	220	27.8
Aniseed (Rodrigues et al. 2003)	0.50	303	8, 10, 14, 18	0.014–0.025	418	2.03
Basil (Reverchon et al. 1993a)	0.17	313	10	0.23	400	3.06
Black pepper (Ferreira et al. 1999; Ferreira and Meireles 2002)	0.080, 0.11	303, 313, 323	15, 20	0.018–0.20	26	29.1
Black pepper (Perakis et al. 2005)	0.18	313, 323	9, 10, 15	0.20–0.59	751	5.45
Boldo (Uquiche et al. submitted)	0.39, 0.40, 2.36	313	10	0.123	5	2.32
Caraway (Sovová et al. 1994a)	0.38	296, 313	9, 10	0.028–0.048	150	5.30
Carqueja (Vargas et al. 2006)	0.50	313, 323, 333, 343	9	0.35	4	4.09
Celery (Papamichail et al. 2000)	0.21, 0.49	318, 328	10, 15	0.167, 0.456	400	2.90
Chamomile (Povh et al. 2001)	0.30	303, 313	10, 12, 16, 20	0.030–0.087	204	4.18
Chamomile (Kotnik et al. 2007)	0.11	303, 313	10, 15	0.17–0.19	55	4.18
Cinnamon of cunha (Sousa et al. 2005)	0.52	288	6.7	0.065, 0.068	222	27.7
Clove (Reverchon and Marrone 1997)	0.37	323	9	0.244–0.488	400	3.06
Clove (Ruetsch et al. 2003)	0.79	323	9, 12	0.38, 0.76	1,500	2.62
Clove (Daghero et al. 2004)	0.79	323	9, 12	0.38, 1.52	1,500	2.62
Clove (Martínez et al. 2007)	0.86	308	10.0	0.039, 0.11	6, 133, 280	0.98, 1.05, 2.20
Eucalyptus (Della Porta et al. 1999)	0.37	323	9.0	0.514	400	6.00
Fennel (Reverchon et al. 1999)	0.37	323	9	0.20–0.61	400	3.06
Ginger (Roy et al. 1996)	0.35	313	11	0.74	2.2	6.67
Ginger (Martínez et al. 2003)	1.02	293, 303, 313	15, 20	0.091–0.12	150	13.3
Hop (Pfaf-Šovljanski et al. 2005)	0.488	313	15	0.050	200	3.98
Ho-sho (Steffani et al. 2006)	0.37, 0.50, 1.00	313, 323, 333	8, 9, 10	0.18–0.71	8	7.31
Lavender (Reverchon et al. 1995a)	1.67	321	9	0.31	400	3.06
Lavender (Akgun et al. 2000)	1.20	308, 313, 323	8, 10, 12, 14	0.44–1.4	39	50.0
Marigold (Campos et al. 2005)	0.62	313	12, 15	0.068, 0.202	139	19.1

Marjoram (Reverchon et al. 1993a)	0.15	313	10.0	0.23	400	3.06
Nutmeg (Spricigo et al. 2001)	0.30, 0.68, 1.45	296	9	0.032–0.053	35	4.76
Nutmeg (Machmudah et al. 2006)	0.56, 0.69, 2.12	313, 318, 323	1.0, 1.5	0.011, 0.068	500	1.86
Orange (Mira et al. (1996)	0.30, 0.50, 1.50, 7.50	323	15	0.084, 0.585	300	2.30
Orange (Mira et al. 1999)	0.30, 0.50, 1.50, 7.50	323	15	0.084, 0.585	300	2.30
Oregano (Esquivel et al. 1996)	1.10	298, 313	7, 10, 15	0.50–0.63	30	3.99
Oregano (Gaspar 2002)	0.36	310, 320	8, 20	0.22, 0.088	196	2.00
Oregano (Gaspar et al. 2003)	0.33, 0.36, 0.70, 1.55	300, 310, 320	7, 8, 10, 15, 20	0.017–0.058	319	0.47
Oregano (Uquiche et al. submitted)	0.35, 0.36, 2.36	313	10	0.123	5	2.32
Parsley (Louli et al. 2004)	0.29, 0.50	308, 318	10, 15	0.16–0.45	185, 209	1.34, 1.52
Pennyroyal (Reis-Vasco et al. 2000)	0.30, 0.50, 0.70	323	10	0.48–0.97	247–379	3.28–5.02
Peppermint (Goto et al. 1993)	0.12	313, 333, 353	8,8, 14.7, 19.6	0.099–0.43	21	2.17
Rosemary (Reverchon et al. 1993a)	0.23	313	10	0.23	400	3.06
Rosemary (Coelho et al. 1997)	0.72, 1.33	308, 313	10, 12.5, 20	0.11–0.43	5	12.9
Rosemary (Bensebia et al. (2009)	0.44	308, 313	10, 12, 15, 18	0.25–0.69	125	13.4
Sage (Catchpole et al. 1996b)	0.50–1.53	291	7	0.19–0.48	2,959	2.41
Sage (Reverchon 1996)	0.25–3.10	323	9	0.85–1.51	400	5.94
Sage (Langa et al. 2009)	0.3, 0.5, 0.8	313, 323	9, 10	0.15–0.34	1,000	6.00
Spearmint (Kim and Hong 2002)	0.30	312, 322	6.9, 8.5, 10.3	0.017–0.068	46	3.54
Thyme (Zekovic et al. 2001)	3.32, 1.46, 0.70	313	10	0.063	200	3.98
Valerian (Zizovic et al. 2007a)	0.40, 0.65, 0.90	313, 323	10, 15	0.072, 0.147	150	2.35
Valerian (Salimi et al. 2008)	0.59	310	17	0.233	10	12.9
Vetiver (Martínez et al. 2007)	0.12	313	20	0.054, 0.150	9, 187	1.45, 1.47
Wild thyme (Stamenić et al. 2008)	0.700	323	10	0.147	150	2.35

whole essential oil were considered, and the most concentrated four families in those cases where five or more were represented in excess of 1% each. Table 17.3 summarizes representative compounds of up to four families for essential oils in Table 17.2. As an example, the lavender essential oil of Reverchon et al. (1995a) has 3.33% MTs (main component, myrcene, representing 35.7% of all MTs), 87.9% OMTs (main component, linalyl acetate, representing 39.4% of all OMTs), 6.14% STs (main component, β-farnesene, representing 36.3 of all STs), and 2.63% OSTs (main component, bisabolol, representing 79.5% of all MTs). The values of V_c were estimated for the representative compounds in the various families using Joback's modification of the Lydersen's group-contribution method (Poling et al. 2000).

Table 17.4 summarizes the estimations of the molecular weight (MW_2) and critical volume (V_{c2}) of the pseudo-solutes representing the essential oils of the different herbs and spices reported in Table 17.3. It is clear that the properties of the pseudo-solutes vary between substrates, as expected, but also for a single substrate because of differences in the substrates or extracts. Indeed, the essential oils exhibit differences due to typical variations in biological samples associated with genetic and processing (e.g., harvest time, drying treatment, and storage condition) factors (Zetzl et al. 2003). In addition, steam distillates, hydrodistillates, and CO_2 extracts from the same substrate exhibit differences due to thermal and/or oxidative degradation of labile components during distillation, or solubilization of additional compounds in CO_2 with increased solvent power (Moyler 1993; Reverchon 1997). Figure 17.3 shows that the composition of sage essential oils extracted with high-pressure CO_2 at 313 K and 9 MPa, or 323 K and 10 MPa, changes depending on process conditions and extraction time.

17.3.1 Axial Dispersion Coefficient

Authors del Valle and de la Fuente (2006) showed consistency in the reported literature values of axial dispersion coefficients for flow of high-pressure CO_2 in a packed bed, when presenting the experimental values in a dimensionless plot of D_{ax}/D_{12} versus Pe_p where Pe_p is the Peclet number for the particle (17.7), which in turn corresponds to the product of the dimensionless numbers of Reynolds (Re, 17.8) and Schmidt (Sc, 17.9).

$$Pe_p\ (= Re \cdot Sc) = \frac{U\, d_p}{D_{12}} \tag{17.7}$$

$$Re = \frac{\rho\, U\, d_p}{\mu} \tag{17.8}$$

$$Sc = \frac{\mu}{\rho\, D_{12}} \tag{17.9}$$

Table 17.3 Summary of compositions of plant essential oils from high-pressure CO_2 extraction studies in Table 17.2. Besides the name of the main component, for each of the up to 4 fractions the compound type,* percent of fraction, and percent of the main component in the fraction are indicated within parenthesis

Plant material	Fraction 1	Fraction 2	Fraction 3	Fraction 4
Basil (Reverchon and Sesti Osséo 1994b)	Estragole (OMT/89/54)	α-*trans* Bergamotene (ST/9.0/46)	T Cadinol (ST/2.2/47)	–
Lavender I (Reverchon et al. 1995a)	Myrcene (MT/3.33/35.7)	Linalyl acetate (OMT/87.9/39.4)	*cis*-β-Farnesene (ST/6.14/36.3)	α-Bisabolol (ST/2.63/79.5)
Lavender II (Akgün et al. 2000)	Camphor (OMT/56.9)	Fenchone (OMT/43.1)	–	–
Marjoram (Jimenez-Carmona et al. 1999)	Sabinene (MT/17.7/42.3)	*cis*-Sabinene hydrate (OMT/78.9/78.6)	β-Caryophyllene (ST/3.46/100)	–
Oregano (Gaspar 2002)	γ-Terpinene (MT/6.78/79.7)	Thymol (OMT/85.8/42.4)	β-Caryophyllene (ST/7.47/100)	–
Pennyroyal (Aghel et al. 2004)	Limonene (MT/14.6/100)	Pulegone (OMT/85.4/60.9)	–	–
Peppermint (Roy et al. 1996)	Limonene (MT/2.86/45.0)	Menthol (OMT/92.8/74.5)	Germacrene (ST/4.35/57.2)	–
Rosemary (Coelho et al. 1997)	Limonene (MT/26.0/47.6)	Camphor (OMT/65.1/57.6)	α-Humulene (ST/7.23/44.1)	Caryophyllene oxide (OST/1.60/100)
Sage I (Reverchon et al. 1995b)	β-Pinene (MT/11.6/21.1)	1,8-Cineole (OMT/70.8/76.8)	β-Caryophyllene (ST/14.5/48.8)	Manool (OST/3.19/56.1)
Sage II (Langa et al. 2009) (313 K/9 MPa)	Myrcene (MT/9.08/35.9)	Camphor (OMT/80.4/62.5)	β-Caryophyllene (ST/6.19/29.2)	Viridoflorol (OST/4.35/39.8)
Sage 2 (Langa et al. 2009) (323 K/10 MPa)	Myrcene (MT/11.4/39.1)	Camphor (OMT/79.9/69.0)	β-Caryophyllene (ST/5.79/30.4)	Caryophyllene oxide (OST/2.88/15.5)
Spearmint (Özer et al. 1996)	Limonene (MT/6.42/81.9)	Carvone (OMT/90.6/89.5)	β-Bourbonene (ST/2.95/78.6)	–
Thyme (Zekovic et al. 2001)	Thymol (OMT/19.6/4.9)	β-Caryophyllene (ST/2.25/100)	Tetradecane (HC/78.2/67.1)	–
Wild thyme (Sefidkon et al. 2004) Before flowering	γ-Terpinene (MT/52.2/42.8)	Thymol (OMT/32.9/58.1)	β-Caryophyllene (ST/14.6/42)	Spathulenol (OST/0.31/33.3)

(*continued*)

Table 17.3 (continued)

Plant material	Fraction 1	Fraction 2	Fraction 3	Fraction 4
Wild thyme (Sefidkon et al. 2004) After flowering	γ-Terpinene (MT/60.20/42.7)	Thymol (OMT/32.09/66.1)	Germacrene-D (ST/6.80/85.0)	Caryophyllene oxide (OST/0.91/87.5)
Anise (Rodrígues et al. 2003) (303 K/8 MPa)	Anethole (OMT/92.0/97.7)	γ-Himachalene (ST/2.27/100)	Isoeugenyl 2-methyl-butyrate (OST/5.76/100)	
Anise (Rodrígues et al. 2003) (303 K/10 MPa)	Anethole (OMT/92.2/98.3)	γ-Himachalene (ST/2.72/100)	Isoeugenyl 2-methyl-butyrate (ST/2.72/100)	
Anise (Rodrígues et al. 2003) (303 K/14 MPa)	Anethole (OMT/91.6/98.2)	γ-Himachalene (ST/2.91/100)	Isoeugenyl 2-methyl-butyrate (OST/5.50/100)	
Caraway (Sovová et al. 1994a)	Limonene (MT/39.8)	Carvone (OMT/60.2)	–	–
Celery (Mišić et al. 2008)	Limonene (MT/28.9/91.7)	Sedanenolide (OMT/64.0/77.7)	β-Selinene (ST/4.89/73.5)	Carotol (OST/2.22/78.3)
Fennel (Simandi et al. 1999)	Limonene (MT/9.37/39.6)	Anethole (OMT/90.6/72.2)	–	–
Parsley (Louli et al. 2004) (10 MPa)	α-Pinene (MT/6.59/49.1)	Myristicin (PhPro/93.4/57.4)	–	–
Parsley (Louli et al. 2004) (15 MPa)	α-Pinene (MT/2.40/55.8)	Myristicin (MT/2.40/55.8)	–	–
Carqueja (Simões-Pires et al. 2005)	β-Pinene (MT/3.42/75.0)	Carquejyl acetate (OMT/42.7/90.7)	Ledol (OST/53.9/38.6)	–
Chamomile I (Povh et al. 2001)	β-Farnesene (ST/39.6/86.3)	α-Bisabolol (OST/60.4/47.0)	–	–
Chamomile II (Kotnik et al. 2007) (303 K/10 MPa)	Matricine (OST/100)	–	–	–
Chamomile II (Kotnik et al. 2007) (303 K/15 MPa)	Matricine (OST/96.5)	–	–	–
Chamomile II (Kotnik et al. 2007) (313 K/10 MPa)	Matricine (OST/97.3)	–	–	–
Chamomile II (Kotnik et al. 2007) (313 K/15 MPa)	Matricine (OST/96.4)	–	–	–
Marigold (Danielski et al. 2007) (313 K/12 MPa)	Tetradecanoic acid (LOHC/2.46/100)	Octacosane (HC/94.6/94.6)	Cholest-4-en-3-one-14-methyl (HOHC/2.94/40.7)	–

Marigold (Danielski et al. 2007) (313 K/15 MPa)	Octacosane (HC/98.7/43.1)	Taraxasterol (H-OHC/1.35/34.2)	–	–
Alecrim pimenta (Sousa et al. 2002)	*p*-Cymene (MT/3.22/45.0)	Thymol (OMT/74.8/67.9)	β-Caryophyllene (ST/20.0/72.2)	Caryophyllene oxide (OST/1.97/100)
Black pepper I (Ferreira et al. 1999)	Limonene (MT/66.2/30.1)	β-Caryophyllene (ST/33.8/21.8)	–	–
Black pepper II (Ferreira et al. 1999)	Limonene (MT/1.00/57.8)	β-Caryophyllene (ST/99.0/70.9)	–	–
Black pepper III (Perakis et al. 2005)	Limonene (MT/31.2/29.8)	Linalool (OMT/1.57/51.3)	β-Caryophyllene (ST/34.2/35.5)	Caryophyllene oxide (OST/33.0/51.5)
Boldo (Miraldi et al. 1996)	p-Cymene (MT/9.28/94.7)	Ascaridole (OMT/81.75/26.5)	Guaizulene (ST/8.96/100)	–
Cinnamon of Cunha (Sousa et al. 2005)	Anethole (OMT/96.5/95.8)	Germacrene (ST/3.51/35.7)	–	–
Clove (Della Porta et al. 1998)	Eugenol (OMT/86.3/77.5)	β-Caryophyllene (ST/13.7/82.2)	–	–
Eucalyptus (Della Porta et al. 1999)	α-Pinene (MT/12.2/86.1)	1,8-Cineole (OMT/67.1/93.3)	Aromadendrene (ST/12.3/65.3)	Guaiol (OST/8.40/50.0)
Ginger (Martínez et al. 2003)	Zingiberene (OMT/9.77/56.7)	α-Zingiberene (ST/45.6/35.6)	Farnesol (OST/3.73/30.3)	6-Gingerol (Ging/40.9/28.9)
Hop (Pfaf-Šovljanski et al. 2005)	α-Humulene (ST/13.5/82.4)	Isohumulone (α-acid/13.0/100)	Lupulone (β-acid/73.5/53)	–
Ho-sho (Bakkali et al. 2005)	Sabinene (MT/21.7/35.5)	1,8-Cineole (OMT/75.0/80.0)	Viridiflorol (OST/3.29/100)	–
Nutmeg I (Spricigo et al. 1999)	Sabinene (MT/78.8/51.9)	Myristicin (OMT/21.2/36.8)	–	–
Nutmeg II (Machmudah et al. 2006)	3-Cyclohexene-1-ol (LOHC/15.7/26.4)	β-Phellandrene (MT/46.3/42.9)	Myristicin (OMT/36.2/89.9)	Copaene (ST/1.83/68.9)
Orange (Budich and Brunner 1999)	Limonene (MT/98.3/97.6)	Linalool (OMT/1.75/28.8)	–	–
Valerian I (Zizovic et al. 2007a) (313 K/10 MPa)	Borneol (OMT/15.9/36.8)	Valerena-4,7(11)-diene (ST/14.1/25.7)	Valerenal (OST/67.4/19.3)	(E)-Valerenyl isovalerate (H-OHC/2.68/70.0)

(*continued*)

Table 17.3 (continued)

Plant material	Fraction 1	Fraction 2	Fraction 3	Fraction 4
Valerian II (Zizovic et al. 2007a) (313 K/10 MPa)	Isovaleric acid (LOHC/6.01/100)	Bornyl acetate (OMT/13.9/59.3)	Valerena-4,7(11)-diene (ST/13.8/17.2)	Valerianol (OST/66.2/19.7)
Valerian II (Zizovic et al. 2007a) (313 K/15 MPa)	Isovaleric acid (LOHC/7.67/100)	Bornyl acetate (OMT/10.7/61.6)	β-Bisabolene (ST/13.2/17.7)	Valerianol (OST/68.4/16.6)
Valerian II (Zizovic et al. 2007a) (323 K/10 MPa)	Isovaleric acid (LOHC/4.37/100)	Bornyl acetate (OMT/12.1/58.9)	Valerena-4,7(11)-diene (ST/13.3/17.1)	Valerianol (OST/70.2/19.2)
Valerian II (Zizovic et al. 2007a) (323 K/15 MPa)	Isovaleric acid (LOHC/3.57/100)	Bornyl acetate (OMT/10.7/59.3)	Valerena-4,7(11)-diene (ST/13.3/17.1)	Valerianol (OST/72.7/20.0)
Valerian III (Zizovic et al. 2007a)	Isovaleric acid (LOHC/9.64/100)	Bornyl acetate (OMT/16.7/52.9)	δ-Elemene (ST/28.6/26.9)	Valerenal (OST/45.0/34.9)

*MT indicates a monoterpene hydrocarbon; OMT, an oxygenated monoterpene; ST, a sesquiterpene hydrocarbon; OST, an oxygenated sesquiterpene; HC, an hydrocarbon; LOHC, a light oxygenated hydrocarbon; HOHC, a heavy oxygenated hydrocarbon; PhPro, a phenyl propanoid; and Ging, a gingerol

Table 17.4 Summary of estimated molecular weights (MW) and critical volumes (V_c) of plant essential oils in Table 17.3

Plant material	Scientific name	Family	Identified compounds (%)	Molecular weight (*MW*, Da)	Critical volume (V_c, cm^3/mol)
Basil	*Ocimum basilicum*	Lamiaceae	99.4	153.0	508.0
Lavender I	*Lavandula angustifolia*	Lamiaceae	100.1	194.5	682.6
Lavender II	*Lavandula angustifolia*	Lamiaceae	76.9	152.2	503.5
Marjoram	*Origanum majorama*	Lamiaceae	36.8	152.0	517.7
Oregano	*Origanum vulgare*	Lamiaceae	87.0	152.2	440.3
Pennyroyal	*Mentha pulegium*	Lamiaceae	100.0	149.7	504.1
Peppermint	*Mentha* × *piperita*	Lamiaceae	99.3	157.2	527.2
Rosemary	*Rosmarinus officinalis*	Lamiaceae	100.0	151.7	523.6
Sage I	*Salvia officinalis*	Lamiaceae	100.0	160.0	546.0
Sage II (313 K/9 MPa)	*Salvia officinalis*	Lamiaceae	81.4	155.2	519.8
Sage II (323 K/10 MPa)	*Salvia officinalis*	Lamiaceae	87.1	153.8	153.8
Spearmint	*Mentha spicata*	Lamiaceae	100.0	150.4	508.5
Thyme	*Thymus vulgaris*	Lamiaceae	11.9	186.8	719.0
Wild thyme, before flowering	*Thymus serpyllum*	Lamiaceae	98.0	148.1	506.6
Wild thyme, after flowering	*Thymus serpyllum*	Lamiaceae	88.2	144.3	500.4
Anise (303 K/8 MPa)	*Pimpinella anisum*	Apiaceae	99.2	152.7	500.0
Anise (303 K/10 MPa)	*Pimpinella anisum*	Apiaceae	97.7	152.5	499.6
Anise (303 K/14 MPa)	*Pimpinella anisum*	Apiaceae	97.0	152.8	500.7
Caraway	*Carum carvi*	Apiaceae	98.0	144.3	505.2
Celery	*Apium graveolens*	Apiaceae	99.8	172.7	585.9
Fennel	*Foeniculum vulgare*	Apiaceae	100.0	147.0	487.7
Parsley (10 MPa)	*Petroselinum crispum*	Apiaceae	83.4	187.1	533.1
Parsley (15 MPa)	*Petroselinum crispum*	Apiaceae	96.2	193.0	552.1
Carqueja	*Baccharis trimera*	Asteraceae	83.7	204.3	678.6
Chamomile I	*Matricaria recutita*	Asteraceae	44.4	214.9	790.6
Chamomile II (303 K/10 MPa)	*Matricaria recutita*	Asteraceae	7.56	306.4	886.5
Chamomile II (303 K/15 MPa)	*Matricaria recutita*	Asteraceae	8.42	306.4	886.5
Chamomile II (313 K/10 MPa)	*Matricaria recutita*	Asteraceae	9.74	306.4	886.5
Chamomile II (313 K/15 MPa)	*Matricaria recutita*	Asteraceae	9.65	306.4	886.5

(*continued*)

Table 17.4 (continued)

Plant material	Scientific name	Family	Identified compounds (%)	Molecular weight (*MW*, Da)	Critical volume (V_c, cm^3/mol)
Marigold (313 K/12 MPa)	*Calendula officinalis*	Asteraceae	30.9	387.9	1,565.1
Marigold (313 K/15 MPa)	*Calendula officinalis*	Asteraceae	28.2	395.2	1,601.4
Alecrim pimenta	*Lippia sidoides*	Verbenaceae	95.2	159.0	470.4
Black pepper I	*Piper nigrum*	Piperaceae	99.6	153.5	562.1
Black pepper II	*Piper nigrum*	Piperaceae	99.2	203.3	719.3
Black pepper III	*Piper nigrum*	Piperaceae	73.3	179.7	633.9
Boldo	*Peumus boldus*	Monimiaceae	98.2	166.6	525.1
Cinnamon of Cunha	*Croton zehntneri*	Euphorbiaceae	95.7	149.6	149.6
Clove	*Syzygium aromaticum*	Myrtaceae	98.5	168.8	454.7
Eucalyptus	*Eucalyptus globules*	Myrtaceae	100.0	155.0	528.6
Ginger	*Zingiber officinale*	Zingiberaceae	71.7	241.1	799.0
Hop	*Humulus lupulus*	Cannabaceae	93.3	364.5	1,224.8
Ho-sho	*Cinnamomum camphora*	Lauraceae	83.7	151.4	516.2
Nutmeg I	*Myristica fragrans*	Myristicaceae	89.6	145.2	498.9
Nutmeg II	*Myristica fragrans*	Myristicaceae	99.6	143.5	143.5
Orange	*Citrus sinensis*	Rutaceae	100	136.5	508.49
Valerian I (313 K/10 MPa)	*Valeriana officinalis*	Valerianaceae	83.5	204.6	712.1
Valerian II (313 K/10 MPa)	*Valeriana officinalis*	Valerianaceae	89.1	201.9	688.4
Valerian II (313 K/15 MPa)	*Valeriana officinalis*	Valerianaceae	86.2	199.2	683.0
Valerian II (323 K/10 MPa)	*Valeriana officinalis*	Valerianaceae	88.7	206.0	703.5
Valerian II (323 K/15 MPa)	*Valeriana officinalis*	Valerianaceae	86.4	208.3	711.8
Valerian III	*Valeriana officinalis*	Valerianaceae	82.7	190.2	662.7

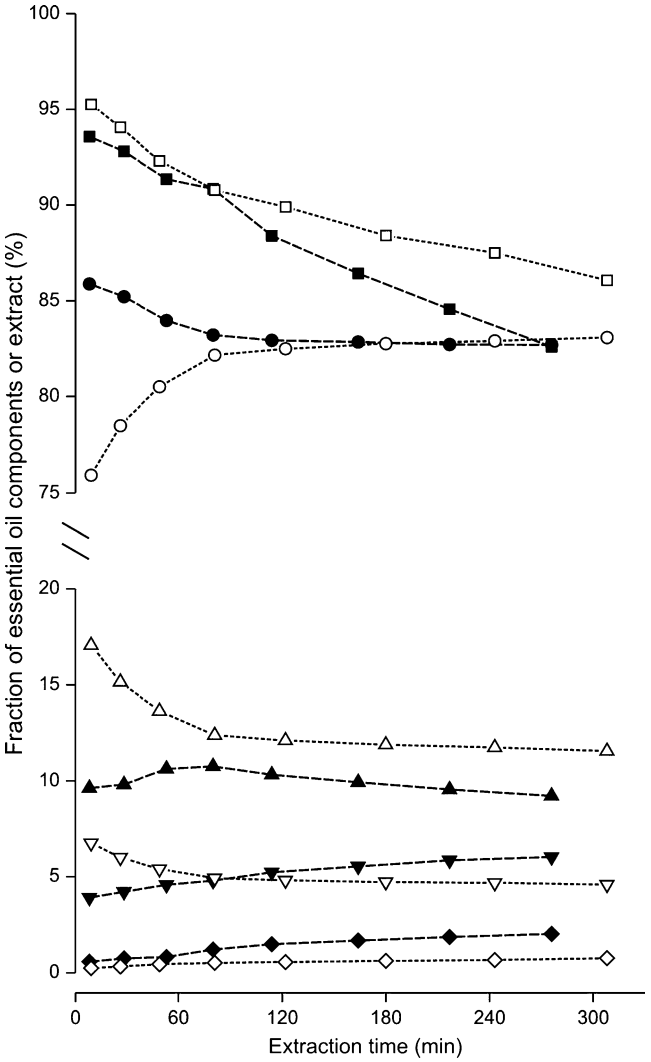

Fig. 17.3 Effect of process time and conditions on the composition of sage essential oils extracted with high-pressure CO_2: (-▲-) monoterpenes, (-●-) oxygenated monoterpenes, (-▼-) sesquiterpenes, (-◆-) oxygenated sesquiterpenes, and (-■-) total essential oil components extracted at 313 K and 9 MPa; and (···△···) monoterpenes, (···○···) oxygenated monoterpenes, (···▽···) sesquiterpenes, (···◇···) oxygenated sesquiterpenes, and (···□···) total essential oil components extracted at 323 K and 10 MPa (Adapted from Langa et al. 2009)

In a related work, del Valle and Catchpole (2005) correlated literature data for the axial dispersion of high-pressure CO_2 in packed beds (Tan and Liou 1989; Catchpole et al. 1996a; Funazukuri et al. 1998; Yu 1998; Ghoreishi and Akgerman 2004). Typical measurements in these studies were conducted by injecting a pulse

of solute (gaseous methane, volatile acetone or hexachlorobenzene, or low-volatility benzoic acid, oleic acid, or squalene) into the high-pressure CO_2 stream before a bed ($0.4 \leq D \leq 50.8$ mm) packed with different materials (sand particles, glass beads, or steel beads ranging in size from $d_p = 0.05$ to $d_p = 3.18$ mm), and evaluating the dispersion (concentration profile) of the solute in the stream leaving the bed. Different flow directions (horizontal, upward, downward) and regimes (from molecular-transport-controlled, $Pe_d \sim 9.1 \times 10^{-3}$, to convection-controlled flow conditions, $Pe_d \sim 1.2 \times 10^3$) were assayed in these studies.

Figure 17.4 summarizes the results of the correlation study of del Valle and Catchpole (2005). When dispersion is controlled by molecular transport ($Pe_d \leq 1$) the ratio D_{ax}/D_{12} has a nearly constant value (slightly below 1 in this particular case), as expected (Dullien 1992). On the other hand, under convention-controlled conditions ($Pe_d > 1$), the ratio D_{ax}/D_{12} increases exponentially with Pe_d, which results in a nearly straight line having a slope between 1 and 2 when presenting the data in a log–log plot, as also expected (Dullien 1992). Data scattering for large values of Pe_d is partially explained by the scale of the measurements; data obtained using large vessels exhibited a larger axial dispersion coefficient than data obtained using small tubes (del Valle and Catchpole 2005). Dispersion typically increases as the length of the bed (L) increases due to the increase in the residence time in the packed bed (Han et al. 1985). Dispersion also increases as the diameter of the bed (D_E) decreases because of the pronounced decrease in local porosity in the radial direction from the wall of the tube or vessel when the ratio D_E/d_p decreases, which increases concentration-gradient-driven radial diffusion and consequently increases

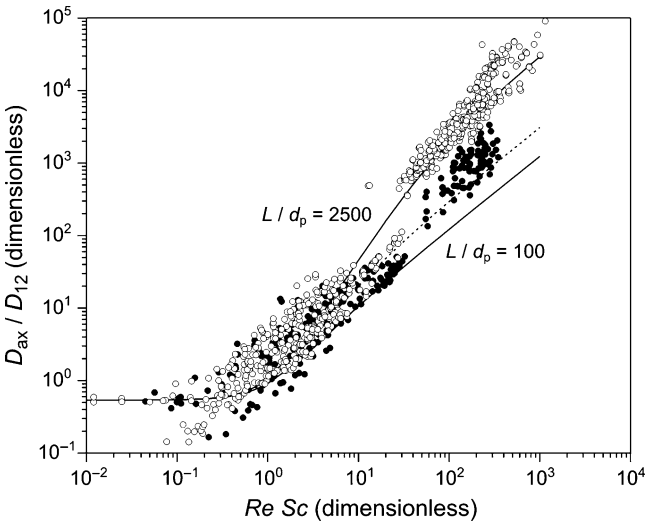

Fig. 17.4 Dimensionless plot of the axial dispersion coefficient (D_{ax}) in a packed bed operating under a high-pressure CO_2 and flow regime. The independent variable is the ratio D_{ax}/D_{12} [where D_{12} is a binary diffusion coefficient of the solute (component 2) in CO_2 (component 1)] and the dependent variable is the Peclet number for the particle (17.5)

axial dispersion of the solute (Fahien and Smith 1955). It is apparent for the results in Fig. 17.4 that the effect of an increase in L/d_p predominates over the effect of an increase in D/d_p, so that the axial dispersion is larger in large vessels than small tubes (for purposes here, $L/d_p \leq 250$ in small packed beds). Thus, del Valle and Catchpole (2005) selected Pe_d and the ratio L/d_p as the independent variables in their correlation for D_{ax}/D_{12} (17.10).

$$\frac{D_{ax}}{D_{12}} = 0.540 + \frac{0.530\left(Pe_p\right)^2}{1 + 42.8\left(\frac{Pe_p}{L/d_p}\right)}. \tag{17.10}$$

Figure 17.4 reports experimental measurements of axial dispersion using closed circles for small packed beds (experimentally $89 \leq L/d_p \leq 234$) and open circles for large beds ($295 \leq L/d_p \leq 2{,}320$), and includes the limit between the two regions predicted by (17.10) for $L/d_p = 250$ in the form of a segmented line.

In this work, the authors believe that a precise estimation of the value of the axial dispersion coefficient is less important than determining whether axial dispersion phenomena affects SCFE of plant essential oils to such an extent that the term with D_{ax} must be included in the differential mass balance equation (last term on the left of (17.1)). This determination is important because axial dispersion phenomena is typically neglected to simplify the fitting of model parameters. del Valle and de la Fuente (2006) analyzed the effect of dispersion in mass transfer for SCFE of oilseeds under typical industrial conditions based on the claim of Goto et al. (1996) that it can be disregarded in mass transfer models when the value of the Peclet number for the packed bed (Pe_L, 17.11) is above *ca.* 100.

$$Pe_L = \frac{U\,L}{D_{ax}\varepsilon} \tag{17.11}$$

Recommended conditions for SCFE of plant essential oils are 323 K and 9 MPa (Reverchon 1997), for which the following values of physical properties were estimated in this work: $\rho = 285$ kg/m^3; $\mu = 2.47 \times 10^{-5}$ Pa s; $D_{12} \cong 3.00 \times 10^{-8}$ m^2/s; and, $Sc = 2.86$. Conditions favoring axial dispersion in the extraction vessel include a large superficial solvent velocity (e.g., $U = 5$ mm/s) (Eggers 1996), a large particle size, a small bed voidage, and a tall vessel (see 17.10 and 17.11). Eggers (1996) mentioned that the aspect ratio (L/D) of a typical extraction vessel is between 4 and 6, while Reverchon (1997) specified that an industrial SCFE facility for plant essential oils (Essences, Salerno, Italy) used vessels of 0.3 m^3, so in this work a packed bed $L = 2.40$ m tall and $D = 40$ cm wide was selected for calculations ($L/D = 6$, $V = 0.3$ m^3). According to the analysis, dispersive effects can be neglected ($Pe_L \geq 100$) for small particles of $d_p \leq 0.71$ mm, but for larger particles, it is necessary to reduce the bed voidage from $\varepsilon \leq 0.59$ for $d_p = 1.0$ mm to $\varepsilon \leq 0.34$ for $d_p = 1.5$ mm.

As shown in Table 17.1, most authors neglect the contribution of axial dispersion in their SCFE models for plant essential oils from solid substrates in packed beds. There are exceptions (studies where the axial dispersion coefficient is estimated using a literature correlation) including Ruetsch et al. (2003) and Daghero et al. (2004), who used the correlation of Wakao and Kaguei (1982); Goodarznia and Eikani (1998), Spricigo et al. (2001), Gaspar et al. (2003), Steffani et al. (2006), Zizovic at al. (2005, 2007a,b,c), Salimi et al. (2008), and Stamenić et al. (2008), who used the correlation of Tan and Liou (1989); and Machmudah et al. (2006), who used the correlation of Funazukuri et al. (1998). On the other hand, Reis-Vasco et al. (2000) used D_{ax} as a fitting parameter for their experimental data, but their best-fit values decreased when the superficial solvent velocity of the CO_2 increased (which was not as expected), and were 31–138 times larger than predicted using (17.10).

17.3.2 External Mass Transfer Coefficient

There are two values of k_f (expressed in, e.g., m/s) and $k_f a_p$ (expressed in, e.g., s^{-1}) reported in the literature as external mass transfer coefficients. Thus, in this work all values were recalculated first in similar units. To do this, the specific surface (a_p), or total particle surface (S_p) per unit volume of the packed bed [$(1 - \varepsilon)\ V_p$], was estimated using (17.12):

$$a_p = \frac{\psi}{(1-\varepsilon)\ d_p}. \tag{17.12}$$

In (17.12), ψ is a factor that depends on the geometry of the particles: ψ tends to 2 for very thin slabs (approaching a so-called infinite slab geometry), for which d_p is the thickness of the slab; and $\psi = 6$ for spheres. The void fraction in the packed bed (ε) in (17.12) ranged from 0.24 for milled black pepper (Ferreira et al. 1999) to 0.901 for rapidly decompressed oregano (Uquiche et al., submitted). We assumed a typical value $\varepsilon = 0.6$ in absence of a reported value (Mira et al. 1996; Papamichail et al. 2000; Louli et al. 2004; Zizovic et al. 2007a).

Figure 17.5 summarizes corrected values of k_f from the literature in a dimensionless plot of $Sh/Sc^{1/3}$ versus Re, where Sh is the dimensionless Sherwood number defined in (17.13):

$$Sh = \frac{k_f d_p}{D_{12}} \tag{17.13}$$

Figure 17.5 also includes reference lines corresponding to correlations in the literature for the external mass transfer coefficient in packed beds operating with liquids, gases, and SCFs. The correlations include the equation of Wakao and Kaguei (1982) for mass transfer in packed beds with low-pressure liquids and

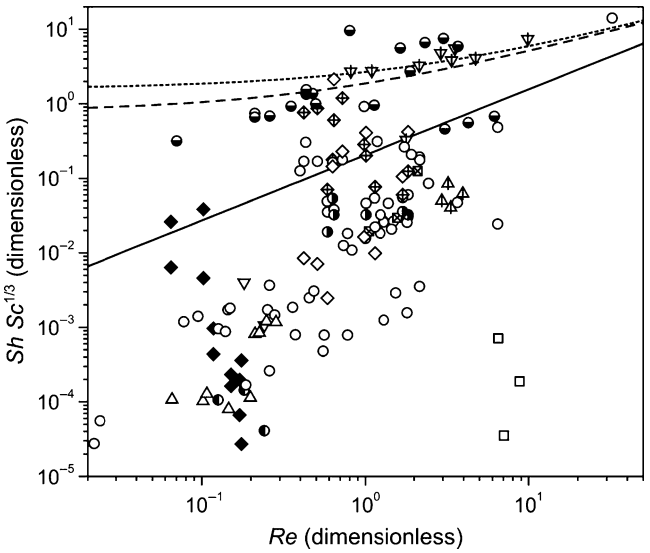

Fig. 17.5 Dimensionless plot of $Sh\ Sc^{-1/3}$ versus Re [where Sh, Sc, and Re are the dimensionless Sherwood (17.11), Schmidt (17.7), and Reynolds (17.6) numbers] for literature values of the external mass transfer coefficient (k_f) in SCFE of plant essential oils as a function of the flow regime in the packed bed. Plotted values were estimated from best-fitting parameters reported by the identified authors using the following models (model names reported in Table 17.1): (△) EMTC model applied by Ferreira et al. (1999) and Kotnik et al. (2007); (◇) R-SO model applied by Papamichail et al. (2000) and Louli et al. (2004); (⊕) LDF/UENA model applied by Papamichail et al. (2000) and Louli et al. (2004); (⧫) LDF/PF/CDIC model applied by Coelho et al. (1997); (□) LDF-Sph/PF model applied by Esquivel et al. (1996); (⊠) LDF/ADPF model applied by Reverchon and Marrone (1997); (○) Sovova's model applied by Mira et al. (1996, 1999), Papamichail et al. (2000), Povh et al. (2001), Ferreira and Meireles (2002), Sousa et al. (2002, 2005), Martínez et al. (2003, 2007), Rodrigues et al. (2003), Louli et al. (2004), Campos et al. (2005), Perakis et al. (2005), Vargas et al. (2006), and Bensebia et al. (2009); (◑) IBC/PF model applied by Louli et al. (2004); (◐) IBC/PFNA model applied by Sovová et al. (1994b); (◒) IBC/PF/PCPR model applied by Sovová (2005), Machmudah et al. (2006), and Langa et al. (2009); (◆) DDD/PM model applied by Kim and Hong (2002); (▽) SC/PF model applied by Germain et al. (2005); and (⧩) SC/ADPF model applied by Steffani et al. (2006)

gases (17.14), which is valid for $3 < Re < 3{,}000$ and $0.5 < \mathrm{Sc} < 10^4$, and the equation of Puiggené et al. (1997) for evaporation of 1,2-dichlorobenzene from glass beads into a high-pressure CO_2 stream (17.15), which is valid for $10 < Re < 100$ and $Sc < 10$.

$$Sh = 2 + 1.1\ Re^{0.6}\ Sc^{0.33} \tag{17.14}$$

$$Sh = 0.206\ Re^{0.8}\ Sc^{0.33} \tag{17.15}$$

The experimental values of Sc for the kinetic studies in Table 17.2 ranged from 2.05 to 17.0, and this result conditioned the selection of values for the two lines

corresponding to the correlation of Wakao and Kaguei (1982) in Fig. 17.5. The values of mass transfer coefficients predicted by Wakao and Kaguei (1982) for liquids and gases (17.14) are above those predicted by the literature correlations for mass transfer in packed beds operating with SCFs under forced convection (del Valle and de la Fuente 2006). Among the specific correlations for mass transfer in packed beds operating with SCFs, the predictions made in the equation of King and Catchpole (1993) are above those made in the equation of Tan et al. (1988), which are in turn above those made in (17.15) (del Valle and de la Fuente 2006). Thus, the expected estimated values of $Sh/Sc^{1/3}$ derived from the studies in Table 17.2 should be seen between the top and bottom lines in Fig. 17.5.

Figure 17.5 shows that experimental values of $Sh/Sc^{1/3}$ for the SCFE of plant essential oils exhibit considerable scattering (a span covering 3 orders of magnitude was observed, e.g., with data of Kim and Hong 2002), and are generally smaller (up to several orders of magnitude) than those predicted by the literature correlations. Most best-fit values were below the predictions of (17.15) with the exception of values of Papamichail et al. (2000) and Martínez et al. (2007), and a single value of Mira et al. (1999) using Sovová's model (Table 17.1), some values of Papamichail et al. (2000) and Louli et al. (2004) using model LDF/UENA, values of Machmudah et al. (2006) and Langa et al. (2009) using model IBC/PF/PCPR, and values of Steffani et al. (2006) using model SC/ADPF (who used (17.14) to get first guess values for k_f). Smaller best-fit values than predictions of literature correlations are probably due to a combination of several factors, including underestimation of the contribution of internal (solid phase) mechanisms to the total resistance to mass transfer, overestimation of the mass transfer area, underestimation of solvent flow heterogeneity effects, and underestimation of natural convection effects.

Some kinetic models assume that the extraction rate is controlled by external resistances to mass transfer (Ferreira et al. 1999; Kotnik et al. 2007). If this is not the case, the best-fit value of k_f would be smaller than in model systems without internal resistance to mass transfer, as those used to obtain the two correlations reported in Fig. 17.5, to compensate the contribution to the total resistance of the solid matrix (del Valle and de la Fuente 2006). This will also occur if the internal resistance to mass transfer is not neglected, but underestimated.

An overestimation of a_p would also be compensated by an underestimation of the value of k_f in cases where an overall mass transfer coefficient ($k_f a_p$) is used as a fitting parameter for experimental data (del Valle and de la Fuente 2006). In the work presented in this chapter the assumption is that the solid particles were spherical ((17.12) for $\psi = 6$), and although spheres have the smallest surface-area-to-volume ratio among regular geometric shapes, not all of the external surface of the particles is fully available for extraction due to tight packing in low-porosity beds (Marrone et al. 1998) or agglomeration of solid particles (Štastová et al. 1996; Eggers et al. 2000; del Valle et al. 2008).

Other causes of a reduction in the extraction rate and an associated reduction in the best-fitting value of k_f are irregularities in the packing of solid particles and other nonidealities that change the interstitial velocity of the high-pressure CO_2 across the extraction vessel (del Valle et al. 2004). Indeed, it is possible to have high-velocity

zones near the wall of an extraction vessel coexisting with low-velocity zones close to the axis of the vessel, with the end result of smaller extraction rates and smaller values of k_f in the axis than near the wall of the vessel (Sovová et al. 1994b; del Valle et al. 2004). These changes in velocity can be explained by the radial variations in bed porosity that result when packing comparatively large particles in small-diameter vessels (i.e., when $d_p/D < 10$ for mono-disperse particles) or radial variations in solvent viscosity when heating the packed-bed contents by conduction through the wall of the extraction vessel. Consequently with this hypothesis Brunner (1994) reported that the residual content of theobromine in ground cocoa seed shells increases when moving from the vessel wall toward the center of the extraction vessel in large-scale extraction experiments, and that these changes in residual solute content are more pronounced when the superficial velocity of high-pressure CO_2 decreases from 3.5 to <1.7 mm/s. The global effect of these changes is a reduction in the average value of the external mass coefficient (del Valle et al. 2004).

The last explanation for the differences between experimental and correlated values of k_f is neglecting the undesirable effects of natural convection on the external mass transfer. The natural convection phenomenon is important in experiments where high-pressure CO_2 moves slowly upwards in a vertical extraction vessel and against the gradient in density ($\Delta\rho = \rho_{sat} - \rho$) that develops when essential oils dissolve into the CO_2 stream, a condition under which the loaded CO_2 phase moves down under the influence of the force of gravity (Stüber et al. 1996; Puiggené et al. 1997; Germain et al. 2005). Thus, the extraction rate in a SCFE system using CO_2 upflow conditions is smaller than in a system using downflow conditions due to the negative influence of natural convection on mass transfer opposed by gravity (Sovová et al. 1994a, b; Stüber et al. 1996; Germain et al. 2005). This is important to consider in SCFE of plant essential oils because of several factors favoring undesirable convection phenomena (Germain et al. 2005): (1) the preference of solvent upflow conditions in industrial practice to improve extraction by fluidization of small particles and avoidance of compaction of the packed bed; (2) the use of near-critical conditions for extraction (Table 17.2); (3) the large solubility of essential oil components in high-pressure CO_2 under typical extraction conditions (Sect. 17.4); and (4) the use of a small superficial solvent velocity in experimental studies, as reported in the literature. Both correlations presented in Fig. 17.5 apply under forced convection conditions, but not when natural convection effects start to dominate as the ratio Gr/Re^2 increases ($>> 1$), where Gr is the dimensionless Grashof number defined in (17.16):

$$Gr = \frac{g\, d_p^3\, \rho^2\, \Delta\rho}{c_{sat}\, \mu^2}. \tag{17.16}$$

Germain et al. (2005) showed that for the extraction of caraway essential oils with high-pressure CO_2 at 313 K and 9–10 MPa ($Sc = 2.13$), another correlation of Puiggené et al. (1997) that takes into account the effect of natural convection

phenomena predicts smaller values of the external mass transfer coefficient when mass transfer is opposed by gravity (CO_2 upflow conditions) than when it is aided by gravity (CO_2 downflow conditions), whereas there are virtually no differences in $Sh/Sc^{1/3}$ for a relatively large Re (e.g., $Re \geq 50$). For a value of Re slightly below ($Re \approx 10$) the value of $Sh/Sc^{1/3}$ drops pronouncedly; this drop is only slightly dependent on the value of Gr (for $10 < Gr < 38{,}000$), but shifts to smaller values of Re as the value of Sc decreases (e.g., $Re \approx 2.5$ for $Sc = 34.4$). This helps to explain some of the experimental results reported in Fig. 17.5.

In selected cases, the value of k_f was not fitted to a cumulative extraction plot, but instead adopted from a literature correlation for forced convection. Goto et al. (1993, 1998), Spricigo et al. (2001), and Steffani et al. (2006) used the equation of Wakao and Kaguei (1982). Several authors used the equation of Tan et al. (1988), including Reverchon et al. (1993a), Reverchon (1996), Goodarznia and Eikani (1998), Perakis et al. (2005), Zizovic et al. (2005, 2007a,b,c), Salimi et al. (2008), and Stamenić et al. (2008). Catchpole et al. (1996b), Gaspar et al. (2003), Ruetsch et al. (2003), Daghero et al. (2004), and Machmudah et al. (2006) used the equation of King and Catchpole (1993). Araus et al. (2009) and Uquiche et al. (submitted) used the equation of Puiggené et al. (1997). It is relevant to mention that in most of these studies, the selected equations were applied for values of Re below the limit where the natural convection effects must be taken into account. Two exceptions where natural convection phenomenon was accounted for are the works of Akgun et al. (2000), who used the equation of Lee and Holder (1995), and Germain et al. (2005), who use an equation of Puiggené et al. (1997).

17.3.3 Effective Diffusivity in the Solid Matrix

To compare the best-fit internal mass transfer parameters in the reviewed studies in this work, the value of a microstructural factor F_M (17.17) that embodies all effects of the substrate and its pretreatment on inner mass transfer was estimated (Aguilera and Stanley 1999; del Valle and de la Fuente 2006; Araus et al. 2009; Uquiche et al. submitted):

$$F_M = \frac{D_{12}}{D_e}. \tag{17.17}$$

The term F_M gives the retarding effect of the solid matrix on the mass transfer rate by indicating how many times smaller the effective diffusivity of the essential oil is in the treated plant material than its binary diffusion coefficient in high-pressure CO_2. It is convenient to use F_M instead of D_e in modeling SCFE processes because it is independent of extraction temperature and pressure, interstitial solvent velocity, and substrate particle size (Araus et al. 2009).

There are some problems in expressing the internal mass transfer parameters as reported in the literature in consistent units. For example, some contributions

describe the best-fit value of an internal mass transfer coefficient k_i (expressed in, e.g., m/s) (Reverchon et al. 1999; Reis-Vasco et al. 2000) or the product $k_i a_p$ (expressed in, e.g., s^{-1}) (Sovová et al. 1994a; Esquivel et al. 1996; Mira et al. 1996, 1999; Coelho et al. 1997; Ferreira et al. 1999; Papamichail et al. 2000; Povh et al. 2001; Ferreira and Meireles 2002; Sousa et al. 2002, 2005; Martínez et al. 2003, 2007; Rodrigues et al. 2003; Louli et al. 2004; Campos et al. 2005; Perakis et al. 2005; Sovová 2005; Machmudah et al. 2006; Vargas et al. 2006; Bensebia et al. 2009; Langa et al. 2009), and in these cases the effective diffusivity was computed using the relationship between D_e and the reciprocal of $k_i a_p$ (or the so-called internal diffusion time t_i, s) proposed by Villermaux (1987) and reported in (17.18):

$$D_e = \frac{k_i d_p}{(1-\varepsilon)\,\xi} \tag{17.18}$$

where the particle-geometry parameter ξ was defined in connection with (17.5) in Sect. 2.3 (ξ = 10 for a sphere, ξ = 6 for a for thin slab).
When values of the effective diffusivity were reported, those cases were distinguished where they referred to the movement of the pseudo-solute in the solid (e.g., diffusion model), from those referring to movement in the fluid phase trapped in the solid (e.g., DDD models, SC models). Under the latter conditions, the values of D_e can be estimated according to (17.19) (del Valle and de la Fuente 2006):

$$D_e = D'_e K \tag{17.19}$$

where D'_e(the effective diffusivity of the pseudo-solute in the fluid trapped within the pores of the solid matrix) is the reported value, and K, the partition of the pseudo-solute between the SCF and the herb or spice which, in absence of a reported value (Sovová et al. 1994a; Mira et al. 1996, 1999; Coelho et al. 1997; Ferreira et al. 1999; Papamichail et al. 2000; Povh et al. 2001; Ferreira and Meireles 2002; Martínez et al. 2003, 2007; Rodrigues et al. 2003; Louli et al. 2004; Campos et al. 2005; Perakis et al. 2005; Vargas et al. 2006; Bensebia et al. 2009), is estimated using (17.20):

$$K = \frac{C_{fo}}{C_{so}} \tag{17.20}$$

Table 17.4 is an example of computed values of F_M in the case of SCFE of essential oils from oregano bracts, reporting the effect on F_M of different independent variables such as extraction temperature, extraction pressure, superficial velocity of the CO_2, sample pretreatment, and sample particle size. It is important to note that in those experiments where Esquivel et al. (1996), Gaspar (2002) (data modeled by Araus et al. 2009), and Gaspar et al. (2003) studied the effect of extraction temperature and/or extraction pressure, they also changed the superficial

velocity of the CO_2, because they kept the mass flow rate constant instead. Indeed, the superficial velocity of the CO_2 (U) depends not only on its mass flow rate (Q), but also on its density (ρ) under process conditions, which is a strong function of the extraction temperature and pressure, especially under near-critical conditions, according to (17.21):

$$U = \frac{4\,Q}{\pi\,D_E^2\,\rho} \tag{17.21}$$

As proposed by Araus et al. (2009), it was expected that the values of F_M are dependent on sample pretreatment, but independent of process temperature, process pressure, CO_2 superficial velocity, and substrate particle size, but clearly this is not the case (Table 17.4). Some of the differences can be imputed to typical variations in biological materials associated with differences in genetic makeup, growing environment, and harvest time (Zetzl et al. 2003). Although some differences were expected between the samples assayed by Esquivel et al. (1996), Gaspar (2002), Gaspar et al. (2003), and Uquiche et al. (submitted), which explains why the differences were smaller between experiments in a single study than among the four studies, the percent differences in estimated values of F_M between experiments in single studies were clearly still large. The very large difference in values of F_M between the sample with $d_p = 1.55$ mm (untreated sample) and all other samples in the study of Gaspar et al. (2003) can be explained by the positive effect of sample milling in reducing internal resistance to mass transfer. Uquiche et al. (submitted) also imputed the differences in values of F_M between their samples to microstructural differences caused by conventional milling, low-temperature milling, and rapid decompression of oregano and provided microscopy evidence of these differences. In work presented in this chapter the composition of the essential oil sample of oregano reported by Gaspar (2002) was used as representative of the extracts obtained in all experiments (Table 17.5); however, this assumption may be erroneous because of the aforementioned variability exhibited by biologic materials, as well as the variability in extract composition with process temperature and process pressure (i.e., extracts obtained using higher density CO_2 are expected to contain heavier and more polar compounds than the sample analyzed by Gaspar). As it will be analyzed later in this section, the errors introduced when not accounting for the actual composition are not as large as those observed in Table 17.5 and, in addition, differences were not expected in extract composition as used in experiments done by Gaspar et al. (2003) to assess the effect on extraction kinetics of the superficial solvent velocity, or the size of milled particles (Table 17.5). In this work, the authors believe mathematical models adopted and their ability to fit the physical picture of the actual extraction process explain the differences among estimated values of F_M reported in Table 17.5 to a large extent. For example, in the work of Gaspar et al. (2003) average values of F_M were 7.32×10^5 (range of value between 2.65×10^5 and 5.72×10^6) using model IBC-Diff (Table 17.5), 4.28×10^5 (range: 1.46×10^5 to 3.81×10^6) using model Diff-Slab/IC, and 4.19×10^5

Table 17.5 Values of microstructural factor for high-pressure CO_2 extraction of essential oils from oregano in selected studies from Tables 17.1 and 17.2 as a function of extraction conditions (system temperature and pressure, superficial velocity) and sample pretreatment and particle size

Studied effect	Independent variable	Microstructural factor (F_M, –)	Reference
Process conditions[a]	$T = 298$ K/$P = 7$ MPa	34,900	Esquivel et al. (1996)
	$T = 313$ K/$P = 10$ MPa	3,600	
	$T = 313$ K/$P = 15$ MPa	1,880	
Process pressure[b]	$P = 7$ MPa	409,000	Gaspar et al. (2003)
	$P = 8$ MPa	313,000	
	$P = 10$ MPa	265,000	
	$P = 15$ MPa	277,000	
Process temperature[c]	$T = 300$ K	277,000	Gaspar et al. (2003)
	$T = 310$ K	308,000	
	$T = 320$ K	390,000	
Superficial solvent velocity[d]	$U = 0.017$ mm/s	593,000	Gaspar et al. (2003)
	$U = 0.029$ mm/s	542,000	
	$U = 0.040$ mm/s	519,000	
	$U = 0.052$ mm/s	479,000	
Sample particle size[e]	$d_p = 0.330$ mm	440,000	Gaspar et al. (2003)
	$d_p = 0.360$ mm	440,000	
	$d_p = 0.700$ mm	477,000	
	$d_p = 1.550$ mm	5,720,000	
Sample pretreatment[f]	Conventionally milled ($d_p = 0.354$ mm)	2,650	Uquiche et al. (submitted)
	Low-temperature-milled ($d_p = 0.339$ mm)	2,540	
	Rapidly decompressed ($d_p = 0.844$ mm)	1,000	

[a] $_p = 1.10$ mm/$Q = 8.33$ g CO_2/min
[b] $d_p = 0.36$ mm/$T = 300$ K/$Q = 8.33$ g CO_2/min
[c] $d_p = 0.36$ mm/$P = 15$ MPa/$Q = 8.33$ g CO_2/min)
[d] $d_p = 0.36$ mm/$T = 310$ K/$P = 10$ MPa
[e] $T = 300$ K/$P = 7$ MPa/$U = 0.017$ mm/s
[f] $T = 313$ K/$P = 10$ MPa/$U = 1.234$ mm/s

(range: 1.38×10^5 to 3.81×10^6) using model Diff-Slab/PM. Furthermore, values of F_M for a selected experiment of Gaspar et al. (2003) – $d_p = 0.360$ mm/$T = 300$ K/$P = 8$ MPa/$Q = 8.33$ g CO_2/min – differed by a factor of more than 10 depending on the model: 3.13×10^5 using model IBC-Diff (Gaspar et al. 2003) and 2.64×10^5 using model Diff-PF (Araus et al. 2009).

Table 17.6 supports the claim that mathematical models and their ability to fit the physical picture of the actual extraction process explain the differences among estimated values of F_M to a great extent in the case of four different substrates. For basil, marjoram, and rosemary average values of F_M were approximately 1.5 times larger using model Diff-Sph/PM (Reverchon et al. 1993a) than model Diff-ADPF (Goodarznia and Eikani 1998), and approximately 70 times larger using model Diff-ADPF than model μS/SGl (Zizovic et al. 2005). For caraway, values of F_M were 20–110 times larger using model IBC/PFNA (Sovová et al. 1994a) than model

Table 17.6 Values of microstructural factor for high-pressure CO_2 extraction of plant essential oils in selected studies from Tables 17.1 and 17.2. All reported values for a single substrate and extraction condition were based on single experiments from an original publication, and fitted by individual authors to different models

Substrate	Original Study	Goodarznia and Eikani (1998)	Zizovic et al. (2005)	Sovová (2005)	Contribution of the authors
Basil (Reverchon et al. 1993a)	91,200	72,000	675	–	–
Marjoram (Reverchon et al. 1993a)	97,100	59,100	894	–	–
Rosemary (Reverchon et al. 1993a)	48,400	28,800	891	–	–
Caraway (Sovová et al. (1994a), extraction at 313 K and 9 MPa)	2,180,000	20,000	–	–	1,860 (Germain et al. 2005)
Caraway (Sovová et al. (1994a), extraction at 313 K and 10 MPa)	680,000	36,000	–	–	3,620 (Germain et al. 2005)
Pennyroyal (Reis-Vasco et al. (2000), d_p = 0.3 mm)	280	–	–	–	436 (Araus et al. 2009)
Pennyroyal (Reis-Vasco et al. (2000), d_p = 0.5 mm)	168	–	–	817	436 (Araus et al. 2009)
Pennyroyal (Reis-Vasco et al. (2000), d_p = 0.7 mm)	120	–	1,278	–	436 (Araus et al. 2009)

Diff-ADPF (Goodarznia and Eikani 1998), and approximately 10 times larger using model Diff-ADPF than model SC/PF (Germain et al. 2005). Finally, for pennyroyal values of F_M were 1.5–3.5 times larger using model Diff-PF (Araus et al. 2009) than model LDF/ADPF (Reis-Vasco et al. 2000), and for selected experiments 6.8 times larger using model IBC/PF/PCPR (Sovová 2005) or 10.7 times larger using model μS/SGl (Zizovic et al. 2005) than using model LDF/ADPF (Reis-Vasco et al. 2000).

Table 17.7 reports the interval of F_M-values estimated for all mass transfer studies in Tables 17.1 and 17.2 that inform best-fit values of internal mass transfer parameters, with the exception of studies in Tables 17.5 and 17.6. The results of the single experiments were collated using the same material based on this chapter's hypothesis that the values of F_M depend on the sample and its pretreatment, but do not depend on the extraction temperature and pressure, CO_2 superficial velocity, and particle diameter (del Valle and de la Fuente 2006; Araus et al. 2009; Uquiche et al. submitted). Explanations of the observed variations in the form of wide intervals for the values of F_M were advanced in the previous paragraphs in explaining some differences in Tables 17.5 and 17.6.

According to (17.17), the validity of reported values of the microstructural correction factor in Tables 17.5–17.7 depends partially on the values of the binary diffusion coefficient (D_{12}) estimated in this chapter using the equation of Catchpole and King (1994). This equation was developed with a large database that did not include typical components in plant essential oils. Table 17.8 displays estimated

Table 17.7 Summary of values of the microstructural factor for high-pressure CO_2 extraction of plant essential oils in studies from Tables 17.1 and 17.2 that are not included in Tables 17.4 or 17.5

Substrate	Pretreatment	Model name[a]	Microstructural factor (F_M, –)
Black pepper (Ferreira and Meireles 2002)	Milled	Sovová	(230–2.40) × 10^7
Black pepper (Perakis et al. 2005)	Milled	Sovová	(12.5–1.47) × 10^3
Valerian II (Zizovic et al. 2007a)	Milled	μS/SCav	(218–6.79) × 10^5
Valerian I (Zizovic et al. 2007a)	Milled	μS/SCav	(7.25–3.58) × 10^6
Valerian III (Zizovic et al. 2007a)	Milled	μS/SCav	(4.63–2.99) × 10^6
Spearmint (Kim and Hong 2002)	Milled	DDD/PM	(30.1–4.17) × 10^4
Marigold (Zizovic et al. 2007a)	Milled	Sovová	(68.2–4.06) × 10^3
Marigold (Zizovic et al. 2007a)	Milled	Diff-Slab/PM	(11.2–4.99) × 10^4
Sage (Reverchon 1996)	Milled	LDF-Slab/PMMS	5.54 × 10^4
Sage (Araus et al. (2009)	Milled	Diff/PF	(39.5–3.95) × 10^3
Sage (Catchpole et al. 1996b)	Chopped	LDF/IMTC	2.52 × 10^3
Sage (Langa et al. 2009)	Milled	IBC/PF/PCPR	49.9–3.75
Rosemary (Coelho et al. 1997)	Milled	LDF/PF/CDIC	(16.9–7.39) × 10^2
Rosemary (Bensebia et al. 2009)	Milled	Sovová	(4.34–1.26) × 10^2
Hop (Pfaf-Šovljanski et al. 2005)	Milled	R-SO	3.20 × 10^4
Aniseed (Rodrigues et al. 2003)	Milled	Sovová	(30.5–2.09) × 10^3
Eucalyptus (Zizovic et al. 2007c)	Milled	μS/SCav	1.58 × 10^4
Chamomile (Povh et al. 2001)	Milled	Sovová	(14.7–7.97) × 10^3
Chamomile (Araus et al. 2009)	Milled	Diff/PF	1.08 × 10^4
Chamomile (Kotnik et al. 2007)	Milled	EMTC	(6.65–3.53) × 10^3
Thyme (Zekovic et al. 2001)	Milled	R-SO	(13.9–1.2) × 10^3
Orange peel (Mira et al. 1996)	Milled	Sovová	(13.5–1.15) × 10^3
Orange peel (Mira et al. (1999)	Milled	Sovová	4290–7.29
Orange peel (Zizovic et al. 2007c)	Milled	μS/SCav	1.68 × 10^2
Ginger (Martínez et al. 2003)	Milled	Sovová	(11.1–2.21) × 10^3
Alecrim pimenta (Sousa et al. 2002)	Triturated	Sovová	1.03 × 10^4
Ho-sho (Steffani et al. 2006)	Milled	SC/ADPF	(83.1–4.44) × 10^2
Parsley (Louli et al. 2004)	Milled	Sovová	(7.53–2.23) × 10^3
Parsley (Louli et al. 2004)	Milled	Sovová	(7.5–2.54) × 10^3
Lavender (Reverchon et al. 1995a)	Milled	R-SO	6.41 × 10^3
Lavender (Akgun et al. 2000)	Manually crushed	SC/PF	(36.8–9.25) × 10^2
Lavender (Araus et al. 2009)[7]	Milled	Diff/PF	2.03 × 10^2
Cinnamon of cunha (Sousa et al. 2005)	Triturated	Sovová	(6.17–4.62) × 10^3
Boldo (Uquiche et al. submitted)	Rapidly decompressed	Diff/PF	5.66 × 10^3
Boldo (Uquiche et al. submitted)	Conventionally milled	Diff/PF	4.75 × 10^3
Boldo (Uquiche et al. submitted)	Low-temperature-milled	Diff/PF	4.18 × 10^3
Nutmeg (Spricigo et al. 2001)	Milled	SC/ADPF	(56.5–3.39) × 10^2
Nutmeg (Machmudah et al. 2006)	Milled	–	–
Fennel (Reverchon et al. 1999)	Milled	LDF/PF	(2.25–2.37) × 10^2
Celery (Papamichail et al. 2000)	Milled	Sovová	(15.1–2.04) × 10^2
Celery (Zizovic et al. 2005)	Milled	μS/SDuct	1.28 × 10^3

(*continued*)

Table 17.7 (continued)

Substrate	Pretreatment	Model name[a]	Microstructural factor (F_M, –)
Carqueja (Vargas et al. 2006)	Milled	Sovová	(4.25–1.79) × 10^2
Carqueja (Vargas et al. 2006)	Milled	R-SO	(8.30–1.58) × 10^2
Clove (Martínez et al. 2007)	Milled	Sovová	84.2–69.6

[a]Model names are specified in Table 17.1

variations in the D_{12} of typical components in plant essential oil extracts in high-pressure CO_2 as a function of CO_2 density and system temperature. Values of D_{12} decrease when decreasing the temperature (a 6.4% decrease from 333 to 313 K), or increasing the density of the CO_2 (a 60% decrease from 285 to 683 kg/m^3), or increasing the size of the solute. However, changing D_{12} to a considerable extent demands extreme changes in extract composition; the reduction is limited to 25% between the heaviest OST (the 17-C farnesyl acetate) and lightest MT (the 10-C limonene), 40% between the wax (the 28-C *n*-octacosane) and limonene, and 56% between the triglyceride (the 57-C triolein) and limonene. According to this analysis, the discrepancies in D_{12} associated with the use of the equation of Catchpole and King (1994) and the adoption of an erroneous pseudo-solute could result in discrepancies that are substantially smaller than discrepancies in values of F_M reported in Tables 17.5–17.7.

Another factor that is partially responsible for errors in the estimation of F_M, according to (17.19), is the erroneous estimation of the partition K of the pseudo-solute between the solid and the fluid. A discussion of errors in the estimation of K can be found in Sect. 4.4.

There are some reports on the estimation of D_e for a porous solid as a function of D_{12} and the inner porosity (ε_p) of the solid substrate (Goto et al. 1993; Ruetsch et al. 2003; Daghero et al. 2004; Perakis et al. 2005). According to the equation of Wakao and Smith (1962), (17.22), F_M can be estimated as follows:

$$F_M = \frac{1}{\varepsilon_p^2} \tag{17.22}$$

Considering that in these studies, inner porosity values for the substrates ranged from $\varepsilon_p = 0.487$ for black pepper (Perakis et al. 2005) to $\varepsilon_p = 0.537$ for peppermint (Goto et al. 1993), the values of F_M estimated using (17.22) ranged from 4.0 to 4.2. Thus, (17.22) produces smaller values of F_M than those reported in Tables 17.5–17.7. Ruetsch et al. (2003) and Daghero et al. (2004) did not measure ε_p, but assumed a value $\varepsilon_p = 0.5$. On the other hand, Perakis et al. (2005) estimated the porosity from experimental values of the true density (ρ_p) of ground particles of black pepper, and the bulk density (ρ_p) of a packed of the particles according to (17.23):

$$\varepsilon = 1 - \frac{\rho_b}{\rho_p} \tag{17.23}$$

Table 17.8 Predicted binary diffusion coefficient D_{12} ($m^2/s \times 10^8$) of selected components in plant essential oils (component 2) in supercritical CO_2 (component 1) as a function of system temperature and CO_2 density

Solute	MW_2 (Da)	V_{c2} (cm^3/mol)	ρ = 285.0 (kg/m^3)			ρ = 682.6 (kg/m^3)		
			313 K (8.1 MPa)	323 K (9.0 MPa)	333 K (9.9 MPa)	313 K (10.0 MPa)	323 K (12.8 MPa)	333 K (15.7 MPa)
Limonene	136.2	507.5	3.38	3.49	3.60	1.37	1.41	1.45
Linalool	154.3	565.5	3.22	3.32	3.42	1.30	1.34	1.38
Linalyl acetate	196.3	682.5	2.95	3.04	3.13	1.19	1.23	1.26
β-Caryophyllene	204.4	722.5	2.88	2.97	3.06	1.16	1.20	1.23
Farnesol	222.4	837.5	2.71	2.79	2.88	1.09	1.13	1.16
Farnesyl acetate	264.4	954.5	2.55	2.63	2.71	1.03	1.061	1.09
n-Octacosane	394.8	1,603.5	2.04	2.11	2.17	0.824	0.850	0.877
Triolein	885.5	3,233.5	1.49	1.54	1.59	0.603	0.622	0.642

The problem with using (17.21) to estimate the inner porosity of the substrate is that ε is the total porosity of the bed instead of ε_p, which is smaller. (17.24) relates the inner porosity of the substrate (ε_p) with the total porosity (ε) and the interparticle porosity of the particles in the packed bed (ε_b):

$$\varepsilon_p = \frac{\varepsilon - \varepsilon_b}{1 - \varepsilon_b} \tag{17.24}$$

Considering that randomly packed spherical particles in a dense bed have a large ratio, D/d_p, for which the expected value of interparticle porosity is $\varepsilon_b = 0.36$ (Carman 1937), it can be estimated using (17.24) that $\varepsilon_p = 0.198$ for $\varepsilon = 0.487$, and then using (17.22) that $F_M = 25.4$, which is still small but closer to the experimental values reported in Tables 17.5–17.7.

This chapter's analysis of the inner mass transfer within the solid substrate up to this point has implicitly considered that the substrate is a homogeneous material. Tables 17.5–17.7 include examples of materials being considered as being composed of broken superficial cells and intact inner cells, and total mass transfer in these heterogeneous materials considers separate extraction of the two fractions according to different controlling mechanisms, respectively external resistance to mass transfer, and internal (diffusive) resistance to mass transfer. These models usually use the ratio of broken to intact cells or the fraction of free solute (α) in the pretreated substrate as a fitting parameter; however, this ratio has to agree with the microstructure of the biological substrate, particularly of the specialized secretory structures where plant essential oils are encapsulated. For a spherical particle obtained by milling of a parenquimatous tissue, α is given by (17.25):

$$\alpha = 1 - \left(1 - \frac{d_c}{d_p}\right)^3 \tag{17.25}$$

where the thickness of a superficial layer of ruptured cells is closely related to the diameter (d_c) of the specialized secretory structure, and d_p is the diameter of the milled particle.

Figure 17.6 shows the effect of the ratio between cell diameter and particle diameter (d_c/d_p) on the best-fit values of fractions of broken cells (α) in milled herbs or spices containing superficial glands, including oregano bracts (Gaspar et al. 2003), pennyroyal leaves (Sovová 2005), rosemary leaves (Bensebia et al. 2009), and sage leaves (Langa et al. 2009); secretary ducts, including caraway fruits (Sovová et al. 1994a), celery seeds (Papamichail et al. 2000), chamomile flowers (Povh et al. 2001), aniseed fruits (Rodrigues et al. 2003), parsley seeds (Louli et al. 2004), and marigold flowers (Campos et al. 2005); or secretory cavities, such as orange peels (Mira et al. 1996, 1999). For calculations, the cell diameters (d_c) estimated from microphotographs in the literature were as follows: for oregano, $d_c = 78$ μm (Svoboda and Svoboda 2000); for pennyroyal, $d_c = 52.5$ μm (Zizovic et al. 2007c); for rosemary, $d_c = 85$ μm (Svoboda and Svoboda 2000); for sage,

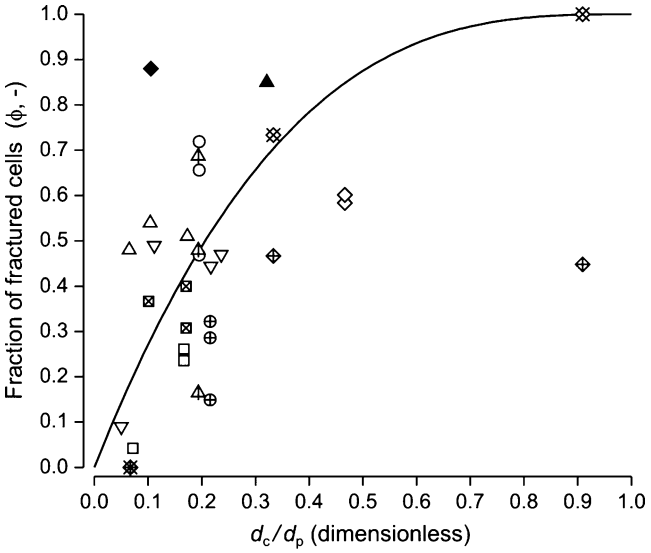

Fig. 17.6 Effect of particle diameter on the best-fit values of the fraction of broken cells in milled herbs or spices. Calculations were made from data of (▲) caraway (Sovová et al. 1994a), (⊕) orange peel (Mira et al. 1996), (⊗) orange peel (Mira et al. 1999), (□) celery (Papamichail et al. 2000), (◇) chamomile (Povh et al. 2001), (▽) oregano (Gaspar et al. 2003), (⊕) aniseed (Rodrigues et al. 2003), (⍋) marigold (Campos et al. 2005), (◆) pennyroyal (Sovová 2005), (⊠) parsley (Louli et al. 2004), (○) rosemary (Bensebia et al. 2009), and (△) sage (Langa et al. 2009)

$d_c = 52$ μm (Serrato-Valenti et al. 1997); for caraway, $d_c = 123$ μm (Svoboda and Svoboda 2000); for celery, $d_c = 35$ μm (Stamenić et al. 2008); for chamomile, $d_c = 140$ μm (Zizovic et al. 2007c); for aniseed, $d_c = 108$ μm (Zizovic et al. 2007c); for parsley, $d_c = 50$ μm (Podlaski et al. 2003); for marigold, $d_c = 120$ μm (Zizovic et al. 2007c); and for orange peels, $d_c = 500$ μm (Svoboda and Svoboda 2000). The line in Fig. 17.6 corresponds to (17.25) which is only valid for size reduction relying on impact or attrition mechanisms that fracture surface cells only. Figure 17.6 shows that (17.25) only partially explains the best-fit values of broken cells reported in the literature, possibly because of differences between the assumed and actual particle shape, microstructure, and fracturing mechanism of the specialized secretory structures in the plant materials.

Zizovic et al. (2005, 2007a, b, c) have contributed a series of studies on the mathematical modeling of SCFE of plant essential oils at the micro-scale that demonstrate the need to include a description of the encapsulating secretory structures in plant tissue to improve the predictive capacity of the model. These structures (glandular trichomes or glands, large or small secretory cavities, and secretory ducts) (Sect. 17.1.1), are not equally affected by pre-treatment, nor by the extraction process. For example, milling causes partial destruction of glandular trichomes or glands in the surface of leaves, terminal shoots, and flowers of *Laminaceae* herbs, and subsequent SCFE causes partial destruction of the

remaining glands by a mechanism involving diffusion of CO_2 through the gland wall, its dissolution into the essential oil, and swelling the CO_2-saturated mixture to the extent of rupturing the gland. Zizovic et al. (2005) obtained microscopical evidence of the rupture of a fraction $\phi \sim 0.35$ of the glands during milling of dried mentha leaves to a final particle diameter of 0.5–1 mm, as well as of the rupture of about $\varphi \sim 0.39$ of the glands after contacting unmilled leaves with high-pressure CO_2 at 313 K and 10 MPa for 1 h. Zizovic et al. (2005) hypothesized that all glands cracked during the process as a result of swelling of the gland contents, become disrupted upon saturation of the essential oil with the CO_2 at a single time that is determined by diffusion of CO_2 through the gland wall, but later Stamenić et al. (2008) proposed a cracking time distribution based on microscopical evidence gathered by exposing wild thyme leaves to high-pressure CO_2 at 313 K and 10 MPa different times between 20 min and 100 min. These models were applied to basil, rosemary, marjoram, and pennyroyal by Zizovic et al. (2005) and to wild thyme by Stamenić et al. (2008).

Unlike superficial glands that can rupture upon swelling of the gland contents by dissolution of CO_2 into the essential oil, inner secretory cavities in plant tissue are ruptured only as a result of a size-reduction pretreatment, with the probability of rupture being dependent on the relative sizes of secretory cavities and milled particles. Since the physical picture for the extraction of essential oil from secretory cavities at the microscale is similar to that of intact and broken cells proposed by Sovová (1994) (Sect. 17.2.3), the mathematical model in this particular case considered simultaneous extraction of essential oils from disrupted cavities controlled by an external mass transfer coefficient, and of essential oils from nondisrupted cavities controlled by a best-fit internal mass transfer coefficient. Zizovic et al. (2007a) estimated the fraction of disrupted cavities in milled valerian roots as the ratio between the cavity diameter (determined by microscopy) and the particle diameter (determined by sieving). Zizovic et al. (2007a) estimated the mean diffusion pathway in nondisrupted cells as half the difference between the particle diameter and cavity diameter, but they did not explain the basis for this assumption. This model was applied to valerian roots by Zizovic et al. (2007a), and to clove buds, ginger rhizomes, and eucalyptus leaves by Zizovic et al. (2007c). Consequently, Zizovic et al. (2007c) developed a separate model for SCFE of plant materials with large secretory cavities, such as citrus peels, where most cavities are cracked.

In the case of plant material with secretory ducts, the size-reduction pretreatment opens each duct on two opposite sides of the particle. The essential oil in the duct becomes saturated with CO_2 during extraction and the swelling of the mixture results in a superficial layer of oil embedding the whole particle. SCFE can be pictured as a two-stage process. In the first stage, when the mass transfer area is the external surface of the particle, the extraction of essential oil is defined by convection of the superficial oil to the CO_2 (mass transfer coefficient from a literature correlation). In the second stage, when the mass transfer area diminishes to that fraction of the external surface of the particle covered with openings of secretory ducts, the essential oil moves from a receding boundary in the pore to the pore

opening by unimpeded diffusion (defined by the binary diffusion coefficient of the oil in CO_2), and then by convection (the same mass transfer coefficient from the first stage) from the pore opening to the bulk of the high-pressure CO_2 phase; the diffusion path for the essential oil in this second stage is half the particle diameter. Zizovic et al. (2007b) proposed a fully predictive mathematical model for SCFE plant material with secretory ducts, which used the diameter of the secretory ducts and their superficial density (number of ducts per unit surface area) as microstructural parameters. The model was applied for fruits of celery (Stamenić et al. 2008), and fruits of fennel, and flowers of chamomile and marigold (Zizovic et al. 2007b).

17.4 Phase Equilibrium Effects in Essential Oil Extraction, Fractionation, and Recovery

In this section, the effect of phase equilibrium on the extraction, fractionation, and recovery of plant essential oils using high-pressure CO_2 is discussed. Firstly, the variations in the solubility of essential oil components in high-pressure CO_2 are discussed as a function of system temperature and pressure (Sect. 17.4.1). Secondly, there is discussion of the selective removal of high-solubility MTs from the remaining OMTs so as to produce citrus essential oils with an improved functionality (more intense aroma, less off-flavors, increased solubility in water) based on high-pressure phase equilibrium data for ternary CO_2 + MT + OMT and more complex systems (Sect. 17.4.2). Next, the thermodynamic solubility in CO_2 of complex essential oil mixtures is compared with the "operational" solubility of the CO_2 extract of the corresponding herb or spice under comparable temperature and pressure (Sect. 17.4.3). Finally, the effect of sorption phenomena on the aforementioned "operational" solubility (Sect. 17.4.4) is discussed.

17.4.1 Solubility in CO_2 of Essential Oil Components in Model (Binary) Systems

There are many experimental studies about the solubility of selected essential oil components in CO_2 as a function of system temperature and pressure, as shown in Table 17.9. The data include four different solute families and CO_2 conditions that span from subcooled liquid, to superheated vapor, and to SCF (equilibrium temperatures of 296–373 K, and equilibrium pressures of 0.81–30.9 MPa). There is abundant information in the literature about the solubility of limonene in high-pressure CO_2, but virtually none about other 10-carbon MT compounds, the only exceptions being *p*-cymene and α-pinene (Table 17.9). On the other hand, there is extensive information on the solubility of OMT compounds in high-pressure CO_2, including anisaldehyde, camphor, carvacrol, carvone, 1,8-cineole (eucalyptol),

Table 17.9 Summary of high-pressure equilibrium CO_2 + plant essential oil component binary systems. The essential oil components were classified as monoterpene hydrocarbons, oxygenated monoterpenes, sesquiterpene hydrocarbons and oxygenated sesquiterpenes, and waxy compounds

Solute	Data points	Temperature(s) or temperature range (K)	Pressure(s) or pressure range (MPa)	Solubility range (mg solute/g CO_2)
Monoterpenes				
p-Cymene (Wagner and Pavlicek 1993)	16	313–323	3.855–9.829	6.73–41.7
Limonene (di Giacomo et al. 1989)	26	308, 315, 323	3.0–10.0	0.681–142
Limonene (Matos et al. 1989)	14	318, 323	8.6–9.8	12.4–106
Limonene (Marteau et al. 1995)	29	310, 320, 323	6.96–9.85	5.58–73.2
Limonene (Iwai et al. 1996)	15	313, 323, 333	3.94–10.26	3.41–24.3
Limonene (Akgun et al. 1999)	22	313, 323, 333	7.04–11–20	1.24–54.8
Limonene (Chang and Chen 1999)	28	314, 323, 333	0.83–11.00	1.55–47.2
Limonene (Vieira de Melo et al. 1999)	16	323, 333, 343	7.00–10.55	4.96–88.2
Limonene (Kim and Hong 1999)	11	312, 322	6.2–9.3	3.10–79.4
Limonene (Berna et al. 2000)	8	318	6.9–10.5	5.27–1,202
Limonene (Gamse and Marr 2000)	42	304, 314, 324	3.1–8.4	2.79–65.4
Limonene (Benvenuti and Gironi 2001)	8	315	3.05–8.50	5.89–18.4
Limonene (Leeke et al. 2001)	15	318, 323	7.32–10.05	2.79–81.3
Limonene (Francisco and Sivik 2002)	8	313, 333	8–25	12.4–89.2
Limonene (Fonseca et al. 2003)	4	323	8.3–9.5	130–244
α-Pinene (Pavlicek and Richter 1993)	72	313, 323, 328	3.25–9.75	3.60–54.3
α-Pinene (Richter and Sovová 1993)	24	296–335	6.14, 7.65	4.15–102
α-Pinene (Akgun et al. 1999)	19	313, 323, 333	7.15–10.93	5.27–53.5
α-Pinene (Francisco and Sivik 2002)	8	313, 333	8–25	9.32–82.7
Oxygenated monoterpenes				
p-Anisaldehyde (Mukhopadhyay and De 1995)	13	323, 373	5.5–13.7	0.619–43.9
Camphor (Akgun et al. 1999)	39	313, 323, 333	7.51–12.61	2.98–139
Camphor (Carvalho et al. 2006)	15	314, 324, 334, 354	8.65–15.71	32.5–275
Carvacrol (Leeke et al. 2001)	49	313, 323	7.70–30.85	9.59–740
Carvone (Kim and Hong 1999)	13	312, 322	6.2–9.6	0.307–59.0
Carvone (Gamse and Marr 2000)	31	304, 314, 324	2.0–10.0	0.683–50.9
1,8-Cineole (Matos et al. 1989)	15	318, 323	7.75–9.80	14.1–82.5
1,8-Cineole (Francisco and Sivik 2002)	8	313, 333	8.0–25.0	10.5–86.2
Citral (di Giacomo et al. 1989)	29	308, 315, 323	3.0–11.0	0.104–78.9
Citral (Marteau et al. 1995)	26	310, 320, 330	7.94–11.93	2.42–4.85
Citral (Benvenuti and Gironi 2001)	10	315	4.70–9.58	0.692–36.0
Citral (Fonseca et al. 2003)	4	323	8.7–10.3	32.5–143
β-Citronellol (Tufeu et al. 1993)	15	309, 316, 321	8.46–15.70	25.8–160
Eugenol (Cheng et al. 2000)	21	308, 318, 328	1.480–12.512	4.48–61.8
Fenchone (Akgun et al. 1999)	21	313, 323, 333	7.04–11.50	1.04–1.04
Geraniol (Tufeu et al. 1993)	9	309, 316, 321	10.82–16.27	37.9–120
Linalool (Chang and Chen 1999)	29	313, 323, 333	0.81–11.06	1.05–35.4
Linalool (Vieira de Melo et al. 1999)	3	323	7.49–8.37	1.75–4.56
Linalool (Berna et al. 2000)	13	318, 328	7.1–11.1	2.39–1,381

(*continued*)

Table 17.9 (continued)

Solute	Data points	Temperature(s) or temperature range (K)	Pressure(s) or pressure range (MPa)	Solubility range (mg solute/g CO_2)
Linalool (Fonseca et al. 2003)	3	323	8.6–9.4	132–196
Linalool (Iwai et al. 1994)	14	313, 323, 333	4.00, 10.96	1.05–27.9
Linalool (Raeissi and Peters 2005)	12	319–348	9.355–13.705	71.5
Menthol (Carvalho et al. 2006)	12	323, 343	6.5–13.5	0.256–218
Menthol (Sovová and Jež 1994)	40	308, 313, 318, 323, 328	6.52–11.56	0.782–47.1
Menthol (Sovová et al. 2007)	47	303, 313, 323, 333	6.64–14.37	1.24–147
Thymol (Carvalho et al. 2006)	12	323, 343	6.5–13.5	19.6–497
Verbenol (Richter and Sovová 1993)	73	313, 323, 328	5.09–13.78	0.208–194
Sesquiterpenes and oxygenated sesquiterpenes				
β-Caryophyllene (Michielin et al. 2009)	86	303, 313, 323, 333, 343	4.5–19.2	18.7–522
Artemisinin (Xing et al. 2003)	36	310, 318, 328, 338	10.0–27.0	0.628–17.1
Farnesol (Núñez et al. 2010)	58	313, 323, 333	9.7–26	0.657–9.67
α-Humulene (Michielin et al. 2009)	77	303, 313, 323, 333, 343	4.7–19.2	18.7–521
Patchoulol (Hybertson 2007)	8	313, 323	10.0–25.0	2.17–48.0
Typical wax component				
Octacosane (Reverchon et al. 1993b)	28	308, 313, 318	8.0–27.5	0.110–3.50
Octacosane (Stassi and Schiraldi 1994)	3	308–318	25	0.610–3.36
Octacosane (Chandler et al. 1996)	14	308, 318	10.0–24.0	0.170–4.22

citral, β-citronellol, eugenol, fenchone, geraniol, linalool, menthol, thymol, and verbenol (Table 17.9). There is less solubility information about the 15-carbon terpene compounds, which is limited to artemisinin (OST), β-caryophyllene (ST), farnesol (OST), α-humulene (ST), and patchoulol (OST). Finally, although there is extensive information in the literature on the solubility of waxy compounds in high-pressure CO_2, Table 17.9 is limited to experimental works with octacosane. Literature on the solubility of waxy compounds includes *n*-alkanes having 9–36 carbon atoms under typical CO_2 extraction conditions, as well as long-chain *n*-alkanes under typical gas-processing conditions (Stassi and Schiraldi 1994; Chandler et al. 1996; Reverchon et al. 1993b). Stahl et al. (1988) conducted a systematic study on the solubility of essential oil components in high-pressure CO_2 including data for limonene, anethole (OMT), carvone, eugenol, β-caryophyllene, and valeranone (OST). This chapter does not include the results of Stahl et al. (1988) in Table 17.9 since they reported trend lines instead of actual experimental data, so their results are of less value for quantitative comparison purposes.

Solubility values of selected essential oil components in high-pressure CO_2 vary widely, as exemplified in Fig. 17.7 for the solubility of limonene in high-pressure

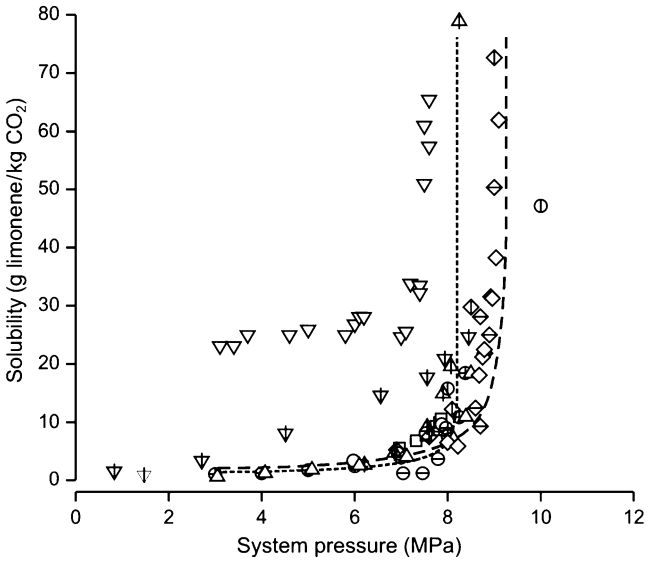

Fig. 17.7 Solubility of limonene in supercritical CO_2 as a function of system pressure (approximately between 1 MPa and 10 MPa) as reported by (⊕) di Giacomo et al. (1989) at 313 K, (◈) Matos et al. (1989) at 318 K, (□) Marteau et al. (1995) at 310 K, (○) Iwai et al. (1996) at 313 K, (⊖) Akgun et al. (1999) at 313 K, (▼) Chang and Chen (1999) at 314 K, (▲) Kim and Hong (1999) at 312 K, (◈) Berna et al. (2000) at 318 K, (▽) Gamse and Marr (2000) at 314 K, (△) Benvenuti and Gironi (2001) at 315 K, (◇) Leeke et al. (2001) at 318 K, and (⊙) Francisco and Sivik (2002) at 313 K. Lines represent the solubility isotherms at (– – –) 311 and (-------) 318 K predicted using the Peng-Robinson-Mathias-Copeman equation of state with the modified Huron-Vidal (MHV1) – UNIFAC mixing rules and model parameters in database of PE 2000 (Pfohl et al. 2000), a shareware software for modeling high-pressure phase equilibria

CO_2 at approximately 313 K (310–318 K) and as a function of system pressure, due to the inherent limitations of methodologies applied to assess phase equilibrium (Raal and Mühlbauer 1998). Limonene is the most abundant MT in plant essential oils, representing >90% (w/w) of some of them, because it acts typically as a carrier of other compounds (mainly OMTs) that impact more definitely on plant aroma. The experimental methods can be broadly classified as analytic (if one or both phases in equilibrium are sampled and analyzed to determine composition) or synthetic (if the global composition of the system is predetermined, and the conditions of the system are changed so as to reach a phase boundary). These broad classes, in turn, can be implemented in static or dynamic equilibrium cells, depending on agitation. In dynamic cells, the time to reach equilibrium is shortened by agitation of the cell contents, or recirculation of one or the two phases in the cell (the so-called multi-pass dynamic systems, where sampling is done in recirculation loops). Measurements using all methods are susceptible to error if true equilibrium conditions are not reached, and no single method is more questionable in this regard than the one-pass dynamic method (di Giacomo et al. 1989; Kim and Hong 1999;

Gamse and Marr 2000; Benvenuti and Gironi 2001; Fonseca et al. 2003). Observation of the cell contents through a window-cell helps to ascertain the quality of stirring and the number and nature of phases in the system. In the case of analytical methods, where system temperature and pressure are kept constant, sampling and analysis of one phase as a function of equilibration time can help to ascertain whether equilibrium conditions have been reached. Another problem with analytic methods occurs when an incomplete picture of the equilibrium is achieved when only the CO_2-rich phase is sampled, and when CO_2 transfers to the solute-rich phase (Matos et al. 1989; Berna et al. 2000). A final problem when using an analytic system is the disturbance of system conditions and the associated shift in equilibrium during sampling, which causes a drop in pressure (Iwai et al. 1996; Vieira de Melo et al. 1999). Since these disturbances are unavoidable, users of analytical methodologies try to minimize the negative effects of sampling by using large cells (Akgun et al. 1999; Leeke et al. 2001), or by reducing the size of the sampled aliquot by coupling the cell with a high-sensitivity instrument such as an infrared absorption device (Marteau et al. 1995), a densitometer (Chang and Chen 1999), or a chromatograph (Francisco and Sivik 2002).

The sampling problem inherent in analytic methods can be avoided by using synthetic methods. Synthetic systems use a variable volume cell to change system pressure while keeping the temperature and global composition constant. Raising the pressure (reducing the inner volume of the cell) to make the CO_2-rich phase collapse to a single bubble (as is the case when the composition of the liquid phase equals the global composition of the system) determines the bubble pressure at the test temperature. Alternatively, decreasing the pressure (increasing the inner volume of the cell) to cause the solute-rich phase collapse to a single drop (as is the case when the composition of the vapor phase equals the global composition of the system) determines the dew point at the test temperature. A problem of the synthetic method is the inherent difficulty in reaching and determining both bubble and dew point conditions for binary and more complex systems (Marteau et al. 1995).

The solubility of limonene in supercritical CO_2 at 313 K increases steadily with system pressure at low pressures ($P < 8$ MPa) and then increases sharply at high pressures ($P > 8$ MPa), with the transition between steady and sharp increase occurring close to the critical point of the mixture (Fig. 17.7). The reported critical point of CO_2 + limonene mixtures at 313 K is 8.3 MPa (Matos et al. 1989) or 8.5 MPa (Tufeu et al. 1993), and under these conditions the composition of the liquid phase coincides with that of the SCF phase (35.1 g limonene/kg CO_2). The binary CO_2 + limonene system exhibits a temperature crossover at ~8 MPa (Akgun et al. 1999; Berna et al. 2000). Thus, as the temperature increases isobarically, solubility of limonene in CO_2 decreases at $P < 8$ MPa due to reduction in the density and solvent power of CO_2, whereas solubility increases at $P > 8$ MPa due to the rise in vapor pressure and volatility of limonene. There is a general consistency between experimental solubility data for <8.5 MPa and for <80 g limonene/kg CO_2, but the data of Chang and Chen (1999) and Gamse and Marr (2000) are ~3 times and ~10 times, respectively, above the general trend. The results of Francisco and Sivik (2002) are questionable because they report limited solubility

of limonene in CO_2 under conditions where the two components are mutually miscible (at 313 K and well above the critical pressure of the CO_2 + limonene mixture). The data are more diverse at pressures >8.5 MPa due to experimental difficulties in measuring solubilities under conditions near the critical point of a mixture.

Figure 17.7 also includes the solubility isotherms at 310 and 318 K of limonene in high-pressure CO_2 predicted using the computer program PE 2000 (Pfohl et al. 2000). PE 2000 models liquid–vapor equilibrium by searching the phase transition corresponding to the bubble-point curve of the CO_2 + limonene system. Phase equilibrium was modeled using the modification of Mathias-Copeman of the Peng-Robinson (PR) equation of state (EoS), or the so-called PR-Mathias-Copeman EoS (Poling et al. 2000), and the first modification (or Modification 1, M1) of the Huron-Vidal (HV) mixing rules with the activity coefficients estimated using UNIFAC, or the so-called MHV1-UNIFAC mixing rules (Poling et al. 2000). The database of PE 2000 included all model parameters for the CO_2 + limonene system. Figure 17.7 shows a reasonable agreement between the predictions of the model and the experimental measurements, including the temperature cross-over at ~8 MPa. This finding is important because the selected model is of a predictive nature, in that the model parameters for the binary system are not estimated using phase equilibrium data; this chapter will expand on the implications of this feature when comparing the solubilities in high-pressure CO_2 of other compounds in Table 17.9.

Table 17.10 compares the solubilities in high-pressure CO_2 of selected solutes from each component family in Table 17.9 to those of limonene, under selected system conditions (313 K and 8 or 9–10 MPa). The density of the CO_2 under the selected system conditions bracket the interval proposed by Reverchon (1997) for SCFE of plant essential oils (250–500 kg/m^3). At the lower end of recommended CO_2 density, ~260 kg/m^3 (at 313 K and 8 MPa), the solubility of limonene in high-pressure CO_2 is approximately 6 g/kg, which is about 50% lower than the solubility of α-pinene reported by Akgun et al. (1999), probably because of the increased volatility (larger vapor pressure) of α-pinene as compared to limonene at 313 K (Table 17.10). The oxygen-bearing functional groups in OMTs increase their molecular weight and polarity, and decrease their vapor pressure as compared to MTs, which causes the solubility of OMTs in high-pressure CO_2 at 313 K and 8 MPa to be about 50% of that of limonene. At the upper end of recommended CO_2 density, ~410 kg/m^3 (at 313 K and 9 MPa), the binary systems of MTs and CO_2 are above their critical points, thus MTs are fully miscible with CO_2. Tufeu et al. (1993) reported the critical points at 314 K of the binary CO_2 + citral (8.76 MPa, 36.4 g citral/kg CO_2) and CO_2 + linalool (8.66 MPa, 11.5 g linalool/kg CO_2) systems, and these critical point values bring into question the limited solubility of citral in high-pressure CO_2 at 313 K and 9 MPa as reported by Benvenuti and Gironi (2001) (Table 17.10). The solubilities in high-pressure CO_2 at 313 K and ~9 MPa of the two OMTs in Table 17.10 (camphor and menthol) are approximately 1 order of magnitude larger than the corresponding solubilities of the ST (β-caryophyllene) and OSTs (artemisinin, farnesol, patchoulol), also included in Table 17.10, which are in turn approximately 2 orders of magnitude above the corresponding solubility

Table 17.10 Solubilities of selected plant essential oil components in high-pressure CO_2 at 313 K and relatively low (approximately 8 MPa) or relatively high pressure (8.6–10 MPa). Essential oil component included representative monoterpene hydrocarbons (limonene and α-pinene) and oxygenated monoterpenes (citral, linalool, and menthol), a sesquiterpene hydrocarbon (β-caryophyllene), an oxygenated sesquiterpene (farnesol), and a hydrocarbon (octacosane)

Compound	Molecular weight (*MW*, Da)	Vapor pressure (P_v, Pa)	Low-pressure			High-pressure		
			Pressure (*P*, MPa)	CO_2 density (ρ, kg/m^3)	Solubility (C_{sat}, mg/g CO_2)	Pressure (*P*, MPa)	CO_2 density (ρ, kg/m^3)	Solubility (C_{sat}, mg/g CO_2)
Limonene (Benvenuti and Gironi 2001)[a]	136.2	515 (Espinosa-Díaz et al. 1999)	8.13	295.6	7.04	9.0	408.4	CM[c]
α-Pinene (Richter and Sovová 1993)	136.2	1,440 (Richter and Sovová 1993)	7.74	252.7	60.1	9.0	408.4	CM
α-Pinene (Akgun et al. 1999)	136.2	1,440 (Richter and Sovová 1993)	7.74	252.7	60.1	–	–	–
Camphor (Akgun et al. 1999)	152.2	133 (Espinosa-Díaz et al. 1999)[b]	7.97	276.1	3.60	8.8	436.1	98.9
Citral (Benvenuti and Gironi 2001) [a]	152.2	30 (Stull 1947)	8.00	261.3	1.30	9.0	408.4	7.66
Linalool (Iwai et al. 1994)	154.2	95 (Espinosa-Díaz et al. 1999)	7.99	278.3	5.27	–	–	–
Menthol (Sovová and Jež 1994)	156.3	<133 (Stull 1947)[b]	7.86	264.3	3.31	9.02	497.9	50.8
β-Caryophyllene (Michielin et al. 2009)	204.4	0.018 (The Good Scents Company 2009a)	–	–	–	8.6	375.9	18.65
Farnesol (Núñez et al. 2010)	222.4	0.192 (The Good Scents Company 2009b)	–	–	–	9.73	609.3	4.29
Octacosane (Chandler et al. 1996)	394.3	~7×10^{-6} (Chandler et al. (1996)	–	–	–	10.0	631.7	0.170

[a]At 315 K
[b]Sublimation pressure
[c]Completely miscible

of a typical wax (*n*-octacosane), 0.015 g/kg CO_2, which is as expected because of the differences in molecular weight (increasing) between OMT compounds, ST/OST compounds, and waxes.

Figure 17.8 expands the results in Table 17.10 to show solubility isotherms of selected compounds in a wider pressure range, together with the estimates of the predictive model in this chapter. In order to use the PR-Mathias-Copeman EoS in PE 2000, an adjustment was made of the so-called model parameters c_1, c_2, and c_3, to vapor pressure data for α-pinene (Daubert and Danner 1989), citral (Hall 2001), linalool (Espinosa-Díaz et al. 1999), β-caryophyllene (Helmig et al. 2003; The Good Scents Company 2009a), farnesol (Helmig et al. 2003; The Good Scents Company 2009b), and *n*-octacosane (Daubert and Danner 1989; Chandler et al. 1996). Other parameters required were the normal boiling point, critical temperature, critical pressure, and acentric factor for the pure compounds. In those cases where no reliable values for these properties were available, values were estimated using group contribution methods. The normal boiling point of *n*-octacosane was

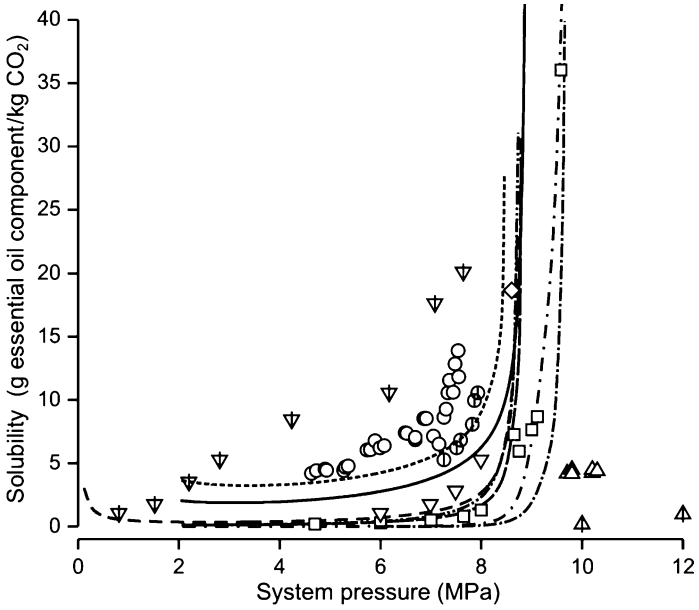

Fig. 17.8 Solubilities of selected plant essential oil components in supercritical CO_2 as a function of system pressure (approximately between 1 MPa and 12 MPa), including (——) limonene at 315.7 K; α-pinene at 313 K, data of (----○) Richter and Sovová (1993) and (----⊕) Akgun et al. (1999); (—-□) citral at 315 K, data of Benvenuti and Gironi (2001); linalool at 313 K, data of (– –▽) Iwai et al. (1994) or (– –▽) Chang and Chen (1999); (–··–◇) caryophyllene at 313 K, data of Michielin et al. (2009); (– · –△) farnesol at 313 K, data of Núñez et al. (2010); and (–··–⏃) octacosane at 313 K, data of Chandler et al. (1996). Lines represent the solubility isotherms at corresponding temperatures predicted by the Peng-Robinson-Mathias-Copeman equation of state with the modified Huron-Vidal (MHV1) – UNIFAC mixing rules using PE 2000 (Pfohl et al. 2000). The solubility isotherm for (——) limonene in supercritical CO_2 at 315.7 K predicted by PE 2000 is included as a reference

estimated using Joback's method (Poling et al. 2000). On the other hand, the critical temperature and critical pressure of citral, linalool, β-caryophyllene, farnesol, and *n*-octacosane were also estimated using Joback's method (Poling et al. 2000), whereas the acentric factor of these same solutes was estimated using the method of Lee-Kesler (Poling et al. 2000). PE 2000 includes all of these group-contribution algorithms for the estimation of physical properties. Figure 17.8 shows that the predictive model implemented in PE 2000 gives values of solubility for typical essential components in high-pressure CO_2 under typical extraction conditions for herbs and spices that are only qualitatively correct; thus, it can be only moderately appropriate for the purpose of discussing equilibrium effects on mass transfer kinetics as attempted in this chapter. An advantage of the method is that it is fully predictive if a group contribution method is applied to estimate the effect of temperature on the vapor or sublimation pressure of the solutes. Obviously, the predictive capabilities of the model improve when including experimental instead of estimated values of relevant physical properties, as suggested by the better fit of the model to experimental solubility data for limonene (Fig. 17.7) than higher molecular solutes such as STs, OSTs, and waxes (Fig. 17.8 compares the experimental data and predicted solubility isotherms for β-caryophyllene, farnesol, and *n*-octacosane).

Differences in solubility between solutes using data for binary CO_2 + solute systems suggest the possibility of selectively recovering a single solute or mixture of solutes in a complex essential oil sample. A general application of this type of fractionation process is the deterpenation of essential oils, which consists of the selective elimination of oxidation-prone and water-immiscible MTs that mask the characteristic aroma of OMTs in an herb or spice, and cause a haze in aqueous essential oil solutions (Stahl et al. 1988; Temelli et al. 1990; Reverchon 1997). Mukhopadhyay and De (1995) proposed the selective recovery of menthol from peppermint oil based on the solubility isotherms at 323 and 343 K of the binary CO_2 + menthol (component 2) and CO_2 + thymol (component 3) systems at pressures ranging from 6.5 to 13.5 MPa. They computed the values of the separation factor between menthol and thymol, R_{23} (17.26), as a function of system temperature and pressure,

$$R_{23} = \frac{y_2}{y_3}, \tag{17.26}$$

and found that $3.37 \leq R_{23} \leq 6.12$, which suggests that it is possible to enrich menthol in the high-pressure CO_2 phase. Mukhopadhyay and De (1995) neglected the molecular interactions between menthol and thymol, which may affect the separation factor, as exemplified next for the separation of limonene and linalool using high-pressure CO_2. It is also important to mention that using the separation factor to draw conclusions about the selective recovery of a component in a binary or multicomponent mixture has limitations in that the analysis should be made by comparing of concentration ratios between the two components in two phases (liquid, SCF) in equilibrium; if these concentration ratios coincide in the two

phases, then it is not possible to selectively recover one of the components using high-pressure CO_2 as the separating agent. Thus, the selectivity of the separation between menthol and thymol, α_{23} (17.27), instead of the separation factor R_{23} should be computed, where:

$$\alpha_{23} = \frac{y_2/y_3}{x_2/x_3} \tag{17.27}$$

Chafer et al. (2001) used composition information from the vapor phase for the ternary CO_2 (1) + limonene (2) + linalool (3) system to estimate the separation factor R_{23} so as to evaluate the possibility of recovering a linalool-enriched fraction. They concluded that the deterpenation of linalool was possible based on R_{23} values of ~2 for mixtures of limonene and linalool containing about 90–95% (mol/mol) of limonene, but also observed that the values of R_{23} were approximately four times higher when estimated on the basis of binary equilibrium data, which reveals a loss of information when solute–solute interactions in the more complex systems are not accounted for. Because of the requirement of ternary data to assess the fractionating capabilities of high-pressure CO_2, this subject is discussed next.

17.4.2 Essential Oil Fractionation in Model (Ternary) Systems and Complex Mixtures

Two CO_2-containing tertiary systems of practical importance that have been extensively analyzed in the literature are CO_2 + limonene + citral and CO_2 + limonene + linalool, because limonene and citral (a mixture of two isomers, geranial and neral) are the key MT and OMT, respectively, in lemon essential oil (Gironi and Maschietti 2008), and linalool replaces citral as the key OMT in orange essential oil (Budich and Brunner 1999). High-pressure CO_2 fractionation allows deterpenation of citrus oils so as to improve their shelf life, solubility in water, and aroma (Stahl et al. 1988; Temelli et al. 1990; Reverchon 1997), and the designing of these two deterpenation processes demands phase equilibria data for the aforementioned model systems (Budich et al. 1999; Gironi and Maschietti 2008).

The phase equilibria of the ternary CO_2 (1) + limonene (2) + citral (3) system was studied by Benvenuti and Gironi (2001) at 315 K and 8.4 or 9.0 MPa, and by Fonseca et al. (2003) at 323 K and 9.5, 9.7, or 10.3 MPa. Fonseca et al. (2003) reported that the selectivity α_{23} for the separation between limonene and citral varied between 1.72 and 2.00, which indicates that the vapor (or CO_2-rich) phase is enriched in limonene, whereas citral remains in the liquid (or essential oil-rich) phase. This agrees with the vapor pressure ratio between limonene and citral, ${P_2}^{Sat}/{P_3}^{Sat} = 17$ (Benvenuti and Gironi 2001), which defines separation under low-solubility (relatively small pressure) conditions. The selectivity α_{23} did not depend on system pressure (9.5–10.3 MPa), nor the composition of the essential oil model mixture (49–73% w/w limonene) (Fonseca et al. 2003). On the other hand, values of

α_{23} estimated by Benvenuti and Gironi (2001) at 315 K ranged from 1 to 62 depending on the limonene content in the CO_2-rich phase and the system pressure (limonene content in a CO_2-free basis ranged 36–90% mol/mol at 8.4 MPa, and 26–74% mol/mol at 9 MPa).

The vapor–liquid equilibria of the CO_2 (1) + limonene (2) + linalool (3) ternary system has been studied by Morotomi et al. (1999) at 313 K and 6.9 MPa, 333 K and 6.9 MPa, or 333 K and 10.0 MPa, by Vieira de Melo et al. (1999) at 323 K and 7.54, 8.08, 8.76, or 8.90 MPa, and by Chafer et al. (2001) at 318 or 328 K, pressures between 7 and 11 MPa, and mixtures having 40% or 60% (w/w) limonene in a CO_2-free basis. The selectivity for the separation between limonene and linalool is $\alpha_{23} > 1.2$ (Morotomi et al. 1999), which suggests the possibility of enriching limonene in the vapor phase, thus making the isolation of linalool in the liquid phase feasible, particularly in essential oil mixtures enriched in oxygenated compounds. Vieira de Melo et al. (1999) reported that α_{23} decreases from 3.75 to 2.14 as the pressure increases from 7.54 to 8.90 MPa, probably as a result of the increase in the solvent power of high-pressure CO_2 for OMTs. The apparent selectivity at 323 K and 8 MPa based on binary data ($\alpha_{23} = 4.6$) was larger than the true selectivity based on ternary data ($\alpha_{23} = 3.6$), thus confirming the need for ternary equilibrium data for the design of deterpenation process (Vieira de Melo et al. 1999). Chafer et al. (2001) reported the composition of the vapor phase only; thus, it was not possible to estimate values of selectivity for the separation of limonene and linalool based on their data.

The use of model systems with a limited number of components is appropriate only as a rough estimate of the behavior of more complex natural mixtures. Because of that, Budich and Brunner (1999) and Budich et al. (1999) recommended the estimation of separation factors and other design parameters for the high-pressure CO_2 deterpenation process by using actual essential oil mixtures. Cold-pressed orange oil is constituted by about 200 components, mainly MTs (~95% w/w) and OMTs. Temelli et al. (1990) measured the solubility in CO_2 of this oil at 313, 323, 333, and 343 K and 8.3, 9.7, 11.0, and 12.4 MPa using a one-pass dynamic method. Experimental results confirmed that CO_2 preferably solubilizes MTs so that the selectivity α_{23} for the separation between limonene (2) and linalool (3), the key components in the MT and OMT fractions, respectively, ranged from 1.10 to 2.83 within the experimental region. Under isothermal conditions, α_{23} reached a maximum at 9.7 MPa and then decreased to a minimum at 12.4 MPa. Temelli et al. (1990) also reported an unusual increment in solubility at 313 K and 12.4 MPa, which they attributed to the formation of a liquid phase, a common occurrence in systems of high-pressure CO_2 and complex liquid mixtures.

Budich and Brunner (1999) studied the equilibrium of CO_2 + orange peel oil at 323, 333, or 343 K and 8–13 MPa. For data analysis they assumed orange peel oil as a binary mixture of 98.25% (w/w) terpenes (*T*, 96.7% w/w limonene) and 1.75% (w/w) oxygenated aroma compounds (*A*, 28.8% w/w linalool). The solubility of the essential oil in high-pressure CO_2 was similar to that of pure limonene, probably because of the elevated content of limonene in orange peel oil. The selectivity α_{TA} ranged from 1.3 to 3.2, which suggests the possibility of

removing the MT fraction using high-pressure CO_2. Under isothermal conditions, α_{TA} decreases as the pressure increases. For low-solubility values (<10 g extract/kg CO_2) α_{TA} decreases with temperature under isobaric conditions because of a more limited increase in the vapor pressure of the OMTs than MTs; for high-solubility values (>50 g extract/kg CO_2) α_{TA} increases with temperature due to the reduction in the density and solvent power of the CO_2; in the intermediate range (10–50 g extract/kg CO_2) there is not a definite trend for the variations in α_{TA} with temperature.

Figure 17.9 compares the values of selectivity measured by Budich et al. (1999) for the multicomponent CO_2 + orange peel oil system at 323 and 333 K with those reported for the CO_2 + limonene + citral or CO_2 + limonene + linalool model systems. For all temperature-solubility pairs, $\alpha_{23} < \alpha_{TA}$, e.g., at 323 K the values of α_{23} reported by de Vieira de Melo et al. (1999) are 25% of the values of α_{TA}, whereas the values of α_{23} reported by de Fonseca et al. (2003) are ~40% of the values of α_{TA}, and at 333 K Morotomi et al. (1999) report values of α_{23} ranging from 16% to 51% of corresponding values of α_{TA} at 333 K. Budich et al. (1999) reported that values of α_{TA} at 333 K and 10 MPa decreased pronouncedly as the content of terpenes in the liquid phase increased, or when replacing the real OMT fraction (α_{TA} ~ 2.2 for a 98.3% w/w MT content in the liquid phase) by pure

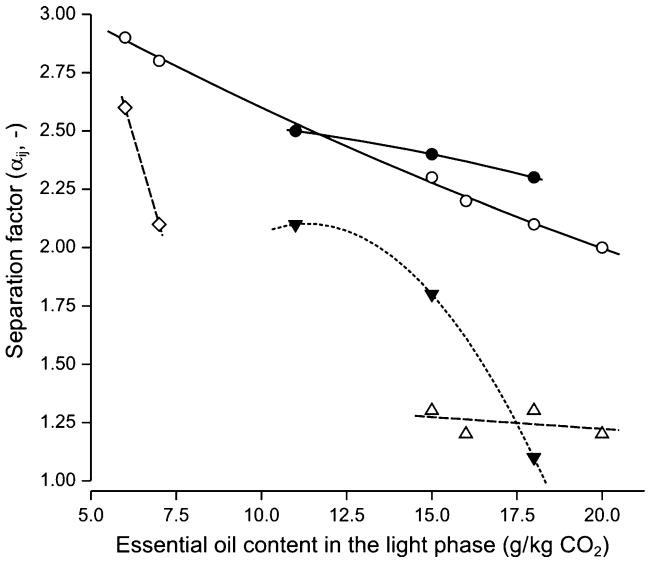

Fig. 17.9 Separation factors between terpenes and aroma (oxygenated) compounds in model and real systems as a function of essential oil concentration in the CO_2 phase: α_{23} for the separation at 323 K of limonene and linalool in a ternary CO_2 + limonene + linalool system reported by (--◇--) Vieira de Melo et al. (1999) and (--△--) Morotomi et al. (1999); (···▼···) α_{23} for the separation at 333 K of limonene and citral in a ternary CO_2 + limonene + citral system (Fonseca et al. 2003); and α_{TA} for the separation at (—○—) 323 K or (—●—) 333 K between terpene and aroma (oxygenated) compounds in orange peel oil (Budich et al. 1999)

linalool ($\alpha_{TA} \sim 1.2$). This result is consistent with the value $\alpha_{23} \sim 1.1$ reported by Morotomi et al. (1999) for the model limonene + linalool system containing 85% w/w MT in the liquid phase. Based on data in Fig. 17.9, Budich et al. (1999) recommended deterpenation of orange oil at $\geq$ 333 K, where both α_{TA} (=1.5) and the solubility of the oil in high-pressure CO_2 are high enough to make the process economical.

17.4.3 Thermodynamic and Operational Solubility in the CO_2 Extraction of Essential Oils

There have been few publications on high-pressure phase equilibria between CO_2 and complex mixtures other than those of Temelli et al. (1990) with cold-pressed orange oil, and those of Budich and Brunner (1999) with orange peel oil. Reported equilibrium isotherms include those of clove bud oil at 303, 308, 313, 318, and 328 K for 5.8–10.8 MPa (Souza et al. 2004); of fennel seed oil at 303, 313, 323, and 333 K for 4.74–21.0 MPa (Moura et al. 2005); of vetiver (*Vetiveria zizanioides*) root oil at 303, 318, and 333 K for 5–30 MPa (Takeuchi et al. 2008); of candeia (*Eremanthus erythropappus*) bark oil at 313, 323, and 333 K for 6.27–25.2 MPa (Teixeira de Souza et al. 2008); and of priprioca (*Cyperus articulatus*) rhizome oil at 313, 323, and 333 K and 4.42–29.9 MPa (Moura et al. 2005). These measurements are usually performed using synthetic methods (Sect. 17.4.1), and are difficult to set up, in that bubble and dew or cloud points are not easily visually identified for complex mixtures of CO_2 and natural extracts. With the exception of vetiver root and priprioca rhizome, these studies complement other studies on SCFE (Table 17.1). Furthermore, besides assisting the analysis of the extraction process, the results of these studies can help to optimize the condition of the separation step of the entire SCFE process. Indeed, the high-pressure phase equilibrium for complex CO_2 + essential oil systems under typical separation conditions in a SCFE plant (e.g., 273–288 K and 2–9 MPa, Reverchon and De Marco 2008) determines the residual solute content in a recycled CO_2 stream, which affects the extraction rate (del Valle et al. 2004), as well as the residual content of CO_2 in the extract, which affected solvent losses during the process (Takeuchi et al. 2008).

Table 17.11 presents the solubilities of essential oil extracts of orange peel, clove bud, fennel seed, and candeia bark under selected temperature and pressure conditions, as taken from the publications of Budich and Brunner (1999), Souza et al. (2004), Moura et al. (2005), and Teixeira de Souza et al. (2008), respectively. Specifically referred to are the values from the *P-y* branch of isotherms in equilibrium diagrams under the conditions where only two phases (a CO_2-rich vapor phase and an essential oil-rich liquid phase) were at equilibrium, which forced the neglect of many data points under conditions where the authors reported partial liquid miscibility. Liquid immiscibility conditions in complex systems result from

Table 17.11 Comparison of estimated thermodynamic solubility and operational solubility for selected studies on high-pressure CO_2 extraction of plant essential oils

Extract	Temperature (T, K)	Pressure (P, MPa)	Solubility (C_{sat}, mg solute/g CO_2)
Orange peel oil			
Limonene (Iwai et al. (1994)	313	7.17	6.2
Linalool (Iwai et al. 1994)	313	7.17	2.1
Model oil mixture[a]	313	7.17	6.0
Actual essential oil (Budich and Brunner 1999)	313	7.17	5.1
Actual essential oil (Budich and Brunner 1999)	313	15	CM*
Ibid. in the presence of substrate (Mira et al. 1996, 1999)	313	15	13.2–19.3
Clove oil			
Eugenol (Cheng et al. 2000)	313	8.06	5.6
β-Caryophyllene (Stahl et al. 1988)	313	8.06	2.3
Model oil mixture[b]	313	8.06	5.0
Actual essential oil (Souza et al. 2004)	313	8.06	11
Ibid. in the presence of substrate (Martínez et al. 2007)	308	10	230
Fennel oil			
Limonene (Iwai et al. 1994)	313	8.02	9.6
Anethole (Stahl et al. 1988)	313	8.02	6
Model oil mixture[c]	313	8.02	5
Actual essential oil (Moura et al. 2005)	313	8.02	26
Ibid. in the presence of substrate (Reverchon et al. 1999)	313	9	2
Candeia oil			
Actual essential oil (Teixeira de Souza et al. 2008)	313	6.17	111
Ibid. in the presence of substrate (Teixeira de Souza et al. 2008)	313	10	4.5

[a]Ideal solubility estimated neglecting interactions between solutes and assuming orange peel oil as a mixture of 98% (w/w) limonene and 2% (w/w) linalool
[b]Ideal solubility estimated neglecting interactions between solutes and assuming clove oil as a mixture of 86% (w/w) eugenol and 14% (w/w) β-caryophyllene
[c]Ideal solubility estimated neglecting interactions between solutes and assuming fennel oil as a mixture of 9% w/w limonene and 91% w/w anethole
*Complete miscibility between the essential oil and high-pressure CO_2

interactions between minor components in the essential oil mixture, and those interactions have large effects on the actual equilibrium. One such effect is a limited dependence on temperature of the equilibrium concentration of the essential oil in the high-pressure CO_2-rich phase. Another effect is unusual variations in essential oil solubility as a function of system temperature and pressure, such as the increase in solubility of cold-pressed orange oil in high-pressure CO_2, as reported by Temelli et al. (1990) at 313 K and 12.4 MPa. Taking further advantage of equilibrium data of essential oils in high-pressure CO_2 collected up to now demands more detailed experimental evidence.

The thermodynamic solubility values reported in Table 17.11 are different from those expected based on measurements for model binary systems of CO_2 and the main MT, OMT, and ST/OST in the actual essential oils. The belief here is that this

finding is due to the effect of minor components in the essential oils which, as mentioned before, interact with each other and the major components in the mixture, thus strongly affecting the equilibrium, as exemplified in the following paragraph.

In general, the solubility of a particular substance in high-pressure CO_2, such as MT or OMT, may be affected by the presence of other substances in the natural product, such as a wax or a triglyceride, which may exhibit a higher or lower solubility in the CO_2. The example of a major MT and a wax is relevant in the particular case of essential oils because, as previously mentioned, they are usually encapsulated within specialized wax-made structures that serve a protective function in herbs (Gaspar et al. 2001). Sovová et al. (2001) reported high-pressure phase equilibria data for a ternary CO_2 + limonene + blackcurrant oil system at 313 K and 8–12 MPa, and showed that the solubility of limonene in high-pressure CO_2 decreased in the presence of triglycerides for pressures up to 20% higher than the critical pressure of the CO_2 + limonene binary mixture ($P_{cm} = 8.44$ MPa).

17.4.4 Operational Solubility and Sorption Phenomena in the CO_2 Extraction of Essential Oils

Figure 17.1b defines the "operational" solubility of plant essential oils as the concentration of the essential oil in high-pressure CO_2 at the outlet of the extraction vessel, provided that CO_2 and the herb or spice reach equilibrium conditions as the CO_2 travels along the vessel, and there is some free solute in the substrate. The initial slope of the cumulative plot of solute yield versus specific CO_2 consumption may represent the actual "operational" solubility only if extraction is preceded by an initial static period to achieve steady temperature and pressure conditions and equilibration between the substrate and the high-pressure CO_2. Table 17.11 shows that the operational solubility (in the presence of the solid substrate) of selected essential oils in high-pressure CO_2 is smaller than the thermodynamic solubility (in the absence of the solid substrate) under equivalent conditions, probably due to binding of the essential oils to the solid matrix or an insufficient amount of essential oils in the herb or spice to saturate the CO_2 (del Valle et al. 2005; Sovová 2005).

Figure 17.10 shows selected values of operational solubility C_{fo} as a function of the ratio between C_{so} and ρ, together with trend lines that can be explained on the basis of either limited availability of the essential oil in the solid matrix or a sufficient amount to saturate the high-pressure CO_2 phase in a case where the essential oil is not bound to the solid matrix. If the porosity of an extraction vessel with an inner volume V packed with a milled herb or spice of inner porosity ε_p is ε, the vessel will contain $V\,[\varepsilon + (1 - \varepsilon)\,\varepsilon_p]\,\rho$ of high-pressure CO_2 at system temperature and pressure (at those conditions the density of the CO_2 is ρ). If the substrate loaded in the extraction vessel (a total weight $V\,(1 - \varepsilon)$

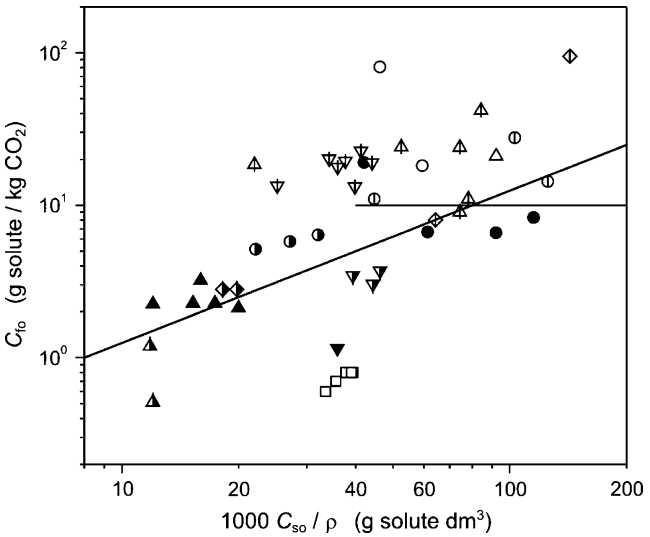

Fig. 17.10 Best-fit values of operational solubility of essential oils in high-pressure CO_2 as a function of the initial essential oil content in the herb or spice. Plotted values include substrates with light essential oils ($v_c \leq 550$ cm^3/mol) extracted with low-density ($\rho \leq 650$ kg/m^3) CO_2 –(○) caraway (Sovová et al. 2004), (△) nutmeg (Machmudah et al. 2006), and (□) sage (Langa et al. 2009) – or high-density ($\rho > 650$ kg/m^3) CO_2 – orange peel (Mira et al. 1996, 1999), (◭) nutmeg (Spricigo et al. 2001; Machmudah et al. 2006), (▽) alecrim pimenta (Sousa et al. 2002), and (◍) aniseed (Rodrigues et al. 2003), as well as substrates with heavy essential oils ($v_c > 550$ cm^3/mol) extracted with low-density ($\rho \leq 650$ kg/m^3) CO_2 –(▼) chamomile (Povh et al. 2001), (●) carqueja (Vargas et al. 2006), and (▲) valerian (Zizovic et al. 2007a) or high-density ($\rho > 650$ kg/m^3) CO_2 (▼) chamomile (Povh et al. 2001), (◑) ginger (Martínez et al. 2003), (◆) marigold (Campos et al. 2005), and (▲) valerian (Zizovic et al. 2007a)

ε_p ρ_s, where ρ_s is the true density of the solid matrix) initially contains a concentration C_{so} of essential oil in a solute-free basis, in a situation where there is not enough solute to saturate the CO_2 following a static extraction period, (17.28) defines the operational solubility:

$$C_{fo} = \frac{1}{\frac{1}{\varepsilon_p}\left(\frac{\varepsilon}{1-\varepsilon}\right) + 1} \frac{\rho_s}{\rho} C_{so} \tag{17.28}$$

where the term $\varepsilon/(1 - \varepsilon)$ represents the ratio of interparticle void volume to apparent particle volume. Equation 17.28 suggests that a plot of C_{fo} versus (C_{so}/ρ) (Fig. 17.10) will result in a straight line with a slope m (17.29):

$$m = \frac{\rho_s}{\frac{1}{\varepsilon_p}\left(\frac{\varepsilon}{1-\varepsilon}\right) + 1} \tag{17.29}$$

On the other hand, if there is enough solute to saturate the CO_2 phase (C_{so}/ρ large), C_{fo} will reach an asymptotic value C_{sat} (the thermodynamic solubility of the complex essential oil mixture in the CO_2 under process conditions). It is difficult to compute the slope m in the absence of precise measurements of the bed porosity (ε), the interparticle porosity (ε_p), and the true density of the matrix (ρ_s), which may vary depending on the substrate and its pretreatment, but the data in Fig. 17.10 were plotted under the simplifying assumption that m changes little between substrates. Regarding the horizontal asymptote, it is important to stress that C_{sat} is a strong function of the essential oil mixture and the system conditions characterized by the temperature and density of the CO_2 (Chrastil 1982).

Figure 17.10 presents selected data that follow the trend suggested by the hypothesis of limited solute in a noninteracting solid matrix. A log–log plot was made to allow a wide range of experimental values in a single plot, and under those conditions a linear relationship such as (17.28) (power relationship with an exponent one) follows a straight line with a unitary slope (such as the trend line included in Fig. 17.10 for values of C_{so}/ρ below 0.05 g dm^3). Fig. 17.10 includes essential oils with relatively low values of critical volume ($V_c \leq 550$ cm^3/mol) enriched in monoterpene hydrocarbons, oxygenated monoterpenes, and related compounds such as those of aniseed, caraway, alecrim pimenta, nutmeg, orange peel, and sage, and extracts with larger values of critical volume ($V_c > 550$ cm^3/mol) that are instead enriched in heavier sesquiterpenes, waxes, and related compounds, such as the extracts of carqueja, chamomile, ginger, marigold, and valerian. Apparently, heavy extracts and essential oils behave the same for low solute contents ($C_{so}/\rho \leq 0.05$ g dm^3) in the solid matrix, as expected; only for high solute contents ($C_{so}/\rho > 0.05$ g dm^3) do the values for heavy extracts level off to an apparent solubility of $C_{sat} \sim 10$ g/kg. Another trend that is apparent in Fig. 17.10 is that the values of C_{fo} for low CO_2 density ($\rho \leq 650$ kg/m^3) tend to be below the values C_{fo} for higher CO_2 densities ($\rho > 650$ kg/m^3), particularly in the upper end of values of C_{so}/ρ, as expected for an increase in solubility with the solvent power of CO_2.

Table 17.12 complements Fig. 17.10, providing values of operational solubility (C_{fo}) reported from studies in Table 17.2 reviewed in this chapter. The data in Fig. 17.10 exhibit scattering because of variations in substrates and their pretreatments, extraction temperatures, and CO_2 densities that are not fully accounted for in the plot, and some additional values in Table 17.12 are not fully consistent with the aforementioned trends. Of all single-measurement C_{fo} values reported in Table 17.12 (boldo, cinnamon of Cunha, fennel, oregano, and pennyroyal), only the one for pennyroyal does not follow the general trends in Fig. 17.10. In the case of rosemary, the data of Coelho et al. (1997) and Bensebia et al. (2009) are inconsistent, and only the C_{fo} values of Coelho et al. (1997), higher, follow the trend lines in Fig. 17.10. The data on clove by Ruetsch et al. (2003) and Martínez et al. (2007) are outside (above and/or to the right) the upper limits selected for Fig. 17.10 and are inconsistent; only the C_{fo} values of Martínez et al. (2007) follow the general trends in Fig. 17.10. The data of Perakis et al. (2005) on black pepper, to the right of the upper limit of C_{so}/ρ (> 0.05 g m^3) in Fig. 17.10, are only slightly below the top

Table 17.12 Summary of operation solubility values in high-pressure CO_2 extraction of plant essential oils studies from Tables 17.1 and 17.2, as a function of the extraction conditions and the initial solute content of the substrates

Substrate	Temperature (T, K)	CO_2 density (ρ, kg/m^3)	Initial solute content (C_{so}, mg solute/g solute-free)	Operational solubility (C_{fo}, mg solute/g CO_2)
Clove (Martínez et al. 2007)	306	713	157	230
Clove (Ruetsch et al. 2003)	323	581	212	34.0
Clove (Ruetsch et al. 2003)	323	288	212	2.50
Orange peel (Mira et al. 1996)	323	700	100.0	95.0
Orange peel (Mira et al. 1996)	323	700	45.0	8.00
Black pepper (Ferreira and Meireles 2002)	313	780	35.8	93.2
Black pepper (Ferreira et al. 1999)	303, 323	698, 847	35.8	89.0–85.8
Black pepper (Ferreira et al. 1999)	303–323	698–847	14.7	35.3–24.2
Black pepper (Perakis et al. 2005)	313, 323	384–780	92.0–155	3.80–2.50
Caraway (Sovová et al. 1994a)	313	623	28.8	80.9
Caraway (Sovová et al. 1994a)	313	484	28.8	18.2
Nutmeg (Spricigo et al. 2001)	296	819	18.0–69.0	67.5
Nutmeg (Machmudah et al. 2006)	313–323	629–780	58.0	24.0–9.00
Parsley (Louli et al. 2004)	318	742	650	33.0
Parsley (Louli et al. 2004)	308, 318	498, 713	120	8.302.80
Cinnamon of Cunhã (Sousa et al. 2005)	288	851	38.5	28.3
Aniseed (Rodrigues et al. 2003)	313	700–836	31.3–105	27.7–11.0
Alecrim pimenta (Sousa et al. 2002)	283–298	728–891	22.4–34.0	22.7–13.2
Carqueja (Vargas et al. 2006)	313–343	208–486	17.5–24.0	19.1–6.60
Celery (Papamichail et al. 2000)	348, 328	498–742	500	8.31–2.12
Celery (Papamichail et al. 2000)	318	498	62.0	2.12
Ginger (Martínez et al. 2003)	293–313	847–905	20.0–25.0	6.41–5.15
Chamomile (Povh et al. 2001)	303, 313	623–809	22.4–34.2	3.71–1.15
Valerian (Zizovic et al. 2007a)	313, 323	384–780	6.14–12.6	3.22–0.511
Marigold (Campos et al. 2005)	313	718, 780	14.2	2.80
Fennel (Reverchon et al. 1999)	323	288	18.3	2.00
Rosemary (Coelho et al. 1997)	308, 313	629–777	7.05	1.98–1.65
Rosemary (Bensebia et al. 2009)	313, 333	290–780	32.0	0.356–0.238
Boldo (Uquiche et al. submitted)	313	632	13.1	1.75
Pennyroyal (Reis-Vasco et al. 2000)	323	384	25.3	1.16
Sage (Langa et al. 2009)	313, 323	384, 486	12.9–19.2	0.800–0.600
Lavender (Akgun et al. 2000)	323	220–670	15.3	0.418–0.234
Oregano (Uquiche et al. submitted)	313	632	6.02	0.390

solubility $C_{sat} \sim 10$ g/kg for heavy extracts. Finally, the data of operational solubility C_{fo} of Ferreira et al. (1999) and Ferreira and Meireles (2002) for black pepper are irregularly high, whereas the data of initial solute content C_{so} of Papamichail et al. (2000) for celery and of Louli et al. (2004) for parsley are too high, considering the typical amount of extractible compounds in those substrates (Moyler 1993).

Goto et al. (1998) showed that the operational solubility of menthol (the main component in the essential oil of mint leaves) is smaller than its thermodynamic solubility in high-pressure CO_2 at 313 K and 13.6 MPa, and suggested that the transfer of menthol to the CO_2 phase was limited by strong interactions between the essential oil and solid matrix. They also claimed weaker interactions between *n*-triacontane (the main component in the cuticular waxes of mint leaves) with the solid matrix than between menthol and the solid matrix because the operational solubility of *n*-triacontane was closer to its thermodynamic solubility than the operational solubility of menthol. As shown in Sect. 17.4.3, solute–solute interactions between the components of the mint leaf extract may be partially responsible for a reduction in the apparent solubilities of menthol and *n*-triacontane in CO_2 when they are a part of a complex essential oil mixture as compared with their corresponding thermodynamic solubilities in the binary CO_2 + menthol or CO_2 + *n*-triacontane systems, but this does not negate the possibility of a reduction in their apparent solubility due to some additional interactions between the solutes and the solid matrix.

The effect of solute binding by the solid matrix, which affects solute availability in SCFE, can be accounted for by an equilibrium sorption isotherm that relates the concentration of solute in the high-pressure CO_2 phase with the residual content of solute in the solid phase (the pretreated herb or spice) under equilibrium conditions. Some authors hypothesize that the operational solubility C_{fo} depends on the substrate and extraction conditions, but does not depend on the solute content in the substrate, as reported in Table 17.12. Other authors hypothesize a constant partition coefficient K (17.20) for essential oils between the high-pressure CO_2 phase and the solid phase, which may correspond to a linear sorption isotherm (17.30a), derived from (17.20) or the initial slope of another sorption isotherm model for a low essential oil content in the pretreated herb or spice, such as the Freundlich (17.30b), Langmuir (17.30c), or Brunauer-Emmett-Teller (BET, (17.30d) models. Finally, selected authors combine the possibility of a constant C_{sat} for large concentrations of essential oil in the solid matrix ($C_{so} > C_{lim}$) and a constant partition coefficient for smaller values of C_{so} ($\leq C_{lim}$) using the so-called isotherm of Perrut et al. (1997). Table 17.13 summarizes the values of the linear partition coefficient K (or equivalent partition coefficient, (17.31)), as reported in studies from Table 17.2 reviewed in this chapter.

The mathematical models for the linear, Freundlich, Langmuir, and BET's sorption isotherms are, respectively, as follows:

$$\bar{C}_s = \frac{C_f}{K} \tag{17.30a}$$

Table 17.13 Summary of values of solute partition coefficients in high-pressure CO_2 extraction of plant essential oils in studies from Tables 17.1 and 17.2, as a function of the extraction conditions and the initial solute content of the substrates

Substrate	Temperature (T, K)	CO_2 density (ρ, kg/m^3)	Initial solute content (C_{so}, mg solute/g solute-free)	Solute partition coefficient (K, –)
Cinnamon of Cunhã (Sousa et al. 2005)	288	851	38.5	2.38–2.00
Carqueja (Vargas et al. 2006)	313	486	20.4	0.813
Carqueja (Vargas et al. 2006)	323	285	17.5	0.694
Carqueja (Vargas et al. 2006)	333	235	21.7	0.104
Carqueja (Vargas et al. 2006)	343	208	24.0	0.067
Clove (Ruetsch et al. 2003)	323	288, 581	212.1	0.314
Clove (Daghero et al. 2004)	323	288, 581	212.1	0.022–0.008
Nutmeg (Machmudah et al. 2006)	313	780	58.0	0.300–0.150
Nutmeg (Machmudah et al. 2006)	323	700, 780	58.0	0.300–0.100
Nutmeg (Machmudah et al. 2006)	318	742	58.0	0.200
Boldo (Uquiche et al. submitted)	313	632	13.1	0.134
Parsley (Louli et al. (2004)	308	713	120	0.067[a]
Parsley (Louli et al. (2004)	318	498, 742	650, 120	0.051–0.023[a]
Parsley (Louli et al. (2004)	308	713	63	0.0099[b]
Parsley (Louli et al. (2004)	318	498, 742	63, 450	0.0076–0.0038[b]
Celery (Papamichail et al. 2000)	328	654	500	0.0605[a]
Celery (Papamichail et al. 2000)	318	498, 742	63, 270	0.0585–0.0471[a]
Celery (Papamichail et al. 2000)	328	654	417	0.0046[b]
Celery (Papamichail et al. 2000)	318	498, 742	417, 476	0.0041–0.00001[b]
Oregano (Uquiche et al. submitted)	313	632	6.02	0.0647
Peppermint (Goto et al. 1993)	313	445, 777	–	0.0506–0.0202
Peppermint (Goto et al. 1993)	333	228, 594	–	0.0331–0.0113
Peppermint (Goto et al. 1993)	353	184, 415	–	0.0248–0.0066
Sage (Langa et al. 2009)	313	486	17.3–19.2	0.047–0.042
Sage (Langa et al. 2009)	323	384	12.9	0.033
Black pepper (Perakis et al. 2005)	313	486, 629	93.0, 134.0	0.0090–0.0025
Black pepper (Perakis et al. 2005)	323	384	84.0	0.0063
Pennyroyal (Sovová 2005)	323	384	25.3	0.063

[a]Sovová's model, model R-SO
[b]Model LDF-UENA

$$\bar{C}_s = \frac{(C_f)^n}{k} \tag{17.30b}$$

$$\bar{C}_s = \frac{k\, C_m C_f}{1 + k\, C_f} \tag{17.30c}$$

$$\bar{C}_s = \frac{k\, C_m C_f}{(C_{sat} - C_f)[C_{sat} + (k-1)C_f]} \tag{17.30d}$$

where k and n are empirical sorption energy parameters, and C_m (the so-called monolayer coverage of the solid surface) is the maximal amount of essential oil that can hold the solid matrix. Ruetsch et al. (2003) and Daghero et al. (2004) arbitrarily assumed that the monolayer coverage corresponded to the initial solute content ($C_m = C_{so}$) in clove. The sorption isotherm models (17.30a–17.30d) are written with C_s instead of C_f as the independent variable because they are adapted from the literature on adsorptive separations. In adsorptive separation processes, where the solute in a fluid phase transfers to a solid phase, there is no upper limit to solute concentration in the fluid phase (for all practical purposes, solute and mobile or fluid phases are mutually miscible), and eventual saturation of the solid matrix imposes an upper limit on the concentration of the solute in the solid for high concentration in the fluid under equilibrium conditions. Depending on the herb or spice and its pretreatment, this upper limit in concentration of solute in the solid substrate is not reached when the concentration of the essential oil in the CO_2 is limited by its solubility under process conditions. Because of that, Ruetsch et al. (2003), Daghero et al. (2004), and Salimi et al. (2008) imposed an upper limit ($C_f \leq C_{sat}$) to the value of solute concentration in the CO_2 phase for high concentrations of solute in the solid phase (Fig. 17.11). Equation 17.31 defines the limit value of K for small value of C_s ($C_s \to 0$) for both Langmuir's and BET's sorption isotherm models (Frendlich's isotherm model predicts limit values, $K = 0$ for $n > 1$ and $K \to \infty$ for $n < 1$):

$$K = \frac{1}{k\, C_m} \tag{17.31}$$

Observation did not reveal special trends in values of the linear partition coefficients (Table 17.13) as a function of the substrate and its essential oil content, the temperature of the system, or the density of the CO_2 (plots not shown). Based on (17.28) for a noninteracting solid matrix, for a packed bed with porosity $\varepsilon = 0.6$, a solid substrate with true density $\rho_s = 1{,}000$ kg/m^3, an inner porosity $\varepsilon_p = 0.1$, and high-pressure CO_2 at 323 K and 9 MPa ($\rho = 287.5$ kg/m^3), the expected value of the partition coefficient in a situation of limited essential oil content in the plant material would be $K = 0.222$, which is between upper and lower limit values reported in Table 17.13. No evidence was found that K increases as the initial essential oil content in the herb or spice increases. Also, no evidence was found that

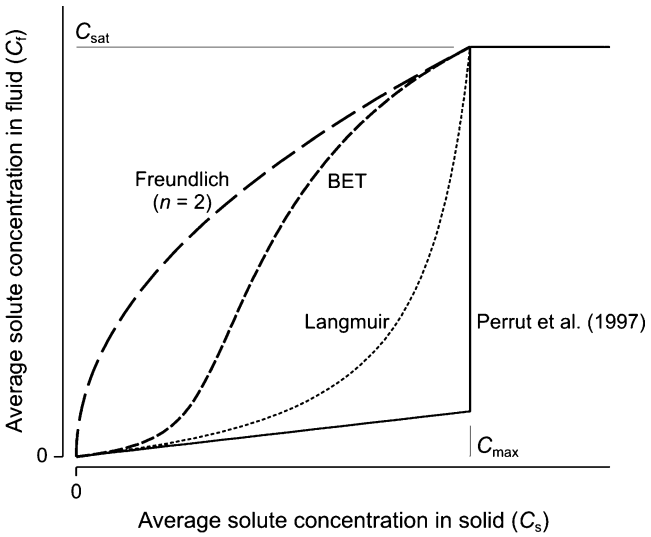

Fig. 17.11 Sorption isotherm models for equilibrium partition of essential oil between high-pressure CO_2 and an herb or a spice as a function of the solute content in the substrate under equilibrium conditions at constant system temperature and pressure

K decreases as the density of the CO_2 increases, as expected (a comparison of (17.28), (17.29), and (17.30a) suggests that $K = m/\rho$ for a situation where the essential oil does not interact with the solid matrix).

17.5 Concluding Remarks

This chapter reviewed mass transfer and phase equilibrium parameters that can be used to design industrial SCFE processes for plant essential oils. Relevant mass transfer parameters include an axial dispersion coefficient (D_{ax}) for the migration of the solute in the SCF along the bed; an external mass transfer coefficient (k_f) for its movement through the stationary SCF film surrounding the solid particles; and an effective diffusivity (D_e) for its movement through the solid matrix, which were computed in the form of a so-called microstructural factor (F_M). This review suggests neglecting axial dispersion effects to simplify the mass transfer models.

Based on this review, it is recommended that SCFE experiments be carried out under forced convection conditions, and that the external mass transfer coefficient (k_f) be estimated using a literature-based correlation between dimensionless variables valid for mass transfer in packed beds operating with SCFs. Best-fitting usually provides underestimations of k_f because of the underestimation of internal resistances to mass transfer, overestimation of the specific surface of the solid

substrate, neglecting of solvent flow heterogeneity effects when using a small D/d_p ratio, and/or neglecting of natural convention effects when using low-*Re* flow conditions.

The values of the microstructural factor for inner mass transfer in the herb or spice estimated in this chapter ranged from $F_M = 10^2$ to $F_M = 10^5$, which suggested pronounced limitations to mass transfer within the solid matrix in the high-pressure CO_2 extraction of plant essential oils. The estimated values of F_M, unlike those expected, depended on the system (temperature, pressure) conditions, the superficial velocity of the CO_2, and/or the particle size of the substrate. Furthermore, for equivalent experiments, the best-fit values of F_M changed dramatically depending on the applied mathematical model, which raised questions about the validity of some of the hypotheses of these mass transfer models. To improve the modeling of high-pressure CO_2 extraction of plant essential oils, extraction experiments should be complemented by measurements using microscopy and allied/complementary techniques to fully characterize the pretreated solid matrix at a relevant scale (Aguilera and Stanley 1999; Zizovic et al. 2005, 2007a, b, c; Stamenić et al. 2008). Such measurements would result in microstructure– extractability relationships, which could be taken advantage of to optimize the pretreatment of the herb or spice samples prior to SCFE.

Regarding phase equilibrium data for designing industrial SCFE processes for plant essential oils, the conclusion here is that their "operational" solubility in high-pressure CO_2 depends markedly on the availability of the solute (the complex essential oil mixture) and its partition between the solid matrix (the herb or spice) and the SCF. The reviewed literature included several phase equilibrium studies using binary systems CO_2 + pure essential oil (mainly MT and OMT) component, few studies using ternary CO_2 + limonene + citral/linalool systems, and limited studies using CO_2 and complex essential oil mixtures (low-pressure CO_2 extracts of herbs or spices). Further advancements in this field will require additional fluid phase equilibrium measurements using binary mixtures of CO_2 and ST or OST compounds, CO_2 + MT + OMT model ternary mixtures representing plant essential oils other than citrus oils, or CO_2 + complex essential oil mixtures. Furthermore, given that the "operational" solubility of essential oils in high-pressure CO_2 does not depend solely on thermodynamic solubility, quantifying the effect of the availability and binding of the solute to the herb or spice demands additional measurements of the solid-SCF phase equilibrium in addition to the aforementioned fluid phase equilibrium data. Because there is no real evidence in the literature that the solute partition between the solid substrate and the SCF is constant, sorption isotherms should be experimentally measured instead of assuming a sorption pattern and achieving best-fit model parameters as part of the data analysis process.

Acknowledgments The present work was funded by the Chilean agency Fondecyt (Regular project 105–0675 and International Cooperation project 703–0033). We are indebted to Verónica Glatzel (PUC) for recalculating from the literature some of the values of external mass transfer coefficient (k_f), and effective diffusivities (D_e) that we report in Sect. 17.3.2 and 17.3.3, respectively; and to Gustavo Lozano (TUHH) for simulating the solubility isotherms for selected

essential oil components included in Figs. 17.7 and 17.8 using the predictive methodology described in Sect. 17.4.1 in PE 2000.

References

Aghel N, Yamini Y, Hadjiakhoondi A, Pourmortazavi SM (2004) Supercritical carbon dioxide extraction of *Mentha pulegium* L. essential oil. Talanta 62:407–411

Aguilera JM, Stanley DW (1999) Microstructural principles of food processing and engineering, 2nd edn. Aspen Publishers, Gaithersburg, MD

Akgun M, Akgun NA, Dincer S (1999) Phase behaviour of essential oil components in supercritical carbon dioxide. J Supercrit Fluids 15:117–125

Akgun M, Akgun NA, Dincer S (2000) Extraction and modeling of lavender flower essential oil using supercritical carbon dioxide. Ind Eng Chem Res 39:473–477

Araus K, Uquiche E, del Valle JM (2009) Matrix effects in supercritical CO_2 extraction of essential oils from plant material. J Food Eng 92:438–447

Bakkali F, Averbeck S, Averbeck D, Zhiri A, Idaomar M (2005) Cytotoxicity and gene induction by some essential oils in the yeast *Saccharomyces cerevisiae*. Mutat Res 585:1–13

Bensebia O, Barth D, Bensebia B, Dahmani A (2009) Supercritical CO_2 extraction of rosemary: Effect of extraction parameters and modelling. J Supercrit Fluids 49:161–166

Benvenuti F, Gironi F (2001) High-pressure equilibrium data in systems containing supercritical carbon dioxide, limonene, and citral. J Chem Eng Data 46:795–799

Berna A, Chafer A, Monton JB (2000) Solubilities of essential oil components of orange in supercritical carbon dioxide. J Chem Eng Data 45:724–727

Brielmann HL, Setzer WN, Kaufman PB, Kirakosyan A, Cseke LJ (2006) Phytochemicals: The chemical components of plants. In: Cseke LJ, Kirakosyan A, Kaufman PB, Warber S, Duke JA, Brielmann HL (eds) Natural products from plants, 2nd edn. CRC Press, Boca Raton, FL, pp 1–49

Brunner G (1984) Mass transfer from solid material in gas extraction. Ber Bunsen Ges Phys Chem 88:887–891

Brunner G (1994) Gas extraction: an introduction to fundamentals of supercritical fluids and the application to separation processes. Springer, New York

Budich M, Brunner G (1999) Vapor–liquid equilibrium data and flooding point measurements of the mixture carbon dioxide + orange peel oil. Fluid Phase Equilib 158–160:759–773

Budich M, Heilig S, Wesse T, Leibküchler V, Brunner G (1999) Countercurrent deterpenation of citrus oils with supercritical CO_2. J Supercrit Fluids 14:105–114

Campos LMAS, Michielin EMZ, Danielski L, Ferreira SRS (2005) Experimental data and modeling the supercritical fluid extraction of marigold (*Calendula officinalis*) oleoresin. J Supercrit Fluids 34:163–170

Carman PC (1937) Fluid flow through granular beds. Trans Inst Chem Eng 15:150–166

Carvalho RN Jr, Corazza ML, Cardozo-Filho L, Meireles MAA (2006) Phase equilibrium for (camphor + CO_2), (camphor + propane), and (camphor + CO_2 + propane). J Chem Eng Data 51:997–1000

Catchpole OJ, King MB (1994) Measurement and correlation of binary diffusion coefficients in near critical fluids. Ind Eng Chem Res 33:1828–1837

Catchpole OJ, Andrews EW, Toikka GN, Wilkinson GT (1994) Mathematical models for the extraction of oils from plant matrices using near-critical solvent. In: Perrut M, Brunner G (eds) Proceedings of the third symposium on supercritical fluids, vol 2. Institut National Polytechnique de Lorraine, Lorraine, France, pp 47–52

Catchpole OJ, Bernig R, Bott MB (1996a) Measurement and correlation of packed-bed axial dispersion coefficients in supercritical carbon dioxide. Ind Eng Chem Res 35:824–828

Catchpole OJ, Grey JB, Smallfield BM (1996b) Near-critical extraction of sage, celery, and coriander seed. J Supercrit Fluids 9:273–279

Chafer A, Berna A, Monton JB, Mulet A (2001) High pressure solubility data of the system limonene plus linalool plus CO_2. J Chem Eng Data 46:1145–1148

Chandler K, Pouillot FLL, Eckert CA (1996) Phase equilibria of alkanes in natural gas systems. 3. Alkanes in carbon dioxide. J Chem Eng Data 41:6–10

Chang CMJ, Chen CC (1999) High-pressure densities and *P–T–x–y* diagrams for carbon dioxide + linalool and carbon dioxide + limonene. Fluid Phase Equilib 163:119–126

Cheng K-W, Kuo S-J, Muoi Tang M, Chen Y-P (2000) Vapor–liquid equilibria at elevated pressures of binary mixtures of carbon dioxide with methyl salicylate, eugenol, and diethyl phthalate. J Supercrit Fluids 18:87–99

Chrastil J (1982) Solubility of solids and liquids in supercritical gases. J Phys Chem 86: 3016–3021

Coelho JAP, Mendes RL, Provost MC, Cabral JMS, Novais JM, Palavra AMF (1997) Supercritical carbon dioxide extraction of volatile compounds from rosemary. In: Abraham MA, Sunol AK (eds) Supercritical fluids. Extraction and pollution prevention. American Chemical Society, Washington, DC, pp 101–109

Coelho JAP, Pereira AP, Mendes RL, Palavra AMF (2003) Supercritical carbon dioxide extraction of *Foeniculum vulgare* volatile oil. Flavour Frag J 18:316–319

Crank J (1975) The mathematics of diffusion, 2nd edn. Oxford University Press, New York

Cygnarowicz-Provost M (1996) Design and economic analysis of supercritical fluid extraction processes. In: King JW, List GR (eds) Supercritical fluid technology in oil and lipid chemistry. AOCS Press, Champaign, IL, pp 155–179

Daghero J, Ruetsch L, Zacchi P, Mattea M (2004) Supercritical CO_2 extraction of herbaceous matrices. Pilot plant experiments and modeling. V Encuentro Brasileño sobre Fluidos Supercríticos (EBFS 2004), Florianopolis, Brasil

Danielski L, Campos LMAS, Bresciani LFV, Hense H, Yunes RA, Ferreira SRS (2007) Marigold (*Calendula officinalis* L.) oleoresin: solubility in SC-CO_2 and composition profile. Chem Eng Process 46:99–106

Daubert TE, Danner RP (1989) Physical and thermodynamic properties of pure chemicals: data compilation. Hemisphere Publishers, New York

del Valle JM, Aguilera JM (1999) Extracción con CO_2 a alta presión. Fundamentos y aplicaciones en la industria de alimentos. Food Sci Technol Int 5:1–24

del Valle JM, Catchpole OJ (2005) Transferencia de masa en lechos empacados operando con fluidos supercríticos. I. Correlación de coeficientes de dispersión axial. XVI Congreso Chileno de Ingeniería Química, Pucón, Chile

del Valle JM, de la Fuente JC, Cardarelli DA (2005) Contributions to supercritical extraction of vegetable substrates in Latin America. J Food Eng 67:35–57

del Valle JM, de la Fuente JC (2006) Supercritical CO_2 extraction of oilseeds: Review of kinetic and equilibrium models. CRC Crit Rev Food Sci Nutr 46:131–160

del Valle JM, Rivera O, Mattea M, Ruetsch L, Daghero J, Flores A (2004) Supercritical CO_2 processing of pretreated rosehip seeds: Effect of process scale on oil extraction kinetics. J Supercrit Fluids 31:159–174

del Valle JM, Mena C, Budinich M (2008) Extraction of garlic with supercritical CO_2 and conventional organic solvents. Braz J Chem Eng 25:535–542

Della Porta G, Taddeo R, D'urso E, Reverchon E (1998) Isolation of clove bud and star anise essential oil by supercritical CO_2 extraction. Lebensm Wiss Technol 31:454–460

Della Porta G, Porcedda S, Marongiu B, Reverchon E (1999) Isolation of eucalyptus oil by supercritical fluid extraction. Flavour Frag J 14:214–218

Denny EFK (1991) Field distillation for herbaceous oils, 2nd edn. Denny, McKenzie Associates, Lilydale (Tasmania), Australia

di Giacomo G, Brandani V, del Re G, Mucciante V (1989) Solubility of essential oil components in compressed supercritical carbon dioxide. Fluid Phase Equilib 52:405–411

Dullien F (1992) Porous media. Fluid transport and pore structure, 2nd edn. Academic, San Diego, CA

Eggers R (1996) Supercritical fluid extraction of oilseeds/lipids in natural products. In: King JW, List GR (eds) Supercritical fluid technology in oil and lipid chemistry. AOCS Press, Champaign, IL, pp 35–64

Eggers R, Ambrogi A, von Schnitzler J (2000) Special features of SFC solid extraction of natural products: Deoling of wheat gluten and extraction of rose hip oil. Braz J Chem Eng 17:329–334

Espinosa-Díaz MA, Guetachew T, Landy P, Jose J, Voilley A (1999) Experimental and estimated saturated vapor pressure of aroma compounds. Fluid Phase Equilib 157:257–270

Esquivel MM, de Sousa CL, Ribeiro MA, Bernardo-Gil MG (1996) Mathematical models for supercritical extraction of oregano "*Origanum virens* L.". In: von Rohr PR, Trepp C (eds) High pressure chemical engineering. Elsevier, Amsterdam, The Netherlands, pp 525–530

Fahien RW, Smith JM (1955) Mass transfer in packed beds. Am Inst Chem Eng J 1:28–37

Ferreira SRS, Meireles MAA (2002) Modeling the supercritical fluid extraction of black pepper (*Piper nigrum* L.) essential oil. J Food Eng 54:263–269

Ferreira SRS, Nikolov ZL, Doraiswamy LK, Meireles MAA, Petentate A (1999) Supercritical fluid extraction of black pepper (*Piper nigrum* L.) essential oil. J Supercrit Fluids 14:235–245

Fonseca J, Simoes PC, Nunes da Ponte M (2003) An apparatus for high-pressure VLE measurements using a static mixer. Results for (CO_2 + limonene + citral) and (CO_2 + limonene + linalool). J Supercrit Fluids 25:7–17

Francisco JD, Sivik B (2002) Solubility of three monoterpenes, their mixtures and eucalyptus leaf oils in dense carbon dioxide. J Supercrit Fluids 23:11–19

Funazukuri T, Kong C, Kagei S (1998) Effective axial dispersion coefficients in packed beds under supercritical conditions. J Supercrit Fluids 13:169–175

Gamse T, Marr R (2000) High-pressure phase equilibria of the binary systems carvone-carbon dioxide and limonene-carbon dioxide at 303, 313 and 323 K. Fluid Phase Equilib 171:165–174

Gardner DS (1993) Commercial scale extraction of alpha acids and hop oils with compressed CO_2. In: King MB, Bott TR (eds) Extraction of natural products using near-critical solvents. Blackie Academic & Professional, London, UK, pp 84–100

Gaspar F (2002) Extraction of essential oils and cuticular waxes with compressed CO_2: Effect of extraction pressure and temperature. Ind Eng Chem Res 41:2497–2503

Gaspar F, Santos R, King MB (2001) Disruption of glandular trichomes with compressed CO_2: Alternative matrix pre-treatment for CO_2 extraction of essential oils. J Supercrit Fluids 21:11–22

Gaspar F, Lu T, Santos R, Al-Duri B (2003) Modelling the extraction of essential oils with compressed carbon dioxide. J Supercrit Fluids 25:247–260

Germain JC, del Valle JM, de la Fuente JC (2005) Natural convection retards supercritical CO_2 extraction of essential oils and lipids from vegetable substrates. Ind Eng Chem Res 44:2879–2886

Ghoreishi SM, Akgerman A (2004) Dispersion coefficients of supercritical fluid in fixed beds. Sep Purif Technol 39:39–50

Gironi F, Maschietti M (2008) Continuous countercurrent deterpenation of lemon essential oil by means of supercritical carbon dioxide: experimental data and process modeling. Chem Eng Sci 63:651–661

Goodarznia I, Eikani M (1998) Supercritical carbon dioxide extraction of essential oils: Modelling and simulation. Chem Eng Sci 53:1387–1395

Goto M, Sato M, Hirose T (1993) Extraction of peppermint oil by supercritical carbon dioxide. J Chem Eng Jpn 26:401–407

Goto M, Roy BC, Hirose T (1996) Shrinking-core leaching model for supercritical-fluid extraction. J Supercrit Fluids 9:128–133

Goto M, Roy B, Kodama A, Hirose T (1998) Modeling supercritical fluid extraction process involving solute-solid interaction. J Chem Eng Jpn 32:171–177

Hall HK (ed) (2001) Landolt-Börnstein: Numerical data and functional relationships in science and technology – New Series. Group 4: Physical chemistry, Vol. 20: Vapor pressure of chemicals. Subvolume B: Vapor pressure and antoine constants for oxygen containing organic compounds. Springer, Berlin, Germany

Han N-H, Bhakta J, Carbonell RG (1985) Longitudinal and lateral dispersion in packed beds: effect of column length and particle size distribution. Am Inst Chem Eng J 31:277–288

Helmig D, Revermann T, Pollmann J, Kaltschmidt O, Jiménez-Hernández A, Bocquet F, David D (2003) Calibration system and analytical considerations for quantitative sesquiterpene measurements in air. J Chromatogr A 1002:193–211

Hong IK, Rho SW, Lee KS, Lee WH, Yoo KP (1990) Modeling of soybean oil bed extraction with supercritical carbon dioxide. Korean J Chem Eng 7:40–46

Hubert P, Vitzthum OG (1978) Fluid extraction of hops, spices and tobacco with supercritical gases. Angew Chem Int Ed Engl 17:710–715

Hybertson BM (2007) Solubility of the sesquiterpene alcohol patchoulol in supercritical carbon dioxide. J Chem Eng Data 52:235–238

Iwai Y, Hosotani N, Morotomi T, Koga Y, Arai Y (1994) High-pressure vapor-liquid-equilibria for carbon-dioxide plus linalool. J Chem Eng Data 39:900–902

Iwai Y, Morotomi T, Sakamoto K, Koga Y, Arai Y (1996) High-pressure vapor-liquid equilibria for carbon dioxide plus limonene. J Chem Eng Data 41:951–952

Jimenez-Carmona MM, Ubera JL, Luque de Castro MD (1999) Comparison of continous subcritical water extraction and hydrodistillation of marjoram essential oil. J Chromatogr A 855:625–632

Kim KH, Hong J (1999) Equilibrium solubilities of spearmint oil components in supercritical carbon dioxide. Fluid Phase Equilib 164:107–115

Kim KH, Hong J (2002) A mass transfer model for super- and near-critical CO_2 extraction of spearmint leaf oil. Sep Sci Technol 37:2271–2288

King MB, Catchpole O (1993) Physico-chemical data required for the design of near-critical fluid extraction process. In: King MB, Bott TR (eds) Extraction of natural products using near-critical solvents. Blackie Academic & Professional, London, UK, pp 184–231

Kotnik P, Skerget M, Knez Z (2007) Supercritical fluid extraction of chamomile flower heads: Comparison with conventional extraction, kinetics and scale-up. J Supercrit Fluids 43: 192–198

Lack E, Seidlitz H (1993) Commercial scale decaffeination of coffee and tea using supercritical CO_2. In: King MB, Bott TR (eds) Extraction of natural products using near-critical solvents. Blackie Academic & Professional, London, UK, pp 101–139

Langa E, Della Porta G, Palavra AMF, Urieta JS, Mainar A (2009) Supercritical fluid extraction of Spanish sage essential oil: Optimization of the process parameters and modelling. J Supercrit Fluids 49:174–181

Lee CH, Holder GD (1995) Use of supercritical fluid chromatography for obtaining mass transfer coefficients in fluid-solid systems at supercritical conditions. Ind Eng Chem Res 34:906–914

Leeke GA, Santos R, King M (2001) Vapor-liquid equilibria for the carbon dioxide plus carvacrol system at elevated pressures. J Chem Eng Data 46:541–545

Louli V, Folas G, Voutsas E, Magoulas K (2004) Extraction of parsley seed oil by supercritical CO_2. J Supercrit Fluids 30:163–174

Ma YH, Evans LB (1968) Transient diffusion from a well-stirred reservoir to a body of arbitrary shape. J Am Inst Chem Eng 14:956–961

Machmudah S, Sulaswatty A, Sasaki M, Goto M, Hirose T (2006) Supercritical CO_2 extraction of nutmeg oil: Experiments and modeling. J Supercrit Fluids 39:30–39

Marrone C, Poletto M, Reverchon E, Stassi A (1998) Almond oil extraction by supercritical CO_2: Experiments and modelling. Chem Eng Sci 53:3711–3718

Marteau Ph, Obriot J, Tufeu R (1995) Experimental determination of vapor-liquid equilibria of CO_2 + limonene and CO_2 + citral mixtures. J Supercrit Fluids 8:20–24

Martin AJP, Synge R (1941) A new form of chromatogram employing two liquid phases. 1. A theory of chromatography. 2. Application to the micro-determination of the higher mono-amino-acids in proteins. Biochem J 35:1358–1368

Martínez J, Monteiro AR, Rosa PTV, Marques MOM, Meireles M (2003) Multicomponent model to describe extraction of ginger oleoresin with supercritical carbon dioxide. Ind Eng Chem Res 42:1057–1063

Martínez J, Rosa PTV, Meireles MAA (2007) Extraction of clove and vetiver oils with supercritical carbon dioxide: modeling and simulation. Open Chem Eng J 1:1–7

Matos HA, Gomes de Azevedo E, Simoes PC, Carrondo MT, Nunes da Ponte M (1989) Phase equilibria of natural flavours and supercritical solvents. Fluid Phase Equilib 52:357–364

Michielin EMZ, Rosso SR, Franceschi E, Borges GR, Corazza ML, Oliveira JV, Ferreira SRS (2009) High-pressure phase equilibrium data for systems with carbon dioxide, α-humulene and *trans*-caryophyllene. J Chem Thermodyn 41:130–137

Mira B, Blasco M, Subirats S, Berna A (1996) Supercritical CO_2 extraction of essential oils from orange peel. J Supercrit Fluids 9:238–243

Mira B, Blasco M, Berna A, Subirats S (1999) Supercritical CO_2 extraction of essential oil from orange peel. Effect of operation conditions on the extract composition. J Supercrit Fluids 14:95–104

Miraldi E, Ferri S, Franchi GG, Giorgi G (1996) *Peumus boldus* essential oil: New constituents and comparison of oils from leaves of different origin. Fitoterapia 67:227–230

Mišić D, Zizovic I, Stamenić M, Ašanin R, Ristić M, Petrović SD, Skala D (2008) Antimicrobial activity of celery fruit isolates and SFE process modeling. Biochem Eng J 42:148–152

Morotomi T, Iwai Y, Yamaguchi H, Arai Y (1999) High-pressure vapor-liquid equilibria for carbon dioxide plus limonene plus linalool. J Chem Eng Data 44:1370–1372

Moura LS, Corazza ML, Cardozo-Filho L, Meireles MAA (2005) Phase equilibrium measurements for the system fennel (*Foeniculum vulgare*) extract + CO_2. J Chem Eng Data 50:1657–1661

Moyler DA (1993) Extraction of flavours and fragrances with compressed CO_2. In: King MB, Bott TR (eds) Extraction of natural products using near-critical solvents. Blackie Academic & Professional, London, UK, pp 140–183

Mukhopadhyay M (2000) Natural extracts using supercritical carbon dioxide. CRC Press, Boca Raton, FL

Mukhopadhyay M, De SK (1995) Fluid-phase behavior of close molecular-weight fine chemicals with supercritical carbon dioxide. J Chem Eng Data 40:909–913

NIST (2000) Fluid Thermodynamic and Transport Properties (version 5.0). http://www.nist.gov/srd/nist23.htm

Núñez GA, del Valle JM, de la Fuente JC (2010) Solubilities in supercritical carbon dioxide of (2E,6E)-3,7,11-trimethyldodeca-2,6,10-trien-1-ol (farnesol) and (2 S)-5,7-dihydroxy-2-(4-hydroxyphenyl)chroman-4-one (naringenin). J Chem Eng Data 55:3863–3868

Özer EÖ, Platin S, Akman U, Hortaçsu Ö (1996) Supercritical carbon dioxide extraction of spearmint oil from mint-plant leaves. Can J Chem Eng 74:920–928

Papamichail I, Louli V, Magoulas K (2000) Supercritical fluid extraction of celery seed oil. J Supercrit Fluids 18:213–226

Pavlicek J, Richter M (1993) High pressure vapour-liquid equilibrium in the carbon dioxide–α-pinene system. Fluid Phase Equilib 90:125–133

Perakis C, Louli V, Magoulas K (2005) Supercritical fluid extraction of black pepper oil. J Food Eng 71:386–393

Perrut M, Clavier JY, Poletto M, Reverchon E (1997) Mathematical modeling of sunflower seed extraction by supercritical CO_2. Ind Eng Chem Res 36:430–435

Pfaf-Šovljanski II, Grujić OS, Peruničić MB, Cvetković IM, Zeković Z (2005) Supercritical carbon dioxide hop extraction. APTEFF 36:111–120

Pfohl O, Petkov S, Brunner G (2000) PE 2000: a powerful tool to correlate phase equilibria. Herbert Utz Verlag, München, Germany

Podlaski S, Chrobak Z, Wyszkowska Z (2003) The effect of parsley seed hydration treatment and pelleting on seed vigour. Plant Soil Environ 49:114–118
Poling BE, Prausnitz JM, O'Connell J (2000) The properties of gases and liquids, 5th edn. McGraw-Hill, New York
Povh NP, Marques MOM, Meireles MAA (2001) Supercritical CO_2 extraction of essential oil and oleoresin from chamomile (*Chamomilla recutita* L.). J Supercrit Fluids 21:245–256
Puiggené J, Larrayoz MA, Recasens F (1997) Free liquid-to-supercritical fluid mass transfer in packed beds. Chem Eng Sci 52:195–212
Quirin K-W, Gerard D (2007) Supercritical fluid extraction (SFE). In: Ziegler H (ed) Flavourings: production, composition, applications, regulations, 2nd edn. Wiley-VCH, Weinheim, Germany, pp 49–65
Raal JD, Mühlbauer AL (1998) Phase equilibria: measurement and computation. Taylor & Francis, Washington, DC
Raeissi S, Peters CJ (2005) Experimental determination of high-pressure phase equilibria of the ternary system carbon dioxide + limonene + linalool. J Supercrit Fluids 35:10–17
Reis-Vasco EMC, Coelho JAP, Palavra AMF, Marrone C, Reverchon E (2000) Mathematical modelling and simulation of pennyroyal essential oil supercritical extraction. Chem Eng Sci 55:2917–2922
Reverchon E (1996) Mathematical modeling of supercritical extraction of sage oil. J Am Inst Chem Eng 42:1765–1771
Reverchon E (1997) Supercritical fluid extraction and fractionation of essential oils and related products. J Supercrit Fluids 10:1–37
Reverchon E, De Marco I (2006) Supercritical fluid extraction and fractionation of natural matter. J Supercrit Fluids 38:146–166
Reverchon E, De Marco I (2008) Essential oils extraction and fractionation using supercritical fluids. In: Martínez JL (ed) Supercritical fluid extraction of nutraceuticals and bioactive compounds. CRC Press, Boca Raton, FL, pp 305–335
Reverchon E, Marrone C (1997) Supercritical extraction of clove bud essential oil: Isolation and mathematical modeling. Chem Eng Sci 52:3421–3428
Reverchon E, Sesti Osséo L (1994a) Modelling the supercritical extraction of basil oil. In: Perrut M, Brunner G (eds) Proceedings of the third symposium on supercritical fluids, Vol. 2., pp 189–196
Reverchon E, Sesti Osséo L (1994b) Supercritical CO_2 extraction of basil oil: Characterization of products and process modeling. J Supercrit Fluids 7:185–190
Reverchon E, Donsi G, Sesti Osséo L (1993a) Modeling of supercritical fluid extraction from herbaceous matrices. Ind Eng Chem Res 32:2721–2726
Reverchon E, Russo P, Stassi A (1993b) Solubilities of solid octacosane and triacontane in supercritical carbon dioxide. J Chem Eng Data 38:458–460
Reverchon E, Della Porta G, Senatore F (1995a) Supercritical CO_2 extraction and fractionation of lavender essential oil and waxes. J Agr Food Chem 43:1654–1658
Reverchon E, Taddeo R, Della Porta G (1995b) Extraction of sage oil by supercritical CO2: Influence of some process parameters. J Supercrit Fluids 8:302–309
Reverchon E, Daghero J, Marrone C, Mattea M, Poletto M (1999) Supercritical fractional extraction of fennel seed oil and essential oil: Experiments and mathematical modeling. Ind Eng Chem Res 38:3069–3075
Richter M, Sovová H (1993) The solubility of 2 monoterpenes in supercritical carbon-dioxide. Fluid Phase Equilib 85:285–300
Rodrigues VM, Rosa PTV, Marques MOM, Petenate AJ, Meireles MAA (2003) Supercritical extraction of essential oil from aniseed (*Pimpinella anisum* L.) using CO_2: Solubility, kinetics, and composition data. J Agric Food Chem 51:1518–1523
Roy BC, Goto M, Hirose T (1996) Extraction of ginger oil with supercritical carbon dioxide: Experiments and modeling. Ind Eng Chem Res 35:607–612
Ruetsch L, Daghero J, Mattea M (2003) Supercritical extraction of solid matrices. Model formulation and experiments. Lat Am Appl Res 33:103–107

Salimi A, Fatemi S, Zakizadeh Nei Nei H, Safaralie A (2008) Mathematical modeling of supercritical extraction of valerenic acid from *Valeriana officinalis* L. Chem Eng Technol 31:1470–1480

Sanders N (1993) Food legislation and the scope for increased use of near-critical fluid extraction operations in the food, flavouring and pharmaceutical industries. In: King MB, Bott TR (eds) Extraction of natural products using near-critical solvents. Blackie Academic & Professional, London, UK, pp 34–49

Sefidkon F, Dabiri M, Mirmostafa SA (2004) The composition of *Thymus serpyllum* L. oil. J Essent Oil Res 16:184–185

Serrato-Valenti G, Bisio A, Cornara L, Ciarallo G (1997) Structural and histochemical investigation of the glandular trichomes of *Salvia aurea* L. leaves, and chemical analysis of the essential oil. Ann Bot 79:329–336

Simandi B, Deák A, Rónyai E, Yanxiang G, Veress T, Lemberkovics E, Then M, Saa-Kiss A, Vámos-Falusi Z (1999) Supercritical carbon dioxide extraction and fractionation of fennel oil. J Agric Food Chem 47:1635–1640

Simões-Pires CA, Debenedetti S, Spegazzini E, Mentz LA, Matzenbacher NI, Limberger RP, Henriques A (2005) Investigation of the essential oil from eight species of *Baccharis* belonging to sect. Caulopterae (Asteraceae, Astereae): A taxonomic approach. Plant Syst Evol 253:23–32

Skerget M, Knez Z (2001) Modelling high pressure extraction processes. Comput Chem Eng 25:879–886

Sousa EMBD, Chiavone-Filho O, Moreno MT, Silva DN, Marques MOM, Meireles MAA (2002) Experimental results for the extraction of essential oil from *Lippia sidoides* Cham. using pressurized carbon dioxide. Braz J Chem Eng 19:229–241

Sousa EMBD, Martínez J, Chiavone-Filho O, Rosa PTV, Domingos T, Meireles MAA (2005) Extraction of volatile oil from *Croton zehntneri* Pax et Hoff with pressurized CO_2: Solubility, composition and kinetics. J Food Eng 69:325–333

Souza AT, Corazza ML, Cardozo-Filho L, Guirardello R, Meireles MAA (2004) Phase equilibrium measurements for the system clove (*Eugenia caryophyllus*) oil + CO_2. J Chem Eng Data 49:352–356

Sovová H (1994) Rate of the vegetable oil extraction with supercritical CO_2.1. Modeling of extraction curves. Chem Eng Sci 49:409–414

Sovová H (2005) Mathematical model for supercritical fluid extraction of natural products and extraction curve evaluation. J Supercrit Fluids 33:35–52

Sovová H, Jež J (1994) Solubility of menthol in supercritical carbon-dioxide. J Chem Eng Data 39:840–841

Sovová H, Komers R, Kucera J, Jež J (1994a) Supercritical carbon dioxide extraction of caraway essential oil. Chem Eng Sci 49:2499–2505

Sovová H, Kucera J, Jez J (1994b) Rate of vegetable oil extraction with supercritical CO_2. 2. Extraction of grape oil. Chem Eng Sci 49:415–420

Sovová H, Stateva RP, Galushko AA (2001) Essential oils from seeds: Solubility of limonene in supercritical CO_2 and how it is affected by fatty oil. J Supercrit Fluids 20:113–129

Sovová H, Stateva RP, Galushko AA (2007) High-pressure equilibrium of menthol + CO_2. J Supercrit Fluids 41:1–9

Spricigo CB, Pinto LT, Bolzan A, Novais AF (1999) Extraction of essential oil and lipids from nutmeg by liquid carbon dioxide. J Supercrit Fluids 15:253–259

Spricigo CB, Bolzan A, Pinto LT (2001) Mathematical modeling of nutmeg essential oil extraction by liquid carbon dioxide. Lat Am Appl Res 31:397–401

Stahl E, Quirin K-W, Gerard D (1988) Dense gases for extraction and refining. Springer-Verlag, Berlin, Germany

Stamenić M, Zizovic I, Orlović A, Skala D (2008) Mathematical modelling of essential SFE on the micro-scale. Classification of plant material. J Supercrit Fluids 46:285–292

Stassi A, Schiraldi A (1994) Solubility of vegetable cuticular waxes in supercritical CO_2 isothermal calorimetry investigations. Thermochim Acta 246:417–425

Šťastová J, Jež J, Bartlová M, Sovová H (1996) Rate of vegetable oil extraction with supercritical CO_2. 3. Extraction from sea buckthorn. Chem Eng Sci 51:4347–4352
Steffani E, Atti-Santos AC, Atti-Serafini L, Pinto LT (2006) Extraction of ho-sho (*Cinnamomum camphora* Nees and Eberm var. *Linaloolifera fujita*) essential oil with supercritical CO_2: Experiments and modeling. Braz J Chem Eng 23:259–266
Stüber F, Vázquez AM, Larrayoz MA, Recasens F (1996) Supercritical fluid extraction of packed beds: External mass transfer in upflow and downflow operation. Ind Eng Chem Res 35:3618–3628
Stüber F, Julien S, Recasens F (1997) Internal mass transfer in sintered metallic pellets filled with supercritical fluid. Chem Eng Sci 52:3527–3542
Stull DR (1947) Vapor pressures of pure substances organic compounds. Ind Eng Chem 39:517–540
Svoboda K, Svoboda T (2000) Secretory structures of aromatic and medicinal plants. A review and atlas of micrographs. Microscopix Publications, Knighton, UK
Takeuchi TM, Leal PF, Favareto R, Cardozo-Filho L, Corazza ML, Rosa PTV, Meireles MAA (2008) Study of the phase equilibrium formed inside the flash tank used at the separation step of a supercritical fluid extraction unit. J Supercrit Fluids 43:447–459
Tan CS, Liou DC (1989) Axial dispersion of supercritical carbon dioxide in packed beds. Ind Eng Chem Res 28:1246–1250
Tan CS, Liang SK, Liou DC (1988) Fluid-solid mass transfer in a supercritical fluid extractor. Chem Eng J 38:17–22
Teixeira de Souza A, Benazzia T, Boer Grings M, Cabral V, da Silva E, Cardozo-Filho L, Ceva Antunes O (2008) Supercritical extraction process and phase equilibrium of candeia (*Eremanthus erythropappus*) oil using supercritical carbon dioxide. J Supercrit Fluids 47:182–187
Temelli F, O'Connell JP, Chen CS, Braddock RJ (1990) Thermodynamic analysis of supercritical carbon dioxide extraction of terpenes from cold-pressed orange oil. Ind Eng Chem Res 29:618–624
The Good Scents Company (2009a) http://www.thegoodscentscompany.com/data/rw1060851.html
The Good Scents Company (2009b) http://www.thegoodscentscompany.com/data/rw1005091.html
Tufeu R, Subra P, Plateaux C (1993) Contribution to the experimental determination of the phase diagrams of some (carbon dioxide + a terpene) mixtures. J Chem Thermodyn 25:1219–1228
Uquiche E, Huerta E, Sandoval A, del Valle JM. Effect of boldo (*Peumus boldus* M.) pretreatment on the kinetics of supercritical CO_2 essential oil extraction. J Food Eng (submitted)
Vargas RMF, Cassel E, Gomes GMF, Longhi LGS, Atti-Serafini L, Atti-Santos AC (2006) Supercritical extraction of *carqueja* essential oil: Experiments and modeling. Braz J Chem Eng 23:375–382
Vieira de Melo SAB, Pallado P, Guarise GB, Bertucco A (1999) High-pressure vapor-liquid equilibrium data for binary and ternary systems formed by supercritical CO_2, limonene and linalool. Braz J Chem Eng 16:7–17
Villermaux J (1987) Chemical engineering approach to dynamic modelling of linear chromatography: A flexible method for representing complex phenomena from simple concepts. J Chromatogr A 406:11–26
Wagner Z, Pavlicek J (1993) Vapour-liquid equilibrium in the carbon dioxide: p-cymene system at high pressure. Fluid Phase Equilib 90:135–141
Wakao N, Kaguei S (1982) Heat and mass transfer in packed beds. Gordon & Breach, New York
Wakao N, Smith JM (1962) Diffusion in catalyst pellets. Chem Eng Sci 17:825–834
Xing H, Yang Y, Su B, Huang M, Ren Q (2003) Solubility of artemisinin in supercritical carbon dioxide. J Chem Eng Data 48:330–332
Yu D (1998) Solute pulse dispersion in soil columns: a comparison of supercritical CO_2, gaseous and aqueous systems. Ph.D. thesis, University of California at Los Angeles, CA

Zekovic Z, Lepojevic Z, Tolic A (2001) Modeling of the thyme-supercritical carbon dioxide extraction system. I. The influence of carbon dioxide flow rate and grinding degree of thyme. Sep Sci Technol 36:2459–3472

Zetzl C, Brunner G, Meireles MAA (2003) Standardized low-cost batch SFE-units for university education and comparative research. In: Brunner G, Kikic I, Perrut M (eds) Proceedings of the 6th international symposium on supercritical fluids. Institut National Polytechnique de Lorraine, Lorraine, France, pp 577–585

Zizovic I, Stamenić M, Orlović A, Skala D (2005) Supercritical carbon dioxide essential oil extraction of Lamiaceae family species: Mathematical modelling on the micro-scale and process optimization. Chem Eng Sci 60:6747–6756

Zizovic I, Stamenić M, Ivanović J, Orlović A, Ristić M, Djordjević S, Petrović SD, Skala D (2007a) Supercritical carbon dioxide extraction of sesquiterpenes from valerian root. J Supercrit Fluids 43:249–258

Zizovic I, Stamenić M, Orlović A, Skala D (2007b) Supercritical carbon dioxide extraction of essential oils from plants with secretory ducts: Mathematical modelling on the micro-scale. J Supercrit Fluids 39:338–346

Zizovic IT, Stamenić MD, Orlović AM, Skala DU (2007c) Supercritical carbon-dioxide extraction of essential oils and mathematical modelling on the micro-scale. In: Berton LP (ed) Chemical engineering research trends. Nova Science Publishers, New York, pp 221–249

Part III
Water Management in Food

Chapter 18
Glass Transitions: Opportunities and Challenges

Yrjö H. Roos and Nattiga Silalai

18.1 Introduction

Glass transition is a well-known transformation of the solid-fluid states of noncrystalline solids and liquids. In food systems the glass transition is often a property of carbohydrates and proteins, as observed in numerous food materials (White and Cakebread 1966; Slade and Levine 1995). Glass transition results in various physicochemical and thermal phenomena associated with the solid–liquid transformation of a supercooled liquid. A number of noncrystalline polymers, as well as sugar melts, exhibit glass transition at approximately 100–150°C below their equilibrium melting temperature (Roos 1993). The glass transition of low water and frozen foods has been recognized as one of the most important factors affecting food properties, processing characteristics, and shelf life (Roos 1995a). Glass transition contributes to numerous engineering properties of foods, their structure and texture, and reaction kinetics. It is also useful in understanding sensory properties, including hardness, crispiness, softness, and flavor release (Slade and Levine 1995; Roos 1995a; Roudaut et al. 2004). Knowledge of molecular mobility and changes in mechanical and physical properties over the glass transition can be used to control the characteristics of food solids, for example, in drying, freeze-drying, freezing, and extrusion. An overview of the importance of the glass transition in food engineering, including selected food systems and processes, as well as challenges in using glass transition data in the control of food properties, food processing, and storage stability, will be highlighted in this review.

Y.H. Roos (✉) and N. Silalai
School of Food and Nutritional Sciences, University College Cork, Cork, Ireland
e-mail: yrjo.roos@ucc.ie

J.M. Aguilera et al. (eds.), *Food Engineering Interfaces*, Food Engineering Series,
DOI 10.1007/978-1-4419-7475-4_18,

18.1.1 Confectionary

The physical state of sugars is important in manufacturing and control of quality changes during storage of confectionery. Formation of noncrystalline solid sugar structures is the basic technology underpinning the manufacturing of hard sugar candies, which are often produced from sugar melts or concentrates by rapidly cooling the product after heating to above melting temperatures. High solids concentration and rapid cooling enhance the formation of solid, transparent, and brittle, glassy materials. White and Cakebread (1966) stated that food materials containing amorphous sugars, such as hard candies, were stable at temperatures below their glass transition. Cotton candy is another example of sugar glass technology. Cotton candy is made by melting crystalline sucrose, which is spun under rapid cooling and dehydration into an amorphous (glassy) solid. At temperatures exceeding the glass transition temperature, T_g, of sucrose, the spun structure collapses as a result of crystallization of the sugar. A hard lump of sucrose crystals imbedded in a partially glassy structure may form, making the shelf life of the product very short (Labuza and Labuza 2004).

18.1.2 Frozen Foods

Crystallization and recrystallization of amorphous food components are time-dependent phase transitions. Crystallization and recrystallization processes are affected by the physical state of food solids and may be controlled by the glass transition. One example is lactose crystallization in frozen desserts and ice cream. Such solute crystallization is a result of freeze concentration of the solutes and subsequent supersaturation. At sufficiently low temperatures the solutes, along with some unfrozen water, vitrify into the solid (glassy) state reducing diffusion and causing crystallization processes to cease. Crystallization and recrystallization processes, however, take place in frozen foods above the onset temperature of ice melting in the maximally freeze-concentrated solute matrix (Roos and Karel 1991b, d; Roos 1995a). As lactose is one the least soluble sugars, lactose crystallization often occurs in ice cream produced without stabilizers. Lactose crystallization causes an undesirable coarse and sandy mouthfeel, while ice recrystallization may be observed from large, coarse ice crystals and flaky ice structure.

Various authors (White and Cakebread 1966; Livney et al. 1995; Roos 1995a) have reported that rates of crystallization processes increase above the glass transition. At temperatures approaching the glass transition, crystallization and recrystallization rates reduce as a result of limited molecular mobility (Roudaut et al. 2004) when the material is transformed into the solid (glassy) state. At temperature below the glass transition, crystallization of food components as well as their recrystallization is unlikely because of the solid-like structure and absence of translational diffusion of molecules (Roos 1995a; Hartel 1996;

Roudaut et al. 2004). Recrystallization phenomena are typical of frozen foods, which often may be stored at fairly high temperatures or exposed to significant temperature fluctuations after manufacturing. Recrystallization of ice is a time-dependent process and generally characterized by an increase in the size of ice crystals with storage time (Roos 1995a; Hagiwara et al. 2005). Roos (1995a) pointed out that rates of ice formation and recrystallization could be controlled by using the temperature difference of the T_g (referred to as $T-T_g$) as the rate-defining factor. The recrystallization rate is strongly reduced below the glass transition of the freeze-concentrated, unfrozen system (Carrington et al. 1996). Thus, the glass transition temperatures, T_g, of the freeze-concentrated solutes and unfrozen water content at temperatures during frozen storage are the most important composition-dependent factors, which then can be used to control the extent of ice formation and ice recrystallization in frozen foods at any given storage temperature.

18.1.3 Cereal Foods

Starch is a mix of carbohydrate polymers and the main component of cereal foods. Starch is present also in legume seeds and tuber plants. The two starch components, amylose and amylopectin, may exist in crystalline, partially crystalline, and amorphous states (Slade and Levine 1991). In native starches, amylose may exist as a noncrystalline component but amylopectin often exhibits partial crystallinity (Roos 1995a). Water in amorphous parts of starch components acts as a plasticizer and decreases the T_g. Glass transition, melting temperatures, and water content are the most important parameters characterizing the state and physical properties of starch components over a wide temperature range in cereals processing and product storage.

Phase transitions associated with gelatinization and loss of native structure in granular starches can define and explain differences in the physical properties of starches and their behavior in food products (Lund 1989). Levine and Slade (1990) pointed out that starch gelatinization is a nonequilibrium melting process that occurs during the heating of starch in the presence of water. Retrogradation of starch is a temperature-, water-content-, and time-dependent crystallization phenomenon and occurs after cooling of gelatinized starch. The rate of retrogradation depends on the presence and ratio of amylopectin and amylose, and the molecular weight of these starch components (Roos 1995a; Jouppila and Roos 1997). After cooling of gelatinized starch, amylose crystallization occurs rapidly, while crystallization of amylopectin may occur during storage of gelatinized starch and cereal foods (Roos 1995a; Ronda and Roos 2008).

Several studies (Le Meste et al. 1992; Jouppila and Roos 1997; Ronda and Roos 2008) indicated that the textural characteristics of cereal foods at different temperatures and water contents could be explained in terms of temperature with respect to T_g. Starch retrogradation, including a basic crystallization process of gelatinized starch components, can be detected by DSC from observed physical

change in a starch gel or paste, and by X-ray diffraction methods (Roos 2007a). Glass transition can control texture- and stability-related phenomena such as gelatinization and retrogradation, which may proceed over the temperature range $T_g < T < T_m$ (Biliaderis 1992; Yoshimura et al. 1996). Crystallization in gelatinized starch (or starch retrogradation) and the loss of water during storage were found to contribute to aging and bread staling above the glass transition (Roos et al. 1996; Champion et al. 2000; Ronda and Roos 2008). Moreover, crispness, which is affected by water content and glass transition, is an essential factor in achieving acceptable quality among numerous cereal and snack foods (Roudaut et al. 2002). Many cereal-based foods, such as breakfast cereals, wafers, and biscuits, have a crispy or crunchy texture when consumed at low water contents (below 10% water); however, crispness may be lost as the water content increases due to water sorption and subsequent water plasticization of amorphous structures (Nicholls et al. 1995; Roos et al. 1998; Hochstetter et al. 2006). A critical water activity (a_w) at which crispness is lost was found to be specific according to each material. A change resulting in loss of crispness often occurred around 0.35–0.50 a_w (Roos 1993; Roos et al. 1996). When the critical water content or water activity is exceeded, the T_g of the material occurs below the ambient temperature (Roos 1993).

18.1.4 Food Powders and Dehydrated Foods

Food powders containing amorphous carbohydrates, such as lactose in dairy powders, may show changes in physical properties, for example, crystallization, clumping, stickiness, and caking during processing, handling, and storage (Levine and Slade 1986). Stickiness and caking phenomena are related to the collapse phenomena occurring in amorphous solids, and often result from increased temperature or exposure of powders to high-humidity conditions.

Caking of powders may be considered as a collapse phenomenon, which occurs when particle surfaces in contact form permanent aggregates and harden causing a loss of free-flowing properties in powder particles. Boonyai et al. (2004) explained the difference between stickiness and caking of food powders. They stated that stickiness is an instantaneous process but caking occurs over a time period. The common cause of stickiness is plasticization of particle surfaces, which allows a sufficient decrease of surface viscosity for the formation of liquid bridges between particles (Downton et al. 1982; Roos 1995a). These phenomena in powders, with amorphous components contributing to stickiness, can be characterized as time-dependent surface flow properties that are controlled by properties of the amorphous components and their flow at temperatures above the glass transition (Roos 1995a). Several researchers (Roos and Karel 1991a, b; Chuy and Labuza 1994; Roos 1995a; Bhandari and Howes 1999) have illustrated possible relationships among stickiness, caking, and glass transition. The food polymer science approach has increased understanding of the state of food materials and its use to control or prevent undesirable physical changes, including powder stability (Bhandari and

Howes 1999). Amorphous solids exist in a supercooled liquid (rubbery state) above the glass transition at which plasticization-dependent viscosity decreases occur rapidly. Glass transition enhances molecular mobility and flow, leading to stickiness and crystallization problems in low-water and frozen foods (Roudaut et al. 2004). Therefore, glass transition is an important and useful concept in observation of parameters, such as temperature and water content for the control or reduction of liquid-like properties of powder components during processing and storage.

Collapse during freeze-drying and collapse of freeze-dried matrices may adversely affect material properties during dehydration and storage, respectively. Collapse is a result of viscous flow of amorphous materials or their components, causing loss of structure, reduction of pore size, and shrinkage. Such collapse is associated with undesirable appearance and loss of texture, and volatile substances (Karel and Flink 1973; Levi and Karel 1995). It occurs above glass transition, the rate of which depends on temperature and water content. Levi and Karel (1995) found that rates of collapse were strongly dependent on the temperature above the glass transition. Increasing water content depressed the T_g and increased the $T–T_g$ at the observed temperature. The flow and rate of collapse above T_g were functions of temperature difference ($T–T_g$), which could be modeled by the Williams-Landel-Ferry (WLF) relationship (Roos 1995a). This suggested that the T_g was an applicable parameter for the prediction and control of collapse during freeze-drying and storage of amorphous foods.

18.2 Glass Transition: Opportunities

An increase in molecular mobility above the glass transition enhances flow of amorphous structures and results in time-dependent physical changes (Roos and Karel 1991a; Bhandari et al. 1997; Bhandari and Howes 1999). This occurs above a critical temperature, or plasticization level, which often refers to the glass transition temperature, T_g, or water activity and water content, respectively (Roos 2007b). Glassy states may form in numerous food processes involving cooling of highly supercooled liquids or removal of water by dehydration or freezing (Fig. 18.1). Glass formation or vitrification of food solids may occur in various glassy, non-equilibrium (solid glassy state) solid structures. These may have different physical appearances, such as freeze-dried or spray dried structures, and also may exhibit varying thermodynamic states (Roos 2008).

18.2.1 Freezing and Freeze-Drying

Ice crystallization and collapse of structure in partially frozen systems are controlled by the molecular mobility of food components in freeze-concentrated, unfrozen water-solute systems (Levi and Karel 1995; Roos 1995a). These changes are time-dependent and reduce in rate as the maximally freeze-concentrated state is

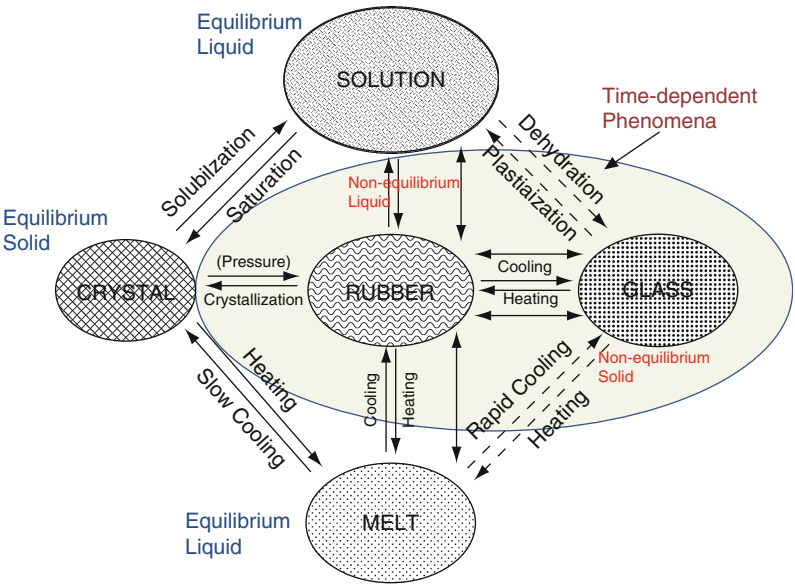

Fig. 18.1 Changes in physical state of amorphous materials around glass transition and time-dependent characteristics (Data are from Roos and Karel 1991a)

approached. The glassy structures of the unfrozen water-solids phases that are formed in maximally freeze-concentrated systems support the structure against flow and collapse, but the structure does not allow further ice formation (Roos and Karel 1991d; Roos 2007a). Freezing and frozen storage conditions, however, affect the size of ice crystals, which could probably be further manipulated by the control of freeze-concentration and ice formation.

Ice formation in foods results in a freeze-concentration of solids and a gradually decreasing freezing temperature as the solute concentration of the unfrozen phase increases. The freeze-concentrated, amorphous unfrozen phase contains unfrozen water and solids; it provides a continuous phase for the dispersed ice crystals and possibly lipids or other nondissolved solid components (Roos 1995a). The glass transition temperature of the maximally freeze-concentrated unfrozen phase (T_g') is independent of the solute concentration prior to freezing and often corresponds with a solute concentration (C_g') of 80% (w/w) (Roos et al. 1996). At temperatures below the T_g' the amorphous unfrozen phase is vitrified and exists as a glassy solid (Roos and Karel 1991d), whereas ice dissolution at temperatures above the onset temperature of ice melting, T_m', decreases the viscosity of the unfrozen phase, which shows viscous flow under gravity. Hence, frozen systems at temperatures above the T_m' cannot support the solid structure (Fig. 18.2) and show collapse or shrinkage (Bhandari and Howes 1999; Le Meste et al. 2002; Alves-Filho and Roos 2006). Stability of frozen foods can be accomplished by manipulation of food composition to increase the T_m' or by using storage temperatures lower than the T_m' (Hartel 1996). However, compositional changes in food formulations are not always possible.

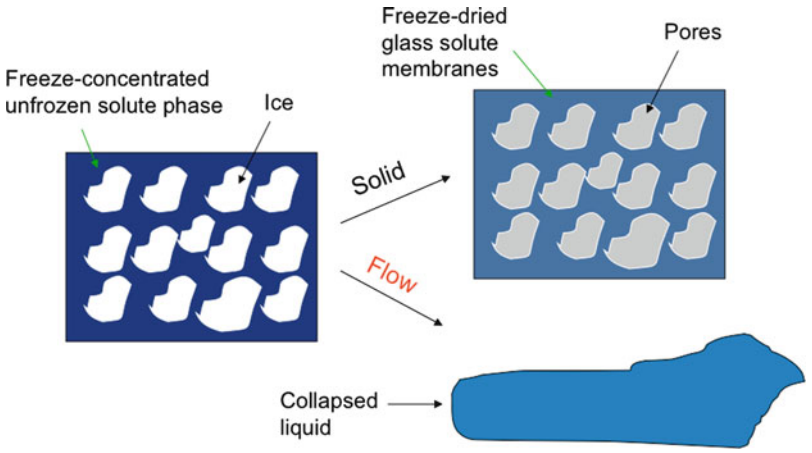

Fig. 18.2 Viscous flow of freeze-concentrated liquid phase in freeze-drying

The control of ice crystal growth in frozen foods and ice cream has been postulated by the T_m' control (Goff et al. 1993). They suggested that polysaccharides provided resistance to thermal deformation and increased subzero viscosity above the T_m'. Hence, ice crystal size and the rate of growth of ice crystals in frozen foods and ice cream containing polysaccharides were smaller than in frozen foods and ice cream without added polysaccharides. Ice formation ceases as a result of kinetic limitations for crystal growth below T_g'; some frozen foods are stable against deteriorative changes because of the glassy state of the unfrozen phase (Levine and Slade 1986; Roos and Karel 1991d). However, some reactions, such as oxidation of sensitive components may accelerate as a result of maximum freeze-concentration of foods. Studies of frozen food stability are relatively few and therefore it requires substantial further attention by researchers. It appears, however, that the control of the glass transition of the unfrozen phase and ice melting is fundamental to freezing and frozen storage as well as freeze-drying.

18.2.2 Spray Drying

Particle stickiness and subsequent deposition of semi-dried particles on dryer surfaces is regarded as one of the most typical problems in spray drying. During drying of sugar-rich foods, such as fruit juices, honey, and some starch derivatives (glucose syrup/maltodextrins with higher dextrose equivalent values), their structures may remain as syrup-like liquids; such particles stick on the drier surfaces leading to lower product yields and operating problems (Bhandari et al. 1997). In industrial applications, sticky-point temperature curves may be generated and used to develop optimal drying operations to minimize stickiness problems.

Stickiness is a time-dependent phenomenon that is related to structural transformations and flow of amorphous solids around the glass transition (Roos and Karel 1991c; Roos 1995a). Measured T_g values have correlated well with sticky-point measurements and the glass transition concept has provided a better fundamental understanding and predictability of stickiness (Roos et al. 1996; Adhikari et al. 2001, 2005). Application of glass transition data is extremely useful in the design of dehydration equipment to minimize the stickiness of sugar-rich food solids (Truong et al. 2005a, 2005b). Truong et al. (2005a, b) suggested that the glass transition approach could be used to reduce stickiness because the difference between the outlet air temperature and the T_g of the solids of the final product ($T-T_g$) was a measurable, stickiness controlling property of the particles in the spray-drying process. The T_g was influenced by solids composition, which affects the physical changes in foods (Ozkan et al. 2002; Fitzpatrick et al. 2007a, b; Nijidam and Langrish 2006; Haque and Roos 2006). Amorphous low-molecular weight substances such as fructose and glucose have a low T_g. High-molecular weight components, such as polysaccharides and proteins, increase the T_g of mixtures containing sugars (Roos and Karel 1991c; Haque and Roos 2004; Shrestha et al. 2007); they also affect the powder characteristics during spray drying as shown in (Fig. 18.3) (Haque and Roos 2006).

Maltodextrins are widely used as food components to reduce stickiness in sugar-rich foods because of their T_g and viscosity increasing property in mixtures with sugars (Bhandari et al. 1997). Addition of low dextrose equivalent (DE) maltodextrins decreases stickiness and caking during drying and storage (Adhikari et al. 2004; Langrish et al. 2007), and provides an excellent opportunity to improve processing and storage characteristics. The effect on mixture properties can be predicted using T_g data. The stickiness behavior can be characterized by various techniques (Lazar et al. 1956; Downton et al. 1982; Chuy and Labuza 1994; Hennigs et al. 2001; Ozkan et al. 2002). The sticky points of powders were found

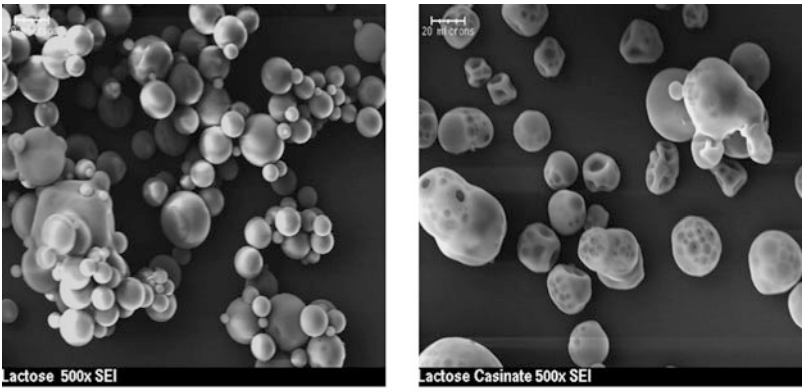

Fig. 18.3 Composition affects glass transition and dehydration characteristics using scanning electron microscopy (SEM) (Further data can be found in Haque and Roos 2006)

to be associated with glass transition temperatures at 10–20°C above the T_g (Roos and Karel 1991b; Roos 1995a; Hennigs et al. 2001; Ozmen and Langrish 2002; Adhikari et al. 2005). This indicated that the glass transition is a useful parameter to control dehydration and powder characteristics, including stickiness, caking, and agglomeration during drying processes and product storage.

18.2.3 Extrusion

Extrusion has become a well-established and widely used food processing method. Extrusion processes often involve conversion of solid ingredients to a viscous but homogeneous mixture followed by formation of dense, solid, or expanded highly porous structures. Biodegradable packaging and edible films may also be manufactured using extrusion processes. The use of extrusion in food applications is often based on empirical knowledge of solids behavior and structure formation. However, the materials science understanding of foods and knowledge of their phase and state transitions are fundamental in the control of extrusion processes and material behavior in structure formation and storage (Slade and Levine 1991, 1995; Roos 1995a). This development also is an opportunity to improve extrusion processes and product quality, particularly in the development of novel extrusion applications.

The formation of the structure of several extruded foods and low-moisture foods, such as snack foods and breakfast cereals, is influenced by temperature and water content. The glass transition can be used to control their plasticization, gelatinization, and the glass formation. In plasticization, increasing the temperature or the water content results in a decrease of the T_g. Water plasticization also controls modulus and tensile strength of extruded films produced by extrusion (Garcia et al. 2004; Roos 1995a; Hochstetter et al. 2006). One of the desired characteristics of extruded snacks and breakfast cereals is a crispy texture. At the expansion of plasticized foods, starchy solids are rapidly dehydrated and the solids vitrify, i.e., the structure of the food solids becomes a glass, forming thin membranes with brittle and crispy characteristics. Details on plasticization and structure formation in extrusion provide new opportunities for controlling the process and the texture and deterioration of extruded products since water plasticization and oxygen permeability can be manipulated during storage (Roos 1995a; Roos et al. 1996; Hochstetter et al. 2006). For example, Garcia et al. (2004) used glass transition data to control the thermal and water plasticization of extruded meat products and to achieve improved water permeability properties of films.

18.2.4 Encapsulation

Encapsulation processes are used to entrap food ingredients, enzymes, cells, or other components in structure-forming, encapsulant materials. Applications of

encapsulation have been increased in the food industry, since this process often aims at improved protection from heat and loss, or otherwise stabilizes sensitive components in food processing and storage. Dispersed droplets and particles in encapsulant matrices show reduced reaction rates and are often protected from surrounding reactants as a result of decreased diffusion through the glassy structure below the glass transition (Roos 1995a). Both temperature and water plasticization of encapsulant matrices may increase structural changes and release of encapsulated substances. Above the glass transition, the amorphous materials exhibit viscous flow and structures of food materials often change, which can result in collapse and release of encapsulated components.

The formulation of encapsulant matrices and control of glass formation may be used to improve encapsulation and stability of food products. For example, highly polymeric compounds such as proteins and hydrocolloids have high glass transition temperatures. These high molecular weight miscible compounds with miscible lower molecular weight components increase the glass transition temperature of the mixture and stabilize the glassy state against higher temperatures and water contents (Roos 2008). There is, however, very little information about the miscibility of carbohydrate polymers and proteins in food systems, as well as on how the use of various processes affects glass formation. Food structures also have heterogeneities that can greatly affect encapsulation, so their role in stability and shelf-life control needs to be investigated further.

18.3 Glass Transition: Challenges

Changes in physicochemical and physical properties of foods are likely to occur around glass transition, the point at which amorphous solids convert to liquids and exhibit viscous flow. The glass transition results in enhanced molecular mobility, which is associated with decreasing relaxation times and a lower viscosity. There have been numerous studies of enthalpy relaxations around the glass transition (Haque et al. 2006). These relaxations are examples of time-dependent glass formation and present challenges in the understanding of glassy structures formed in food processing.

Food processes, such as freezing and freeze-drying, spray drying or extrusion, may produce structures specific to the product composition, process, and processing parameters. These factors, together with thermal and water effects in storage, contribute to the properties and quality of food systems at the time of consumption. Understanding the state of glassy food materials and their time-dependent characteristics may require rigorous experimental studies, as such research would clarify the role of glassy states in the control of reaction rates and stabilization of highly sensitive food systems.

It is generally agreed that endothermic enthalpy relaxations increase with increasing aging time and temperature below the glass transition (Haque et al. 2006). Relaxations may also indicate exothermic enthalphy changes as translational

mobility of molecules appears around the glass transition (Roos 1995a, 2008). These relaxations show qualitative and quantitative information on the enthalpy state of molecules within a glass. As translational mobility of molecules appears around the glass transition materials may either require (endothermal relaxation) or release (exothermal relaxation) heat as they respond to the increasing temperature. Molecular mobility and the time-dependent nature of the glass transition can also be observed from mechanical and dielectric properties of materials (Champion et al. 2000; Le Meste et al. 2002; Roudaut et al. 2004; Roos 2008). Both dielectric and dynamic mechanical properties show the α-relaxation around the glass transition.

The α-relaxation can be observed using dielectric analysis (DEA) or dynamic-mechanical analysis (DMA) (Laaksonen and Labuza 2001; Laaksonen and Roos 2001; Royall et al. 2005; Hochstetter et al. 2006; Roos 2008). The α-relaxation temperatures obtained are frequency-dependent, indicating the nonequilibrium and time-dependent nature of the system. These relaxations may be used to describe mechanical properties of food materials, such as stickiness and caking of amorphous powders. Silalai et al. (2009a) found that the α-relaxation of dairy powders shifted to higher temperatures with increasing frequencies of DEA and DMA measurements (Fig. 18.4). The frequency-dependence of the α-relaxation followed the Arrhenius relationship (Talja and Roos 2001), and a frequency corresponding to the glass transition temperature could be identified. The glass transition measured by DSC and the α-relaxation temperatures (T_α) determined by DMA and DEA correlated closely with the sticky-point temperatures obtained using an empirical measurement (Silalai et al. 2009b).

Solids composition also affects structural formation and the quality of foods during processing and storage. For example, powders containing high amounts of lactose exhibited high adhesion of powder particles with increasing temperature and water content as a result of surface plasticization. Surface plasticization caused

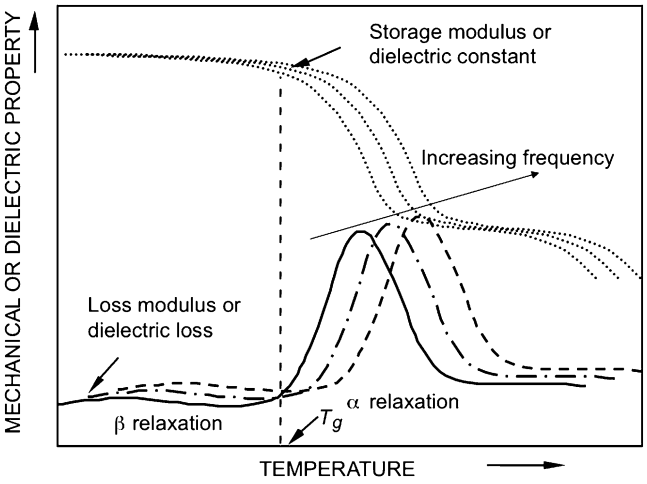

Fig. 18.4 Time-dependent characteristics and relaxations of the amorphous state

a decrease in sticky-point temperatures (Silalai et al. 2009b). Although many researchers (Roos and Karel 1991b; Chuy and Labuza 1994; Roos 2002) have demonstrated that stickiness and caking of dairy powders are related to glass transition, the time-dependent flow and contact time measurements still remain as challenging areas in glass transition research. However, composition, plasticization, and temperature are the main causes leading to a sufficient decrease in surface viscosity and higher adhesion and cohesion of powder particles. It was also shown by Downton et al. (1982) that powders were free-flowing particles at temperatures below glass transition; they became plasticized at above these temperatures, at decreasing viscosity in the range 10^7 to 10^9 Pa s.

Crystallization of amorphous components, particularly sugars in low-water and frozen foods, and starch components in gelatinized starch-containing foods, is often the most dramatic change in food systems. Numerous examples are available on lactose crystallization in dairy powders (Jouppila et al. 1997) and ice cream (Hartel 1996), as well as on starch retrogradation, including amylopectin crystallization (Jouppila et al. 1997). Crystallization is affected by water content and other components in low-water and frozen foods. Haque and Roos (2004) found that the T_g of spray-dried lactose–protein mixtures increased as a result of added protein components. The rate of crystallization of amorphous lactose was also reduced in spray-dried lactose–protein mixtures (Fig. 18.5). The data suggested that various proteins may affect lactose crystallization properties differently; studies of crystallization with salts showed that salts may further complicate crystallization (Omar and Roos 2007). These findings with information on water plasticization and component miscibility are fundamental in describing the spray-drying characteristics and product stability of sugar-containing food solids. The practical applications of these data are numerous but may require a systematic materials science approach in product formulation and equipment design.

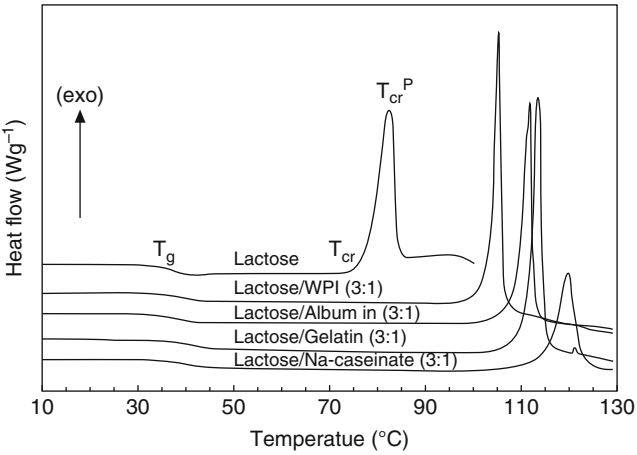

Fig. 18.5 Glass transition and crystallization temperatures of amorphous lactose in the presence of various proteins (From Haque and Roos 2004)

The effects of food components in mixtures on dielectric and mechanical properties around the glass transition have been reported in several studies (Kalichevsky et al. 1993; Nilolaidis and Labuza 1996; Talja and Roos 2001; Laaksonen and Labuza 2001; Laaksonen et al. 2002; Laaksonen and Roos 2001, 2003; Hashimoto et al. 2003). According to Silalai et al. (2009a, 2009b), dairy powders with increased protein content exhibited higher T_g values as measured by DSC. This was in agreement with increased T_α values as determined by DEA and DMA. There were also other changes in mechanical and dielectric relaxations. Dielectric and mechanical properties of powders with high lactose contents changed considerably around the glass transition as compared to powders with high protein contents (Figs. 18.6 and 18.7).

In frozen and freeze-drying systems, solids composition affects the glass transition of the maximally freeze-concentrated unfrozen phase, T_g', and onset temperature of ice melting, T_m' (Roos and Karel 1991d; Goff et al. 1993). The α-relaxations of frozen systems were also affected by composition and frequency, as observed from dielectric and dynamic-mechanical relaxations (Laaksonen and Roos 2001; Laaksonen et al. 2002). These data are of significant importance in the control of freezing and freeze-drying properties of food and other biological materials. The challenges in the control of freezing properties, frozen food stability, as well as freeze-drying can be addressed by understanding the state and phase transitions of freeze-concentrated systems. For example, polymeric materials in mixtures containing sugar lower the T_g' but increase the T_m'. This increases the broadness of the transition

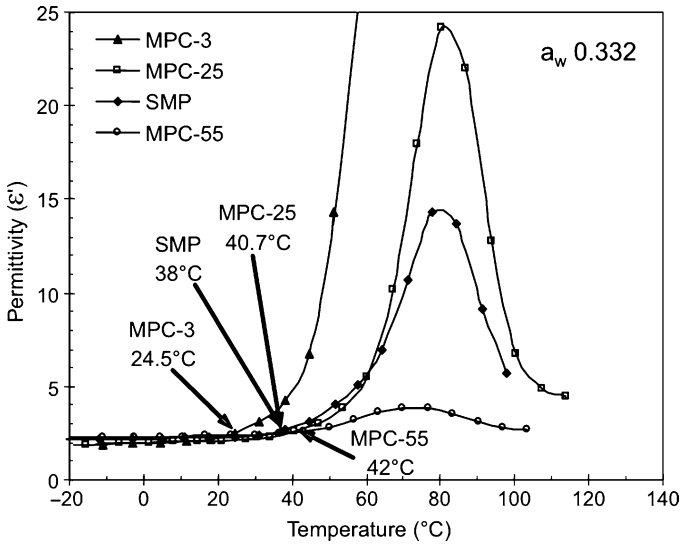

Fig. 18.6 Dielectric thermal analysis (*DEA*) thermograms showing the effect of carbohydrate–protein composition on dielectric relaxations of nonfat milk solids at water activity of 0.332. The carbohydrate–protein ratios for MPC-3, MPC-25, SMP, and MPC-55 were 15:74, 27:59, 40:48, and 56:32 (% of total solids, w/w), respectively

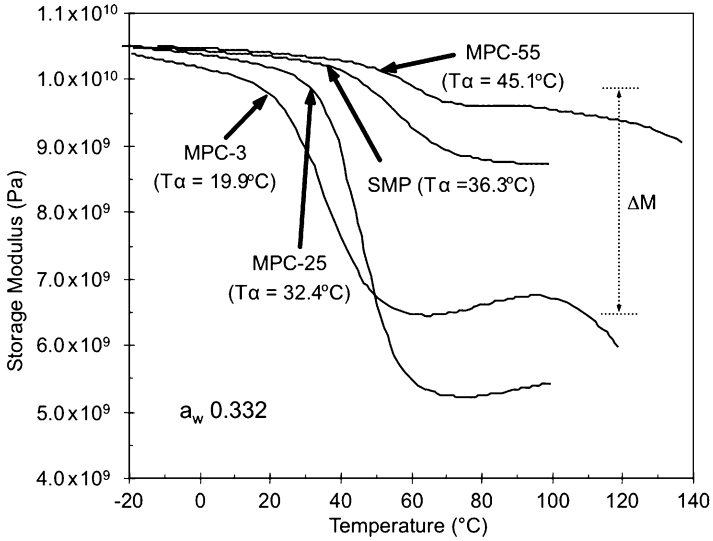

Fig. 18.7 Dynamic mechanical analysis (*DMA*) thermograms showing the effect of carbohydrate–protein composition on dielectric relaxations of nonfat milk solids at water activity of 0.332. The carbohydrate–protein ratios for MPC-3, MPC-25, SMP, and MPC-55 were 15:74, 27:59, 40:48, and 56:32 (% of total solids, w/w), respectively

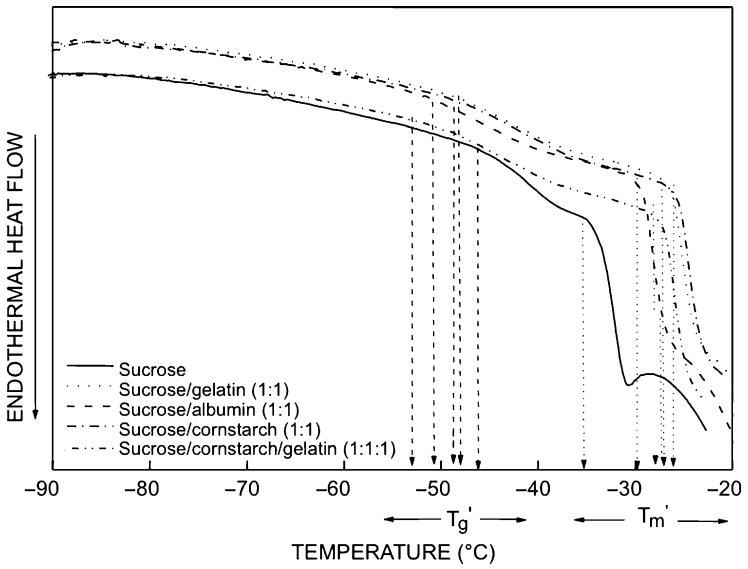

Fig. 18.8 Differential scanning calorimetry (*DSC*) thermograms showing glass transition and ice melting in sucrose and protein–starch systems (Data are from Singh and Roos 2005)

temperature range and suggests that ice formation is affected by the composition and diffusional characteristics of the unfrozen matrix. It seems that polymeric compounds, such as gelatin and corn starch, as shown in (Fig. 18.8), inhibit ice formation resulting in a higher unfrozen water content with corresponding lowering of the T_g' and increase of the T_m' (onset of melting occurred at a higher temperature corresponding to a lower ice content and higher melting temperature) (Singh and Roos 2005). Although it appears that compositional changes affect food properties in freeze-concentrated systems, their complex structure makes experiments and collection of low temperature data complicated. However, further analysis of heterogeneities and time-dependent changes in composition and microstructure in frozen systems will be useful in the design of freezing processes and formulation of frozen foods with improved quality and stability.

18.4 Conclusion

Significant progress has been made in understanding the role of glass transitions in food materials during food processing and storage. Glass transitions in foods have been shown to affect the flow properties of concentrated systems and, therefore, challenges exist in processes such as dehydration, extrusion, and freezing. The glass transitions and water plasticization behavior of food solids may affect structural changes, crystallization processes, as well as deteriorative reactions, which often limit the shelf life of low-water and frozen foods. Novel thermal analytical systems and other techniques are crucial to further understanding the complex nature of food systems, as well as the translation of knowledge of glass transition properties to the benefit of processing equipment and food product design for meeting processing needs and establishing the highest quality standards.

References

Adhikari BP, Howes T, Bhandari BR, Troung V (2001) Stickiness in foods: a review of mechanisms and test methods. Int J Food Prop 4(1):1–33

Adhikari B, Howes T, Bhandari BR, Troung V (2004) Effect of addition of maltodextrin on drying kinetics and stickiness of sugar and acid-rich foods during convective drying: experiments and modeling. J Food Eng 62:53–68

Adhikari B, Howes T, Lecomte D, Bhandari BR (2005) A glass transition temperature approach for the prediction of the surface stickiness of a drying droplet during spray drying. Powder Technol 149:168–179

Alves-Filho O, Roos YH (2006) Advances in multi-purpose drying operations with phase and state transitions. Dry Technol 24:383–396

Bhandari BR, Datta N, Howes T (1997) Problems associated with spray drying of sugar-rich foods. Dry Technol 15(2):671–684

Bhandari BR, Howes T (1999) Implication of glass transition for the drying and stability of dried foods. J Food Eng 40:71–79

Biliaderis CG (1992) Structures and phase transitions of starch in food systems. Food Technol 46(6):98–109

Boonyai P, Bhandari BR, Howes T (2004) Stickiness measurement techniques for food powders: a review. Powder Technol 145:34–46
Carrington AK, Goff HD, Stanley DW (1996) Structure and stability of the glassy state in rapidly and slowly cooled carbohydrate solutions. Food Res Int 29(2):207–213
Champion D, Le Meste M, Simatos D (2000) Towards on improved understanding of glass transition and relaxations in foods: molecular mobility in the glass transition range. Food Sci Technol 11:41–55
Chuy LE, Labuza TP (1994) Caking and stickiness of dairy-based food powders as related to glass transition. J Food Sci 59(1):43–46
Downton GE, Flores-Luna JL, King CJ (1982) Mechanism of stickiness in hygroscopic amorphous powders. Indus Eng Chem Fund 21:447–451
Fitzpatrick JJ, Hodnett M, Twomey M, Cerqueira PSM, O'Flynn J, Roos YH (2007a) Glass transition and the flowability and caking of powders containing amorphous lactose. Powder Technol 178(2):119–28
Fitzpatrick JJ, Barry K, Cerqueira PSM, Iqbal T, O'Neill J, Roos YH (2007b) Effect of composition and storage conditions on the flow ability of dairy powders. Int Dairy J 17:383–392
Garcia RA, Onwulata CI, Ashby RD (2004) Water plasticization of extruded material made from meat and bone meal and sodium caseinate. J Agr Food Chem 52:3776–3779
Goff HD, Caldwell KB, Stanley DW (1993) The influence of polysaccharides on the glass transition in frozen sucrose solutions and ice cream. J Dairy Sci 76:1268–1277
Hagiwara T, Mao J, Suzuki T, Takai R (2005) Ice recrystallization in sucrose solutions stored in a temperature range of −21°C to −50°C. Food Sci Technol Res 11(4):407–411
Haque K, Roos YH (2004) Water plasticization and crystallization of lactose in spray-dried lactose/protein mixtures. J Food Sci 69(1):23–29
Haque K, Roos YH (2006) Differences in the physical state and thermal behaviour of spray-dried and freeze-dried lactose and lactose/protein mixtures. Innovative Food Sci Emerg Technol 7:62–73
Haque K, Kawai K, Suzuki T (2006) Glass transition and enthalpy relaxation of amorphous lactose glass. Carbohyd Res 341:1884–1889
Hartel RW (1996) Ice crystallization during manufacture of ice cream. Trends Food Sci Technol 7:315–321
Hashimoto T, Hagiwara T, Suzuki T, Takai R (2003) Study on glass transition Katsuobushi (boiled and dried bonito fish stick) by differential scanning calorimetry and dynamic mechanical analysis. Fisheries Sci 69:1290–1297
Hennigs C, Kockel TK, Langrish TAG (2001) New measurements of the sticky behavior of skim milk powders. Dry Technol 19(3&4):471–484
Hochstetter A, Talja RA, Helen HJ, Hyvonen L, Jouppila K (2006) Properties of gluten-based sheet produced by twin-screw extruder. Lebensm Wiss Technol 39:893–901
Jouppila K, Roos YH (1997) The physical state of amorphous corn starch and its impact on crystallization. Carbohyd Polym 32:95–104
Jouppila K, Kansikas J, Roos YH (1997) Glass transition, water plasticization, and lactose crystallization in skim milk powder. J Dairy Sci 80(12):3152–3160
Kalichevsky MT, Blanshard JMV, Tokarczuk PF (1993) Effect of water content and sugars on the glass transition of casein and sodium caseinate. Int J Food Sci Tech 28:139–151
Karel M, Flink JM (1973) Influence of frozen state reactions on freeze-dried foods. J Agr Food Chem 21:16–21
Laaksonen TJ, Labuza TP (2001) Effects of moisture, sucrose, NaCl, and arabinoxylan on relaxation in wheat dough as measured by DMTA. Int J Food Prop 4(2):311–325
Laaksonen TJ, Roos YH (2001) Dielectric relaxations of frozen wheat doughs containing sucrose, NaCl, ascorbic acid and their mixtures. J Cereal Sci 33:331–340
Laaksonen TJ, Roos YH (2003) Water sorption and dielectric relaxations of wheat doughs (containing sucrose, NaCl, ascorbic acid, and their mixtures). J Cereal Sci 37:319–326
Laaksonen TJ, Jouppila K, Roos YH (2002) Effects of arabinoxylans on thermal behaviour of frozen wheat doughs as measured by DSC, DMA, and DEA. J Food Sci 67(1):223–230

Labuza TP, Labuza PS (2004) Influence of temperature and relative humidity on the physical states of cotton candy. J Food Process Pres 28(4):274–287
Langrish TAG, Chan WC, Kota K (2007) Comparison of maltodextrin and skim milk wall deposition rates in a pilot-scale spray dryer. Powder Technol 179:84–89
Lazar ME, Brown AH, Smith GS, Wong FF, Linquist FE (1956) Experimental production of tomato powder by spray drying. Food Technol 10:129–134
Le Meste M, Huang VT, Panama J, Anderson G, Lentz R (1992) Glass transition of bread. Cereal Food World 37:164–267
Le Meste M, Champion D, Roudaut G, Blond G, Simatos D (2002) Glass transition and food technology: a critical appraisal. J Food Sci 67(7):2444–2458
Levi G, Karel M (1995) Volumetric shrinkage (collapse) in freeze-dried carbohydrates above their glass transition temperature. Food Res Int 28(2):145–151
Levine H, Slade L (1986) A polymer physicochemical approach to the study of commercial starch hydrolysis products (SHP's). Carbohyd Polym 6:213–244
Levine H, Slade L (1990) Influences of the glassy and rubbery states on the thermal, mechanical and structural properties of doughs and baked products. In: Faridi H, Faubion JM (eds) Dough rheology and baked product texture. AVI, New York, pp 157–330
Livney YD, Donhowe DP, Hartel RW (1995) Influence of temperature on crystallization of lactose in ice-cream. Int J Food Sci Tech 30(3):311–320
Lund DB (1989) Starch gelatinization. In: Singh RP, Medina AG (eds) Food properties and computer-aided engineering of food processing systems. Kluwer, The Netherlands, pp 299–311
Nicholls RJ, Appelqvist IAM, Davies AP, Ingman SJ, Lillford PJ (1995) Glass transitions and the fracture behaviour of gluten and starches within the glassy state. J Cereal Sci 21:25–36
Nijidam JJ, Langrish TAG (2006) The effect of surface composition on the functional properties of milk powders. J Food Eng 77:919–925
Nikolaidis A, Labuza TP (1996) Glass transition state diagram of a baked cracker and its relationship to gluten. J Food Sci 61(4):803–806
Omar AME, Roos YH (2007) Glass transition and crystallization behaviour of freeze-dried lactose-salt mixtures. Lebensm Wiss Technol 40(3):536–543
Ozkan N, Walisinghe N, Chen XD (2002) Characterization of stickiness and cake formation in whole milk and skim milk powders. J Food Eng 55:293–303
Ozmen L, Langrish TAG (2002) Comparison of glass transition temperature and sticky point temperature for skim milk powder. Dry Technol 20(6):1177–1192
Ronda F, Roos YH (2008) Gelatinization and freeze-concentration effects on recrystallization in corn and potato starch gels. Carbohyd Res 343:903–911
Roos YH (1995a) Phase transitions in foods. Academic, San Diego
Roos YH (1995b) Characterization of food polymers using state diagrams. J Food Eng 24:339–360
Roos YH (2002) Importance of glass transition and water activity to spray drying and stability of dairy powders. Lait 82:475–484
Roos YH (2004) Phase and state transitions in dehydration of biomaterials and foods. In: Mujumdar AS (ed) Dehydration of products of biological origin. Science Publishers, Enfield, NH, pp 3–22
Roos YH (2007a) Phase transitions and transformations in food systems. In: Heldman DR, Lund DB (eds) Handbook of food engineering, 2nd edn. CRC Press, New York, pp 284–352
Roos YH (2007b) Water activity and the glass transition. In: Barbosa-Cánovas GV, Fontana AJ, Schmidt SJ, Labuza TP (eds) Water activity in foods. Fundamentals and applications. IFT Press/Blackwell, Ames, IA, pp 29–45
Roos YH (2008) The glassy state. In: Aguilera JM, Lifford PJ (eds) Food materials science. Principles and practice. Springer, New York, pp 67–82
Roos YH, Karel M (1991a) Applying state diagrams to food processing and development. Food Technol 12:66, 68–71, 107
Roos YH, Karel M (1991b) Plasticizing effect of water on thermal behavior and crystallization of amorphous food models. J Food Sci 56(1):38–43

Roos YH, Karel M (1991c) Phase transitions of mixtures of amorphous polysaccharides and sugars. Biotechnol Progr 7:49–53
Roos YH, Karel M (1991d) Phase transitions of amorphous sucrose and frozen sucrose solutions. J Food Sci 56:266–267
Roos YH, Karel M, Kokini JL (1996) Glass transitions in low moisture and frozen foods: effect on shelf life and quality. Food Technol 50:95–108
Roos YH, Roininen K, Jouppila K, Tuorila H (1998) Glass transition and water plasticization effects on crispness of a snack food extrudate. Int J Food Prop 1:163–180
Rosenberg M, Sheu TY (1996) Microencapsulation of volatiles by spray drying in whey protein-based wall systems. Int Dairy J 6(3):273–284
Roudaut G, Dacremont C, Vallès Pàmies B, Colas B, Le Meste M (2002) Crispness: a critical review on sensory and material science approaches. Trends Food Sci Technol 13:217–227
Roudaut G, Simatos D, Champion D, Contreras-Lopez E, Le Meste M (2004) Molecular mobility around the glass transition temperature: a mini review. Innovative Food Sci Emerg Technol 5:127–134
Royall PG, Huang C, Tang SJ, Duncan J, Van-de-Velde G, Brown MB (2005) The development of DMA for the detection of amorphous content in pharmaceutical powdered materials. Int J Pharm 301:181–191
Shrestha AK, Howes T, Adhikari BP, Wood BJ, Bhandar BR (2007) Effect of protein concentration on the surface composition, water sorption and glass transition temperature of spray-dried skim milk powders. Food Chem 104:1436–1444
Silalai N, Hogan S, O'Callaghan D, Roos YH (2009a) Dielectric relaxations and stickiness of dairy powders influenced by glass transition. In: Fisher P, Pollard M, Windhab EJ (eds) Proceedings of the 5th International Symposium on Food Rheology and Structure – ISFRS 2009, June 15–18, 2009, Zürich, Switzerland, pp 428–430
Silalai N, Hogan S, O'Callaghan D, Roos YH (2009b) The control of dairy powder characteristics using alpha-relaxation and glass transition data. In: Devahastin S (ed) *Drying 2009* – Proceedings of the 6th Asia-Pacific Drying Conference (ADC2009), October 19–21, 2009, Bangkok, Thailand, pp 61–64
Singh KJ, Roos YH (2005) Frozen state transitions of sucrose-protein cornstarch mixtures. J Food Sci Technol 70(3):E198–204
Singh KJ, Roos YH (2006) State transitions and freeze concentration in trehalose-protein-cornstarch mixtures. LWT 39:930–938
Slade L, Levine H (1991) Beyond water activity: Recent advances based on an alternative approach to the assessment of food quality and safety. Crit Rev Food Sci Nutr 30 (2–3):115–360
Slade L, Levine H (1995) Water and the glass transition-dependence of the glass transition on composition and chemical structure: Special implications for flour functionality in cookie baking. J Food Eng 24(4):431–509
Talja RA, Roos YH (2001) Phase and state transition effects on dielectric, mechanical, and thermal properties of polyols. Thermochim Acta 380:109–121
Truong V, Bhandari BR, Howes T (2005a) Optimization of co-current spray drying process of sugar-rich foods. Part I-Moisture and glass transition temperature profile during drying. J Food Eng 71:55–65
Truong V, Bhandari BR, Howes T (2005b) Optimization of co-current spray drying process of sugar-rich foods. Part II-Optimization of spray drying process based on glass transition concept. J Food Eng 71:66–72
White GW, Cakebread SH (1966) The glassy state in certain sugar containing food products. J Food Technol 1:73–82
Yoshimura M, Takaya T, Nishinari K (1996) Effects of konjacglucomannan on the gelatinization and retrogradation of corn starch as determined by rheology and differential scanning calorimetry. J Agr Food Chem 44:2970–2976

Chapter 19
Caking of Water-Soluble Amorphous and Crystalline Food Powders

Stefan Palzer and Karl Sommer

19.1 Introduction

Time consolidation during storage, often called caking, is a major problem when handling water-soluble powders in a humid and hot environment. Caking requires grinding to transform the powder cake into single particles or agglomerates. Sometimes even whole silos are blocked by caked powder and the powder can only be removed manually using mining techniques. Furthermore, the quality of powder a products is negatively affected by caking during storage or transport. Instead of a free-flowing powder, large powder lumps are delivered to the consumer. To reduce the processing costs caused by the required grinding or sieving and to increase the quality of the end product, such caking has to be avoided.

Mainly powders that contain a major amount of water-soluble amorphous substances are sensitive to caking. Examples of such amorphous substances are: powdered vegetable-, yeast-, and meat extracts, hydrolyzed fish proteins, and hydrolyzed plant proteins, flavoring powders, various food additives such as starch hydrolysates, amorphous lactose, amorphous dextrose, amorphous sucrose, maltose, and amorphous organic acids such as citric- and ascorbic acid and spray-dried dairy powders (Peleg and Mannheim 1977; Wallack and King 1988; Aguilera et al. 1993; Aguilera et al. 1995).

Occasionally caking of fine water-soluble crystalline powders is also observed. Sodium chloride, crystalline citric acid, urea, and sucrose are examples of crystalline powders that consolidate during storage at high relative humidity of the surrounding air. Figure 19.1 shows scanning electron microscopic pictures of different caked powders containing major amounts of amorphous substances. Some inter-particle bridges are highlighted by white circles.

S. Palzer (✉)
Nestle Product Technology Centre York, Nestec York Ltd, P.O. Box 204/Haxby Road, York YO91 1XY, UK
e-mail: stefan.palzer@rdyo.nestle.com

K. Sommer
Department of Process Engineering of Disperse Systems, Technical University of Munich, Am Forum 2, 85354 Freising, Germany

J.M. Aguilera et al. (eds.), *Food Engineering Interfaces*, Food Engineering Series,
DOI 10.1007/978-1-4419-7475-4_19,

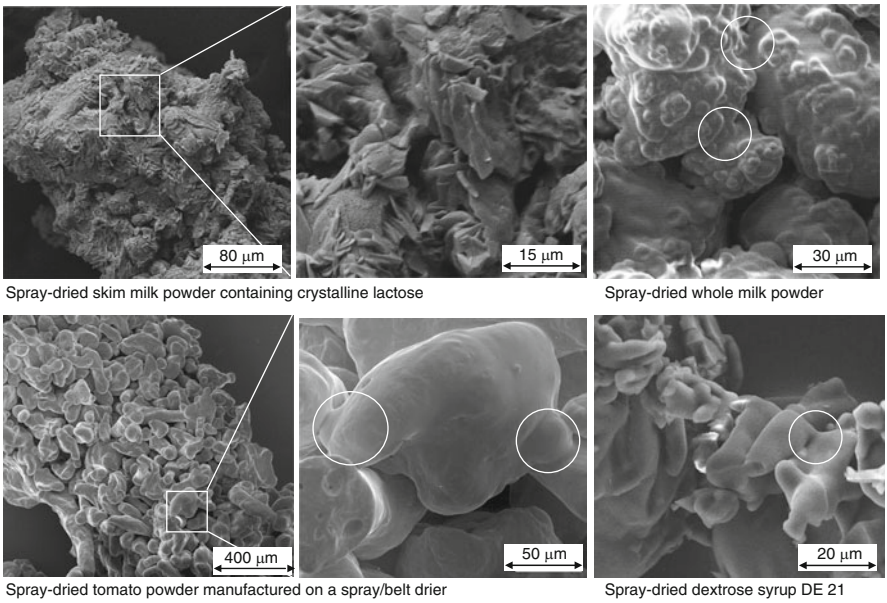

Fig. 19.1 Scanning electron microscopic pictures of caked powders (bridges highlighted by white circles)

As demonstrated in the current study, the chemical composition, supra-molecular structure, and microstructure as well as external factors such as stress, humidity, and temperature are decisive in determining the caking mechanism and the caking kinetic.

19.2 Scientific Background

19.2.1 Supra-molecular Structure and Material Properties

The increase in adhesion forces between single particles causing caking depends on the material properties and the storage or processing conditions. The material properties are a function of the environmental conditions. They also strongly depend on the supra-molecular structure of the material. The relation between supra-molecular structure and material properties has been discussed extensively in previously published scientific articles (e.g., Palzer 2006, 2009a, b). Generally, one can distinguish between polar and nonpolar materials with amorphous, crystalline, and semi-crystalline supra-molecular structures. Amorphous water-soluble structures composed of polar molecules are able to incorporate significant amounts of water. Depending on the vapor pressure or water activity they absorb water molecules, which are then stored inside the free volume in the molecular matrix. The absorbed water increases the mobility of the molecules composing the amorphous

matrix and thus decreases the viscosity of the amorphous material. Furthermore, amorphous matrices are thermo-sensitive. Their viscosity decreases markedly with increasing temperature. Accordingly, a decrease in viscosity, which might cause an increase in adhesion forces, can be equally achieved by increasing temperature or moisture content. Crystalline substances, which might contain crystal water, absorb practically no water molecules until they dissolve, while exceeding their critical relative humidity. Thus, below the critical relative humidity, variations in air humidity do not affect the mechanical properties of the material. Furthermore, temperature variations below the melting temperature do not change the mechanical material properties of crystalline structures significantly. When exceeding the melting temperature the material liquefies completely at constant temperature.

In addition delisquence phenomena might further increase the moisture sensitivity of particle mixtures.

19.2.2 Adhesion Mechanisms

Increasing adhesion forces between particles are a prerequisite for any caking process. Adhesion can be either linked to the development of material bridges or increasing of Van der Waals forces between neighboring particles. For most caking processes the following adhesion mechanisms are relevant:

- Increasing Van der Waals forces due to visco-elastic or plastic deformation
- Liquid bridges with low viscosity containing a low concentration of mono-, oligo- or polymers or ions
- Liquid bridges with medium or high viscosity containing a high concentration of dissolved oligomers or polymers
- Amorphous solid bridges
- Crystalline solid bridges

There is no clear transition from high viscous liquid bridges to amorphous solid bridges. Generally, an amorphous solid is discussed if the viscosity exceeds 10^{10}–10^{11} Pa·s. Depending on the nature of the particles, these listed adhesion mechanisms can contribute to increasing the adhesion force F holding neighboring particles together. The tensile strength of manufactured agglomerates depends on the strength of these adhesion forces acting between primary particles. According to Rumpf (1970), the tensile strength of an agglomerate composed of spheres with a diameter a can be estimated through (19.1):

$$\sigma_t = \frac{1-\varepsilon}{\pi \cdot a^2} \cdot K \cdot F \qquad K \approx \frac{\pi}{\varepsilon} \tag{19.1}$$

where F is the adhesion force between two spheres, ε is the porosity of the agglomerate, and K represents the coordination number of the primary particles of the agglomerate. For spherical particles K is approximately equal to π/ε (Rumpf 1970).

Adhesion between food particles can be linked to increasing Van der Waals forces, which are electrostatic forces generated by temporary load shifts in neighboring molecules. The Van der Waals force F_{vdW} between two deformed particles can be estimated according to Lifshitz (1956) and Hamaker (1937). Except for plastically deformable particles, most caking processes are not caused by increasing Van der Waals forces. However, plastic or visco-elastic deformation of particles leading to increasing number of contact points, increasing contact area, and decreasing distance between neighboring particle surfaces might enhance caking caused by sintering of amorphous substances.

Caking might be also linked to dissolution and re-crystallization of crystalline material. The required water can be liberated in a powder bulk by condensation of humidity from the air or re-crystallization of humid amorphous material. If sufficient water is liberated, liquid bridges between the particles are generated. Dissolution of low molecular weight substances in the liquid changes the viscosity of the liquid bridges only slightly. Thus, the strength of liquid bridges containing mainly dissolved low-molecular substances or a low concentration of polymers mainly depends on capillary forces. The capillary pressure p_c in a liquid bridge can be calculated based on the surface tension γ, the wetting angle Θ, the radius s of the meniscus of the liquid bridge, and the radius x of the cross-section area of the bridge. Assuming that the particles are spherical, the tensile strength σ_t of a humid powder bulk or agglomerate, stabilized by liquid bridges exhibiting a low viscosity, can be estimated according to Rumpf (1958) through (19.2):

$$\sigma_t = S \cdot C \cdot \frac{1-\varepsilon}{\varepsilon} \cdot \frac{2 \cdot \gamma}{a} \cdot cos\,\theta \tag{19.2}$$

where S is the saturation of the porous agglomerate with liquid (ratio of liquid volume versus total void volume within the agglomerate), C is a constant parameter (monodisperse spheres: $C = 6$) (Rumpf 1958), ε is the porosity of the agglomerate, γ is the surface tension of the liquid, a is the diameter of the primary particles, and Θ represents the contact angle between the liquid and the solid substance.

The adhesion forces caused by aqueous liquid bridges containing dissolved substances can be further increased by drying. Finally, the liquid bridge is transformed into a solid bridge (Fig. 19.2). Depending on the drying velocity, solid bridges with amorphous or crystalline structures are obtained.

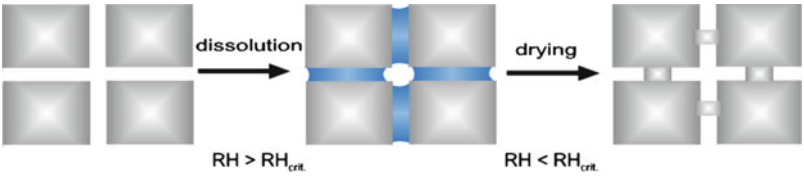

Fig. 19.2 Formation of liquid and solid bridges between crystalline particles (e.g., due to storage at varying relative humidity RH or delisquence)

Changes in the tensile strength σ_t of agglomerates due to dehydration of liquid bridges can be predicted according to Rumpf (1958) by using (19.3):

$$\sigma_t = \frac{V_{diss}}{V_{agglo}} \cdot (1 - \varepsilon) \cdot \sigma_s \tag{19.3}$$

where V_{diss} is the dissolved solid volume within the entire agglomerate, V_{agglo} is the volume of the agglomerate, σ_s represents the tensile strength of the solid substance building the bridge after drying, and ε is the agglomerate porosity. The tensile strength of liquid bridges containing polymer molecules also depends on the strain rate applied during the measurement.

For many powders sintering is the main mechanism leading to time consolidation of the powder bulk. Like low-viscosity liquid droplets, amorphous particles tend to adopt a spherical shape. By bringing two amorphous particles into contact with each other, they can be considered as one new single particle. To minimize the free surface area of this newly created particle, molecules are transported to the contact point between the two primary particles (Fig. 19.3). Such a process is called sintering. The driving force behind the sinter process is the difference between the capillary pressure at the contact point between the particles and the Laplace pressure in the volume of the two initial particles.

Since the capillary pressure is directly linked to the vapor pressure in the continuous gas phase surrounding the particles, a gradient of the vapor pressure exists across the particle. Based on these local differences between capillary and vapor pressure and depending on how big the substances vapor pressure of the substance is, different molecular transport mechanisms are observed. The relevant literature (Kuczynski 1949; Schatt 1992; Wagner 1997) distinguishes between transport of molecules through the vapor phase, surface diffusion, volume diffusion, and grain-boundary diffusion. Substances having a medium or high vapor pressure can be transported via the gas phase surrounding the particles. The sintering substance evaporates at convex particle surfaces, which exhibit a high vapor pressure. Following the evaporation, molecules are transported by diffusion through the gas phase to the concave meniscus of the bridge between two particles. Such concave structures are characterized by a lower vapor pressure. The material condenses at the contact point between the particles and builds a sinter bridge

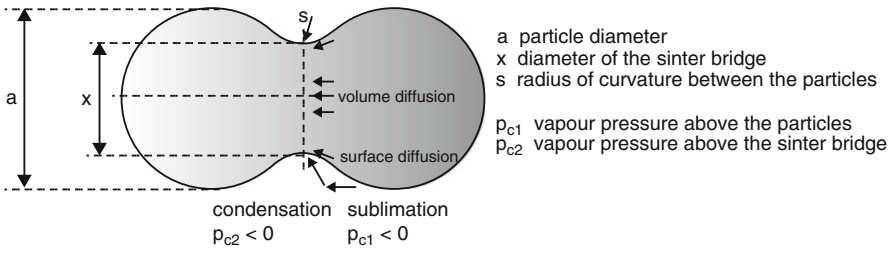

Fig. 19.3 Sintering mechanisms

between them. This evaporation and condensation of substances can contribute significantly to the growth of the sinter bridge if the vapor pressure of the sintering substance is high enough. Since the vapor pressure of most major food components is comparably low, a molecular transport through the gas phase seems to be less relevant for sintering of amorphous food particles. Molecules can also be transported by surface or volume diffusion. Such diffusion of molecules inside the particles, sometimes also referred to as viscous flow, seems to be the most relevant mechanism for sintering of water-soluble amorphous food particles.

The kinetic of such transport processes strongly depends on the diffusion coefficient, which is a function of viscosity. The viscosity of amorphous solids depends on the temperature as well as on the plasticizer content of the material. Thus, sintering of amorphous water-soluble particles can be controlled by adjusting the temperature and/or the water content of the system.

Different sinter phases are usually distinguished according to the observed structural changes in the particle package (Fig. 19.4). In an initial phase, when the sinter bridges are still very thin, the particles adhere to each other. Macroscopically, a reduction of the powder's flowability (often described as "stickiness") is observed. With advancing sinter time the diameter of the sinter bridge grows, which leads to increasing adhesion forces between the particles. Open pores are gradually eliminated and the particles lose their structural integrity. The powder and particle structure collapses, while the system is progressively transformed from a powder into a foam-like system where the air is enclosed in an amorphous melt.

For modeling the sintering of organic particles by viscous flow, Frenkel (1945) published equation (19.4). Assuming the spherical particles have a diameter a, the diameter of the sinter bridge x can be calculated depending on the sinter time t, the surface tension γ, and the viscosity η:

$$\left(\frac{x}{a}\right)^2 = \frac{1}{6} \cdot \frac{\gamma}{a} \cdot \frac{t}{\eta} \tag{19.4}$$

Alternatively, the sinter kinetic can be predicted according to Rumpf et al. (1976). Assuming a punctual contact between the particles and neglecting changes in particle geometry during sintering, they modeled the viscous flow based on the Navier–Stokes equations, where F_t represents the force with which the particles are pressed together.

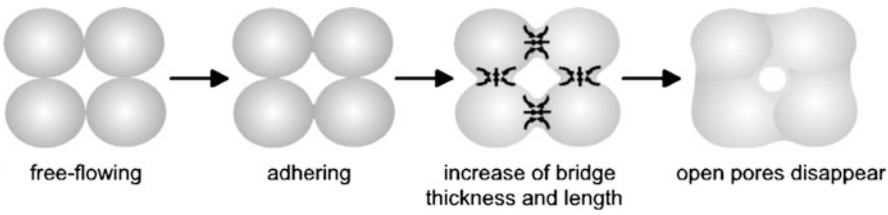

Fig. 19.4 Different phases of the sintering process

$$\left(\frac{x}{a}\right)^2 = \left(\frac{4}{5}\cdot\frac{\gamma}{a} + \frac{2\cdot F_t}{5\cdot\pi\cdot a^2}\right)\cdot\frac{t}{\eta} \tag{19.5}$$

Both equation (19.4) and (19.5) are only valid for the initial phase of the sinter process. For nonspherical particles, the relevant radius a must be estimated based on the curvature radius at the contact point between the particles. A prerequisite for a sinter process is molecular contact between the particles. A moderate force (e.g., caused by weight of particles) pressing the particles together ensures a continuous contact between the particles during sintering. Except for pressure agglomeration the impact of the force F_t on the sinter kinetic can be neglected. Variations in surface tension are mostly limited. Hence, viscosity (which might vary by magnitudes) (Palzer 2006, 2009a) governs the sinter kinetic. As mentioned before, the viscosity of water-soluble amorphous substances depends on their moisture content w and the temperature T. Combining the Gordon-Taylor equation with the Williams-Landel-Ferry equation (Palzer 2009a), and considering the fact that due to sorption or desorption processes the humidity of the amorphous substance might change as a function of time, equation (19.6) is obtained:

$$\left(\frac{x}{a}\right)^2 = \int_{t=0}^{t_{\max}} \left(\frac{4}{5}\cdot\frac{\gamma}{a} + \frac{2\cdot F_t}{5\cdot\ \pi\cdot a^2}\right)\cdot\eta_g^{-1}\cdot 10^{\frac{-C\cdot(T-T_g(t))}{B+(T-T_g(t))}}\cdot dt \tag{19.6}$$

Where t_{max} is the time available for the sinter process. By combining (19.1) with (19.6) the tensile strength of sintered agglomerates can be estimated.

$$\sigma_t = \frac{(1/\varepsilon)\cdot\pi}{\varepsilon}\cdot\sigma_s(T,w,\omega)\cdot\int_{t=0}^{t_{\max}} \left(\frac{4}{5}\cdot\frac{\gamma}{a} + \frac{2\cdot F_t}{5\cdot\ \pi\cdot a^2}\right)\cdot\eta_g^{-1}\cdot 10^{\frac{-C\cdot(T-T_g(t))}{B+(T-T_g(t))}}\cdot dt \tag{19.7}$$

However, in practice it remains difficult to predict the tensile strength of sintered agglomerates because of the geometrical diversity of primary particles and the visco-elastic nature of the built sinter bridges. According to Downtown et al. (1982) a significant adhesion force F between the particles is observed if the diameter ratio x/a exceeds a value of 0.01. Wallack and King (1988) reported that a value x/a of 0.1 is required for adhesion.

19.2.3 Caking Processes

Several of the mentioned adhesion mechanisms can lead to a time consolidation of powders (Tomas 1996). As demonstrated in the current study, mainly sintering is responsible for the observed caking of amorphous food powders. For caking caused by sintering of amorphous particles, several stages can be distinguished. In the

initial phase of the process the powder starts to become sticky and particles adhere to each other. They form brittle lumps, and with progressing sintering, a mechanically stable powder cake is obtained. During a later phase of sintering, particles missing a stabilizing inner structure (built of non-dissolving substances) lose their structure and shape. The powder structure collapses, open pores in the particle package disappear, and finally a highly viscous, amorphous melt is obtained. The shape of some particles (e.g., dehydrated vegetable or fruit pieces) is preserved by an insoluble matrix (e.g., composed of cellulose, fat, or proteins) and, thus, no structural collapse of such powders is observed.

When water-soluble amorphous substances are stored in a high-humidity environment they absorb water and thus their viscosity decreases. Although sintering is accelerated due to the decreasing viscosity, the tensile strength of the growing sinter bridges decreases with increasing water content. Due to the progressing absorption of water, the strength of the powder cake first increases and then in a later phase of the process decreases again. At low moisture content, or in the early phase of the sintering process, the diameter of the sinter bridge limits the stability of the particle cake. The growing diameter of the sinter bridges leads to an increasing strength of the cake. With progressing moisture absorption the viscosity of the bridge decreases and thus the strength of the powder cake decreases again. Finally, the powder structure collapses and a pasty mass is obtained. The viscosity of amorphous substances is also reduced at elevated temperatures, leading to an accelerated sintering of the particles and a steadily increasing strength of the powder cake.

Crystalline water-soluble powders behave differently when exposed to high humidity or temperature. If their critical humidity is temporarily exceeded they will partially dissolve. The formed low viscosity liquid bridges are often rather fragile. However, a stable powder cake can be formed if the absorbed water evaporates again enabling a re-crystallization of the dissolved substance. Caking of crystalline powders stored in closed containers can thus be induced by condensation and evaporation of moisture due to temperature variations. The condensate builds liquid bridges between the particles. After a short time span the liquid forming these bridges is saturated with the dissolving substance. If the condensed water is later evaporated at increasing temperature stable bridges between the particles are formed.

19.2.4 Powder Flowability and Stress States

Caking is characterized by significantly decreasing powder flowability. Increasing adhesion forces lead to decreasing powder flowability. Yielding of a powder bulk strongly depends on such adhesion forces, and the magnitude and direction of the different stresses to which it is exposed. The stress state in a powder can be analyzed by establishing force balances around a prism-shaped powder element. The powder element is exposed to normal stresses σ and shear stresses τ. The position

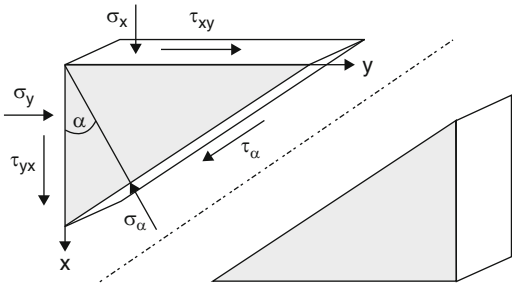

Fig. 19.5 Normal and shear stresses acting on a prism-shaped powder element

of the plane separating the powder prism from the remaining powder volume is characterized by the angle α. The normal and shear stresses acting on or in this plane are σ_α and τ_α (Fig. 19.5).

A necessary condition for yielding of the powder is that the two shear stresses acting on the powder prism are equal to each other ($\tau_{xy} = \tau_{yx}$). By establishing the force balances for the prism-shaped powder element shown in Fig. 19.5, the equations for calculating the shear stress τ_α and the normal stress σ_a acting in the inclined shear plane can be deducted ((19.8) and (19.9)), where *dh* is the depth of the element and *dl* represents the length of the shear plane.

$$\begin{aligned}\sigma_\alpha \cdot dl \cdot dh &= \sigma_y \cdot sin\,\alpha \cdot dh \cdot sin\,\alpha \cdot dl + \sigma_x \cdot cos\,\alpha \cdot dh \cdot cos \cdot dl \\ &\quad + \tau_{yx} \cdot cos\,\alpha \cdot dh \cdot sin\,\alpha \cdot dl + \tau_{xy} \cdot sin\,\alpha \cdot dh \cdot cos\,\alpha \cdot dl \\ \Leftrightarrow\ \sigma_\alpha &= \sigma_y \cdot sin^2\,\alpha + \sigma_x \cdot cos^2\alpha + 2 \cdot \tau_{xy} \cdot sin\,\alpha \cdot cos\,\alpha \\ \Leftrightarrow\ \sigma_\alpha &= \frac{\sigma_x + \sigma_y}{2} + \frac{\sigma_x - \sigma_y}{2} \cdot cos\,2\alpha + \tau_{xy} \cdot sin\,2\alpha\end{aligned} \tag{19.8}$$

$$\begin{aligned}\tau_\alpha \cdot dl \cdot dh &= \sigma_y \cdot dl \cdot sin\,\alpha \cdot dh \cdot cos\,\alpha - \sigma_x \cdot dl \cdot cos\,\alpha \cdot dh \cdot sin\,\alpha \\ &\quad - \tau_{xy} \cdot dl \cdot sin\,\alpha \cdot dh \cdot sin\,\alpha + \tau_{xy} \cdot dl \cdot cos\,\alpha \cdot dh \cdot cos\,\alpha \\ \Leftrightarrow \tau_\alpha &= -\frac{\sigma_x + \sigma_y}{2} \cdot sin\,2\alpha + \tau_{xy} \cdot cos\,2\alpha\end{aligned} \tag{19.9}$$

There are two values for the angle α for which the shear stress τ_α in the shear plane equals zero.

$$\begin{aligned}&\alpha = \frac{1}{2} \cdot \arctan\left(\frac{2 \cdot \tau_{xy}}{\sigma_x - \sigma_y}\right) \quad or \quad \alpha = \frac{1}{2} \cdot \arctan\left(\frac{2 \cdot \tau_{xy}}{\sigma_x - \sigma_y}\right) - \frac{\pi}{2} \\ &\Rightarrow\ \tau_\alpha = 0\end{aligned} \tag{19.10}$$

The normal stresses in the shear plane corresponding to these two angles are called main consolidation stress σ_1 and σ_2. Knowing σ_1, σ_2, and the inclination

angle α allows calculation of the normal stress and the shear stress acting on the powder element.

$$\sigma_{xy} = \frac{\sigma_1 + \sigma_2}{2} \pm \frac{\sigma_1 - \sigma_2}{2} \cdot cos\, 2\alpha$$
$$\tau_{xy} = -\frac{\sigma_1 - \sigma_2}{2} \cdot sin\, 2\alpha \tag{19.11}$$

By varying the inclination angle α, a number of corresponding σ/τ combinations are obtained. The so-called Mohr's circle can be constructed by plotting these σ/τ pairs in a σ/τ diagram. The Mohr's stress circle represents all possible stress states of a bulk solid element.

If σ_2 equals zero, the mono-axial stress state is given. In the mono-axial stress state, the bulk solid element is exposed to stress in only one direction. For the mono-axial and the bi-axial stress states, the Mohr circles are shown in Fig. 19.6. In the bi-axial stress state both main consolidation stresses are larger than zero.

Complementary to the stress state, in a confined powder volume the flow properties of the powder have to be analyzed. Only the combination of possible stress states with the material properties will allow a prediction of the powder's behavior. The powder flowability is characterized by the combination of normal and shear stress, which leads to yielding of the powder bulk. The powder is always pre-sheared to provide a constant bulk density and then sheared under varying normal loads to identify the shear stress required for yielding. The obtained σ/τ combinations build the so-called yield locus, which can be plotted in a σ/τ diagram (Fig. 19.7). According to the theory of Mohr and Coulomb the obtained σ/τ combinations form a straight line in the σ/τ diagram running through the origin:

$$\tau = tan\, \varphi \cdot \sigma + C \tag{19.12}$$

where φ_e is the angle for stationary flow and φ is the flow angle of incipient flow.

Following the theory of the mono-axial and the bi-axial stress states, two Mohr circles can be constructed to which the yield locus is tangential. The pre-shear point

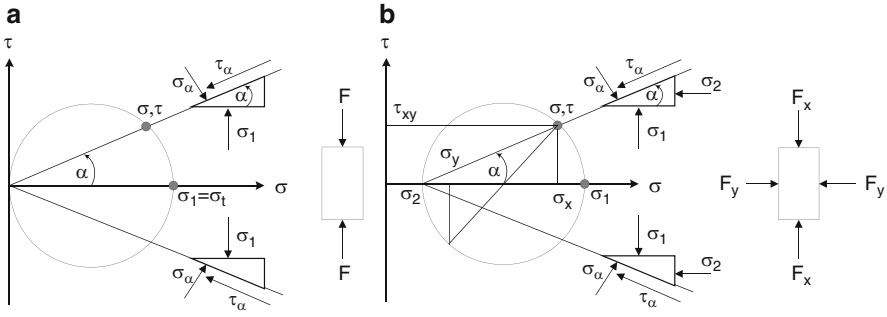

Fig. 19.6 Mohr's circle for the mono-axial (**a**) and bi-axial (**b**) stress states

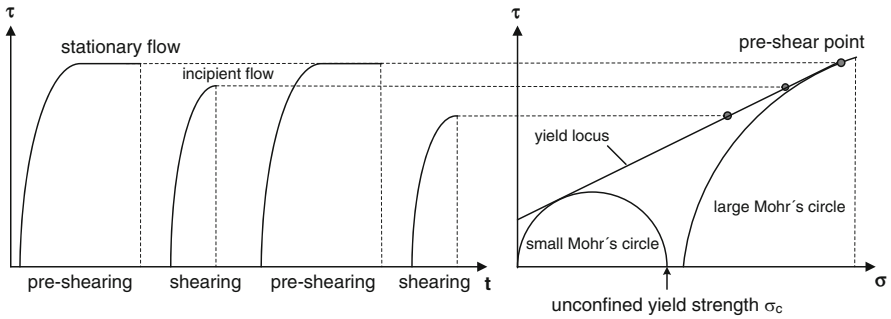

Fig. 19.7 Determining the yield locus based on results from shear tests

is located on the larger Mohr circle, which represents the bi-axial stress state. The normal stress at which the smaller Mohr circle intersects with the vertical stress axis is called unconfined yield strength σ_c. The unconfined yield strength is a measure of the stability of the powder cake and can thus be used to quantify caking. The normal stress at which the larger of the two Mohr circles intersects with the vertical stress axis is called principle consolidation stress σ_1 (Fig. 19.7).

The flow factor *ffc* of a powder is calculated as the ratio between the principle consolidation stress σ_1 and the unconfined yield stress σ_c. It characterizes the powder's flowability at the powder density achieved during pre-shearing.

$$ff_c = \frac{\sigma_1}{\sigma_c} \tag{19.13}$$

Based on the flow factor, Jenicke (1970) published the following scale for grouping powders concerning their flowability.

$ff_c < 1$ hardened
$1 < ff_c < 2$ very cohesive
$2 < ff_c < 4$ cohesive
$4 < ff_c < 10$ easy flowing
$ff_c > 10$ free flowing

19.3 Materials and Methods

19.3.1 Materials

The spray-dried dextrose syrup used in the reported trials has a dextrose equivalent (DE) of 20–23, an initial water content of 4% (db) (water activity, $a_w = 0.18$), and a mean particle diameter $x_{50,3}$ of (150 ± 25) µm. The yeast extract is characterized by a mean particle diameter $x_{50,3}$ of (101 ± 34) µm. The sodium chloride has a mean

particle diameter $x_{50,3}$ of (507 ± 75) μm and a water content below 0.1% (db). The sucrose used is purified (99% pure sucrose). The crystalline sucrose powder has a particle diameter $x_{50,3}$ of (643 ± 66) μm and contains less than 0.1% water (db). The spray-dried amorphous sucrose powder has a diameter $x_{50,3}$ of (135 ± 22) μm.

19.3.2 Method for Measuring Caking

The flowability of the powder sample is evaluated through ring-shear tests. Figure 19.8a illustrates the principle of the used ring-shear tester and Fig. 19.8b shows the shear-cells used for time consolidation trials.

For each test the sample is filled into a cell having the form of a ring. The cell is then closed with a cover ring that has some baffles reaching into the powder. This cover ring lying on the powder bulk and can be turned using a motor. The torque required to turn the cover ring against the cell body is measured depending on the normal stress acting on the ring cover. By taking the ring geometry into consideration, the measured torque can be transformed into a shear stress. The shear stress τ is the stress required to initiate yielding the powder which is exposed to a defined normal stress σ. Each powder sample is sheared twice: by pre-shearing, a constant density is assured for all samples, whereas subsequent shearing delivers information about the powder's flowability. For pre-shearing, the sample is filled into the ring cell and the ring cover is loaded with a defined weight exposing the powder to a defined normal stress. Then the ring cover is turned until a constant torque is obtained. This torque can be transformed into the shear stress required for stationary flow of the powder at a constant density. After performing such pre-shearing the powder has a defined density. Now the normal stress acting on the ring cover is reduced and the powder is sheared again. The shear stress at which the powder starts yielding is measured. This procedure has to be repeated by applying the same normal stress for pre-shearing and varying the normal stress during shearing. The obtained σ/τ pairs are only valid

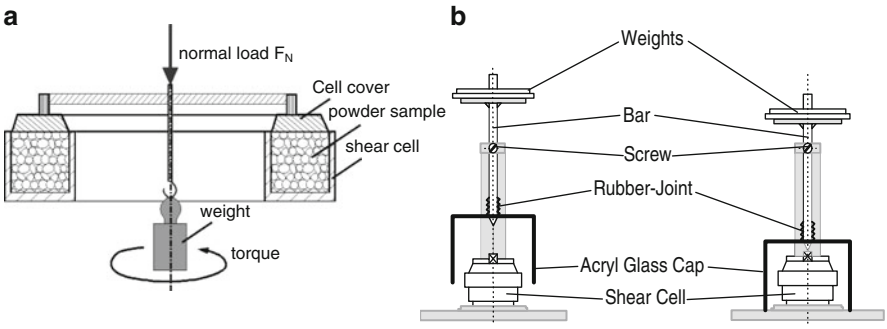

Fig. 19.8 Principle of a ring shear tester (**a**) and cells used for time consolidation trials (**b**)

for the constant powder density achieved by the chosen normal stress used for pre-shearing.

Time-consolidation trials using a ring shear tester are performed as follows: The samples are filled in ring-shear cells. A pre-shearing of the samples provides a defined powder density. Next, the shear cells are stored under controlled conditions for a defined time. The cover ring of the cell lying on the powder carries a defined weight during storage. Each cell has a housing in which the temperature and the relative humidity of the air can be adjusted individually (Fig. 19.8b). Before and after storage, the flowability of the powder sample stored in the ring cell is measured in a shear tester (Fig. 19.8a). The observed increase in unconfined yield strength and the calculated increase of the flow-factor are appropriate measures to quantify the intensity of caking.

To quantify the caking intensity, the unconfined yield strength σ_c of the initial sample and the stored powder has to be compared with each other. Either the increase in unconfined yield strength σ_{ct} or the decrease in the flow factor *ffc* can be used for quantifying the degree of caking. Empirically, it has been found that strong caking corresponds to an increase in unconfined yield strength of more than 500–1,000 Pa.

One of the major drawbacks of time consolidation experiments in ring-shear cells is the hampered exchange of moisture between the air and the sample during the consolidation phase. Contrary to such test conditions, in practice moisture absorption and time consolidation are often parallel processes, which are difficult to separate from each other.

19.4 Results and Discussion

19.4.1 Caking of Amorphous Water-Soluble Powders

In the current study caking of pure dextrose syrup (DE 21) was investigated. In the first series of trials the sintering of two amorphous dextrose syrup particles (DE 21) was monitored. Two particles were exposed at constant temperature of 25°C to relative humidity of 70%. Both particles were placed on a silanized hydrophobic glass plate and the relative humidity of the surrounding air was adjusted by using a saturated salt solution. Figure 19.9 shows the water content of the particles dependent on storage time and images of the growing sinter bridge developed between the two particles.

The absorbed moisture leads to a decreasing viscosity of the amorphous matrix and thus sintering is accelerated. A stable sinter bridge is obtained after 3–6 h of storage. Finally, the two particles coalesce and form a single viscous droplet. Such changes also happen in a bulk of amorphous water-soluble particles stored at elevated humidity and temperature.

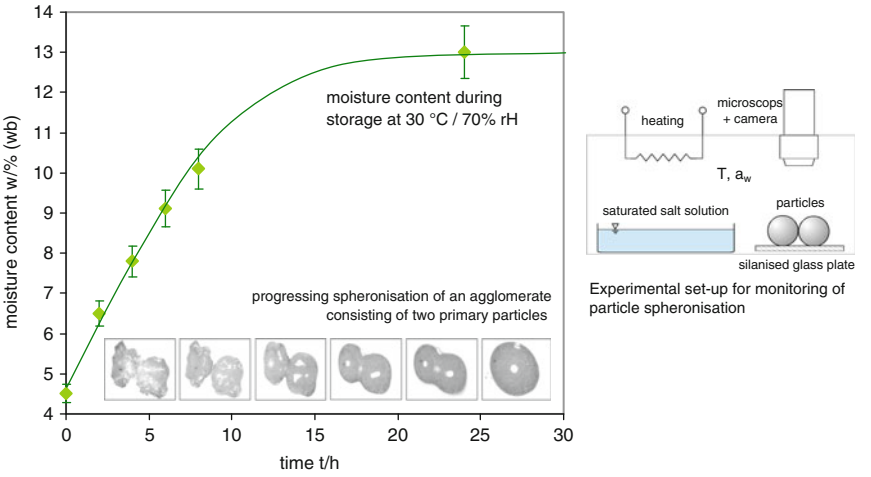

Fig. 19.9 Moisture content and visual appearance of two dextrose syrup particles (DE 21) stored at 25°C and 70% RH as a function of storage time

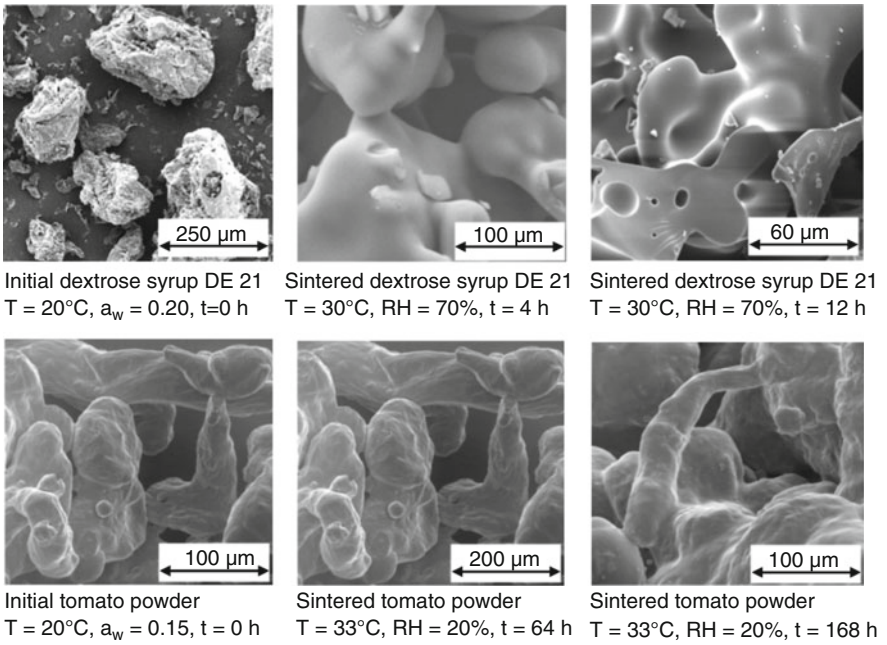

Fig. 19.10 Sintering of spray-dried tomato and spray-dried dextrose syrup (DE 21) powders stored at 10–20°C above their glass transition temperatures

Figure 19.10 shows a dextrose syrup powder and a tomato powder, which were both stored at 10–20°C above their glass transition temperatures. With progressing storage time the dextrose syrup particles sinter together and finally the powder completely loses its structure. The tomato powder particles also sinter together. However, dehydrated cell walls, which are mainly composed of water insoluble cellulose and hemicellulose, preserve their structure. Thus, no complete collapse of the particle structure is observed.

As already discussed, the sinter bridge diameter can also be calculated using equations (19.5) or (19.6). Figure 19.11 shows a comparison of the calculated sinter bridge diameter (19.6) with the measured sinter bridge diameter between two dextrose syrup particles stored at 30°C and 70% RH (see also Fig. 19.9).

The calculated kinetics of sintering is in good agreement with the measured increase of the diameter of the sinter bridge. Despite the various assumptions and simplifications made, equation (19.6) allows a satisfying prediction of the sinter kinetic of amorphous water-soluble particles. Possibly, the accuracy of the prediction can be further improved by taking into account a moisture gradient along the particle diameter. Using the Navier–Stokes equations for a pair of sintering particles, the viscosity gradient corresponding to the moisture distribution inside the particles has to be considered.

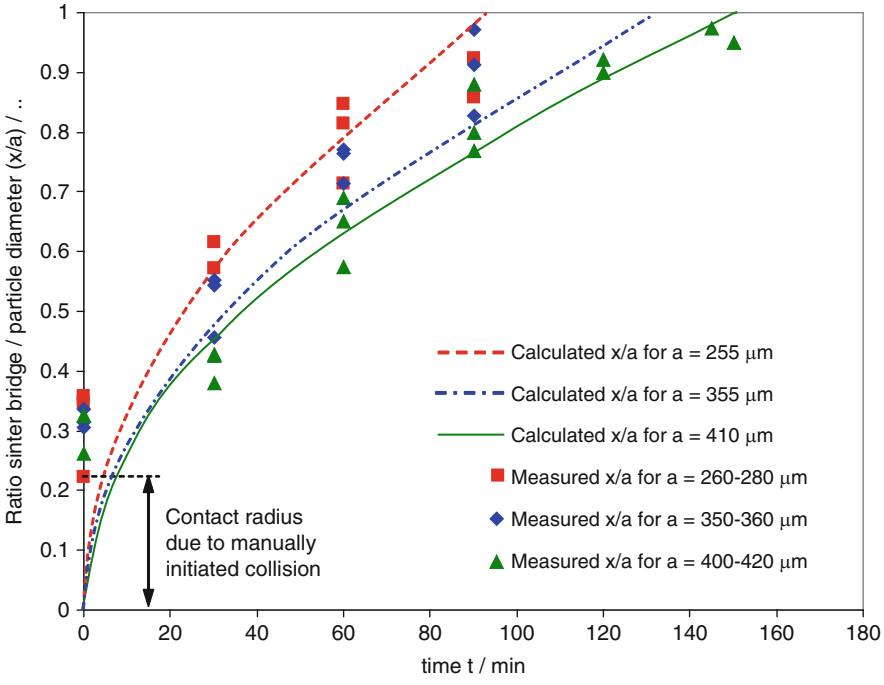

Fig. 19.11 Comparison between the calculated and measured sinter bridge/particle diameter ratio for pairs of spray-dried dextrose syrup particles (DE 21) stored at 30°C and 75% RH ($T_g = -4$°C; $\gamma_{l,g} = 70$ mNm, $\eta = 10^6$ Pa·s)

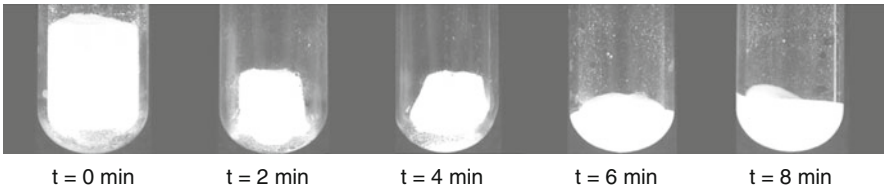

Fig. 19.12 Collapse of a package of dextrose syrup particles exposed to increasing temperature (DE 21; 10% moisture (wb); heated in an oil bath at oil temperature of 90°C)

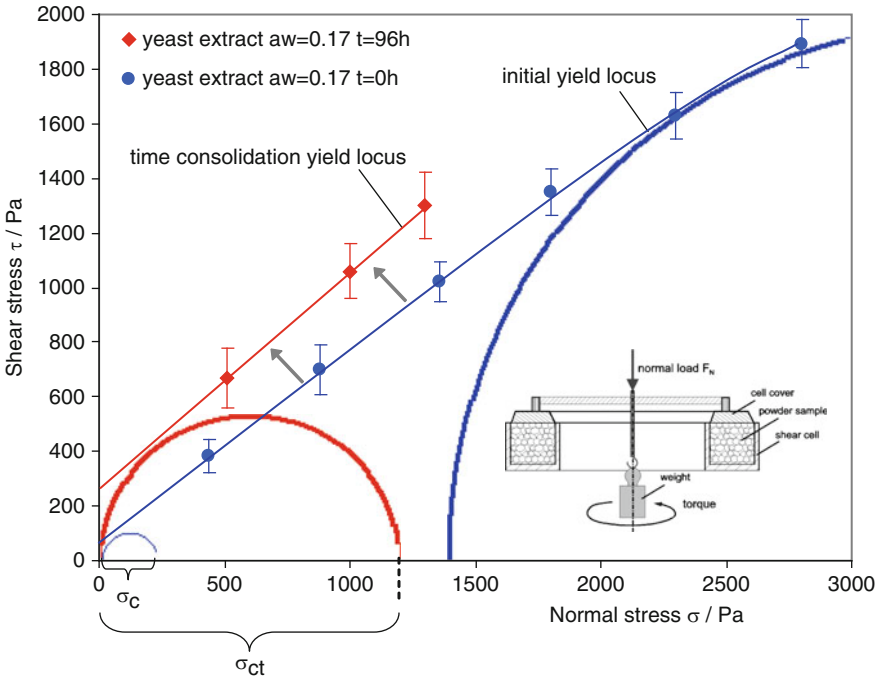

Fig. 19.13 Initial shear locus of yeast extract and shear locus of yeast extract stored for 5 days at 10°C above T_g (ring shear tester; $T = 25$°C; $a_w = 0.17$, $t = 96$ h; consolidation stress 1,200 Pa)

A number of macroscopically visible changes in the powder bulk are linked to the described sinter processes. Figure 19.12 shows a glass tube filled with a dextrose syrup powder (DE 21; water content 10%). The tube is heated in an oil bath at 90°C. A loss of porosity and a shrinking of the powder package are observed. In the final stage of the process the particle package collapses and a viscous melt is obtained.

The development of sinter bridges between the particles leads to a decreasing flowability of the powder bulk. Figure 19.13 shows the shift of the yield locus and the increase in unconfined yield strength σ_{ct} of yeast extract with a water activity of 0.17, stored for 5 days at 10°C above its glass transition temperature. The yeast

extract shown in Fig. 19.13 exhibits a strong caking that corresponds with an increase in unconfined yield strength of roughly 1,000 Pa·s. Similar results can be obtained using dextrose syrup, maltodextrine powders, or other water-soluble amorphous food powders.

It is necessary to predict such caking of amorphous powders in order to reduce manufacturing costs and to avoid a decrease in quality of the final product. Assuming a constant viscosity of the amorphous substance forming the bridge, the unconfined yield strength should be a function of the average sinter bridge diameter. In Fig. 19.14 the unconfined yield strength of spray-dried tomato powder, dextrose syrup, and hydrolyzed whey permeate (Teunou and Fitzpatrick 1999a, b) is plotted against the calculated squared ratio between the diameter of the sinter bridge and the particle diameter $(x/a)^2$. The ratio $(x/a)^2$ is calculated through (19.6). According to the results obtained, the unconfined yield strength increases with the increasing ratio $(x/a)^2$ more or less linearly for $(x/a)^2$ values exceeding 0.05. The observed onset of consolidation is in agreement with the studies of Downtown et al. (1982), Wallack and King (1988), and Aguilera et al. (1993) who observed a caking if the ratio between the radius of the sinter bridge and the particle diameter x/a exceeds a value ranging from 0.01 to 0.1. According to (19.7) the unconfined yield strength of the powder cake should theoretically increase linearly with $(x/a)^2$. Such correlation can be confirmed for values of $(x/a)^2$ exceeding 0.05 (Fig. 19.14).

In the initial phase of the storage process the growth of the sinter bridge might be delayed due to incomplete contact between the particles. The gap at the contact points between single particles has to be bridged before the development of the bridge is initiated. Such a delay of the sinter process might explain why a theoretical ratio $(x/a)^2$ of 0.05 has to be exceeded before a linear increase in tensile strength is observed. Another explanation is that the initial powder is in disequilibrium with

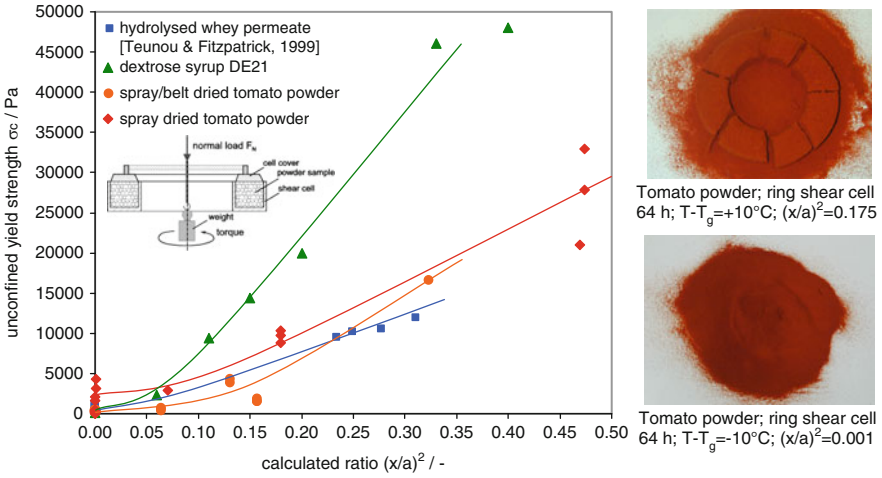

Fig. 19.14 Measured unconfined yield strength of tomato powder, dextrose syrup DE 21, and hydrolyzed whey permeate plotted against the calculated ratio $(x/a)^2$ (19.6)

the surrounding air and in the early phase of the experiments moisture still migrates into the particles. Only the moisture content on the particle surface is used for calculating the diameter of the sinter bridge, although the viscosity of the particle inside is also relevant for sintering by viscous flow. Hence, a calculation based purely on the initial moisture content of the particle surface at the beginning of the process yields too large bridge diameters.

Apparently, the risk of caking can be predicted through the calculated sinter bridge diameter. It is important to notice that equation (19.6) used for calculating the theoretical ratio $(x/a)^2$ is valid only for the initial phase of the sintering process. Furthermore, dehydrated cell structures in the tomato powder particles bind the strongly plasticized amorphous substance through capillary forces and some substances might crystallize. Thus, the availability of amorphous material (which builds the sinter bridges) might be limited. Consequently, the real growth kinetic of the sinter bridge can deviate significantly from the predicted growth rate.

Despite all the mentioned effects, it has been demonstrated that the risk of caking of water-soluble amorphous powders can be predicted by calculating the theoretical sinter bridge diameter. The influence of viscosity, which might vary by order of magnitudes due to increasing moisture and/or increasing temperature, dominates by far most of the other effects. The general conclusion is that caking can be expected when the calculated $(x/a)^2$ value exceeds 0.05.

19.4.2 Caking of Crystalline Powders

Crystalline particles show no time consolidation at constant moisture content. If the relative humidity of the air exceeds temporarily, or locally, the critical humidity of the crystalline substance, a partial superficial dissolution is observed. With decreasing of the relative humidity, the generated liquid bridges dry out again. The dissolved substance re-crystallizes and builds solid bridges between the particles. Such changes might be observed especially when storing the powder in closed storage containers, excluding a convective moisture transfer to the environment. To estimate the risk of caking, it is sufficient to analyze the expected variations in temperature, and to estimate the corresponding changes in relative humidity of the air through the Mollier diagram for humid air. If the predicted maximum relative air humidity inside the powder bulk exceeds the critical humidity of the crystalline substance, the probability of caking is high.

19.4.3 Caking of Powder Mixes

Dehydrated food products are often mixes of different powdered components. Caking of such powder mixes depends on the physico-chemical properties of their components, the amount of each component, and the distribution of the different

components in the mix. There are very few scientific studies that investigate the caking of complex powder mixes in view of the particle size distribution and the particle shape of single components.

In the current study, the caking of binary mixes of amorphous spray-dried yeast extract and amorphous spray-dried dextrose syrup powder (DE 21) was investigated through time consolidation experiments performed in ring-shear cells. The two powders are characterized by a similar particle size distribution. Both powder components were stored for 3 days in the form of a thin powder layer at 25°C and a relative humidity (RH) of 17 or 35%. Because the yeast extract powder starts to cake during storage at a relative humidity of 35%, it was sieved again before being mixed with a varying amount of dextrose syrup powder. The powder mixes, characterized by a water activity of 0.17 or 0.35 and containing different amounts of yeast extract and dextrose syrup, were filled into the shear cells, pre-sheared, and stored at 25°C for 96 h under a consolidation (normal) stress of 1,100–1,300 Pa. At relative humidity of 35% the dextrose syrup has a glass transition temperature of 50–60°C, while that of the yeast extract is roughly −15°C. Thus, it can be expected that the yeast extract particles will be strongly plasticized as the dextrose syrup remains glassy. Figure 19.15 shows the measured yield loci dependent on storage time, humidity, and composition of the blend.

At water activity of 0.17 and corresponding relative humidity of 17%, the shear stress required for yielding for all powder blends is comparably low. All dextrose syrup/yeast extract blends are free-flowing. The flowability of powder blends containing yeast extract, which was conditioned at relative humidity of 35%, significantly decreases if the blend contains more than 25% yeast extract.

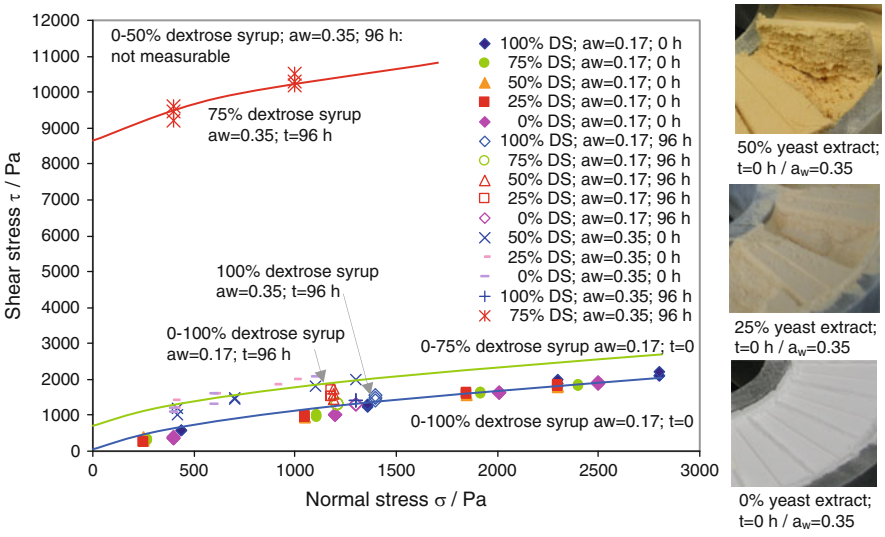

Fig. 19.15 Yield loci of different dextrose syrup/yeast extract blends at a water activity of 17% or 35% (storage time 0 h and 96 h; consolidation stress 1,100–1,300 Pa; bulk density 480–490 kg/m^3)

To analyze the experimental data and to characterize the flowability of the samples, the unconfined yield strength can be plotted against the corresponding principle consolidation stress (Fig. 19.16). In addition, lines of constant flow factor *ffc* (19.13) can be included in the established graph to characterize the flowability of the samples. A flow factor smaller than 1 is equivalent to a hard powder cake. A flow factor between 1 and 2 represents a very cohesive powder. In Fig. 19.16 the unconfined yield strength of the non-stored powder mixes is plotted against their principle consolidation stress.

Apparently, the flowability of pure dextrose syrup only slightly decreases if the water activity is increased from 0.17 to 0.35. As already mentioned, the flowability of powdered mixes containing at least 25% yeast extract significantly decreases if the water activity of the mix is increased from 0.17 to 0.35. A hard powder cake is obtained at a yeast extract concentration of more than 50%. At this concentration the macroscopic behavior of the powder mix is governed only by the yeast extract. At a yeast extract concentration of below 25%, the flowability of the entire powder mixture is identical to that of pure dextrose syrup.

In Fig. 19.17 the unconfined yield strength of non-stored ($t = 0$ h) powder blends, with water activity of 0.35, is compared with the unconfined yield strength of identical samples stored for 96 h.

The flowability of all powder mixes with water activity of 0.17 remains nearly unchanged during storage. The same result is obtained for pure dextrose syrup with water activity of 0.35. However, the flowability of mixes with water activity of 0.35 and containing at least 25% yeast extract strongly decreases during storage. Powder blends containing a higher amount of yeast extract are

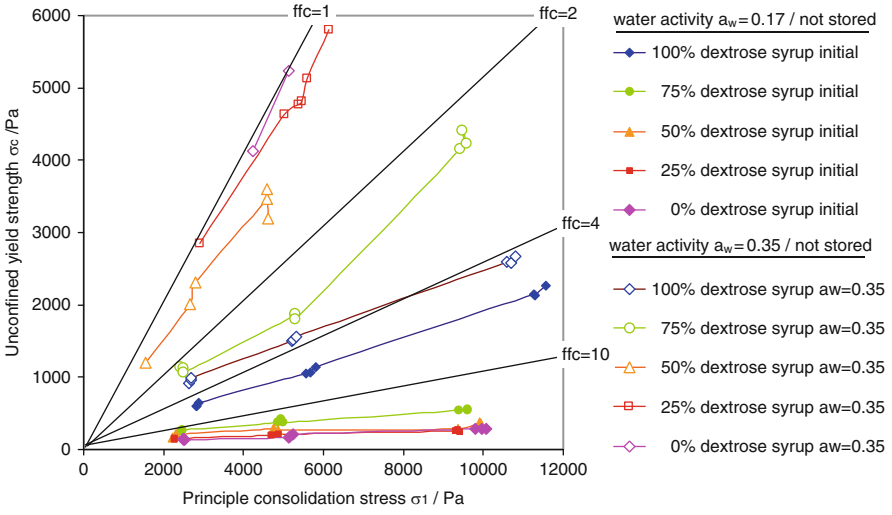

Fig. 19.16 Unconfined yield strength dependent on the principle consolidation stress for different *non-stored* dextrose syrup/yeast extract blends with different water activity (storage time 0 h; pre-shear stress 1,100–1,300 Pa; powder density 480–490 kg/m^3)

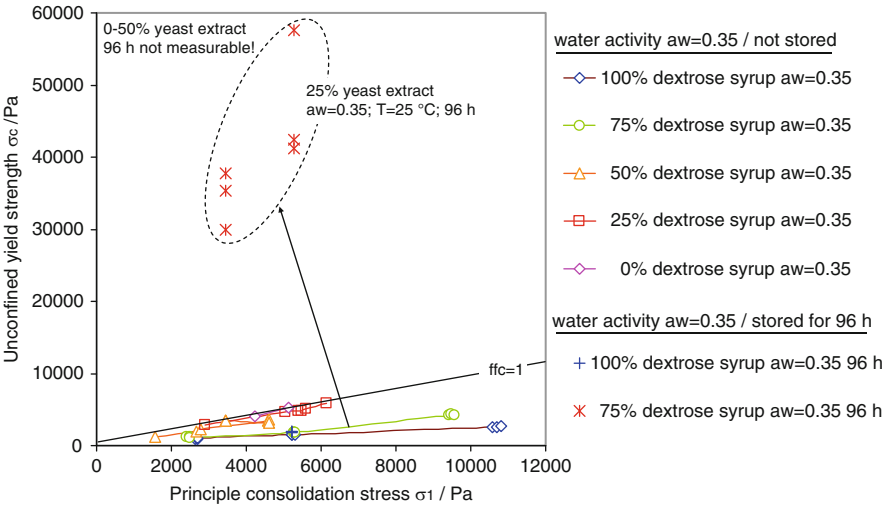

Fig. 19.17 Unconfined yield strength dependent on the principle consolidation stress for different *stored* dextrose syrup/yeast extract blends with water activity a_w of 0.35 (storage time $t = 0$ h and $t = 96$ h; pre-shear stress 1,100–1,300 Pa; powder density 480–490 kg/m^3)

strongly plasticized and, thus, ring shear tests are not the appropriate method to characterize their flowability. Hence, flowability of these powder mixes was described only qualitatively.

In a second series of trials the caking of powder blends composed of amorphous spray-dried dextrose syrup (DE 21; $a_w = 0.17$) and amorphous maltodextrine (DE 6; $a_w = 0.20$) was investigated. Both spray-dried powders, which are mixes of different dextrose oligomers, have a similar particle size distribution. Different blends of the components of these two powders were stored in the form of a thin layer in open tins at 30°C and 70% RH. The caking intensity of the different powder blends is described using a predefined semi-quantitative scale. Contrary to the time consolidation trials in ring-shear cells, an exchange of moisture between the powder layer in the tins and the surrounding air is possible. At 30°C and relative humidity of 70% the glass transition temperature T_g of the dextrose syrup is exceeded by 30°C, whereas for the maltodextrine the difference between storage temperature T and T_g is smaller than 5°C. Accordingly, it can be expected that only the dextrose syrup particles will sinter together with solid surfaces or neighboring particles. The results of the trials are summarized in Table 19.1.

Apparently, a concentration of 17–20% of the sintering component is required for time consolidation of the entire powder blend (Palzer 2006). Assuming a systematic mix of powder fractions, a similar size of the particles, and a cubic particle package, one adhesive particle should be able to bind six surrounding non-adhesive particles. This theoretical ratio (1:6) is equal to a mass fraction of 14%. Since the adhesive particles are neither systematically distributed within the mix nor is an ideal cubic particle package given, it is not surprising that the experimentally determined

Table 19.1 Caking of dextrose syrup DE 21/maltodextrine DE 6 blends stored at 30°C/70% RH

Concentration of dextrose syrup/% (DE 21: DE 6)	0	10 (1:9)	14 (1:6)	17 (1:5)	20 (1:4)	33 (1:2)	50 (1:1)	67 (2:1)	80 (4:1)	83 (5:1)	86 (6:1)	100
Storage time $t = 0$ h	–	–	–	–	–	–	–	–	–	–	–	–
Storage time $t = 24$ h	–	–	–	–	+	+	+	+	+	+	+	+
Storage time $t = 72$ h	–	–	–	+	+	+	+	+	+	+	+	+
Storage time $t = 168$ h	–	–	–	+	+	+	+	+	+	+	+	+

(−) free flowing; (+) caked

concentration of the adhesive particles required for caking is a few percentages higher than the theoretical value.

It can be expected that the smaller the particles of one powder fraction, the larger their influence on the macroscopic behavior of the mix. To avoid caking of powder masses and to improve their flowability, 0.2–3.0% of a flow agent (e.g., silicid acid or starch) is often added to powders that tend to exhibit strong caking. The efficiency of such anti-caking agents can be improved by reducing their mean particle diameter. However, it should be considered that the anti-caking agents used in amorphous powders are only effective for a limited storage time. With progressing time these small particles, acting as distance pieces between the amorphous particles, are absorbed into the amorphous matrix due to sinter processes.

Sometimes caking of blends of water-soluble crystalline and amorphous particles is observed at humidity/temperature combinations, in which case neither the pure amorphous substance nor the pure crystalline substance is sufficiently plasticized, and starts to dissolve. At the contact point between the crystals and amorphous particles a tertiary molecular mix composed of both substances and water is formed. The sorption isotherm of this particle mix deviates significantly from the sorption isotherm obtained by combining the isotherms of the pure substances according to their percentage in the mix. Accordingly, a partial dissolution of the substances is often observed at conditions in which the pure components of the powder mix are stable. Bringing the particles of both components in contact with each other increases their moisture sensitivity. This phenomena is sometimes also refered to as delisquence. Thus caking is observed at a relative humidity value which is significantly below the humidity, leading to time consolidation of the pure components of the powder mix (Schreyer et al. 2008).

19.4.4 Influence of Re-crystallization of Amorphous Substances on Caking

Crystallization of amorphous substances during storage influences caking because only amorphous substances sinter together at the given low temperatures. Furthermore, crystallization processes affect caking due to the different moisture capacity

Table 19.2 Caking intensity and crystallinity of skim milk powder stored at 30°C/70% RH

Storage time t/h	0	2	4	6	8	10	12	14	18	20	22	24
Caking intensity	–	–	–	–	(+)	(+)	(+)	(+)	(+)	(+)	(+)	(+)
Crystallinity of lactose (% of total lactose)	8	52	74	84	86	87	87	96	97	100	100	100

(−) free flowing; (+) slightly caked

between amorphous and crystalline matrices. The water capacity of crystalline structures is limited to their crystal water. With some exceptions the amount of moisture that can be bound in a crystalline structure is small. Hence, in most cases water is liberated during crystallization of amorphous water-soluble substances. The liberated humidity has an autocatalytic effect on the crystallization process and it accelerates sintering of the remaining amorphous substance. On the other hand, it transforms the amorphous material, which builds the sinter bridges between the particles into stable crystalline structures. Taking these two effects into account it can be expected that in the initial phase of the process crystallization accelerates caking, whereas toward the end of crystallization a shortage of amorphous substance will limit the growth of the sinter bridges.

Caking and crystallization of amorphous lactose or spray-dried milk powder containing amorphous lactose is a well-known phenomenon (Lloyd et al. 1996). In this chapter, the impact of lactose crystallization on the caking of spray-dried skim milk powder is discussed. The milk powder was stored at 30°C and relative humidity of 70%. Table 19.2 shows the degree of crystallinity (quantified by light microscopy with polarized light and image analysis) and the caking intensity observed for different storage times.

Exposing the skim milk powder to the test climate, crystallization immediately starts and the amount of available amorphous lactose decreases. In the mean time, water is liberated due to the transformation of the hygroscopic amorphous lactose into its crystalline state. After 6 h of storage, 84% of the total lactose has already been crystallized. After storage for 8 h a caking of the powder is observed. During the following hours the hardness of the obtained skim milk powder cake does not increase further. This observation might be explained by a shortage in amorphous lactose due to the progressing crystallization.

19.5 Summary and Conclusions

As shown in the current study caking of water-soluble powders is linked to either sintering of the amorphous substances or partial dissolution and re-crystallization of crystalline materials. The kinetic of caking of amorphous particles can be predicted based on the calculated theoretical sinter bridge diameter. The risk of caking of crystalline substances can be estimated by comparing the critical relative humidity leading to dissolution with the relative humidity of the surrounding air. Caking of binary mixes of water-soluble amorphous particles (similar size) is determined by sintering of the most moisture sensitive component, i.e., if the amount of this

component exceeds 15–20% in the mix. However, due to interactions between the different substances, time consolidation of mixes of water-soluble crystalline and amorphous powders is sometimes observed at temperature/moisture conditions in which the isolated pure components of the mix remain free flowing.

References

Aguilera J, Levi G, Karel M (1993) Effect of water content on the glass transition and caking of fish protein hydrolysates. Biotechnol Prog 9:651–654

Aguilera J, Valle J, Karel M (1995) Caking phenomena in amorphous food powders. Trends Food Sci Technol 6:149

Downtown G, Flores-Luna J, King C (1982) Mechanism of stickiness in hygroscopic, amorphous powders. Ind Eng Chem Fundam 21:447–451

Frenkel J (1945) Viscous flow of crystalline bodies under action of surface tension. J Phys (USSR) 9(5):385–391

Hamaker H (1937) The London-Van der Waals attraction between spherical particles. Physica 4(10):1058–1072

Jenike, A.W. (1970) Storage and flow of solids. Bull. 123, Eng. Exp. Station, University of Utah, Salt Lake City/US

Kuczynski G (1949) Self-diffusion in sintering of metallic particles. J Metal 1(2):169–178

Lifshitz E (1956) The theory of molecular attraction forces between solids. Soviet Phys JETP 2(1):73–83

Lloyd R, Chen X, Hargreaves J (1996) Glass transition and caking of spray-dried lactose. Journal of Food Science Technology 31:305–311

PalzerS (2006) Influence of supra-molecular structure and storage conditions on the caking of powders. Proceedings of the 5th World Congress on Particle Technology 2006, paper no. 231a

Palzer S (2009a) Influence of material properties on the agglomeration of water-soluble amorphous particles. Powder Technol 189:318–326

Palzer S (2010) Relating the supra-molecular structure of water-soluble food solids with their material properties. Trends in Food Science and Technology 21(1):12–25

Peleg M, Mannheim C (1977) The mechanism of caking of powdered onion. J Food Proc Preserv 1:3

Rumpf H (1958) Grundlagen und Methoden des Granulierens. Chem Ing Techn 30(3):144–158

Rumpf H (1970) Zur Theorie der Zugfestigkeit von Agglomeraten bei Kraftübertragung an Kontaktpunkten. Chem Ing Techn 42(8):538–540

Rumpf H, Sommer K, Steier K (1976) Mechanismen der Haftkraftverstärkung bei der Partikelhaftung durch plastisches Verformen. Sintern und viskoelastisches Fliessen. Chem Ing Tech 48(4):300–307

Schatt W (1992) Sintervorgänge – Grundlagen. VDI Verlag, Düsseldorf/G

Schreyer E, Palzer S, Sommer K (2008) Sorption, sintering and caking behaviour of binary mixtures of amorphous and crystalline particles. Workshop on Particle & Powder Technology as applied to foods, nutraceuticals and pharmaceuticals. Massy Paris/France

Teunou E, Fitzpatrick J (1999a) Characterization of food powder flowability. J Food Eng 39:31–37

Teunou E, Fitzpatrick J (1999b) Effect of relative humidity and temperature on food powder flowability. J Food Eng 42:109–116

Tomas J (1996) Zum Verfestigungsprozeß von Schüttgütern – Mikroprozesse, Kinetikmodelle und Anwendungen. Schüttgut 2(1):31–50

Wagner T (1997) Kaltsprühen ein- und mehrphasiger Flüssigkeiten. Ph.D. thesis, Food Process Engineering, Department of Food Science, ETH Zürich/CH

Wallack D, King C (1988) Sticking and agglomeration of hygroscopic, amorphous carbohydrates and food powders. Biotechnol Prog 4:31–35

Chapter 20
Effective Drying Zones and Nonlinear Dynamics in a Laboratory Spray Dryer

Ulises Ramón Morales-Durán, Liliana Alamilla-Beltrán, Humberto Hernández-Sánchez, Jose Jorge Chanona-Pérez, Antonio Ruperto Jiménez-Aparicio, and Gustavo Fidel Gutiérrez-López

20.1 Introduction

Extensive experimental spray drying tests have been carried out by various researchers to assess drying kinetics inside the chamber (Zbicinski et al. 2002). At the beginning of this decade, about 20,000 spray dryers were used commercially for processing agrochemical, biotechnological, chemical, pharmaceutical, and food products. Evaporative capacities of spray drying equipment are in the range of 1–10 L/h for laboratory units and up to about 200 t/h for large-scale processing (Mujumdar and Devahastin 2000). Use of inadequate drying systems and incorrect drying conditions may lead to obtaining products in which added value and physical and chemical properties do not meet the required specifications. Also, in some cases, deposition of wet or rubbery product on the wall of the drying chamber may occur, causing enormous economical losses (Goula and Adamopoulos 2004). Selecting drying conditions, atomizing device, and size and geometry of the drying chamber must take into account the desired characteristics of the product and, in most cases, involve complex mass and heat transfer calculations. The most common food powders are baby foods, dairy products, proteins, coffee and tea extracts, flavors and encapsulated fats (Chen and Patel 2008; Goula and Adamopoulos 2008). The amount of moisture removed from a droplet inside the drying chamber depends on the mechanisms that govern the evaporation rate and the residence time of the droplet in each zone of the equipment. This phenomenon can be described using transport equations, CFD (Seydel et al. 2006; Zbicinski and Li 2006) and nonlinear considerations (Van den Bleek et al. 2002).

U.R. Morales-Durán, L. Alamilla-Beltrán, H. Hernández-Sánchez, J.J. Chanona-Pérez, and G.F. Gutiérrez-López (✉)
Departamento de Graduados e Investigación en Alimentos, Escuela Nacional de Ciencias Biológicas, Instituto Politécnico Nacional, Carpioy Plan de Ayala, s/n CP. 11340, México DF, Edomex, Mexico
e-mail: gusfgl@gmail.com

A.R. Jiménez-Aparicio
Carretera Yautepec-Jojutla, Km. 6, calle CEPROBI No. 8, Col. San Isidro, Yautepec, Morelos, C.P. 62731, México

J.M. Aguilera et al. (eds.), *Food Engineering Interfaces*, Food Engineering Series,
DOI 10.1007/978-1-4419-7475-4_20,

Some authors consider that atomization is a key stage in the process (Allen and Bakker 1994; Furuta et al. 1994; Oakley 1994). Type of atomizer and feed partially determine the kind of drying chamber to be used and the energy spent in atomizing. Size distribution of the spray as well as particle trajectory and velocity inside the chamber and powder collection system will also contribute to the overall quality of the operation (Filoková and Mujumdar 1995; Chawla 1994). Moreover, in some cases particles can produce turbulence, which in time can lead to different rates of transport that may affect the quality of the product using the same equipment (Van den Bleek et al. 2002).

Special attention should be given to drying times, trajectories of particles, and the time that droplets take to reach the wall of the dryer. Chamber diameter and volume play a key role regarding this issue (Gutiérrez et al. 1997, 1998). Droplets of variable size and different morphology should reach the wall and leave the dryer at the desired final moisture content. For certain foods, drops in spray dryers often approach and reach the boiling temperature of the dissolvent (water in most food related applications); vapor generation may cause particles to grow in size and then collapse. Bubbles may form and collapse repeatedly in a process known as morphological development (Hecht and King 2000). The complexity of the spray drying process makes experimental study of mass transfer from individual drops impractical, which has induced research on predicting moisture content as well as on morphological characteristics of particles during the process by suspending a drop of the material under study in a fixed position (Adhikari et al. 2000; Ferrari et al. 1989). In this context, digital image analysis can play an important role when evaluating changes in particle size, formation of crust, shrinkage, inflation, blow-up, presence of holes, etc. (Adhikari et al. 2000; Aguilera and Stanley 1999). Reports on the prediction of various thermal and hydrodynamic conditions have made it possible to distinguish among different phenomena associated with droplet morphology and have allowed the recognition of periods and actual drying zones in drying chambers (Dolinsky 2001).

Identification of drying zones inside the chamber and change of moisture content during dehydration may help to establish relationships between dryer design and product quality. In this work, effective drying zones evaluated as heat transfer units in the chamber as well as the morphological development of the particle using digital image analysis are reported for a two-fluid nozzle laboratory co-current spray dryer. Also, computational fluid dynamics (CFD) has been used in this work to evaluate hydrodynamics to assess the effects of particle-gas interactions in the effective drying zones. This has allowed the establishment of correlations between lumped models and nonlinear considerations of air-particle interactions, including the evaluation of Lyapunov coefficients and formation of attractors for trajectories (Van den Bleek et al. 2002). Computer vision systems may be applied to aid discussion of the usefulness of traditional design calculations and findings derived from intensive computing exercises, as well as from advanced theories on chaotic behavior.

20.2 Materials and Methods

20.2.1 Testing Material

Testing material was, in all cases, 40% TS maltodextrin solution (20 ED) supplied by Arancia Corn Products S.A. (Mexico). Experiments on trajectories of particles were performed by using powdered maltodextrin (20 ED) supplied by the same company.

20.2.2 Spray Dryer

The spray dryer used in this work was a two-fluid nozzle co-current laboratory spray dryer equipped with a peristaltic pump for feed fine control and cyclone for powder collection. The dryer is depicted in Fig. 20.1. The dimensions of the drying chamber were diameter 0.38 m, height 0.60 m, and height of cone 0.40 m. Details of design and construction of the experimental dryer are given elsewhere (Alamilla-Beltrán et al. 2001). The evaporative capacity of the dryer is 0.8 kg of evaporated

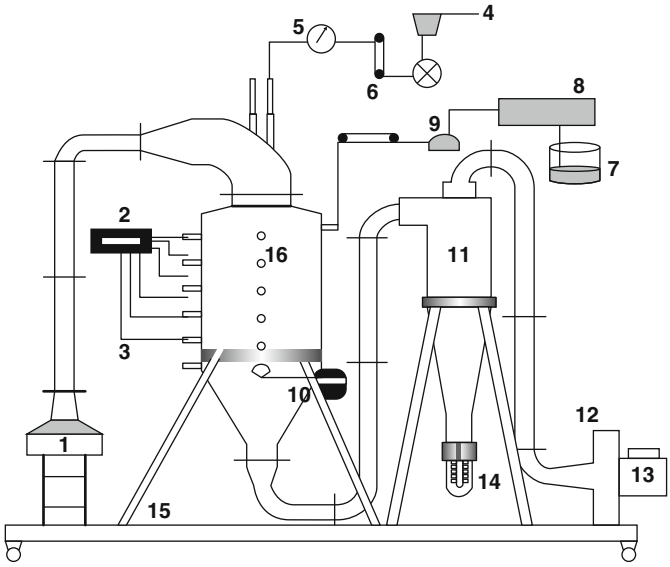

Fig. 20.1 Diagram of spray dryer. (**a**) Heater; (**b**) temperature recorder; (**c**) thermocouples; (**d**) air to nozzle; (**e**) manometer; (**f**) rotameter; (**g**) liquid feed; (**h**) feed pump; (**i**) pulse dampener; (**j**) thermoanemometer; (**k**) cyclone; (**l**) fan; (**m**) motor; (**n**) powder collector; (**o**) supporting structure; (**p**) drying chamber

water/h (similar to laboratory-scale dryers, e.g., SDMicro™ Spray Dryer, Niro; Mini Spray Dryer B-290, Büchi).

Experiments were conducted under the following drying conditions: inlet/outlet temperatures of 200/173°C (denoted as high-temperature drying), and 170/145°C (denoted as low-temperature drying) and volumetric airflow of 75 m^3/h. Feed rate was, in all cases, 1.39 kg/h. The nozzle was located at 0.1 m from the top of the chamber. A J-type thermocouple was used to measure the inlet air drying temperature. At the bottom of the chamber the outlet air drying temperature was evaluated.

20.2.3 Moisture Content and Sampling of Material

Sampling of material inside the chamber was performed using a bayonet-type sampler previously described (Alamilla-Beltrán et al. 2005). It was introduced to the dryer through specially constructed tapped devices separated 0.10 m from each other. A diagram of the dryer showing the measuring points is presented in Fig. 20.2. Average moisture content was evaluated following AOAC 32.1.03 method (AOAC 1995) for the different heights of the chamber in which each sample was collected. Sampling was performed once drying proceeded in a constant regime.

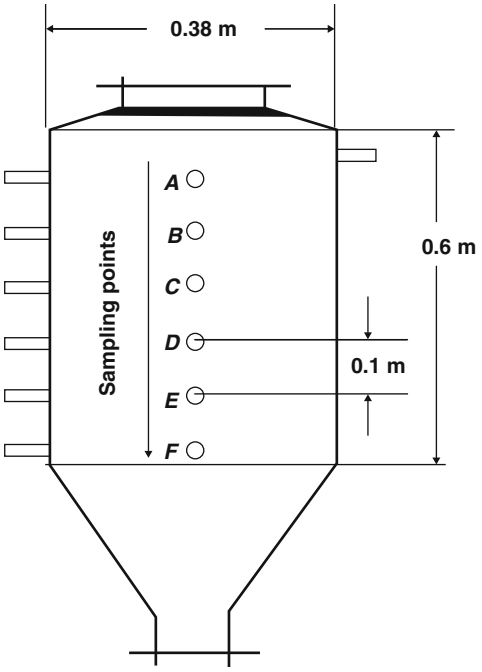

Fig. 20.2 Diagram of the longitudinal section of the dryer showing sampling points and chamber dimensions

20.2.4 Evaluation of Air and Product Temperature

The air drying temperature was evaluated using thermocouples type J. One thermocouple was fitted at the air inlet. A second thermocouple was positioned at the air outlet duct at the bottom of the chamber. This thermocouple was used to measure the outlet air drying temperature. The thermocouples were adapted to a digital register, Barnant (model 692). The wet bulb temperature was measured at the same points and inside the chamber at the sampling points (Fig. 20.2) during the drying process. With dry bulb temperature and wet bulb temperatures, the enthalpy was calculated. The product temperature was measured using the thermocouple collocated at the sampling point A.

20.2.5 Mean Particle Diameter During Drying

Particles obtained during drying experiments were observed using light microscopy. The microscope (Zeiss Axiophot) was fitted with a 20× objective and blue filter (total magnification 100× and 200×, depending on drying experiment). The illumination was provided by a light-field source. Images were obtained by means of a digital camera (ZVS-47DE) with resolution of 640 × 480 pixels and captured in a PC. KS400 ver. 3.01 software was used to process images and to determine the diameter of individual particles. Mean diameter of particles at different heights in the chamber was reported as the corresponding average value for powders collected at the center of the spray-cone and at different heights along the drying chamber as depicted in Fig. 20.2. Initial diameter of the droplet was measured using a particle analyzer Malvern Series 2,600 at the feed rate and atomizing air pressure used in the drying operation.

20.2.6 Measurement of the Mass Flow Rate

Mass flow rate of air (Gs) was evaluated by measuring the mean air velocity in the air exhaust duct of the dryer with a hot-wire anemometer (Digital Thermoanemometer TSI Inc., model 8330-M, USA). Mass flow rate of liquid (L) was evaluated using a peristaltic pump (Masterflex-Cole Parmer Instrument, model 7521–40). Spraying air was controlled by means of a rotameter (Blue White).

20.2.7 Effective Drying Height

In this work, a proposal for the calculation of the effective drying height based on the application of transfer units was applied. This methodology considers that the longitude along which one of the fluids travels through the dryer is formed

by the number of transfer units (N_{tOG}) corresponding to a dimensionless function of the difference of temperatures and the driving force for heat transfer. The height of the transfer unit (H_{tOG}) is a function of the conditions of flow.

The evaluation of the effective drying height was based on the consideration that the drying process is similar to the humidification operation, with the exception of the influence of the solids (Foust et al. 1993). This influence is important and in this proposal it was considered that the drying air is humidified in adiabatic form during the process. The flow diagram for the proposal is presented in Figs. 20.3 and 20.4. Figure 20.3 illustrates calculations of the product temperature at different points along the dryer, and Fig. 20.4 shows the evaluation of the effective drying height.

The number of transfer units is related to its capacity to transfer heat and may be evaluated by using (20.1).

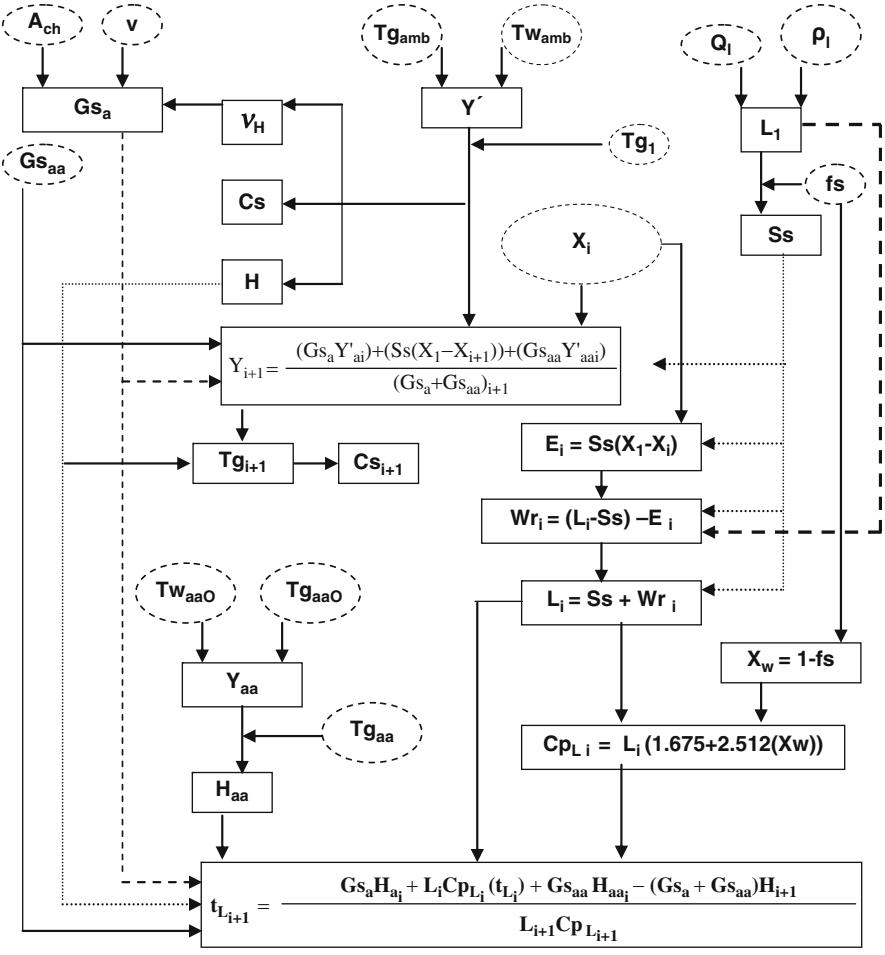

Fig. 20.3 Flow diagram of evaluation of product temperature

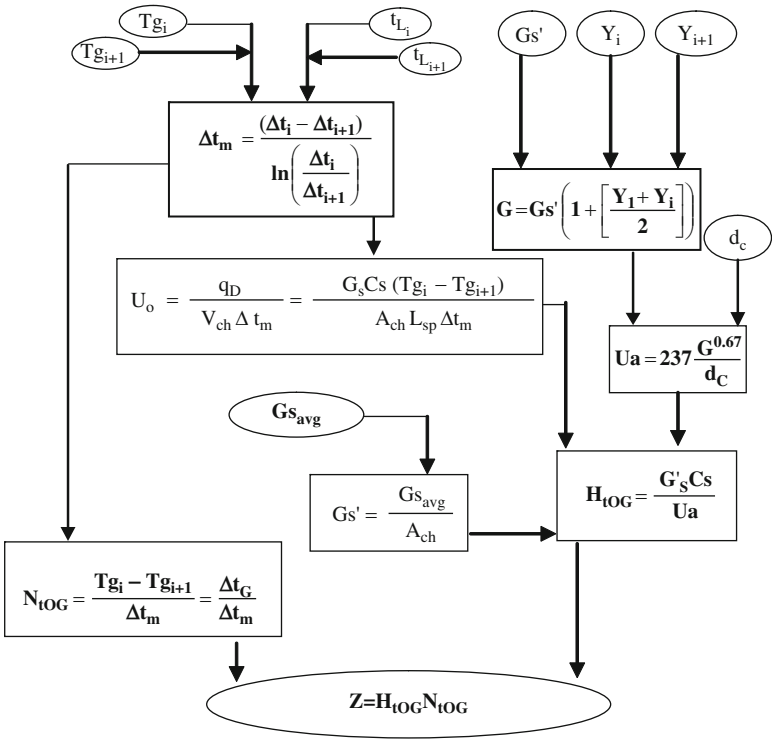

Fig. 20.4 Flow diagram of evaluation of effective drying height

The height of the heat transfer unit depends on the volumetric coefficient of heat transfer and the volumetric airflow. It can be calculated as follows (Treybal 1996):

$$N_{\mathrm{tOG}} = \frac{Tg_{\mathrm{i}} - Tg_{\mathrm{i+1}}}{\Delta t_{\mathrm{m}}} = \frac{\Delta T_{\mathrm{g}}}{\Delta T_{\mathrm{m}}} \tag{20.1}$$

In the case of rotational dryers (in which air flows through a mass of dispersed solids), the volumetric coefficient of heat transfer in kJ/(h) (m^3 of dryer) (°C) can be calculated with (20.3). This equation is based on the flow mass of drying air by unit of transversal area, and the diameter of the same one (Friedman and Marshall 1949; McCormick 1962).

$$H_{\mathrm{tOG}} = \frac{G'_{\mathrm{s}} C_{\mathrm{s}}}{\mathrm{Ua}} \tag{20.2}$$

An increase in the speed of the gas will increase the exposed surface. The contact air-particle consists of a mass of humid material in dispersed phase in contact with drying air in the continuous phase.

$$\mathrm{Ua} = 237\ \frac{G^{0.67}}{d_c} \tag{20.3}$$

The number of transfer units and the length of a transfer unit are related by means of (20.4) (Treybal 1996). This relationship allows determination of the value of the effective drying height (Z) inside the drying chamber.

$$Z = N_{\mathrm{tOG}}\ H_{\mathrm{tOG}} \tag{20.4}$$

20.2.8 Computational Fluid Dynamics Simulation

Simulation of the drying process was carried out using CFX 10.0. Drying air velocity field was simulated using the k–ε (Southwell and Langrish 2000; Langrish et al. 2004). The Lagrangian–Euler approach was selected for the resolution of the discrete phase. Drag force was assessed using the Schiller–Nauman correlation. Airflow and particles-air interactions were also evaluated.

20.2.9 Simulation of Airflow Profiles

To simulate the air-velocity of drying air, a three-dimensional representation of the equipment was made. Domain was divided in a 138,717 elements. Boundary conditions were established, with inlet air taken as 1.54×10^{-2} kg/s according to experimental data. Atomizing air inlet was 116 m/s corresponding to 1.54×10^{-4} kg/s evaluated by considering the flow divided by the area of annulus of the nozzle. At the outlet zone of the dryer, a relative static pressure of 0 Pa was considered. A steady-state simulation was carried out until reaching an average relative error of 10^{-4}. Steady-state simulation was used as the initial value of nonsteady-state flow for 10 s, using a 0.24 s resolution. The need for these sorts of experiments and CFD simulation has been noted by Fletcher et al. (2006).

20.2.10 Nonlinear Dynamics of the System

Dynamics of a dispersed maltodextrin powdered phase in the chamber was evaluated under airflow drying conditions. Fifty grams per minute of powdered maltodextrin having a range of particle sizes of 5–45 μm was fed into the dryer. A 200 mW laser beam was fitted to the dryer to axially illuminate the trajectories of the particles. Images of the trajectories were taken using a webcam (iSlim 2020 AF. Genius, USA) every 0.24 s. Images were taken at 0.1 m and 0.3 m from the

atomizing nozzle in the axial direction, which also corresponded to air velocity-measuring points. Crops of images were obtained and fractal dimension of texture (FDT) was evaluated by using the SDBC plugging of ImageJ (Chen et al. 2003). Series 2 min long were recorded to observe oscillations of the FDT values. Time series so obtained were processed to derive the corresponding Lyapunov coefficients of the system and the phase-space of reflected light (Wolf et al. 1985). These calculations could render useful information on the nonlinear (chaotic) behavior of the system and allow the derivation of important conclusions on overall tendencies of flow into the dryer by calculating Kolmogorov Entropy values.

20.3 Results and Discussion

Evaluation of the number of transfer units allowed recognition of the three different stages during drying. The experimental evidence of water removed from the product (moisture content), temperatures of the drying air and the product (inside the aspersion cone), along with changes in particle size (shrink and expansion) have been associated with the stages of drying. Two of these factors are related to water evaporated and shrinkage and a third with particle growth.

Initially, a first zone called the first drying stage was observed, in which elimination of water solely occurs without the generation of powder. It would be possible to assume that the flow in drying zones is less mixed than for zone 3 (or that a controlling flow induced by the nozzle is generated). This section coincides with the characteristics of stages I and II as reported by Dolinsky (2001).

A second zone, called the second drying stage was observed in which the formation of the shell of the particle generates a powdered product with almost the equivalent of the final moisture of the solid. For the low-temperature operation, a 93% loss of moisture was reached, while for high-temperature drying, the loss of total humidity was 97%. In both cases, the temperature of the air reached minimum value. Also, shrinkage of the particle was observed along with an incipient expansion. At 200°C, particles shrank, mainly within the spraying cone. This could not be appreciated at 170°C, but it is probable that similar phenomena would be observed between 0.2 m and 0.3 m below the nozzle. At the same time, the temperature of the product increased from the adiabatic-saturation temperature until the boiling temperature of water was reached. Likewise, in this stage, the volumetric coefficient of heat transfer had the highest value, suggesting the existence of a pattern of mixed-flow. This section agrees with the characteristics of the stage III reported by Dolinsky (2001). A better description of this mixed-flow can be carried out by applying CFD techniques such as those described in the Materials and Methods section.

After the drying stages, a third zone, denominated as the expansion stage was detected. In this phase it was observed that after shrinkage the particle begins to expand. The size of the particle increased twofold and occasionally presented cracking, and in some cases, explosion of the material and rupture of the shell were observed. Particles that exploded were, in general, hollow spheres presenting

thin crusts for high-temperature drying conditions and thick crusts for low-temperature drying conditions. The presence of this stage is related to the temperature of the drying air, the moisture of the particle, and the gradient of pressures between the interior and the exterior of the droplet. In this zone, the loss of humidity was not significant and it could be considered as not important for drying. Also, in this zone, the temperature of the solid remained constant at its higher value. In this stage, the volumetric coefficient of heat transfer presented its lower value. Stages IV and V as reported by Dolinsky (2001) coincide with this expansion stage. The effective height of drying represents the minimum longitude to carry out effective drying.

On the other hand, solids concentration of the feed, inlet air drying temperature, mass flow of inlet product, mass flow of atomizing air, and type of feed can modify the morphological development of the particle and, in consequence, the final characteristics of the product. Changes in operating conditions will cause different effective heights of drying. However, drying and expansion stages will be present for this material. In Figs. 20.5 and 20.6, a pictorial representation of punctual temperatures of air and images of the product are presented for both experimental conditions. The shadowed areas represent each of the recognized drying stages.

In Fig. 20.7 a representation of nonsteady-state air patterns inside the chamber is presented. No influence of the nozzle in this case was considered. It should be noted that there is a recirculating airflow with a central downward jet similar to a flow in an infinite plenum surrounded by an upward stream of air. The highest density of upward flow vectors was found in the first and part of the second drying zone corresponding to the effective drying zones evaluated earlier through the evaluation

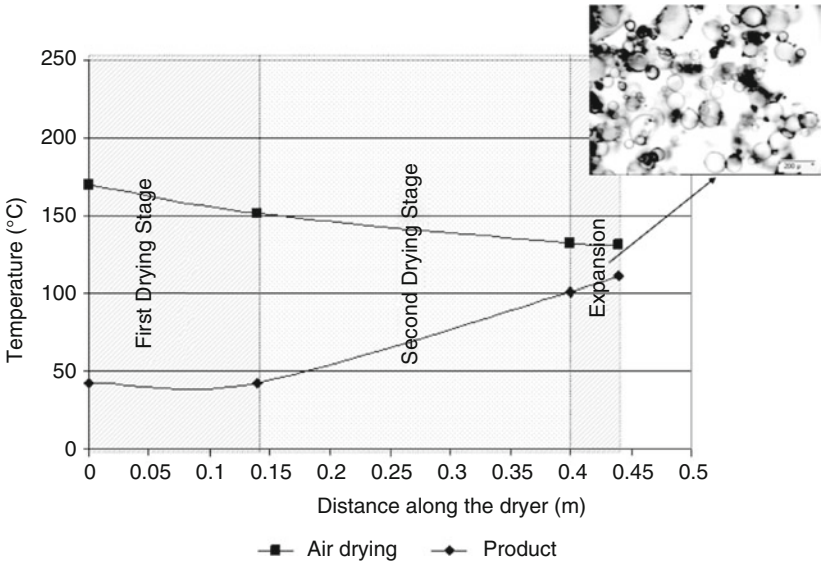

Fig. 20.5 Temperature profile of drying air and product inside the dryer and an image of the final dried product, corresponding to the condition 170/145°C

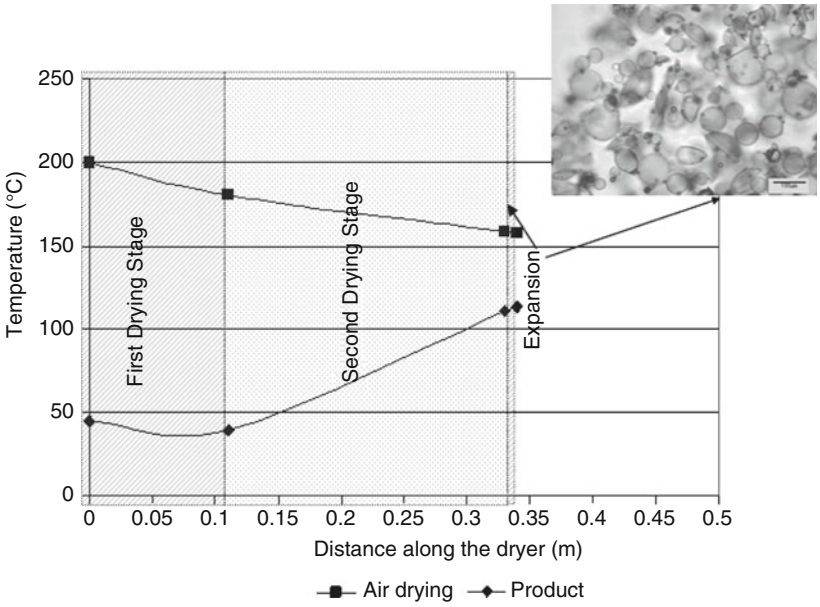

Fig. 20.6 Temperature profile of drying air and product in the dryer and an image of the final dried product, corresponding to the condition 200/173°C

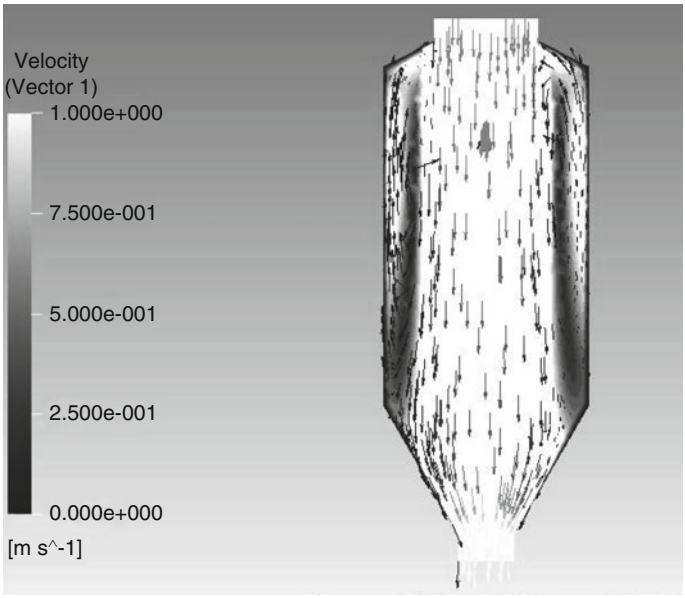

Fig. 20.7 CFD representation of non steady-state air patterns inside the chamber with no influence of the nozzle

of the transfer units, which may explain the intense drying in this region. In Fig. 20.8, the representation of nonsteady-state air patterns with influence of the nozzle is presented at different times of simulation. It is possible to observe that a nonstable air pattern was found. However, in all cases, a denser zone of mixed

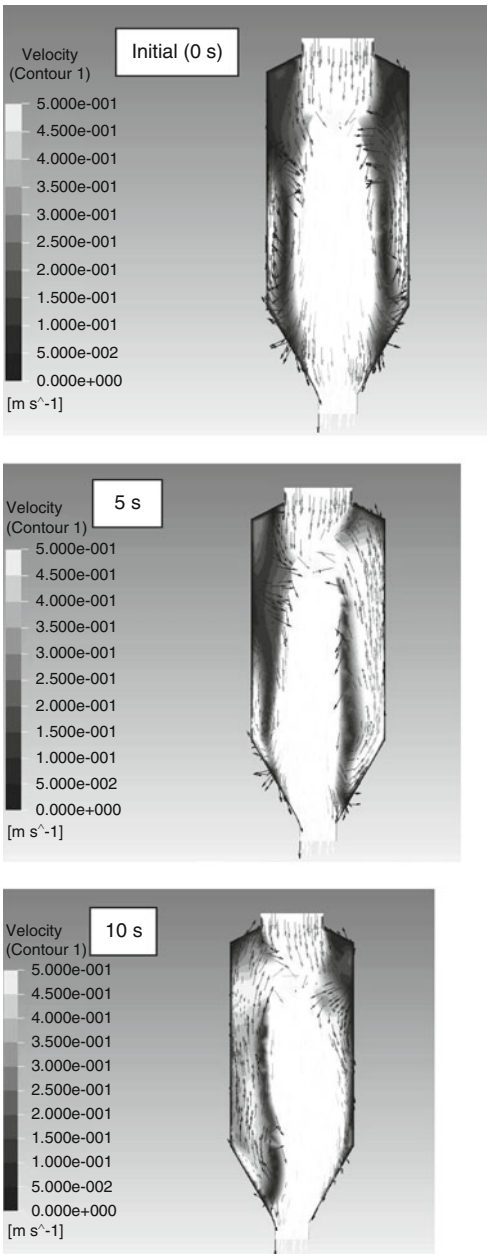

Fig. 20.8 Representation of nonsteady-state air patterns with influence of the nozzle presented at 0, 5, and 10 s of simulation

(upward and downward) flow was found, which confirms that effective drying zones are found in the first zone (first and second drying zones) of the chamber.

In Fig. 20.9, it is possible to observe the simulated trajectories of the particles used as tracers with no influence of the atomizing nozzle. Most particles were directed to the bottom of dryer since drag dominated the process. However, when the nozzle was considered in the simulation (Fig. 20.10), an imbalance of trajectories was caused and the nozzle governed hydrodynamics. This phenomenon was validated experimentally by feeding particles to the drying chamber. Images of an air-particles mix were taken by illuminating the field with the laser beam. Reflected light was scattered and seemed to present irregular patterns that were evaluated by calculating their fractal dimension at different times. Surface 3.D plots of gray-level intensity are shown in Fig. 20.11; they show the heterogeneity of laser beam reflection in the particles and are an indicator of oscillation of the air-particle flow. FDT was presented in the form of phase-space graphs, and the formation of attractors was evident. For 10 cm axial distance from the top, Lyapunov coefficients in the range of 3.46–13.62 were obtained, while for 30 cm the coefficients were

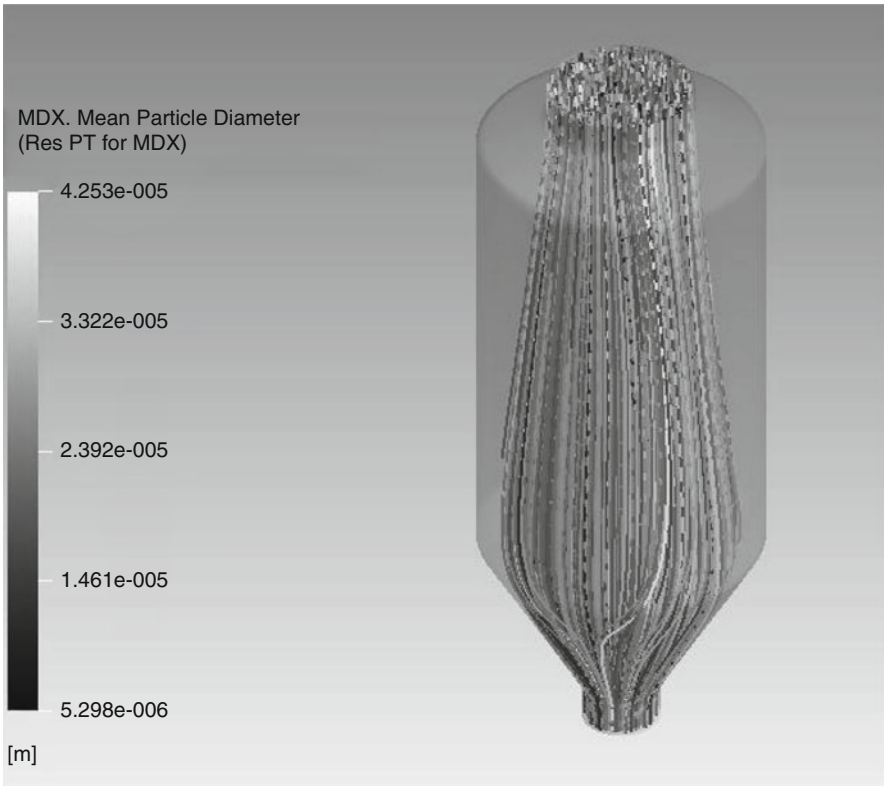

Fig. 20.9 Simulated trajectories of the particles used as tracers with no influence of the atomizing nozzle; most particles were directed to the bottom of the dryer since drag dominated the process

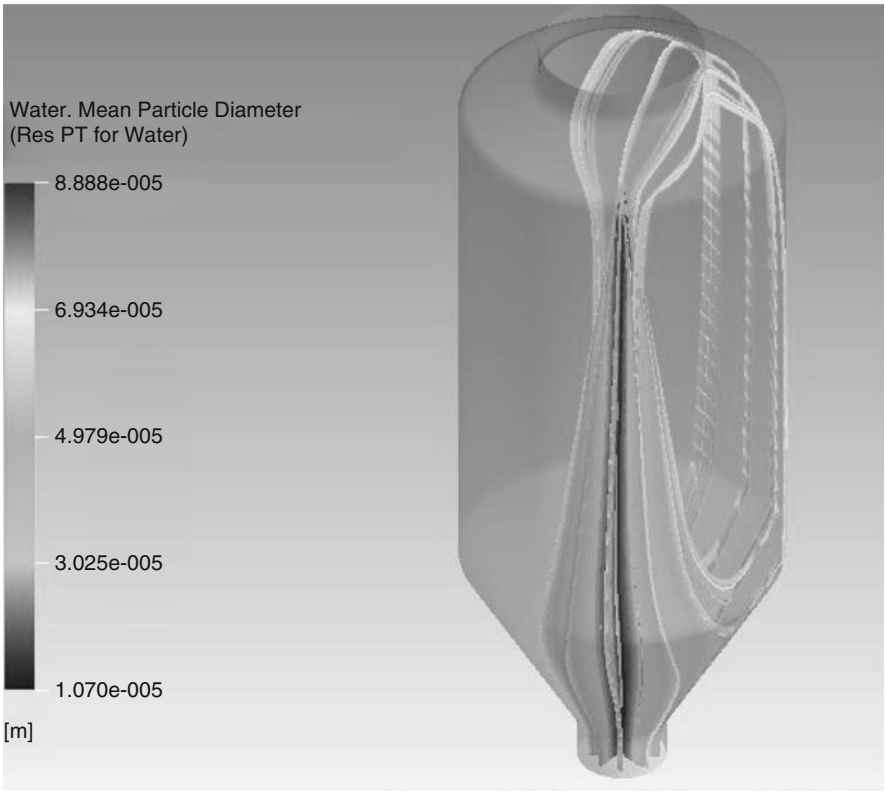

Fig. 20.10 Simulated trajectories of the particles used as tracers with the presence of the atomizing nozzle showing an imbalance of trajectories

5.44–11.63. These results also confirmed that more turbulent zones are found around the atomizer and within the first drying zone evaluated earlier through the evaluation of the transfer units, which may explain the intense drying in this region. These results also agree with those obtained by Huang et al. (2005) who used a k–ε model and found that the highest turbulence was around the atomizing device. In Figs. 20.12 and 20.13, graphs on the oscillations of FDT and corresponding Lyapunov coefficients are presented, as well as phase-space diagrams showing the obtained attractors at 10 and 30 cm axial distance from the top of the dryer.

20.4 Conclusions

The application of the concept of the number of transfer units in spray drying allowed the establishment of three stages related to the drying of the material. An initial first drying stage was identified, in which the product temperature remained

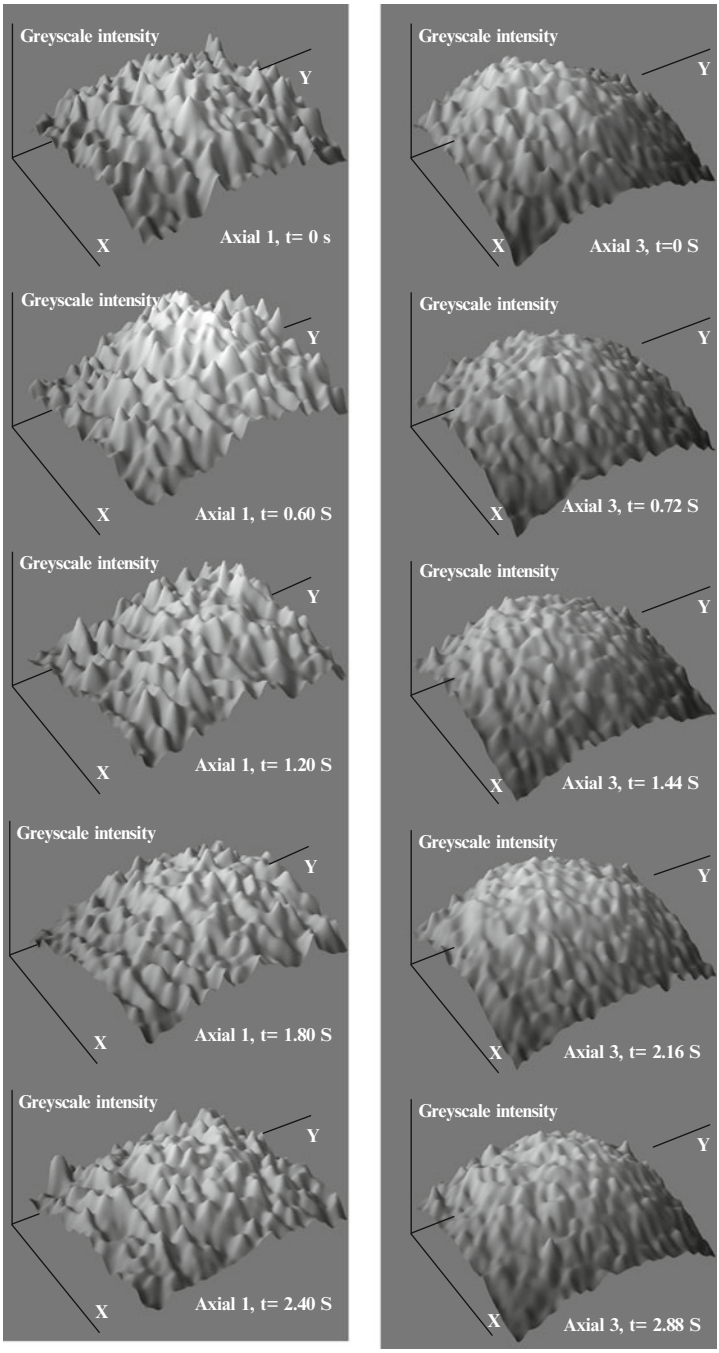

Fig. 20.11 Surface 3-D plots of gray-level intensity corresponding to laser beam reflection on particles, showing heterogeneity of flow at: (**a**) 10 cm and (**b**) 30 cm axial distance from the nozzle

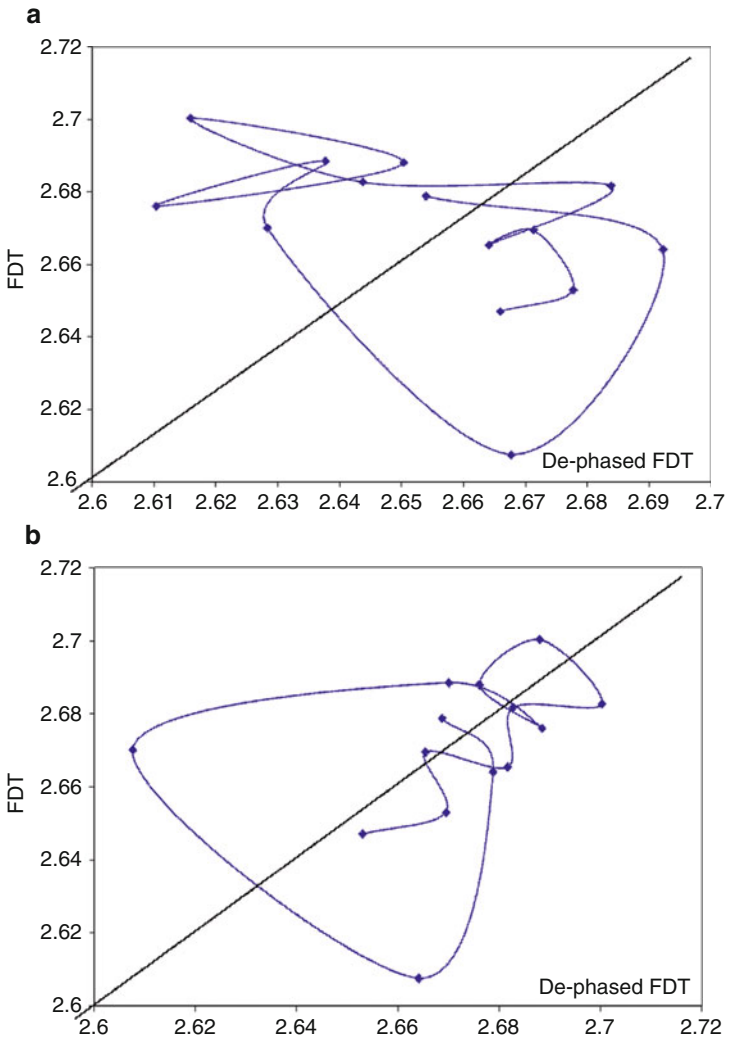

Fig. 20.12 Phase-space diagrams of FDT showing the presence of an attractor at: (**a**) 10 cm and (**b**) 30 cm axial distance from the nozzle. The 45° straight line shows the nearest neighboring points

constant and near to the adiabatic saturation temperature of the drying air. A second drying stage was identified, which showed an increase in the product temperature with the presence of dry powder. A third expansion stage was then identified in which an increment in the size of the particle was observed. The first and second drying stages represent the area in which an effective drying inside the spraying chamber was carried out. The calculated values of the volumetric coefficient of heat transfer allowed the assumption that in the second drying stage a pattern of mixed

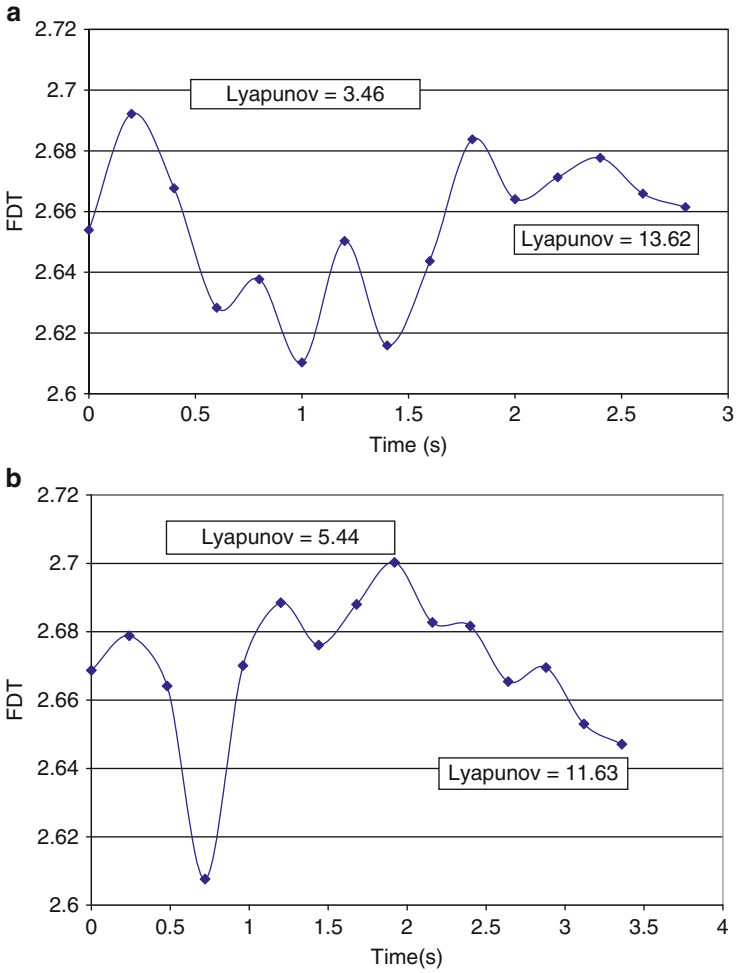

Fig. 20.13 Oscillations of FDT and corresponding Lyapunov coefficients for: (**a**) 10 cm and (**b**) 30 cm axial distance from the nozzle. Distance of text-box covers points used for calculation

flow was present. Drying zones presented according to CFD simulation (and experimental validation) a high deal of air-particle recirculation phenomena. Nonlinear dynamics could characterize these recirculation zones by using Lyapunov coefficients and by the presence of attractors related to fractal dimension of texture of the reflected laser beam cropped images. Highest simulated and validated turbulence was found in the upper part of the dryer. Steady and nonsteady-state simulations allowed insight into the nonlinear properties of generated turbulence. While the transfer units approach is useful for construction of lumped models, CFD and experiments based on air-particle trajectories constitute a good approach for the

understanding of turbulence inside the dryer. Both approaches may be useful and could complement each other for design purposes.

20.5 Symbols

A_{ch} Chamber area (m)
Cp_L Heat capacity of liquid
C_s Heat capacity of moist air (kJ/kg°C)
E Mass flow rate of water evaporated (kg of water/h)
F_s Fraction of solids
Gs Mass flow rate of air (kg/h)
Gs′ Mass flux of air (kg/h m^2)
Gs_m Average mass flow rate of air
H Enthalpy of air (kJ/kg of dry air)
H_{tOG} Length of heat-transfer units (m)
L Mass flow rate of liquid (kg/h)
L_{sp} Distance between sampling points (m)
N_{tOG} Number of heat-transfer units
Q_l Volumetric flow rate of liquid (m^3/h)
q_D Rate of heat flow (kJ/h)
t_L Temperature of the solution or dry solid (°C)
T_g Temperature of drying air (°C)
T_w Wet bulb temperature of drying air (°C)
Uo Volumetric heat transfer-coefficient (kJ/h m^3°C)
Uo_m Average volumetric heat transfer-coefficient (kJ/h m^3°C)
v Air velocity (m/s)
V_{ch} Volume of cylindrical section of the spray chamber (m^3)
v_h Humid volume (m^3/kg dry air)
Wr Water in the solution (kg of water/h)
X Moisture content (dry basis) (kg of water/kg of dry solid)
Xw Moisture content (wet basis) (kg of water/kg of solution)
Y Absolute humidity of air (kg of water/kg of dry air)
Z Effective length of drying, m

20.5.1 Greek Letters

Δt Temperature difference between air and dry solid or solution (°C)
Δt_G Change in gas temperature owing to heat transfer to solid only (°C)
ρ_l Density of liquid (kg/m^3)
Δt_m Logarithmic-mean temperature difference (°C)
ω Dry solid

20.5.2 Subscripts

1 At the inlet conditions of spray dryer
2 At the outlet conditions of spray dryer
aa Atomizing air
aa_O Atomizing air at ambient conditions
amb Ambient
a Drying air
i Sampling point, inlet conditions of spray dryer

Acknowledgment Author U.R. Morales-Durán thanks Biotecsa-México for their support. The authors also thank IPN-México and CONACYT-México (project 84287) for their financial support.

References

Adhikari B, Howes T, Bhandari B, Truong V (2000) Experimental studies and kinetics of single drop drying and their relevance in drying of sugar-rich foods: a review. Int J Food Prop 3(3):323–351

Aguilera J, Stanley D (1999) Simultaneous heat and mass transfer: Dehydration. In: Microstructural principles of food processing and engineering, 2nd edn. Aspen Publishers, New York, pp 373–411

Alamilla-Beltrán L, Hernández-Parada A, Chanona-Pérez J, Jiménez-Aparicio A, Suárez-Fernández O, Santiago-Pineda T, Gutierrez-Lopez G (2001) Design and performance of a spray dryer for food processing. Proceedings of the 8th International Conference on Engineering and Food. ICEF 8, Technomic Pub. Co, USA, pp 1151–1155

Alamilla-Beltrán L, Chanona-Pérez J, Jiménez-Aparicio A, Gutiérrez-López G (2005) Description of morphological changes of particles along spray drying. J Food Eng 67(1–2):179–184

Allen R, Bakker H (1994) Spray dryer control-based on line particle size analysis. Trans IChemE Part A: Chem Eng Res Design 72:251–254

AOAC (1995) Official methods of analysis of AOAC International, 16th edn. AOAC International, USA, pp 31–32

Chawla J (1994) Effect of the droplet agglomeration on the design of spray dryer towers. Drying Technol 12(6):1357–1365

Chen X, Patel K (2008) Manufacturing better quality food powders from spray drying and subsequent treatments. Dry Technol 26(11):1313–1318

Chen W-S, Yuan S-Y, Hsieh C-M (2003) Two algorithms to estimate fractal dimension of gray-level images. Opt Eng 42(8):2452–2464

Dolinsky A (2001) High-temperature spray drying. Dry Technol 19(5):785–806

Ferrari G, Meerdink G, Walstra P (1989) Drying kinetics for a single droplet of skim milk. J Food Eng 10:215–230

Filoková I, Mujumdar A (1995) Industrial spray drying systems. In: Mujumdar A (ed) Handbook of spray drying. Marcel Dekker, New York, pp 263–307

Fletcher D, Guo B, Harvie D, Langrish T, Nijdam J, Williams J (2006) What is important in the simulation of spray dryer performance and how do current CFD models perform? Appl Math Model 30(11):1281–1292

Foust A, Wenzel L, Clump C (1993) Principles of unit operations. CECSA, México

Friedman S, Marshall W Jr (1949) Studies in rotary drying. Part II – heat and mass transfer. Chem Eng Prog 45(9):573–588

Furuta T, Hayashi H, Ohashis T (1994) Some criteria of spray drying design for food liquid. Dry Technol 12(1–2):151–177

Goula A, Adamopoulos K (2004) Influence of spray drying conditions on residue accumulation: Simulation using CFD. Dry Technol 22(5):1107–1128

Goula A, Adamopoulos K (2008) Effect of maltodextrin addition during spray drying of tomato pulp in dehumidified air: I. Drying kinetics and product recovery. Dry Technol 26(6): 714–725

Gutiérrez G, Ordorica C, Osorio G, Hernández A, Patiño R, Jiménez A, Santiago T (1997) ASCON-programa para el establecimiento de las condiciones de operación en secadores por aspersión de disco rotatorio. In: Mulet A, Ordorica C, Benedito J (eds) Herramientas de cálculo en ingeniería de alimentos III. Univ. Politécnica de Valencia, Instituto Politécnico Nacional, España-México, pp 93–103

Gutiérrez G, Osorio G, Jiménez A, Pyle L (1998) An assessment of droplet-air contact and spray drying performance in bioprocess engineering. In: Galindo E, Ramírez O (eds) Advances in bioprocess engineering II. Kluwer, The Netherlands, pp 251–275

Hecht J, King C (2000) Spray drying: influence of developing drop morphology on drying rates and retention of volatile substances. 1. Single-drop experiments. Indus Eng Chem Res 39:1756–1765

Huang L, Passos M, Kumar K, Mujumdar A (2005) A three-dimensional simulation of a spray dryer fitted with a rotary atomizer. Dry Technol 23(9–11):1859–1873

Langrish T, Williams J, Fletcher D (2004) Simulation of the effects of inlet swirl on gas flow patterns in a pilot-scale spray dryer. Chem Eng Res Des 82(7):821–833

McCormick P (1962) Gas velocity effects on heat transfer in direct heat rotary dryers. Chem Eng Prog 58(6):57–61

Mujumdar A, Devahastin S (2000) Mujumdar's practical guide to industrial drying. Exergex Corporation, Canada

Oakley D (1994) Scale-up of spray dryers with the aid of computational fluid dynamics. Dry Technol 12(1–2):217–233

Seydel P, Blömer J, Bertling J (2006) Modeling particle formation at spray drying using population balances. Dry Technol 24(2):137–146

Southwell D, Langrish T (2000) Observations of flow patterns in a spray dryer. Dry Technol 18(3):661–685

Treybal R (1996) Mass transfer operations. McGraw-Hill, México

Van den Bleek C, Coppens M-O, Schouten J (2002) Application of chaos analysis to multiphase reactors. Chem Eng Sci 57(22–23):4763–4778

Wolf A, Swift J, Swinney H, Vastano J (1985) Determining Lyapunov exponents from a time series. Physica D 16(3):285–317

Zbicinski I, Li X (2006) Conditions for accurate CFD modeling of spray-drying process. Dry Technol 24(9):1109–1114

Zbicinski I, Delag A, Strumillo C, Adamiec J (2002) Advanced experimental analysis of drying kinetics in spray drying. Chem Eng J 28:207–216

Chapter 21
Rehydration Modeling of Food Particulates Utilizing Principles of Water Transport in Porous Media

I. Sam Saguy, Oranit Troygot, Alejandro Marabi, and Rony Wallach

21.1 Introduction

In the last decade, there has been a continuous rise in the demand for convenience foods, including dehydrated products, mainly due to modern lifestyles (Marabi and Saguy 2009; Saguy et al. 2007). This trend is accompanied by a decrease in the ability, desire or time to prepare food and an increase in financial means, leading consumers to choose foods that are readily available, convenient, and require only minimal or no preparation before consumption (Tillotson 2003). The rehydration of dried foods is a fundamental unit operation in the food industry. The quality of rehydrated and reconstituted products is affected by the drying conditions and rehydration processes utilized, ultimately influencing consumer acceptance. During the drying process, physicochemical changes, including textural and structural modifications, migration of solutes, loss of volatiles and nutrients occur in an irreversible manner, and have an impact on the quality of the final product. Therefore, the drying process needs to be understood and controlled, to create a dried product with optimal nutritional, sensorial, and rehydration characteristics (Saguy et al. 2007). In addition to medium uptake, leaching of solids from the food product to the medium is another important aspect during rehydration. To address

I.S. Saguy (✉) and O. Troygot
Institute of Biochemistry, Food Science and Nutrition, Robert H. Smith Faculty of Agricultural, Food and Environment, The Hebrew University of Jerusalem, P.O. Box 12, Rehovot, 76100, Israel
e-mail: ssaguy@agri.huji.ac.il

A. Marabi
Institute of Biochemistry, Food Science and Nutrition, Robert H. Smith Faculty of Agricultural, Food and Environment, The Hebrew University of Jerusalem, P.O. Box 12, Rehovot, 76100, Israel
and
Solid Products, Department of Food Science & Technology, Nestlé Research Center, Vers-Chez-Les-Blanc CH-1000, Lausanne 26, Switzerland

R. Wallach
Department of Soil and Water Sciences, Robert H. Smith Faculty of Agricultural, Food and Environment, The Hebrew University of Jerusalem, P.O. Box 12, Rehovot, 76100, Israel

J.M. Aguilera et al. (eds.), *Food Engineering Interfaces*, Food Engineering Series,
DOI 10.1007/978-1-4419-7475-4_21,

this phenomenon, nondissolvable solids were proposed (Marabi et al. 2004a) and utilized in the determination of the rehydration ratio(RR).

21.2 Mathematical Modeling

In recent years, the food domain has experienced an encouraging transition from the empirically-based to physically-based models. Nevertheless, most rehydration studies reported in the literature still include empirical and semiempirical models to describe the mechanisms of liquid uptake, solids leaching, and the kinetics of the processes (Marabi and Saguy 2009).

Mathematical modeling facilitates an understanding of process characteristics, providing insight into the governing mechanisms taking place, and thus it could be utilized to improve the process for better products. Liquid uptake is typically modeled by applying a mechanistic approach or employing an empirical approach. Fick's second law of diffusion is a typical example of a mechanistic approach, whereas the first-order model is merely a curve-fitting empirical model. The development of empirical models requires considerably less effort and therefore, they are utilized frequently. However, empirical models are limited and nontransferable (Saguy et al. 2005b).

21.2.1 Empirical and Semiempirical Models

Five models that are often used (Saguy et al. 2007) include: the *exponential model* (Misra and Brooker 1980), *Peleg's model* (Cunningham et al. 2007; Garcia-Pascual et al. 2006; Giraldo et al. 2006; Peleg 1988), *first-order kinetics* (Gowen et al. 2007; Krokida and Philippopoulos 2005); the *Weibull distribution function* (Cunha et al. 1998a, b; Cunningham et al. 2007; Garcia-Pascual et al. 2006; Machado et al. 1997), and the *normalized Weibull distribution function* (Marabi et al. 2003, 2004a, b; Marabi and Saguy 2004; Marabi and Saguy 2005).

Among the empirical models, the Weibull distribution function is used frequently and has recently been improved to describe the rehydration of dried foods. It is important to note however, that all of these empirical models offer rather limited insight into the fundamental principles involved, and in some cases, hinder understanding of the transport mechanism(s) (Marabi and Saguy 2009). Nevertheless, they provide an excellent basis for curve-fitting and allow process representation as a function of physical properties and rehydration conditions.

21.2.2 The Diffusion Model

The diffusion model is a combination of physical and empirical approaches, founded on Fick's first and second laws. Solving Fick's second law requires making

numerous assumptions and simplifications (Saguy et al. 2007). To overcome some of these difficulties, the effective diffusion coefficient D_{eff} is utilized, which is derived from experimental data and is an apparent value that encompasses all intrinsic hydraulic properties of the particles. The effective diffusivity is linked to both the porosity and tortuosity. A typical D_{eff} value for moisture in foods ranges from 10^{-8} to 10^{-12} m^2/s, generally being closer to 10^{-10} m^2/s (Maroulis et al. 2001), and is influenced by temperature, water content, pressure, physical properties, and the dried food's structure. However, it is well documented that some or most of the above assumptions made to solve Fick's laws are not valid. Moreover, mechanisms of mass transfer other than molecular or Fickian diffusion may also occur. Some of the drawbacks of the Fickian approach were recently discussed (Saguy et al. 2007).

21.3 Paradigm Shift: Capillary Flow in Porous Media

As most empirical models are primarily utilized to avoid more complex considerations and complications such as changes occurring within the product, the actual microstructure is not considered. The alternative is to apply a physically-based approach utilizing the porous media where the actual microstructure and void channels are important. This may sound straightforward, but it requires a paradigm shift and an interdisciplinary approach is suggested (Saguy et al. 2007). The approach is based on integrating the know-how developed in other domains such as soil science to study the porous media and fluid transport in foods.

Rehydration is a very complex phenomenon involving different transport mechanisms, including molecular diffusion, convection, hydraulic flow, and capillary flow (Saravacos and Maroulis 2001). Liquid imbibition follows various mechanisms occurring in tandem (Chiralt and Fito 2003; Marabi et al. 2003; Marabi and Saguy 2005; Oliveira and Ilincanu 1999). However, the contribution of mechanisms involving mass flux due to a temperature gradient (Soret effect) is considered insignificant and therefore often is disregarded (Datta 2007a). Several studies utilizing the Washburn equation to represent the movement of liquids into porous food matrices were reviewed recently (Marabi and Saguy 2009; Saguy et al. 2007).

It is however worth noting that the rehydration mechanism is no longer relying solely on the common postulation that it is governed by Fickian diffusion. Other mathematical models based on capillary flow in porous media are also utilized. These models are derived from the well-known Lucas (1918) and Washburn (1921) equations (also called the Lucas-Washburn or Washburn-Rideal equation). This approach is based on utilization of several well-known derivations known as the Laplace, Poiseuille, and Lucas-Washburn equations (Marabi and Saguy 2009).

After imbibition of water into dried porous foods it was shown that the process followed the Washburn equation (Lee et al. 2005; Saguy et al. 2005a). However, discrepancies related to the utilization of a single "effective" cylindrical capillary radius and constant contact angle were also reported (Saguy et al. 2005a). An additional factor that may be responsible for the inaccuracies encountered when

comparing experimental data with the Washburn equation may be related to the tortuosity of the pores within the food sample. The pore network is often regarded as a bundle of cylindrical and straight capillaries with a determined effective radius (Saguy et al. 2007). Thus, the Washburn equation may be utilized in its original form (Aguilera et al. 2004), or otherwise corrected with a tortuosity factor (Carbonell et al. 2004).

Other studies also concluded that there is water movement during various food processes. For instance, water transfer during vacuum osmotic drying was described as a combination of traditional Fickian diffusion and vacuum capillary flow. In this case, water transfer was closely related to the porosity of the fruit being tested (Shi and Fito-Maupoey 1994). Radial NMR micro-imaging technique utilized to study pasta rehydration indicated a non-Fickian process (Hills et al. 1996). Capillary penetration or another fast transport mechanism occurring near the interface in the rehydration of apples was also suggested (Salvatori et al. 1999).

21.4 Flow in Unsaturated Porous Media

21.4.1 Capillarity and Tension Head

Water that has entered a porous medium but has not drained out of the sample will be retained in the pores by capillary forces or will surround the surface of the particles by molecular forces of adhesion and cohesion. Therefore, a simple measurement of water content in the medium is not sufficient to enumerate the complete status of the medium's water. While the quantity of water present in the medium is very important, the potential or affinity with which the water is retained is perhaps more important, mainly if the dynamics of this water is considered (Saguy et al. 2007). This potential may be defined as the amount of work done or potential energy stored, per unit volume, in moving a mass of water from the reference state (typically chosen as pure free water). Matric potential could be considered as potential energy per unit volume (J m^{-3}), which is also expressed as Pascal. This clarifies the use of the terminology "pressure potential" by soil physicists referring to matric potential as soil pressure, or if divided by bulk density, as pressure head (Wallach 2007).

Capillarity deals with both the macroscopic and statistical behavior of interfaces, rather than their molecular structure. Capillarity is also referred to as surface tension, γ (work per unit area expressed as J m^{-2}). This phenomenon is extremely important in water retention in porous media. Surface tension occurs at the molecular level and involves two types of molecular forces: adhesive forces, which are the attractive forces of molecules of dissimilar substances and cohesive forces, which are the attractions between molecules in similar substances. Cohesive forces decrease rapidly with distance and are the strongest in solids, less strong in liquids, and the weakest in gases (Saguy et al. 2007).

As water rises in a capillary, the meniscus is spherical in shape and concave upward. By letting r equal the tube radius, the excess pressure above the meniscus compared to the pressure directly below can be described under various assumptions by $2\gamma/r$. As the pressure on the water surface outside the capillary tube is atmospheric, the pressure in the liquid below the meniscus will be less than the atmospheric pressure above the meniscus by $2\gamma/r$. This will force the fluid up the tube until the hydrostatic pressure of the fluid column within the tube equals the excess pressure of $2\gamma/r$. The total force (upward) supports the weight of the fluid column to the height h_c. The height of the capillary rise can be expressed as (Laplace equation):

$$h_c = \frac{2\gamma \cos\theta_a}{\rho g r} \tag{21.1}$$

where hc = capillary rise (water tension head) (m); g = gravity (m/s^2); θ_a= apparent contact angle (^{o}).

21.4.2 Water Retention Curve

The water characteristic curve of porous media is also known as the water retension curve (RC), which describes the functional relationship between the volumetric water content θ and matric potential ψ under equilibrium conditions. The matric potential is usually replaced by the pressure potential head h (m), which is the energy per unit weight of water. As the water in the unsaturated porous media is at subatmospheric pressure, the pressure potential head is commonly called "tension head." This curve is an important property related to the distribution of pore space (sizes, interconnectedness), which is strongly affected by texture and structure, as well as related factors including organic matter content. The RC indicates the amount of water in the porous medium at a given tension head (Saguy et al. 2007). It is also a primary hydraulic property required for modeling water flow in porous media. RCs are highly nonlinear functions and relatively difficult to obtain accurately (Hillel 1998; Wallach 2007).

The traditional method of determining water retention involves establishing a series of equilibria between water in the porous medium sample and a body of water at known water tensions. The medium-water system is in hydraulic contact with the body of water via a water-wetted porous plate or membrane. At each equilibrium, the volumetric water content of the medium is determined and paired with a value of the tension head (h), determined from the pressure in the body of water and the gas phase pressure in the substrate. The data pair (θ, h) forms one point on an RC. A summary of methods frequently used in soil science to determine the RC can be found in the literature (e.g., Klute 1986). It is worth noting that RC quantification resembles sorption isotherm determination in foods (Fontana and Campbell 2007; Saguy et al. 2007).

Measured values of water content and tension head (θ -h) are often fragmentary and usually based on relatively few measurements over the wetness range of interest. For modeling and analysis purposes, and characterization and comparison of different substrates and scenarios, it is essential to represent the RC in continuous and parametric form. A parametric expression of an RC model should contain as few parameters as possible, to simplify its estimation and to describe the behavior at the limits (wet and dry ends), while closely fitting the nonlinear shape of the θ -h data (Saguy et al. 2007).

Many models have been suggested to describe RC in soil science (Hillel 1998; Jury and Gardner 1991). The most frequently used are those of Brooks and Corey (1966), denoted as B-C model, and van Genuchten (1980), denoted as VG model. The parameters of the models are typically determined by curve-fitting of experimental data. B-C model follows:

$$\begin{cases} \dfrac{\theta-\theta_r}{\theta_s-\theta_r} = S_e = \left(\dfrac{h}{h_b}\right)^{\lambda} & h > h_b \\ \dfrac{\theta-\theta_r}{\theta_s-\theta_r} = S_e = 1 & h \le h_b \end{cases}$$
$$\begin{cases} K(h) = K_s \cdot {S_e}^{2+2/(m_v+\tau)} & h > h_b \\ K(h) = K_s & h \le h_b \end{cases} \tag{21.2}$$

where S_e = effective saturation (-); h_b = air entry value (m); λ = "pore size index" empirically-determined parameter (-); θ, θ_r, θ_s = current, residual, and saturated volumetric water contents, respectively (m^3/m^3); K_s = saturated hydraulic conductivity (m/s); m_v = empiric parameter (-).

The residual water content is somewhat arbitrarily defined as the water content at which the corresponding hydraulic conductivity is essentially zero, but very often it is used as an empirical constant when fitting hydraulic functions. As opposed to θ_s, which has a clear physical significance, the meaning of θ_r and its estimation have not yet been resolved (Wallach 2007).When $\theta_r = 0$ (m^3/m^3), S_e approaches S. Note that S_e varies between zero and one.

The other common parametric model for relating water content to the tension head was proposed by VG:

$$S_e = \frac{\theta-\theta_r}{\theta_s-\theta_r}\left[\frac{1}{1+(\alpha_h \cdot h)^n}\right]^{m_v} \tag{21.3}$$

where α_h (m^{-1}) and m_v (-) are empirical parameters (determining the shape of the RC; derived by curve-fitting techniques).

The value of the hydraulic conductivity of a saturated porous medium (K_s) depends on the properties of the medium and the flowing fluid. This dependence can be separated into two factors: fluidity f (defined as $\rho g/\eta$; η = *viscosity* (Pa s)) and intrinsic permeability k (m^2):

$$K_s = kf = \frac{k\rho g}{\eta} \tag{21.4}$$

The intrinsic permeability of a medium is a function of pore structure and geometry. Particles of smaller-sized individual grains have a larger specific surface area, increasing the drag on water molecules flowing through the medium, which results in a reduced intrinsic permeability and K_s.

21.4.3 Richards Equation, Boundary, and Initial Conditions

The Darcy law describes the flow equation in saturated media:

$$J = -K_s \frac{\Delta H}{\Delta s} \tag{21.5}$$

where H = the hydraulic head (m); s = distance along a stream line in the flow field (m); $\Delta H/\Delta s$ = the hydraulic-head gradient along the stream line (-); and J = flux density or flow per unit area opposite the direction defined by hydraulic-head gradient (m/s).

The Darcy law can be coupled with the conservation of mass principles to derive a continuity equation. Using one horizontal dimension leads to:

$$\frac{\partial \theta}{\partial t} = \frac{\partial}{\partial x}\left[K(h)\frac{\partial h}{\partial x}\right] \tag{21.6}$$

Equation (21.6) contains two unknowns, namely θ and h; applying the chain rule for the left hand side of (21.6) provides the h-based continuity equation:

$$C(h)\frac{\partial h}{\partial t} = \frac{\partial}{\partial x}\left[K(h)\frac{\partial h}{\partial x}\right] \tag{21.7}$$

where $C(h) = \partial\theta/\partial h$ is the slope of the RC and is called the specific moisture capacity (1/m).

Applying the chain rule for the derivative to the right hand side of (21.6) provides the θ-based continuity equation, which is a diffusion-type (nonlinear) equation:

$$\frac{\partial \theta}{\partial t} = \frac{\partial}{\partial x}\left(D_h(\theta)\frac{\partial \theta}{\partial x}\right) \tag{21.8}$$

where $D_h(\theta) = K(h)\cdot\partial h/\partial\theta$ (m^2/s) is denoted as hydraulic diffusivity and is the ratio of the unsaturated hydraulic conductivity to the specific moisture capacity.

The advantage of the θ-based form is that $D_h(\theta)$ does not vary with θ nearly as much as $K(h)$ varies with h. The last two equations, along with their various alternative formulations, are known as the Richards equation.

21.4.4 Developing the Theory of Flow in Porous Media

To utilize the theory of flow in porous-media in rehydration of dry food particulates, the RC of these particulates is needed. The B-C and VG and other functions used to model the RCs have significant limitations at low-liquid saturations in that they use a parameter called residual saturation, which is the minimum liquid saturation calculated by these equations. At low water content, vapor diffusion is predominantly driven by vapor pressure differences, which in turn is driven by local vapor pressure lowering (related to capillary pressure through Kelvin's equation). Hence, vapor flow is significantly influenced by the RC at low water contents.

The limitations of the two-phase characteristic curves in the low water content region lead to errors in liquid and vapor transport, and in the prediction of the actual water content in this region. This value is important in the transition from liquid–solid sorption to vapor-solid sorption, which is typically at 4–6 monomolecular layers, or liquid saturation of 0.11–0.16 (m^3/m^3) based on soil surface area of 25 m^2/g (Webb 2000). At higher liquid saturations, adsorption is primarily via liquid–solid processes. As the liquid saturation decreases, however, vapor-solid sorption contributes to the adsorption process more and more and may dominate at low values of liquid saturation.

Physically-based modification of the RC has been suggested by a number of authors (e.g., Campbell and Shiozawa 1992; Morel-Seytoux and Nimmo 1999; Ross et al. 1991; Rossi and Nimmo 1994). Campbell and Shiozawa (1992) observed that the capillary pressure in the dry region is a linear function of liquid saturation on a semilog plot; using this relationship, they added a VG water content relationship to obtain the full capillary pressure curve, where the parameters in the VG equation were refit to the data assuming zero liquid residual saturation. Subsequent models have all used the linear relationship observed by Campbell and Shiozawa (1992). The model proposed by Rossi and Nimmo (1994) is based on the B-C model with zero residual saturation, which is equivalent to the expression of Campbell (1974), with the dry region function proposed by Campbell and Shiozawa (1992) in the low water content region. Morel-Seytoux and Nimmo (1999) slightly modified the Rossi and Nimmo (1994) model. Webb (2000) presented a similar approach to the dry region modification of Morel-Seytoux and Nimmo (1999) in that it merges an existing RC with a dry region expression. However, the approach of Morel-Seytoux and Nimmo (1999) requires the simultaneous solution of two nonlinear equations, while the Webb (2000) approach only requires a few iterations in a single equation.

Following these approaches, we suggested a new method to predict the RCs of porous media (food particulates in particular) from measured water sorption isotherms. This method is based on a four-step procedure (Saguy et al. 2007):

1. Water sorption isotherm
   The suggested method adopts the fundamental water isotherm approach to describe the relationship between water content and water activity in the dry zone. This selection is straightforward and takes into consideration the knowledge bank on the relationship between food stability and water activity. Although the utilization of glass transition theory could also be considered, in this case the relationship between water and the gas phase is of interest. The conversion from water activity to tension head is carried out by utilizing the Kelvin equation:

$$h = \frac{RT}{\rho_w g M_w} \ln(a_w) \tag{21.9}$$

where R = gas constant ($J \cdot K^{-1} \cdot mol^{-1}$); M_w = molecular water mass (0.018 kg/mol); T = absolute temperature (K); ρ_w = water density (1,000 kg/m^3); a_w = water activity (-).

   However, the theoretical aspects of the Kelvin equation at low water activities are still under development and further studies are required. A typical water sorption isotherm is depicted in (Fig. 21.1) for microcrystalline cellulose (MCC).
2. Retention curve
   Initially, the sorption isotherm data is converted to water retention data and plotted as tension head vs. volumetric volume of water to comply with the RC presentation. Note that the moisture content for each data point of the sorption

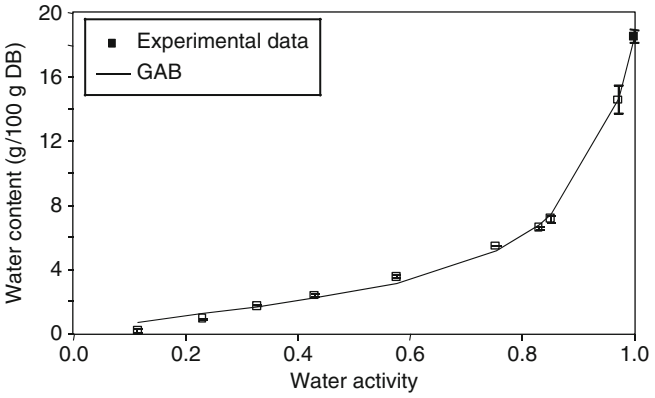

Fig. 21.1 Typical water sorption isotherm for microcrystalline cellulose at 25°C (Adapted from Saguy et al. 2007)

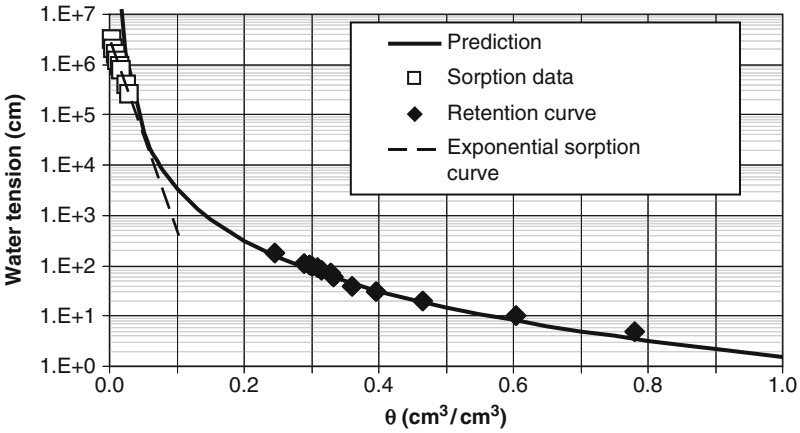

Fig. 21.2 Typical water sorption and water retention data for microcrystalline cellulose at 25°C (prediction made using B-C model) (Adapted from Saguy et al. 2007)

isotherm (m, a_w) is converted to (h, θ) by utilizing the Kelvin equation (21.9), transforming the moisture content to its volumetric value:

$$\theta = m\frac{\rho_b}{\rho_w} \tag{21.10}$$

where m = moisture content (kg H_2O/kg dry solids; DB); ρ_b = bulk density (kg/m^3). Typical values are presented in (Fig. 21.2).

3. Prediction and validation of RC from a_w data

   The sorption isotherm data after transformation to the adequate RC scale was utilized to derive the B-C model using the two aforementioned requirements, namely continuity and smoothness at a point defined as θ^*, h^*. This yielded two equations from which θ^* and λ were derived. Once θ^* is known, it can be placed in one of the equations to derive λ and the B-C function can be drawn. Note that in our first approach, and for simplicity of treatment, it was assumed that the sorption isotherm is a linear function on a semilogarithmic scale (e.g., Webb 2000). Another requirement for using the B-C function, when physical data is absent, is to know the values of its parameters: h_b, θ_s (saturated water content), θ_r (residual water content), and λ (pore index parameter). The first two parameters can be experimentally measured (although adaptation to food systems is required): θ_r is an approximated parameter while λ is evaluated through model equations. Applying this approach in a VG model (instead of B-C one) requires an additional parameter, which adds to the complexity of the solution without gaining any further conceptual insight into the overall approach, and as such is not covered herewith.

   Validation was then carried out, in which RC was measured using the hanging column method (Klute 1986) and the fit obtained, as depicted in (Fig. 21.2).

Since methods used in this case for soils are probably difficult for implementation in most food systems, measurements of only a few points is recommended, starting from the wet end of the curve.

4. Retention curve validation
   Once the water RC is known, the unsaturated hydraulic conductivity function (21.2) can be determined and the Richards equation (21.8) solved. As for the saturated hydraulic conductivity, it is independently measured. Again, certain adaptations are necessary for evaluating K_s in food systems. Both the measurement and prediction of 10-cm column dry MCC rehydration are depicted in (Fig. 21.3). Simulations were made using Hydrus 1-D software (a code for simulating one-dimensional movement), based on the Richards equations for water flow (Simunek et al. 2005) for the following boundary and initial conditions: constant upper boundary flux and constant tension head at bottom boundary set to zero. The initial moisture content was assumed as oven-dry. The simulation predicted the cumulative bottom flux, was then multiplied with the sample cross-section, yielding the volume of water absorbed by the sample.
5. Typical experimental data on foods
   To demonstrate the applicability of the above four-step procedure, imbibition tests were carried out using freeze-dried wheat groats (burghul). Simulations (not showed) illustrated that although the B-C characteristic-curve based on water absorption model yielded a shape similar to the experimental data for early times (ca. 500 s), a significant discrepancy was clearly observed at relatively long times. Rehydration times longer than ca. 1,000 s are quite lengthy, compared to the shorter duration utilized for typical "instant" consumer products. Conversely, the B-C model was quite accurate at shorter times (e.g., less than 300 s). Thus, these data suggest that prolonged food rehydration is more complex and requires additional consideration. A similar conclusion was reached after

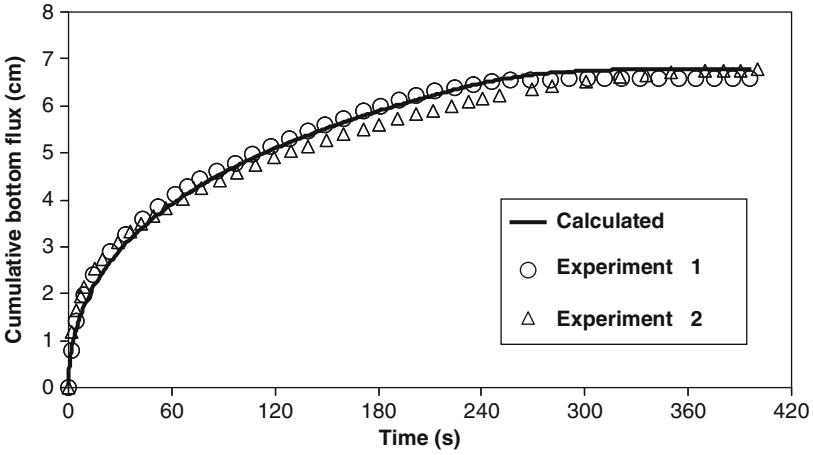

Fig. 21.3 Typical rehydration data for microcrystalline cellulose at 25°C (Adapted from Saguy et al. 2007)

repeating the long-time rehydration experiments with freeze-dried carrots (data not shown).

Next, an empirical approach was applied using a "double" Weibull model to account for diffusion and relaxation, as both could have a completely different time scale:

$$w_t = w_{\infty 1}\left\{1 - \exp\left[-(t/\alpha_1)^{\beta_1}\right]\right\} + w_{\infty 2}\left\{1 - \exp\left[-(t/\alpha_2)^{\beta_2}\right]\right\} \qquad (21.11)$$

where w_t, $w_{\infty 1}$, and $w_{\infty 2}$ = the momentary weight, infinite-weight due to diffusion, and relaxation, respectively (kg H_2O/kg dry solids); t = time (s), α and β = scale parameter (s), and Weibull shape parameter (–); 1 = diffusion and 2 = relaxation.

When the combined model was utilized, the fitted data showed an excellent fit for short and long rehydration times. The model was used to simulate the contribution of each individual mechanism, namely diffusion and relaxation. As expected, relaxation lags diffusion markedly. This could explain some of the literature data in which both diffusion and nondiffusion mechanisms were reported.

The criterion utilized to differentiate between the diffusion and relaxation mechanisms is derived from the value of the Weibull shape parameter. Values of 0.6–0.8 were defined as capillary flow, while values above 1.0 were characterized as relaxation (Marabi et al. 2003). Figure 21.4 shows the ratio between relaxation and diffusion; it is clear that at short rehydration time the freeze-dried product depicts that the diffusion mechanism is dominating; however, as time progresses, relaxation also starts to play a significant role.

This data suggests that additional considerations are required especially for long rehydration time during which water flow is not capillary-driven. It is suggested that the porosity of a dried food product (e.g., freeze-dried carrot, freeze-dried

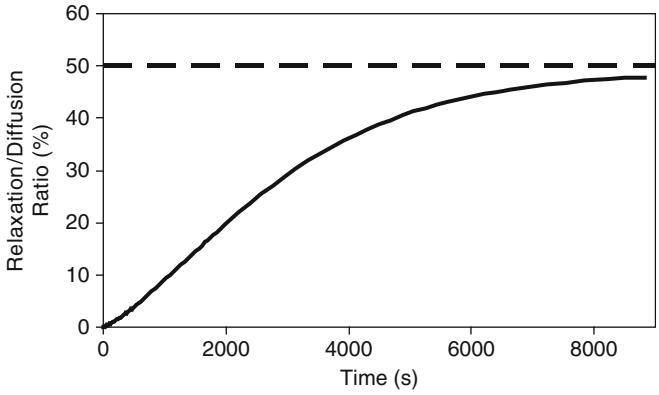

Fig. 21.4 Simulated ratios ("double" Weibull model) between water uptake due to diffusion and relaxation (freeze-dried wheat groats, burghul, 25°C)

wheat groats) is hierarchical (i.e., made of pores: between- and within- the particles. The former pores are inter-porosity, while the latter are intra-porosity, which are typically dead-ended). While water flow is driven by capillarity in the interpores, it is also driven by moisture content gradients in the intrapores. This concept (also known as "mobile-immobile") is currently under development and preliminary results are encouraging supporting the overall hypothesis that physically-based model for the simulations of porous foodstuffs rehydration is feasible.

This important topic will become apparent once internal structure data are available (see recommendations below).

21.4.5 Rehydration of Foods Using Porous Media: Additional Considerations

The theory of capillary imbibition for modeling the rehydration of foods was applied by several other groups. For instance, a capillary-flow approach was utilized (Weerts et al. 2003a, b) to model the temperature and anisotropy effects during the rehydration of tea leaves. The predicted values agreed well with the experimental data derived from NMR measurements, leading to the conclusion that the physically based constitutive relationships of water activity and hydraulic conductivity could be utilized to overcome the simplification of modeling water transport as a process governed by Fick's laws. The approach could be extended to include gravity and osmotic pressure effects and also coupled with heat and solute transport in porous media for modeling heat, water, and chemical transport in general hydration and drying operations of porous food materials.

Another study (Singh et al. 2004) noted that one of the salient features of fluid transport through biological systems is the complex flow path presented by the biopolymeric matrix, thus expanding the above approach. Similarly, it was recently proposed that use of an "effective" single cylindrical capillary radius is the simplest possible model to describe capillary penetration into a porous medium. However, this model may be insufficient in many cases (Saguy et al. 2005a), especially when a significant distribution of pore size exists (Marmur and Cohen 1997), as previously shown for dried foods (Karathanos et al. 1996). More specifically, and depending upon the type of food and its processing history, it may contain pores ranging in radius from 0.1 to 300 μm, those in the 10–300 μm range being the most common (Bell and Labuza 2000).

Although numerous models have been proposed and frequently applied, additional improvements are required before modeling of the process based on the real mechanism(s) occurring becomes possible. Nevertheless, recent studies focused on more fundamental physical-based approaches have taken on a central role. Hence, significant progress is anticipated.

21.5 New Approaches and Other Advances

The rehydration of dried foods involves different physical mechanisms, among them water imbibition, internal diffusion (in the solid and pores), convection and diffusion at the surface and within large open pores, hydraulic flow, capillary flow, and relaxation of the solid matrix (Marabi and Saguy 2009; Saguy et al. 2007). Additionally, we have highlighted the utilization of a double Weibull model as well as mobile-immobile model. A growing body of data as well as ours indicates that simplification of the rehydration process may not be fully warranted, or in some cases, might even result in misleading conclusions (Datta 2007a, b; Saguy et al. 2005b; Weerts et al. 2003a, b). This realization is relatively new and important insights are coming to light from the merging of different scientific disciplines, including food and soil sciences, biophysics, environmental sciences, and petroleum and chemical engineering. The ultimate goal of these interdisciplinary efforts is to provide more advanced and accurate physical models that describe the mechanism(s) taking place during the rehydration process (Saguy et al. 2007).

The models recently developed and successfully applied to the flow of liquids into dried foods are based on theories usually termed as "capillary-flow approach" and/or "flow in porous media." The theories are already well developed in other fields, as are the methodologies needed to generate the required experimental data. However, there is still a considerable lack of data and, more importantly, standard methods allowing collection of the relevant physical properties of the food matrix and its interaction with the liquid. It is expected in the near future that collaborative studies will provide the information needed to apply these theories.

The common starting point for developing models that account for fluid flow in porous media is Darcy's equation and its Navier–Stokes analog (Datta 2007a; Saguy et al. 2005b; Weerts et al. 2003b). In addition, the main roles of the food particles' physical properties (e.g., pore-size distribution, heterogeneity, tortuosity), the embedding liquid (e.g., density, dynamic viscosity), the external conditions (e.g., temperature, pressure), and the interface (e.g., contact angle) are also considered in order to quantify the changes occurring during drying and to facilitate the modeling of the rehydration process. These studies on fluid flow in porous media have presented, in adequate detail, the development of the models, and the reader is referred to them for more detailed information (Saguy et al. 2007).

Recent studies focusing on the various transport mechanisms in porous media include:

- Molecular diffusion of gases, including water vapor: Darcy flow of gases resulting from pressure and liquid flow due to gas and capillary pressures (Datta 2007a).
- Utilization of Lucas-Washburn equation in modeling rehydration of dried foods (Lee et al. 2005; Machado et al. 1997; Saguy et al. 2005a).
- New methods and technologies to obtain experimental data (Datta 2007a, b; Saguy et al. 2005b) including: (1) density, porosity, thermal conductivity, and specific heat of solid material, (2) molecular, capillary, and effective diffusivities, (3) moisture isotherms, (4) vapor and liquid permeability, and (5) water-potential

curves; data in the last two categories is either nonexistent for foods or very difficult to obtain.

It is worth noting that new technology and utilization of X-ray MCT capabilities are spreading. X-ray MCT is a powerful tool for detailed observations of microstructure of porous foods and is expected to become a pertinent method for obtaining detailed information that can be further utilized in computational simulations of the imbibition of liquids into porous media. Hence, it could open new avenues for ultimately quantifying and modeling internal changes during both drying and rehydration, thereby providing the necessary information for studying the mechanism(s) involved, and enabling better control and quality improvements.

21.6 Research Needs

Future research needs to focus on the accomplishment of four main goals, as recently summarized (Saguy et al. 2007): (1) expand the theory and approach outline above to different a_w, and RC models and foods, (2) apply "transport in porous media" theories to model the fate of dissolved and retained substances in food particulates, (3) develop physical-based models-multidisciplinary research integrating/assimilating theories and knowledge from other fields, and (4) perform in-situ quantification–development of new methods/techniques, for in-situ quantifying of changes in food matrix microstructure, and water/vapor movement.

21.7 Conclusions

We have highlighted how porous media physics could be implemented for modeling the rehydration of foods. The main conclusions can be summarized as:

- Sorption isotherm data could be extended to a complete RC for use in a rehydration model.
- Flow in porous media theory, as demonstrated, is applicable to the rehydration of food particulates.
- Moving from empirical models to physically-based ones for foods was demonstrated and therefore, is recommended.
- Multidisciplinary collaboration is paramount and synergistic in opening new avenues of research.

The field is entering a new era in which innovative approaches and multidisciplinary teams will provide fresh insights, resulting in new discoveries and a better and deeper understanding of the phenomena. This will ultimately lead to much better control of the structure and rehydration, leading to improved food products with enhanced consumer appeal and acceptability.

References

Aguilera JM, Michel M, Mayor G (2004) Fat migration in chocolate: diffusion or capillary flow in a particulate solid? A hypothesis paper. J Food Sci 69:R167–R174

Bell LN, Labuza TP (2000) Moisture sorption – practical aspects of isotherm measurement and use. American Association of Cereal Chemists, St. Paul

Brooks RH, Corey AT (1966) Properties of porous media affecting fluid flow. J Irrig Drain E-Asce 2:61–68

Campbell GS (1974) A simple method for determining unsaturated conductivity from moisture retention data. Soil Sci l17:311–314

Campbell GS, Shiozawa S (1992) Prediction of hydraulic properties of soils using particle-size distribution and bulk density data. International Workshop on Indirect Methods for Estimating the Hydraulic Properties of Unsaturated Soils. University of California, Riverside, CA

Carbonell S, Hey MJ, Mitchell JR, Roberts CJ, Hipkiss J, Vercauteren J (2004) Capillary flow and rheology measurements on chocolate crum/sunflower oil mixtures. J Food Sci 69:E465–E470

Chiralt A, Fito P (2003) Transport mechanisms in osmotic dehydration: the role of the structure. Food Sci Technol Int 9:179–186

Cunha LM, Oliveira FAR, Ilincanu LA (1998a) Application of the probabilistic Weibull distribution to rehydration kinetics: relationship between the model parameters and the underlying physical mechanisms. In: Oliveira JC, Oliveira FAR (eds) Proceedings of the 3rd workshop of the Copernicus project, Leuven, Belgium

Cunha LM, Oliveira FAR, Oliveira JC (1998b) Optimal experimental design for estimating the kinetic parameters of processes described by the Weibull probability distribution function. J Food Eng 37:175–191

Cunningham SE, McMinn WAM, Magee TRA, Richardson PS (2007) Modelling water absorption of pasta during soaking. J Food Eng 82:600–607

Datta AK (2007a) Porous media approaches to studying simultaneous heat and mass transfer in food processes. I: problem formulations. J Food Eng 80:90–95

Datta AK (2007b) Porous media approaches to studying simultaneous heat and mass transfer in food processes. II: property data and representative results. J Food Eng 80:96–110

Fontana AJ Jr, Campbell GS (2007) Applications of water activity in non food systems. In: Barbosa-Canovas GV, Fontana AJ Jr, Schmidt SJ, Labuza TP (eds). Water Activity in Foods: Fundamentals and Applications. Chapter 14. IFT Press/Blackwell, Ames, IA

Garcia-Pascual P, Sanjuan N, Melis R, Mulet A (2006) Morchella esculenta (morel) rehydration process modelling. J Food Eng 72:346–353

Giraldo G, Vazquez R, Martin-Esparza ME, Chiralt A (2006) Rehydration kinetics and soluble solids lixiviation of candied mango fruit as affected by sucrose concentration. J Food Eng 77:825–834

Gowen A, Abu-Ghannam N, Frias J, Oliveira J (2007) Modelling the water absorption process in chickpeas (Cicer arietinum L.) – the effect of blanching pre-treatment on water intake and texture kinetics. J Food Eng 78:810–819

Hillel D (1998) Environmental soil physics. Academic, San Diego

Hills BP, Babonneau F, Quantin VM, Gaudet F, Belton PS (1996) Radial NMR microimaging studies of the rehydration of extruded pasta. J Food Eng 27:71–86

Jury WA, Gardner WR (1991) Soil physics. Wiley, New York

Karathanos VT, Kanellopoulos NK, Belessiotis VG (1996) Development of porous structure during air drying of agricultural plant products. J Food Eng 29:167–183

Klute A (1986) Water retention: Laboratory methods. In: Klute A (ed) Methods of soil analysis. Part I, physical and mineralogical methods, 2nd edn. American Society of Agronomy, Madison

Krokida MK, Philippopoulos C (2005) Rehydration of dehydrated foods. Drying Technol 23:799–830

Lee KT, Farid M, Nguang SK (2005) The mathematical modelling of the rehydration characteristics of fruits. J Food Eng 72:16–23

Lucas R (1918) Ueber das zeitgesetz des kapillar aufstiegs von Flussigkeiten. Kolloid-Zeitschrift 23:15–22

Machado MF, Oliveira FAR, Gekas V (1997) Modeling water uptake and soluble solids losses by puffed breakfast cereal immersed in water or milk. In: Jowitt R (ed) Proceedings of the seventh international congress on engineering and food – Part I. Sheffield Academic Press, Sheffield, UK

Marabi A, Dilak C, Shah J, Saguy IS (2004a) Kinetics of solids leaching during rehydration of particulate dry vegetables. J Food Sci 69:FEP91–FEP96

Marabi A, Jacobson M, Livings S, Saguy IS (2004b) Effect of mixing and viscosity on rehydration of dry food particulates. Eur Food Res Technol 218:339–344

Marabi A, Livings S, Jacobson M, Saguy IS (2003) Normalized Weibull distribution for modeling rehydration of food particulates. Eur Food Res Technol 217:311–318

Marabi A, Saguy IS (2004) Effect of porosity on rehydration of dry food particulates. J Sci Food Agr 84:1105–1110

Marabi A, Saguy IS (2005) Viscosity and starch particle size effects on rehydration of freeze-dried carrots. J Sci Food Agr 85:700–706

Marabi A, Saguy IS (2009) Rehydration and Reconstitution of Foods. In: Ratti C (ed) Advances in food dehydration. CRC Press, Boca Raton

Marmur A, Cohen RD (1997) Characterization of porous media by the kinetics of liquid penetration: the vertical capillaries model. J Colloid Interf Sci 189:299–304

Maroulis ZB, Saravacos GD, Panagiotou NM, Krokida MK (2001) Moisture diffusivity data compilation for foodstuffs: effect of material moisture content and temperature. Int J Food Prop 4:225–237

Misra MK, Brooker DB (1980) Thin-layer drying and rewetting equations for shelled yellow corn. Trans ASAE 23:1254–1260

Morel-Seytoux HJ, Nimmo JR (1999) Soil water retention and maximum capillary drive from saturation to oven dryness. Water Resour Res 35:2031–2041

Oliveira FAR, Ilincanu L (1999) Rehydration of dried plant tissues: Basic concepts and mathematical modeling. In: Oliveira FAR, Oliveira JC (eds) Processing foods. CRC Press, Boca Raton

Peleg M (1988) An empirical-model for the description of moisture sorption curves. J Food Sci 53:1216–1219

Ross PJ, Williams J, Bristow KL (1991) Equation for extending water-retention curves to dryness. Soil Sci Soc Am J 55:923–927

Rossi C, Nimmo JR (1994) Modeling of soil water retention from saturation to oven dryness. Water Resour Res 30:701–708

Saguy IS, Marabi A, Wallach R (2005a) Liquid imbibition during rehydration of dry porous foods. Innov Food Sci Emerg Technol 6:37–43

Saguy IS, Marabi A, Wallach R (2005b) New approach to model rehydration of dry food particulates utilizing principles of liquid transport in porous media. Trends Food Sci Technol 16:495–506

Saguy IS, Troygot O, Marabi A, Wallach R (2007) Rehydration modeling of food particulates utilizing principles of water transport in porous media. Bangkok: 10th International Symposium on the Properties of Water (ISOPOW X). (Also Chapter 17. In: Reid DS, Sajjaanantakul T, Lillford PJ, Charoenrein S (eds) Water properties in food, health, pharmaceutical and biological systems: ISOPOW 10). Wiley-Blackwell, 2010)

Salvatori D, Andres A, Chiralt A, Fito P (1999) Osmotic dehydration progression in apple tissue II: generalized equations for concentration prediction. J Food Eng 42:133–138

Saravacos GD, Maroulis ZB (2001) Transport of water in food materials. Transport properties of foods. Marcel Dekker, New York

Shi XQ, Fito-Maupoey P (1994) Mass transfer in vacuum osmotic dehydration of fruits: a mathematical model approach. Lebensm Wiss Technol 27:67–72

Simunek J, van Genuchten MTh, Sejna M (2005) The HYDRUS-1D Software package for simulating the movement of water, heat, and multiple solutes in variably saturated media. [Version 3.0] Department of Environmental Sciences, University of California, Riverside

Singh PP, Maier DE, Cushman JH, Haghighi K, Corvalan C (2004) Effect of viscoelastic relaxation on moisture transport in foods. Part I: Solution of general transport equation. J Math Biol 49:1–19

Tillotson JE (2003) Convenience foods. In: Trugo L, Finglas PM (eds) Encyclopedia food sciences and nutrition, 2nd edn. Academic, Oxford

van Genuchten MTh (1980) A closed-form equation for predicting the hydraulic conductivity of unsaturated soils. Soil Sci Soc Am J 44:892–898

Wallach R (2007) Physical characteristics of soilless media. In: Raviv M, Lieth JH (eds) Soilless culture: theory and practice. Elsevier, London

Washburn EW (1921) The dynamics of capillary flow. Phys Rev 17:273–283

Webb SW (2000) A simple extension of two-phase characteristic curves to include the dry region. Water Resour Res 36:1425–1430

Weerts AH, Lian G, Martin D (2003a) Modeling rehydration of porous biomaterials: anisotropy effects. J Food Sci 68:937–942

Weerts AH, Lian G, Martin DR (2003b) Modeling the hydration of foodstuffs: temperature effects. AIChE J 49:1334–1339

Chapter 22
Responses of Living Organisms to Freezing and Drying: Potential Applications in Food Technology

María del Pilar Buera

22.1 Introduction

Some living organisms can survive under extreme stresses by adapting to situations that would otherwise be lethal. They develop various mechanisms for adaptation, surviving adverse environmental conditions such as lack of water (cryptobiosis or anhydrobiosis) and freezing temperatures (cryobiosis) (Carpenter et al. 1986; Crowe et al. 1998, Watanabe et al. 2002). Since water is required to hydrate molecules (e.g., folding of proteins into active molecules cannot proceed without water), and their macromolecular structure and functionality are sensitively determined by their interactions with water, in many cases the stress is governed by interference from interaction with biomolecules (Franks 1982, 1995). At cold temperature, water freezes and forms disruptive ice crystals that can damage cellular structures. In conditions of low humidity or high osmolality, water leaves the cells, thus altering the hydration of macromolecules and their ability to participate in reactions necessary for life.

Various strategies can protect cells against extreme temperatures and dehydration, enabling their survival. Since these tolerant organisms face the same problems of protection during food preservation as their important biomolecules do, by studying the strategies used in nature, innovative procedures can be developed for use in food technology. By analyzing and interpreting these mechanisms, systems and processes can be engineered to preserve food quality during processing and to extend product shelf life (Aguilera and Karel 1997).

M. del Pilar Buera
Departamentos de Industrias y de Química Orgánica, Ciudad Universitaria, 1428 Ciudad de Buenos Aires, Argentina
e-mail: pilar@di.fcen.uba.ar

J.M. Aguilera et al. (eds.), *Food Engineering Interfaces*, Food Engineering Series,
DOI 10.1007/978-1-4419-7475-4_22,

22.2 Desiccation Strategies: Glass Formation and Solute-Protecting Interactions in Anhydrobiotes

Glass formation is a natural mechanism for the preservation of complex anhydrobiotic organisms, which can tolerate desiccation and survive extended periods of time in the dry state (Crowe et al. 1998). In response to dehydration the cytoplasm of desiccation-tolerant organisms forms glasses; these organisms contain large amounts of soluble nonreducing sugars and their state diagrams resemble those of simple sugar mixtures. Some of the organisms (e.g., *Artemia salina*, yeast cells, and tardigrades) accumulate α, α –trehalose, while others (pollen, seeds and resurrection plants, e.g., *Selaginella lepidophyl)* accumulate sucrose and other nonreducing β-furanosides (e.g., raffinose, stachyose, and verbascose). Other examples of living systems that exploit the formation of glass to preserve life are some species of the simple flatworm (Tunnacliffe and Lapinski 2003).

The insect *Polypedilum vanderplanki* Hint. is the largest multicellular animal known to tolerate almost complete dehydration without deterioration (Watanabe et al. 2002). Their anhydrobiotic larvae show extremely high thermal tolerance (−270°C to +102°C) and can recover soon after prolonged dehydration up to 17 years (Hinton 1960). Watanabe et al. (2002) showed that rapid accumulation of trehalose (up to 18% of dry body mass) plays a key role in the successful induction of anhydrobiosis of these larvae and that it is possible to store their individual organs, and cells from them, at room temperature under dehydrated conditions.

Crowe et al. (1998) reported that vitrification of the structure is necessary to improve enzyme and liposome stability, but specific hydrogen-bond interactions between sugars and the biomaterial are also needed. Besides forming glasses, in which kinetic restrictions for physico-chemical changes such as chemical reactions and crystallization operate, sugars develop the ability to protect proteins and membranes through hydrogen bond interactions with the active biomolecules. Dried yeast cells have been observed to have glass transition temperatures (T_g) and water sorption isotherms that are independent of the amount of trehalose. However, their viability was dramatically dependent on the quantity of disaccharides present (Cerrutti et al. 2000).

Desiccation-sensitive organisms, on the other hand, generally lose their viability during drying at water contents at which the glassy state has not yet been formed (Buitink and Leprince 2004). Besides, sugars, proteins (dehydrines), salts, and amino acids are accumulated by organisms resistant to dehydration; they act in different ways, stabilizing proteins and membranes, contributing to osmotic adjustment, or act as free radical scavengers.

The potential applications of intracellular disaccharides in animal cell biopreservation are limited by the inability of mammalian cells to synthesize or actively accumulate sugars such as trehalose (Holovati and Acker 2007). The use of liposomes as a permeabilization strategy for the intracellular delivery of trehalose has been investigated as a useful cell delivery vehicle for membrane-impermeant

biologically active compounds, including drugs, enzymes, hormones, and genetic material, and also for improved cell recovery following low-temperature exposure (Holovati and Acker 2007).

22.3 Survival in Frozen Environments: Managing the Kinetics of Ice Nucleation or Ice Crystal Growth

Many organisms exist in habitats where temperatures fall below the freezing point of water. Intracellular ice formation changes the chemical environments of biomolecules. Particularly, pH change and ionic force increase may be a cause of protein and nucleic acid damage (Franks 1982). In parallel, injuries due to mechanical changes affect the systems: large ice crystals disrupt tissue structure and thus regulation of ice crystal growth may be important for the survival of these organisms in winter. Some plants and animals have evolved to prevent the lethal effects of ice crystal formation in cells. The mechanisms by which organisms survive extreme low temperatures are (1) extracellular water crystallization (formation of crystals outside cell membrane), (2) use of antifreeze proteins (AFPs) or by the formation of a glass (Clark et al. 2007).

One of the most studied groups of organisms is the Collembola (arthropods or springtails) (Clark et al. 2007). In many freeze-tolerant insects, very potent ice nucleators are present in the hemolymph. Among vertebrates, hatchling painted turtles (*Chrysemys picta*) provide another example of "natural freeze-tolerance" (Packard and Packard 2004; Costanzo et al. 2008). In freeze-tolerant species, proteinaceous ice nucleators (INAs) trigger extracellular freezing at high subzero temperatures, either to provide cold protection from released heat of fusion or to establish a protective extracellular freezing, which drives water out of the cells, further decreasing the temperature at which intracellular ice forms (Costanzo et al. 2008).

Alternatively, some organisms will die if frozen and avoid freezing by maintaining their body fluids in the liquid state even at extremely low subzero temperatures. Freeze-avoiding species increase their supercooling potential by removing ice nucleators and accumulating polyols. Terrestrial invertebrates and polar marine fish stabilize their supercooled state by means of noncolligatively-acting AFPs. Fish, insects, and some plants that live in Arctic regions have evolved to produce AFPs, which inhibit the growth of ice crystals by adsorption to the ice surface (Zachariassen and Kristiansen 2000). These organisms (specifically insects) also have the mechanisms to inactivate INAs, minimizing the risk of inoculation by ice and INAs. Antinucleating protein of bacterial origin inhibits the fluctuation of ice nucleus formation via foreign particles (Kawahara 2002).

Many nonfreezing tolerant arthropods and insects use freeze avoidance, but others, such as the Arctic springtail *Onychiurus arcticus* or some insects, use the strategy of protective dehydration (Clark et al. 2007). In protective dehydration,

loss of water occurs across a diffusion gradient between the super-cooled cell fluids and ice in its surroundings, such that freezing point depression always exceeds the environmental temperature, and eventually the organisms lose sufficient water and desiccate to ensure that a freezing event cannot occur. Studies have shown with the springtail *O. Arcticus* or the freshwater snail, *P. canaliculata*, that exposure to subzero temperatures and low water vapor pressure induces extensive dehydration through a highly permeable cuticle; in combination with rapid synthesis and accumulation of membrane/protein cryoprotectant trehalose and some low molecular weight compounds, cold hardiness is enhanced (Clark et al. 2007; Matsukura et al. 2008). As a result, water in the cells freezes at −40°C (Zachariassen et al. 2004).

Table 22.1 summarizes the main strategies that allow some living organisms to survive adverse conditions, showing representative examples of each group. It should be noted that some species can switch between freeze avoidance and freeze tolerance, depending on prevailing physiological and environmental conditions (Costanzo et al. 2008).

22.4 Some Theoretical Considerations

Before interpreting different strategies depicted in previous sections, some theoretical concepts should be introduced. Removal of water, either by drying or freezing, induces supersaturation of cytosolic components, leading to an increase in cohesive forces between molecules and restriction of molecular mobility within cytoplasm. Although both drying and freezing are considered to promote damage by hydric stress, different protective mechanisms operate in each process (Carpenter et al. 1986).

The strategies for avoiding the above-mentioned injuries caused by dehydration and freezing can be analyzed through simplified temperature-composition state diagrams (shown schematically in Fig. 22.1), in arbitrary units, but they are generically designed by approximating the composition of cell cytosol, similar to that also observed for seeds and different tissues (Levine and Slade 1992; Buitink and Leprince 2004; Espinosa et al. 2006; Matiacevich et al. 2006).

In such supplemented diagrams the curves corresponding to equilibrium conditions (liquidus, T_m, and solubility, T_s curves) and T_g of systems are plotted as a function of water content (w). Since different curves in Fig. 22.1 delimit regions where main dynamic changes could happen as a consequence of phase/state changes (Levine and Slade 1992), this kind of diagram can predict whether systems are under thermodynamic or kinetic control, for given composition-temperature conditions, provided thermal history of samples is known (Levine and Slade 1986; Roos and Karel 1991a; Levine and Slade 1992). Of particular interest for analysis of involved phenomena are the formation of glasses and freezing characteristics of systems.

Table 22.1 The main strategies allowing some living organisms to survive adverse conditions; involved mechanisms and representative examples

Type of organism	Mechanisms	Action	Involved solutes		Examples
Anhydro-biotes	Glass formation at low water content	Reduce molecular mobility, protective hydrogen bond interactions	Protective non-reducing sugars Proteins: dehydrines	Trehalose	*Artemia salina*, yeast cells (*Saccharomyces cerevisiae*), tardigrades, flatworm, insects (larvae of chironomid *Polypedilum vanderplanki)*, rotifers (*Philodina roseola*); resurrection plants (*Selaginella spp.)*
				sucrose, raffinose, stachyose	pollen, orthodox seeds, resurrection plants (*Selaginella lepidophyl*)
Freeze-tolerant	Promote extracellular water crystallization	Decrease supercooling, increase ice nucleation temperature, decrease freezing time	Adaptive INAs		Insects, arthropods or springtails (snow flea), vertebrates (hatchling painted turtles)
Freeze-avoiding	Inhibit growth of ice crystals by adsorption to ice surface	Increase supercooling, decrease freezing temperature	AFPs (non-colligative)		Polar marine fishes, terrestrial invertebrates, insects, arthropods, nematodes, plants, fungi
	Inactivation of ubiquos INAs	Inhibit fluctuation of ice nucleus formation by a foreign particle	Proteins, polymers		Antarctic bacteria (*Pseudomonas fluorescens*)
	Vitrification at high water content	Reduce molecular mobility	Low molecular weight compounds: polyols		freshwater snail (*P. canaliculata*), fly (*Eurosta solidaginis*), frog (*Rana sylvatica*)

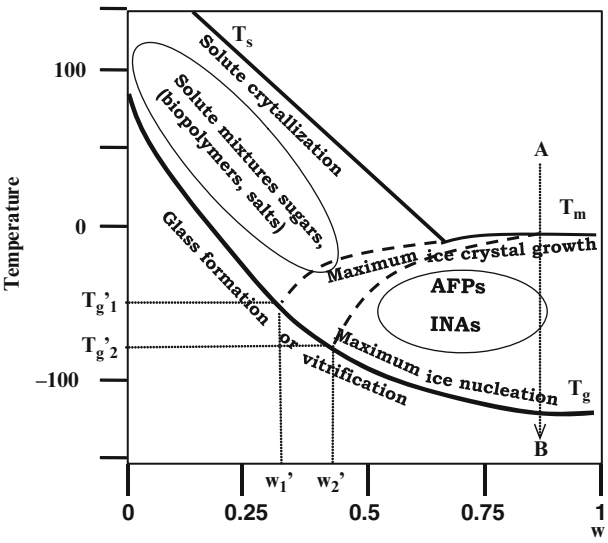

Fig. 22.1 Supplemented state diagram showing the equilibrium curves (solubility, T_s; ice melting, T_m) and nonequilibrium glass transition curve (T_g). The main expected changes are indicated, as are the mechanisms for avoiding damage (see text)

Amorphous glasses are formed by a continuous process in which no interface or solidification front is involved. Their structure is comparable to that of a liquid (some short-range order is observed, but no long-range order), but their properties are those of a solid. Glasses are characterized by a critical temperature T_g, above which most physical changes (including solute crystallization) result from sharp increase in molecular mobility, which occurs above their T_g (Levine and Slade 1986; Roos and Karel 1991a, b, c; Slade and Levine 1991). As shown in Fig. 22.1, T_g of a material is a function of the relative proportion of its glass-forming components and water content. Inclusion of T_g curve in supplemented state diagrams (corresponding to nonequilibrium transition) allows including the concept of time in which a certain event will take place or changes, which will be kinetically delayed/inhibited under certain conditions.

In region below T_m, as ice separates out during freezing, solute concentration of unfrozen phase in contact with ice increases. The combined effects of lowering temperature and increasing concentration impose molecular mobility restrictions on systems. Concentration of the unfrozen phase increases as temperature decreases. The point at which the liquidus curve, T_m, intercepts T_g curve defines the point (T_g'; w_g'), which represents the particular temperature/solute concentration below which water crystallization is kinetically inhibited. w_g' represents the lowest mass fraction of water that can be obtained by solute concentration in amorphous matrix due to ice crystallization. T_g' is the glass transition temperature of maximum ice-concentrated solution (Fig. 22.1). It should be noted that material composition will affect T_g' and w_g', thus affecting the amount of water remaining unfrozen in the

matrix ($w_g'_1$ and $w_g'_2$ in Fig. 22.1) and temperature range at which the process should be performed (Fig. 22.1). Due to predominantly nonequilibrium conditions of naturally-occurring frozen or dehydrated systems, they are subjected to dynamical (time-dependent) changes. Thus, the extent of damage will be related to the mentioned variables, to the rate and temperature of cooling, and should be taken into account in the design of processes and system formulation.

Freezing is a process of ice crystallization from supercooled water. In this process, water should undergo a stage of ice nucleation, followed by growth of ice. Nucleation is the initial stage and one of the most important steps toward creating ice. Without this step, ice would never occur in supercooled water. Nucleation can be regarded as a kinetic process for ice nuclei to overcome a kinetics barrier, the so-called nucleation barrier under a given thermodynamic driving force, which is proportional to the supercooling.

Ice growth is thermodynamically favored in water at temperatures below 0°C. However, ice nucleation is not kinetically favored in pure water and can remain liquid up to nearly −40°C, the homogeneous nucleation temperature (T_h), if free of ice nucleating species. A supercooled system is that in which no crystallization has occurred, even if it is below the liquidus curves (T_s and T_m in Fig. 22.1). Ice nucleation at temperatures greater than T_h is induced by heterogeneous INAs (Wowk and Fahy 2002). Almost all organic and inorganic substances can catalyze ice formation (i.e., serve as ice nuclei) at temperatures between −15°C and −40°C.

The degree of supercooling is the thermodynamic impulsive force for crystallization, defined as:

$$\Delta T = T_m - T \tag{22.1}$$

where T is actual subzero temperature and T_m is equilibrium melting point of ice.

The transient ice-like embryos formed by aggregation of water molecules is subjected to continuous fluctuation in size due to incorporation of new molecules and detachment of others. For a given temperature, there will be a critical radius that defines the minimum size a nucleus can have to be a stable crystal. Heneghan et al. (2002) defined the supercooling point, which is often approximated in biological studies as the temperature at which, on an average, 50% of samples are frozen. The supercooling capacity of an organism, also frequently mentioned in literature, is thus inversely related to this supercooling point: the lower the supercooling point (i.e., the lower the ice crystallization temperature), the higher the supercooling capacity of an organism. Supercooling is limited by heterogeneous nucleation in the presence of solid impurities. Certain compounds can serve as nuclei at temperatures as high as −6°C, and the wide variety of impurities present in natural systems makes homogeneous nucleation impossible. Ice nucleation preferentially occurs on these impurities, such as mold walls or cell membranes (nonadaptive INAs); since they are points with high excess energy, they lower the energy required to form the interface between the existing phase and new phase. Removing heterogeneities is one effective way of decreasing temperature at which ice forms, i.e., increasing difficulty of freezing. Some proteins have the function of

inhibiting nucleating activities of nonadaptive INAs. The critical radius decreases with decreasing temperature below T_m, and the rate of nucleation would increase with temperature below T_m. This effect is limited by decrease in molecular mobility at lower temperatures; the curves showing actual variation of nucleation frequency with temperature, crystal growth, and overall crystallization are shown as full lines in Fig. 22.2a, b.

Once initiated, crystal growth is slowed and often terminated with increasing viscosity (MacKenzie 1977). Because the free energy barrier of three-dimensional

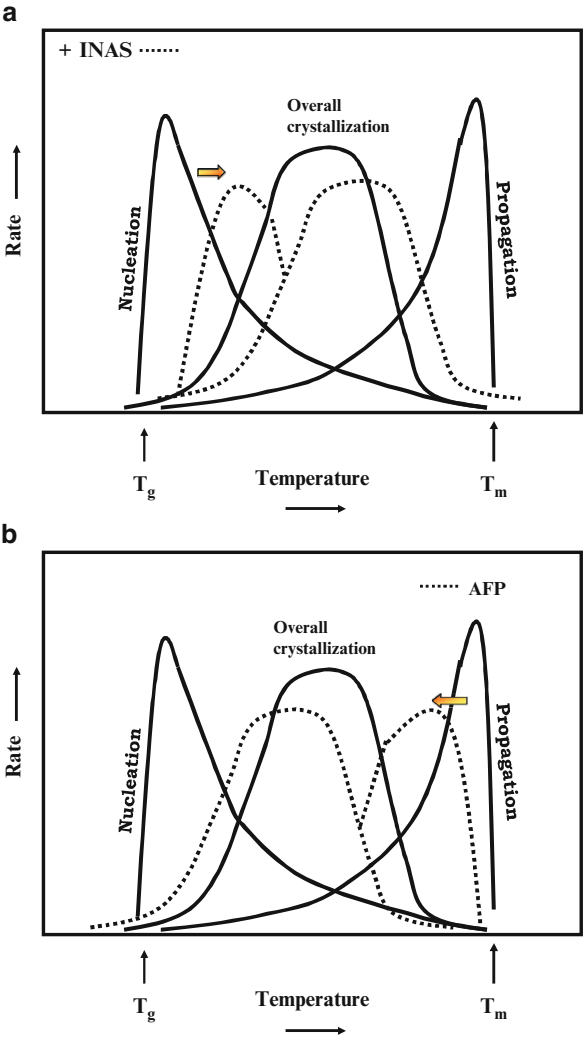

Fig. 22.2 Schematic curves showing ice nucleation and crystal growth rates, and overall crystallization rate (*full lines*) and their potential modification (*dotted lines*) by the presence of (**a**) ice nucleating agents (*INAs*) or (**b**)antifreeze proteins (*AFPs*)

nucleation is much higher than that of growth, in the case of ice crystals, growth normally becomes much easier than nucleation: once ice nuclei are formed, the rapid growth rate leads to instant freezing (Du et al. 2003). To control nucleation systematically, the upper size needs to be controlled.

22.5 Involved Mechanisms

22.5.1 Avoidance of Solids Crystallization in Supercooled State

Anhydrobiotes are dehydrated systems that have the ability to form glasses and can be located in the low **w** region of Fig. 22.1. Amorphous glasses are metastable materials in a nonequilibrium state, as these systems are located below the saturation curve, T_s, in the temperature-composition state diagram (Fig. 22.1), in which the stable form is crystal. However, in the glassy state, most structural changes occur very slowly and only small motions of molecules, mainly rotational motions of side chains and vibrations, may occur (Levine and Slade 1986; Slade and Levine 1991). Thus, crystallization of amorphous solids is kinetically delayed if sample remains in the glassy state, below T_g. Since direct interaction of sugars with molecules imbedded in the glassy matrix will prevent protein denaturation and lead to optimal preservation (Arakawa and Timasheff 1982), it is important that sugars remain in a noncrystalline state, either glassy or supercooled. It should be noted that when solute crystallization occurs, composition of the noncrystalline phase changes, and often an increase of deteriorative reaction rates is observed (Buera et al. 2005).

In the case of seeds, embryos and plant tissues, presence of several oligosaccharides has been related to seed longevity due to protection given to proteins and membranes, and to prevention of sucrose crystallization (Obendorf 1997; Murthy et al. 2003).

The influence of different yeast (e.g., *Saccharomyces cerevisiae*) cellular fractions was studied in an attempt to gain knowledge on the feasibility of trehalose crystallization in yeast cells. Certain constituents of *S. cerevisiae* cells inhibited/delayed trehalose crystallization upon humidification at high R.Hs. (Espinosa et al. 2006). This reveals that cellular structures naturally have components that act in delaying or inhibiting sugar crystallization in the interior of cells. Although crystallization of sugars in the cytoplasm has been considered as a cause of viability loss, no evidence of sugar crystallization in cells or tissues was ever reported (Buitink and Leprince 2004; Espinosa et al. 2006; Matiacevich et al. 2006). In fact, sugar crystallization has not been evident in any published, seed, fruit, or tissue thermogram during rewarming of systems from below to above glass transition temperature.

The effect of a mixture of several sugars on crystallization and stability of embedded enzymes was analyzed in freeze-dried model systems. In trehalose-lactose systems, the time to crystallization of lactose increased when trehalose

was added (Mazzobre et al. 2001). The addition of raffinose also had a retarding effect on sucrose crystallization (Buera et al. 2005). The onset temperature for trehalose or sucrose crystallization, determined by DSC, increased when raffinose or lactose was added and was even avoided during the run if enough of the second sugar was present (Mazzobre at al. 2001). Buera et al. (2005) showed that the presence of proteins delayed sugar crystallization and, in parallel, sugars retarded protein denaturation**.** Santagapita et al. (2008) have also reported delay of trehalose crystallization with the presence of polymers or salts. Because of this, when simple sugars or polyol matrices are designed to protect biomolecules, a common practice in pharmaceuticals or food ingredient formulations, a second excipient is needed.

22.5.2 Increase of Extracellular Ice Nucleation Rate: INAs

Many biological systems promote extracellular heterogeneous nucleation by the presence of a variety of INAs, which may be either incidental or adaptive. Incidental INAs (e.g., cell walls or dust particles) promote heterogeneous nucleation only as a normally unwanted side effect. Adaptive INAs are generally lipoproteins of about 30 kD; they reduce supercooling capacity by increasing supercooling temperature to as little as $-1°C$, nucleating ice crystals between cells. The amino acids within proteins form templates for ice, which serve as embryos for ice formation. Among the most efficient INAs in nature are ice nucleating proteins found on the surface of certain bacteria, such as *Pseudomonas syringae*, *Erwinia herbicola*, and *Pseudomonas fluorescens* (Kawahara 2002), commonly found on plant leaves, and other above-ground plant parts. Such proteins must assume a rigid, ice-like conformation larger than 10 nm and be able to aggregate. A thin layer of ice can always form on the surface of an INA. However, this will not lead to spontaneous ice growth unless the INA is of a certain critical size above which free ice growth will occur. Consequently, a larger INA gives a smaller required supercooling and a higher T_n. As they have the tendency to form protein aggregates of large spatial extent (larger than 10 nm) (Kajava and Lindow 1993), they act as strong heterogeneous ice nuclei in dewdrops, and ice crystals thus formed grow and break plant tissues, causing frost injury to host plants (Lindow 1983). The effects of INAs on nucleation kinetics, and further crystal growth, are schematized in Fig. 22.2a. It can be seen that supercooling point is decreased in the presence of INAs and consequently, supercooling capacity of organisms is decreased.

In natural settings, inhibition of bacterial INA is of considerable interest for environmental ice control, particularly in the prevention of frost damage to crops (Wowk and Fahy 2002). Ingestion of these ice-nucleating bacteria caused an abrupt decrease in supercooling capacity of the Colorado potato beetle (*Leptinotarsa decemlineata Say*), a freeze-intolerant species that overwinters as adults in shallow, terrestrial burrows (Costanzo et al. 1998). The ice-nucleating-active bacterium *Pseudomonas syringae* was employed as pest control in grain silos, to increase

mortality of the granary weevil *Sitophilus granarius* (L.) and saw-toothed grain beetle *Oryzaephilus surinamensis* (L.) (Mignon et al. 1998).

22.5.3 Inhibition of Ice Crystal Growth: AFP

Freeze avoidance is often achieved by a high capacity for supercooling, minimizing the risk of inoculation by ice and INAs. At low temperatures, many plants and microorganisms produce colligative protectants such as proline or sucrose. However, some organisms are also capable of producing AFPs and antifreeze glycoproteins (AFGPs), protecting them from the negative effects of freezing. AFPs and AFGPs were first identified in 1970 in Antarctic fish varieties that can survive in seawater colder than the freezing temperature of their blood; AFPs and AFGPs were then found in microorganisms, insects, plants, and nematodes. Their molecular weight ranged between 2,600 and 33,000 Da. Although they were thought to act by colligative effect, decreasing melting point of water, it was later observed that they act by avoiding growth of ice crystals, having a low effect on colligative properties.

AFPs act at concentrations in the order of 10^{-5} M and inhibit ice crystal growth by adsorption-inhibition. The nuclear magnetic resonance, x-ray structure, and many spectroscopic studies with AFPs have been helpful in determining the structure-function relationship. Mutational studies have indicated the importance of hydrophobic residues in ice binding (Venketesh and Dayananda 2008). Ice crystals can grow along six a-axes, all in the same plane, or along the c-axis, which is perpendicular to the plane of the six a-axes. Ice crystal growth at temperatures close to T_m typically occurs along the a-axes, which accounts for the typical hexagonal shape of snowflakes. The c-axis growth results in needle-like ice crystals, which are potentially damaging (Davies and Hew 1990). The morphology of ice crystals will depend on the planes in which growth inhibition is performed by AFP. AFPs typically found in Arctic fish specifically adsorb to basal ice (a-axis), growing planes and avoiding propagation, and behave as "structural ice inhibitor agents" (Pertaya et al. 2007a, b); ice crystal growth occurs in bipyramidal shape. By contrast, AFPs from Arctic insects typically inhibit c-axis growth, forming brown flat discs.

All AFPs tested to date show both antifreeze activity and inhibition of ice recrystallization, suggesting a common mechanism for these two effects mediated through ice binding. To visualize the binding of AFP to ice, Pertaya et al. (2007a, b, 2008) labeled the spruce budworm AFP with enhanced green fluorescent protein (GFP) and observed the AFP-GFP molecules directly on ice crystals using confocal microscopy. Melt-growth-melt sequences in low concentrations of AFPs revealed that the same general behavior of an apparently rotated crystal, observed in pure ice under high pressure, is reproduced in ice under the influence of AFP at ambient pressure and temperatures near 0°C.

While AFPs lower the freezing point, the melting point is unaltered. The separation of melting and freezing temperature is usually referred to as thermal hysteresis (TH), and temperature of ice growth is referred to as hysteresis freezing point. The hysteresis is the result of an adsorption of AFPs to crystal surface. This causes ice to grow as convex surface regions between adjacent adsorbed AFPs, thus lowering temperature at which the crystal can visibly expand (Kristiansen and Zachariassen 2005). Within the resulting TH gap, ice crystals appear to be kinetically stable, neither growing nor melting. The level of TH is directly related to intrinsic activity of specific AF(G)P and to their concentration. Results by Evans et al. (2007) showed that when AF(G)P are dissolved in salt solutions, such as NaCl, at concentrations they could encounter in nature, there is a synergistic effect on TH that is positively related to salt concentration. This enhancement could have resulted from the hydration shell of dissolved ions, which reduces freezable water. Alternatively, salt could influence the hydration shell surrounding AF(G)P, increasing protein surface area available to adsorb to ice/water interface (Evans et al. 2007).

Five AFP types have been isolated from fish, six from plants, and two from insects; five bacteria produce AFPs and show no related structures, varying in protein size and specific activity (Davies and Hew 1990; Brush et al. 1994; Davies et al. 2002; Gilbert et al. 2004). The AFPs found in certain insects (which allow them to survive winters at temperatures as low as −30°C) are up to 100 times more powerful than similar proteins in fish (Graether et al. 2000). Although TH activity of plant AFPs is low compared to that of fish and insects, their inhibition of ice recrystallization is comparable or even greater (Smallwood et al. 1999). The effect of AFP on kinetic control of ice crystallization is shown schematically in Fig. 22.2b (dotted lines).

22.5.4 Vitrification at High Water Content (Liquid N and/ or with Concentrated Solutes)

The alternative route to remove ice crystallization is rapid cooling into the glassy state, or vitrification (line A–B in Fig. 22.1). Vitrification as a cryopreservation method has many primary benefits, such as no ice crystal formation through increased speed of temperature conduction, which provides a significant increase in cooling rates. This can eliminate structural damage during freezing, but mass transfer rates limit the sample size in which this can be achieved and thawing is never rapid enough to prevent crystallization from causing extensive damage (Lillford and Holt 2002). It should be noted that the maximum ice nucleation occurs just above T_g and the maximum ice-crystal growth-rate occurs just below T_m (Fig. 22.1). Thus, the many nuclei formed when cooling can cause massive ice growth when rewarming. This leads to devitrification. The main concern with cooling is the maximum nucleation range near T_g. The addition of a cryoprotectant may allow cooling up to the T_g region without forming any nuclei, if cooling is

quick enough. If nuclei are formed, the rapid cooling and high viscosity near T_g in the presence of cryoprotectant will not allow the nuclei to grow very much and thus prevents them from being harmful. Increasing cryoprotectant concentrations lowers both T_h and T_m, but the effect is more dramatic on T_h than T_m. Enough cryoprotectant to lower T_m will lower temperature of nucleation to T_g, thereby delaying nucleation. Northern frogs use glucose as a cryoprotectant (Mietchen et al. 2008). When temperatures drop, the liver of these frogs produces large amounts of glucose, which a special form of insulin allows to enter into their cells in large quantities. Except for the heart and brain, much of the frog's body freezes. The two disaccharides that most protect proteins and cell membranes against chilling, freezing, and dehydration are sucrose and trehalose.

Dissolved polymers form glasses readily once they are freeze-concentrated. Below T_g, no further ice forms, and crystal growth rates and sintering of ice are kinetically slowed to almost zero. The damage caused by the amount of ice present and temperature at which it is stabilized against growth and/or recrystallization should be balanced (Lillford and Holt 2002). Increasing speed of thermal conduction and decreasing concentration of cryoprotectant are challenges to overcome with vitrification methods. The convenience of vitrification could push development of this technique beyond most presently common clinical uses for embryos and tissue preservation (Kattera and Chen 2006).

22.5.5 The Problem of Recalcitrant Seeds

Orthodox seeds undergo a programmed desiccation at termination of their development. Vitrification of cytoplasm components in orthodox seeds is proposed to be advantageous for germplasm stability, and their transitions may affect seed viability (Walters 2004). The cytoplasmic glass of seeds is composed mainly of sugars (sucrose and oligosaccharides comprise over 10–20% of dry weight), high molecular weight oligosaccharides, and proteins. As storage temperature or water content increases, seeds undergo glass-to-liquid transition (T_g), resulting in an increase in molecular mobility. As T_g is a function of water content, whether seed tissues are in the glassy state or not, it will depend on both seed water content and storage temperature (Buitink and Leprince 2004; Matiacevich et al. 2006). Investigations have led to the suggestion that seeds induce glass formation as water content is depressed, thus limiting deteriorative reactions (Murthy et al. 2003). The seed's tolerance to desiccation (orthodox) can be attributed to the presence of the soluble carbohydrates raffinose and sucrose in the cytoplasmasm of embryo cells. In contrast, recalcitrant seeds (*Araucaria angustifolia*, palm) do not tolerate a reduction in water below a relatively high level without loss of viability. Conventional storage techniques are thus not applicable to these seeds and cryopreservation is the only feasible alternative for their long-term storage. Panza et al. (2006) have observed that at necessary water contents (or relative humidities (R.Hs.)) at

which embryos of recalcitrant *Araucaria angustifolia* seeds retain their viability (at and above R.H. 85%), water freezes upon cooling at subzero temperatures. Their high-freezable water content promotes injuries, and their conservation at low-temperatures represents a challenge. Thus, recalcitrant seeds are good models for analyzing the impact of freezing rate, storage time, and temperature on degree of injury. If plant tissues are exposed to rapid cooling only minor damage occurs (−196°C). Seeds with lower amounts of frozen water would be more easily cryopreserved. The preservation of recalcitrant seeds could be improved by vitrification, either by dehydration, after imbibition of embryos with protecting agents, or by freezing, avoiding ice formation, but this is an area of further research, of interest in biodiversity preservation, for example.

22.6 Applications in Food Technology

The implications of glass formation and glass transitions in food technology have been extensively analyzed since the pioneering work by Levine and Slade in the 1980s (Levine and Slade 1986, 1992), based on polymer science approaches. Afterwards, many scientific publications evolved (Roos 1995). Parallel advances in the area of preservation mechanisms of living organisms under extreme conditions promoted the study of sugar properties in relation to their protective effects on labile biomolecules (Arakawa and Timasheff 1982; Crowe et al. 1998; Clegg 2001). Fundamental research areas were also focused on dynamic aspects related to glass-forming properties of sugars, and on molecular interactions that sugars are capable of developing in hydrogen bonding.

According to the discussed aspects, possible strategies to avoid sugar crystallization for food and ingredient formulation in low water content systems may include vitrification or sugar crystallization delay in supercooled media, which can be achieved by combinations with biopolymers, salts, or other sugars. Recently, Leinen and Labuza (2006) and Belcourt and Labuza 2007) successfully suppressed sucrose recrystallization by addition of raffinose to the formulation of cotton candy and soft cookies, respectively, which consequently improved technological properties of products.

The efficiency of freezing and resulting food quality is affected by two important factors: supercooling (cooling of liquid below its freezing point, without freezing) and nucleation (initiation of crystallization of liquid water into solid ice) (Li and Lee 1995). Both phenomena are modified by the presence of two kinds of proteins showing opposite behavior (Hew and Yang 1992; Li and Sun 2002), which provide enormous technological potential in industrial processes (Lillford and Holt 2002).

INAs, on the one hand, decrease supercooling and increase nucleation temperature (T_n), thus decreasing freezing time and forming a large number of ice crystals with a dendritic structure (Feeney and Yeh 1998; Li and Lee 1995; Li and Sun 2002). AFPs, on the other hand, increase supercooling, generate very small ice crystals, lower freezing temperature, and retard recrystallization in frozen storage.

Lillford and Holt (2002) and Li and Sun (2002) have reviewed the main potential applications of INAs and AFPs. The beneficial effects of INAs are manifested in decreasing energy cost and crystal size, favoring quality improvements and increased shelf life. Bacterial ice nucleators were employed in the freezing of meat (Payne et al. 1994), and in products difficult to concentrate or freeze-dried products, such as fruit juices or pastes (Li and Lee 1995). The management of ice nucleation and crystallization times can also be employed for the development of new products. For example, freeze-texturing of protein products may generate foods with special characteristics (Watanabe and Arai 1994).

AFPs behave both as antinucleators and as growth inhibitors, preventing heterogeneous nuclei from growing (Lillford and Holt 2002). One of the most interesting applications is the performance of AFP after ice is nucleated or in conditions where ice crystals would normally grow and sinter (Griffith and Ewart 1995). The presence of AFPs in these products may inhibit ice crystal growth at fluctuating subzero temperatures during storage or transportation, thus preserving food quality and decreasing operative costs.

AFPs are natural products that form part of a normal diet through their occurrence at high concentrations in food fish and vegetables (Smallwood et al. 1999). Simple natural extracts that are purified or partially purified are likely to meet consumer acceptance. The AFPs from vegetables have a number of potential applications. For example, Zhang et al. (2007a) improved the texture of frozen dough and the effect of volatile compounds in crumb foods by the addition of a concentrated carrot extract containing carrot AFP. AFP is efficient at relatively low concentration, but the cost of extraction from natural sources restricts their use only to applications with very high added value. Strategies for improving AFP production from natural sources can be developed. Naturally-occurring "antifreeze" has been found in carrots, winter wheat, and rye (Li and Lee 1995). Desjardins et al. (2007) showed that the thermal regimen of wolffish can be manipulated to enhance their tolerance to subzero temperatures and also their ability to produce AFP. Abundant AFPs could also be generated as by-products in processing certain fish species for food (Griffith and Ewart 1995).

Alternatively, AFP genes can also be introduced into microorganisms used to produce frozen yogurt (Yeh et al. 2008). Recent advances in biotechnology and control of heterologous gene expression may make them potentially accessible in high quantities. The multiple forms of AFPs synthesized within each organism, and demonstrated possibilities for useful modification through protein engineering, make it feasible to choose the most appropriate AFP, with a suitable level of activity for addition to a particular product or expression in a particular plant or animal (Griffith and Ewart 1995; Li and Lee 1995; Lillford and Holt 2002). Further, the ability to modify the rate and shape of crystal growth and to protect cellular membranes during lipid-phase transitions have resulted in identification of a number of potential applications of AFGPs as food additives, and in the cryopreservation and hypothermal storage of cells and tissues (Harding et al. 2003).

22.7 Future Prospects

The study of delay/inhibition of sugar crystallization in supercooled liquids at low water content may increase the range of applications of sugar as excipients for food ingredient formulation for specific purposes. Currently, relative long-term storage of living cells in the high water content range can be done only in cryoprotectant solution at extremely low subzero temperatures, and most of the time media formulations are performed on an empirical basis. A standardized vitrification protocol for cryopreservation on a scientific basis has yet to be defined, taking into account the many variables that can profoundly influence its effectiveness and potential to improve survival rates of vitrified cells (e.g., type and concentration of cryoprotectant; temperature of vitrification solution at exposure; duration of exposure to final cryoprotectant before plunging into LN2).

Liquid-to-solid nucleation of a supercooled aqueous solution seems to be a simple phenomenon, but it remains a poorly understood process of evolution of a metastable state to its final equilibrium state. Inputs from fundamental research in this area are also needed (Heneghan et al. 2002). Careful design of experiments for measuring temperatures and times of nucleation and crystal growth should be developed (Chapsky and Rubinsky 1997; Heneghan et al. 2002; Du et al. 2003; Zachariassen et al. 2004; Yin et al. 2005).

The presence of ice surfaces was reported as a cause of freeze-induced perturbations of protein native fold, but these interactions are poorly understood. Gabellieri and Stambrini (2006) reported that a binding method using a fluorescence probe may find practical utility in testing the effectiveness of various additives employed in frozen or freeze-dried protein formulations. Research work in this area would be helpful in the development of "ice managing" additives. Besides, the quantitative relationships between the activity of INAs and AFPs and variable parameters that affect the measurement of activity should be established to elucidate the mechanism and organize the research findings.

Fundamental research also on freeze tolerance mechanisms may allow identification of secondary metabolic products that prepare organisms for stress from ice formation, osmotic dehydration or freeze concentration; further, molecules that have applications in industrial settings could be produced in large quantities once their functions are elucidated (Feeney and Yeh 1998; Lillford and Holt 2002). The effect of proteins and polysaccharides involved in INA inactivation should also be further investigated to explore their potential applications (Kawahara 2002; Wowk and Fahy 2007).

Although many advances have been achieved in the last 10 years, additional research is still needed to define the relationship between molecular structure and the function of INAs and AFPs. The developments of infrared thermography, microscopic and magnetic resonance spectroscopy, and imaging techniques for cryobiological investigations were demonstrated as powerful tools for interpretation of mechanisms of action for different AFPs (Wisniewski et al. 2001; Pertaya et al. 2007a, b, 2008; Mietchen et al. 2008), and are expected to further contribute to advances in these areas.

The availability of ice nucleators or antinucleators for food uses involves development of purification protocols of potential AFPs and INAs and effective ways for their characterization (Kawahara et al. 2006; Zhang et al. 2007b). Besides being nontoxic, nonpathogenic, and environmentally safe, they should be palatable (Lillford and Holt 2002). Sensory evaluation should thus be performed on processed products with these additives before being commercialized.

The chemical synthesis of AFPs is an attractive alternative to their difficult isolation and purification from natural sources, and this would permit quality control and mass production (Matsumoto et al. 2006). The successful synthesis of small AFGPs using solution methods and solid-phase chemistry provides the opportunity to perform key structure-activity studies that would clarify important residues and functional groups required for activity (Harding et al. 2003). The possibility of production using different molecular biological techniques, which will help increase the yield, is also dealt with (Venketesh and Dayananda 2008).

Improving the efficiency of AFPs by the presence of simple molecules normally present in foods, such as electrolytes (Du and Liu 2008), provides another new insight into the antifreeze mechanism of AFPs on ice crystallization.

AFPs can display both protective and cytotoxic actions, and both nucleation of ice and inhibition of ice crystal growth; they have also been shown to either stabilize or disrupt the membrane, depending on several factors (membrane composition, type, and concentration of AFP) (Wang 2000; Tomczak et al. 2001). At certain levels, AFP-ice interactions may induce the complexes to aggregate, promoting ice nucleation, and loss of ability to inhibit recrystallization. Although at low concentrations AFPs can be employed very effectively to maintain texture and flavor of frozen foods, it should be noted that bipyramidal or spicular ice crystals, which grow in solutions containing high concentrations of AFP, are so detrimental for cell survival that they are proposed as an important tool in cryosurgery (Matsumoto et al. 2006). These properties indicate that careful consideration of concentrations and type of AFP used require further study in order to understand the mechanisms by which they occur and their potential usefulness in food technology.

The use of gene transfer to generate food organisms that produce AFPs needs to be carried out. Since one important consideration is that of consumer acceptance of transgenic products, transfer of genes from INA^+ bacteria to other microorganisms commonly used in production of foods (Yeh et al., 2008), or AFP genes from cereal grains (e.g., winter wheat or rye) to plants for production of more freezing-resistant fruits, is expected to be better accepted by consumers than the use of fish AFPs or bacterial INAs (Lillford and Holt 2002). The addition of INAs or AFPs to food products could involve significant modification in formulation and handling procedures. Thus, a further analysis of phase/state diagrams is necessary before large-scale food production.

The relatively high cost of freezing processes currently used in the food industry and the search for products with special structures could be the major impulse toward new innovations in freezing techniques. Additional work to analyze cost-benefit, balancing the energy savings, and product-quality improvements, is essential before final commercialization of application in the food industry (Lillford and

Holt 2002). The discussed aspects are examples of how the tools from cryobiology may stimulate those innovations.

It is interesting to note that the different aspects referred to in this chapter show the synergistic interaction of multidisciplinary interfaces of physics, chemistry, medicine, biotechnology, food science and technology, pharmacy, and biology, which are faced with preservation of living organisms such as embryos and cells, structures like liposomes, as well as labile molecules, such as enzymes, antibodies, and hormones.

Acknowledgments The author acknowledges the invaluable help of her collaborators Drs. Florencia Mazzobre, Carolina Schebor, Beatriz Elizalde, Silvia Matiacevich, Nuria Acevedo, Patricio Santagapita, Abel Farroni, and Nora Gutiérrez. Financial support by CONICET–PIP 5977, ANPCyT–PICT 20545, and UBACYT X024 is also acknowledged.

References

Aguilera JM, Karel M (1997) Preservation of biological materials under desiccation. Crit Rev Food Sci Nutr 37:287–309

Arakawa T, Timasheff SN (1982) Stabilization of protein structure by sugars. Biochemistry 21:6536–6544

Belcourt LA, Labuza TP (2007) Effect of raffinose on sucrose recrystallization and textural changes in soft cookies. J Food Sci 72:C065–C071

Brush RA, Griffith M, Mlynarz A (1994) Characterization and quantification of intrinsic ice nucleators in winter rye (*Secale cereale*) leaves. Plant Physiol 104:725–735

Buera P, Schebor C, Elizalde B (2005) Carbohydrate crystallization phenomena in dehydrated food and ingredient formulations: involved factors, consequences and prevention. J Food Eng 67:157–165

Buitink J, Leprince O (2004) Glass formation in plant anhydrobiotes: survival in the dry state. Cryobiology 48:215–228

Carpenter JF, Crowe JH, Arakawa T (1986) Comparison of solute-induced protein stabilization in aqueous solution and in the frozen and dried states. J Dairy Sci 73:3627–3636

Cerrutti P, Segovia M, Galvagno M, Schebor C, Buera MP (2000) Commercial yeast stability during dehydration and thermal treatment as affected by intracellular content and external presence of trehalose. Appl Microbiol Biotechnol 54:575–580

Chapsky L, Rubinsky B (1997) Kinetics of antifreeze protein-induced ice growth inhibition. FEBS Lett 412:241–244

Clark MS, Thorne MAS, Purać J, Grubor-Lajšić G, Kube M, Reinhardt R, Worland MR (2007) Surviving extreme polar winters by desiccation: clues from Arctic springtail (*Onychiurus arcticus*). BMC Genomics 8:475–467

Clegg JS (2001) Cryptobiosis: a peculiar state of biological organization. Comp Biochem Physiol 128B:613–624

Costanzo JP, Litzgus JD, Iverson JB, Lee RE (1998) Soil hydric characteristics and environmental ice nuclei influence supercooling capacity of hatchling painted turtles *Chrysemys picta*. J Exp Biol 201:3105–3112

Costanzo JP, Lee RE Jr, Ultsch GRJ (2008) Physiological ecology of overwintering in hatchling turtles. J Exp Zool A Ecol Genet Physiol 309:297–379

Crowe JH, Carpenter JF, Crowe LM (1998) The Role of vitrification in anhidrobiosis. Annu Rev Physiol 60:73–103

Davies PL, Hew CL (1990) Biochemistry of fish antifreeze proteins. FASEB 4:2460–2468

Davies PL, Baardsnes J, Kuiper MJ, Walker VK (2002) Structure and function of antifreeze proteins. Phil Trans R Soc B 357:927–935

Desjardins M, Le François NR, Fletcher GL, Blier PU (2007) High antifreeze protein levels in wolffish (*Anarhichas lupus*) make them an ideal candidate for culture in cold, potentially ice laden waters. Aquaculture 272:667–674

Du N, Liu XY (2008) Enhanced antifreeze effect of antifreeze protein on ice nucleation by electrolyte. Cryst Growth Des 8:3290–3294

Du N, Liu XY, Hew CL (2003) Ice nucleation inhibition: mechanism of antifreeze by antifreeze protein. J Biol Chem 278:36000–36004

Espinosa L, Schebor C, Buera MP, Moreno S, Chirife J (2006) Inhibition of trehalose crystallization by cytoplasmic yeast components. Cryobiology 52:157–160

Evans RP, Hobbs RS, Goddard SV, Fletcher GL (2007) The importance of dissolved salts to the in vivo efficacy of antifreeze proteins. Comp Biochem Physiol A Mol Integr Physiol 148:556–561

Feeney RE, Yeh Y (1998) Antifreeze proteins: current status and possible food uses. Trends Food Sci Technol 9:102–106

Franks F (1982) The properties of aqueous solutions at subzero temperatures. In: Franks F (ed) Water, a comprehensive treatise, vol 7. Plenum, London

Franks F (1995) Biophysics and biochemistry at low temperatures. Cambridge University Press, Cambridge

Gabellieri E, Strambini GB (2006) ANS fluorescence detects widespread perturbations of protein tertiary structure in ice. Biophys J 90:3239–3245

Gilbert JA, Hill PJ, Dodd CER, Laybourn-Parry J (2004) Demonstration of antifreeze protein activity in Antarctic lake bacteria. Microbiology 150:171–180

Graether SP, Kuiper MJ, Gagne SM, Walker VK, Jia Z, Sykes BD, Davies PL (2000) Beta-helix structure and ice-binding properties of a hyperactive antifreeze protein from an insect. Nature 406:325–328

Griffith M, Ewart KV (1995) Antifreeze proteins and their potential use in frozen foods. Biotechnol Adv 13:375–402

Harding MM, Anderberg PI, Haymet AD (2003) "Antifreeze" glycoproteins from polar fish. Eur J Biochem 270:1381–1392

Heneghan AF, Wilson PW, Haymet ADJ (2002) Heterogeneous nucleation of supercooled water, and the effect of an added catalyst. Proc Natl Acad Sci USA 99:9631–9634

Hew CL, Yang DS (1992) Protein interaction with ice. Eur J Biochem 203:33–42

Hinton HE (1960) A fly larva that tolerates dehydration and temperatures of −270°C to +102°C. Nature 188:336–337

Holovati JL, Acker JP (2007) Spectrophotometric measurement of intraliposomal trehalose. Cryobiology 55:98–107

Kajava AV, Lindow SE (1993) A model for the three dimensional structure of ice nucleating proteins. J Mol Biol 232:709–717

Kattera S, Chen C (2006) Cryopreservation of embryos by vitrification: current development. Int Surg 91:S55–S62

Kawahara H (2002) The structures and functions of ice crystal-controlling proteins from bacteria. J Biosci Bioeng 94:492–496

Kawahara H, Kawakami H, Obata H (2006) Purification and characterization of antifreeze protein from a mushroom Flammulina velutipes. Cryobiology 53:428

Kristiansen E, Zachariassen KE (2005) The mechanism by which fish antifreeze proteins cause thermal hysteresis. Cryobiol 51:262–280

Leinen KM, Labuza TP (2006) Crystallization inhibition of an amorphous sucrose system using raffinose. J Zhejiang Univ Sci 7(2):85–89

Levine H, Slade L (1986) A polymer physico-chemical approach to the study of commercial starch hydrolysis products (SHPs). Carbohydr Polym 6:213–244

Levine H, Slade L (1992) Glass transitions in foods. In: Schwartzberg H, Hartel R (eds) Physical chemistry of foods. Marcel Dekker, New York, pp 83–221

Li B, Sun D-W (2002) Novel methods for rapid freezing and thawing of foods–a review. J Food Eng 54:175–182
Li J, Lee T-C (1995) Bacterial ice nucleation and its potential application in the food industry. Trends Food Sci Technol 6:259–265
Lillford PJ, Holt CB (2002) In vitro uses of biological cryoprotectants. Philos Trans R Soc Lond B Biol Sci 357:945–951
Lindow SE (1983) The role of bacterial ice nucleation in frost injury to plants. Annu Rev Phytopathol 68:523–527
MacKenzie AP (1977) Non-equilibrium freezing behaviour of aqueous systems. Philos Trans R Soc Lond B Biol Sci 278:167–189
Matiacevich SB, Castellión ML, Maldonado SB, Buera MP (2006) Water-dependent thermal transitions in quinoa embryos. Thermochimica Acta 448:117–122
Matsukura K, Tsumuki H, Izumi Y, Wada T (2008) Changes in chemical components in the freshwater apple snail, *Pomacea canaliculata* (*Gastropoda: Ampullariidae*), in relation to development of its cold hardiness. Cryobiol 56:131–137
Matsumoto S, Matsusita M, Morita T, Kamachi H, Tsukiyama S, Furukawa Y, Koshida S, Tachibana Y, Nishimura S, Todo S (2006) Effects of synthetic antifreeze glycoprotein analogue on islet cell survival and function during cryopreservation. Cryobiol 52:90–98
Mazzobre MF, Soto G, Aguilera JM, Buera MP (2001) Crystallization kinetics of lactose in systems co-lyofilized with trehalose. Analysis by differential scanning calorimetry. Food Res Int 34:903–911
Mietchen D, Manz D, Volke F, Storey K (2008) Vivo assessment of cold adaptation in insect larvae by magnetic resonance imaging and magnetic resonance spectroscopy. PLoS ONE 3(12):e3826, 1–10
Mignon J, Haubruge E, Gaspar Ch (1998) Effect of ice-nucleating bacteria (*Pseudomonas syringae* Van Hall) on insect susceptibility to sub-zero temperatures. J Stor Prod Res 34:81–86
Murthy UMN, Kumar PP, Sun WQ (2003) Mechanisms of seed aging under different storage conditions for *Vigna radiata* (L.) Wilczek: lipid peroxidation, sugar hydrolysis, maillard reactions and their relationship to glass state transition. J Exp Bot 54:1057–1067
Obendorf RL (1997) Oligosaccharides and galactosyl cyclitols in seed desiccation tolerance. Seed Sci Res 7:63–74
Packard GC, Packard MJ (2004) To freeze or not to freeze: adaptations for overwintering by hatchlings of the North American painted turtle. J Exp Biol 207:2897–2906
Panza V, Láinez V, Maldonado SB, Maroder H, Buera P (2006) Storage changes and subcellular freezing injuries in recalcitrant *Araucaria angustifolia* embryos. In: Water properties of food, pharmaceutical and biological materials, eds. M.P. Buera, J. Welti-Chanes, P. Lillford and H.R. Corti. Boca Raton, FL: CRC Press/Taylor & Francis
Payne SR, Stanford D, Harris A, Young OA (1994) The effects of antifreeze proteins on chilled and frozen meat. Meat Sci 37:429–438
Pertaya N, Marshall CB, DiPrinzio CL, Wilen L, Thomson ES, Wettlaufer JS, Davies PL, Braslavsky I (2007a) Fluorescence microscopy evidence for quasi-permanent attachment of antifreeze proteins to ice surfaces. Biophys J 92:3663–3673
Pertaya N, Celik Y, DiPrinzio CL, Wettlaufer JS, Davies PL, Braslavsky I (2007b) Growth–melt asymmetry in ice crystals under the influence of spruce budworm antifreeze protein. J Phys Condens Matter 19:412101, 12 pp
Pertaya N, Marshall CB, Celik Y, Davies PL, Braslavsky I (2008) Direct visualization of spruce budworm antifreeze protein interacting with ice crystals: basal plane affinity confers hyperactivity. Biophys J 95:333–341
Roos YH (1995) Water and phase transitions. In: Steve Taylor (ed) Phase transitions in foods. Academic, London, pp 73–107, chapter 4
Roos Y, Karel M (1991a) Applying state diagrams to food processing and development. Food Technol 45:66–71

Roos Y, Karel M (1991b) Amorphous state and delays ice formation in sucrose solutions. Int J Food Sci Technol 26:553–566

Roos Y, Karel M (1991c) Nonequilibrium ice formation in carbohydrate solutions. Cryo Lett 12:367–376

Santagapita PR, Gómez Brizuela L, Mazzobre MF, Villalonga Santana R, Corti HR, Buera MP (2008) Structure/function relationships of several biopolymers as related to β-fructofuranosidase stability in dehydrated systems. Biomacromol 9:741–747

Slade L, Levine H (1991) Beyond water activity: recent advances based on an alternative approach to the assessment of food quality and safety. Crit Rev Food Sci Nutr 30:115–360

Smallwood M, Worrall D, Byass L, Elias L, Ashford D, Doucet CJ, Holt C, Telford J, Lillford P, Bowles DJ (1999) Isolation and characterization of a novel antifreeze protein from carrot (*Daucus carota*). Biochem J 340:385–391

Tomczak MM, Hincha DK, Estrada SD, Feeney RE, Crowe JH (2001) Antifreeze proteins differentially affect model membranes during freezing. Biochem Biophys Acta (BBA) – Biomembranes 1511:255–263

Tunnacliffe A, Lapinski J (2003) Resurrecting Van Leeuwenhoek's rotifers: a reappraisal of the role of disaccharides in anhydrobiosis. Phil Trans R Soc Lond B 358:1755–1771

Venketesh S, Dayananda C (2008) Properties, potentials, and prospects of antifreeze proteins. Crit Rev Biotechnol 28:57–82

Walters C (2004) Temperature dependency of molecular mobility in preserved seeds. Biophys J 86:1253–1258

Wang J-H (2000) A comprehensive evaluation of the effects and mechanisms of antifreeze proteins during low-temperature preservation. Cryobiology 41:1–9

Watanabe M, Arai S (1994) Bacterial ice-nucleation activity and its application to freeze concentration of fresh foods for modification of their properties. J Food Eng 22:453–473

Watanabe M, Kikawada T, Minagawa N, Yukuhiro F, Okuda T (2002) Mechanism allowing an insect to survive complete dehydration and extreme temperatures. J Exp Biol 205:2799–2802

Wisniewski M, Fuller M, Glenn DM, Palta J, Carter J, Gusta L, Griffith M, Duman J (2001) Factors involved in ice nucleation and propagation in plants: an overview based on new insights gained from the use of infrared thermography. J Agr Sci 14:41–47

Wowk B, Fahy GM (2002) Inhibition of bacterial ice nucleation by polyglycerol polymers. Cryobiology 44:14–23

Wowk B, Fahy GM (2007) Ice nucleation and growth in concentrated vitrification solutions. Cryobiology 55:330

Yeh C-M, Huang X-H, Sue C-W (2008) Functional secretion of a type 1 antifreeze protein analogue by optimization of promoter, signal peptide, prosequence, and terminator in *Lactococcus lactis*. J Agric Food Chem 56:8442–8450

Yin LJK, Chen ML, Tzeng SS, Chiou T-K, Jiang ST (2005) Properties of extracellular ice-nucleating substances from Pseudomonas fluorescens MACK-4 and its effect on the freezing of some food materials. Fisheries Sci 71:941–947

Zachariassen KE, Kristiansen E, Pedersen SA, Hammel HT (2004) Ice nucleation in solutions and freeze-avoiding insects – homogeneous or heterogeneous? Cryobiology 48:309–321

Zachariassen KE, Kristiansen E (2000) Ice nucleation and antinucleation in nature. Cryobiology 41:257–279

Zhang C, Zhang H, Wang L, Gao H, Guo XN, Yao HY (2007a) Improvement of texture properties and flavor of frozen dough by carrot (Daucus carota) antifreeze protein supplementation. J Agric Food Chem 55:9620–9626

Zhang C, Zhang H, Wang L, Zhang J, Yao H (2007b) Purification of antifreeze protein from wheat bran (*Triticum aestivum L.*) based on its hydrophilicity and ice-binding capacity. J Agric Food Chem 55:7654–7658

Part IV
Food Microstructure

Chapter 23
Food Microstructures for Health, Well-being, and Pleasure

José Miguel Aguilera

23.1 Introduction

For centuries, mankind has converted natural materials into an edible state, since apart from some fruits, vegetables, and nuts, most plant and animal tissues are not easily eaten. As large numbers of people flocked into cities, massive food production became necessary with the concomitant problems of transporting, storing, processing, and distributing millions of unitized and safe products. Presently, the packaged food industry is the world's largest business, with an annual turnover of almost $1.6 trillion, and approximately 70% of the food consumed in homes in large urban centers is purchased in supermarkets. Moreover, consumer food products are now cheaper and more abundant than ever before in the past. In this sense, food manufacturing is the most prominent application of bioprocess engineering. Yet, food is not distributed equally and it is estimated that 17% of the total population in the world does not have enough food (FAO 2005). For those who barely surpass the survival level, cereals, legumes, and tubers provide well over 50% of all calories. Rice alone, which undergoes only basic processing, provides 20% of the world's food calories. As a result of intensive processing, the developed world spends more than double the kcal per nutritional kcal compared to the less-developed countries (LDCs), most of which comes from nonrenewable energy sources (as opposed to burned biomass) (Giampietro et al. 1994).

Foods are processed to make them more palatable and safe, to improve their shelf-life and convenience, and to expand the variety of the culinary supply. As is the case of many materials typical in our daily life, some of the most desirable properties of foods are related to events that occur at length scales below 100 μm. Thus, food processing has been defined as a controlled effort to preserve, destroy, and transform the microstructure of foods (Aguilera and Stanley 1999). For

J.M. Aguilera
Department of Chemical and Bioprocess Engineering, Pontificia Universidad Católica de Chile, Santiago, Chile
e-mail: jmaguile@ing.puc.cl

J.M. Aguilera et al. (eds.), *Food Engineering Interfaces*, Food Engineering Series,
DOI 10.1007/978-1-4419-7475-4_23,

example, the structure of fruits and vegetables must be preserved after harvest so that we can enjoy their natural flavors and textures, as is the case with muscle tissue after slaughter. Wheat has to be ground into fine particles, a prerequisite to mixing the flour with other ingredients. The structure of oilseeds and sugar beets needs to be partly obliterated so that the extracted products, oil and sugar, respectively, are easily recovered from plant cells with minimal downstream processing. But it is the transformation and creation of safe, healthy, and palatable structures which is the main thrust of the food processing industry of the future.

23.2 Foods Are Unique Materials

People depict the perception of foods in terms typical of the mechanics and flow of materials (e.g., tough, soft or thick, sticky, thin, etc.) and scientists try to characterize them according to the principles of materials science (Aguilera and Lillford 2008). But when it comes to "design" foods, they exhibit their own uniqueness. Foods are unique among materials in daily life in that they are ingested, and become part of our body. (*Note*: foods are not the only products we put in our mouth and swallow. Pharmaceutical tablets and capsules also find their way into our bodies; however, they do not have to taste good or look good!). Foods are exceptional among engineering materials in that they have to fail in the mouth and disintegrate in the digestive tract. This immediately adds several extra dimensions to their intrinsic properties as materials: foods have to be palatable, chewable, and degradable. Imperfections produced during fabrication (e.g., gas bubbles, surface cracks, etc.) that are intolerable in engineering materials are part of the intrinsic quality of some foods. For example, Swiss cheese must possess well-developed round or slightly oval-shaped "eyes" that are relatively uniform in size and distribution (USDA 2001). Unlike the case of engineering materials, food properties have no absolute value, but instead depend largely on several characteristics assigned by consumers (i.e., age of product, physiological state, etc.), including the consumer's personal judgment, which is largely based on traditions and learning. Moreover, some foods may elicit different physiological responses in different individuals, as is the case of food allergies.

23.3 Food Structure Matters

In foods, structure matters because it is responsible for many of food's desirable properties, such as appearance, texture, flavor release, and nutrient bioavailability (Aguilera 2005; Parada and Aguilera 2007). Processed foods (e.g., baked and confectionery products, dried pasta, processed meats, etc.) are structured mixed systems in which individual components (proteins, fats, carbohydrates, etc.) are usually reassembled into colloidal, amorphous or crystalline states or separated into

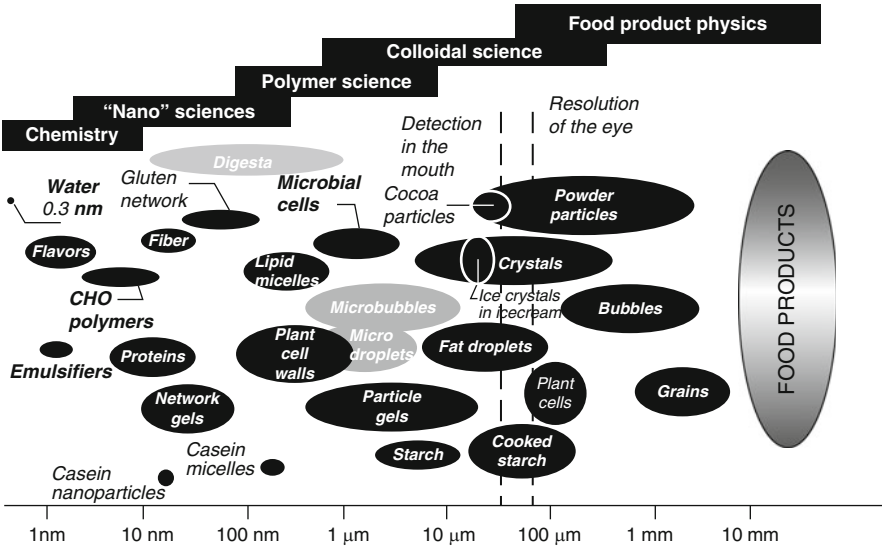

Fig. 23.1 The scale of some microstructural elements important in foods (approximate values)

concentrated phases after heating/cooling and the application of shear. By food microstructure we understand the spatial arrangement of identifiable elements in a food and their interactions (Aguilera and Stanley 1999). Typical microstructural elements in foods are plant cell walls, starch granules, water and oil droplets, fibers, fat and ice crystals, gas bubbles, etc. Most of these elements cannot be seen by the naked eye but their abundance, size, and size distribution are easily recognized as texture, which is perceived in the mouth (Fig. 23.1).

The design challenges to food fabricators have evolved and expanded through time. Until the late 1980s, the main structural properties assessed by scientists were those associated with the physical states of products as they moved from producers to consumers along the supply chain. The emerging concerns of consumers for health and well-being have brought about new structural properties targeted at the brain-gut axis, which will increasingly be the discriminating attributes that determine success in the marketplace. For the first time in the history of food and nutrition, we have the knowledge and tools to design food for health, well-being, and pleasure.

23.4 Nature Is the Ultimate Provider of Food Structures

Palatable foods are easily recognized by the sensations experienced during mastication. Foods produced by nature are generally organized hierarchically from molecules into assemblies and organelles (e.g., protein bodies, fat deposits, cell

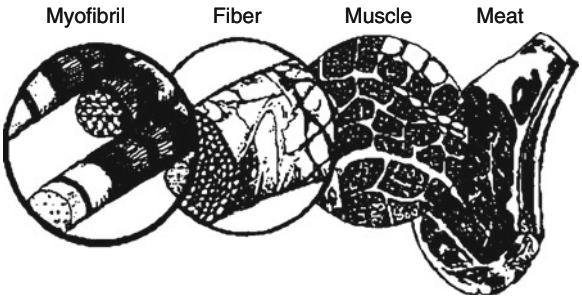

Fig. 23.2 An example of hierarchical scales in muscle tissue

walls, etc.) that are later compartmentalized into cells (some in the form of fibers) and tissues. "Natural" food structures may be classified into four broad categories: (i) Fibrous structures assembled hierarchically from small molecules (glucose) or macromolecules (proteins) into tissues for specific functionality (e.g., muscles) and held together at different levels by specific interfacial interactions (Fig. 23.2); (ii) fleshy materials from plants that are hierarchal composites of hydrated cells that exhibit internal (turgor) pressure of about 1 MPa (10 atm) and are bonded together at the cell walls (e.g., tubers, fruits, and vegetables); (iii) encapsulated embryos of plants that contain a dispersion of starch, protein, and lipids assembled into discrete packets (e.g., in grains and pulses); and (iv) a unique complex fluid called milk, intended for nutrition of the young mammal containing several nutrients in a state of dispersion.

Structures in nature have been regarded as the inspiration for the design of better-fabricated foods. There is ample awareness among cooks and food technologists that destroying the structure of natural foods results in rapid and uncontrolled deterioration. Nature stabilizes structures against unwanted reactions mainly by three means:

- At the molecular level by complexing reactants into passive forms.
- By compartmentalizing and segregating substrates and catalysts. Take garlic, for example. When the tissue is disrupted the odorless precursor is placed in contact with an enzyme that triggers a series of reactions leading to diallyl disulfide, the powerful component of garlic odor.
- In seeds, nature "freezes" biological activity at ambient temperature by immobilization of the whole system into an amorphous matrix.

Copying nature, however, has not always resulted in good food analogs. Margarine and other spreadable fats made from vegetable oils have a microstructure radically different from that of the "natural product" butter. In margarine, crystallized fat forms a fine network of interconnected platelets composed of single crystals and "sheet-like" crystal aggregates that occlude an emulsion of water and liquid oil (Heertje 1993); in butter, fat remains largely as fat globules.

23.5 Atomic Doping by Nature and the Color of Some Foods

The presence or absence of specific atoms does make a difference in how we enjoy our foods, and nature does a fabulous job in doping complex molecules with selected atoms for this purpose. Chlorophyll, the green pigment that we appreciate in all green vegetables and fruits, is similar in structure to hemoglobin, which provides the red coloring in meat (Fig. 23.3). The notable difference between these two substances is that in the center of the chlorophyll molecule is a magnesium atom, while in the center of hemoglobin is iron. During thermal processing the Mg atom is displaced by two hydrogen atoms, resulting in the olive-brown pigment pheophytin.

23.6 The Cow's Udder: A Fantastic Microfluidic Device

It is remarkable that the wide assortment of dairy products is derived from structures formed by three types of building blocks: casein micelles (CM), globular whey proteins, and fat globules (FG). Emulsions (cream), foams (whipped cream), gels (yoghurt), a plastic solid (butter), and cheeses of many textures are the result of interactions between these two types of elements.

CM and FG are assembled inside the mammary cells of the cow's udder. Casein, β-lactoglobulin, and α-lactalbumin are synthesized from amino acids at the polysomes (poly-ribosomes) on the rough endoplasmic reticulum (RER). Synthesized proteins are transferred from the RER to the Golgi apparatus where they are processed for transport out of the cell. Casein is secreted from the Golgi apparatus

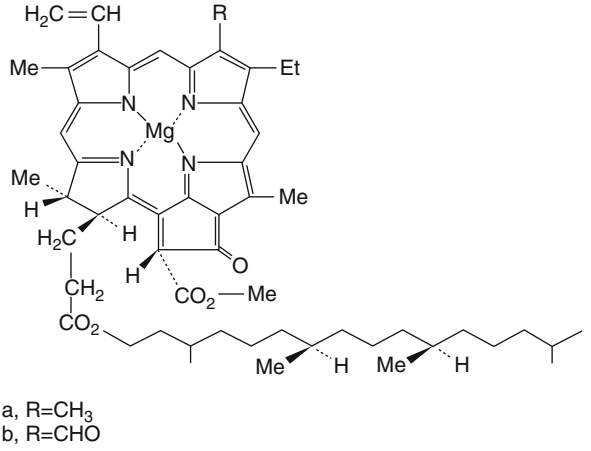

Fig. 23.3 Structure of chlorophyll molecule that gives green color to vegetables. Note the Mg atom at the center

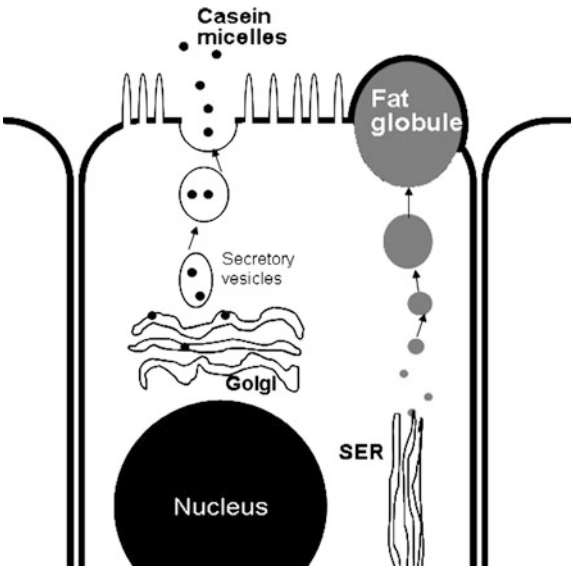

Fig. 23.4 Scheme of a mammary cell in cow's udder, indicating location of synthesis, assembly, and release of casein micelles and fat globules into the lumen

as a micelle assembled from the subcasein molecules, calcium, and phosphorous (Fig. 23.4). Milk fat triglycerides are synthesized on the smooth endoplasmic reticulum. Numerous small lipid droplets fuse together as they move toward the apical membrane, and a large lipid droplet forces out the membrane of the cell, becomes surrounded by it and enters the lumen (Heid and Keenan 2005). Consequently, each fat globule in milk is covered by a biological membrane, the fat globule membrane (Fig. 23.4). Thus, the mammary cell is an amazing microdevice for the assemblage and release of individual particles of colloidal size.

23.7 The Kinetics of Structure Formation: The Case of Whipped Cream

In contrast to natural materials, the morphological features of structures in fabricated foods are, to a certain extent, within our control. Origin of the many structures of foods, even those made from a single raw material (e.g., cow's milk), lies in the ingredients mix, the interaction between structural elements, and the fact that thermodynamic equilibrium is practically never achieved during processing. Usually, metastable structures are attained because they are favored kinetically, i.e., the approach to equilibrium is slow. Physical and chemical changes occur simultaneously with the formation of the matrix. At a certain point during the development of a particular structure a process of shape stabilization sets in, usually by vitrification, high viscosity effects, partial crystallization, phase separation, and/or formation of a network.

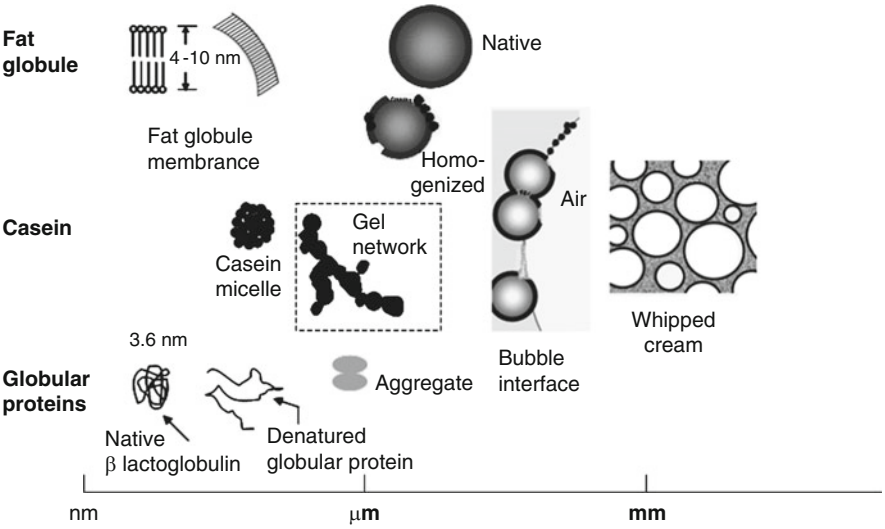

Fig. 23.5 The main building blocks for structure formation in milk are fat globules, casein, and globular whey proteins (only β-lactoglobulin is shown). Structure formation leading to a stable whipped cream proceeds to the right (larger microstructures). At the center is shown the association of destabilized casein micelles into a gel network, the basis of cheese-making

Whipped cream is a foam, stabilized by particles located at the air/liquid interface (Fig. 23.5). Bubble stabilization is mostly achieved by partly-solid fat globules (ca. 1–4 μm diameter, see below) rather than by surface active agents (as in beaten egg whites). This is why cream that has less than 30% fat will not whip. Temperature strongly influences the physical state (i.e., ratio of solid fat to liquid fat) and consequently the properties of fat globules. To stabilize the foam, fat crystals must collect at the bubble interface to impede coalescence. Foam formation and stabilization can basically be explained as a multistage process, with some significant differences between nonhomogenized (pasteurized cream) and ultra high temperature (UHT, held at 140°C for 4 s) homogenized creams (Kulozik 2008). These differences originate from the size and state of fat globules in each particular system prior to whipping (Fig. 23.5). In nonhomogenized cream, fat globules are surrounded by the native fat-globule membrane, while in homogenized UHT cream they are covered by a modified membrane of proteins (casein and globular proteins). Also, in the former case fat globules are larger than in the latter (~4 vs ~1 μm).

23.8 Hierarchical Arrangements in Fats

Molecular transformations and structure-building properties of proteins and polysaccharides are more or less well understood. Denaturation, aggregation, and gelation of properties of several proteins are documented, as well as the

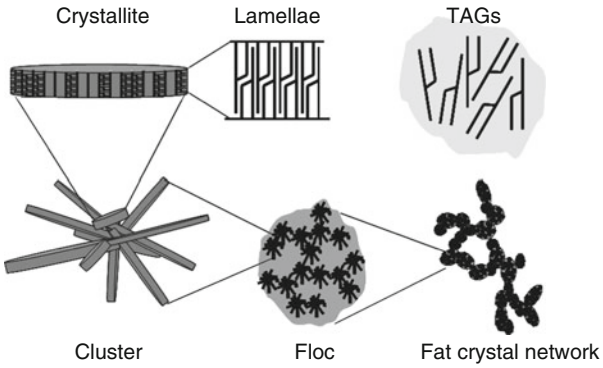

Fig. 23.6 Structural hierarchy of fat crystal networks (from *top right*, counter clockwise) (Adapted from Narine and Marangoni 1999)

gelatinization and gel formation of starches and other hydrocolloids. Hierarchical structures also develop spontaneously in the case of fats that influence the functional properties of products (spreadability, mouth-feel, etc.). Fats and oils comprise primarily triacylglycerides (TAGs). As the temperature of a molten fat (oil) is reduced below melting temperature it becomes supersaturated, with regards to the higher-melting fraction of TAGs, and crystallization starts to take place. It is typical of fats to exhibit polymorphism, that is, they can crystallize into different forms. Moreover, hierarchical structures are assembled that span from thin crystalline lamellas to a network of crystal flocs (Fig. 23.6). This is important because the rheological properties of products containing fats depend on the microstructures and bonding mechanisms holding the units together at different levels (Narine and Marangoni 1999).

Due to their amphiphilic nature, monoglycerides and phospholipids form various self-assembly structures (association colloids) when dissolved in water, for example, lamellar, micellar, cubic or hexagonal mesophases in the range of 10–100 nm. In molecular self-assembly, the final structure is "encoded" in the properties of the molecules rather than obtained through chemical reactions. Liquid crystalline phases arranged as a multilamellar α-coagel can incorporate large amounts of water between ordered bilayers, and have been used in the design of low-calorie fat spreads (Heertje et al. 1998).

23.9 Microstructures for Health

A next generation of processed foods will be designed for the brain-body axis. As such, they will be enjoyable to eat, will be nutritionally efficient, and will make us feel better. For example, many of these foods will be structured in such a way as to

control the release of flavors or bioactive molecules, the rate of stomach emptying, etc. (Norton et al. 2007). As we understand more about how food components interact with the human genome and metabolism, new perspectives for the prevention of nutrition-related diseases will become available (German et al. 2004). One approach is personalized nutrition or matching metabolic needs with specific foods and diets. The challenge will be to make foods that are appealing to the health-conscious consumer, have the right proportion of beneficial ingredients, and are pleasant to be eaten.

In the last 10 years, evidence has shown that food structure plays a key role in digestion and absorption and that these processes are not as simple and direct as previously thought. People have become more concerned about the fraction of specific nutrients reaching systemic circulation (bioavailability) than with the total amount present in our food before ingestion. Before absorption into the gut a nutrient must become bioaccessible, meaning that it has to be at the molecular level, in a colloidal state, or in a micellar state, in the case of hydrophobic compounds (Duchateau and Klaffke 2008).

The structural organization of the food matrix as well as its nature have been demonstrated to affect the slow degradation of starch in pasta (Fardet et al. 1998) and the possible influence on the postprandial glycemic response (Ricciardi et al. 2003). Resistant or slowly digestible starches, as well as control of the degree of starch gelatinization, may be used to modulate the glucose concentration in the blood (Parada and Aguilera 2009). The rate and extent of lipid digestion depends on the breakdown of the matrix in which the lipid phase is embedded. Matrices occluding lipids may be designed by gelation, extrusion, or drying of biopolymers and sugars (McClements et al. 2008). It has been suggested that the controlled physiological response of lipid emulsions may be affected by proper design of the adsorbed layer on lipid droplets and their size (Singh et al. 2009). The role of food structure in the availability of several nutrients (carotenoids, xanthophylls, etc.) has been recently reviewed by Parada and Aguilera (2007). As we increase our understanding of how food structures are formed during processing and cooking, and broken down during digestion, the ability to design healthy products will be enhanced (Leser et al. 2003).

To control the microstructure of processed foods, traditional unit operations will have to be scaled down to the micron level and below. Current technologies used by food processors are largely based on breaking down structure into smaller elements by the application of mechanical energy to the bulk phase (e.g., grinding, homogenization, spray drying). The ratio between the structure-forming device (e.g., gap in the homogenizing valve) and the microstructural elements formed (liquid droplets) may be of several orders of magnitude. In the future, structure operations will be more like the cow's udder where assembly and release of microstructures will occur at the individual element's level. One interesting application is the use of membranes and microfluidic devices in the formation of multiple emulsions and foams (Skurtys and Aguilera 2008; Muschiolik 2007).

23.10 Microstructures for Pleasure

With the advent of gastronomy in the nineteenth century came the first restaurant. Presently, annual sales in the restaurant business around the world are between $1 and 1.5 trillion dollars. At restaurants one can experience the delights of almost any traditional and ethnic cuisine and the creativity of talented chefs for a price. This is in opposition to the concept of cheap and standardized "fast food" and can only be explained by the desires of people to experience the full pleasure of their senses.

Some modern chefs have broken with old culinary routines, designing dishes based on sophisticated techniques and guided by scientific principles explored in their own laboratories. Taking science into the chef's domain has been called molecular gastronomy (Vega and Ubbink 2008; This 2006). For example, food science and gastronomy have merged in the kitchen in the preparation of artificial caviar, cryogenic desserts, innovative gels, and "airs" or foams (3-D sauces), among other creations. These structural creations are the envy of food technologists who have had experience with these novelties but have not succeeded in placing them on supermarket shelves due to the high costs involved and lack of demand. Nonetheless, top chefs nowadays have gained the trust of people who have been seduced by their creations, and they are probably the most innovative professionals in the food industry. Playing gastronomic engineering in the chef's kitchen does not require sizing the market or scaling up processes, since the minimal portions prepared in the kitchen are almost under laboratory conditions (Aguilera 2009). Therefore, chefs and food scientists/engineers alike are called to unite and expand the offer of good food and the appreciation for taste and quality.

23.11 Conclusions

Most of the desirable food properties depend on the way a food is structured, either by nature or processing. Throughout time, millions of "popular scientists" have experimented with foods in the kitchen, so it is not surprising that many creative food structures have originated either by trial-and-error (or just error!) or by serendipity. It is only in the last few decades that we have gained a basic understanding of how food microstructures are formed from the molecular level to that of products. This has initiated the era of food materials science and the bottom-up design of food products. New technologies, most notably the use of membranes and microdevices, promise to bring the scale of fabrication closer to that of key microstructural elements. On the demand side, increasing evidence linking diets and some nontransmissible diseases (cardiovascular diseases and some cancers) will open new opportunities to tailor products that may help prevent or ameliorate the effects of these diseases. Novel ingredients and nutraceuticals that are used in the food health and well-being market need to be structured in attractive formats. In the coming years, structuring foods for the brain (pleasure), the gut (gut health),

and the cells (health and vitality) will become increasingly important as new knowledge emerges from studies of neurophysiology, consumer preferences, nutrition and digestion, nanoscience, and nutrigenomics as well as other –omics.

Acknowledgments Research has been partly funded by the Fondecyt project 1095199 and the Marcel Loncin Award of IFT.

References

Aguilera JM (2005) Why food microstructure? J Food Eng 67:3–11

Aguilera JM (2009) Gastronomic engineering. In: Moskowitz H, Saguy IS, Straus T (eds) An Integrated approach to new food product development. Taylor & Francis, Boca Raton, FL, pp 317–328

Aguilera JM, Lillford PJ (2008) Food materials science: principles and practice. Springer, New York

Aguilera JM, Stanley DW (1999) Microstructural principles of food processing and engineering, 2nd edn. Aspen, Gaitherburg, MD

Duchateau G, Klaffke W (2008) Product composition, structure and bioavailability. Food Biophys 3:207–212

FAO (2005) The state of food insecurity in the world 2005. Food and Agriculture Organization, Rome, Italy

Fardet A, Hoebler C, Baldwin PM, Bouchet B, Gallant DJ, Barry J-L (1998) Involvement of the protein network in the in vitro degradation of starch from spaghetti and lasagna: a microscopic and enzymic study. J Cereal Sci 27:133–145

German JB, Yeretzian C, Watzke HJ (2004) Personalizing foods for health and preference. Food Technol 58(12):26–31

Giampietro M, Bukkens SGF, Pimentel D (1994) Models of energy analysis to assess the performance of food systems. Agric Syst 45:19–41

Heertje I (1993) Structure and function of food products. Food Struct 12:343–364

Heertje I, Roijers EC, Hendrickx HACM (1998) Liquid crystalline phases in the structuring of food products. Lebems-Wiss u- Technol 31:387–396

Heid HW, Keenan TW (2005) Intracellular origin and secretion of milk fat globules. Eur J Cell Biol 84:245–258

Kulozik U (2008) Structured dairy products: Processing and matrix design. In: Aguilera JM, Lillford PJ (eds) Food materials science. Springer, New York, pp 439–473

Leser ME, Michel M, Watzke H (2003) Food goes nano–New horizons for food structure research. In: Dickinson E, van Vliet T (eds) Food colloids: biopolymers and materials. Royal Society of Chemistry, Oxford, pp 3–13

McClements DJ, Decker EA, Park Y, Weiss J (2008) Designing food structure to control stability, digestion, release and absorption of lipophilic food components. Food Biophys 3:219–228

Muschiolik G (2007) Multiple emulsions for food use. Curr Opin Colloid Interf Sci 12:213–220

Narine SS, Marangoni AG (1999) Relating structure of fat crystal networks to mechanical properties: a review. Food Res Intern 12:227–248

Norton I, Moore S, Fryer P (2007) Understanding food structuring and breakdown: engineering approaches to obesity. Obes Rev 8(suppl1):83–88

Parada J, Aguilera JM (2007) Food microstructure affects the bioavailability of several nutrients. J Food Sci 72:R21–R32

Parada J, Aguilera JM (2009) In vitro digestibility and glycemic response of potato starch is related to granule size and degree of gelatinization. J Food Sci 74:E34–E38

Riccardi G, Clemente G, Giacco R (2003) Glycemic index of local foods and diets: the Mediterranean experience. Nutr Rev 61:56–60
Singh H, Ye A, Horne D (2009) Structuring food emulsions in the gastrointestinal tract to modify lipid digestion. Progr Lipid Res 48:92–100
Skurtys O, Aguilera JM (2008) Applications of microfluidic devices in food engineering. Food Biophys 3:1–15
This H (2006) Molecular gastronomy: exploring the science of flavor. Columbia University Press, New York
Vega C, Ubbink J (2008) Molecular gastronomy: a food fad or science supporting innovative cuisine? Trends Food Sci Technol 19:372–382
USDA (2001) United States standards for grades of Swiss cheese, emmentaler cheese. §58.2574 Specifications for US grades. The United States Department of Agriculture, Washington, DC

Chapter 24
Fruit Microstructure Evaluation Using Synchrotron X-Ray Computed Tomography

Pieter Verboven, Quang Tri Ho, Els Herremans, Hibru Kelemu Mebatsion, Bart Nicolaï, Greet Kerckhofs, Martine Wevers, and Peter Cloetens

24.1 Fruit Quality and Microstructure

Fruits and vegetables cover 16.6% of the EU production of agricultural food.[1] Fruit is after milk (but leading over cereals) the most important food item consumed in the EU (over 400 g/capita/day). Yearly, the production amounts to 38.3 million tons of fruit and 66 million tons of vegetables. Fresh apples and pears are products of many countries in the EU, with main production in France, Spain, Italy, Germany, Poland, Austria, Belgium, and The Netherlands. Exports (3€ billion in 2005) are growing for both fruits and vegetables, but imports are more than four times higher and are competing strongly in the home market.

Fruit represents an important category of biological food products with high water content and cellular microstructure. Fruit's visual, textural, and nutritional qualities have direct economic impact for fresh consumption as well as processing. A fruit consists of different tissue types such as the epidermis (with cuticle), cortex parenchyma tissue, core tissue, and vascular tissue, each with a different microstructural composition. From macro- to nano-scale, the physical properties of fruit are affected by type of tissue, geometric properties of cells, presence of an adhesive middle lamella between individual cells, cellular water potential, mechanical properties of cell wall, presence of intercellular spaces, and subcellular features, such as plasma-membrane, plasmodesmata, and aquaporins (Fig. 24.1). Degradation of

[1] http://ec.europa.eu/agriculture/capreform/fruitveg/presentations/fresh_en.pdf

P. Verboven (✉), Q.T. Ho,, E. Herremans,, H.K. Mebatsion, and B. Nicolaï,
Division BIOSYST-MeBioS, K.U. Leuven, W. de Croylaan 42, P.O. Box 2428, BE-3001 Leuven, Belgium
e-mail: Pieter.verboven@biw.kuleuven.be

G. Kerckhofs and M. Wevers,
Research group of Materials Performance and Non-destructive Evaluation, Katholieke Universiteit Leuven, Kasteelpark Arenberg 44, BE-3001 Leuven, Belgium

P. Cloetens
ID19 High-resolution Diffraction Topography Beamline, European Synchrotron Radiation Facility, 6 rue Jules Horowitz, BP220, 38043 Grenoble Cedex, France

J.M. Aguilera et al. (eds.), *Food Engineering Interfaces*, Food Engineering Series,
DOI 10.1007/978-1-4419-7475-4_24,

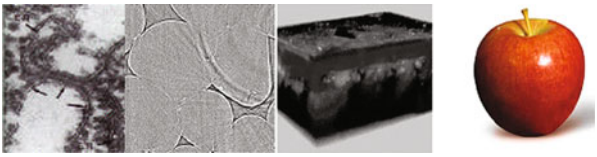

Fig. 24.1 Some features of apple microstructure (*left* to *right*): cross-section of cell wall with plasmodesmata; cross-section of cells with intercellular pores; and epidermis with wax layer

fruit's microstructure after harvest quickly leads to interior quality defects. The amount of loss due to internal disorders that develop during storage varies from year to year, but for some cultivars this is always significant. Peak losses of fruit have been recorded as high as 20–30% in some years and locations.

Several disorders may occur that reduce the commercial value of the fruit. Pome fruit, for example, is often stored for up to 10 months at a low temperature (typically around 0°C) in combination with reduced O_2 and increased CO_2 partial pressure (so-called "Controlled Atmosphere (CA) storage") to reduce their respiration rate and, hence, extend their storage life. However, the optimal gas composition is critical, as too low O_2 partial pressure in combination with too high CO_2 partial pressure may lead to physiological disorders and off-flavors. In fact, under suboptimal conditions some fruits may develop browning and core breakdown. This storage disorder is characterized by the development of brown internal tissue, which further develops into cavities so that the fruit can no longer be commercialized. This disorder has been monitored nondestructively by means of MRI and X-ray CT (Lammertyn et al. 2003). How it relates to microstructure is unknown.

The incidence of senescent breakdown in apple with symptoms similar to browning varies from year to year, apparently affected by preharvest growing conditions. This disorder is related to the age of the fruit, and occurs more often in large, over-mature apples. Late harvest, delay in cooling, and storage at temperatures above those recommended favor the occurrence. Incidence of senescent breakdown usually indicates that storage life has passed.

Water core is a disease that appears as hard glassy regions near the core in apples. Apples that have been exposed to high temperatures and sunlight near maturity are more susceptible to water core development. Water core does not develop in storage and may even disappear when originally present in a mild form.

Bitter pit symptoms are mainly found in the cortex apple tissue near the skin and first appear as soft, brown areas, which eventually become desiccated due to the collapse of surrounding cells, forming a dry cavity or "pit." The disorder is due to preharvest factors including the fruit's mineral status and the climate in the orchard. The microstructure of fresh pome fruit (apple and pear) has recently been investigated by means of light microscopy (Schotsmans et al. 2004), scanning electron microscopy and confocal microscopy (Veraverbeke et al. 2001), and very recently, by X-ray computed microtomography (Mendoza et al. 2007; Mebatsion et al. 2006; Verboven et al. 2008).

Internal disorders in fruit can cause extreme losses during the storage season. Since fruits normally have to be cut to detect internal disorders, they are often only observed upon quality inspection of the whole batch after shipping. This typically leads to refusal and subsequent destruction of the whole batch, which may cause large financial loss. By using new microstructure sensors and improved understanding of the effect of microstructure on such disorders, their occurrence may be detected earlier or even in advance, resulting in more high quality fruit.

24.2 X-Ray Computed Tomography

X-ray CT is a relatively new technique developed in the late 1970s that enables the nondestructive visualization of the internal structure of objects. The first, mainly medical CT scanners had a pixel resolution of about 1 mm. In the 1980s, after some technological advances towards micro-focus X-ray sources and high-tech detection systems, it was possible to develop a micro-CT (or μCT) system, which nowadays has a pixel resolution of 1,000 times better than medical CT scanners. The technique of X-ray (micro)-CT is based on the interaction of X-rays with matter. When X-rays pass through an object they are attenuated depending on the density and atomic number of the object under investigation and the applied X-ray energy. By using projection images obtained from different angles, a reconstruction can be made of a virtual slice through the object. After different consecutive slices are reconstructed, a 3-D visualization can be obtained. Next to μCT technology, new in-situ stages (rotatable support platforms for samples) can be developed, which increase the possibilities of the tomographic systems. An example of such in-situ stages is the environmental stage (or cooling stage), which is an interesting tool in the study of fresh food products.

As a noninvasive technique, μCT has been applied to the study of internal 3-D structures for several food products, e.g., marshmallow, aerated chocolate, and chocolate muffins (Lim and Barigou 2004). Kuroki et al. (2004) obtained 3-D spatial information on gas-filled intercellular spaces in cucumber fruit. Babin et al. (2005) studied the microstructure of cellular cereal products captured by synchrotron radiation μCT. Leonard et al. (2008) used μCT on processed banana. Synchrotron radiation μCT has been applied by K.U. Leuven (Katholieke Universiteit Leuven) with success to more difficult products, such as apple and pear, with resolutions below 1 μm (Mendoza et al. 2007; Verboven et al. 2008).

A new challenge in technology is the nano-CT system that has opened up a new era in X-ray imaging with a spatial resolution in the range of hundreds of nanometers. Proceeding to submicron pixel sizes requires increased performance of the X-ray source, rotation stage, and X-ray detector. The fact that the object can be scanned under normal environmental conditions without any coating, vacuum treatment, or other preparation techniques makes it an interesting tool as such, as well as a reference source for interpreting microstructure measurements with other methods.

24.3 Synchrotron X-Ray CT of Fruit Tissue

Visualization of microstructure by X-ray microtomography of plant tissues in their natural state has been difficult because of the low contrast and limited resolution (Westneat et al. 2003; Kuroki et al. 2004; Kim et al. 2006; Rau et al. 2006; Mendoza et al. 2007). Important structural features such as small voids between cells, vascular capillaries, or cell walls could therefore not be visualized, rendering incorrect connectivity information (Fig. 24.2).

High resolution tomography using synchrotron radiation offers a means to explore at submicrometer resolution 3-D fruit tissues with high water content in their natural state. As explained by Salvo et al. (2003), synchrotron radiation X-ray tomography has important advantages over the X-ray tube tomography of conventional X-ray CT equipment. X-ray tube tomography produces a divergent beam; therefore, the resolution is limited by the beam angle and required field of view. The beam angle may also produce artifacts in the reconstructed images. The parallel beam produced by synchrotron radiation, with good spatial coherence, makes a quantitative reconstruction that is free of geometrical and beam hardening artifacts possible. These conditions can only be achieved at large scale facilities with high energy flux sources and long distances between the source and tomography set-up (around 100 m). The facility at ESRF (Grenoble, France) was accessible to the authors on the basis of a successful research proposal.

Phase contrast imaging with synchrotron X-rays has been developed for edge enhancement on tomographs with low absorption mode contrast (Davis et al. 1995; Cloetens et al. 1999). High resolution phase tomography of biological tissues at a pixel size close to 1 μm has only recently been achieved (Plouraboue et al. 2004; Thurner et al. 2005), but it required sample preparation to improve contrast in the images. For in vivo observations, high resolution phase tomography has thus far been applied to relatively dry or hard biological samples, such as plant seeds (Stuppy et al. 2003; Cloetens et al. 2006), as well as wet soft samples more prone to damage by X-rays (Cloetens et al. 2006; Verboven et al. 2008). Figure 24.2c demonstrates the power of the technique for imaging cells, cell walls, and pores in pear fruit tissues.

24.4 3-D Imaging of Fruit Microstructure

24.4.1 Fruit and Methods

Pears (cv. Conference) were harvested (September 13, 2006) at the experimental station Fruitteeltcentrum (Rillaar, Belgium). Apples (cv. Jonagold) were picked during the pre-climacteric stage (September 25, 2006) at another experimental station, PCFruit (Velm, Belgium). Some fruits with “Early” and “Late” picking dates were also harvested 14 days before and after the given dates, respectively. All fruits

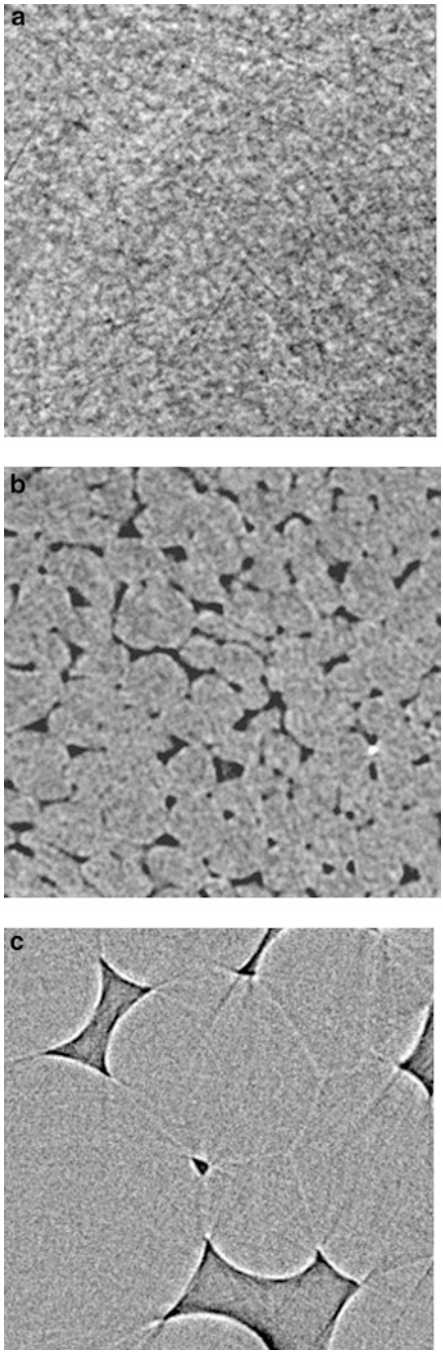

Fig. 24.2 (**a**) Microfocus X-ray CT of pear at 9.5 μm pixel size, image size 256*256 pixels. (**b**) High resolution X-ray CT of pear at 4.8 μm pixel size, image size 256*256 pixels. (**c**) Synchrotron X-ray CT (phase contrast) of pear at 0.7 μm pixel size, image size 256*256 pixels. Dark areas indicate air-filled pores, lighter colored zones are cells

were cooled and stored under controlled atmospheric conditions (2.5 kPa O_2, 0.7 kPa CO_2 – 1°C for pear; 1 kPa O_2, 2 kPa CO_2 – 0.8°C for apple) up to time of experiments (Nov. 3–6, 2006). Picking data and cooling procedures are optimal commercial practices to preserve fruit quality during long-term storage. Cylindrical samples, 5 mm diameter and 1–2 cm length, were removed from the fruit tissues of apple and pear using a cork bore in the radial direction on the equator of the fruit. The samples were mounted in a polymethyl methacrylatetube and covered with polymer foil to avoid dehydration. As stated previously, the experiments were conducted on beamline ID19 at the ESRF, Grenoble, France i.e., a long (150 m) imaging beamline where the spatial coherence of the beam is particularly large (transverse coherence length in the order of 100 μm). The system provided a field of view of 1.43×1.43 mm^2 and, at best, an image pixel size of 0.7 μm. 3-D stacks of $2{,}048 \times 2{,}048 \times 2{,}048$ pixels were obtained. Volume renderings and quantitative measurements on the sample were obtained by 3-D image segmentation and isosurface representations with Amira (Mercury Computer Systems, Chelmsford, MA), and dedicated software written for virtual tissue generation (Mebatsion et al. 2009).

24.4.2 Microstructure of Apple and Pear Fruit

Figure 24.3 shows the microstructure of different tissues of Jonagold apple and Conference pear fruit obtained by synchrotron radiation X-ray imaging. The dermal tissue presents a dense assembly of cells with little or no voids. Both fruits are aerated by voids in between the cells of the parenchyma that makes up the bulk of the cortex tissue of the fruit. The vascular tissue in the mature fruit contains empty xylem vessels surrounded by dense tissue without any air voids. The parenchyma in the pear fruit consists of smaller cells and air voids compared to the apple.

The structure of the voids is significantly different in the two fruits. In apple, the voids are the size of the cells, while in pear the voids are small channel-like structures. The total fraction of voids is also significantly larger in the Jonagold apple than in the Conference pear. Verboven et al. (2008) used the microstructure characteristics presented in Fig. 24.3 to interpret the apparent gas exchange properties of the two fruits in relation to storability and internal disorders.

24.4.3 Multiscale Modeling

One purpose of microstructure data is in modeling. As there are no good methods at present to measure in vivo internal concentrations of constituents in plant tissues, a mathematical modeling approach provides an alternative to predicting these concentrations. Such a model could be used conveniently to perform in silico experiments to evaluate, for example, the effect of changing storage or processing conditions on the internal quality. The multiscale modeling paradigm (Ho et al. 2009) provides

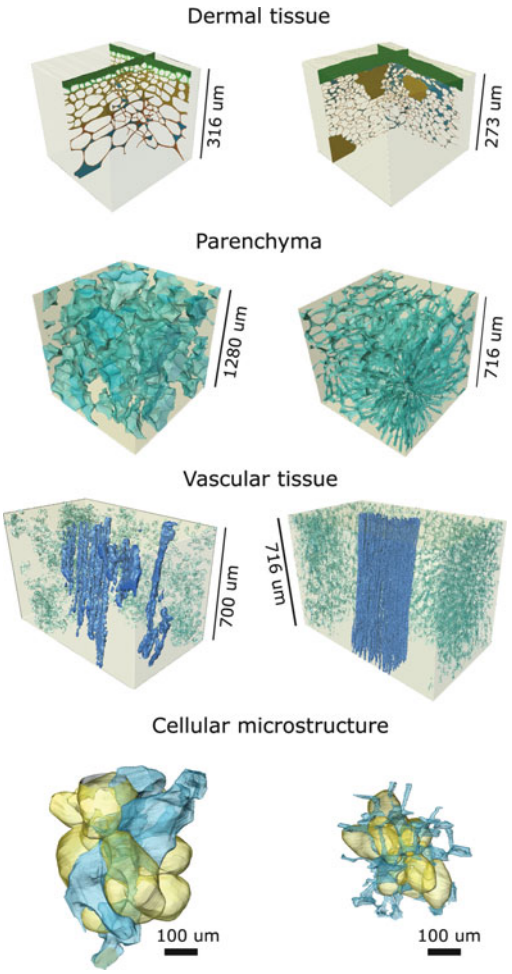

Fig. 24.3 The 3-D microstructure of apple cv. Jonagold (*left*) versus pear cv. Conference (*right*) obtained from synchrotron radiation X-ray tomography. Air-filled pores are colored in blue, cells in yellow, cell walls and sclereids in brown. Details of results are given in Verboven et al. (2008)

a means to combining the relative simplicity of continuum-type models defined at the macroscale level with the level of detail of models incorporating the microscale features that need to be obtained from 3-D microstructural imaging. To this end, X-ray images must be introduced into the models. This can be conveniently done using solid modeling suitable for volume meshing with elements to be used in solution methods such as the finite element method (Mebatsion et al. 2009). Figure 24.4 shows a way to achieve such a microscale model. The coordinates of individual cells in the X-ray images (Fig. 24.4a) across a series of slices were estimated after the transformation of digital images to representative polygons defined by points on the natural boundaries of the cells. Once the 3-D coordinates of individual cells were established, ellipsoids that fit these sets of points were generated using a Least Squared Fitted Ellipsoid

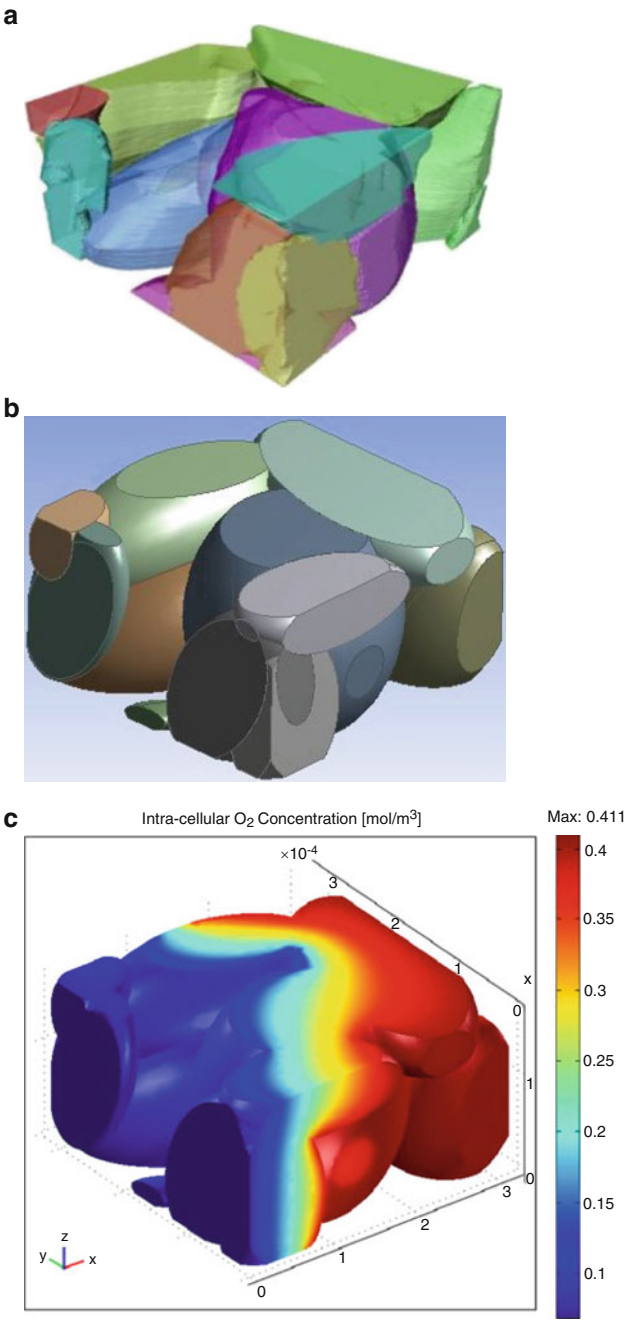

Fig. 24.4 Use of apple 3-D microstructure images for modeling: (**a**) Synchrotron radiation X-ray image. (**b**) Ellipsoid-fitted solid model of X-ray image using method of Mebatsion et al. (2009) and (**c**) Computed O_2 profile in tissue using model of Ho et al. (2009)

algorithm developed by Mebatsion et al. (2008b). The model tissue geometry (Fig. 24.4b) was generated from the ellipsoids, which were truncated when neighboring volumes overlapped. As a result, as many truncated ellipsoids as there are cellular images were generated, producing a virtual tissue representative of the fruit microstructure. Figure 24.4c demonstrates the results of the gas exchange model by Ho et al. (2009) as applied to the 3-D microstructure model of apple. In a future step, such models could be used to evaluate the tissue properties of fruit to evaluate the effect of storage and processing conditions.

24.5 Conclusions

Today, internal defects in fruits can only be detected when the fruit is cut. The whole batch is then assigned as lost; economic risks are therefore high. Early and nondestructive detection of interior defects and/or aspects that initiate these defects can prevent severe economicloss. To that end, the role of the fruit microstructure must be understood and measurement of relevant features online during preservation and transformation of the fruit should be targeted. With respect to the first objective, it was demonstrated that the method of synchrotron radiation X-ray tomography provides a suitable tool to probe the microstructure of *in vivo* tissues. To develop fast and cheap online measurement technologies (e.g., X-ray radiography, nuclear magnetic resonance relaxometry and diffusometry, diffuse spectroscopy, or optical coherence tomography) the presented method serves as a reference.

Acknowledgments The K.U. Leuven Interfaculty Council for Development Co-operation (IRO), the K.U. Leuven Research Council (project OT-08023), the Fund for Scientific Research (project G.06.03.08), and the Institute for the Promotion of Innovation by Science and Technology in Flanders (projects IWT-060720 and IWT-050633) are gratefully acknowledged for financial support. Pieter Verboven is Fellow of the Industrial Research Fund of the K.U. Leuven. The results were obtained with a beamtime project of the European Synchrotron Radiation Facility in Grenoble, France (experiment MA222).

References

Babin P, Della Valle G, Dendievel R, Lassoued N, Salvo L (2005) Mechanical properties of bread crumbs from tomography based finite element simulations. J Mater Sci 40:5867–5873

Cloetens P, Ludwig W, Baruchel J, Van Dyck D, Van Landuyt J, Guigay JP, Schlenker M (1999) Holotomography: quantitative phase tomography with micrometer resolution using hard synchrotron radiation x rays. Appl Phys Lett 75:2912–2914

Cloetens P, Mache R, Schlenker M, Lerbs-Mache S (2006) Quantitative phase tomography of Arabidopsis seeds reveals intercellular void network. Proc Natl Acad Sci USA 103:14626–14630

Davis TJ, Gao D, Gureyev TE, Stevenson AW, Wilkins SW (1995) Phase contrast imaging of weakly absorbing materials using hard X-rays. Nature 373:595–598

Ho Q, Verboven P, Mebatsion H, Verlinden B, Vandewalle S, Nicolaï B (2009) Microscale mechanisms of gas exchange in fruit tissue. New Phytol 182:163–174

Kim SA, Punshon A, Lanzirotti A, Li L, Alonso JM, Ecker JR, Kaplan J, Guerinot ML (2006) Localization of iron in Arabidopsis seed requires the vacuolar membrane transporter VIT1. Science 314:1295–1298

Kuroki S, Oshita S, Sotome I, Kawagoe Y, Seo Y (2004) Visualization of 3-D network of gas-filled intercellular spaces in cucumber fruit after harvest. Postharvest Biol Technol 33:255–262

Lammertyn J, Dresselaers T, Van Hecke P, Jancsok P, Wevers M, Nicolaï BM (2003) Magn Reson Imaging 21:805–815

Léonard A, Blacher S, Nimmol C, Devahastin S (2008) Effect of far-infrared radiation assisted drying on microstructure of banana slices: an illustrative use of X-ray microtomography in microstructural evaluation of a food product. J Food Eng 85:154–162

Lim KS, Barigou M (2004) X-ray micro-computed tomography of aerated cellular food products. Food Res Int 37:1001–1012

Mebatsion HK, Verboven P, Ho QT, Mendoza F, Verlinden BE, Nguyen TA, Nicolaï BM (2006) Modeling fruit microstructure using novel ellipse tessellation algorithm. CMES-Comp Model Eng 14:1–14

Mebatsion H, Verboven P, Ho Q, Verlinden B, Nicolaï B (2008a) Modelling fruit (micro) structures, why and how? Trends Food Sci Technol 19:59–66

Mebatsion HK, Verboven P, Jancsók PT, Ho QT, Verlinden B, Nicolaï BM (2008b) Modeling 3-D fruit tissue microstructure using a novel ellipsoid tessellation algorithm. CMES-Comp Model Eng 29:137–149

Mebatsion HK, Verboven P, Melese Endalew A, Billen J, Ho QT, Nicolaï BM (2009) A novel method for 3-D microstructure modeling of pome fruit tissue using synchrotron radiation tomography images. J Food Eng 93(2):141–148

Mendoza F, Verboven P, Mebatsion HK, Kerckhofs G, Wevers M, Nicolaï B (2007) Three-dimensional pore space quantification of apple tissue using X-ray computed microtomography. Planta 226:559–570

Plouraboue F, Cloetens P, Fonta C, Steyer A, Lauwers A, Marc-Vergnes J-P (2004) X-ray high-resolution vascular network imaging. J Microsc–Oxford 215:139–148

Rau C, Robinson IK, Richter CP (2006) Visualizing soft tissue in the mammalian cochlea with coherent hard X-rays. Microsc Res Tech 69:660–665

Salvo L, Cloetens P, Maire E, Zabler S, Blandin JJ, Buffière JY, Ludwig W, Boller E, Bellet D, Josserond C (2003) X-ray micro-tomography an attractive characterisation technique in materials science. Nucl Instrum Meth B 200:273–286

Schotsmans W, Verlinden BE, Lammertyn J, Nicolaï BM (2004) The relationship between gas transport properties and the histology of apple. J Sci Food Agric 84:1131–1140

Stuppy WH, Maisano JA, Colbert MW, Rudall PJ, Rowe TB (2003) Three-dimensional analysis of plant structure using high-resolution X-ray computed tomography. Trends Plant Sci 8:2–6

Thurner P, Muller R, Raeber G, Sennhauser U, Hubbell J (2005) 3D Morphology of cell cultures: a quantitative approach using micrometer synchrotron light tomography. Microsc Res Tech 66: 289–298

Veraverbeke EA, Van Bruaene N, Van Oostveldt P, Nicolaï BM (2001) Non destructive analysis of the wax layer of apple (Malus domestica Borkh.) by means of confocal laser scanning microscopy. Planta 213:525–533

Verboven P, Kerckhofs G, Mebatsion H, Ho Q, Temst K, Wevers M, Cloetens P, Nicolaï B (2008) Three-dimensional gas exchange pathways in pome fruit characterized by synchrotron X-ray computed tomography. Plant Physiol 147:518–527

Westneat MW, Betz O, Blob RW, Fezzaa K, Cooper WJ, Lee W-K (2003) Tracheal respiration in insects visualized with synchrotron X-ray imaging. Science 299:558–560

Chapter 25
Multifractal Characterization of Apple Pore and Ham Fat-Connective Tissue Size Distributions Using Image Analysis

Fernando Mendoza, Nektarios Valous, Adriana Delgado, and Da-Wen Sun

25.1 Application of Fractal and Multifractal Analysis to Biological Material

Fractal and multifractal concepts have been increasingly applied in various fields of science to describe the complexity and self-similarity of nature. A fractal describes a rough or fragmented geometric shape that can be subdivided into parts, each of which is at least approximately a reduced-size copy of the whole. Fractal dimensions offer a systematic approach to quantifying irregular patterns that contain an internal structure repeated over a range of scales (Mandelbrot 1992). Estimations of fractal dimension are based on the box-counting technique, which allows obtaining the scaling properties of 2-D fractal objects (e.g., from binary images) by covering the images with boxes size ε and counting the number of boxes containing at least one pixel representing the object or structure under study. However, the disadvantage of the box-counting technique is that the process does not consider the amount of mass inside a box and therefore is not able to resolve regions with high or low density of mass. Biological materials are frequently complex in the distribution of their components or structures, which could be of interest to characterize and to quantify, and therefore, simple fractal dimension estimations may not be enough to appropriately characterize these materials.

By contrast, multifractal methods are suitable for characterizing a complex spatial arrangement of mass because they can resolve local densities (Vicsek 1992). Multifractal formalisms involve decomposing self-similar measures into intertwined fractal sets, which are characterized by their singularity strength and fractal dimension. Multifractal characterization does not require a single dimension, but rather a sequence of generalized fractal dimensions. Thus, a combination of all the fractal sets produces a multifractal spectrum that can characterize variability and heterogeneity of the studied variables (Kravchenko et al. 1999). The advantage of

F. Mendoza (✉), N. Valous, A. Delgado, and D.-W. Sun
FRCFT Group, Biosystems Engineering, UCD Agriculture & Food Science Centre, University College Dublin, Belfield D4, Ireland
e-mail: fmendoza@ing.puc.cl; dawen.sun@ucd.ie

J.M. Aguilera et al. (eds.), *Food Engineering Interfaces*, Food Engineering Series,
DOI 10.1007/978-1-4419-7475-4_25,

the multifractal approach is that multifractal parameters can be independent of the size of the studied objects (Cox and Wang 1993), and that no assumptions are required about the data following any specific distribution (Scheuring and Riedi 1994). This type of analysis has been successfully applied to plant science, ecology, and agronomy research for study of vegetation patterns (Scheuring and Riedi 1994), zooplankton biomass (Pascual et al. 1995), root systems of legumes (Ketipearachchi and Tatsumi 2000), spatial and temporal variability of residual soil NO_3–N and corn grain yield (Eghball et al. 2003), and soil structure under long-term wastewater irrigation (Xiaoyan et al. 2007), among others. However, very little further information exists about the multifractality in food samples at micro and macro levels and their related properties.

The objective of this chapter is to give an overview of the multifractal theory as applied to natural objects and systems, and to illustrate with two examples the complete application of this approach for characterizing contrasting PSD in apple tissue and FSD in cooked pork ham images. The identification of potential multifractal parameters useful for quality characterization and classification of these samples will be a final aim as well. PSD in apple tissue and FSD in pork hams are the fundamental physical properties analyzed in assessing their quality. In apple tissue, PSD is related to the mass-transport phenomena characteristics and complexity of O_2 and CO_2 diffusivity, and in the case of hams, FSD is related to the sensory properties such as texture, taste, quality of raw meat, and visual appearance. In both food products, accurate representation of these microstructural properties is needed for objective quality characterization and prediction during apple preservation and ham formulation.

25.2 Theory of MFA

Measurement of multifractals mainly involves measuring a statistical distribution, which in turn yields useful information even if the underlying structure does not show a self-similar or self-affine behavior (Plotnick et al. 1996). In a homogeneous system, the number N of features of a certain size ε varies (Chhabra and Jensen 1989; Everstz and Mandelbrot 1992; Vicsek 1992):

$$N(\varepsilon) \propto \varepsilon^{-D_0}, \tag{25.1}$$

where the fractal dimension D_0,

$$D_0 = \lim_{\varepsilon \to 0} \frac{\log N(\varepsilon)}{\log \frac{1}{\varepsilon}} \tag{25.2}$$

can be measured by counting number N of boxes needed to cover the object under investigation for increasing box size ε and estimating the slope of a log-log plot

(i.e., using box-counting method). For heterogeneous or nonuniform systems, the probability within the *i*th region P_i scales as:

$$P_i(\varepsilon) = \varepsilon^{\alpha_i} \tag{25.3}$$

where α_i is the Lipschitz-Hölder exponent characterizing density in the *i*th box (Halsey et al. 1986). One technique to determine multifractal parameters is to cover a measure with boxes size ε. The number of boxes $N(\alpha)$ where the probability has values in the interval $(\alpha, \alpha + d\alpha)$ is found to scale as (Halsey et al. 1986; Chhabra and Jensen 1989):

$$N(\alpha) \propto \varepsilon^{-f(\alpha)} \tag{25.4}$$

where $f(\alpha)$ can be defined as the fractal dimension of the set of boxes with singularities α. The exponent α can take on values from the interval $(\alpha_{-\infty}, \alpha_{+\infty})$, and $f(\alpha)$ is usually a single-humped function with a maximum at $df(\alpha(q))/d\alpha(q) = 0$, where $q = 0$, $f_{\max}$ is equal to the box-counting or D_0 (Vicsek 1992; Gouyet 1996). In practice, using the box-counting method, for every box i the probability of a *containing object*, also called the partition function, is obtained for different moments q, which can vary from $-\infty$ to $+\infty$. The partition function is represented by $\mu(q,\varepsilon)$ and defined as (Chhabra and Jensen 1989):

$$\mu(q, \varepsilon) = \sum_{i=1}^{N(\varepsilon)} P_i^q(\varepsilon) \tag{25.5}$$

Multifractal sets can also be characterized on the basis of the generalized dimensions of the *qth* moment orders of a distribution, D_q (Hentchel and Procaccia 1983). Based on the work of Rényi (1995) they are defined as:

$$D_q = \lim_{\varepsilon \to 0} \frac{1}{1-q} \frac{\log \sum_{i=1}^{n(\varepsilon)} P_i^q}{\log \varepsilon} \tag{25.6}$$

and when $q = 1$, things become tricky and can be computed as:

$$D_1 = \lim_{\varepsilon \to 0} \frac{\sum_{i=1}^{n(\varepsilon)} P_i \log P_i}{\log \varepsilon} \tag{25.7}$$

The generalized dimension D_q is a monotone decreasing function for all real q values within the interval $(-\infty, +\infty)$. When $q < 0$, μ emphasizes regions in the distribution with less concentration of a measure, whereas the opposite is true for $q > 0$ (Chhabra and Jensen 1989). This means that the sum in the numerator of

(25.10) is dominated by the highest values of P_i for $q > 0$, and the lowest values of P_i for $q < 0$.

The partition function (a log-log plot of the quantity $\mu(q,\varepsilon)$ over ε for different q yields) scales as:

$$\mu(q,\varepsilon) \propto \varepsilon^{-\tau(q)} \tag{25.8a}$$

or

$$\tau_q = \lim_{\varepsilon \to 0} \frac{\log \mu(q,\varepsilon)}{\log \frac{1}{\varepsilon}} \tag{25.8b}$$

where $\tau(q)$ is the mass or correlation exponent of the qth order defined as (Halsey et al. 1986):

$$\tau(q) = (q-1)D_q \tag{25.9}$$

The connection between the power exponents $f(\alpha)$ (25.4) and $\tau(q)$ (25.6) is made via the Legendre transformation (Callen 1985; Halsey et al. 1986; Chhabra and Jensen 1989):

$$f(\alpha(q)) = q\alpha(q) - \tau(q) \tag{25.10}$$

and

$$\alpha(q) = \frac{\mathrm{d}\tau(q)}{\mathrm{d}q} \tag{25.11}$$

The $f(\alpha)$ spectrum and the generalized dimensions contain the same information, both characterizing an interwoven ensemble of fractal dimensions $f(\alpha_i)$. In each of the ith fractals, the observable P_i scales with the Lipschitz-Hölder-exponent α_i.

The generalized dimensions for $q = 0$, 1, and 2 mathematically describe the defined fractal dimensions known as D_0, D_1, and D_2. D_0 is also known as a capacity dimension; it is independent of q and provides global (or average) information on the system (Voss 1988). D_1 is related to the information or Shannon entropy (Shannon and Weaver 1949), and quantifies the degree of disorder present in a distribution. According to Gouyet (1996), for a measure $\mu \in (0,1)$, the value of D_1 is in the range of $0 < D_1 < 1$. A D_1; a value close to 1.0 characterizes a system uniformly distributed throughout all scales, whereas a D_1 close to 0 reflects a subset of the scale in which the irregularities are concentrated. D_2 is mathematically associated with the correlation function (Grassberger and Procaccia 1983) and computes the correlation of measures contained in intervals of size ε. The relationship between D_0, D_1, and D_2 is $D_2 \leq D_1 \leq D_0$, where the equality $D_0 = D_1 = D_2$ occurs only if the fractal is statistically or exactly self-similar and homogeneous (i.e., monofractal) (Korvin 1992).

25.3 Multifractal Characterization of PSD in Fresh and Frozen-Thawed Apple Tissue

An apple fruit is mainly composed of the fleshy tissue of parenchyma cells permeated with vascular and intercellular air spaces (Esau 1977). The structural geometry of these intercellular spaces, or porous media, plays a fundamental role in governing the fluid and gas transport through its tissue (Celia et al. 1995; Dražeta et al. 2004). In general, the gas-filled intercellular spaces in plant organs are considered as the predominant pathways for gas transport through the plant and are greatly related to the characteristics of gas exchange (Raven 1996; Kuroki et al. 2004). The volume of air increases during fruit growth and occupies a considerable proportion of the fruit at harvest (Harker and Ferguson 1988; Yamaki and Ino 1992). This increase in air space is accompanied by a proportional decline in fruit density, while the density of the fruit cells themselves remains roughly constant (Westwood et al. 1967; Baoping 1999). In addition, the microstructure and fraction of intercellular air differs between cultivars and also between positions in the parenchyma tissue of the same fruit (Baumann and Henze 1983; Vincent 1989). Larger fruits of the same cultivar have a higher proportion of air than smaller fruits (Volz et al. 2004). Therefore, the characterization of these intercellular air spaces and distribution based on microstructural properties and realistic percolation models have important agricultural applications, since they are related to the understanding of fruit physiology and postharvest quality of the fruit during preservation. Fruits with greater fractional air volumes have been shown to be softer (Yearsley et al. 1997a, b; Volz et al. 2004), or more mealy (Harker and Hallet 1992), and to have greater internal gas diffusion rates (Rajapakse et al. 1990; Ho et al. 2006). Furthermore, the volume of these intercellular air spaces continues to increase during storage, and therefore, its measurement can be used to define the age of the fruit and also to characterize the effects of different storage conditions on its quality (Khan and Vincent 1990; Harker et al. 1999). All these features could be related to its known susceptibility to internal tissue browning and breakdown (Cheng et al. 1998).

On the other hand, freezing is a well-known preservation method widely used in the food industry. It involves lowering the product temperature generally to $-18°C$ or below. At temperatures lower than $-10°C$, few microorganisms can develop, chemical reactions rates are greatly reduced, and cellular metabolic reactions are also delayed (Delgado and Sun 2001). One of the key issues in maintaining the shelf-life and other quality attributes of frozen food is ice crystallization (Kennedy 2003). The freezing process combines the favorable effect of low temperatures with the conversion of water into ice. The water–ice transition has the advantage of fixing the tissue structure and separating the water fraction in the form of ice crystals in such a way that water is not available either as a solvent or a reactive component (Delgado and Sun 2001). However, the size and location of the ice crystals may damage cell membranes and break down the physical structure. Thus, the cause of the undesirable physico-chemical modifications during freezing

is the crystallization of water and sometimes solutes (Martino et al. 1998; Delgado and Sun 2001). Slow freezing generally leads to large ice crystals formed exclusively on extracellular areas, which can damage cell structure and affect the thaw behavior as well as have an effect on the sensory properties and nutritional value of foodstuffs, while high freezing rates produce small crystals evenly distributed all over the tissue. Therefore, extended research has been carried out to control the crystal size. Conventional cooling methods, such as air blast, plate contact, circulating brine, and liquid nitrogen (ordered in increasing values of the heat transfer coefficient) are the most common methods used for food freezing (Sun 2001). Among these traditional methods, the immersion freezing process offers numerous advantages, e.g., high-heat-transfer coefficients, individualized freezing, good product quality, energy savings, etc.

We believe that the spectrum of local fractal dimensions could be an indication of geometric characteristics of PSD in fresh and frozen-thawed apples. This hope is solidly based on the fact that the fractal approach provides multifractal outputs that can be adjusted in order to fit multifractal spectra obtained from experimental data. Furthermore, it is well known that deviation from local fractal dimensions is greater for nonuniforms or natural plant structures such as pore distribution in apples; therefore, local fractal dimensions measured within a small region may vary from point to point, and the object can be characterized by a spectrum of fractal dimensions. Multifractal analysis (MFA) may improve characterization and discrimination of changes with high precision in apple tissue microstructure due to processing and preservation.

25.3.1 Experimental Procedure for Apple Tissue

Figure 25.1 illustrates the experimental procedure for apple sampling, the reconstructed X-ray image acquisition projection, and the stack of cropped X-ray images used for further processing and MFA. In this example, a Granny Smith apple (*Malus domestica*) with ~8.5 cm dia. (86.9% w/w moisture and ~12°Brix) was selected from a local market in Dublin (Ireland) and stored at 4 ± 1°C for use later that same day. This apple variety was chosen as a test material due to the uniformity of its tissues and its structural stability in storage (Sterling 1968). In addition, the Granny Smith variety was available all over Ireland that year at a fairly constant quality. In spite of this, it is well known that high microstructural variability exists among apples even coming from the same lot, and therefore for analysis, the samples were extracted from the same apple. The apple cylinders (i.e., two fresh and two frozen samples) measuring 1.8 cm dia. and 2.5 cm high were cut using a cork borer in radial orientation from the middle parenchyma (~10 mm from the skin; Fig. 25.1a) and the same spatial position around the fruit. What remained of the fruit tissue was used for initial water content and soluble solids determination.

Frozen samples were obtained by immersing samples in a bath system filled with a freezing solution of 50% ethylene glycol and 50% water in volume. All samples

(fresh and frozen) were loosely wrapped in tissue paper saturated with water to prevent browning reactions, and kept together in a refrigerator for 24 h at 4 ± 1°C to achieve uniform initial temperature and thawing of the frozen samples, and until apple cylinders were imaged. Moisture loss or water uptake during this period was considered to have little effect.

Samples were scanned with an X-ray micro-CT scanner (SCANCO MEDICAL AG, μCT-40, Bassersdorf, Switzerland) over the interval 0°–180° (using a 0.9° scan step) at a linear resolution of 10 μm by pixel, operating voltage of 70 kV, current of 114 μA, and exposure time of 8.4 s. To account for the nonuniformities in the X-ray beam and nonuniform response of the CCD detector, the raw images were corrected for dark and white fields by averaging the flat field correction references collected at the beginning of the experiment. Each sample was enclosed in a plastic tube to avoid dehydration without any special preparation. The imaging process took approximately 25 min per sample.

The X-ray shadow projections of the 3-D object, digitalized as 2,048 × 2,048 pixels, were processed using a mathematical back-projection procedure to obtain reconstructed cross-section images of linear attenuation coefficient values with 256 gradations (8-bit) (Fig. 25.1b). Thus, a stack of 200 cross-sections of grey images of the object (considering apple tissue and image background), with a 10 μm interslice distance, was obtained from each scanned apple sample. Thus, for each set of radiographic images, to extract only the apple tissue image, a fixed area in the midsection of the scanned region (1,024 × 1,024 pixels, equivalent to 104.9 cm^2) was cropped and then subjected to image analysis (Fig. 25.1c).

To obtain binary images for the consecutive MFA, the pores need to be identified and segmented at a certain threshold. However, the distinctions among the voids and solid phases in the radiographic images of apple tissue are frequently not sharp. They do not show a bimodal distribution due to the amount of peak overlap in the attenuation coefficient histogram (Mendoza et al. 2007); as a result, dedicated segmentation algorithms need to be used to closely represent the pore structure in the images. Therefore, partition of apple tissue images into pores and cellular

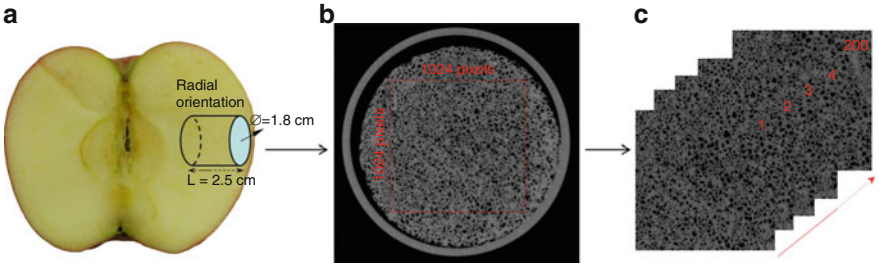

Fig. 25.1 Illustration of experimental procedure for MFA of a fresh apple sample: (**a**) Sampling in radial orientation; (**b**) representative X-ray cross-sectional image reconstructed with 256 gradations, showing the *cropped region* (1,024 × 1,024 $pixels^2$; *black regions* represent pores; *gray regions* represent cellular material); (**c**) stack of cropped radiographic images used for further processing and MFA

material was performed using the kriging-based segmentation algorithm developed by Oh and Lindquist (1999). The algorithm is a nonparametric formulation able to analyze regions of uncertainty based on the estimation of spatial covariance of the image in conjunction with the indicator kriging to determine object edges (Mardia and Hainsworth 1988). More details about the scanning process and segmentation algorithm of radiographic apple tissue images can be found in Mendoza et al. (2007).

25.3.2 Extracted Features and Multifractal Spectrum Computation

The fractal properties were extracted from digitized binary images of fat-connective tissue structures; 200 images from each type of apple sample, fresh or frozen-thawed, were evaluated. Parameters calculated from each multifractal spectrum were: the *Hausdorff dimension*, $f(\alpha)$; the *singularities of strength*, α; and their *generalized fractal dimension*, D_q; all were calculated in the range of moment orders (q) between -10 and $+10$ taken at 0.1 lag increments. In addition, the bulk porosity of each apple sample, representing the void space as a fraction of the total volume, was calculated from the binary segmented images by a simple count of the pixels in the pore space divided by the total number of pixels in the image. Since the X-ray CT technique gave a stack of 200 images per sample, the average value of the computed multifractal parameters and spectrums from each stack of images and repetition were reported and used in further analyses.

To calculate the $f(\alpha)$-spectra, the method developed by Chhabra and Jensen (1989) was implemented in Matlab v7.0 (MathWorks, Inc., USA). Figure 25.2 illustrates the multifractal theory applied to a binary image of fresh apple tissue corresponding to the cropped image shown in Fig. 25.1b. Thus, images were partitioned using the box-counting algorithm to estimate the probability of containing pores (voids) for each box size ε, from 2 to 1,024 (i.e., in steps of 2^k, $1 < k < 10$). From this information the partition functions and mass or correlation exponent of the qth order $\tau(q)$ were obtained, as shown in Fig. 25.2b, c. Doing this for images that are 1,024 × 1,024 pixels avoids artifacts, which occur when boxes do not entirely cover the image at the borders. A family of normalized measures, $\mu_i(q,\varepsilon)$, was constructed for positive and negative values of q covering variable ranges in steps of 0.1:

$$\mu_i(q,\varepsilon) = \frac{P_i^q(\varepsilon)}{\sum_{i=1}^{N(\varepsilon)} P_i^q(\varepsilon)} \tag{25.12}$$

where $P_i(\varepsilon)$ is the fraction (or probability) of pores contained in each ith box size ε. Note that for any value of q, the normalized measures take values in the interval (0, 1). The direct computation of $f(\alpha)$ values was made using the simplified relations proposed by Chhaabra et al. (1989), and Chhabra and Jensen (1989):

$$f(q) = \lim_{\varepsilon \to 0} \frac{\sum_{i=1}^{N(\varepsilon)} \mu(q,\varepsilon) \cdot \log[\mu_i(q,\varepsilon)]}{\log \varepsilon} \tag{25.13}$$

Similarly, values of $\alpha(q)$were computed by evaluating:

$$\alpha(q) = \lim_{\varepsilon \to 0} \frac{\sum_{i=1}^{N(\varepsilon)} \mu(q,\varepsilon) \cdot \log[P_i(\varepsilon)]}{\log \varepsilon} \tag{25.14}$$

For each q, values $f(q)$ and $\alpha(q)$were obtained from the slope of plots of the numerators in (25.13) and (25.14) versus log ε over the entire range of ε values considered. The range of q values over which both functions were linear (Δq) was selected considering the coefficients of determination (R^2) of both fits (Fig. 25.2d, e). The $f(q)$ and $\alpha(q)$ functions (Fig. 25.2f) obtained over a given Δq were used to construct $f(\alpha)$-spectra as an implicit function of q and ε. The symmetry of multifractal spectra was evaluated by comparing the width of the spectra from their center [$\alpha(0)$] to $\alpha(|q_i|)$. Values of $|q_i|$ were the same in both the positive and negative domains and equal to the smaller of the two defining the Δq interval.

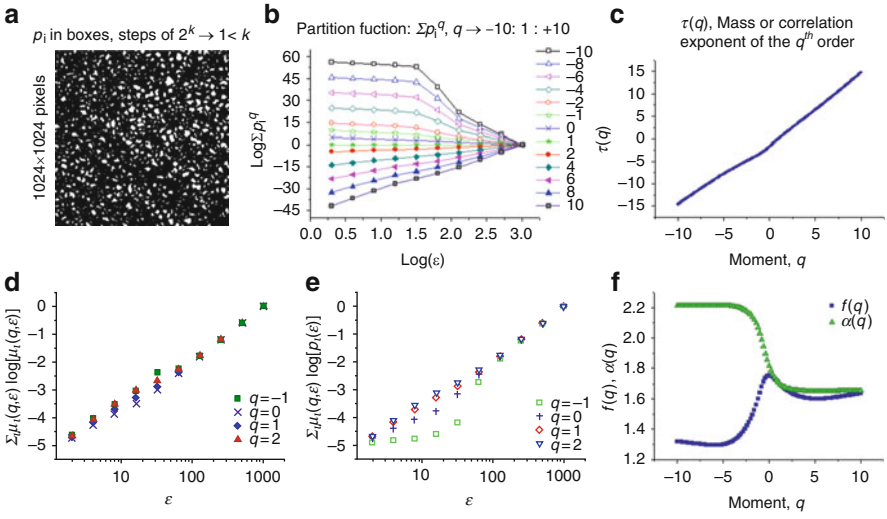

Fig. 25.2 Illustration of multifractal theory applied to a binary image of fresh apple tissue (corresponding to *cropped image* in Fig. 25.1**b**): (**a**) Binary image (pores are represented by *white pixels*); (**b**) partition functions calculated in range of moment orders (q) between −10 and +10, but showing only lag increments of 2; (**c**) mass or correlation exponent of the *qth* order $\tau(q)$; (**d**) and (**e**) Plots of (25.14) and (25.13), respectively, as a function of ε; (**f**) Illustration of $f(q)$ and $\alpha(q)$ spectrums

On the other hand, generalized dimensions were obtained as the slope of the partition function over box size, both taken as logarithms (25.8) and (25.9). This method is known as the method of moments (Everstz and Mandelbrot 1992) or Rényi spectrum (Rényi 1995), as D_q is estimated for every moment q.

25.3.3 Results of MFA for PSD in Apples

To give a better idea about the microstructure of apple tissue, Fig. 25.3 shows representative radiographic images extracted from fresh and frozen-thawed apple tissue. The samples are characterized by different porous structures, illustrating the deleterious effect of freezing on the apple's microstructure. In the frozen-thawed sample, the cell disruption and tissue due to ice crystal formation is evident, wherein the pores are larger and rounded compared to fresh apple tissue. Also, differences (heterogeneity) in the bulk porosity distribution between cultivars are visually evident (Table 25.1). The average porosity computed from two stacks of apple images extracted from the same fruit (taken parallel to the medial axis of each fruit, 0° and 180° around the fruit; 200 images per stack, area per image = 104.9 cm^2) showed values 14.1 ± 0.8% for fresh and 20.7 ± 1.4% for frozen-thawed tissue. ANOVA analysis of the average porosity confirmed the differences (*P-value* <0.05) between apple samples and revealed a higher variability between images from frozen-thawed tissue than those computed from fresh tissue, as represented by their standard deviations.

A crucial step in MFA is to determine the range of both ε and the moments of order q over which a multifractal method is applicable. This means determining the range of ε and q in which the numerators of (25.13) and (25.14) are linear functions of log ε. The range of q values was selected considering the coefficients of determination (R^2) of the fits (Fig. 25.2d, e). In this study, the general criterion was to choose the range of moments with R^2 equal or larger than 0.95. Thus, the condition was met for $\alpha(q)$ in the range Δq of −10 to +10, and for $f(q)$ in the range Δq of −1.4 to +5.8, for both fresh and frozen-thawed samples.

The corresponding $f(\alpha)$-spectra and Rényi spectra (range of moment order q between −10 and +10) for each apple type are shown in Fig. 25.4a, b, respectively. The $f(\alpha)$-spectra shows the typical hump-shape observed for multifractal objects, but there are distinct differences in shape and symmetry between the fresh and frozen-thawed apple samples (Fig. 25.4a). The curvature and symmetry

Table 25.1 Selected multifractal parameters and standard deviations from the analysis of binary images of pores for fresh and frozen-thawed apple tissue

	Porosity (%)	$\alpha(0) - \alpha(1)$	$\alpha(-1) - \alpha(0)$	$D_0 - D_1$	$f[\alpha(-1)] - D_0$	D_1/D_0
Fresh	14.1 ± 0.8^x	0.214 ± 0.015^x	0.602 ± 0.084^x	0.090 ± 0.006^x	0.190 ± 0.015^x	0.955 ± 0.003^x
Frozen	20.7 ± 1.4^y	0.229 ± 0.016^y	0.791 ± 0.129^y	0.092 ± 0.008^y	0.238 ± 0.025^y	0.954 ± 0.003^y

x–y, values with different letters within each column indicate significant differences among fresh and frozen apples ($p < 0.05$)

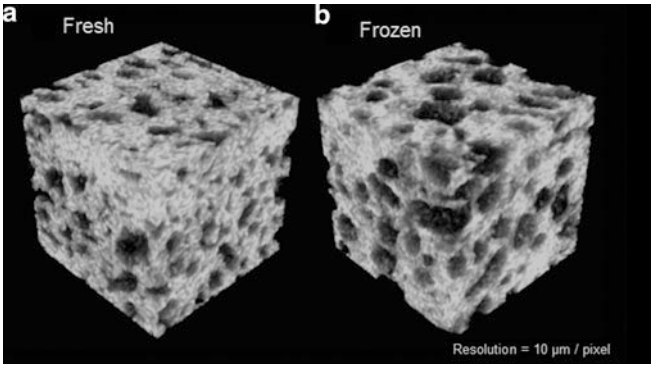

Fig. 25.3 Reconstructed 3-D X-ray apple tissue images (200^3 pixels$^3 \approx 8$ mm^3): (**a**) Fresh; (**b**) frozen-thawed tissue (*dark regions* represent pores; *clear regions* represent cellular material). The pore space in frozen-thawed tissue appears larger and apparently more heterogeneous in size than in fresh apple tissue, evidencing the deleterious effect of freezing on the apple microstructure

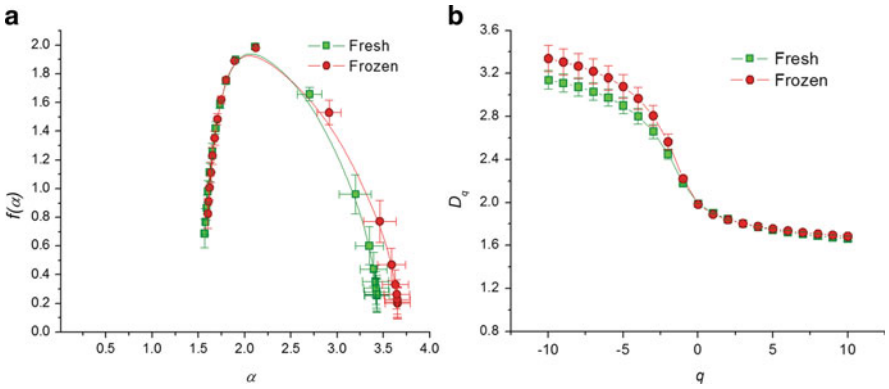

Fig. 25.4 Multifractal spectrums of PSD in fresh and frozen-thawed apple tissues expressed by: (**a**) $f(\alpha)$-spectra; (**b**) Rényi dimensions spectra, D_q

of the $f(\alpha)$-spectra provide information on the heterogeneity of a system, defined by the diversity of scaling exponents needed to characterize it. A homogeneous fractal exhibits a narrow $f(\alpha)$-spectra, whereas the opposite is true for a heterogeneous fractal. Thus, PSD in fresh apple tissue is more homogeneous than in frozen-thawed tissue as revealed by their $f(\alpha)$-spectra in Fig. 25.4a.

On the other hand, the Rényi spectra or generalized dimensions of the long transect are sigma-shaped curves with a clear asymmetry with respect to the cut point and the vertical axis; there is much more curvature for negative values of q than for positive values, which tend to be constant (Fig. 25.4b). More specifically, they exhibited pronounced decreasing D_q values with increasing q, and showed clear statistical differences between apple samples for D_q values with moments lower than $q = 0$. In this example, the evaluated range of D_q ran from $D_{-10} = 3.140 \pm 0.086$

to $D_{+10} = 1.664 \pm 0.022$ for fresh apple tissue, and from $D_{-10} = 3.339 \pm 0.122$ to $D_{+10} = 1.686 \pm 0.021$ for frozen-thawed tissue. However, the width of the D_q-spectra was greater in the frozen-thawed tissue, which indicated that the heterogeneity of PSDs in the parenchyma tissue was more apparent than in fresh apple, also confirming that the visual differences appreciated in the reconstructed 3-D images in Fig. 25.3.

In addition, heterogeneity can be assessed at $q = 0$ by the magnitude of differences in the values D_0 and $\alpha(0)$, or more generally, by the magnitude of changes around D_0 in both $f(\alpha)$ and α axes. Table 25.1 shows selected multifractal parameters for characterizing the heterogeneity of fresh and frozen-thawed apple samples. In the present example, except for D_1/D_0, the computed parameters ($\alpha(0) - \alpha(1)$, $\alpha(-1) - \alpha(0)$, $D_0 - D_1$, and $f[\alpha(-1)] - D_0$) showed statistical differences (*P-value* <0.05) between apple samples. In a symmetric spectrum, the widths ranging from $\alpha(0)$ to $\alpha(|q_i|)$, and D_0 to $D_{(|qi|)}$ are expected to be similar and smaller. In this sense, the results presented in Table 25.1 clearly confirm that PSD in fresh apple tissue is more homogeneous than that of frozen-thawed tissue. This tendency toward homogeneity implies that regions with high and low concentration of mass (pores) scale similarly.

25.4 Multifractal Characterization of FSD for Two Qualities of Presliced Pork Hams

In ham products, FSD is a fundamental physical property analyzed in assessing product quality. Here, FSD is related to sensory properties such as texture, taste, quality of the raw meat, and visual appearance. Therefore, accurate representation of this microstructural property is needed for an objective quality characterization and prediction during ham formulation. Moreover, ham slices in general have complex and inhomogeneous colored surfaces, and textures do not contain any detectable periodic or quasiperiodic structure. Instead, textures exhibit random but persistent patterns that result in a cloud-like appearance (Mendoza et al. 2009). These inhomogeneities can be attributed mainly to formulation, presence of pores/defects and fat-connective tissue, and color variations (Valous et al. 2009). Thus, for objective characterization, image analysis techniques need to take into account the high variability in texture appearance. Consequently, fractal metrics and concepts have been recently applied to investigate and describe the complexities and self-similarities of a variety of ham surfaces (Mendoza et al. 2009; Valous et al. 2009).

Similar to the multifractal characterization of PSD in fresh and frozen-thawed apple tissues (10 μm/pixel), we have presented an application of multifractal theory for characterization of FSD in two qualities of presliced pork hams typically consumed in Ireland. Here, the extracted multifractal parameters and spectrums were computed using the same principles and conditions mentioned above; nevertheless, it is important to note that the MFA in this case was tested for characterization of structures segmented from ham images captured at the macroscale level (0.102 mm/pixel).

25.4.1 Experimental Procedure for Ham Samples

Two qualities of pork hams were manufactured at Dawn Farm Foods Co. (Kildare, Ireland), using different muscle sections and various percentages of brine solutions (wet curing by injection). Specifically, the *high yield ham* (low quality) had a 50% brine injection and was made from pork muscle called Silverside PAD (biceps femoris), cut to 100 mm width. The injected muscle was vacuum-tumbled at 1,500 rpm for 12 h and vacuum-filled into PVC casings, clipped, and cooked at 82°C to a core temperature of 72°C. The *medium-yield ham* (intermediate quality) had a 30% brine injection and contained three leg muscles: Topside, Silverside, and Knuckle. The injected muscle was vacuum-tumbled at 500 rpm for 5 h and vacuum-filled into PVC casings, clipped, and cooked at 82°C to a core temperature of 72°C. All pork ham samples were chilled to 4°C before slicing. Images were acquired immediately after slicing (100 slices per type of ham quality).

To ensure reproducibility in the preprocessing and MFA of ham images, a color-calibrated computer vision system (CVS) as described by Valous et al. (2009) was used for image acquisition (spatial resolution 0.102 mm/pixel). Then, a polynomial transform was used for signal calibration of the captured images (Valous et al. 2009), which mapped the raw RGB primary signals into the sRGB color standard (IEC 1999). These color-calibrated images were used in the identification and segmentation of fat-connective tissue structures. For analysis, due to the large variation in size and shape between the two presliced ham qualities, the images were subsequently cropped in the central region to produce 512 × 512 pixel images (equivalent to 2,727.4 mm^2). The software package MATLAB (MathWorks, USA) was used for image processing and multifractal computations.

The fat-connective tissue segmentation was performed using the green (G) intensity images (from sRGB), since visually this color channel better represented the edges of the fat-connective tissue structures of the two evaluated hams. Thus, the green (G) intensity image was preprocessed with a median filter (3 × 3) to remove impulse noise. Then, a morphological closing filter (3 × 3) was applied to remove pores; a decrease in the intensity variations of the background pixels (more "flat" background in relation to fat-connective tissue) was also carried out. A hi-pass filter (15 × 15) was applied for increasing sharpness and contrast. This operation introduced some random noise, which was then removed using the median filtering operation (3 × 3), while a subsequent histogram-based segmentation using a unique threshold value of 200 produced the binary images (Valous et al. 2009).

Figure 25.5 shows representative images of the two evaluated pork ham qualities as well as the experimental procedure for cropping and binarization of the fat-connective tissue structures. The original ham images were cropped to obtain three square regions (512 × 512 $pixels^2$) from each slice; since not all ham slices had the same spatial dimensions, this process allowed receiving representative information from each quality sample, facilitating better scrutiny and interpretation, and also keeping computation times manageable. Also, the depicted binary images confirm the performance of the segmentation method used in this investigation.

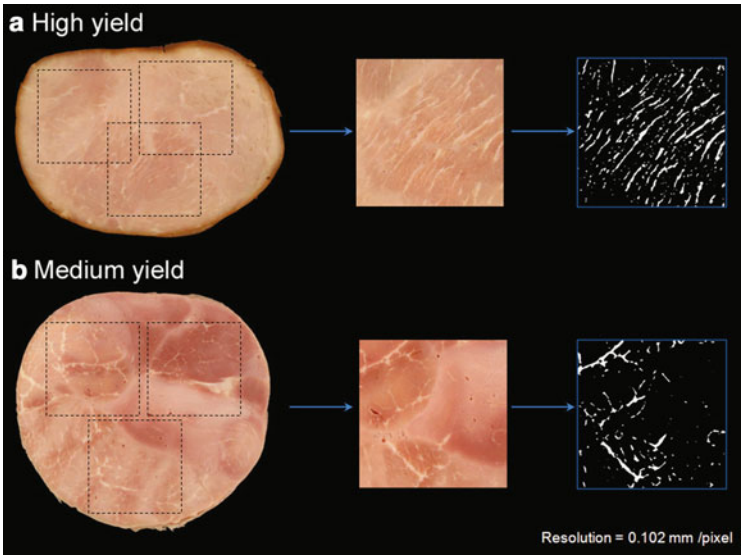

Fig. 25.5 Illustration of experimental procedure for MFA using ham samples: (**a**) Representative images of the two evaluated pork ham qualities; (**b**) cropped color regions (512 × 512 pixels^2); (**c**) corresponding binary images of segmented fat-connective tissue structures used for further processing and MFA

25.4.2 Results of MFA for FSD in Hams

As observed in Fig. 25.5, the evaluated ham qualities are characterized by different contents and distributions of fat-connective tissue structures; they also show a high variability in the textural appearance of slices from the same quality type. Fat-connective tissue estimations (average of 300 square images per quality type) showed values for high yield of 6.2 ± 2.1% and for medium yield 2.9 ± 1.6%. The statistical differences (*P-value* <0.05) were evident between these average indices (Table 25.2).

The range of q values for ham samples, considering the coefficients of determination (R^2) equal or larger than 0.95, for the plot of numerators (25.13) and (25.14) versus log ε, were for $\alpha(q)$ in the range Δq of -1.7 to +10 and for $f(q)$ in the range Δq of -1.6 to +3.1 for both ham qualities.

Figures 25.6a, b depict the average $f(\alpha)$-spectra and Rényi spectra for each ham quality and their standard deviations for each point, respectively. The $f(\alpha)$-spectra revealed that FSD in medium-yield hams is slightly more homogeneous than in high-yield hams (Fig. 25.6a), as indicated by the shorter amplitude and symmetric shape of the average $f(\alpha)$-spectra for the medium-yield ham. Similarly, the Rényi spectra (Fig. 25.6b) exhibited pronounced decreased D_q values with increasing q, and showed clear statistical differences between the ham qualities in the entire range of D_q values (with q moments ranging from -10 to $+10$). In this example, the

Table 25.2 Selected multifractal parameters and standard deviations from the analysis of binary images of fat-connective tissue for the two qualities of presliced hams

	Fat-connective tissue index (%)	$\alpha(0) - \alpha(1)$	$\alpha(-1) - \alpha(0)$	$D_0 - D_1$	$f[\alpha(-1)] - D_0$	D_1/D_0
High	6.23 ± 2.07^x	0.385 ± 0.042^x	0.616 ± 0.069^x	0.164 ± 0.020^x	0.267 ± 0.023^x	0.909 ± 0.013^x
Medium	2.89 ± 1.56^y	0.393 ± 0.070^x	0.470 ± 0.119^y	0.174 ± 0.029^y	0.233 ± 0.054^y	0.888 ± 0.021^y

x–y, values with different letters within each column indicate significant differences among ham qualities ($p < 0.05$)

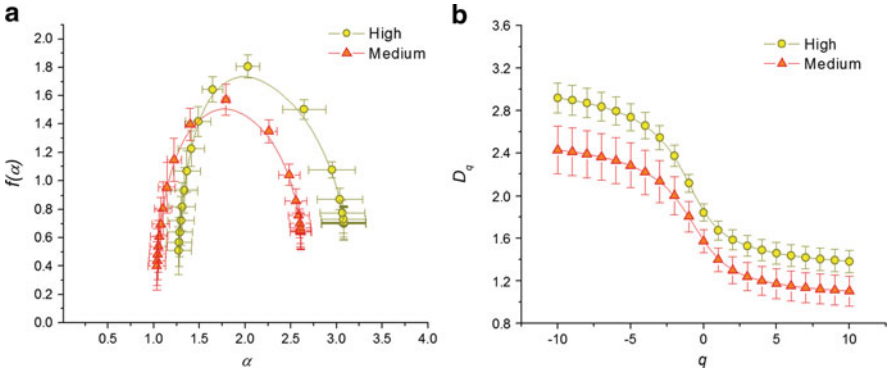

Fig. 25.6 Multifractal spectrums of FSD in two qualities of presliced hams expressed as: (**a**) $f(\alpha)$-spectra; (**b**) Rényi dimensions spectra, D_q

evaluated range of D_q ran from $D_{-10} = 2.920 \pm 0.142$ to $D_{+10} = 1.382 \pm 0.107$ for high-yield hams and $D_{-10} = 2.429 \pm 0.226$ to $D_{+10} = 1.326 \pm 0.140$ for medium-yield hams, with an average D_0 dimension for high- and medium-yield hams of 1.808 ± 0.080 and 1.572 ± 0.180, respectively. Nonetheless, the width of D_q-spectra is greater in high-yield hams, which indicates that the heterogeneity of FSDs in the ham matrix is more apparent than in medium-yield types. In general, both multifractal spectrums allowed for a robust characterization of these two types of ham. The selected multifractal parameters presented in Table 25.2 confirm that, with exception of the difference $\alpha(0) - \alpha(1)$ and in spite of the high variability of samples coming from the same quality, the computed parameters $\alpha(-1) - \alpha(0)$, $D_0 - D_1$, $f[\alpha(-1)] - D_0$, and D_1/D_0 are all statistically different (*P-value* <0.05) and therefore could be used as quality predictors of hams.

25.5 Conclusions and Outlook

In this chapter, multifractal spectrum and the generalized dimensions of apple pore structure are computed with data obtained from X-ray images (10 μm/pixel) of fresh and frozen-thawed apple samples (Granny Smith), as well as color images (0.102 mm/pixel) of two different qualities of presliced pork hams typically

consumed in Ireland. The extracted multiscaling properties from binary images (of pores or fat-connective tissue structures) allowed evaluating and revealing the significance of the method in discrimination of morphology and distribution of pores and fat-connective tissue structures in these particular samples.

Multifractal parameters were found to reflect the major aspects of variability in the PSD of apple tissue and FSD of ham fat-connective tissue, providing a unique quantitative characterization of the spatial distribution data. The irregularity and complexity of apple pore structure and ham fat-connective tissue, together with its scale-invariant features suggest that multifractal distribution is a suitable and natural model.

The results of both examples have also demonstrated that MFA has significant benefits for quantitative analysis of the complex microstructure of biological materials from images, allowing conclusions to be drawn on the exact topography of, for example, PSD and FSD of apple tissue and presliced cooked pork hams. Potential multifractal parameters for characterizing contrasting PSD and FSD are D_0, D_1, $\alpha(0) - \alpha(1)$, $\alpha(-1) - \alpha(0)$, $D_0 - D_1$, $f[\alpha(-1)] - D_0$, and D_1/D_0. Furthermore, modeling apple and ham images with multifractal spectrums, such as $f(\alpha)$-spectra and D_q-spectra, allows the capture of differentiating microstructural features and makes possible the automatic characterization, not only between apple varieties and ham types, but also between roughness degrees or image textures, due to the capability of the multifractal parameters to resolve local densities from images. Multifractal parameters are promising descriptors for type identification and quality assessment of apple and ham samples. Moreover, this multiscaling procedure and image analysis technique should provide valuable opportunities for further research of other natural and processed foods.

Acknowledgements The authors gratefully acknowledge the Food Institutional Research Measure (FIRM) strategic research initiative, as administered by the Irish Department of Agriculture and Food, for their financial support.

References

Baoping J (1999) Nondestructive technology for fruits grading. In: Proceedings of 1999 international conference on agricultural engineering, Beijing, China, pp IV127–IV133

Baumann H, Henze J (1983) Intercellular space volume of fruit. Acta Hort 138:107–111

Callen HB (1985) Thermodynamics and an introduction to thermostatistics, 2nd edn. Wiley, New York

Celia M, Reeves P, Ferrand L (1995) Recent advances in pore scale models for multiphase flow in porous media. Rev Geophys Suppl 33:1049–1057

Cheng Q, Banks NH, Nicholson SE, Kingsley AM, Mackay BR (1998) Effects of temperature on gas exchange of "Braeburn" apples. NZ J Crop Hort Sci 26:299–306

Chhabra A, Jensen RV (1989) Direct determination of the f(alpha) singularity spectrum. Phys Rev Lett 62(12):1327–1330

Chhaabra AB, Meneveu C, Jensen RV, Sreenivasan KR (1989) Direct determination of the f(alpha) singularity spectrum and its application to fully developed turbulence. Phys Rev A 40:5284–5294

Cox LB, Wang JSY (1993) Fractal surfaces: measurements and applications in earth sciences. Fractals 1:87–117
Delgado AE, Sun D-W (2001) Heat and mass transfer models for predicting freezing process – a review. J Food Eng 47(3):157–174
Dražeta L, Lang A, Alistair JH, Richard KV, Paula EJ (2004) Air volume measurement of "Braeburn" apple fruit. J Exp Bot 55:1061–1069
Eghball B, Schepers JS, Negahban M, Schlemmer MR (2003) Spatial and temporal variability of soil nitrate and corn yield: multifractal analysis. Agron J 95:339–346
Esau K (1977) Anatomy of seed plants. Wiley, New York
Everstz CJG, Mandelbrot BB (1992) Multifractal measures. In: Peitgen H, Jürgens H, Saupe D (eds) Chaos and fractals. Springer, Berlin, pp 922–953
Gouyet J-F (1996) Physics and fractal structures. Springer, New York
Grassberger P, Procaccia I (1983) Characterization of strange attractors. Phys Rev Lett 50(5):346–349
Halsey TC, Jensen MH, Kadanoff LP, Procaccia I, Shraiman BI (1986) Fractal measures and their singularities: the characterization of strange sets. Phys Rev A 33(2):1141–1151
Harker FR, Ferguson IB (1988) Calcium ion transport across discs of the cortical flesh of apple fruit in relation to fruit development. Physiol Plant 74:695–700
Harker FR, Hallet IC (1992) Physiological changes associated with development of mealiness of apple fruit during cool storage. HortScience 27:1291–1294
Harker FR, Watkins CB, Brookfield PL, Miller MJ, Reid S, Jackson PJ, Bieleski RL, Bartley T (1999) Maturity and regional influences on watercore development and its postharvest disappearance in "Fuji" apples. J Am Soc Hortic Sci 124:166–172
Hentchel HGE, Procaccia I (1983) The infinite number of generalized dimensions of fractals and strange attractors. Physica D 8:435–444
Ho QT, Verlinden BE, Verboven P, Nicolaï BM (2006) Gas diffusion properties at different positions in the pear. Postharvest Biol Technol 41:113–120
IEC (1999) IEC 61966–2–1: multimedia systems and equipment – colour measurements and management – Part 2–1: colour management – default RGB color space – sRGB. International Electrotechnical Commission (IEC), Geneva, Switzerland
Kennedy C (2003) Developments in freezing. In: Zeuthen P, Bøgh-Sørensen L (eds) Food preservation techniques. CRC Press, Cambridge/England, pp 228–240
Ketipearachchi KW, Tatsumi J (2000) Local fractal dimensions and multifractal analysis of the root system of legumes. Plant Prod Sci 3:289–295
Khan AA, Vincent JFV (1990) Anisotropy of apple parenchyma. J Sci Food Agric 52:455–466
Korvin G (1992) Fractals models in the earth sciences. Elsevier, Amsterdam, The Netherlands
Kravchenko AN, Boast CW, Bullock DG (1999) Multifractal analysis of soil variability. Agron J 91:1033–1041
Kuroki S, Oshita S, Sotome I, Kawagoe Y, Seo Y (2004) Visualization of 3-D network of gas-filled intercellular spaces in cucumber fruit after harvest. Postharvest Biol Technol 33:255–262
Mandelbrot BB (1992) The fractal geometry of nature, 2nd edn. W.H. Freeman, New York
Mardia KV, Hainsworth TJ (1988) A spatial thresholding method for image segmentation. IEEE Trans Pattern Anal Mach Intell 6:919–927
Martino MN, Otero L, Sanz PD, Zaritzky NE (1998) Size and location of ice crystals in pork frozen by high-pressure-assisted freezing as compared to classical methods. Meat Sci 50(3):303–313
Mendoza F, Verboven P, Mebatsion HK, Kerckhofs G, Wevers M, Nicolaï BM (2007) Three-dimensional pore space quantification of apple tissue using x-ray computed microtomography. Planta 226:559–570
Mendoza F, Valous NA, Allen P, Kenny TA, Ward P, Sun D-W (2009) Analysis and classification of commercial ham slice images using directional fractal dimension features. Meat Sci 81(2):313–320
Oh W, Lindquist W (1999) Image thresholding by indicator kriging. IEEE Trans Pattern Anal Mach Intell 21:590–602

Pascual M, Ascioti FA, Caswell H (1995) Intermittency in the plankton: a multifractal analysis of zooplankton biomass variability. J Plankton Res 17:1209–1232

Plotnick RE, Gardner RH, Hargrove WW, Prestegaard K, Perlmutter M (1996) Lacunarity analysis: a general technique for the analysis of spatial patterns. Phys Rev E 53(5):5461–5468

Rajapakse NC, Banks NH, Hewett EW, Cleland DJ (1990) Development of oxygen concentration gradients in flesh tissues of bulky plant organs. J Am Soc Hortic Sci 115:793–797

Raven JA (1996) Into the voids: the distribution, function, development and maintenance of gas spaces in plants. Ann Bot 78:137–142

Rényi A (1995) On a new axiomatic theory of probability. Acta Mathematica Hungarica VI 3–4:285–335

Scheuring I, Riedi RH (1994) Application of multifractals to the analysis of vegetation pattern. J Veg Sci 5:489–496

Shannon CE, Weaver W (1949) The mathematical theory of communication. University of Illinois Press, Chicago

Sterling C (1968) Effect of low temperature on structure and firmness of apple tissue. J Food Sci 33:577–580

Sun D-W (ed) (2001) Advances in food refrigeration. Leatherhead Publishing, LFRA Ltd, Surrey

Valous NA, Mendoza F, Sun D-W, Allen P (2009) Colour calibration of a laboratory computer vision system for quality evaluation of pre-sliced hams. Meat Sci 81(1):132–141

Vicsek T (1992) Fractal growth phenomena, 2nd edn. Word Scientific Publishing, Singapore

Vincent JFV (1989) Relationships between density and stiffness of apple flesh. J Sci Food Agric 31:267–276

Volz RK, Harker FR, Hallet IC, Lang A (2004) Development of texture in apple fruit – a biophysical perspective. Acta Hort 636:473–479

Voss RF (1988) Fractals in nature: from characterization to simulation. In: Peitgen H-O, Saupe D (eds) The sciences of fractal images. Springer, New York, pp 21–69

Westwood MN, Batjer LP, Billingsley HD (1967) Cell size, cell number and fruit density of apples as related to fruit size, position in the cluster and thinning method. Proc Am Soc Hort Sci 91:51–62

Xiaoyan G, Peiling Y, Shumei R, Yunkai L (2007) Multifractal analysis of soil structure under long-term wastewater irrigation based on digital image technology. NZ J Agric Res 50:789–796

Yamaki S, Ino M (1992) Alteration of cellular compartmentation and membrane permeability to sugars in immature and mature apple fruit. J Am Soc Hortic Sci 117:951–954

Yearsley CW, Banks NH, Ganesh S (1997a) Temperature effects on the internal lower oxygen limits of apple fruit. Postharvest Biol Technol 11:73–83

Yearsley CW, Banks NH, Ganesh S (1997b) Effects of carbon dioxide on the internal lower oxygen limits of apple fruit. Postharvest Biol Technol 12:1–13

Part V
Food Packaging

Chapter 26
New Packaging Materials Based on Renewable Resources: Properties, Applications, and Prospects

Stéphane Guilbert, Carole Guillaume, and Nathalie Gontard

26.1 Introduction

Since the 1980s, research programs on high-value materials based on renewable resources have boomed as a result of a larger demand for packaging materials with better environmental balance and/or new or original properties, such as biodegradability, versatility according to physico-chemical conditions, controlled release or adsorption, etc. These new materials are designed to have a better environmental impact than conventional plastics. They are considered "bio-plastics" (Guilbert et al. 2005) even if the definition of this term is not clear: the polymer's origin might be a fossil or from renewable resources, its synthesis can be chemical or naturally made, and its end-life, conventional/biodegradable or compostable. The different ways to obtain bio-plastics (commercially available or under development) are presented in Fig. 26.1.

Materials based on "extractible" agropolymers such as starch, cellulose, or proteins have been obtained through either casting techniques or thermoplastic processing. Their water and temperature sensitivity can be built on to react to fresh food physiology and/or to trigger responses adaptive to environmental change. These materials also exhibit interesting properties related to mass transport characteristics: they generally have a high carbon dioxide/oxygen (CO_2/O_2) selectivity ratio associated with high gas permeability. Such bio-plastics, which can be combined with paper or bio-polyesters for mechanical resistance, are able to create unique modified atmospheres favorable to the preservation of fresh fruits and vegetables (Gontard and Guillaume 2009). Bio-plastics based on proteins are also used as an inclusion matrix for a controlled release of volatile antimicrobial agents to increase food shelf-life. Their release kinetics and thus antimicrobial efficiency can be modulated thanks to physically induced crosslinking treatments or introduction of nanoparticules to suit to the food distribution chain (Guillaume et al. 2008;

S. Guilbert (✉), C. Guillaume, and N. Gontard
Joint Research Unit, Agropolymers Engineering and Emerging Technologies, Montpellier SupAgro, INRA, UM II, CIRAD, 34060 Montpellier, France
e-mail: guilbert@supagro.inra.fr

J.M. Aguilera et al. (eds.), *Food Engineering Interfaces*, Food Engineering Series,
DOI 10.1007/978-1-4419-7475-4_26,

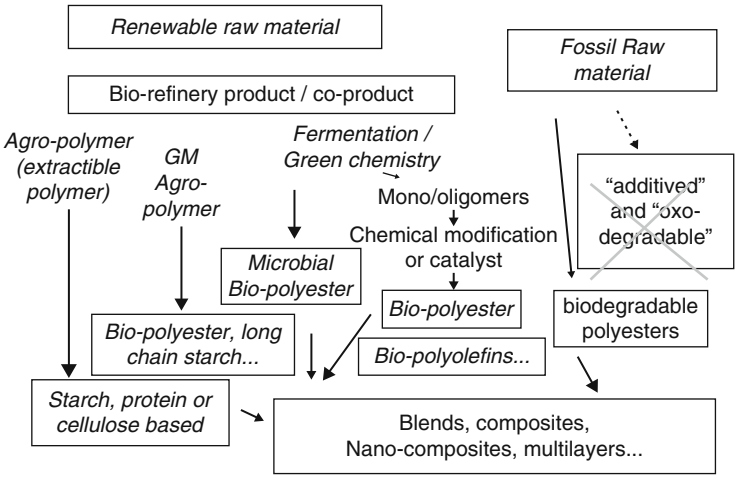

Fig. 26.1 Actual bio-plastics, commercial or under development

Gontard and Guillaume 2009). Nonconventional extractible polyesters are also now produced either by microorganisms or genetically modified (GM) plants (Fig. 26.1).

Apart from extractible polymers, *bio-sourced plastic polymers* are produced by chemical synthesis of monomers obtained by fermentation of renewable substrates. Today, they are bio-polyesters, bio-polyolefins, and bio-elastomers. Some are still under development, and others, such as polylactic acid (PLA), are already commercialized for the formulation of packaging materials (Fig. 26.1). Their properties are identical or close to conventional material properties, with renewability as a strong functional and commercial advantage. Some of these bio-sourced polymers (e.g., bio-polyesters) are biodegradable or compostable (e.g., PLA).

Biodegradable fossil-based plastic materials (generally, polyesters) have been developed in order to facilitate processability optimization and to improve mechanical, barrier, optical, and biodegradability properties. Their combination with extractible agropolymer materials, or bio-sourced polyester materials, or fibers, to form blends or composite materials, has given good test results. This could be a solution to optimize production costs and modulate the biodegradability kinetics and mechanical and transport properties.

26.2 Bio-plastics: Where Are We Now?

Bio-plastics can be classified into three categories according to chemistry used to synthesize the polymer (conventional/biosynthesis), origin (natural/fossil), and end-life (conventional/biodegradation or composting). Reference to the term "bio" can be assigned to either of these categories (Table 26.1). A fourth category called "additived polymers" is sometimes cited as "degradable" or even "biodegradable"

Table 26.1 The main groups of bio-plastics

Polymer group	Origin	Chemistry	End life	Examples
Nature-made polymers	Renewable	Naturally engineered	Biodegradable or compostable	Starch, cellulose, proteins, PHAs
Chemically synthesized polymers	Renewable	Conventional synthesis	Biodegradable or compostable	PLA
	Fossil	Conventional synthesis	Biodegradable or compostable	PCL, PBAT, PBSA
	Renewable	Conventional synthesis	Not biodegradable	Bio-sourced polyolefins, PE, PP

(Fig. 26.1). It refers to conventional polymers (e.g., polyethylene [PE] and polypropylene [PP]) mixed with 1–5% additives, which are supposed to promote the degradation of the entire material. Additives are organic materials such as starch, cellulose or ethylene vinyl alcohol (called "Additived with organic materials"), or transition metals (e.g., cobalt, zinc, manganese) that catalyze oxidation and chain scission (called "oxo-degradable"). In the first case, only a small portion of the material biodegrades; the material is considered "fragmentable." In the second case, the pro-oxidation catalysts promote polymer chain scission when the material is exposed to an abiotic environment (temperature, O_2, UV, etc.). Both types of additived polymers do not meet the standard specifications for compostable or biodegradable plastics (ASTM D64000 or D6868). In addition, the environmental consequences of their usage are largely unknown (e.g., ecotoxicity or accumulation of nano-size products of chain scission). Therefore, additive polymers should definitively be excluded from the bio-plastics family.

The *first group of bio-plastics refers to "nature-made polymers"* that have been naturally engineered by vegetal or microbial cells (i.e., crop plants, industrial microorganisms), which are then extracted, purified, and eventually modified. These polymers are renewable. The main benefits are high yields from natural fabrication and excellent carbon and energy balance. In addition, functional properties (e.g., mass transport properties) are often original and far from conventional plastic properties, thus paving the way for new applications such as active or intelligent materials (see Sect. 26.3). The formulation of bio-plastic materials based on extractible agropolymers implies the use of polyesters, polysaccharides or proteins. These polymers have the capability to form a matrix with sufficient cohesion and continuity, a crystalline or amorphous continuous structure, under certain conditions. Starch is the most commonly used agricultural raw material, and is inexpensive, widely available, and relatively easy to handle. "All-starch" bio-plastics are made from thermoplastic starch and are formed with standard techniques (as used for synthetic polymer films) such as extrusion or injection molding. The use of thermoplastic proteins was also investigated (Gontard and Guilbert 1994; Guilbert et al. 2006), but commercial applications are still expected. Among the proteins, milk proteins (casein, whey proteins), soya proteins, and cereal proteins (wheat gluten, zein, etc.) have been more extensively studied (Guilbert and Cuq 2002).

The glass transition temperature and melting temperature of polysaccharides and proteins are very high (above degradation temperature); thus, the use of plasticizers, such as water, glycerol or lactic acid is required. One of the inconveniences using water-soluble plasticizers is the migration towards and contact with the product (food), leading to either a loss of material properties or pollution of the product. This type of material based on a continuous hydrocolloid matrix is generally not very resistant to water, as moisture-barrier properties are poor. In some cases, water solubility or sensitivity to water is a functional advantage, e.g., in the formulation of soluble sachets. For the majority of usages, reducing the plasticizer's migration and the improvement of water resistance and water-barrier properties are of prime importance. Chemical modifications, such as grafting with hydrophobic compounds or usage of specific additives (cross-linking agents or nonwater-soluble plasticizers), adapted to the polymer structure have been proposed but with poor success. In most cases, gains in water or mechanical resistance are counterbalanced by a strong loss in elongation at strength. Regarding these developments, internal plasticization through chemical grafting or design of copolymer materials (e.g., protein/polyesters) is the most promising (Auvergne et al. 2008). Another interesting development is the formation of nano-reinforced materials, for example with exfoliated nanoclays.

Commercial water-resistant, starch-based bio-plastics are produced by using fine molecular blends of biodegradable synthetic polymers (see below) and starch. These materials are made with gelatinized starch (up to 60%) and hydrophilic (e.g., ethylene vinyl alcohol copolymer [EVOH]) or hydrophobic synthetic biodegradable polymers (e.g., polycaprolactone [PCL], or polybutylene adipateterephthalate [PBAT], known as "Ecoflex®") and compatibility agents (Fritz et al. 1994). The polyesters form the continuous phase leading to materials presenting a relative water resistance and acceptable barrier and mechanical properties. The most important starch-/polyester-based materials on the market are those proposed by Novamont as Materbi® or by Sphere as Bioplast.® Actual production of these starch/polyester blends is estimated between 50 and 80 kT/year with a price between 1.2 and 3.0€/kg according to the grade considered.

Microbial polyesters (e.g., polyhydroxyalkanoates [PHAs]) are excreted or stored by microorganisms cultivated on starch hydrolysates or lipidic mediums. PHAs are unbranched polymers predominantly composed of R-3-hydroxyalkanoic acid monomers, ranging from 3 to 14 carbons in length with hydrogen or alkyl up to nonyl radicals. Copolymers of different length monomers or introduction of other monomers are often proposed. Isolation and purification costs could be high for these products, as they are obtained from complex mixtures. Monsanto stopped the commercialization of the poly(3)-hydroxybutyrate-hydroxyvalerate (PHB/V) product Biopol® in 1999. Since that date, others have entered the market and have built new facilities for pilot plant production of microbial PHA, as in the case of Tianan Biologic Material produced in Ningbo (China), Biocycle® by PHB Industrial in Brazil, or "Telles," a Metabolix/Archer Daniels Midland joint venture that plans to produce "Mirel." DSM (Nl) announced a $20 million dollar investment in China in partnership with TIANJIN to produce 10,000 t/year of PHA. Recently, the production of PHAs with GM crop

plants was proposed with the potential for producing large amounts of bio-polymers at a low cost. A commercially relevant yield of 7–14% dry weight has been achieved with transgenic sugarcane or switch grass. Metabolix is one of the major industrial actors in this field.

PHA-based plastic properties look like PE ones but their rigidity is much higher due to a higher glass transition temperature (+5°/+10°C, compared to −120°C for PE). Actual production of these microbial polyesters is still very low (between 0.6 and 1.2 kT/year) with cost between 1.8 and 5.0€/kg according to the quality and production process.

The *second group of bio-plastics refers to "chemical synthesis"* polymers, which are also sometimes called "artificial bio-polymers." They can be: (i) bio-sourced (renewable origin) and biodegradable or compostable (e.g., PLA), (ii) bio-sourced and nonbiodegradable (e.g., bio-PE, bio PP), or (iii) petrol-based (fossil origin) but biodegradable (e.g., PBAT or PBSA). These polymers are synthesized by conventional chemical polymerization of monomers issued either from fossil oil cracking or renewable resource "deconstruction" (e.g., products of a plant biorefinery). These may benefit from the possibility of designed tailor-made polymers with controlled properties but the environmental impact is sometimes controversial.

Polylactic (and polyglycolic) acids are mainly produced by chemical polymerization of lactic acid (and glycolic acid) obtained by Lactobacillus fermentation. Biomass is used for fermentation derivatives of corn flour (corn starch hydrolysates), but use of the whole plant (including straw and lignocellulosic parts) is expected in the near future (second generation). Commercial applications of PLA materials are growing very rapidly under the trademarks of Ingeo™ from Cargill (USA) or Purasorb from Purac (NL). PLA-based plastic properties are similar to PE properties but their rigidity is much higher due to a higher glass transition temperature (+5°/+60°C, instead of −120°C for PE). PLA biodegrades at temperatures higher than Tg; the standard PLA (Tg = +50/+60°C) is not considered as biodegradable according to the ASTM standards but is compostable. In 2008, PLA production was slightly above 70 kT/year with an average price of 1.3–2.6€/kg.

Bio-sourced but not biodegradable/compostable plastics polymers (biopolyolefins, biopolyurethan, polycarbonate, etc.), produced with monomers from renewable resources and "green chemistry" transformation, have been announced for the near future. For example, Braskem, Brazil's largest petrochemical firm, invested US$150 million in a 200 KT plant to produce PE from sugarcane-based ethanol in 2009.

Petrol-based biodegradable polyesters are produced mainly by chemical synthesis, by companies such as Basf with Ecoflex (-PBAT-), Showa Highpolymer with Bionolle (polybutene succinate adipate -PBSA-), and Solvay with Capa (Polycaprolactone -PCL-). Actual production of these polyesters is between 10 and 25 kT/year with price around 2.0–3.0€/kg. Several research projects to replace these last fossil biodegradable polyesters with renewable ones are underway. Some are based on plant oil, fatty acid or glycerol chemical modification, including polymerization. Other projects are based on the production by fermentation of some monomers for copolymer building. As an example, Roquette (FR) and DSM (NL) announced the

future building of a pilot plant for the production by fermentation of succinic acid for PBSA fabrication.

26.3 Applications of Bio-plastics

All commercial bio-plastic materials can be processed using conventional shaping processes (e.g., extrusion, injection, injection molding) or coating processes (casting of solution in adequate solvents). Their applications can be classified into four categories: (i) plastics to be composted; (in fields where reuse or fine recovery is difficult; for short shelf-life products such as disposable items or fast food packaging; in fields where recycling is not industrially feasible, such as fiber composite), (ii) plastics used in natural environments (in fields where recovery is not economically or practically feasible, such as mulching of plastics for agriculture), (iii) specialty plastics (in fields with specific features where bio-plastics possess preferential properties), and (iv) commodity plastic substitutes with renewable origin (supposedly has a better environmental impact than nonbio-sourced ones).

Due to their relatively high cost and low availability, actual commercial applications of biodegradable plastics are limited to special niches with environmental considerations. Loose fill packaging and compost bags are the two major end uses, constituting nearly 50% of demand in 2008 but applications in the field of agriculture and food packaging are expected to dominate in the near future.

Actual commercial bio-plastic materials have different features that can be matched with different applications. For instance, considering the two major products on the market, Mater-bi material of Novamont and PLA of Cargill, the Mater-bi material is more suitable for films or bags, while PLA is mostly used for packaging and trays (unless plasticized). Manufacturers presently have a double function as both buyer and provider. Further, producers using the same applications are not yet competitive; they blend polymers from one producer to another to obtain specific or intended material properties.

Commercial applications of biodegradable materials are growing very rapidly, but because they are complex to develop and sometimes hard to produce, the total production of "thermoplastic bio-plastics" is actually low, with a total world consumption (2008) of only 120,000–150,000 t. Thus, large-scale application is not possible. This value is inferior to the production capacity of bio-plastics, which is around 300,000 t; a 2-year shift from capacity is observed.

The market for biodegradable plastics is young compared to that of traditional plastics. It started 20 years ago and has been booming for 2 or 3 years (Advanced Bioplastics 2003). World production passed from the pilot scale (during 1990s) to the industrial scale. However, this amount represents 0.2–0.3% of the total plastic market distributed using biodegradable polymers, ranging from fossil origin (50,000 t) to renewable resources (250,000 t). The global production capacity of biodegradable polymers is expected to reach 1,000,000 t in 2015.

Nonbiodegradable, bio-sourced plastics are under development and/or are at the pilot plant production stage (e.g., bio-sourced PE from sugarcane alcohol in Brazil). Completion of the first commercial products is expected in 2010 (but prices are not available). Expected markets are linked to public or private markets requiring a minimal and mandatory ratio for renewable based materials (e.g., plastic- or fiber-based material for construction).

Presently, the bio-plastic market is under the authority of a limited number of producers, such as American Cargill, Italian Novamont, and German BASF, and to a lesser extent, French Sphere and Biolice. Others entering the market are American Dupont, Procter & Gamble, Novomer and Metabolix, British UCB, Brazilan Biocycle and Braskem, French Roquette, and Dutch DSM.

Actual manufacturers expect to expand their production capacity, and construction of numerous plants is planned in Europe, USA, Brazil, and China. However, the existing economic crisis combined with some uncertainty about the environmental impact of bio-plastics (few global life cycle analyses [LCAs]) might hamper these ambitions.

26.4 Original Properties and Active Materials for Food Packaging

There are very few reliable data concerning the environmental footprint of bioplastics. Some life cycle analysis (LCA) is available but the scope of such is generally limited to the factory (from cradle to gate). Without cradle to tomb analysis (e.g., cradle to composting) or better, cradle to cradle, it is very difficult to advise on the real environmental impact (compared to conventional plastic materials). It is also true that due to the absence of an optimized supply chain on one part, and industrial local composting facilities on another part, it is unfair to compare an emerging chain to a well-established one. For these reasons, governmental agencies generally support the R&D effort in the domain of bio-plastics study, to help and promote the emergence of a viable industry.

Beyond environmental consideration, the development of bioplastics is driven by their unique and original properties when compared to conventional plastics. This is mainly due to very different molecular architecture and in most cases their hydrophilic character. These specific properties, mainly observed for extractible agropolymers, can be of great interest for designing gas selective or active materials for food packaging. Gas selectivity, obtained by the ratio of gas permeability, represents the ability of materials to favor transfer of one gas compared with another. For instance, various CO_2/O_2 permeation ratio is expected in modified atmosphere packaging (MAP) to meet physiological requirements of a large range of fresh produces. Active packaging has deliberately incorporated active agents that are intended to release or absorb substances into, onto or from the packaged food or the environment surrounding the food, and is defined in the food contact material

framework regulation 1935/2004 (Danielli et al. 2008). Such new packaging technologies are expected to play a major role in response to consumer demand for more convenient, safer, and mildly preserved products with longer storage duration. In addition, globalization of markets results in longer distribution distances and major challenges in the food packaging industry, acting as a driving force for development of packaging concepts that extend shelf-life while maintaining food quality and safety. This concept is developing throughout Europe and is enhancing the competitiveness of the food and packaging industry, with a huge potential market. Japan and the USA share more than 50% and 22% of the global Active and Intelligent (A&I) packaging market, respectively, against only 15% for EU. Simultaneously, the use of modified atmosphere packaging (MAP), passive packaging with gas-selective materials, or active packaging with additional gas (or vapor or any other volatile agent) emitter or absorber for the preservation of fresh or minimally processed fruits and vegetables constitutes one of the most important challenges.

To illustrate these properties, we chose to develop the case of an extractible agropolymer: wheat gluten proteins. Wheat gluten films appears to be of great interest because of their high gas permeability, adapted to the respiration of fresh fruits and vegetable, and high selectivity values (CO_2 permeability/O_2 permeability), which are able to create a unique low O_2 and CO_2 atmosphere adaptable to the preservation of CO_2-sensitive commodities (Gontard et al. 1996; Barron et al. 2002). However, despite their low cost and interesting functional properties for food packaging, these protein-based materials needs to be combined with:

- fiber-based materials, such as paper to overcome its poor mechanical properties (Han and Krochta 1999; Rhim et al. 2006; Gastaldi et al. 2007),
- or nanofillers such as montmorillonite (MMT) to reduce moisture sensitivity (Wang et al. 2005; Hedenqvist et al. 2006; Olabarrieta et al. 2006; Tunc et al. 2007).

An experimental support paper was coated with an acid wheat gluten solution (20% w/v, pH4) containing or not MMT (2.5% w/w of proteins) to produce composite or nanocomposite materials, respectively. O_2 and CO_2 permeability of composite and nanocomposite materials was evaluated at 25°C, and 80% and 90% relative humidity (RH), respectively, in comparison to control uncoated materials. The continuous layer formed by wheat gluten proteins on support paper greatly reduced gas permeability of the paper. Coated paper could thus not be considered as porous any longer. O_2 and CO_2 permeability values were not significantly affected by the presence of MMT in the wheat gluten network regardless of RH. Since permeability is known to be governed by two mechanisms, diffusion and sorption, it was assumed that introduction of MMT did not change solubility nor diffusivity of O_2 and CO_2, as observed in a previous study (Tunc et al. 2007). It should be pointed out that O_2 and CO_2 permeability of both composite and nanocomposite materials increased when increasing RH. This phenomenon was also observed on pure wheat gluten films [Gontard et al. 1996], suggesting that the wheat gluten-based coating layer is the key element of gas-barrier properties in the studied materials (composite and nanocomposite). The increasing RH effect was attributed to a modification of the wheat gluten network structure and polymeric chain mobility and is related to

the change from the glassy to the rubbery state (Gontard et al. 1996; Gontard and Ring 1996). The increase of CO_2 permeability was more pronounced than O_2 permeability. This phenomenon was explained by a selective sorption of CO_2 due to the specific interactions occurring between CO_2 and the water-plasticized protein matrix, especially the high-content amide groups of wheat gluten protein (Pochat-Bohatier et al. 2006). At high RH value, adsorption of water should provide better accessibility to active sites of CO_2 sorption located on the mobile polymeric protein chains. As a consequence, gas selectivity (COE permeability/O_2 permeability) was highly affected by RH (from 80 to 90% RH) and rose from 1.9 to 7.9 and 1.5 to 7.5 for composite and nanocomposite materials, respectively. These results show that the unique gas selectivity properties are preserved when combined with paper or MMTs. If we consider the potential use of the nanocomposite material for MAP of fresh produces at 90% RH, CO_2 should go out the packaging headspace at a rate 7.5-fold higher than O_2 comes in.

Passive MAP experiments were conducted on parsley with the uncoated support paper as a control and the nanocomposite material at a controlled RH of 80%. As expected for a highly porous material, O_2 and CO_2 partial pressures at the steady state obtained using control paper were close to air composition (21 and 0 kPa, respectively). Such an atmosphere was detrimental to the quality of the produce. After only 4 days of storage, more than 50% of ascorbic acid and chlorophyll were lost, and parsley leaves were fully yellow. Nanocomposite material generated a headspace atmosphere containing lower O_2 (11 kPa) and higher CO_2 (4 kPa) content. This steady atmosphere clearly improved the quality attributes of parsley during storage by maintaining a high chlorophyll content (directly linked to parsley's green color) and ascorbic acid during 8 days of storage. A critical level of 60% initial vitamin C content was reached after only 3 days of storage with uncoated paper, against more than 8 days for composite material. The use of nanocomposite materials for MAP of parsley led to equilibrium atmosphere favorable to maintaining parsley quality, by slowing down oxidation and physiological reactions responsible for product degradation. Similar results were obtained with mushrooms, and other fruits and vegetables.

Another promising application of extractible agropolymers, and in particular protein-based materials, is their use as active antimicrobial packaging. This relies on the ability of bio-based polymers to entrap active compounds and to release these compounds in a controlled way, with a moisture- and temperature-triggering effect (Carlin et al. 2001; Gennadios and Weller 1991; Guilbert et al. 1997). Protein-based materials have also been demonstrated to be efficient for antimicrobial packaging because of their ability to control, in a relevant way, the release of volatile extracts of various essential oils (allylisothyocyanate, carvacrol, cinnamaldehyde, and eugenol) (Ben Arfa et al. 2007a, b; Chalier et al. 2007) that could open new routes for the development of active MAP.

It has been shown that the release of the compound carvacrol from paper coated with wheat gluten is RH-dependent with or without the addition of nano-particles of MMTs. Release of this volatile compound was assessed at 25°C on all materials as a function of time, using a two-step gradient for RH. Composite material lost more

than 70% of carvacrol within 20 days of storage at 60% RH. This meant that only 30% of active agent would be available for release into the food during storage within packaging. Placed at 100% RH, 30% of active agent was entirely released within 8 days. In the presence of MMT introduced into the wheat gluten network (nanocomposite material), only 20% of carvacrol was released during 20 days of storage at 60% RH. Consequently, 80% of the volatile active agent remained available for release during the period food is packaged. Placed at 100% RH, 80% of active agent was entirely released within 13 days (from day 22 to 35). It can be concluded from these results that the release of cavacrol from wheat gluten-coated paper is RH-dependent with or without MMT. Such behavior is highly interesting for both limiting volatile active agent losses before using the material as food packaging, and for triggering the active agent release in the presence of the food.

26.5 Conclusions

Considering the relative novelty of packaging materials based on renewable resources, the following conclusions or question can be drawn:

- There is no clear definition of "bio-plastic," and different concepts sometimes contradictory are emerging accordingly in reference to polymer origin (natural/fossil), chemistry (conventional/biosynthesis), and/or end-life (conventional/biodegradable).
- Properties of biodegradable polymers are still far from conventional plastics (i.e., glass transition temperature, melting temperature, processability, mechanical properties, and water sensitivity).
- The necessity to use plasticizers for many extractible polymers-based materials is a major drawback for food contact materials (how to control their migration into the product).
- Biodegradable packaging is often not suitable for packaging of long shelf-life products with high water content (water sensitivity of materials and growth of microorganisms on packaging, e.g., on some made of proteins that need a combination with nanofillers to overcome this drawback).
- Prices are still high and susceptible to change according to the cost of renewable raw materials.
- Some of the most promising polymers are obtained through GMO plant or GMO microorganism origins (e.g., PLA, PHA, etc.), whereas "GMO" origin is not compatible with the "green" image of biodegradable or bio-sourced products.
- Apart from extractible polymers, which are of limited application, other bio-plastics are obtained through a deconstruction/reconstruction procedure (e.g., natural polymer hydrolysis, followed by fermentation, purification, polymerization stages, etc.). What is the rationality for such a complex and costly procedure?
- In actual context, it is difficult to analyze the life cycle of bio-plastics from cradle to cradle due to poor availability of materials, lack of composting facilities, the

necessity to collect materials separately, and the sorting of bio-plastic material waste for correct treatment to avoid pollution and interaction with industrial recycling facilities for conventional materials (e.g., PET recycling).

– What is the economic and environmental rationality for bio-sourced conventional plastics? Orientation on extractible plant and microbial polymers (starch, protein, cellulose, bio-polyesters, etc.) is probably more rational than producing monomers from natural origins (i.e., deconstruction of high-value natural polymers) for reconstruction of bio-sourced plastic. Due to competition in the food/nonfood usage of agricultural products (even if relatively low land surface is required for production of bio-plastics compared to other usages such as energy or food), the rationality is to use limited volumes; one can also recommend that bio-plastics be reserved for high-value specialty plastics (materials with original/specific properties such as biodegradability, respirability, gas selectivity, controlled release, etc.), not for substitution of commodity plastics.

These conclusions sound very negative but this is mainly due to the lack of reliable data on the subject, and to the fact that some materials or concepts (e.g., bio-sourced conventional plastics) are very new and to the tendency of scientific and economic actors to treat the subject in a passion mode. More research is needed in polymer/materials science, plasturgy, properties enhancement, migration studies, safety issues of biodegradable food contact materials, eco-conception, LCA, etc.

References

Auvergne R, Morel M-H, Menut P, Guilbert S, Robin JJ (2008) Reactivity of Wheat gluten protein during mechanical mixing: radical and nucleophilic reactions for the addition of molecules on sulfur. Biomacromolecules 9:664–671

Barron C, Varoquaux P, Guilbert S, Gontard N, Gouble B (2002) Modified atmosphere packaging of cultivated mushroom (*Agaricus bisporus* L.) with hydrophilic films. J Food Sci 67:251–255

Ben Arfa A, Chrakabandhu Y, Presiozi-Belloy L, Chalier P, Gontard N (2007a) Coating paper with soy protein isolates as inclusion matrix of carvacrol. Food Res Int 40:22–32

Ben Arfa A, Presiozi-Belloy L, Chalier P, Gontard N (2007b) Antimicrobial paper based on soy protein isolate or modified starch coating including carvacrol and cinnamaldehyde. J Agric Food Chem 55:2155–2162

Chalier P, Ben Arfa A, Presiozi-Belloy L, Gontard N (2007) Carvacrol losses from antimicrobial soy protein coated papers as a function of drying paper conditions. J Appl Polym Sci 106:611–620

Carlin F, Gontard N, Reich M, Nguyen-The C (2001) Utilization of zein coating and sorbic acid to reduce *Listeria monocytogenes* growth on cooked sweet corn. J Food Sci 66:1385–1389

Fritz HG, Seidenstücker T, Bölz U, Juza M, Schroeter J, Endres HJ (1994) Study on production of thermoplastics and fibers based mainly on biological materials. Science Research Development. European Comission, EUR 16102EN

Gastaldi E, Chalier P, Guillemin A, Gontard N (2007) Microstructure of protein-coated paper as affected by physico-chemical properties of coating solutions. Colloid Surf A 301:301–310

Gennadios A, Weller CL (1991) Edible films and coatings from soymilk and soy protein. Cereal Food World 36:1004–1009

Gontard N, Guilbert S, Cuq JL (1993) Water and glycerol as plasticizers affect mechanical and water vapor barrier properties of an edible wheat gluten film. J Food Sci 58(1):206–211

Gontard N, Guilbert S (1994) Bio-packaging: technology and properties of edible and/or biodegradable material of agricultural origin. In: Mathlouthi M (ed) Food packaging and preservation. Blackie Academic & Professional, Glasgow, pp 159–181

Gontard N, Thibault R, Cuq B, Guilbert S (1996) Influence of relative humidity and film composition on oxygen and carbon dioxide permeabilities of edible films. J Agric Food Chem 44:1064–1069

Gontard N, Ring S (1996) Edible wheat gluten film: influence of water content on glass transition temperature. J Agric Food Chem 44:3474–3478

Gontard N, Guillaume C (2009) Food packaging and the shelf life of fruits and vegetables. In: Robertson GL (ed) Food packaging and shelf life: a practical guide. CRC Press, Boca Raton, FL, chapter 16

Guilbert S, Cuq B, Gontard N (1997) Recent innovations in edible and/or biodegradable packaging materials. Food Addit Contam 14:741–751

Guilbert S, Cuq B (2002) Protein as raw material for biodegradable products. In: Bastioli C (ed) Handbook of biodegradable polymers. Rapra tech Ltd. London

Guilbert S, Feuilloley P, Bellon Fontaine V (2005) Biodegradable polymers in agricultural applications. In: Smith R (ed) Biodegradable polymers for industrial applications. Woodhead Publishing, Cambridge, chapter 25

Guilbert S, Morel MH, Gontard N, Cuq B (2006) Protein-based plastics and composites as smart green materials. In: Bozell JJ, Patel MK (eds) Feedstocks for the future: renewables for the production of chemicals and materials. Oxford University Press, New York, pp 334–350, (n 921). American Chemical Society

Guillaume C, Chalier P, Gontard N (2008) Modified atmosphere packaging using environmentally compatible and active food packaging materials. In: Chiellini E (ed) Environmentally compatible food packaging. Woodhead Publishing, Cambridge, pp 396–418

Han JH, Krochta JM (1999) Wetting properties and water vapor permeability of whey-protein-coated paper. Tranns ASAE 42:1375–1382

Hedenqvist MS, Backman A, Gallstedt M, Boyd RH, Gedde UW (2006) Morphology and diffusion properties of whey/montmorillonite nanocomposites. Compos Sci Technol 66:2350–2359

Olabarrieta I, Gallstedt M, Ispizua I, Sarasua JR, Hedenqvist MS (2006) Properties of aged montmorillionite-wheat gluten composite films. J Agric Food Chem 54:1283–1288

Pochat-Bohatier C, Sanchez J, Gontard N (2006) Influence of relative humidity on carbon dioxide sorption in wheat gluten films. J Food Eng 77:983–991

Rhim JW, Lee JH, Hong SI (2006) Water resistance and mechanical properties of biopolymer (alginate and soy protein) coated paperboards. LWT Food Sci Technol 39:806–813

Tunc S, Angellier H, Cahyana Y, Chalier P, Gontard N, Gastaldi E (2007) Functional properties of wheat gluten/montmorillonite films processed by casting. J Membr Sci 289:159–168

Wang SF, Shen L, Tong YJ, Chen L, Phang IY, Lim PQ, Liu TX (2005) Biopolymer chitosan/montmorillonite nanocomposites: preparation and characterization. Polym Degrad Stab 90:123–131

Chapter 27
Edible Coatings to Improve Food Quality and Safety

Noemí Zaritzky

27.1 Introduction

Edible films and coatings are useful materials mainly produced from edible biopolymers and food-grade additives (GRAS). Films are usually made from polymers that are able to provide mechanical strength to a stand-alone thin structure (Han 2005; Han and Gennadios 2005). Coatings are a particular form of films directly applied to the surface of materials. An edible coating has a close and continuous association with the food until consumption and it is regarded as a part of the final product. Edible coatings enhance the quality of food products, protecting them from physical, chemical, and biological deterioration (Kester and Fennema 1986; Han and Gennadios 2005).

The application of edible coatings can improve the physical strength of food products, reduce particle clustering, and improve visual and tactile features on product surfaces (Cuq et al. 1995; Cisneros-Zevallos et al. 1997). The coatings can also protect food products from moisture migration, microbial growth on the surface, light-induced chemical changes, oxidation of nutrients, etc. Edible coatings can act as barriers against oils, gases, or vapors and as carriers of active substances (antioxidants, antimicrobials, colors, and flavors) (Kester and Fennema 1986; Gennadios and Weller 1990; Guilbert and Gontard 1995; Krochta and De Mulder-Johnston 1997; Miller et al. 1998). These functions enhance the quality of food products, resulting in shelf-life extension and safety improvement. Further, edible coatings can be utilized as active films when applied to modify the atmosphere of food surface conditions (Cuq et al. 1995; Guilbert and Gontard 2005).

As an example of edible films, yuba (soy-milk skin) has been traditionally used in Asian countries since the fifteenth century (Wu and Bates 1972; Park et al. 2002). Wax coatings were applied to citrus fruits in the twelfth and thirteenth centuries, but only

N. Zaritzky
Centro de Investigación y Desarrollo en Criotecnología de Alimentos (CIDCA), Universidad Nacional de La Plata (UNLP) – CONICET La Plata and Depto de Ingeniería Química, La Plata, Argentina
e-mail: zaritzky@ing.unlp.edu.ar

J.M. Aguilera et al. (eds.), *Food Engineering Interfaces*, Food Engineering Series,
DOI 10.1007/978-1-4419-7475-4_27,

commercially utilized on apples and pears since 1930 (Baldwin 1994; Debeaufort et al. 1998; Park 1999). Lipid coatings (larding) on meats and cheeses have been used since the Middle Ages for shrinkage prevention (Donhowe and Fennema 1994).

The objectives of this presentation are to: (1) discuss the basic concepts of food coating applications, (2) review the most significant publications in this area, and (3) describe the different experiments carried out in our laboratory studying the performance of edible coatings to improve food quality and safety.

27.2 Edible Coating Materials

Coating materials can be either hydrophilic or hydrophobic; the main film-forming materials are biopolymers, such as proteins and polysaccharides (carbohydrates and gums); lipids and resins are also used, however they are not biopolymers (Gennadios et al. 1997). Coating materials can be used alone or in combinations (Krochta et al. 1994; Baldwin et al. 1997). The formulation of bioplastics or edible films implies the use of at least one component able to form a matrix, having sufficient cohesion and continuity (Nussinovitch 2003).

Polysaccharides: The most common polysaccharides used for edible coatings are methyl cellulose (MC), carboxymethyl cellulose (CMC), hydroxypropyl cellulose (HPC), hydroxypropyl methyl cellulose (HPMC), starch, modified starches, amylose, hydroxypropyl amylose (HPA), alginate, carrageenan, pectin, chitosan, gellan gum, xanthan gum, etc. The occurrence of relatively large numbers of hydroxyl groups in the structure of polysaccharides indicates that hydrogen bonds may play significant roles in film formation and characteristics. Starch is the most common agricultural raw material used for biodegradable and edible films formulation, and is an appropriate matrix-forming material with lower cost compared to other alternatives. Starch is also widely available and relatively easy to handle; amylose is responsible for the film-forming capacity of starch (Guilbert and Gontard 2005). Cellulose derivatives are composed of linear chains of β (1–4) glucosidic units with methyl, hydroxypropyl, or carboxyl substituents. MC has excellent film-making properties, as well as high solubility and efficient O_2 and lipid-barrier properties (Donhowe and Fennema 1994; Nisperos-Carriedo 1994). Two other examples, chitin and its deacetylated product, chitosan, have received much interest regarding application in the food industry due to their biocompatibility, biodegradability, and bioactivity.

Proteins: Different proteins such as whey protein, casein, collagen, gelatin, egg white protein, keratin, fish, myofibrillar protein, corn zein, wheat gluten, soy protein, pea protein, peanut protein, cottonseed protein, rice bran protein, etc., have been used in edible coatings. The most distinctive characteristics of proteins, compared to other film-forming materials, would be the conformational denaturation, electrostatic charges, and amphiphilic nature of proteins. Many factors can affect the conformation of proteins, such as charge density and hydrophilic-hydrophobic balance, which in turn can affect the physical and mechanical properties of films and coatings.

Protein film-forming materials are derived from animal tissues, milk, eggs, grains, and oil seeds (Krochta 1997, 2002). Among the proteins considered, milk proteins (casein, whey proteins), soy proteins, and cereal proteins (wheat gluten, zein) have been more extensively studied (Gennadios et al. 1994; Guilbert et al. 2001). Since several edible food coatings are made with proteins that can cause allergic responses in some consumers and problems in people affected by Celiac disease (gluten intolerance), the use of a food coating with a known allergen or the presence of gluten in a food must be appropriately declared and clearly labeled on the product.

Waxes/Lipids/Resins: In this group, beeswax, candelilla wax, carnauba wax, cocoa butter, milk fat fractions, acetylated monoglycerides, fatty acids, and resins (shellac, terpene) are used in edible coatings. It should be noted that lipids and resins are not biopolymers; nevertheless, they are edible, biodegradable, and considered to be cohesive water barrier biomaterials. Most lipids and edible resins are soft-solids at room temperature and show characteristic phase transition temperatures. Films or coatings made from lipids have very high water resistance and low surface energy, due to their hydrophobic nature. Lipids are generally applied in thin layers or as a composite with a polymeric matrix. Lipids can be combined with other film-forming materials, such as proteins or polysaccharides, as emulsion particles or as multilayer coatings in order to increase the resistance to water penetration (Greener and Fennema 1989; Greener and Fennema 1992; Baldwin et al. 1997; Gennadios et al. 1997; Perez-Gago and Krochta 2002; Perez-Gago and Krochta 2005).

Plasticizers: The structures of films containing polysaccharides and proteins are often brittle and stiff due to extensive interactions between the polymer molecules (Krochta 2002). The film-forming mechanisms of biopolymers include intermolecular forces such as covalent bonds (e.g., disulfide bonds and cross-linking) and/or electrostatic, hydrophobic, or ionic interactions. The addition of plasticizers overcomes this film brittleness and improves flexibility and extensibility. Plasticizers are low molecular weight agents incorporated into the polymeric film-forming material; the plasticizer positions itself between the polymer molecules and interferes with the polymer-polymer interaction, increasing the flexibility and processability of the material (Guilbert and Gontard 1995). Plasticizers must be compatible with the film-forming polymer; they reduce the intermolecular forces and increase the mobility of polymer chains. Plasticizers increase the free volume of polymer structures or the molecular mobility of polymer molecules (Sothornvit and Krochta 2000, 2001), decreasing the ratio between the crystalline and the amorphous regions, and decreasing the glass transition temperature (T_g) of the polymer (Krochta 2002; Guilbert and Gontard 2005). Most plasticizers are very hydrophilic and hygroscopic; they attract water molecules and form a large hydrodynamic plasticizer-water complex. Hydrophilic compounds, such as polyols (glycerol, sorbitol, and polyethylene glycol) are commonly used as plasticizers in hydrophilic film formulations.

Functional additives: This group includes antioxidants, antimicrobials, nutrients, nutraceuticals, flavors, and colorants, which can be combined with film-forming biopolymers to modify the functionality of films or coatings. The most beneficial characteristics of edible films and coatings are their edibility and inherent

biodegradability (Guilbert et al. 1996). To maintain edibility, all film components (i.e., biopolymers, plasticizers, and other additives) should be food-grade ingredients and all process facilities should be acceptable for food processing; solvents used should be restricted to water and ethanol.

27.3 Application and Distribution of Edible Coatings on the Food Surface

The application and distribution of the film-coating material in a liquid form can be achieved by hand spreading with a paint brush, spraying, falling film enrobing, dipping and subsequent dripping, and distribution in a revolving pan (pan coating), etc. (Guilbert 1986). Edible coating formulations must be wet when spread on the food's surface; upon drying the formulation must form a film coating with adequate adhesion, cohesion, and durability to function properly.

Different tests can be performed on the filmogenic suspensions before the coating is applied on a foodstuff. Rheological analysis and viscoelastic properties of the suspensions help to determine the suitability of the food coating method (immersion, spraying, etc.). Rheological behaviors (flow curves) are normally evaluated using viscometers; oscillatory rheometers allow measurement of the viscoelastic parameters of the film-forming suspension (García et al. 2004b, 2006; Lopez et al. 2008).

Some negatively charged gums, such as alginate, pectin, and CMC, show significantly different rheological properties in acidic conditions as opposed to neutral or alkaline conditions. Rheological behavior and surface tension of the film-forming suspension are important factors linked to suspension spreadability and coating adhesion capacity. A decrease in the surface tension of the filmogenic suspension leads to a better coating adhesion to foodstuffs. The peel or surface of many vegetables has low surface tension for protection purposes; however, this natural advantage is a drawback in the case of aqueous coating applications. The properties of the edible coating depend on the type of film-forming materials and especially on their structural characteristics (Han and Gennadios 2005).

Cohesion is the attractive force between the molecules of the same substance; it depends on the structure of the polymer, the molecular length, geometry, and molecular weight distribution, and on the type and position of the lateral groups. Cohesion of film-forming materials influences the mechanical strength of the films (Guilbert et al. 1996). If the film-forming material contains different components that are not compatible with the main biopolymers, the cohesion decreases and film strength weakens. Plasticizers reduce the cohesion of film-forming polymers.

Adhesion of film-forming materials is an important parameter for film casting and coating processes (Guilbert and Gontard 2005). Adhesion is an attractive force between the surface molecules of coating materials and food surfaces. A low

adhesion force leads to an incomplete coating on the food surface. A large difference between the surface energy of a coating material, and the uncoated product surface, results in a poor coating performance. Surface active agents, such as emulsifiers in the film-forming solution, reduce the surface tension of the coating solution; then the difference between the solid surface energy and the surface tension of the coating solution decreases, increasing the work of adhesion (Cuq et al. 1995; Guilbert and Gontard 2005).

27.4 Edible Coating Characteristics as Related to Polymer Structure and Physico-chemical Properties

The physical and chemical characteristics of the biopolymers greatly influence the properties of resulting films and coatings. An edible film is essentially a dried and extensively interacting polymer network of a three-dimensional structure. The film-forming mechanisms of biopolymers include intermolecular forces such as covalent bonds (e.g., disulfide bonds and cross-linking) and/or electrostatic, hydrophobic, or ionic interactions. It is important to determine the relationship between the polymer structural chemistry and the physico-chemical and mechanical properties of the film or coating. Several techniques can be used to characterize the structure of the biopolymers forming the coatings, such as scanning electron microscopy (SEM), X-ray diffraction, differential scanning calorimetry (DSC), thermal mechanical analysis (TMA), dynamic mechanical thermal analysis (DMTA), and Fourier transform infrared spectroscopy (FTIR), etc. The main properties of a coating are as follows: moisture and gas permeation (barrier properties), water vapor sorption isotherms, optical attributes (light transmittance, color), thermoplastic characteristics, crystallinity, mechanical properties of the film (strength, elasticity), and film solubility in water and oil.

The optical properties impact the surface appearance of coated foods. Surface film color is generally measured using a colorimeter and opacity is determined by spectrophotometry. Film opacity is a critical property of a food coating; it can be measured using the method proposed by Gontard et al. (1992), in which the absorption spectrum is recorded in the visible range. The opacity is estimated as the area below the absorption curve; this area has a very low value for transparent films. The color, shininess, and transparency of edible films and coating layers vary significantly depending on the chemical composition and the structure of the polymer used. For example, the color stability of whey protein isolate (WPI) coatings is affected by Maillard reactions (produced by milk proteins during storage), causing yellowing.

The water sorption isotherms of the coatings can be measured on films formed under standard conditions. They are useful to estimate stability at different ambient conditions, mainly because the hydrocolloid film properties are highly dependent

on relative humidity (RH). The presence of plasticizers, such as glycerol or sorbitol increases the hygroscopic characteristics of the films.

Microstructure characterization of the coatings helps to understand the performance of the different formulations. Light microscopy observation (stereomicroscopy) is used to analyze coating thickness and uniformity; SEM permits evaluation of film homogeneity, the presence of different layers, pores, and cracks, and the smoothness of the coated surface. FTIR is a useful technique for composite film microstructure characterization since it allows evaluation of interactions and compatibility between the components (Lacroix and Le Tien 2005), and permits identification of the functional groups in the polymers after modifications.

The spectral regions 3,300–3,000 cm^{-1} are generally used for elucidation of the free or interacting hydroxyl groups; 2,950–2,850 cm^{-1} for alkyl (-CH_2-) chains; at 1,750–1,650 cm^{-1} the bands represent carbonyl groups and amides bands. Pinotti et al. (2007) applied FTIR spectrometry to determine the possible interactions between chitosan and MC composite systems.

X-ray diffraction patterns of the films are characterized by sharp peaks associated with the crystalline fraction and amorphous zones. The amorphous fraction of the sample can be estimated by the area between the smooth curve, drawn to follow the scattering hump, and the baseline joining the background within the low- and high-angle points; the crystalline fraction can be estimated by the upper region above the smooth curve. X-rays can also detect the recrystallization process during storage, such as retrogradation in starch-based films and coatings (García et al. 2000b; Mali et al. 2002, 2006)

Glass transition is a reversible change that takes place in the polymer between the rubbery and glassy states; the temperature at which it occurs is the T_g. The properties of amorphous or semicrystalline materials are seriously modified when the temperature of the compounds rises above T_g. Generally, fully amorphous bioplastic applications are limited by the fact that T_g of a polymer is highly affected by the RH (especially for hydrophilic polymers). Below T_g the material is rigid, and above T_g, it becomes rubbery and visco-elastic (Guilbert and Gontard 2005). Below T_g, weak and non-cooperative local vibrations and rotation movements of the molecules are possible; above T_g, strong and cooperative movements of whole molecules and polymer segments can be observed. The knowledge of T_g is important since it determines both the mechanical and barrier properties (Mali et al. 2005, 2006). DSC and DMTA techniques can be used to determine T_g. DMTA is considered the most sensitive method for measuring the T_g of a material. In DMTA, an oscillating strain is applied to a sample and the resulting stress developed in the sample is measured. The output signals are analyzed, and, using established mathematical methods, the rheological parameters are also computed. The ratio of viscous modulus (E'') to elastic modulus (E') is the tangent of the phase angle shift between the stress and strain vectors ($E''/E' = \tan \delta$); it measures the damping ability of the material. The glass transition of a film is detected as a sudden and marked decrease in the elastic modulus E´ and a peak in the tan delta curve as temperature increases. Plasticization decreases the intermolecular forces between polymer chains, and reduces T_g.

27.5 Barrier Properties

The quality of most food products deteriorates from moisture absorption, O_2 invasion, flavor loss, undesirable odor absorption, and migration of packaging components into the food (Kester and Fennema 1986; Debeaufort et al. 1998; Miller et al. 1998; Krochta 2002). These mass transfer phenomena can occur between the food and the environment, the food and packaging materials, or among heterogeneous ingredients in the food product itself (Krochta 1997). The diffusion of atmospheric O_2 into foods causes oxidation of food ingredients; dried foods can absorb moisture from the environment or from other wet zones in the food, leading to the loss of crispness. Edible films and coatings may be used to wrap these food products or located between the heterogeneous parts of food products to prevent migration phenomena and to preserve quality (Guilbert et al. 1997; Krochta 2002).

To characterize the barrier properties of edible films and coatings, the transmission rates of specific migrants should be determined using stand-alone edible films (McHugh and Krochta 1994). Most of the research on this subject reports the water vapor, O_2, CO_2 and flavor permeabilities, and oil resistance of edible films. However, barrier properties of films and coatings determine their applicability to improving the storage life of different products. Permeability depends not only on the diffusion coefficient but also on the solubility of permeants in the system. Barrier properties are strongly related to film structure since permeants are moved through the amorphous zone. Film formulation, especially with the addition of plasticizers, affects both the barrier and mechanical properties because these properties modify film structure, chain mobility, and diffusion coefficients of permeants.

27.5.1 Water Vapor Permeability

Water vapor permeability (WVP) determinations can be performed using commercial instruments; in addition, many researchers applied the ASTM (1995) method E96 with the modifications introduced by Gennadios et al. (1994). In this method the film sample is sealed over a circular opening of known area in a permeation cell that is stored at constant temperature in a dissecator. Anhydrous calcium chloride or silica gel (0% RH) is placed inside the cell and a saturated solution (constant RH) is used in the dissecator; thus water vapor transport is determined from the weight gain of the permeation cell (García et al. 1999, 2000a, 2004b, 2006; Romero-Bastida et al. 2005).

Synthetic moisture-barrier films such as low-density polyethylene (LDPE) show low values of WVP $= 9.14 \times 10^{-13}$ g m^{-1} s^{-1} Pa^{-1} in comparison with polysaccharides and proteins, which are polymeric and hydrophilic by nature and poor moisture barriers. The WVP permeabilities of proteins, such as gluten and zein plastified with glycerol, range between 7.00×10^{-10} and 8.90×10^{-10} g m^{-1} s^{-1} Pa^{-1}.

Lower WVP values were reported for several polysaccharides; sorbitol plastified yam starch (3%) and corn starch (2%) films have WVP values of 1.50×10^{-10} and 1.75×10^{-10} g m^{-1} s^{-1} Pa^{-1}, respectively (Mali et al. 2002, 2004, 2006). Films of MC (1%) and Chitosan (1%) have WVP values similar to that of cellophane ranging between 7.55×10^{-11} and 9.03×10^{-11} g m^{-1} s^{-1} Pa^{-1} (Pinotti et al. 2007).

It is important to remark that edible films made of proteins and polysaccharides have low water-vapor barrier properties, with WVP values at one and two orders of magnitude higher than that of LDPE; therefore, they can only be used as protective barriers to limit moisture exchange in short-term applications. However, these edible films can be of considerable value for numerous processes, as in the case of modified atmosphere packaging of fresh, minimally processed or fermented foods (fish, meat, fruits, vegetables, and cheeses).

Lipids or waxes for edible applications show better water-vapor barrier properties than starch or protein-based materials do, but they still have significantly lower water-vapor barrier properties than most synthetic plastic films; WVP values ranging between 2.75 and 3.1×10^{-12} g m^{-1} s^{-1} Pa^{-1} were reported for beeswax and carnauba wax (Shellhammer and Krochta 1997; Perez-Gago and Krochta 2005).

Lipid compounds, such as animal and vegetable fats (natural waxes and derivatives, acetoglycerides, surfactants, etc.), could be proposed as components of edible coatings given their excellent moisture-barrier properties; however, they can cause textural and sensory problems due to oxidation and a waxy taste; further, their nonpolymeric nature limits the ability to form cohesive films (Perez-Gago and Krochta 2005). The addition of lipids to polysaccharide-and protein-based films decreases WVP due to hydrophobicity; this is an important property in the case of fresh fruits and vegetables because composite coatings retard moisture loss and shriveling in fresh products.

27.5.2 Gas Permeabilities

CO_2 and O_2 barrier properties are important in understanding the quality and physiological aspects of coated food during storage and determine food coatings applications. Gas permeability is commonly measured on isolated films. O_2 permeability can be measured using available commercial equipment; moreover, CO_2 and O_2 permeability of films can be assessed by the accumulation method in a specially designed cell (García et al. 1999, 2000b; Bifani et al. 2007). This quasistatic method was based on measuring the amount of gas diffusing through a film, quantified by gas chromatography.

García et al. (1999) measured gaseous permeabilities to O_2 (PO_2) and CO_2 (PCO_2) for different starch-based films; values of $PO_2 = 5.69 \times 10^{-9}$ cm^3 $m^{-1}s^{-1}$ Pa^{-1} and $PCO_2 = 0.248 \times 10^{-9}$ cm^3 m^{-1} s^{-1} Pa^{-1} were reported for corn starch films plasticized with glycerol. All tested starch-based films, plasticized with either glycerol or sorbitol, showed higher gas permeability to CO_2 than O_2, with a ratio of permeability (PCO_2/PO_2) ranging between 8 and 10 (selectivity

coefficient). These results can be attributed to a higher solubility of CO_2 than O_2 in the coatings (McHugh and Krochta 1994). Synthetic materials such as LDPE have lower selectivity coefficients between CO_2 and O_2 (around 4) compared to an average ratio of 9 in the case of starch-based films (Cuq et al. 1998; García et al. 1998ab; Park 1999). Cuq et al. (1995) compared the CO_2 to O_2 permeability ratio for several synthetic and edible films and reported that edible films show higher selectivity than synthetic ones, with ratios in the range of 8–30. Very high gas selectivity is particularly interesting for modified atmosphere packaging of cheeses (to control proliferation of microflora), and for fresh fruits and vegetables (to control respiration rates).

Gas permeability is strongly related to crystallinity of polymeric chains, where in general, the higher the degree of crystallinity, the lower the permeability. As for synthetic materials, gas and vapor permeabilities depend on several factors, such as the ratio between crystalline and amorphous zones, polymeric chain mobility, and specific interactions between the functional groups in the polymers and gases in the amorphous zones. Permeability increases with a decreasing crystalline-amorphous ratio because permeation occurs through the amorphous zones of the film.

Starch and proteins have gas-barrier properties in dry conditions, especially against O_2. For example, the O_2 permeability of a wheat gluten film was 800 times lower than that of LDPE. However, O_2 permeability is very sensitive to RH (Guilbert et al. 1997). At higher RH conditions, O_2 permeability increases significantly; thus, it is important to maintain low RH in the environment to maximize the effectiveness of edible films as gas barriers. Values of the selectivity coefficient between CO_2 and O_2 ranging between 4 and 35 were reported by Gontard et al. (1996); this selectivity coefficient is very sensitive to moisture and temperature for gluten films, whereas for synthetic polymers it remains relatively constant ranging between 4 and 6 (Guilbert and Gontard 2005).

27.6 Composite Film Formation

Composite films and coatings can be formulated to combine the advantages of each component. Biopolymer composites can modify film properties and create film structures for specific applications (Wu et al. 2002). A composite film that combines lipids and hydrocolloids can be produced as either a bi-layer or a stable emulsion. In bi-layer composite films, the lipid forms a second layer over the polysaccharide or protein layer. In emulsion composite films, the lipid is dispersed and entrapped in the supporting matrix of protein or polysaccharide (Perez-Gago and Krochta 2005). The emulsifying character of proteins makes them appropriate for this technique; however, in the case of polysaccharides, the addition of an emulsifier is required to improve emulsion stability. Emulsion preparation parameters, such as stirring velocity and emulsifier addition are important factors in obtaining homogenous films and coatings, since they determine emulsion stability.

27.7 Examples of Coating Applications

In general, an ideal coating should be safe, unperceived by the consumer, have no off-flavor and taste, be a desirable moisture and gas barrier, and have a certain mechanical strength. Many factors determine the success of edible coatings in improving the quality and extending the shelf-life of foods. Factors such as chemical composition, structure, methods used to form the films or coatings, storage conditions, and properties of the food itself (maturity stage in the case of fruits and vegetables, moisture and lipid content, etc.) are all important. When applying edible films and coatings, these factors have to be carefully considered (Zhao and McDaniel 2005).

Quality maintenance and product enhancement are significant functions of edible films and coatings (Krochta 1997). They can retard surface dehydration, moisture absorption, oxidation of ingredients, aroma loss, frying oil absorption, ripening/aging, and microbial deterioration of food products. In addition to the physical and chemical quality enhancements, edible films and coatings contribute to visual quality, surface smoothness, flavor carriage, edible color print, and other marketing-related quality factors. Edible films and coatings may be used to preserve the quality of several food commodities. The O_2-barrier property of films and coating layers can prevent oxidation of lipid ingredients, colorants, and flavors of food products such as nuts, confectionary, and fried foods (Baldwin et al. 1997). This property is also used to retard the respiration rate of fruits and vegetables (Baldwin et al. 1995). Many climacteric fruits and vegetables can be coated with edible film-forming materials to slow down their respiration rate (Park 1999; Amarante and Banks 2001).

High-fat meat and fish products, such as sausages and fillets, can be protected from oxidation using O_2 barrier edible coatings. Moisture loss is the most critical quality degradation factor in fresh produce (Guilbert et al. 1997). Moisture-barrier properties of edible films and coatings can protect fresh fruits and vegetables from dehydration. The moisture-barrier property can also be utilized to prevent moisture migration between heterogeneous food product ingredients, for example between raisins and breakfast cereals (Kester and Fennema 1986), pie fillings, and crusts, etc. Different materials used in edible-coating formulation have been reported in literature (Kester and Fennema 1986; Gennadios and Weller 1990; Krochta et al. 1994; Krochta and De Moulder Johnston 1997; Debeaufort et al. 1998; Zhao and McDaniel 2005; Lin and Zhao 2007).

Some selected examples are listed below:

- Wheat gluten, whey proteins, corn zein, waxes (beeswax, carnauba, candelilla), cellulose derivatives and pectins for fruits, grains, and vegetables as O_2 and moisture barriers
- Waxes or fatty acids on fruits and vegetables to delay spoilage and to reduce water loss and, on cheeses, to prevent mold growth

- Gelatin, seaweed, and pectinate to eliminate dripping, and as moisture barriers on cheese, ice cream, and yogurt
- Corn zein, milk and whey proteins, waxes, and methyl cellulose in confections
- Cellulose derivatives on fried foods to reduce oil absorption
- Gelatin, carrageenan and alginate, whey protein, collagen, casein, and cellulose derivatives on poultry, beef, fish and seafood
- Acetylated monoglyceride and whey protein on frozen salmon to reduce moisture loss and lipid oxidation
- Casein, xanthan gum on peeled carrots to reduce dehydration and white blush formation
- Chitosan on strawberries to delay spoilage, and on tomatoes, to extend shelf-life
- Cellulose, chitosan, and sodium caseinate on bell peppers to reduce O_2 and CO_2 permeability
- Starch in coated prunes, strawberries, and nuts to prolong storage life
- Dextrin on apples to delay oxidative browning
- Corn zein on tomatoes to delay color changes and loss of firmness
- Wheat gluten, cellulose, soy protein, and whey protein applied individually on egg shells to improve shell strength and to reduce microbial contamination
- Starch, corn zein, whey protein, and acetylated monoglyceride on nuts to delay rancidity
- Soy protein on apples to retard changes in firmness and color
- Chitosan-based coatings to reduce drip loss on frozen-thawed raspberries
- Alginate on fresh meat, poultry, and precooked ground pork to reduce shrinkage, oxidative rancidity, moisture migration, and oil absorption
- Mixtures of stearic-palmitic acids and hydroxypropyl cellulose, and MC and palmitic acid coatings, as moisture barriers for heterogeneous foods (puree, cake, ice cream cones)

27.8 Incorporating Functional Ingredients into Edible Films and Coatings

A unique feature of edible films and coatings is their capacity to carry many functional ingredients, including antioxidants, antimicrobial agents, flavorings, and colorants. Integration of these ingredients can enhance food stability, quality, functionality, and safety. For instance, food microbial stability can be improved using edible-active layers, which act as surface-retention agents to limit the diffusion of food additives into the food core; these layers can be used with simultaneous treatments such as controlled atmosphere and refrigeration. In another example, high concentration of a chemical preservative incorporated into an edible coating may allow a decrease in the total amount of the preservative in the food, attaining similar performance.

27.8.1 Antioxidant Edible Coatings

Antioxidants, such as tocopherol and butylated hydroxytoluene (BHT) were integrated into edible coatings to inhibit lipid oxidation in precooked beef patties and fish muscle, respectively (Zhao and McDaniel 2005). The antioxidant effects of ascorbic acid in whey protein film coatings applied on roasted peanuts for the control of lipid oxidation were also studied by Min and Krochta. (2007). By measuring the peroxide values and the thiobarbituric acid reactive substances, it was shown that the addition of ascorbic acid to the coating retarded lipid oxidation in peanuts.

27.8.2 Antimicrobial Edible Films

The concept of active packaging was introduced with antimicrobial films and coatings. Edible films can serve as carriers of antimicrobials to extend product shelf-life and to reduce the risk of pathogen growth on food surfaces. Edible films have been developed that can reduce, inhibit, or delay the growth of microorganisms on the surface of coated foods. Excellent reviews on antimicrobial edible films have been published by different authors (Han 2000, 2002, 2003a, b; Franssen and Krochta 2003; Cagri et al. 2004).

Chitosan: A polysaccharide obtained by deacetylation of chitin, chitosan originates from crustacean exoskeleton and fungal cell walls. It has been widely used in antimicrobial films and coatings due to its property of inhibiting the growth of many pathogenic bacteria and fungi. In some fungi, chitosan can alter membrane functions by interacting with the strongly electronegative microbial surface, leading to changes in permeability, metabolic disturbances, and eventually death.

Natural preservatives: There has been a tendency in the last several years to use natural preservatives in edible-coating formulations. Some of the most commonly used preservatives and antimicrobials are:

- Organic acids (acetic, benzoic, lactic, propionic, sorbic)
- Parabens (methyl paraben)
- Fatty acid esters (glyceryl monolaurate)
- Polypeptides (lysozyme, peroxidase, lactoferrin, nisin)
- Nitrites (potassium nitrite, sodium nitrite)
- Sulfites (potassium sulfite, sodium sulfite)
- Natural preservatives (essential oils, spices, extracts such as cinnamon, sage, allicin, and liquid smoke)
- Other preservatives (atamycin, EDTA)

These agents can be used in protein-, polysaccharide-, and lipid-based edible coatings and films.

Benzoic acid and sodium benzoate: These two are among the first chemical preservatives permitted in foods by the Food and Drug Administration. Benzoic acid (pKa = 4.20) and sodium benzoate are generally regarded as safe preservatives at levels up to 0.1%. Sodium benzoate and benzoic acid are inhibitory to mold, yeast, and pathogenic and psychrotrophic spoilage bacteria. Sodium benzoate is one of the most commonly used antimicrobials in edible films because it is soluble in most film solutions and remains active after film preparation. Organic acids are more effective in the undissociated form and, therefore, the antimicrobial activity is related to pH. At pH = 4.0, 60% of benzoic acid is undissociated (Cagri et al. 2004).This antimicrobial can be incorporated into MC, collagen, and chitosan films, all of which have a relatively low pH. Edible films containing benzoic acid and its sodium salt are adequate for acidic foods like cheeses and fermented meat products.

Sorbic acid: This is a straight chain unsaturated monocarboxylic acid; the carboxyl group reacts to form calcium, sodium, or potassium salts. Potassium sorbate is highly soluble in water (58.2% at 20°C). Edible films containing potassium sorbate are most effective at pH < 6.0. Sorbic acid salts were widely used as antimicrobial agents in carbohydrate- and protein-based edible films formulated with MC, WPI, and chitosan. Films containing sorbates have been tested against spoilage bacteria, pathogenic bacteria, yeasts, and molds in laboratory media.

Propionic acid: This acid is commonly used as a food preservative because of its wide spectrum of activity. Propionic acid, which is a monocarboxylic acid, is produced by *Propionibacterium freudenreichii subsp. shermanii*. Antimicrobial activity of propionates is also pH dependent. Although this acid is primarily active against molds, some yeasts and bacteria are also inhibited. The amount of propionate used in foods is generally less than 0.4% (Cagri et al. 2004).

Parabens: Produced by esterification of the carboxyl group of benzoic acid, most parabens are active at pH 3.0–8.0. The methyl, propyl, and heptyl parabens can be used as food preservatives in most countries. Parabens can also be used effectively in a wide range of foods; they are generally more active against molds and yeasts than bacteria. For complete inhibition of bacteria and fungi, concentrations of esters of p-hydroxybenzoic acid ranging between 0.033 and 1.0 mg/L are necessary (Cagri et al. 2004).

Free fatty acids: Low concentrations of long-chain fatty acids are inhibitory to microorganisms, especially gram-positive bacteria and yeasts. Saturated fatty acids with chain lengths of C12 to C16 and C10 to C12 have the most antimicrobial activity against bacteria and yeasts, respectively (Cagri et al. 2004). Fatty acids are more active at low pH (5.0), and both fatty acids and monoglycerides are inhibitory to many bacterial species. Monoesters of glycerols and esters of sucrose are more antimicrobial than their corresponding free acids.

Acetic acid and sodium diacetate: Both are active against various spoilage and pathogenic bacteria and have been used in many foods. Like other organic acids, acetic acid can be used to acidify edible coatings containing chitosan, alginate, collagen, and WPI.

Lactic acid: This acid is used for improving and controlling the quality and microbial stability of foods. Lactic acid sprays (1–3% solutions) have been widely

used to sanitize meat carcass surfaces, with gram-negative psychrotrophs generally being more sensitive to treatment than gram-positive organisms. Lactic acid can be used as an acidulant in chitosan and collagen films.

Nisin: The first bacteriocin used in the food industry, nisin is one of the most investigated bacteriocins in antimicrobial edible films. It is produced by fermentation using *Lactococcus lactis subsp. Lactis*. It was recognized as a safe biological food preservative by a joint FAO/World Health Organization commission on food additives in 1968, and accepted by the Food and Drug Administration in 1988. Nisin is a polycyclic peptide antibacterial with 34 amino acids residues. It is obtained commercially from natural substrates, including milk, and is not chemically synthesized. It inhibits gram-positive spoilage and pathogenic bacteria (*Listeria monocytogenes, Staphylococcus aureus, Clostridium botulinum*). Incorporation of nisin into packaging materials inhibits the growth of gram-positive bacteria but does not inhibit gram-negative bacteria such as *E. coli*.

Nisin can be incorporated into the film suspension or applied directly to the film surface after casting. Various nisin-containing protein-based films (e.g., whey protein, corn zein, wheat protein, soy protein) have been assessed for antimicrobial activity against gram-positive bacteria such as *L. monocytogenes* and lactic acid bacteria (Cagri et al. 2004).

Pediocins: Produced by *Pediococcus acidilactici*, this group of bacteriocins can be used in edible films and coatings because of their wide spectrum of antimicrobial activity and effectiveness over a wide range of pH values and temperatures. Antimicrobial activity of pediocin is retained at 100°C, decreasing at 121°C, and is most evident at pH values between 4 and 7, with substantial losses at pH 3 and 9. Pediocin remains active following treatment with lipase, phospholipase C, lysozyme, DNase, or RNase, but its activity is destroyed by protease, papain, and a-chymotrypsin (Cagri et al. 2004).

Lysozyme: This enzyme is found in egg whites, human tears, and other secretions. It is responsible for breaking down the polysaccharide walls of many kinds of bacteria and thus it provides some protection against infection. The enzyme is formed by 129 amino acids cross-linked by four disulfide bonds. Dried egg white, the commercial source for lysozyme, contains about 3.5% lysozyme. It is heat stable (100°C) at pH 5.3 but inactivated at lower temperatures when pH is increased. Lysozyme is most active against gram-positive bacteria (Cagri et al. 2004).

Spices, herbs, and essential oils: Essential oils are responsible for the odor, aroma, and flavor of spices and herbs. These compounds can be added to edible films to modify flavor, aroma, and odor and to introduce antimicrobial properties. Films containing these ethanol-soluble compounds show activity against both gram-negative and gram-positive bacteria. Essential oils (cardamom, cinnamon, cloves, coriander, garlic, nutmeg, oregano, parsley, rosemary, sage, thyme, etc.) are inhibitory to various spoilage or pathogenic bacteria, molds, and yeasts. However, the use of these oils as food additives is limited due to their strong flavor.

Lactoferrin (lactotransferrin): This iron-binding glycoprotein is present in bovine milk. It inhibits the growth of some bacteria; however, other bacteria with

low iron requirements, such as lactic acid bacteria, are not inhibited by lactoferrin. *Pseudomonas fluorescens, Enterococcus faecalis, and Bifidobacterium bifidum* strains are highly resistant to this peptide. The mode of action of lactoferrin has not been fully elucidated, but presumably it alters membrane permeability because of its cationic nature.

Liquid smoke: Used in processed meats, sausages, and cheeses, liquid smoke contains phenols and acetic acid, which are bactericidal at relatively low concentrations. It can inactivate common food-borne pathogens, including *E. coli, Salmonella, Staphylococcus aureus*, and *L. monocytogenes*. It is generally very acidic and has antimicrobial, antioxidant, and flavor properties, making it a potentially attractive edible coating additive. However, incorporation of liquid smoke has only been studied for edible collagen casings.

Cha and Chinnan (2004) reviewed important aspects of biopolymer-based antimicrobial packaging. The incorporation of several antimicrobial agents (EDTA) and grapefruit seed extract into films, made of Na-alginate and K-carrageenan, produced a strong inhibition against *Micrococcus luteus, L. innocua, Salmonella enteritidis, E. coli,* and *S. aureus*; sodium alginate-based films, with the addition of nisin, lysozyme, and EDTA, showed the strongest inhibition against the same bacterial strains. Chitosan films containing nisin showed a high antimicrobial activity against *M. luteus*. Whey protein film coating was used as a vehicle for combining antimicrobials (grape seed extract, nisin, malic acid, and EDTA) (Cha and Chinnan 2004).

The primary advantage of antimicrobial edible films is that the inhibitory agents in these films can be specifically targeted to postprocessing contaminants on the food surface. It is important to predict and control the preservative release (Torres and Karel 1985; Torres et al. 1985; Redl et al. 1996).The diffusion rate of the antimicrobial into the product is partially controlled by agents incorporated into the film. The edible film matrix entraps the antimicrobial and decreases its diffusion during storage; thus, lower levels of preservative addition would be needed in an edible coating to achieve a targeted shelf-life, as compared to spraying the antimicrobial on the surface.

Controlling the antimicrobial release from edible films is very important; therefore, measurement of the diffusion coefficients of the antimicrobials in edible films should be carried out under controlled conditions (Vojdani and Torres 1990; Brody et al. 2001; Min et al. 2008). While antimicrobial coatings may extend the shelf-life and protect food products, it must be emphasized that such advantages are never substitutes for proper handling, storage, and good manufacturing practices.

27.8.3 Edible Coatings as Carriers of Nutraceutical Ingredients

There is an increasing consumer interest in the health-enhancing roles of specific foods and physiologically active food components (nutraceuticals or functional foods). Edible coatings could provide an excellent way to enhance the nutritional

value of foods by carrying nutrients or nutraceuticals that are lacking, or present in low quantities (Mei and Zhao 2003; Park and Zhao 2004; Park 2004). Zhao and Mc Daniel (2005) integrated high concentrations of minerals and vitamins into edible films and coatings.

Mei et al. (2002) developed xanthan gum coatings containing a high concentration of calcium and vitamin E, and applied such coatings to fresh baby carrots. Han et al. (2004) applied chitosan coatings with high concentrations of calcium or vitamin E on fresh and frozen strawberries and red raspberries.

27.9 Edible Coatings to Improve Quality and Extend Shelf Life of Foods - Case Studies

27.9.1 Edible Coatings Acting as Oil Barriers in Fried Products

One of the applications of coatings is to reduce the OU of products during deep-fat frying (Balasubramaniam et al. 1997). The excess of fat in the diet has been linked to coronary heart disease; thus, coatings applied to food before frying can help reduce health problems associated with fat consumption. Frying occurs during the immersion of the product in oil at temperatures higher than the boiling temperature of water (150–200°C). Deep-fat frying is a complex process involving simultaneous heat and mass transfer (Bertolini Suarez et al. 2008)

Various hydrocolloids, especially cellulose derivatives, can be used as edible coatings to decrease oil content during frying. Williams and Mittal (1999) found that MC films showed the best barrier properties, reducing fat uptake more than hydroxypropylcellulose and gellan gum films. Cellulose derivatives, including MC and HPMC exhibit thermal gelation. When suspensions are heated a gel is formed that reverts back below the gelation temperature, and the original suspension viscosity is recovered. MC forms a gel at high temperatures; hydrophobic polymer chain interactions are involved in the thermal gelation process with a predominance of intermolecular hydrogen bonding over intramolecular hydrogen bonding within the cellulose ether. Extensive research on edible coatings from cellulose derivatives was carried out in our laboratories (García et al. 2002, 2004a; Bertolini Suarez et al. 2008). The objectives of the experiments were to analyze the coating performance in reducing OU in French fries and fried pastry.

Aqueous suspensions of 1% Methocel A4M (based on MC), 2% K100LV, and 2% E15LV (based on MC and HPMC), with and without sorbitol (0.25–1%), were used for coating applications. The rheological behavior of the suspensions and the viscoelastic moduli were measured with an oscillatory rheometer. MC suspensions were selected for coating application because they showed the highest elastic (G') and complex (G^*) moduli.

Model dough discs (60 mm dia. and 7 mm thick) were prepared with refined wheat flour and distilled water. Samples were dipped in coating suspensions for 30 s

and drained. Coated and uncoated samples were fried in sunflower oil under controlled temperature conditions (160 ± 0.5°C, previously determined by a sensory panel). Surface color (lightness and chromaticity parameters), firmness (instrumental texture analysis), and OU of the control and coated fried samples were measured at different frying times.

During frying of both the coated and uncoated samples a moving boundary was produced within the product, separating the dehydrated zone from the wet core (Fig. 27.1). A protective layer (approximately 15 μm thick) was formed on the surface of the coated samples during the initial stages of frying, due to MC thermal gelation above 60°C; the coating was becoming dehydrated and remained attached to the surface of the product. SEM observations showed the integrity of the MC layer and good adhesion of this coating to the fried product (Fig. 27.1); the addition of a plasticizer (sorbitol) in the coating formulation was necessary to achieve coating integrity and uniformity.

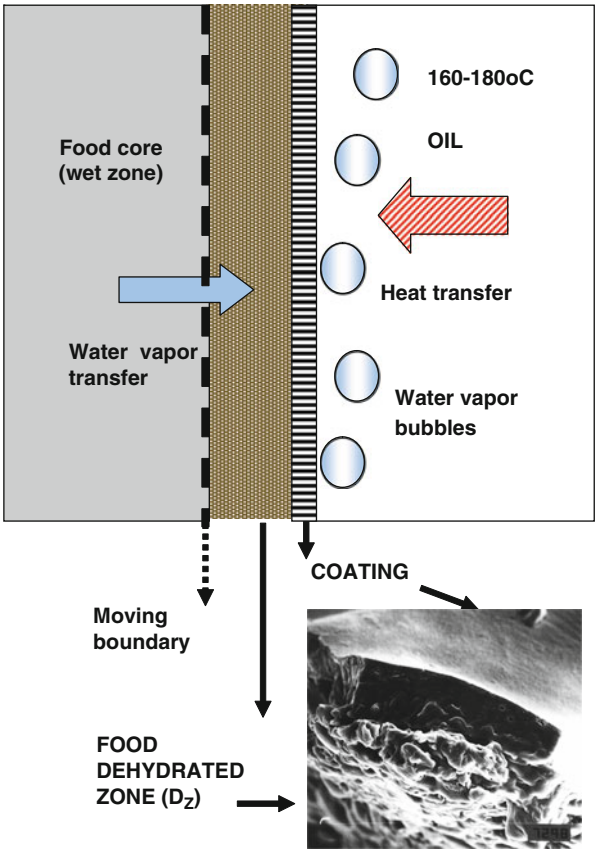

Fig. 27.1 Schematic description of frying process in a coated product, and scanning electron microscopy (*SEM*) micrograph of the methylcellulose coating applied on a fried dough sample

OU was determined by combining a preliminary batch extraction process with a semicontinuous extraction in a Soxhlet; the extracted lipid phases were analyzed by HPLC (García et al. 2002, 2004a). MC coatings (1% A4M and 0.75% sorbitol) were effective in decreasing oil content without affecting the water content of the samples (Bertolini Suarez et al. 2008); the OU in coated samples was 30% lower than in the uncoated ones at the final frying time (Fig. 27.2).

Concerning the quality attributes of the fried dough, differences between the instrumental color parameters and firmness values of coated and uncoated samples were not significant, during the frying process ($t < 720$ s); besides, the panelists could not distinguish the differences between the control and coated samples. These results demonstrate the effectiveness of the MC coating to reduce OU without affecting the sensory attributes of the samples (García et al. 2002).

The frying process was mathematically modeled (Bertolini Suarez et al. 2008) and experimentally validated; temperature profiles and water-content distributions were predicted by the model. Nonlinear-coupled energy and mass transfer partial differential equations, under unsteady state conditions, considering a moving boundary, were numerically solved considering both thermal and physical properties change with temperature and moisture content. The model simulated appropriately the experimental data of temperature and water content during the different frying stages.

Microstructural changes are produced during the frying process; the heat and mass transfer model predicted the position of the vaporization front and the thickness of the dehydrated zone (dZ) as a function of frying time (Fig. 27.2). In addition, water content correlated linearly with the vaporization front position corresponding to the thickness of the humidity core (Bertolini Suarez et al. 2008).

During frying the vapor leaves voids in the product and allows for the oil to enter later; OU is mainly produced when the product is removed from the frying medium.

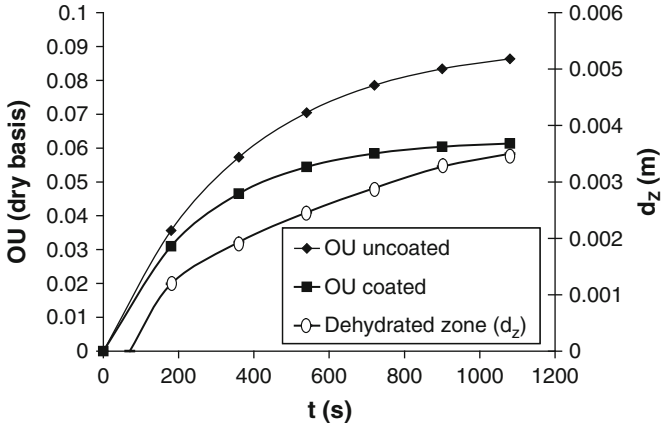

Fig. 27.2 Effect of methylcellulose coating on oil uptake in fried dough. The presence of coating decreases oil uptake. Oil uptake curve can be closely related to increase of dehydrated zone thickness (*dZ*)

OU is affected by the microstructure of the dehydrated zone and is dependent on the balance between the oil retained on the surface and the oil drained after retrieval of the product from the oil bath; the oil retained by the surface penetrates into the pores left by the water evaporation. The amount of oil retained at the sample surface is limited, due to the oil surface wetting, the property related to the interfacial tension that governs these phenomena. Figure 27.2 shows similar shapes for the OU curves (experimental data) and the thickness of the dehydrated zone (predicted values). From these results, OU was linearly correlated with the thickness of the dehydrated zone during the initial frying period (Bertolini-Suarez et al. 2008).

Other results obtained in our laboratory on using edible coatings to reduce OU during frying (4 min/180°C) showed a reduction of 40.6% in oil content of French fries (0.7 × 0.7 × 5 cm) using MC (1%) and sorbitol, without causing detrimental effects on the quality attributes (surface color and texture).

27.9.2 Starch-Based Edible Coatings to Prolong Storage Life of Refrigerated Highly Perishable Fruits

The strategies explored to extend postharvest life of fruits should consider several challenges, such as extending maturation and senescence periods, reducing dehydration, and reducing onset and rate of microbial growth. Edible films and coatings could offer solutions to all such challenges simultaneously, the use of which has been reported by several researchers for different vegetables and fruits (Drake and Nelson 1990; El Gaouth et al. 1991; Park 1999, 2003, Park et al. 2005). The use of coatings with selective permeabilities on fruits has also been shown to have an influence on fruit physiology in retarding ripening and postharvest metabolism, thus, extending the fruit's storage life (Baldwin 1994).

Edible coatings can be made from food materials regarded as GRAS, such as proteins, lipids, cellulose derivatives, starch, and other polysaccharides. Composite films can be formulated to combine the advantages of both lipid and hydrocolloid components (Guilbert 1986). In the case of fruit and vegetable conservation, the lipid component in coating formulation can serve as a good barrier against water vapor, while the hydrocolloid component can provide a selective barrier against O_2 and CO_2 and the necessary supporting matrix. The functional, organoleptic, nutritional, and mechanical properties of an edible film can be modified with the addition of various chemicals in minor amounts, such as plasticizers, antimicrobial agents, and lipids.

Strawberries (Fragaria × ananassa), a typical soft fruit variety, have high physiological postharvest activity that transforms them into a highly perishable fruit with a low period of commercialization, which is mainly limited by fungal infection. As a consequence, strawberries have short ripening and senescence periods, which makes coating this fruit a good alternative for extending storage life. In this case, the effect of adding plasticizer and lipid and antimicrobial agents to

starch-based coatings, on their performance, applied to strawberries is discussed (García et al. 1998a, b, 2001).

Strawberries (Fragaria × ananassa, cv Selva) at the commercial ripening stage (75% red color), grown on a local farm in greenhouses, were harvested and immediately treated. The strawberries were dipped in chlorinated water (0.25 g Cl_2/L), dried with air, dipped in coating suspensions, and dried again with air (1.2 m/s, 20°C and 84.8% RH). Uncoated fruit (control) was treated similarly, replacing immersion in starch suspensions with distilled water. Samples were stored in a cold chamber at 0°C and 84.8% RH.

Two different starches were used for coating formulations: commercial corn starch with 25% amylose and a high amylose corn starch; and amylomaize (Amylomaize VII, Amaizo, USA) with 65% amylose. Starches were cold-gelatinized using sodium hydroxide; suspensions were neutralized with H3P04. The gelatinization method was selected to comply with the dipping procedure for coating application, and the heat-sensitive characteristic of strawberries. Glycerol or sorbitol was added as plasticizer at a concentration of 20 g/L. Additionally, 2 g/L sunflower oil were added and emulsions were homogenized at 7,800 rpm. Potassium sorbate (2 g/L) and citric acid (to reach pH 4) were also included in the formulations as antimicrobial agents.

Rheological behavior of coating suspensions was analyzed. The suspensions showed pseudoplastic behavior ($n < 1$) and the Power law rheological model satisfactorily fit experimental data ($r^2 > 0.96$). Plasticizer and lipid addition to corn and amylomaize suspensions decreased the flow behavior index and increased the consistency index. Apparent viscosity of corn starch suspensions also decreased with plasticizer and lipid addition.

Microstructure characterization of the coatings contributed to understanding the performance of the different formulations. This characterization included light microscopy observation (stereomicroscopy) and SEM. The stereomicroscope was used to determine coating thickness (40–50 μm) and to check coating uniformity; coated samples were stained with iodine solution to improve coating visualization. Polarized light microscopy observations revealed that starch was totally gelatinized in the filmogenic suspensions (García et al. 1998a, b). SEM observations showed that plasticizer addition was necessary for film integrity, to avoid pores and cracks. Plasticized films containing lipid (Fig. 27.3b) exhibited smooth surfaces and a compact structure, thereby indicating the homogeneous dispersion of lipids in the film matrix (García et al. 1999, 2000a, b).

Modifications of the crystalline structure of films stored at 20°C and 63.8% RH were evaluated by DSC and x-ray diffraction, using Kα Cu radiation ($\lambda = 1.5418$ Å). X-rays detected the starch recrystallization process during storage. In the case of starch-based films, peak width slightly decreased and peak intensities increased with storage time, showing a tendency toward increase in crystallite size, which can be attributed to a slow recrystallization process (García et al. 2000b, 2001). In the case of starch coatings obtained by alkaline treatment, X-ray diffraction patterns showed that both corn and amylomaize films attained a common crystalline structure of higher stability with storage time, exhibiting an A-type starch pattern

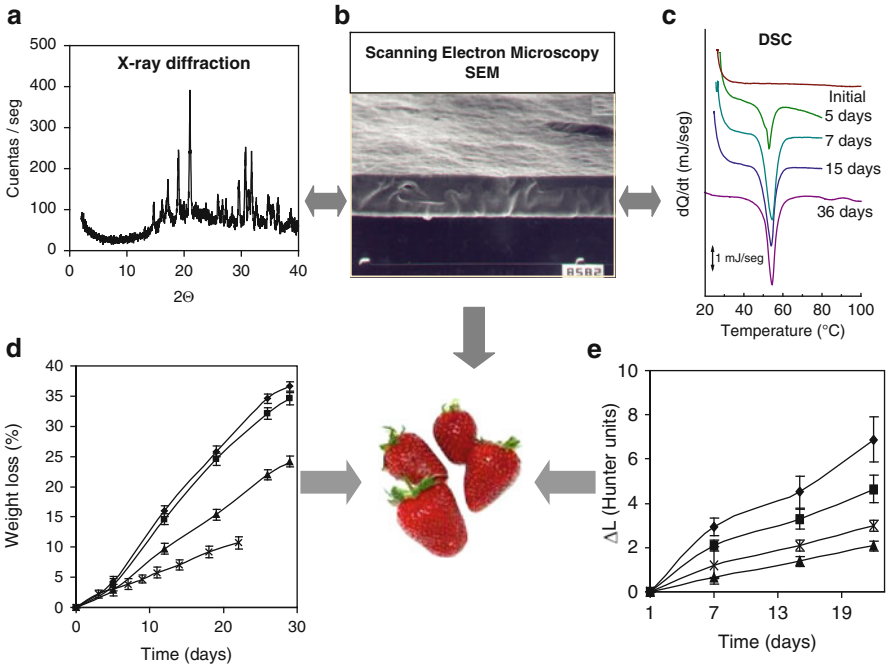

Fig. 27.3 Application of starch-based coatings to prolong storage life of refrigerated strawberries. (**a**, **b**, **c**) Coating characterization; (**a**) X-Ray diffraction pattern of amylomaize coating containing 20 g/L glycerol and 2 g/L sunflower oil; (**b**) SEM micrograph of corn starch-based films with 20 g/L sorbitol and 2 g/L sunflower oil. Magnification: 100 μm between marks; (**c**) DSC thermograms of amylomaize film stored at 20°C and 63.8% relative humidity. (**d**, **e**) Effect of coating formulation on quality parameters of refrigerated strawberries during storage at 0°C and 84% RH; (**d**) weight losses, (**e**) lightness differences. Control samples, uncoated fruits, (○); composition of coating formulation: (□) amylomaize without plasticizer; (Δ) amylomaize with 20 g/L sorbitol; and (◇) amylomaize with 20 g/L sorbitol and 2 g/L sunflower oil. *Bars* indicate standard errors

(Fig. 27.3a). Films without plasticizer showed higher crystallinity (higher peaks) than films containing plasticizer, which showed a larger amorphous zone and lower peaks.

Amylomaize films containing neither plasticizer nor lipid showed a higher crystallinity (higher numbers of peaks) than films containing plasticizer and lipid. These results agree with the DSC studies that showed endothermic transitions with lower peak temperatures and lower ΔH in films with plasticizer and lipid than in control films. Presence of lipid and plasticizer in film formulations did not alter the x-ray pattern of the most stable structure developed in stored control films; peaks maintained their initial positions.

Crystalline evolution of the film matrix during storage was also evaluated by DSC; this technique also allowed determining the T_g. Starch coatings obtained by alkaline treatment, showed an endothermic transition with a peak temperature around 50°C during storage; this peak became narrower and its temperature and the corresponding enthalpy (ΔH) increased with storage time (Fig. 27.3c).

Table 27.1 Barrier properties of starch-based coatings: water vapor permeability (WVP) and gaseous permeabilities

Starch-based coating	Additives	WVP $\times 10^{10}$ (g m^{-1} s^{-1} Pa^{-1})	CO_2 permeability[a] $\times$ 10^9 (g m^{-1} s^{-1} Pa^{-1})	O_2 permeability[a] $\times 10^9$ (g m^{-1} s^{-1} Pa^{-1})
Corn	Without additives	3.68 ± 2.24[b]	29.21 ± 13.89	1.59 ± 0.30
	G	2.57 ± 1.04	5.69 ± 0.97	0.46 ± 0.05
	G + SO	1.92 ± 0.47	5.87 ± 0.58	ND
	S	1.75 ± 0.14	4.19 ± 0.81	0.24 ± 0.03
	S + SO	1.22 ± 0.11	4.72 ± 0.65	ND
Amylo-maize	Without additives	2.62 ± 1.39	28.05 ± 7.37	2.64 ± 0.25
	G	2.14 ± 0.75	3.85 ± 1.28	0.321 ± 0.02
	G + SO	1.76 ± 0.37	4.39 ± 0.90	ND
	S	1.21 ± 0.15	2.96 ± 0.46	0.23 ± 0.03
	S + SO	0.97 ± 0.08	3.43 ± 0.21	ND

G glycerol (20 g/L), *S* sorbitol (20 g/L), *SO* sunflower oil (2 g/L), *ND* not determined
[a]At standard pressure and temperature conditions
[b]Value ± standard deviation

Barrier properties, which include water vapor (WVP), and O_2 and CO_2 permeabilities of starch-based coating formulations, were determined on films obtained by casting (García et al. 2000b). The addition of lipids to starch-based films decreased WVP due to its hydrophobicity (Table 27.1). This is an important property in the case of fresh fruits and vegetables because composite coatings retard moisture loss and subsequent shriveling of fresh products. Table 27.1 shows that O_2 permeabilities were much lower than those of CO_2, indicating a selective action of these films on gas permeabilities. Amylomaize films with higher amylose content showed higher crystallinity and therefore, lower permeabilities than corn starch films. The development of edible coatings with selective gas permeabilities is a good example of active packaging's role in controlling respiratory exchange and improving the conservation of fresh vegetables. Moreover, the addition of lipid, which is necessary to reduce WVP, maintained the selective gas permeability property since CO_2 and O_2 permeabilities did not differ from those of plasticized starch-based films.

The effect of coatings on the quality attributes of refrigerated strawberries was analyzed and the following results were obtained:

Weight loss: The same fruits were weighed at the beginning of the experiment and during storage; weight loss was expressed as percentage loss of initial weight. All the tested coatings showed a beneficial effect on weight loss (Fig. 27.3d). Weight loss in fruits coated with starch formulations, without plasticizer, was similar to those of control fruits due to pores and cracks. Coatings with sorbitol led to significantly lower fruit weight loss than glycerol, regardless of starch type. However, weight loss was unacceptable after 3 weeks of storage for coated fruits without lipid. The addition of sunflower oil was necessary to reduce weight loss

significantly ($P < 0.05$) and to increase storage life, provided the microbial counts were below the established limit (10^6 CFU/g fruit), even at 28 days of storage. The maximum weight loss reduction at 28 days of storage was 63.2%, obtained with coating formulations that included sunflower oil (García et al. 2001).

Texture changes: Important modifications in texture can occur in fruits and vegetables during storage, determining the postharvest storage life of the product. Fruit softening is generally attributed to degradation of the cell wall components, mainly pectins, due to the activity of specific enzymes such as polygalacturonase. The rate and extension of firmness loss during ripening of soft fruits, such as strawberries, is one of the main factors; for both control and coated fruits, the breaking force decreased as a function of storage time. The formulations that minimized weight loss maintained better firmness, since this attribute is also highly influenced by water content.

Color changes: The effect of coatings on surface color modifications in strawberries was also analyzed, because this quality attribute may determine consumer acceptability of the fruit. Lightness (L) and chromaticity parameters (a and b) were recorded at 1st, 8th, 15th and 22nd days of storage. Both plasticizers significantly delayed surface color development. Formulations containing glycerol gave better surface color results compared to those containing sorbitol. Oil addition did not modify surface color results significantly, regardless of plasticizer used in formulation (Fig. 27.3e).

Physiological parameters of fruit, such as titratable acids, pH, anthocyanin, and sugar content are good indicators of maturation and senescence. Coatings may alter natural physiological behavior, modifying the organoleptic characteristics of fruit such as color, taste, or flavor. In coated strawberries, these physiological parameters were slowed down but reached commercially acceptable values. The results indicate that starch-based coatings retard the metabolic reactions, and thus, senescence of coated refrigerated fruits is delayed. This result is attributed to the differential gaseous permeability of films. The O_2 and CO_2 barriers lead to a reduction in respiration rate by limiting the exposure to ambient O_2, increasing internal CO_2, delaying ripening, senescence, and extending storage life of treated fruits (Baldwin 1994; Avena-Bustillos et al. 1997; García et al. 1998a, b, 2001).

In microbiological analysis, surface microbial growth is the main cause of spoilage for many food products. Microorganisms growing on strawberries were mainly yeasts, molds, and sugar-fermenting bacteria. Aerobic mesophilic and psychrotrophic bacteria, molds and yeasts, and coliform microorganisms were analyzed at different storage times. Viable counts were expressed as log CFU/g fruit. Microbial counts in unplasticized, coated strawberries did not differ significantly from the control. Coatings with potassium sorbate, a well-known effective antifungal agent, significantly decreased ($P < 0.05$) yeast and mold counts on coated strawberries. Since the undissociated form is the active antimicrobial agent of sorbic acid, citric acid at fruit pH was added to coating formulation to increase potassium sorbate effectiveness. The addition of 0.2 g/L potassium sorbate

and critic acid to the starch-based coating was the most effective formulation for decreasing microbial counts. This active coating allows using lower amounts of preservatives, maintaining the same antimicrobial efficacy as traditional techniques, with consequent health and economic benefits.

The storage life of a refrigerated fruit, defined as the time necessary to reach 10^6 CFU/g, was determined for the different formulations. At 0°C, the storage life of the uncoated fruit was 14 days; coatings with sorbitol extended fruit storage life to 21 days. At maximum storage time assayed (28 days), formulations with sorbitol and potassium sorbate showed microbial counts below 10^6 CFU/g in fruit. The addition of potassium sorbate enhanced the effectiveness of starch coatings; moreover, the addition of citric acid (to reach pH 4) increased the antimicrobial action of potassium sorbate, leading to a shelf-life of more than 28 days for coated strawberry.

The presence of antimicrobial agents in the coating provided a local high and effective concentration of the preservative. Edible films and coatings act as surface-retention agents and limit preservative diffusion in the food core. This allows reducing the total amount of preservative added to a food compared to traditional methods (e.g., dipping in chemical preservative solutions) (García et al. 1998a, b, 2001).

In conclusion, starch-based coatings with selective gaseous permeabilities proved to extend the storage life of refrigerated strawberries. Plasticizer and lipid addition improved coating performance by decreasing WVP. Weight losses were reduced, color changes delayed, and firmness of tissue and fruit appearance improved. Modifications of the physiological parameters of the fruit were slowed down but reached commercially acceptable values. Starch-based coatings containing potassium sorbate and citric acid helped decrease microbial growth; as a result, shelf-life of the fruit was extended to more than 28 days compared with 14 days for uncoated fruits.

27.10 Final Remarks

Edible films and coatings enhance the quality of food products, protecting them from physical, chemical, and biological deterioration, which results in extended shelf-life and improved safety. They can be used on fruits, vegetables, seafood, meats, and confectionery products. Edible coatings can help retain or improve food product quality by:

- Forming an efficient barrier to prevent moisture loss.
- Delaying ripening process in vegetables, through selective permeability to gases that affects postharvest metabolism, extending the storage life.
- Reducing OU in frying process.
- Adding vitamins or other functional ingredients to enhance quality.

- Incorporating active additives such as antimicrobial agents and antioxidants. Active components are located at the surface of the product, where their action is required. Coating matrix limits diffusion into the core of the food and thus, minor additive concentrations are needed compared to bulk addition.

The factors contributing to renewed interest in the development of edible coatings include:

- Consumer demand for safe and high quality foods, with longer shelf-life.
- Interest of food processors in new storage techniques.
- Opportunities for creating new markets for film-forming ingredients derived from under-utilized agricultural commodities.

Successful growth in the area of edible films will require strong interaction between food technologies and polymer science. Collaborative research work will allow edible coatings to be used in target applications. Moreover, the development of new technologies (functionalization, cross-linking, etc.) to improve the film properties (control release, bioactivity protection, resistance to water etc.) of active packaging and coatings is a major focus for future research.

References

Amarante C, Banks NH (2001) Post harvest physiology and quality of coated fruits and vegetables. Hort Rev 26:161–238

ASTM (1995) Standard test methods for water vapor transmission of material. In: Annual book of ASTM. American Society for Testing and Materials, Philadelphia, PA, pp E96–95

Avena-Bustillos RJ, Krochta JM, Saltveit ME (1997) Water vapor resistance of red delicious apples and celery sticks coated with edible caseinate-acetylated mono-glyceride films. J Food Sci 62(2):351–354

Balasubramaniam M, Chinnan MS, Mallikarjunan P, Phillips RD (1997) The effect of edible film on oil uptake and moisture retention of a deep-fat fried poultry product. J Food Process Eng 20:17–29

Baldwin EA (1994) Edible coatings for fresh fruits and vegetables: past, present and future. In: Krochta JM, Baldwin EA, Nisperos-Carriedo M (eds) Edible coatings and films to improve food quality. Technomic Publishing, Lancaster, PA, pp 25–64

Baldwin EA, Nispero-Carriedo MO, Baker RA (1995) Edible coatings for lightly processed fruits and vegetables. Hort Sci 30(1):35–38

Baldwin EA, Nispero-Carriedo MO, Hagenmaier RD, Baker RA (1997) Use of lipids in coatings for food products. Food Technol 51(6):56–64

Bertolini Suarez R, Campañone LA, García MA, Zaritzky NE (2008) Comparison of the deep frying process in coated and uncoated dough systems. J Food Eng 84:383–393

Bifani V, Ramírez C, Ihla M, Rubilara M, García MA, Zaritzky N (2007) Effects of murta (Ugni molinae Turcz) extract on gas and water vapor permeability of carboxymethylcellulose based edible films. Lebensm Wiss Technol-Food Sci Technol 40:1473–1481

Brody AL, Strupinsky ER, Kline LR (2001) Antimicrobial packaging. In: Active packaging for food applications. CRC, Boca Raton, FL, pp 131–194

Cagri A, Ustunol Z, Ryser ET (2004) Antimicrobial edible films and coatings. J Food Prot 67(4):833–848

Cha DS, Chinnan MS (2004) Biopolymer-based antimicrobial packaging: a review. Crit Rev Food Sci Nutr 44:223–237

Cisneros-Zevallos L, Saltveit ME, Krochta JM (1997) Hygroscopic coatings control surface white discoloration of peeled (minimally processes) carrots during storage. J Food Sci 62(2):363–366, 398

Cuq B, Gontard N, Guilbert S (1995) Edible films and coatings as active layers. In: Rooney M (ed) Active food packaging. Blackie Academic and Professional, Glasgow, UK, pp 111–142

Cuq B, Gontard N, Guilbert S (1998) Proteins as agricultural polymers for packaging production. Cereal Chem 75(1):1–9

Debeaufort F, Quezada-Gallo JA, Voilley A (1998) Edible films and coatings: tomorrow's packaging: a review. Crit Rev Food Sci Nutr 38(4):299–313

Donhowe IG, Fennema O (1994) Edible films and coatings: characteristics, formation, definitions, and testing methods. In: Krochta JM, Baldwin EA, Nisperos-Carriedo M (eds) Edible coatings and films to improve food quality. Technomic Publishing, Lancaster, PA, pp 1–24

Drake SR, Nelson JW (1990) Storage quality of waxed and nonwaxed "Delicious" and "Golden Delicious" apples. J Food Qual 13:331–334

El Gaouth A, Arul J, Ponnampalam R, Boulet M (1991) Chitosan coating effect on storability and quality of fresh strawberry. J Food Sci 56(6):618–1620

Franssen LR, Krochta JM (2003) Edible coatings containing natural antimicrobials for processed foods. In: Roller S (ed) Natural antimicrobials for the minimal processing of foods. Woodhead Publishing Limited, Cambridge, UK

García MA, Martino MN, Zaritzky NE (1998a) Plasticizer effect on starch-based coatings applied to strawberries (Fragaria × ananassa). J Agr Food Chem 46:3758–3767

García MA, Martino MN, Zaritzky NE (1998b) Starch-based coatings: effect on refrigerated strawberry (Fragaria ananassa) quality. J Sci Food Agric 76(3):411–420

García MA, Martino MN, Zaritzky NE (1999) Edible starch films and coatings characterization: scanning electron microscopy, water vapor, and gas permeabilities. Scanning 21(5):348–353

García MA, Martino MN, Zaritzky NE (2000a) Lipid addition to improve barrier properties of edible starch-based films and coatings. J Food Sci 65(6):941–947

García MA, Martino MN, Zaritzky NE (2000b) Microstructural characterization of plasticized starch-based films. Starch/Staerke 52(4):118–124

García MA, Martino MN, Zaritzky NE (2001) Composite starch-based coatings applied to strawberries (Fragaria ananassa). Nahrung 45(4):267–272

García MA, Ferrero C, Campana A, Bértola N, Martino M, Zaritzky N (2004a) Methylcellulose coatings applied to reduce oil uptake in fried products. Food Sci Technol Int 10(5):339–346

García MA, Pinotti A, Martino MN, Zaritzky NE (2004b) Characterization of composite hydrocolloid films. Carbohydr Polym 56(3):339–345

García MA, Pinotti A, Zaritzky NE (2006) Physicochemical, water vapor barrier and mechanical properties of corn starch and chitosan composite films. Starch/Staerke 58(9):453–463

Garcìa MA, Ferrero C, Bértola N, Martino M, Zaritzky N (2002) Edible coatings from cellulose derivatives to reduce oil uptake in fried products. Innovative Food Sci Emerg Technol 3(4):391–397

Gennadios A, Weller CL (1990) Edible films and coatings from wheat and corn proteins. Food Technol 44(10):63–69

Gennadios A, McHugh TH, Weller CL, Krochta JM (1994) Edible coatings and film based proteins. In: Krochta JM, Baldwin EA, Nisperos-Carriedo M (eds) Edible coatings and films to improve food quality. Technomic Publishing, Lancaster, PA, pp 201–277

Gennadios A, Hanna MA, Kurth LB (1997) Application of edible coatings on meats, poultry and seafoods: a review. Lebensm Wiss Technol 30(4):337–350

Gontard N, Guilbert S, Cuq JL (1992) Edible wheat gluten films: influence of the main process variables on film properties using response surface methodology. J Food Sci 57(190–195):199

Gontard N, Thibault R, Cuq B, Guilbert S (1996) Influence of relative humidity and film composition on oxygen and carbon dioxide permeabilities of edible films. J Agr Food Chem 44(4):1064–1069

Greener IK, Fennema O (1989) Barrier properties and surface characteristics of edible, bilayer films. J Food Sci 54:1393–1399
Greener IK, Fennema O (1992) Lipid-based edible films and coatings. Lipid Technol 4:34–38
Guilbert S (1986) Technology and application of edible protective films. In: Mathlouthi M (ed) Food packaging and preservation. Theory and practice. Elsevier Applied Science Publishing Co, London, UK, pp 371–394
Guilbert S, Gontard N (1995) Edible and biodegradable food packaging. In: Ackermann P, Jagerstad M, Ohlsson T (eds) Foods and packaging materials – chemical interactions. The Royal Society of Chemistry, Cambridge, England, pp 159–168
Guilbert S, Gontard N (2005) Agro-polymers for edible and biodegradable films: review of agricultural polymeric materials, physical and mechanical characteristics, Chapter 4.16. In: Han JH (ed) Innovations in food packaging. Elsevier Academic, Oxford, England, pp 263–276
Guilbert S, Gontard N, Gorris LGM (1996) Prolongation of the shelf life of perishable food products using biodegradable films and coatings. Lebensm Wiss Technol-Food Sci Technol 29:10–17
Guilbert S, Cuq B, Gontard N (1997) Recent innovations in edible and/or biodegradable packaging materials. Food Addit Contam 14(6–7):741–751
Guilbert S, Gontard N, Morel MH, Chalier P, Micard X, Redl A (2001) Formation and properties of wheat gluten films and coatings. In: Gennadios A (ed) Protein-based films and coatings. CRC, Boca Raton, FL, pp 69–122
Han JH (2000) Antimicrobial food packaging. Food Technol 54(3):56–65
Han JH (2002) Protein-based edible films and coatings carrying antimicrobial agents. In: Gennadios A (ed) Protein-based films and coatings. CRC, Boca Raton, FL, pp 485–499
Han JH (2003a) Antimicrobial food packaging. In: Ahvenainen R (ed) Novel food packaging techniques. Woodhead Publishing Ltd, Cambridge, UK, pp 50–70
Han JH (2003b) Design of antimicrobial packaging systems. Int Rev Food Sci Technol 11:106–109
Han JH (2005) New technologies in food packaging: overview. In: Han JH (ed) Innovations in food packaging. Elsevier Academic, Oxford, England, pp 3–11
Han JH, Gennadios A (2005) Edible films and coatings: a review. In: Han JH (ed) Innovations in food packaging. Elsevier Academic, Oxford, England, pp 239–262
Han C, Zhao Y, Leonard SW, Traber MG (2004) Edible coatings to improve storability and enhance nutritional value of fresh and frozen strawberries (*Fragaria ananassa*) and raspberries (*Rubus ideaus*). Postharvest Biol Technol 33(1):67–78
Kester JJ, Fennema OR (1986) Edible films and coatings: a review. Food Technol 48(12):47–59
Krochta JM (1997) Edible protein films and coatings. In: Damodaran S, Paraf A (eds) Food proteins and their applications. Marcel Dekker, New York, pp 529–549
Krochta JM (2002) Proteins as raw materials for films and coatings: definitions, current status, and opportunities. In: Gennadios A (ed) Protein-based films and coatings. CRC, Boca Raton, FL, pp 1–41
Krochta JM, De Mulder-Johnston C (1997) Edible and biodegradable polymer films: challenges and opportunities. Food Technol 51(2):61–74
Krochta JM, Baldwin EA, Nisperos-Carriedo MO (1994) Edible coatings and films to improve food quality. Technomic, Lancaster, PA
Lacroix M, Le Tien C (2005) Edible films and coatings from nonstarch polysaccharides. In: Han JH (ed) Innovations in food packaging. Elsevier Academic, Oxford, England, pp 338–359
Lin D, Zhao Y (2007) Innovations in the development and application of edible coatings for fresh and minimally processed fruits and vegetables. Compr Rev Food Sci Food Safety 6:60–74
Lopez OV, Garcia MA, Zaritzky N (2008) Film forming capacity of chemically modified corn starches. Carbohydr Polym 73:573–581
Mali S, Grossmann MVE, Garcia MA, Martino MN, Zaritzky NE (2002) Microstructural characterization of yam starch films. Carbohydr Polym 50(4):379–386
Mali S, Grossmann MVE, Garcia MA, Martino MN, Zaritzky NE (2004) Barrier, mechanical and optical properties of plasticized yam starch films. Carbohydr Polym 56(2):129–135

Mali S, Grossmann MVE, García MA, Martino MN, Zaritzky NE (2005) Mechanical and thermal properties of yam starch films. Food Hydrocolloids 19(1):157–164
Mali S, Grossmann MVE, Garcia MA, Martino MN, Zaritzky NE (2006) Effects of controlled storage on thermal, mechanical and barrier properties of plasticized films from different starch sources. J Food Eng 75(4):453–460
McHugh TH, Krochta JM (1994) Permeability properties of edible films. In: Krochta JM, Baldwin EA, Nisperos-Carriedo M (eds) Edible coatings and films to improve food quality. Technomic, Lancaster, PA, pp 139–187
Mei Y, Zhao Y (2003) Barrier and mechanical properties of milk protein-based edible films incorporated with nutraceuticals. J Agr Food Chem 51(7):1914–1918
Mei Y, Zhao Y, Farr H (2002) Enhancement of nutritional and sensory qualities of fresh baby carrots by edible coatings. J Food Sci 67(5):1964–1968
Miller KS, Upadhyaya SK, Krochta JM (1998) Permeability of d-limonene in whey protein films. J Food Sci 63(2):244–247
Min S, Krochta JM (2007) Ascorbic acid-containing whey protein film coatings for control of oxidation. J Agr Food Chem 55(8):2964–2969
Min S, Rumsey TR, Krochta JM (2008) Diffusion of the antimicrobial lysozyme from a whey protein coating on smoked salmon. J Food Eng 84:39–47
Nisperos-Carriedo MO (1994) Edible films and coatings based on polysaccharides. In: Krochta JM, Baldwin EA, Nisperos-Carriedo MO (eds) Edible coatings and films to improve food quality. Technomic Publishing, Lancaster, PA, pp 305–335
Nussinovitch A (2003) Water soluble polymer applications in foods. Blackwell Science, Oxford, UK, pp 29–69
Park HJ (1999) Development of advanced edible coatings for fruits. Trends Food Sci Technol 10:254–260
Park HJ (2005) Edible coatings for fruit. In: Jongen W (ed) Fruit and vegetable processing. CRC, Boca Raton, FL
Park SI, Zhao Y (2004) Incorporation of a high concentration of mineral or vitamin into chitosan-based films. J Agr Food Chem 52:1933–1939
Park SK, Hettiarachchy NS, Ju ZY, Gennadios A (2002) Formation and properties of soy protein films and coatings. In: Gennadios A (ed) Protein-based films and coatings. CRC, Boca Raton, FL, pp 123–137
Park SI, Daeschel MA, Zhao Y (2004) Functional properties of antimicrobial lysozyme chitosan composite films. J Food Sci 69:215–221
Park SI, Stan SD, Daeschel MA, Zhao Y (2005) Antifungal coatings on fresh strawberries (Fragaria × ananassa) to control mold growth during cold storage. J Food Sci 70:202–207
Pérez-Gago MB, Krochta JM (2005) Emulsion and bi-layer edible films. In: Han JH (ed) Innovations in food packaging. Elsevier Academic, Oxford, England, pp 384–402
Pinotti A, García MA, Martino MN, Zaritzky NE (2007) Study on microstructure and physical properties of composite films based on chitosan and methylcellulose. Food Hydrocolloids 21(1):66–72
Redl A, Gontard N, Guilbert S (1996) Determination of sorbic acid diffusivity in edible wheat gluten and lipid based films. J Food Sci 61:116–120
Romero-Bastida CA, Bello-Pérez LA, García MA, Martino MN, Solorza-Feria J, Zaritzky NE (2005) Physicochemical and microstructural characterization of films prepared by thermal and cold gelatinization from non-conventional sources of starches. Carbohydr Polym 60(2):235–244
Shellhammer TH, Krochta JM (1997) Whey protein emulsion film performance as affected by lipid type amount. J Food Sci 62(2):390–394
Sothornvit R, Krochta JM (2000) Plasticizer effect on oxygen permeability of beta -lactoglobulin films. J Agr Food Chem 48:6298–6302
Sothornvit R, Krochta JM (2001) Plasticizer effect on mechanical properties of beta -lactoglobulin films. J Food Eng 50:149–155

Torres JA, Karel M (1985) Microbial stabilization of intermediate moisture food surfaces III. Effects of surface preservative concentration and surface pH control on microbial stability of an intermediate moisture cheese analog. J Food Process Preserv 9:107–119

Torres JA, Bouzas J0, Karel M (1985) Microbial stabilization of intermediate moisture food surfaces II. Control of surface pH. J Food Process Preserv 9:93–106

Vojdani F, Torres JA (1990) Potassium sorbate permeability of methylcellulose and hydroxypropyl methylcellulose coatings: effect of fatty acid. J Food Sci 55:841–846

Williams R, Mittal GS (1999) Low-fat fried foods with edible coatings: modeling and simulation. J Food Sci 64:317–322

Wu LC, Bates RF (1972) Soy protein-lipid films. I. Studies on the film formation phenomenon. J Food Sci 37(1):36–39

Wu Y, Weller CL, Hamouz F, Cuppett SL, Schnepf M (2002) Development and application of multicomponent edible coatings and films: a review. Adv Food Nutr Res 44:347–394

Zhao Y, McDaniel M (2005) Sensory quality of foods associated with edible film and coating systems and shelf life extension. In: Han JH (ed) Innovations in food packaging. Elsevier Academic, Oxford, England, pp 434–453

Chapter 28
Physical Properties of Edible Gelatin Films Colored with Chlorophyllide

Paulo J.A. Sobral, Rosemary A. Carvalho, and Carmen S. Fávaro-Trindade

28.1 Introduction

The question of the environmental impact of synthetic packaging has generally favored research on edible films and, in particular, biodegradable films, which are flexible materials elaborated with biological macromolecules capable of forming a continuous matrix (Gontard and Guilbert 1996; Krochta and De-Mulder-Johnston 1997; Van de Velde and Kiekens 2002; Tharanathan 2003). The main biopolymers of agricultural origin used in the elaboration of films are polysaccharides (Nisperos-Carriedo 1994) and proteins (Gennadios et al. 1994; Torres 1994). Synthetic biopolymers have also been studied in depth in recent decades (Van de Velde and Kiekens 2002).

Among the proteins, gelatin has stimulated much interest due to its excellent filmogenic properties (Arvanitoyannis 2002). Gelatin was one of the first macromolecules used in the production of films, and has continued to be widely studied for this purpose due to its functional properties, large scale production, and competitive prices (Arvanitoyannis 2002).

The properties of the macromolecules directly influence the final characteristics of the edible films. The properties of protein-based films are determined by the protein-protein and protein-water interactions, which can be controlled by the preparation conditions of the FFS and by the addition of plasticizers (Gennadios et al. 1994; Torres 1994; Gontard and Guilbert 1996; Arvanitoyannis 2002). Plasticizers are low molecular weight molecules and therefore can penetrate the biopolymeric matrix, increasing the free space between the macromolecular chains, causing a decrease in the intermolecular forces throughout the matrix (Banker 1966; Krochta and De-Mulder-Johnston 1997).

In practical terms, the final characteristics of edible and/or biodegradable films are the result of numerous parameters, such as the characteristics and concentrations of the macromolecule and other constituents (solvent, plasticizer, etc.); pH;

P.J.A. Sobral (✉), R.A. Carvalho, and C.S. Fávaro-Trindade
Department of Food Engineering, University of São Paulo, Pirassununga (SP), Brazil
e-mail: pjsobral@usp.br

J.M. Aguilera et al. (eds.), *Food Engineering Interfaces*, Food Engineering Series,
DOI 10.1007/978-1-4419-7475-4_28,

denaturation conditions (in the case of proteins); type of support used; drying conditions; and environmental conditions (temperature and humidity).

Protein-based films, including those from gelatin, generally present excellent gas-barrier properties and good mechanical properties. In addition, they can serve as a support for active substances such as antioxidants, antimicrobial agents, etc. (Gómez-Guillén et al. 2007; López-Carballo et al. 2008; Gómez-Estaca et al. 2009). On another side, two papers on biopolymer-based films containing natural pigments can be found, in which the pigments in both cases are derived from chlorophyll (Corat et al. 2007; López-Carballo et al. 2008).

Since chlorophyll is a pigment, it can confer a green color on the material, which can be an added attraction. However, the properties of the material, notably the light-barrier properties, may be affected by the presence of this pigment (Corat et al. 2007). Thus, this chapter will present and discuss the effects of adding chlorophyll to the formulation of gelatin-based edible films, which would also permit the production of more attractive packaging with improved light-barrier properties.

28.2 Gelatin and Edible Films

Gelatin is a protein of animal origin resulting from the acidic or basic hydrolysis of the collagen obtained from bones, bovine or swine hides, or connective tissue (Gennadios et al. 1994). Configuration of the peptide chain in gelatin is normally controlled by interactions between the solvent and the amino acids in the main chain, and by certain preferential orientations of the peptide bonds, such that the amino acid sequence is responsible for the characteristics of the gelatin (Veis 1964). In general, glycine, proline, and hydroxyproline constitute one-third of the total amino acids in gelatin (Veis 1964; Gennadios et al. 1994).

The molecular weight of gelatin depends on the type of raw material and process conditions used, varying from 3,000 to 200,000 Da (Gennadios et al. 1994). According to the type of pretreatment used to remove impurities and to start the hydrolysis of the raw material, the gelatin is classified as Type A when an acid pretreatment is used, resulting in an isoelectric point between 7.0 and 9.4; or Type B, when a basic pretreatment is used, resulting in an isoelectric point between 4.5 and 5.3 (Veis 1964).

Gelatin is soluble in water at temperatures above 30°C. When submitted to temperatures above its melting point, the gelatin swells, dissolves, and forms heat-reversible gels when the temperature returns to room temperature (Slade and Levine 1987). At the molecular level, the formation of a gelatin gel involves restructuring of the proteins, implying transformation from a disordered state to an ordered state, formed by triple-helix structures characteristic of collagen in the active state, the structure and physical properties of these gels being a result of the formation of microcrystalline links (Slade and Levine 1987; Achet and He 1995; Ziegler and Foegeding 1990).

Various studies involving the formation of edible and/or biodegradable films have been carried out with mammalian (Arvanitoyannis et al. 1997, 1998a, b; Lim et al. 1999; Menegalli et al. 1999; Sobral 1999; Sobral et al. 2001; Carvalho and Grosso 2004; Bertan et al. 2005; Thomazine et al. 2005; Vanin et al. 2005; Carvalho and Grosso 2006; Carvalho et al. 2008a) and fish (Jongjareonrak et al. 2006a, b; Gómez-Guillén et al. 2007; Zhang et al. 2007; Carvalho et al. 2008b) gelatin. In general, gelatin-based films show good mechanical resistance but reduced efficiency as a water vapor barrier. On the other hand, due to the hydrophilic characteristics of gelatin, these films show an elevated susceptibility to environmental conditions, making the films difficult to use as packaging materials. Various alternatives have been studied in an attempt to improve these characteristics, such as enzymatic modifications (Lim et al. 1999; Carvalho and Grosso 2004), chemical modifications (Bigi et al. 2001; Carvalho and Grosso 2004, 2006; Cao et al. 2007; Carvalho et al. 2008a), the incorporation of different types of plasticizers (Vanin et al. 2005), the use of plasticizer blends (Thomazine et al. 2005), and lipid incorporation (Bertan et al. 2005), among others. In general, no significant improvements were observed with respect to the water vapor barrier and mechanical properties.

Another alternative used in an attempt to improve the mechanical resistance of these materials was the mixture of the biopolymers with synthetic polymers (Tharanathan 2003). One very interesting synthetic polymer for this type of study is the polyvinyl alcohol (PVA), which, despite being synthetic, is hydrophilic and biodegradable (Matsumura et al. 1999). Some films based on blends of PVA with gelatin have been developed (Chiellini et al. 2001; Bergo et al. 2006; Mendieta-Taboada et al. 2008; Maria et al. 2008; Silva et al. 2008; Carvalho et al. 2009). However, all these films were colorless, that is, the inclusion of pigments to make them more attractive was not studied.

28.3 Chlorophylls

Chlorophylls are the most abundant natural pigments in plants. They occur in the chloroplasts of leaves and other vegetable tissues, being very common in fruits and vegetables (Streit et al. 2005; Humphrey 2004). Precursors and derivatives of the chlorophylls are used in photodynamic medical treatments (Schoefs 2002). In addition, chlorophyllian pigments are currently of great industrial importance, since they can be used both as pigments and as antioxidants, although there is controversy in the research studies with respect to the latter property (Lanfer-Marquez 2003).

Due to their color and physical properties, the chlorophylls are also used as colorants for food products (Humphrey 2004; Chattopadhyay et al. 2008). Most chlorophyll colorants exist in a water-soluble form and are used in dairy products, soups, oils, sugar confections, drinks, and cosmetics (Francis 2002).

In plants, the chlorophyll molecules are associated with proteins, carotenoids, and tocopherols by way of noncovalent interactions, which give them certain stability (Delgado-Vargas and Paredes-López 2002). After their extraction from the vegetable tissues, these pigments are chemically unstable and can easily be altered or destroyed, modifying the perception and quality of the products. In general, the chlorophylls are relatively unstable and sensitive to light, heating, oxygen, and chemical degradation (Kidmose et al. 2002; Schoefs 2002).

Chlorophylls are molecules formed from complex porphyrin derivatives, constituting the most important subgroup of pigments within the tetrapyrrole group (Fig. 28.1) (Chattopadhyay et al. 2008). Structurally, they are formed by four pyrrolic rings and a fifth isocyclic ring located at the side of the third pyrrolic ring, bonded to each other via methylenic bridges and containing one magnesium atom on their inside. A molecule of propionic acid esterified to a long chain acyclic alcohol, usually a phytol, can be found on the fourth pyrrolic ring, conferring a hydrophobic character to the chlorophyll (Delgado-Vargas and Paredes-López 2002; Francis 2002; Lanfer-Marquez 2003; Humphrey 2004; Chattopadhyay et al. 2008). Porphyrin is a stable ring-shaped molecule around which electrons are free to migrate. Because the electrons move freely, the ring has the potential to gain or lose electrons easily, and thus to provide energized electrons to other molecules. This is the fundamental process by which chlorophyll captures the energy of sunlight (Wilska-Jeszka 2007).

Two chlorophylls, chlorophyll A and chlorophyll B, are currently important as food dyes (Chattopadhyay et al. 2008). These pigments are obtained from plants and only differ with respect to the position of the functional groups $–CH_3$ and –CHO, respectively, on carbon 3 (Kidmose et al. 2002; Humphrey 2004). These differences in the structure of the chlorophyll are sufficient to produce different

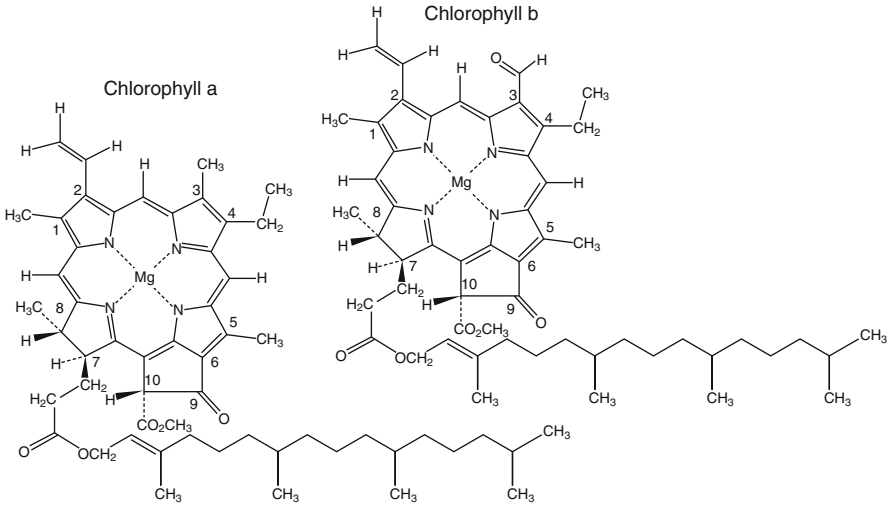

Fig. 28.1 Chemical structure of chlorophylls

wavelength absorptions and hence a variety of different green hues. The colors vary from greenish-yellow to greenish-blue, and the derivatives of these chlorophylls would be probable producers of orange hues or, under drastic chemical conditions, a red color (Delgado-Vargas and Paredes-López 2002).

Moreover, chlorophyllide is a green pigment obtained by removal of the phytyl group of chlorophyll through hydrolysis in dilute alkali or the action of chlorophyllase, and is thus water soluble (Kidmose et al. 2002; Lanfer-Marquez 2003). These chlorophylls are green in color because they absorb strongly in the red and blue regions of the visible spectrum (Kidmose et al. 2002).

28.4 Experimental Considerations

The films were produced from FFSs containing 2 g gelatin/100 g FFS and 25 g sorbitol/100 g gelatin. Pigskin gelatin was used, provided by Gelita South America (São Paulo, Brazil). To prepare these solutions, the gelatin was first hydrated for 30 min. at room temperature, followed by dissolution at 55°C in a water bath (TE 184-Tecnal) (Sobral et al. 2001). After dissolution the plasticizer previously dissolved in water and the chlorophyll pigment were added. A water soluble form of chlorophyll, the chlorophyllide (10% solution of chlorophyll 70008) provided by *Germinal aditivos para alimentos* (Cabreúva, Brazil), was used for practical reasons. To test the effect of the pigment concentrations, 0, 2, 4, 6, 8, and 10 g of chlorophyll solution/100 g gelatin were added to the FFS.

After drying in an oven with air circulation (MA 037-TECNAL) at 30°C for about 24 h, easily handled films were obtained with thicknesses between 0.075 and 0.081 mm, determined using a Mitutoyo digital micrometer (±0.001 mm). The films were then characterized after preconditioning in desiccators containing NaBr (relative humidity 58%) at 25°C for at least 7 days. The film characteristics (mechanical properties, solubility, moisture content, water vapor, and optical barrier properties) were determined in an acclimatized room with a temperature of about 22°C and relative humidity between 55% and 65%.

The moisture content of the films was determined in an oven at 105°C to constant weight. The water solubility of the films was determined after 24 h of immersion, according to Gontard et al. (1993), and expressed in terms of dissolved dry mass. Water vapor permeability was determined using the method proposed by Gontard et al. (1993). The films were fixed in cells containing silica gel, which were then placed in desiccators containing distilled water and maintained at 25°C in an oven (BOD TE 390 TECNAL) (±0.2°C). Weight gain of the system was determined at 24 h intervals, over a period of 120 h. Water vapor permeability (WVP) was calculated from (28.1) (Gontard et al. 1993).

$$\mathrm{WVP} = \frac{w}{tA}\,\frac{x}{\Delta P} \tag{28.1}$$

where x is the mean film thickness (mm), A is the permeation area (cm^2), ΔP is the partial vapor pressure difference between the inside of the cell (silica gel, $P_1 = 0$ Pa) and the distilled water ($P_2 = 3{,}166$ Pa), and the term w/t corresponds to the angular coefficient of the linear regression of the graph of mass versus time (g/h).

The mechanical properties (stress at break, elongation at break, and elastic modulus) of the films were determined by a tensile stress test using the TA.XT2*i* texturometer (Stable Micro Systems) with the tensile grip probe, moving at 0.9 mm/s, according to Thomazine et al. (2005). The color parameters (a^*, b^*, and L^*), the total color difference (ΔE^*), and the opacity were determined according to Sobral (1999) using the Miniscan XE (HunterLab) colorimeter. The parameters a^*, b^*, and L^* were determined by the superimposition of the films on a white standard and the total difference in color according to (28.2) (Gennadios et al. 1996).

$$\Delta E* = \left[(\Delta L*)^2 + (\Delta a*)^2 + (\Delta b*)^2 \right]^{0,5} \tag{28.2}$$

where $\Delta L^* = L^*_{\text{standard}} - L^*_{\text{sample}}$, $\Delta a^* = a^*_{\text{standard}} - a^*_{\text{sample}}$, $\Delta b^* = b^*_{\text{standard}} - b^*_{\text{sample}}$.

Opacity was determined according to Sobral (2000) with the same apparatus and computer program used to measure the color, and was calculated as the ratio between the opacity of the film superimposed on the black standard (Y_b) and that on the white standard (Y_w) ($Y = Y_b/Y_w$). The gloss of the films was determined using the Rhopoint NGL 20/60 glossimeter at an angle of 20° according to Villalobos et al. (2005). This angle was sufficient because gelatin-based films have high gloss values (Maria et al. 2008; Silva et al. 2008). The UV and visible light barrier properties were measured at wavelengths varying from 190 to 800 nm, using a UV-Visible spectrophotometer (Biochrom, Libra S22), as described by Fang et al. (2002). The Duncan test was used to compare the means of these results ($\alpha = 5\%$) using the SAS computer program (version 6.8, SAS Inc., Carry, NC, USA).

The color parameters were also evaluated in relation to the variation in film thickness. This study was carried out by superimposing the films from each formulation and of known thickness, one on top of the other. A colorimeter reading was made after the addition of each film. The regression analyses were carried out using the software Statistica 8.0 (StatSoft, Inc.).

28.5 Physical Properties of Gelatin-Based Films Colored with Chlorophyllide

In general the chlorophyllide concentration in the FFS affected the main physical properties studied, although with no logical sequence, that is, one could not affirm that the properties presented in Table 28.1 increased or decreased as a function of increase in chlorophyllide concentration, despite observing significant differences

Table 28.1 Range of variation in physical properties of colored gelatin films

Properties	Range
Moisture content	12.0–13.8 g water/100 g film
Solubility in water	38.6–44.1 g/100 g dry film
Water vapor permeability	3.4–6.7 $\times$ 10^{-8} g mm/h cm^2 Pa
Tensile strength	45.6–53.0 MPa
Elongation at break	11.3–24.1%
Elasticity modulus	13.6–18.1 MPa/%
Gloss at 20°	134–198
Opacity	0.3–0.4

($P < 0.05$) between the means in some cases. The moisture content of the films colored with chlorophyll were similar to those determined by Sobral et al. (2001) and Thomazine et al. (2005) for gelatin-based films plasticized with sorbitol and conditioned in the same way.

The addition of chlorophyllide did not significantly ($P > 0.05$) affect the water solubility of the films, independent of the concentration added. These water solubility result values were slightly higher than those observed by Carvalho and Grosso (2004, 2006) for gelatin-based (25–30 g/100 g of film) films that were modified chemically and enzymatically and plasticized with glycerol.

The water vapor permeability oscillated between 3 and 7 $\times$ 10^8 g mm/h cm^2 Pa, with no clear behavior as a function of increase in chlorophyllide concentration in the film. Despite some significant differences ($P < 0.05$) observed between some of the mean values, such variation did not constitute an important effect, that is, all the films continued to be highly permeable to water vapor.

The addition of chlorophyllide to the film did affect the mechanical resistance, although there was no direct relationship between the pigment concentration and the stress at break. The observed stresses at break values were similar to those obtained by Thomazine et al. (2005) for gelatin-based films plasticized with sorbitol (25 g sorbitol/100 g of gelatin). On the other hand, it was observed that an increase in chlorophyllide concentration caused a greater variation in elongation at break. Independent of the addition of chlorophyllide, the elongation at break values was higher than that observed by Thomazine et al. (2005). With respect to the elastic modulus, the property that indicates the rigidity of the material, an increase in chlorophyllide concentration did not cause significant variations in this property. Apparently, the incorporation of chlorophyll can affect the mobility of the polymeric matrix due to its structure and possible interaction with protein, a behavior typical of plasticizing agents. In fact, such behavior can also be observed with synthetic materials. According to Durston (2006), there are limits to the amount of colored pigment that can be added to polyethylene, without affecting the mechanical properties of the film.

High gloss samples are better differentiated using measurements at smaller angles (Villalobos et al. 2005). Thus, only the results obtained at 20° were presented in Table 28.1. In general, the addition of chlorophyllide caused an increase in gloss on the film surface, indicating that the incorporation of pigment favored the morphology of the polymeric matrix, that is, decreased surface roughness as

compared to pure gelatin. The films developed in the present study presented greater gloss than whey protein isolate-based films dried in a microwave dryer, with gloss values between 87 and 96 (Kaya and Kaya 2000), or hydroxypropyl methylcellulose-based films with gloss values below 100 (Villalobos et al. 2005). The opposite behavior is normally observed with synthetic materials, for which a specific coloring process should be used to prevent it from adversely affecting the surface gloss of the films (Durston 2006).

Opacity was also not significantly ($P > 0.05$) affected by increases in the chlorophyllide concentration in the gelatin films. Thus, it could be suggested that the inclusion of chlorophyllide in the film formulation, at the concentrations studied, did not affect the translucence of the films, which continued similar to that of pure gelatin films, which are extremely transparent (very low opacity) (Sobral 1999; Vanin et al. 2005). Since many packaging applications require the contents to be visible, film transparency is of considerable interest (Hanlon et al. 1998).

In addition, this result for opacity suggests that the chlorophyllide was completely dissolved in the polymeric matrix, since it is known that the presence of a dispersed, nonmiscible phase promotes opacity as a function of the differences in refractive indexes of the phases and the concentration and particle size of the dispersed phase (Villalobos et al. 2005).

28.6 UV and Light Barrier Properties of Gelatin-Based Films Colored with Chlorophyllide

Although gelatin constitutes an excellent UV light barrier (Fig. 28.2) the presence of chlorophyllide in the gelatin-based films contributed to an increase in this property, since the films showed no transmittance at 200 nm, and between 2.6 and 6.0 at 280 nm. The chlorophyllide absorbed UV radiation, having a protective effect against the degradation of the material (Hanlon et al. 1998) and the packaged foodstuff (Coltro et al. 2003). Thus, films colored with chlorophyllide show excellent UV barrier properties, suggesting that this type of material could be used to package foods rich in lipids and/or oxygen-susceptible vitamins (Bekbolet 1990; Fang et al. 2002; Artharn et al. 2007). According to Saffert et al. (2009), light is known to have a damaging effect on several foodstuffs, such as milk and other dairy products, due to the presence of light-sensitive vitamins like vitamins A and B_2. The most pronounced effect of light catalyzed reactions is observed with light in the lower wavelengths of the visible spectrum and in the UV spectrum (Bekbolet 1990).

Contrarily, Shiku et al. (2004) working on films based on fish sarcoplasmic proteins, and Artharn et al. (2007), working on films based on fish muscle proteins, determined no transmittance between 200 and 280 nm. It is highly possible that this excellent capacity as a UV barrier was caused by the presence of nondissolved proteins, constituting physical barriers (Villalobos et al. 2005; Monedero et al. 2009). However, Fang et al. (2002), in working with whey-based films, obtained

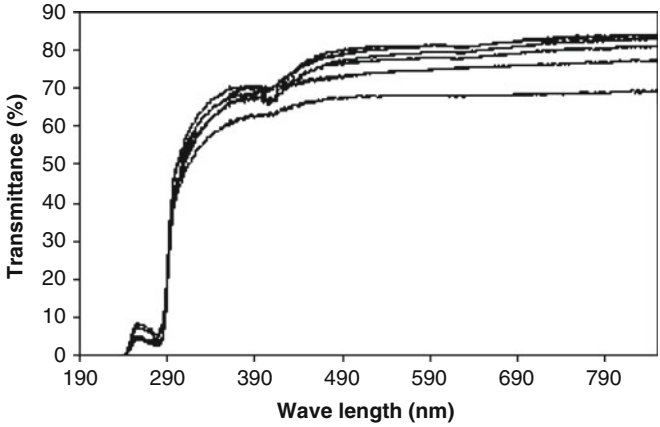

Fig. 28.2 Spectra of gelatin films colored with chlorophyllide

values for transmittance between 6 and 7 also between 200 and 280 nm. The great barrier property of gelatin-based films could be explained by the presence of amino acids containing aromatic rings in their residues, as can be seen in the aminogram determined by Sobral et al. (2001).

28.7 Color Characteristics of Gelatin-Based Films Colored with Chlorophyllide

The addition of chlorophyllide to the gelatin films caused significant alterations in the parameters a^* and b^* (Fig. 28.3), but did not affect parameter L^*, remaining practically constant at about 91, which is almost equivalent to the parameter of the white standard used as the support.

The parameter a^*, which varies from green (−) to red (+) decreased linearly with the pigment concentration (C_p) (28.3), indicating, effectively, that the material became greener with increase in concentration of the pigment as expected. On the other hand, the parameter b^*, which varies from blue (−) to yellow (+), increased linearly with increase in the pigment concentration (28.4), suggesting that the films presented a yellowy green coloration.

$$a^* = -0.94 - 0.14\, C_p, \qquad R^2 = 0.987 \tag{28.3}$$

$$b^* = 2.75 + 0.19\, C_p, \qquad R^2 = 0.963 \tag{28.4}$$

The values of the color parameters determined in the present study were similar to those obtained by López-Carballo et al. (2008), who characterized edible films prepared with 10 g of gelatin/100 mL, 2.5 g glycerol/100 mL and 80 μg of

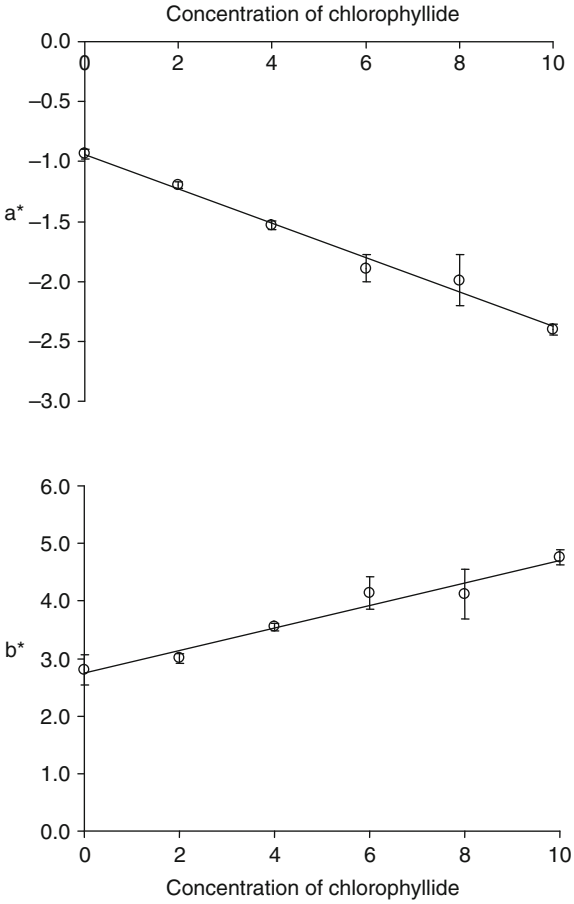

Fig. 28.3 Parameters a^* (*top*) and b^* (*bottom*) of gelatin films containing different chlorophyllide concentrations

chlorophyllin E-140 or E-141/mL: $a^* = -3.2$ and -4.4, $b^* = 7.2$ and 4.6, and $L^* = 85$ and 87, respectively. According to these authors, the films had a vivid green-yellow color as compared to the gelatin films.

An increase in chlorophyllide concentration also caused a linear increase (28.5) in the total color difference (Fig. 28.4), signifying that the films containing additive evidently became more colored with greater pigment concentration.

$$\Delta E* = 3.51 + 0.19\, C_p, \qquad R^2 = 0.864 \tag{28.5}$$

Nevertheless, the values for ΔE^* were not as high as those that would have been expected from the presence of pigment in the formulation. Although the gelatin films with added chlorophyll were more colored than films based on various other proteins without the addition of pigments, such as gelatin (Vanin et al. 2005) and ovoalbumins

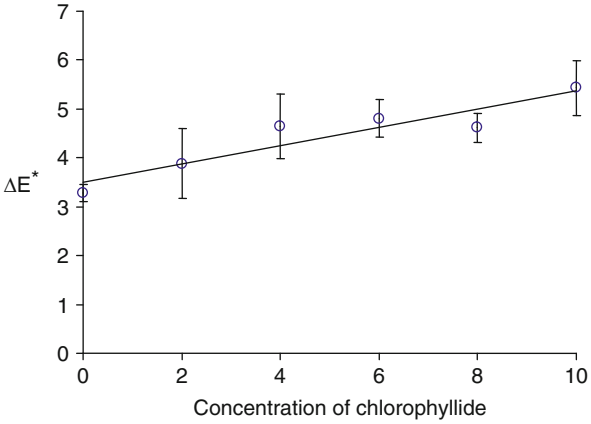

Fig. 28.4 Color difference (ΔE^*) in gelatin films containing different chlorophyllide concentrations

Table 28.2 Examples of color parameters in protein-based edible films

Films	ΔE^i	a^i	b^i	L^i	References
Egg albumen films, 40 g glycerol/100 g protein. (i = 1)	1.7	−0.5	3.5	96	Gennadios et al. (1996)
Water-soluble fish proteins films, 25 g sorbitol/100 g protein. (i = *)	7.0	−0.8	8	33	Bourtoom et al. (2006)
Laboratory-prepared soy protein isolate films, 30 g glycerol/100 g protein. (i = 1)	8.5	−2.3	9.9	95	Kunte et al. (1997)
Films based on Amaranth flour, 22.5 g glycerol/100 g flour. (i = *)	8.9	−1.2	8.1	90	Tápia-Blácido et al. (2007)
Round scad mince based film, dark muscle, 50 g glycerol/100 g protein. (i = *)	–	−2.5	20.7	84	Artharn et al. (2007)
Wheat gluten films, 30 g glycerol/100 g protein, heat treated at 140°C/15 min. (i = *)	–	10.5	45.4	75	Micard et al. (2000)
Fish muscle protein, 40 g glycerol/100 g protein, heat treated at 40°C/30 min. (i = *)	8.5	−1.6	8.9	97	Paschoalick et al. (2003)
Mammalian gelatin, 53 g glycerin/100 g gelatin (i = *)	3	−1	2.8	91	Sobral (1999)
Blends of gelatin and PVA, hydrolysis degree of 95.7%, 25 g glycerol/100 g macromolecules (i = *)	3.2	−1	2.6	92	Maria et al. (2008)
Fish skin gelatin, 25 g glycerol/100 g proteins. (i = *)	–	−0.4	1.6	9.5	Jongjareonrak et al. (2006a)

(i = 1): HunterLab; (i = *): CIELab

(Gennadios et al. 1996), they were apparently less colored than other films, also those containing no pigments such as films based on Nile Tilapia myofibrillar proteins (Sobral 2000) and soy proteins (Kunte et al. 1997) (Table 28.2).

However, despite the behavior of increasing coloration with increasing chlorophyll concentration in the film formulation, the coloration was practically imperceptible to the eye. According to Nassau (1996), the appearance of color as detected by the eye and interpreted by the brain depends significantly on the exact viewing circumstances, including sample transparency. In fact, the color of a pigmented medium, such as a plastic, depends on both transmittance and reflectance, which in turn are different if the material is opaque or transparent (Saunderson 1942). Moreover, according to Hanlon et al. (1998), in some plastics the thickness of translucent material has a direct bearing on the chroma $\{C^* = [(a^*)^2 + (b^*)^2]^{0.5}\}$.

Thus, considering that, although transparent, the opacity of gelatin films increases with increase in thickness (Sobral 1999), the perception of the color of the material would be different depending on the thickness of the films. Thus, analyses of the color of superimposed films, simulating films with increasing thickness, allowed for the confirmation that the thickness effectively influenced film coloration.

Figures 28.5 and 28.6 show that the parameters a^*, b^*, L^* and the total color difference (ΔE^*) varied linearly with the thickness (x) of the films, with different slopes, depending on the chlorophyllide concentrations (C_p) in the film formulation. Thus, these data were submitted to a multilinear regression analysis to observe both effects of x and C_p (28.6)–(28.9):

$$a* = 0.89 - 0.57x - 0.77\,C_p, \qquad R^2 = 0.886 \tag{28.6}$$

$$b* = -0.70 + 0.73x + 0.60\,C_p, \qquad R^2 = 0.927 \tag{28.7}$$

$$L* = 95.76 - 0.97x - 0.26\,C_p, \qquad R^2 = 0.985 \tag{28.8}$$

$$\Delta E* = -2.79 + 0.91x + 0.42\,C_p, \qquad R^2 = 0.969 \tag{28.9}$$

The quality of fitting can be also observed in Fig. 28.7, where it is possible to observe the capacity of all models to predict the experimental data. The data are closely banded around the straight line with a slope of 45°, which indicates the effectiveness of the (28.6)–(28.9) in describing the effect of pigment concentration and thickness on color parameters.

The linear behavior between the total color difference and thickness of biopolymer-based films was verified by Sobral (1999, 2000) working with gelatin and Tilapia myofibrillar protein films (respectively). However, no paper was found in the specialized literature on the effect of the concentration of a pigment on the actual effect of the thickness.

Moreover, it can be noted now that the thicker films ($x \rightarrow 0.400$ mm) presented very high color difference values ($\Delta E^* \cong 23$), much higher than those observed for colorless films (Table 28.2).

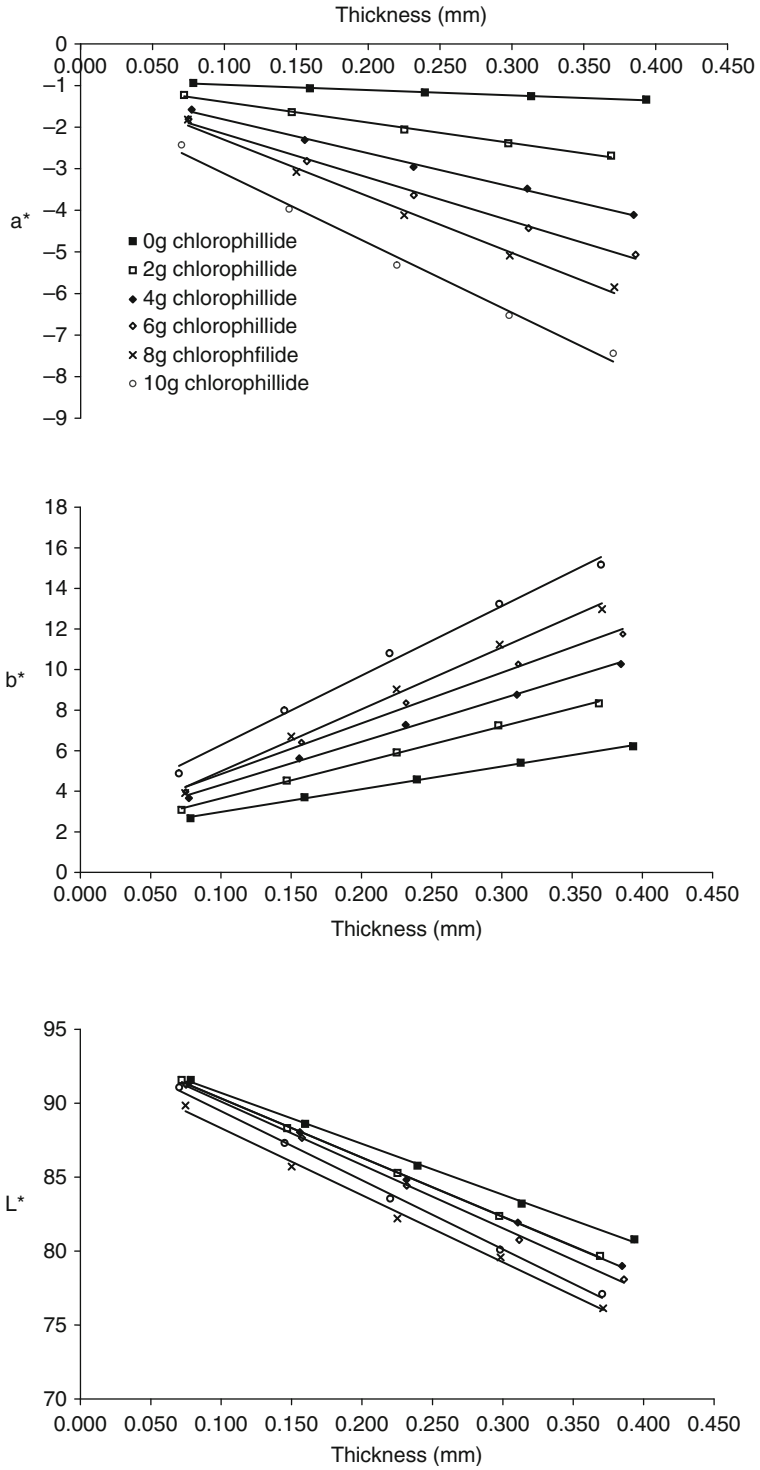

Fig. 28.5 Parameters *a** (*top*), *b** (*middle*), and *L** (*bottom*) of gelatin films containing different chlorophyllide concentrations, as a function of thickness

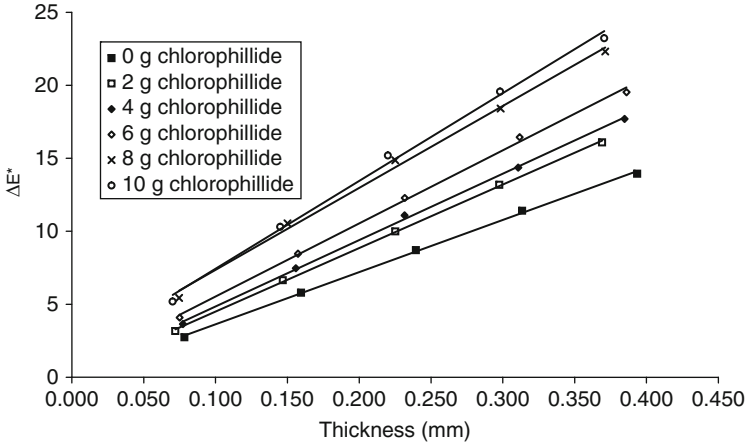

Fig. 28.6 Total color difference (ΔE^*) in gelatin films containing different chlorophyllide concentrations, as a function of thickness

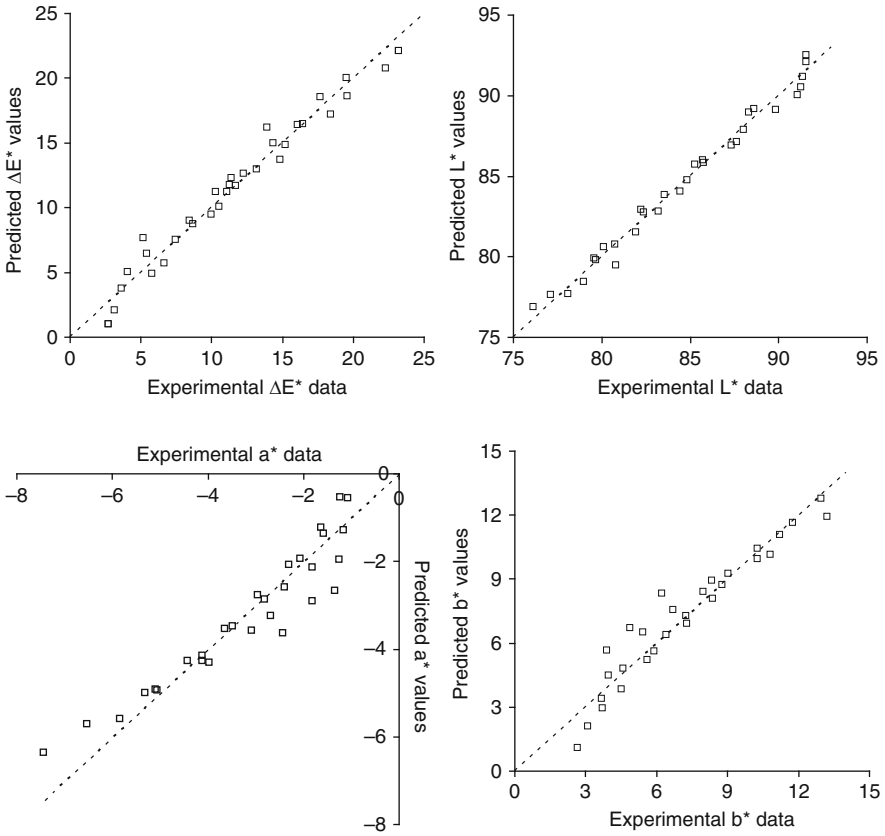

Fig. 28.7 Predicted values using (28.7)–(28.9) against experimental data of color parameters (slope of straight lines is 45°)

28.8 Conclusion

The use of a water-soluble pigment such as chlorophyll in the form of chlorophyllide is perfectly viable in edible film technology. The addition of this pigment does not affect the principal physical or functional properties of the material as compared to pure gelatin. However, perception of the green coloration is difficult, since the material is transparent. An increase in film thickness could contribute to a better perception of the color provided by the pigment.

Acknowledgements to the Foundation for Research Support of the State of São Paulo (FAPESP) and the National Council for Scientific and Technological Development (CNPq) for their support.

References

Achet DÇ, He XW (1995) Determination of the renaturation level in gelatin films. Polymer 36(4):787–791

Artharn A, Benjakul S, Prodpran T, Tanaka M (2007) Properties of a protein-based film from round scad (*Decapterus maruadsi*) as affected by muscle types and washing. Food Chem 103:867–874

Arvanitoyannis IS (2002) Formation and properties of collagen and gelatin films and coatings. In: Gennadios A (ed) Protein-based films and coatings. CRC Press, Boca Raton, pp 275–304

Arvanitoyannis I, Psomiadou E, Nakayama A, Aiba S, Yamamoto N (1997) Edible films made from gelatin, soluble starch and polyols, Part 3. Food Chem 60(4):593–604

Arvanitoyannis I, Nakayama A, Aiba S (1998a) Edible films made from hydroxypropyl starch and gelatin and plasticized by polyols and water. Carbohydr Polym 36:105–119

Arvanitoyannis I, Nakayama A, Aiba S (1998b) Chitosan and gelatin-based edible films: state diagrams, mechanical and permeation properties. Carbohydr Polym 37:371–382

Banker GS (1966) Film coating, theory and practice. J Pharmacol Sci 55:81–89

Bekbolet M (1990) Light effects on food. J Food Prot 53:430–440

Bergo PV, Carvalho RA, Sobral PJA, Bevilacqua FRS, Pinto JKC, Souza JP (2006) Microwave insertion loss measurements in gelatin-based films. Meas Sci Technol 17:3261–3264

Bertan LC, Tanada-Palmu PS, Siani ACC, Grosso RF (2005) Effect of fatty acids and 'Brazilian elemi' on composite films based on gelatin. Food Hydrocolloids 19(1):73–82

Bigi A, Cojazzi G, Panzavolta S, Rubini K, Roveri N (2001) Mechanical and thermal properties of gelatin films at different degrees of glutaraldehyde crosslinking. Biomaterials 22(7):763–768

Bourtoom T, Chinnan MS, Jantawat P, Sanguandeeku R (2006) Effect of select parameters on the properties of edible film from water-soluble fish proteins in surimi wash-water. Lebensmittel Wiss Technol 39:405–418

Cao N, Fu Y, He J (2007) Mechanical properties of gelatin films cross-linked, respectively, by ferulic acid and tannin acid. Food Hydrocolloids 21(4):575–584

Carvalho RA, Grosso CRF (2004) Characterization of gelatin based films modified with transglutaminase, glyoxal and formaldehyde. Food Hydrocolloids 18:717–726

Carvalho RA, Grosso CRF (2006) Properties of chemically modified gelatin films. Braz J Chem Eng 23(1):45–53

Carvalho RA, Grosso CRF, Sobral PJA (2008a) Effect of chemical treatment on the mechanical properties, water vapour permeability and sorption isotherms of gelatin-based films. Packag Technol Sci 21:165–169

Carvalho RA, Sobral PJA, Thomazine M, Habitante AMQB, Giménez B, Guillen CG, Montero P (2008b) Development of edible films based on differently processed Atlantic halibut (*Hippoglossus hippoglossus*) skin gelatin. Food Hydrocolloids 22:1117–1123

Carvalho RA, Moraes ICF, Bergo PVA, Kamimura ES, Habitante AMQB, Sobral PJA (2009) Study of some physical properties of biodegradable films based on blends of gelatin and poly (vinyl alcohol) using a response-surface methodology. Mater Sci Eng, C 29:485–491

Chattopadhyay P, Chatterjee S, Sen SK (2008) Biotechnological potential of natural food grade biocolorants. Afr J Biotechnol 7(17):2972–2985

Chiellini E, Cinelli P, Fernandes EG, Kenawy ES, Lazzeri A (2001) Gelatin-based blends and composites. Morphological and thermal mechanical characterization. Biomacromolecules 2:806–811

Coltro L, Padula M, Saron ES, Borghetti J, Buratin AEP (2003) Evaluation of a UV absorber added to PET bottles for edible oil packaging. Packag Technol Sci 16(1):15–20

Corat M, Carvalho RA, Trindade CSF, Sobral PJA (2007) Produção e caracterização de filmes a base de gelatina coloridos com clorofila. Alimentos: Ciencia e Ingeniería 16:94–96

Delgado-Vargas F, Paredes-López O (2002) Natural colorants for food and nutraceutical uses. CRC Press, Boca Raton

Durston J (2006) Flexible package closures and sealing systems. In: Theobald N, Winder B (eds) Package closures and sealing systems. CRC Press, Boca Raton, pp 204–230

Fang Y, Tung MA, Britt IJ, Yada S, Dalgleish DG (2002) Tensile and barrier properties of edible films made from whey proteins. J Food Sci 67:188–193

Francis FJ (2002) Food colorings. In: MacDougall DB (ed) Colour in food. CRC Press, New York, pp 307–340

Gennadios A, McHugh TH, Weller CL, Krochta JM (1994) Edible coating and films based on proteins. In: Krochta JM, Baldwin EA, Nisperos-Carriedo MO (eds) Edible coatings and to improve food quality. Technomic Publishing Company, Lancaster, pp 201–277

Gennadios A, Weller CL, Handa MA, Froning GW (1996) Mechanical properties of egg albumen films. J Food Sci 61(3):585–589

Gómez-Estaca J, Giménez B, Montero P, Gómez-Guillén MC (2009) Incorporation of antioxidant borage extract into edible films based on sole skin gelatin or a commercial fish gelatin. J Food Eng 92(1):78–85

Gómez-Guillén MC, Ihl M, Bifani V, Silva A, Montero P (2007) Edible films made from tuna-fish gelatin with antioxidant extracts of two different murta ecotypes leaves (*Ugni molinae* Turcz). Food Hydrocolloids 21:1133–1143

Gontard N, Guilbert S (1996) Bio-packaging: technology and properties of edible and/or biodegradable material of agricultural origin. Boletim da SBCTA 30(1):3–15

Gontard N, Guilbert S, Cuq J-L (1993) Water and glycerol as plasticizers effect mechanical and water vapor barrier properties of an edible wheat gluten film. J Agr Food Chem 58:206–211

Hanlon JF, Kelsey RJ, Forcinio HE (1998) Handbook of package engineering, 3rd edn. Technomic Publishing Company Inc., Lancaster

Humphrey AM (2004) Chlorophyll as a color and functional ingredient. J Food Sci 69(5): C422–C425

Jongjareonrak A, Benjakul S, Visessanguan W, Prodpran T, Tanaka M (2006a) Characterization of edible films from skin gelatin of brownstripe red snapper and bigeye snapper. Food Hydrocolloids 20(4):492–501

Jongjareonrak A, Benjakul S, Visessanguan W, Tanaka M (2006b) Effects of plasticizers on the properties of edible films from skin gelatin of bigeye snapper and brownstripe red snapper. Eur Food Res Technol 222:229–235

Kaya S, Kaya A (2000) Microwave drying effects on properties of whey protein isolate edible. J Food Eng 43:91–96

Kidmose U, Edelenbos M, Nørbæk R, Christensen LP (2002) Colour stability in vegetables. In: MacDougall DB (ed) Colour in food. CRC Press, New York, pp 189–242

Krochta JM, De-Mulder-Johnston CD (1997) Edible and biodegradable polymer films: challenges and opportunities. Food Technol 51:61–74

Kunte LA, Gennadios A, Cuppett SL, Hanna MA, Weller CL (1997) Cast films from soy protein isolates and fractions. Cereal Chem 74(2):115–118

Lanfer-Marquez UM (2003) O papel da clorofila na alimentação: uma revisão. Braz J Pharm Sci 39(3):227–242

Lim LT, Mine Y, Tung A (1999) Barrier and tensile properties of transglutaminase cross-linked gelatin films as affect by relative humidity, temperature, and glycerol content. J Food Sci 64(4):616–622

López-Carballo G, Hernández-Muñoz P, Gavara R, Ocio MJ (2008) Photoactivated chlorophyllin-based gelatin films and coatings to prevent microbial contamination of food products. Int J Food Microbiol 126:65–70

Maria TMC, Carvalho RA, Sobral PJA, Habitante AMBQ, Solorza-Feria JS (2008) The effect of the degree of hydrolysis of the PVA and the plasticizer concentration on the color, opacity, and thermal and mechanical properties of films based on PVA and gelatin blends. J Food Eng 87:191–199

Matsumura S, Tomizawa N, Toki A, Nishikawa K, Toshima K (1999) Novel poly(vinyl alcohol)-degrading enzyme and the degradation mechanism. Macromolecules 32:7753–7761

Mendieta-Taboada OWM, Sobral PJA, Carvalho RA, Habitante AMBQ (2008) Thermomechanical properties of biodegradable films based on blends of gelatin and poly(vinyl alcohol). Food Hydrocolloids 22:1485–1492

Menegalli FC, Sobral PJA, Roques M, Laurent S (1999) Characteristics of gelatin biofilms in relation to drying process conditions near melting. Drying Technol 17:1697–1706

Micard V, Balamri R, Morel M-H, Guilbert S (2000) Properties of chemically and physically treated wheat gluten films. J Agric Food Chem 48(7):2948–2953

Monedero FM, Fabra MJ, Talens P, Chiralt A (2009) Effect of oleic acid-beeswax mixtures on mechanical, optical and water barrier properties of soy protein isolate based films. J Food Eng 91(4):509–515

Nassau K (1996) Fundamentals of color science. In: Nassau K (ed) Color for science, art and technology. North Holland, Lebanon, pp 1–30

Nisperos-Carriedo MO (1994) Edible coatings and films based on polysaccharides. In: Krochta JM, Baldwin EA, Nisperos-Carriedo M (eds) Edible coatings and films to improve food quality. Technomic Publishing Company, Lancaster, pp 305–336

Paschoalick TM, Garcia FT, Sobral PJA, Habitante AMQB (2003) Characterization of some functional properties of edible films based on muscle proteins of Nile Tilapia. Food Hydrocolloids 17:419–427

Saffert A, Pieper G, Jetten J (2009) Effect of package light transmittance on the vitamin content of milk, part 3: fortified UHT low-fat milk. Packag Technol Sci 22:31–37

Saunderson JL (1942) Calculation of the color of pigmented plastics. J Opt Soc Am 32(12): 727–729

Schoefs B (2002) Chlorophyll and carotenoid analysis in food products. Properties of the pigments and methods of analysis. Trends Food Sci Technol 13:361–371

Shiku Y, Hamaguchi PY, Benjakul S, Visessanguan W, Tanaka M (2004) Effect of surimi quality on properties of edible films based on Alaska Pollack. Food Chem 86:493–499

Silva GGD, Sobral PJA, Carvalho RA, Bergo PVA, Mendieta-Taboada OW, Habitante AMQB (2008) Biodegradable films based on blends of gelatin and poly (vinyl alcohol): effect of PVA type or concentration on some physical properties of films. J Polym Environ 16:276–285

Slade L, Levine H (1987) Polymer-chemical properties of gelatin in foods. In: Pearson AM, Dutson TR, Bailey AJ (eds) Advances in meat research, collagen as a food. Elsevier Applied Science, London, pp 251–266

Sobral PJA (1999) Propriedades funcionais de biofilmes de gelatina em função da espessura. Ciência & Engenharia 8:60–67

Sobral PJA (2000) Influência da espessura sobre certas propriedades de biofilmes à base de proteínas miofibrilares. Pesqui Agropecu Bras 35:1251–1259

Sobral PJA, Menegalli FC, Hubinguer MD, Roques MA (2001) Mechanical, water vapor barrier and thermal properties of gelatin based edible films. Food Hydrocolloids 15:423–32

Streit MN, Canterle LP, Canto MW, Hecktheuer LHH (2005) As clorofilas. Ciência Rural 35:748–755

Tapia-BLácido DT, Mauri A, Menegalli FC, Sobral PJA, Añon MC (2007) Contribution of the starch, protein and lipid fractions to the physical, thermal and structural properties of amaranth (*amaranthus caudatus*) flour films. J Food Sci 72:E293–E300

Tharanathan RN (2003) Biodegradable films and composite coatings: past, present and future. Trends Food Sci Technol 14:71–78

Thomazine M, Carvalho RA, Sobral PJA (2005) Physical properties of gelatin films plasticized by blends of glycerol and sorbitol. J Food Sci 70:172–176

Torres JA (1994) Edible films and coatings from proteins. In: Hettiarachy NS, Ziegler GR (eds) Protein functionality in food systems. Marcel Dekker, New York, pp 467–507

Van de Velde K, Kiekens P (2002) Biopolymers: overview of several properties and consequences on their applications. Polym Test 21(4):433–442

Vanin FM, Sobral PJA, Menegalli FC, Carvalho RA, Habitante AMQB (2005) Effects of plasticizers and their concentrations on thermal and functional properties of gelatin based films. Food Hydrocolloids 70:172–176

Veis A (1964) The molecular characterization of gelatin. In: The macromolecular chemistry of gelatin. Academic, New York

Villalobos R, Chanona J, Hernández P, Gutiérrez G, Chiralt A (2005) Gloss and transparency of hydroxypropyl methylcellulose films containing surfactants as affected by their microstructure. Food Hydrocolloids 19:53–61

Wilska-Jeszka J (2007) Food Colorants. In: Sikorski ZE (ed) Chemical and functional properties of food components. CRC Press, Boca Raton, pp 245–274

Zhang S, Wang Y, Herring JL, Oh J-H (2007) Characterization of edible film fabricated with channel catfish (*Ictalurus punctatus*) gelatin extract using selected pretreatment methods. J Food Sci 72(9):C498–C503

Ziegler CR, Foegeding EA (1990) The gelation of proteins. Adv Food Nutr Res 34:203–298

Index

J.M. Aguilera et al. (eds.), *Food Engineering Interfaces*, Food Engineering Series,
DOI 10.1007/978-1-4419-7475-4, © Springer Science+Business Media, LLC 2011